รายงานวิจัยฉบับสมบูรณ์

โครงการส่งเสริมกลุ่มวิจัย (เมธีวิจัยอาวุโส)

การวิจัยและพัฒนาใหม่ ๆ ของวัสดุพอลิเมอร์สีเขียวและประโยชน์ใช้งาน

โดย

ศาสตราจารย์ ดร. สุดา เกียรติกำจรวงศ์

กรกฎาคม 2554

สัญญาเลขที่ RTA5080004

รายงานวิจัยฉบับสมบูรณ์

โครงการส่งเสริมกลุ่มวิจัย (เมธีวิจัยอาวุโส)

การวิจัยและพัฒนาใหม่ ๆ ของวัสดุพอลิเมอร์สีเขียวและประโยชน์ใช้งาน

ศาสตราจารย์ ดร. สุดา เกียรติกำจรวงศ์
ภาควิชาวิทยาศาสตร์ทางภาพถ่ายและเทคโนโลยีทางการพิมพ์
คณะวิทยาศาสตร์ จุฬาลงกรณ์มหาวิทยาลัย

สนับสนุนโดยสำนักงานกองทุนสนับสนุนการวิจัย

(ความเห็นในรายงานนี้เป็นของผู้วิจัย สกว. ไม่จำเป็นต้องเห็นด้วยเสมอไป)

กิตติกรรมประกาศ

รายงานวิจัยฉบับนี้ เป็นผลงานจากโครงการเมธีวิจัยอาวุโส ระยะที่ 2 หรือ โครงการส่งเสริมกลุ่มวิจัย ประจำปี 2550 – 2553 ได้รับการสนับสนุนจากสำนักงานกองทุนสนับสนุนการวิจัย (สกว.) และสำนักงานคณะกรรมการการอุดมศึกษา (สกอ.) เรื่อง **การวิจัยและพัฒนาใหม่ ๆ ของวัสดุพอลิเมอร์สีเขียวและประโยชน์ใช้งาน (Novel Research and Development in Green Polymer Materials and Their Applications)**

ด้วยปรารถนาของหัวหน้าโครงการวิจัยที่จะรวบรวมผลงานต่าง ๆ ให้สมบูรณ์ที่สุด จึงได้ขยายเวลาวิจัยจากปกติใช้เวลา 3 ปี มาเป็นเวลา 4 ปี (พ.ศ. 2554) หัวหน้าโครงการซาบซึ้งในการสนับสนุนอย่างเต็มที่ของสำนักงาน สกว. ทั้งในช่วงเวลาปกติ และช่วงที่ขยายเวลาออกไปอีก 1 ปี ทำให้สามารถผลิตนิสิตระดับบัณฑิตศึกษาได้อีก 3 คน พร้อมบทความที่จะเกิดขึ้นอีกจำนวนหนึ่ง ในฐานะหัวหน้าโครงการเมธีวิจัยอาวุโส ระยะที่ 2 ขอกราบขอบพระคุณสำนักงานกองทุนสนับสนุนการวิจัย โดยเฉพาะอย่างยิ่ง อดีตผู้อำนวยการฝ่ายวิชาการ (ศาสตราจารย์ ดร. วิชัย บุญแสง) ที่ให้กำลังใจมาตลอดเวลา 3 ปี ที่ท่านอยู่ในตำแหน่ง โดยท่านให้ความกรุณามาเปิดงานประชุมวิชาการประจำปีทุกปีอย่างสม่ำเสมอ ให้ข้อแนะนำ ให้กำลังใจ และช่วยเสนอวิธีแก้ปัญหามาตลอด ขอขอบพระคุณท่านรักษาการผู้อำนวยการฝ่ายวิชาการคนใหม่ (ศาสตราจารย์ ดร. สวัสดิ์ ตันตระรัตน์) ที่ให้การสนับสนุนอย่างดีเช่นกันใน 1 ปี ที่ผ่านมา

นอกจากนี้ คณะวิจัยขอบพระคุณหน่วยงานเจ้าสังกัดของนักวิจัยทุกท่านที่อนุเคราะห์สถานที่และให้ใช้อุปกรณ์ประกอบการวิจัย เป็นอย่างดีตลอดมา ขอขอบคุณบริษัทและโรงงานผู้ผลิตที่เอื้อเฟื้อสารเคมีบางประเภทที่ได้กล่าวไว้ในรายงานความก้าวหน้าการวิจัยและในบทความที่พิมพ์เผยแพร่ในวารสารวิชาการ อย่างไรก็ตาม หัวหน้าโครงการนี้จะขอกราบขอบพระคุณอีกครั้งหนึ่งสำหรับทุกสิ่งทุกอย่างที่ท่านได้ให้การสนับสนุนทั้งที่มีการกล่าวถึงและไม่ได้กล่าวถึง

ศาสตราจารย์ ดร. สุดา เกียรติกำจรวงศ์

หัวหน้าโครงการเมธีวิจัยอาวุโส ระยะที่ 2

พ.ศ. 2550 - 2554

การวิจัยและพัฒนาใหม่ ๆ ของวัสดุพอลิเมอร์สีเขียวและประโยชน์ใช้งาน

Novel Research and Development in Green Polymer Materials and Their Applications

บทคัดย่อ

บทนำ

โครงการนี้เป็นโครงการเมธีวิจัยอาวุโสระยะที่สอง ประจำปี พ.ศ. 2550 – พ.ศ. 2553 มีโครงการย่อยในโครงการหลักนี้ 10 โครงการย่อย ระยะเวลาวิจัยแต่ละโครงการตั้งแต่ 1 ปี ถึง 3 ปี เนื่องจากมีโครงการย่อยจำนวนมากและครอบคลุมสาระวิชาหลายแขนง จึงทำให้ทำวิจัยไม่เสร็จทันเวลาที่กำหนด ด้วยความกรุณาของผู้อำนวยการฝ่ายวิชาการ จึงได้รับการอนุมัติให้ขยายเวลาวิจัยออกไปอีก 1 ปี สิ้นสุดโครงการวันที่ 31 กรกฎาคม 2554 เพื่อให้โครงการสมบูรณ์และผู้ช่วยวิจัยสามารถทำวิจัยเสร็จและสำเร็จการศึกษาจำนวนหนึ่ง โครงการย่อยทั้งหมดมีดังนี้

โครงการวิจัยย่อยที่ 1

Reactive Blending of Cassava Starch and Acrylamide and Its Application in Thermoplastic Vulcanizates of NR/PP blends

รีแอ็กทีฟเบลนดิงของแป้งมันสำปะหลังกับอะคริลาไมด์และเทอร์โมพลาสติกวัลคะไนเซตส์ของยางธรรมชาติกับพอลิโพรไพลีนเบลนด์

โครงการวิจัยย่อยที่ 2

Biomedical Applications of Surface-Charged Chitosan Particles and Assembled Thin Film of Charged Derivatives of Chitosan

การประยุกต์ทางชีวการแพทย์ของอนุภาคไคโทซานที่พื้นผิวมีประจุและฟิล์มประกอบแบบบางของอนุพันธ์ที่มีประจุของไคโตซาน

โครงการวิจัยย่อยที่ 3

3.1 Synthesis and Performance of Grafted Chitosan/Mica Nanocomposite for Antibacterial Activities

การสังเคราะห์และสมรรถนะของไคโทซานกราฟต์/ไมกานาโนคอมพอสิตสำหรับต้านเชื้อแบคทีเรีย

3.2 Synthesis and Characterization of Controlled Release NPK Fertilizer Hydrogel

การสังเคราะห์และการตรวจสอบเอกลักษณ์ของปุ๋ยไฮโดรเจลเอ็นพีเคที่ควบคุมการปลดปล่อย

โครงการวิจัยย่อยที่ 4

Microencapsulation via Glass Membrane Emulsification and Controlled Release of Menthol

ไมโครเอนแคปซูเลชันของเมนทอลโดยกลาสเมมเบรนอิมัลซิฟิเคชันและการปลดปล่อยแบบควบคุม

โครงการวิจัยย่อยที่ 5

Synthesis of Acrylamide-Based Copolymeric Superabsorbents with Thermal Stability and Flame Retardant Properties

การสังเคราะห์ซูเปอร์แอบซอร์แบนต์นาโนคอมพอสิตที่มีสมบัติความเสถียรทางความร้อนและหน่วงการติดไฟ

โครงการวิจัยย่อยที่ 6

Surface Modification of Electrospun Chitosan Nanofibers for Antibacterial Activity

การดัดแปรผิวของไคโทซานนาโนไฟเบอร์จาการปั่นเส้นใยเพื่อต้านฤทธิ์เชื้อแบคทีเรีย

โครงการวิจัยย่อยที่ 7

Synthesis of Hydrogel from Collagen

การสังเคราะห์ไฮโดรเจลจากคอลลาเจน

โครงการวิจัยย่อยที่ 8

Pretreatment of Kapok Fiber for Pulping and Papermaking

การปรับสภาพเส้นใยนุ่นเพื่อการผลิตเยื่อและกระดาษ

โครงการวิจัยย่อยที่ 9

9.1 Simulation of Printed Images on Silk Fabric by Ink Jet Printer

การจำลองภาพพิมพ์บนผ้าไหมด้วยเครื่องพิมพ์อิงก์เจ็ต

9.2 Textile Fabric Pretreatment and Pretreated Fabric Ink-jet Ink Printing

การปรับผิวเส้นใยผ้าและการพิมพ์ผ้าที่ปรับผิวแล้วด้วยหมึกพิมพ์อิงก์เจ็ต

โครงการวิจัยย่อยที่ 10

Reinforcement of Dipped Natural Rubber Film by *In Situ* Generated Silica

การเสริมแรงฟิล์มยางธรรมชาติแบบจุ่มด้วยซิลิกาที่เกิดขึ้นภายใน ณ จุดเกิดปฏิกิริยา

เนื่องจากครงการวิจัยนี้มีโครงการย่อยจำนวนมากที่ใช้สารตั้งต้น หรือวัตถุประสงค์ปลายทางคล้ายกัน จึงเห็นว่า ควรนำมารวมกลุ่มงานวิจัยได้ 7 กลุ่มโครงการวิจัยที่มีวัตถุประสงค์ตรงกัน เพื่อให้เห็นภาพของงานวิจัยได้ชัดเจนขึ้น ง่ายต่อการอ่านและด้านนำไปใช้งานได้ชัดเจนขึ้นในอนาคต ดังนี้

กลุ่มโครงการวิจัยที่ 1 ยางธรรมชาติและการดัดแปรคุณลักษณะของยางธรรมชาติ มีงานวิจัย 4 เรื่อง ดังนี้

1.1 Preparation of Cassava Starch-Graft-Polyacrylamide Superabsorbent Polymers and Associated Superabsorbent Polymer Composites by Reactive Blending

1.2 Synthesis and Characterization of Water Swellable Natural Rubber Composites

1.3 Reinforcement of Dipped Natural Rubber Film by *In Situ* Generated Silica

1.4 Silica Formation inside Natural Rubber Grafted with Methyl Methacrylate/ Methacryloxypropyl Trimethoxysilane

กลุ่มโครงการวิจัยที่ 2 ไคโทซานและการพัฒนาไคโทซานสำหรับการใช้งานทางชีวการแพทย์ มี 2 เรื่องหลัก 5 หัวข้อย่อย ดังนี้

2.1 Biomedical Applications of Surface-Charged Chitosan Particles and Assembled Thin Film of Charged Derivatives of Chitosan มี 2 เรื่องย่อย

2.1.1 Surface-quaternized Chitosan Particles as Alternative and Effective Organic Antibacterial Fillers

2.1.2 Multilayer Thin Films Assembled from Charged Derivatives of Chitosan: Formation and Biological Responses

2.2 Syntheses, Characterization and Antibacterial Activity of Chitosan Grafted Hydrogels and Associated Mica Containing Nanocomposite Hydrogels

2.3 Surface Modification of Electrospun Chitosan Nanofibers for Antibacterial Activity

กลุ่มโครงการวิจัยที่ 3 ไฮโดรเจลสำหรับสิ่งแวดล้อม มีงานวิจัย 3 เรื่อง

3.1 Synthesis of Acrylamide/Acrylic Acid-Based Aluminum Flocculant for Dye Reduction and Textile Wastewater Treatment

3.2 Photocatalytic Efficiency of TiO_2/Poly[Acrylamide-*co*-(Acrylic Acid)] Composite for Textile Dye Degradation

3.3 Acrylamide-Based Composite Hydrogel Initiated by TiO_2 Photocatalyst for Dye and Hydrogel Degradation

กลุ่มโครงการวิจัยที่ 4 ไฮโดรเจลกับการใช้งานเฉพาะทาง มี 5 เรื่อง

4.1 Gel Strength and Swelling of Acrylamide-Protic Acid Superabsorbent Copolymers

4.2 Acrylamide–Itaconic Acid Superabsorbent Polymers and Superabsorbent Polymer/Mica Nanocomposites

4.3 Synthesis of Acrylamide-*co*-(Itaconic Acid) Superabsorbent Polymers and Associated Silica Superabsorbent Polymer Composites

4.4 Acrylamide/2-acrylamido-2-methylpropane Sulfonic Acid and Associated Sodium Salt Superabsorbent Copolymers with Mica Nanocomposites as Fire Retardants

4.5 Effect of Fire Retardant on Flammability of Acrylamide and 2-Acrylamido-2-Methylpropane Sodium Sulfonate Copolymer Composites

4.6 Swelling Properties and Strength of Poly[Acrylamide-*co*-(Itaconic Acid)] Gel and Clay-Modified Poly[Acrylamide-*co*-(Itaconic Acid)] Gel

กลุ่มโครงการวิจัยที่ 5 ไมโครเอนแคปซูเลชันและการควบคุมการปล่อยของวัสดุอินทรีย์/อินทรีย์ มีงานวิจัย 4 เรื่อง

5.1 Microencapsulation of Menthol via Glass Membrane Emulsification and Controlled Release

5.2 Synthesis of Microcapsules of Eucalyptus Oil via Shirasu Porous Glass Membrane Emulsification and Controlled Release

5.3 Synthesis and Characterization of Controlled Release Compound NPK Fertilizer Hydrogel

5.4 Synthesis and Characterization of Hydrogel for Insulin Released from Collagen Grafted Poly[(Acrylic Acid)-*co*-(Methacrylic Acid)]

กลุ่มโครงการวิจัยที่ 6 การผลิตเส้นใยและกระดาษจากนุ่น มีงานวิจัย 3 เรื่อง

6.1 Kapok I: Properties Investigation of Kapok Fiber as a Potential Pulp Source for Papermaking

6.2 Kapok II: Pretreatment of Kapok Fibers for Pulping and Papermaking

6.3 Kapok III: Use of Kapok Pulp to Improve Properties of Recycled Paper

กลุ่มโครงการวิจัยที่ 7 การปรับผิวผ้าและการพิมพ์ผ้าด้วยหมึกพิมพ์อิงก์เจ็ต

7.1 Modified Chitosan Pretreatment of Polyester Fabric for Printing by Ink Jet Ink

7.2 Anionically Surface-Modified Pigment/Binder Ink Jet Inks for Silk Fabric Printing

7.3 Simulation of Printed Images on Silk Fabric by Ink Jet Printer

7.4 Effects of Chitosan and Glycine Pretreatment on Polyester Fabric Printed by Ink Jet Ink

7.5 Effects of Ink Formulation Containing Surface-Modified Pigmented Jet Inks on Jettability

ดังนั้น จึงขอรายงานบทคัดย่อของงานวิจัยนี้ตามลำดับเนื้องานวิจัยดังกล่าวข้างต้น

กลุ่มโครงการวิจัยที่ 1 ยางธรรมชาติและการดัดแปรคุณลักษณะของยางธรรมชาติ

1.1 Preparation of Cassava Starch-Graft-Polyacrylamide Superabsorbent Polymers and Associated Superabsorbent Polymer Composites by Reactive Blending

Cassava starch-*g*-polyacrylamide (PAM) was successfully prepared by a reactive batch processing using a specially designed batch reactor resulting in a superabsorbent polymer (SAP) with water absorption of 605 g/g being obtained under the optimized reaction conditions. The occurrence of a graft copolymer was confirmed by FT-IR spectra, where it was found to exhibit all characteristic bands of both starch and acrylamide (AM) units. SEM micrographs of the starch granules showed an irregular shape and varied particle sizes with a smooth surface, while the graft copolymers had a coarse porous structure and broad network. Various types of inorganic filler were added to the graft copolymer to prepare the SAP composites (SAPC). It was found that the SAPC with bentonite clay exhibited the highest water absorption of approximately 730 g/g. Conversely, the incorporation of silica to the graft copolymer gave a significantly lower water absorption capability than the copolymer alone.

Key words: Acrylamide, Batch reactor, Cassava starch, Superabsorbent polymer composite

การเตรียมพอลิเมอร์ซูเปอร์แอบซอร์เบนต์ของแป้งมันสำปะหลังกราฟต์พอลิอะคริลาไมด์และคอมพอสิตแอบซอร์เบนต์ที่สอดคล้องกัน

โครงการนี้ได้เตรียมแป้งมันสำปะหลังกราฟต์พอลิอะคริลาไมด์ (พีเอเอ็ม หรือ PAM) ด้วยวิธีรีแอกทีฟแบบกะในปฏิกรณ์ที่ออกแบบพิเศษ ทำให้ได้พอลิเมอร์ซูเปอร์แอบซอร์เบนต์ (เอสเอพี หรือ SAP) ที่มีค่าการดูดซึมน้ำ 605 กรัมต่อกรัมของสารแห้ง ภายใต้ภาวะของปฏิกิริยาที่ควบคุมให้เหมาะสม เทคนิค FTIR ตรวจพบลักษณะเฉพาะของพีกหรือแบนด์ทั้งในแป้งและพอลิอะคริลไมด์ (PAM) ภาพอิเล็กตรอนไมโครกราฟแสดงเม็ดแป้งที่มีขนาดไม่แน่นอน แต่มีผิวเรียบ ในขณะที่ภาพของกราฟต์โคพอลิเมอร์มีโครงสร้างหยาบ พร้อมรูพรุนและโครงข่ายกว้าง ได้ใส่สารเติมแต่งอนินทรีย์หลายชนิดให้แก่กราฟต์โคพอลิเมอร์เพื่อเตรียมพอลิเมอร์ซูเปอร์แอบซอร์เบนต์คอมพอสิต (SAPC) พบว่า SAPC ที่ผสมแร่ดินเบนโทไนต์ มีค่าการดูดซึมน้ำมากสุด 730 กรัมต่อกรัมของสารแห้ง ในทางตรงกันข้าม การใส่ผงซิลิกาในกราฟต์โคพอลิเมอร์ลดค่าการดูดซึมน้ำลงมากอย่างมีนัยสำคัญเมื่อเปรียบเทียบกับโคพอลิเมอร์ที่ไม่เติมผงซิลิกา

คำสำคัญ: อะคริลาไมด์, ปฏิกิริยาแบบกะ, แป้งมันสำปะหลัง, ซูเปอร์แอบซอร์เบนต์พอลิเมอร์คอมพอสิต

1.2 Synthesis and Characterization of Water Swellable Natural Rubber Composites

Superabsorbent polymer (SAP) based on cassava starch-*g*-polyacrylamide was prepared by a reactive batch processing using a specially designed batch reactor. The SAP composites (SAPCs) were prepared by blending with 20 phr of bentonite clay. The clay was used to increase water absorbency of the SAP from 605 g/g to SAPC of 730 g/g. Water swellable natural rubber (WSNR) was then prepared by blending high ammonia natural rubber (HANR) latex, and dry blending of epoxidized natural rubber (ENR), and maleated natural rubber (MNR) with SAPC, poly(ethylene oxide) (PEO) and trimethylol propane trimethacrylate coupling agent (TMPTMA). Curing, mechanical, morphological properties and water absorbency of WSNRs were characterized. The WSNR with PEO and TMPTMA gave higher mechanical strength and water absorbency. Increasing PEO loadings rendered higher absorbency with lower mechanical strength at its contents higher than 10 phr. A higher scorch time, cure time with a low crosslinking density, and cure rate index were found in the MNR base WSNRs compared with those of the unmodified NR and ENR base WSNRs. The ENR base WSNR exhibited the highest water absorbency with lower mechanical strength compared with the unmodified NR base WSNR.

Key words: Coupling agent, Poly(ethylene oxide), Superabsorbent polymer, Superabsorbent polymer composite, Trimethylol propane trimethacrylate, Water swellable natural rubber.

การสังเคราะห์และการตรวจลักษณะเฉพาะของยางธรรมชาติคอมพอสิตบวมน้ำ

ได้เตรียมพอลิเมอร์ซูเปอร์แอบซอร์เบนต์ (SAP) ของแป้งมันสำปะหลังกราฟต์พอลิอะคริลาไมด์ โดยทำปฏิกิริยาในปฏิกรณ์แบบกะที่ออกแบบพิเศษ และเตรียมพอลิเมอร์ซูเปอร์แอบซอร์เบนต์คอมพอสิต (SAPC) โดยผสมแร่ดินเบนโทไนต์ 20 พีเอชอาร์ การใช้แร่ดินก็เพื่อเพิ่มความแข็งแรงและค่าการดูดซึมน้ำของ SAP จาก 605 กรัมต่อกรัมของสารแห้ง เป็นค่า 730 กรัมต่อกรัมของสารแห้งใน SAPC เตรียมยางธรรรมชาติบวมน้ำจากการผสมเลเท็กซ์ของยางธรรมชาติที่มีความเข้มข้นของแอมโมเนียมาก และผลิตยางธรรมชาติดัดแปรบวมน้ำมากอีก 2 ประเภท คือ ยางธรรมชาติอิพอกซิไดส์ (ENR) และยางธรรมชาติมาลิเอต (MNR) ผสมยางธรรมชาติแต่ละประเภทด้วย SAPC พอลิเอทิลีนออกไซด์ (PEO)

และสารคู่ควบไทรเมทิลอลโพรเพนไทรเมทาคริเลต (TMPTMA) ตรวจคุณลักษณะด้านการบ่ม ด้านสัณฐานวิทยา สมบัติเชิงกล และค่าการดูดซึมน้ำ พบว่า ยางธรรมชาติไม่ดัดแปรที่มี PEO และ TMPTMA ให้ค่าสมบัติเชิงกลและค่าการดูดซึมน้ำดีขึ้น เมื่อเติม PEO 10 พีเอชอาร์ ทำให้ยางธรรมชาติบวมน้ำมีค่าการดูดซึมมากขึ้นแต่ความแข็งแรงเชิงกลลดลง และใช้เวลาทำให้ยางสุกและเกรียมนานขึ้น แต่ยังมีค่าความหนาแน่นของการเชื่อมขวางต่ำลง ในยางธรรมชาติบวมน้ำมาลิเอกมีค่าดัชนีของอัตราการบ่มสูงขึ้นเมื่อเทียบกับยางธรรมชาติบวมน้ำที่ไม่มีการดัดแปรโครงสร้างของยางและยางธรรมชาติบวมน้ำอีพอกซิไดส์ นอกจากนี้พบว่า ยางธรรมชาติบวมน้ำอีพอกซิไดส์ให้ค่าการดูดซึมน้ำมากกว่าและมีค่าสมบัติเชิงกลต่ำลงกว่ายางธรรมชาติบวมน้ำที่ไม่ดัดแปรโครงสร้าง

คำสำคัญ: สารคู่ควบ, พอลิเอทิลีนออกไซด์, พอลิเมอร์ซูเปอร์แอบซอร์เบนต์, พอลิเมอร์ซูเปอร์แอบซอร์เบนต์คอมพอสิต, ไทรเมทิลอลโพรเพนไทรเมทาคริเลต, ยางธรรมชาติบวมน้ำ

1.3 Reinforcement of Dipped Natural Rubber Film by *In Situ* Generated Silica

A method for preparing silica-reinforced rubber thin film by latex dipping process was established. The latex used in the dipping step was pre-mixed with alkoxysilane precursor and sulfur curing agents. By one heating step, both *in situ* silica formation and rubber curing took place successfully in the rubber thin films. This work focused on the use of two alkoxysilane precursors that contained one vinyl group, i.e., vinyl triethoxysilane (VTOS), and methacryloxypropyl trimethoxysilane (MPS). Both were able to covalently link to the double bonds in NR chains via sulfur or radical crosslinking. Therefore, the size and distribution of *in situ* silica as well as its reinforcement capability on the NR vulcanizates were investigated as a function of the type and amount of added alkoxysilanes.

Key words: Particle-reinforcement, Mechanical properties, Sol-gel process.

การเสริมแรงฟิล์มยางธรรมชาติแบบจุ่มด้วยซิลิกาที่เกิดขึ้นภายใน ณ จุดเกิดปฏิกิริยา

งานวิจัยได้ศึกษากรรมวิธีการเตรียมฟิล์มบางของลาเท็กซ์ยางธรรมชาติแบบจุ่ม เลเท็กซ์นี้ต้องผสมกับแอลคอกซิไซเลนพรีเคอร์เซอร์และสารบ่มซัลเฟอร์ก่อน แค่ให้ความร้อนเพียงขั้นเดียวก็ทำให้เกิดผงซิลิกาจากสารพรีเคอร์เซอร์พร้อมกับเกิดการบ่มฟิล์มยางอย่างสมบูรณ์ งานวิจัยนี้เน้นการใช้แอลคอกซิไซเลนพรีเคอร์เซอร์ที่มีหมู่ไวนิลเพียง 1 หมู่ 2 ชนิด คือ ไวนิลไทรเอทอกซิไซเลน (VTOS) และเมทาคริลอ

ซิโพรพิลไทรเมทอกซิไซเลน (MPS) สารทั้งสองนี้สามารถเกิดพันธะโควาเลนต์กับพันธะคู่ในสายโซ่ของยางธรรมชาติผ่านซัลเฟอร์ หรือการเชื่อมขวางด้วยอนุมูลอิสระ ดังนั้น จึงศึกษาขนาดและการกระจายขนาดของผงซิลิกาที่เกิดขึ้นระหว่างการบ่มกับความสามารถในการเสริมแรงของยางวัลคะไนเซตส์ ซึ่งเป็นตัวแปรของชนิดและปริมาณของแอลคอกซีไซเลนที่เติมลงไป

คำสำคัญ: การเสริมแสงด้วยอนุภาค สมบัติเชิงกล, กระบวนการโซล-เจล

1.4 Silica Formation inside Natural Rubber Grafted with Methyl Methacrylate/Gamma-Methacryloxypropyl Trimethoxysilane

Methyl methacrylate (MMA) and γ-methacryloxypropyl trimethoxysilane (γ-MPS) were both grafted onto isoprene units of natural rubber (NR) with the aim to prepare rubber-silica hybrid. The methoxy silane units of γ-MPS were allowed to undergo hydrolysis and condensation reaction by heating the cast film of the grafted latex at 50°C to form silica particles within the rubber matrix. The formation of this rubber-silica hybrid was confirmed by ATR-FTIR, TEM and SEM. The γ-MPS coupling agent could also transform into silica inside the rubber. The addition of tetraethoxysilane (TEOS) resulted in an increase of *in situ* silica of up to 6 phr. The grafting efficiency of MMA onto rubber was around 80%, while that of γ-MPS was about 48%. The final composition of the hybrid rubber was 86:12:2.0 (by weight) of NR: MMA:γ-MPS.

Key words: In situ silica*,* Methyl methacrylate*,* γ-methacryloxypropyl trimethoxysilane, Natural rubber

การเกิดซิลิกาภายในยางธรรมชาติกราฟต์ด้วยเมทิลเมทาคริเลต / เมทาคริลอกซีโพรพิลไทรเมทอกซีไซเลน

โครงการนี้ได้เตรียมยางธรรมชาติผสมผงซิลิกาโดยกราฟต์เมทิลเมทาคริเลต (MMA) และแกมมา-เมทอะคริลอกซีโพรพิลไทรเมทอกซีไซเลน (γ-MPS) บนหน่วยไอโซพรินของยางธรรมชาติ หน่วยเมทอกซีไซเลนของ γ-MPS เกิดไฮโดรไลซิสและปฏิกิริยาควบแน่นได้โดยให้ความร้อน 50 องศาเซลเซียส แก่ฟิล์มจุ่มของเลเท็กซ์กราฟต์เพื่อให้เกิดอนุภาคซิลิกา ณ จุดเกิดปฏิกิริยาแก่เมทริกซ์ของยาง ยืนยันเอกลักษณ์และการเกิดผงซิลิกาในยางผสมซิลิกาด้วยเทคนิค ATR-FTIR, TEM และ SEM สารคู่ควบ γ-

MPS นี้สามารถเปลี่ยนรูปและเกิดซิลิกา ณ จุดเกิดปฏิกิริยาอยู่ภายในยางธรรมชาติด้วย การเติมเททระเอทอกซีไซเลน (TEOS) ทำให้เพิ่มปริมาณซิลิกาที่เกิด ณ จุดเกิดปฏิกิริยาเพิ่มขึ้นถึง 6 phr ประสิทธิ์ภาพการกราฟต์ของ MMA บนยางธรรมชาติอยู่ที่ร้อยละ 80 ในขณะที่การกราฟต์ด้วย γ-MPS มีประสิทธิ์ภาพเพียงร้อยละ 48 องค์ประกอบสุดท้ายของยางผสมผงซิลิกามีสัดส่วนของยางธรรมชาติ : MMA : γ--MPS เป็น 86:12:2

คำสำคัญ: ซิลิกาที่เกิด ณ จุดเกิดปฏิกิริยา, เมทิลเมทาคริเลต, แกมมา-เมทอะคริโลซีโพรพิลไทรเมทอกซิไซเลน, ยางธรรมชาติ

กลุ่มโครงการวิจัยที่ 2 ไคโทซานและการพัฒนาไคโทซานสำหรับการใช้งานทางชีวการแพทย์

2. Biomedical Applications of Surface-Charged Chitosan Particles and Assembled Thin Film of Charged Derivatives of Chitosan

Chitosan is a partially deacetylated form of chitin, a natural substance found abundantly in the exoskeletons of insects, shells of crustaceans, and fungal cell walls. Because of its favorable physicochemical and biological properties such as biocompatible, non-toxic, antibacterial, chitosan is considered as an attractive material that can be potentially used in many biomedical-related applications. The repeating units of chitosan constitute a large number of hydroxyl and amino groups. These two functional groups offer several possibilities for derivatization and immobilization of biologically active species. Taking advantages of functional group availability for chemical reactions of chitosan and the diversified bioactivity of chitosan and its charged derivatives, this research aimed to explore the applicability of charge-functionalized chitosan. The research was divided into two parts. The first part concentrated on the formation of multilayer films from charged derivatives of chitosan via layer-by-layer adsorption. The charged derivatives that were of our interest are *N*-sulfofurfuryl chitosan (SFC), *N*-succinyl chitosan (SCC), and *N*-[(2-hydroxyl-3-trimethylammonium)propyl] chitosan chloride (HTACC). The assembly process and viscoelastic properties were monitored by quartz crystal microbalance (QCM). Stratification of the multilayer film was demonstrated by water contact angle analysis. The coverage of the assembled films was characterized by atomic force microscopy and ATR-FTIR spectroscopy. Biological responses of the selected assembled films were assessed in term of *in vitro* cell adhesion and proliferation of fibroblasts, antibacterial activity, and platelet adhesion.

Keywords: Chitosan, Charged derivative, Multilayer film, Biocompatibility, Particles, Antibacterial activity, Biosensor, DNA, PNA, Ion exchanger

ไคโทซานได้จากการกำจัดหมู่แอซิทิลบางส่วนของไคทิน สารธรรมชาติที่พบมากในเปลือกของแมลง สัตว์มีกระดอง และผนังเซลล์ของเห็ดและราบางชนิด เนื่องจากสมบัติทางกายภาพ เคมี และชีวภาพที่น่าสนใจของไคโทซาน เช่น เข้ากันได้กับสิ่งมีชีวิต ไม่เป็นพิษ และต้านแบคทีเรีย ทำให้ไคโท

ซานเป็นวัสดุที่น่าสนใจและมีศักยภาพในการพัฒนาเพื่อการประยุกต์ในงานที่เกี่ยวข้องกับชีวการแพทย์ หน่วยซ้ำของไคโทซานประกอบด้วยหมู่ไฮดรอกซิลและหมู่แอมิโนที่สามารถนำไปใช้ในเปลี่ยนเป็นอนุพันธ์ต่างๆ หรือการตรึงสารที่ไวทางชีวภาพได้ ใช้ประโยชน์จากการมีหมู่ฟังก์ชันที่สามารถนำไปใช้ในการดัดแปรทางเคมีของไคโทซานและสมบัติทางชีวภาพที่หลากหลายของอนุพันธ์ที่มีประจุของไคโทซาน งานวิจัยนี้มีเป้าหมายที่จะศึกษาการใช้อนุพันธ์ที่มีประจุของไคโทซาน งานวิจัยแบ่งออกเป็นสองส่วน ส่วนแรกเป็นการศึกษาการเกิดเป็นฟิล์มมัลติเลเยอร์ของอนุพันธ์ที่มีประจุของไคโทซานด้วยการประกอบแบบชั้นต่อชั้น อนุพันธ์มีประจุของไคโทซานที่สนใจศึกษาในงานวิจัยนี้ ได้แก่ เอ็น-ซัลโฟเฟอร์ฟูริลไคโทซาน, เอ็น-ซักซินิลไคโทซาน, และ เอ็น-[(2-ไฮดรอกซิล-3-ไทรเมทิล แอมโมเนียม)โพรพิล]ไคโทซานคลอไรด์ ติดตามกระบวนการประกอบเป็นฟิล์มและสมบัติวิสโคอิลาสติซิตีด้วยควอร์ตซ์คริสทัลไมโครบาลานซ์ วิเคราะห์การสลับชั้นด้วยการวัดมุมสัมผัสของน้ำ ตรวจสอบการปกคลุมของฟิล์มที่ประกอบขึ้นด้วยอะตอมมิกฟอร์ซไมโครสโกปีและเอทีอาร์เอฟทีไออาร์สเปกโทรสโกปี ศึกษาการตอบสนองทางชีวภาพของฟิล์มที่ประกอบขึ้นบางระบบในแง่ของการยึดเกาะและการเพิ่มจำนวนของเซลล์ไฟโบรบลาสต์ในหลอดทดลอง ฤทธิ์ยับยั้งแบคทีเรีย และการเกาะของเกล็ดเลือด

2.1.1 Surface-quaternized Chitosan Particles as Alternative and Effective Organic Antibacterial Fillers

Taking advantage of the large surface area that is covered with permanent positive charges of quaternary ammonium entities, this research aimed to develop environmentally friendly, organic antibacterial fillers from quaternized chitosan particles that may be applicable for biomedical devices, health and textile industries. The particles were formulated by ionic crosslinking of chitosan with tripolyphosphate followed by quaternization that was conducted under heterogeneous condition via either direct methylation or reductive *N*alkylation with a selected aldehyde followed by methylation. Sub-micron, spherical, and positively charged quaternized chitosan particles were formed, as determined by 1H-NMR, FT-IR, PCS, and TEM analysis. Antibacterial activity tests performed by viable cell counts suggested that all quaternized chitosan particles exhibited superior antibacterial activity against the model Gram-positive bacteria, *S.aureus*, as compared to the native chitosan particles at neutral pH. Only some quaternized chitosan particles, especially those having a high charge density and bearing large alkyl substituent groups, were capable of suppressing the growth of the model Gram-

negative bacteria, *E. coli*. The inhibitory efficiency of the quaternized chitosan particles was quantified in terms of the minimum inhibitory concentration (MIC).

Keywords: chitosan; particle; heterogeneous quaternization; minimum inhibitory concentration

อนุภาคไคโทซานควอเตอร์ไนซ์ที่ผิวเป็นฟิลเลอร์อินทรีย์ทางเลือกที่มีประสิทธ์ภาพด้านการต้านเชื้อแบคทีเรีย

ใช้ประโยชน์จากการมีพื้นที่ผิวสูงและการถูกปกคลุมด้วยประจุถาวรของหมู่ควอเทอร์นารีแอมโมเนียมของอนุภาคควอเทอร์ไนซ์ไคโทซาน งานวิจัยในส่วนที่สองสนใจศึกษาการใช้อนุภาคดังกล่าวเพื่อวัตถุประ- สงค์ สองประการ คือ เป็นสารยับยั้งแบคทีเรีย และเป็นตัวแลกเปลี่ยนแอนไอออนสำหรับการประยุกต์ทางไบโอเซ็นเซอร์ ทั้งนี้เตรียมอนุภาคด้วยการเชื่อมขวางแบบไอออนิกของไคโทซานด้วยไทรพอลิฟอสเฟส ตามด้วยควอเทอร์ไนเซชันซึ่งส่วนใหญ่เป็นการทำปฏิกิริยาแบบวิวิธพันธ์ผ่านเมทิลเลชันหรือเอ็น-รีดักทีฟแอลคิเลชัน/เมทิลเลชัน จากการยืนยันการเกิดอนุภาคโดยการวิเคราะห์ด้วยเทคนิคฟูเรียทรานส์ฟอร์มอินฟราเรดสเปกโทรสโกปี, โฟตอนคอร์รีเลชันสเปกโทรสโกปี และกล้องจุลทรรศน์อิเล็กตรอนแบบส่งกราด ผ่านพบว่า อนุภาคที่ได้มีขนาดเล็กกว่า 1 ไมครอเมตร มีลักษณะเป็นทรงกลมและมีประจุเป็นบวก จากการทดสอบฤทธิ์ในการยับยั้งแบคทีเรียด้วยการนับจำนวนแบคทีเรียที่รอดชีวิตพบว่าอนุภาคควอเทอร์ไนซ์ไคโทซานทุกชนิดมีฤทธิ์ในการยับยั้ง *S.aureus* ซึ่งเป็นแบคทีเรียแกรมบวกที่เหนือกว่าอนุภาคไคโทซานในสภาวะที่มีพีเอชเป็นกลาง ในขณะที่มีเพียงอนุภาคควอเทอร์ไนซ์ไคโทซานบางชนิดโดยเฉพาะอย่างยิ่งที่มีความหนาแน่นประจุสูงและมีหมู่แทนที่แอลคิลขนาดใหญ่ที่สามารถยับยั้งการเติบโตของ *E.coli* ซึ่งเป็นแบคทีเรีย แกรมลบ นอกจากนี้ยังพบว่าประสิทธิภาพในการยับยั้งขึ้นกับปริมาณของอนุภาคซึ่งประเมินค่าเชิงปริมาณได้จากความเข้มข้นต่ำสุดที่ทำให้เกิดการยับยั้ง งานวิจัยอีกส่วนหนึ่งเป็นการศึกษาการใช้อนุภาคควอเทอไนซ์ไคโทซานเป็นตัวแลกเปลี่ยนแอนไอออนร่วมกับพิโรลิดินิลเพปไทด์นิวคลีอิกแอซิดที่มีคอนฟอร์เมชันถูกจำกัด (พีเอ็นเอ) สำหรับการตรวจลำดับเบสของดีเอ็นเอ จากการวิเคราะห์ด้วยมัลดิ-ทอฟแมสสเปกโทรเมทรีพบว่าอนุภาคควอเทอไนซ์ไคโทซานสามารถใช้ร่วมกับพีเอ็นเอที่มีลำดับเบสเป็น T9 ในการบอกความแตกต่างระหว่างดีเอ็นเอที่มีลำดับเบสเป็นคู่สมจากดีเอ็นเอที่มีลำดับเบสไม่เป็นคู่สม (มีลำดับเบสผิดไปหนึ่งตำแหน่งหรือทุกตำแหน่ง) ได้

คำหลัก: ไคโทซาน, อนุพันธ์มีประจุ, ฟิล์มมัลติเลเยอร์, ความเข้ากันได้กับสิ่งมีชีวิต, อนุภาค, ฤทธิ์ยับยั้งแบคทีเรีย, ไบโอเซนเซอร์, ดีเอ็นเอ, พีเอ็นเอ, ตัวแลกเปลี่ยนไอออน

2.1.2 Multilayer Thin Films Assembled from Charged Derivatives of Chitosan: Formation and Biological Responses

Charged derivatives of chitosan, *N*-sulfofurfuryl chitosan (SFC) and *N*-[(2-hydroxyl-3-trimethylammonium)propyl] chitosan chloride (HTACC), were prepared by reductive alkylation using 5-formyl-2-furansulfonic acid, sodium salt (FFSA) as a reagent and ring opening of glycidyltrimethylammonium chloride (GTMAC) by amino groups of chitosan(CHI), respectively. Multilayer thin film of chitosan and its charged derivatives was fabricated by alternate layer-by-layer adsorption onto a surface-treated poly(ethylene terephthalate) (treated PET) substrate. Assembly process was monitored by quartz crystal microbalance (QCM). Stratification of the multilayer film was demonstrated by water contact angle data. The coverage of the assembled films was characterized by AFM and ATR-FTIR analyses. Alternate biological responses of the assembled films were assessed by protein adsorption and *in vitro* cell adhesion and proliferation.

Keywords: Chitosan, Charged derivative, Layer-by-layer adsorption, Multilayer film, Polyelectrolyte

ฟิล์มหลายชั้นประกอบจากอนุพันธ์ที่มีประจุของไคโตซาน: การเกิดและตอบสนองทางชีวภาพ

อนุพันธ์ที่มีประจุของไคโตซาน, เอ็น-ซัลโฟเฟอร์ฟูริลไคโตซาน (เอสเอฟซี) และเอ็น-[(2-ไฮดรอกซิล-3-ไตรเมทิลแอมโมเนียม)โพรพิล]ไคโตซานคลอไรด์ (เอชทีเอซีซี) เตรียมขึ้นโดยปฏิกิริยารีดักทีฟแอลคิลเลชันโดยใช้เกลือโซเดียมของ 5-ฟอร์มิล-2-ฟิวแรนซัลโฟนิกแอซิดเป็นรีเอเจนต์ และปฏิกิริยาการเปิดวงของไกลซิดิลไทรเมทิลแอมโมเนียมคลอไรด์ (จีทีเอ็มเอซี) ด้วยหมู่แอมิโนของไคโตซานตามลำดับ เตรียมมัลติเลเยอร์ฟิล์มของไคโตซานและอนุพันธ์ที่มีประจุของไคโตซานบนผิวของพอลิเอทิลีนเทเรฟทาเลตที่มีการดัดแปรด้วยวิธีการดูดซับแบบประกอบชั้นต่อชั้นของพอลิอิเล็กโทรไลต์ที่มีประจุตรงข้ามกัน ติดตามกระบวนการประกอบเป็นฟิล์มด้วยเทคนิคควอร์ทซ์คริสตัลไมโครบาลานซ์ (คิวซีเอ็ม) สามารถยืนยันการสลับชั้นของฟิล์มหลายชั้นได้จากผลการวัดมุมสัมผัสของน้ำ วิเคราะห์ลักษณะและโครงสร้างทางเคมีบนพื้นผิวของมัลติเลเยอร์ฟิล์มด้วยอะตอมมิกฟอร์ซไมโครสโกปี (เอเอฟเอ็ม) และเอทีอาร์-เอฟทีไออาร์ ตรวจสอบการตอบสนองทางชีวภาพแบบสลับของฟิล์มที่ประกอบขึ้นโดยศึกษาการดูดซับของโปรตีน การยึดเกาะและการแพร่กระจายของเซลล์ในหลอดทดลอง

คำสำคัญ: ไคโทซาน, อนุพันธ์มีประจุ, การดูดซับแบบชั้นต่อชั้น, ฟิล์มหลายชั้น, พอลิอิเล็กทรอไลต์

2.2 Syntheses, Characterization and Antibacterial Activity of Chitosan Grafted Hydrogels and Associated Mica Containing Nanocomposite Hydrogels

Chitosan (CS) grafted poly[(acrylic acid)-*co*-(2-hydroxyethyl methacrylate)] (CS-*g*-poly(AA-*co*-HEMA)) at different molar ratios of AA and HEMA, and the associated nanocomposite hydrogels of CS-*g*-poly(AA-*co*-HEMA)/mica were synthesized by radical copolymerization. The grafting positions at the amino or hydroxyl groups in the CS were identified by Fourier transform infrared spectroscopy. CS-*g*-poly(AA-*co*-HEMA) hydrogels were intercalated in the mica and the amount of hydrogel insertion did not affect the spacing of the silicate layers in mica. The higher mica loadings produced rougher surfaces of the nanocomposite hydrogel. The water absorbency of the CS-*g*-poly(AA-*co*-HEMA)/mica nanocomposite hydrogels decreased with increasing levels of mica loading to a lower level than those of the CS*g*-poly(AA-*co*-HEMA) hydrogels. Both CS-*g*-poly(AA) and CS-*g*-poly(AA-*co*-HEMA)/mica nanocomposite hydrogels exhibited a higher antiproliferative activity against *Staphylococcus aureus* than did the neat CS hydrogel with CS-*g*-poly(AA) revealing a very pronounced minimum inhibition concentration (MIC) of 1.56 mg ml^{-1}. The extent of mica loading in the CS-*g*- poly(AA-*co*-HEMA) nanocomposite hydrogels did not affect the MIC (12.5 mg ml^{-1}).

Keywords: Chitosan, Acrylic acid, 2-hydroxyethyl methacrylate, Mica, Nanocomposite hydrogel, Antibacterial property

การสังเคราะห์ การตรวจคุณลักษณะ และการตรวจสอบฤทธิ์ต้านแบคทีเรียของไฮโดรเจลไคโทซานและไฮโดรเจลไคโทซานนาโนคอมพอสิตที่มีไมกา

สังเคราะห์ไคโทซานกราฟต์พอลิเมอร์ร่วมอะคริลิกแอซิดและ 2-ไฮดรอกซีเอทิลเมทาคริเลต (CS-*g*-poly(AA-*co*-HEMA)) ที่อัตราส่วนโดยโมลต่าง ๆ ของ AA และ HEMA และไฮโดรเจลนาโนคอมพอสิตของ CS-*g*-poly(AA-*co*-HEMA)/mica ด้วยปฏิกิริยาการเกิดพอลิเมอร์แบบอนุมูลอิสระ หาตำแหน่งการกราฟต์ด้วยเทคนิค FTIR พบว่า เกิดกราฟต์ที่หมู่แอมิโนหรือไฮดรอกซิลในไคโทซาน ไฮโดรเจลนาโนคอมพอสิตของ CS-*g*-poly(AA-*co*-HEMA) เกิดลักษณะอินเทอร์คาเลต ซึ่งมีการแทรกสอดของสายโซ่พอลิเมอร์ในชั้นซิลิเกตของไมกา และปริมาณการสอดแทรกของไฮโดรเจลไม่มีผลต่อระยะห่างของชั้นซิลิ

เกตในไมกา ปริมาณไมกาที่เพิ่มขึ้นทำให้ไฮโดรเจลนาโนคอมพอสิตมีพื้นผิวขรุขระมากขึ้น การดูดซึมน้ำของ CS-*g*-poly(AA-*co*-HEMA)/mica nanocomposite ลดลง จากการเพิ่มปริมาณไมกาในการสังเคราะห์ และค่านี้ลดลงมากกว่าค่าการดูดซึมน้ำของ CS-*g*-poly(AA-*co*-HEMA) hydrogel ทั้ง CS-*g*-poly(AA) และ CS-*g*-poly(AA-*co*-HEMA)/mica composite แสดงฤทธิ์ยับยั้งการแบ่งตัวของเซลล์ (antiproliferative activity) ต่อเชื้อสเตปฟิโลคอกคัสออเรียส มากกว่าที่ไคโทซานไฮโดรเจลจะทำได้ ความเข้มข้นน้อยที่สุดที่ยับยั้งเชื้อนี้ได้ของ CS-*g*-poly(AA) มีค่า 1.56 มิลลิกรัมต่อมิลลิลิตร ปริมาณไมกาใน CS-*g*-poly(AA-*co*-HEMA)/mica nanocomposite hydrogel ไม่มีผลต่อค่า MIC ซึ่งให้ค่าเท่ากัน คือ 12.5 มิลลิกรัมต่อมิลลิลิตร

คำสำคัญ: *ไคโทซาน, อะคริลิกแอซิด, 2-ไฮดรอกซีเอทิลเมทาคริเลต, ไมกา, ไฮโดรเจลนาโนคอมพอสิต, ต้านฤทธิ์เชื้อแบคทีเรีย*

2.3 Surface Modification of Electrospun Chitosan Nanofibers for Antibacterial Activity

Chitosan with a degree of deacetylation of 95% in its blend with poly(ethylene oxide) (PEO) was fabricated into nanofibrous membranes by electrospinning. The introduction of PEO was to facilitate the fiber formation. The spinning solution was 6.7% w/v chitosan and 0.3% w/v PEO in 70:30 v/v trifluoroacetic acid/dichloromethane. The obtained fibers were smooth without the presence of beads, as confirmed by scanning electron microscopy (SEM). The diameters of the individual fibers were 272 $\pm$ 56 nm. The surface of the obtained chitosan fibers was modified with *N*-(2-hydroxyl) propyl-3-trimethyl ammonium chloride (HTAC) with an aim of making the chitosan nanofibrous membranes into a quaternary ammonium salt (HTACC). The reaction was characterized by Fourier-transformed infrared spectroscopy (FTIR) and degree of swelling. The resulting chitosan fibers were tested with two types of bacteria and the antibacterial activities were compared and discussed.

Keywords: Surface modification, Electrospinning, Chitosan, Derivative of chitosan, Nanofiber, Antibacterial activity

การดัดแปรผิวของเส้นใยไคโทซานขนาดนาโนเมตรปั่นด้วยไฟฟ้าเพื่อต้านฤทธิ์แบคทีเรีย

ได้ผลิตเมมเบรนของเส้นใยไคโทซานขนาดนาโนเมตรจากไคโทซานที่มีระดับดีแอเซตทิเลชันร้อยละ 95 ผสมกับพอลิเอทิลีนออกไซด์ (PEO) ด้วยเทคนิคอิเล็กทรอสปินนิง การใส่ PEO ก็เพื่อช่วยในการฉีดเส้นใย สารละลายสปินนิงประกอบด้วยไคโทซานร้อยละ 6.7 โดยน้ำหนัก และ PEO ร้อยละ 0.3 โดยน้ำหนัก ในสารละลายผสมระหว่างไทรฟูลออโรแอซิติกแอซิดกับไดคลอโรมีเทนสัดส่วน 70:30 โดยปริมาตร เส้นใยเมมเบรนที่ได้มีความเรียบ ไม่มีปุ่มหรือปมตลอดเส้น ซึ่งตรวจสอบได้ด้วยกล้องจุลทรรศน์อิเล็กทรอนแบบส่องกราด เส้นผ่าศูนย์กลางของเส้นใยมีค่า 272 $\pm$ 56 นาโนเมตร นำสารเอ็น-2-ไฮดรอกซีพรอพิล-3-ไทรเมทิลแอมโมเนียมคลอไรด์ *(N*-(2-hydroxyl) propyl-3-trimethyl ammonium chloride) (HTAC) มาดัดแปรผิวหน้าของเส้นใยไคโทซานที่ได้ เพื่อทำให้ผิวเส้นใยเหล่านี้มีเกลือของควอเตอร์นารี (HTACC) ซึ่งยืนยันได้ด้วยเทคนิค FTIR และระดับขั้นของการดูดซึมน้ำ นำเส้นใยที่ได้ทั้งหมดมาทดสอบฤทธิ์การต้านเชื้อแบคทีเรีย งานนี้ได้นำเสนอผลและวิพากย์ฤทธิ์การต้านแบคทีเรีย

คำสำคัญ: การดัดแปรผิว, อิเล็กทรอสปินนิง, ไคโทซาน, อนุพันธ์ของไคโทซาน, นาโนไฟเบอร์, ฤทธิ์ต้านแบคทีเรีย

กลุ่มโครงการวิจัยที่ 3 ไฮโดรเจลสำหรับสิ่งแวดล้อม

3.1 Synthesis of Acrylamide/Acrylic Acid-Based Aluminum Flocculant for Dye Reduction and Textile Wastewater Treatment

Aluminum hydroxide-poly[acrylamide-*co*-(acrylic acid)], AHAMAA, was synthesized with a redox initiator by solution polymerization in which the effects of reactant contents were optimized. The effects of pH, temperature, and initial dye concentration on Congo red reduction were investigated. A mixture of Congo red and direct blue 71, and the composite textile dye wastewater were investigated. Adsorptions of both dyes were more effective in the non-buffered solution than those in the buffered solution, and Congo red were adsorbed more than direct blue 71 at all pHs. The adsorption of Congo red increased with increasing temperature and its initial concentration. Both dyes obeyed the Freundlich adsorption isotherm. The maximum adsorptions in 100 mg dm^{-3} solution were 109±0.5 mg g^{-1} and 62±6.6 mg g^{-1} for Congo red and direct blue 71, respectively. At 150 mg dm^{-3} of the mixed Congo red and direct blue 71, the adsorption was 142±2 mg g^{-1} by 643±3 mg dm^{-3} AHAMAA. The 40 mg g^{-1} dyes of the textile effluent wastewater were adsorbed by 500 mg dm^{-3} AHAMAA. AHAMAA could decrease turbidity of the composite wastewater containing a mixture of reactive and direct dyes from 405 to 23 NTU.

Keywords: Aluminum flocculant, Poly[acrylamide-co-(acrylic acid)], Dye adsorption, Turbidity reduction, Wastewater

การสังเคราะห์สารจับกลุ่มก้อนอะลูมิเนียมฐานอะคริลาไมด์/อะคริลิกแอซิดสำหรับการลดสีย้อมและการบำบัดน้ำเสียสิ่งทอ

สารก่อการจับกลุ่มพอลิเมอร์อะลูมิเนียมไฮดรอกไซด์-โคพอลิเมอร์ของอะคริลาไมด์และอะคริลิกแอซิด (AHAMAA) สังเคราะห์ได้โดยใช้สารริเริ่มปฏิกิริยารีดอกซ์ในปฏิกิริยาพอลิเมอไรเซชันแบบสารละลาย ปรับปริมาณสารตั้งต้นให้เหมาะสมในการสังเคราะห์ นำสารที่สังเคราะห์ได้มาศึกษาผลของค่าความเป็นกรด-เบส อุณหภูมิ และความเข้มข้นเริ่มต้นของสีย้อมต่อการลดสีย้อม Congo red และ direct blue 71 ในน้ำเสียสังเคราะห์ และคอมพอสิตของสีย้อมในน้ำเสียจากโรงงานอุตสาหกรรมสิ่งทอ จากผล

การทดลองพบว่า AHAMAA ดูดซับสีย้อม Congo red และ direct blue 71 ในน้ำเสียสังเคราะห์ที่ภาวะไม่มีสารควบคุมค่าความเป็นกรด-เบสดีกว่าน้ำเสียสังเคราะห์ที่มีสารควบคุมความเป็นกรด-เบส และดูดซับสีย้อม Congo red ดีกว่า direct blue 71 ทุกค่าความเป็นกรด-เบส การดูดซับสีย้อม Congo red เพิ่มขึ้น เมื่อเพิ่มความเข้มข้นเริ่มต้นของสีย้อม และอุณหภูมิ การดูดซับสีย้อมของ AHAMAA เป็นแบบ Freundlich isotherm เมื่อความเข้มข้นเริ่มต้นของสีย้อมเป็น 100 มิลลิกรัมต่อลูกบาศก์เดซิเมตร AHAMAA ดูดซับ Congo red ได้มากสุด 109 $\pm$ 0.5 มิลลิกรัมต่อกรัม และดูดซับ direct blue 71 ได้มากสุด 62 $\pm$ 6.6 มิลลิกรัมต่อกรัม ในน้ำเสียสังเคราะห์ที่มีสีย้อมทั้งสองผสมกันที่ความเข้มข้นรวมเป็น 150 มิลลิกรัมต่อลูกบาศก์เดซิเมตร เมื่อใช้ AHAMAA ความเข้มข้น 643 $\pm$ 3 มิลลิกรัมต่อลูกบาศก์เดซิเมตร สามารถดูดซับสีย้อมรวมได้ 142$\pm$2 มิลลิกรัมต่อกรัม และ AHAMAA ความเข้มข้น 500 มิลลิกรัมต่อลูกบาศก์เดซิเมตร สามารถดูดซับสีย้อมในน้ำเสียจากโรงงานอุตสาหกรรมสิ่งทอได้ 40 มิลลิกรัมต่อกรัม นอกจากนี้ AHAMAA ยังสามารถลดความขุ่นของน้ำเสียจากอุตสาหกรรมสิ่งทอที่มีสีย้อม reactive dye ผสมกับ direct dye จากความขุ่น 405 เป็น 23 NTU

คำสำคัญ: สารก่อการจับกลุ่มชนิดอะลูมิเนียม, โคพอลิเมอร์ของอะคริลาไมด์และอะคริลิกแอซิด, การดูดซับสีย้อม, การลดความขุ่น, น้ำเสีย

3.2 Photocatalytic Efficiency of TiO_2/Poly[Acrylamide-*Co*-(Acrylic Acid)] Composite for Textile Dye Degradation

Poly[acrylamide-*co*-(acrylic acid)], (poly[AAm-*co*-(AAc)]), and TiO_2/Poly[AAm-*co*-(AAc)] composite were synthesized by an aqueous solution polymerization method. Poly[AAm-*co*-(AAc)] and TiO_2/Poly[AAm-*co*-(AAc)] composite had equilibrium water absorbency of 823±2 and 455$\pm$8 times their dry weights, respectively. The efficiency of the composite to absorb methylene blue was determined using UV-visible spectrophotometry. The results showed that 88% of 5 mg L^{-1} of methylene blue solution was absorbed with an absorption rate of 0.1344 min^{-1}. Influential factors on the photocatalytic degradation, namely type of TiO_2, wavelength and intensity of UV radiation, were investigated. In the presence of UV radiation at 365 nm, TiO_2/Poly[AAm-*co*-(AAc)] composite can degrade as high as 91% of the dye in 40 min. In contrast, poly[AAm-*co*-(AAc)] could degrade only 3% of the dye. Degradation of the dye was not observed neither in TiO_2/Poly[AAm-*co*-(AAc)] composite nor poly[AAm-*co*-(AAc)] without

exposure to UV radiation when the dye was incorporated into the system. The reused efficiency of TiO_2/Poly[AAm-*co*-(AAc)] composite understudy was found that the TiO_2/Poly[AAm-*co*-(AAc)] composite could be reused for only 2 times before it became slurry. This result indicated that TiO_2/Poly[AAm-*co*-(AAc)] composite not only degraded the methylene blue but also decomposed itself under UV irradiation. This leads to a conclusion that the system does not cause any environmental problems.

Keywords: Composite, Photocatalysts, Photodegradation, Titanium dioxide

ประสิทธิภาพด้านโฟโตแคตทาลิสของคอมพอสิตไทเทเนียมไดออกไซด์/พอลิ(อะคริลาไมด์-*โค*-อะคริลิกแอซิด) สำหรับการแตกสลายของสีย้อม

ได้สังเคราะห์พอลิ(อะคริลาไมด์-*โค*-กรดอะคริลิก) และคอมพอสิตของพอลิ(อะคริลาไมด์-*โค*-กรดอะคริลิก) ที่มีไทเทเนียมไดออกไซด์โดยปฏิกิริยาพอลิเมอไรเซชันแบบสารละลาย พบว่า พอลิเมอร์ร่วมและคอมพอสิตของพอลิเมอร์ร่วมที่เตรียมได้มีค่าการดูดซึมน้ำ 823±2 และ 455±8 เท่าของน้ำหนักพอลิเมอร์แห้ง ตามลำดับ ได้ศึกษาประสิทธิภาพการดูดซึมสีเมทิลีนบลูในสารละลายด้วยเทคนิคยูวีวิสซิเบิลสเปกโทรโฟโตเมตรีพบว่า คอมพอสิตที่เตรียมได้สามารถดูดซึมสีเมทิลีนบลูที่ความเข้มข้น 5 มิลลิกรัมต่อลิตรได้ร้อยละ 88 โดยมีค่าคงตัวอัตราการดูดซึมสี 0.1344 ต่อนาที ศึกษาการแตกสลายของโมเลกุลสีเมทิลีนบลูที่ถูกดูดซึมบนคอมพอสิตด้วยการศึกษาอิทธิพลของตัวแปร ได้แก่ ชนิดของอนุภาคไทเทเนียมไดออกไซด์ ความยาวคลื่นและความเข้มของรังสียูวี พบว่า ไทเทเนียมไดออกไซด์พอลิเมอร์คอมพอสิตมีประสิทธิภาพในการแตกสลายสีเมทิลีนบลูได้มากถึงร้อยละ 91 ใช้เวลา 40 นาที ฉายด้วยรังสียูวีความยาวคลื่น 365 นาโนเมตร ในทางตรงกันข้าม พบการแตกสลายของสีย้อมด้วยพอลิเมอร์ร่วมที่ไม่มีไทเทเนียมไดออกไซด์เพียงร้อยละ 3 และไม่เกิดการแตกสลายสีย้อมในที่มืดของพอลิเมอร์ร่วมและคอมพอสิต ศึกษาประสิทธิภาพการใช้ซ้ำของพอลิเมอร์คอมพอสิตภายใต้ภาวะที่ฉายด้วยรังสียูวี พบว่าสามารถนำกลับมาใช้ใหม่ได้ 2 ครั้งก่อนที่พอลิเมอร์คอมพอสิตจะกลายเป็นของหนืด ผลการทดลองนี้แสดงว่า พอลิเมอร์คอมพอสิตไม่เพียงแตกสลายสีเมทิลีนบลู ยังแตกสลายตัวพอลิเมอร์เองภายใต้รังสียูวี งานวิจัยนี้นำไปสู่การสรุปว่า ระบบนี้ไม่ก่อปัญหาสิ่งแวดล้อม

คำหลัก: คอมพอสิต, โฟโตแคตทาลิสต์, การแตกสลายด้วยแสง, ไทเทเนียมไดออกไซด์

3.3 Acrylamide-Based Composite Hydrogels Initiated by Titanium Dioxide Photocatalyst for Dye and Composite Hydrogel Degradations

To synthesize the composite hydrogels, nano-sized titanium hydroxide particles were dispersed in distilled water and exposed to ultraviolet radiation (UV) for a set time while the dispersion was being stirred. When the titanium hydroxide had reacted with water to generate hydroxyl radicals, monomers and crosslinking agent were added and exposed to UV again while stirring the reaction mixture. A composite hydrogel was resulted in at the specified time, acrylamide with its co monomers namely acrylic acid and/or itaconic acid and crosslinking monomer of *N, N'*-methylenebisacrylamide were used for the synthesis. The resulting composite hydrogels were tested for water absorption in distilled water and dye solution such as Congo red or other dye solutions. The composite hydrogel and adsorbed dye degradations are to be experimented under UV radiation. This project is still ongoing since it has just started in January 2011.

Keywords: Acrylamide-based composite hydrogel, TiO_2 photocatalyst, Hydrogel degradations, Dye degradation

ไฮโดรเจลคอมพอสิตฐานอะคริลาไมด์ริเริ่มโดยโฟโตแคตทาลิสต์ไทเทเนียมไดออกไซด์สำหรับการแตกสลายของสีย้อมและไฮโดรเจล

สังเคราะห์ไฮโดรเจลคอมพอสิตเริ่มด้วยการนำอนุภาคไทเทเนียมไดออกไซด์ระดับนาโนเมตรมากวนในน้ำ แล้วกวนพร้อมกับฉายรังสีอัลตราไวโอเลตเป็นระยะเวลาหนึ่ง เพื่อให้ไทเทเนียมไดออกไซด์ทำปฏิกิริยากับน้ำแล้วเกิดอนุมูลไฮดรอกซิลขึ้น เติมมอนอเมอร์และสารเชื่อมขวาง แล้วกวนต่อไปพร้อมกับฉายรังสีอัลตราไวโอเลต จนกระทั่งเกิดเป็นไฮโดรเจลคอมพอสิตขึ้น มอนอเมอร์ที่ใช้ในการสังเคราะห์คือ อะคริลาไมด์ ซึ่งมีมอนอเมอร์ร่วมคือ กรดอะคริลิก หรือกรดอิทาโคนิก และสารเชื่อมขวางที่ใช้คือ *เอ็น, เอ็น*-เมทิลีนบิสอะคริลาไมด์ นำไฮโดรเจลที่สังเคราะห์ไปวิเคราะห์หาความสามารถในการดูดซึมน้ำและสีย้อม Congo red พร้อมกับตรวจสอบเอกลักษณ์ต่าง ๆ ของรูปแบบการดูดซับสี ตรวจสอบการแตกสลายของไฮโดรเจลคอมพอสิตและแตกสลายของสีย้อมที่ถูกดูดซับบนไฮโดรเจลคอมพอสิตด้วยปฏิกิริยาเคมีทางแสง โครงการนี้เพิ่งเริ่มวิจัยเมื่อเดือนมกราคม 2554

คำสำคัญ: ไฮโดรเจลคอมพอสิตฐานอะคริลาไมด์, ไทเทเนียมไดออกไซด์โฟโตแคตาลิสต์, การแตกสลายของไฮโดรเจล, การแตกสลายของสีย้อม

กลุ่มโครงการวิจัยที่ 4 ไฮโดรเจลกับการใช้งานเฉพาะทาง

4.1 Gel Strength and Swelling of Acrylamide-Protic Acid Superabsorbent Copolymers

The viscoelastic and swelling properties of polyacrylamide-based superabsorbent copolymers were investigated as a function of the ionic comonomer structure. Superabsorbent copolymers were synthesized by free-radical crosslinking copolymerization of acrylamide and one of the monoprotic acids (acrylic acid and crotonic acid) or the diprotic acids (maleic acid and itaconic acid) as the investigated ionic comonomer. The reaction composition of all components, i.e. monomer, comonomer, initiator, co-initiator and crosslinker, was fixed to be the same for the synthesis of all four superabsorbent copolymer systems. Viscoelastic measurements were performed in all systems where the particles were closely packed. The network structures of all systems were evaluated via viscoelastic and swelling measurements. The results indicated that superabsorbent polymers with high water absorbency were accompanied by low gel strength and the calculated high value of molecular weight between crosslinks ($\overline{M}_c$) and low value of effective crosslinking density (ν_e). Diprotic acid-containing superabsorbent polymers showed higher water absorbency over monoprotic acid-containing and nonionic ones. The differences in $\overline{M}_c$ and ν_e values of each system were explained with respect to the differences in the monomer reactivity ratio and hydrophilicity of the comonomers.

Keywords: Superabsorbent polymers, Swelling, Viscoelastic, Molecular weight between crosslinks, Crosslinking density

ความแข็งแรงของเจลและการบวมตัวของโคพอลิเมอร์ซูเปอร์แอบซอร์เบนต์ฐานอะครลาไมด์-กรดโปรติก

การวิจัยนี้เพื่อศึกษาโครงสร้างของไอออนิกโคพอลิเมอร์ที่มีต่อสมบัติความหยุ่นหนืดและสมบัติการบวมตัวของโคพอลิเมอร์ซูเปอร์แอบซอร์เบนต์อะครลาไมด์-กรดโปรติก ได้สังเคราะห์โคพอลิเมอร์ซูเปอร์แอบซอร์เบนต์โดยวิธีการเกิดปฏิกิริยาโคพอลิเมอไรเซชันแบบอนุมูลอิสระของมอนอเมอร์อะคริลาไมด์กับกรดมอนอเมอร์โปรตอนเดียว (อะคริลิกแอซิดและโครโทนิกแอซิด) หรือกรดมอนอเมอร์สองโปรตอน (มาเลอิกแอซิดและอิทาโคนิกแอซิด) ซึ่งทำหน้าที่เป็นมอนอเมอร์ร่วมแบบมีประจุ กำหนดองค์ประกอบของสารต่าง ๆ ในปฏิกิริยา เช่น มอนอเมอร์ มอนอเมอร์ร่วม อินิชิเอเตอร์ อินิชิเอเตอร์ร่วม และสารเชื่อม

ขวาง ให้เป็นต่าคงตัวและมีค่าเท่ากันสำหรับการสังเคราะห์โคพอลิเมอร์ซูเปอร์แอบซอร์เบนต์ 4 ชนิดนี้ วัดสมบัติความหยุ่นหนืดของโคพอลิเมอร์ซูเปอร์แอบซอร์เบนต์ทั้ง 4 ชนิด เมื่อกำหนดให้อนุภาคของโคพอลิเมอร์เหล่านี้มีลักษณะเกาะกันแน่นเป็นก้อนปิด (closely packed) ประเมินโครงสร้างของเครือข่ายของโคพอลิเมอร์ทั้ง 4 ชนิดจากสมบัติความหยุ่นหนืดและการบวมตัว ผลที่ได้แสดงว่า โคพอลิเมอร์ซูเปอร์แอบซอร์เบนต์มีค่าการดูดซึมน้ำมากเมื่อพอลิเมอร์เจลมีความแข็งแรงต่ำ มีค่าน้ำหนักโมเลกุลเฉลี่ยระหว่างโซ่เชื่อมขวางสูง และมีค่าความหนาแน่นของการเชื่อมขวางต่ำ โคพอลิเมอร์ซูเปอร์แอบซอร์เบนต์ชนิดสองโปรตอนมีค่าการดูดซึมน้ำมากกว่าโคพอลิเมอร์ซูเปอร์แอบซอร์เบนต์ชนิดหนึ่งโปรตอนและพอลิเมอร์ซูเปอร์แอบซอร์เบนต์ชนิดไม่มีประจุ ความแตกต่างระหว่างค่าน้ำหนักโมเลกุลเฉลี่ยระหว่างโซ่เชื่อมขวางและค่าความหนาแน่นของการเชื่อมขวางของโคพอลิเมอร์ซูเปอร์แอบซอร์เบนต์มีความสัมพันธ์กับค่าความไวของมอนอเมอร์และความชอบน้ำของมอนอเมอร์ร่วม

คำสำคัญ พอลิเมอร์ซูเปอร์แอบซอร์เบนต์, การบวมตัว, สมบัติความหยุ่นหนืด, น้ำหนักโมเลกุลระหว่างโซ่เชื่อมขวาง, ค่าความหนาแน่นของการเชื่อมขวาง

4.2 Acrylamide–Itaconic Acid Superabsorbent Polymers and Superabsorbent Polymer/ Mica Nanocomposites

Superabsorbent polymer and its nanocomposite of acrylamide (AM)/itaconic acid (IA) were synthesized by solution polymerization in an aqueous solution of AM with IA comonomer and mica used as an inorganic additive. This reaction was initiated by a redox initiator couple of ammonium persulfate and *N, N, N′, N′*-tetramethylethylenediamine in the presence of *N, N′*-methylenebisacrylamide crosslinker. The influences of the concentrations of IA, the crosslinker and mica at several reaction temperatures on water absorption of the superabsorbent polymer systems were examined. The superabsorbent copolymers and their nanocomposites were tested with a load of 0.28 or 0.70 psi in both distilled water and artificial urine. Transmission electron micrographs and X-ray diffraction confirmed that the polymer chains were successfully intercalated into the silicate layers in the mica. The water absorbency and the artificial urine absorbency of the composite with an AM-to-IA mole ratio of 95:5, 0.2% mol N-MBA, and 5% w/w mica were 748±5 and 76±2 g g^{-1}, respectively, whilst the neat copolymer achieved only 640±7 and 72±2g g^{-1} in water and artificial urine, respectively. The viscoelastic behavior

suggested that the swollen gel of the nanocomposites exhibited mechanical stability and elasticity.

Keywords: Superabsorbent nanocomposites, Mica, Water absorbency, Intercalation

ซูเปอร์แอบซอร์แบนต์พอลิเมอร์ของอะคริลาไมด์/อิทาโคนิกแอซิดและไมกานาโนคอมพอสิตซูเปอร์แอบซอร์แบนต์พอลิเมอร์

ได้สังเคราะห์ซูเปอร์แอบซอร์แบนต์พอลิเมอร์และคอมพอสิตของซูเปอร์แอบซอร์แบนต์พอลิเมอร์ของอะครลาไมด์และอิทาโคนิกแอซิด โดยการเกิดพอลิเมอไรเซชันในสารละลายของอะคริลาไมด์และอิทาโคนิกแอซิดโคมอนอเมอร์กับผงไมกาซึ่งเป็นสารเติมแต่งอนินทรีย์ ปฏิกิริยาได้เกิดขึ้นโดยคู่รีดอกซ์อินิชิเอเตอร์ของแอมโมเนียมเพอร์ซัลเฟตและ*เอ็น,เอ็น,เอ็น',เอ็น'*,-เททระเมทิลเอทิลีนไดแอมีนและมี*เอ็น,เอ็น'*-เมทิลีนบิสอะคริลาไมด์เป็นสารเชื่อมขวาง อิทธิพลของความเข้มข้นของอิทาโคนิกแอซิด สารเชื่อมขวาง และไมกาที่อุณหภูมิต่าง ๆ ของการเกิดปฏิกิริยามีผลต่อการดูดซึมน้ำของซูเปอร์แอบซอร์แบนต์พอลิเมอร์และคอมพอสิตของพอลิเมอร์ วัดค่าการดูดซึมน้ำของซูเปอร์แอบซอร์แบนต์พอลิเมอร์ทั้งสองภายใต้แรงกดทับ 0.28 or 0.70 ปอนด์ต่อตารางนิ้ว ในน้ำกลั่นและในปัสสาวะเทียม ภาพจากกล้องจุลทรรศน์แบบส่องผ่านและเส้นกราฟของการเลี้ยวเบนด้วยรังสีเอกซ์บ่งบอกว่า โซ่พอลิเมอร์ได้สอดแทรกเข้าไปในชั้นซิลิเกตของไมกา การดูดซึมน้ำและน้ำปัสสาวะเทียมของพอลิเมอร์คอมพอสิตที่มีสัดส่วนโมลของอะคริลาไมด์ต่ออิทาโคนิกแอซิด 95:5, 0.2% โดยโมลของสารเชื่อมขวาง และปริมาณไมการ้อยละ 5 โดยน้ำหนัก มีค่า 748±5 และ 76±2 กรัมต่อกรัมของสารแห้ง ตามลำดับ พฤติกรรมด้านความหยุ่นหนืดบ่งว่า เจลที่บวมตัวเต็มที่ของคอมพอสิตซูเปอร์แอบซอร์แบนต์พอลิเมอร์มีความเสถียรเชิงกลและมีความยืดหยุ่น

คำสำคัญ: นาโนคอมพอสิตซูเปอร์แอบซอร์เบนต์, ไมกา, การดูดซึมน้ำ, การสอดแทรก

4.3 Synthesis of Acrylamide-*co*-(Itaconic Acid) Superabsorbent Polymers and Associated Silica Superabsorbent Polymer Composites

Superabsorbent polymers (SAPs) were synthesized from acrylamide (AM) and itaconic acid (IA) *via* a crosslinking polymerization. SAP composites (SAPCs) were formed by the incorporation of silica with three particle sizes into the polymerization to increase the gel strength of SAPs. Effects of AM: IA molar ratios, silica types and concentrations on water

absorbency, absorbency rate and absorbency under loadings (AUL) of the composites were investigated. The highest water absorbency of the SAP is 233 ± 8 g g^{-1} at an AM: IA molar ratio of 97:3 with absorbency rate of 149 ± 2 g g^{-1} within 15 min. The highest AUL of the SAPC with 0.5-2.0% w w^{-1} silica is 13 g g^{-1} by 1.93 x 10^3 Pa load. A pseudo-second-order kinetics for water absorbency was found in both SAPs and *in situ* SAPCs. *In situ* SAPCs and the mechanically mixed SAPCs in vertical and horizontal direction yielded similar water absorbency values. This research suggested that SAPCs can be economically prepared by mixing SAP with silica powders in a mixing machine to obtain a high water absorption capacity from SAPC.

Keywords: Acrylamide-co-(Itaconic Acid) Superabsorbent Polymers, silica, composite, mechanical mixing, vertical mixing, horizontal mixing

การสังเคราะห์พอลิเมอร์ซูเปอร์แอบซอร์เบนต์ของอะคราไมด์-*โค*-อิทาโคนิกแอซิดกับซิลิกาคอมพอสิตของพอลิเมอร์ซูเปอร์แอบซอร์เบนต์อะคราไมด์-โค-อิทาโคนิกแอซิด

ได้สังเคราะห์พอลิเมอร์ซูเปอร์แอบซอร์เบนต์ (SAP) ของอะคราไมด์-โค-อิทาโคนิกแอซิด จากอะคริลาไมด์ (AM) และอิทาโคนิกแอซิด (IA) โดยการเกิดปฏิกิริยาแบบเชื่อมขวาง คอมพอสิตของ SAP (SAPC) เกิดจากการผสมซิลิกาที่มีขนาดอนุภาคระดับนาโนเมตร 3 ขนาด เข้าไปขณะที่เกิดปฏิกิริยาพอลิเมอไรเซชันเพื่อเพิ่มความแข็งแรงต่อเจลพอลิเมอร์ ผลของสัดส่วนโดยโมลของ AM: IA, ชนิดและปริมารของซิลิกาต่อค่าการดูดซึมน้ำ อัตราการดูดซึมน้ำ และการดูดซึมน้ำภายใต้แรงกดทับ (AUL) ของ SAPC ค่าการดูดซึมน้ำมากสุดของ SAP คือ 233 ± 8 กรัมต่อกรัมของสารแห้ง ที่สัดส่วนโดยโมลของ AM:IA 97:3 และมีอัตรการดูดซึมที่ 149 ± 2 กรัมต่อกรัมของสารแห้ง ภายใน 15 นาที AUL ของ SAPC ที่มีปริมาณซิลิการ้อยละ 0.5-2 มีค่า 13 กรัมต่อกรัมของสารแห้ง โดยแรงกดทับ 1.93 x 10^3 พัสคาล จลนศาสตร์ของการดูดซึมน้ำของ SAP และ SAPC ที่เกิดพร้อมกันกับพอลิเมอร์มีลักษณะเป็น pseudo-second-order เหมือนกัน การดูดซึมน้ำของ SAPCs ที่เกิดขึ้นพร้อมการเกิดพอลิเมอร์ กับ SAPCs ที่เกิดจาการผสมโดยเขย่า SAP ในแนวตั้ง หรือแนวนอนด้วยเครื่องมือเขย่าแบบรอบแกนแนวตั้ง หรือเครื่องหมุนแบบลูกกลิ้งรอบแนวนอนมีค่าเท่ากัน งานวิจัยนี้เสนอแนะว่า การเตรียม SAPCs ที่ประหยัดโดยการผสม SAPs กับผงซิลิกาในเครื่องผสม สามารถผลิต SAPCs ที่มีค่าการดูดซึมน้ำมากได้

คำสำคัญ: พอลิเมอร์ซูเปอร์แอบซอร์เบนต์อะคริลาไมดี-โค-อิทาโคนิกแอซิด, ซิลิกา, คอมพอสิต, การผสมเชิงกล, การผสมในแนวตั้ง, การผสมในแนวนอน

4.4 Acrylamide/2-acrylamido-2-methylpropane Sulfonic Acid and Associated Sodium Salt Superabsorbent Copolymers with Mica Nanocomposites as Fire Retardants

Superabsorbent polymers (SAPs) of poly[acrylamide-*co*-(2-acrylamido-2-methylpropane sulfonic acid)], poly(AM-*co*-AMPS-H^+), and its sodium salt, poly(AM-*co*-AMPS-Na^+), were synthesized by free-radical crosslinking polymerization. A maximum water absorbency in deionized water of 1212 g g^{-1} was achieved for poly(AM-*co*-AMPS-Na^+) at an 85% mol of AMPS-Na^+. The inclusion of mica at 5 – 30% (w w^{-1}) into the preparation of poly(AM-*co*-AMPS-Na^+) SAP leads to an intercalated structure, as detected by XRD and TEM analyses. Poly(AM-*co*-AMPS-Na^+)/30% (w w^{-1}) mica SAP nanocomposite showed a tap-water absorbency of 593 g g^{-1} with a better thermal stability, compared to the pure SAP. Cone calorimetric analyses revealed that the wood specimens coated with the prepared poly(AM-*co*-AMPS-Na^+) SAP or its 30% (w w^{-1}) mica nanocomposite provided excellent protection in delaying the ignition time after exposure to an open flame when compared to that observed with the uncoated specimen (186, 136 and 13 s, respectively). The maximum reduction in the peak heat release rate, the greatest extension of time at peak heat release rate and the minimum in total heat release rate were observed with the mica SAP nanocomposite-coated surface. Intercalating structure of mica in the SAP nanocomposites provided a better shielding effect against external heat sources, and the capability of poly(AM-*co*-AMPS-Na^+) SAP in holding a large amount of water.

Keywords: Superabsorbent; Acrylamide; 2-acrylamido-2-methylpropane sulfonic acid sodium salt; Mica; Nanocomposites; Cone calorimetry.

สารหน่วงไฟของอะคริลาไมด์/2-อะคริลามิโด-2-เมทิลโพรเพนซัลโฟนิกแอซิดและเกลือโซเดียมของโคพอลิเมอร์ซูเปอร์แอบซอร์เบนต์กับไมกานาโนคอมพอสิต

ได้สังเคราะห์ซูเปอร์แอบซอร์เบนต์พอลิเมอร์ (SAP) ของพอลิ(อะคริลาไมด์-*โค*-2-อะคริลามิโด-2-เมทิลโพรเพนซัลโฟนิกแอซิด) หรือ poly(AM-*co*-AMPS-H^+) และเกลือโซเดียมของพอลิเมอร์ poly(AM-*co*-AMPS-Na^+) โดยวิธีการเกิดพอลิเมอร์แบบเชื่อมขวางด้วยอนุมูลอิสระ ค่าการดูดซึมน้ำมากที่สุดในน้ำกลั่น คือ 1212 กรัมต่อกรัม ของสารแห้ง ที่สังเคราะห์ได้จาก poly(AM-*co*-AMPS-Na^+) ที่ร้อยละ 85 โดย

โมลของ 2-อะคริลามิโด-2-เมทิลโพรเพนโซเดียมซัลโฟเนต (AMPS-Na^+) การใส่ผงไมการ้อยละ 5 -30 โดยน้ำหนักเข้าไปใน poly(AM-*co*-AMPS-Na^+) SAP ทำให้เกิดโครงสร้างแบบสอดแทรกของโซ่พอลิเมอร์เข้าไปในไมกา ดังที่ตรวจสอบได้ด้วยภาพจากกล้องจุลทรรศน์แบบสองผ่านและภาพจากการเลี้ยวเบนของรังสีเอกซ์ นาโนคอมพอสิตของ poly(AM-*co*-AMPS-Na^+) ที่มีผงไมการ้อยละ 30 สามารถดูดซึมน้ำประปาได้ 593 กรัมต่อกรัมของสารแห้ง พร้อมมีสภาพต้านความร้อนที่อุณหภูมิสูงได้เมื่อเปรียบเทียบกับ poly(AM-*co*-AMPS-Na^+) SAP การวิเคราะห์เชิงความร้อนด้วยโคนแคลอริเมทรีเปิดเผยว่า ชิ้นไม้ที่เคลือบด้วย poly(AM-*co*-AMPS-Na^+)/30 ไมกานาโนคอมพอสิต สามารถป้องกันชิ้นไม้โดยหน่วงการติดไฟภายหลังได้รับการสัมผัสโดยตรงกับเปลวไฟเมื่อเปรียบเทียบกับไม้ที่เคลือบเฉพาะ poly(AM-*co*-AMPS-Na^+) และไม้ที่ไม่ได้เคลือบเป็นเวลา 186, 136 และ 13 วินาที ตามลำดับ พบความสามารถในการลดอัตราการปล่อยความร้อน ณ จุดยอดของพีกมากที่สุดใน poly(AM-*co*-AMPS-Na^+)/30 ไมกานาโนคอมพอสิต การหน่วงเวลาไหม้ไฟมากที่สุด ณ จุดยอดของพีกที่ปลดปล่อยความร้อน และปริมาณความร้อนน้อยที่สุดที่ปล่อยออกมาที่ผิวของไม้ที่กำลังไหม้ไฟที่มีการเคลือบด้วยนาโนคอมพอสิต โครงสร้างการสอดแทรกของโซ่พอลิเมอร์ของ poly(AM-*co*-AMPS-Na^+) เข้าไปในไมกา เป็นฉนวนป้องกันความร้อนจากภายนอกเข้าไปไหม้เนื้อไม้ที่เคลือบสารนี้ พร้อมกับน้ำปริมาณมากที่สารนี้กักเก็บไว้จะถูกปล่อยออกมาเพื่อลดอุณหภูมิของชิ้นไม้ที่ไหม้ไฟ

คำสำคัญ: ซูเปอร์แอบซอร์เบนต์, อะคริลาไมด์, 2-อะคริลามิโด-2-เมทิลโพรเพนโซเดียมซัลโฟเนต, ไมกา, นาโนคอมพอสิต, โคนแคลอริเมทรี

4.5 Effect of fire retardant on flammability of acrylamide and 2-acrylamido-2-methylpropane sodium sulfonate copolymer nanocomposites

Poly[acrylamide-*co*-(2-acrylamido-2-methylpropane sodium sulfonate)] superabsor- bents and superabsorbent composites (SAPCs) with zinc borate and/or melamine as fire retardants were synthesized. Water absorbencies decreased inversely to added amount of fire retardant. Thermal stability of SAPC/zinc borate increases with increasing zinc borate. Incorporating melamine improved thermal stability of the SAPC until 300°C. Flammability analysis demonstrated that wood surface coated with SAP or SAPC emulsions extended time to ignition of the wood. Peak heat release rate and total heat release are smallest in specimens coated with SAPC/30%melamine. Wood coated with SAPC incorporating 20% zinc borate/10% melamine mixture gave the longest time to ignition at 4½ min.

Keywords: Superabsorbent, Zinc borate, Melamine, Fire retardant, Cone calorimetry.

ผลของสารหน่วงการติดไฟต่อการไหม้ไฟของนาโนคอมพอสิตโคพอลิเมอร์ของอะคริลาไมด์และ2-อะคริลามิโด-2-เมทิลโพนเพนโซเดียมซัลโฟเนต

ได้สังเคราะห์สารหน่วงไฟที่ประกอบด้วยซูเปอร์แอบซอร์เบนต์พอลิเมอร์ของพอลิ(อะคริลาไมด์-โค-2-อะคริลามิโด-2-เมทิลโพรเพนโซเดียมซัลโฟเนต) และคอมพอสิตของซูเปอร์แอบซอร์เบนต์พอลิเมอร์หน่วงไฟของพอลิ(อะคริลาไมด์-โค-2-อะคริลามิโด-2-เมทิลโพรเพนโซเดียมซัลโฟเนต) ซึ่งผสมกับซิงก์บอร์เรต และ/หรือเมลามีน ค่าการดูดซึมน้ำลดลงเป็นสัดส่วนผกผันกลับกับปริมาณของสารหน่วงไฟอนินทรีย์ ความเสถียรเชิงความร้อนของ SAPC/ซิงก์บอร์เรตเพิ่มขึ้นตามปริมาณของซิงก์บอเรตที่เพิ่มขึ้น การเติมเมลามีนเข้าไปในนาโนคอมพอสิตของซูเปอร์แอบซอร์เบนต์พอลิเมอร์ปรับปรุงความเสภียรเชิงความร้อนได้ถึงอุณหภูมิสูงสุดที่ 300 องศาเซลเซียส การวิเคราะห์การไหม้ไฟของชิ้นไม้ พบว่า ชิ้นไม้ที่เคลือบด้วยอิมัลชันของ SAP หรือ SAPC สามารถยืดเวลาติดไฟของไม้ได้ อัตราการปล่อยความร้อน ณ จุดพีก และปริมาณความร้อนที่ปล่อยมากที่สุด มีค่าน้อยที่สุดในชิ้นไม้ที่เคลือบด้วย SAPC/30% เมลามีน ชิ้นไม้ที่เคลือบด้วย SAPC/20% ซิงก์บอเรต/10%เมลามีน สามารถหน่วงการติดไฟได้นานที่สุดถึง 4 นาที 30 วินาที

คำสำคัญ ซูเปอร์แอบซอร์เบนต์, ซิงก์บอเรต, เมลามีน, สารหน่วงไฟ, โคนแคลอริเมทรี

4.6 Swelling Properties and Strength of Poly[Acrylamide-*co*-(Itaconic Acid)] Gel and Clay-Modified Poly[Acrylamide-*co*-(Itaconic Acid)] Gel

Three types of clay (montmorillonite, bentonite and mica) and chemically modified clays were investigated for creating better superabsorbent polymer nanocomposites (SAPCs) with stronger gel strength and higher water swelling at under loading conditions. The selected types of clay were treated by two methods, one with inorganic acids (HCl, H_2SO_4) and another with organic compound, such as cetyltrimethylammonium bromide ($C_{19}H_{42}BrN$) and anionic surfactant (hexadecanoic acid) were used. Ionic exchange capacity and its interaction through acid-base were consideration. The SAPCs were synthesized through free radical crosslinking polymerization of acrylamide and itaconic acid in the presence of clays and modified clays.

Reaction conditions were controlled to give the optimized water absorption and high gel strength. This project has just started in January 2011.

Keyword: Superabsorbent, Clays, Modified Clays, Gel strength, AUL, Water absorption

สมบัติการบวมตัวและความแข็งแรงของเจลพอลิ(อะคริลาไมด์-*โค*-อิทาโคนิกแอซิด) และเจลของพอลิ(อะคริลาไมด์-*โค*-อิทาโคนิกแอซิด) ที่ผสมแร่ดินและแร่ดินดัดแปร

ศึกษาชนิดของแร่ดิน (มอนต์มอริลลอไนต์ เบนโทไนต์ และไมกา) และการดัดแปรแร่ดินด้วยวิธีทางเคมี เพื่อทำให้ได้วัสดุเชิงประกอบพอลิเมอร์ดูดซึมน้ำมาก (superabsorbent polymer composites, SAPCs) ที่มีความแข็งแรงภายใต้ภาวะกดทับและยังคงมีความสามารถในการบวมตัวมาก ใช้การดัดแปรแร่ดินด้วยวิธีทางเคมี 2 วิธี คือ ทำปฏิกิริยาการกระตุ้นด้วยกรด (กรดเกลือ และกรดซัลฟิวริก) และทำปฏิกิริยากับสารอินทรีย์ เช่น ซีทิลไทรเมทิลแอมโมเนียมโบรไมด์ ($C_{19}H_{42}BrN$) และแอนไอออนิกเซอร์แฟกเตนต์ (เฮกซะเดกคาโนอิกแอซิด) การแลกเปลี่ยนประสิทธิภาพของและปฏิสัมพันธ์ระหว่างกรดและเบสจะนำมาพิจารณา ได้สังเคราะห์ SAPCs ผ่านกระบวนการเกิดพอลิเมอร์แบบอนุมูลอิสระในสารละลายของพอลิเมอร์ร่วมระหว่างอะคริลาไมด์กับอิทาโคนิกแอซิดซึ่งมีแร่ดินกระจายตัวอยู่ ควบคุมภาวะการเกิดปฏิกิริยาเพื่อหาค่าการดูดซึมน้ำมากที่สุดและมีความแข็งแรงของเจลที่ดี โครงการนี้เพิ่งเริ่มวิจัยในเดือนมกราคม 2554

คำสำคัญ ซูเปอร์แอบซอร์เบนต์, แร่ดิน, แร่ดินดัดแปร, ความแข็งแรงของเจล, ค่าการดูดซึมน้ำภายใต้แรงกดทับ, ค่าการดูดซึมน้ำ

กลุ่มโครงการวิจัยที่ 5 ไมโครเอนแคปซูเลชันและการควบคุมการปล่อยของวัสดุอินทรีย์/อินทรีย์

5.1 Microencapsulation of menthol via glass membrane emulsification and controlled release

This research studied the preparation of microcapsules of menthol with the Shirasu porous glass (SPG) membrane emulsification technique combined with a high-speed disperser. The oil-in water emulsion from the SPG membrane was prepared by controlling operation pressures, the amounts of surfactant and stabilizer, and the amount of menthol loading. The average droplet size ($\overline{d_e}$) and coefficient variation (CV) of the emulsion droplets were systemically investigated. The emulsions of menthol so prepared were mixed with the chitosan solution prepared by the high-speed disperser. Tripolyphosphate (TPP) crosslinker solution was gradually dropped in the emulsion mixture. The effects of crosslinking time and pH of microcapsules on the properties of the microcapsules were investigated. The mechanism of menthol release of microcapsules was studied. The flow behavior of microcapsules formulated in a leave–on hair conditioner was also investigated. It was found that the emulsions of menthol were successfully prepared via the SPG membrane pore sizes of 5.2 μm. The droplets having the $\overline{d_e}$, of 19.6±2.3 μm and the coefficient variation (CV) of 11.5% were achieved. When the menthol loading in the dispersed phase increased from 5 to 10%wt, the size of emulsion droplets decreased but the size distribution was broader. The optimal condition of emulsion prepared with the high-speed disperser was 14000 rpm at 90 s mixing in 1.5 %w v^{-1} of chitosan solution. Chitosan layer of microcapsule shell was crosslinked via ionic bonding between the positive charge of chitosan and the negative charge of TPP. The average size of microcapsules was 27.6±7.2 μm with the CV of 26.3 %. The pH of emulsion of the microcapsules was in the range of 5-7 which is good for uses in hair applications. The mechanism of menthol release was a diffusion control which depended on the amount of chitosan-to-tripolyphosphate ratio (by mole) and crosslinking time. The microcapsules formulated in a leave–on hair conditioner were found to exhibit the pseudoplastic/thixotropic flow behavior. The conditioner was stability and applicable at temperatures not higher than 40 ºC. Its coating on human hair rendered soft hair and easy hair combing.

Keywords: Microencapsulation, Menthol, Glass membrane emulsification, SPG, Controlled release

ไมโครแอนแคปซูเลชันของเมนทอลผ่านกลาสเมมเบรนอิมัลซิฟิเคชันและการปล่อยแบบควบคุม

งานวิจัยนี้เป็นการศึกษาการเตรียมไมโครแคปซูลของเมนทอลด้วยเทคนิคชิราสุพอรัสกลาสเมมเบรน (เอสพีจี) อิมัลซิฟิเคชันร่วมกับเครื่องกวนสารละลายความเร็วรอบสูง เตรียมอิมัลชันของน้ำมันในน้ำจากเอสพีจีเมมเบรน ปรับความดันที่ใช้ เปลี่ยนปริมาณของสารลดแรงตึงผิว สารเพิ่มเสถียรภาพ และปริมาณเมนทอล วัดขนาดและการกระจายของหยดน้ำมันในน้ำที่เตรียมได้ นำอิมัลชันของเมนทอลที่เตรียมได้จากเอสพีจีเมมเบรนผสมกับอิมัลชันที่มีไคโทซานซึ่งเตรียมด้วยการกวนด้วยเครื่องกวนสารละลาย ค่อย ๆ หยดสารละลายเชื่อมขวางไทรพอลิฟอสเฟต ศึกษาผลของเวลาเชื่อมขวาง และค่าความเป็นกรด-เบสต่อสมบัติของอิมัลชันที่เตรียมได้ ศึกษากลไกการปล่อยเมนทอลจากไมโครแคปซูล และสมบัติการไหลของครีมบำรุงเส้นผมชนิดที่ไม่ต้องล้างออกที่เตรียมด้วยไมโครแคปซูล พบว่าสามารถเตรียมหยดของน้ำมันในน้ำด้วยเอสพีจีเมมเบรนที่มีขนาดรูพรุน 5.2 ไมโครเมตร หยดน้ำมันที่ได้มีขนาดเฉลี่ย 19.6±2.3 ไมโครเมตร และมีค่าสัมประสิทธิ์การแปรปรวนประมาณร้อยละ 11.5 เมื่อปริมาณเมนทอลเพิ่มขึ้นจากร้อยละ 5 เป็น 10 โดยน้ำหนัก หยดน้ำมันมีขนาดเล็กลง แต่มีการกระจายตัวของขนาดกว้างขึ้น ภาวะที่เหมาะสมสำหรับการเตรียมหยดน้ำมันในน้ำด้วยเครื่องกวนสารละลายความเร็วรอบสูง คือ ความเร็วการกวน 14000 รอบต่อนาที เวลา 90 วินาที และความเข้มข้นของสารละลายไคโทซานร้อยละ 1.5 โดยน้ำหนักต่อปริมาตร เปลือกของแคปซูลไคโทซานเกิดการเชื่อมขวางด้วยพันธะไอออนิกระหว่างประจุบวกของไคโทซานกับประจุลบของไทรพอลิฟอสเฟต เกิดเป็นไมโครแคปซูลที่มีขนาดเฉลี่ย 27.6±7.2 ไมโครเมตร และมีค่าสัมประสิทธิ์การแปรปรวนร้อยละ 26.3 ความเป็นกรด-เบสของระบบอิมัลชันที่จะนำไมโครแคปซูลไปใช้งานด้านเส้นผมควรอยู่ในช่วง 5 ถึง 7 กลไกการปล่อยเมนทอลจากไมโครแคปซูลเป็นการควบคุมแบบการแพร่ ซึ่งขึ้นอยู่กับปริมาณไทรพอลิฟอสเฟต สัดส่วนโดยโมลของไคโทซานต่อไทรพอลิฟอสเฟต และเวลาการเชื่อมขวาง เมื่อใช้ไมโครแคปซูลเตรียมเป็นครีมบำรุงเส้นผมชนิดที่ไม่ต้องล้างออก ครีมที่ได้มีพฤติกรรมการไหลแบบซูโดพลาสติก/ทิกโซทรอปี และครีมบำรุงผมมีเสถียรภาพที่ดี ใช้งานได้ดีที่อุณหภูมิไม่สูงกว่า 40 องศาเซลเซียส และเคลือบติดบนเส้นผมมนุษย์ได้ ทำให้เส้นผมนุ่มลื่นและหวีง่ายขึ้น

คำสำคัญ: ไมโครเอ็นแคปซูเลชัน, เมนทอล, กลาสเมมเบรนอิมัลซิฟิเคชัน, เอสพีจี, การปล่อยแบบควบคุม

5.2 Synthesis of Microcapsules Containing Eucalyptus Oil via Shirasu Porous Glass Membrane Emulsification

The emulsion of eucalyptus oil was encapsulated by sodium alginate via Shirasu Porous Glass Membrane which possesses uniform pore size. The eucalyptus oil, liquid paraffin and petroleum ether were used to compose the dispersed phase while sodium dodecylsulfate surfactant and poly(vinyl alcohol) stabilizer were used as ingredients in the continuous phase to realize an oil-in-water emulsion. Calcium carbonate was used a crosslinking agent. The reaction parameters of importance namely the concentrations of encapsulating sodium alginate, and the crosslinking agent and the crosslinking time on physical and morphological properties, microcapsule size and size distribution were investigated. The extent of encapsulation and controlled release of eucalyptus oil were experimented. This project has just started in early January 2011.

Keywords: Eucalyptus oil, Sodium alginate, Shirasu Porous Glass Membrane, Microcapsules, Encapsulation, Controlled release

การสังเคราะห์ไมโครแคปซูลบรรจุน้ำมันยูคาลิปตัสโดยอิมัลซิฟิเคชันผ่านชิราซุพอรัสกลาสเมมเบรน

เตรียมอิมัลชันของน้ำมันยูคาลิปตัสที่ถูกห่อหุ้มด้วยโซเดียมแอลจิเนต ผ่านชิราสุพอรัสกลาสเมมเบรน (Shirasu Porous Glass Membrane) ที่มีขนาดรูพรุนสม่ำเสมอ ใช้น้ำมันยูคาลิปตัส พาราฟินเหลวและปิโตรเลียมอีเทอร์เป็นวัฏภาคกระจาย ใช้โซเดียมแอลจิเนต สารลดแรงตึงผิวโซเดียมโดเดกซิลซัลเฟต และสารเพิ่มความเสถียรแก่อิมัลชันพอลิไวนิลแอลกอฮอล์เป็นวัฏภาคต่อเนื่อง ใช้ระบบอิมัลชันแบบน้ำมันในน้ำ สารเชื่อมขวางเป็นแคลเซียมคาร์บอเนต ศึกษาผลของตัวแปรต่าง ๆ ได้แก่ ความเข้มข้นของสารห่อหุ้มโซเดียมแอลจิเนต ความเข้มข้นของสารเชื่อมขวาง เวลาที่ใช้ในการทำปฏิกิริยาเชื่อมขวาง ต่อสมบัติทางกายภาพ วัดขนาดและการกระจายตัวของไมโครแคปซูล ตรวจสอบสัณฐานวิทยาของไมโครแคปซูล ศึกษาปริมาณที่กักเก็บได้และการปล่อยน้ำมันยูคาลิปตัสจากไมโครแคปซูล ได้ไมโครแคปซูลของน้ำมันยูคาลิปตัสที่มีขนาดอนุภาคสม่ำเสมอ มีการกระจายตัวของขนาดอนุภาคที่แคบ และสามารถควบคุมการปล่อยน้ำมันยูคาลิปตัสในภาวะการใช้งานได้ โครงการนี้ได้เริ่มวิจัยเมื่อต้นเดือนมกราคม 2554

คำสำคัญ: น้ำมันยูคาลิปตัส, โซเดียมแอลจิเนต, ชิราสุพอรัสกลาสเมมเบรน, ไมโครแคปซูล, การห่อหุ้ม, การปล่อยแบบควบคุม

5.3 Synthesis and Characterization of Controlled Release NPK Compound Fertilizer Hydrogel

This research studied the synthesis of controlled-release NPK compound fertilizer hydrogels. The controlled-release fertilizer hydrogels were prepared by dipping the fertilizer granules in poly(vinyl alcohol) (PVA) solution and then in chitosan (CS) solution. The PVA- and CS-coated fertilizer granules were crosslinked via vapor deposition of glutaraldehyde (GA) solution in a 2.9-L closed chamber. Water dissolution times of the un-coated fertilizer granules and the coated fertilizer granules were investigated. The fertilizer hydrogel were synthesized by grafting the crosslinked-CS layer of coated fertilizer with acrylamide (AM) and acrylic acid (AA) via inverse suspension polymerization. The existences of functional groups of the crosslinked-CS and the grafted fertilizer hydrogel were confirmed by FTIR spectroscopy. The morphologies of the un-coated and coated granules were viewed by optical microscopy. The surface morphology of hydrogel layer after swelling was also investigated by scanning electron microscopy. The effect of reactants on water absorbency of compound fertilizer hydrogel was observed. Release behaviors of the compound fertilizer hydrogel granules were investigated. It was found that water dissolution times of the grafted fertilizer increased with increasing the frequency of coating. To synthesize the compound fertilizer hydrogel, the optimal ratio of AM-to-AA was 3:97% mol and the optimal contents of *N,N,N',N'*-tetramethylethylenediamine (*N,N,N',N'*-TEMED), ammonium persulfate (APS) and *N,N'*-methylenebisacrylamide (*N*-MBA) was 0.13, 0.13 and 0.01% by mol of monomers, respectively. Water absorbency of the compound fertilizer hydrogel was 233±5 g/g in distilled water at room temperature within 24 h of immersion. The release nutrient order in 30-days of compound fertilizer hydrogel granules was 84±18, 63±12 and 36±15%, of N, P and K nutrients, respectively. The release data of the N and P nutrients of the fertilizer granules hydrogel obeyed the Korsmeyer-Peppas model while the K nutrient release followed the exponential behavior.

Keywords: NPK Compound Fertilizer, Poly(vinyl alcohol), Chitosan, Glutaraldehyde crosslinker, Fertilizer hydrogel

การสังเคราะห์และการตรวจสอบลักษณะของปุ๋ยไฮโดรเจลคอมพาวนด์เอ็นพีเคที่มีการปล่อยแบบควบคุม

งานวิจัยนี้มุ่งศึกษาการเตรียมปุ๋ยไฮโดรเจลคอมพาวนด์ชนิดควบคุมการปล่อยธาตุ NPK ได้เตรียมปุ๋ยไฮโดรเจลด้วยการจุ่มเม็ดปุ๋ยลงในสารละลายพอลิไวนิลแอลกอฮอล์ ตามด้วยการจุ่มในสารละลายไคโทซานและเชื่อมขวางด้วยไอของสารละลายกลูทารัลดีไฮด์ หาเวลาที่ปุ๋ยไม่เคลือบและปุ๋ยเคลือบละลายน้ำหมด นำปุ๋ยเคลือบพอลิไวนิลแอลกอฮอล์และไคโทซานที่เชื่อมขวางแล้วมาสังเคราะห์เป็นปุ๋ยไฮโดรเจล ด้วยการทำปฏิกิริยาการเกิดพอลิเมอร์แบบแขวนลอยของมอนอเมอร์อะคริลาไมด์และอะคริลิกแอซิด ตรวจสอบหมู่ฟังก์ชันของของปุ๋ยไฮโดรเจลด้วยเทคนิคฟูเรียร์ทรานฟอร์มอินฟราเรดส-เปกโทรสโกปี ศึกษาสัณฐานวิทยาของเม็ดปุ๋ยที่ไม่เคลือบและเคลือบด้วยเทคนิคกล้องจุลทรรศน์แบบแสง และตรวจสอบสัณฐานวิทยาของชั้นไฮโดรเจลที่เคลือบเม็ดปุ๋ยหลังจากบวมน้ำด้วยกล้องจุลทรรศน์อิเล็กตรอนแบบส่องกราด ศึกษาผลของสารตั้งต้นต่อค่าการดูดซึมน้ำของปุ๋ยไฮโดรเจลคอมพาวนด์ และศึกษาการปล่อยธาตุอาหารเอ็นพีเคในปุ๋ยไฮโดรเจลคอมพาวนด์ พบว่า เวลาในการละลายน้ำของปุ๋ยเพิ่มขึ้นด้วยการเพิ่มจำนวนครั้งในการเคลือบ ปริมาณสารตั้งต้นที่เหมาะสมในการสังเคราะห์ปุ๋ยไฮโดรเจลคอมพาวนด์ คือ อัตราส่วนของมอนอเมอร์อะคริลาไมด์ต่ออะคริลิกแอซิดมีค่าร้อยละ 3:97 โดยโมล ใช้*เอ็น,เอ็น,เอ็น', เอ็น'*-เททระเมทิลเอทิลีนไดแอมีน แอมโมเนียมเพอร์ซัลเฟต และ*เอ็น, เอ็น'*-เมทิลีนบิสอะคริลาไมด์มีค่า 0.13, 0.13 และ 0.01% โมลของมอนอเมอร์ทั้งหมด ให้ค่าการดูดซึมน้ำ 233±5 กรัมต่อน้ำหนักแห้งในน้ำกลั่น ที่อุณหภูมิห้อง ภายในเวลา 24 ชั่วโมง เม็ดปุ๋ยไฮโดรเจลคอมพาวนด์ปล่อยธาตุอาหารเอ็นพีเคได้ร้อยละ 84±18, 63±12 และ 36±15 ตามลำดับ ภายในเวลา 30 วัน ในน้ำกลั่น ค่าการปล่อยธาตุอาหารไนโตรเจนและฟอสฟอรัสสอดคล้องกับแบบจำลองจลนศาสตร์การปล่อยของ Korsmeyer-Peppas ส่วนการปล่อยธาตุอาหารโพแทสเซียมเป็นแบบเอกซ์โพเนนเชียล

คำสำคัญ: ปุ๋ยคอมพาวนด์เอ็นพีเค, พอลิไวนิลแอลกอฮอล์, ไคโทซาน, สารเชื่อมขวางกลูทารัลดีไฮด์, ปุ๋ยไฮโดรเจล

5.4 Synthesis and characterization of hydrogel for insulin released from hydrolyzed collagen grafted poly[(acrylic acid)-*co*-(methacrylic acid)]

Hydrolyzed collagen grafted poly[(acrylic acid)-*co*-(methacrylic acid)] hydrogels were synthesized by solution polymerization. Acrylic acid (AA) and methacrylic acid (MAA), ammonium persulfate (APS), *N, N, N', N'*-tetramethylethylenediamine (TEMED), and *N, N'*-

methylenebisacrylamide (N-MBA) were used as a pair of monomer, an initiator, a co-initiator, and a crosslinking agent, respectively. The effects of reagents on the performance and water absorbency of synthesized hydrogels were investigated. The grafted hydrolyzed collagen hydrogel was confirmed by FTIR technique. The effects of pH in buffered and non-buffered solutions, sodium chloride solution, and temperature on the swelling behavior of the grafted hydrolyzed collagen hydrogel were examined. The released behavior of insulin or methylene blue (as a smaller-sized model drug) was also investigated in simulated gastric and intestinal fluids. It was found that when the APS contents were too high or low, the synthesized products were not in the hydrogel form and the water absorbency cannot be determined. The high water absorbency of grafted hydrogel was reached 476±9 gg^{-1}, when the ratio of AA-to-MAA was 92:8 and the contents of TEMED, APS and N-MBA were 0.015, 0.2 and 0.12 % by mol of monomers, respectively. The grafted hydrolyzed collagen hydrogel in the acidic and neutral pH solution was suitable for drug delivery application at a target site. It showed that the abilities to release of insulin and methylene blue were slightly less in the simulated gastric fluid and relatively high in the simulated intestinal fluid. The results obtained were in good agreement with the pH responses of the synthesized hydrogel. Thus, the hydrolyzed collagen grafted poly[(acrylic acid)-*co*-(methacrylic acid)] hydrogel exhibits itself as the insulin controlled release medium.

Keywords: Hydrogel, Hydrolyzed collagen, Grafted collagen, Acrylic acid, Methacrylic acid

การสังเคราะห์และการตรวจสอบคุณลักษณะเฉพาะของไฮโรเจลสำหรับการปล่อยอินซูลินจากคอลลาเจนไฮโดรไลซ์กราฟต์พอลิ(อะคริลิกแอซิด-*โค*-เมทาคริลิกแอซิด)

สังเคราะห์ไฮโดรเจลจากคอลลาเจนไฮโดรไลซ์กราฟต์พอลิเมอร์ร่วมอะคริลิกแอซิด-เมทาคริลิกแอซิด โดยปฏิกิริยาการเกิดพอลิเมอร์ในสารละลาย ใช้อะคริลิกแอซิดเป็นมอนอเมอร์ เมทาคริลิกแอซิดเป็นมอนอเมอร์ร่วม แอมโมเนียมเพอร์ซัลเฟตเป็นสารริเริ่มปฏิกิริยา และ *เอ็น, เอ็น, เอ็น', เอ็น'*-เททระเมทิลเอทิลีนไดแอมีนเป็นสารริเริ่มปฏิกิริยาร่วม และ *เอ็น, เอ็น'*-เมทิลีนบิสอะคริลาไมด์เป็นสารเชื่อมขวาง ศึกษาผลของสารตั้งต้นต่อค่าการดูดซึมน้ำของไฮโดรเจลที่สังเคราะห์ได้ ยืนยันการเกิดการกราฟต์ของไฮโดรเจลจากคอลลาเจนไฮโดรไลซ์ด้วยเทคนิค FTIR ศึกษาผลของค่าความเป็นกรด-เบสในสารละลายไม่มีบัฟเฟอร์และสารละลายบัฟเฟอร์ ความเข้มข้นของสารละลายเกลือโซเดียมคลอไรด์ และอุณหภูมิต่อ

การตอบสนองของการดูดซึมน้ำของไฮโดรเจลจากกราฟต์คอลลาเจนไฮโดรไลซ์ ศึกษาการนำส่งยาของอินซูลินและเมทิลีนบลูที่ใช้เป็นแบบจำลองการปล่อยยา โดยเลียนแบบสารละลายในกระเพาะอาหาร และสารละลายภายในลำไส้ พบว่า เมื่อปริมาณสารเริ่มปฏิกิริยามีมากหรือน้อยเกินไป สารที่สังเคราะห์ได้ไม่อยู่ในรูปของไฮโดรเจล และไม่สามารถหาค่าการดูดซึมน้ำ กราฟต์ไฮโดรเจลที่สังเคราะห์ได้มีค่าการดูดซึมน้ำมากเท่ากับ 476±9 เท่าของน้ำหนักสารแห้ง เมื่อใช้สัดส่วนของอะคริลิกแอซิดต่อเมทาคริลิกแอซิด 92:8 โดยโมล ปริมาณแอมโมเนียมเพอร์ซัลเฟต *เอ็น, เอ็น, เอ็น', เอ็น'*-เททระเมทิลเอทิลีนไดแอมีน และ *เอ็น, เอ็น'*-เมทิลีนบิสอะคริลาไมด์ เท่ากับ 0.015, 0.2 และ 0.12 โดยโมลของมอนอเมอร์ตามลำดับ ไฮโดรเจลจากกราฟต์คอลลาเจนไฮโดรไลซ์มีการตอบสนองในภาวะกรดและภาวะเป็นกลางที่เหมาะสมกับการนำไปประยุกต์ในการนำส่งยาไปยังอวัยวะเป้าหมาย ไฮโดรเจลปล่อยอินซูลินและเมทิลีนบลูออกมาน้อยในสารละลายเลียนแบบกระเพาะอาหารที่มีสภาพเป็นกรด เมื่อไฮโดรเจลอยู่ในสารละลายเลียนแบบลำไส้ที่มีภาวะเป็นกลาง สามารถปล่อยอินซูลินและเมทิลีนบลูออกมาในปริมาณมาก ซึ่งสอดคล้องกับผลการทดลองในส่วนของการตอบสนองต่อค่าความเป็นกรด-เบสของไฮโดรเจลที่สังเคราะห์ได้ ดังนั้น ไฮโดรเจลจากคอลลาเจนไฮโดรไลซ์กราฟต์พอลิเมอร์ร่วมอะคริลิกแอซิด-เมทาคริลิกแอซิด สามารถแสดงผลเป็นตัวกลางควบคุมการปล่อยอินซูลินได้ดี

คำสำคัญ: ไฮโดรเจล, คอลลาเจนไฮโดรไลซ์, กราฟเทดคอลลาเจน, อะคริลิกแอซิด, เมทาคริลิกแอซิด

กลุ่มโครงการวิจัยที่ 6 การผลิตเส้นใยและกระดาษจากนุ่น

6.1 Kapok I: Properties investigation of kapok fiber as a potential pulp source for papermaking

The potential use of kapok fiber as a new source for pulping and papermaking has been investigated. The experiment was started by cooking kapok fibers with different dosages of sodium hydroxide. Then, the pulp was refined twice using a disc refiner with a disc gap of 1/100 inch. Handsheets were made and their strength properties were evaluated to determine the optimal dosage of sodium hydroxide. The optimized pulping condition was then used to prepare kapok pulp. Then, this kapok pulp was mixed with commercial hardwood pulp and/or softwood pulp at different blend ratios to make papers. Addition of the kapok pulp to the mixed pulps improved the tensile and burst strengths of the sheets but decreased the tear resistance. Water repellency of the sheets prepared from the kapok pulp mixed with the commercial pulps was also improved. These results indicate that kapok fiber can be a quality pulp source for papermaking, especially for packaging paper.

Keywords: Kapok fiber; Paper properties, Raw material, Papermaking

นุ่น I: การประเมินสมบัติของเส้นใยนุ่นเป็นแหล่งเยื่อที่มีศักยภาพเพื่อการผลิตกระดาษ

โครงการนี้ได้ประเมินศักยภาพและความเหมาะสมของเส้นใยนุ่นเพื่อเป็นแหล่งเยื่อและการผลิตกระดาษชนิดใหม่ เริ่มต้นด้วยการต้มเยื่อนุ่นในสารละลายโซเดียมไฮดรอกไซด์ปริมาณต่าง ๆ นำเยื่อที่ต้มแล้วมาบด 2 ครั้งในเครื่องบดเยื่อแบบจาน ใช้ระยะห่างระหว่างจานบด 1/1000 นิ้ว ผลิตกระดาษแฮนด์ชิตจากเยื่อที่บดได้ ประเมินสมบัติด้านความแข็งแรงของแฮนด์ชิตเพื่อหาปริมาณโซเดียมไฮดรอกไซด์ที่เหมาะสม เมื่อได้ภาวะการต้มเยื่อที่เหมาะสมแล้ว นำภาวะนี้ไปผลิตเยื่ออีกครั้งหนึ่ง นำเยื่อที่ผลิตได้ใหม่ด้วยภาวะนี้ไปผสมกับเยื่อจากไม้เนื้อแข็ง เยื่อจากไม้เนื้ออ่อน และเยื่อผสมระหว่าเยื่อทั้งสองชนิด เยื่อนุ่นที่เติมลงไปในเยื่อผสมปรับปรุงสมบัติเทนไซล์และความแข็งแรงทนแรงระเบิดของกระดาษแฮนด์ชิต แต่ลดความต้านทานต่อแรงฉีกขาด จากการวัดมุมสัมผัสของน้ำบนกระดาษแฮนด์ชิตที่เตรียมได้ กระดาษแฮนด์ชิตขับน้ำกลั่นที่หยดบนกระดาษนุ่นผสมเยื่อผสมทั้งสองชนิดมากขึ้น ผลที่ได้เหล่านี้บ่งชี้ว่า เยื่อนุ่นสามารถเป็นแหล่งเยื่อที่มีคุณภาพสำหรับการผลิตกระดาษ โดยเฉพาะอย่างสำหรับกระดาษบรรจุภัณฑ์

คำสำคัญ: เส้นใยนุ่น, สมบัติของกระดาษ, วัตถุดิบ, การผลิตกระดาษ

6.2 Kapok II: Pretreatment of Kapok Fibers for Pulping and Papermaking

Kapok fiber is naturally coated with wax and cutin which render it hydrophobic. To obtain the fiber suitable for pulping, it must be immersed in water for as long as three to four weeks. This research investigated the effects of fiber pretreatments by chemical method or biological method for varied immersion times before it could be subjected to soda pulping. These pretreatments were compared with those obtained from the controlled fiber where the kapok fibers were immersed in tap water for 3 weeks (as controlled kapok). For the chemical pretreatment, the doses of sodium hydroxide (5 and 10% based on O.D. fiber weight) were used with various immersion times (1, 2 and 3 weeks). For the biological pretreatment, the enzyme lipase doses (0.25 and 0.5% based on O.D. fiber weight) was used under the immersion times (1, 3 and 5 hours). All the pretreatment results were compared with those obtained from the control. After the kapok fibers had passed the soda pulping process and further processes, the pulp and their handsheets having 60 g/m^2 from each pretreatment were characterized for the pulping efficiency, physical properties and optical properties. This research elucidated the results and causes of each effect and suggested their benefits for the pulp and paper making.

Keywords: Kapok fiber, Chemical pretreatment, Biological pretreatment, Soda pulping, Lipase, Immersion times, Paper making

นุ่น II: การปรับสภาพผิวของเส้นใยนุ่นสำหรับการผลิตเยื่อและการผลิตกระดาษ

เส้นใยนุ่นมีขี้ผึ้งและเคอร์ทินเคลือบอยู่ตามธรรมชาติ จึงทำให้นุ่นไม่ชอบน้ำ ในการผลิตเยื่อจากนุ่นจำเป็นต้องแช่นุ่นในน้ำเป็นเวลานานถึง 3-4 สัปดาห์ งานวิจัยจึงได้ศึกษาผลของการปรับสภาพเส้นใยแบบเคมี หรือแบบชีวภาพของเส้นใยนุ่น ก่อนนำเส้นใยนุ่นไปเข้ากระบวนการโซดา และเทียบผลกับเส้นใยนุ่นที่แช่ในน้ำประปาอย่างเดียว เป็นเวลา 3 สัปดาห์ (นุ่นควบคุม) ได้ศึกษาผลจากปริมาณโซเดียมไฮดรอกไซด์ของการปรับสภาพแบบเคมี (ร้อยละ 5 และ 10 เมื่อเทียบกับน้ำหนักของนุ่นที่อบแห้ง) และเวลาแช่นุ่น (1, 2 และ 3 สัปดาห์) ส่วนการปรับสภาพด้วยวิธีทางชีวภาพใช้เอนไซม์ไลเปส (ร้อยละ 0.25 และ 0.50 เมื่อเทียบ

กับน้ำหนักของนุ่นที่อบแห้ง) และเวลาแช่นุ่น (1, 3 และ 5 ชั่วโมง) ภายหลังที่เส้นใยนุ่นผ่านกระบวนการโซดา และขึ้นแผ่นกระดาษแล้ว ได้ศึกษาประสิทธิภาพในการผลิต สมบัติเชิงกลและสมบัติทางแสงของเยื่อและกระดาษที่ได้จากแต่ละกระบวนการปรับสภาพ อธิบายผลและเหตุที่ได้จากตัวแปรพร้อมทั้งเสนอแนะการใช้ประโยชน์ของเยื่อและกระดาษ

คำสำคัญ: เส้นใยนุ่น, การปรับสภาพเชิงเคมี, การปรับสภาพเชิงชีวภาพ, การต้มเยื่อด้วยโซดา, เอ็นไซม์ไลเปส, เวลาการแช่, การผลิตกระดาษ

Kapok III: Use of Kapok Pulp to Improve Properties of Recycled Paper

Using recycled paper is one way to reduce environment problems. However, higher cycle numbers of recycling leads to reduction of paper strength; thus, improvement of recycled paper properties is very important. One way to improve strength of recycled paper is to use kapok pulp because kapok is the long fiber with good enough pulp and paper properties. In this study, paper was made using kapok and recycled pulp to compare with those using softwood-to-recycled pulp ratios at 100:0, 10:90, 20:80, 30:70 and 0:100. As a result, it was found that recycling up to three cycles had a small effect on paper properties. Higher amount of kapok pulp in the mixed pulp between kapok pulp and recycled pulp increased porosity, opacity, density and tensile index but decreased brightness and whiteness of handsheets. On the other hand, higher amount of softwood pulp led to higher tear index only. So, the combination of the mixed pulps and amount of pulps used are really dependent on the final paper property required.

Keywords: Recycled paper, Kapok fiber, Softwood, Paper properties

นุ่น III: การใช้เส้นใยนุ่นในการปรับปรุงสมบัติของกระดาษที่ผลิตจากเยื่อเวียนทำใหม่

งานวิจัยในส่วนนี้ศึกษาผลของการใช้เยื่อนุ่นในการปรับปรุงสมบัติของกระดาษที่ผลิตจากเยื่อเวียนทำใหม่ แต่อย่างไรก็ตาม จำนวนรอบของการเวียนทำใหม่มากเกินไปจะลดความแข็งแรงของกระดาษเวียนทำใหม่ ดังนั้น การปรับปรุงสมบัติของกระดาษเวียนทำใหม่มีความสำคัญมาก วิธีหนึ่งที่จะเพิ่มความแข็งแรงแก่กระดาษเวียนทำใหม่คือ การใส่เยื่อนุ่น เพราะเยื่อนุ่นเป็นเยื่อใยยาวซึ่งมีสมบัติของเยื่อและ

กระดาษที่ดีพอ การทดลองเริ่มต้นจากการนำเยื่อนุ่นมาผสมกับเยื่อเวียนทำใหม่ ในสัดส่วน เยื่อนุ่น: เยื่อเวียนทำใหม่ 100:0, 10:90, 20:80, 30:70 *และ* 0:100 ในแต่ละรอบของการเวียนทำใหม่ ตั้งแต่ 1- 3 รอบ นอกจากนี้ ยังนำเยื่อใยยาว (เยื่อจากไม้เนื้ออ่อน) มาผสมเยื่อเวียนทำใหม่แทนเยื่อนุ่น เพื่อใช้เปรียบเทียบประสิทธิภาพการปรับปรุงสมบัติของเยื่อเวียนทำใหม่ผสมระหว่างเยื่อนุ่นกับเยื่อยาว จากการทดลองพบว่า เมื่อเปรียบเทียบกับเยื่อใยยาวแล้ว การใช้ปริมาณสัดส่วนเยื่อนุ่นที่มากขึ้นในการผลิตกระดาษจากเยื่อเวียนทำใหม่ ส่งผลให้ค่าความแข็งแรงต่อแรงดึง ความหนาแน่น ความพรุน ความเรียบ และความทึบแสงของกระดาษเพิ่มมากขึ้น ในขณะที่เมื่อเปรียบเทียบกับเยื่อนุ่นในสัดส่วนที่เท่ากันแล้ว การใช้เยื่อใยยาวในสัดส่วนที่เพิ่มขึ้นส่งผลให้ค่าความต้านทานแรงฉีกมีค่าสูงขึ้นมากกว่าการใช้เยื่อนุ่น ดังนั้น การผสมผสานการใช้เส้นใยผสมและปริมาณที่พอเหมาะขึ้นกับสมบัติสุดท้ายของกระดาษที่ต้องการ

คำสำคัญ: กระดาษเวียนทำใหม่, เส้นใยนุ่น, ไม้เนื้ออ่อน, สมบัติของกระดาษ

กลุ่มโครงการวิจัย ที่ 7 ผ้าไหมและการพิมพ์ผ้าไหมด้วยหมึกพิมพ์อิงก์เจ็ต

7.1 Modified chitosan pretreatment of polyester fabric for printing by ink jet ink

The present research deals with the use of pretreatment solutions of chitosan (CH), *N*-[(4-dimethyl aminobenzyl)imino] chitosan (DBIC), *N*-[(2-hydroxy-3-trimethylammonium) propyl] chitosan chloride (HTACC), glycine (Gly), and a mixture of CH and Gly, for padding polyester fabrics prior to printing with a set of seven-color pigmented water-based ink jet inks. After padding the fabrics with the above cationic pretreatments, they were printed with a piezo-electric drop-on-demand jet printer. CH, DBIC and HTACC were characterized by IR and NMR spectroscopy. The zeta potentials of the pretreatment solutions, the inks and the fabrics were measured. The K/S values, color gamut, tone reproduction, outline sharpness, and the surface appearance of the fabrics were characterized. Statistical evaluation of the significance of the results was performed. Among the pretreatments, the HTACC at 0.1% (w/v) yielded fabrics with the highest K/S values, widest color gamut and gamut volume, more color saturation with good tonal reproduction, and the sharpest and smoothest outline of printed character, and a smooth fabric surface with less stiffness. The proposed ionic interactions between the protonated amino groups of CH and the anionic portion of the encapsulated ink pigments, and van der Waals and hydrophobic interactions between the polyester and the pigments are likely reasons for these enhanced properties of the printed fabrics.

*Keywords: Chitosan; glycine, N-[(4-dimethyl aminobenzyl)imino] chitosan, N-[(2-hydroxy-3-*trimethylammonium)propyl] chitosan chloride, Color properties**,** Outline sharpness**,** Stiffness

การปรับสภาพผิวผ้าพอลิเอสเทอร์ด้วยไคโทซานดัดแปรสำหรับการพิมพ์โดยหมึกอิงก์เจ็ต

งานวิจัยนี้เป็นการศึกษาผลของสารละลายปรับสภาพผิวผ้าพอลิเอสเทอร์ 5 ชนิด คือ ไคโทซาน ไคโทซานดัดแปร เอ็น-4-ไดเมทิลแอมิโนเบนซิลอิมิโน (*N*-[(4-dimethyl aminobenzyl)imino] chitosan, DBIC) เอ็น-2-ไฮดรอกซี-3-ไทรเมทิลแอมโมเนียมพรอพิลไคโทซานคลอไรด์ (*N*-[(2-hydroxyl-3-trimethylammonium)propyl] chitosan chloride, HTACC) ไกลซีน และของผสมระหว่างไคโทซานกับไกลซีน สำหรับการแพดดิงผ้าก่อนการพิมพ์ด้วยหมึกพิมพ์อิงก์เจ็ตฐานน้ำชนิดสารสี 7 สี ด้วยเครื่องพิมพ์อิงก์เจ็ตแบบ piezo-electric drop-on-demand ตรวจสอบลักษณะเฉพาะของไคโทซาน ไคโท

ซานดัดแปร DBIC และ HTACC ด้วยเทคเนิค IR and NMR วัดค่า zeta potentials ของสารละลายปรับสภาพผิว และผ้าพอลิเอส- เทอร์ วัดความเข้มสี ขอบเขตสี การผลิตน้ำหนักสี ความคมชัดของตัวอักษร และตรวจสอบลักษณะพื้นผิวผ้าที่ปรับสภาพ พบว่า HTACC ความเข้มข้นร้อยละ 0.1 โดยน้ำหนัก ให้ความเข้มสีมากสุด ขอบเขตสีและปริมาตรสีกว้างสุด ความอิ่มตัวสีและการผลิตน้ำหนักสีดี ความคมชัดของตัวอักษรมากสุด และพื้นผิวผ้ามีความกระด้างน้อยสุด ด้วยปฏิกิริยาระหว่างประจุบวกของสารปรับสภาพผิวผ้ากับประจุลบของสารสีในหมึกพิมพ์ และแรง van der Waals และความไม่ชอบน้ำของผ้าพอลิเอสเทอร์และสารสีที่มีผลเพิ่มคุณภาพผ้าพิมพ์พอลิเอสเทอร์ด้วยระบบการพิมพ์อิงก์เจ็ต

คำสำคัญ: ไคโทซาน, ไกลซีน, ไคโทซานดัดแปร เอ็น-4-ไดเมทิลแอมิโนเบนซิลอิมิโน, เอ็น-2-ไฮดรอกซี-3-พรอพิลไทรเมทิลแอมโมเนียมไคโทซานคลอไรด์, สมบัติทางสี, ความคมชัดของเส้น, ความกระด้าง

7.2 Anionically surface-modified pigment/binder ink jet inks for silk fabric printing

The purpose of this research was to prepare anionically surface-modified organic pigment/binder ink jet inks for printing on chitosan-pre-treated silk fabrics. Anionically surface-modified organic pigment/binder ink jet inks were prepared in four colours (cyan, magenta, yellow and black). The pigment-to-binder ratio was controlled at 1:6.4 for the cyan, magenta and yellow inks, and 1:3.4 for the black ink. Ink formulations (by weight) were assembled and mixed as follows: 8% pigment dispersion, 10% diethylene glycol, 12% glycerol, 5% urea, 10% polyacrylate emulsion binder and 55% deionised water. The inks were mixed and filtered with a special type of membrane to remove the oversized particles. They were characterised in terms of their particle size, zeta potential, particle morphology, viscosity, surface tension and pH. The inks were printed onto silk or the chitosan pre-treated silk fabrics using a piezo-type ink jet printer. The fabrics were then heat cured and analysed for the effect of chitosan pre-treatment on colour gamut, wash fastness and crock fastness. The formulated ink jet inks yielded an acceptably good ink jetting reliability, one–year stability and printability. The chitosan pre-treated silk fabrics gave a wider colour gamut and colour saturation than the non-treated one. Crock fastness and wash fastness of the chitosan pre-treated fabrics where relatively better than those of non-treated fabrics. The surface modified pigments are transparent and thus their inks printed on the chitosan pre-treated fabrics produced slightly low K/S values of CMYK colours because the limited chitosan concentration in the pre-treatment is controlled by its solubility in

acidic solution. The higher loading of chitosan pre-treatment gave higher K/S values and a stiffer touch of the fabrics which is uncomfortable for users. Water-based pigmented inks having the sulphonate group on the pigment surface can be printed on the fabric surface pre-treated with chitosan molecules which have the protonated amino groups to give good color appearance. It is anticipated that this type of ink can be applied to any textile surface which has been pre-treated with the protonated chitosan. Ionic interactions between the sulphonate group of the pigment and protonated amino groups of chitosan in conjunction with polyacrylate binder enhance colour strength, widen colour gamut and chroma, and produce good adhesion for fabric operational properties such as wash fastness and crock fastness.

Keywords: Anionic functional group, Surface-modified pigments, Ink jet, Fabric pre-treatment, Chitosan, Silk fabric, Polyacrylate emulsion binder

การพิมพ์ผ้าไหมด้วยหมึกพิมพ์อิงก์เจ็ตชนิดผิวสารสีมีประจุลบ/สารยึด

วัตถุประสงค์ของงานวิจัยนี้เพื่อเตรียมหมึกพิมพ์อิงก์เจ็ตชนิดผิวสารสีมีประจุลบผสมกับสารยึดเพื่อพิมพ์ผ้าไหมปรับผิวผ้าด้วยสารละลายไคโทซานประจุลบ นำสารสีผิวมีประจุลบ 4 สี ได้แก่ สีฟ้าเขียว สีม่วงแดง สีเหลือง และสีดำ ใช้สัดส่วนของสารสีต่อสารยึด เป็น 1: 6.4 สำหรับสีหมึกพิมพ์สีฟ้าเขียว สีม่วงแดงและสีเหลือง ส่วนสีหมึกพิมพ์สีดำมีสัดส่วนเป็น 1:3.4 ผสมองค์ประกอบในหมึกพิมพ์ตามลำดับดังนี้ สารละลายของสารสีซึ่งการกระจายมาแล้วในพอลิเมอร์ ร้อยละ 8 ไดเอทิลีนไกลคอลร้อยละ 10 ไกลคอลร้อยละ 5 ยูเรียร้อยละ 10 อิมัลชันพอลิอะคริเลตไบน์เดอร์ร้อยละ 10 และน้ำกลั่นร้อยละ 55 ผสมและเขย่าให้เข้ากัน กรองด้วยเมมเบรนพิเศษเพื่อกรองอนุภาคขนาดใหญ่ออกไป นำหมึกพิมพ์ที่เตรียมได้ทั้งหมดไปวัดขนาดอนุภาค ความต่างศักย์ซีตา สัณฐานวิทยาของอนุภาค ความหนืด แรงตึงผิว และค่าความเป็นกรด-เบสของหมึกพิมพ์ นำหมึกพิมพ์ทั้งสี่สีบรรจุในตลับพิมพ์และนำไปพิมพ์ผ้าไหมที่ไม่ผ่านการจุ่มรีดและผ้าที่ผ่านการจุ่มรีดด้วยสารละลายไคโทซานด้วยเครื่องพิมพ์อิงก์เจ็ตที่ขับเคลื่อนการพิมพ์ด้วยแรงดันเปียร์โซ นำผ้าพิมพ์เหล่านี้ไปอบและวิเคราะห์คุณภาพของสีพิมพ์ด้านแกมุตสี ความทนการซัก และความทนการขัดข่วนและขัดถู หมึกพิมพ์สูตรชุดนี้ที่กำหนดสามารถพ่นหมึกได้เส้นหมึกพิมพ์สมบูรณ์ ลักษณะการพ่นหมึกเชื่อถือได้ และมีความเสถียรของสารสีในหมึกพิมพ์เก็บได้นาน 1 ปี ผ้าพิมพ์ที่ปรับผิวด้วยไคโทซานมีค่าแกมุตสีกว้างกว่าและมีความอิ่มตัวของสีมากกว่าผ้าที่ไม่ได้ปรับผิว ความทนการขัดข่วนและขัดถู และความทนการซักของผ้าพิมพ์ที่ปรับผิวมีค่ามากกว่าผ้าพิมพ์ที่ไม่ปรับผิว สารสีที่ดัดแปรด้วยสารเคมีที่ผิวมีความโปร่งใสมาก สีพิมพ์ที่ได้บนผ้าไหมที่จุ่มรีดด้วยสารละลายไค

โทซานจึงมีค่า K/S ไม่สูง เพราะปริมาณที่จำกัดของไคโทซานที่ละลายได้เฉพาะในกรดที่มีค่าความเป็นกรด-เบสต่ำกว่า 4 และปริมาณไคโทซามที่มากขึ้นบนผ้าไหมก็จะทำให้สีพิมพ์มีค่า K/S มากขึ้นแต่ผ้าพิมพ์มีความกระด้างมากขึ้น ผู้ใช้จับต้องไม่สบายมือและไม่สบายเมื่อสวมใส่ หมึกพิมพ์อิงก์เจ็ตฐานน้ำที่มีกลุ่มซัลโฟเนตประจุบนผิวของสารสีพิมพ์ได้สีเข้มดีขึ้นบนผ้าที่ปรับผิวด้วยไคโทซานที่มีประจุบวกจากการเติมโปรตอนที่กลุ่มแอมิโน เป็นที่คาดว่า หมึกพิมพ์กลุ่มนี้สามารถใช้ได้กับผ้าได้ทุกชนิดที่ได้รับการปรับผิวก่อนพิมพ์ด้วยไคโทซานประจุบวก พันธะไอออนระหว่างกลุ่มซัลโฟเนตประจุลบกับสารไคโทซานประจุบวกเมื่อเสริมกับสารยึดพอลิอะคริเลต จะช่วยส่งให้สีพิมพ์มีความอิ่มตัวมากขึ้น สีในแกมุตกว้างขึ้น และเกิดแรงยึดติดมากขึ้น ทำให้ทนการซักและการขีดข่วนและการขัดถูมากขึ้น

คำสำคัญ: หมู่ฟังก์ชันประจุลบ, สารสีดัดแปรผิว, หมึกพิมพ์อิงก์เจ็ต, สารปรับผิวผ้า, ไคโทซาน, ผ้าไหม, สารยึดอิมัลชันพอลิอะคริเลต

7.3 Simulation of Printed Images on Silk Fabric by Ink Jet Printer

Silk fabric is a fabric in which its gloss is perceived differently in comparison with other fabrics due to its specific reflectance. This research measured a Bidirectional Reflectance Distribution Function (BRDF) of three types of silk fabric having different weaving styles in conjunction with reflectance characteristics. We measured BRDF of the silk fabrics and its reflection model was then proposed. The proposed reflection model incorporates a specular reflection lobe and diffuse reflection lobe. The proposed model and the measured BRDF of the three silk fabrics were fitted by the least-square error method. The measured BRDF of the silk fabric were also fitted with Phong reflection model, Oren-Nayar reflection model and Torrance-Sparrow reflection. It was found that the proposed model fitted better with the measured BRDF than did the general models of Phong-reflection, Oren-Nayar reflection, and Torrance-reflection. The proposed model can thus be used to approximate, analyze and elucidate the characteristics of light reflection of the three silk fabrics.

Key words: BRDF, silk fabrics, reflection model.

การวัด Bidirectional Reflectance Distribution Function และการจำลองแบบการสะท้อนแสงของผ้าไหม

ผ้าไหมเป็นสิ่งทอที่มีความมันวาวมากกว่าสิ่งทอประเภทอื่น เนื่องจากผ้าไหมมีลักษณะการสะท้อนแสงที่มีความเฉพาะตัว ดังนั้น งานวิจัยนี้จึงศึกษาลักษณะการสะท้อนแสงของผ้าไหม โดยวัดค่า BRDF (Bidirectional Reflectance Distribution Function) และนำเสนอแบบจำลองการสะท้อนแสงของพื้นผิวผ้าไหมที่คำนึงถึงการสะท้อนของแสงฟุ้งและแสงกล้า โดยใช้วิธีการหาค่าความผิดพลาดกำลังสองน้อยที่สุด (least-square error) หาความสัมพันธ์ระหว่างค่าที่วัดกับแบบจำลอง เมื่อทดสอบแบบจำลองที่ได้พบว่า แบบจำลองที่นำเสนอนี้มีความสัมพันธ์กับ BRDF ที่วัดได้ของผ้าไหมมากกว่าแบบจำลองการสะท้อนแสงที่มีอยู่ทั่วไป ได้แก่ แบบจำลองการสะท้อนแสงของ Phong reflection model, แบบจำลองการสะท้อนแสงของ Oren-Nayar reflection model และแบบจำลองการสะท้อนแสงของ Torrance-Sparrow reflection model ผู้วิจัยสามารถพยากรณ์ค่าการสะท้อนแสง วิเคราะห์ และอธิบายลักษณะการสะท้อนแสงของผ้าไหมได้จากแบบจำลองที่นำเสนอนี้

คำสำคัญ : บีอาร์ดีเอฟ, ผ้าไหม, แบบจำลองการสะท้อนแสง

7.4 Effects of Chitosan and Glycine Pretreatment on Polyester Fabric Printed by Ink Jet Ink

The effects of pretreatment solutions of chitosan (CS) and glycine (Gly) on polyester fabric and their printing results were investigated. The polyester fabrics were padded with CS (4% w/v) or Gly (5% w/v) solution prior to printing with a set of seven-color pigmented water-based jet inks from a piezo-electric jet printer. Hydrophobicity/hydrophilicity of the untreated and treated polyester fabrics was measured by wicking test. K/S values and color difference of the polyester printed fabrics were investigated. The printed fabric with Gly pretreatment had the higher K/S values and color difference than those with CS pretreatment due to its interaction with color inks. Gly increased hydrophilicity of the treated polyester fabric, while CS markedly decreased the hydrophilicity. Interaction between the pretreatment agent and the active groups on pigment color development was elucidated.

Keywords: Chitosan, Glycine, Polyester fabric, Ink jet printing

ผลของการปรับผิวด้วยไคโทซานและไกลซีนบนผ้าพอลิเอสเทอร์พิมพ์ด้วยหมึกพิมพ์อิงก์เจ็ต

ได้ศึกษาและวิเคราะห์ผลของการปรับผิวด้วยสารละลายไคโทซาน (CS) และไกลซีน (Gly) บนผ้าพอลิเอสเทอร์และผลการพิมพ์ด้วยหมึกพิมพ์อิงก์เจ็ต นำผ้าพอลิเอสเทอร์ไปจุ่มรีดด้วยสารละลายไคโทซานความเข้มข้นร้อยละ 4 โดยน้ำหนักต่อปริมาตรตัวทำละลาย หรือ Gly ร้อยละ 5 ก่อนพิมพ์ด้วยชุดหมึกพิมพ์อิงก์เจ็ตสารสีฐานน้ำ 7 สี จากเครื่องพิมพ์แบบเปียร์โซ หาความไม่ชอบน้ำและความชอบน้ำบนผิวผ้าที่ไม่ปรับผิวและปรับผิวด้วยวิธีวัดการซึมน้ำ (wicking test) วัดค่า K/S และ ΔE (ความแตกต่าง) ของสีบนผ้าพิมพ์ ผ้าพิมพ์ที่ปรับผิวด้วย Gly ให้ค่า K/S และ ΔE ของสีพิมพ์มากกว่าผ้าพิมพ์ที่ปรับผิวด้วย CS ส่วน Gly เพิ่มความชอบน้ำของผ้าพอลิเอสเทอร์ ในขณะที่ CS ลดความชอบน้ำอย่างมีนัยสำคัญ เนื่องจากชนิดของสารปรับผิวมีปฏิสัมพันธ์กับสารสีของหมึกพิมพ์แตกต่างกัน งานวิจัยนี้จึงได้อธิบายความสัมพันธ์ระหว่างสารปรับผิวกับหมู่ฟังก์ชันที่ไวต่อการพัฒนาสีของสารสี

คำสำคัญ: ไคโทซาน, ไกลซีน, พอลิเอสเทอร์, การพิมพ์อิงก์เจ็ต

7.5 Effects of Ink Formulation Containing Surface-Modified Pigmented Jet Inks on Jettability

Six surface-modified pigmented inkjet inks comprising black, cyan, magenta, yellow, light cyan, and light magenta colors were prepared with a pigment-to-binder ratio of 1:2. Styrene-acrylic acid emulsion was used as a binder. Fluid system composed of diethylene glycol and glycerol was examined by varying their ratios to adjust the ink viscosity. Overall particle size of pigment and polymer emulsion was controlled within the range of 100 to 300 nm. Surface tensions were varied by surfactant concentration. The range of viscosity and surface tension affecting the jettability were investigated. Good jettability range was found in a viscosity-surface tension operation window in each series of ink formulation 5 which could produce the complete test patterns.

Key words: Ink formulation, Surface modified pigment, Viscosity, Surface tension, Ink jet ink, Jetting

ผลขององค์ประกอบของหมึกพิมพ์ในหมึกพิมพ์อิงก์เจ็ตที่มีสารสีดัดแปรผิวต่อการพ่นหมึก

ได้เตรียมหมึกพิมพ์อิงก์เจ็ตประเภทสารสีจากสารสีดัดแปรผิว 6 ชนิด ซึ่งมีสารสีสีดำ สีฟ้าเขียว สีเหลือง สีม่วงแดง สีฟ้าเขียวอ่อน และสีม่วงแดงอ่อน ในสัดส่วนของสารสีต่อสารยึด 1 ต่อ 2 โดยมีอิมัลชันของสไตรีนและอะคริลิกแอซิดเป็นสารยึด แปรสัดส่วนของไดเอทีลีนไกลคอลและกลีเซอรอลซึ่งเป็นระบบของไหลของหมึกพิมพ์ เพื่อปรับความหนืดของหมึกพิมพ์ให้ทำงานได้ ปรับขนาดอนุภาคของสารสีและขนาดของอนุภาคอิมัลชันพอลิเมอร์โดยเฉลี่ยให้อยู่ในช่วง 100 ถึง 300 นาโนเมตร ปรับแรงตึงผิวของหมึกพิมพ์ด้วยความเข้มข้นของสารลดแรงตึงผิวที่คัดเลือก ช่วงของความหนืดและแรงตึงผิวของหมึกพิมพ์แต่ละสีมีผลต่อความสามารถในการพ่นหมึกพิมพ์ ได้ศึกษาช่วงหน้าต่างที่ให้ขอบเขตของความหนืดและแรงตึงผิวที่พ่นหมึกพิมพ์ได้ของหมึกพิมพ์แต่ละสีในแต่ละสูตรหมึก พบว่า หมึกพิมพ์อิงก์เจ็ตสูตร 5 ซึ่งสามารถพิมพ์เส้นหมึกทุกสีได้รูปแบบของเส้นสมบูรณ์ที่สุด

คำสำคัญ: สูตรหมึกพิมพ์, สารสีดัดแปรผิว, ความหนืด, แรงตึงผิว, หมึกพิพม์อิงก์เจ็ต, การพ่นหยดหมึก

4. ผลงานที่ได้จากโครงการ

4.1 ผลงานตีพิมพ์ในวารสารวิชาการนานาชาติ/หนังสือ/สิทธิบัตร

ก. ในวารสารวิชาการระดับนานาชาติ

1. Nakason, C., Wohmang, T.; Kaesaman, A., Kiatkamjornwong, S. 2010. Preparation of Cassava Starch-Graft-Polyacrylamide Superabsorbents and Associated Composites by Reactive Blending, Carbohydrate Polymers, 81, 348–357.

2. Vallapa, N., Wiarachai, O., Thongchul, N., Pan, J., Tangpasuthadol, V., Kiatkamjornwong, S., Hoven, P. V. 2011. Enhancing antibacterial activity of chitosan surface by heterogeneous quaternization, Carbohydrate Polymers, 83, 868－875.

3. Noppakundilograt, S., Nanakorn, P., Jinsart, W., Kiatkamjornwong, S. 2010. Synthesis of Acrylamide/acrylic acid-Based Aluminum Flocculant for Dye Reduction and Textile Wastewater Treatment, Polymer Engineering and Science, 50(8), 1535－1546.

4. Kangwansupamonkon, W, Jitbunpot, W., Kiatkamjornwong, S. 2010. Photocatalytic efficiency of TiO_2/poly[acrylamide-*co*-(acrylicacid)] composite for textile dye degradation, Polymer Degradation and Stability, 95, 1894 － 1902.

5. Seetapan, N., Wongsawaeng, J., Kiatkamjornwong, S., 2011, Gel strength and swelling of acrylamide-protic acid superabsorbent copolymers, Polymer for Advanced Technologies, DOI: 10.1002/pat.1658, online.

6. Foungfung, D., Seetapan, N., Phattanarudee, S., Kiatkamjornwong, S. 2011. Synthesis of acrylamide /itaconic acid superabsorbent polymers and superabsorbent polymer/mica nanocomposites. Polymer for Advanced Technologies, 22, 635 － 647.

7. Limparyoon, N., Seetapan, N., Kiatkamjornwong, S. 2011. Acrylamide/2-acrylamido-2-methylpropane Sulfonic Acid and Associated Sodium Salt Superabsorbent Copolymers with Mica Nanocomposites as Fire Retardants, Polymer Degradation and Stability, 96, 1054 －1063

8. Seetapan, N., Nattawut Limparyoon, N., Kiatkamjornwong, S. 2011. Effect of fire retardant on flammability of acrylamide and 2-acrylamido-2-methylpropane sodium sulfonate copolymer nanocomposites, Polymer Degradation and Stability, doi:10.1016/j.polymdegradstab.2011.06.014

9. Seetapan, N., Srisithipantakul, N., and Kiatkamjornwong, S. 2011. Synthesis of acrylamide-*co*-(itaconic acid) superabsorbent polymers and associated silica superabsorbent polymer composites, Polymer Engineering and Science, 51(4), 764－775.

10. Noppakundilograt, S., Buranagul, P. Graisuwan, W., Chawan Koopipat, C., Kiatkamjornwong, S. 2010. Modified Chitosan Pretreatment of Polyester Fabric for Printing by Ink Jet Ink, Carbohydrate Polymers, 82, 1124－1135.

11. Chakvattanatham, K., Phattanarudee, S., Kiatkamjornwong, S. 2010. Anionically surface-modified pigment/binder in jet inks for silk fabric printing. Pigment & Resin Technology, 39(6), 327－341.

ข. วารสารในประเทศ

12. Suda Kiatkamjornwong, Boonyakiat Chaitepprasith, Chawan Koopipat, 2010. Measurement of BRDF and Modeling Reflectance of Silk Fabrics, Journal of the Royal Institute of Thailand, 35(1), 109－117.

ค. บทความที่อยู่ระหว่างการแก้ไขและการพิจารณาของวารสาร

13. Somporn Chaiarrekij, Apiporn Apirakchaiskul, Kuntinee Suvarnakich, and Suda Kiatkamjornwong, 2011. Kapok I: Properties investigation of kapok fiber as a potential pulp source for papermaking, Bioresources, under revision.

14. Noppakundilograt, S., Sonjaipanich, K., Thongchul, N., Kiatkamjornwong, S. 2011. Syntheses, Characterization and Antibacterial Activity of Chitosan Grafted Hydrogels and associated mica containing nanocomposite hydrogels, Journal of Applied Polymer Science, under revision.

15. Oraphan Wiarachai, Nuttha Thongchul, Suda Kiatkamjornwong, Voravee P. Hoven, Surface-quaternized chitosan particles as an alternative and effective organic antibacterial filler, Colloids and Surfaces B: Biointerfaces, under review.

16. Navagan Rachanark, Varawut Tangpasuthadol, Suda Kiatkamjornwong, Improvement of tensile modulus and tear strength of natural rubber dipped films by vinylated silica generated in situ, Polymer International, under review.

17. Stéphane Dubascoux, Chalao Thepchalerm, Eric Dubreucq, Suwaluk Wisunthorn, Laurent Vaysse, Suda Kiatkamjornwong, Charoen Nakason, Frédéric Bonfils. Comparative

study of the mesostructure of natural and synthetic polyisoprene by SEC-MALS and AF4-MALS, Journal of Chromatography A., under review.

18. Graisuwan, W.; Ananthanawat, C.; Wiarachai, O.; Puthong, S.; Su, X. D.; Thongchul, N.; Kiatkamjornwong, S.; Hoven, V. P. Multilayer Thin Films Assembled from Charged Derivatives of Chitosan: Formation and Biological Responses, Langmuir, in language check.

19. Somporn Chaiarrekij, Thippawan Hommaivai, Kuntinee Suvarnakich, and Suda Kiatkamjornwong, Kapok II: Pretreatment of kapok fibers for pulping and papermaking Bioresources, in revision before submitting to Bioresources.

20. Roongkarn Nuisin, Jaruwan Krongsil, Suda Kiatkamjornwong Microencapsulation of menthol via glass membrane emulsification and controlled release, to be submitted to Colloids and Surfaces A: Physicochemicals and Engineering Aspects, in language check.

21. Charoen Nakason, Yeampon Nakaramontee, Azizon Kaesaman, Wiyong Kangwansukpamonkon, and Suda Kiatkamjornwong' Synthesis and Characterization of Water Swellable Natural Rubber Composites, in final check of figures and tables.

ง. บทความที่จะร่างจากงานวิจัยที่เพิ่งปิดโครงการวิจัยเมื่อเดือนพฤษภาคม 2554

22. Supaporn Noppakundilograt, Thayarat Petcharat, Suda Kiatkamjornwong. Synthesis and characterization of controlled released NPK fertilizer hydrogel.

23. Wiyong Kangwansupamonkon, Wailawan Tiertrakulwattana, Pitt Suphapol, Suda Kiatkamjornwong. Surface modification of electrospun chitosan nanofiber for antibacterial activity.

24. Wasinee Sakathok, Suda Kiatkamjornwong, Varawut Tangpasuthadol. Physical properties of MMA grafted natural rubber film reinforced with *in situ* generated silica.

25. Sopinya Choopromkaw, Supaporn Noppakundilograt, Suda Kiatkamjornwong, 2010, Synthesis, characterization and controlled release of hydrogel from collagen grafted poly[(acrylic acid)-*co*-(methacrylic acid)]

จ. สิทธิบัตร

1. สุดา เกียรติกำจรวงศ์, วลาสินี จิตบรรพต, วิยงค์ กังวานศุภมงคล, กนิษฐา บุญภาวาณิชกุล คอมพอสิตพอลิเมอร์ดูดซึมน้ำมากที่สามารถแตกสลายตัวเองได้โดยอาศัยการกระตุ้นด้วยรังสีอัลตราไวโอ เลต เลขที่คำขอ 1001001273 วันที่ 26 กันยายน 2553

2. สุดา เกียรติกำจรวงศ์, ณัฐวุฒิ ลิมประยูร, นิสภา ศีตปันย์ 2553 เจลอิมัลชันวัสดุเชิงประกอบพอลิเมอร์ดูดซึมน้ำมากและเจลอิมัลชันพอลิเมอร์ดูดซึมน้ำมากที่มีสมบัติหน่วงการติดไฟ เลขที่คำขอ 1101000208 วันที่ 15 กุมภาพันธ์ 2554

3. สุดา เกียรติกำจรวงศ์ สุภาภรณ์ นพคุณดิลกรัตน์ ณัฏฐ์ธยาน์ เพชรรัตน์ ปุ๋ยละลายช้าและกรรมวิธีการผลิตปุ๋ยละลายช้าดังกล่าว ยื่นผ่านสถาบันทรัพย์สินทางปัญญาเมื่อ 1 มิถุนายน 2554 ขณะนี้รอทางสถาบันพิจารณาแก้ไขเนื้อหาในแง่กฎหมาย คาดว่าจะสามารถส่งไปยังกรมทรัพย์สินทางปัญญาในเดือนกันยายน 2554

4. สุดา เกียรติกำจรวงศ์ สุภาภรณ์ นพคุณดิลกรัตน์ สวเนตร์ วงศ์แป้น ลิตสา วงศ์ศิริทรัพย์ สารปรับสภาพผิวผ้าจากไคโทซานดัดแปรละลายน้ำได้สำหรับการพิมพ์ระบบอิงก์เจ็ต ยื่นผ่านสถาบันทรัพย์สินทางปัญญาเมื่อ 10 พฤษภาคม 2554 ขณะนี้รอทางสถาบันพิจารณาแก้ไขเนื้อหาในแง่กฎหมาย คาดว่าจะสามารถส่งไปยังกรมทรัพย์สินทางปัญญาในเดือนกันยายน 2554

5. สุดา เกียรติกำจรวงศ์ สุภาภรณ์ นพคุณดิลกรัตน์ ปัญฑ์ธร บูรณะกูล สารปรับสภาพผิวผ้าจากไคโท ซานดัดแปรสำหรับผ้าพิมพ์ด้วยหมึกพิมพ์อิงก์เจ็ต ยื่นผ่านสถาบันทรัพย์สินทางปัญญาเมื่อ 2 มิถุนายน 2554 ขณะนี้รอทางสถาบันพิจารณาแก้ไขเนื้อหาในแง่กฎหมาย คาดว่าจะสามารถส่งไปยังกรมทรัพย์สินทางปัญญาในเดือนกันยายน 2554

4.2 ความก้าวหน้าในการสร้างทีมวิจัย

4.2.1 การสำเร็จการศึกษาของนักศึกษาปริญญาเอกและปริญญาโท

1. นางสาวจิราพร วงแสวง นิสิตปริญญามหาบัณฑิต สาขาวิชาปิโตรเคมีและวิทยาศาสตร์พอลิเมอร์ คณะวิทยาศาสตร์ จุฬาลงกรณ์มหาวิทยาลัย สำเร็จการศึกษาเดือนพฤษภาคม พ.ศ. 2551

2. นางสาววิไลพร ไกรสุวรรณ ปริญญาโท หลักสูตรปิโตรเคมีและวิทยาศาสตร์พอลิเมอร์ คณะวิทยาศาสตร์ จุฬาลงกรณ์มหาวิทยาลัย สำเร็จการศึกษาในเดือน พฤษภาคม พ.ศ. 2551

3. นางสาวรันยา บุญเวช สาขาเทคโนโลยียางและวิทยาการพอลิเมอร์ มหาวิทยาลัยสงขลานครินทร์ วิทยาเขตปัตตานี สำเร็จการศึกษาเดือนพฤษภาคม พ.ศ. 2551

4. นางสาววลาสินี จิตรบรรพต นิสิตปริญญามหาบัณฑิต สาขาวิชาปิโตรเคมีและวิทยาศาสตร์พอลิเมอร์ คณะวิทยาศาสตร์ จุฬาลงกรณ์มหาวิทยาลัย สำเร็จการศึกษาเดือนพฤษภาคม พ.ศ. 2551

5. นายอภิพร อภิรักษ์ชัยสกุล ปริญญาโท หลักสูตรเทคโนโลยีเยื่อและกระดาษ คณะวิทยาศาสตร์จุฬาลงกรณ์มหาวิทยาลัย สำเร็จการศึกษาในเดือนพฤษภาคม พ.ศ. 2551

6. นายกิตติชัย สนใจพาณิชย์ ปริญญาโท หลักสูตรปิโตรเคมีและวิทยาศาสตร์พอลิเมอร์ คณะวิทยาศาสตร์ จุฬาลงกรณ์มหาวิทยาลัย สำเร็จการศึกษาในเดือนพฤษภาคม พ.ศ. 2552

7. นางสาวซารีนา ซะยานัย สาขาเทคโนโลยียางและวิทยาการพอลิเมอร์มหาวิทยาลัยสงขลานครินทร์ วิทยาเขตปัตตานี สำเร็จการศึกษาเดือนพฤษภาคม พ.ศ. 2552

8. นางสาวอรพรรณ เวียระชัย ปริญญาโท หลักสูตรปิโตรเคมีและวิทยาศาสตร์พอลิเมอร์ คณะวิทยาศาสตร์ จุฬาลงกรณ์มหาวิทยาลัย สำเร็จการศึกษาในเดือนพฤษภาคม พ.ศ. 2553

9. นายนายตออา เวอะเม็ง สาขาเทคโนโลยียางและวิทยาการพอลิเมอร์มหาวิทยาลัยสงขลานครินทร์ วิทยาเขตปัตตานี สำเร็จการศึกษาเดือนพฤษภาคม พ.ศ. 2553

10. นายเยี่ยมพล นัครามนตรี สาขาเทคโนโลยียางและวิทยาการพอลิเมอร์มหาวิทยาลัยสงขลานครินทร์ วิทยาเขตปัตตานี สำเร็จการศึกษาเดือนพฤษภาคม พ.ศ. 2553

11. นายณัฐวุฒ ลิ้มประยูร ปริญญาโท หลักสูตรปิโตรเคมีและวิทยาศาสตร์พอลิเมอร์ คณะวิทยาศาสตร์ จุฬาลงกรณ์มหาวิทยาลัย สำเร็จการศึกษาในเดือนพฤษภาคม พ.ศ. 2553

12. นางสาวจิตติมา มีบึงพร้าว ปริญญาโท หลักสูตรปิโตรเคมีและวิทยาศาสตร์พอลิเมอร์ คณะวิทยาศาสตร์ จุฬาลงกรณ์มหาวิทยาลัย สำเร็จการศึกษาในเดือนพฤษภาคม พ.ศ. 2553

13. นายนวกานต์ ราชนาค ปริญญาโท หลักสูตรปิโตรเคมีและวิทยาศาสตร์พอลิเมอร์ คณะวิทยาศาสตร์ จุฬาลงกรณ์มหาวิทยาลัย สำเร็จการศึกษาในเดือนพฤษภาคม พ.ศ. 2553

14. นายบุญยเกียรติ ฉายเทพประสิทธิ์ ปริญญาโท หลักสูตรเทคโนโลยีทางภาพ คณะวิทยาศาสตร์ จุฬาลงกรณ์มหาวิทยาลัย สำเร็จการศึกษาในเดือนพฤษภาคม พ.ศ. 2553

15. นางสาวทิพย์วรรณ หอมไม่วาย ปริญญาโท หลักสูตรเทคโนโลยีเยื่อและกระดาษ คณะวิทยาศาสตร์ จุฬาลงกรณ์มหาวิทยาลัย สำเร็จการศึกษาในเดือนพฤษภาคม พ.ศ. 2554

16. นางสาวณัฏฐ์ธยาน์ เพชรรัตน์ นิสิตปริญญาโท หลักสูตรปิโตรเคมีและวิทยาศาสตร์พอลิเมอร์ คณะวิทยาศาสตร์ จุฬาลงกรณ์มหาวิทยาลัย สำเร็จการศึกษาในเดือนพฤษภาคม พ.ศ. 2554

17. นางสาวจารุวรรณ ครองศิลป์ นิสิตปริญญาโท หลักสูตรปิโตรเคมีและวิทยาศาสตร์พอลิเมอร์ คณะวิทยาศาสตร์ จุฬาลงกรณ์มหาวิทยาลัย สำเร็จการศึกษาในเดือนพฤษภาคม พ.ศ. 2554

18. นางสาวโสภิญญา ชูพรมแก้ว นิสิตปริญญาโท หลักสูตรปิโตรเคมีและวิทยาศาสตร์พอลิเมอร์ คณะวิทยาศาสตร์ จุฬาลงกรณ์มหาวิทยาลัย สำเร็จการศึกษาในเดือนพฤษภาคม พ.ศ. 2554

19. นางสาวสันนิภา พัฒนปิยะทรัพย์ นิสิตปริญญาตรี หลักสูตรเทคโนโลยีทางภาพและการพิมพ์ คณะวิทยาศาสตร์ จุฬาลงกรณ์มหาวิทยาลัย สำเร็จการศึกษาในเดือนพฤษภาคม พ.ศ. 2554

20. นางสาวสุทธาทิพย์ เลขาลาวัณย์นิสิตปริญญาตรี หลักสูตรเทคโนโลยีทางภาพและการพิมพ์ คณะวิทยาศาสตร์ จุฬาลงกรณ์มหาวิทยาลัย สำเร็จการศึกษาในเดือนพฤษภาคม พ.ศ. 2554

21. นางสาวสุภาณี พิพัฒน์วิทยา นิสิตปริญญาตรี หลักสูตรเทคโนโลยีทางภาพและการพิมพ์ คณะวิทยาศาสตร์ จุฬาลงกรณ์มหาวิทยาลัย สำเร็จการศึกษาในเดือนพฤษภาคม พ.ศ. 2554

4.2.2 จำนวนหัวหน้าโครงการและนักวิจัยประจำโครงการ ณ วันที่ 1 สิงหาคม 2554

รายนามกลุ่มวิจัย ปี 2550-2554

1. อาจารย์นักวิจัย

ชื่อ-นามสกุล	เริ่มร่วมเข้าโครงการ			สถานภาพปัจจุบัน	
	ตำแหน่งวิชาการ	สังกัด	ตำแหน่งในโครงการ	ตำแหน่งวิชาการ	ตำแหน่งอื่น
1. ดร. สุดา เกียรติกำจรวงศ์	ศาสตราจารย์ 11	ภาควิชา วท. ภาพถ่ายและเทคโนโลยีทางการพิมพ์ คณะวิทยาศาสตร์ จุฬาลงกรณ์มหาวิทยาลัย	หัวหน้าโครงการ	ศาสตราจารย์ 11 หรือ ศาสตราจารย์ A 1	
2. ดร. พิชช์ ศุภผล	รองศาสตราจารย์ 9	วิทยาลัยปิโครเลียมและปิโตรเคมี จุฬาลงกรร์มหาวิทยาลัย	นักวิจัยและอาจารย์ที่ปรึกษาร่วม	ศาสตราจารย์ A2 (ศาสตราจารย์ ระดับ 10)	
3. ดร. เจริญ นาคะสรรค์	รองศาสตราจารย์ 9	ภาควิชาเทคโนโลยียางและพอลิเมอร์ คณะวิทยาศาสตร์ และเทคโนโลยี มหาวิทยาลัยสงขลานครินทร์ วิทยาเขตปัตตานี	หัวหน้าโครงการย่อย	รองศาสตราจารย์ 9	คณบดี คณะวิทยาศาสตร์และเทคโนโลยี มหาวิทยาลัยสงขลานครินทร์ วิทยาเขตปัตตานี
4. ดร. วรวีร์ โฮ่เวน	ผู้ช่วยศาสตราจารย์ 8	ภาควิชาเคมี คณะวิทยาศาสตร์ จุฬาลงกรณ์มหาวิทยาลัย	หัวหน้าโครงการย่อย	รองศาสตราจารย์ 9	
5. ดร. ธีรยุทธ วิไลวัลย์	รองศาสตราจารย์ 9	ภาควิชาเคมี คณะวิทยาศาสตร์ จุฬาลงกรณ์มหาวิทยาลัย	นักวิจัยและอาจารย์ที่ปรึกษา	รองศาสตราจารย์ 9	อยู่ในขั้นตอนการพิจารณาตำแหน่ง ศาสตราจารย์ ระดับ 10

			ร่วม		
6. ดร. วราวุฒิ ตั้งพสุธาดล	ผู้ช่วยศาสตราจารย์ 7	ภาควิชาเคมี คณะวิทยาศาสตร์ จุฬาลงกรณ์มหาวิทยาลัย	หัวหน้าโครงการย่อย	ผู้ช่วยศาสตราจารย์ 8	
7. อาซีซัน แกสมาน	รองศาสตราจารย์ 8	ภาควิชาเทคโนโลยียางและพอลิเมอร์ คณะวิทยาศาสตร์ และเทคโนโลยี มหาวิทยาลัยสงขลานครินทร์ วิทยาเขตปัตตานี	นักวิจัย	รองศาสตราจารย์ 9	รองคณบดี คณะวิทยาศาสตร์และเทคโนโลยี มหาวิทยาลัยสงขลานครินทร์
8. ดร. สุภาภรณ์ นพคุณดิลกรัตน์	ผู้ช่วยศาสตราจารย์ 7	ภาควิชา วท. ภาพถ่ายและเทคโนโลยีทางการพิมพ์ คณะวิทยาศาสตร์ จุฬาลงกรณ์มหาวิทยาลัย	หัวหน้าโครงการย่อย	ผู้ช่วยศาสตราจารย์ 8	รองหัวหน้าภาควิชา ภาควิชา วท. ภาพถ่ายและเทคโนโลยีทางการพิมพ์ คณะวิทยาศาสตร์ จุฬาลงกรณ์มหาวิทยาลัย
9. ดร. ชวาล คูร์พิพัฒน์	ผู้ช่วยศาสตราจารย์ ระดับ 7	ภาควิชา วท. ภาพถ่ายและเทคโนโลยีทางการพิมพ์ คณะวิทยาศาสตร์ จุฬาลงกรณ์มหาวิทยาลัย	หัวหน้าโครงการย่อย	นักวิจัย	
10. ดร. นิสภา คีตปันย์	นักวิจัย P 3	ศูนย์เทคโนโลยีโลหะและวัสดุแห่งชาติ สำนักพัฒนาวิทยาศาสตร์และเทคโนโลยีแห่งชาติ กระทรวงวิทยาศาสตร์และเทคโนโลยี	หัวหน้าโครงการย่อย	นักวิจัย P 3	
11. ดร. รุ่งกานต์	อาจารย์พนักงาน	ภาควิชาวิทยาศาสตร์ทั่วไป	หัวหน้าโครงการ	ผู้ช่วยศาสตราจารย์	

นุ้ยสินธุ์	มหาวิทยาลัย A 5	คณะวิทยาศาสตร์ จุฬาลงกรณ์มหาวิทยาลัย	ย่อย	พนักงานมหาวิทยาลัย A 4	
12. ดร. วิยงค์ กังวานศุภมงคล	นักวิจัย P 3	ศูนย์นาโนเทคโนโลยีแห่งชาติ สำนักพัฒนาวิทยาศาสตร์และเทคโนโลยีแห่งชาติ กระทรวงวิทยาศาสตร์ และเทคโนโลยี	หัวหน้าโครงการย่อย	นักวิจัย P 3	หัวหน้าโครงการศูนย์วิจัย ศูนย์นาโนเทคโนโลยีแห่งชาติ
13. สมพร ชัยอารีย์กิจ	อาจารย์พนักงานมหาวิทยาลัย A 5	ภาควิชา วท. ภาพถ่ายและเทคโนโลยีทางการพิมพ์ คณะวิทยาศาสตร์ จุฬาลงกรณ์มหาวิทยาลัย	หัวหน้าโครงการย่อย	อาจารย์พนักงานมหาวิทยาลัย A 5	
14 ดร. กุนทินี สุวรรณกิจ	อาจารย์พนักงานมหาวิทยาลัย A 5	ภาควิชา วท. ภาพถ่ายและเทคโนโลยีทางการพิมพ์ คณะวิทยาศาสตร์ จุฬาลงกรณ์มหาวิทยาลัย	นักวิจัย	อาจารย์พนักงานมหาวิทยาลัย A 5	

2. รายนามนิสิตผู้ช่วยวิจัยที่กำลังศึกษา

ชื่อ-นามสกุล	เริ่มร่วมเข้าโครงการ		
	สาขา/ระดับการศึกษา	สังกัด	ประมาณการการสำเร็จการศึกษา
นางสาววลัยวัลย์ เตียวตระกูลวัฒน	ปิโตรเคมี ฯ /โท	คณะวิทยาศาสตร์ จุฬาลงกรณ์มหาวิทยาลัย	ภาคต้น ปีการศึกษา 2554
นางสาววาสินี สากะโทก	ปิโตรเคมี ฯ /โท	คณะวิทยาศาสตร์ จุฬาลงกรณ์มหาวิทยาลัย	ภาคต้น ปีการศึกษา 2555
นางสาวเพียงหทัย พิบูลย์	ปิโตรเคมี ฯ /โท	คณะวิทยาศาสตร์ จุฬาลงกรณ์มหาวิทยาลัย	ภาคต้น ปีการศึกษา 2555
นางสาวนิสารัตน์ อณสุววรณ์	ปิโตรเคมี ฯ /โท	คณะวิทยาศาสตร์ จุฬาลงกรณ์มหาวิทยาลัย	ภาคต้น ปีการศึกษา 2555
นายนที คล้ายแก้ว	ปิโตรเคมี ฯ /โท	คณะวิทยาศาสตร์ จุฬาลงกรณ์มหาวิทยาลัย	ภาคต้น ปีการศึกษา 2555
นางสาวปิยะพร อรรคฮาต	ปิโตรเคมี/เอก	คณะวิทยาศาสตร์ จุฬาลงกรณ์มหาวิทยาลัย	ภาคปลาย ปีการศึกษา 2554
นางสาววิไลพร ไกรสุวรรณ	ปิโตรเคมี/เอก	คณะวิทยาศาสตร์ จุฬาลงกรณ์มหาวิทยาลัย	ภาคต้น ปีการศึกษา 2555
นางสาวเฉลา เทพเฉลิม	เทคโนโลยีพอลิเมอร์/เอก	คณะบัณฑิตวิทยาลัย มหาวิทยาลัยสงขลานครินทร์ (วิทยาเขตปัตตานี)	ภาคต้น ปีการศึกษา 2556

4.3 การนำผลจากโครงการไปใช้ประโยชน์

ได้ประชาสัมพันธ์ผลงานบางประเภทสู่นักข่าวและหนังสือพิมพ์ ดังตัวอย่างข่าวที่ได้ประชาสัมพันธ์ไปยังสื่อต่าง ๆ ดังตัวอย่างการประชาสัมพันธ์ 1 เรื่อง

ข่าวประชาสัมพันธ์

นักวิจัยจุฬาฯ ผลิตกรีนพอลิเมอร์ย่อยสลายเร็วด้วยรังสีอัลตราไวโอเลต

ปัจจุบันพอลิเมอร์ดูดซึมน้ำมาก หรือไฮโดรเจล เป็นที่สนใจและถูกนำไปใช้ประโยชน์ในอุตสาหกรรมหลายด้าน เนื่องจากมีความสามารถในการดูดซึมน้ำได้สูง มีสมบัติในการบวมน้ำและสามารถเก็บกักน้ำไว้ในโครงสร้างได้มากกว่า 20 เท่าของน้ำหนักพอลิเมอร์แห้งและไม่ละลายน้ำ

ในด้านเกษตรกรรม มีการนำพอลิเมอร์ดูดซึมน้ำมากไปใช้ในการทำสวนประดับ ซึ่งจะช่วยในการปรับปรุงคุณภาพดิน โดยเพิ่มความสามารถในการกักเก็บน้ำ และปล่อยน้ำสู่ดินและรากพืช เป็นการรักษาความสมดุลของความชื้นในดิน และช่วยกักเก็บสารอาหารของพืชที่ละลายในเจลพอลิเมอร์

ขณะที่ด้านอุตสาหกรรม มีการนำพอลิเมอร์ดูดซึมน้ำมากมาใช้ทำผลิตภัณฑ์เพื่อสุขอนามัย ผ้าอ้อมเด็ก ผ้าอ้อมผู้สูงวัย และผ้าอ้อมผู้ป่วย กระดาษชำระ เป็นต้น ด้านการแพทย์ได้นำไปทำผ้าพันแผล ใช้เป็นสารควบคุมอัตราการปล่อยยาสำหรับผู้ป่วย ด้านอาหารนำมาใช้เป็นสารป้องกันการรั่วซึมของของเหลวในภาชนะบรรจุอาหาร นอกจากนี้ยังนำมาใช้ในงานด้านอื่น ๆเช่น สารดับเพลิง หิมะเทียม หมึกพิมพ์ เป็นต้น

อย่างไรก็ตามพอลิเมอร์ดังกล่าวส่วนใหญ่เป็นผลิตภัณฑ์จากปิโตรเคมี ซึ่งต้องใช้ระยะเวลายาวนานหลายร้อยปีในการแตกสลาย หรือไม่สามารถแตกสลายได้เองตามธรรมชาติ ประกอบกับปัจจุบันมีแนวโน้มการใช้พอลิเมอร์ดูดซึมน้ำมากเพิ่มขึ้นอย่างชัดเจน จึงก่อให้ขยะและปัญหาด้าน

สิ่งแวดล้อมตามมา ขณะนี้หลายประเทศเริ่มตื่นตัวและพยายามหาทางแก้ไขพัฒนาวัสดุต่าง ๆ ที่จะสามารถแตกสลายได้เองตามธรรมชาติ

ศ.ดร.สุดา เกียรติกำจรวงศ์ เมธีวิจัยอาวุโส สกว. ภาควิชาวิทยาศาสตร์ทางการพิมพ์และเทคโนโลยีทางการพิมพ์ คณะวิทยาศาสตร์ จุฬาลงกรณ์มหาวิทยาลัย ได้รับการสนับสนุนทุนวิจัยจากฝ่ายวิชาการ สำนักงานกองทุนสนับสนุนการวิจัย (สกว.) เพื่อทำวิจัยและพัฒนาวัสดุพอลิเมอร์สีเขียวและประโยชน์ใช้งาน

ศ.ดร.สุดา เปิดเผยว่า คณะวิจัยได้ผลิตพอลิเมอร์คอมพอสิตดูดซึมน้ำมากที่มีลักษณะเป็นก้อนวุ้นหรือเจลใส หรือเป็นของเหลวที่มีความหนืดสูงและตกตะกอนก้อนเจลที่ได้เป็นก้อนแข็งและบดให้มีขนาดเล็กต่อไป พอลิเมอร์ที่ผลิตได้นี้สามารถดูดซับสีย้อมสิ่งทอและสามารถแตกสลายทั้งสีย้อมและตนเองได้ โดยอาศัยการกระตุ้นด้วยรังสีอัลตราไวโอเลตจากแหล่งกำเนิดรังสีหรือจากดวงอาทิตย์ที่มากพอ ทำให้เกิดการเปลี่ยนแปลงสมบัติและโครงสร้างทางเคมีจนแตกสลายภายในเวลาอันรวดเร็วเพียงพอที่จะไม่ทำให้เกิดการสะสมของเสียต่อภาวะแวดล้อม นอกจากนี้พอลิเมอร์คอมพอสิตดูดซึมน้ำมากยังสามารถดูดซับและแตกสลายสีย้อมสิ่งทอที่ก่อให้เกิดน้ำเสียหลังกระบวนการย้อมเสร็จสิ้นได้อีกด้วย

จากการทดสอบการแตกสลายสีย้อมของสิ่งทอ พบว่าสีย้อมที่ถูกดูดซับด้วยพอลิเมอร์คอมพอสิตดูดซึมน้ำมาก จะแตกสลายได้หมดภายใต้รังสีอัลตราไวโอเลตเป็นเวลา 20-40 นาที และเมื่อฉายในระยะเวลา 24 ชั่วโมง พอลิเมอร์คอมพอสิตดูดซึมน้ำมากจะแตกสลายกลายเป็นของเหลวใสจนเหลือเพียงอนุภาคไททาเนียมไดออกไซด์ปริมาณน้อยมาก

“พอลิเมอร์ดังกล่าวจัดได้เป็นวัสดุสีเขียวที่สามารถช่วยลดปัญหาสิ่งแวดล้อม และเป็นวัสดุที่สามารถนำมาใช้กับอุตสาหกรรมได้หลากหลายประเภท เนื่องจากมีความสามารถในการแตกสลายตัวเองได้ภายใต้รังสีอัลตราไวโอเลตในระยะเวลาอันสั้น จึงมีประโยชน์ทั้งในด้านธุรกิจ สังคม และสิ่งแวดล้อม อีกทั้งสามารถตอบสนองความต้องการของผู้บริโภคอีกด้วย ซึ่งงานวิจัยนี้ได้ยื่นจดสิทธิบัตรเป็นที่เรียบร้อยแล้ว” ศ.ดร.สุดากล่าวสรุป

****

นิธิปรียา จันทวงษ์
เจ้าหน้าที่บริหารโครงการ
ฝ่ายวิชาการ สกว.
0-2278-8249

5 กิจกรรมอื่น ๆ ที่ เกี่ยวข้อง

5.1 ผลงานอื่น ๆ เช่น การไปเสนอผลงาน การได้รับเชิญไปเป็นวิทยากร การได้รับรางวัล

ก. การนำเสนอผลงานของผู้ช่วยวิจัยระดับปริญญาโทในการประชุมต่าง ๆ ดังนี้

1. อภิพร อภิรักษ์ชัยสกุล, กุนทินี สุวรรณกิจ, สมพร ชัยอารีย์กิจ และ สุดา เกียรติกำจรวงศ์, “การใช้เส้นใยนุ่นในการปรับปรุงสมบัติกระดาษ”, การประชุมวิชาการ “นเรศวรวิจัย” ครั้งที่ 4: การบริหารนวัตกรรม, คณะวิทยาศาสตร์ มหาวิทยาลัยนเรศวร, พิษณุโลก, 28-29 กรกฎาคม 2551.

2. Graisuwan, W.; Kiatkamjornwong, S. Hoven, V. P. Formation and Biocompatibility of Multilayer Film Assembled From Charged Derivatives of Chitosan 33rd Congress on Science and Technology of Thailand at Walailak University, October 18-20, 2007, บทความผู้จัดทำหายไปจากเอกสารการประชุม จึงไม่มีข้อมูลของเอกสาร

3. Graisuwan, W.; Kiatkamjornwong, S. Hoven, V. P. Formation and Biocompatibility of Multilayer Film Assembled From Charged Derivatives of Chitosan, Proceedings of the 3rd Mathematics & Physical Science International Graduate Congress, December 12-14, 2007, A038 with a poster, pp. 322-326.

4. Walasinee Jitbunpot, Wiyong Kangwansupamonkon, Suda Kiatkamjornwong, “Removal Efficiency of Methylene Blue Dye Using TiO_2/Poly[acrylamide-*co*-(acrylic acid)] Composites”, Proceedings of the 34th Congress on Science and Technology of Thailand 2008, The Queen Sirikit National Convention Center, Bangkok, Thailand, Oct 31- Nov 2, 2008, STT 34_F_F0003.

5. Walasinee Jitbunpot, Suda Kiatkamjornwong, Wiyong Kangwansupamonkon, “Preparation and Dye Removal Efficiency Study Using Nano TiO_2/Poly[acrylamide-*co*-(acrylic acid)] Composite”, Proceedings of the 1st Biannual NanoThailand Symposium, 2008, The Queen Sirikit National Convention Center, Bangkok, Thailand, Nov 6-8, 2008, T64, pp. 290-294.

6. Hoven, V. P.; Vallapa, N.; Thongchul, N.; Tangpasuthadol, V.; Kiatkamjornwong, S. “Antibacterial Activity of Surface-quaternized Chitosan” *The 42nd IUPAC World Polymer Congress (MACRO 2008), Polymer at Frontiers of Science and Technology*, June 29 – July 4, 2008, Taipei, Taiwan, Poster.

7. Punthorn Buranagul, Supaporn Noppakundilograt, Suda Kiatkamjornwong. Pretreatment of Polyester Fabric Surface with Chitosan Solution for Ink Jet Printing, Proceedings of 34th Congress on Science and Technology of Thailand at Queen Sirikit National Convention Center, October 31-November 2, 2008, STT34_E_E0118.

8. Kittichai Sonjaipanich, Supaporn Noppakundilograt, Nuttha Thongchul, Suda Kiatkamjornwong, Synthesis of Grafted Chitosan Poly[(acrylic acid)-*co*-(2-hydroxyethyl methacrylate)] Hydrogels for Antibacterial Activity, Proceedings of 34th Congress on Science and Technology of Thailand at Queen Sirikit National Convention Center, October 31 - November 2, 2008, STT34_E_E0051.

9. Wiarachai, O.; Thongchul, N.; Kiatkamjornwong, S.; Hoven, V. P. "Development of Antibacterial Fillers from Quaternized Chitosan Particles" *The* 5th *National Chitin-Chitosan Conference* July 24-25, **2008**, Bangkok, Thailand, Oral

10. Graisuwan, W.; Puthong, S.; Kiatkamjornwong, S.; Hoven, V. P. "Formation and Biocompatibility of Multilayer Films Assembled from Charged Derivatives of Chitosan" *The* 5th *National Chitin-Chitosan Conference* July 24-25, **2008**, Bangkok, Thailand, Oral

11. Meebungpraw, J.; Vilaivan, T.; Kiatkamjornwong, S.; Hoven, V. P. "Determination of DNA Sequences Using Quaternized Chitosan Particles in Combination with MALDI-TOF Mass Spectrometry" *The 2nd Polymer Graduate Conference in Thailand*, May 21-22, **2009**, Chulalongkorn University, Bangkok, Thailand, Poster

12. Wiarachai, O.; Thongchul, N.; Kiatkamjornwong, S.; Hoven, V. P. "Quaternary Ammonium-containing Chitosan Particles: Preparation and Antibacterial Activity" *Pure and Applied Chemistry International Conference 2009*, January 14-16, **2009**, Naresuan University, Phitsanulok, Thailand, Poster

13. Meebungpraw, J.; Vilaivan, T.; Kiatkamjornwong, S.; Hoven, V. P. "Detection of DNA-PNA Hybridization using Quaternized Chitosan Particles in Combination with MALDI-TOF Mass Spectrometry" *Pure and Applied Chemistry International Conference 2009*, January 14-16, **2009**, Naresuan University, Phitsanulok, Thailand, Poster.

14. Meebungpraw, J.; Vilaivan, T.; Kiatkamjornwong, S.; Hoven, V. P. "Determination of DNA Sequences using Peptide Nucleic Acid in Combination with Chitosan Particles by MALDI-TOF Mass Spectrometry" *The 11th Pacific Polymer Conference*, December 6-10, **2009**, Cairns, Australia, Poster.

15. Limprayoon, N., Seetapan, N., and Kiatkamjornwong, S., "Water absorbency of superabsorbent copolymer of acrylamide/2-acrylamido-2-methylpropane sulfonic acid and its sodium salt" *presented in The 2nd Polymer Graduate Conference of Thailand, 21-22 May 2009*, Bangkok, Thailand, pp. 57-61.

16. Jaruwan Krongsin, Supaporn Noppakundilograt, Roongkan Nuisin, Suda Kiatkamjornwong, 2010. Microencapsulation of menthol by crosslinked chitosan via porous glass membrane emulsification technique, Proceedings of the First Polymer Conference of Thailand, October 7-8, 2010 at the Convention Center, Chulabhorn Research Institute, Bangkok, pp. 264-269.

17. Natthaya Pheatcharat, Supaporn Noppakundilograt, Suda Kiatkamjornwong, 2010, Synthesis and characterization of prolonged-dissolution NPK fertilizer hydrogel, Proceedings of the First Polymer Conference of Thailand, October 7-8, 2010 at the Convention Center, Chulabhorn Research Institute, Bangkok, pp. 124-129.

18. Sopinya Choopromkaw, Supaporn Noppakundilograt, Suda Kiatkamjornwong, 2010, Synthesis and characterization of hydrogel from collagen grafted poly[(acrylic acid)-*co*-(methacrylic acid)], Proceedings of the First Polymer Conference of Thailand, October 7-8, 2010 at the Convention Center, Chulabhorn Research Institute, Bangkok, pp. 165-170.

19. Wilaiwan.Tiawtrakoonwat Pitt Supapho, Wiyong Kangwansupamonkon, Suda Kiatkamjornwong, Surface modification of electrospun chitosan nanofiber, Pure and Applied Chemistry International Conference (PACCON2011), Jan 5-7 2011 at the Miracle Grand Hotel, Bangkok, pp. 465-468.

20. Chawan Koopipat, Boonyakiat Chaitepprasith and Suda Kiatkamjornwong, Modeling BRDF of Silk Fabric by modifying Phong Reflection Model, oral presentation in The 31st International Congress on Imaging Science (ICIS2010) Beijing May 12 - 16, 2010, in Proceedings, pp. 98-101.

21. Hommaivai, T., Suvarnakich, K., Chaiarrekij, S., and Kiatkamjornwong, S., “Alkali Pretreatment of Kapok Fibers for Pulping and Papermaking”, the 1st Polymer Conference of Thailand, the Convention Center of Chulabhorn Research Institute, Bangkok, Thailand, October 7-8, 2010 pages 118-123. (หมายเหตุ: ได้รับรางวัล the best oral presentation award in Polymers for Food and Agriculture).

22. สันนิภา พัฒนปิยะทรัพย์, สุทธาทิพย์ เลขาลาวัณย์, สุภาณี พิพัฒน์วิทยา, สมพร ชัยอารีย์กิจ และ สุดา เกียรติกำจรวงศ์, “การใช้เยื่อนุ่นในการปรับปรุงสมบัติของกระดาษรีไซเคิล”, การประชุมวิชาการครั้งที่ 19 ประจำปี 2554 (The Science Forum 2011), คณะวิทยาศาสตร์ จุฬาลงกรณ์มหาวิทยาลัย, กรุงเทพมหานคร, 10-11 มีนาคม 2554 (หมายเหตุ: ได้รับรางวัลชนะเลิศอันดับที่ 1 The Hitachi Trophy 2011 สาขาวิทยาศาสตร์ประยุกต์และเทคโนโลยี) บทคัดย่อ

23. Sae-ung, P.; Meebungpraw, J.; Tumcharern, G.; Vilaivan, V.; Kiatkamjornwong, S.; Hoven, V. P. "Featuring Biosensing Applications of Chitosan" *Pure and Applied Chemistry International Conference 2011*, January 5 - 7, 2011, Miracle Grand Hotel, Bangkok, Thailand, Invited presentation.

24. Chalao Thepchalerm, Stephane Dubascoux1, Eric Dubreucq, Suwaluk Wisunthorn, Laurent Vaysse, Suda Kiatkamjornwong, Charoen Nakason, Frederic Bonfils. Characterization of Natural Rubber Mesostructure by Size-Exclusion Chromatography (SEC) and Asymmetric Flow Field-Flow Fractionation (AF4) Coupled with an Online Multi-Angle Light Scattering Detector (MALS), Together for Hevea and Natural Rubber Research, The Third Annual Seminar of HRPP: Prince of Songkla University, Surat Thani Campus, May 10th, 2011. Abstract.

ข. อาจารย์นักวิจัยและนิสิตในโครงการวิจัยที่ได้รับรางวัล

อาจารย์

1. **รองศาสตราจารย์ ดร. เจริญ นาคะสรร ได้รับรางวัลดังต่อไปนี้**

1.1 รางวัลนักวิจัยดีเด่นแห่งชาติ สภาวิจัยแห่งชาติ ประจำปี พ.ศ. 2553 สาขาวิทยาศาสตร์กายภาพและคณิตศาสตร์ **และ**

1.2 รางวัลวิทยาศาสตร์และเทคโนโลยีดีเด่นสาขาพอลิเมอร์ มูลนิธิโทเร ประเทศไทย ประจำปี พ.ศ. 2553

2. **รองศาสตราจารย์ ดร. ธีรยุทธ วิไลวัลย์** รางวัลนักวิจัยดีเด่นแห่งชาติ สภาวิจัยแห่งชาติ ประจำปี พ.ศ. 2553 สาขาวิทยาศาสตร์เคมีและเภสัช

นิสิต

1. **นางสาวอรพรรณ เวียรชัย** ได้รับรางวัลชนะเลิศ การแข่งขันเสนอผลงานประเภทโปสเตอร์ ในสาขา Nanomaterials จากงานวิจัยในหัวข้อเรื่อง "Development of Antibacterial Fillers from Quaternized Chitosan Particles"จากการประชุม The 16th Science Forum ซึ่งจัดขึ้นที่คณะวิทยาศาสตร์ จุฬาลงกรณ์มหาวิทยาลัย ในระหว่างวันที่ 13-14 มีนาคม 2551

2. **นางสาวจิตติมา มีบึงพร้าว** ได้รับรางวัล The Outstanding Poster Presentation Award สาขา Material Science and Nanotechnology จากงานวิจัยในหัวข้อเรื่อง "Determination of DNA Sequences using Peptide Nucleic Acid in Combination with Chitosan Particles by MALDI-TOF Mass Spectrometry" จากการประชุม Pure and Applied Chemistry International Conference (PACCON 2009) ซึ่งจัดขึ้นที่มหาวิทยาลัยนเรศวร ในระหว่างวันที่ 14-16 มกราคม 2552

3. **นางสาวทิพวรรณ หอมไม่วาย** ได้รับรางวัล the best oral presentation award in Polymers for Food and Agriculture โดยการนำเสนอผลงาน Alkali Pretreatment of Kapok Fibers

for Pulping and Papermaking" Hommaivai, T., Suvarnakich, K., Chaiarrekij, S., and Kiatkamjornwong, S., in the 1st Polymer Conference of Thailand, the Convention Center of Chulabhorn Research Institute, Bangkok, Thailand, October 7-8, 2010 pages 118-123.

4. **นางสาวสันนิภา พัฒนปิยะทรัพย์, นางสาวสุทธาทิพย์ เลขาลาวัณย์, นางสาวสุภาณี พิพัฒน์วิทยา** นำเสนองานวิจัยเรื่อง การใช้เยื่อนุ่นในการปรับปรุงสมบัติของกระดาษรีไซเคิล ได้รับรางวัลบรรยายชนะเลิศอันดับที่ 1 The Hitachi Trophy 2011 สาขาวิทยาศาสตร์ประยุกต์และเทคโนโลยี) การประชุมวิชาการครั้งที่ 19 ประจำปี 2554 (The Science Forum 2011), คณะวิทยาศาสตร์ จุฬาลงกรณ์มหาวิทยาลัย, กรุงเทพมหานคร, 10-11 มีนาคม 2554

ค. ข้อมูลนิสิตที่ได้รับทุนเครือข่าย

1. ชื่อนิสิต: นางสาวปิยะพร อรรคฮาต

หลักสูตร: ปิโตรเคมี

หัวข้อวิทยานิพนธ์: Synthesis and sensor application of carboxyl-containing polymer brushes

อาจารย์ที่ปรึกษาหลัก: รองศาสตราจารย์ ดร. วรวีร์ โฮเว่น ภาควิชาเคมี คณะวิทยาศาสตร์ จุฬาลงกรณ์มหาวิทยาลัย

อาจารย์ที่ปรึกษาร่วม: ศาสตราจารย์ ดร. สุดา เกียรติกำจรวงศ์ ภาควิชาวิทยาศาสตร์ทางภาพถ่ายและเทคโนโลยีทางการพิมพ์ คณะวิทยาศาสตร์ จุฬาลงกรณ์มหาวิทยาลัย

อาจารย์ที่ปรึกษาร่วม: Professor Dr. Yasuhiko Iwasaki, Department of Chemistry and Materials Engineering, Faculty of Chemistry, Materials and Bioengineeringม Kansai University, Japan

ปีที่เข้าศึกษา: 2549

สถานภาพปัจจุบัน: สอบป้องกันวิทยานิพนธ์แล้วในเดือนเมษายน 2554 ขณะนี้อยู่ระหว่างการแก้ไขบทความเพื่อส่งตีพิมพ์ในวารสารวิชาการระดับนานาชาติ นิสิตจะจบการศึกษาเมื่อบทความได้รับการตีพิมพ์ในวารสารวิชาการระดับนานาชาติแล้ว

หน่วยงานที่จะเข้าทำงานหลังจากจบการศึกษา: ภาควิชาเคมี คณะวิทยาศาสตร์ มหา-วิทยาลัยบูรพา

2. ชื่อนิสิต: นางสาววิไลพร ไกรสุวรรณ

หลักสูตร: ปิโตรเคมี

หัวข้อวิทยานิพนธ์: Synthesis and characterization of active functional copolymers of *N*-isopropylacrylamide

อาจารย์ที่ปรึกษาหลัก: รองศาสตราจารย์ ดร. วรวีร์ โฮเว่น ภาควิชาเคมี คณะวิทยาศาสตร์ จุฬาลงกรณ์มหาวิทยาลัย

อาจารย์ที่ปรึกษาร่วม: ศาสตราจารย์ ดร. สุดา เกียรติกำจรวงศ์ ภาควิชาวิทยาศาสตร์ทางภาพถ่ายและเทคโนโลยีทางการพิมพ์ คณะวิทยาศาสตร์ จุฬาลงกรณ์มหาวิทยาลัย

ปีที่เข้าศึกษา: 2551

สถานภาพปัจจุบัน: สอบโครงร่างวิทยานิพนธ์แล้วในเดือนธันวาคม 2553 ขณะนี้อยู่ระหว่างการทำวิจัย

หน่วยงานที่จะเข้าทำงานหลังจากจบการศึกษา: ยังไม่มี

3. ชื่อนักศึกษา: นางสาวเฉลา เทพเฉลิม

หลักสูตร ปรัชญาดุษฎีบัณฑิต (เทคโนโลยีพอลิเมอร์) คณะ บัณฑิตวิทยาลัย มหาวิทยาลัยสงขลานครินทร์ (วิทยาเขตปัตตานี)

หัวข้อวิทยานิพนธ์ทั้งไทยและอังกฤษ

ภาษาไทย ปรากฏการณ์แข็งขึ้นของยางธรรมชาติ: กลไกเชิงโมเลกุลและความเกี่ยวข้องของส่วนที่ไม่ใช่ยางที่มีผลกระทบต่อโครงสร้างและสมบัติการไหล

ภาษาอังกฤษ Storage hardening of natural rubber: Molecular mechanisms and non-isoprene compounds involved: influence of the phenomenon on structure and rheological properties.

ชื่ออาจารย์ที่ปรึกษาทั้งคนไทยและต่างประเทศ พร้อมสถานที่ทำงานของอาจารย์ที่ปรึกษาทั้งหมด

1) Dr. Frederic Bonfils (UMR IATE 1208, CIRAD, INRA, Montpellier SupAgro, UMII, 2 Place Viala, 34060 Montpellier Cedex 1, France)

2) Dr. Laurent Vaysse ([1]UMR IATE 1208, CIRAD, INRA, Montpellier SupAgro, UMII, [2]KU-CIRAD laboratory Agroindustry building 3, 7th Floor, Kasetsart University, Bangkok 10900, Thailand)

3) Dr. Suwaluk Wisunthorn (Faculty of Science and Industrial Technology, Prince of Songkla University, Surat Thani Campus, Muang District, Surat Thani, Thailand)

4) Assoc. Prof. Dr. Charoen Nakason (Center of Excellence in Natural Rubber Technology, Faculty of Science & Technology, Prince of Songkla University, Pattani campus, Thailand)

5) Prof. Dr. Suda Kiatkamjornwong (Department of Imaging and Printing Technology, Faculty of Science, Chulalongkorn University, Bangkok, Thailand)

4. **ความร่วมมือกับเครือข่ายต่างประเทศ**

1) CIRAD (Agricultural Research for Development), Montpellier, France

2) Mixed Research Unit (Unité Mixte de Recherche, UMR), Montpellier, France

3) Montpellier SupAgro (International Center for Higher Education in Agricultural Sciences), France

5. **ความก้าวหน้าของการทำวิจัย** ผลการนำเสนอผลงานวิจัย เช่น การประชุมวิชาการในประเทศ นอกประเทศ การส่งบทความไปยังวารสารนานาชาติ

1) การประชุมวิชาการ The 3rd “Hevea Research Platform in Partnership” (HRPP) Annual Seminar, Workshop and Field trip ณ มหาวิทยาลัยสงขลานครินทร์ วิทยาเขตสุราษฎร์ธานี, วันที่ 10 - 12 พฤษภาคม 2554

2) ชื่อที่สอง ในการตีพิมพ์วารสาร Journal of Chromatography A (Submitted paper on June 7, 2011) ดังนี้ Stephane Dubascoux, Chalao Thepchalerm, Eric Dubreucq, Suwaluk Wisunthorn, Laurent Vaysse, Suda Kiatkamjornwong, Charoen Nakason, Frederic Bonfils Comparative study of the mesostructure of natural and synthetic polyisoprene by SEC-MALS and AF4-MALS. Journal of Chromatography A, submitted.

6. รางวัลที่ได้ของนักศึกษา ยังไม่มี

7. การคาดคะเนเวลาที่จะจบการศึกษา ประมาณเดือนธันวาคม พ.ศ.2555 ถึงเดือนมิถุนายน พ.ศ. 2556

8. การคาดคะเนวิชาชีพในอนาคต อาจารย์ในสังกัดมหาวิทยาลัยของรัฐบาล

เอกสารแนบ

บทความพิมพ์เผยแพร่ในวารสาร

Carbohydrate Polymers 81 (2010) 348–357

Contents lists available at ScienceDirect

Carbohydrate Polymers

journal homepage: www.elsevier.com/locate/carbpol

Preparation of cassava starch-graft-polyacrylamide superabsorbents and associated composites by reactive blending

Charoen Nakason[a], Toha Wohmang[a], Azizon Kaesaman[a], Suda Kiatkamjornwong[b,*]

[a] Center of Excellence in Natural Rubber Technology, Department of Rubber Technology and Polymer Science, Faculty of Science and Technology, Prince of Songkla University, Pattani, 94000, Thailand
[b] Multidisciplinary Program of Petrochemistry and Polymer Science, Department of Imaging and Printing Technology, Faculty of Science, Chulalongkorn University, Bangkok, 10330, Thailand

ARTICLE INFO

Article history:
Received 11 January 2010
Received in revised form 11 February 2010
Accepted 15 February 2010
Available online 4 March 2010

Keywords:
Batch reactor
High water absorbing polymer
Cassava starch
Acrylamide

ABSTRACT

Cassava starch-*g*-polyacrylamide (PAM) was successfully prepared by a reactive batch processing using a specially designed batch reactor resulting in a superabsorbent polymer (SAP) with water absorption of 605 g/g being obtained under the optimized reaction conditions. The occurrence of a graft copolymer was confirmed by FT-IR spectra, where it was found to exhibit all characteristic bands of both starch and acrylamide (AM) units. SEM micrographs of the starch granules showed an irregular shape and varied particle sizes with a smooth surface, while the graft copolymers had a coarse porous structure and broad network. Various types of inorganic filler were added to the graft copolymer to prepare the SAP composites (SAPC). It was found that the SAPC with bentonite clay exhibited the highest water absorption of approximately 730 g/g. Conversely, the incorporation of silica to the graft copolymer gave a significantly lower water absorption capability than the copolymer alone.

© 2010 Elsevier Ltd. All rights reserved.

1. Introduction

Biodegradable polymers have drawn considerable attention in both academia and industry due to the problem of environmental pollution caused by the disposal of synthetic polymer waste. Therefore, the development of biodegradable polymers has been one of the main areas of current interest. One of the simple practical approaches to prepare biodegradable polymers is to blend polymers with various types of starch. Since Thailand is one of the world's largest exporters of cassava products it, therefore, has a great opportunity to search for a reliable process to use cassava starch by modifying its molecular structure to produce biodegradable products, such as superabsorbent polymers (SAPs) (Lanthong, Nuisin, & Kiatkamjornwong, 2006). SAPs are a lightly crosslinked network of hydrophilic polymer chains that can absorb and retain a large quantity of aqueous fluids, and where the absorbed fluids are hardly removed even under pressure (Zhang, Li, & Wang, 2006). Most of the current SAPs are synthetic polymers that have a poor biodegradability leading to environmental problems with their disposal. The development of starch-based SAPs could potentially be used to solve this problem. Potential applications of starch-based SAPs are fairly diverse and include personal care products, fire-fighting gels, agricultural uses, and so forth (Willett & Finkenstadt, 2006). Starch-based SAPs are developed by grafting starch with unsaturated hydrophilic monomers, such as acrylic, acrylamide (AM) (Athawale & Lele, 1998; Karadağ, Üzüm, & Saraydin, 2005; Lanthong et al., 2006; Mostafa, 1995; Willett & Finkenstadt, 2006; Zhang et al., 2006) and ε-caprolactone (Chen et al., 2005), and can be formed by radical chain copolymerization via chemical initiation (Athawale & Lele, 2000; Chen, Park, & Park, 1999) or by the use of γ-ray irradiation (Caykara, Bozkaya, & Kantoğlu, 2003; Kiatkamjornwong, Mongkolsawat, & Sonsuk, 2002).

Although reactive extrusion has been used as a continuous process (Carr, Kim, Yoon, & Stanley, 1992; Willett & Finkenstadt, 2006; Yoon, Carr, & Bagley, 1992), processing of most starch-based graft copolymers is typically done in a batch process, but this consumes a large amount of water (Fanta, 1996; Weaver et al., 1977). Starch-*g*-polyacrylamide (PAM) has been successfully prepared before using a co-rotating twin screw extruder (Finkenstadt & Willett, 2005; Willett & Finkenstadt, 2003), but the maximum water absorption capacity of the SAPs obtained using this process was relatively low at only approximately 300 times their dry weight in water (Carr et al., 1992).

In this work, a specially designed batch reactor was built and used to prepare starch-*g*-PAM based SAPs via reactive processing with low quantities of water. This was aimed to enhance the water retention capability of the saponified starch-*g*-PAM SAP obtained and also to improve some other important properties (see below). The influence of the reaction time, temperature, concentration of

* Corresponding author. Tel.: +66 2 218 5587; fax: +66 2 255 3021.
E-mail addresses: ncharoen@bunga.pn.psu.ac.th (C. Nakason), ksuda@chula.ac.th (S. Kiatkamjornwong).

0144-8617/$ – see front matter © 2010 Elsevier Ltd. All rights reserved.
doi:10.1016/j.carbpol.2010.02.030

the initiator and the molar ratio of starch:AM on the conversion, graft efficiency, graft content and water absorbency were investigated. SAP composites (SAPC) of the starch-*g*-PAM with silica, bentonite clay and China clay were also prepared and their water absorption was tested.

2. Experimental

2.1. Materials

The cassava starch used as the polymer substrate was obtained from Siam Starch (1966) Co., Ltd., Rayong, Thailand. AM, used as a grafting monomer, was manufactured by Fluka (Buchs, Switzerland). Potassium persulfate (KPS), used as a free radical initiator, was manufactured by Asia Pacific Specialty Chemicals Ltd. (Seven Hills, Australia). Hydroquinone, used as a free radical scavenger, was manufactured by Merck (Darmstadt, Germany). *N*,*N*′-Methylenebisacrylamide (*N*,*N*′-MBA), used as a crosslinker, was manufactured by Fluka (Buchs, Switzerland). For the preparation of SAPCs, Ultrasil VN 3 GR silica obtained from Evonik Degussa GmbH (Essen, Germany), bentonite clay, grade SAC-1, manufactured by Thai Nippon Chemical Industry, Co., Ltd. (Samut Sakhon, Thailand) and China clay manufactured by Renuka Minchem Pvt. Ltd. (Udaipur, India) were each mixed in the reactive batch processing.

2.2. Reactive polymerization

Reactive batch processing was performed using an in-house specially designed and built batch reactor with a capacity of approx-

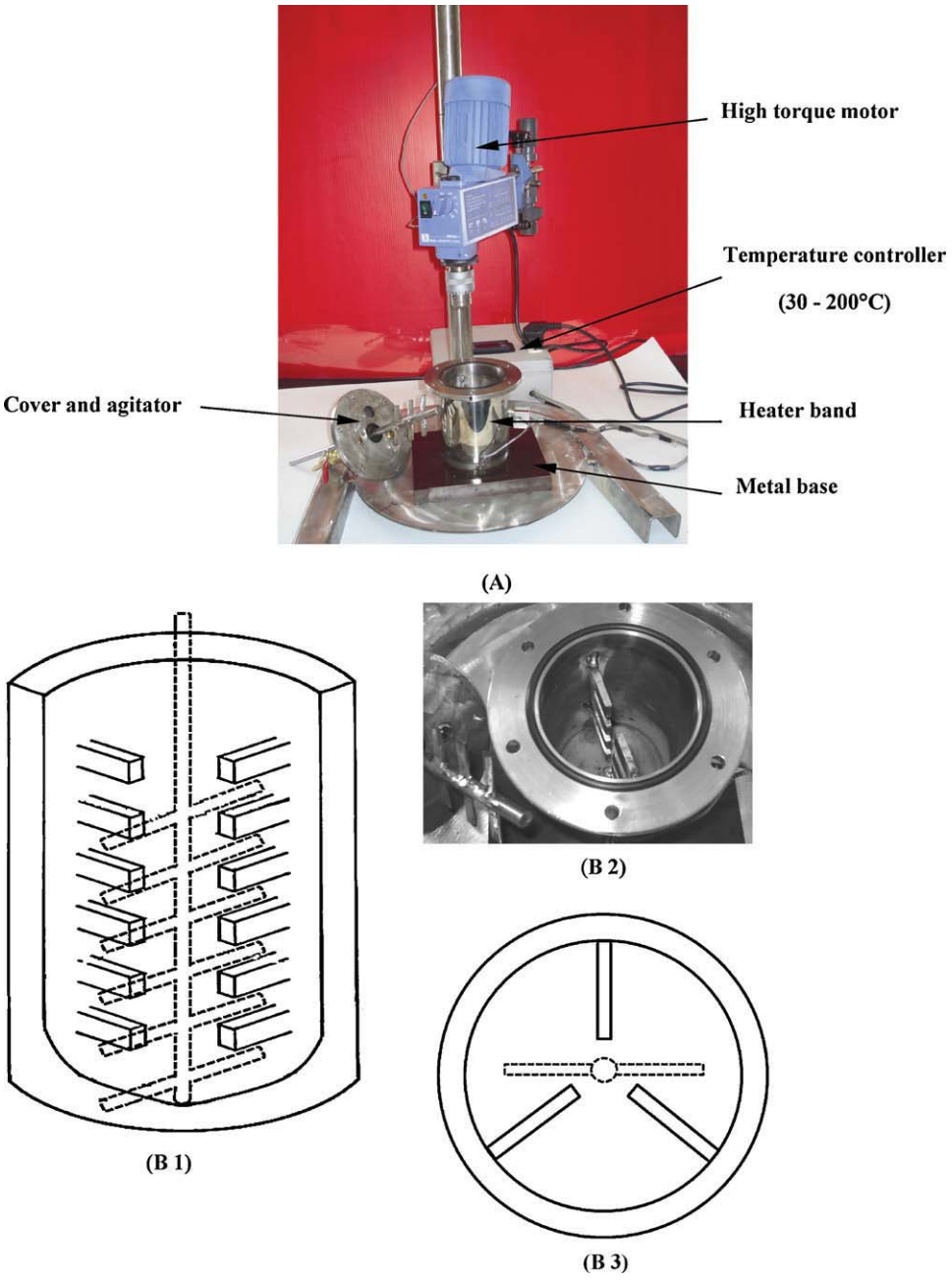

Fig. 1. Components of a specially designed batch reactor. A: Batch reactor, and B: specially designed mixing elements showing (B1) side view of total stirring blades, (B2) top view of the reactor stirring blades, and (B3) top view of total stirring blades.

Table 1
Relationship of the Reynolds number and mixing speed.

Reynolds number	Mixing speed
<10	Low speed for laminar flow
$10 < N_{rev} < 10^4$	Medium speed for transition
$>10^4$	High speed for turbulent flow

imately 1 L, as shown in Fig. 1. It is a stainless steel reactor with a specially designed internal geometry containing an agitator. A programmable heating element surrounded the outside cylinder of the reactor, and a stainless steel cover for the inlet and outlet of nitrogen gas was also built. A high torque motor with a maximum torque of 3000 N cm (RW 47D High-Viscosity Mechanical Overhead Stirrer powered by a 3 × 230 V, 60 Hz, 570 W, IKA, Staufen Germany) was fitted to an in-house made specially designed agitator to cause a thorough mixing of the highly viscous material during the graft copolymerization.

Graft copolymerization was begun by drying cassava starch in a hot air oven for at least 4 h at 60 °C before incorporating it into the batch reactor. Nitrogen gas was purged thoroughly into the reactor and stirred for at least 1 min to eliminate oxygen gas. Distilled water and cassava starch was added at a 1:1 (w/w) ratio and stirred at 60 °C for 20 min to form the gelatinized starch. The temperature of the mix was then increased to 80 °C and stirred for 2 min before incorporating 3.70 mM KPS initiator and then stirring continuously for another 30 min. An aqueous solution of 23.81% (w/w) AM was then added drop wise to the reactor with a continual stirring for the indicated time intervals (a range of 110–260 min). The actual concentration of the starch was also 23.81% (w/w) of the total mass, i.e., starch:AM = 1:1 by weight. The reactor is capable of handling gelatinized starch at this mixture ratio with the small amount of water because the high torque motor is used. In this part of experiment, no crosslinker was incorporated for characterization purposes. Then, the ungrafted homopolymer (PAM) was soluble in ethanol/water whereas the starch grafted PAM was insoluble.

The reaction and newly synthesized product was then quenched by adding 0.5% (w/w) of hydroquinone in ethanol and left overnight to remove the un-reacted monomer. The solid products were finally collected by filtration and dried.

2.3. Saponification

To enhance the water absorbing capability of the resultant SAP, 40 g of the graft copolymer was transferred to a flask containing 100 mL of 1 mol/L of sodium hydroxide solution and 100 mL of distilled water and the content was saponified at 90 °C for 2 h. The final concentration of the graft copolymer in NaOH solution was 16.67% (w/w) of the total mass, i.e., 40 g of the graft copolymer in 240 g of the mixture. The pH of the saponified products was then adjusted to 7 by the addition of a 1 M HCl solution and the graft copolymer was coagulated and precipitated by the rapid addition of an excess amount of methanol. The solid saponified copolymer was then filtered and washed thoroughly to remove the ungrafted starch as well as the un-reacted monomer. The thoroughly washed products were then dried in a vacuum oven at 60 °C until the weight of the polymer was constant. They were then ground and filtered through an 80-mesh screen to leave the powdery SAP.

2.3.1. Influence of the inorganic filler

Three types of inorganic filler, namely silica, China clay and bentonite clay, were incorporated in the starch-*g*-PAM copolymer SAP to form SAPCs. The graft copolymer was first prepared using a 1:1 (w/w) ratio of starch:AM at a reaction time and temperature of 140 min and 80 °C with KPS at 1.5 wt% of starch and 0.3 wt% of *N*,*N*′-

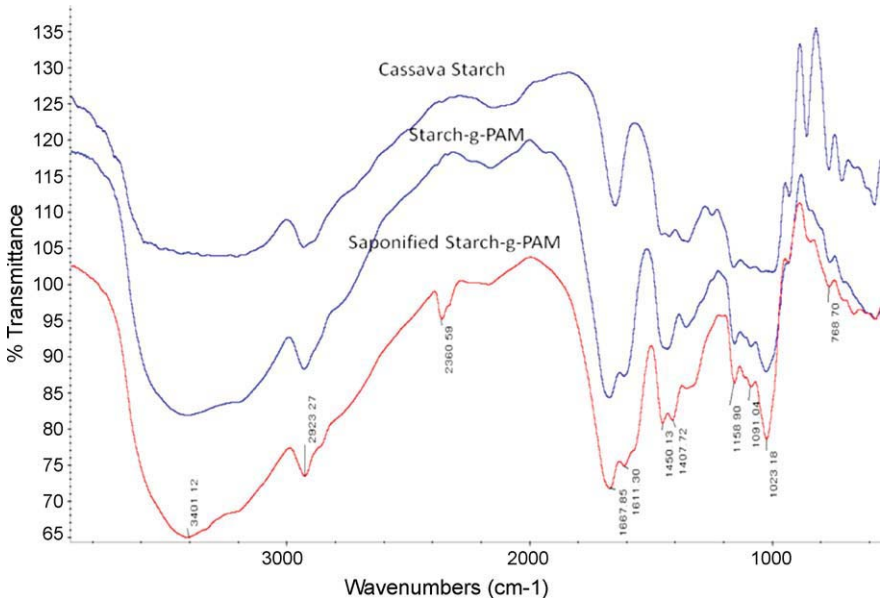

Fig. 2. Representative FT-IR spectra of cassava starch, the starch-*g*-PAM copolymer and its saponified product.

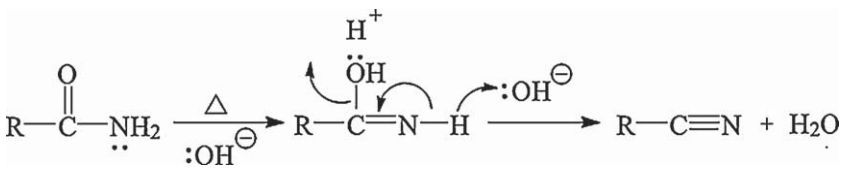

Scheme 1. Proposed mechanism for the formation of nitrile group from dehydration of amide group by alkaline hydrolysis at 90 °C.

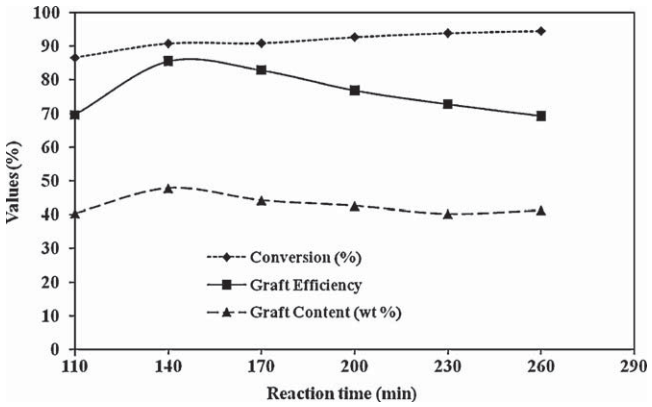

Fig. 3. Relationship between the level of conversion, graft efficiency and graft content of the saponified starch-g-PAM copolymer SAP against the reaction time employed for the copolymer formation.

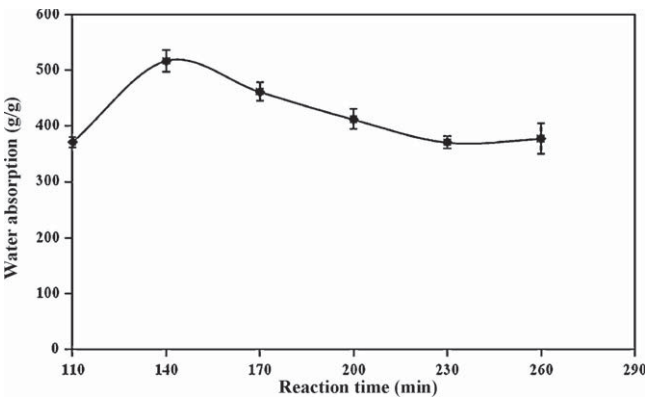

Fig. 4. Relationship between the reaction time used for the starch-g-PAM copolymer SAP formation and the resultant water absorption obtained by the SAP. Data are shown as the mean ± 1 S.D. and are derived from 3 replicate samples.

MBA under a stirring speed of 300 rpm. The fillers were filtered through a 325-mesh stainless steel screen before incorporating in the reaction mixture at a loading level of 10 wt% of graft copolymer.

2.4. Water absorbency

The powdery SAP (0.1 g) was immersed in distilled water (250 mL) for 24 h at ambient temperature (25–30 °C) to reach an equilibrium swelling. The residual water was removed by filtration through an 80-mesh stainless steel screen with the water absorbed polymer left on the screen for at least 1 h to drain off the additional unabsorbed water. During this period, the screen was gently shaken with an alternate lined angle of 15–20° to ensure that most of the un-absorbed water was separated. The un-absorbed water which was held in the free spaces among the SAP particles, due to variation in particle sizes, by capillary force must be excluded. The water absorption was determined by weighing the swollen graft copolymer and its dried polymer in Eq. (1) as follows:

$$\text{water absorbency (g/g)} = \frac{W_1 - W_0}{W_0}, \tag{1}$$

where W_0 is the weight of the dried SAP and W_1 is the weight of the swollen sample.

2.4.1. Characterization

The nitrogen contents were measured using a Kjeldahl digestion unit consisting of Kjeldatherm block digestion units (702001 KBL 20S), a programmable distillation unit with a titration unit (Vapodest 45s) and a scrubber unit, all manufactured by Gerhardt (Königswinter, Germany). Details for the determination of nitrogen content were as described elsewhere (McGill & Figueiredo, 1993). The conversion, graft content and graft efficiency were each calculated using the following equations (2)–(4) (Willett & Finkenstadt, 2003):

$$\text{conversion} = \frac{100N_{crud}}{N_f}, \tag{2}$$

$$\text{graft content} = \frac{100N_i}{19.72}, \tag{3}$$

$$\text{graft efficiency} = \frac{100(1-f)N_i}{(1-f)N_i + fN_s}, \tag{4}$$

where N_{crud} is the nitrogen content (wt%) of the newly synthesized (crude) product. N_f is the theoretical nitrogen content based on the feeding amount of the monomer. N_i is the nitrogen content of the EtOH/H_2O-insoluble fraction and f is the weight of the soluble fraction in the EtOH/H_2O. The nitrogen content of the PAM was 19.72 wt% by the above method. Graft efficiency is based on the amount of monomer polymerized, and is equal to the ratio

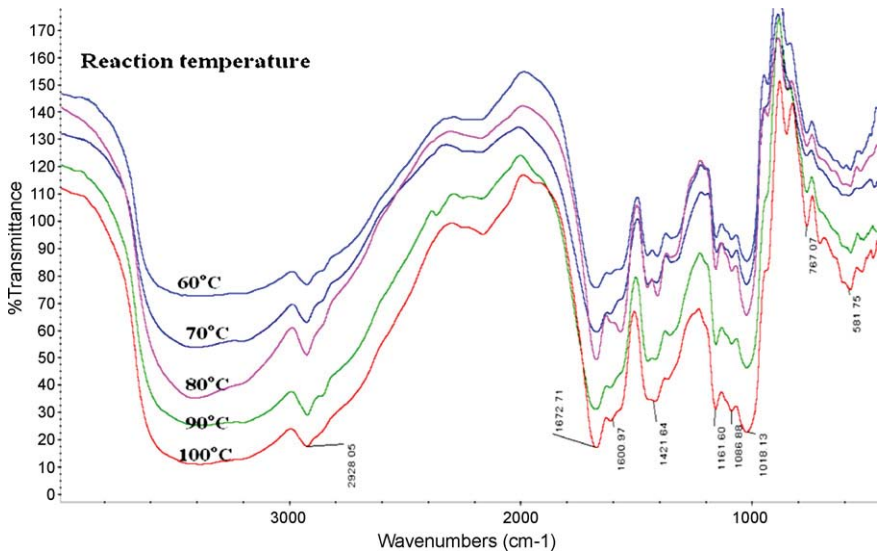

Fig. 5. Representative FT-IR spectra of the purified starch-g-PAM copolymer prepared at the indicated five different reaction temperatures.

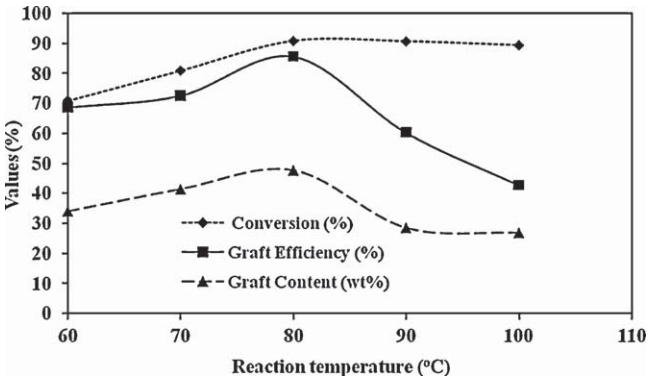

Fig. 6. Relationship between the reaction temperature used to form the starch-*g*-PAM copolymer SAP and the level of conversion, graft efficiency and graft content of the obtained SAP.

of the insoluble amount of PAM to the total amount of PAM (the insoluble and soluble parts). It should be mentioned that GE was calculated only in the reaction system without incorporation of the crosslinking agent.

2.4.1.1. Morphology of SAP and SAPC. The SAP and SAPC samples were dried at 105 °C for 2 h to eliminate moisture. They were cooled in a desiccator, and coated with gold and characterized using a scanning electron microscopy (JOEL SEM, JSM-5200, Tokyo, Japan) at 15 kV.

3. Results and discussion

Based on the specially designed reactor (Fig. 1), the mixing speeds for the polymerization reaction can be controlled based on the relationship between the Reynolds number of the reactor and the mixing speed of the reaction mixture (Table 1). The Reynolds number (N_{Re}) equation is shown in Eq. (5):

$$N_{Re} = \frac{\rho n D^2}{\mu}, \quad (5)$$

where D is the diameter of the propeller (0.31 in), n is the speed of the propeller (300 rpm), ρ is the initial density of the starch (1.50 g/cm^3) and μ is the initial viscosity of the starch (0.018 Pa s). Based on Eq. (5), the specially designed reactor has a Reynolds number of 224.7 and it is possible to state that the reactor is capable of handling viscous dispersion and thus it can mix the reaction mixture by the transition mode at a medium speed (see Table 1).

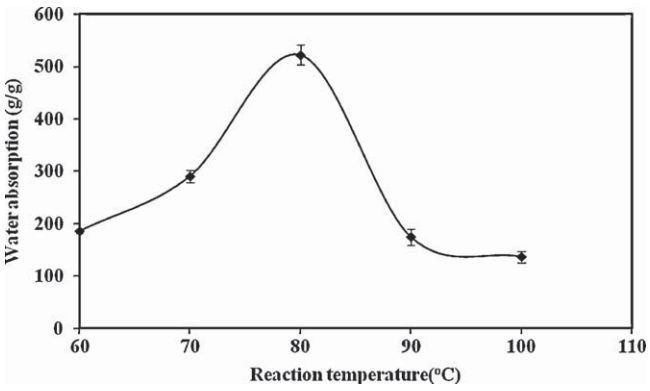

Fig. 7. Relationship between the reaction temperature used to form the starch-*g*-PAM copolymer SAP and the level of water absorption of the obtained SAP. Data are shown as the mean ± 1 S.D. and are derived from 3 replicate sample.

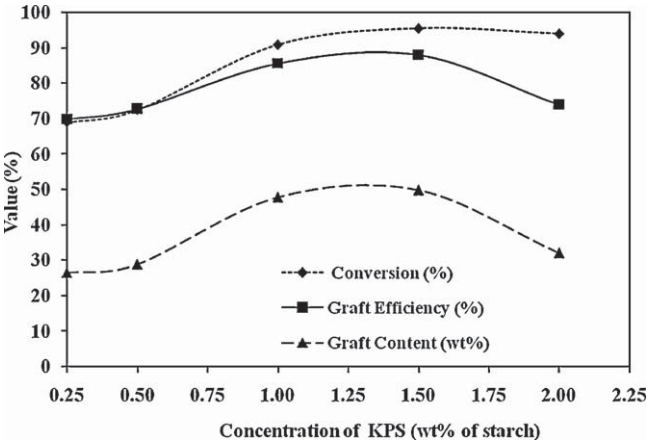

Fig. 8. Relationship between the KPS concentration used to form the starch-*g*-PAM copolymer SAP and the level of conversion, graft efficiency and graft content of the obtained SAP.

3.1. Influence of reaction time

The total time from the start of stirring, to mix the starch with water, until the end of the stirring is termed the reaction time. In this work, the reaction time was varied at 110, 140, 170, 200, 230 and 260 min, with a fixed 1:1 (w/w) ratio of starch:AM, KPS at 1 wt% of starch, a reaction temperature of 80 °C with a stirring speed of 300 rpm.

Fig. 2 shows the representative FT-IR spectra of the cassava starch, the purified starch-*g*-PAM and its saponified product. The broad absorption bands in the region of wave number 3550–3200 cm^{-1}, which represent the O–H stretching vibration, are clearly seen, and the medium absorption peak at 2923 cm^{-1} represents the C–H stretching vibration. Furthermore, the triplet peaks with a strong absorption at 1156, 1051 and 1023 cm^{-1} indicate the presence of the C–O–C stretching vibration. The IR spectrum of the starch-*g*-PAM copolymer gives all the absorption bands of cassava starch plus, additionally, the absorption peaks at 3401, 1667 and 1611 cm^{-1}, which indicate the N–H stretching, C=O stretching and N–H bending of the amide groups, respectively. Therefore, these are the characteristics of the –$CONH_2$ groups in the grafted PAM. Furthermore, the peak at 1407 cm^{-1} that represents –C–N stretching, and that at 766–710 cm^{-1} that represents the weak band of N–H out of plane bending, all are also characteristic bands of the amide grafted onto the cassava starch backbone. After the saponification, the following absorption peaks were observed

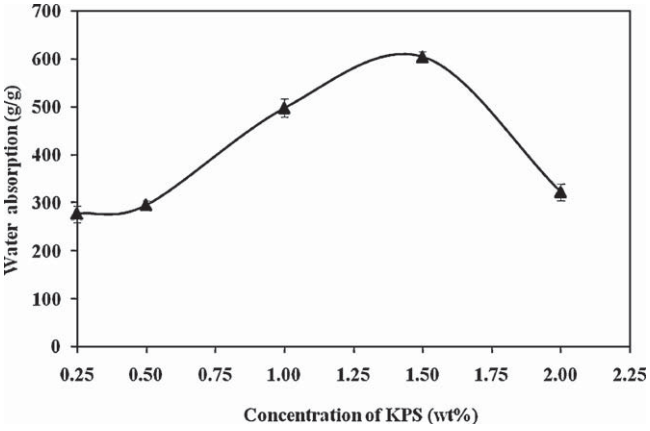

Fig. 9. Relationship between the KPS concentration used to form the starch-*g*-PAM copolymer SAP and the level of water absorption of the obtained SAP. Data are shown as the mean ± 1 S.D. and are derived from 3 replicate samples.

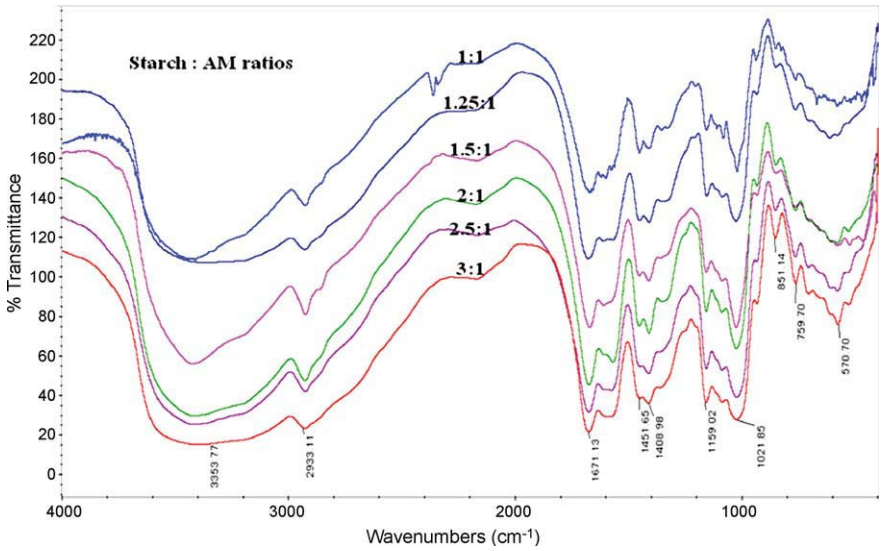

Fig. 10. Representative FT-IR spectra of the purified starch-*g*-PAM copolymer prepared from six different (w/w) ratios of starch:AM.

that confirm the occurrence of PAM; the N–H stretching of O=C–NH (amide band), the C=O stretching, the N–H bending at 1450 cm^{-1} for the –C–N stretching and a relatively intense and sharp peak at 2360 cm^{-1} which is the –C≡N (nitrile or cyanyl) peak, an intermediate peak from the saponification in alkaline solution of the amide group converted to the nitrile or cyanyl group. Although an amide is considered a neutral functional group, it is both weak acid and weak basic, and amide is hydrolyzed by strong acid or strong base. Even though $POCl_3$ is widely used as a dehydrating agent to convert O=C–NH (amide) to R–C≡N (nitrile or cyanyl) (Wade, 1991) it is possible that heat generated at the saponification condition can act as a dehydrating agent to dehydrate acrylamide moiety to nitrile moiety for the SAP prepared from high content of acrylamide (starch:AM = 1:1). This is because the two hydrogen atoms of the amino group can be abstracted by the hydroxide anion under heat. The carbonyl oxygen of acrylamide moiety is simultaneously protonated to become the hydroxyl group as a leaving group which can promote the formation of the nitrile or cyanyl group as shown in Scheme 1.

It is further observed (see the effect of starch:AM ratio) that at the higher starch:AM ratios, this peak (2360 cm^{-1} peak) disappeared because more starch active sites were available for AM grafting.

Fig. 3 shows the influence of the reaction time on the conversion from monomer to polymer, graft efficiency and graft content (based on Eqs. (2)–(4)). The conversion level slightly increased with increasing reaction time from ~88% at 100 min to a maximum value of approximately 95% at a reaction time of 260 min (the longest reaction time). On the other hand, the graft efficiency and graft content initially increased more significantly as the reaction time was increased from 110 to 140 min (70–85% and 40–50%, respectively), and then decreased with longer reaction times. The decrease in graft efficiency with longer reaction times was slightly more marked for graft content but nevertheless the maximum graft efficiency and content were both attained at a reaction time of 140 min. This might be attributed to a higher level of PAM homopolymer formation with reaction times of longer than 140 min. Furthermore, there is a possibility that the crosslinked PAM can be simply degraded by mechanical shear into lower molecular weight fragments during a prolonged reaction time. Regardless, the graft copolymer prepared with a reaction time of 140 min incorporated the highest grafted PAM, content and this corresponded to the highest water absorption capability of the saponified graft copolymer (Fig. 4) which was also obtained from a reaction time of 140 min at ca. 520 g/g). Increasing the reaction time above 140 min caused a decreased water absorption capability, and this is also likely to be due to a lower amount of the grafted PAM which becomes saponified and so more hydrophilic in nature.

Given that reaction times over 140 min only slightly increased the level of conversion but markedly reduced that of the graft efficiency, graft content and water absorbance, a reaction time of 140 min was selected for further investigation.

3.2. Influence of the reaction temperature

Fig. 5 shows the representative FT-IR spectra of the purified starch-*g*-PAM copolymer prepared from five different reaction temperatures (60, 70, 80, 90 and 100 °C) with a fixed reaction time of 140 min, a starch:AM (w/w) ratio of 1, KPS at 1% (w/w) and a stirring speed of 300 rpm. The characteristic bands of cassava starch and amide groups are present, similar to those observed for the purified starch-*g*-PAM copolymer in Fig. 2, which confirms the formation of a cassava starch-*g*-PAM copolymer. The influence of the reaction temperature upon the graft efficiency, graft con-

Table 2
Properties of the cassava starch-*g*-PAM copolymer SAP derived from various (w/w) ratios of starch:AM.

Starch:AM (w/w) ratio	Conversion (%)	Graft efficiency (%)	Graft content (wt%)	Absorbency in DI water (g/g)
1:1	90.9 ± 1.5	85.6 ± 2.1	47.8 ± 1.7	606 ± 10.2
1.25:1	86.7 ± 1.8	80.6 ± 3.5	44.0 ± 3.7	479 ± 9.8
1.5:1	76.4 ± 2.1	76.7 ± 3.9	31.3 ± 3.1	407 ± 11.1
2:1	73.2 ± 3.2	71.1 ± 2.7	28.3 ± 4.7	349 ± 9.7
2.5:1	61.7 ± 3.8	55.6 ± 3.9	23.1 ± 3.1	222 ± 8.9
3:1	48.2 ± 2.7	39.4 ± 4.1	16.8 ± 2.9	132 ± 10.4

The experiment was carried out in triplicate and the data was presented within ±1 S.D.

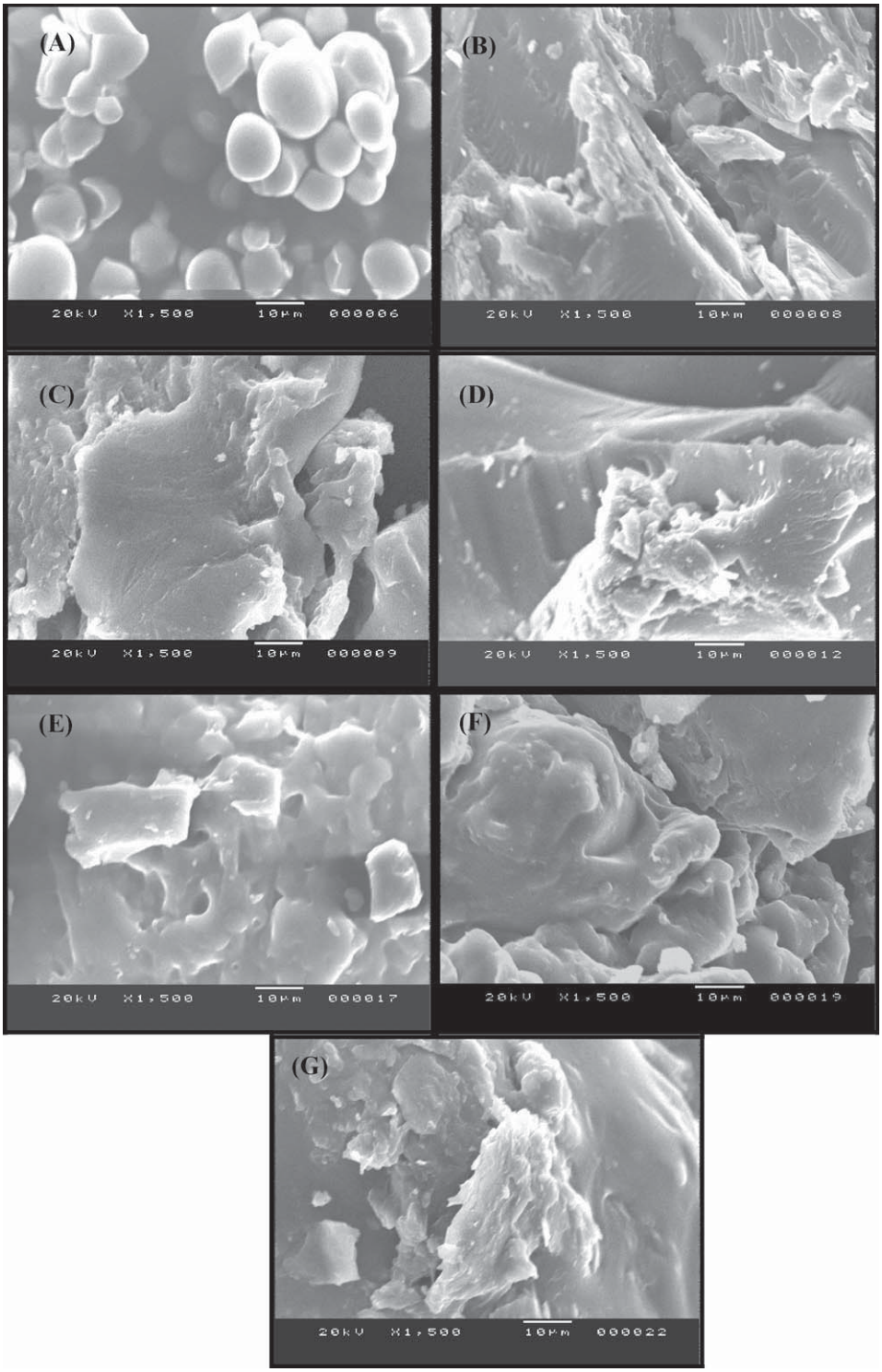

Fig. 11. Representative SEM micrographs of (A) cassava starch, and the purified starch-*g*-PAM copolymer SAP prepared from starch:AM (w/w) ratios of (B) 1:1, (C) 1.25:1, (D) 1.5:1, (E) 2:1, (F) 2.50:1 and (G) 3:1.

tent and level of conversion of monomer to polymers is shown in Fig. 6, where the conversion linearly and significantly increases with increasing temperature within the range of 60–80 °C and then reaches a smooth plateau (or mild decrease) region at reaction temperatures higher than 80 °C. This might be related to the optimum decomposition temperature of KPS at 80 °C, where at temperatures lower than 80 °C the initiator molecules decompose less to give fewer free radicals. On the other hand, at temperatures higher than 80 °C too high a rate of free radical generation is attained which then recombine and so reduce the efficiency of the initiator. The graft efficiency and graft content also increased with increasing reaction temperatures up to 80 °C, and thereafter at higher temperatures an abrupt decrease in the graft efficiency and graft content was observed (Fig. 6). This is attributed to the increasing rate of graft copolymerization in reaction temperatures in the range of 60–80 °C, but at higher temperatures a greater rate of PAM homopolymer formation occurred at the expense of the graft copolymerization. In addition, chain transfer at higher

temperatures is likely to significantly reduce the extent of graft copolymerization. These results correlated well with the water absorption ability of the saponified starch-*g*-PAM copolymer based SAP at various reaction temperatures, where the maximum water absorption was obtained in the saponified starch-*g*-PAM copolymer prepared at 80 °C (Fig. 7). This is because the graft copolymer contains the highest grafted PAM that thereafter was hydrolyzed by the saponification process to result in the presence of the more hydrophilic carboxamide and carboxylic acid groups and therefore a greater level of water absorption.

3.3. Influence of the concentration of potassium persulfate initiator

The conversion level, graft efficiency and graft content of the starch-*g*-PAM copolymer prepared using KPS at five different concentrations (0.25, 0.50, 1.00, 1.50 and 2.00 wt% of the cassava starch), with a fixed starch:monomer (w/w) ratio of 1, a 140 min reaction time at 80 °C and a stirring speed of 300 rpm is summarized in Fig. 8. The conversion level obtained increased with increasing KPS concentrations up to a maximum conversion value at 1.50–2.00 wt% KPS. This may be attributed to the increasing availability of reactive free radicals to initiate the polymerization of PAM to form the grafted PAM and PAM homopolymer. Increasing the concentration of KPS from 1.50–2 wt% did not cause any further significant effect upon the conversion level, although a slight numerical decrease was seen. Although an abundant level of free radicals were formed in the system, the amount of monomer available for the reaction was limiting and, therefore, any further excess production of free radicals might recombine.

The graft efficiency and graft content of the starch-*g*-PAM copolymer also increased with increasing KPS concentrations within the range of 0.25–1.00 by 1.50 wt% KPS, with the maximum values observed between 1 and 1.5 wt%. Likewise, the graft efficiency and content both decreased with further increases in the KPS concentration above 1.50 wt% (Fig. 8). The higher concentrations of initiator (KPS) produced a higher grafted PAM level in cassava starch molecules but at 2 wt% the KPS concentration is too high and chain transfer to monomer or homopolymer formation was more pronounced causing lower graft content and graft efficiency (Fig. 8) as well as the lower water absorption capability (Fig. 9). Indeed, as expected, the water absorption of the saponified cassava starch-*g*-PAM copolymer prepared using KPS at 1.50 wt% exhibited the highest water absorption capability (ca. 605 g/g), which is approximately 2–3 times higher than those of the graft copolymers prepared by reactive extrusion reported elsewhere (Willett & Finkenstadt, 2006).

3.4. Influence of the starch:acrylamide ratios

The influence of the starch:AM ratios, at six different (w/w) ratios of 1:1, 1.25:1, 1.5:1, 2:1, 2.5:1 and 3:1, was analyzed using a 140-min reaction time at 80 °C, a stirring speed of 300 rpm and a KPS concentration of 1.5 wt% of the starch.

The FT-IR spectra of the purified starch-*g*-PAM derived from the six different starch:AM (w/w) ratios revealed all the characteristic bands of both cassava starch and PAM (Fig. 10), as shown respectively in Figs. 2 and 5, supporting the formation of a starch-*g*-PAM copolymer in all six different starch:AM (w/w) ratios. The characteristics and properties of these six different starch-*g*-PAM copolymers based SAPs are shown in Table 2, where it is clear that increasing the starch content decreased the level of conversion, graft efficiency, graft content and water absorption of the SAP. This is attributed to the lowering level of the newly formed graft PAM, which plays the main role in water absorption of the polymer. Therefore, a starch:AM (w/w) ratio of 1:1 was selected to prepare the graft copolymer for further studies.

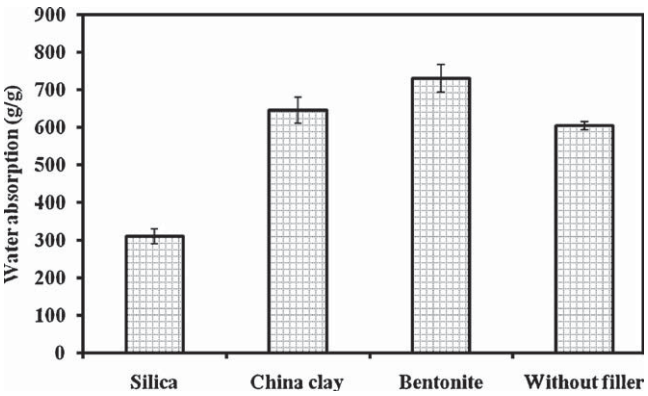

Fig. 12. Water absorption of the saponified starch-*g*-PAM copolymer SAP (without filler) and the derived composite based SAPCs with the indicated inorganic fillers. Data are shown as the mean ± 1 S.D. and are derived from 3 replicate samples.

Representative SEM micrographs of starch and of the starch-*g*-PAM copolymers with different starch:AM (w/w) ratios are illustrated in Fig. 11. Starch granules (Fig. 11(A)) had an irregularly oval shape and a fairly diverse array of particle sizes (in the range of 0.3–1.2 μm in diameter) with a smooth surface. On the other hand, the graft copolymers had a clearly different surface morphology in that the oval particle shape was absent but rather they had a coarse and broad network structure with a rather rough surface. This yields a higher water absorption capability for the copolymer, especially in the case of the SAP derived from a starch:AM (w/w) ratio of 1:1 (Fig. 11(B).

3.5. Influence of inorganic fillers

The water absorption of the saponified starch-*g*-PAM copolymer based SAP and the three SAPCs derived from the SAP is shown in Fig. 12, where the water absorption of the bentonite (730 g/g) and China clay (650 g/g) based SAPCs are significantly higher than those of the base SAP, i.e., without filler (606 g/g) or the silica based SAPC (310 g/g). This is because the hydration of bentonite powder is higher than that of China clay and especially silica and also that the bentonite powder dispersed more readily and produced more particulates in water than did either the China clay or the silica. Unfortunately, the incorporation of the silica resulted in a significantly lower water absorption of the resulting SAPC than that of the original starch-*g*-PAM copolymer based SAP. Perhaps this type of silica caused a smooth surface with a low content of coarse pores, a notion that is supported to some extent by the SEM micrographs (Fig. 13(A)). In contrast, the SAPCs formed with bentonite clay (Fig. 13(C)) and China clay (Fig. 13(B)) both showed a more porous surface which allowed a higher water intension capability of the composite.

Bentonite is an aluminium phyllosilicate absorbent and consists mostly of montmorillonite. Both bentonite and China clay are hydrous aluminium phyllosilicates, while silica is a porous silica dioxide. The former two phyllosilicates can both graft and intercalate the polymer chains but the latter cannot. The work (Foungfung, Seetapan, Phattanarudee, & Kiatkamjornwong, 2010) showed that the inclusion of phyllosilicate clay at an appropriate amount in the *in situ* polymerization of the monomer both enhances the superabsorbent polymer strength and gives a higher level of water absorption. The bentonite, after alkaline saponification, becomes

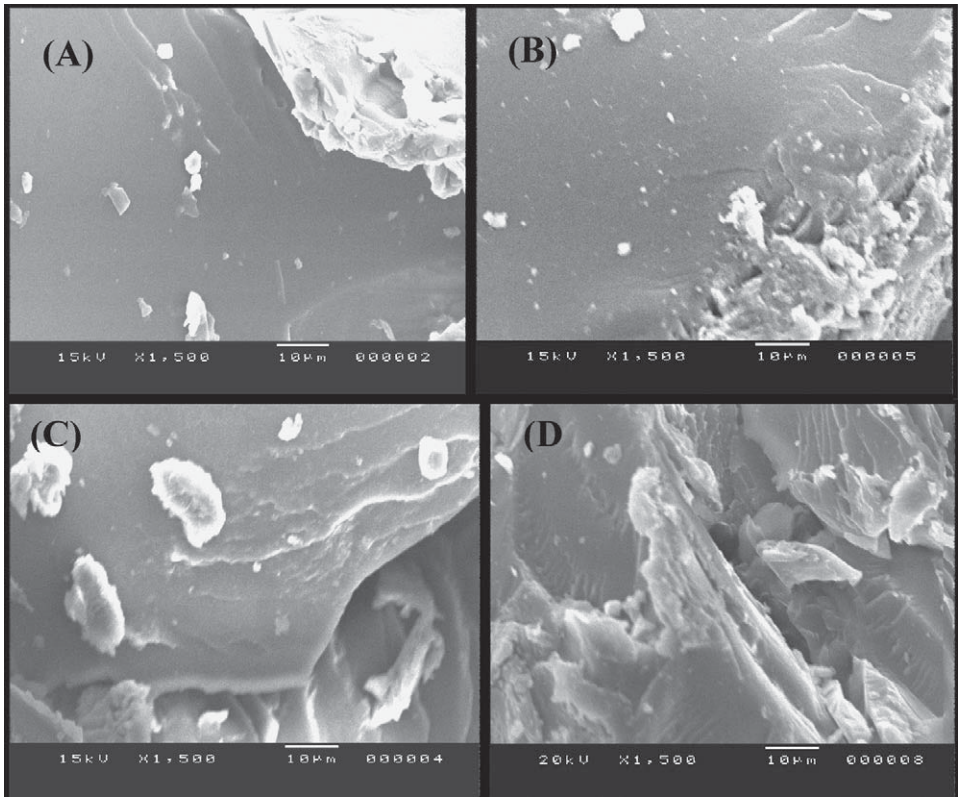

Fig. 13. Representative SEM micrographs of the purified starch-*g*-polyacrylamide composites with (A) silica, (B) China clay, (C) bentonite clay, and (D) without filler.

sodium bentonite which can increase the water absorption more than the kaolinite in the China clay. The *N*,*N*′-MBA crosslinker at 0.3 wt% was used for connecting the acrylamide units to starch or the acrylamide itself. Then the crosslinker could be used to crosslink the ungrafted PAM to be the crosslinked homopolymeric SAPC which can influence water absorption of the whole system. Besides, the clay powder can act as a crosslinking point and plays an important role in the formation of network structure of the SAPC (Wu, Wei, Lin, & Wu, 2003). Likewise, the *N*-MBA crosslinker might also crosslink the active site of the clay with acrylamide monomer or the starch graft PAM SAP (Foungfung et al., 2010; Wu et al., 2003).

4. Conclusions

A high water absorbing copolymer, based on the graft copolymerization of cassava starch and AM, was successfully prepared by reactive batch processing using a specially designed batch reactor. The reactor has a Reynold number of 224.7 and can mix the mixture effectively even at low water content. The highest obtained water absorption capability of the saponified starch-*g*-PAM copolymer was 605 g/g when prepared with a reaction time and temperature of 140 min and 80 °C, a KPS concentration of 1.5 wt% of starch and a starch:AM (w/w) ratio of 1:1. The FT-IR spectra confirmed the formation of saponified starch-*g*-PAM copolymer by exhibiting all the characteristic bands of both starch and AM units. The starch granules, as viewed by SEM, had irregularly oval shaped particles of variable sizes with a smooth surface. However, the graft copolymers exhibited coarse porous structures and a broad network, which may contribute to the higher water absorption capability of the copolymer and the SAPCs over the SAP. The bentonite clay SAPC exhibited the highest water absorption capability (ca. 730 g/g), significantly higher than that of the unfilled graft copolymer SAP (606 g/g). This is due to larger hydration of bentonite powder than those of the China clay and silica.

Acknowledgements

The authors thank the Thailand Research Fund for funding the research project under the Senior Scholarly Consolidation (Grant no. RTA5080004). Many thanks go to the Prince of Songkla University (Pattani Campus) and Chulalongkorn University for research facilities and other support from Publication Consultation Unit of the Research Division, Faculty of Science, Chulalongkorn University.

References

Athawale, V. D., & Lele, V. (1998). Graft copolymerization onto starch. II. Grafting of acrylic acid and preparation of it's hydrogels. *Carbohydrate Polymers*, *35*(1–2), 21–27.

Athawale, V. D., & Lele, V. (2000). Thermal studies on granular maize starch and its graft copolymers with vinyl monomers. *Starch/Stärke*, *52*(6–7), 205–213.

Carr, M. E., Kim, S., Yoon, K. J., & Stanley, K. D. (1992). Graft polymerization of cationic methacrylate, acrylamide, and acrylonitrile monomers onto starch by reactive extrusion. *Cereal Chemistry*, *69*, 70–75.

Caykara, T., Bozkaya, U., & Kantoğlu, Ö. (2003). Network structure and swelling behavior of poly(acrylamide/crotonic acid) hydrogels in aqueous salt solutions. *Journal of Polymer Science Part B: Polymer Physics*, *41*(14), 1589–1778.

Chen, J., Park, H., & Park, K. (1999). Synthesis of superporous hydrogels: Hydrogels with fast swelling and superabsorbent properties. *Journal of Biomedical Materials Research Part A*, *44*, 53–62.

Chen, L., Ni, Y., Bian, X., Qiu, X., Zhang, X., Chen, X., et al. (2005). A novel approach to grafting polymerization of ε-caprolactone onto starch granules. *Carbohydrate Polymers*, *60*(1), 103–109.

Fanta, G. F. (1996). Starch graft copolymers. In J. C. Salamone (Ed.), *Polymeric materials encyclopedia* (pp. 7901–7910). Florida: CRC Press.

Finkenstadt, V. L., & Willett, J. L. (2005). Reactive extrusion of starch-polyacrylamide graft copolymers: Effects of monomer/starch ratio and moisture content. *Macromolecular Chemistry and Physics*, *206*(16), 1648–1652.

Foungfung, D., Seetapan, N., Phattanarudee, S., & Kiatkamjornwong, S. (2010). Acrylamide-itaconic acid superabsorbent polymers and superabsorbent polymer/mica nanocomposites. *Polymers for Advanced Technologies*, 10.1002/pat.1559.

Karadağ, E., Üzüm, O. B., & Saraydin, D. (2005). Water uptake in chemically crosslinked poly(acrylamide-*co*-crotonic acid) hydrogels. *Materials & Design*, *26*(4), 265–270.

Kiatkamjornwong, S., Mongkolsawat, K., & Sonsuk, M. (2002). Synthesis and property characterization of cassava starch-*g*-poly[acrylamide-*co*-(maleic acid)] via gamma-irradiation. *Polymer*, *43*(14), 3915–3924.

Lanthong, P., Nuisin, R., & Kiatkamjornwong, S. (2006). Graft copolymerization, characterization and degradation of cassava starch-*g*-acrylamide/itaconic acid superabsorbents. *Carbohydrate Polymers*, *66*, 229–245.

McGill, W. B., & Figueiredo, C. T. (1993). Chapter 22, Total nitrogen. In M. R. Carter (Ed.), *Soil sampling and methods of analysis* (pp. 201–211). Boca Raton: Lewis.

Mostafa, Kh. M. (1995). Graft polymerization of acrylic acid onto starch using potassium permanganate acid (redox system). *Journal of Applied Polymer Science*, *56*(2), 263–269.

Wade, L. G., Jr. (1991). *Organic chemistry* (p. 967). Englewood Cliffs: Prentice Hall.

Weaver, M. O., Montgomery, R. R., Miller, L. D., Sohns, V. E., Fanta, G. F., & Doane, W. M. (1977). A practical process for the preparation of Super Slurper, a starch-based polymer with a large capacity to absorb water. *Starch/Stärke*, *29*(12), 413–422.

Willett, J. L., & Finkenstadt, V. L. (2003). Preparation of starch-graft-polyacrylamide copolymers by reactive extrusion. *Polymer Engineering and Science*, *43*(10), 1666–1674.

Willett, J. L., & Finkenstadt, V. L. (2006). Reactive extrusion of starch–polyacrylamide graft copolymers using various starches. *Journal of Polymers and the Environment*, *14*(2), 125–129.

Wu, J, Wei, Y., Lin, J., & Wu, S. L. (2003). Study of starch-graft-acrylamide/mineral powder superabsorbent composite. *Polymer*, *44*(21), 6513–6520.

Yoon, D. J., Carr, M. E., & Bagley, E. B. (1992). Reactive extrusion vs. batch preparation of starch-*g*-polyacrylonitrile. *Journal of Applied Polymer Science*, *45*(6), 1093–1100.

Zhang, J., Li, A., & Wang, A. (2006). Study on superabsorbent composite. VI. Preparation, characterization and swelling behaviors of starch phosphate-graft-acrylamide/attapulgite superabsorbent composite. *Carbohydrate Polymers*, *65*(2), 150–158.

Carbohydrate Polymers 83 (2011) 868–875

Contents lists available at ScienceDirect

Carbohydrate Polymers

journal homepage: www.elsevier.com/locate/carbpol

Enhancing antibacterial activity of chitosan surface by heterogeneous quaternization

Napanporn Vallapa[a,b], Oraphan Wiarachai[a,b], Nuttha Thongchul[c], Jisheng Pan[d], Varawut Tangpasuthadol[e], Suda Kiatkamjornwong[f], Voravee P. Hoven[e,*]

[a] Program in Petrochemistry and Polymer Science, Faculty of Science, Chulalongkorn University, Phayathai Road, Pathumwan, Bangkok 10330, Thailand
[b] Center for Petroleum, Petrochemicals, and Advanced Materials, Chulalongkorn University, Phayathai Road, Pathumwan, Bangkok 10330, Thailand
[c] Institute of Biotechnology and Genetic Engineering, Chulalongkorn University, Phayathai Road, Pathumwan, Bangkok 10330, Thailand
[d] Institute of Materials Research and Engineering, A*STAR (Agency for Science, Technology and Research), Research Link, Singapore 117602, Singapore
[e] Organic Synthesis Research Unit, Department of Chemistry, Faculty of Science, Chulalongkorn University, Phayathai Road, Pathumwan, Bangkok 10330, Thailand
[f] Department of Imaging and Printing Technology, Faculty of Science, Chulalongkorn University, Phayathai Road, Pathumwan, Bangkok 10330, Thailand

ARTICLE INFO

Article history:
Received 24 July 2010
Received in revised form 26 August 2010
Accepted 29 August 2010
Available online 6 September 2010

Keywords:
Chitosan
Antibacterial activity
Quaternary ammonium group
Hydrophobicity
Surface modification

ABSTRACT

This research aimed to increase the antibacterial activity of the chitosan surface by introducing quaternary ammonium groups via a heterogeneous two-step process: reductive alkylation using a series of different aldehydes followed by methylation with methyl iodide. ATR-FTIR and XPS analyses, together with water contact angle and zeta potential measurements, confirmed the success of the surface quaternization. The antibacterial activity of the surface-quaternized chitosan film against *Staphylococcus aureus* and *Escherichia coli*, as model Gram-positive and Gram-negative bacteria, respectively, were superior to that of the virgin chitosan film. The apparent damaged bacterial morphology upon contact with the surface-quaternized chitosan film was verified by SEM. Thus, the introduction of additional positive charges to the chitosan surface via the versatile and yet simple process of heterogeneous quaternization can significantly improve the antibacterial activity of the chitosan surface, especially in a neutral environment.

© 2010 Elsevier Ltd. All rights reserved.

1. Introduction

Chitosan has progressively attracted attention due to its multiple bioactivities, such as antimicrobial (Lim & Hudson, 2004; Ong, Wu, Moochhala, Tan, & Lu, 2008) and antitumor (Gorbach et al., 1994). The antibacterial activity, in particular, has been followed with great interest. Chitosan inhibits the growth of a fairly diverse range of bacteria (Choi et al., 2001; Fujimoto, Tsuchiya, Terao, Nakamura, & Yamamoto, 2006) and thus offer great benefit to a wide variety of applications, ranging from medical (Alves & Mano, 2008) to agriculture (Campaniello, Bevilacqua, Sinigaglia, & Corbo, 2008) The exact mechanism of the antimicrobial action of chitosan is still ambiguous, although six main mechanisms, none of which are mutually exclusive, have been proposed (Raafat, von Bargen, Haas, & Sahl, 2008; Rabea, Badawy, Stevens, Smagghe, & Steurbaut, 2003) as follows: (1) Interactions between the positively charged moieties on the chitosan molecules and those negatively charged ones on the microbial cell outer membranes leads to changes in the cell membrane structure and permeability inducing the leakage of proteinaceous and other intracellular constituents and so challenging the biochemical and physiological competency of the bacteria leading to loss of replicative ability and eventual death. (2) Chitosan acts as a chelating agent that selectively binds trace metals and subsequently inhibits the production of toxins and microbial growth. (3) Chitosan activates several defense processes in the host tissue, acts as a water binding agent and inhibits various enzymes. (4) Low molecular weight chitosan penetrates the cytosol of the microorganisms and, through the binding of chitosan with DNA, results in the interference with the synthesis of mRNA and proteins. (5) Chitosan on the surface of the cell can form an impermeable polymeric layer which alters the cell permeability and prevents nutrients from entering the cell. (6) Finally, since chitosan can adsorb the electronegative substances in the cell and flocculate them, it disturbs the physiological activities of the microorganism leading to their death.

Nonetheless, chitosan, shows its antibacterial activity only in acidic medium, which is ascribed to the poor solubility of chitosan above its pK_a (pH 6.5). For this reason, a number of chitosan derivatives have been developed not only to expand the use of chitosan into a broader pH range and so media but also to improve the bactericidal actions of chitosan. Amongst all the derivatives that exhibit superior antibacterial activity to native

* Corresponding author. Tel.: +66 2218 7626–7; fax: +66 2218 7598.
E-mail address: vipavee.p@chula.ac.th (V.P. Hoven).

0144-8617/$ – see front matter © 2010 Elsevier Ltd. All rights reserved.
doi:10.1016/j.carbpol.2010.08.075

chitosan, quaternary ammonium-containing ones have gained the most attention. They are typically synthesized either by direct quaternization of the amino groups of chitosan using alkyl halides under alkaline conditions (Domard, Rinaudo, & Terrassin, 1986; Polnok, Borchard, Verhoef, Sarisuta, & Junginger, 2004), by reductive *N*-alkylation reaction of chitosan with aldehydes via Schiff's base intermediates followed by quaternization with methyl iodide (Muzzarelli & Tanfani, 1985; Sajomsang, Gonil, & Saesoo, 2009) or by reductive *N*-alkylation reaction of chitosan with quaternary ammonium-type aldehydes (Suzuki, Oda, Shinobu, Saimoto, & Shigemasa, 2000). Reaction of the amino groups of chitosan with glycidyltrimethylammonium chloride (GTMAC) has been introduced as an alternative for *N*-selective reaction under acidic and neutral conditions (Seong, Whang, & Ko, 2000; Sun, Du, Fan, Chen, & Yang, 2006). A recent review on the synthesis and applications of quaternized derivatives of chitosan have been available in published literatures (Mourya & Inamdar, 2009; Sajomsang, 2010).

Chitosan in its solid form (film, fiber or particles) holds promising values in many applications for which interfacial contact inhibition is sufficient, although its bactericidal action is only favorable in acidic media (pH < 6.5) when most of its amino groups hold their cationic character. As a means to permanently introduce a positive charge to solid chitosan, without having to incorporate additional cationic species or altering the processability of chitosan, heterogeneous quaternization seems to be an attractive approach. The reactions can be accomplished in the absence of tedious purification process that are certainly required if the quaternization is done homogeneously in solution. Chitosan can be fabricated into the desired solid form (film, fiber or particle) prior to the surface modification. Previously, we have demonstrated that it is conceivable to tune the surface properties of chitosan, namely hydrophilicity/hydrophobicity, and protein adsorption, by chemical modification of the chitosan surface by choosing the suitable reagents under a heterogeneous condition (Amornchai, Hoven, & Tangpasuthadol, 2004; Hoven, Tangpasuthadol, Angkitpaiboon, Vallapa, & Kiatkamjornwong, 2007; Tangpasuthadol, Pongchaisirikul, & Hoven, 2003).

This research aimed to conduct the quaternization of chitosan by a well-developed chemistry based on a two-step approach using firstly a reductive *N*-alkylation reaction of chitosan with aldehydes via the formation of Schiff's base intermediates, followed by quaternization with methyl iodide. Besides the positive charge of quaternary ammonium groups, it is envisaged that the hydrophobicity introduced from the hydrocarbon chains of the different aldehydes should help elevate the antibacterial activities, as has been formerly described by others (Badawy, 2010; Kim & Choi, 2002; Ye et al., 2007).

2. Materials and methods

2.1. Materials

Chitosan flakes (DAC of 92%, M_V = 550,000 Da) were purchased from Seafresh Chitosan (Lab) Co., Ltd. (Thailand). Chitosan films and particles were prepared according to the published procedure by Hoven et al. (2007) and Qi, Xu, Jiang, Hu, and Zou (2004), respectively. Methanol, as commercial grade, was distilled over 4A molecular sieves prior to use. Methyl iodide (CH_3I), acetaldehyde, glutaraldehyde, sodium borohydride ($NaBH_4$), sodium iodide (NaI) and were all purchased from Fluka (Switzerland), and used as received. Benzaldehyde and butyraldehyde were purchased from Merck (Germany) and Sigma Chemical Co. (USA), respectively, and used as received. *Staphylococcus aureus* (*S. aureus*) and *Escherichia coli* (*E. coli*) were purchased from the National Center for Genetic Engineering and Biotechnology (Thailand). Trypicase soy agar (TSA) and Trypicase soy broth (TSB) were purchased from PPL System Co., Ltd. (Thailand). Phosphate buffer saline (PBS) was supplied by Aldrich (USA). Ultrapure distilled water was obtained after purification using a Millipore Milli-Q system (USA).

2.2. Preparation of N-alkyl chitosan films or particles

An anhydrous methanol solution of each selected aldehyde (10 mL) at the desired concentration (0.4–1 M) was added into a flask containing chitosan films (2 cm × 2 cm) or particles (0.03 g). After stirring for a given time at ambient temperature (~28–30 °C), $NaBH_4$ (0.3 g, 0.8 mol) was added into the reaction mixture and the solution was stirred for 24 h. The films were removed from the solution, rinsed thoroughly with methanol, and dried *in vacuo*. In the case of particles, they were isolated by centrifugation at 6000 rpm. The supernatant was discarded and the particles were re-suspended in and centrifugally washed with methanol three times prior to being dried *in vacuo*.

2.3. Preparation of quaternized N-alkyl chitosan films or particles

An anhydrous methanol solution of NaI (0.2 M) was added via syringe into a flask containing *N*-alkyl chitosan films (2 cm × 2 cm) or particles (0.03 g) and NaOH (0.13 g, 0.3 mol). The total volume of the reaction mixture was 10 mL and the concentration of CH_3I was varied within a range of 0.4–2.4 M. The reaction mixture was stirred at 50 °C for the indicated time and then the films were removed from the solution, rinsed thoroughly with methanol, and dried *in vacuo*. In the case of particles, they were isolated by centrifugation, washed with methanol and dried *in vacuo* as detailed above.

2.4. Characterization of surface-quaternized chitosan films/particles

A contact angle goniometer, model 100-00, equipped with a Gilmont syringe and a 24-gauge flat-tipped needle (Ramé-Hart, Inc., USA), was used for the determination of water contact angles. The reported angle expressed as the mean ±1 standard deviation is the average of five measurements on different areas of each sample. All attenuated total reflectance-Fourier transform infrared (ATR-FTIR) spectra were collected at a resolution of 4 cm^{-1} and for 128 scans using a Nicolet Magna 750 FT-IR spectrometer (USA) equipped with a liquid-nitrogen-cooled mercury-cadmium-telluride (MCT) detector using a variable angle reflection accessory (Seagull™, Harrick Scientific, USA) with a hemispherical Ge IRE. X-ray photoelectron spectroscopy (XPS) analysis was performed using a VG ESCALAB 220i-XL instrument (UK) equipped with a monochromatic Al Kα (1486.7 eV photons) and an unmonochromated Mg Kα X-ray source (1253.6 eV photons). The zeta potential of chitosan particles was determined using a Zetasizer Nano-ZS (Malvern Instruments, UK) at 25 °C using a scattering angle of 173°. All data are displayed as the mean ± 1 standard deviation and are derived from at least three independent experiments.

2.5. Evaluation of antibacterial activity

All glasswares used for the tests were sterilized in an autoclave at 121 °C for 15 min prior to use. The quaternized *N*-alkyl chitosan films or particles were sterilized by exposing to UV radiation for 30 min prior to the tests. The quaternized *N*-alkyl chitosan films (1 cm × 1 cm) were placed one per well of a 24-well plate containing 2 mL TSB. Then 12 μL of bacterial suspension in distilled water (OD_{600} = 0.5) was pipetted into each well and the plate incubated in a shaking incubator (Model G-25, New Brunswick Scientific Co., Inc., USA) at 37 °C, 110 rpm, for 24 h. The bacterial suspension (100 μL) was then transferred from each well into a well of a 96-well plate

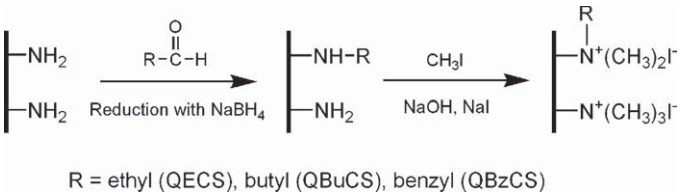

Scheme 1. Surface quaternization of chitosan.

to determine the OD_{600} by UV–vis spectroscopy (Multi-Detection Microplate Reader Model All, Bio-Tek™ Instruments Inc., USA). Another 100 μL of each of the bacterial suspensions was diluted 10^{10} times and 100 μL of this diluted bacterial suspension was then spread onto TSA. After incubating at 37 °C for 24 h, the number of colonies, and thus replication competent bacteria were then counted as a measure of assumed viability. The results, after correction for the dilution factor, were expressed as the mean number of colony forming units per volume (CFU/mL). All tests of antibacterial activity were performed in triplicate per sample and upon at least three independent samples. The antibacterial ratio was calculated using the following relationship:

$$\text{antibacterial ratio (\%)} = \frac{A - B}{A} \times 100 \quad (1)$$

where *A* is a number of original viable bacterial cell after incubation in media alone (control) and *B* is a number of viable bacterial cell after incubation with the designated chitosan film.

Statistical analysis was performed using the Statistical Package for the Social Science (SPSS) version 17.0 software. Statistical comparisons were made by One-Way Analysis of Variance (ANOVA) with the Least Square Difference (LSD) tests post hoc evaluations of differences between groups. The threshold level for accepting statistical significance was set at $p < 0.05$.

2.6. Determination of bacterial morphology

Bacterial morphology on the quaternized *N*-alkyl chitosan films was examined under a scanning electron microscope (SEM, JEOL Model JSM-5800L, Japan). After incubation with the bacterial suspension ($OD_{600} = 0.5$) for 24 h, the quaternized *N*-alkyl chitosan films were removed from the bacterial suspension by sterile forceps and immersed in 3% (w/v) glutaraldehyde solution at 4 °C in order to fix the adherent bacteria on the films. After 24 h, the glutaraldehyde solution was removed and the films were washed with PBS, followed by a stepwise dehydration with 30%, 50%, 70%, 90% and 100% (v/v) ethanol in water for 10 min each. The films were then dried and sputter-coated with a thin film of gold before being characterized by SEM.

3. Results and discussion

3.1. Surface quaternization

The methods used for modifying the chitosan surface are outlined in Scheme 1. The reaction introduces quaternary ammonium groups via a heterogeneous two-step process, the reductive *N*-alkylation using selected aldehydes followed by methylation with methyl iodide to form quaternized *N*-alkyl chitosan surface. Contact angle analysis was used to monitor the extent of both reductive *N*-alkylation and quaternization as a function of reaction time and reagent concentrations. As shown in Fig. S1 (Supplementary data), the reaction with butyraldehyde and benzaldehyde, but not acetaldehyde, intrinsically introduced additional hydrophobicity to the chitosan films. Water contact angle of the virgin chitosan film is 79.8 ± 3.1°. The trend was reversed, however, in the case of acetaldehyde. Upon using the optimized condition that yield the maximum extent of surface reductive *N*-alkylation (summarized in Table S1, Supplementary data), the water contact angle of *N*-ethyl chitosan film, *N*-butyl chitosan film, and *N*-benzyl chitosan film was 82.1 ± 0.7°, 93.8 ± 0.8°, and 93.0 ± 2.3°, respectively. A series of quaternized *N*-alkyl chitosan films were subsequently obtained by methylation of these three different *N*-alkyl chitosan films. According to Fig. S2 shown in the Supplementary data, the surface of all *N*-alkyl chitosan films essentially became more hydrophilic after quaternization. Upon using a reaction time of 12 h, the optimized methyl iodide [CH_3I] for the step of methylation of all *N*-alkyl chitosan substrates together with their lowest water contact angles obtained are displayed in Table S2 (Supplementary data).

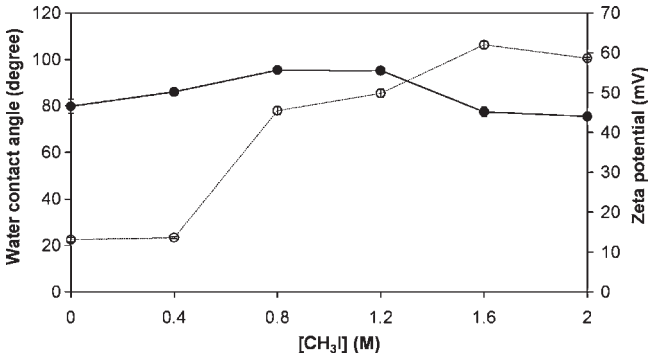

Fig. 1. Water contact angle (●) and zeta potential (○) of the quaternized *N*-benzyl chitosan film/particle prepared by methylation of the *N*-benzyl chitosan film/particle using varied [CH_3I].

In order to verify that the reductive *N*-alkylation followed by methylation can increase the magnitude of positive charges on the chitosan surface, a series of surface-quaternized chitosan particles prepared by conditions equivalent to those used for the films were subjected to zeta potential measurements. The results, also summarized in Table S2, reveal that, as anticipated, all surface-quaternized chitosan particles possessed higher zeta potential values than the virgin unmodified chitosan particles (zeta potential = +13.11 ± 0.6 mV). The highest zeta potential (+58.60 ± 0.3 mV) was achieved in the case of the quaternized *N*-benzyl chitosan (QBzCS) particles implying that its charge magnitude can be broadly tailored. To test this hypothesis, a series of QBzCS films/particles were prepared from *N*-benzyl chitosan films/particles using varied concentrations of CH_3I (Fig. 1), where the degree of quaternization, expressed in terms of zeta potential value, clearly increased as a function of the CH_3I concentration used. The water contact angle, on the other hand, was initially raised as the CH_3I concentration was increased up to 0.8–1.2 M, reaching a maximal value of ~95°, but the surface then became more hydrophilic as the CH_3I concentration was increased further to 1.6–2.0 M. This trend can be explained as a result of the balance between two competing effects. The methyl groups introduced from CH_3I during quaternization enhance the hydrophobicity of the *N*-benzyl chitosan film. However, the higher level of methylation leads to the greater magnitude of surface positive charge density due to the formation of quaternary ammonium groups. The surface of the modified chitosan film thus became more hydrophilic at high levels of quaternization. The lowest water contact angle obtained in the series was ~75°.

ATR-FTIR spectroscopy was also used to confirm the success of quaternization of *N*-alkyl chitosan (Fig. 2). Absorption peaks at 1650 cm^{-1} and 1590 cm^{-1} were assigned to the C=O stretching (Amide I) and N–H bending (Amide II) of the glucosamine unit, respectively. After the reaction, the peak intensity of the N–H bending of chitosan at 1590 cm^{-1} correspondingly decreased, whereas the intensity of C–H deformation peaks at 1470 cm^{-1} increased, indicating that the substitution of the alkyl groups occurred at the

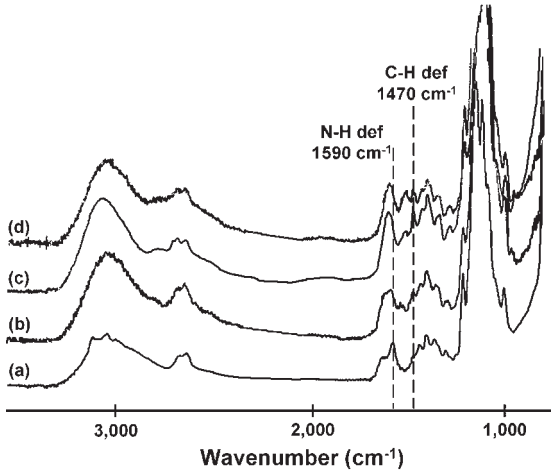

Fig. 2. ATR-FTIR spectra of the (a) chitosan, (b) QECS, (c) QBuCS, and (d) QBzCS films.

amino group of the chitosan film. The results from the ATR-FTIR analysis apparently indicated that the reaction should proceed to a depth of at least 1–2 μm (estimated depth of ATR-FTIR sensitivity).

XPS analysis further supports the success of surface quaternization on QBuCS and QBzCS films (Fig. 3), which were selected as representative samples from the series to be characterized by XPS. Besides C, O, and N, the basic elements already present in the chitosan film, there were no additional elements introduced to the chitosan surface after reductive *N*-alkylation and methylation. The only way to detect the quaternary ammonium groups after surface modification is by considering the N 1s spectrum of the surface-quaternized chitosan film in comparison with the virgin chitosan film. As seen from Fig. 3(a), the N 1s peak of the virgin chitosan film can be fitted with one peak at 400 eV. The N 1s signals of both QBuCS and QBzCS films (Fig. 3(b) and (c)), on the other hand, can be split into two peaks. One appears at the same binding energy as the chitosan film (Peak A). The other having higher binding energy emerges at 403 eV (Peak B). This latter peak can be regarded as a signal from the positively charged nitrogen atom of the quaternary

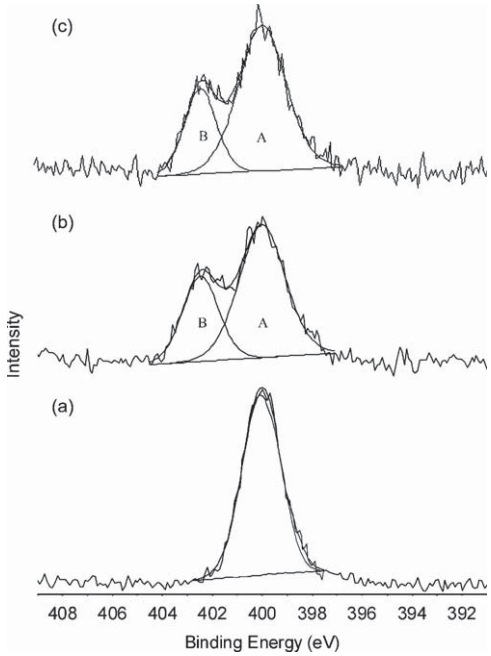

Fig. 3. XPS N 1s spectra of (a) chitosan, (b) QBuCS, and (c) QBzCS films.

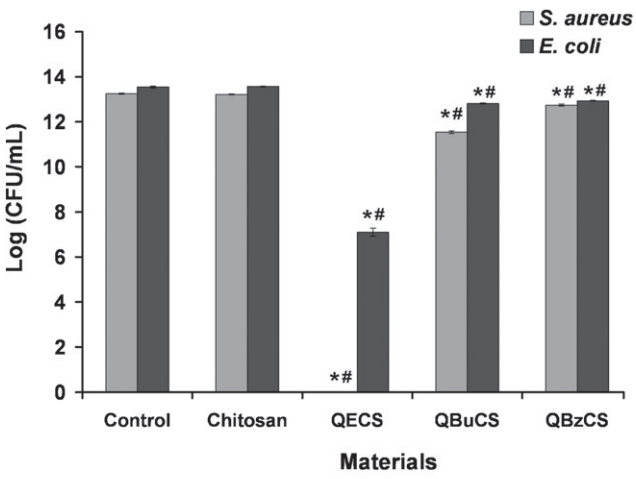

% Antibacterial ratio					
S.aureus	0.00	7.80	100.00	98.04	69.27
E.coli	0.00	0.00	99.99	81.00	75.00

Fig. 4. Total replication competent (viable) cell counts of bacteria grown for 24 h in media alone (control) or in the presence of chitosan and different quaternized *N*-alkyl chitosan films, and below in the table, the corresponding antibacterial ratio. Statistical significance with $p < 0.05$ of the viable count is compared with the control (*) and the chitosan film (#).

ammonium moiety. The %DQ in the surface region could be estimated from the relative ratio of atomic composition of Peak A to Peak B. For the QBzCS series, it was found that the %DQ of the *N*-benzyl chitosan film after quaternization with 0.4 M and 1.6 M CH_3I was equal to 19.2% and 39.6%, respectively. To some extent, these values corresponded with the zeta potential values measured on the quaternized chitosan particles (see Fig. 1 for comparison).

3.2. Evaluation of antibacterial activity

The antibacterial activity of the quaternized *N*-alkyl chitosan films was tested against the Gram-positive and Gram-negative representative bacteria, *S. aureus* and *E. coli*, respectively, in terms of the total number of replication competent (viable) cells as mean colony forming units per volume (CFU/mL). In order to determine the effect of the alkyl substituent on the antibacterial activity of the three quaternized *N*-alkyl chitosan films, QECS, QBuCS and QBzCS, having a similar zeta potential of ~30 mV were selected for the investigation. It is interesting to see from Fig. 4 that the chitosan film, at pH 7.4, showed almost no antibacterial action in comparison with the control of which the bacteria were grown in the absence of chitosan film. This is not quite unexpected, considering that the amino groups on the surface of chitosan films are in the neutral form, not positively charged, at that pH. This also implied that the chelation of the amino groups of chitosan, which has been proposed by others (Cuero, Osuji, & Washington, 1991; Kong et al., 2008) as one of the antibacterial mechanism, does not play a major role in this particular case. This outcome, in fact, suggests a potential significance for the surface quaternization in promoting antibacterial activity under a neutral environment.

Apparently, the QECS and QBuCS films exhibited a greater antibacterial activity than the QBzCS film against both bacterial species. Among all surface-quaternized chitosan films, it seems that the greater the hydrophobicity of the film was, the lower the antibacterial activity was obtained considering that all samples having the similar zeta potential. With the highest water contact angle value (93.0 ± 1.4°), the QBzCS film was not the best

substrate to interact with the bacteria, as previously anticipated based on the assumption that the hydrophobic character should favor the interaction with the lipid bilayers, another major component of the bacterial membrane and subsequently enhances the antibacterial activity. The QECS, on the other hand, exhibited the highest antibacterial activity despite its lowest water contact angle ($71.7 \pm 0.9^{\circ}$) in the series. This somewhat suggested that the bactericidal action of the surface-quaternized chitosan film may take place through not only the contact-inhibitory mechanism as previously expected, but also through a release-inhibitory mechanism similar to what has been observed for soluble chitosan and its quaternized derivatives. A similar speculation that the surface leaching of a soluble protonated glucosamine fraction from the chitosan film as being responsible for the antibacterial activity has also been made recently by Fernandez-Saiz, Lagaron, and Ocio (2009). The extent of weight loss which is presumably caused by surface erosion of all surface-quaternized chitosan films determined by gravimetric analysis was varied roughly in a similar range of 0.1–0.2%. Although there was no specific correlation between the magnitude of weight loss and the type of quaternized derivative, it should be more likely for the QECS to possess the greatest ability to erode out considering its lowest hydrophobicity in the series. It should be noted that there was no detectable weight loss in the case of the virgin, unmodified chitosan film.

The QECS film was detrimental to both *S. aureus* and *E. coli*, although perhaps at a greater magnitude to *S. aureus*, where it yielded a 100% and almost a 100% antibacterial ratio against *S. aureus* and *E. coli*, respectively. The QBuCS film delivered a better inhibitory effect on the Gram-positive bacteria, *S. aureus* than the Gram-negative bacteria, *E. coli*, but neither was as strong as that seen for the QECS film. It is conceivable that the absence of an outer membrane and the presence of negatively charged teichoic acid within a thick peptidoglycan layer (20–80 nm) on the surface of *S. aureus* (Talaro, 2005) should make them more attractive to the positively charged, quaternized chitosan films and easier to be damaged through the contact-inhibitory mechanism than *E. coli* (Fernandez-Saiz et al., 2009). Although *E. coli*, with its thinner double protective layer (the outer lipopolysaccharide layer embedded with a number of small channels of porins and the inner peptidoglycan layer (7–8 nm)) (Talaro, 2005) should be more structurally vulnerable to damage than *S. aureus*, which has a peptidoglycan layer that is several magnitudes thicker than that of *E. coli*, it has been recently been reported, based on AFM analysis, that the stiffness of *S. aureus* is indeed lower than that of *E. coli* (Fernandez-Saiz et al., 2009). However, that did not seem to be the case for the QBzCS films. The antibacterial activity against *E. coli* was relatively comparable to that against *S. aureus*. In fact, the higher susceptibility of *E. coli* than *S. aureus* towards chitosan has also been reported before by others (Chung et al., 2004; Devlieghere, Vermeulen, & Debevere, 2004) For comparison, the investigation was also conducted on the chitosan film that was quaternized by direct methylation with 1.2 M CH_3I for 8 h. It was found that the methylated chitosan film having a comparable zeta potential of +29.3 mV exhibited %antibacterial ratio of ~26 and 29% against *S. aureus* and *E. coli*, respectively. These significantly lower antibacterial efficiency values as opposed to those of the QECS, QBuCS, and QBzCS films helped verifying the indispensable role of the alkyl groups namely ethyl, butyl, and benzyl, respectively, introduced in the step of reductive alkylation, in enhancing the antibacterial activity of the chitosan surface via heterogeneous quaternization.

To further demonstrate the influence of the chitosan surface positive charge density on the antibacterial activity, the latter was examined against *E. coli* and *S. aureus* on a series of QBzCS films in which the charge magnitude was varied as a function of the CH_3I concentration used in the quaternization step. It should be noted that the number written in front of QBzCS displayed in the horizontal axis of Fig. 5 represents the CH_3I concentration used for preparing each QBzCS film. The viable count data shown in Fig. 5 suggested that the antibacterial activity of the surface-quaternized chitosan carrying the same hydrocarbon moiety from the step of *N*-reductive alkylation, benzyl group in this case, can be proportionally tailored as a function of the CH_3I concentration. Besides the increase in charge density, the elevated hydrophilicity introduced by quaternization may also help promote antibacterial activity of the QBzCS films, perhaps through the same mechanism previously described based on surface erosion. This may be the reason why the highly quaternized QBzCS films that were prepared from 1.6 M and 2.0 M of CH_3I and possessed relatively low water contact angles (see Fig. 1 for data) are so potent that they can almost entirely suppress the bacterial growth (~100% antibacterial ratio).

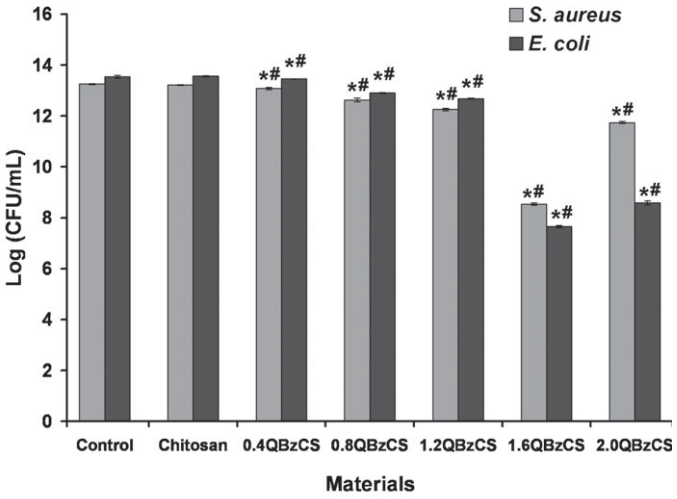

	% Antibacterial ratio						
S.aureus	0.00	7.80	27.00	75.90	89.94	99.99	96.92
E.coli	0.00	0.00	17.00	77.00	86.28	99.99	99.99

Fig. 5. Total replication competent (viable) cell counts of bacteria grown for 24 h in media alone (control) or in the presence of chitosan and QBzCS films having different degree of quaternization (varied as a function of the CH_3I concentration) and below in the table, the corresponding antibacterial ratio. Statistical significance with $p < 0.05$ of the viable count is compared with the control (*) and the chitosan film (#).

In order to determine the morphological changes of bacteria upon prolonged contact with the surface-quaternized chitosan, and to be able to simultaneously correlate the extent of damage with charge magnitude of the chitosan surface, SEM analysis was conducted on the surface of the series of QBzCS films having varied charge magnitude which can be manipulated as a function of CH_3I concentration. It was our intention not to rinse the surface-quaternized film after incubation with the bacterial suspension in order to keep as many bacterial cells adhered onto the film surface as possible, so that both normal and damaged cells can be observed in case they, as is likely, vary in their adherent strength. As revealed in Fig. 6(a) and (b), the typical spherical shape and clustered formation of *S. aureus* cells (Eaton, Fernandes, Pereira, Pintado, & Malcata, 2008) was evident on the surface of chitosan and 0.4QBzCS films with no detectable signs of damage. This corresponds quite well with the fact that the CS and 0.4QBzCS film exhibited no and low antibacterial action against *S. aureus*, respectively. Although most of bacteria on the surface of the 0.8QBzCS and 1.2QBzCS films appear normal in morphology, the cells became less clustered and apparent morphological damage can be easily visualized, especially by those pointed out by arrows and magnified images shown in the inset in Fig. 6(c) and (d). Some cells were ruptured with broken

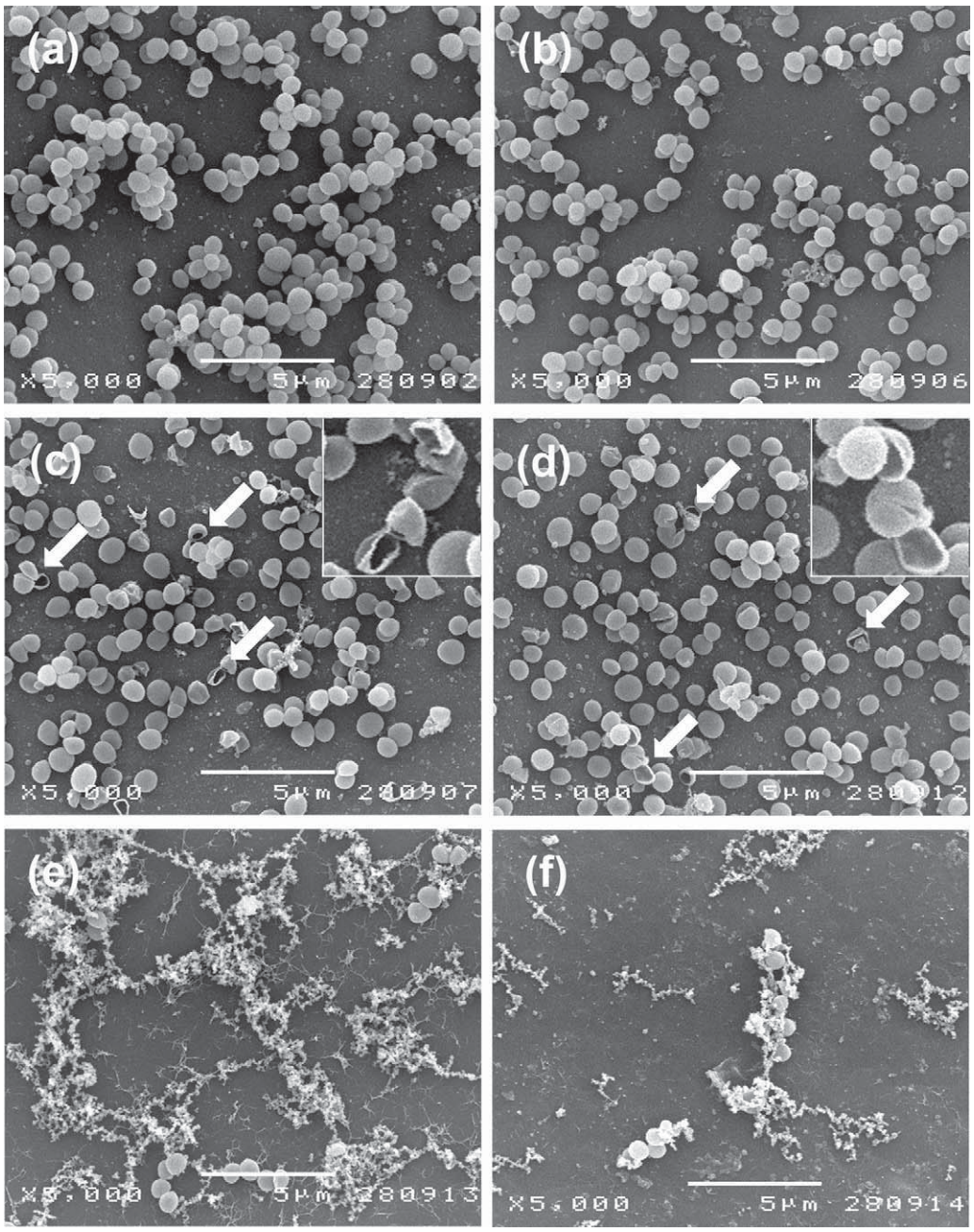

Fig. 6. SEM micrographs of (a) chitosan, (b) 0.4QBzCS, (c) 0.8QBzCS, (d) 1.2QBzCS, (e) 1.6QBzCS, and (f) 2.0QBzCS films after being incubated with the suspension of *S. aureus* (OD_{600} = 0.5) for 24 h. Micrographs shown are representative of at least 5 such fields of view per sample and 3 independent samples.

cell membranes, others were deformed, collapsed and shrunken in size. A further increase in the surface charge density caused extensive lysis of the cells and only few intact bacteria remained on the surface of the 1.6QBzCS and 2.0QBzCS films (Fig. 6(e) and (f)). It is feasible that what appear on those surfaces are fragments of disrupted cytoplasmic membrane and/or intracellular components of the bacteria.

Similar destructive features were also observed in the case of *E. coli* (Fig. 7), even though there was a higher density of *E. coli* cells in the suspension containing chitosan and 0.4QBzCS films than those containing other QBzCS films (see Fig. 5), very few of them adhered onto the surface of chitosan and 0.4QBzCS films, even despite the absence of agitation and washing prior to fixation of the samples, as can be seen from Fig. 7(a) and (b). This may imply that there are no particular attractive forces between the virgin and slightly surface-modified chitosan films under a neutral pH environment. This is entirely the opposite behavior to that observed for *S. aureus* under the same conditions. Nevertheless, the damage to *E. coli* cells became apparent with the QBzCS films having a greater extent of quaternization. As indicated by the arrows, and shown in the insets, in Fig. 7(c)–(f), *E. coli* were severely damaged and appeared in the form of deformed and collapsed rods. Fewer *E. coli* cells in the suspension, together with remnants of destroyed cell membranes and/or intracellular materials of the bacteria that were left on the surface of the 2.0QBzCS film (Fig. 7(f)), indicate that most of them were lysed and did not survive. This outcome is in excellent agreement with the antibacterial activity based on the total viable cell count data.

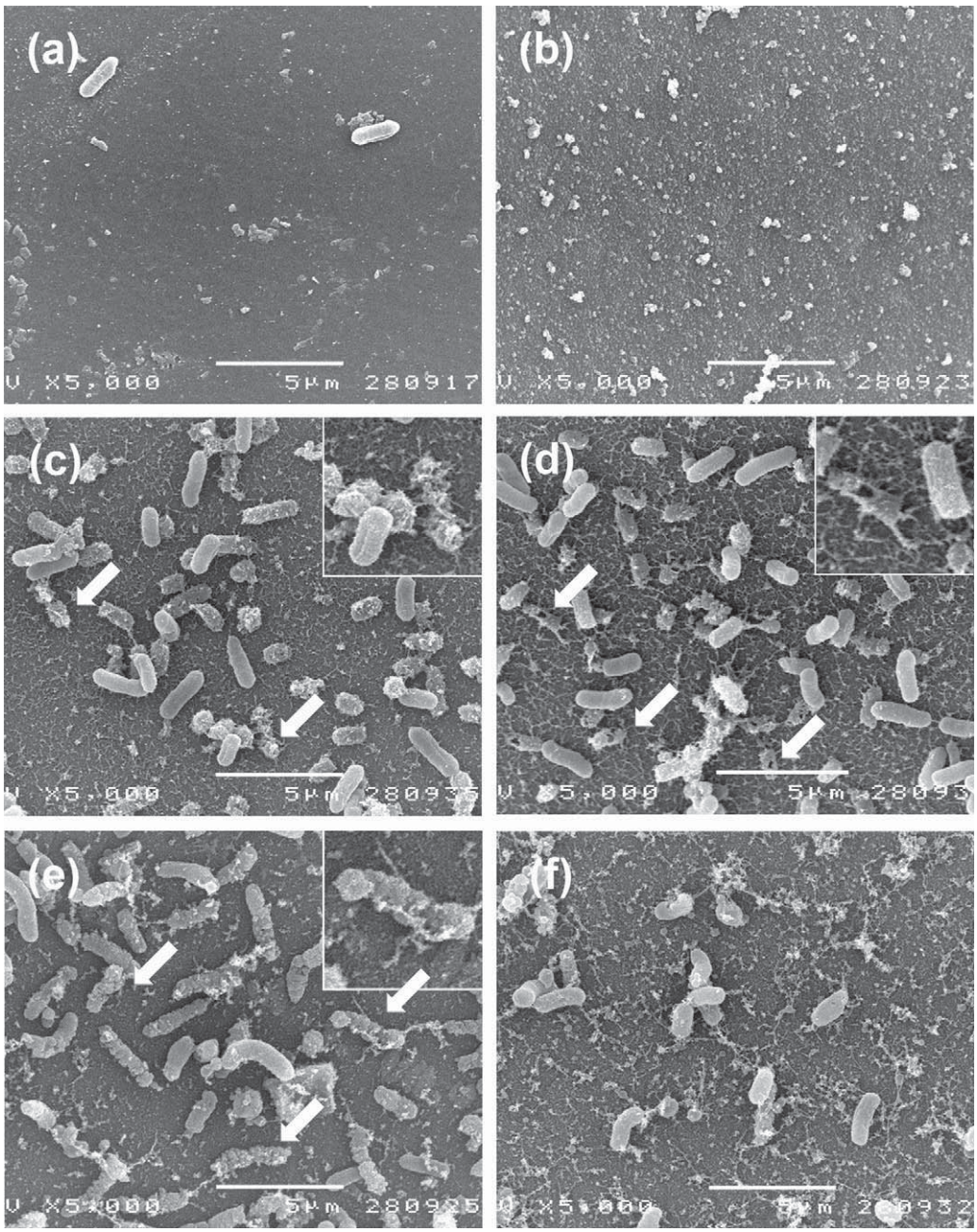

Fig. 7. SEM micrographs of the (a) chitosan, (b) 0.4QBzCS, (c) 0.8QBzCS, (d) 1.2QBzCS, (e) 1.6QBzCS, and (f) 2.0QBzCS chitosan films after being incubated with the suspension of *E. coli* (OD_{600} = 0.5) for 24 h. Micrographs shown are representative of at least 5 such fields of view per sample and 3 independent samples.

4. Conclusions

Quaternized *N*-alkyl chitosan films/particles having different alkyl substituents were successfully prepared. Conventional antibacterial test based on total viable plate counts, as well as microscopic evidences obtained from SEM analysis, support that all surface-modified chitosan samples exhibited greater antibacterial activity against *S. aureus* (Gram-positive bacteria) and *E. coli* (Gram-negative bacteria) than the virgin chitosan surface at neutral pH. The additional positive charges introduced by surface quaternization apparently made the chitosan films more antibacterial. The ability to fine tune the antibacterial activity of the chitosan surface by controlling the degree of quaternization which can readily be varied as a function of CH_3I concentration, renders the heterogeneous quaternization a powerful route for enhancing the antibacterial efficacy of chitosan. This is particularly desirable considering that the process can be done simply on the pre-fabricated solid form of chitosan without the need for a tedious purification process. These surface-quaternized chitosan films/particles should potentially be useful for many technologically important applications requiring antibacterial activity.

Acknowledgements

This research is supported financially by Research Team Promotion Grant from the Thailand Research Fund (RTA47800004). The authors are indebted to Associate Professor Sanong Ekgasit of Chulalongkorn University for the access to the ATR-FTIR facility. Contact angle goniometer provided by the National Metal and Materials Technology Center (MTEC) is gratefully acknowledged.

The authors appreciated a language editing service provided by Dr. Robert Butcher, the Publication Counselling Unit (PCU), Faculty of Science, Chulalongkorn University.

Appendix A. Supplementary data

Supplementary data associated with this article can be found, in the online version, at doi:10.1016/j.carbpol.2010.08.075.

References

Alves, N. M., & Mano, J. F. (2008). Chitosan derivatives obtained by chemical modifications for biomedical and environmental applications. *International Journal of Biological Macromolecules*, *43*(5), 401–414.

Amornchai, W., Hoven, V. P., & Tangpasuthadol, V. (2004). Surface modification of chitosan films-grafting ethylene glycol oligomer and its effect on protein adsorption. *Macromolecular Symposia*, *216*, 99–107.

Badawy, M. E. I. (2010). Structure and antimicrobial activity relationship of quaternary *N*-alkyl chitosan derivatives against some plant pathogens. *Journal of Applied Polymer Science*, *117*(2), 960–969.

Campaniello, D., Bevilacqua, A., Sinigaglia, M., & Corbo, M. R. (2008). Chitosan: Antimicrobial activity and potential applications for preserving minimally processed strawberries. *Food Microbiology*, *25*(8), 992–1000.

Choi, B. K., Kim, K. Y., Yoo, Y. J., Oh, S. J., Choi, J. H., & Kim, C. Y. (2001). In vitro antimicrobial activity of a chitooligosaccharide mixture against *Actinobacillus actinomycetemcomitans* and *Streptococcus mutans*. *International Journal of Antimicrobial Agents*, *18*(6), 553–557.

Chung, Y. C., Su, Y. P., Chen, C. C., Jia, G., Wang, H. I., Wu, J. C. G., et al. (2004). Relationship between antibacterial activity of chitosan and surface characteristics of cell wall. *Acta Pharmacologica Sinica*, *25*(7), 932–936.

Cuero, R. G., Osuji, G., & Washington, A. (1991). *N*-Carboxymethylchitosan inhibition of aflatoxin production: Role of zinc. *Biotechnology Letters*, *13*(6), 441–444.

Devlieghere, F., Vermeulen, A., & Debevere, J. (2004). Chitosan: Antimicrobial activity, interactions with food components and applicability as a coating on fruit and vegetables. *Food Microbiology*, *21*(6), 703–714.

Domard, A., Rinaudo, M., & Terrassin, C. (1986). New method for the quaternization of chitosan. *International Journal of Biological Macromolecules*, *8*(2), 105–107.

Eaton, P., Fernandes, J. C., Pereira, E., Pintado, M. E., & Malcata, F. X. (2008). Atomic force microscopy study of the antibacterial effects of chitosans on *Escherichia coli* and *Staphylococcus aureus*. *Ultramicroscopy*, *108*(10), 1128–1134.

Fernandez-Saiz, P., Lagaron, J. M., & Ocio, M. J. (2009). Optimization of the biocide properties of chitosan for its application in the design of active films of interest in the food area. *Food Hydrocolloids*, *23*(3), 913–921.

Fujimoto, T., Tsuchiya, Y., Terao, M., Nakamura, K., & Yamamoto, M. (2006). Antibacterial effects of chitosan solutions® against *Legionella pneumophila*, *Escherichia coli*, and *Staphylococcus aureus*. *International Journal of Food Microbiology*, *112*(2), 96–101.

Gorbach, V. I., Krasikova, I. N., Lukyanov, P. A., Loenko, Y. N., Soloveva, T. F., Ovodov, Y. S., et al. (1994). New glycolipids (chitooligosaccharide derivatives) possessing immunostimulating and antitumor activities. *Carbohydrate Research*, *260*(1), 73–82.

Hoven, V. P., Tangpasuthadol, V., Angkitpaiboon, Y., Vallapa, N., & Kiatkamjornwong, S. (2007). Surface-charged chitosan: Preparation and protein adsorption. *Carbohydrate Polymers*, *68*(1), 44–53.

Kim, C. H., & Choi, K. S. (2002). Synthesis and antibacterial activity of quaternized chitosan derivatives having different methylene spacers. *Journal of Industrial and Engineering Chemistry*, *8*(1), 71–76.

Kong, M., Chen, X. G., Liu, C. S., Liu, C. G., Meng, X. H., & Yu, L. J. (2008). Antibacterial mechanism of chitosan microspheres in a solid dispersing system against *E. coli*. *Colloids and Surfaces B: Biointerfaces*, *65*(2), 197–202.

Lim, S. H., & Hudson, S. M. (2004). Synthesis and antimicrobial activity of a water-soluble chitosan derivative with a fiber-reactive group. *Carbohydrate Research*, *339*(2), 313–319.

Mourya, V. K., & Inamdar, N. N. (2009). Trimethyl chitosan and its applications in drug delivery. *Journal of Materials Science: Materials in Medicine*, *20*(5), 1057–1079.

Muzzarelli, R. A. A., & Tanfani, F. (1985). The *N*-permethylation of chitosan and the preparation of *N*-trimethyl chitosan iodide. *Carbohydrate Polymers*, *5*(4), 297–307.

Ong, S. Y., Wu, J., Moochhala, S. M., Tan, M. H., & Lu, J. (2008). Development of a chitosan-based wound dressing with improved hemostatic and antimicrobial properties. *Biomaterials*, *29*(32), 4323–4332.

Polnok, A., Borchard, G., Verhoef, J. C., Sarisuta, N., & Junginger, H. E. (2004). Influence of methylation process on the degree of quaternization of *N*-trimethyl chitosan chloride. *European Journal of Pharmaceutics and Biopharmaceutics*, *57*(1), 77–83.

Qi, L. F., Xu, Z. R., Jiang, X., Hu, C. H., & Zou, X. F. (2004). Preparation and antibacterial activity of chitosan nanoparticles. *Carbohydrate Research*, *339*(16), 2693–2700.

Raafat, D., von Bargen, K., Haas, A., & Sahl, H.-G. (2008). Insights into the mode of action of chitosan as an antibacterial compound. *Applied and Environmental Microbiology*, *74*(12), 3764–3773.

Rabea, E. I., Badawy, M. E. T., Stevens, C. V., Smagghe, G., & Steurbaut, W. (2003). Chitosan as antimicrobial agent: Applications and mode of action. *Biomacromolecules*, *4*(6), 1457–1465.

Sajomsang, W. (2010). Synthetic methods and applications of chitosan containing pyridylmethyl moiety and its quaternized derivatives: A review. *Carbohydrate Polymers*, *80*(3), 631–647.

Sajomsang, W., Gonil, P., & Saesoo, S. (2009). Synthesis and antibacterial activity of methylated *N*-(4-*N*,*N*-dimethylaminocinnamyl) chitosan chloride. *European Polymer Journal*, *45*(8), 2319–2328.

Seong, H. S., Whang, H. S., & Ko, S. W. (2000). Synthesis of a quaternary ammonium derivative of chito-oligosaccharide as antimicrobial agent for cellulosic fibers. *Journal of Applied Polymer Science*, *76*(14), 2009–2015.

Sun, L. P., Du, Y. M., Fan, L. H., Chen, X., & Yang, J. H. (2006). Preparation, characterization and antimicrobial activity of quaternized carboxymethyl chitosan and application as pulp-cap. *Polymer*, *47*(6), 1796–1804.

Suzuki, K., Oda, D., Shinobu, T., Saimoto, H., & Shigemasa, Y. (2000). New selectively *N*-substituted quaternary ammonium chitosan derivatives. *Polymer Journal*, *32*(4), 334–338.

Talaro, K. P. (2005). *Foundations in microbiology*. New York: McGraw-Hill.

Tangpasuthadol, V., Pongchaisirikul, N., & Hoven, V. P. (2003). Surface modification of chitosan films: Effects of hydrophobicity on protein adsorption. *Carbohydrate Research*, *338*(9), 937–942.

Ye, X. L., Li, X. G., Yuan, L. J., Ge, L. H., Zhang, B. S., & Zhou, S. B. (2007). Interaction of houttuyfonate homologues with the cell membrane of gram-positive and gram-negative bacteria. *Colloids and Surfaces A: Physicochemical and Engineering Aspects*, *301*(1–3), 412–418.

Synthesis of Acrylamide/Acrylic Acid-Based Aluminum Flocculant for Dye Reduction and Textile Wastewater Treatment

Supaporn Noppakundilograt,[1] Praon Nanakorn,[2] Wanida Jinsart,[3] Suda Kiatkamjornwong[1]
[1] *Department of Imaging and Printing Technology, Faculty of Science, Chulalongkorn University, Bangkok 10330, Thailand*

[2] *Program of Petrochemistry and Polymer Science, Faculty of Science, Chulalongkorn University, Bangkok 10330, Thailand*

[3] *Department of General Science, Faculty of Science, Chulalongkorn University, Bangkok 10330, Thailand*

Aluminum hydroxide-poly[acrylamide-*co*-(acrylic acid)], AHAMAA, was synthesized with a redox initiator by solution polymerization in which the effects of reactant contents were optimized. The effects of pH, temperature, and initial dye concentration on Congo red reduction were investigated. A mixture of Congo red and direct blue 71, and the composite textile dye wastewater were investigated. Adsorptions of both dyes were more effective in the nonbuffered solution than those in the buffered solution, and Congo red adsorbed more than direct blue 71 at all pHs. The adsorption of Congo red increased with increasing temperature and its initial concentration. Both dyes obeyed the Freundlich adsorption isotherm. The maximum adsorptions in 100 mg dm^{-3} solution were 109 $\pm$ 0.5 mg g^{-1} and 62 $\pm$ 6.6 mg g^{-1} for Congo red and direct blue 71, respectively. At 150 mg dm^{-3} of the mixed Congo red and direct blue 71, the adsorption was 142 $\pm$ 2 mg g^{-1} by 643 $\pm$ 3 mg dm^{-3} AHAMAA. The 40 mg g^{-1} dyes of the textile effluent wastewater were adsorbed by 500 mg dm^{-3} AHAMAA. AHAMAA could decrease turbidity of the composite wastewater containing a mixture of reactive and direct dyes from 405 to 23 NTU. POLYM. ENG. SCI., 50:1535–1546, 2010.
© 2010 Society of Plastics Engineers

INTRODUCTION

Wastewater from the textile dyeing and finishing industries is often polluted by azo dyes which can decompose to hazardous aromatic amines that are highly carcinogenic. These potent pollutants are highly toxic to organisms and cause skin irritation, cancer, and mutation of aquatic organisms and humans [1, 2]. Therefore, it is mandated to remove those hazardous chemicals before discharging the wastewater into natural water sources [3–6].

Congo red, C.I. 22120, is a hazardous azo dye [7], and its use in many countries is prohibited but in those where it is allowed it has gained favor for textile dyeing especially in silk due to its vivid, bright, and striking color. However, it is difficult to degrade, making its disposal from wastewater which is a severe problem. Attempts to remove Congo red from wastewater by several kinds of absorbents, such as activated carbon [8], fly ash [9], chitosan [10], acid activated red mud [11], and electrocoagulated metal hydroxide sludge [12] have been reported. Some low-cost absorbents have typically attained a low adsorption capacity. Direct blue 71, C.I. 34140, having a slightly larger structure than Congo red, it is also widely used in the textile industry but in contrast to Congo red, there have been a few research work reporting its adsorption isotherm [13, 14].

Anionic polymeric flocculant hydrogels have been reported to be able to remove cationic dyes [15] but not for anionic dyes such as Congo red [16]. In general, the usage of polymeric flocculants could decrease the consumption of alum or aluminum complex and may be an alternative method for solving the problematic Alzheimer's disease in human, which is induced from the leaking aluminum ions from aluminum complex in the drinking water. Moreover, an increase in the concentration of residual Al ions in sewage sludge became a potential problem as a toxic source in water treatment processes [17–19].

Correspondence to: Suda Kiatkamjornwong; e-mail: ksuda@chula.ac.th
Contract grant sponsor: Senior Scholar Research Team Consolidation Grants (Thailand Research Fund); contract grant numbers: RTA4780004, RTA5080004.
DOI 10.1002/pen.21694
Published online in Wiley InterScience (www.interscience.wiley.com).
© 2010 Society of Plastics Engineers

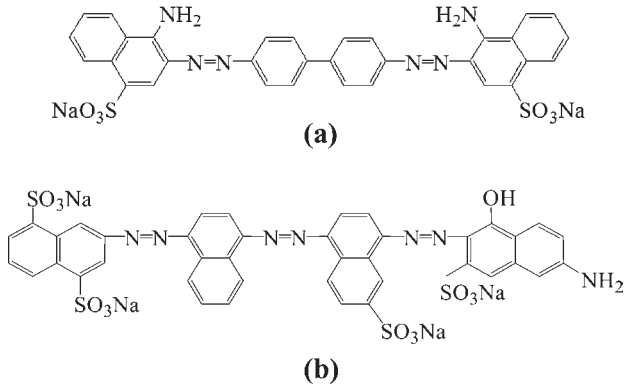

FIG. 1. The molecular structures of (a) Congo red (C.I. 21120) and (b) direct blue 71 (C.I. 34140).

However, there are still needs to have some new adsorbents for treating a wide variety of textile wastewater. The synthetic polymer of aluminum hydroxide poly[acrylamide-*co*-(acrylic acid)], AHAMAA, used for turbidity reduction in synthetic wastewater as a complex polymeric flocculant (CPF) [20] has been reported. In the research, decreases in Congo red and direct blue 71 by AHAMAA considered as a model of anionic dye in wastewater are evaluated since AHAMAA can be an alternative remedy material for the textile industry. Here we report on the synthesis and characterization of AHAMAA, the active ingredients needed for synthesizing the AHAMAA and its capacities to adsorb and decrease the dye concentrations under different pHs and initial dye concentrations. The adsorption isotherms of the two dyes by AHAMAA are studied. Decreases in color and turbidity, by AHAMAA, of the textile effluents containing mixtures of reactive, acid, and direct dyes from the two textile finishing plants are also investigated.

EXPERIMENTAL

Materials

Acrylamide (AM) was provided by Siam Chemical Industry Co. (Bangkok, Thailand). Acrylic acid (AA), *N*,*N*′-methylenebisacrylamide (N-MBA) and *N*,*N*,*N*′,*N*′-tetramethylethylenediamine (TEMED) were purchased from Fluka (Buchs, Switzerland) and used as a co-monomer, crosslinking agent, and polymeric modifier, respectively. Ammonium persulfate initiator (APS) was purchased from Merck (Hohenbrunn, Germany). Sodium carbonate and aluminum sulfate (both were AR grade) were supplied by BDH (Poole, U.K.). Congo red (molecular weight = 696.68) in Fig. 1a [11], and direct blue 71 (molecular weight = 965.94) in Fig. 1b [13], were purchased from Fluka (Buchs, Switzerland) and Sigma-Aldrich (St. Louis, USA), respectively. Deionized water was processed by Elga Deionizer (Model LA611, Buckinghamshire, U.K.). Composite mixtures of reactive dyes, direct dyes, and acid dyes from the textile dyeing and finishing effluents were supplied from two volunteer factories.

Synthesis of Aluminum Hydroxide Suspension

A suspension of $Al(OH)_3$ was prepared by slowly dropping 22.5 cm^3 of 0.2 M sodium carbonate into 20 cm^3 of 0.1 M aluminum sulfate at a constant rate with stirring at room temperature. The $Al(OH)_3$ suspension was then used as it was.

Synthesis of Polymeric Flocculants of Aluminum hydroxide-poly[acrylamide-(acrylic acid)] (AHAMAA)

AHAMAA was synthesized by the polymerization of AM and AA in the presence of the $Al(OH)_3$ suspension. AM and AA were added to a 500-cm^3 four-necked round-bottomed reaction flask containing the newly prepared $Al(OH)_3$ suspension. This reaction flask was equipped with a mechanical stirrer, a condenser, and an inlet tube for nitrogen gas feed, and it was then immersed in a water bath at a controlled temperature of 45°C ± 2°C. The mixture was stirred with a small bladed propeller at 250 rpm under a constant nitrogen gas atmosphere fed through the gas inlet tube for 30 min. The crosslinking agent (N-MBA), initiator (APS), and TEMED were subsequently added (see Table 1) and stirred for another 30 min. The copolymer was filtered, dehydrated with acetone, cut into small pieces of ~1 cm × 1 cm, and dried in a vacuum oven at 50°C for 24 h to a constant weight. The dried samples were then milled and sieved through a 100-mesh sieve. Existence of the synthesized polymers was identified by Fourier Transform Infrared Spectroscopy (FTIR, model Nicolet Impact 410, Madison, WI), and ^{27}Al nuclear magnetic resonance (^{27}Al-NMR, model Unity Inova-500, Palo Alto, CA). The ^{27}Al-NMR measurement was performed in a solid state method and the frequency of ^{27}Al was at 130 MHz. The sample powder was put in a cylindrical sample cell (0.64 cm diameter and 2.0 cm height) and it was then measured at 26°C. The measurement conditions were set as follows: relaxation delay was 1.000 s (first pulse at 58.5° and the second pulse at 9.0°), acquisition time was 0.006 s, and a total time was 16 min 15 s.

TABLE 1. The synthesis parameters of AHAMAA.

Reactants	Quantity
Acrylamide: acrylic acid ($\times 10^{-3}$ mol)	98:2, 96:4, 94:6, 92:8, 90:10
N-MBA ($\times 10^{-4}$ mol)	1.2, 2.3, 4.6, 9.2
APS ($\times 10^{-4}$ mol)	0.8, 1.6, 3.1, 6.2
TEMED ($\times 10^{-4}$ mol)	1.5, 3.0, 6.0, 12.0
Synthesized $Al(OH)_3$ suspension (cm^3)	42.5

DOI 10.1002/pen

Stability of AHAMAA in Water

Stability of the AHAMAA in water was performed by determining the leaching aluminum ion concentration from its complex. Portions of the dry AHAMAA polymer composite material weighing 0.04 g were added into 200 cm^3 of deionized water and kept covered at room temperature for 15, 30, 45, and 60 days. The swollen material was filtered through a 100-mesh aluminum screen sieve. The filtrate was then collected and the aluminum ion concentration in the filtrate was determined by the ICP-AES (PerkinElmer model PLASMA-1000, Waltham, MA).

Effect of the Reactant Contents on Dye Reduction of AHAMAA

The effects of the AM:AA, N-MBA, APS, and TEMED contents on the efficiency of the resultant AHAMAA polymer to decrease Congo red were investigated at room temperature and pH 5. A 50 cm^3 solution containing 24 mg dm^{-3} of Congo red was added to 0.03 g of the dry AHAMAA powder and they were allowed to swell for 24 h. The swollen material was then filtered through a 100-mesh aluminum screen sieve at ambient temperature. The filtrate absorption was measured by a UV–visible spectrophotometer (UV-2550, Shimadzu, Tokyo, Japan) at a wavelength of 497 nm and the amount of the decreased dye expressed as dye removal can be calculated from *Eq. 1*:

$$\%\text{Dye removal} = \frac{C_i - C_e}{C_i} \times 100 \quad (1)$$

where C_i is the initial dye concentration and C_e is the equilibrium dye concentration.

Evaluation of the equilibrium water absorbency of each AHAMAA polymer was carried out using the deionized water at room temperature in a closed system. The deionized water (200 cm^3) was added to 0.1 g of dry AHAMAA, which was then allowed to reach equilibrium swelling for 24 h. The swollen material was then filtered through a 100-mesh aluminum sieve screen for 2 h. The water absorbency was then obtained from the increased weight in the cross-linked AHAMAA and was recorded as water absorbency (Q) expressed as a weight ratio of the absorbed water in the polymer over the dry polymer, calculated from *Eq. 2*:

$$\text{Water absorbency}\,(Q) = (W_s - W_d)/W_d \quad (2)$$

where W_d is the weight of dry AHAMAA (g), and W_s is the weight of the equilibrium swollen material (g). The resultant water absorption is the average of three replications with one standard deviation.

Effect of pH upon Dye Adsorption by AHAMAA

The AHAMAA polymer was prepared from AM, AA, N-MBA, APS and TEMED contents at 96 $\times$ 10^{-3}, 4 $\times$ 10^{-3}, 2.3 $\times$ 10^{-4}, 1.6 $\times$ 10^{-4}, and 12 $\times$ 10^{-4} mol, respectively. The dye adsorption was tested at room temperature using 50 cm^3 solution containing 50 mg dm^{-3} of Congo red or direct blue 71 in 0.3 g dry weight of the polymer material in the two systems. The first system is the nonbuffered solution where pH of the dye solution was adjusted to within the range of 5–11 by using 0.1 M HCl or 0.1 M NaOH. The buffered solution as the second system in which pH of the dye solution was adjusted with a buffer solution consisting of a mixture of 0.2 M boric acid, 0.05 M citric acid, and 0.1 M tri-sodium phosphate, and the pH was maintained in the same range as those in the nonbuffered system [21]. The absorption was measured by the same UV–visible spectrophotometer (UV-2550, Shimadzu, Tokyo, Japan) at their maximum absorptions at 497 nm and 587 nm for Congo red and direct blue 71, respectively.

Effect of Temperature upon Dye Adsorption by AHAMAA

The effect of solution temperature on the decrease of Congo red by AHAMAA was studied at 35, 40, and 50°C using 50 cm^3 of the dye solution containing 100 mg dm^{-3} of Congo red at pH 7 in the nonbuffered system.

Effect of the Initial Dye Concentration

The effect of the initial dye concentration on Congo red reduction was evaluated using the dye solution concentrations of 24, 50, 75, and 100 mg dm^{-3} in the nonbuffered system.

Adsorption Isotherm

The dye solutions of Congo red and direct blue 71 were prepared. Each solution was measured by the same UV–visible spectrophotometer at their maximum absorption wavelength. The amount of the dye adsorbed was calculated from *Eq. 3*:

$$q_e = (C_0 - C_e)\frac{v}{m} \quad (3)$$

where q_e is the equilibrium amount of the dye adsorbed per unit weight of AHAMAA (mg g^{-1}), C_0 is the initial concentration of Congo red or direct blue 71 (mg dm^{-3}), C_e is the concentration of dye at equilibrium (mg dm^{-3}), v is the solution volume (dm^{-3}), and m is the mass of AHAMAA (g) [4].

A linear form of the Langmuir isotherm represents a model of monolayer adsorption on a surface containing a finite number of identical sites. This isotherm is given in *Eq. 4*:

$$\frac{C_e}{q_e} = \frac{1}{Q_{max}K_L} + \frac{C_e}{Q_{max}} \quad (4)$$

where C_e is the concentration of the dye solution (mg dm^{-3}) at equilibrium, q_e is the amount of dye adsorbed per unit weight of AHAMAA (mg g^{-1}), Q_{max} is the monolayer capacity of the adsorbent (mg g^{-1}) and K_L is the Langmuir adsorption constant (dm^3 mg^{-1}). A plot of C_e/q_e against C_e gives a linear line where the Q_{max} and K_L values are obtained from the slope and intercept, respectively.

The Freundlich isotherm reveals a multilayer adsorption model on a heterogeneous surface. This model is formulated in a linear form as shown in *Eq. 5* [22]:

$$\ln q_e = \ln K_F + \frac{1}{n} \ln C_e \quad (5)$$

where C_e is the concentration of dye solution (mg dm^{-3}) at equilibrium, K_F is the adsorption capacity representing a quantity of dye adsorbed onto adsorbent (mg g^{-1}) and n is an empirical parameter representing a heterogeneity factor for measuring the deviation from linearity of the adsorption between solution concentration and adsorption. A plot of ln q_e versus ln C_e gives n and K_F values from the slope and intercept, respectively.

Wastewater Treatment

The decreases in color and turbidity were investigated by AHAMAA from textile wastewater provided by the two textile factories. The sample from the Factory A, named as sample A, contained a mixture of reactive and direct dyes, whereas the sample from the Factory B was mainly acid dye, named as sample B1, and a mixture of disperse and acid dyes, named as sample B2. A synthetic wastewater was also prepared from a mixture of 75 mg dm^{-3} Congo red and 75 mg dm^{-3} direct blue 71 as a model dye wastewater for the quantitative analysis of the color.

The amount of 500 mg dm^{-3} AHAMAA was added into 500 cm^3 of each wastewater sample from which the solution pH was adjusted to 7. It was stirred at 120 rpm for 3 min and at 30 rpm for 30 min. It was then filtered and the color and turbidity of the filtrate were measured. Turbidity of the textile wastewater was measured by a portable turbidity meter (model 2100P, Hach, Loveland, CO). The decrease in turbidity by AHAMAA was calculated from the turbidity before and after the AHAMAA addition.

The decrease in color by AHAMAA for the wastewater treatment was measured using a simple spectrophotometric technique. The filtrate was measured at its maximum absorbance wavelength. The dye concentrations were measured before and after the AHAMAA addition.

The absorption spectral data of the wastewater samples were recorded from 200 to 700 nm. For a quantitative analysis, a calibration curve of the mixture of model dye concentration (mg dm^{-3}) against the absorbance at the λ_{max} of 519 nm was plotted. The dye concentrations were quantified according to the calibration curve of the mixed model dye. Then the decrease in relative dye concentration of the textile wastewater was calculated.

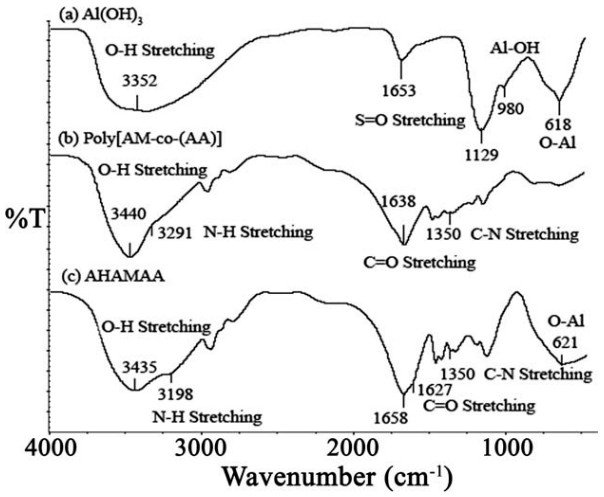

FIG. 2. FTIR spectra of (a) $Al(OH)_3$, (b) poly[AM-*co*-(AA)], and (c) AHAMAA.

RESULTS AND DISCUSSION

Characterization of Functional Groups by FTIR Spectroscopy

The FTIR spectra of the synthesized $Al(OH)_3$ and AHAMAA are shown in Fig. 2 in which $Al(OH)_3$ in spectrum (a) shows a peak of —OH stretching at 3352 cm^{-1} indicating the presence of the hydroxide group. In addition, it also shows the peaks of Al—OH and O—Al at 980 and 618 cm^{-1}, respectively. The strong and broad absorption band centered at 618 cm^{-1} is probably resulted from the combined absorptions of sulfate, the Al—O stretching vibrations and the Al—OH wagging vibration mode of molecular water [23]. This result strongly supports that the hydrolysis product of the aluminum sulfate was aluminum hydroxide, and the absorption peaks at 1129 and 1653 cm^{-1} are the sulfate group of residual aluminum sulfate within the $Al(OH)_3$ suspension [24]. The IR spectrum (b) of poly[AM-*co*-AA] shows the peaks of O—H stretching and C=O stretching of carboxylic acid group at 3440 and 1638 cm^{-1}, respectively. Moreover, it shows the peaks of N—H stretching and C—N stretching of carboxamide group at 3291 and 1350 cm^{-1}, respectively. The spectrum (c) (see Fig. 2) of AHAMAA shows evidence of the coordination between the carboxylate anion and aluminum ion at the strong absorption peak of 1658 cm^{-1}, indicating a complex formation of the poly[AM-*co*-AA] and $Al(OH)_3$ [23]. This result also supports the presence of the carboxylic acid group (3435 and 1627 cm^{-1}) and carboxamide group (3198 and 1350 cm^{-1}) in the three-dimensional crosslinked structure of the copolymer.

 DOI 10.1002/pen

Characterization of $Al(OH)_3$ and AHAMAA by ^{27}Al-NMR

Figure 3 indicates the form of $Al(OH)_3$, and the coordination of the aluminum ions from the ^{27}Al-NMR signals. There is one signal at 9.132 ppm designated for $Al(OH)_3$ in spectrum (a) which indicates that $Al(OH)_3$ was the monomeric species because its signal appears near 0 ppm [25]. On the other hand, the AHAMAA gave the signal at 8.008 ppm of peak (b). It confirms that the aluminum atoms in AHAMAA were mostly in an octahedral coordination [26]. A possible structure of AHAMAA is postulated in Fig. 4.

Stability of the AHAMAA in Water

The amount of aluminum ions leached from AHAMAA in deionized water was found to be in the range of 0.09–0.2 mg dm^{-3} regardless of the soaking time (15–60 days), which suggests that the stability of the aluminum ions in the AHAMAA is high. Under these conditions, the free aluminum ion concentration remained in the treated water is not likely to be harmful to fish, plant, or human health. For example, the aluminum ions in natural groundwater are found from 0.4 mg dm^{-3} to 5 mg dm^{-3} in acidic soils, and the maximum contaminant level of aluminum ions in the human body is not higher than 0.2 mg dm^{-3} [27]. Indeed, the highest stringent amount that is limited by WHO for aluminum ions in human drinking water is as high as 0.2 mg dm^{-3}. Thus, the AHAMAA seems to be quite stable and is safe to be used as a sorbent in aqueous solution to decrease Congo red or direct blue 71 before discharging the treated water to natural water resources.

Dye Decreasing Efficiency

Congo red was used a model to investigate the dye decreasing efficiency of AHAMAA. Considering the molecular structure of Congo red (Fig. 1a) and AHAMAA (see Fig. 3), there are several active points, namely the amino and azo groups, which can interact with the carboxylic acid groups of AHAMAA. To achieve the optimized performance of AHAMAA in decreasing the dye content, the comonomer is a key factor. Other important factors for the dye adsorption are dye permeability, the extent of contact surface and interaction between the dye and the adsorbent via carboxylic acid and aluminum ion. Water absorption can be one of the indicators for the dye molecules to access and permeate into the adsorbent.

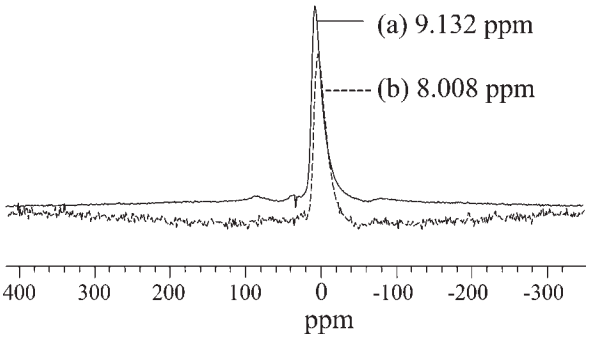

FIG. 3. The ^{27}Al-NMR spectra of (a) $Al(OH)_3$ and (b) AHAMAA synthesized with 4×10^{-3} mol AA, 2.3×10^{-4} mol N-MBA, 1.6×10^{-4} mol APS, and 12×10^{-4} mol TEMED.

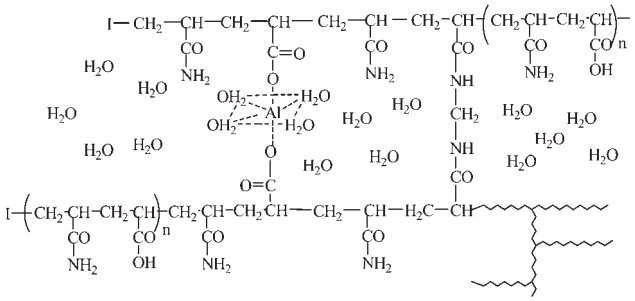

FIG. 4. The structure of AHAMAA.

Effects of Reactant Contents in AHAMAA Polymerization on Decreasing Congo Red Content

Monomer Contents. Basically, Congo red is a dipolar molecule which exists in a cationic form with positively charged azo ($—N{=}N^+—H$) and amino ($—N^+H_2$) groups at pH 5 [8]. Thus, subjecting to the solution pH relative to the dye and the AHAMAA respective p*K*a values, AHAMAA can remove Congo red through the ionic interactions between the negatively charged carboxylate anion of AHAMAA and the positively charged azo or amino groups of Congo red [4]. The efficiency of Congo red reduction (q_e) by the crosslinked AHAMAA synthesized with different contents of AA and N-MBA are illustrated in Fig. 5. The Congo red reduction efficiency increased with increasing the AA content, which is likely to be due to the increasing amount of the resultant carboxylate anions, leading to more ion–ion interactions between AHAMAA and Congo red. In addition, a twofold increase in the AA content also caused water absorbency to increase by 1.3-folds due to increases in hydrophilicity of the polymer chains with increasing levels of the carboxylate anions [28]. The higher the repulsion between carboxylate groups in crosslinked polymer chains, the greater the water absorbency [29]. The highest water absorbency was achieved when the AA content was 4×10^{-3} mol and declined slightly afterward but not significantly with further increases in AA contents (Fig. 5a). This could be caused by a complex formation between the carboxylate anions and the aluminum cations, similarly to another type of crosslinking reaction, to yield a more rigid chain structure. Moreover, this complex structure can certainly decrease the anionic repulsion, which lowers the water absorption [30, 31]. Likewise, the formation of complex along with the decreased amount of free carboxylate anions in AHAMAA may account for the lower Congo

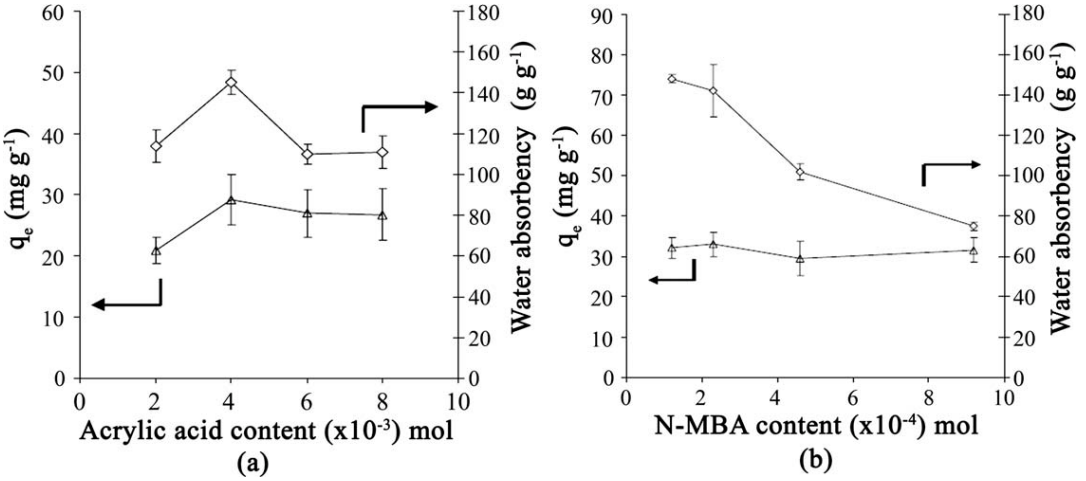

FIG. 5. Effect of the acrylic acid and N-MBA contents on Congo red adsorption efficiency and water absorbency of AHAMAA synthesized by 3.2×10^{-4} mol APS, 12×10^{-4} mol TEMED, 250 rpm, at 45°C and 1 h polymerization time with: (a) 4.6×10^{-4} mol N-MBA with varied contents of AA and (b) 4×10^{-3} mol AA with varied contents of N-MBA.

red reduction efficiency by AHAMAA polymers synthesized with the higher amounts of AA. Thus, when all other conditions remain constant, the Congo red reduction efficiency by AHAMAA was optimal when the AA amount was 4×10^{-3} mol.

Since the crosslinked AHAMAA may principally remove Congo red via the contributions of the negatively charged carboxylate group, any positive effect on decreasing Congo red content could not be expected when increasing the amount of N-MBA. Changing the N-MBA contents did not impose any significant effect on the dye reduction efficiency of AHAMAA (Fig. 5b) because N-MBA is a crosslinking agent, which affects only the double bonds in the network structure but not the number of cations or anions on the polymeric backbone. However, the increasing N-MBA levels did decrease the water absorbency of the resultant AHAMAA polymer (Fig. 5b). This is because increasing rigidity of the crosslinked chains [32] is in a sense analogous to that with AA contents higher than 4×10^{-3} mol as discussed above. From these findings, 4×10^{-3} mol of AA and 2.3×10^{-4} mol of N-MBA were selected to synthesize AHAMAA to investigate the effect of APS content on decreasing Congo red content.

Effect of Initiator and TEMED Contents. In the redox initiated polymerization by APS and TEMED, TEMED is normally the coinitiator or starter to induce the decomposition of the APS initiator. The role of APS is to generate free radicals to control the length of polymer chains, which affects the water absorbency. The water absorbency was low when using low contents of APS in the polymerization (Fig. 6a) because a few radicals were generated and led to short polymer chains having a few carboxylate anions to induce low anionic repulsions. However, increasing the APS level by twofold to 1.6×10^{-4} mol yielded a 10% increase in water absorbency. Further increase in AA contents decreased the water absorption gradually and markedly by 30% at further increases in APS content. Basically, an abundance of radicals was generated at the higher APS contents resulting in the formation of too many short polymer chains in the AHAMAA. The chains can swell less due to the lower chain flexibility and the less repulsion caused by the smaller number of carboxylate groups [32]. Surprisingly, increasing APS contents did not increase Congo red reduction efficiency at all (Fig. 6a), which may be caused by the limited amount of ions in the polymer chains. However, 4×10^{-3} mol of AA, 2.3×10^{-4} mol of N-MBA, and 1.6×10^{-4} mol of APS were selected to synthesize AHAMAA to investigate the effect of TEMED content on dye decreasing efficiency of AHAMAA.

The water absorbency increased markedly with increasing TEMED concentrations in the polymerization reaction (Fig. 6b). In the APS/TEMED initiation, the free radicals $[(CH_3)_2NCH_2CH_2(CH_3)N^{\cdot}CH_2)]$ and $(^{\cdot}OSO_3H)$ are both responsible for the initiation of vinyl polymerization [33]; thus, TEMED accelerates free radical production rates resulting in longer and more flexible polymer chains. The lower the TEMED content, the lower the water absorption (Fig. 6b). The highest Congo red reduction efficiency by AHAMAA polymers was observed at 91% (36 mg g^{-1}) when TEMED content used was 12×10^{-4} mol. The low TEMED content at 1.5×10^{-4} mol can produce AHAMAA polymer that removes 25 mg g^{-1} of Congo red, despite its low water absorption (27 ± 2 g g^{-1}). The decrease in dye content depends more or less upon water absorption because water is a medium, where dye is dissolved, diffused, and transported to the AHAMAA gel.

It is necessary to mention that TEMED is a strong base having a pH value of 11. This implies that TEMED can hydrolyze the carboxamide in acrylamide moiety to give

 DOI 10.1002/pen

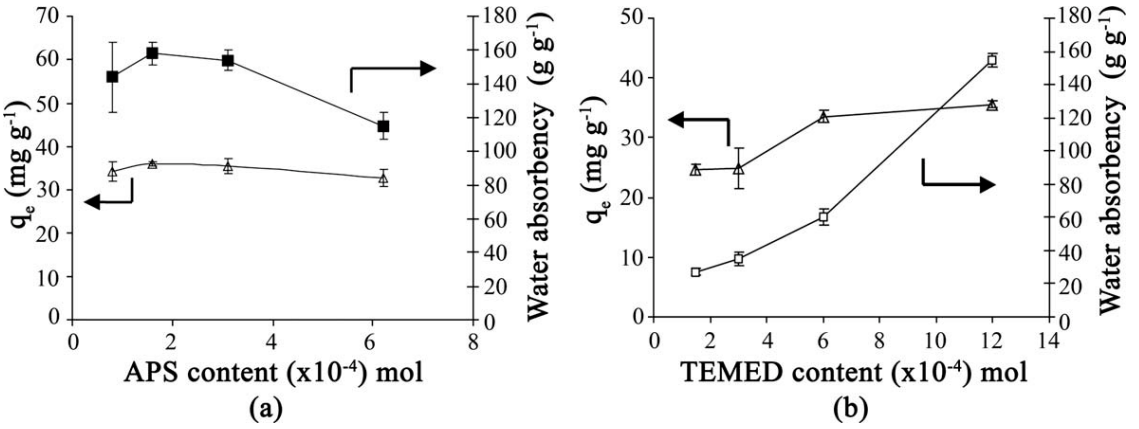

FIG. 6. Effect of the initiator and TEMED contents on Congo red adsorption efficiency and water absorbency of AHAMAA synthesized by 4×10^{-3} mol AA, 2.3×10^{-4} mol N-MBA, 250 rpm, at 45°C and 1 h polymerization time with: (a) 12×10^{-4} mol TEMED with varied contents of APS and (b) 1.6×10^{-4} mol APS with varied contents of TEMED.

the carboxylate group which is the functionality in acrylic acid. Such a hydrolysis at the solution temperature of 45°C which is similar to the NaOH saponification of polyacrylamide could be another attribute to the higher water absorption when higher concentrations of TEMED are used.

Effect of pH on Dye Reduction by AHAMAA Polymer

In a Low Ion Content, the Nonbuffered System. Congo red has a propensity to form ribbon-like micellar mesophases in water solution [34], and is pH dependence (p*K*a of the azo, sulfonate, and amine functional groups). The molecular form of Congo red in a solution medium changed markedly in the pH range of 3–5, and at a high alkaline pH of 12, e.g., the color of Congo red changes from dark blue at pH 3–5 to red at pH 12 from the original red in a solid form [11]. Therefore, pH of the 50 mg dm^{-3} Congo red solution was adjusted to pH 5, 7, 9, or 11 with 0.1 M HCl or 0.1 M NaOH.

At pH 5, the dipolar Congo red exists in a cationic form which is positively charged at the azo (—N=N$^+$—H) and the amino (=N$^+$H$_2$) groups [8]. Thus, AHAMAA can remove Congo red from the solution by strong ionic interactions between the positive charge of the dye and the negative charge of the carboxylate groups in AHAMAA outcompeting the hydrogen bonding of water with the dye, leading to a rather highly dye decreasing level (89% ± 1%) at pH 5, as summarized in Table 2. On the other hand, at pH 7, Congo red in an anionic form is negatively charged at the sulfonate group [8], again allowing Congo red reduction by AHAMAA via ionic interactions, but this time between the aluminum ion in the complex of AHAMAA and the sulfonate anion of the dye, at an apparently higher dye removal efficiency (95% ± 1%). Further increases in pH to 9 and to 11 resulted in a predominance of deprotonated carboxylate groups of AHAMAA, leading to the repulsion between the sulfonate and carboxylate anions of the dye and AHAMAA, respectively, and a lower decreasing efficiency from 95% ± 1% at pH 7 to 43% ± 2% at pH 9 and none at all at pH 11. In addition, the aluminum ion (the cationic part) in AHAMAA might react with the hydroxide ion at the higher pH values instead of the anionic group of the dye [35], leading to a smaller deplete in the dye content.

Direct blue 71 is a triazo dye (Fig. 1b), where the azo form appears to be the predominant species in solution, and it has a tendency to form a nonaggregated state due to the four negatively charged sulfonate groups [36]. Here, AHAMAA was able to moderately deplete direct blue 71 from the solution at pH 5 (59% ± 3%) when the sulfonate groups are partially protonated and thus are weakly anionic. However, as direct blue 71 has a more sulfonate group per molecule than does Congo red, and thus the higher net charge density and repulsion from the AHAMAA carboxylate anions, the efficiency of AHAMAA in removing direct blue 71 was, of course, lower than that observed for Congo red at all pH values tested

TABLE 2. Effect of pH in the buffered and nonbuffered systems on the dye removal efficiency of the synthesized AHAMAA.[a]

	% Dye removal			
	Congo red		Direct blue 71	
pH	Buffer	Nonbuffer	Buffer	Nonbuffer
5	62 ± 2	89 ± 1	ND[b]	59 ± 3
7	13 ± 2	95 ± 1	ND[b]	43 ± 1
9	ND[b]	43 ± 2	ND[b]	35 ± 3
11	ND[b]	ND[b]	ND[b]	ND[b]

[a] Polymerization reactions were carried out with 4×10^{-3} mol AA, 2.3×10^{-4} mol N-MBA, 1.6×10^{-4} mol APS, 12×10^{-4} mol TEMED, 42.5 cm^3 Al(OH)$_3$, 250 rpm, at 45°C and 1 h polymerization.

[b] Cannot be detected.

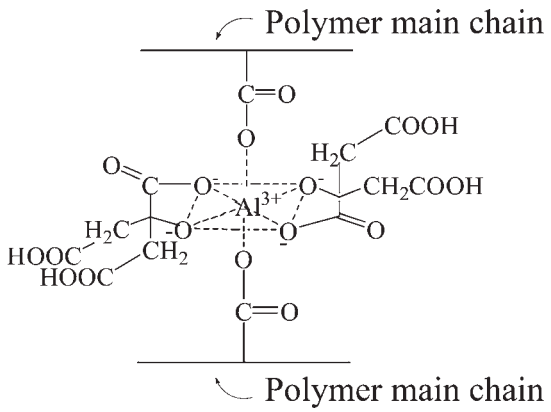

FIG. 7. A possible structure of Al-citrate complex in the buffered system.

(5, 7, 9, and 11), and especially at the higher pH values. Thus, as the pH increases to 7, 9, and 11, the direct blue 71 reduction efficiency by AHAMAA (Table 2) decreases with no detectable decrease in color at pH 11 as discussed above in the case of Congo red.

In a Relatively High Ion Content, the Buffered System. Very interestingly, the dye reduction efficiency in the nonbuffered (a low ion content) system of AHAMAA was significantly greater than that of the buffered system (relatively high ion content) at pHs 5, 7, and 9 (Table 2). This is because the low molecular weight citrate and borate anions of the buffer system created a complex formation with the aluminum ion complexes in AHAMAA [26, 37] as shown in Fig. 7, leading to a decreased ionic attraction between the aluminum cations in the AHAMAA polymer and the sulfonate anions in the dye, and thus resulted in a lower dye reduction. Moreover, the repulsion between the citrate and sulfonate anions would further decrease the dye reduction efficiency.

Effect of Temperature on Congo red Reduction by AHAMAA

The adsorption capacity of dye reduction generally depends on the temperature of the dye solution [38, 39], whilst Congo red has been reported to have a high water solubility of 50–100 g dm^{-3} at 80°C [3]. Thus, the effect of temperature on Congo red adsorption by AHAMAA was studied at 35, 40, and 50°C at pH 7 with a 100 mg dm^{-3} Congo red solution. Its adsorption capacity on AHAMAA in the nonbuffered system increased with increasing solution temperatures (Table 3) because thermal energy enhances the adsorbent to swell more and facilitates higher diffusion of Congo red molecules onto the adsorbent surface and causes more dye penetration into the internal structure of AHAMAA [40].

TABLE 3. Effect of the temperature on the Congo red removal efficiency of the synthesized AHAMAA.[a]

Temperature (°C)	Adsorption capacity (mg g^{-1})
35	109 ± 1
40	110 ± 0.3
50	118 ± 0.6

[a] Polymerization reactions were carried out with 4×10^{-3} mol AA, 2.3×10^{-4} mol N-MBA, 1.6×10^{-4} mol APS, 12×10^{-4} mol TEMED, 42.5 cm^3 $Al(OH)_3$, 250 rpm, at 45°C and 1 h polymerization time.

Effect of the Initial Dye Concentration on Congo Red Reduction

The effect of the initial Congo red concentration on dye reduction by AHAMAA at 30°C at pH 7 was investigated with four Congo red concentrations at 24, 50, 75, and 100 mg dm^{-3}. The results in Fig. 8 indicate that when the initial Congo red concentration increased from 24 to 100 mg dm^{-3}, the adsorption capacity for Congo red increased from 38 to 109 mg g^{-1}, i.e., the dye content was gradually decreased. The dose-dependent response at the low dye concentrations (0–50 mg dm^{-3}) is linear but the response declines as a linear asymptote at the higher dye concentrations (75–100 mg dm^{-3}). The higher Congo red concentrations adsorbed on the AHAMAA gel could be caused by the absorbed water as a medium to dissolve and transport the dye to the gel.

Adsorption Isotherm Analysis

The adsorption isotherms of Congo red and direct blue 71 by AHAMAA did not obey the Langmuir isotherm at all. The data (not shown here) did not fit well to the Langmuir isotherm model with nonlinearity when a plot of C_e/q_e versus C_e was constructed, and the correlation coefficient R^2 values of the lines were 0.6273 and 0.0037 for Congo red and direct blue 71, respectively. The Lang-

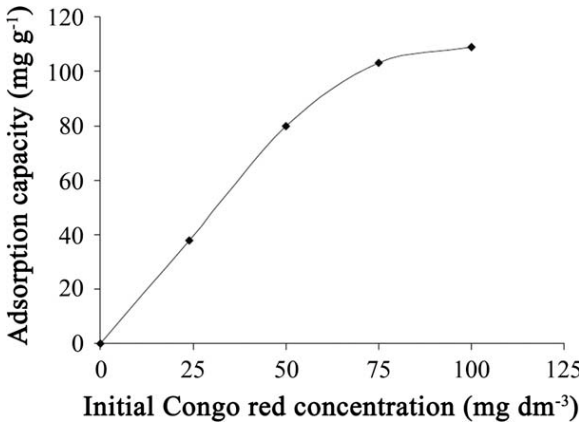

FIG. 8. Effect of the initial dye concentration on the Congo red removal by AHAMAA.

 DOI 10.1002/pen

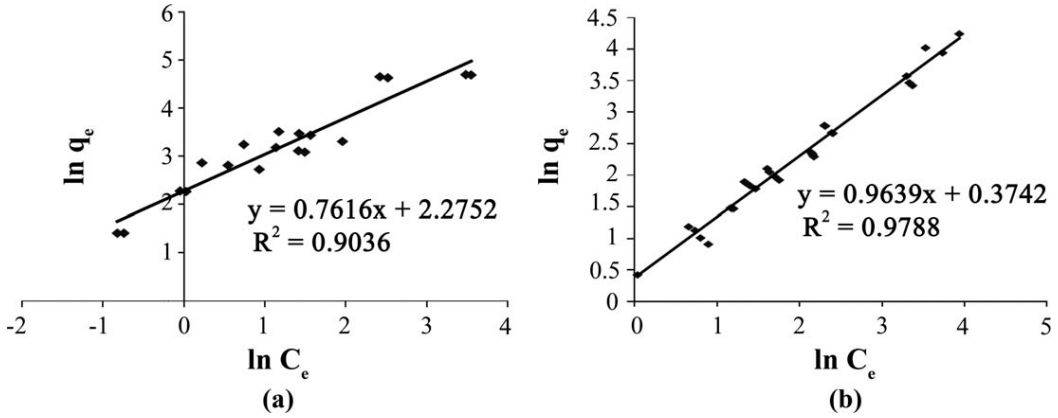

FIG. 9. Freundlich isotherm of: (a) Congo red by AHAMAA and (b) direct blue 71 by AHAMAA.

muir adsorption isotherm is only valid for adsorption of a solute from a solution as a monolayer on an adsorbent surface containing a finite number of identical sites with uniform energy of adsorption.

In contrast, the plots of ln q_e versus ln C_e (Fig. 9a and b) give a linear relationship with R^2 of 0.9036 and 0.9788 for Congo red and direct blue 71, respectively. That is, the result fits well with the Freundlich isotherm, which characterizes a multilayer adsorption model and describes the adsorption behavior on a heterogeneous surface [22]. In fact, the polyacrylamide-based hydrogel synthesized by a redox initiation is a heterogeneous gel. For Congo red and direct blue 71, the K_F values were 9.73 and 1.45, respectively, whereas the n values were 1.31 and 1.04, respectively. The n value of Congo red (1.31) is higher than unity and also higher than that of direct blue (1.04), indicates that the adsorption of Congo red favors a physical process rather than a chemical process. However, one can also state that both dye adsorptions took place by a physical process such as Van der Waal force and electrostatic force. The difference in K_F between the two dyes reflects the higher q_e value of Congo red, and that AHAMAA can adsorb more Congo red than direct blue 71. These results are in good agreement with those presented the above section in the dye reduction. The maximum dye adsorption capacities were 109 ± 0.5 mg g^{-1}

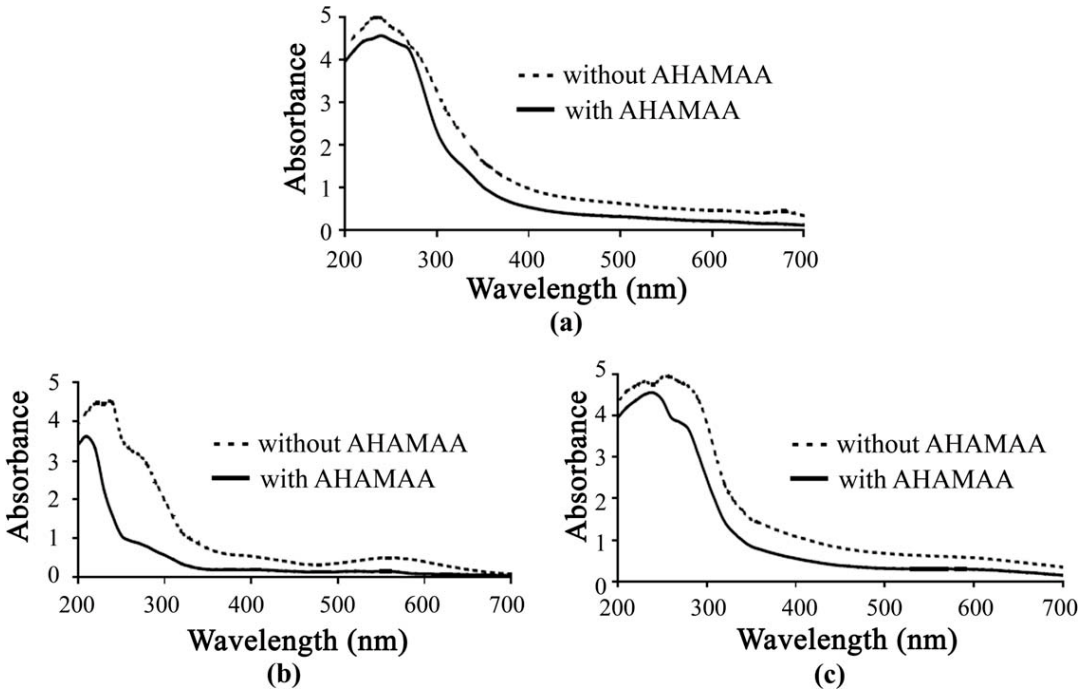

FIG. 10. Absorption spectra of wastewater from factories without and with AHAMAA: (a) A (mixture of reactive and direct dyes), (b) B1 (acid dyes), and (c) B2 (mixture of disperse and acid dyes).

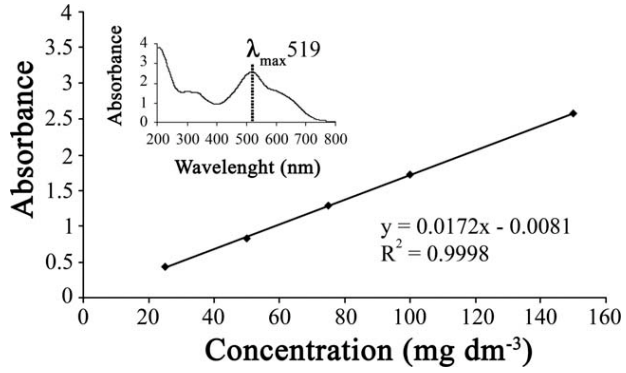

FIG. 11. Calibration line of the mixed dye solutions of Congo red and direct blue 71 (inset figure of absorption spectrum of a mixed aqueous solution of Congo red and direct blue 71).

(65% ± 1%) and 62 ± 6.6 mg g^{-1} (42% ± 6%) for Congo red and direct blue 71, respectively, from a 100 mg dm^{-3} solution of each dye.

Wastewater Treatment

The spectral absorptions of the industrial wastewater of sample A (a mixture of reactive dyes and direct dyes), sample B1 (only acid dyes) and sample B2 (a mixture of disperse dyes and acid dyes) before and after AHAMAA addition are shown in Fig. 10. All of the absorbances were dramatically decreased with wavelengths after the AHAMAA treatment. That means that the AHAMAA is an effective polymer flocculant in decreasing dye contents of the three samples.

The estimated dye concentrations were quantified from the synthetic dye wastewater. A calibration curve of the mixture of Congo red and direct blue 71 was constructed as shown in Fig. 11 in which an inset for the maximum absorption of the mixed dyes at λ_{max} at 519 nm is illustrated. The decrease in dye content in the mixed dye system was 92 ± 3 mg dm^{-3} (61% ± 2%) using 643 ± 3 mg dm^{-3} of AHAMAA. The adsorption capacity in the mixed dye system was 142 ± 2 mg g^{-1}. Table 4 presents the dye contents by measuring the dye absorbance and converting their absorbance to dye concentrations without and with 500 mg dm^{-3} of AHAMAA. The result shows that AHAMAA is able to decrease color of the textile wastewater containing reactive, direct, and acid dyes. The highest dye decrease was 68% (19.9 mg dm^{-3}) for 40 mg g^{-1} of the B1 nondiluted sample containing only acid dyes. The dye reduction decreased with increasing dilution of the wastewater. It is also found that the presence of impurity and unknown additives in the textile effluent wastewater might decrease the dye reduction efficiency of AHAMAA, which could be caused by the charge neutralization or destabilization of the polymer bridge.

Generally, textile wastewater is comprised not only dye molecules but also various negatively charged compounds, such as, anionic detergents, dispersing agents and inorganic compounds such as salts. The flocculation mechanism of anionic textile dyes of reactive, acid, and direct dyes involved the electrostatic interaction between negative charges of the dye with positive charges of AHAMAA. The hydrophobic disperse dyes interacted with negatively charged compounds in textile wastewater to form a dye anionic compound, which behaved as an anionic dye. It interacted then with AHAMAA via the electrostatic attraction [41], resulting in a color reduction of the dyes in textile wastewater.

Based on the ICP analysis, the amount of aluminum ion of AHAMAA is 12 ± 2 mg dm^{-3} and it is responsible for the turbidity experiment. Table 5 shows that the turbidity of the textile wastewater is decreased in the presence of AHAMAA. The initial turbidity of wastewater from factories A and B was decreased with dilution. This may be caused by increasing amounts of the soluble dye and contaminated anionic compounds with water addition. The highest turbidity reduction was found in sample A at 94.4%. Interaction between the colloidal reactive and direct dyes and contaminated anionic compounds with AHAMAA flocculant can take place via the charge neutralization and bridge formation with the AHAMAA [25]. However, AHAMAA did not affect the turbidity of wastewater in sample A/100 having 1.84 NTU because the very low initial turbidity might not be sensitively detected by

TABLE 4. Dye removal of industrial wastewater by AHAMAA.

Wastewater (factory/dilution)	λ_{max} (nm)	Without AHAMAA		With AHAMAA		Dye removal (%)
		Absorbance	Conc. (mg dm^{-3})	Absorbance	Conc. (mg dm^{-3})	
A/0	509	0.60	35.1	0.30	17.8	50
A/10		0.14	8.3	0.07	4.5	45
A/100		0.04	2.6	0.02	1.5	42
B1/0	557	0.50	29.4	0.16	9.5	68
B1/5		0.12	7.3	0.05	2.9	60
B1/10		0.07	4.4	0.04	2.6	40
B2/0	549	0.61	35.8	0.29	17.3	52
B2/5		0.15	8.7	0.08	5.0	42
B2/10		0.09	5.4	0.08	4.7	13

 DOI 10.1002/pen

TABLE 5. Turbidity reduction of industrial wastewater by AHAMAA.

Properties	Industrial wastewater (factory/dilution)							
	A	A/10	A/100	B1	B1/5	B1/10	B2	B2/10
Initial turbidity (NTU)	405	22.7	1.84	52.9	12.7	9.49	86.7	8.8
Turbidity after AHAMAA treatment (NTU)	23.0	8.5	1.97	24.3	5.23	3.94	74.5	8.8
% Reduction	94.4	62.6	NA	54.1	58.9	58.5	14.1	NA

the meter. The turbidity reduction for the sample B1, B1/5, and B1/10 were in the range of 54.1–58.9% at a similar initial turbidity. In sample B2, the turbidity reduction was only 14.1% even if its initial turbidity was rather high (86.7 NTU). This is because sample B2 contained the disperse dyes which cannot react directly with AHAMAA leading to the low turbidity reduction. Thus, when sample B2 was diluted by 10 times to become sample B2/10, AHAMAA cannot decrease its turbidity because of its low initial turbidity (8 NTU).

The investigation indicated that AHAMAA functions as an adsorbent and a flocculant. Because it can be applied in wastewater treatment as a flocculant to make flocs in the turbidity reduction of the kaolin suspension as described [20], and it can also be applied for the removal of dyes in the wastewater by the adsorption mechanism. Thus, it functions as an adsorbent as well.

CONCLUSIONS

AHAMAA was prepared by radical chain copolymerization in solution in which the residual aluminum ion concentration of AHAMAA in water was found in the range of 0.09–0.2 mg dm^{-3} regardless of the soaking time which indicates that AHAMAA is highly stable. AHAMAA can adsorb Congo red and direct blue 71, as validated by the Freundlich isotherm, through ionic interactions between the positively charged aluminum ion of AHAMAA and the sulfonate anion of the dyes. Both dyes are better removed by AHAMAA at pH 5–9 in the nonbuffered system. The dye reduction efficiency in the buffered system is lower than that of the nonbuffered. The adsorption capacity of AHAMAA for Congo red increases with increasing temperature and initial concentration of the dye solution. By adding AHAMAA, the color of the synthetic wastewater was decreased by 61% $\pm$ 2% with the addition of 643 $\pm$ 3 mg dm^{-3} of AHAMAA, and 68% reduction for the industrial wastewater by 500 mg dm^{-3} of AHAMAA. The turbidity reduction of the wastewater from Factory A by AHAMAA was 94.4% when the initial turbidity was 405 NTU to become 23 NTU after the treatment. This new compound was designed to apply in wastewater treatment to reduce or replace alum consumption in a convention method. Although the cost of AHAMAAA is somewhat higher than the conventional alum they are ecological friendly and safe.

ACKNOWLEDGMENTS

Research facilities provided by the Imaging Polymer Laboratory of Chulalongkorn University's Imaging and Printing Technology Department are gratefully acknowledged. The authors thank the Publication Counseling Unit of the Research Division, Faculty of Science, Chulalongkorn University, for language corrections. Many thanks to Ms. Arunnee Sodsree for the dye and wastewater measurement.

REFERENCES

1. C. Novotny, N. Dias, A. Kapanen, K. Malachova, M. Vandrovcova, M. Itavaara, and N. Lima, *Chemosphere*, **63**, 1436 (2006).
2. L.E. Gray and J.S. Ostby, *Fundam. Appl. Toxicol.*, **20**, 177 (1993).
3. B. Acemioglu, *J. Colloid Interface Sci.*, **274**, 371 (2004).
4. P. Baskaralingam, M. Pulikesi, V. Ramamurthi, and S. Sivanesan, *J. Hazard. Mater. B*, **136**, 989 (2006).
5. M. Alkan, S. Celikcapa, O. Demirbas, and M. Dogan, *Dyes Pigm.*, **65**, 251 (2005).
6. T. Robinson, B. Chandran, and P. Nigam, *Water Res.*, **36**, 2824 (2002).
7. L.E. Gray, J.S. Ostby, R.J. Kavlock, and R. Marshall, *Fundam. Appl. Toxicol.*, **19**, 411 (1992).
8. M.K. Purkait, A. Maiti, S. DasGupta, and S. De, *J. Hazard. Mater.*, **145**, 287 (2007).
9. V.V. Basava Rao and S. Ram Mohan Rao, *Chem. Eng. J.*, **16**, 77 (2006).
10. S. Chatterjee, S. Chatterjee, B.P. Chatterjee, and A.K. Guha, *Colloids Surf. A*, **299**, 146 (2007).
11. A. Tor and Y. Cengeloglu, *J. Hazard. Mater. B*, **138**, 409 (2006).
12. A.K. Golder, A.N. Samanta, and S. Ray, *Chem. Eng. J.*, **122**, 107 (2006).
13. A.A. Ahmad, B.H. Hameed, and N. Aziz, *J. Hazard. Mater.*, **141**, 70 (2007).
14. Y. Bulut, N. Gozubenli, and H. Aydin, *J. Hazard. Mater.*, **144**, 300 (2007).
15. E. Karadag, D. Saraydin, and O. Guven, *Water Air Soil Pollut.*, **106**, 369 (1998).
16. S. Duran, D. Solpan, and O. Guven, *Nucl. Instrum. Methods B*, **151**, 196 (1999).
17. O.S. Fatoki and A.O. Ogunfowokan, *Water SA.*, **28**, 293 (2002).
18. N. Kaneko, T. Sugioka, and H. Sakurai, *J. Inorg. Biochem.*, **101**, 967 (2007).

19. M. Kabsch-Korbutowicz, *Desalination*, **185**, 327 (2005).
20. S. Noppakundilograt, P. Nanakorn, K. Sonjaipanich, N. Seetapan, and S. Kiatkamjornwong, *J. Appl. Polym. Sci.*, **114**, 2564 (2009).
21. G.L. Shugar and J.A. Dean, *The Chemist's Ready Handbook*, McGraw-Hill, New York (1990).
22. E.Y. Ozmen and M. Yilmaz, *J. Hazard. Mater.*, **148**, 303 (2007).
23. C.A. Contreras, S. Sugita, and E. Ramos, *AZojomo*, **2**, 3 (2006).
24. G.A. Mazzocchin, F. Agnoli, and S. Mazzocchin, *Anal. Chim. Acta.*, **475**, 181 (2003).
25. B.Y. Gao, Y.B. Chu, Q.Y. Yue, B.J. Wang, and S.G. Wang, *J. Environ. Manage.*, **76**, 143 (2005).
26. W.H. Kuan, M.K. Wang, P.M. Huang, C.W. Wu, C.M. Chang, and S.L. Wang, *Water Res.*, **39**, 3457 (2005).
27. S.M.Z. Al-Kindy, S.S. Al-Ghamari, and F.E. Suliman, *Spectrochim. Acta A*, **68**, 1174 (2007).
28. J. Gregory, "Polymer Adsorption and Flocculation," in *Industrial Water Soluble Polymers*, C.A. Finch, Ed., The Royal Society of Chemistry, London, 62 (1996).
29. T. Caykara, I. Akcakaya, *Eur. Polym. J.*, **42**, 1437 (2006).
30. N.A. Peppas and A.R. Khare, *Adv. Drug. Deliv. Rev.*, **11**, 1 (1993).
31. Z. Chen, M. Liu, and S. Ma, *React. Funct. Polym.*, **62**, 85 (2005).
32. P. Lanthong, R. Nuisin, and S. Kiatkamjornwong, *Carbohydr. Polym.*, **66**, 229 (2006).
33. S. Kiatkamjornwong and R. Wongwathansatien, "Superabsorbent Polymer of Poly[acrylamide-co-(acrylic acid)] by Foamed Polymerization. I. Synthesis and Water Swelling Properties." in *Fundamentals and Applications of Polymer Gels*, Macromolucule Symposia Series 207, R.A. Siegel, Ed., Wiley-VCH, Weinheim, New York, 229 (2004).
34. M. Skowronek, I. Roterman, L. Konieczny, B. Stopa, J. Rybarska, B. Piekarska, A. Gorecki, and M. Krol, *Comput. Chem.*, **24**, 429 (2000).
35. B.C. Faust, W.B. Labiosa, K.H. Dai, J.S. MacFall, B.A. Browne, A.A. Ribeiro, and D.D. Richter, *Geochim. Cosmochim. Acta*, **61**, 3261 (1997).
36. T. Ren, Z. Yuan and B. Su, *Colloids Surf. A*, **300**, 79 (2007).
37. B. Tagirov, J. Schott, J.-C. Harrichoury, and J. Escalier, *Geochim. Cosmochim. Acta*, **68**, 1333 (2004).
38. L. Wang and A. Wang, *J. Hazard. Mater.*, **147**, 979 (2007).
39. F.A. Pavan, S.L.P. Dias, E.C. Lima, and E.V. Benvenutti, *Dyes Pigm.*, **76**, 64 (2008).
40. L. Wang and A. Wang, *Bioresour. Technol.*, **99**, 1403 (2008).
41. R.J. Zemaitaitiene, E. Zliobaite, R. Klimaviciute, and A. Zemaitaitis, *Colloids Surf. A*, **214**, 37 (2003).

 DOI 10.1002/pen

Polymer Degradation and Stability 95 (2010) 1894–1902

Contents lists available at ScienceDirect

Polymer Degradation and Stability

journal homepage: www.elsevier.com/locate/polydegstab

Photocatalytic efficiency of TiO_2/poly[acrylamide-*co*-(acrylic acid)] composite for textile dye degradation

Wiyong Kangwansupamonkon [a], Walasinee Jitbunpot [b], Suda Kiatkamjornwong [c,*]

[a] National Nanotechnology Center, National Science and Technology Development Agency; 111 Thailand Science Park, Paholyothin Road, Klong 1, Klong Luang, Pathumthani 12120, Thailand
[b] Program of Petrochemistry and Polymer Science, Faculty of Science, Chulalongkorn University, Phyathai Road, Bangkok 10330, Thailand
[c] Department of Imaging and Printing Technology, Faculty of Science, Chulalongkorn University, Phyathai Road, Bangkok 10330, Thailand

ARTICLE INFO

Article history:
Received 13 February 2010
Accepted 23 April 2010
Available online 12 May 2010

Keywords:
TiO_2
Hydrogel
Photocatalytic degradation
Dye removal

ABSTRACT

A novel photocatalytically degradable TiO_2/poly[acrylamide-*co*-(acrylic acid)] composite hydrogel (TiO_2/poly[AAm-*co*-AAc]) was synthesized by polymerization in an aqueous solution with *N*,*N*′-methylenebisacrylamide as the crosslinker and ammonium persulphate and TEMED as the initiator pair. The combined and separate effects of photodegradation and adsorption processes for dye removal were evaluated using methylene blue (MB) as the model dye for a photodegradation target, and compared with those of the neat poly[AAm-*co*-AAc], and a commercially available TiO_2 photocatalyst (Degussa P-25). Without photodegradation (i.e. in the dark), the TiO_2/poly[AAm-*co*-AAc] composite adsorbed up to 85% of the MB from a 5 mg L^{-1} MB solution in 15 min compared to only 10% for the pristine TiO_2. The reproducibility in photodegradation of the reused poly[AAm-*co*-AAc] composite was also investigated, where poly[AAm-*co*-AAc] was found to be photocatalytically degraded under UV irradiation. Therefore, the TiO_2/poly[AAm-*co*-AAc] composite hydrogel is a good dye adsorber with self-photodegradability and it also can easily be separated from the reaction by simple filtration. With these properties, the TiO_2/poly[AAm-*co*-AAc] hydrogel can be called a green polymer for use in the photodegradation–adsorption process for the abatement of various pollutants.

© 2010 Elsevier Ltd. All rights reserved.

1. Introduction

In recent years, pollution from dye wastewater has become a serious environmental problem due to the vast and increasing uses of a variety of dyes [1–4]. The dyes usually have a synthetic origin and typically have complex aromatic molecular structures that are more stable and difficult to degrade. The textile, paper, plastics and cosmetic industries use a wide variety of dyes to color their products and discharge large amounts of effluents, including dyes, which are toxic and could cause serious ecological problems. Therefore, dye pollution in water, such as discharge effluent into streams and ground water, is a major environmental problem.

Methylene blue (MB) has wide applications, which includes coloring paper, temporary hair colorant, dyeing cottons and wools. Although it is not strongly hazardous, it can cause some harmful effects, such as heartbeat increase, vomiting, shock, cyanosis, jaundice, quadriplegia, and tissue necrosis in humans. Color removal from effluents polluted with dyes of textile industries has been considered a challenge due to the difficulty of treating such wastewaters by conventional methods. The effluents of the manufacturing and textile industries are discarded into rivers and lakes, changing their biological life [5,6].

The current methods of dye removal from industrial wastewaters can require many processes and steps, such as biological treatment, coagulation, flotation, electrochemical techniques, adsorption and oxidation. Among these methods, adsorption is generally preferred due to its high efficiency, ease of handling and the availability of different adsorbents [7]. However, new environmental laws may consider the used adsorbents or sludge as hazardous waste materials themselves that will require further treatment prior to disposal. Consequently, novel technologies with a higher efficiency and lower energy consumption are required and have stimulated intensive research. An alternative to conventional methods includes the advanced oxidation processes (AOPs), which are based on the generation of very reactive species, such as hydroxyl radicals (•OH), that oxidize a broad range of organic pollutants quickly and non-selectively.

Photocatalytic oxidation using a semiconductor, such as TiO_2 as a photocatalyst, is one of the AOPs being developed. When TiO_2 is

* Corresponding author. Tel.: +662 2185587; fax: +662 2553021.
E-mail addresses: wiyong@nanotec.or.th (W. Kangwansupamonkon), yoghurt55@hotmail.com (W. Jitbunpot), ksuda@chula.ac.th (S. Kiatkamjornwong).

0141-3910/$ – see front matter © 2010 Elsevier Ltd. All rights reserved.
doi:10.1016/j.polymdegradstab.2010.04.019

illuminated by radiation with a wavelength below 380 nm, the photons excite the valence band electrons across the band gap into the conduction band, leaving holes behind in the valence band that will then react with water molecules or hydroxide ions (OH^-) to produce hydroxyl radicals (•OH) [8]. Oxygen is usually supplied as an electron acceptor to prolong the recombination of electron-hole pairs during the photocatalytic oxidation. TiO_2 photocatalysts have been successfully used to purify water and air, to degrade some organic pollutants and to kill microbes including bacteria [9–12]. Several investigations have reported that TiO_2 based photocatalysis is an effective method for discoloring and oxidizing organic dyes in wastewater, [13–15] including optimization of the method with the model dye, methylene blue (MB) [16–19].

However, as a photocatalyst TiO_2 is usually used in a powdery form in aqueous suspension, which requires separation of the TiO_2 particles from the purified water after the discoloring reaction. In addition, the process is generally equipped with an artificial UV radiation source, leading to a considerable increase in the operation and environmental costs. These drawbacks may be an obstacle to the use of TiO_2 photocatalysis for practical applications.

The development of new adsorbents having superior properties, such as a high adsorption capacity, fast adsorption rate and mechanical strength, has generated a great deal of interest in their application for wastewater treatment. Using several polymers with different functional groups is of increasing importance due to their high adsorption capacities and, especially, their regeneration abilities allowing repeated use or application in a continuous treatment processes [20,21]. Hydrogels possessing different functional groups have also been investigated for this purpose [22–24]. Hydrogels can be defined as water-swollen, three-dimensional networks. They can absorb a large amount of water compared to other water absorbing materials, and can also show stimuli-responsive properties to various external stimuli, such as temperature, pH, solvent composition and ionic strength in salt composition, depending on the type of functional groups in the materials [25,26]. In recent years, the preparation of hydrogel composites has spurred research efforts to produce new materials and novel applications in different areas, such as drug delivery, medical materials, agriculture industry and various fractionation/separation processes. However, investigation of the potential applicability of hydrogel composites in the dye removal process is less well studied. Hafez et al. [27] reported the photocatalytic efficiency of TiO_2 immobilized on a PVP/AAc hydrogel for the removal of Remazol Red RB-133 textile dye and under the same experimental conditions (an equal amount of TiO_2 and pH), the PVP/AAc hydrogel supported catalysts rendered 58% and 35% efficiency relative to the non-supported ones of the commercially available Degussa P-25, and freshly prepared colloidal photocatalysts, respectively. Tang et al. [28] studied the use of a TiO_2/polyacrylamide hydrogel composite for the removal and photodegradability of the methyl orange dye, and the TiO_2/PAAm composite had a good photocatalytic degradability, the composite also possessed a good reproducibility of photocatalytic degradability, which is possible to be applied for a practical process.

In the work reported here, a novel hydrogel composite (TiO_2/poly[AAm-*co*-AAc]) was prepared with acrylamide (AAm), acrylic acid (AAc) and TiO_2, and was then evaluated for the ability to remove MB dye from aqueous solutions. The combined effect of photodegradation–adsorption mediated by the TiO_2/poly[AAm-*co*-AAc] composite was investigated. The photocatalytic degradation process utilizing TiO_2 has been shown to be very effective for the degradation of various organic pollutants, but it is ineffective for the abatement of heavy metal ions which are generally non-degradable [29] and only reactive under UV irradiation. In contrast, poly[AAm-*co*-AAc] is known to have a very promising capability in this regard. Therefore, it was expected, and here is evaluated and reported, that TiO_2 and poly[AAm-*co*-AAc] could complement each other with their own advantages and so provide a comprehensive method in the abatement of various wastewater pollutants. Composite gels also have many other advantages, such as a low cost and easy separation from the reaction solution.

2. Experimental

2.1. Materials

AAm and AAc (both commercial grade) were obtained from Siam Chemical Industry, Thailand. *N,N'*-methylenebisacrylamide (*N*-MBA, Fluka, analytical grade) was used as a crosslinking agent. The photocatalyst employed was titanium dioxide (TiO_2, commercial grade, P-25, Degussa Corporation). According to the manufacturer's specification, P-25 has an elementary particle size of 30 nm and a BET surface area of ca. 54 $m^2\ g^{-1}$. Ammonium persulfate (APS, analytical grade, Merck, Germany) and *N,N,N'N'*-tetramethylenediamine (TEMED, analytical grade, Aldrich, Germany) were used as a redox initiator pair for the free radical polymerization reaction. Methanol (MeOH, commercial grade, BDH U.K.) was used for dehydrating water from the gel. Basic blue 9 (MB having a C.I. of 52015, a light blue dye powder) was from Dystar Thai Co. Ltd. (Bangkok, Thailand) and was used as received. All other chemicals were used without further purification.

2.2. Preparation of TiO_2/poly[acrylamide-co-(acrylic acid)] composite hydrogel

The TiO_2/poly[acrylamide-*co*-(acrylic acid)] composite hydrogel was synthesized by polymerization from an aqueous solution containing acrylic acid (2.5×10^{-1} M) and acrylamide (2.5×10^{-1} M) in a four-necked round bottomed flask, equipped with a mechanical stirrer set at 200 rpm and an inlet tube for feeding nitrogen gas. The reaction temperature was controlled at 60 °C. Then 2.5×10^{-2} M of *N*-MBA, 2.5×10^{-3} M of APS, 5–20 %wt of TiO_2 and 0.5 mL of TEMED were sequentially added to the reaction mixture. The mixture was stirred for 30 min and the resulting polymer was dehydrated with methanol, cut into small pieces of about 4–5 mm in diameter, and then dried at 50 °C for 24 h.

2.3. Characterization

2.3.1. Morphological study by SEM

The surface morphologies of TiO_2, poly[AAm-*co*-AAc] and the TiO_2/poly[AAm-*co*-AAc] composite were investigated using scanning electron microscopy (SEM, model JSM-T 220A, JEOL, Japan) without cross-section. The thickness of gold coating on the copolymer and its composites was 25 nm, and the SEM was operated with an accelerating voltage of 15 kV. The elemental analyses from SEM micrographs were used to calculate the percentage (in weight) of titanium by energy dispersive X-ray spectrometry (EDXS).

2.3.2. X-ray diffraction analysis

X-ray diffraction measurements of TiO_2, poly[AAm-*co*-AAc] and the TiO_2/poly[AAm-*co*-AAc] composite were carried out using a JOEL JDX-3530 diffractometer (CuK$\propto$ radiation, $\lambda = 0.15405$ nm, 2 kW). The X-ray diffraction (XRD) patterns were recorded from 10° to 60° in 2θ at a scanning rate of 0.02° min^{-1}. The dried copolymer powder was mounted on a sample holder with smooth double-sided adhesive tape.

2.3.3. The decolorization of the dye solution in the dark

Dye removal behavior from aqueous suspension of the TiO_2/poly[AAm-*co*-AAc] composite in comparison with the pristine TiO_2 was

investigated in continuous adsorption equilibrium experiments using the MB dye solution in the dark (to exclude photodegredation) as follows. A sample of the TiO_2/poly[AAm-*co*-AAc] composite weighing 0.2 g, or 0.0153 g of the pristine TiO_2 (the weight was selected from the TGA results), was transferred directly into a 200 mL aqueous solution of 5 mg L^{-1} MB. The MB solution in each sample was agitated magnetically at a moderate speed and then allowed to sediment. At various time intervals, *t*, an aliquot of the solution was taken and the remaining dye concentration in the solution was subsequently monitored by a UV–visible spectrophotometer (Perkin–Elmer, model Lambda 650, Shelton, Connecticut, U.S.A) at an incident wavelength, λ_{max}, of 664 nm. The initial and equilibrium dye concentrations are determined using a calibration curve based on the absorbance at λ_{max} versus dye concentration in standard dye solutions.

To construct a calibration curve, the MB concentrations of 0.5, 1.0, 2.5, 5.0, 7.5 and 10 mg L^{-1} were prepared in volumetric flasks and the absorbance of each of the standard MB solutions was measured at the maximum absorption wavelength of 664 nm. Therefore, the concentration of MB could be calculated from the regression equation: $y = 0.1777\times$, $R^2 = 0.9892$ as shown in Fig. 1. The amount of dye adsorbed per unit mass of the sample at equilibrium, q_{max} (mg g^{-1}), is calculated by using Equation (1):

$$q_{max} = (C_0 - C_{eq}) \times V/M \quad (1)$$

where C_0 and C_{eq} (mg L^{-1}) are the liquid phase concentrations of dye initially and at equilibrium, respectively, and the dye removal of MB from solution was calculated by Equation (2):

$$\%\ \text{Dye Removal} = \frac{C_0 - C_1}{C_0} \times 100 \quad (2)$$

where C_1 (mg L^{-1}) is the liquid phase concentrations at time, *t*.

2.3.4. Photocatalytic degradation of methylene blue

Photocatalytic degradation of the MB dye was studied using 0.2 g of the TiO_2/poly[AAm-*co*-AAc] composite or the poly[AAm-*co*-AAc] without TiO_2 (as a control). Each sample was poured into a 200 mL MB solution (5 mg L^{-1}) and kept at room temperature for 24 h. After the equilibrium absorption, the unabsorbed dye solution was removed by filtration over a 100-mesh sieve aluminum screen and left for 30 min to drain off the unabsorbed solution. The swollen hydrogels were placed in a quartz cuvette having a path length of 1 cm, capped and exposed on its side to 365 nm UV radiation by a UV lamp at an intensity of 1 mW cm^{-2}. The decolorization of MB at the equilibrium absorption of the neat poly[AAm-*co*-AAc] and TiO_2/poly[AAm-*co*-AAc] composite were measured at the indicated time intervals between 0 and 40 min exposure to UV radiation by a UV–visible spectrophotometer at a wavelength of 608 nm.

The absorbance measurements of the dye concentration in solution were performed with the UV–visible absorption spectroscopy at $\lambda_{max} = 664$ nm and the absorbance measurements of the dye concentration in poly[AAm-*co*-AAc] hydrogel and TiO_2/poly[AAm-*co*-AAc] composite were performed at $\lambda_{max} = 608$ nm. The experimental conditions show that the maximum absorption occurred at 664 and 608 nm at pHs 1–7 as depicted in Fig. 2. The latter absorption band was selected to monitor the temporal concentration changes of methylene blue in poly[AAm-*co*-AAc] and TiO_2/poly[AAm-*co*-AAc] composite. The blue shifts of the absorption bands of methylene blue in poly[AAm-*co*-AAc] and TiO_2/poly[AAm-*co*-AAc] composite are pH dependent as that shown in Equation (3): [18]

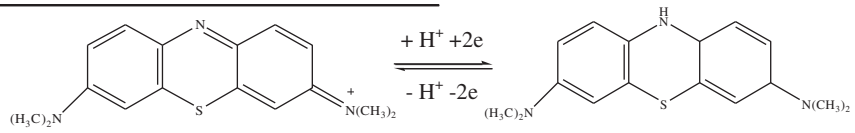

methylene blue leucomethylene blue (3)

The dye removal of MB from within the hydrogel under different conditions, such as in darkness (without UV irradiation) or under UV irradiation, was calculated by Equation (2) where C_0 and C_1 are the concentrations of MB dye measured at 608 nm in equilibrium absorption of the hydrogel before and after the irradiation, respectively.

As per the preliminary kinetics study, it showed that the degradation of MB by the TiO_2/poly[AAm-*co*-AAc] composite was best fitted by pseudo-first-order kinetics. The related kinetic model is shown in Equation (4):

$$-\ln\left(\frac{C}{C_0}\right) = kt \quad (4)$$

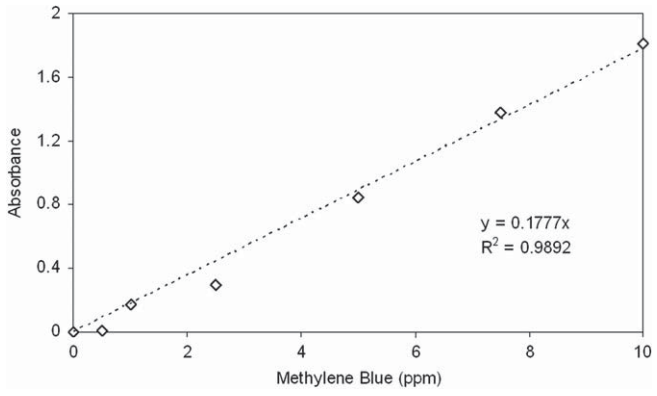

Fig. 1. Calibration curve for MB dye detection by absorbance at 664 nm.

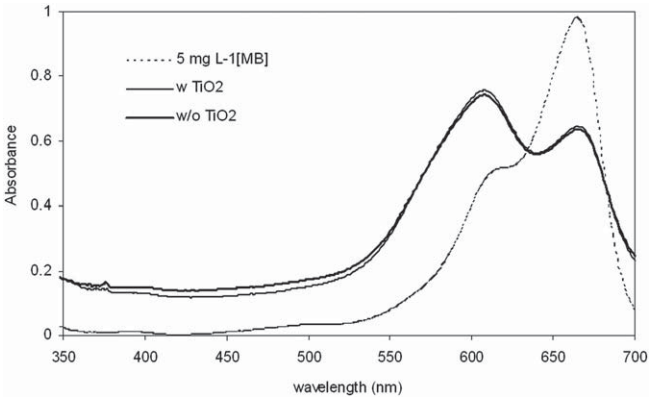

Fig. 2. Temporal spectral changes of MB in TiO_2/poly[AAm-*co*-AAc] composite and poly[AAm-*co*-AAc].

where C_0 and C are the initial dye concentration and that at time t (min), respectively, t is the irradiation time (min) and k is the rate constant (min^{-1}) [30].

2.3.5. Rheological measurement of the TiO_2/poly[AAm-co-AAc] composite for degradation evaluation

The degradation of the TiO_2/poly[AAm-*co*-AAc] composite hydrogel was evaluated by rheological measurements using a strain controlled rheometer (Bohlin Gemini HR nano, Malvern, UK) with parallel plates of 25 mm diameter. Oscillatory experiments and mechanical spectra were recorded in the frequency range of 0.01–35 Hz at 37 °C. The linear viscoelastic region was assessed at 0.1 Hz by assaying the strain sweep with a constant deformation strain of 0.5%. The samples were analyzed 24 h after sample preparation to attain the maximum swelling. The storage or elastic (G') and loss or viscous (G'') moduli were determined as a function of the frequency.

2.3.6. Photodegradation of the TiO_2/uncrosslinked poly[AAm-co-AAc] by GPC

The TiO_2/uncrosslinked poly[AAm-*co*-AAc] was synthesized by polymerization from an aqueous solution as detailed above except that the *N*-MBA crosslinker was omitted in the synthesis step. The TiO_2/uncrosslinked poly[AAm-*co*-AAc] was then irradiated with 365 nm UV radiation at an intensity of 1.6 mW cm^{-2} for 4 h and 24 h and compared to the neat uncrosslinked poly[AAm-*co*-AAc] synthesized under the same conditions. The number average molecular weight ($\overline{M}_n$), weight average molecular weight ($\overline{M}_w$) and polydispersity index (PDI) were analyzed by gel permeation chromatography (GPC). It is important to state that the TiO_2/uncrosslinked poly[AAm-*co*-AAc] must be totally soluble in water. Samples of the polymer composite weighing 10 mg was dissolved in 5 mL of sodium bicarbonate buffer at pH 11, filtered through a 0.45 μm filter, and then the solution was transferred to the autosampler vial for molecular weight determination by GPC.

3. Results and discussion

3.1. Morphological study by SEM

The morphologies of TiO_2 (Degussa P-25) particles, poly[AAm-*co*-AAc] and TiO_2/poly[AAm-*co*-AAc] composite, as observed by SEM, are shown in Fig. 3. TiO_2 (P-25) particles, utilized as a nanocatalyst, were largely small spherical particles of 35–67 nm diameter (mean 50 ± 7 nm) but tended to agglomerate together (Fig. 3 (a)). The pulverized poly[AAm-*co*-AAc], obtained from the radical chain polymerization in aqueous solution, was essentially a smooth sheet free of any significant particulate nature (Fig. 3 (b)). The TiO_2 loadings at 15 and 20%wt were immobilized in the TiO_2/poly[AAm-*co*-AAc] composite showed the TiO_2 particles to be well dispersed and so were found to reside on both the surface and the inner depths (Fig. 3 (c,d)). The TiO_2 particle distribution increased with increasing TiO_2 content. However, the fine nanoscaled TiO_2 particles are susceptible to agglomerate when their content was raised to 20%wt of TiO_2/poly[AAm-*co*-AAc] composite (Fig. 3 (d)).

3.2. X-ray diffraction analysis

To get some information on the TiO_2 content and structure in the hydrogel composites, XRD analysis was performed and typical diffractogram patterns are shown in Fig. 4.

No diffraction peaks in the spectrum for the synthesized poly[AAm-*co*-AAc] hydrogel were obtained. In contrast, a number of sharp peaks were clearly visible in the TiO_2/poly[AAm-*co*-AAc] composite, indicating the presence of crystalline moieties in the composite samples. The (101) and (110) basal plane spacing of TiO_2

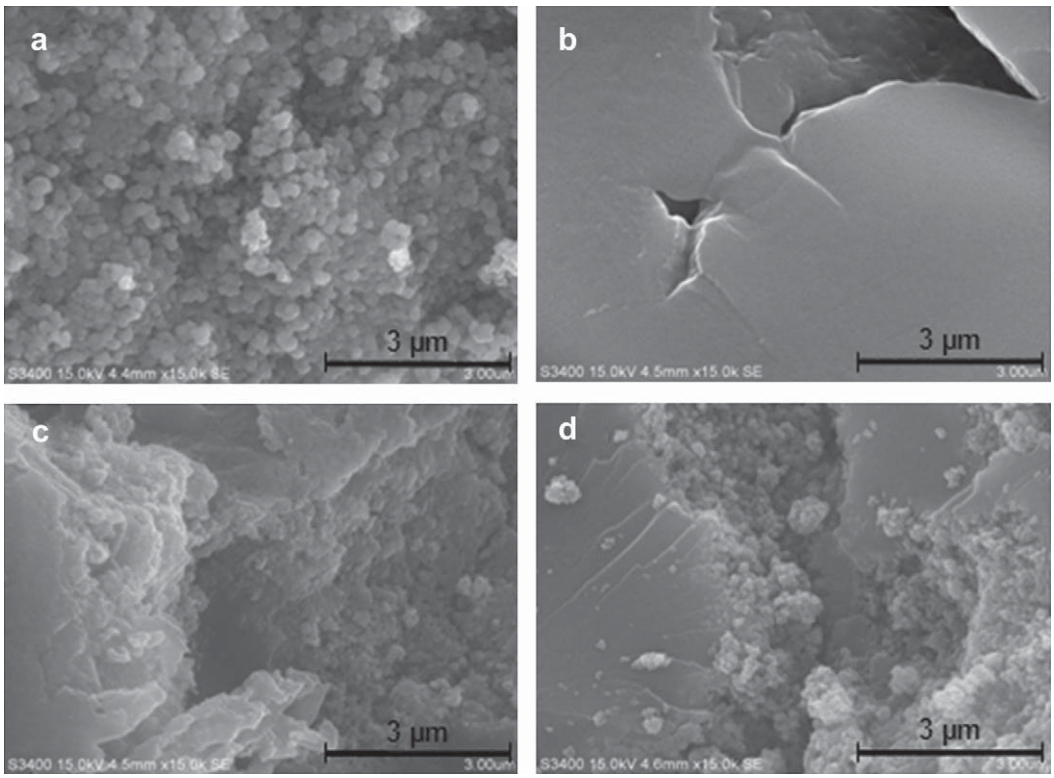

Fig. 3. Representative SEM micrographs of the (a) pristine TiO_2 (P-25), (b) neat poly[AAm-*co*-AAc] hydrogel, (c) 15%wt TiO_2/Poly[AAm-*co*-AAc] composite, and the (d) 20%wt TiO_2/Poly[AAm-*co*-AAc] composite. (Images are taken at 15,000× magnification representing at least 3 of such fields of view per sample and 3 independent samples).

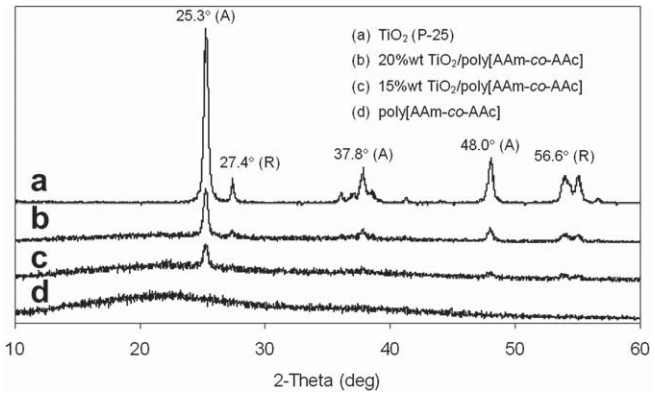

Fig. 4. Representative XRD patterns of (a) TiO_2 (P-25), (b) 20%wt TiO_2 (P-25)/poly[AAm-*co*-AAc], (c) 15%wt TiO_2(P-25)/poly[AAm-*co*-AAc] and (d) poly[AAm-*co*-AAc] (Diffractograms shown are representative of 3 independent samples).

are reported to be the anatase and rutile crystalline phases at $2\theta = 25.3°$ and 27.4°, respectively [31]. The result here shows that the TiO_2 (P-25)/poly[AAm-*co*-AAc] composites have observed peaks at $2\theta = 25.3°$, 37.8° and 48.0° for the anatase crystalline phase and at $2\theta = 27.4°$ and 56.6° for the rutile crystalline phase (Fig. 4 (b,c)).

The intensity of the characteristic TiO_2 peaks increased with increasing amounts of TiO_2 loading in the TiO_2/poly[AAm-*co*-AAc] composite, in comparison with the poly[AAm-*co*-AAc] without TiO_2 (Fig. 4 (b,c)). This confirms that TiO_2 is incorporated in the poly[AAm-*co*-AAc] matrix, and therefore that the poly[AAm-*co*-AAc] and the TiO_2/poly[AAm-*co*-AAc] composite were successfully synthesized.

3.3. Effect of TiO_2 content on photocatalytic degradation

The photocatalytic degradation of the MB dye within the adsorbent, after exposure to a 200 mL 5 mg L^{-1} MB solution and subsequent removal of the solution by filtration, was carried out in a quartz cuvette as described previously. The effects of TiO_2 loading from 5 to 20%wt in the hydrogel on dye degradation, measured with a UV–visible spectrophotometer at a wavelength of 608 nm, were evaluated following exposure to a 365 nm wavelength UV radiation source at an intensity of 1 mW cm^{-2} for 0 or 40 min (Fig. 5).

The dependence of the MB dye removal from the adsorbent hydrogel on the TiO_2 loading in the hydrogel (Fig. 5), evaluated as either %wt TiO_2 or the % Ti element content, indicates that the dye removal efficiency increases with increasing TiO_2 concentration until 15%wt of TiO_2 (5.9% Ti elemental composition). Although TiO_2 is a good photocatalytic degradation agent, and so as the TiO_2 amount in the polymer increased, the photocatalytic degradation is enhanced by the increased number of available catalyst active sites, the TiO_2 nanoparticles are, however, prone to conglomerate at concentrations above 15%wt TiO_2 loading, which results in a decreased photocatalytic degradability due to the decrease in the number of available catalyst active sites.

3.4. Photocatalytic degradation of methylene blue in the hydrogel composite

The photodegradation of MB dye within the adsorbent hydrogel was found to be enhanced in the presence of TiO_2/poly[AAm-*co*-AAc] composite (Fig. 6). Thus, in the presence of 15%wt TiO_2/poly[AAm-*co*-AAc] composite, approximately 91% of the dye was degraded after 40 min UV irradiation at room temperature, in contrast to the 3% seen following UV irradiation without TiO_2.

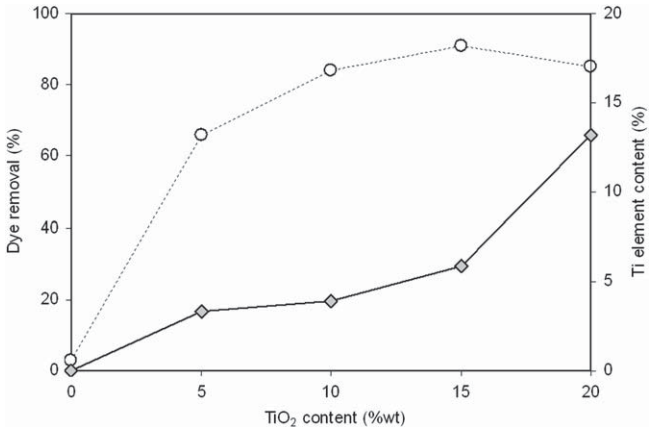

Fig. 5. MB dye removal from the hydrogel as a function of the TiO_2 (P-25) loading (%wt TiO_2 and the % elemental Ti) in the poly[AAm-*co*-AAc] hydrogel, when exposing to 365 nm wavelength UV irradiation at 1 mW cm^{-2} for 40 min (Data are shown as the mean ± 1 S.D. and are derived from 3 replications). Means with a different letter are significantly different ($p < 0.05$; Mann–Whitney *U* test).

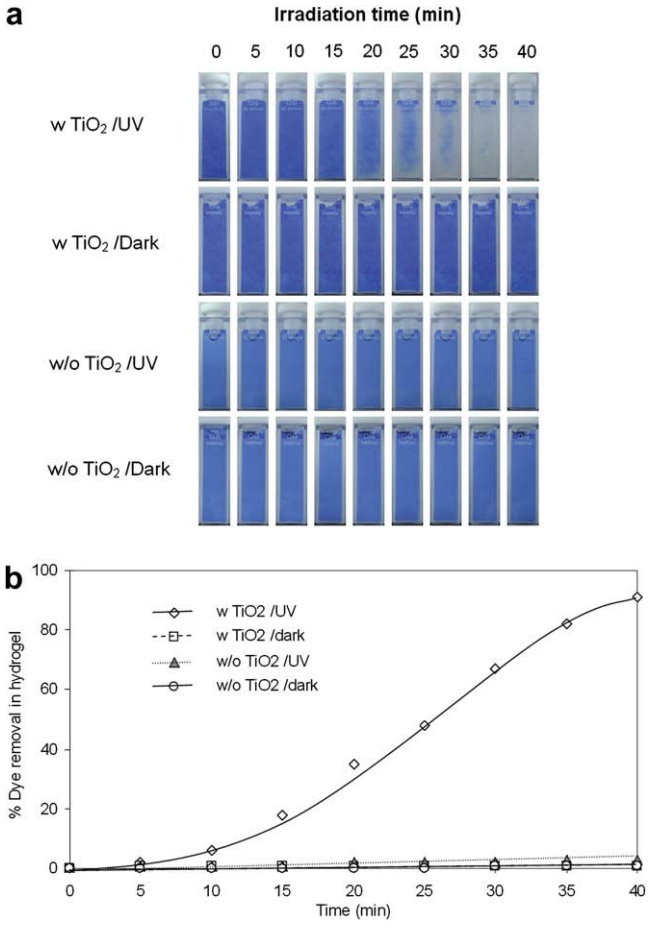

Fig. 6. MB dye removal from the hydrogel with time with (UV) or without (dark) exposure to 365 nm UV radiation at 1 mW cm^{-2} in the presence (w TiO_2) or absence (w/o TiO_2) of 15%wt TiO_2 in the poly[AAm-*co*-AAc] hydrogel. The dye concentration was 5 mg L^{-1} MB (200 mL). (a) Color appearance of MB degradation, where each cuvette is representative of 3 independent repeats. (b) MB dye removal vs. irradiation time, where data are shown as the mean ± 1 S.D., derived from 3 replications.

Likewise, there were no changes in the dye concentration, when poly[AAm-*co*-AAc] or TiO_2/poly[AAm-*co*-AAc] composites were used in the dark (i.e., without UV irradiation). Thus, both UV radiation and the TiO_2 photocatalyst are needed for the effective destruction of MB. Following UV radiation, the irradiated MB molecule is excited and acts as a photosensitizer capable of injecting electrons into the conduction band of the TiO_2 semiconductor particles to form oxidized radicals, whilst the oxidized species of the MB molecules then undergo further degradation, such as via peroxylated or hydroxylated intermediates to further degradation products such as mineralized products [16,32].

3.5. Dye removal from solution in the dark and photocatalytic degradation of methylene blue

Fig. 7 shows the comparison of MB dye removal via adsorption by TiO_2 (P-25), poly[AAm-*co*-AAc] and the TiO_2/poly[AAm-*co*-AAc] composite in contact with the MB solution in the dark (to exclude photodegradation). The poly[AAm-*co*-AAc] hydrogel and TiO_2/poly[AAm-*co*-AAc] composite both adsorbed MB dye to a significant extent with similar kinetics, with essentially equilibrium adsorption, $q_{max} = 5.3$ mg g^{-1}, (% dye removal = ~ 87%) being attained within 15 min. In contrast, the TiO_2 (P-25) alone was a poor adsorbent, reaching a much lower equilibrium (saturation) level of only 0.7 mg g^{-1} (% dye removal = 12%) absorbance after 30–45 min. Thus, the role of poly[AAm-*co*-AAc] as an adsorbent, with the formation of an ionic complex between the MB molecules and the poly[AAm-*co*-AAc] hydrogel [33], and potentially aiding TiO_2 photooxidation should not be ignored.

The adsorption rate constants are summarized in Table 1, where the close $k_{removal}$ values for the poly[AAm-*co*-AAc] and the TiO_2/poly[AAm-*co*-AAc] composite before UV irradiation, compared to the large difference between them after the UV irradiation, are due to interaction of the charged groups of the polymer networks and the dye imines groups to support the adsorption [34]. In contrast, a very small amount of MB molecules could be adsorbed onto the surface of TiO_2 (P-25), although the BET surface area of TiO_2 (P-25) is 54 m^2 g^{-1}. Thus, the ionic functional groups on the poly[AAm-*co*-AAc] backbone can adsorb and trap the cationic dye through ionic interactions. With the TiO_2 alone, the k_{degrad} is very low but it is better than that of poly[AAm-*co*-AAc] alone. To ascertain more details on the photocatalytic degradation of MB, the amount of MB dye removed by the TiO_2/poly[AAm-*co*-AAc] composite, poly[AAm-*co*-AAc] and TiO_2 (P-25) were plotted (Fig. 8). The TiO_2/poly[AAm-*co*-AAc] composite starts with a weak dye removal process within 5 min, accelerates to an almost linear rate between 15 and 30 min and reaches equilibrium at approximately 40 min with a maximum dye removal of 91%. In contrast, the dye removal by TiO_2 (P-25) particles is only 53% at 40 min, but is not yet at equilibrium. Note that the MB dye removal by poly[AAm-*co*-AAc] showed only a very slight increase, attaining only some 3% removal by a 40-min adsorption. According to the rate of photodegradation after the irradiation (Table 1), the extent of dye degradation strongly depended on the presence of TiO_2 particles while poly[AAm-*co*-AAc] did not change the dye degradation at all. However, the k_{degrad} values for the dye removal by the TiO_2/poly[AAm-*co*-AAc] composite and TiO_2 particles alone were significantly greater (145- and 23.1-fold higher, respectively) than that for the poly[AAm-*co*-AAc] alone which had a very low k_{degrad} value (Table 1). Besides its effectiveness in dye removal and the practical advantages of the ease of separation, the photocatalyst can be reused to some extent and then degraded which is described below.

Table 1
Equilibrium dye adsorption, dye removal rate and photodegradation rate constants of MB dye by the pristine TiO_2, TiO_2/poly[AAm-*co*-AAc] and the neat poly[AAm-*co*-AAc].

Sample	q_{max} (mg g^{-1})	Rate constant (k), min^{-1}			
		$k_{removal}$[a]	R^2	k_{degrad}[b]	R^2
Poly[AAm-*co*-AAc]	5.3	0.1346	1	0.0008	0.9865
TiO_2/Poly[AAm-*co*-AAc]*	5.3	0.1344	1	0.1161	0.9936
TiO_2 (P-25)	0.7	0.0006	0.9103	0.0185	0.9916

*loaded with 15%wt TiO_2. UV irradiation at a wavelength of 365 nm and 1 mW cm^{-2}.
[a] $k_{removal}$ were calculated from the curve of Fig. 7 (in the dark).
[b] k_{degrad} was calculated from the curve of Fig. 8 (under UV irradiation).

3.6. Reproducibility of the reused TiO_2/poly[AAm-co-AAc] composite

The reproducibility of the photocatalytic degradation activity of a 0.2 g sample TiO_2 (P-25)/poly[AAm-*co*-AAc] composite performed on a 5 mg L^{-1} MB dye solution (200 mL) is expressed as the number of cycles (Fig. 9), where the photocatalytic degradation of TiO_2/poly[AAm-*co*-AAc] composite was reduced from 91% on the first usage to 82, 22 and 17% after the second, third and fourth cycles of reuse, respectively. This reduced dye photodegradation activity is in accord with the appearance of the recycled TiO_2/poly[AAm-*co*-AAc] composite, which was clearly changed in the morphology as a hydrogel due to the photodegradation (Fig. 10).

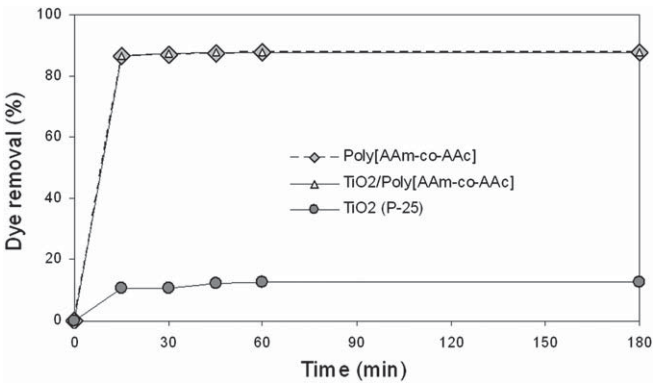

Fig. 7. Adsorption of a 5 mg L^{-1} MB solution (200 mL) by TiO_2 immobilized in poly[AAm-*co*-AAc], neat poly[AAm-*co*-AAc] or the pristine TiO_2 (Degussa P-25) in the dark. Data are shown as the mean ± 1 S.D., derived from 3 replications.

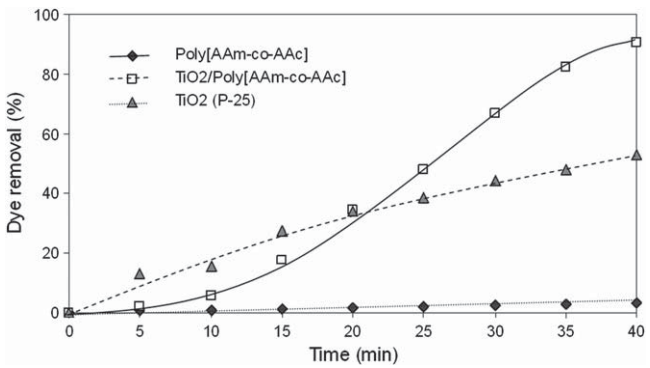

Fig. 8. Photocatalytic degradation of a 5 mg L^{-1} MB solution (200 mL) by TiO_2 immobilized in poly[AAm-*co*-AAc], the neat poly[AAm-*co*-AAc] and the pristine TiO_2 (Degussa P-25) following 365 nm wavelength UV irradiation at 1 mW cm^{-2} for the indicated time. Data are shown as the mean ± 1 S.D., derived from 3 replications.

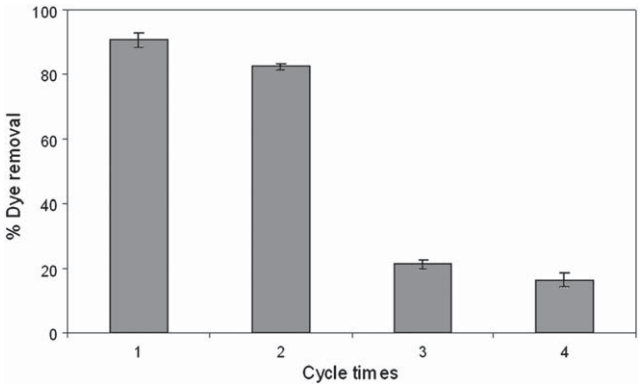

Fig. 9. Photocatalytic degradation of MB with 15%wt TiO_2/poly[AAm-*co*-AAc] composite after the indicated number of recycling times. Data are shown as the mean ± 1 S.D., derived from 3 replications.

3.7. Degradation of TiO_2/poly[AAm-co-AAc] hydrogel composite by rheological measurement

The storage modulus or elasticity modulus (G'), is a measure of the gel elastic behavior associated with the storage of energy, and the loss modulus or viscous modulus (G''), is a measure of the gel viscous behavior associated with the dissipation of energy. The frequency dependence of the storage moduli and loss moduli of poly[AAm-*co*-AAc] and the TiO_2/poly[AAm-*co*-AAc] composite before and after UV irradiation for 8 and 24 h is shown in Fig. 11. It can be seen that G' for both the poly[AAm-*co*-AAc] and the TiO_2/poly[AAm-*co*-AAc] composite before UV irradiation was higher than their corresponding G'' values, which indicates that the elastic response of the material is stronger than the viscous response. After 8 h of UV irradiation, the G' value for the poly[AAm-*co*-AAc] still remained higher than the corresponding G'' but the G'' value for the TiO_2/poly[AAm-*co*-AAc] composite was largely higher than the corresponding G' value. It is well known that the storage modulus can be considered as a measure of the extent of the gel network formation and that the higher the G' value of the gel, the stronger is the gel elasticity. This indicates that the swollen TiO_2/poly[AAm-*co*-AAc] hydrogel composite can be photodegraded faster than the swollen poly[AAm-*co*-AAc] hydrogel without TiO_2 after 8-h UV irradiation, presumably by both photocleavage and photocatalytic reactions. Furthermore, after 24-h of UV irradiation time, the G'' values of both the poly[AAm-*co*-AAc] and the TiO_2/poly[AAm-*co*-AAc] composite were mostly higher than the G', indicating that the viscous response of the material is more predominant than the elastic response and these hydrogel systems displayed a liquid-like behavior. Thus, as well as degrading the MB dye molecules adsorbed into the network, the existence of TiO_2 nanoparticles in the hydrogel composite can also assist the self-degradation of the hydrogel matrix. From the bond energies available (Table 2), the crosslinking molecules in the hydrogel networks can be easily photodegraded because of the lower bond energy (305 kJ mol^{-1}) of the C–N linkage via the *N*-MBA crosslinker.

3.8. Photodegradation of TiO_2/uncrosslinked poly[AAm-co-AAc] by GPC

The initiation step in the photocatalytic degradation process of poly[AAm-*co*-AAc] can be quite different. According to the literature [32–34], TiO_2 molecules are stimulated by absorbing UV radiation of a wavelength lower than 390 nm to generate various active oxygen species. The photocatalytic degradation of the poly[AAm-*co*-AAc] matrix [35–37] may be initiated at the same time as MB photodegradation [16–18] by active oxygen species, such as $O_2^{\bullet -}$, HOO• and HO•, forming on the surface of the TiO_2. These active oxygen species then attack the neighboring polymer chains to extract a hydrogen atom and form carbon-centered radicals, such as $-CH_2^{\bullet}CONH_2^-$ and $-CH_2^{\bullet}COCOOH-$. Their successive reactions

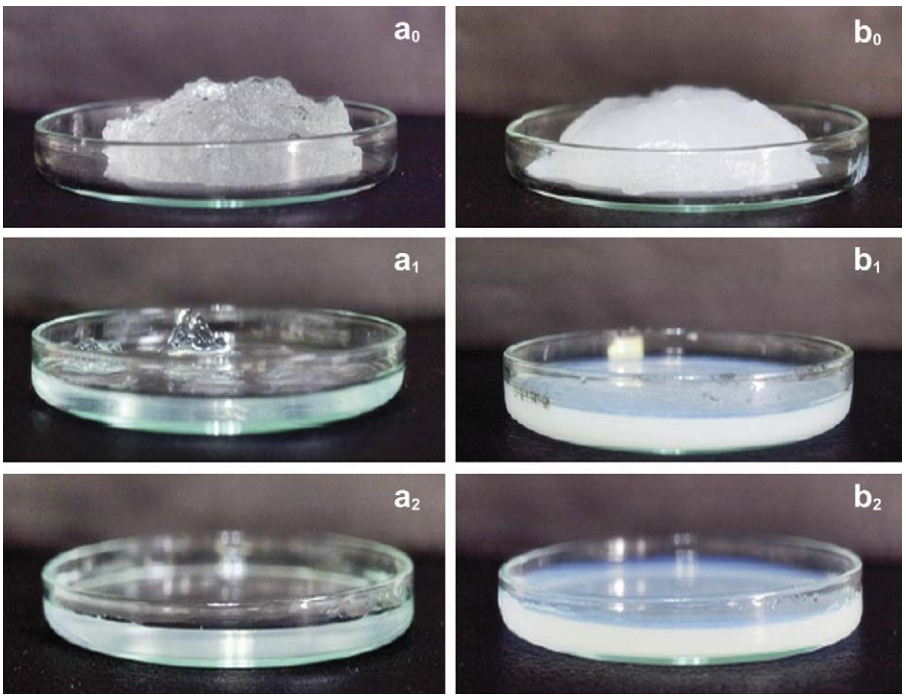

Fig. 10. Appearance of the (a) poly[AAm-*co*-AAc] hydrogel and (b) 15%wt TiO_2/Poly[AAm-*co*-AAc] composite after UV irradiation at 365 nm and 1 mW cm^{-1} for (0) 0 h, (1) 8 h and (2) 24 h. Images shown are representative of 3 independent replications.

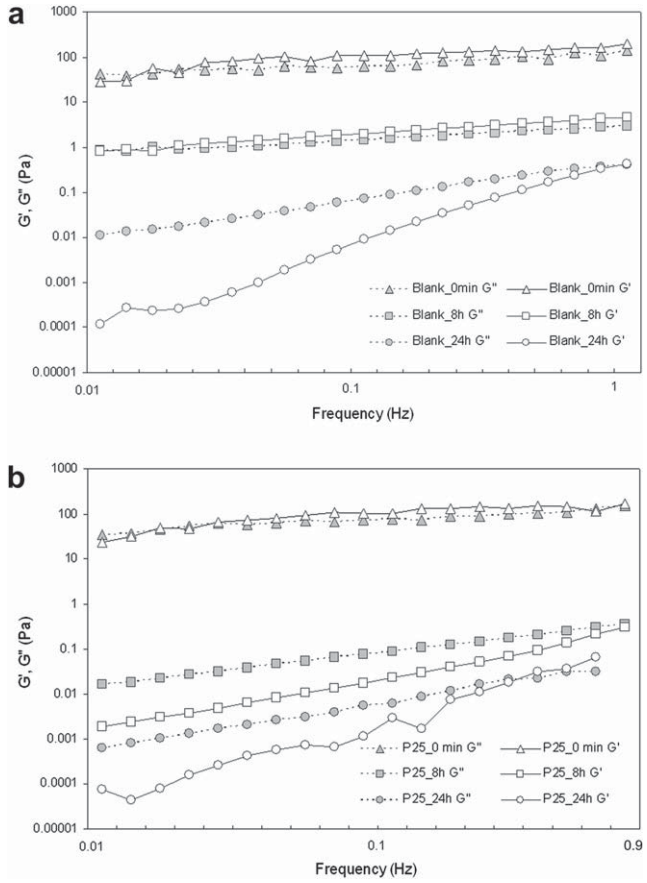

Fig. 11. Frequency dependence of the dynamic storage modulus (G') and the dynamic loss modulus (G'') of the (a) poly[AAm-*co*-AAc] hydrogel and (b) 15%wt TiO_2/Poly [AAm-*co*-AAc] composite after exposure to 365 nm wavelength UV irradiation at 1 mW cm^{-1} for the indicated periods of time. Data are shown as the mean ± 1 S.D., derived from 3 replications.

with $O_2^{\bullet -}$, HOO• and HO• produce hydroxyl derivatives and carbonyl intermediates, leading to the cleavage of the carbon chains and finally the release of carbon dioxide.

The photocatalytic degradation of the uncrosslinked poly [AAm-*co*-AAc] was accompanied by a decrease in the molecular weight of the uncrosslinked poly[AAm-*co*-AAc], as measured by GPC (Table 3). The $\overline{M}_w$ of poly[AAm-*co*-AAc] homopolymer incorporated with TiO_2 decreased some 40% from 991 × 10^3 to 596 × 10^3 g mol^{-1} after 24 h of UV irradiation, a decrease in the $\overline{M}_w$ of ~400 kg mol^{-1}. A similar analysis for the neat poly[AAm-*co*-AAc] shows that the $\overline{M}_w$ was only decreased ~200 kg mol^{-1} and so may imply that the bond scission in the polymer backbone of the TiO_2/poly[AAm-*co*-AAc] composite is caused by both the direct photolytic and the TiO_2 photocatalytic reactions.

Table 2
Average energy for selected bond types.

Type of bond	Energy (kJ mol^{-1})
C–N	305
C–C	347
C–O	358
N–H	391
C–H	413
O–H	467
C=C	614
C=O	745

Table 3
The variation of molecular weights of poly[AAm-*co*-AAc] with irradiation time.

Sample	$\overline{M}_n$[a] (10^{-3} g mol^{-1})	$\overline{M}_w$[b] (10^{-3} g mol^{-1})	PDI
Poly[AAm-*co*-AAc]. *before irradiation*	234	1000	4.3
Poly[AAm-*co*-AAc]. *365 nm, 4 h*	222	972	4.4
Poly[AAm-*co*-AAc]. *365 nm, 24 h*	174	790	4.6
TiO_2/Poly[AAm-*co*-AAc]; *before irradiation*	242	991	4.1
TiO_2/Poly[AAm-*co*-AAc]; *365 nm, 4 h*	220	950	4.3
TiO_2/Poly[AAm-*co*-AAc]; *365 nm, 24 h*	196	596	3.1

[a] $\overline{M}_n$: number average molecular weight.
[b] $\overline{M}_w$: weight average molecular weight.

4. Conclusions

A photocatalytically degradable TiO_2/poly[AAm-*co*-AAc] hydrogel composite was prepared by polymerization from an aqueous solution. XRD and SEM characterizations of the composite indicated that the TiO_2 particles were dispersed throughout the poly[AAm-*co*-AAc] hydrogel composite. TiO_2/poly[AAm-*co*-AAc] composite adsorbed at least 85% of a 5 mg L^{-1} MB solution in 15 min, compared to only 10% by pristine TiO_2 without photodegradation (in the dark). Approximately, 91% of the total MB present was photocatalytically degraded. The obtained results indicate that the newly prepared TiO_2/poly[AAm-*co*-AAc] is capable of removing the MB dye via the combined effect of adsorption-photodegradation. The ease of separation and removal of TiO_2/poly[AAm-*co*-AAc] hydrogel composite from the reactors by filtration and self-photcatalytic degradation, render it a potentially somewhat more green material by coupling with the photodegradation–adsorption process in the abatement of various wastewater pollutants.

Acknowledgments

This research is financially supported by a Research Team Consolidation Grant for Senior Research Scholars from the Thailand Research Fund – Higher Education Commission (contract number RTA5080004). The authors are also grateful for the partial research funding from the National Nanotechnology Center, NSTDA, Thailand (Grant number P-00-60064). Research facilities provided by the Polymer Imaging Laboratory of Chulalongkorn University's Imaging and Printing Technology Department and the National Nanotechnology Center, National Science and Technology Development Agency, are highly appreciated. Research materials donated by the mentioned manufacturers are also acknowledged.

References

[1] Sanghi R, Bhattacharya B, Singh V. *Cassia angustifolia* seed gum as an effective natural coagulant for decolourisation of dye solutions. Green Chem 2002;4:252–4.
[2] Namasivayam C, Arasi DJSE. Removal of Congo red from wastewater by adsorption onto waste red mud. Chemosphere 1997;34:401–17.
[3] Moozyckine AU, Davies DM. Green S as a prototype for an environmentally-degradable dye: the concept of a 'green dye' in future. Green Chem 2002;4:452–8.
[4] Akhtar S, Khan AA, Husain Q. Potential of immobilized bitter gourd (*Momordica charantia*) peroxidases in the decolorization and removal of textile dyes from polluted wastewater and dyeing effluent. Chemosphere 2005;60:291–301.
[5] Ho YS, Mckay G. The kinetics of adsorption of basic dyes from aqueous solutions by sphagnum moss peat. Can J Chem Eng 1998;76:822–7.
[6] Walker GM, Hansen L, Hanna JA, Allen SJ. Kinetics of a reactive dye adsorption onto dolomitic sorbents. Water Res 2003;37:2081–9.
[7] Crini G. Recent developments in polysaccharide-based materials used as adsorbents in wastewater treatment. Progress Polym Sci 2005;30:38–70.

[8] Crittenden JC, Zhang Y, Hand DW, Perram DL, Marchand EG. Solar detoxification of fuel-contaminated groundwater using fixed-bed photocatalysts. Water Environ Res 1996;68:270–8.
[9] Hou H, Zhu D, Cheng J. Application of nanometer TiO_2 photocatalysis material in air purification. Proceedings of the Int Conf Integrat Commercial Micro & Nanosystems; 2007:89.
[10] Li BJ, Yang DH, Wu SQ, Li BS, Meng H, Jiang SP, et al. Application of nano-sized TiO_2 photocatalysis to air purification and sterilization. Zhonghua yu fang yi xue za zhi [Chinese Journal of Preventive Medicine] 2008;42(11):831–5.
[11] Rajeshwar K, Osugi ME, Chanmanee W, Chenthamarakshan CR, Zanoni MVB, Kajitvichyanukul P, et al. Heterogeneous photocatalytic treatment of organic dyes in air and aqueous media. J Photochem Photobio C: Photochem Rev 2008;9(4):171–92.
[12] Kangwansupamonkon W, Lauruengtana V, Surassmo S, Ruktanonchai U. Antibacterial effect of apatite-coated titanium dioxide for textiles applications. Nanomedicine: Nanotech Bio Med 2009;5(2):240–9.
[13] Matthews LR, Avnir D, Modestov AD, Sampath S, Lev O. The incorporation of Titania into modified silicates for solar photodegradation of aqueous species. J Sol-Gel Sci Technol 1997;8:619–23.
[14] Zhan H, Chen K, Tian H. Photocatalytic degradation of acid azo dyes in aqueous TiO_2 suspension II. The effect of pH values. Dyes Pigm 1998;37:241–7.
[15] Li XZ, Zhao YG. Advanced treatment of dyeing wastewater for reuse. Water Sci Technol 1999;39:24955.
[16] Kuo WS, Ho PH. Solar photocatalytic decolorization of methylene blue in water. Chemosphere 2001;45:77–83.
[17] Houas A, Lachheb H, Ksibi M, Elaloui E, Guillard C, Herrmann JM. Photocatalytic degradation pathway of methylene blue in water. Appl Cat B: Environ 2001;31:145–57.
[18] Zhang T, Oyama T, Aoshima A, Hidaka H, Zhao J, Serpone N. Photooxidative N-demethylation of methylene blue in aqueous TiO_2 dispersions under UV irradiation. J Photochem Photobio A: Chem 2001;140:163–9.
[19] Yu Z, Chuang SSC. The effect of Pt on the photocatalytic degradation pathway of methylene blue over TiO_2 under ambient conditions. Appl Cat B: Environ 2008;83:277–85.
[20] Senkal BF, Yavuz E. Preparation of poly(vinyl pyrrolidone) grafted sulfonamide based polystyrene resin and its use for the removal of dye from water. Polym Adv Technol 2006;17:928–31.
[21] Hashem A, Abdel-Halim ES, Sokker HH. Bi-functional starch composites prepared by γ-irradiation for removal of anionic and cationic dyes from aqueous solutions. Polymer Plast Technol Eng 2007;46:71–7.
[22] Kasgoz H. Aminofunctionalized acrylamide-maleic acid hydrogels: adsorption of indigo carmine. Colloids Surf A: Physicochem Eng Aspects 2005; 266:44–50.
[23] Kasgoz H. New sorbent hydrogels for removal of acidic dyes and metal ions from aqueous solutions. Polym Bull 2006;56:517–28.
[24] Dadhaniya PV, Patel MP, Patel RG. Removal of anionic dyes from aqueous solution using poly[*N*-vinyl pyrrolidone/2-(methacryloyloxyethyl) trimethyl ammonium chloride] super-swelling hydrogels. Polym Bull 2007;58: 359–69.
[25] Ohmine I, Tanaka T. Salt effects on the phase transition of ionic gels. J Chem Phys 1982;77:5725–9.
[26] Katayama S, Hirokawa Y, Tanaka T. Reentrant phase transition in acrylamide-derivative copolymer gels. Macromolecules 1984;17(12):2641–3.
[27] Hafez HS, El-Hag Ali A, Abdel-Mottaleb MSA. Photocatalytic efficiency of titanium dioxide immobilized on PVP/AAc hydrogel membranes: a comparative study for safe disposal of wastewater of Remazol Red RB-133 textile dye. Int J Photoenergy 2005;7:181–5.
[28] Tang Q, Lin J, Wu Z, Wu J. Preparation and photocatalytic degradability of TiO_2/polyacrylamide composite. Euro Polym J 2007;43(6):2214–20.
[29] Chen D, Ray AK. Removal of toxic metal ions from wastewater by semiconductor photocatalysis. Chem Eng Sci 2001;56:1561–70.
[30] Abbasi M, Asl NR. Sonochemical degradation of Basic Blue 41 dye assisted by nanoTiO_2 and H_2O_2. J Hazard Mater 2008;153(3):942–7.
[31] Mozia S, Morawski AW, Toyada M, Inagaki M. Application of anatase-phase TiO_2 for decomposition of azo dye in a photocatalytic membrane reactor. Desalination 2009;241(1–3):97–105.
[32] Zainal Z, Hui LK, Hussein MZ, Abdullah AH, Hamadneh IMKR. Characterization of TiO_2-Chitosan/Glass photocatalyst for the removal of a monoazo dye via photodegradation–adsorption process. J Hazard Mater 2009;164:138–45.
[33] Paulino AT, Guilherme MR, Resi AV, Campese GM. Removal of methylene blue from an aqueous media using superabsorbent hydrogel supported on modified polysaccharide. J Colloid Interface Sci 2006;301(1):55–62.
[34] Solpan D, Duran S, Torun M. Removal of cationic dyes by poly(acrylamide-co-acrylic acid) hydrogels in aqueous solutions. Rad Phys Chem 2008; 77:447–55.
[35] Shukla NB, Daraboina N, Madras G. Oxidative and photooxidative degradation of poly(acrylic acid). Polym Degrad Stab 2009;94(8):1238–44.
[36] Vijayalakshmi SP, Madras G. Photocatalytic degradation of poly(ethylene oxide) and polyacrylamide. J Appl Polym Sci 2006;100:3997–4003.
[37] Vinu R, Madras G. Photocatalytic degradation of poly(acrylamide-*co*-acrylic acid). J Phys Chem B 2008;112:8928–35.

Research Article

polymers advanced technologies

Received: 28 October 2008, Revised: 1 June 2009, Accepted: 28 August 2009, Published online in Wiley Online Library: 23 September 2009

(wileyonlinelibrary.com) DOI: 10.1002/pat.1559

Acrylamide–itaconic acid superabsorbent polymers and superabsorbent polymer/mica nanocomposites

Daungtawan Foungfung[a], Siriwan Phattanarudee[b], Nispa Seetapan[c] and Suda Kiatkamjornwong[b]*

Superabsorbent polymer acrylamide (AM)/itaconic acid (IA) and its nanocomposite were synthesized by redox polymerization in an aqueous solution of both monomers with mica used as an inorganic additive. The influences of IA concentration, mica content, and crosslinker concentration on the water absorption and physical properties of the superabsorbent polymer and its nanocomposite were examined. Water absorbency in artificial urine by the synthesized copolymers, and the gel strength of the superabsorbent copolymers and their nanocomposites, were tested with loads of 0.28 or 0.70 psi. Transmission electron micrographs and X-ray diffraction confirmed that the polymer chains were successfully intercalated into the silicate layers in the mica. The water absorbency and the artificial urine absorbency of the composite with an AM-to-IA mole ratio of 95:5, 0.2% mol N-MBA, and 5% w/w mica were 748 ± 5 and $76 \pm 2\,g\,g^{-1}$, respectively, whilst the neat copolymer achieved only 640 ± 7 and $72 \pm 2\,g\,g^{-1}$ in water and artificial urine, respectively. The viscoelastic behavior suggested that the swollen gel of the nanocomposites exhibited mechanical stability and elasticity. Copyright © 2009 John Wiley & Sons, Ltd.

Keywords: superabsorbent polymer; superabsorbent polymer nanocomposite; mica; water absorbency

INTRODUCTION

Superabsorbent polymers are lightly crosslinked hydrophilic polymers that can absorb, swell, and retain aqueous solutions or fluids up to hundreds of times their own dry weight giving them many advantages over traditional water absorbing materials such as cotton, pulp, or sponges. They are widely used in agriculture, horticulture, disposable diapers, cosmetics, controlled drug delivery systems, and wound dressings.[1–9] The first superabsorbent polymer was reported by the US Department of Agriculture in 1961,[10] whilst later research has focused upon attempting to modify these absorbent polymers to enhance their absorbency, gel strength, and absorption rate.[11–15]

In recent years, increasing attention has been paid to the incorporation of inorganic materials in the preparation of superabsorbent polymers including kaolin,[16] montmorillonite,[17,18] attapulgite,[19–22] laponite,[23] vermiculite,[24] bentonite,[25] and mica.[8,26–28] The incorporation of these mineral powders can reduce production costs as well as improve water absorption, gel strength, and the mechanical and thermal stabilities of superabsorbent polymers. Among these clays is mica, a plate-like crystalline aluminosilicate with a 2:1 phyllosilicate type structure with an octahedral Al sheet and two tetrahedral Si sheets. Mica has been widely used as a reinforcing filler in polymeric matrices due to its excellent mechanical, electrical, and thermal properties.[29] Lin *et al.* synthesized a poly(acrylic acid)/mica superabsorbent composite by a graft polymerization reaction between partially neutralized acrylic acid and ultrafine mica powder. The water absorbency of the composite was higher than $1100\,g\,g^{-1}$ at a 10% w/w mica addition.[26] However, further increase in the mica content decreased the water absorbency. The influence of the degree of neutralization of the acrylic acid was found to be optimal at 65%. A series of superabsorbent polymers based on sodium acrylate, mica, and *N*, *N*′-methylenebisacrylamide (N-MBA) were prepared by inverse suspension polymerization.[27] The results showed that the water absorbency and the initial absorption rate gradually decreased with increasing amounts of pure K^+–mica and intercalated mica. In addition, the water absorbency of the composite gels obtained from K^+–mica was higher than that of gels from intercalated-mica. The water absorbency of these gels decreased with increase in the ionic strength of the external salt solution. Zhang and Wang[28] researched a series of clay-based superabsorbent composites prepared from acrylamide (AM) and

* *Correspondence to: S. Kiatkamjornwong, Department of Imaging and Printing Technology, Faculty of Science, Chulalongkorn University, Phayathai Road, Bangkok 10330, Thailand.*
E-mail: ksuda@chula.ac.th

a *D. Foungfung*
Petrochemistry and Polymer Science, Faculty of Science, Chulalongkorn University, Phayathai Road, Bangkok 10330, Thailand

b *S. Phattanarudee, S. Kiatkamjornwong*
Department of Imaging and Printing Technology, Faculty of Science, Chulalongkorn University, Phayathai Road, Bangkok 10330, Thailand

c *N. Seetapan*
National Metal and Materials Technology Center, National Science and Technology Development Agency, 114 Thailand Science Park, Paholyothin Rd, Klong 1, Klong Luang, Pathumthani 12120, Thailand

Contract/grant sponsor: Thailand Research Fund, Senior Research Grant. Grantcontract/grant number: RTA4780004.

Copyright © 2009 John Wiley & Sons, Ltd.

various clays, and reported that mica incorporation improved the thermal stability of superabsorbent composites to a higher degree than the other tested clays. The effect of intercalant content of mica on the properties of the charged nanocomposite poly(*N*-isopropyl acrylamide) hydrogels was investigated. The mica was first intercalated with different levels of intercalant, trimethyl (acrylamido propyl) ammonium chloride (TMAACl), based on the cationic exchange capacity (CEC) of mica.[8] The results showed that mica could intercalate with TMAACl under a low CEC value with the significantly enhanced swelling behavior and mechanical properties being related to the intercalated mica content and CEC values.

AM can be used to copolymerize with a number of vinyl monomers to synthesize superabsorbent polymers. Graft copolymer of starch with acrylic acid/AM,[30,31] AM/maleic acid,[32] acrylic acid/itaconic acid (IA),[33] as superabsorbent polymers could be used for agricultural and environmental applications. Copolymerization of partially hydrolyzed AM with *n*-vinyl pyrrolidone produced superabsorbent polymers for oil recovery applications.[34–36] AM can be also used with acrylic acid,[37] methacrylic acid,[38] and crotonic[39] to produce various properties of superabsorbent polymers for enzyme immobilization or dye removal. However, none of them has involved the inclusion of filler into superabsorbent polymers. For the present investigation, swelling synthetic mica was chosen for *in situ* polymerization of AM–IA superabsorbent polymer nanocomposites. The main aim for adding the mica particles was to form composites with increased swollen gel strength and without loss of water absorbency for personal care products such as baby disposal diapers.

EXPERIMENTAL

Materials

AM (Siam Resin and Chemicals, Thailand) and ionic comonomer, IA (Merck, Hohenbrunn, Germany), were used as monomers. N-MBA (Fluka, Buchs, Switzerland) was utilized as a crosslinker. Ammonium persulphate (APS, Merck, Hohenbrunn, Germany) and *N, N, N′, N′*-tetramethylethylenediamine (TEMED, Fluka, Buchs, Switzerland) were added as a redox initiator pair. The swelling mica with exchangeable sodium ions and a CEC of about 120 meq/100 g was purchased from Wako Pure Chemical Industries, Osaka, Japan. The average particle size, as measured by SEM, was approximately 3 μm. The deionized water used in the experiment was obtained from ELGA Labwater (model reservoir 25L, purelab option, UK). All the materials were used as received.

Preparation of the superabsorbent nanocomposite

A mixture of 60 cm^3 aqueous solution containing AM, IA monomers, and mica was placed in a 500-cm^3 four-necked round-bottomed flask. The mixture was mechanically stirred by a small-bladed propeller at 250 rpm, within a temperature range of $50 \pm 2^{\circ}C$ for 2 hr for monomer intercalation. Then, 20 cm^3 (0.2% mole) of N-MBA aqueous solution was added within 5 min. The mixture was purged with N_2 gas to remove oxygen from the solution during the reaction. Next, 0.3 mole (20 cm^3) of the APS aqueous solution was added and stirred for 5 min. Lastly, 1.2% mole (0.2 cm^3) of the co-initiator (TEMED) was added and the polymerization was continued for 30 min. The resulting polymer was then dewatered with methanol, cut into small pieces, with diameters of about 0.5 cm, and dried at 50°C for 24 hr in a vacuum oven to constant weight. The dried polymer was then milled and separated through a 100-mesh aluminum screening sieve to form the superabsorbent composite particles (powder). Superabsorbent nanocomposites at other AM/IA ratios, different mica contents, and various crosslinker concentrations, listed in Table 1, were prepared in the same manner.

Table 1. Composition variables investigated in crosslinked polymerization of poly(AM-*co*-IA)/mica nanocomposites

Ingredients	Amount
Monomer (AM/IA) ratios (% mol)	99/1, 98/2, 97/3, 96/4, 95/5
Mica (% w/w)	0, 2, 5, 10, 15
N, N′-methylenebisacrylamide (% mole)[a]	0.2, 0.5, 0.7, 0.9
Ammonium persulfate (% mole)[a]	0.3
N, N, N′, N′-tetramethyl-ethylenediamine (% mole)[a]	1.2
Reaction temperature (°C)	50
Agitation speed (rpm)	250
Reaction time (min)	30

[a] % mole based on the monomer concentration.

Determination of the unreacted amount of AM monomer in the superabsorbent polymer by gas chromatography

The superabsorbent polymer derived from the polymerization reaction was stirred in 300 cm^3 of deionized water at room temperature for 30 min. Then 50 cm^3 of the solution was used to determine the trace amounts of AM monomer in the polymerization reaction by Method 8032A,[40] which consists of three steps: bromination, extraction, and calibration. Bromination of the AM double bond gave 2, 3-dibromopropionamide which was extracted from the reaction mixture with ethyl acetate. After salting out with sodium sulfate, the extract was analyzed by gas chromatography.

Determination of density of the superabsorbent nanocomposite

The standard method (ASTM D 792) for determining the polymer density was used to evaluate the densities of mica, poly(AM-*co*-IA), and poly(AM-*co*-IA)/mica nanocomposites in *n*-heptane in a pycnometer.

Measurement of water absorbency

In deinoized water and its absorption with time

Deionized water (200 g) was added to 0.1 g of the superabsorbent polymers or its nanocomposites in a 250 cm^3 glass beaker at room temperature. The nanocomposite was allowed to swell for 24 hr. The residual water was removed by filtration with a 100-mesh screen sieve for 2 hr in a closed system at room temperature and the swollen gel was weighed. The water absorbency, as grams of water per gram of sample ($g\,g^{-1}$) was

 Copyright © 2009 John Wiley & Sons, Ltd.

calculated as shown in eqn (1), from a minimum number of at least three repeats.

$$\text{Water absorbency } (Q) = \frac{B - A}{A} \quad (1)$$

where A and B are the weights of the dry polymer and the swollen gel, respectively.

Deionized water (200 g) was added to 0.1 g of the dried nanocomposites in a 250 ml glass beaker covered with a glass lid. The polymer was allowed to swell first for 1 min. The swollen gel was then separated from the water by filtering it through a 100-mesh sieve aluminum screen for 2 hr at room temperature to drain out the unbound water, and the swollen copolymer was then weighed. Similar experiments were carried out for each gel at the swelling times of 1, 5, 10, 30, 60, 180, 300, and 480 min.

In artificial urine

The same experimental procedures as described above were carried out using artificial reference urine (ARU) instead of deionized water. The ARU was prepared by mixing equal amounts of 0.1055 M sodium chloride, 0.0323 M sodium dihydrogen phosphate, 0.00321 M sodium citrate, 0.00385 M magnesium sulphate, 0.01695 M sodium sulfate, and 0.0637 M potassium chloride. The pH was adjusted to 6.5. The ARU had an ionic strength of 0.0747 mol-ion dm^{-3}, based on the method of Skoog *et al.*[41,42]

Absorbency under load

Deionized water (25 cm^3) was placed in a Petri dish as shown in Fig. 1. Dried copolymer weighing about 0.16 g was carefully sprinkled onto the filter screen of the testing device, which was comprised of an aluminum cylinder with a stainless steel cloth 100-mesh screen sieve placed at the bottom of the cylinder. The device has a diameter of 26 mm and a height of 35 mm. A piston assembly, including appropriate weights to achieve a load of either 0.28 or 0.70 psi, was placed on top of the dry copolymer. After assembly with added dry copolymer with appropriate weight (for a load of 0.28 or 0.70 psi), the entire device was weighed and then placed in the water filled Petri dish for 1 hr to allow the absorption to reach equilibrium, whereupon the entire device was reweighed. The absorbency under load (AUL), as gram of water absorbed per gram of the dry copolymer (g g^{-1}) was calculated as eqn (2).[43]

$$\text{Absorbency under load } (\text{AUL}) = \frac{B - A}{A} \quad (2)$$

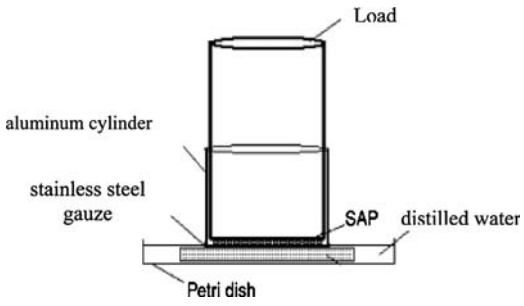

Figure 1. Scheme of the absorbency under load (AUL) setup.

where A and B are the weights of the dry polymer and the swollen gel, respectively. The water absorbency was calculated as gram of water per gram of sample. The number of repeats was not less than three.

Characterization of the superabsorbent nanocomposites

Identification of the functional groups

The functional groups of the copolymers and nanocomposites were identified using Fourier-Transform Infrared Spectrometry (FT-IR) (Nicolet Infrared Spectrometer, model Impact 410). The dried sample was ground with the dried KBr powder. The KBr disk was dried again, pressed, and subjected to the FT-IR spectrometry.

Morphology by scanning and transmission electron microscopic analyses

The surface morphology of the superabsorbent composites was investigated using scanning electron microscopy (SEM, model JSM-6400, JEOL, Japan), without cross-section. The thickness of the gold coating on the sample was 25 nm, and SEM was operated with an accelerating voltage of 15–20 kV to give good image contrast.

For TEM analysis, the superabsorbent nanocomposite particles were dispersed in ethyl alcohol and the suspension was then sonicated for 5 min. The diluted suspension was then dropped onto a 300-mesh copper grid, and left to dry in a control room atmosphere before performing the TEM analysis. TEM micrographs of the samples were obtained at an acceleration voltage of 120 kV (JEOL JEM-2100, Japan).

X-ray diffraction analysis

X-ray diffraction measurements were performed using an X-ray diffractometer, Bruker AXS Model D8 Discover (Cu Kα radiation, 40 kV, 40 mA, with $\lambda = 0.15406$ nm and $n = 1$) at a scanning range from 2 to 25° and a scanning rate of 0.025° min^{-1}. The interlayer spacing (d) of mica and mica-superabsorbent nanocomposites was calculated using Bragg's equation (eqn 3):

$$n\lambda = 2d\sin\theta \quad (3)$$

where d is the interplanar distance of the (001) reflection plane, θ is the diffraction angle, and λ is the wavelength.

Viscoelastic properties

The rheological experiments of the swollen gel particles having an irregular shape were carried out in a strain-controlled rheometer (ARES, TA Inc., New Castle, USA) equipped with a solvent trap to prevent water evaporation during measurements. The experiments were operated at 25°C using parallel plate geometry (50 mm diameter, 1 mm gap) made of stainless steel. The strain sweeps, at a fixed frequency of 1 rad sec^{-1}, were conducted in a range of 0.1–100% for determining a linear viscoelastic (LVE) range, where G' (storage modulus) and G'' (loss modulus) are independent of the strain amplitude. After a strain sweep test, the dynamic frequency sweeps were performed within the determined LVE range. The samples were prepared as follows. A dry superabsorbent (0.1 g) was dispersed in 200 cm^3 distilled water and allowed to swell for 24 hr to reach equilibrium swelling. The swollen superabsorbent was filtered through a

 Copyright © 2009 John Wiley & Sons, Ltd. View this article online at wileyonlinelibrary.com

100-mesh aluminum screen for 2 hr. Pieces of tissue papers were used to rub off the unabsorbed water at the bottom of the screen until the swollen gel did not flow when the screen was held vertically. Afterwards, the swollen gel particles were removed from the screen to investigate their rheological behavior.

Thermal stability analysis

The superabsorbent composites were investigated using a PerkinElmer TGA-7 thermogravimetric analyzer for their thermal property. The measurements were carried out over a temperature range of 25–800°C at a heating rate of 10°C min^{-1} with a nitrogen flow rate of 60 cm^3 min^{-1}. In order to compare the residue of the superabsorbent composite, the polymer was burned in an oven. The dry nanocomposite copolymer samples, weighing 1.00 ± 0.01 g, were each individually placed in a 25 cm^3 porcelain crucible, weighed, and transferred into a furnace at 800°C for 10 hr or until combustion of the remaining white mica powder had been completed. The crucible was removed from the furnace, cooled to room temperature, weighed, and the remaining mica weight was evaluated.

RESULTS AND DISCUSSION

FT-IR spectra of mica, synthesized copolymer, and superabsorbent nanocomposites

The FT-IR spectra of mica, poly[acrylamide-*co*-(itaconic acid)], and poly[acrylamide-*co*-(itaconic acid)]/mica nanocomposites are shown in Fig. 2. The absorption bands at 3452 cm^{-1} (broad) and 1638 cm^{-1} (Fig. 2a) correspond to the O–H stretching and interlayer water vibration present in the mica, whilst those at 1003 cm^{-1} (broad peak), 702, and 476 cm^{-1} are the Si–O stretching, Al–O stretching, and Si–O bending, respectively. The copolymer exhibits a broad absorption band at 3400 cm^{-1}, and strong peaks were observed at 1659 and 1448 cm^{-1}, which correspond to O–H stretching, C=O stretching of $–COO^-$, and C–N stretching of O=C–N–H, present in the IA and AM monomers

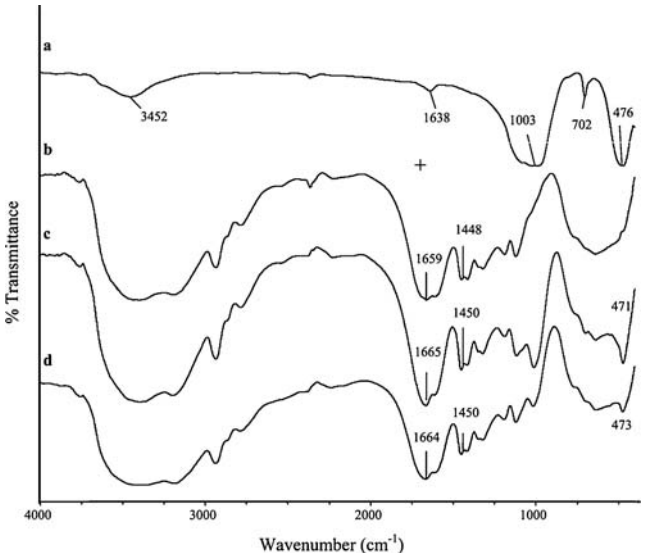

Figure 2. FT-IR spectra of (a) mica, (b) poly(AM-*co*-IA) copolymer, (c, d) poly(AM-*co*-IA)/mica nanocomposite at a 97:3 mole ratio crosslinked by 0.2% mole N-MBA with either (c) 15% w/w of mica or (d) 5% w/w of mica.

(Fig.2b). In comparing the spectra of pure mica and the copolymer, the spectra of nanocomposites synthesized using 5 and 15% (w/w) mica showed a similar broad band in the 3400–3370 cm^{-1} range and strong peaks at 1665–1664 cm^{-1} and 1450 cm^{-1} for the $–COO^-$ indicating the characteristics of the copolymer. However, the $–COO^-$ group on the IA might have experienced a conformation change during the reaction.[16] With mica addition, the absorption band of the –C–N stretching ($–CONH_2$) was shifted from 1448 to 1450 cm^{-1}. Furthermore, the weak absorption bands at 1016–1011 cm^{-1}, and the strong bands at 473–471 cm^{-1} intimate the existence of a Si–OH group in the nanocomposites (Fig. 2c,d), which have possibly acquired a conformation change during the reaction. Taken together, these observed peaks strongly support that the reaction product is the desired composite. Since the characteristic absorption peaks for the $–COO^-$ group on the IA and the mica Si–OH group are changed after the copolymerization, it is suggested that they have reacted together during the copolymerization.[16] One possible reaction is a grafting reaction (via the esterification reaction) of the OH groups on mica with the $–COO^-$ group on the IA,[44,45] where the OH groups in mica esterifies with the $–COO^-$ group on the IA and then radical chain polymerization takes place. Another possible mechanism is that the hydroxyl groups may react with the radicals and liberate free radicals on the mica structure and the graft polymerization can take place on these free radicals, giving IA–AM branches on the mica backbone.[45] We favor the latter suggestion that the grafting reaction takes place on the mica surface since it is observed that the amount of mica present influences the interaction between AM/IA and mica, as well as the swelling properties of the corresponding superabsorbent nanocomposites.

Micro-morphology and TEM analyses

The representative SEM micrograph of mica particles is shown in Fig. 3a which reveals their platelet and flake-like appearance with an average particle size of 3 μm. In contrast, surface of the copolymer without mica is rather smooth (Fig. 3b). Upon mica incorporation, the mica particles were evenly and well dispersed in the matrix of the superabsorbent nanocomposite, but as clusters (loose agglomerates or tight aggregates) of about 30–50 μm, rather than individual particles, imbedded in the polymer matrix (Fig. 3c,d). Strong particle adhesive forces might have caused this agglomeration. Mica has a plate-like structure (platelet) with a high aspect ratio of reinforcing particles and it has good adhesion to the matrix polymer. Both are of great importance because they control the final properties of the composites.

Internal structures of the nanocomposites, on a nanometer scale, were investigated using TEM since this allows a qualitative understanding of the internal structure through direct observation. It was postulated that some of the polymer chains, polymerized by the incorporation of the monomers, are distributed between the silicate layers resulting from the initial intercalation of both acrylate monomers with mica in solution. In some support for this notion was that poly(AM-*co*-IA)/2% w/w mica nanocomposites had a partially intercalated structure, displayed as the dark cross lines, indicating the parts of the polymeric intercalation into the interlayer spacing of mica (Fig. 4). The thickness of the cross lines were approximately 1 nm, which corresponds to the typical thickness of the clay layers, whereas the distance between the cross lines are the interlayer spaces,

 Copyright © 2009 John Wiley & Sons, Ltd.

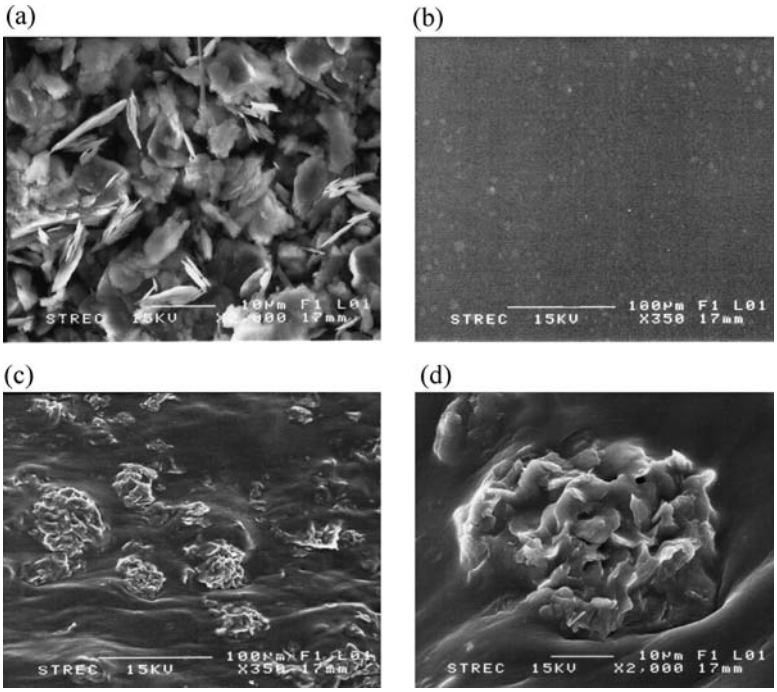

Figure 3. Representative SEM micrographs of (a) mica, (b) mica-free superabsorbent polymer, and (c, d) superabsorbent polymer/mica nanocomposites at a magnification of either (c) 350 × or (d) at 12,000 ×.

and the gray bases are the polymer matrix. These micrographs demonstrate that the inorganic phase (the mica particles) is dispersed at the nanometer level in the organic phase (copolymer). Consequently, the nanocomposites exhibit unique properties not being shared by their micro-scale counterparts or conventionally filled polymer.[46] The interlayer distance of mica in the nanocomposites obtained from TEM micrograph is about 13 Å, correlating well with the interlayer spacing characterized by XRD analysis.

X-ray diffraction analysis

XRD patterns supply very useful information on the gallery size of the final intercalated nanocomposites by measuring the increase in the basal (001) *d*-spacing, as depicted in the representative X-ray diffractograms in Fig. 5. The measured d_{001} of mica is 12.4 Å ($2\theta = 7.1^{\circ}$), and that of the mica composites (AM/IA mole ratio of 97:3) with 15 and 5% w/w mica have peaks at about $d = 14$ and 13.8 Å, corresponding to $2\theta = 6.3$ and 6.4°, respectively. According to the above TEM results, the increase in the basal interlayer spacing of mica implies that there is polymer intercalation within the stacked silicate galleries of mica.[46] A substantial increase in the intensity of the XRD peak is observed for the mica loading from 5 to 15% w/w which corresponds to the increased content in intercalated mica.

Table 2 summarizes the XRD analysis results which show that the peak position of the (001) basal plane remained approximately the same at different AM/IA ratios and mica contents, and thus the basal spacing is apparently independent of the content of IA and mica (within these tested ranges) in the prepared composites. However, the differing amounts of IA and mica at 0.2% mole N-MBA are responsible for the different water absorptions of the composites, which might imply that the limited amount of AM and IA monomers penetrated between the layers of clay during the dispersion of the clay into the monomer mixture. Hence, after the polymerization, the interlayer spacing of mica is widened due to the presence of the intercalated copolymer chains. The rest of the added IA content, which cannot penetrate within the clay interlayer, distributes within the mixture and copolymerizes with AM resulting in the enhancement of the water absorbency as the content of IA increases. Additionally, the increase in the hydrogen-bonding formation from the interaction of the carboxylic groups of IA with clay outside the gallery leads to the improved water absorbency. A 2-dimensional schematic representation of the composites containing low and high IA content is shown in Scheme 1. The data summarized in Table 2 also reveals that the different mica contents influence the water absorption capacity of the composite, which will be discussed later in "Effect of IA concentration and mica content on water absorbency" section.

Density of the synthesized poly(AM-*co*-IA)/mica nanocomposites

The main application of synthesized superabsorbent nanocomposites is to produce personal care products such as adult and baby diapers. Importantly then, the desired superabsorbent polymer or composite should not add extra weight to the diapers and this would provide discomfort to users. The densities relative to the poly(AM-*co*-IA) nanocomposite at 95:5 mole ratio of AM/IA, the poly(AM-*co*-IA)/mica nanocomposite densities were increased to 8.76 and 20.44% for 5 and 15% w/w of mica inclusion, respectively (Table 3). Given that optimal water absorption was attained at 5% w/w mica (Table 2) which inflicts only an 8.8% increase in the density of the polymer nanocomposites (Table 3), this should not prevent the development of an optimum product design that is comfortable for users.

 Copyright © 2009 John Wiley & Sons, Ltd. View this article online at wileyonlinelibrary.com

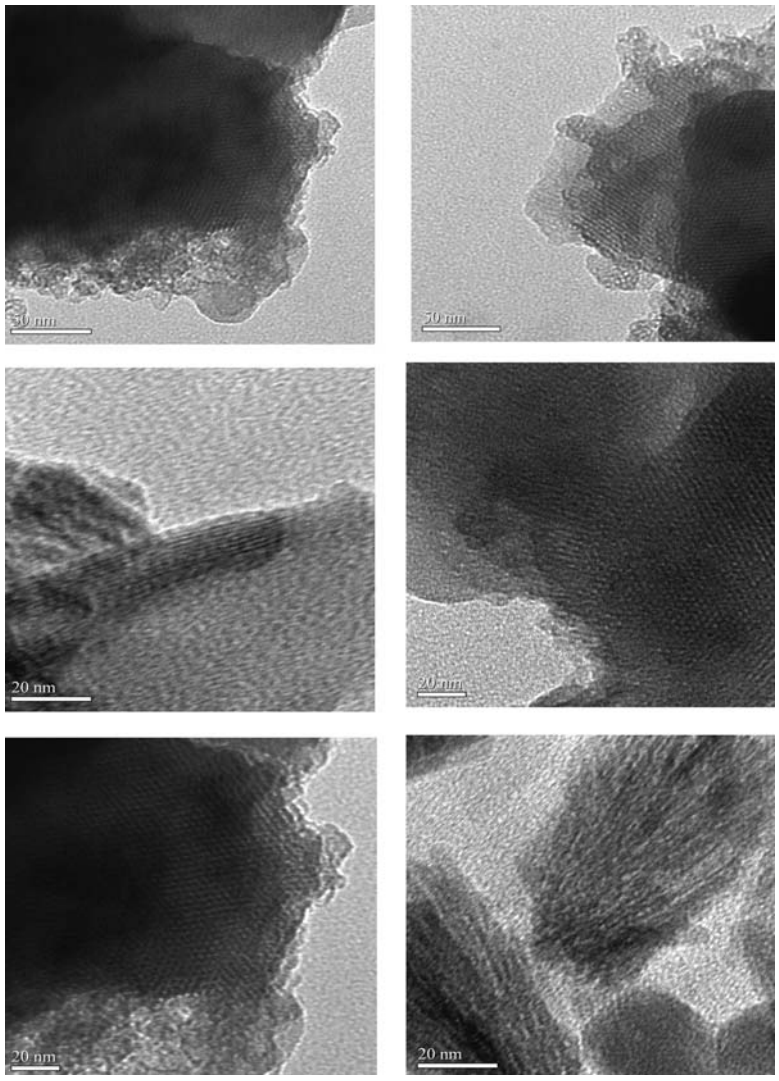

Figure 4. Representative TEM micrographs of poly(AM-*co*-IA)/mica nanocomposites at a 97:3 mole ratio with 2% w/w mica and crosslinked by 0.2% mole N-MBA.

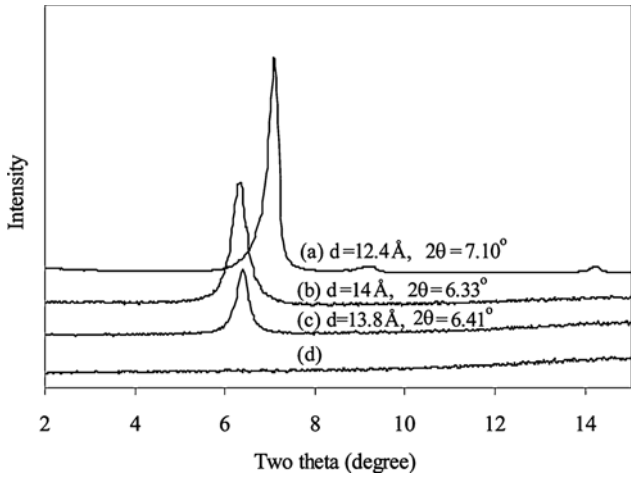

Figure 5. Representative X-ray diffraction patterns of (a) mica powder, (b, c) poly(AM-*co*-IA)/mica nanocomposites with either (b) 15 w/w mica or (c) 5% w/w mica, and (d) poly(AM-*co*-IA) copolymer. All copolymers had an AM/IA mole ratio of 97:3 and were crosslinked with 0.2% mole N-MBA.

The effect of N-MBA and IA concentrations on water absorbency

The relationship between water absorbency and N-MBA crosslinker concentration at three levels of IA concentration and two levels of mica incorporation is summarized in Fig. 6. The results show that the effect of mica addition at 5% w/w enhances the water absorbency and this is more marked at the high levels (5% mole) of IA and low N-MBA concentrations (0.2% mole). For the composite with 1% mole IA, the effect of the crosslinker is less effective when its contents were higher than 0.5% mole, implying that the crosslinker has crosslinked most of the IA molecules due to the higher reactivity ratios of N-MBA and IA. Thus, the crosslinking effect dominates the other minor effects to give nearly constant water absorption at higher N-MBA and mica contents. The effect of N-MBA crosslinker on decreasing the water absorption of the copolymers and their nanocomposites was obviously discernable at low levels of the crosslinker. However, at a higher concentration of crosslinker, the water absorption decreased gradually and was seen to level off. This behavior results from the cyclization and the multiple crosslinking reactions at pendant vinyl groups of the N-MBA.[47]

 Copyright © 2009 John Wiley & Sons, Ltd.

Table 2. The effect of AM/IA ratios and mica content on the XRD patterns and water absorption of crosslinked poly(AM-*co*-IA) and nanocomposites with 5 and 15% w/w mica

AM/IA ratio of composite	Mica content (% w/w)	Typical diffraction peak (°)	Basal spacing (Å)	Water absorption ($g\,g^{-1}$)
—	100	7.1	12.4	—
99:1	5	6.3	14	330
	15	6.4	13.9	250
97:3	5	6.4	13.8	420
	15	6.3	14	390
95:5	5	6.3	14	750
	15	6.4	13.9	590

Residual amount of AM monomer in the superabsorbents polymer

The residual amount of AM monomer in the superabsorbents polymer is another important issue of concern because the AM monomer is classified as a probable carcinogen and a known cumulative neurotoxin in humans. On the other hand, polyacrylamide is not known to display either bioactivity or harmful and is not considered hazardous for users.[48] The unreacted AM level in (nano) composites is summarized in Table 4. Note that although residual N-MBA will also be detected as well as free monomer by this method, this will serve to increase and not hide the free monomer estimates and thus they can be seen as conservative estimates of safe levels. In any case, and to err on the side of caution, we consider that such errors are likely to be small because the reactivity ratio, r_1 and r_2, values for AM/N-MBA are 0.64 and 1.77, respectively,[49] and N-MBA was only added at a final concentration of 2% mole, and thus would have rapidly reacted with the other monomers. Thus the analyzed value of the residual monomer will principally reflect the level of the AM monomer. Regardless, the residual amount of the AM monomer retained in the polymer was very low (about 0.1%) and its content will not be harmful to users because users are not in direct

Table 3. The densities of mica, crosslinked poly(AM-*co*-IA), and poly(AM-*co*-IA)/mica nanocomposites

Crosslinked poly(AM-*co*-IA), % w/w	Mica Content Added, % w/w	Density ($g\,cm^{-3}$)[a] of AM/IA at 95:5 mole ratio
—	100	1.94 ± 0.03
100	0	1.37 ± 0.04
100	5	1.49 ± 0.01
100	15	1.65 ± 0.03

[a] Data are displayed as the average $\pm$ 1 SD and are derived from four independent repeats.

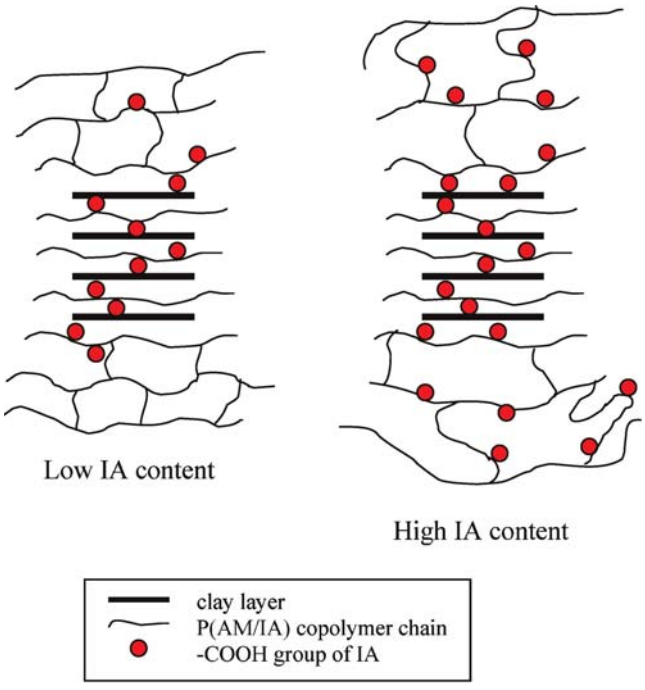

Scheme 1. A two-dimensional schematic representation of poly(AM-*co*-IA) intercalated within the mica galleries and grafted on the mica surface at low (1% mole) and high (5% mole) IA contents.

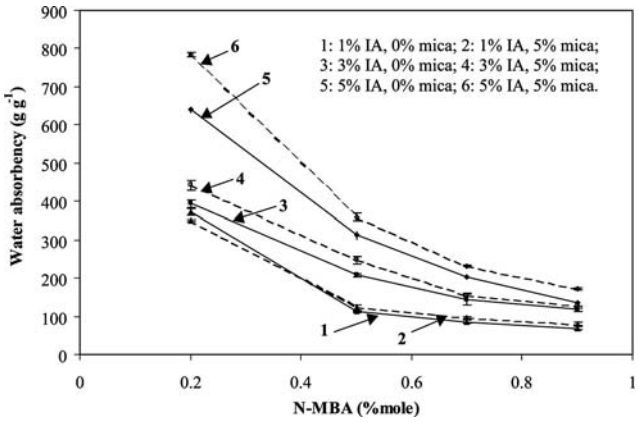

Figure 6. The effect of varying the N-MBA crosslinker concentration on the water absorbency (Q) of the crosslinked poly(AM-*co*-IA) copolymers and their nanocomposites with 5% w/w of mica addition at various IA concentrations.

 Copyright © 2009 John Wiley & Sons, Ltd. View this article online at wileyonlinelibrary.com

Table 4. The residual amounts of acrylamide monomer in the crosslinked polymer and polymer nanocomposites

AM/IA ratio	Initial acrylamide monomer concentration (ppm)	Residual acrylamide monomer in the crosslinked polymer[a]	
		ppm	%
100:0	71,080	94.2	0.13
99:1	70,369	54.7	0.08
95:5	67,526	56.5	0.08

[a] Data are displayed as the mean ± 1 SD and are derived from two independent repeats.

contact with the superabsorbent polymer enveloped in a napkin pad.

Effect of IA concentration and mica content on water absorbency

In deinoized water

Polyacrylamide superabsorbent prepared with 0.2% mole of crosslinker can absorb water at $35 \pm 1\,g\,g^{-1}$ dry weight, whereas the water absorbency of the synthesized poly(AM-*co*-IA) superabsorbents using the same amount of crosslinker vary from 372 ± 9 to $640 \pm 7\,g\,g^{-1}$ dry weight corresponding to the addition of 1–5% mole IA (as seen in Fig. 7 without the addition of mica). The increase in water absorbency of the copolymers is caused by the addition of IA into the polymer network. An increase in the IA concentrations increases the amount of free carboxyl groups (–COOH), and thus increases the electrostatic repulsive forces between the charge sites on the carboxylate ions upon their complete dissociation,[50] leading to expansion of the structure. The expanded structure with high IA contents causes a high degree of swelling and higher water absorption of the superabsorbent polymers and their composites.

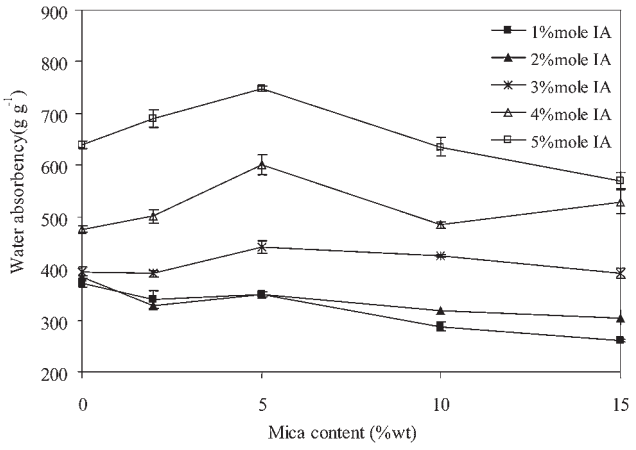

Figure 7. The effect of mica content on water absorbency (*Q*) of the 0.2% mole of N-MBA crosslinked poly(AM-*co*-IA)/mica nanocomposites.

In our superabsorbent preparation, we observed the formation of slurry if an IA content of higher than 5% mole was employed in the reaction mixture. This prohibits its use in personal care applications. The product cannot be dewatered with methanol and the dry gel could not be obtained. This result is in good agreement with the findings by Pulat and Eksi,[50] who reported that increase in the IA levels in copolymeric structures decreased the effective crosslinking densities of the polymer networks. As IA could not form superabsorbent polymers by itself, an excessive amount of IA in the monomer mixture made it more difficult to form a copolymer gel. The degree of swelling of the synthesized copolymers of AM and IA mainly depended on the repulsive forces between the hydrophilic pendants (amide and carboxylic groups) in their structures. The reactivity ratios of AM, IA, and N-MBA are 0.77, 1.36, and 1.77, respectively,[51] *i.e.* IA molecules are used up via a crosslinking reaction with N-MBA before AM monomer, even if the monomer feed concentrations are equal or higher. In the present case, the structure of the copolymer contained more units of uncrosslinked PAM moiety than crosslinked IA units owing to a higher AM concentration.

The water absorbency of superabsorbent polymer nanocomposites shows a similar trend to that of poly(AM-*co*-IA) copolymer in which the water absorbency increases with an increase in IA concentration (Fig. 7). The same rationale described previously is applicable here, where the highest swelling and the largest basal spacing of the superabsorbent polymer nanocomposites were achieved at 5% mole of IA. The result shows that the water absorbency tends to increase as the mica content increases from 0–5% w/w for the nanocomposite systems containing 3–5% mole IA, whereas the highest water absorption was found at 5% w/w mica. However, above a 5% w/w mica content, the water absorbency decreased, suggesting a rigidity effect from the added mica on the copolymer. As described in the previous section, it is likely that the intercalated structure was increased in the composite and the grafting reaction took place on the surface of mica. Increase in the mica levels will increase the crosslinking density of superabsorbent nanocomposites with decrease in the entropy of the chains as they become stiffer, giving a stronger gel with fewer available spaces for water to enter, and a decreased water swelling capacity.[27]

In contrast, mica inclusion does not significantly improve the water absorbency of the superabsorbent nanocomposites with 1 and 2% mole IA. As discussed above, the water absorbency of all the nanocomposites is decreased as the mica content increases beyond 5% w/w.

The mechanisms of the intercalation are complex and are not known in much detail. Gao[52] conjectured that there are three states in the composite structure. Here, we present such interactions occurring in our system using the speculation of Gao as indicated in Scheme 1. The first stage involves the polymer molecules intercalating into the interlayer spaces of the clay facilitated by Van der Waals interactions and hydrogen bonding between the polymer molecules (containing ionic groups from IA) and the hydrated interlayer cations and the silicate layer. The second stage is the binding of polymer chains to the outer surface of the clay particles via hydrogen bonds. Lastly, polymer chains located far from clay particles form networks by reacting with the N-MBA crosslinking agent. The latter has no interaction with the clay particles. Therefore, the overall structure of the composite would be quite complex. Understanding this complex structure will assist in predicting or searching the composite properties.

 Copyright © 2009 John Wiley & Sons, Ltd.

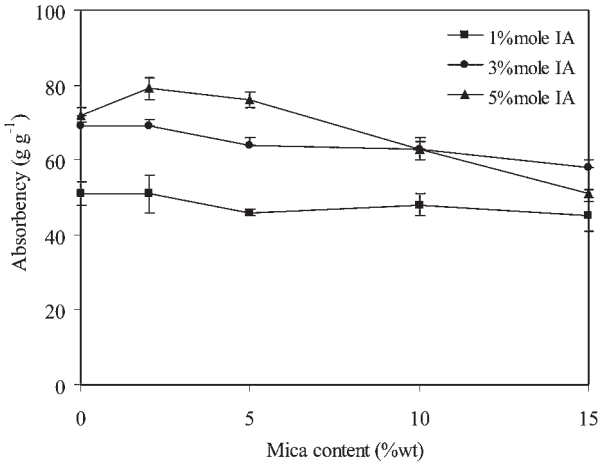

Figure 8. Water absorbency in artificial urine of the superabsorbent nanocomposites at AM/IA ratios of 99:1, 97:3, and 95:5, 0.2% mole of N-MBA, with various levels of mica content.

In ARU

A critical property in selecting a superabsorbent product for commercial use in personal care applications is the extent of swelling in ionic and osmoactive body-waste liquids such as urine and blood.[53] An acceptable swelling capacity is approximately 20–40 g of urine per gram of polymer. The amount of urine absorbed by various poly(AM-*co*-IA)/mica nanocomposites prepared with AM/IA ratios of 99:1, 97:3, and 95:5, at different mica contents were investigated and the results are summarized in Fig. 8. In general, the swelling of the superabsorbent nanocomposite in ARU is much lower than the swelling obtained in deinoized water due to the presence of salts in the urine solution, leading to a decrease in expansion of the gel networks caused by the repulsive forces of counter ions on the polymeric chain shielded by the bound ionic charges. Therefore, the osmotic pressure differences between the gel network and the external solution decrease with increase in ionic strength of the artificial urine.[54] The forces for the absorption of ionic solutions are attributed to the osmotic pressure based on the movable counter ions, the polymer-solvent affinity, and the rubber elasticity. The ionic strength of the artificial urine used in these studies was calculated[42] to be 0.0747 mol-ion dm^{-3} or 74.7 mM. Normal urine usually has an ionic strength of 10–800 mM or up to 1500 mM ionic strength in the mild dehydration, a superabsorbent polymer with higher urine absorption is needed to compensate the reduction of urine absorption caused by the salt effect. The ionic strength of the swelling liquid (e.g. urine) has an inversely proportional effect on the equilibrium-swelling ratio. The results show that the urine absorbency of the nanocomposites containing 1 and 3% mole of IA decreased slightly with increase in the content of mica. However, the nanocomposite with 5% mole IA yielded the highest urine absorption of all the samples, and this was maximal with the addition of 2% w/w mica, with higher mica levels significantly decreasing the urine absorbency of the nanocomposite. Likely, the decrease in the concentration difference of counterions inside and outside the superabsorbent particles is responsible for the decrease in urine absorption. Nanocomposites with high IA content (5% mole) showed a slight increase in urine absorbency with small mica additions (2 and 5% w/w), which is probably due to the increase in the osmotic pressure difference in the low chemically-crosslinking density system. However, why nanocomposites with 5% mole IA should show such a marked decrease in water absorption, with increasing mica levels above 5% w/w compared to those with lower IA levels, cannot currently be explained.

Water AUL

The poly(AM-*co*-IA) and poly(AM-*co*-IA)/mica nanocomposites with 5 and 15% w/w mica can absorb water up without load to 251 ± 4, 239 ± 10, and 201 ± 9 g g^{-1} of the dry copolymer within 1 min, respectively. The results shown in Table 5 indicate that the more the mica content in the nanocomposites, the lower the absorption rate for poly(AM-*co*-IA)/mica nanocomposites due to

Table 5. Effect of swelling time on water absorbency of the superabsorbent polymer*

poly(AM-*co*-IA) copolymer		Poly(AM-*co*-IA)/mica nanocompsoite			
		5%wt mica		15%wt mica	
Time (min)	Water absorbency (Q) g g^{-1}	Time (min)	Water absorbency (Q) g g^{-1}	Time (min)	Water absorbency (Q) g g^{-1}
1	251 ± 4	1	239 ± 10	1	201 ± 9
5	310 ± 7	5	290 ± 9	5	212 ± 8
10	313 ± 6	10	305 ± 7	10	230 ± 8
30	337 ± 9	30	327 ± 5	30	238 ± 7
60	340 ± 6	60	330 ± 4	60	235 ± 6
180	347 ± 8	180	341 ± 7	180	248 ± 10
300	357 ± 4	300	348 ± 8	300	255 ± 5
480	371 ± 10	480	350 ± 8	480	350 ± 9

*Polymerizations were carried out at the AM/IA ratio of 99:1, 0.2% mole of N-MBA, 0.3% mole of APS, 1.2% mole of TEMED, mica contents at 5 and 15% wt, 50°C, and 30 min. Each result was an average of three repeats with one standard deviation.

 Copyright © 2009 John Wiley & Sons, Ltd. View this article online at wileyonlinelibrary.com

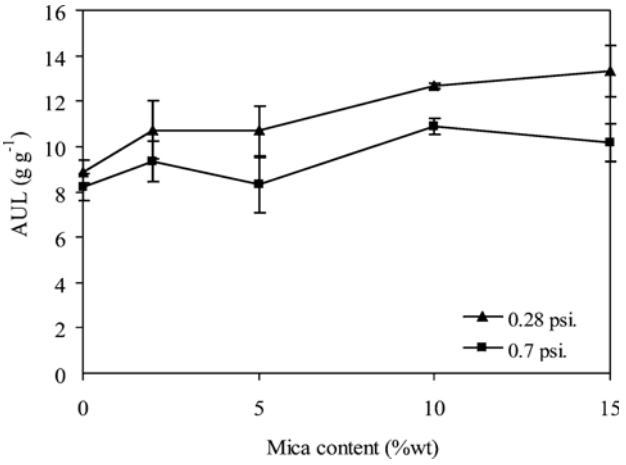

Figure 9. The effect of mica content on the absorbency under load (AUL) of the 0.2% mole of N-MBA crosslinked poly(AM-*co*-IA)/mica nanocomposites at a AM/IA mole ratio of 99:1.

the rigidity of the polymer chains resulting from a larger number of the crosslink density of the nanocomposites. The absorption rate sharply increased in the beginning, and the equilibrium absorbency could be achieved in 60 min for all of the polymers. Therefore, it is logical to carry out water AUL for 1 hr based on the extent of water absorbency and a few hours used as personal care products.

AUL measures the ability of a polymer to absorb fluid under a static load, and can be considered as a measurement of gel stability or gel strength. A high value of AUL correlates to a high gel strength. The water AUL (0.28 and 0.7 psi) of the poly(AM-*co*-IA)/mica nanocomposites in Fig. 9 was drastically reduced compared to those without a load, as depicted in Fig. 8. The heavier load at 0.7 psi yields a significantly lower absorbency at all levels of mica inclusion tested (0–15% w/w), presumably a larger compressive load restricts the flexibility and mobility of the polymer chains resulting in the lower water absorbency. Interestingly, the water AUL increased with the increase in the mica content, which is attributed to the fact that the mica particles act as crosslink points in combination with the polymer intercalation. When the mica levels are increased, the polymer crosslink density and rigid structure are simultaneously enhanced, thereby increasing the gel strength at the expense of water absorption underweight loading. Consistent with this notion, the results presented in Table 6 indicate that the gel strength attained in the nanocomposites of other AM/IA ratios also tend to increase with the mica content as well.

Viscoelastic properties of poly(AM-*co*-IA)/mica nanocomposites

The storage (G') and loss (G'') moduli, as a function of frequency, for the superabsorbents (AM/IA mole ratios of 99:1 and 97:3) at various mica contents are summarized in Fig. 10. The experiments were performed within the LVE region, as predetermined from stress sweep experiments (data not shown here). All the superabsorbents behaved as elastic networks where G' was approximately tenfolds larger than G'' at all studied frequencies. An elastic network is endowed with the formation of chemical crosslinking between the copolymers and N-MBA, and the physical interaction of the copolymer chains and mica particles.[55] The more distinct frequency-independent G' was observed in the system of 99:1 mole ratio of AM/IA, which means that this gel system has a more stable network structure when exposed to high frequencies. In contrast, the nanocomposites with a 97:3 mole ratio of AM/IA showed obvious frequency-dependent G' and G'' due to the ability of the superabsorbent to absorb high levels of water molecules. The frequency-dependent G' is characteristic of soft gels, which is sensitive to the applied frequency, especially at high frequency. Since the G' of all the nanocomposites were weak if they were frequency-dependent at the low frequency range, the equilibrium modulus (G_e), corresponding to the effective crosslink density, was determined from the value of G' at 0.1 rad sec^{-1}. Unfortunately, the experiments for nanocomposites with AM/IA ratios of 96:4 and 95:5 could not be performed due to the soft gel formation, which could not be used for the test.

Figure 11 shows the plots of equilibrium modulus and tan δ of the superabsorbents, extracted from the information in Fig. 10, as a function of mica contents. Tan δ is taken from the ratio of G''/G' and a value of tan $\delta < 1$ means that the system is elastic. In contrast, if tan $\delta > 1$, the system shows fluid-like behavior. The increase in G_e (the equilibrium modulus) with an increase in mica

Table 6. Water absorption under load of the crosslinked poly(AM-*co*-IA) and its nanocomposites at various mica contents

		Water absorbency under load (g g^{-1}) at AM/IA mole ratio				
Load (psi)	Mica (% w/w)	99:1	98:2	97:3	96:4	95:5
0.28	0	8.9 ± 0.5	9.6 ± 1.05	10.5 ± 0.4	10.6 ± 0.1	10.4 ± 0.2
	5	10.7 ± 1.1	9.7 ± 0.6	12.1 ± 0.5	10.6 ± 1.5	10.6 ± 0.1
	10	12.7 ± 0.1	11.7 ± 0.4	12.4 ± 0.6	11.7 ± 1.7	9.5 ± 0.8
0.7	0	8.2 ± 0.6	7.2 ± 1.4	8.9 ± 1.3	9.2 ± 0.9	7.6 ± 1.3
	5	8.3 ± 1.2	9.2 ± 0.1	10 ± 0.7	7.7 ± 0.4	8.1 ± 0.5
	10	10.9 ± 0.4	8.7 ± 0.3	10.5 ± 0.4	9.3 ± 1.0	7.7 ± 0.5

Data are displayed as the mean ± 1 SD and are derived from three independent repeats at the N-MBA content of 0.2% mole based on the monomer concentration.

 Copyright © 2009 John Wiley & Sons, Ltd.

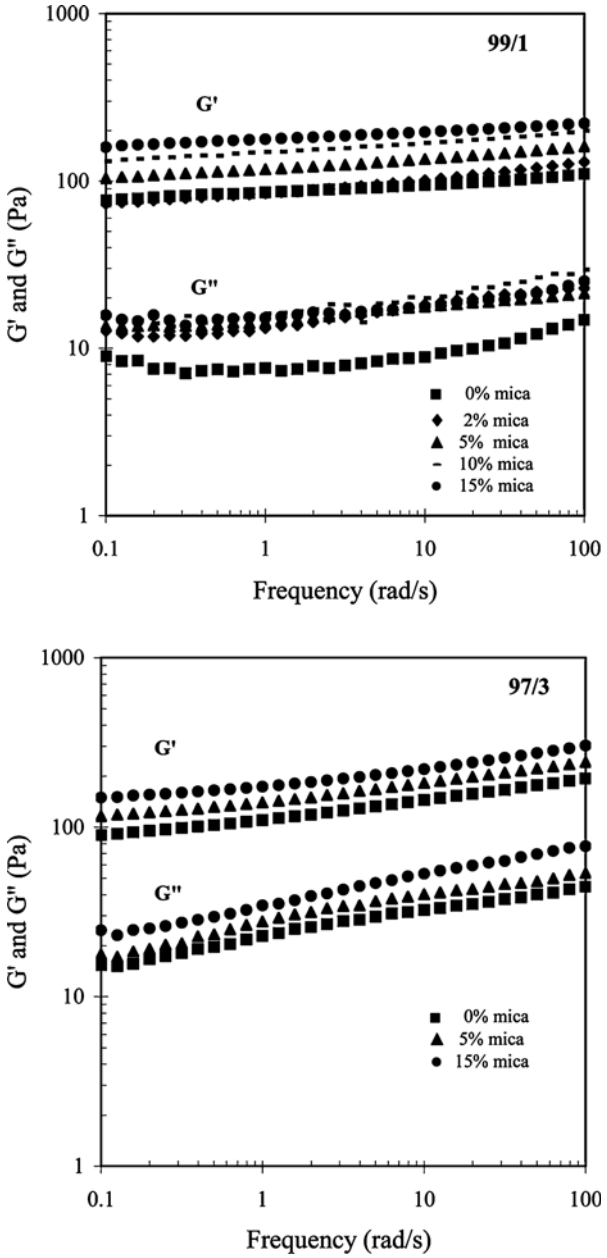

Figure 10. Angular frequency dependence of G' and G'' at the constant strain (1% strain) for the synthesized poly(AM-*co*-IA)/mica nanocomposites at the AM/IA ratio of 99:1 and 97:3, 0.2% mole of N-MBA, and at various mica contents.

content of both superabsorbent systems indicates an increase in the additional crosslinking density acquired from the formation of network structures between the copolymer chains and the mica particles. Typically, the increase in G_e due to an increase in network density results in a decrease in water absorbency (Q), as seen in composites with a 99:1 mole ratio of AM/IA (Fig. 11 inset). However, for composites containing 3% mole IA, although the network density increases (corresponding to an increase in G_e), Q increases as well up to 5% w/w mica addition. This strange behavior might be due to the alteration in the osmotic pressure exerted in the superabsorbent particles from the presence of counterions of the added mica; the more the counterion

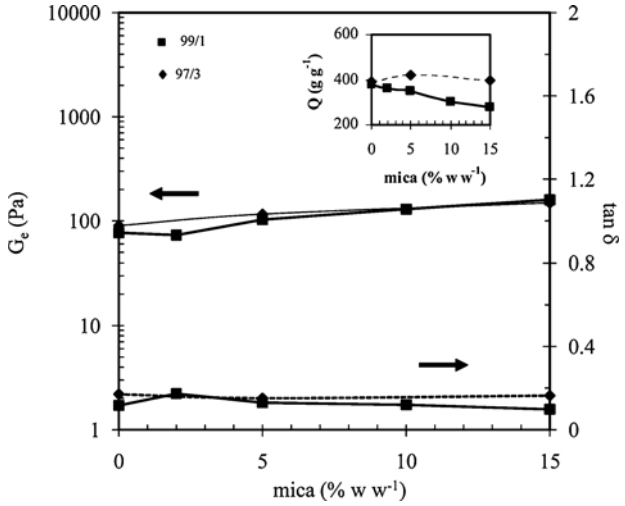

Figure 11. Equilibrium modulus (G_e) and tanδ (at 0.1 rad sec^{-1} where the G_e was taken) of the superabsorbent copolymers and the nanocomposite copolymer hydrogels prepared from AM/IA ratio of 99:1, 97:3 and at various mica contents. An inset is a plot of water absorption (Q) vs. mica content redrawn for a discussion.

concentration within the superabsorbent increases then so does the osmotic pressure. Therefore, the ionic nature of mica predominates its crosslinker effect and so the increase in superabsorbent swelling is induced by increase in the mica content.[55] Nevertheless, for both 1 and 3% mole composites, as the mica content is further increased, the crosslinking effect dominated.

Thermal properties of poly(AM-*co*-IA)/mica nanocomposites

For poly(AM-*co*-IA)/mica nanocomposites, the thermal stability of mica and composite residues at 800°C are both increased with increase in the mica content in comparison with the poly(AM-*co*-IA) without mica. The TGA results are shown in Fig. 12a–c. The increase in the thermal stability can be attributed to the high thermal stability of mica and to the interaction between the mica particles and the polymer matrix.[46] Moreover, the thermal stability of the composites is enhanced with increase in the mica contents from 5 to 15% w/w, which provides additional evidence of mica dispersion within the polymer matrix. Under mild stirring for a certain mixing time, the mica powder could be well dispersed and stabilized in the monomer solution. Mica acts as a heat barrier, thus delaying the diffusion of volatile thermo-oxidation products into gas, which results in the enhanced thermal stability of the system.[54] The amount of mica retained in the composites are in the range of 79–80%, regardless of the mica content added, as determined by the furnace test, which suggests that most of the mica was intercalated into the polymer network or was grafted, and a smaller amount (approximately 20% w/w) was dispersed in the suspension during the preparation of the superabsorbent polymer and was not used in the reactions and was removed during the process. Based on the above characterized properties of absorbency, viscoelastic, and thermal stability properties, we conclude that the gas permeability properties of the composites should not be affected in comparison with the neat polymer.

 Copyright © 2009 John Wiley & Sons, Ltd.

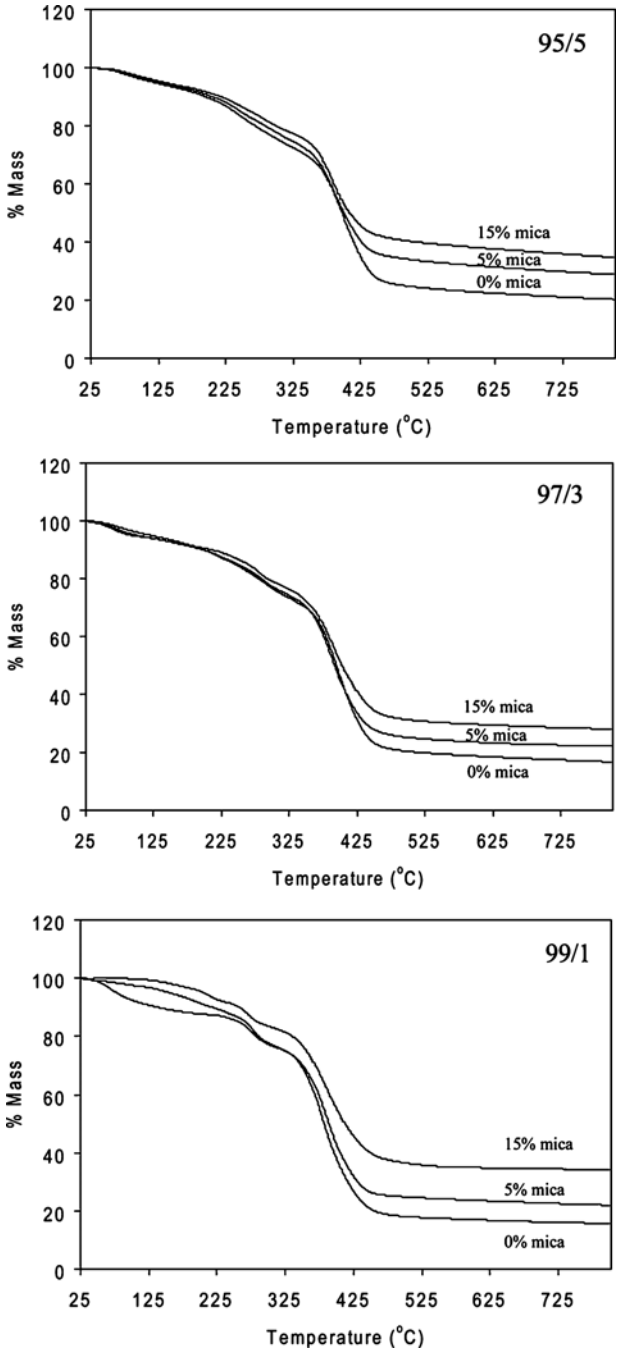

Figure 12. Representative TGA thermograms of the 0.2% mole of N-MBA crosslinked poly(AM-*co*-IA)/mica nanocomposites at AM/IA mole ratios of: (a) 99:1, (b) 97:3, and (c) 95:5, with various mica contents.

CONCLUSIONS

Crosslinked poly(AM-*co*-IA) copolymers and poly(AM-*co*-IA)/mica nanocomposites were successfully prepared in solution by redox polymerization. The FTIR characterization of the poly(AM-*co*-IA)/mica nanocomposites also gave the characteristic absorption peaks of $-COO^-$ from the carboxylic acid group in the IA moiety at 1665–1664 cm^{-1} and the absorption peaks of Si–OH group in mica at 1016–1011 cm^{-1} and 473–471 cm^{-1}. Increasing the IA concentration in the copolymer resulted in enhanced water absorbency of the superabsorbent polymers or polymer composites. By dispersing mica prior to polymerization, the swollen gel strength was increased as verified by the AUL and viscoelastic behavior. The TEM and XRD analyses of the composites indicated that the interlayer spacings of mica were enlarged, suggesting that the intercalation was successfully achieved. The addition of small (up to 5% w/w) mica content increased water absorption of the nanocomposites containing IA molecules at 3% mole and higher, but water absorption decreased with further increase in the mica content. The artificial urine absorption was found to decrease slightly with increase in the content of mica in the nanocomposites. However, at the AM/IA mole ratio of 95:5 with 2% w/w of mica, the water absorbency in the ARU of the superabsorbent nanocomposite reached its maximum at approximately 80 g g^{-1}. Thermal gravimetric analysis showed enhanced physical properties evidenced from the increased thermal stability with increasing mica content. Increase in the crosslinker concentration decreased the water absorbency of the nanocomposites. The residual amounts of AM monomer in the polymer and a high mica amount incorporated indicates that the solution polymerization is an acceptable synthesis route to prepare the superabsorbent polymer and superabsorbent polymer nanocomposite.

Acknowledgements

The authors are thankful for research facilities provided by the Polymer Imaging Laboratory of Chulalongkorn University's Imaging and Printing Technology Department, Faculty of Science. The authors would also like to thank the Publication Counseling Unit, especially Dr Robert Butcher, of the Research Division, Faculty of Science, Chulalongkorn University, for language correction and valuable suggestions.

REFERENCES

[1] F. L. Buchholz, A. T. Graham, Chapter 1. *Modern Superabsorbent Polymer Technology*. Wiley-VCH, New York, **1998**,
[2] G. Xu, G. Y. Wu, L. Li, *Special Petrochem.* **2002**, *1*, 42–44.
[3] T. Sakiyama, C. H. Chu, T. Fujii, T. Yano, *J. Appl. Poly. Sci.* **1993**, *50*, 2021–2025.
[4] T. Shiga, Y. Hirose, A. Okada, T. Kurauchi, *J. Appl. Polym. Sci.* **1992**, *44*, 249–253.
[5] T. Shiga, Y. Hirose, A. Okada, T. Kurauchi, *J. Appl. Polym. Sci.* **1993**, *47*, 113–119.
[6] P. Riccardo, J. Macromol, *Sci., Rev. Macromol. Chem. Phys.* **1994**, *34*, 607–662.
[7] A. Kikuchi, T. Okano, *Adv. Drug. Deliver. Rev.* **2002**, *54*, 53–77.
[8] W. F. Lee, K. T. Tsao, *J. Appl. Polym. Sci.* **2007**, *104*, 2277–2287.
[9] M. Kokabi, M. Sirousazar, Z. M. Hassan, *Eur. Polym. J.* **2007**, *43*, 773–781.
[10] United States Department of Agriculture. US Patent 3,981,100, **1961**.
[11] M. Yoshinobu, M. Morita, I. Sakata, *J. Appl. Polym. Sci.* **1992**, *45*, 805–812.
[12] M. J. Molina, M. R. Gómez-Antón, I. F. Piérola, *Macromol. Chem. Phys.* **2002**, *203*, 2075–2082.
[13] W. F. Lee, Y. C. Chen, *J. Appl. Polym. Sci.* **2005**, *97*, 855–861.
[14] X. Li, W. Wu, J. Wang, Y. Duan, *Carbohydr. Polym.* **2006**, *66*, 473–479.
[15] J. Z. Yi, L. M. Zhang, *Eur. Polym. J.* **2007**, *43*, 3215–3221.
[16] J. Wu, Y. Wei, J. Lin, S. Lin, *Polymer* **2003**, *44*, 6513–6520.
[17] W. F. Lee, L. G. Yang, *J. Appl. Polym. Sci.* **2004**, *92*, 3422–3429.
[18] Z. Weian, L. Wei, F. Yue'e, *Mater. Lett.* **2005**, *59*, 2876–2880.
[19] A. Li, A. Wang, *Eur. Polym. J.* **2005**, *41*, 1630–1637.
[20] J. Zhang, H. Chen, A. Wang, *Eur. Polym. J.* **2005**, *41*, 2434–2442.
[21] J. Zhang, H. Chen, A. Wang., *Eur. Polym. J.* **2006**, *42*, 101–108.
[22] Y. Xiang, Z. Peng, D. Chen, *Eur. Polym. J.* **2006**, *42*, 2125–2132.
[23] J. Z. Yi, L. M. Zhang, *Eur. Polym. J.* **2007**, *43*, 3215–3221.

 Copyright © 2009 John Wiley & Sons, Ltd.

[24] Y. Zheng, P. Li, J. Zhang, A. Wang., *Eur. Polym. J.* **2007**, *43*, 1691–1698.
[25] F. Santiago, A. E. Mucientes, M. Osorio, C. Rivera, *Eur. Polym. J.* **2007**, *43*, 1–9.
[26] J. Lin, J. Wu, Z. Yang, M. Pu, *Macromol. Rapid. Commun.* **2001**, *22*, 422–424.
[27] W. F. Lee, Y. C. Chen, *Eur. Polym. J.* **2005**, *41*, 1605–1612.
[28] J. Zhang, A. Wang, *React. Funct. Polym.* **2007**, *67*, 737–745.
[29] I. S. Miles, S. Rostami, *Multicomponent Polymer Systems*. Wiley, New York, **1992**.
[30] S. Kiatkamjornwong, W. Chomsaksakul, M. Sonsuk, *Radiat. Phys. Chem.* **2000**, *59*, 413–427.
[31] W. Jiraprasertkul, R. Nuisin, W. Jinsart, S. Kiatkamjornwong, *J. Appl. Polym. Sci.* **2006**, *102*, 2915–2928.
[32] S. Kiatkamjornwong, K. Mongkolsawat, M. Sonsuk, *Polymer* **2006**, *43*, 3915–3924.
[33] P. Lanthong, R. Nuisin, S. Kiatkamjornwong, *Carbohydr. Polym.* **2006**, *66*, 229–245.
[34] S. Kiatkamjornwong, P. Suwanmala, *Radiat. Phys. Chem.* **1997**, *50*, 617–624.
[35] S. Kiatkamjornwong, P. Suwanmala, *Radiat. Phys. Chem.* **1998**, *52*, 217–221.
[36] S. Kiatkamjornwong, P. Suwanmala, *J. Appl. Polym. Sci.* **1998**, *68*, 191–203.
[37] S. Kiatkamjornwong, R. Wongwatthanasatien, *Macromol. Symp.* **2004**, *207*, 229–240.
[38] S. Kiatkamjornwong, N. Siwarungson, A. Nganbunsri, *J. Appl. Polym. Sci.* **1999**, *73*, 2273–2291.
[39] D. Yiamsawas, W. Kangwansupamonkon, O. Chailapakul, S. Kiatkamjornwong, *React. Funct. Polym.* **2007**, *67*, 865–882.
[40] U.S. EPA Method8032A. SW-846 Rev 1. U.S. Environmental Protection Agency. Office of Solid Waste; 1996: http://www.ultrasci.com/analytical method.aspx?analyticalmethod (accessed April14, 2007).
[41] V. S. Joshi, M. J. Parekh, M. J. Joshi, A. D. B. Vaidya, *Urol. Res.* **2005**, *33*, 80–86.
[42] D. A. Skoog, D. M. West, F. J. Holler, *Fundamentals of Analytical Chemistry* (7th edn), Harcourt Brace & Company, Florida, **1991**.
[43] M. J. Ramazani-Harandi, M. J. Zohuriaan-Mehr, A. A. Yousefi, A. Ershad-Langroudi, K. Kabiri, *Polym. Test* **2006**, *25*, 470–474.
[44] P. S. Liu, L. Li, N. L. Zhou, J. Zhang, S. H. Wei, J. Shen, *J. Appl. Polym. Sci.* **2006**, *102*, 5725–5730.
[45] F. Zhang, Z. Guo, H. Gao, Y. Li, L. Ren, L. Shi, L. Wang, *Polym. Bull.* **2005**, *55*, 419–428.
[46] J. H. Chang, Y. U. An, D. Cho, E. P. Giannelis, *Polymer* **2003**, *44*, 3715–3720.
[47] J. N. Hamid, O. Oguz, *J. Appl. Polym. Sci.* **1996**, *60*, 971–979.
[48] A. Y. Gamel, H. A. Al-Maskati, A. Y. Ali, M. G. Dairi, *Mutat. Res.* **1993**, *300*, 91–97.
[49] J. Baselga, M. A. Llorente, J. L. Nieto, I. F. P. Hernández-Fuentes, *Eur. Polym. J.* **1988**, *24*, 161–165.
[50] M. Pulat, H. Eksi, *J. Appl. Polym. Sci.* **2006**, *102*, 5994–5999.
[51] N. Uyanik, C. Erbil, *Eur. Polym. J.* **2000**, *36*, 2651–2654.
[52] D. Gao, Superabsorbent polymer composite (SAPC) materials and their industrial and high-tech applications. *Ph.D. Thesis*, **2003**, Bergakademie, Freiberg University, Freiberg.
[53] H. A. Abd El-Rehim, *Radiat. Phys. Chem.* **2005**, *74*, 111–117.
[54] P. S. Keshava, Y. Mohan, J. Sreeramulu, K. Mohana, *React. Funct. Polym.* **2006**, *66*, 1482–1493.
[55] O. Okay, W. Oppermann, *Macromolecules* **2007**, *40*, 3378–3387.

 Copyright © 2009 John Wiley & Sons, Ltd.

Research Article

polymers advanced technologies

Received: 17 July 2009, Revised: 19 November 2009, Accepted: 18 December 2009, Published online in Wiley InterScience: 2010

(www.interscience.wiley.com) DOI: 10.1002/pat.1658

Gel strength and swelling of acrylamide-protic acid superabsorbent copolymers

Nispa Seetapan[a], Jiraporn Wongsawaeng[b] and Suda Kiatkamjornwong[b]*

The viscoelastic and swelling properties of polyacrylamide-based superabsorbent copolymers were investigated as a function of the ionic comonomer structure. Superabsorbent copolymers were synthesized by free-radical crosslinking copolymerization of acrylamide and one of the monoprotic acids (acrylic acid and crotonic acid) or the diprotic acids (maleic acid and itaconic acid) as the investigated ionic comonomer. The reaction composition of all components, i.e. monomer, comonomer, initiator, co-initiator, and crosslinker, was fixed to be the same for the synthesis of all four superabsorbent copolymer systems. Viscoelastic measurements were performed in all systems where the particles were closely packed. The network structures of all systems were evaluated via viscoelastic and swelling measurements. The results indicated that superabsorbent polymers (SAPs) with high water absorbency were accompanied by low gel strength and the calculated high value of molecular weight between crosslinks ($\overline{M}_c$) and low value of effective crosslinking density (ν_e). Diprotic acid-containing SAPs showed higher water absorbency over monoprotic acid-containing and non-ionic ones. The differences in $\overline{M}_c$ and ν_e values of each system were explained with respect to the differences in the monomer reactivity ratio and hydrophilicity of the comonomers. Copyright © 2010 John Wiley & Sons, Ltd.

Keywords: superabsorbent polymers; swelling; viscoelastic; molecular weight between crosslinks; crosslinking density

INTRODUCTION

Superabsorbent polymers (SAPs) are polymers that can absorb and retain water, saline solutions, or physiological fluids up to thousands times their dry weight. These properties correspond to the three-dimensional hydrophilic network structure of the polymers. They have received considerable attention not only in the fields of personal care products, biosorbent, biomaterials,[1] but also for agricultural soil,[2] wastewater treatment,[3–7] and other applications where water absorbency or water retention is important. Besides their hydrophilic nature, SAPs containing an ionic moiety have enhanced water absorbency compared to non-ionic ones.[8] Several ionic vinyl monomers, i.e. acrylic acid, itaconic acid, and so forth, have been selected to copolymerize with a non-ionic hydrophilic monomer like acrylamide to prepare SAPs with high degree of swelling.[6,7,9,10] Besides, one of the desired characteristics of SAPs is the optimum gel strength suitable for many applications. Both the desired properties (high swelling capacity and optimum gel strength) are in correlation with the network structure within the SAPs, which can be expressed as the average molecular weight between crosslinks ($\overline{M}_c$) and the effective crosslinking density (ν_e). The degree of crosslinking, the type and degree of ionic comonomer incorporated can be used to control the network structure, and thus the degree of swelling of SAPs.

Unlike the extensive determination of swelling behavior, few studies on the characterization of swollen gel strength of SAPs have been reported; for instance, Ramazani-Harandi *et al.*[11] recently determined the swollen gel strength of the commercial acrylic-based SAP polymer via rheological characterization based on non-destructive oscillatory measurements. Oscillatory measurement is typically used to measure viscoelastic properties of material.[12,13] Basically, the material is exposed to a small amplitude oscillatory stress (or strain), which is smaller than the critical value; the resulting strain (or stress) and phase lag between the input stress and the output strain are measured. This type of deformation can provide information on elastic energy storage and viscous energy dissipation, quantitatively represented as storage modulus (G') and loss modulus (G''), respectively. G' is proportional to the extent of the elastic component and G'' is rational to the extent of the viscous component of the system. The strength of materials is measured by the magnitude of $\tan\delta$ (the ratio G''/G'), where δ is a phase angle.

In this study, the gel strength and equilibrium water absorption capacity of acrylamide-based SAPs were examined through viscoelastic and swelling measurements, respectively. Four representative mono- and di-protic acids comonomers, namely,

* *Correspondence to: S. Kiatkamjornwong, Multidisciplinary Program of Petrochemistry and Polymer Science, Department of Imaging and Printing Technology, Faculty of Science, Chulalongkorn University, Phayathai Road, Bangkok 10330, Thailand.*
E-mail: ksuda@chula.ac.th

a *N. Seetapan*
National Metal and Materials Technology Center, National Science and Technology Development Agency, 114 Thailand Science Park, Paholyothin Road, Pathumthani 12120, Thailand

b *J. Wongsawaeng, S. Kiatkamjornwong*
Multidisciplinary Program of Petrochemistry and Polymer Science, Department of Imaging and Printing Technology, Faculty of Science, Chulalongkorn University, Phayathai Road, Bangkok 10330, Thailand

Contract/grant sponsor: Thailand Research Fund; contract/grant number: RTA5080004.

Copyright © 2010 John Wiley & Sons, Ltd.

acrylic, crotonic, maleic, and itaconic acids, having different hydrophilicity and monomer reactivity ratios toward the growing radicals, were selected to copolymerize with acrylamide. For comparison, acrylamide-based SAPs having four ionic comonomers were synthesized. All SAPs were synthesized via free-radical crosslinking polymerization. The reaction components, i.e. monomer, comonomer, initiator, co-initiator, and crosslinker, were fixed to be the same for all copolymeric systems. The network structure of each system was calculated via the equilibrium elastic modulus, obtained from the viscoelastic measurement using the polymer network theory. Likewise, the determination of the network structure in the prepared SAPs was performed using swelling data. Based on the monomer reactivity ratio and the hydrophilicity of comonomers, the obtained $\overline{M}_c$ and v_e were correlated to the network structure, swelling behavior, and the measured gel strength of the SAPs.

EXPERIMENTAL

Materials

Acrylamide monomer (AM, 99% (w w^{-1}) purity) received from Siam Chemical Industry, Samutprakarn, Thailand, was used as a monomer. Acrylic acid (AA, Fluka, Buchs, Switzerland), crotonic acid (CA, Fluka, Buchs, Switzerland), maleic acid (MA, Merck, Darmstadts, Germany), and itaconic acid (IA, Merck, Darmstadts, Germany), were used as received. The chemical structures of the acrylamide monomer and comonomers are shown in Fig. 1. Ammonium persulfate (APS, Merck, Darmstadts, Germany), *N,N,N′,N′*-tetramethylethylenediamine (TEMED, Fluka, Buchs, Switzerland), and methylenebisacrylamide (MBA, Fluka, Buchs, Switzerland) were used as the initiator, coinitiator, and crosslinker, respectively. Glacial acetic acid (CH_3COOH, BDH, Poole, England), phosphoric acid (H_3PO_4, 85% (w w^{-1}), Ajax, Sevenhills, Australia), boric acid (H_3BO_3, Merck, Darmstadts, Germany), and standardized sodium hydroxide (NaOH, Ajax, Sevenhills, Australia) were used to prepare 0.1 M Britton–Robinson buffers with pH values of the buffer adjusted to between 2 and 9 as desired by the addition of the appropriate amount of 0.2 M NaOH.[14] Deionized water (Elga Deionizer, Model LA611, Buckinghamshire, UK) was used for all solutions.

Preparation of polyacrylamide and acrylamide superabsorbent copolymers

SAPs were prepared by free-radical crosslinking polymerization. The concentrations of APS (initiator), TEMED (co-initiator), and MBA (crosslinker) were selected at 1.0, 2.0, and 1.0% by weight of the monomers, respectively. For the synthesis of copolymers, the molar ratio of acrylamide: anionic comonomer was fixed at 96:4. The reaction compositions for all (co)polymer synthesis are summarized in Table 1. Briefly, a mixture containing AM, comonomer, MBA, APS, and 100 cm^3 of deionized water was placed in a 500-cm^3 four-necked round-bottomed flask equipped with a mechanical stirrer (IKA Euro-ST B, Germany), a condenser, and an inlet tube of nitrogen gas. The reaction flask was immersed in a controlled thermostat water bath (Mammert, Swabach, Germany) and heated to 45°C with stirring at 250 rpm for 5 min. Then, TEMED was added to the mixture and polymerization was allowed to proceed for 30 min to ensure a complete polymerization.[7] The obtained product was dried at 60°C for 24 hr, milled, and then sieved through a 100-mesh sieve aluminum screen to obtain a dry irregular-shape powder with particle sizes <150 μm. To extract the uncrosslinked polymer and/or residual monomers from the gel particles, 1 g of the dry SAPs was then stirred in 300 cm^3 of distilled water at room temperature for 24 hr. The mixture was then separated to obtain the washed SAP and an aqueous extract. The washed SAP was dehydrated in methanol, dried at 60°C for 24 hr, ground, and then sieved via a 100-mesh sieve aluminum screen. To detect the unreacted comonomers, the aqueous extract was titrated with 0.05 M NaOH to a phenolphthalein end point. The existence of the synthesized superabsorbent copolymers was confirmed by Raman spectroscopy (Perkin Elmer, Spectrum GX, Massachusetts, USA).

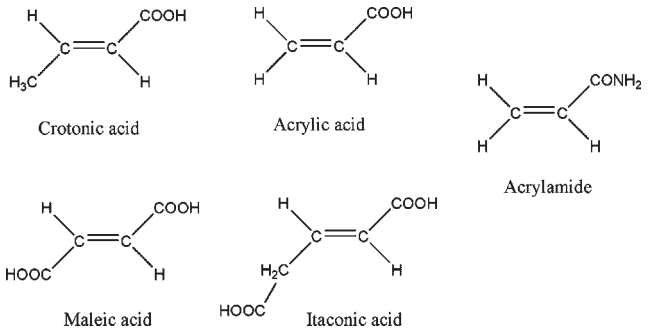

Figure 1. Chemical structures of acrylamide monomer and comonomers employed in the polymerization.

Swelling measurements

The swelling measurements of the superabsorbent copolymer particles were performed at room temperature. Deionized water and Britton–Robinson buffers at a pH ranging from 2 to 9, all with an ionic strength of 0.1 M, were employed as swelling media. The obtained 0.1 g of dry particles were allowed to swell in the 200 cm^3 deionized water for 24 hr to ensure the equilibrium (or maximum) swelling of the superabsorbent copolymers (based on our kinetic study of swelling). Subsequently, the fully swollen particles were separated from the unabsorbed medium by filtering through a 100-mesh sieve aluminum screen for 2 hr. Pieces of soft paper towel were used to absorb the unabsorbed water at the bottom of the screen until the swollen gel did not flow when the screen was held vertically. The swollen gel particle was then weighed and the water absorbency at equilibrium (Q_e, g g^{-1}) was calculated by

$$Q_e = \frac{\text{mass of fully swollen particle} - \text{mass of dry particle}}{\text{mass of dry particle}} = q_w - 1 \quad (1)$$

where q_w is the equilibrium weight swelling ratio of the superabsorbent copolymer particles.

The equilibrium volume swelling ratio (q_v) was then determined by eqn (2):

$$q_v = 1 + Q_e \left(\frac{\rho_{\text{polymer}}}{\rho_{\text{water}}} \right) \quad (2)$$

where ρ_{polymer} and ρ_{water} are densities of the dry SAP particles and water, respectively.

Copyright © 2010 John Wiley & Sons, Ltd.

Table 1. Feeding composition of monomers, crosslinker, initiator, coinitiator, and water[a] for the synthesized superabsorbent polymers

Superabsorbent polymers	Monomers		Crosslinker MBA (g)	Initiator APS (g)	Co-initiator TEMED (g)
	AM (g)	Comonomer (g)			
PAM	7.1080	—	0.0711	0.0711	0.1085
P(AM/AA)	6.8238	0.2838	0.0713	0.0714	0.1395
P(AM/CA)	6.8237	0.3446	0.0718	0.0717	0.1395
P(AM/MA)	6.8238	0.4644	0.0730	0.0729	0.1473
P(AM/IA)	6.8238	0.5204	0.0730	0.0735	0.1473

[a] Deionized water of 100 cm^3 was used for each SAP.

Swelling measurements were done in triplicate to obtain the average value of the water absorbency at equilibrium swelling.

Density measurements

The density of polyacrylamide superabsorbent and their copolymers was determined by the Ultrapycnometer 1000 (Quantachrome, Boynton Beach, Florida, USA), involving Archimedes' principle of fluid displacement and Boyle's law to determine the sample volume. The displacing material is helium gas, which can penetrate pores within samples. The experiment was performed by purging helium gas into the SAP samples at 23°C. The density was reported as an average value from five measurements, with the standard deviation (not shown here) being less than 0.002 g cm^{-3} for all samples.

Viscoelastic measurements

The viscoelastic experiments of the fully swollen SAP particles were carried out in a stress-controlled Gemini HR^{nano} rheometer (Malvern Instruments Ltd., Worcestershire, UK), and equipped with a solvent-trap and moisture controlling systems to prevent water evaporation during measurements. The operating temperature was 25°C, which was controlled by a peltier plate. The experiments were performed using acrylic parallel plate geometry (40 mm diameter, 1 mm gap). Firstly, a linear viscoelastic (LVE) region, where G' and G'' are independent of the stress amplitude, was determined by performing a dynamic stress sweep from 0.1–100 Pa at a fixed frequency of 1 Hz. Subsequent dynamic frequency sweep experiments were carried out within the evaluated LVE range.

The swollen SAP particles, after removing the unabsorbed water by filtering through the 100-mesh screen for 2 hr, were removed from the screen and placed on the measuring acrylic parallel plate of the rheometer. After loading the samples, they were allowed to relax for 10 min before carrying out each measurement in order to eliminate shear history from the sample loading. After the stress sweep experiment, a new swollen sample was loaded to perform the frequency sweep experiment at a fixed stress in the pre-determined LVE range. Three repetitions of viscoelastic measurements were performed for each sample and the obtained values of moduli were checked for reproducibility.

RESULTS AND DISCUSSION

Synthesis of acrylamide-based superabsorbent copolymers

The synthesized superabsorbent copolymers along with their functional groups were confirmed via Raman spectrometry (whose spectra are not shown here). The strong peak of the carboxylate group at 1648–1651 cm^{-1} for all SAPs, attributed to the C=O stretching, corresponds to a conformational change during the crosslinking reaction. The peaks at 3330, 3200, 2920, and 1320 cm^{-1} represent N–H, O–H, C–H, and C–N stretching, respectively. The results indicate that all SAP samples are acrylamide-based copolymers. Based on the titration experiment of the extracted solution, the end point detection was very low. Thus, one may conclude that acrylamide and anionic comonomer were essentially completely consumed in the crosslinking copolymerization.

Swelling experiments

Swelling in deionized water

As summarized in Table 2, the equilibrium water absorbency (Q_e) of each of the crosslinked ionic copolymers in deionized water was larger than that of crosslinked PAM, most likely as a result of the ionic (carboxylic acid) pendants in the copolymer structure to increase osmotic pressure inside the gel. The superabsorbent copolymers containing diprotic acid moieties, P(AM/MA) and

Table 2. Equilibrium water absorbency (Q_e), equilibrium volume swelling ratio (q_v), and equilibrium elastic modulus (G_e) of the superabsorbent polymers swollen in deionized water

Superabsorbent polymers	Q_e (g g^{-1})	q_v	G_e (Pa)
PAM	33 ± 1	46 ± 2	1,020 ± 20
P(AM/AA)	131 ± 7	174 ± 10	480 ± 15
P(AM/CA)	44 ± 2	59 ± 4	870 ± 20
P(AM/MA)	160 ± 4	210 ± 6	330 ± 15
P(AM/IA)	294 ± 6	393 ± 9	200 ± 15

The data were obtained from three replicates.

 Copyright © 2010 John Wiley & Sons, Ltd.

P(AM/IA), absorbed more water than the monoprotic acid-containing superabsorbent copolymers, P(AM/AA) and P(AM/CA). The possible reason is that more resultant density of ionic groups present in the copolymer network derived from the diprotic acid comonomers leads to an increase in electrostatic repulsive forces between charged sites on the carboxylate anions upon their complete dissociation and thus leads to a more extended configuration.[9] The result also showed that although the P(AM/CA)-SAPs contain monoprotic acid in the network structure, the water absorbency was insignificantly different from that of the non-ionic PAM-SAPs. We postulate that the reason might be attributed to the huge difference in the reactivity ratio between AM and CA, and the relatively low hydrophilicity of CA (to be discussed below).

Swelling in Britton–Robinson buffer at various pHs

Figure 2 summarizes the data showing the pH dependence of the equilibrium water absorbency of PAM and the four copolymeric SAPs in Britton–Robinson buffers with pH values from 2 to 9 and a fixed ionic strength of 0.1 M. The water absorbency of pure PAM was not influenced by the pH of the swelling medium, as expected due to its non-ionic hydrophilic nature. In contrast, the swelling behavior of three of the four anionic SAPs, P(AM/AA), P(AM/MA), and P(AM/IA), increased with increase in the pH of the swelling medium, due to their polyelectrolyte nature. However, the swelling behavior of the P(AM/CA)-SAPs merely responded to the variation in the pH of medium. This result is consistent with those of Çaykara *et al.*,[15] who reported that there was very little effect of pH on the swelling behavior of crosslinked P(AM/CA) synthesized at a 95.3:4.7 molar ratio of AM:CA, which is very similar to the 96:4 ratio used here. However, as the content of CA in the copolymer was increased, so the pH-dependent swelling behavior of the copolymer was apparently increased, and they concluded that the equilibrium volume swelling depended greatly on the mole fraction of ionizable carboxylic acid groups in the network.[15] We postulate that other reasons for the fairly pH-sensitive swelling of P(AM/CA) (96:4 molar ratio) might be attributed to the significant difference of the reactivity ratio between AM and CA, and the hydrophobicity of CA (to be discussed below).

Swelling of an ionic network is expected to significantly increase with a higher content of the ionic moiety within its structure. Anionic copolymeric SAPs are ionizable because of the presence of charged carboxylic acid groups. Each of the two monoprotic acids tested has a single dissociation constant with a

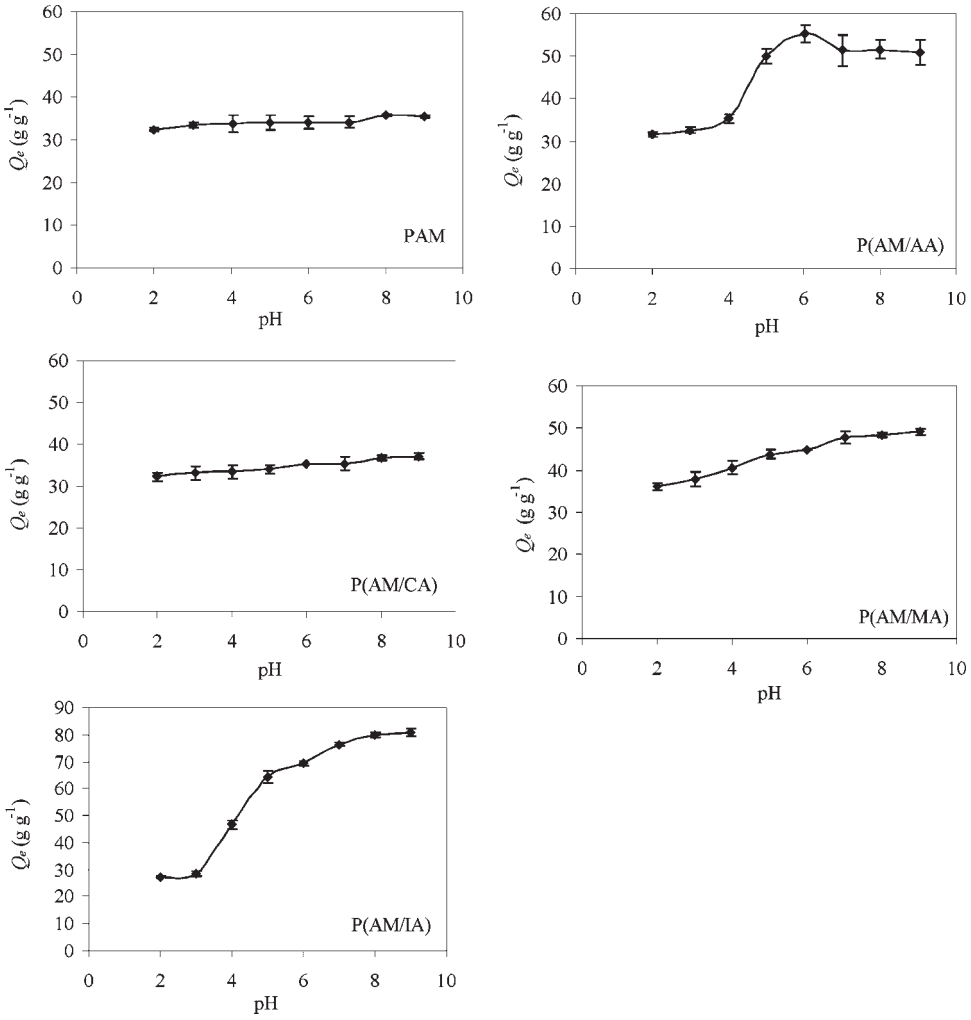

Figure 2. The effect of pH on the equilibrium water absorbency (Q_e) of SAPs: PAM, P(AM/AA), P(AM/CA), P(AM/MA), and P(AM/IA).

Copyright © 2010 John Wiley & Sons, Ltd.

polymers advanced technologies

pK_a of 4.25 and 4.69 for AA and CA, respectively, whilst the two diprotic acids have two dissociation constants, i.e. a pK_{a1} of 1.83 and 3.85, and a pK_{a2} of 6.07 and 5.45 for MA and IA, respectively.[14] Theoretically, as the pH is increased there should be a sudden increase in the gel swelling as the pH nears the pK_a of the monoprotic acid containing SAPs, with a two-step swelling pattern for diprotic acid containing SAPs corresponding to their respective pK_{a1} and pK_{a2}. Of course, experimentally, these may be less sharp due to local environments changing some of the effective pK_a values within the copolymer and, if the two dissociation constants are relatively close, their overlapping (merging) would lead to a single broad swelling of the network at around these pH values, as was reported for crosslinked poly[(*N*-vinyl-2-pyrrolidone)-*co*-(itaconic acid)].[16]

In this study (Fig. 2), an increase in the buffer pH resulted in an increase in the equilibrium water absorbency. At a low pH, ionization of the ionic groups in the SAPs is suppressed by H^+ ions in the swelling medium and so flexibility of the chain is rather low. As the pH is increased, the ionic units dissociate and attract cations into the SAPs to replace H^+ ions. The concentration of mobile ions inside the SAPs is, therefore, enhanced, which causes an increase in the ion swelling pressure. As a consequence, the equilibrium water absorbency increases. Such a trend is clearly seen for P(AM/AA)- and P(AM/IA)-SAPs, the latter showing the expected partial mergence of the pK_{a1} and pK_{a2} responses, whilst allowing for the fact that the pK_{a1} of IA is below the pH range tested, the expected trend for gel swelling around the pK_{a2} range was also noted for P(AM-IA). However, no such a trend was easily discernable for P(AM-CA)-SAPs (Fig. 2)

Viscoelastic experiments

Viscoelastic studies of our swollen SAP particles in deionized water were determined by means of the rheological method. Our investigated swollen particles consist completely of a system of closely packed gel particles. Their viscoelastic behaviors could be explained by interparticle interactions. The strength of such interactions, therefore, determined viscoelastic properties of the systems. Firstly, stress sweep experiments were performed to determine the LVE regime, where G' and G'' are independent of the stress amplitude, as shown in Fig. 3(a). The storage modulus was always larger than the loss modulus at the LVE regime. The extent of LVE range extended differently in each sample as observed from the deviation of the value of both moduli from linearity as the applied stress increased. The maximum stress up to which G' remains constant is called the critical stress (σ_c) which indicates a transition between linear and nonlinear regimes. The critical stress can be taken as the dynamic yield stress value. This means that below the critical stress the system behaves like an elastic solid. At the external applied stress beyond σ_c, the internal network structure started to break down and subsequently material flowed like a liquid. The result showed that the LVE range and the critical stress increased in sequence of P(AM/IA) < P(AM/MA) < P(AM/AA) < P(AM/CA) < PAM. The wide LVE region and large σ_c indicated that the system had good ability to resist external stresses to a greater extent. Furthermore, the values of tan δ are plotted in Fig. 3(b). Tan δ is the ratio of G''/G', where δ is a phase angle. If the value of tan δ is larger than 1 ($G'' > G'$), the system behaves like a liquid; whereas, if the value of tan δ is smaller than 1 ($G'' < G'$), the system shows solid-like (gel or network) behavior. Therefore, the strength of the interaction or internal structure is basically measured by the magnitude of tan δ. The smaller the tan δ is, the stronger the interaction becomes. The results indicated that the strength of SAP particles inversely correlated to the water absorption capability. As a comparison to other systems, PAM and P(AM/CA) SAPs had indifferent ability to hold water and could absorb a small amount of water; thus, the larger G' and the smaller tan δ were found in both the systems. On the contrary, P(AM/IA) SAP had ability to absorb the largest amount of water, and thus, it possessed the lowest gel strength.

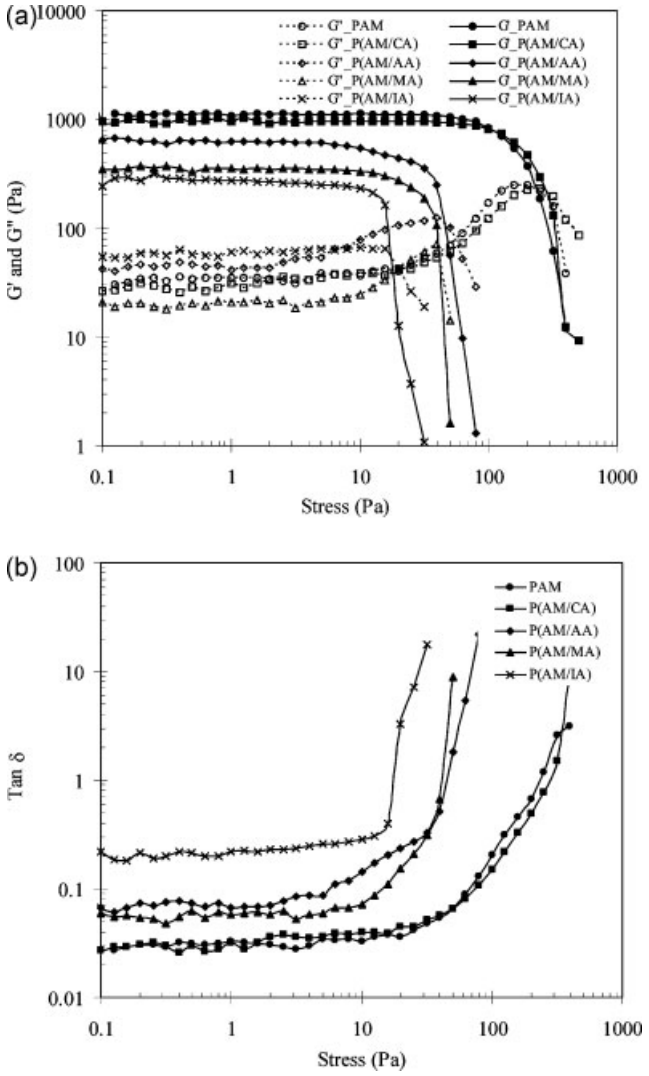

Figure 3. Viscoelastic properties of the SAPs swollen in deionized water, (a). storage (G') and loss (G'') moduli, and (b). tan δ as a function of stress.

It is interesting to note that for all the systems, except P(AM/IA), above the critical stress where a destruction of the gel particles occurred, a maximum in G'' was observed at a stress level close to where the viscoelastic response became primarily dissipative (tan $\delta \sim 1$) and subsequently dropped at the larger applied stress. This behavior was very similar to a characteristic of nonlinearity, observed in the behavior of close-packed colloidal dispersions.[17–19] A slightly gradual drop in G' whereas G'' began to increase and reflected the onset of nonlinear, yielding when the stress approached a critical value where the particles were forced

 Copyright © 2010 John Wiley & Sons, Ltd.

to exchange positions with their neighbors, and hence the material could more effectively dissipate energy. At a larger stress where a progressive drop in G' was observed in association with a decrease in G'' after passing through a maximum, indicating the onset of plastic flow region.

Unlike the others, the SAP of P(AM/IA) did not show a maximum in G'' when the applied stress was increased. However, it behaved somewhat like a linear polymer solution. This was likely from the ability to absorb a large amount of water in P(AM/IA). As a result, when the applied stress approached the critical stress, the swollen particles, which were comparatively very soft, did not have enough strength to hop over the neighboring particles; therefore, the system flowed instead, which was consistent to the decreases in both moduli beyond the LVE region.

Figure 4 summarizes the observed storage (G') and loss (G'') moduli as a function of frequency for all the swollen SAP particles. The experiments were performed within the LVE region, as determined from stress sweep experiments. The viscoelastic behavior was dominated by an elastic character where G' was 10-fold larger than G'' at all frequencies studied (0.01–10 Hz). Additionally, no significant frequency-dependent changes in G' were observed for SAPs of PAM, P(AM/CA), P(AM/AA), and P(AM/MA), whereas a slightly frequency-sensitive G' was observed for the P(AM/IA)-SAPs over the whole range of tested frequencies. Systems containing a higher level of small molecules (water molecules in this case) can dissipate more energy and thus, at a high frequency (corresponding to a short time scale), an increase in G'' is expected for a system absorbing a large amount of water such as P(AM/IA) SAPs. The flatness of G' over an appreciable decade of frequencies indicates a characteristic of a gel system.[12] Since G' of all the systems at a low frequency range was not distinctly frequency-dependent, the equilibrium modulus (G_e), shown in Table 2, was determined from G' at 0.01 Hz. Table 2 indicates that Q_e was found to be inversely correlated with G_e. A higher amount of water molecules inside the SAPs causes a higher mobility of the network chains and so leads to a lower strength of the system as observed from a lower G_e and larger $\tan\delta$.

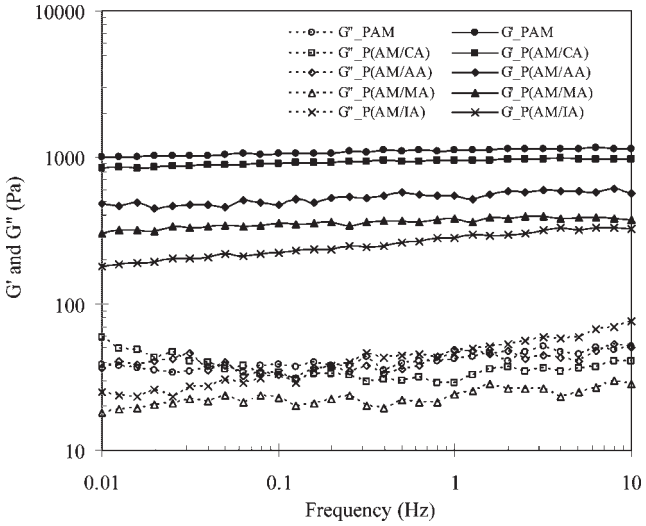

Figure 4. Storage (G') and loss (G'') moduli as a function of frequency for SAP particles swollen in deionized water.

Determination of $\overline{M}_c$ from viscoelastic and swelling experiments

Viscoelastic behavior of particle dispersions is influenced by particle size, particle dispersity, volume fraction occupied by particles, and the gel strength of particles. Our investigated dried SAP particles with classified particle size were allowed to swell into an equilibrium stage. Each system had different ability to absorb water depending on the type of ionic comonomer, degree of crosslinking density within the particles, and the balanced osmotic pressure of the system. Therefore, the swollen particle size of each system was unequal. However, all systems were characterized in the close-packed region, where all of the spaces were occupied by the swollen particles. The swollen particles contacted one another; as a result, the elastic response dominated over the dissipative energy. Within this region, the magnitude of storage modulus and the strength of the system were strongly influenced by the degree of crosslinking within the particles. Crosslinking density is related to the average molecular weight between crosslinks ($\overline{M}_c$), which can be determined via viscoelastic measurements. The theory of polymer networks predicts the equilibrium elastic modulus (G_e) for polymer gels obtained by the crosslinking polymerization as given in

$$G_e = \left(1 - \frac{2}{\phi}\right)\left(\frac{\rho_2}{\overline{M}_c}\right) RT {\nu_{2r}}^{2/3} {\nu_{2m}}^{1/3} \tag{3}$$

where ϕ is the number for branches originating from a crosslinking site ($\phi = 4$ for tetrafunctional networks), ρ_2 is the polymer network density, R is the gas constant, and T is the temperature.[20] The factor $(1 - 2/\phi)$ is introduced for systems in a highly swollen state such as hydrogel (Phantom networks). The value of G_e is reported in Table 2. The ν_{2m} is the volume fraction of polymer network, which can be calculated by

$$\nu_{2m} = \frac{1}{q_v} \tag{4}$$

The ν_{2r} is the volume fraction of the network after the polymerization, which can be identified as shown in eqn (5):

$$\nu_{2r} = c_o V_r \tag{5}$$

where c_o is the initial concentration of monomers (mol cm^{-3}).[21] V_r is the average molar volume of polymer repeating units, and can be calculated as shown in eqn (6):

$$V_r = M_r/\rho_2 \tag{6}$$

where M_r is the molecular weight of the repeating unit in the copolymers,[21] and is determined from eqn (7):

$$M_r = [M_n(1 - f_i) + M_i(f_i)] \tag{7}$$

where M_n is molecular weight of a neutral unit (acrylamide monomer), and M_i is the molecular weight of an ionic unit (comonomer) in the system, f_i is a mol fraction of the ionic unit in the system ($f_i = 0.04$). Table 3 contains parameters essential for calculating $\overline{M}_c$, according to eqn (3). The determined values of $\overline{M}_c$ (from eqn (3)) obtained from viscoelastic measurement are listed in Table 4. The result indicated that SAPs with higher swelling capability exhibited lower gel strength as a result of the larger $\overline{M}_c$.

Copyright © 2010 John Wiley & Sons, Ltd.

Table 3. Density and essential parameters used to determine network parameters

Superabsorbent polymers	ρ_2 (g cm^{-3})	M_r (g mol^{-1})	V_r (cm^3 mol^{-1})	c_o (mol cm^{-3})	ν_{2r}
PAM	1.3669	71.08	52.00	0.001	0.0519
P(AM/AA)	1.3174	71.12	53.98	0.001	0.0537
P(AM/CA)	1.3369	71.68	54.41	0.001	0.0543
P(AM/MA)	1.3116	72.88	55.57	0.001	0.0555
P(AM/IA)	1.3321	73.44	55.13	0.001	0.0550

We attempted to determine $\overline{M}_c$ of all prepared SAPs from the equilibrium degrees of swelling. The average molecular weight between crosslinks for non-ionic phantom networks is expressed as shown in

$$\overline{M}_c = -\frac{\left(1-\frac{2}{\phi}\right)V_1\rho_2{\nu_{2r}}^{2/3}{\nu_{2m}}^{1/3}}{[\ln(1-\nu_{2m})+\nu_{2m}+\chi\nu_{2m}^2]} \quad (8)$$

where V_1 is the molar volume of the swelling agent, and χ is the Flory polymer–solvent interaction parameter.[22] Therefore, as also shown in Table 4, the $\overline{M}_{c\ \mathrm{swelling}}$ values of PAM superabsorbents were calculated according to eqn (8) using the literature reported χ values.[23–25] It has to be noted that a small difference in the reported χ values gives a very large difference in the calculated $\overline{M}_c$. Mahmudi *et al.*[26] suggested that the values of $\overline{M}_c$ and crosslink density can be correctly determined from swelling experiments if the χ parameter is reliably accepted or experimentally evaluated.

The swelling behavior of non-ionic network is thermodynamically dominated by contributions from the chemical potentials of mixing and elasticity. Upon swelling in an aqueous solvent, the diffusion of water into the network is driven by forces generated from the difference between the chemical potential of water inside and outside of the network until the equilibrium swelling is reached. This elastic contribution prevents the network from becoming completely dissolved. If networks contain ionizable groups within polymer chains, an additional force from the ionic contribution influences the swelling, where an increase in swelling is expected due to charge localization within the ionic network.[27,28] Therefore, the equation to determine $\overline{M}_c$ of monoprotic acid-containing networks synthesized by the simultaneous polymerization and crosslinking reaction of the monomers was derived, as shown in eqn (9):

$$\left[\frac{K_a}{10^{-\mathrm{pH}}+K_a}\right]^2\frac{V_1 f_i^2}{4I\overline{V}_r^2}-\nu_{2m}^{-2}\ln(1-\nu_{2m})-\nu_{2m}^{-1} = \chi+\frac{\left(1-\frac{2}{\phi}\right)V_1\rho_2\nu_{2r}^{2/3}\nu_{2m}^{-5/3}}{\overline{M}_c} \quad (9)$$

where K_a is the dissociation constant of monoprotic acid, I is the ionic strength of the swelling medium, and f_i is the weight fraction of ionizable polymer in the gel system.[15]

In case of diprotic-acid containing networks, the equation was proposed by Çaykara *et al.*[29] as given in

$$\left[\frac{2K_{a1}K_{a2}+10^{-\mathrm{pH}}K_{a1}}{2\left[(10^{-\mathrm{pH}})^2+10^{-\mathrm{pH}}K_{a1}+K_{a1}K_{a2}\right]}\right]^2\frac{V_1 f_i^2}{4I\overline{V}_r^2} - \nu_{2m}^{-2}\ln(1-\nu_{2m})-\nu_{2m}^{-1} = \chi+\frac{\left(1-\frac{2}{\phi}\right)V_1\rho_2{\nu_{2r}}^{2/3}{\nu_{2m}}^{-5/3}}{\overline{M}_c} \quad (10)$$

where K_{a1} and K_{a2} are the first and second dissociation constants of diprotic acid, respectively.

Therefore, data obtained from swelling experiments as a function of the pH (Fig. 2) were used to evaluate $\overline{M}_c$ using eqns (9) and (10) for mono- and di- protic acid-containing copolymeric SAPs, respectively. The equations also provided the χ parameter of each system. If one defines the left-hand side, and the coefficient of $1/\overline{M}_c$ on the right-hand side of eqns (9) and (10) to be constant values of A and B, respectively, as described in

Table 4. Network parameters of the superabsorbent particles

Superabsorbent polymers	$\overline{M}_{c\ \mathrm{viscoelastic}}$ (g mol^{-1})	$\overline{M}_{c\ \mathrm{swelling}}$ (g mol^{-1})	χ_{swelling}	$\overline{M}_{c\ \mathrm{stoi}}$ (g mol^{-1})
PAM	65,000 ± 1,800	37,000*, 76,000**	0.480*, 0.494**	7,726
P(AM/AA)	87,000 ± 3,800	51,200 ± 2,800	0.491 ± 0.001	7,730
P(AM/CA)	70,000 ± 2,300	8,750 ± 150	0.401 ± 0.004	7,625
P(AM/MA)	120,000 ± 7,700	3,6450 ± 50	0.477 ± 0.003	7,753
P(AM/IA)	163,000 ± 17,000	184,000 ± 3,400	0.503 ± 0.001	7,650

* Literature reported χ values[23,24].
** Literature reported χ values[25].

 Copyright © 2010 John Wiley & Sons, Ltd.

eqn (11), the plot of A against B correspondingly gives χ and $\overline{M}_c$ as the intercept and inverse slope via a linear regression analysis.

$$A = \chi + B/\overline{M}_c \tag{11}$$

In this study, the related experimental parameters used with eqns (9) and (10) are the ionic strength of the swelling medium ($I = 1 \times 10^{-4}$ mol cm^{-3}), the molar volume of the swelling medium (water) ($V_1 = 18$ cm^3 mol^{-1}), and the others as shown in Table 3.

The plots of eqn (11) for each copolymeric SAPs are shown in Fig. 5. The determined $\overline{M}_c$ and χ values of the SAPs from their swelling behavior are listed in Table 4.

On the other hand, if one assumes that all MBA crosslinkers were involved in the formation of effective crosslinks in the network, the stoichiometric molecular weight between crosslinks, $M_{c\ (stoi.)}$, can be then calculated by

$$M_c(\text{stoi}) = M_r/2X \tag{12}$$

where X is crosslinking ratio (the mol ratio of crosslinker to monomers).[10]

Table 4 shows that the experimentally calculated $\overline{M}_c$ values from both measurements of all SAP particles are higher than their respective stoichiometrically calculated values. This difference is attributed to the fact that a significant portion of the divinyl crosslinker (MBA) may not be employed in the crosslinking copolymerization. It is well known that gelation during free-radical crosslinking copolymerization occurs non-randomly, probably due to the cyclization and the multiple crosslinking reactions at pendant vinyl groups of MBA.[30,31] In addition, several researchers have reported that a high degree of monomer dilution during SAPs preparation and a higher crosslinker reactivity are predominantly accountable for these cyclizations and multiple crosslinking reactions, which lead to a heterogeneous crosslinking distribution in the system.[32,33] The inhomogeneously crosslinking density distribution, known as the spatial gel inhomogeneity, is disadvantageous because it drastically reduces the optical clarity and strength of gels.[34] Since the spatial gel inhomogeneity results in local concentration fluctuations in gels, scattering methods, such as small angle X-ray scattering,[35,36] small angle neutron scattering,[37] and light scattering,[38,39] have been employed to investigate such inhomogeneity. Scattering theories of inhomogeneous gel have been proposed.[40–42] A more comprehensive theory has been recently constructed by Panyukov and Rabin[43,44] for a randomly crosslinked neutral polymer gels. Subsequently, the scattering theory was extended by Rabin and Panyukov[45] to describe weakly charged polymer gels.

The experimentally determined values of $\overline{M}_c$ were used to calculate the effective crosslinking densities (ν_e) from the ratio of $\rho_2/\overline{M}_c$, which are shown in Fig. 6 along with the values of Q_e for all copolymeric SAPs. Although the absolute values of ν_e from both techniques were not in good agreement with each other, the same tendency was observed; that is, the effective crosslinking density decreased as the equilibrium water absorbency increased. It is interesting to note that large difference in both of the determined ν_e values was observed in SAPs containing crotonic acid as a comonomer.

Interpretation of the calculated network parameters from the reactivity ratio and structure of the ionic comonomers

The prepared copolymeric SAPs exhibited different degrees of crosslinking density, responding to the discrepancy in water absorbency and gel strength, although the content of MBA

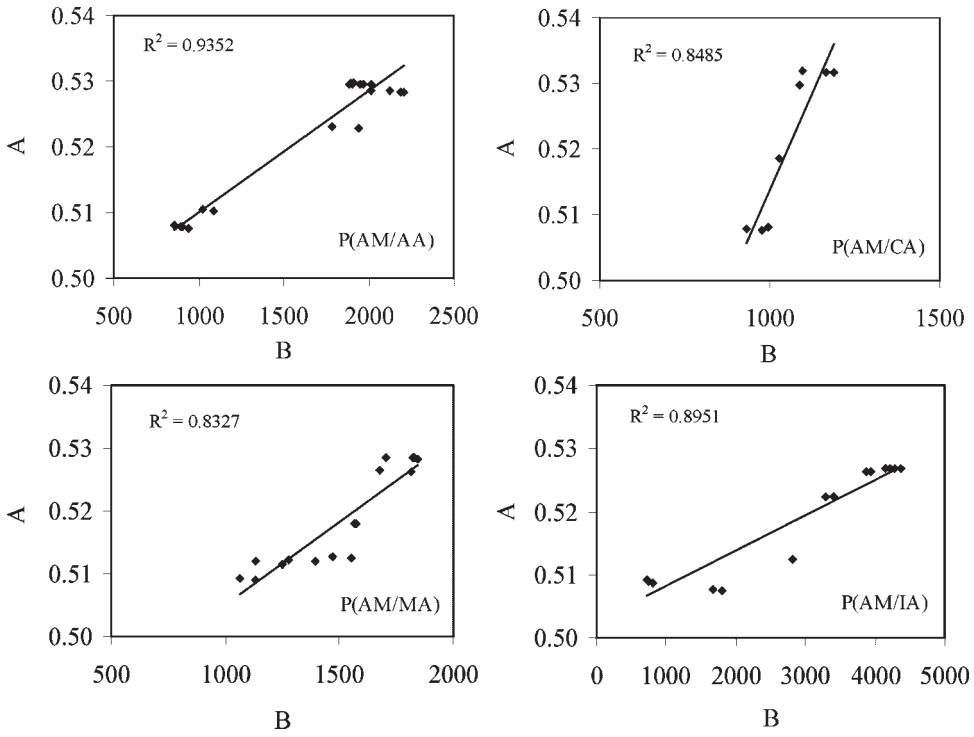

Figure 5. Determination of χ and $\overline{M}_c$ values from the equilibrium swelling behaviors of copolymeric SAPs: P(AM/AA), P(AM/CA), P(AM/MA), and P(AM/IA). See the text for an explanation of A and B.

Copyright © 2010 John Wiley & Sons, Ltd.

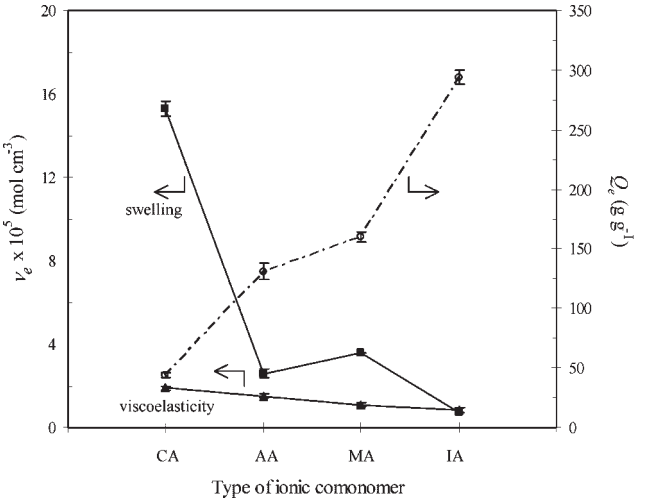

Figure 6. Effective crosslinking density (ν_e) and equilibrium water absorbency (Q_e) of polyacrylamide-SAPs containing various types of ionic comonomer.

crosslinker was equal in all preparations. Therefore, the type of ionic comonomer present in the SAP particles strongly influenced their network structure, which was discussed via the reactivity ratio and the structure of the employed ionic comonomers.

Acrylamide-based copolymer containing monoprotic acid monomer

Poly[acrylamide-co-(crotonic acid)]. In radical copolymerization, the monomer reactivity ratios (r) of a pair of monomers generally determine the distribution of each composition along the copolymer chain. It involves the reactivity of a monomer toward a radical.[46] For P(AM/CA), r_{AM} is 4.72–5.32 and r_{CA} is 0.11–0.12.[47] Due to its very low reactivity ratio, CA does not homopolymerize efficiently under these conditions. In a crosslinking copolymerization, the reactivity of the crosslinking agent MBA must also be considered, i.e. r_{AM} and r_{MBA} are 0.64 and 1.77, respectively.[33] The MBA has a high tendency to homopolymerize unless steric effects prevent its self-polymerization. Therefore, AM preferentially reacts with MBA to form a PAM crosslinked polymer. However, as mentioned previously, a high amount of MBA in the crosslinking reaction was used for cyclization and multiple crosslinking reactions.[30] In view of the extent of monomer reactivity and the relative concentration of all the components in the reaction, one may state that AM was crosslinked by MBA when the polymerization reaction was initially started but that as the AM and MBA were locally depleted, then CA was increasingly subsequently reacted to the growing radicals to yield an SAP with the CA moieties at the chain ends.[7] Thus, the obtained SAP might be in the form of the crosslinked AM/MBA at the center with peripherally-distributed CA chains. This is consistent with the observed poor swelling of the P(AM/CA)-SAPs and the large magnitude of G_e similar to that of PAM superabsorbents.

The low reactivity ratio of CA is due to the steric hindrance of the methyl group adjacent to vinyl group and the induction or resonance effects. The methyl group is an electron donating group which increases the electron density on the vinyl group and may facilitate its bonding to a cationic species. At the same time, the carboxylate anion in the carboxylic acid at the α carbon tends to ionize and delocalize between the carbon and oxygen atoms, facilitating the attack of an anionic species by decreasing the electron density on the carbon–carbon double bond. Due to the balance between the electron donating and withdrawing effects, CA could be effectively neutral and, without stringent requirements for the attacking of the π-bond, stabilization of the propagating radical species can take place.[7,46] Thus, in this scenario the effect of steric hindrance is the dominant effect for radical chain polymerization, which limits the amount of CA distributed within the copolymer network, and the water absorption is restricted. Moreover, the hydrophobic nature of CA could limit the level of water absorption of the copolymer.

Poly[acrylamide-co-(acrylic acid)]. In comparison to P(AM/CA), a higher amount of AA incorporated within the copolymer network of P(AM/AA) is expected due to the higher reactivity ratio of AA than that of CA (r_{AM} is 1.08–1.34 and r_{AA} is 0.29–0.34).[7,47] The higher amount of incorporated hydrophilic moieties will then create greater water absorption to P(AM/AA). Due to the high reactivity ratio of MBA, MBA will tend to incorporate into the polymer chain and can crosslink both AM and AA. This leads to a higher density of ionic components within the copolymer, and then the growing chains presume a more extended conformation resulting in the larger $\overline{M}_c$ and, thus, the smaller ν_e.

Acrylamide-based copolymer containing diprotic acid monomer

Poly[acrylamide-co-(maleic acid)]. The reactivity ratios of the AM and MA pair have not been reported in the literature. However, as a result of its 1, 2-disubstituted vinyl structure, MA has low tendency to copolymerize. Yet, it is still much greater than its reactivity toward homopolymerization to such an extent that MA does not homopolymerize,[48] and the 1, 2-disubstituted vinyl monomer structure decreases its reactivity toward growing radicals due to steric hindrance.[46] However, in the presence of a monomer with a high polymerization tendency, such as AM, MA is randomly incorporated along the copolymer backbone,[49] which may account for the lower observed Q_e and the larger ν_e when compared to those seen with the P(AM/IA)-SAPs.

Poly[acrylamide-co-(itaconic acid)]. The IA contains a methylene group, connected to one carboxylic group, at the β carbon, whereas MA has no methylene group (Fig. 1). The presence of the methylene group renders a high reactivity ratio of IA, i.e. the r_{AM} is 0.48–0.88 and r_{IA} is 1.24–1.65.[47] Due to its significantly higher reactivity ratio over AM, IA has a larger tendency to incorporate into the growing polymer chains. As a result, IA might be incorporated as a block in the copolymer backbone. The presence of a higher density of negative charges from the carboxylic groups along the backbone can cause the growing chains to extend more than the system of P(AM/MA) due to the higher electrostatic repulsion. The more extended conformation normally lowers the tendency of growing radicals to cyclize, and to form crosslinked and multiple crosslinked branches during free-radical crosslinking copolymerization. Thus, a relatively low value of ν_e was obtained.

Besides, Table 4 also shows the values of χ parameter determined via swelling experiments. The result shows that the obtained χ values of P(AM/AA)-, P(AM/MA)-, and P(AM/IA)-SAPs were close to that of crosslinked PAM (reported to be 0.48[23,24]

 Copyright © 2010 John Wiley & Sons, Ltd.

and 0.494[25]); whereas the χ value of P(AM/CA)- SAPs was lower (0.401 ± 0.004). Note that χ is also used to analyze the polymer–solvent miscibility, where lower χ values represent a greater miscibility between the polymer and solvent. Flory stated that if $\chi < 0.5$, then the polymer and solvent are completely miscible.[27] The χ values of P(AM/AA)-, P(AM/MA)-, and P(AM/IA)-SAPs were close to 0.5, which may suggest that those copolymers are likely to be miscible with their swelling medium, but cannot dissolve due to the presence of the crosslinked junctions. However, the still lower χ value of the P(AM/CA)-SAPs, which is less than 0.5, was neither matched by a complete dissolution of the SAPs in the swelling medium, nor a better miscibility with the medium over the other SAPs. Rather, it might result from the indifferent ability to absorb water at the various pHs of the SAPs. As shown in Fig. 2, the observed water absorbency of the P(AM/CA)-SAPs was somewhat pH-independent (over the pH range from 2 to 9), despite the presence of ionic groups from CA ($pK_a = 4.69$). The increase in water absorption of the P(AM/CA)-SAPs over that of PAM-SAPs is rather more likely to be due to the increase in hydrogen bonding between the carboxylic groups and water molecules at $pH < pK_a$. Since most CA may be located at the end of the crosslinked copolymer chains, or may be present as dangling chains, due to its very low reactivity (as discussed previously), the dissociation of its ionic groups (carboxylic groups) at pHs above its pK_a will not radically influence the swelling of the network. That is, the inclusion of CA at a 4% molar ratio did not effectively change the osmotic pressure exerted by the counterions in the network. In contrast, the addition of the other three ionic comonomers at the same molar ratio rapidly increased the water absorption of the systems (at $pH > pK_a$) as a consequence of the increased osmotic pressure due to the concentration difference between the counterions inside and outside of the SAPs. Therefore, the application of eqn (9), which includes the ionic contribution on swelling into the chemical potential of the system and the inclusion of ionic moieties into the system, to calculate χ and $\overline{M}_c$ is not suitable for our P(AM/CA)-SAPs, which may result in the low value of χ and the large magnitude of v_e determined from the swelling experiments.

As a result, this study suggested that to enhance the water swelling capacity of the SAPs, an ionic comonomer is typically included in the polymerization system. However, a loss of the SAPs mechanical properties might be observed as a trade-off consequence. Experimental data from our findings reveal that if one needs to synthesize SAPs with good swelling and mechanical properties, it is essential to carefully consider the structure and hydrophilicity of the selected ionic comonomer since these parameters determine the distribution of the ionic comonomer in the SAPs system which controls the final desired properties, such as high swelling capacity, fast swelling rate, and sufficient gel strength for a particular application.

CONCLUSION

Four types of acrylamide-based SAPs, derived from two monoprotic acid monomers and two diprotic acid monomers, were synthesized at a fixed molar ratio of acrylamide to anionic comonomer of 96:4 under the same reaction conditions with APS, MBA, and TEMED at 1, 1, and 2% (w w^{-1}) of monomers, respectively. The SAPs were allowed to freely swell into an equilibrium state and the water absorbency was measured. Viscoelastic behavior was determined in a system of closely packed swollen superabsorbent particles. SAPs containing diprotic acid predominantly influenced on the increased water absorbency. An increase in swelling capability led to a decrease in gel strength. Viscoelastic and swelling approaches in determining the network structure parameters provided the similar tendency in which the values of $\overline{M}_c$ and v_e of the prepared SAPs decreased with increase in the swelling capability. The postulations on these observations were elucidated from the reactivity ratios and hydrophilicity of the ionic comonomers.

Acknowledgements

The authors gratefully acknowledge the kind support from the Thailand Research Fund under the Research Scholar Team Consolidation Program Contract no. RTA5080004. Research facilities provided by the Imaging Polymer Laboratory of Chulalongkorn University's Department of Imaging and Printing Technology, Faculty of Science are gratefully acknowledged. The authors would like to thank the Publication Counseling Unit of the Research Division, Faculty of Science, Chulalongkorn University, for language suggestions.

REFERENCES

[1] D. Saraydin, S. Unver-Saraydin, E. Karadağ, E. Koptagel, O. Güven, *Nucl. Instr. Meth. B* **2004**, *217*, 281.
[2] E. Karadağ, D. Saraydin, Y. Caldiran, O. Güven, *Polym. Adv. Technol.* **2000**, *11*, 59.
[3] S. Duran, D. Solpan, O. Güven, *Nucl. Instr. Meth. B* **1999**, *151*, 196.
[4] E. Karadağ, O. B. Uzüm, D. Saraydin, *Eur. Polym. J.* **2002**, *38*, 2133.
[5] H. K. Can, B. Kirci, S. Kavalak, A. Güner, *Radiat. Phys. Chem.* **2003**, *68*, 811.
[6] W. Jiraprasertkul, R. Nuisin, W. Jinsart, S. Kiatkamjornwong, *J. Appl. Polym. Sci.* **2006**, *102*, 2915.
[7] D. Yiamsawas, W. Kangwansupamonkon, O. Chailapakul, S. Kiatkamjornwong, *React. Funct. Polym.* **2007**, *67*, 865.
[8] S. Kiatkamjornwong, W. Chomsaksakul, M. Sonsuk, *Radiat. Phys. Chem.* **2000**, *59*, 413.
[9] B. Taşdelen, N. Kayaman-Apohan, O. Güven, B. M. Baysal, *Int. J. Pharm.* **2004**, *278*, 343.
[10] O. Okay, S. B. Sarıışık, *Eur. Polym. J.* **2000**, *36*, 393.
[11] M. Ramazani-Harandi, M. Zohuriaan-Mehr, A. Yousefi, A. Ershad-Langroudi, K. Kabiri, *Polym. Test.* **2006**, *25*, 470.
[12] G. M. Kavanagh, S. B. Ross-Murphy, *Prog. Polym. Sci.* **1998**, *23*, 533.
[13] S. Gunasekaran, M. Mehmet Ak, *Trends Food Sci. Tech.* **2000**, *11*, 115.
[14] J. A. Dean, *Lange's Handbook of Chemistry* (15th edn), McGraw-Hill, Inc., New York, **1999**.
[15] T. Çaykara, U. Bozkaya, O. Kantoğlu, *J. Polym. Sci. Part B: Polym. Phys.* **2003**, *41*, 1656.
[16] M. Şen, A. Yakar, O. Güven, *Polymer* **1999**, *40*, 2969.
[17] R. J. Keltz, R. K. Prud'homme, W. W. Graessely, *Rheo. Acta* **1988**, *27*, 531.
[18] C. Raquois, J. F. Tassin, S. Rezaiguia, A. V. Gindre, *Prog. Org. Coat.* **1995**, *26*, 239.
[19] I. Kaneda, A. Sogobe, *Colloids Surf. A Physicochem. Eng. Asp.* **2005**, *270–271*, 163.
[20] G. Hild, *Prog. Polym. Sci.* **1998**, *23*, 1019.
[21] T. Çaykara, İ. Akçakaya, *Eur. Polym. J.* **2006**, *42*, 1437.
[22] J. E. Mark, B. Erman, *Rubberlike Elasticity a Molecular Primer*. Wiley, New York, **1988**.
[23] J. P. Baker, L. H. Hong, H. W. Blanch, J. M. Prausnitz, *Macromolecules* **1994**, *27*, 1446.
[24] M. Y. Kizilay, O. Okay, *Macromolecules* **2003**, *36*, 6856.
[25] J. Rosiak, K. Burczak, T. Zolozynzka, W. Pekala, *Radiat. Phys. Chem.* **1983**, *22*, 917.

 Copyright © 2010 John Wiley & Sons, Ltd.

[26] N. Mahmudi, M. Şen, S. Rendevski, O. Güven, *Nucl. Instr. Meth. B* **2007**, *265*, 375.
[27] P. J. Flory, *Principles of Polymer Chemistry*. Cornell University, Ithaca, NY, **1953**.
[28] H. H. Hooper, J. P. Baker, H. W. Blanch, J. M. Prausnitz, *Macromolecules* **1990**, *23*, 1096.
[29] T. Çaykara, M. Doğmuş, Ö. Kantoğlu, *J. Polym. Sci. Part B: Polym. Phys.* **2004**, *42*, 2586.
[30] H. J. Naghash, O. Okay, *J. Appl. Polym. Sci.* **1996**, *60*, 971.
[31] E. A. Kuru, N. Orakdogen, O. Okay, *Eur. Polym. J.* **2007**, *43*, 2913.
[32] H. Tobita, A. E. Hamielec, *Polymer* **1990**, *31*, 1546.
[33] J. Baselga, M. A. Llorente, J. L. Nieto, I. Hernández-Fuentes, I. F. Piérola, *Eur. Polym. J.* **1988**, *24*, 161.
[34] I. Yazici, O. Okay, *Polymer* **2005**, *46*, 2595.
[35] S. Mallam, F. Horkay, A. M. Hecht, E. Geissler, *Macromolecules* **1989**, *22*, 3356.
[36] Y. Cohen, O. Ramon, I. J. Kopelman, S. Mizraki, *J. Polym. Sci. Polym. Phys. Ed.* **1992**, *30*, 1055.
[37] T. Norisuye, N. Masui, Y. Kida, D. Ikuta, E. Kokufuta, S. Ito, S. Panyukov, M. Shibayama, *Polymer* **2002**, *43*, 5289.
[38] M. Y. Kizilay, O. Okay, *Polymer* **2003**, *44*, 5239.
[39] M. Y. Kizilay, O. Okay, *Polymer* **2004**, *45*, 2567.
[40] S. J. Candau, C. Y. Toung, T. Tanaka, P. Lemarechal, J. Bastide, *J. Chem. Phys.* **1979**, *70*, 4694.
[41] P. N. Pusey, W. van Megen, *Physica A* **1989**, *157*, 705.
[42] A. Onuki, *J. Phys. II France* **1992**, *2*, 45.
[43] S. Panyukov, Y. Rabin, *Phys. Rep.* **1996**, *269*, 1.
[44] S. Panyukov, Y. Rabin, *Macromolecules* **1996**, *29*, 7960.
[45] Y. Rabin, S. Panyukov, *Macromolecules* **1997**, *30*, 301.
[46] G. Odian, *Principles of Polymerization* (3rd edn), Wiley-Interscience, New Jersey, **2004**.
[47] R. J. Andrews, E. A. Grulke, *Polymer Handbook*, (Eds. A. Brundorf S. Immergut), John Wiley & Sons, New York, **1999**.
[48] P. Akkas, O. Güven, *J. Appl. Polym. Sci.* **2000**, *78*, 284.
[49] D. Saraydin, E. Karadağ, O. Güven, *Polym. Adv. Technol.* **1995**, *6*, 719.

 Copyright © 2010 John Wiley & Sons, Ltd.

Polymer Degradation and Stability 96 (2011) 1054–1063

Contents lists available at ScienceDirect

Polymer Degradation and Stability

journal homepage: www.elsevier.com/locate/polydegstab

Acrylamide/2-acrylamido-2-methylpropane sulfonic acid and associated sodium salt superabsorbent copolymer nanocomposites with mica as fire retardants

Nattawut Limparyoon [a,1], Nispa Seetapan [b,2], Suda Kiatkamjornwong [c,*]

[a] Program of Petrochemistry and Polymer Science, Faculty of Science, Chulalongkorn University, Bangkok 10330, Thailand
[b] National Metal and Materials Technology Center, 114 Thailand Science Park, Paholyothin Rd., Klong 1, Klong Luang, Pathumthani 12120, Thailand
[c] Department of Printing and Imaging Technology, Faculty of Science, Chulalongkorn University, Bangkok 10330, Thailand

ARTICLE INFO

Article history:
Received 28 November 2010
Received in revised form
15 March 2011
Accepted 27 March 2011
Available online 2 April 2011

Keywords:
Superabsorbent
Acrylamide
2-Acrylamido-2-methylpropane sulfonic acid sodium salt
Mica
Nanocomposites
Cone calorimetry

ABSTRACT

Acrylamide (AM) and 2-acrylamido-2-methylpropane sulfonic acid (AMPS-H^+) or its sodium salt (AMPS-Na^+) were copolymerised by free-radical crosslinking polymerization to obtain poly(AM-*co*-AMPS-H^+) and poly(AM-*co*-AMPS-Na^+) superabsorbent polymers (SAPs). A maximum water absorbency in deionised water of 1200 g g^{-1} was achieved for poly(AM-*co*-AMPS-Na^+) at a 85% mol of AMPS-Na^+. The inclusion of mica at 5–30% (w w^{-1}) into the preparation of poly(AM-*co*-AMPS-Na^+) SAP leads to an intercalated structure, as detected by XRD and TEM analyses. Poly(AM-*co*-AMPS-Na^+)/30% (w w^{-1}) mica SAP nanocomposite showed a tap water absorbency of 593 g g^{-1} with a better thermal stability, compared to the pure SAP. Cone calorimetric analyses revealed that the wood specimens coated with the prepared poly(AM-*co*-AMPS-Na^+) SAP or its 30% (w w^{-1}) mica nanocomposite provided excellent protection in delaying the ignition time after exposure to an open flame when compared to that observed with the uncoated specimen. The maximum reduction in the peak heat release rate and the greatest extension of time at peak heat release rate were observed with the nanocomposite-coated surface, but the total heat release rate was increased. The delayed burning mechanism is brought by the intercalating structure of mica in the SAP nanocomposites, which provided a better shielding effect against external heat sources, and the capability of the SAP nanocomposite in holding a large amount of water.

© 2011 Elsevier Ltd. All rights reserved.

1. Introduction

Superabsorbent polymers (SAPs) are polymers that can absorb and retain water, saline solutions or physiological fluids up to several thousand times their dry weight. These properties correspond to the three-dimensional hydrophilic network structure of the polymers. Besides their hydrophilic nature, SAPs containing an ionic moiety have an enhanced water absorbency compared to non-ionic ones. This is due to the fact that the ionic groups in the copolymer network lead to an increase in electrostatic repulsive forces between charged sites along the copolymer chains and so a more extended copolymer network [1,2]. Several ionic vinyl monomers; i.e. acrylic acid, itaconic acid, and so forth, have been selected to copolymerise with a non-ionic hydrophilic monomer, like acrylamide (AM), to prepare SAPs with a high degree of swelling [3–7]. The sodium salt form of the ionic monomer 2-acrylamido-2-methylpropane sulfonic acid (AMPS-H^+), that is AMPS-Na^+ has been of great interest in the past few years since the strongly ionisable sulfonate groups can totally dissociate in the overall pH range [1,8–15], resulting in copolymeric hydrogels with a pH-independent swelling behaviour. Based on their superior water swellable characteristics, SAPs have been widely used not only in the fields of personal care products, biosorbents and biomaterials [16], but also for agricultural soil [17], wastewater treatment [5,6,18–20] and other applications where water absorbency or water retention is important, including fire-fighting applications [21–24]. In this last scenario water is typically used to extinguish fires or to prevent combustible objects from burning by reducing the temperature of the combustible material below the burning temperature. However, when a fire is extinguished by spraying water onto it, less than about 10% of the water is generally effective in extinguishing the fire, due to the loss of the rest of the water, such as by run-off or pre-evaporation of the water away from the material surface. Therefore, SAPs have been proposed as a method to greatly improve the resistance to combustion of

* Corresponding author. Tel.: +66 2218 5587; fax: +66 2255 3021.
E-mail addresses: winny047@hotmail.com (N. Limparyoon), nispam@mtec.or.th (N. Seetapan), ksuda@chula.ac.th, ksuda@sc.chula.ac.th (S. Kiatkamjornwong).
[1] Tel.: +66 2 594 1344.
[2] Tel.: +66 2 564 6500.

0141-3910/$ – see front matter © 2011 Elsevier Ltd. All rights reserved.
doi:10.1016/j.polymdegradstab.2011.03.012

objects, or to prevent the penetration of extreme heat or fire to combustible materials. To prevent the spreading of fire, a sufficient amount of swollen SAP has to be sprayed onto the burnable objects to continuously coat their surface when nearby the burning fire. The mechanism of preventing the fire spreading is to cool the surface of the object and to reduce the quantity of oxygen from the surface of the burnable object to such a degree that the flame is extinguished [22]. However, SAPs are organic materials which lose their thermal stability when exposed to high temperatures. Typically, their structures are degraded to more than 50% of their original weight at 400 °C. Therefore, for fire-fighting applications, SAP nanocomposites with the inorganic fillers can be a promising system due to the ability to absorb a high amount of water together with the thermal stability provided by the added inorganic materials. Unlike the extensive studies on improving the fire-retardant properties of thermoplastics, thermosets and elastomers [25–29], the investigation of SAPs with enhanced thermal stability for fire-fighting applications is now drawing much more interest than before due to global warming and the need to preserve the environment [30].

Therefore, in this study, SAPs of AM and an ionic comonomer (AMPS-H^+ or AMPS-Na^+) with a high water swelling capacity were synthesized using free-radical crosslinking polymerization. AMPS-Na^+ was selected as the ionic comonomer because of its strongly ionisable sulfonate groups. For comparison, the free acid form (AMPS-H^+) was also employed to synthesize the network copolymer in order to investigate if the form of the ionic comonomer (either the salt or the acid) yielded SAPs with a higher swelling capability in water. The quantities of ionic comonomer, initiator, co-initiator and crosslinker, and the amount of reaction medium (water) on the water absorbency of the obtained poly(AM-*co*-AMPS-Na^+) and poly(AM-*co*-AMPS-H^+) SAPs were investigated. Furthermore, poly(AM-*co*-AMPS-Na^+)/mica nanocomposites were prepared in order to attempt to form SAP nanocomposites with an enhanced thermal stability, since polymer nanocomposites with various types of clay, such as attapulgite, kaolinite, mica, vermiculite and montmorillonite, have been reported to contribute remarkably improved thermal properties to the polymer matrix [31–34]. The range of mica content introduced into the poly(AM-*co*-AMPS-Na^+) SAP matrix was varied from 0 to 30% w w^{-1}. The water absorbency capacity in both deionised and tap waters, and the morphology and thermal properties of the poly(AM-*co*-AMPS-Na^+)/mica SAP nanocomposites were evaluated. Furthermore, the flammability of the prepared poly(AM-*co*-AMPS-Na^+) SAP and its poly(AM-*co*-AMPS-Na^+)/mica nanocomposite was examined using a cone calorimeter by coating these different types of SAPs on the wood specimen. All the data were then correlated to determine the poly(AM-*co*-AMPS-Na^+)/mica SAP nanocomposite with the most suitable properties for inhibiting the spreading of fire.

2. Experimental

2.1. Materials

Acrylamide (AM) was gifted from Siam Chemical Industry Co., Ltd. (Bangkok, Thailand). 2-acrylamido-2-methylpropane sulfonic acid sodium salt (AMPS-Na^+) and 2-acrylamido-2-methylpropane sulfonic acid (AMPS-H^+) were purchased from Aldrich (Steinheim, Germany). The chemical structures of the monomers are shown in Fig. 1. *N,N′*-methylenebisacrylamide (N-MBA) and *N,N,N′,N′*-tetramethylethylenediamine (TEMED) were received from Fluka (Buchs, Switzerland). Ammonium persulfate (APS) was from Ajax (Seven Hills, Australia). Swelling mica (industrial grade) was from Wako Pure Chemical Industries, Osaka, Japan. Deionised water (Elga Deionizer, Model LA611, U.K.) was used for the synthesis and the swelling experiment.

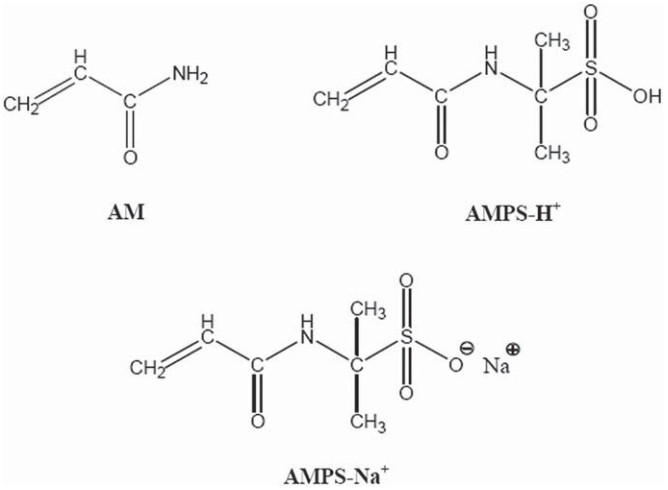

Fig. 1. Chemical structures of the monomers employed in polymerization: acrylamide (AM), 2-acrylamido-2-methylpropane sulfonic acid (AMPS-H^+) and 2-acrylamido-2-methylpropane sulfonic acid sodium salt (AMPS-Na^+).

2.2. Preparation of poly(AM-co-AMPS-H^+) and poly(AM-co-AMPS-Na^+) SAPs and their mica-containing nanocomposites

Poly(AM-*co*-AMPS-Na^+) and poly(AM-*co*-AMPS-H^+) SAPs were prepared by free-radical crosslinking polymerization. The concentrations of APS (initiator), TEMED (co-initiator) and N-MBA (crosslinker) were selected at 1.2, 1.2 and 0.2% mol of the monomers, respectively. For the synthesis of copolymers, the molar ratio of AM:ionic comonomer was varied from 98:2 to 15:85. AM was dissolved in 20 cm^3 of deionised water in a 1000-cm^3 four-necked round-bottomed reactor equipped with a mechanical stirrer, a condenser and an inlet tube of nitrogen gas. The ionic comonomer (AMPS-Na^+ or AMPS-H^+) was added, and the mixture was stirred at room temperature for 5 min before being heated to 60 °C under a nitrogen atmosphere. N-MBA and APS were sequentially dissolved in 5 ml of deionised water, added to the mixture and stirred for 5 min. Finally, TEMED was added to the mixture and the reaction proceeded for 30 min to ensure complete polymerization. The product obtained was dewatered with acetone, dried, milled and then sieved through a 100-mesh sieve aluminium screen.

The amount of water, crosslinker, co-initiator and initiator present in the polymerization reaction was investigated in order to obtain the SAP with maximum water absorbency. Poly(AM-*co*-AMPS-Na^+)/mica SAP nanocomposites were prepared using the same procedure as above but with the addition of the mica (ranging from 5 to 30% w w^{-1}) into the aqueous solution of monomers prior to the polymerization reaction.

2.3. Fourier Transform Infrared Spectroscopy (FT-IR)

The existence of the functional groups of the synthesized copolymers and the mica nanocomposites was confirmed by Fourier Transform Infrared Spectroscopy (FT-IR; System 2000, Perkin Elmer, U.S.A.). The dried sample and KBr powder were mixed, ground, pressed, and then subjected to the FT-IR spectrometry.

2.4. Water absorbency

The water absorbencies of the poly(AM-*co*-AMPS-Na^+) and poly(AM-*co*-AMPS-H^+) SAPs and the poly(AM-*co*-AMPS-Na^+)/mica SAP nanocomposites were evaluated out in deionised and tap water at room temperature. Each 0.1 g portion of dry SAP was allowed to swell in 200 cm^3 of deionised or tap water for 24 h. Subsequently, the fully swollen SAPs were separated from the unabsorbed medium by filtering through a 100-mesh sieve aluminium screen for 2 h and then weighed. The water absorbency at equilibrium (g g^{-1}) was calculated by Equation (1):

$$\textit{Water absorbency} = \frac{\textit{weight of swollen gel} - \textit{weight of dry gel}}{\textit{weight of dry gel}} \quad (1)$$

Swelling measurements were done in triplicate for each system to obtain the average and standard deviation of the water absorbency at equilibrium swelling.

2.5. Transmission electron microscopy (TEM)

Morphologies of the poly(AM-*co*-AMPS-Na^+) SAP and its respective mica-containing SAP nanocomposite were characterized by transmission electron microscopy (TEM). The particles were dispersed in ethyl alcohol and the mixture was then sonicated for 5 min. The diluted suspension was then dropped onto a 300-mesh copper grid and left to dry in a controlled atmosphere. TEM micrographs of the samples were then obtained from the transmission electron microscopy (JOEL JEM-2100, Japan) at an acceleration voltage of 120 kV.

2.6. X-ray diffraction (XRD) analysis

X-ray diffraction (XRD) measurements were performed using an X-ray diffractometry (Bruker AXS Model D8 Discover, CuKα radiation, 40 kV, 40 mA, with $\lambda = 0.15406$ nm and $n = 1$) at a scanning range from 1 to 15° and a scanning rate of 0.5° min^{-1}. The interlayer spacings (d) of mica and poly(AM-*co*-AMPS-Na^+)/mica SAP nanocomposites were calculated using Bragg's equation (Equation (2)):

$$n\lambda = 2d\sin\theta \quad (2)$$

where d is the interplanar distance of the (001) reflection plane, θ is the diffraction angle and λ is the wavelength.

2.7. Thermal stability analysis

The thermal properties of the poly(AM-*co*-AMPS-Na^+) SAP and the poly(AM-*co*-AMPS-Na^+)/mica SAP nanocomposites were investigated using a thermogravimetric analyzer (TGA/SDTA 851^e, Mettler Toledo Corporation, Switzerland). The measurements were carried out over a temperature range of 25–800 °C at a heating rate of 10 °C min^{-1} and with a nitrogen flow rate of 60 cm^3 min^{-1}. In addition, TGA under a zero air atmosphere at a flow rate of 60 cm^3 min^{-1} was examined as well.

2.8. Flammability test

Flammability analysis was evaluated using a cone calorimeter (Fire Testing Technology Ltd., UK), according to ISO 5660, at an incident heat flux (50 kW m^{-2}) in an air atmosphere, and under the free convective air flow condition. The SAPs were prepared in the form of an oil-in-water emulsion by adopting the procedure of Sortwell [35] as follows.

The dry poly(AM-*co*-AMPS-Na^+)SAPs and their respective mica-containing SAP nanocomposites were dispersed at 40% w w^{-1} in a mixture of 50% w w^{-1} of palm oil and 10% w w^{-1} of a non-ionic surfactant blend (54% w w^{-1} of Tween 80 or polyoxyethylenesorbitan monooleate/46% w w^{-1} of Span 80 or sorbitan (Z)-mono-9-octadecenoate), having a net hydrophilic/lipophilic balance (HLB) value of 10. Then, a 5% v v^{-1} of the poly(AM-*co*-AMPS-Na^+) SAP or poly(AM-*co*-AMPS-Na^+)/mica SAP nanocomposite suspension in the oil was dispersed in tap water, which resulted in the formation of a viscous slurry gel. This poly(AM-*co*-AMPS-Na^+) SAP or poly(AM-*co*-AMPS-Na^+)/mica SAP nanocomposite dispersion was then coated to give a 3-mm thickness layer on a 100 × 100 × 3 mm^3 wood (Apocynaceae, Wrightia religiosa *Benth.*) board surface. The surfaces of the SAP- and mica-containing SAP nanocomposite-coated wood specimens were exposed directly to an open flame generated by a propane gas jet. The distance between the bottom surface of the cone heater and the specimen surface is adjusted to 25 mm. An uncoated wood board (from the same batch of wood as those coated) was used as the reference control. The time to ignition, time to burn through the coatings, and the heat release rate were recorded. The charred samples left from the experiments were captured by a digital camera after the specimen self-extinguished.

3. Results and discussion

3.1. Preparation and characterization of poly(AM-co-AMPS-H^+) and poly(AM-co-AMPS-Na^+) SAPs

3.1.1. Effect of acid and salt forms of the AMPS ionic monomer on the swelling behaviour in deionised water

Poly(AM-*co*-AMPS-H^+) and poly(AM-*co*-AMPS-Na^+) SAPs were synthesized by varying the molar ratios of AM:ionic comonomer (AMPS-H^+ or AMPS-Na^+) from 98:2 to 15:85 with the concentration of APS, TEMED and N-MBA fixed at 1.2, 1.2 and 0.2% mol, respectively. The presence of the functional groups of the SAPs was evaluated via FT-IR spectra (Fig. 2). Both spectra show a broad coupling peak of N–H and O–H stretching at around 3000–3500 cm^{-1}, peaks of C–H stretching of CH and CH_2 at around 2900–3000 cm^{-1}, a sharp peak of C=O stretching of the amide I at around 1663 cm^{-1} (Fig. 2(a)) and 1664 cm^{-1} (Fig. 2(b)) and a strong peak of the N–H bending of amide II at 1552 cm^{-1} (Fig. 2(a)) and 1542 cm^{-1} (Fig. 2(b)). The relative weak peaks at 1450 cm^{-1}

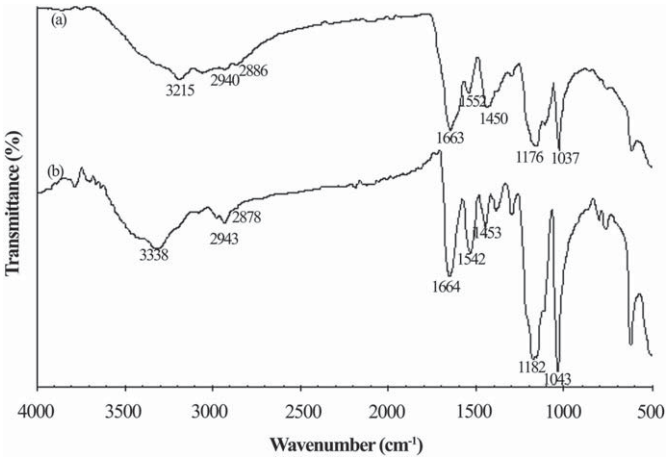

Fig. 2. Representative FT-IR spectra of the (a) poly(AM-*co*-AMPS-H^+) and (b) poly(AM-*co*-AMPS-Na^+) SAPs prepared from a 20:80% mol AM: ionic comonomer with 1.2% mol of APS, 1.2% mol of TEMED and 0.2% mol of MBA.

(Fig. 2(a)) and 1453 cm^{-1} (Fig. 2(b)) along with those at 1663 cm^{-1} and 1664 cm^{-1} are the symmetrical and asymmetrical $C(=O)_2$ stretching. Importantly, the sharp and strong peaks of the S=O stretching of AMPS-H^+ and AMPS-Na^+ at 1037 cm^{-1} (Fig. 2(a)) [36] and 1043 cm^{-1} (Fig. 2(b)) [1] were observed, respectively. Another two strong and sharp peaks at 1176 cm^{-1} (Fig. 2(a)) and 1182 cm^{-1} (Fig. 2(b)) arose from the C–C(=O)–O stretching. A relatively board and strong peak at 3338 cm^{-1} in Fig. 2(b) is for the NH or the OH stretching of poly(AM-*co*-AMPS-Na^+) where that for poly(AM-*co*-AMPS-H^+) (Fig. 2(a)) becomes very board at 3215 cm^{-1} because the OH group in the free acid superimposed the NH stretching of acrylamide moiety. Therefore, the SAP samples synthesized are poly(AM-*co*-AMPS-H^+) and poly(AM-*co*-AMPS-Na^+).

The water absorbency of the poly(AM-*co*-AMPS-Na^+) SAP was found to increase sharply just over four-fold (from 60 to 244 g g^{-1}) when the content of AMPS-Na^+ in the SAP was increased from 2 to 10% mol (Fig. 3(a)). Beyond this content, the water absorbency increased continuously but gradually until it reached 516 g g^{-1} at 60% mol of AMPS-Na^+. Further increases in the AMPS-Na^+ content abruptly enhanced the water absorbency to a maximum of 986 ± 31 g g^{-1} at 85% mol of AMPS-Na^+. The increase in water absorbency corresponded to the increase in the ionic group content (sulfonate groups) in the prepared SAPs. At 90% mol AMPS-Na^+ gel formation could not be obtained but rather weak gel slurry was achieved instead.

By adopting the proposed model from Buchholz and Burgert [37], the mechanism of the swelling and water absorbency of the poly(AM-*co*-AMPS-Na^+) SAPs can be postulated as follows. The SAP consists of many hydrophilic polymer chains with sulfonate groups and crosslinking points between the chains to prevent an infinite swelling. The dissociated sodium sulfonate groups increase the osmotic pressure inside the polymer, and the negative charges of sulfonate groups repel each other to expand the polymer coils, but are compensated for by the positive charges of the sodium salt to prevent an infinite expansion. When the polymer is in contact with water, water diffuses into the polymer network and solvates the sodium ions and the negatively charged sulfonates. The driving force for swelling is the difference between the osmotic pressure inside and outside the polymer membrane.

The water absorbency of poly(AM-*co*-AMPS-H^+) SAP (Fig. 3(b)) also increased constantly with the content of AMPS-H^+ up to 60% mol, but to a much less marked degree (1.81- to two-fold lower over the 10–60% mol range) than that of the poly(AM-*co*-AMPS-Na^+) SAP (Fig. 3(a)) at the same mol % content of ionic comonomer.

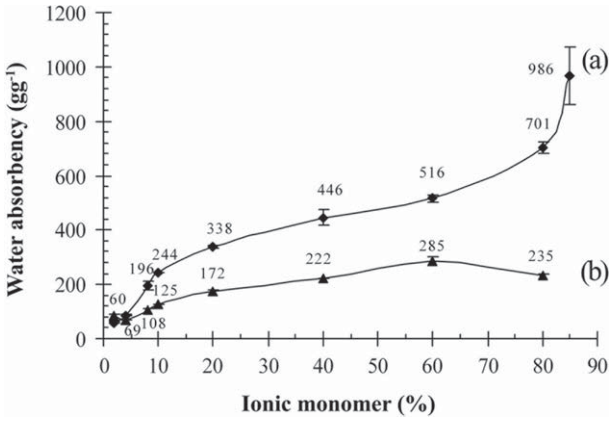

Fig. 3. Water absorbency of the (a) poly(AM-*co*-AMPS-Na^+) and (b) poly(AM-*co*-AMPS-H^+) SAPs as a function of the ionic comonomer contents (% mol). All SAPs were prepared using 1.2% mol of APS, 1.2% mol of TEMED and 0.2% mol of MBA.

The higher water absorbency of poly(AM-*co*-AMPS-Na^+) can be explained by three attributes: 1) the presence of the salt form (AMPS-Na^+) yielded a higher difference in the ionic osmotic pressures between the hydrogel and the swelling medium (water); 2) the larger Na^+ ions trapped in the SAP can induce the copolymer chain between crosslinking points to presume a more extended conformation; and 3) the strong acidity of AMPS-H^+ might induce a chain scission reaction [38] in the copolymer, as observed from the developed yellowish colour in the product attributed by the increased in AMPS-H^+ content.

3.1.2. Effect of the initial degree of monomer dilution and the crosslinker content on the swelling behaviour in deionised water of poly(AM-co-AMPS-Na^+) SAP

In solution polymerization, the initial degree of dilution of the monomers has been shown to strongly influence the obtained hydrogel structure and properties [39–42]. As the water present in the polymerization increases, the network structure becomes increasingly loose. Since this is especially the case when using ionic monomers, then SAPs were prepared with 85% mol of the AMPS-Na^+ ionic monomer rather than the AMPS-H^+ form, using both 10 and 40 ml of water reaction volume, and a crosslinker (N-MBA) content of 0.05, 0.10 or 0.20% mol. The water absorbencies of the poly(AM-*co*-AMPS-Na^+) SAPs obtained from these preparations are reported in Table 1, where it was clear that increasing the N-MBA content in the SAPs formed in a 10-ml reaction volume system led to a significant decrease in the water absorbency (1.35- and 2.77-fold as the N-MBA was increased from 0.05 to 0.1 and 0.2% mol, respectively). This is likely to be due to the increase in the crosslinking density that will then restrict the movement of the copolymer chains and limit the swelling capability of the SAPs. When the polymerization reaction was performed in 40 ml water, gel formation could not be achieved at the two lower N-MBA concentrations (0.05 and 0.10% mol) indicating that the continuous network could not be formed with this amount of water in the polymerization reaction [43].

3.1.3. Effect of the co-initiator and the initiator concentrations on the swelling behaviour of poly(AM-co-AMPS-Na^+) SAPs in deionised water

In a redox polymerization, an oxidant and a reductant pair is generally used to generate one radical and a cation and anion pair as the reaction by-product. The use of APS and TEMED is an example of an oxidation–reduction reaction to produce radicals that can initiate polymerization. The APS oxidant needs to receive an electron from a reductant to start the radical initiation reaction.

The effect of varying the TEMED content (0.6–1.8% mol) on the water absorbency of the formed poly(AM-*co*-AMPS-Na^+) SAPs is shown in Table 2. The water absorbency of the poly(AM-*co*-AMPS-Na^+) SAPs increased as the co-initiator concentration was increased up to 1.2% mol, with then no significant further increase in the

Table 1
Water absorbency of the poly(AM-*co*-AMPS-Na^+) SAP[a] as a function of the amount of water present in the polymerization reaction and the amount of N-MBA crosslinker.

Amount of water (ml)	Amount of N-MBA (% mol)	Water absorbency (g g^{-1})
10	0.05	1006 ± 95
	0.10	746 ± 26
	0.20	399 ± 31
40	0.05	No gel formation
	0.10	No gel formation
	0.20	986 ± 31

[a] AM: AMPS-Na^+ of 15:85% mol, 1.2% mol of APS and 1.2% mol of TEMED.

Table 2
Water absorbency of the poly(AM-*co*-AMPS-Na^+) SAPs[a] as a function of the amount of reactants.

Amount of reactants (% mol)			Water absorbency (g g^{-1})
N-MBA	TEMED	APS	
0.10	0.6	1.2	580 ± 13
	0.9		573 ± 12
	1.2		746 ± 26
	1.8		738 ± 23
0.05	0.6	1.2	981 ± 8
	0.9		983 ± 21
	1.2		1006 ± 95
	1.8		No gel formation
0.05	0.6	0.6	1212 ± 54
		1.2	981 ± 8
		1.8	797 ± 85

[a] AM: AMPS-Na^+ of 15:85% mol in 10 ml of water as the reaction medium.

water absorbency as the TEMED concentration increased further to 1.8% mol. Since TEMED is the co-initiator or starter to induce the decomposition of the APS initiator, then at low TEMED concentrations the concentration of activated TEMED molecules is not enough to produce hydroxyl radicals. Thus, long polymer chains are not produced, resulting in the low water absorbency. In contrast, at high TEMED concentrations, short polymer chains were produced which could recombine to create many long-chains polymers, thus providing the high water absorbency. In addition, TEMED is a strong base so it may hydrolyze or neutralize the sulfonate groups to enhance water absorbency.

The effect of the APS initiator concentration on the water absorbency of the resultant poly(AM-*co*-AMPS-Na^+) SAPs is shown in Table 2, where increasing the APS concentration from 0.6% to 1.2 and 1.8% mol led to a significant decrease (1.23- and 1.52-fold) in the equilibrium water absorbency. At a low APS concentration, a few radicals were generated allowing the polymer chain to propagate into long chains and so a large amount of water was absorbed into the SAP. In contrast, at high APS concentrations too many radicals were generated resulting in short polymer chains being produced and so the poly(AM-*co*-AMPS-Na^+) SAP formed cannot swell to such a large extent.

3.2. Preparation and characterization of poly(AM-co-AMPS-Na^+)/mica SAP nanocomposite

3.2.1. Water absorbency measurement in deionised water and tap water

The results from the previous section revealed the maximum water absorbency in deionised water of 1212 g g^{-1} was attained from SAPs synthesized from a 15:85% mol ratio of AM:AMPS-Na^+ in the presence of 10 ml of reaction medium (water), and with 0.6% mol of APS, 0.6% mol of TEMED and 0.05% mol of N-MBA. Thus, poly(AM-*co*-AMPS-Na^+)/mica SAP nanocomposites were prepared as above except with mica loadings from 0 to 30% w w^{-1} in order to evaluate any enhanced thermal stability that was afforded by the inclusion of mica into the prepared SAPs for the fire-retardant applications whilst maintaining their high water absorbency. The functional groups of the prepared nanocomposites investigated via FT-IR spectra are shown in Fig. 4. A strong peak of Si–O stretching at 972 cm^{-1} and a sharp peak of Al–O stretching at 694 cm^{-1} were evident in the pristine mica [44]. The spectra of the poly(AM-*co*-AMPS-Na^+)/mica SAP nanocomposites show the overlapped broad peak of N–H stretching and O–H stretching at 3418 cm^{-1} and 3307 cm^{-1}, the strong peak of C=O stretching of amide I at 1641 cm^{-1} [45], the strong peak of the N–H bending of amide II at

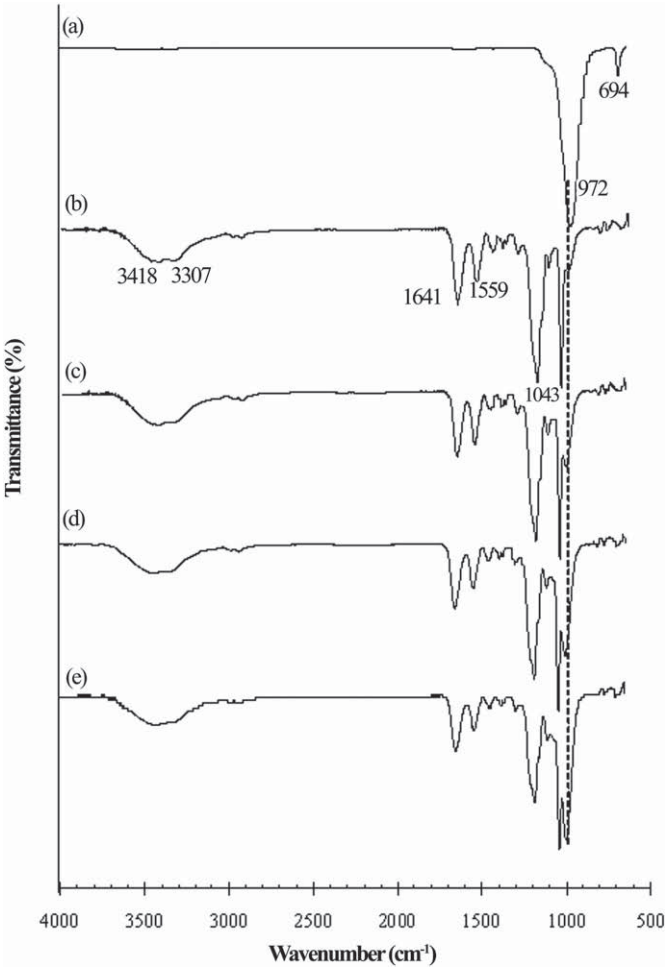

Fig. 4. Representative FT-IR spectra of (a) pristine mica, and poly(AM-*co*-AMPS-Na^+)/mica nanocomposites with mica contents of (b) 5%, (c) 10%, (d) 20% and (e) 30% w w^{-1}. All SAPs were prepared from a AM: ionic comonomer of 15:85% mol, 0.6% mol of APS, 0.6% mol of TEMED and 0.05% mol of MBA.

1559 cm^{-1}, the sharp peak of the S=O group of AMPS-Na^+ at 1043 cm^{-1} [1], and a characteristic peak of the Si–O stretching at 972 cm^{-1} that increases in peak area in relationship to the amount of mica loaded in the synthesized nanocomposites. The results indicated that the resulting products were the desired poly(AM-*co*-AMPS-Na^+)/mica SAP nanocomposites.

The water absorbency capacities in deionised and tap waters of the poly(AM-*co*-AMPS-Na^+)/mica SAP nanocomposites with different mica loadings are shown in Fig. 5. In all cases the water absorbency level in tap water was lower than that in the deionised water, due to the presence of several major cations, such as Fe^{3+} (7.2 ppm), Ca^{2+} (27.2 ppm) and Mg^{2+} (0.05 ppm), provided by the Metropolitan Waterworks Authority. These cations cause a decrease in the gel expansion because the repulsive forces of the anionic groups along the polymer chains were shielded by the bound ionic charges. Therefore, the difference in osmotic pressure between the gel network and the external solution decreases as the quantity of the cations in the swelling medium increases. Note, however, that this difference between the swelling level in deionised and tap water becomes less marked with the inclusion of increasing mica levels in the poly(AM-*co*-AMPS-Na^+)/mica nanocomposite. In addition, the water absorbency decreased with increasing mica content, showing a pronounced reduction in water absorbency (1.46- and 1.12-fold in deionised and tap waters,

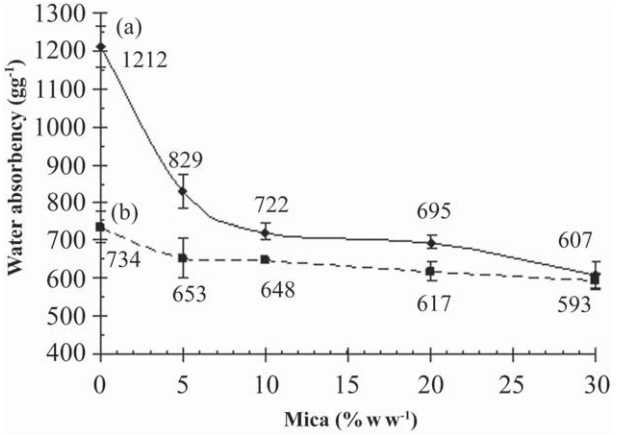

Fig. 5. Water absorbency of the poly(AM-*co*-AMPS-Na^+) SAP and poly(AM-*co*-AMPS-Na^+)/mica SAP nanocomposites in (a) deionised water and (b) tap water as a function of the mica loading levels. SAPs were prepared using 15:85% mol AM:AMPS-Na^+ with 0.6% mol of APS, 0.6% mol of TEMED and 0.05% mol of MBA in 10 ml of water.

respectively) when 5% (w w^{-1}) of mica was added into the neat SAP. Beyond this value, a steady but slight reduction in the water swelling was observed with increasing mica levels. The presence of mica in the poly(AM-*co*-AMPS-Na^+)/mica SAP nanocomposites acts as a physical crosslink junction within the composite in which the polymer chain intercalated within the layers of mica. Thus, the water absorbency reduces proportionally to the content of mica [34].

3.2.2. XRD and TEM analyses

The intercalated structures of the prepared poly(AM-*co*-AMPS-Na^+)/mica SAP nanocomposites were investigated via XRD and TEM analyses. XRD patterns provide useful information related to the variation in the basal (001) *d*-spacing of the final nanocomposites and representative diffractograms are shown in Fig. 6. The measured d_{001} of mica is 12.4 Å ($2\theta = 7.2°$) and the mica composites at 5, 10, 20 and 30% w w^{-1} of mica have a d_{001} spacing at 13.9, 13.9, 13.7 and 13.1 Å, corresponding to the peaks of 2θ at 6.4, 6.4, 6.5 and 6.6°, respectively. Thus, the *in-situ* intercalated nature of the mica within the polymerised poly(AM-*co*-AMPS-Na^+)/mica

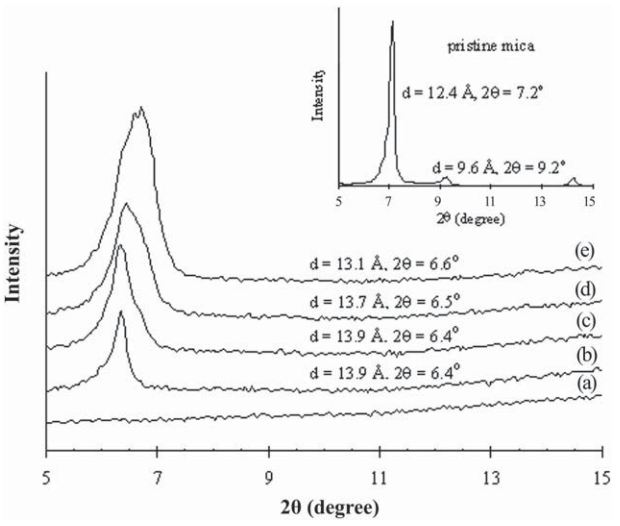

Fig. 6. Representative XRD patterns of poly(AM-*co*-AMPS-Na^+)/mica SAP nanocomposites as a function of the mica loadings for (a): 0%, (b): 5%, (c): 10%, (d): 20% and (e): 30%. The inset shows the XRD pattern of pristine mica.

SAP nanocomposite is revealed. In addition, a slight increase in the value of 2θ was observed with increasing mica contents representing a decrease in the distance between the interlayers of mica.

TEM micrographs (Fig. 7) support the intercalated poly(AM-*co*-AMPS-Na^+)/mica SAP nanocomposite structure obtained from the XRD data. The dark cross lines indicate the parts of the polymer intercalated into the interlayer spacing of mica. The thickness of the cross lines is approximately 1 nm, corresponding to the typical thickness of the clay layers, whereas the distance between the cross lines are interlayer spaces and the grey bases are the polymer matrix. These micrographs demonstrate that mica particles are dispersed at the nanometer level in the SAP matrix. The interlayer distance of mica in the nanocomposites obtained from the TEM micrographs is approximately 13 Å, correlating well with the interlayer spacing characterized by XRD analysis.

3.2.3. Thermal gravimetric analysis (TGA)

The thermal stability of the poly(AM-*co*-AMPS-Na^+)/mica SAP nanocomposites and the pristine mica was evaluated using TGA under a nitrogen atmosphere, with representative thermograms shown in Fig. 8(a). Pure mica had a single degradation stage at 68–87 °C with a weight loss of 7.3%, which was the loss of the moisture retained in the mica. Thermograms of poly(AM-*co*-AMPS-Na^+)/mica SAP nanocomposites at mica loadings of 10, 20 and 30% w w^{-1} are similar to the thermal decomposition of poly(AM-*co*-AMPS-Na^+) SAPs without mica in that the four similar stages of decomposition are seen. The first stage of degradation takes place in the range of 40–125 °C and corresponds to the absorbed and bound water. The second sharp degradation stage, in the range of 307–329 °C, is ascribed to the amide side group of the AMPS-Na^+. The third stage, in the range of 329–413 °C, is interpreted as the amide side group of AM and the crosslinker. The final stage in the range of 450–800 °C is assigned to the thermal degradation of the backbone chain [32].

From these TGA thermograms, the temperature at which a 50% weight loss occurs was found to increase from 380 to 415 °C as the mica loading increased from 0 to 30% w w^{-1}. The thermal stability of the nanocomposites and the amount of residue at 800 °C increased as the amount of mica present in the systems increased. This improvement in the thermal stability of the nanocomposites could be attributed to the pronounced thermal stability of mica and to the interaction between the mica particles and the polymer matrix [46]. By calculating the amount of residues left at 800 °C from the thermograms, 70% by weight of the mica was retained in the SAP nanocomposites regardless of the mica content loaded. Thus, the remaining amount of mica (~30%) was not incorporated into the SAPs and was removed during the precipitation process.

Prior to the flammability analysis, the thermal stability under air of poly(AM-*co*-AMPS-Na^+) SAP and its 30% w w^{-1} mica-containing nanocomposite was examined as a model system to represent the thermal degradation of the materials exposed to a normal air atmosphere. TGA analysis under an air atmosphere shows a significantly increased temperature at which a 50% weight loss was attained (340–480 °C as the mica level increases from 0 to 30% w w^{-1}) (Fig. 8(b)) and residual weight content of the char residue (36% in comparison to the 20% weight of residue from poly(AM-*co*-AMPS-Na^+)) at 800 °C. DTG thermograms (Fig. 8(c)) revealed similar thermal decomposition stages for the poly(AM-*co*-AMPS-Na^+) SAP and its mica-containing nanocomposite. The first stage of degradation is from the loss of absorbed and bound water at 90–100 °C. The second stage, where the maximum weight loss rate was detected at 330 °C, corresponds to degradation of the amide side chain. The third degradation stage occurs at 580 °C and corresponds to the main chain pyrolysis. Therefore, these results confirm that mica inclusion led to an improved thermal stability for the poly(AM-*co*-AMPS-Na^+)/mica

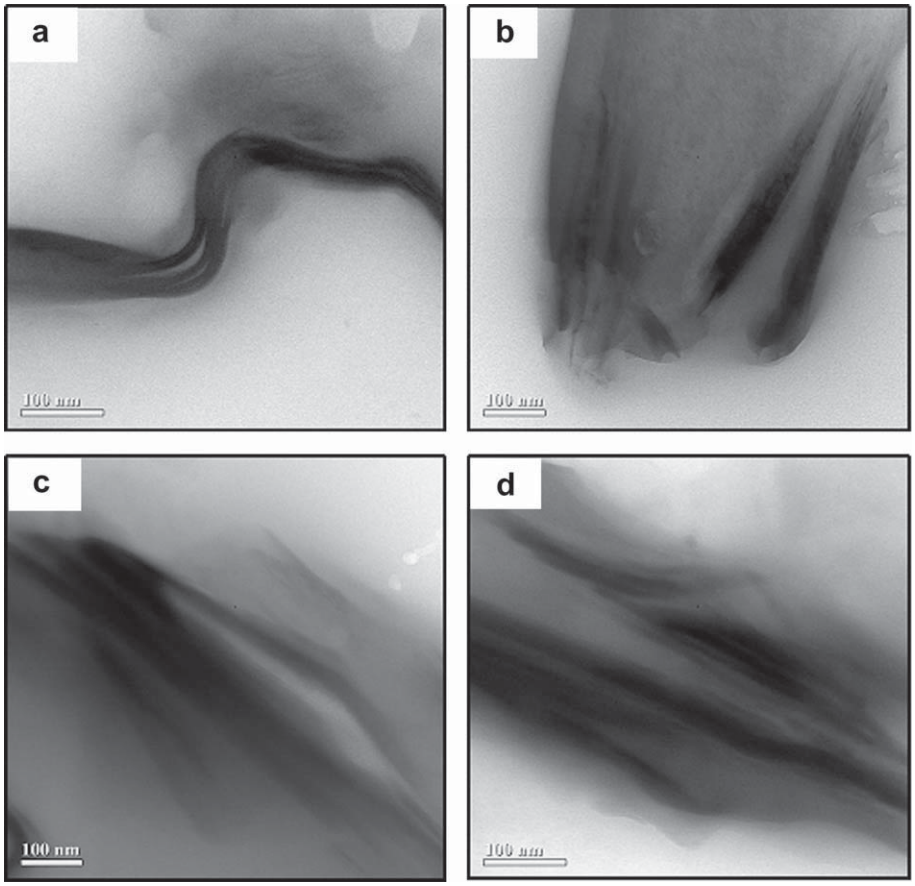

Fig. 7. Representative TEM micrographs of poly(AM-*co*-AMPS-Na^+)/mica SAP nanocomposites with mica loading levels of 5, 10, 20 and 30% w w^{-1} for a,b,c and d, respectively.

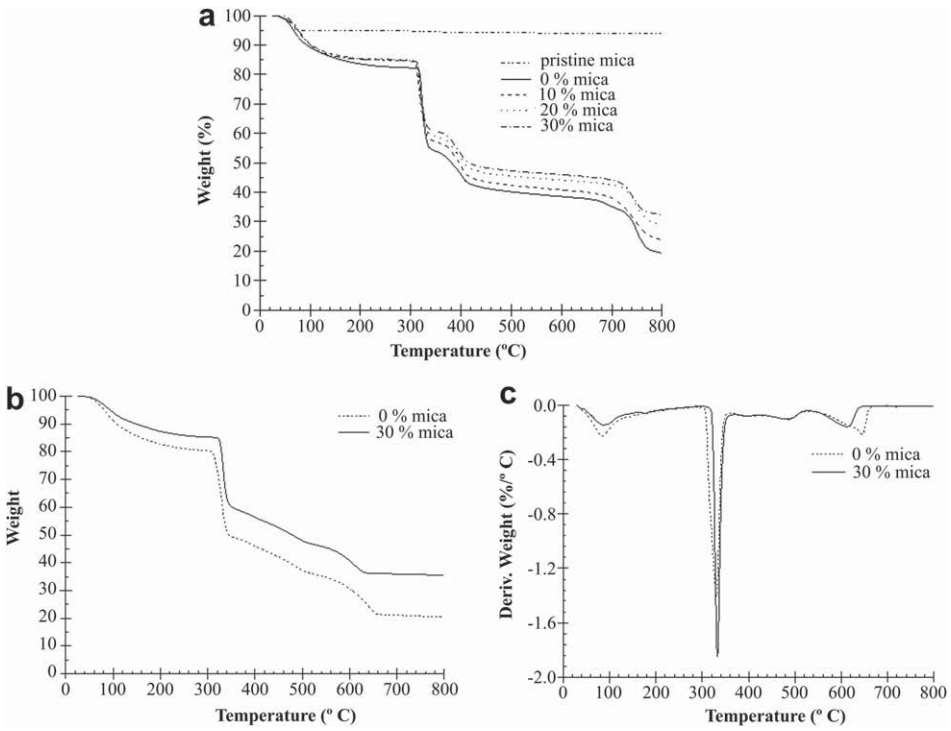

Fig. 8. Representative TGA thermograms, obtained under a N_2 atmosphere, of (a) poly(AM-*co*-AMPS-Na^+)/mica SAP nanocomposites at various mica loadings (0–30% w w^{-1}), shown in comparison with that for pristine mica; (b) TGA and (c) DTG thermograms, obtained under a zero air atmosphere, of poly(AM-*co*-AMPS-Na^+) SAPs and poly(AM-*co*-AMPS-Na^+)/30% w w^{-1} mica SAP nanocomposites.

Table 3
Cone calorimetric data for the uncoated, mica-free and 30% w w^{-1} mica-containing SAP-coated wood specimens.

Specimen	Time to ignition (s)	Time to burn the coated gel[a] (s)	Peak HRR (kW m^{-2})	Time at peak HRR (s)	Total HRR (MJ m^{-2})
Uncoated wood	13 ± 2	–	309	79	22
SAP-coated wood	125 ± 2	4 ± 2	222	224	26
SAP/30% mica-coated wood	186 ± 3	84 ± 6	213	302	25

[a] Time to burn the coated gel was measured after sample ignition.

SAP nanocomposites at all temperature ranges because the mica acts as a heat barrier to delay the diffusion of volatile thermo-oxidation products to gas, and the escape of gas from the nanocomposite [34,47].

3.2.4. Flammability analysis

Cone calorimetric analyses were investigated for the poly(AM-*co*-AMPS-Na^+)/30% w w^{-1} mica SAP nanocomposite-coated wood surface due to its superior thermal stability among the other poly(AM-*co*-AMPS-Na^+)/mica SAP nanocomposites studied. Poly(AM-*co*-AMPS-Na^+) SAP-coated wood and uncoated wood specimens from the same wood batch were used as controls. The flammability characterization was carried out at an incident heat flux of 50 kW m^{-2}, in an air atmosphere with a flame temperature of 885 °C. After being exposed to the direct flame, the time to ignition of each specimen was fast for the uncoated wood board (13 s), but was about ten-fold longer for the poly(AM-*co*-AMPS-Na^+) SAP-coated specimens, illustrating the excellent protection in delaying the ignition time after exposing to an open flame (Table 3).

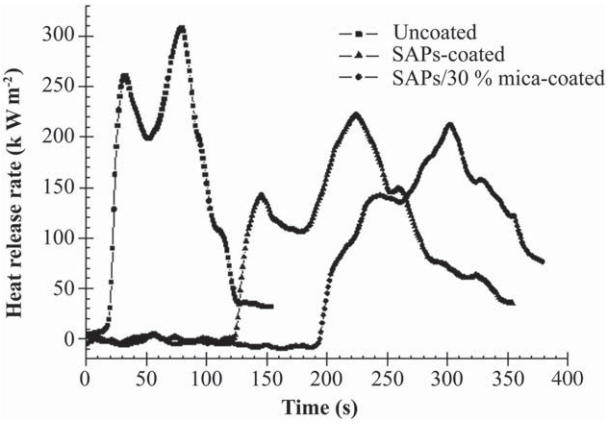

Fig. 9. Representative heat release rate per burning surface area of the uncoated, the poly(AM-*co*-AMPS-Na^+) SAP-coated, and the poly(AM-*co*-AMPS-Na^+)/30% w w^{-1} mica SAP nanocomposite-coated wood boards.

Moreover, the presence of 30% w w^{-1} mica significantly enhanced the thermal barrier, retarded the diffusion of heat and slowed down the burning, as observed from the longer time to ignition (1.49- and 14.31-fold longer than the mica-free SAP treated and untreated wood, respectively) and the 21-fold longer time to burn the coated gel (Table 3).

Heat release is defined as the heat generated due to various chemical reactions when a material is exposed to fire, and provides information on the size of the fire and hence the corresponding fire hazard [26]. Materials with a low heat release rate gives less damage to the surroundings than those with high heat release rate. Thus, the heat release rate, particularly the peak value, is the primary characteristic in determining the size, growth and suppression requirements of a fire environment [48]. A 1.39-fold reduced peak heat release rate per unit of burning surface (PHRR) and a 2.83-fold prolonged time at the PHRR (t_{PHRR}) were found in the poly(AM-*co*-AMPS-Na^+) SAP-coated specimens compared to the uncoated one (Table 3 and Fig. 9), which might be attributed by the cooling effect of water trapped within the SAP particles and the formation of chars covering on the surface of the coated specimens. The inclusion of 30% w w^{-1} mica into the poly(AM-*co*-AMPS-Na^+)/mica SAP nanocomposite slightly decreased further (1.04-fold) the PHRR and markedly increased (1.35-fold) the t_{PHRR} over that seen with the mica-free poly(AM-*co*-AMPS-Na^+) SAP alone. This enhanced slow burning process is brought by the formation of clay barrier, which provided a better shielding effect against external heat sources, as well as the capability of the SAP nanocomposite in holding a large amount of water.

However, when considering the total heat release rate (THRR) defined as a total heat at the end of burning. As mentioned in this study, the combustion experiment was performed until flame was self-extinguished. It was found that, for the uncoated specimen, the observed THRR of 22 MJ m^{-2} was obtained from the combustion of the wood itself. Flame eventually extinguished because the entire wood specimen was completely burnt out. When comparing with the uncoated wood surface, it is interesting to mention that THRR values of the mica-free and mica-added poly(AM-*co*-AMPS-Na^+) SAPs-coated specimens were found increased to 26 MJ m^{-2} and 25 MJ m^{-2}, respectively. The explanation could be from the fact that the neat SAP and the SAP/mica nanocomposite are both fuels which

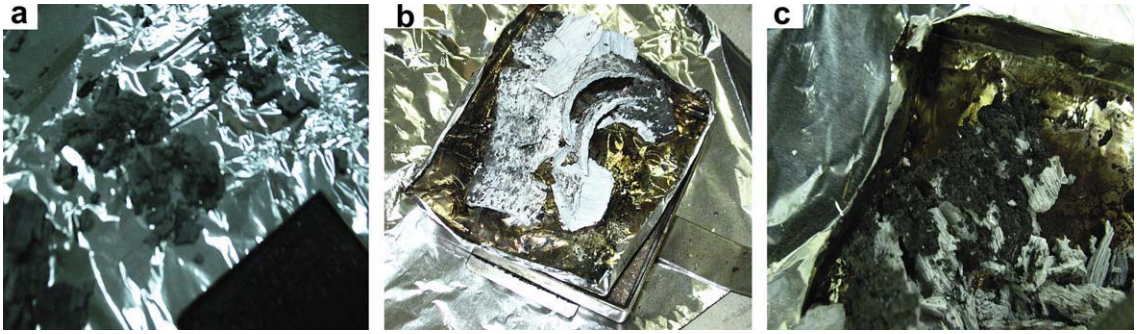

Fig. 10. Representative optical photographs of the charred specimens of (a) the uncoated wood, (b) poly(AM-*co*-AMPS-Na^+) SAP-coated wood and (c) poly(AM-*co*-AMPS-Na^+)/30% w w^{-1} mica SAP nanocomposite-coated wood.

finally combusted under heat, consecutively with the burnout of wood to cause an increased THRR as compared to the uncoated wood surface. This means that both coated specimens can only delay the fire ignition, reduce PHRR and increase time at PHRR, but do not reduce THRR. This observation has been previously observed for polymer/clay nanocomposite where HRR is significantly reduced in the nanocomposite, but THRR remains unaffected [49] or increased [50].

Fig. 10 shows the char characteristics after the flame was self-extinguished. The uncoated wood gave a dark grey char, whereas the chars of the wood boards coated with the mica-free poly(AM-*co*-AMPS-Na^+) SAPs are white and those coated with the poly(AM-*co*-AMPS-Na^+)/30% w w^{-1} nanocomposite are black lump char. Furthermore, the maximum reduction in PHRR and the greatest extension of t_{PHRR} were observed in the poly(AM-*co*-AMPS-Na^+)/mica SAP nanocomposite-coated surface, possibly due to the intercalating structure of the mica in the nanocomposite providing a better barrier against external heat [51].

4. Conclusions

Poly(AM-*co*-AMPS-Na^+) and poly(AM-*co*-AMPS-H^+) SAPs were synthesized by free-radical crosslinking polymerization. The water absorbency of poly(AM-*co*-AMPS-H^+) was lower than that of poly(AM-*co*-AMPS-Na^+), presumably because the strong acidity of the AMPS-H^+ monomer resulted in a chain scission reaction in the SAP. Poly(AM-*co*-AMPS-Na^+)/mica SAP nanocomposite at 30% w w^{-1} mica showed a tap water absorbency of 593 g g^{-1} and a better thermal stability compared to the pure poly(AM-*co*-AMPS-Na^+) SAP. The emulsions of the swollen poly(AM-*co*-AMPS-Na^+) SAP and its 30% w w^{-1} mica-containing nanocomposite were made by mixing with vegetable oil and surfactant, and subsequently were coated on the wood specimens. Flammability analysis revealed that both coated wood specimens showed an excellent reduction in the peak heat release rate, and prolonged the time at peak heat release rate. However, the total heat release rate was found increased. This might be from the fact that poly(AM-*co*-AMPS-Na^+) SAP and its mica nanocomposite are both fuels, which finally combusted under heat.

Acknowledgements

The authors are indebted for the full financial support from the Thailand Research Fund under the Research Team Aided Program Contract no. RTA5080004. The provision of research facilities by the Imaging Polymer Laboratory of Chulalongkorn University's Department of Imaging and Printing Technology, Faculty of Science is highly acknowledged. Cone Calorimetric experiment provided by the Department of Civil Engineering, Faculty of Engineering, Chulalongkorn University, and English edition of the manuscript by the Publication Counsellor Unit of the Research Division, Faculty of Science, Chulalongkorn University, are highly appreciated. The authors thank Siam Chemical Industry Co., Ltd., for donating acrylamide monomer for the research.

References

[1] Durmaz S, Okay O. Acrylamide/2-acrylamido-2-methylpropane sulfonic acid sodium salt-based hydrogels: synthesis and characterization. Polymer 2000; 41:3693–704.
[2] Kiatkamjornwong S, Chomsaksakul W, Sonsuk M. Radiation modification of water absorption of cassava starch by acrylic acid/acrylamide. Radiat Phys Chem 2000;59:413–27.
[3] Okay O, Sarıışık SB. Swelling behaviour of poly(acrylamide-co-sodium acrylate) hydrogels in aqueous salt solutions: theory versus experiments. Eur Polym J 2000;36:393–9.
[4] Taşdelen B, Kayaman-Apohan N, Güven O, Baysal BM. Preparation of poly(*N*-isopropylacrylamide/itaconic acid) copolymeric hydrogels and their drug release behaviour. Int J Pharm 2004;278:343–51.
[5] Jiraprasertkul W, Nuisin R, Jinsart W, Kiatkamjornwong S. Synthesis and characterization of cassava starch graft poly(acrylic acid) and poly[(acrylic acid)-co-acrylamide] and polymer flocculants for wastewater treatment. J Appl Polym Sci 2006;102:2915–28.
[6] Yiamsawas D, Kangwansupamonkon W, Chailapakul O, Kiatkamjornwong S. Synthesis and swelling properties of poly[acrylamide-*co*-(crotonic acid)] superabsorbents. React Funct Polym 2007;67:865–82.
[7] Seetapan N, Wongsawaeng J, Kiatkamjornwong S. Gel strength and swelling of acrylamide-protic acid superabsorbent copolymers. Polym Adv Technol; 2010. doi:10.1002/pat.1658.
[8] Tong Z, Liu X. Swelling equilibria volume phase transition in hydrogels with strongly dissociating electrolytes. Macromolecules 1994;27:844–8.
[9] Liu X, Tong Z, Hu O. Swelling equilibria of hydrogels with sulfonate groups in water and in aqueous salt solutions. Macromolecules 1995;28: 3813–7.
[10] Fisher LW, Sochor AR, Tan JS. Chain characteristics of poly(2-acrylamido-2-methylpropanesulfonate) polymers. 1. Light-scattering and intrinsic-viscosity studies. Macromolecules 1977;10:949–54.
[11] Churochkina NA, Starodoubtsev SG, Khokhlov AR. Swelling and collapse of the gel composites based on neutral and slightly charged poly(acrylamide) gels containing Na-montmorillonite. Polym Gels Netw 1998;6:205–15.
[12] Okay O, Sarıışık SB, Zor SD. Swelling behavior of anionic acrylamide-based hydrogels in aqueous salt solutions: comparison of experiment with theory. J Appl Polym Sci 1998;70:567–75.
[13] Ozmen MM, Okay O. Superfast responsive ionic hydrogels with controllable pore size. Polymer 2005;46:8119–27.
[14] Gad YH. Preparation and characterization of poly(2-acrylamido-2-methylpropanesulfonic acid)/chitosan hydrogel using gamma irradiation and its application in wastewater treatment. Radiat Phys Chem 2008;77:1101–7.
[15] Kaşgöz H, Durmuş A, Kaşgöz A. Enhanced swelling and adsorption properties of AAM-AMPSNa/clay hydrogel nanocomposites for heavy metal ion removal. Polym Adv Technol 2008;19:213–20.
[16] Saraydin D, Unver-Saraydin S, Karadağ E, Koptagel E, Güven O. In vivo biocompatibility of radiation crosslinked acrylamide copolymers. Nucl Instrum Meth B 2004;217:281–92.
[17] Karadağ E, Saraydin D, Caldiran Y, Güven O. Swelling studies of copolymeric acrylamide/crotonic acid hydrogels as carriers for agricultural uses. Polym Adv Technol 2000;11:59–68.
[18] Duran S, Solpan D, Güven O. Synthesis and characterization of acrylamide-acrylic acid hydrogels and adsorption of some textile dyes. Nucl Instrum Meth B 1999;151:196–9.
[19] Karadağ E, Uzüm OB, Saraydin D. Swelling equilibria and dye adsorption studies of chemically crosslinked superabsorbent acrylamide/maleic acid hydrogels. Eur Polym J 2002;38:2133–41.
[20] Can HK, Kirci B, Kavalak S, Güner A. Removal of some textile dyes from aqueous solutions by poly(*N*-vinyl-2-pyrrolidone) and poly(*N*-vinyl-2-pyrrolidone)/$K_2S_2O_8$ hydrogels. Radiat Phys Chem 2003;68:811–8.
[21] Bashaw RN, Harper BG. Method for controlling the spread of fire. US patent 3229769; 1966.
[22] Pascente JE, Pascente TJ. Method of preventing combustion by applying an aqueous superabsorbent polymer composition. US patent 5849210; 1998.
[23] Beck M, Champ S, Tonnessen M, Ziemer A, Goebel G, Pfeiffer M. Fire extinguishing and/or fire retarding compositions. US patent 2007/0289752 A1; 2007.
[24] Erdner S, Pakan D. Fire control composition and method. US patent 7670513 B2; 2010.
[25] Beyer G. Organoclays as flame retardants for PVC. Polym Adv Technol 2008; 19:485–8.
[26] Chigwada G, Wang D, Jiang DD, Wilkie CA. Styrenic nanocomposites prepared using a novel biphenyl-containing modified clay. Polym Degrad Stabil 2006; 91:755–62.
[27] Glodek TE, Boyd SE, McAninch IM, LaScala JJ. Properties and performance of fire resistant eco-composites using polyhedral oligomeric silsesquioxane (POSS) fire retardants. Compos Sci Technol 2008;68:2994–3001.
[28] Karlsson L, Lundgren A, Jungqvist J, Hjertberg T. Influence of melt behaviour on the flame retardant properties of ethylene copolymers modified with calcium carbonate and silicone elastomer. Polym Degrad Stabil 2009;94: 527–32.
[29] Morgan AB. Flame retarded polymer layered silicate nanocomposites: a review of commercial and open literature systems. Polym Adv Technol 2006;17:206–17.
[30] Bordado JCM, Gomes JFP. New technologies for effective forest fire fighting. Int J Environ Stud 2007;64:243–51.
[31] Zeng QH, Yu AB, Lu GQ, Paul DR. Clay-based polymer nanocomposites: research and commercial development. J Nanosci Nanotechnol 2005;5: 1574–92.
[32] Zhang J, Wang A. Study on superabsorbent composites. IX: synthesis, characterization and swelling behaviors of polyacrylamide/clay composites based on various clays. React Funct Polym 2007;67:737–45.
[33] Lu H, Hu Y, Li M, Song L. Clay intercalation and influence on flammability and crystallization behaviors of POE-based nanocomposites. Polym Composite 2008;29:1358–63.

[34] Foungfung D, Phattanarudee S, Seetapan N, Kiatkamjornwong S. Acrylamide-itaconic acid superabsorbent polymers and superabsorbent polymer/mica nanocomposites. Polym Adv Technol; 2010. doi:10.1002/pat.1559.
[35] Sortwell ET. Method of preventing or extinguishing fires. US patent 2009/0151963 A1; 2009.
[36] Lin SB, Yuan CH, Ke AR, Quan ZL. Electrical response characterization of PVA–P(AA/AMPS) IPN hydrogels in aqueous Na_2SO_4 solution. Sens Actuators B 2008;134:281–6.
[37] Buchholz FL, Burgert JH. Synthesis and application of superabsorbent polymers. In: Finch CA, editor. Industrial water soluble polymers. Cambridge: Royal Society of Chemistry; 1996. p. 93.
[38] Odian G. Principles of polymerization. 4th ed. New Jersey: John Wiley & Sons, Inc; 2004.
[39] Ilavsky M, Prins W. Rheo-optics of poly(2-hydroxyethyl methacrylate) gels. II. Effect of cross-linking density and stage of dilution during network formation. Macromolecules 1970;3:425–33.
[40] Dusek K, Janacek J. Hydrophilic gels based on copolymers of 2-hydroxyethyl methacrylate with methacrylamide and acrylamide. J Appl Polym Sci 1975;19:3061–75.
[41] Baker JP, Hong L-H, Blanch HW, Prausnitz JM. Effect of initial total monomer concentration on the swelling behaviour of cationic acrylamide-based hydrogels. Macromolecules 1994;27:1446–54.
[42] Naghash HJ, Okay O. Formation and structure of polyacrylamide gels. J Appl Polym Sci 1996;60:971–9.
[43] Huang Y, Seitz U, Funk W. Synthesis and characterization of bisacrylamide microgels containing sulfo groups. Macromol Chem 1985;186:273–81.
[44] Dai H, Li H, Wang F. An alternative process for the preparation of Cu-coated mica composite powder. Surf Coat Tech 2006;201:2859–66.
[45] Tang Q, Wu J, Sun H, Fan S, Hu D, Lin J. Superabsorbent conducting hydrogel from poly(acrylamide-aniline) with thermo-sensitivity and release properties. Carbohydr Polym 2008;73:473–81.
[46] Chang JH, An YU, Cho D, Giannelis EP. Polylactide nanocomposites: comparison of their properties with montmorillonite and synthetic mica (II). Polymer 2003;44:3715–20.
[47] Zhang J, Wang Q, Wang A. Synthesis and characterization of chitosan-*g*-poly(acrylic acid)/attapulgite superabsorbent composites. Carbohydr Polym 2007;68:367–74.
[48] Koo JH, editor. Polymer nanocomposites: processing, characterization, and applications. New York: The McGraw-Hill Companies, Inc; 2006.
[49] Bartholmai M, Schartel B. Layered silicate polymer nanocomposites: new approach or illusion for fire retardancy? Investigations of the potentials and the tasks using a model system. Polym Adv Technol 2004;15:355–64.
[50] Hussain M, Varley RJ, Mathys Z, Cheng YB, Simon GP. Effect of organo-phosphorus and nano-clay materials on the thermal and fire performance of epoxy resins. J Appl Polym Sci 2004;91:1233–53.
[51] Schartel B, Bartholmai M, Knoll U. Some comments on the main fire retardancy mechanisms in polymer nanocomposites. Polym Adv Technol 2006;17:772–7.

Polymer Degradation and Stability xxx (2011) 1–7

Contents lists available at ScienceDirect

Polymer Degradation and Stability

journal homepage: www.elsevier.com/locate/polydegstab

Effect of fire retardant on flammability of acrylamide and 2-acrylamido-2-methylpropane sodium sulfonate copolymer composites

Nispa Seetapan [a,1], Nattawut Limparyoon [b,2], Suda Kiatkamjornwong [c,*]

[a] National Metal and Materials Technology Center, 114 Thailand Science Park, Paholyothin Rd., Klong 1, Klong Luang, Pathumthani 12120, Thailand
[b] Program of Petrochemistry and Polymer Science, Faculty of Science, Chulalongkorn University, Bangkok 10330, Thailand
[c] Department of Printing and Imaging Technology, Faculty of Science, Chulalongkorn University, Bangkok 10330, Thailand

ARTICLE INFO

Article history:
Received 9 April 2011
Received in revised form
1 June 2011
Accepted 22 June 2011
Available online xxx

Keywords:
Superabsorbent
Zinc borate
Melamine
Fire retardant
Cone calorimetry

ABSTRACT

Poly[acrylamide-*co*-(2-acrylamido-2-methylpropane sodium sulfonate)] superabsorbents and superabsorbent composites (SAPCs) with zinc borate and/or melamine as fire retardants were synthesized. Water absorbencies decreased inversely to added amount of fire retardant. Thermal stability of SAPC/zinc borate increases with increasing zinc borate. Incorporating melamine improved thermal stability of the SAPC until 300 °C. Flammability analysis demonstrated that wood surface coated with SAP or SAPC emulsions extended time to ignition of the wood. Peak heat release rate and total heat release are smallest in specimens coated with SAPC/30% melamine. Wood coated with SAPC incorporating 20% zinc borate/10% melamine mixture gave the longest time to ignition at 4½ min.

© 2011 Elsevier Ltd. All rights reserved.

1. Introduction

Superabsorbent polymers (SAPs) are lightly crosslinked hydrophilic polymers that can absorb and retain water, saline solutions, or physiological fluids up to thousands times their dry weight. Several ionic vinyl monomers have been copolymerized with a nonionic hydrophilic monomer to prepare SAPs with high degree of swelling [1–7]. Based on the superior water swellable characteristic, SAPs have been widely used in the fields of personal care products [8], agricultural soil [9], wastewater treatment [5,6,10–14], as well as in fire-fighting application [15–17]. In the later case, water is typically used to extinguish the fire or to prevent combustible objects from burning by reducing the temperature of the combustible material below the burning temperature. However, when a fire is extinguished by spraying water onto it, only a small amount of the total water applied is generally effective in extinguishing the fire, due to loss of most of the water, such as by run-off or evaporation of the water. Therefore, SAPs have been proposed as a method to prolong a combustible object from burning, or to prevent the penetration of extreme heat or fire to a combustible material. To prevent the spreading of fire, a sufficient amount of swollen SAPs have to be sprayed onto an ignitable or burnable object so as to continuously coat the surface of the object nearby the burning fire. Here, the mechanism of preventing the fire spreading is to both cool the surface of the object below the ignition temperature and to reduce the quantity of oxygen at the surface of the burnable object to a degree such that the flame is extinguished [16]. However, SAPs are organic materials which lose their thermal stability when exposed to high temperatures. Therefore, for fire-fighting applications, the incorporation of a fire retardant into SAPs can offer thermal protection from fire due to the ability to absorb high amount of water together with the thermal stability provided by the added inorganic materials. However, unlike the extensive studies on improving fire-retardant property of thermoplastics, thermosets, elastomer, and wood [18–22], the investigation of SAPs with thermal stability and fire-retardant properties for fire-fighting applications is rather limited [23,24]. Our previously published results on flammability analysis using cone calorimetry technique revealed that the wood specimens coated with SAP or SAP/mica nanocomposite showed an excellent reduction in the peak heat release rate, and extended the time at peak heat release rate, but did not reduce the total heat release [24].

Among several characterized fire retardants, zinc borate has been found to be an effective inorganic fire retardant that possesses

* Corresponding author. Tel.: +66 2218 5587; fax: +66 2255 3021.
E-mail addresses: nispam@mtec.or.th (N. Seetapan), winny047@hotmail.com (N. Limparyoon), ksuda@chula.ac.th (S. Kiatkamjornwong).
[1] Tel.: +662 564 6500.
[2] Tel.: +662 594 1344.

0141-3910/$ – see front matter © 2011 Elsevier Ltd. All rights reserved.
doi:10.1016/j.polymdegradstab.2011.06.014

Please cite this article in press as: Seetapan N, et al., Effect of fire retardant on flammability of acrylamide and 2-acrylamido-2-methylpropane sodium sulfonate copolymer composites, Polymer Degradation and Stability (2011), doi:10.1016/j.polymdegradstab.2011.06.014

key characteristic properties of flame retardants, such as smoke suppression and promoting charring, and so on [25], that are required by new fire standards. It has been postulated that the mechanism of the zinc borate induced flame retardancy in polymeric materials involves the formation of a protective char layer at surface of the materials, which then obstructs the access of oxygen and subsequently prevents the oxidation of carbon [26]. As such, zinc borate is commonly used as a multifunctional flame retardant in combination with other halogenated or halogenated free flame retardant systems to boost flame retardancy properties [27]. Melamine is another type of nitrogen-containing flame retardants and has been used in thermoplastics [28,29]. The mechanism of melamine's fire retardancy has been reviewed and is proposed to be due to the sublimation and vapor-phase dissociation, where it is converted to non-volatile products and ammonia [30]. Therefore, in this study, we have incorporated different loadings of zinc borate and melamine into the synthesis of acrylamide (AM) and 2-acrylamido-2-methylpropane sodium sulfonate (AMPS-Na^+) SAPs. These potential fire retardants of the obtained superabsorbent composites (SAPCs) were evaluated for their water absorbency, thermal stability and flammability. AMPS-Na^+ was chosen because its strongly ionizable sulfonate groups can provide SAPs with a high water swelling capability. The novel fire retardant incorporating SAPCs that showed the best tap-water swelling, thermal stability and flammability might be appropriate for inhibiting the spreading of fire.

2. Experimental

2.1. Materials

Acrylamide (AM) was gifted from Siam Chemical Industry Co., Ltd. (Bangkok, Thailand). 2-acrylamido-2-methylpropane sodium sulfonate (AMPS-Na^+) was purchased from Aldrich (Steinhiem, Germany). *N*,*N*′-methylenebisacrylamide (MBA) and *N*,*N*,*N*′,*N*′-tetramethylethylenediamine (TEMED) were received from Fluka (Buchs, Switzerland). Ammonium persulfate (APS) was from Ajax (Seven Hills, Australia). Zinc borate ($2ZnO_2B_2O_3 \cdot 3H_2O$, Aldrich, Steinhiem, Germany) and melamine ($C_3H_6N_6$, Thai Mitsui Specialty Chemicals Co., Ltd., Chachoengsao, Thailand) were employed as fire retardants. Deionized water (Elga Deionizer, Model LA611, U.K.) was used for the synthesis and the swelling experiment.

2.2. Preparation of AM-co-AMPS-Na^+ SAPs

SAPs were synthesized by free-radical crosslinking polymerization of AM and AMPS-Na^+ at the molar ratio of 15:85, with 0.05% mol of MBA (crosslinker). An equal concentration of APS (initiator) and TEMED (co-initiator) was used at 1.2% by mol of the monomers. These concentrations were selected as being found previously to yield the SAP with the highest water absorbencies [24]. Firstly, AM was dissolved in deionized water in a 500-cm^3 reactor equipped with a mechanical stirrer, a condenser, and an inlet tube of nitrogen gas. AMPS-Na^+ was then added and the mixture was stirred at room temperature for 5 min, before heating to 60 °C under nitrogen atmosphere. Next, MBA and APS were sequentially added to the mixture and stirred for 5 min. Finally, TEMED was added and the polymerization was proceeded for 30 min to ensure complete polymerization. The obtained product was dehydrated with acetone, dried, milled, and then sieved through a 100-mesh sieve aluminum screen.

SAPs/fire retardant composites were synthesized by incorporating the desired amount of fire retardant into the polymerization mixture before MBA, APS, and TEMED were added. In this study, zinc borate, melamine, and their mixtures were chosen as fire retardant systems.

2.3. Fourier transform infrared spectroscopy (FT-IR)

The existence of the components of each SAP or SAPC was evaluated by analysis of their respective functional groups by Fourier Transform Infrared Spectroscopy (FTIR; System 2000, Perkin Elmer, U.S.A.). The dried sample and KBr powder were mixed, ground, pressed, and then subjected to the FT-IR spectrometry.

2.4. Water absorbency measurement

The water absorbency of the SAP and its derived SAPCs containing zinc borate, melamine or both, was carried out at room temperature. Each 0.1 g aliquot of dried SAP or SAPC product was allowed to swell in 200 cm^3 of deionized or tap water for 24 h. Subsequently, the fully swollen superabsorbents were separated from the unabsorbed medium by filtering through a 100-mesh sieve aluminum screen for 2 h. The swollen superabsorbents were then weighed and the water absorbency at equilibrium (g g^{-1}) was calculated by Eq. (1) and they were performed in triplicate for each system:

$$\text{Water absorbency} = \frac{\text{weight of swollen gel} - \text{weight of dry gel}}{\text{weight of dry gel}} \quad (1)$$

2.5. Thermal stability analysis

The SAP and its derived SAPCs were investigated for thermal properties using a TGA/SDTA 851e (Mettler Toledo Corporation, Switzerland). The measurements were carried out over a temperature range of 25–800 °C at a heating rate of 10 °C min^{-1} with a nitrogen gas flow rate of 60 cm^3 min^{-1}.

2.6. Flammability test

Flammability analysis was evaluated using a cone calorimeter (Fire Testing Technology Ltd., UK), according to ISO 5660, at an incident heat flux (50 kW m^{-2}) in an air atmosphere, and under the free convective air flow condition. The SAPs were prepared in the form of an oil-in-water dispersion as follows [31].

The dry SAPs or SAPCs (40% w w^{-1}) were dispersed in a mixture of 50% w w^{-1} of palm oil and 10% w w^{-1} of nonionic surfactant blends containing 54% w w^{-1} of Tween 80 or poly(oxyethylenesorbitan monooleate) having the HLB of 15 and 46% w w^{-1} of Span 80 or sorbitan (Z)-mono-9-octadecenoate having the HLB of 4.3 to give the HLB value of the blend is 10. Each suspension (5% v v^{-1}) in the oil-surfactant mixture was then dispersed in tap water, to subsequently obtain a viscous slurry gel that was used as an emulsion to coat wood (Apocynaceae, *Wrightia religiosa* Benth.) board dimension 100 × 100 × 3 mm to a surface depth of 3 mm. The surface of the wood, both uncoated and coated from the same batch, was subsequently exposed directly to an open flame generated by a propane gas jet. The uncoated wood board was used as the relative control to compare the effectiveness of the SAP and SAPC gels as fire retardants. The time to ignition (t_{ign}), peak of heat release rate (PHRR), time to PHRR (t_{PHRR}) and total heat release (THR) were recorded. The charred samples left after the flame extinguished were photographed by a digital camera.

3. Results and discussion

3.1. Synthesis of poly(AM-co-AMPS-Na^+)/fire retardant SAPCs

The IR spectra shown in Fig. 1(a)–(e) of zinc borate alone and that after the nominal incorporation of 5, 10, 20, and 30% w w^{-1} into the SAPCs revealed that the zinc borate alone shows peaks as

Please cite this article in press as: Seetapan N, et al., Effect of fire retardant on flammability of acrylamide and 2-acrylamido-2-methylpropane sodium sulfonate copolymer composites, Polymer Degradation and Stability (2011), doi:10.1016/j.polymdegradstab.2011.06.014

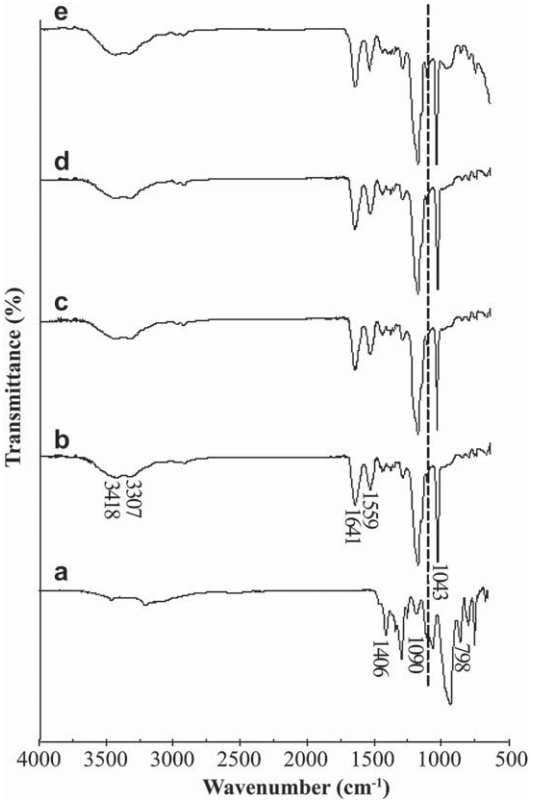

Fig. 1. Representative FT-IR spectra of (a) zinc borate, and poly(AM-*co*-AMPS-Na^+)/zinc borate SAPCs with nominal zinc borate loadings of (b) 5%, (c) 10%, (d) 20% and (e) 30% (w w^{-1}).

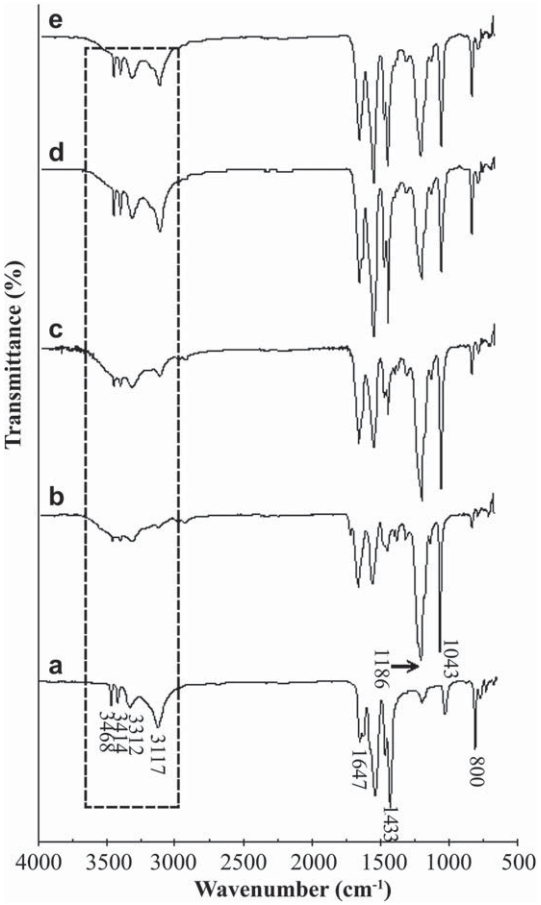

Fig. 2. Representative FT-IR spectra of (a) melamine and poly(AM-*co*-AMPS-Na^+)/melamine SAPCs with nominal melamine loadings of (b) 5%, (c) 10%, (d) 20% and (e) 30% (w w^{-1}).

follows: 1406 cm^{-1} (s), $\nu_{B(3)-O\ as}$; 1090 cm^{-1} (sh) and 798 cm^{-1} (sh), $\nu_{B(4)-O}$ [32]. For zinc borate SAPCs, the overlapping peaks of ν_{N-H} and ν_{O-H} are found at 3418 cm^{-1} (b) and 3307 cm^{-1} (b), respectively; the $\nu_{C=O}$ peak amide I at 1641 cm^{-1} (s) [33], the δ_{N-H} peak of amide II at 1559 cm^{-1} (s) and the $\nu_{S=O}$ peak of AMPS-Na^+ at 1043 cm^{-1} (sh) [2]. The $\nu_{B(4)-O}$ peak at 1090 cm^{-1} was also present and increased in relation to the amount of zinc borate in the synthesized composites. However, when a nominal of 30% w w^{-1} loading of zinc borate was prepared, some zinc borate was seen to precipitate and so separate from the obtained SAPC.

The FT-IR spectra of melamine and poly(AM-*co*-AMPS-Na^+)/melamine SAPCs with melamine contents of 5, 10, 20, and 30% w w^{-1} in Fig. 2(a)–(e) show the characteristic peaks of melamine as follows: 3468–3117 cm^{-1} (s), ν_{N-H}; 1647 cm^{-1}(s), $\nu_{C=N}$; 1535 cm^{-1} (sh), δ_{N-H}; 1433 cm^{-1} (sh), ν_{C-N}; ~800 cm^{-1}, $\delta_{N-H\ (op)}$ [34]. Besides, the overlapping peak of ν_{N-H} and ν_{O-H} peaks are found at ~3500–3000 cm^{-1} (b), the δ_{C-H} at 1186 cm^{-1} (s), and the $\nu_{S=O}$ peak of AMPS-Na^+ at 1043 cm^{-1} (sh) [2]. The ν_{N-H} and $\delta_{N-H\ (op)}$ peaks of melamine increased in relation to the amount of melamine loaded in the SAPCs.

Mixtures of zinc borate and melamine at 20:10, 15:15, and 10:20 by % w were incorporated in the respective SAPCs. The FT-IR spectra (Fig. 3(a)–(c)) of these prepared SAPCs showed the characteristic peaks of both zinc borate and melamine at about 1090 cm^{-1} and 3468–3117 cm^{-1}, respectively.

3.2. Swelling behavior of poly(AM-co-AMPS-Na^+)/fire retardant SAPCs

Water absorbency in tap water of the SAP and zinc borate containing SAPCs were always significantly lower than those in deionized water (Fig. 4(a)), being about 1.65-fold lower for the SAP and from 2.56- to 3.93-fold lower for the SAPCs (the difference increases as the nominal zinc level increases). The same trend was also seen for melamine containing SAPCs, but the difference between the water absorbency in tap and deionized water was less marked (Fig. 4(b)). The difference in water absorption is caused by the presence of ions in the tap water, which was used here contains Fe^{3+} (7.2 ppm), Ca^{2+} (27.2 ppm) and Mg^{2+} (0.05 ppm) as the dominant ions. The main reason is the shielding or screening effects of the cations that reduce the osmotic pressure of SAPCs. Comparing the effect of the ions on the SAPCs, one can see that the zinc borate incorporated SAPCs were affected more than melamine because the water absorption was reduced the most (Fig. 4(a) and (b)). One possible cause is the negatively synergistic effect of Zn^{2+} in the SAPC with the three main cations (Fe^{3+}, Ca^{2+} and Mg^{2+}). For the SAPC incorporating melamine, the effect of the cation salts in tap water on the water absorbency was not so strong due to the lower polarity of melamine (Fig. 4(b)).

The equilibrium water absorbency of the mixed zinc borate and melamine SAPCs synthesized with 30% w w^{-1} fire retardant in Fig. 5 for the three zinc borate-to-melamine w w^{-1} ratios shows that the zinc borate-to-melamine ratio at 20:10 (% w w^{-1}) strongly decreases the equilibrium water absorbency in deionized and tap water by 1.76- and 1.50-fold respectively compared with poly(AM-*co*-AMPS-Na^+) SAP (Fig. 4(b)). As the zinc borate-to-melamine ratios (% w w^{-1}) were decreased to 15:15 and 10:20, the equilibrium water absorbency in both tap and deionized water slightly

Please cite this article in press as: Seetapan N, et al., Effect of fire retardant on flammability of acrylamide and 2-acrylamido-2-methylpropane sodium sulfonate copolymer composites, Polymer Degradation and Stability (2011), doi:10.1016/j.polymdegradstab.2011.06.014

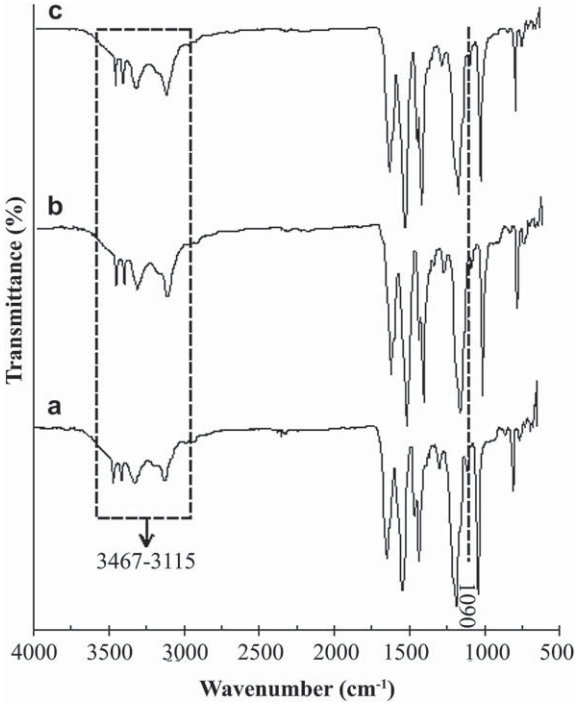

Fig. 3. Representative FT-IR spectra poly(AM-*co*-AMPS-Na^+)/zinc borate and melamine SAPCs loaded with nominal zinc borate: melamine w w^{-1} ratios of (a) 20:10, (b) 15:15 and (c) 10:20.

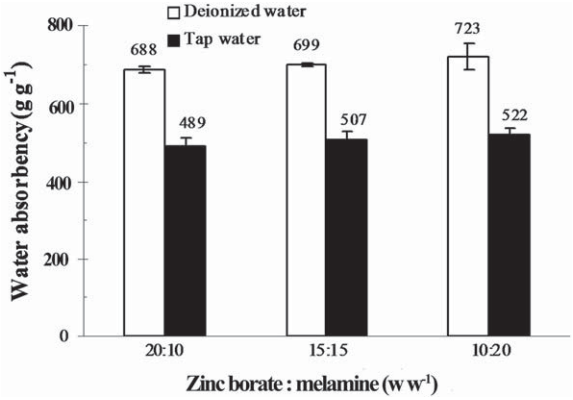

Fig. 5. Effect of the zinc borate-to-melamine ratios on the equilibrium water absorbency in deionized water and tap water of poly(AM-*co*-AMPS-Na^+)/mixed zinc borate and melamine SAPCs at zinc borate: melamine ratios of 20:10, 15:15 and 10:20% w w^{-1} of total monomers.

increased (compared with zinc borate-to-melamine ratios of 20:10 (% w w^{-1})). This is because the polarity of the SAPCs increases with increasing melamine contents.

3.3. Thermal analysis of poly(AM-co-AMPS-Na^+)/fire retardant SAPCs

The thermal behaviors of poly(AM-*co*-AMPS-Na^+)/zinc borate SAPCs were similar to that seen with poly(AM-*co*-AMPS-Na^+) SAP, as revealed by TGA thermograph analyses shown in Fig. 6. Zinc borate degraded via the dehydration of zinc borate crystals in the range of 341–416 °C [35]. The first degradation stage (~100 °C) of all SAPs and SAPCs takes place due to the loss of absorbed and bound water. The second (313–328 °C) and third (325–433 °C) stages of degradation are ascribed to the amide side group of the AMPS-Na^+ and AM, respectively [36], and the dehydration of zinc borate crystal. The final decomposition stage (711–800 °C) is assigned to the degradation of chain backbone and rearranged zinc borate [35]. The results indicated the enhanced thermal stability at all the tested temperatures was detected as a function of zinc borate loading because zinc borate rearranges its structure and so acts as a heat barrier to delay the diffusion of volatile thermo-oxidation products to gas, and gas to the composite [35].

Pure melamine shows two degradation stages (Fig. 7), the generation of nitrogen volatile side groups in the first stage (315–381 °C) and then, in the second stage (416–748 °C), the decomposition of main chain and nitrogen volatiles from the first stage [37]. In comparison, thermograms of the poly(AM-*co*-AMPS-Na^+)/melamine SAPCs show a first degradation stage (~100 °C), due to the loss of absorbed and bound water, whilst the second stage (282–310 °C) is ascribed to the decomposition of the nitrogen compounds from melamine. The third (313–346 °C) and fourth (345–412 °C) stages are interpreted as the degradation of AMPS-Na^+ and AM, respectively, whilst the final decomposition stage (742–800 °C) is assigned to the degradation of the backbone chain (Fig. 7). Overall, the incorporation of melamine improved the thermal stability of the SAPCs up to about 310 °C but thereafter melamine started to show an almost complete decomposition at higher temperature due to the loss of nitrogen compounds [38], and was completely decomposed at about 750 °C. Therefore, beyond ~330 °C, the thermal stability of the melamine-based SAPCs decreased with increasing melamine loadings.

The TGA thermograms of the SAPCs composed of poly(AM-*co*-AMPS-Na^+) with either zinc borate or melamine incorporated to make SAPCs, revealed that the incorporation of zinc borate apparently promoted the thermal stability to the SAPCs over the studied temperature range (0–800 °C) (Fig. 6), whilst melamine showed a better thermal stability at temperatures only below 310 °C (Fig. 7).

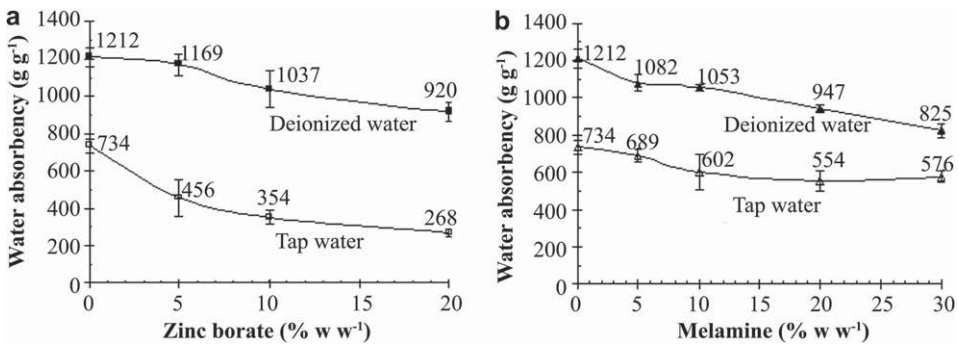

Fig. 4. Water absorbency of (a) zinc borate, and (b) melamine incorporated SAPC in deionized water and tap water.

Please cite this article in press as: Seetapan N, et al., Effect of fire retardant on flammability of acrylamide and 2-acrylamido-2-methylpropane sodium sulfonate copolymer composites, Polymer Degradation and Stability (2011), doi:10.1016/j.polymdegradstab.2011.06.014

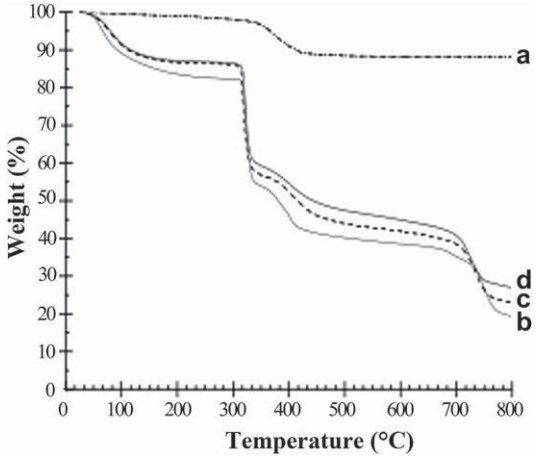

Fig. 6. Representative TGA thermograms of (a) zinc borate, (b) poly(AM-*co*-AMPS-Na^+) SAPs and the zinc borate derived SAPCs with (c) 10 and (d) 20% w w^{-1} nominal loadings of zinc borate.

The latter is because at higher temperatures most of the melamine dissociated to the vapor phase [30] that can then dilute the content of oxygen gas in the area of burning objects. Therefore, the addition of both zinc borate and melamine into SAPCs could potentially offer a better thermal protection over the wide temperature from 0 to 800 °C and so was evaluated next. The TGA thermograms of the mixed zinc borate and melamine SAPCs, at a zinc borate-to-melamine addition ratios of 20:10, 15:15, and 10:20 (% w w^{-1}) of total monomers (Fig. 8) were similar to that seen for both melamine SAPC (Fig. 7) and zinc borate SAPC (Fig. 6). At temperatures below about 300 °C there was no different weight loss in thermal decomposition profiles among all the composites with varying melamine contents (Fig. 8). In addition, thermal stability was found to increase with an increasing zinc borate ratio at temperatures above 350 °C. Compared to the parental SAP, these derived SAPCs show a better thermal stability at all evaluated temperatures (0–800 °C).

3.4. Flammability analysis

Heat release is defined as the heat generated due to various chemical reactions when a material is exposed to fire, and provides information on the size of the fire and hence the corresponding fire hazard [18]. Materials with a low heat release rate (HRR) gives less damage to the surroundings than those with high HRR. Thus, the

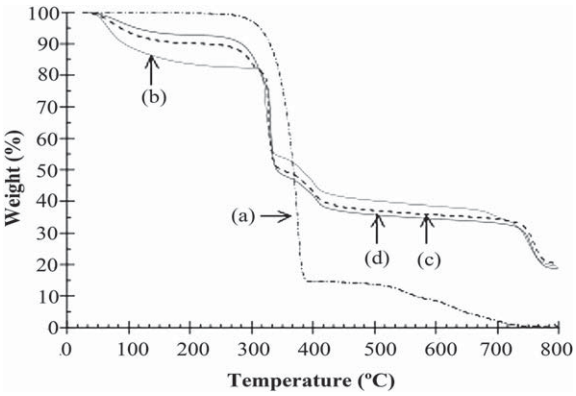

Fig. 7. Representative TGA thermograms of (a) melamine, (b) poly(AM-*co*-AMPS-Na^+) SAPs and the melamine derived SAPCs with (c) 20 and (d) 30% w w^{-1} nominal loadings of melamine.

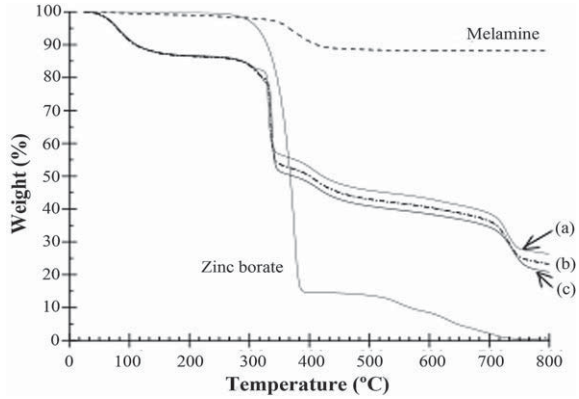

Fig. 8. Representative TGA thermograms of poly(AM-*co*-AMPS-Na^+)/mixed zinc borate and melamine SAPCs at nominal zinc borate:-to-melamine ratios of (a) 20:10, (b) 15:15, and (c) 10:20% w w^{-1} of total monomers. Redrawn for a discussion are thermograms of zinc borate and melamine.

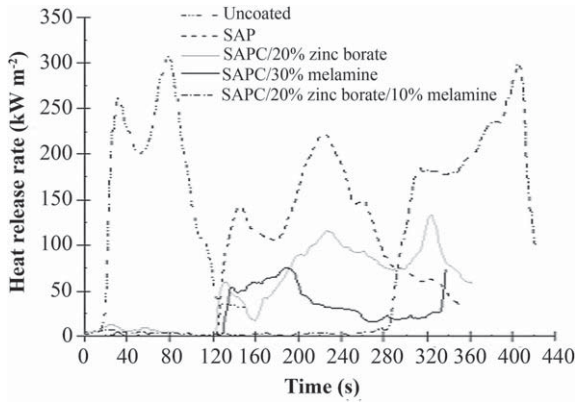

Fig. 9. Heat release rate plots for the uncoated wood and the woods coated with different emulsion systems.

HRR, and particularly the PHRR, is the primary characteristic in determining the size, growth and suppression requirements of a fire environment [39]. The THR is defined as a total heat release at the end of burning. In this study, the combustion experiment was performed until flame was self-extinguished. The HRR plots for the uncoated and the coated wood specimens revealed that the t_{ign} was fastest for the uncoated wood board (13 s), but was about ten-fold to twenty-fold longer for all the SAP- or SAPC-coated specimens (Fig. 9), illustrating the excellent protection obtained in delaying the flammability after exposure to an open flame (Table 1). For the uncoated specimen, the observed THR of 22 MJ m^{-2} was obtained from the combustion of the wood itself, where the flame eventually extinguished because the entire wood specimen was completely

Table 1
Flammability parameters obtained from the cone calorimetry.

Specimen	t_{ign} (s)	PHRR (kW m^{-2})	t_{PHRR} (s)	THR (MJ m^{-2})
Uncoated wood	13	309	79	22
Wood coated with SAPs	125	222	224	26
Wood coated with SAPs, 20% zinc borate	118	132	324	18
Wood coated with SAPs, 30% melamine	117	75	188	8
Wood coated with SAPs, 20% zinc borate and 10% melamine	278	300	405	26

t_{ign}, time to ignition; PHRR, peak heat release rate; t_{PHRR}, time to PHRR; THR, total heat release.

Please cite this article in press as: Seetapan N, et al., Effect of fire retardant on flammability of acrylamide and 2-acrylamido-2-methylpropane sodium sulfonate copolymer composites, Polymer Degradation and Stability (2011), doi:10.1016/j.polymdegradstab.2011.06.014

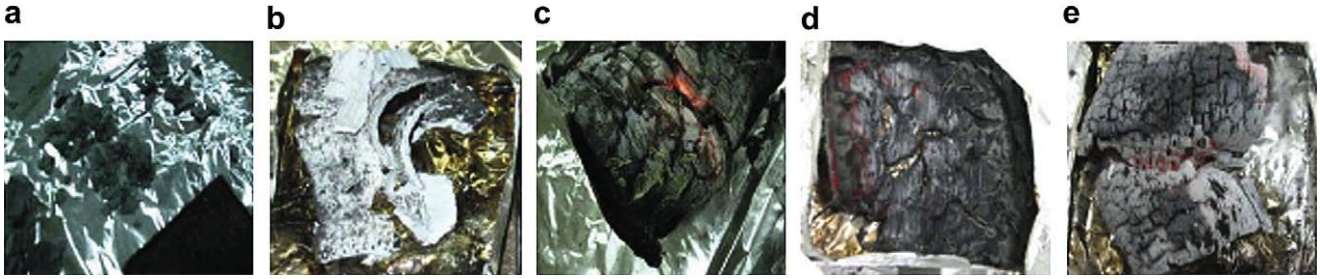

Fig. 10. Charred samples of (a) the uncoated, (b) the poly(AM-*co*-AMPS-Na^+) SAP-coated, (c) the poly(AM-*co*-AMPS-Na^+)/20% zinc borate SAPC-coated, (d) the poly(AM-*co*-AMPS-Na^+)/30% melamine SAPC-coated, and (e) the poly(AM-*co*-AMPS-Na^+)/20% zinc borate/10% melamine SAPC-coated wood boards.

burnt out. PHRR and t_{PHRR} were observed at 309 kW m^{-2} and 79 s, respectively, for the uncoated wood specimen.

When compared to the uncoated wood surface, that coated with the neat SAP gel reduced the PHRR 1.39-fold, and delayed both the t_{ign} 9.62-fold to 125 s and the t_{PHRR} 2.83-fold to 224 s, whereas the THR was increased slightly (1.18-fold) to 26 MJ m^{-2}. This delayed-burning mechanism is explained as being due to the cooling effect of water trapped within the SAP particles. After ignition, the trapped water is slowly released causing a lower HRR for the duration of the burning process. After all water evaporated, the neat SAP, which is a fuel itself, finally combusted under heat, consecutively with the burnout of wood, and so increased the THR compared to the uncoated wood surface.

In case of the wood coated with the SAPC gels incorporating either of 20% w w^{-1} zinc borate or 30% w w^{-1} melamine, the t_{ign} values were broadly similar to that of the neat SAP-coated specimen, but showed a clear reduction in the PHRR, being 1.68-fold and 2.96-fold lower, respectively, and is due to the fire retardant effect of zinc borate and melamine. The role of zinc borate is likely to be due to formation of a protective zinc oxide covering on the surface during combustion, which will obstruct the access of oxygen and so preventing complete combustion. The presence of melamine in the coating gel offers high potential in reducing the PHRR, due to the conversion of melamine to non-volatile products and ammonia [30], then effectively diluted the oxygen gas during combustion. Experimentally, 120 s after the specimen started to flame, it self-extinguished for about 80 s and then, at about 330 s, the flame ignited itself, as observed by the increase in the HRR (Fig. 9), due to the depletion of volatile phase and the remaining wood specimen.

The wood coated with the mixture of zinc borate and melamine containing SAPC gel provided the best delay in fire ignition (t_{ign} = 258 s), some 21.4-fold longer than the untreated wood and 2.2–2.4-fold long than the other SAP or SAPC treated samples, presumably attributed to the combined effect of zinc borate and melamine. However, after ignition, the specimen demonstrated a rapid increase in the HRR and the PHRR, the latter at 300 kW m^{-2}, which is a level broadly similar to that seen in the uncoated specimen. This is likely due to the burning of both wood specimen and SAP particles.

Fig. 10 shows representative images of the residues after the flame was self-extinguished. The uncoated wood gave a dark gray ash (Fig. 10(a)), whereas the residue of the wood coated with the poly(AM-*co*-AMPS-Na^+) SAP after burning appeared as a white charred layer and a dark gray residue, representing the combustion of the coated SAP particles and the wood, respectively (Fig. 10(b)). The char was found to be fragile and easily cracked. Specimens coated with the SAPC containing either zinc borate (Fig. 10(c)) or melamine (Fig. 10(d)) showed a more compact black char protective layer, preventing the penetration of gases and the complete combustion. As a result, there was a reduction in the PHRR and THR in both coated samples (Table 1). In case of a mixed zinc borate and melamine containing SAPC-coated specimen (Fig. 10(e)), the residual char was white and gray indicating a complete burning of the SAP particles and wood.

4. Conclusion

Poly(AM-*co*-AMPS-Na^+) SAPs and their zinc borate and/or melamine containing SAPCs as fire retardants were synthesized by free-radical crosslinking polymerization. Water absorbencies of SAPCs decreased inversely to the amount of added fire retardant. The thermal stability of SAPCs increased as the zinc borate loadings increased, whilst melamine incorporation improved the thermal stability up to 300 °C. Both SAP and SAPC gels, coated onto the wood surface, delayed the specimen fire ignition, reduced the PHRR and extended the t_{PHRR}. The SAPC/30% w w^{-1} melamine provided the lowest PHRR and THR. The co-incorporation of 20% w w^{-1} zinc borate and 10% w w^{-1} melamine in the SAPC gel provided an excellent coating system with the time to ignition of the coated specimen being delayed to about 4.5 min compared to 13 s and 2 min for the uncoated and SAP-coated wood, respectively. This may allow sufficient time for the evacuation of premises and prevention fires from spreading.

Acknowledgments

The authors would like to acknowledge the financial support from the Thailand Research Fund under the Research Scholar Team Consolidation Program Contract no. RTA5080004. Research facilities provided by the Imaging Polymer Laboratory of Chulalongkorn University's Department of Imaging and Printing Technology, Faculty of Science are highly appreciated. English edition of the manuscript by the Publication Counselor Unit of the Research Division, Faculty of Science, Chulalongkorn University, are highly appreciated.

References

[1] Kiatkamjornwong S, Chomsaksakul W, Sonsuk M. Radiation modification of water absorption of cassava starch by acrylic acid/acrylamide. Radiat Phys Chem 2000;59:413–27.
[2] Durmaz S, Okay O. Acrylamide/2-acrylamido-2-methylpropane sulfonic acid sodium salt-based hydrogels: synthesis and characterization. Polymer 2000; 41:3693–704.
[3] Okay O, Sarıışık SB. Swelling behavior of poly(acrylamide-*co*-sodium acrylate) hydrogels in aqueous salt solutions: theory versus experiments. Eur Polym J 2000;36(2):393–9.
[4] Taşdelen B, Kayaman-Apohan N, Güven O, Baysal BM. Preparation of poly(N-isopropylacrylamide/itaconic acid) copolymeric hydrogels and their drug release behavior. Int J Pharm 2004;278:343–51.
[5] Jiraprasertkul W, Nuisin R, Jinsart W, Kiatkamjornwong S. Synthesis and characterization of cassava starch graft poly(acrylic acid) and poly[(acrylic acid)-co-acrylamide] and polymer flocculants for wastewater treatment. J Appl Polym Sci 2006;102:2915–28.

Please cite this article in press as: Seetapan N, et al., Effect of fire retardant on flammability of acrylamide and 2-acrylamido-2-methylpropane sodium sulfonate copolymer composites, Polymer Degradation and Stability (2011), doi:10.1016/j.polymdegradstab.2011.06.014

[6] Yiamsawas D, Kangwansupamonkon W, Chailapakul O, Kiatkamjornwong S. Synthesis and swelling properties of poly[acrylamide-*co*-(crotonic acid)] superabsorbents. React Funct Polym 2007;67:865–82.
[7] Seetapan N, Wongsawaeng J, Kiatkamjornwong S. Gel strength and swelling of acrylamide-protic acid superabsorbent copolymers. Polym Adv Technol; 2010. doi:10.1002/pat.1658.
[8] Saraydin D, Unver-Saraydin S, Karadağ E, Koptagel E, Güven O. In vivo biocompatibility of radiation crosslinked acrylamide copolymers. Nucl Instr Meth B 2004;217:281–92.
[9] Karadağ E, Saraydin D, Caldiran Y, Güven O. Swelling studies of copolymeric acrylamide/crotonic acid hydrogels as carriers for agricultural uses. Polym Adv Technol 2000;11(2):59–68.
[10] Duran S, Solpan D, Güven O. Synthesis and characterization of acrylamide-acrylic add hydrogels and adsorption of some textile dyes. Nucl Instr Meth B 1999;151(1–4):196–9.
[11] Karadağ E, Uzüm OB, Saraydin D. Swelling equilibria and dye adsorption studies of chemically crosslinked superabsorbent acrylamide/maleic acid hydrogels. Eur Polym J 2002;38:2133–41.
[12] Can HK, Kirci B, Kavalak S, Güner A. Removal of some textile dyes from aqueous solutions by poly(*N*-vinyl-2-pyrrolidone) and poly(*N*-vinyl-2-pyrrolidone)/$K_2S_2O_8$ hydrogels. Radiat Phy Chem 2003;68:811–8.
[13] Noppakundilograt S, Nanakorn P, Sonjaipanich K, Seetapan N, Kiatkamjornwong S. Synthesis and characterization of acrylamide-based aluminium flocculants for wastewater treatment. J Appl Polym Sci 2009;114:2564–75.
[14] Noppakundilograt S, Nanakorn P, Jinsart W, Kiatkamjornwong S. Synthesis of acrylamide/acrylic acid-based aluminum flocculant for dye reduction and textile wastewater treatment. Polym Eng Sci 2010;50(8):1535–46.
[15] Bashaw RN, Harper BG. Method for controlling the spread of fire. US patent 3229769; 1966.
[16] Pascente JE, Pascente TJ. Method of preventing combustion by applying an aqueous superabsorbent polymer composition. US patent 5849210; 1998.
[17] Beck M, Champ S, Tonnessen M, Ziemer A, Goebel G, Pfeiffer M. Fire extinguishing and/or fire retarding compositions. US patent 2007/0289752 A1; 2007.
[18] Chigwada G, Wang D, Jiang DD, Wilkie CA. Styrenic nanocomposites prepared using a novel biphenyl-containing modified clay. Polym Degrad Stab 2006;91:755–62.
[19] Karlsson L, Lundgren A, Jungqvist J, Hjertberg T. Influence of melt behaviour on the flame retardant properties of ethylene copolymers modified with calcium carbonate and silicone elastomer. Polym Degrad Stab 2009;94:527–32.
[20] Morgan AB. Flame retarded polymer layered silicate nanocomposites: a review of commercial and open literature systems. Polym Adv Technol 2006;17:206–17.
[21] Hirata T, Kawamoto T, Nishimoto T. Thermogravimetry of wood treated with water-soluble retardants and a proposal for development of fire retarded wood materials. Fire Mater 1991;15:27–36.
[22] Hagen M, Hereid J, Delichatsios MA, Zhang J, Bakirtzis D. Flammability assessment of fire-retarded Nordic Spruce wood using thermogravimetric analyses and cone calorimetry. Fire Saf J 2009;44:1053–66.
[23] Bordado JCM, Gomes JFP. New technologies for effective forest fire fighting. Int J Environ Stud 2007;64:243–51.
[24] Limparyoon N, Seetapan N, Kiatkamjornwong S. Acrylamide/2-acrylamido-2-methylpropane sulfonic acid and associated sodium salt superabsorbent copolymers with mica nanocomposites as fire retardants. Polym Deg Stab 2011;96:1054–63.
[25] Nazare S, Kandola BK, Horrocks AR. Smoke, CO, and CO_2 measurements and evaluation using different fire testing techniques for flame retardant unsaturated polyester resin formulations. J Fire Sci 2008;26:215–42.
[26] Chen L, Wang Y-Z. A review on flame retardant technology in China. Part I: development of flame retardants. Polym Adv Technol 2010;21:1–26.
[27] Wu W, Yang CQ. Comparison of different reactive organophosphorus flame retardant agents for cotton. Part II: Fabric flame resistant performance and physical properties. Polym Deg Stab 2007;92:363–9.
[28] Levchik SV, Balabanovich AI, Levchik GF, Costa L. Effect of melamine and its salts on combustion and thermal decomposition of polyamide 6. Fire Mater 1997;21:75–83.
[29] Balabanovich AI. The effect of melamine on the combustion and thermal decomposition behaviour of poly(butylenes terephatalate). Polym Deg Stab 2004;84:451–8.
[30] Weil ED, Choudhary V. Flame-retarding plastics and elastomers with melamine. J Fire Sci 1995;13:104–26.
[31] Sortwell ET. Method of preventing or extinguishing fires. US patent 2009/0151963 A1; 2009.
[32] Yongzhong J, Shiyang G, Shuping X, Jun L. FT-IR spectroscopy of supersaturated aqueous solutions of magnesium borate. Spectrochim Acta A 1999;56(7):1291–7.
[33] Tang Q, Wu J, Sun H, Fan S, Hu D, Lin J. Superabsorbent conducting hydrogel from poly(acrylamide-aniline) with thermo-sensitivity and release properties. Carbohyd Polym 2008;73:473–81.
[34] Hu Y, Ye L, Zhao X. Synthesis of the melamine–formaldehyde polycondensate and its thermal stabilization effect on polyoxymethylene. Polymer 2006;47:2649–59.
[35] Genovese A, Shanks RA. Structural and thermal interpretation of the synergy and interactions between the fire retardants magnesium hydroxide and zinc borate. Polym Deg Stab 2007;92:2–13.
[36] Zhang J, Wang A. Study on superabsorbent composites. IX: synthesis, characterization and swelling behaviors of polyacrylamide/clay composites based on various clays. React Funct Polym 2007;67:737–45.
[37] Liang H, Asif A, Shi W. Thermal degradation and flame retardancy of a novel methacrylated phenolic melamine used for UV curable flame retardant coatings. Polym Deg Stab 2005;87:495–501.
[38] Costa L, Camino G, Luda di Cortemiglia MP. Mechanism of thermal degradation of fire-retardant melamine salts. In: Nelson G, editor. Fire and polymers: hazards identification and prevention. ACS Symposium Series 425. Washington, DC: ACS; 1990. p. 211e38.
[39] Koo JH, editor. Polymer nanocomposites: processing, characterization, and applications. New York: The McGraw-Hill Companies, Inc.; 2006.

Please cite this article in press as: Seetapan N, et al., Effect of fire retardant on flammability of acrylamide and 2-acrylamido-2-methylpropane sodium sulfonate copolymer composites, Polymer Degradation and Stability (2011), doi:10.1016/j.polymdegradstab.2011.06.014

Synthesis of Acrylamide-*Co*-(Itaconic Acid) Superabsorbent Polymers and Associated Silica Superabsorbent Polymer Composites

Nispa Seetapan,[1] Natsiri Srisithipantakul,[2] Suda Kiatkamjornwong[3]
[1] *National Metal and Materials Technology Center, National Science and Technology Development Agency, Pathumthani 12120, Thailand*

[2] *Faculty of Science, Chulalongkorn University, Bangkok 10330, Thailand*

[3] *Program of Petrochemistry and Polymer Science, Faculty of Science, Chulalongkorn University, Bangkok 10330, Thailand*

Superabsorbent polymers (SAPs) were synthesized from acrylamide (AM) and itaconic acid (IA) via a crosslinking polymerization. SAP composites (SAPCs) were formed by the incorporation of silica with three particle sizes into the polymerization to increase the gel strength of SAPs. Effects of AM: IA molar ratios, silica types and concentrations on water absorbency, absorbency rate and absorbency under loadings (AUL) of the composites were investigated. The highest water absorbency of the SAP is 233 ± 8 g g^{-1} at an AM: IA molar ratio of 97:3 with absorbency of 149 ± 2 g g^{-1} within 15 min. The highest AUL of the SAPC with 0.5%–2.0% w w^{-1} silica is 13 g g^{-1} by 1.93 × 10^3 Pa load. A pseudo-second-order kinetics for water absorbency was found in both SAPs and in situ SAPCs. In situ SAPCs and the mechanically mixed SAPCs in vertical and horizontal direction yielded similar water absorbency values. POLYM. ENG. SCI., 51:764–775, 2011.
© 2011 Society of Plastics Engineers

INTRODUCTION

Superabsorbent polymers (SAPs) and their associated SAP composites (SAPCs) have drawn much interest since the early 1970s. During that period, Fanta et al. investigated graft copolymerization of vinyl acrylate or acrylonitrile onto starch and other polysaccharides, which yielded products that could absorb from several hundred to several thousand times their own weight in water and also had a high water holding capacity under pressure, also known as absorbency under load (AUL) [1], and thus the name "superabsorbent polymer" was adopted. Research and development into SAPs have focused on their extraordinarily high-water absorbency and applications. Indeed, over 80% of SAPs have found extensive commercial applications as sorbents in personal care products, such as infant diapers [2], feminine hygiene products, and incontinence products [3]. Not only that, but also many new applications have already been investigated through such active research and development, leading to the successful application of SAPs in new fields, such as matrices for enzyme immobilization [4, 5], bio-sorbents in preparative chromatography [6], materials for agricultural mulches and fertilizers [7, 8], matrices for controlled release devices [9], drug delivery [10], bioactive scaffolds for bone engineering [11], bio-separation [12], moisture retention in soil [13, 14], SAPCs as a sealing material [15], debris flow control, artificial snow [16, 17], a gel actuator [18], and fire fighting [19]. The desired features of superabsorbents are a high swelling capacity, high swelling rate, and a greater strength of the swollen gel. The majority of the reported superabsorbents comprise of only the first mentioned feature, i.e., a high absorbency, but there are few studies concerning improvements of the absorbency rate and gel strength. Absorbent particles are conventionally strengthened through surface crosslinking [20]. Traditionally, an inorganic component is used as a filling material for the purpose of improving the material properties and reducing the product cost. The addition of inorganic powder (usually <5% w w^{-1}) to a SAP provides a method for increasing the gel strength [21–23]. The utility of the inorganic nanoparticles as additives to enhance the polymer performance has been increased. Such inorganic materials for the preparation of SAPCs can be laponite

Correspondence to: Suda Kiatkamjornwong; e-mail: ksuda@chula.ac.th
Contract grant sponsor: Thailand Research Fund; contract grant number: RTA5080004; contract grant sponsor: Imaging Polymer Laboratory of the Faculty of Science's Department of Imaging and Printing Technology, Chulalongkorn University.
DOI 10.1002/pen.21882
Published online in Wiley Online Library (wileyonlinelibrary.com).
© 2011 Society of Plastics Engineers

[21], kaolin [24], montmorillonite [22, 25], attapulgite [26–28], mica [23, 29], bentonite [30], sercite [31], or rectorite [32] to form the layered silicate structures.

A novel SAPC based upon starch-*g*-AM/mineral powder, with a water absorbency of about 4000 times its own weight, was synthesized by a graft-copolymerization reaction of AM, potato starch, and mineral ultrafine powder, followed by hydrolysis with sodium hydroxide [33]. The SAPCs doped with kaolinite powder possessed a higher water absorbency than those doped with bentonite or sercite powder, since the kaolinite powder can moderately disperse in the water and crosslink with the AM and starch. Moreover, the collaborative absorbent effect of —$CONH_2$, —COONa, and —COOH groups has been found to be superior to that of a single —$CONH_2$, —COONa, or —COOH group. The ultrafine mineral powder as a crosslinking point plays an important role in the formation of a network structure in SAPCs. Incorporation of kaolin into hydrogel SAPCs caused a reduced equilibrium swelling and swelling rate to as low as 17–31% and 19–29% (w w^{-1}), respectively, but resulted in an enhanced gel strength by as much as 21–35% above that of the corresponding SAP as a control [34]. Grafted sodium carboxymethylcellulose (CMC) - silica gel SAPC with a water absorbency capacity as high as 4000 g g^{-1} in distilled water has been reported [35]. Super porous hydrogel composites with the inclusion of modified cellulose gum or an internally cross-linked form of CMC typically gave a significant improvement in the properties of superporous hydrogels, such as a high mechanical strength and a high swelling ratio. Indeed, the inclusion of a suitable composite material typically increases the physical crosslinking density and so provides a high strength and prevents the polymer chains from collapsing during air drying [36]. The in situ sol-gel method used to prepare bioactive hydrogels [11, 37, 38] is considered to be quite expensive for industrial use. Therefore, the use of amorphous silica powder to form the non-layered silica SAPCs is a cheaper way for industries to manufacture personal care products. On the other hand, the mechanical mixing of SAP with silicate powder can be another economical way to prepare SAPCs.

In this research, poly[acrylamide-*co*-(itaconic acid)]/silica composites as potential SAPCs were made by in situ solution polymerization with three different sizes of silica. The SAPCs with a high water absorbency rate and capacities were compared with the SAPCs prepared by mechanical mixing between the P(AM-IA) SAP and silica powder of the same composition.

TABLE 1. Silica types and their physical properties.

Physical properties	Aerosil 90	Aerosil 200	Aerosil 300
BET surface area, (m^2 g^{-1})	90 ± 15	200 ± 25	300 ± 30
Average primary particle size, (nm)	20	12	7
pH	3.7−4.7	3.7−4.7	3.7−4.7
SiO_2 (% w w^{-1})	>99.8	>99.8	>99.8
Al_2O_3 (% w w^{-1})	<0.05	<0.05	<0.05
Fe_2O_3 (% w w^{-1})	<0.003	<0.003	<0.003
HCl (% w w^{-1})	<0.025	<0.025	<0.025

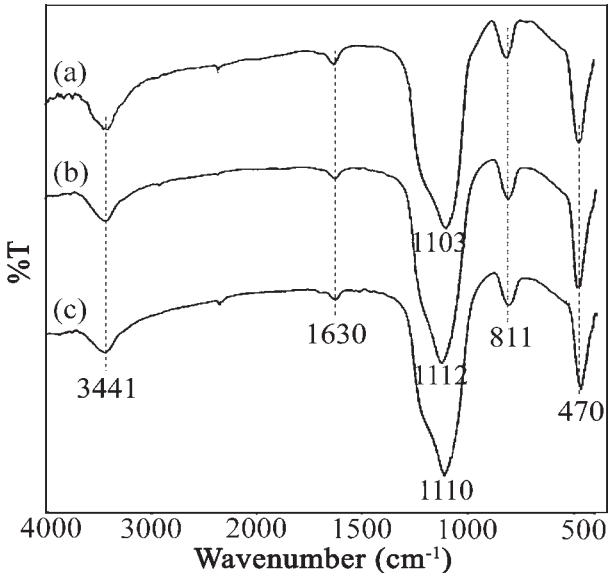

FIG. 1. IR spectra of the three types of silica used in the synthesis: (a) Aerosil 90, (b) Aerosil 200, and (c) Aerosil 300.

EXPERIMENTAL PROCEDURES

Materials and Methods

Acrylamide (AM, Siam Chemicals, Bangkok, Thailand), itaconic acid (IA, Merck, Hohenbrunn, Germany), *N,N′*-methylenebisacrylamide (*N*-MBA, Fluka, Buchs, Switzerland), ammonium persulfate (APS, Merck, Hohenbrunn, Germany), *N,N,N′,N′*-tetramethylethylenediamine (TEMED, Fluka, Buchs, Switzerland), and silica (SiO_2, J.J-Degussa-Huts, Thailand) were used. The three types of silica used in this research, and their properties, are shown in Table 1 and their IR spectra are given in Fig. 1.

Polymerization

A 100-cm^3 mixture of AM: IA of 100:0, 99:1, 98:2, and 97:3 (by % molar ratios) was supplemented with 0.5% w w^{-1} *N*-MBA crosslinker, the initiator couple of APS (1.0% w w^{-1}) and TEMED (0.20 cm^3), and then poured into a 500-cm^3 four-necked round-bottomed flask equipped with a mechanical stirrer (Ika-Ruhrwerke RW20, Staufen, Germany), a spiral condenser and a thermometer. The polymerization reaction was allowed to proceed at 45°C in a water bath (WBU 45 Memmert, Schwabach, West Germany) under a nitrogen gas atmosphere for 30 min with stirring at 250 rpm The resulting polymer was dehydrated with methanol, cut into small pieces of half a centimeter in diameter, dried in a vacuum

TABLE 2. Basic formulation for the preparation of P(AM-IA) SAPs and P(AM-IA)/silica SAPCs.

Ingredient	In situ polymerization method	Mechanical mixing method
AM / IA (mole/mole)	100/0, 99/1, 98/2, 97/3	100/0, 99/1, 98/2, 97/3
Aerosil 90 silica (w w^{-1})	0.1, 0.2, 0.5, 2.0	0.1, 0.5, 2.0
Aerosil 200 silica (w w^{-1})	0.1, 0.2, 0.5, 2.0	—
Aerosil 300 silica (w w^{-1})	0.1, 0.2, 0.5, 2.0	0.1, 0.5, 2.0
N-MBA (w w^{-1})	0.5	0.5
APS (w w^{-1})	1.0	1.0
TEMED (cm^3)	0.2	0.2
Horizontal mixing (rpm)	600	600
Vertical mixing (rpm)	100	100

oven (Hotpack, USA) for 24 h to a constant weight, and then milled. The obtained copolymer powders were then investigated for their water absorbency capacity. The monomer AM: IA molar ratio from which the synthesized P(AM-IA) copolymer possessed the highest water absorbency was then selected to prepare the P(AM-IA)/silica SAPC.

To prepare the SAPCs, three types of silica, namely Aerosil 90, Aerosil 200, and Aerosil 300, each at four different concentrations of 0.1, 0.2, 0.5, and 2% w w^{-1}, were added in situ with the other ingredients in the polymerization process as shown in Table 2.

Characterization of the Copolymers

Identification of the Functional Groups of the Synthesized Copolymers. The functional groups of the copolymers were investigated by Fourier transform infrared spectroscopy (FTIR model Nicolet Impact 410) using a KBr pellet method with 32 scans and 4 cm^{-1} resolution. The interface software (Nicolet Omnic) was connected to the Nicolet FTIR in a data acquisition system.

Surface Morphology of the Synthesized Copolymers. The surface morphology of the copolymers was investigated using scanning electron microscopy (SEM, model JSM-6400, Japan) without cross-sectioning. The thickness of gold coated on the copolymer was 25 nm, and SEM was operated with a 15 kV accelerating voltage. The elemental analyses of the SEM micrographs were investigated by energy dispersive X-ray spectrometry (EDXS).

Equilibrium Water Absorbency

In deionized Water. Deionized water (150 g) was added to 0.1 g of the dry copolymer (*A*) in a 250 cm^3 glass beaker covered with a lid and it was allowed to swell for 30 min. The completely swollen copolymer gel was filtered through 100-mesh aluminum sieve screen for 3 h and the remaining swollen copolymer gel was weighed (*B*). The water absorbency (g g^{-1} of the dry copolymer) was calculated by *Eq. 1* shown below:

$$\text{Water absorbency of copolymer}\,(\text{g g}^{-1}) = (B - A)/A \quad (1)$$

Absorbency Under Load (AUL). Deionized water (25 cm^3) was placed in a Petri dish. A 0.16 g (*A*) aliquot of the dry copolymer was carefully scattered onto the filter screen of the test device (a flexiglass cylinder of 26 mm diameter, 35 mm height, and a 100 mesh stainless steel cloth in the bottom). A piston assembly, including an additional weight to achieve a load of 0.28 psi (1.93×10^3 Pa) was placed on the top of the dry copolymer. After weighing the assembly device (*B*), it was placed on the Petri dish, and absorbency was allowed to proceed for 1 h after which time the entire device was reweighed (*C*). Similar experiments were carried out for a load of 0.70 psi (4.83×10^3 Pa). The AUL (g g^{-1}) was calculated by *Eq. 2*:

$$\text{AUL}(\text{g g}^{-1}) = (C - B)/A \quad (2)$$

Swelling Kinetics of the SAPs and SAPCs. Deionized water of 1000 cm^3 was placed in a 2-dm^3 beaker. The dry copolymer of 0.1 g was sealed in a teabag and placed in a beaker where it was allowed to swell for 15 min. The soaked teabag was removed from the beaker and the swollen copolymer was weighed after excess water on the bag was blotted out on filter paper. Similar experiments were carried out but for gel swelling times of 15, 45, 105, 225, 1125, and 1605 min. Schott's equation [39], as shown in *Eq. 3*, is used to describe a well-known pseudo second-order absorbency kinetics equation and was used in these studies to test for pseudo second-order absorbency kinetics of water absorbency by the SAPs and SAPCs. Since:

$$t/Q_t = t/Q_\infty + 1/kQ_\infty^2, \quad (3)$$

where Q_t and Q_∞ are the absorbencies at time t and infinite time for full swelling and k is the absorbency coefficient which describes the rate constant of swelling, then by plotting t/Q_t vs. t, Q_∞ and k can be calculated.

The Level of Retained Silica in the P(AM-IA) Gel. A 1.00 g (*A*) aliquot of the dry copolymer was placed in a 100 cm^3 porcelain crucible on a hot plate and heated at 100°C for 45 min before being placed in a muffle furnace (Vulcan 3-550 PD) at 600°C for 90 min until all the powder became white. The crucible was removed from the furnace and cool. The white powder was weighed (*B*), and the amount of retained silica in the gel was calculated by *Eq. 4*:

$$\text{Silica retained in the gel} = (B - A)/A \quad (4)$$

 DOI 10.1002/pen

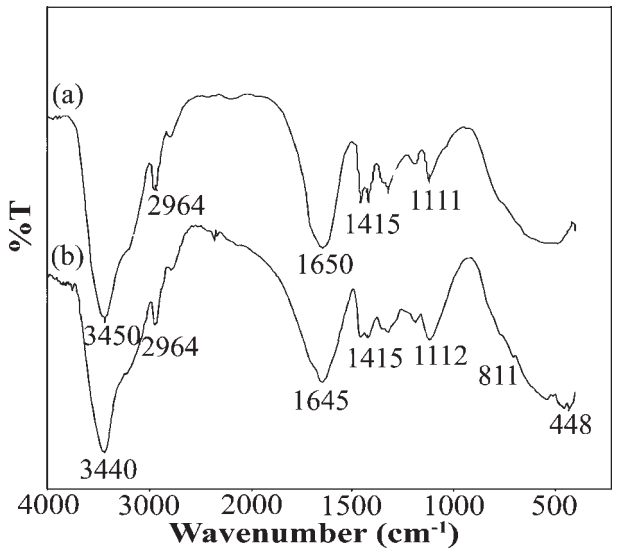

FIG. 2. IR spectra of (a) P(AM), and (b) P(AM)/Aerosil 90 silica composite.

SAPCs by Mechanical Mixing. A 0.2 g aliquot of the dried P(AM-IA) copolymer powder having a mesh size of not larger than 100 and the specified amount of silica were mixed in the bottle by a home-made mixing rotator with a controllable speed at 600 rpm for 30 min for horizontal mixing (HM). For the vertical mixing (VM), the mixture was shaken with a speed of 100 rpm in a rolling type mixer (MS1 Minishaker, IKA-Work, Inc, Wilmington). After mixing (either HM or VM), the sample was transferred for the water absorbency experiment. The types of silica and copolymer used for the mixing are shown in Table 2.

RESULTS AND DISCUSSION

The assignments of the FTIR spectra of the three silicas are shown in Fig. 1. All three types of silica (Aerosil 90, Aerosil 200, and Aerosil 300) gave the similar IR peaks with a medium OH stretching peak at 3444–3441 cm^{-1}, a weak C=O stretching peak at 1630 cm^{-1}, a strong peak at 1112–1103 cm^{-1} for Si—O—Si bending, a medium peak at 811–810 cm^{-1} for Si—OH and a sharp peak at 474–470 cm^{-1} for Si—O—Si bending. Table 1 shows that their BET surface areas and average primary particle sizes are significantly different.

The peaks of P(AM) (Fig. 2a), P(AM)/Aerosil 90 silica SAPC (Fig. 2b, P(AM-IA) (Fig. 3a) and P(AM-IA)/Aerosil 90 silica SAPC (Fig. 3b) indicated that silica was attached onto both the AM and IA moieties via covalent bonding. All copolymers showed the strong peak at 3450–3440 cm^{-1} for the N—H stretching overlapping with the OH— stretching, the medium peak at 2939–2936 cm^{-1} for the C—H stretching, the medium peak at about 1650 cm^{-1} of the C=O stretching for amide I, the peak at 1415–1452 cm^{-1} for the C—H bending of amide, and the medium peak at 1112–1120 cm^{-1} for the N—H (amide II) bending. Besides the aforementioned peaks, the Si—O—Si sharp peak of Aerosil 90 silica at 470 cm^{-1} was shifted to 448 cm^{-1} in the P(AM)/Aerosil 90 silica (Fig. 2b) and to 447 cm^{-1} in the P(AM-IA)/Aerosil 90 silica SAPCs (Fig. 3b). Other SAPCs with either Aerosil 200 or Aerosil 300 silica addition demonstrated the similar spectra (not shown here) as the Aerosil 90 silica-copolymer composites.

The existence of silica particles in the SAPCs was confirmed by SEM micrographs (see Fig. 4). PAM and P(AM-IA) copolymers have a rough morphology (Fig. 4a and b), while the micrograph of P(AM-IA)/Aerosil 90 silica composite shows a similar morphology but with large agglomerates of white particles of silica trapped on the rough surface of polymer matrix (Fig. 4c). EDXS analysis of P(AM-IA) and P(AM-IA)/Aerosil 90 silica composite (Fig. 4d and e) indicates that besides common elements such as carbon and oxygen found in both copolymers, the presence of silicon element was also detected in the prepared copolymer composite at the energy peak at 1.75 keV. Therefore, data from SEM-EDXS confirmed that the silica particles were retained within the SAPCs.

Effect of Itaconic Acid Concentration

The Water Absorbency of the Synthesized Copolymer. The water absorbency of the copolymers synthesized in situ by solution polymerization with three concentrations (0, 1, 2, and 3% molar ratio) of IA is shown in Table 3. Because the reactivity ratios r_1 and r_2 values for AM/*N*-MBA are 0.64 and 1.77, respectively, the PAM was thus rigid due to more effective crosslinking density to cause the low water absorbency [40]. The effective

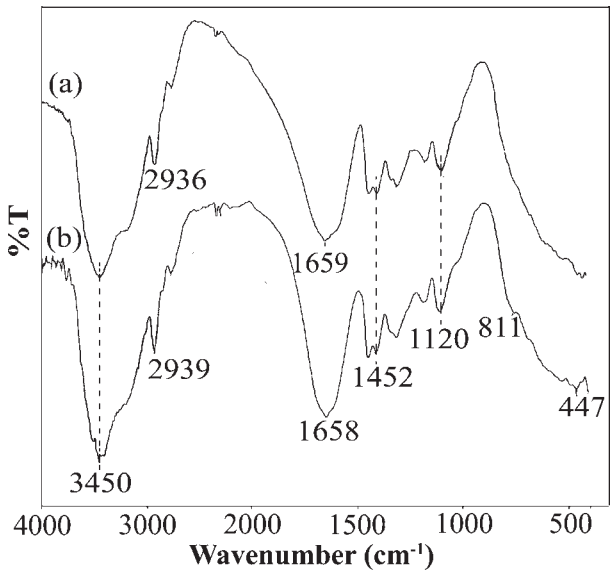

FIG. 3. IR spectra of (a) P(AM-IA), and (b) P(AM-IA)/Aerosil 90 silica composite.

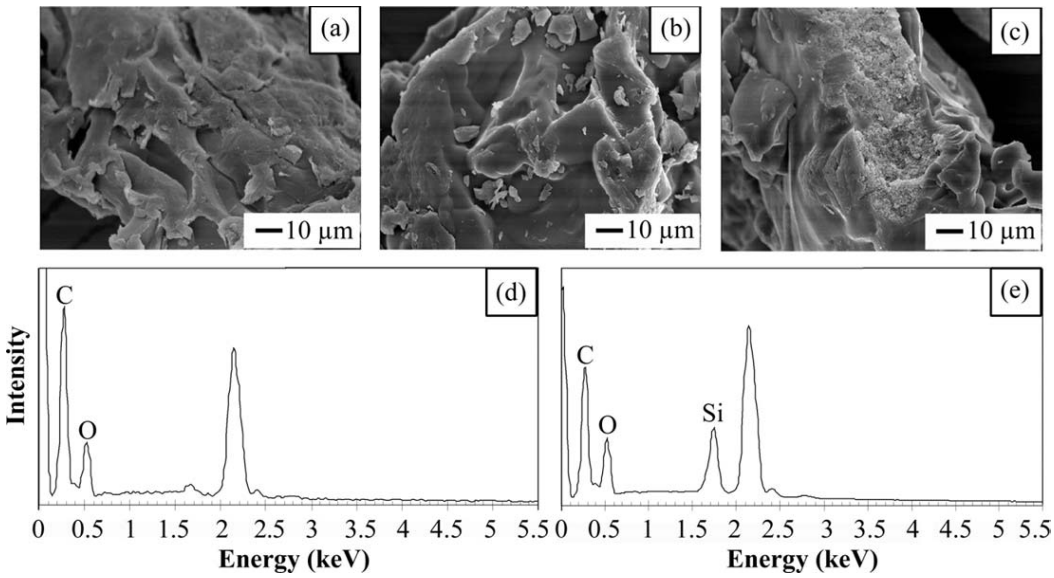

FIG. 4. SEM micrographs of (a) P(AM), (b) P(AM-IA), and (c) P(AM-IA)/Aerosil 90 silica composite; and EDXS spectra of (d) P(AM-IA) and (e) P(AM-IA)/Aerosil 90 silica composite.

crosslinking density is defined as the number of moles of elastically effective crosslinks per unit volume of polymer. Therefore, an increase of hydrophilic monomer (IA) in the SAPs enhances the swelling capability and, hence, decreases the effective crosslinking density. This statement has been investigated by several researches. Our previous investigation, for example, found that SAPs with high water absorbency were accompanied by low gel strength and the calculated low value of effective crosslinking density [41]. The water absorbency increases with increasing concentrations of the hydrophilic and ionic functional groups of IA, in good agreement with the previous findings by Uyanik and Erbil [42] and Pulat and Eksi [43], who reported that increasing IA concentrations in copolymer structures decreases the effective crosslinking densities of the polymer networks. As IA cannot form superabsorbent polymers by itself, an excessive amount of IA in the monomer mixture made it more difficult to form a copolymer gel. Thus, here we could show the results of IA concentrations up to only 3% (molar ratio). The degree of swelling of the synthesized P(AM-IA) copolymers mainly depends on the repulsive forces between the hydrophilic pendants (amide and carboxylic groups) in their structures. For AM/IA copolymer, IA was reported to be more reactive than AM ($r_{IA} > r_{AM}$) [42]. Therefore, IA molecules are used up via a crosslinking reaction with *N*-MBA before AM monomer, even if AM feed concentrations are higher. In the present case, the structure of the copolymer should contain more units of the uncrosslinked PAM moiety than crosslinked IA units owing to a higher AM concentration and higher reactivity of *N*-MBA. The synthesized copolymer must have an optimum ratio of AM-to-IA to balance hydrophilic or ionic functional groups and chain flexibility to produce the copolymer with the highest water absorbency capacity. The copolymer synthesized by an AM: IA molar ratio of 97:3 can absorb deionized water to as high as 233 ± 8 g g^{-1} (Table 3). However, the AUL values were nearly constant at 11–12 g g^{-1} and 12–14 g g^{-1} for a load of 0.28 psi (1.93×10^3 Pa) and 0.70 psi (4.83×10^3 Pa), respectively, regardless of the IA concentration. Thus, the AUL was essentially constant regardless of the loads and the concentration of the hydrophilic or ionic functional groups and chain flexibility.

The AUL is a measure of the ability of an SAP to absorb a liquid while the SAP is under an application of load or restraining force. The value of AUL is altered proportionally to the strength of the swollen gel, thus, AUL is often reported in the technical data sheets and patent articles in order to quantify the gel strength suitable for a particular application such as diapers for baby and adult [44, 45].

In free swelling (without an application of external load), the presence of ionic charges along polymer chains significantly increases the swelling of SAPs due to an increase in electrostatic repulsive forces between charged

TABLE 3. Effect of itaconic acid concentration (molar ratio) on the water absorbency of the P(AM-IA) SAP.

Itaconic acid concentration (% molar ratio)	Water absorbency under load (AUL [Pa]) of		
	0	1.93×10^3	4.83×10^3
0	51 ± 2	14	12
1	157 ± 9	14	12
2	191 ± 6	13	11
3	233 ± 8	12	11

APS, 1.0% w w^{-1}; *N*-MBA, 0.5% w w^{-1}; at 45°C, 250 rpm, 30 min.

 DOI 10.1002/pen

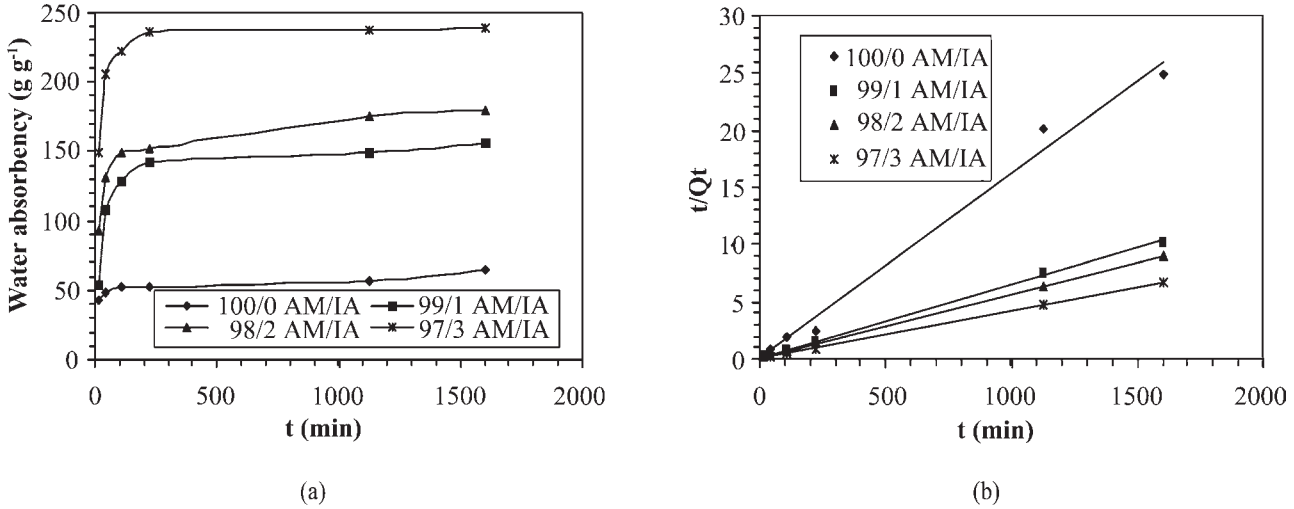

FIG. 5. Effect of the itaconic acid concentration (molar ratio) on the swelling kinetics of: (a) water absorbency vs. absorption time, (b) t/Q_t vs. absorption time (the linear regression equations and correlation coefficients were given in Table 4).

sites on the carboxylate anions (in case of IA) upon their complete dissociation and thus leads to a more extended configuration, as seen in Table 3 that the copolymer system of 3% mole of IA yielded the water absorbency of around 233 g g^{-1}, while the water absorbency of the P(AM) SAP was about 51 g g^{-1}.

However, under an application of load, the swelling ability of SAP is decreased with respect to the load-free absorbency (see Table 3) as a result of the restricted mobility of polymer chain. Therefore, the diffusion of a liquid into the SAP particle is counterbalanced by the external pressure applied on the SAP particles. As a result, our data imply that the extended conformations of the main chain, especially in SAP containing ionic charges, are prohibited under an application of load. Therefore, the observed AUL value was insignificantly altered irrespective of the applied loads and the concentration of ionic groups within the SAP.

The Swelling Kinetics of the Synthesized Copolymers. In practical applications, not only is a higher absorbency capacity required for the absorbent, but also a high swelling rate. The swelling kinetics of hydrogels have been characterized as occurring in two stages; an initial first order (Fickian diffusion model) stage followed by a later second order (Schott model) stage. In the initial stage, the swelling of hydrogel in water is governed by a first order diffusion process which involves migration of water to fill the spaces between polymer chains. The Fick model is thus valid for the initial swell stage where the fractional swelling value (Q_t/Q_∞) is less than or equal to 0.6 [46]. The Schott model is used for longer swelling times when the density of the hydrogel has increased. At this second order swelling, the swelling kinetic is not controlled by diffusion, but by the relaxation of the polymer chains [39, 47]. The evaluated swelling kinetics of the P(AM-IA) copolymer, synthesized by in situ solution polymerization of various concentrations (0, 1, 2, and 3% molar ratios) of IA revealed that the higher the IA concentration, the larger the water absorbency became (Fig. 5a). In other words, the P(AM) SAP gave the lowest water absorbency and the 97:3 (molar ratio) P(AM-IA) SAP gave the highest water absorbency (233 ± 8 g g^{-1}) due to the hydrophilic nature of the carboxylic acid of the IA monomer. The 97:3 (molar ratio) P(AM-IA) SAP could absorb deionized water up to 149 ± 2 g g^{-1} of the dry copolymer within 15 min and reached the highest absorbency within 200 min. A plot of t/Q_t vs. t reveals that all the absorbency data almost perfectly fit in a linear line with small positive intercepts and high r^2 values, in support of pseudo-second order kinetics (Fig. 5b). The fitting equation and the r^2 value are reported in Table 4. Indeed, the experimentally determined water absorbency values fit the theoretically determined values from the

TABLE 4. Equilibrium water absorbency (Q_∞) and rate constant of swelling of P(AM-IA) SAPs prepared from various IA contents.

IA content (% molar)	Q_∞ (Schott model)	K (min^{-1})	Q_∞ (experimental)	Fitting second order kinetic equation	r^2
0	62	6.14e-3	51 ± 2	$y = 0.0161x + 0.0422$	0.9894
1	156	2.53e-4	157 ± 9	$y = 0.0064x + 0.162$	0.9996
2	182	2.27e-4	191 ± 6	$y = 0.0055x + 0.1333$	0.9997
3	238	5.44e-4	233 ± 8	$y = 0.0042x + 0.0324$	1

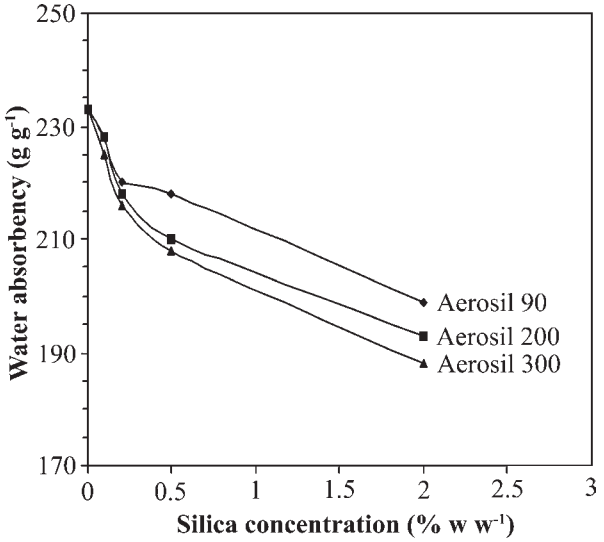

FIG. 6. Effect of silica concentration on water absorbency of SAPCs synthesized from 97:3% molar ratio of AM:IA.

Schott model (*Eq. 3*) supporting pseudo-second order kinetics for the swelling behavior of the P(AM-IA) SAPs (Table 4). In comparison to the P(AM) SAP, the presence of IA in the hydrogel lowered the swelling rate constant (k), although the k value at a 3% molar ratio of IA was higher than that for 1 and 2% IA but still less than that seen in the P(AM) SAP (Table 4). Likewise, the first order kinetics model also tested (not shown here) does not give a good straight line but gives low regression values.

Effect of Silica

Type and Concentration of Silica on the Water Absorbency of SAPCs. The incorporation of each type of silica (Aerosil 90, 200, and 300) into the 97:3 (molar ratio) P(AM-IA) copolymer to form P(AM-IA)/silica composites reduced the water absorbency of the SAPC in a dose dependent manner, reaching a level of some 15–20% lower at 2% w w^{-1} silica than that seen without silica, 0% (see Fig. 6). In addition, there was a dependency upon the type of silica, with the larger silica particles yielding a SAPC with lower water absorbency at the same nominal silica concentration. For example, compared to that at 0% silica, the water absorbency was decreased from 233 ± 8 g g^{-1} to 199 ± 4, 193 ± 6, and 188 ± 1 g g^{-1}, a reduction of 15, 17, and 20%, with the incorporation of Aerosil 90, Aerosil 200, and Aerosil 300 at 2% w w^{-1}, respectively. This is to be expected since water absorbency is related to the higher hydrophilic properties of the hydrophilic chain and the silica particle size, as shown in Table 1, the BET surface areas of the three silicas differ significantly. As to the dose-dependent effect, the silica particles present in SAPs act as crosslinking points [5], and so more crosslinking points are available with the increased addition of SiO_2 in addition to the *N*-MBA crosslinking agent. Although more hydrogen bonding takes place between the hydrophilic silanol group on the silica, water absorbency through this bonding may increase the rigidity of the chain. Since the surface physical–chemical properties are the same, and so do not differentially affect the water absorbency of the SAPCs, their surface areas and average primary particle size are, therefore, the important attributes controlling the extent of water absorbency.

Type of Silica and Silica Content on the Swelling Kinetics. The swelling kinetics of the SAPCs, synthesized from a 97:3 molar ratio of AM:IA with in situ incorporation of 2.0% w w^{-1} of silica were essentially the same for all three types of silica (Fig. 7a) and showed pseudo second-order absorbency kinetics regardless of the

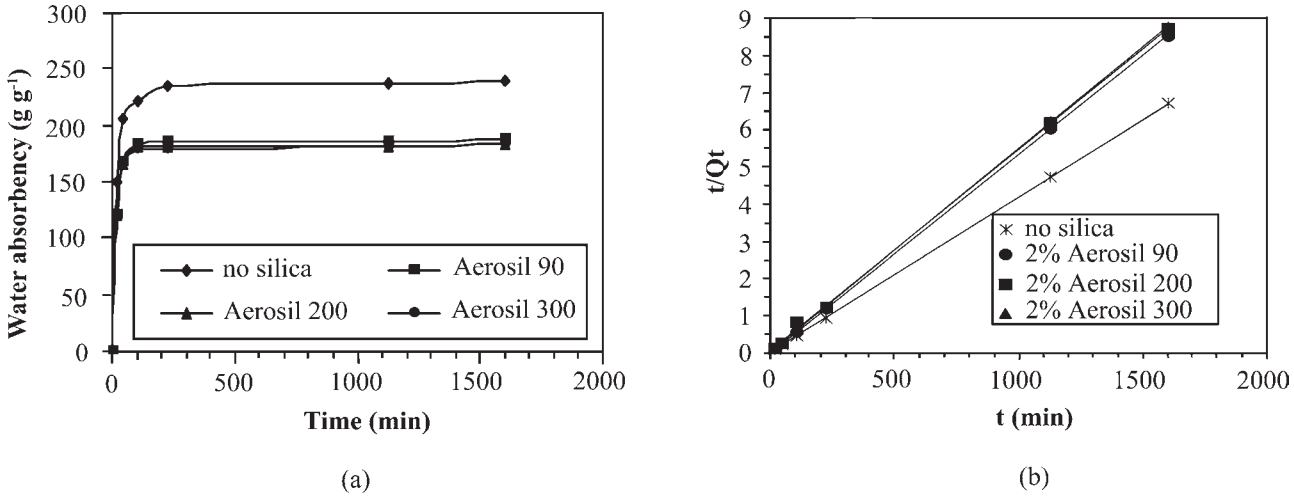

FIG. 7. Effect of the type of silica on the swelling kinetics of a P(AM-IA)/2% w w^{-1} silica composite (97:3 molar ratio of AM: IA) showing the (a) water absorbency vs. absorption time, and (b) t/Q_t vs. absorption time (the linear regression equations and correlation coefficients were given in Table 5).

 DOI 10.1002/pen

TABLE 5. Equilibrium water absorbency (Q_∞) and rate constant of swelling (k): of SAPCs prepared from P(AM-IA)/2% w w w[1]silica (97:3 molar ratio of AM: IA), with the indicated different types of silica particles.

System	Q_∞ (Schott model)	k (min^{-1})	Q_∞ (experimental)	Fitting second order kinetic equation	r^2
No silica	238	5.44e-4	233 ± 8	$y = 0.0042x + 0.0324$	1
Aerosil 90	189	9.03e-4	188 ± 6	$y = 0.0053x + 0.0311$	1
Aerosil 200	185	3.14e-4	184 ± 2	$y = 0.0054x + 0.0928$	0.9994
Aerosil 300	182	6.53e-4	183 ± 4	$y = 0.0055x + 0.0463$	1

presence of silica and its concentration (Fig. 7b). The high quality of linear curve fitting is represented by the value of r^2 equal to 1 (Table 5). Again the experimental water absorbency values were very close to those derived theoretically from the Schott model of pseudo second-order kinetics (Table 5). In the presence of 2.0% w w^{-1} silica, the resulting 97:3 molar ratio P(AM-IA)/silica SAPC could absorb water at the very similar values of 121 ± 8, 119 ± 8, and 118 ± 8 g g^{-1} of the dry polymer within 15 min for Aerosil 90, Aerosil 200, and Aerosil 300, respectively. The dependence of swelling time on the equilibrium swelling rate arises because the mass of liquid absorbed during the swelling, so that the rate increases until constant at the absorbency time longer than 300 min. The water swelling rate depends on the equilibrium swelling capacity of the polymer. The swelling absorbency values of the 97:3 P(AM-IA)/silica SAPCs with Aerosil 90, Aerosil 200, and Aerosil 300 are not much different to each other but decreased with increasing concentrations of silica (Table 6). As mentioned before, the fine silica particles act as additional crosslinking junctions and so the crosslink density increased with increasing silica levels, leading to a decreased swelling.

The swelling kinetics of the P(AM-IA)/silica SAPCs, synthesized from a 97:3 molar ratio of AM: IA with four contents of Aerosil 90, are shown in Fig. 8a, and replotted as t/Q_t vs. t in Fig. 8b. As mentioned earlier, all the t/Q_t vs. t plots are linear and fit well with the calculated values using the Schott's pseudo second-order absorbency kinetics model (Table 7). The incorporation of silica causes a dose-dependent decrease in the water absorbency, but the rate constant of swelling (k) was accelerated by increasing silica contents, due to the increasing level of crosslinking density within the SAPCs.

In view of the second-order absorbency kinetics observed in a later time course (Figs. 5, 7, and 8), one can describe the absorbency behavior as follows. When the P(AM-IA) SAP or P(AM-IA)/silica SAPC contacts with the excess amount of water, diffusion takes place which is governed by a first-order process on a short time scale (Fick model), and then subsequently the rate of swelling at long swelling times is not governed by the diffusion, but rather is mainly controlled by stress relaxation of the amorphous regions of the polymer network which follows a pseudo second-order kinetics control (Scott model).

The Effect of the Type of Silica and its Content on the Water AUL of the Synthesized Copolymers. The water AUL (1.93×10^3 Pa and 4.83×10^3 Pa) of the P(AM-IA)/silica SAPCs, synthesized from a 97:3 molar ratio of AM: IA in the presence of the three silica types (Aerosol 90, 200, and 300) and four contents (0.1, 0.2, 0.5, and 2% w w^{-1}) of silica is shown in Table 6. The AULs at 1.93×10^3 Pa and 4.83×10^3 Pa for the 97:3 P(AM-IA) SAP were very similar at 12 g g^{-1} and 11 g g^{-1}, respectively (Table 3), and were not significantly changed by the addition of silica, type or concentration, with all tested P(AM-IA)/silica SAPCs having an AUL of 11–13 g g^{-1} at both evaluated loads.

In general, silica has been used to help improve the gel strength so as to provide a higher AUL to swollen gels with an otherwise reduced water absorbency. The swelling in the present work was observed to decrease slightly with increasing contents of silica in the P(AM-IA)/silica composite. The additional amounts of silica probably act as nonreactive filler dispersed in the network. It may be attributed to the fact that fine silica particles act as additional junctions. Therefore, silica imposes effects on gel strength or AUL improvement, in that the higher the silica concentration, the higher the gel strength becomes.

TABLE 6. Effect of silica types and concentrations on the water absorbency of SAPCs (97:3 molar ratio of AM:IA).

Concentration of silica (% w w^{-1})	Water absorbency (g g^{-1}) under loads (Pa) of								
	0			1.93×10^3			4.83×10^3		
	Aerosil 90	Aerosil 200	Aerosil 300	Aerosil 90	Aerosil 200	Aerosil 300	Aerosil 90	Aerosil 200	Aerosil 300
0.1	228 ± 1	228 ± 7	225 ± 2	12	12	12	11	11	11
0.2	220 ± 1	218 ± 2	216 ± 3	12	12	13	11	11	12
0.5	218 ± 1	210 ± 5	208 ± 5	13	13	13	12	12	12
2.0	199 ± 4	193 ± 6	188 ± 1	13	13	13	12	12	12

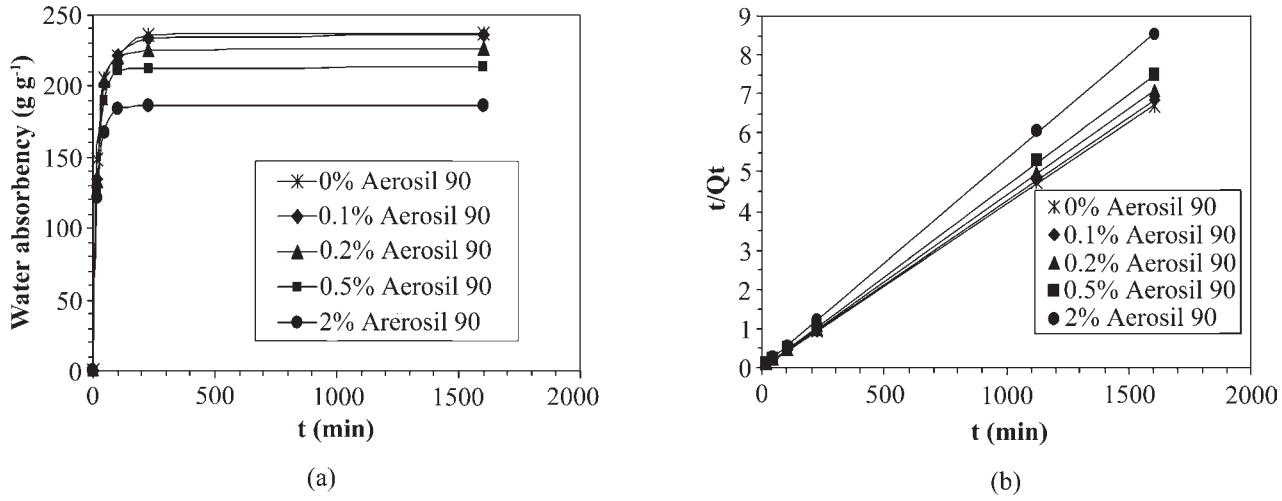

FIG. 8. Effect of silica concentration on the (a) water absorbency vs. absorption time and (b) t/Q_t vs. absorption time for a P(AM-IA)/Aerosil 90 silica composite (97:3 molar ratio of AM: IA) (the linear regression equations and correlation coefficients were given in Table 7).

Besides the crosslinking reaction, these characteristics may be attributed to the fact that the fine silica particles act as additional junctions for grafting reaction on their surface to increase the SAPC density. Increasing silica contents led to increased gel strength, although the water absorbency value of the SAPCs with different silica types (particle sizes) is not different at all. Increasing the water absorbency was achieved by a lower crosslinking reaction, AUL decreased because the swollen particles easily deformed and clumped together under load, liquid supplying voids or spaces were closed. If this is the case, then to increase the AUL, a second polymerization on the surface with a small amount of additional crosslinking density may be needed.

The Retained Silica in the Gel

The actual amount of silica that is incorporated into the 97:3 P(AM-IA)/silica SAPC was evaluated by the difference in silica contents between those in the initial prepolymerization and the final products after the polymerization (Table 8). The amounts of silica retained in the SAPCs are lower than the added amounts of silica added, i.e., the whole amount of silica is not incorporated into the polymer network, but rather only some 86–95% is retained. This is not linearly dependent upon the silica content in the polymerization reaction and, although their average primary particle sizes are significantly different, the interaction between SAPCs and the three different silica types cannot be differentiated. The retention of silica within the SAPCs is in agreement with the IR spectra (see Fig. 3) and the SEM-EDXS data (see Fig. 4).

Effect of Mechanical Mixing on Water Absorbency of SAPCs

Since it is possible to mix or blend the SAP with the silica particles as an organic and inorganic composite, it is of interest if the resulting composite will perform similarly to the in situ polymerized SAPCs. That is, the performance of the silica-filled SAPC can match that the in situ silica SAPC arises because the silica can leak out from the composite. Then, its strength might be somewhat lower compared to the in situ polymerized SAPCs.

Effect of the Mixing Method

The VM motion uses an eccentric motion in the vertical direction with a constant speed of 100 rpm while the

TABLE 7. Equilibrium water absorbency (Q_∞) and rate constant of swelling (k): of SAPCs prepared from P(AM-IA)/Aerosil 90 silica (97:3 molar ratio of AM: IA) with the incorporation of the indicated final Aerosil 90 concentration.

Aerosil 90 (w w^{-1})	Q_∞ (Schott model)	k (min^{-1})	Q_∞ (experimental)	Fitting second order kinetic equation	R^2
0	238	5.44e-4	233 ± 8	$y = 0.0042x + 0.0324$	1
0.1	238	5.78e-4	235 ± 6	$y = 0.0042x + 0.0305$	1
0.2	227	7.53e-4	227 ± 1	$y = 0.0044x + 0.0257$	1
0.5	213	8.09e-4	214 ± 6	$y = 0.0047x + 0.0273$	1
2	189	9.39e-4	188 ± 6	$y = 0.0053x + 0.0299$	1

 DOI 10.1002/pen

TABLE 8. The silica retained in the gel at various silica concentrations.

Type of Aerosil	Silica concentration added in polymerization (% w w^{-1})	Silica concentration after sintering (% w w^{-1})	Silica concentration retained in the gel (% w w^{-1})
Aerosil 90	0.1	0.09	90
	0.2	0.19	95
	0.5	0.44	88
	2.0	1.79	90
Aerosil 200	2.0	1.85	93
Aerosil 300	2.0	1.71	86

HM method uses a constant rotation speed of 600 rpm in the horizontal direction. To this are added the SAP particles with silica powder, and dispersion of the components in the cylindrical bottle is accomplished by rotating the bottle and its contents about the horizontal axis of the cylindrical bottle at a rate sufficient to lift the silica particles to one side and then cause them to roll, slide and tumble or cascade to the lower side. At this speed, the rotation movement is the cascade manner. When the HM rotation of SAP and silica particles in the cylindrical bottle takes place, some parts of the particles contact with the cylindrical wall in the diameter direction of the roller movement, contact sites of the SAPs for silica particles decrease when the movement of the cylindrical bottle is continued. In the VM motion, both the SAPs and silica particles move up and down along the length of the cylindrical bottle. Therefore, the contact sites of the SAPs and silica particles in the VM direction are higher than the HM motion leading to the larger probability of silica particles in adhering to the SAP surface. The adsorption of silica is strengthened by hydrogen bonding between hydroxyl groups on silica surface and carboxylic and amine groups on P(AM-IA) SAP. Based on the mixing mechanism and speed, the Aerosil 300 having larger surface area (BET surface area of 300 ± 30 m^2 g^{-1} and 7 nm particle size) adsorbed on SAP particles more than the Aerosil 90 silica did (BET surface area of 90 ± 15 m^2 g^{-1} and 20 nm particle size). As a result Aerosil 300-SAPC should provide the lower water absorbency since the adsorbed silica might interrupt the diffusion or the binding of water into the SAP particle. However, the results in Table 9 indicated that both the mixing direction and types of the investigated silica particles did not significantly alter the water absorbency of the SAPC comparative to the in situ SAPC polymerization.

When the mixture of SAPs and silica particles is mixed by an eccentric rotation (VM), they move up and down along the length of the cylindrical bottle. Therefore, the mixing force is controlled by a centrifugal acceleration, α, as shown in *Eq. 5* [48, 49]:

$$\alpha = (r_b + r_e)\omega^2 \tag{5}$$

where r_b is the radius of the glass bottle, r_e is the eccentric radius, and ω is the rotation angular velocity. According to the theory of the elasticity contact between spheres [48], the contact area S increases as indicated in *Eq. 6:*

$$S\alpha F^{2/3} \tag{6}$$

where F is the force worked on the spheres. The Aerosil 300 silica has a stronger force to hold silica particles on the surface of the SAP due to its larger surface area and smaller size. Thus, the SAPs and Aerosil 300 can physically interact, aggregate, or agglomerate together more strongly than those of Aerosil 90.

It is necessary to mention that SAPs at various AM:IA ratios without silica were also mixed horizontally or vertically as for a control purpose at the same condition for the SAPCs. The mixing force given to SAPs actually helps only disperse the particle agglomeration and imposes a slight effect on water absorbency as shown in Table 9. Regardless of the dependence of the mixing time on the SAPs-silica contact, the HM rotation rate is higher than the VM rotation and, therefore, the force between the SAP and silica particles by HM rotation increases rapidly. The mixing force between the SAP and silica particles can be divided into three regions: elastic, plastic and destructive. In the low mixing force region, the con-

TABLE 9. Mechanical mixing of the superabsorbent copolymer with silica by horizontal mixing or vertical mixing.

Silica surface area (m^2 g^{-1})	Silica content (% w)	Water absorbency (g g^{-1}) of SAPCs from AM/IA (mol %)											
		100/0			99/1			98/2			97/3		
		In situ	VM	HM	In situ	VM	HM	In situ	VM	HM	In situ	VM	HM
90	0	51 ± 2	35 ± 1	35 ± 1	157 ± 9	144 ± 8	144 ± 8	191 ± 6	201 ± 5	201 ± 5	233 ± 8	225 ± 4	225 ± 4
	0.1	—	36 ± 2	19 ± 2	—	177 ± 7	182 ± 41	—	178 ± 9	174 ± 9	228 ± 1	239 ± 29	228 ± 17
	0.5	—	37 ± 5	20 ± 3	—	165 ± 2	183 ± 24	—	155 ± 7	176 ± 11	218 ± 1	250 ± 13	340 ± 63
	2.0	—	34 ± 0	21 ± 3	—	189 ± 35	136 ± 19	—	165 ± 19	164 ± 6	199 ± 4	225 ± 22	228 ± 8
300	0	51 ± 2	35 ± 1	35 ± 1	157 ± 9	144 ± 8	144 ± 8	191 ± 6	201 ± 5	201 ± 5	233 ± 8	225 ± 4	225 ± 4
	0.1	—	41 ± 2	37 ± 1	—	147 ± 19	151 ± 6	—	191 ± 6	213 ± 51	225 ± 2	166 ± 5	220 ± 48
	0.5	—	40 ± 1	40 ± 1	—	143 ± 8	132 ± 12	—	198 ± 14	208 ± 5	208 ± 2	209 ± 23	195 ± 23
	2.0	—	40 ± 2	42 ± 2	—	141 ± 19	135 ± 3	—	193 ± 6	205 ± 2	188 ± 1	201 ± 3	212 ± 5

0.2 g sample, mixing time = 30 min, vertical mixing (VM) at 100 rpm and horizontal mixing (HM) at 600 rpm, "—" for do not measure.

tact between SAPs and silica particles is supposed to be elastic, in good approximation, and after the mixing, the shapes of SAPs and silica do not change. Over the elastic force range, some plastic region can be observed, and if the force becomes greater than plastic region, SAP destruction may arise.

The results in Table 9 indicate that all the SAPs having various silica types and contents mixed under VM or HM motions are linear and it can be concluded that their mixing forces are elastic because the water absorbency values are in a linear trend. The extent of water absorbency of the in situ SAPCs containing a 97:3 molar AM: IA ratio with various silica contents used in comparison with the mechanical mixing SAPCs at the same monomer ratio are similar with only a small deviation in most cases.

The Role of Silica in SAPCs

The preparation of SAPs needs to have a crosslinking agent to control the gel properties. However, when a crosslinking agent, such as *N*-MBA, is used, the water absorbency decreased. To control the desirable level of water absorbency through the chemical crosslinking reaction, a well-designed recipe and reaction condition must be strictly controlled. Inorganic particulate filler with a hydrophilic surface, such as silica, is normally recommended for incorporation during the polymerization of SAPs as another crosslinking site or grafting site for the in situ prepared SAPCs or mechanical mixing of SAPs and silica to give SAPCs. As shown above, the silica particles can be embedded in the polymer to give a better overall strength. Moreover, the presence of silica in the SAPCs reduces the load-free water absorbency very slightly. Data from the water AUL, however, were not significantly different between the SAP and SAPCs due to the aforementioned discussion. When the SAPCs are assembled as a baby diaper or famine napkins, the absorbed fluid is still held within the superabsorbent network and silica also helps the polymer to flow easily from the sack and can improve fluid permeability of the hydrated SAPs. In this work, we tuned the combination between the chemical crosslinking reaction by *N*-MBA and the minimum silica incorporation to obtain the desirable water absorbency behavior.

CONCLUSIONS

The P(AM-IA) SAPs prepared by in situ solution polymerization produced a high level of water absorbency and a much lower AUL water absorbency. Increasing the IA concentration in the SAPs significantly increased the water absorbency. In situ polymerized SAPCs containing various molar ratios of AM: IA and incorporating three types of silica particles at various contents were synthesized. The water absorbency of SAPCs was lower than those of SAPs, the extent of which depended on the amount of silica incorporated. However, the AUL of SAPs and SAPCs at a 97:3 molar ratio of AM: IA was almost unchanged regardless of the type and amount of silica added. The amounts of silica retained in the SAPCs of the three silica types and contents were in the range of 88–95% by weight. Water absorbency kinetics of the P(AM-IA) SAPs or the P(AM-IA)/silica SAPCs obeys Langmuir absorbency isotherm with a pseudo second-order absorbency phenomenon. Horizontal or vertical mixed SAPs with two types of silica at 0.1, 0.5, and 2% by weight did not give significant differences in water absorbency. In addition, the levels of water absorbency of the mechanically mixed SAPCs did not significantly vary from the levels obtained from the in situ SAPCs. Therefore, the obtained results indicated that in order to prepare SAP with improved mechanical properties via the addition of silica particles, one could avoid the complicated in situ polymerization reaction in the presence of the silica particles by mechanical mixing the neat SAP with silica particles to obtain the associated SAPC.

ACKNOWLEDGMENTS

The authors thank Publication Counseling Unit (PCU) for the language check and some useful suggestion.

REFERENCES

1. F.L. Buchholz, "Preparation and Structure of Polyacrylate," in *Absorbent Polymer Technology*, L. Brannon-Peppas and R.S. Harland, Eds., Amsterdam, Elsevier Science, 23 (1990).
2. K. Kosemund, H. Schlatter, J.L. Ochsenhirt, E.L. Krause, D.S. Marsman, and G.N. Erasala, *Regul. Toxicol. Pharmacol.*, **53**(**2**), 81 (2008).
3. F. Masuda, "Trends in the Development of Superabsorbent Polymers for Diaper," in *Superabsorbent Polymers: Science and Technology*; ACS Symposium Series # 573, F.L. Buchholz and N.A. Peppas, Eds., The American Chemical Society, Washington, DC, 88 (1994).
4. R. Chandra and R. Rustgi, *Prog. Polym. Sci.*, **23**, 1273 (1998).
5. M.J. Ham and Y.H. Kim, *Polym. Eng. Sci.*, **48**, 2439 (2008).
6. S. Dalal, S. Raghava, and M.N. Gupta, *Biochem. Eng. J.*, **42**, 301 (2008).
7. R. Liang, M. Liu, and L. Wu, *React. Funct. Polym.*, **67**, 769 (2007).
8. R.E. Sojka, D.L. Bjorneberg, J.A. Entry, R.D. Lentz, and W.J. Orts, *Adv. Agronomy*, **92**, 75 (2007).
9. A. P. Nikolaos and R.K. Atul, *Adv. Drug Delivery Rev.*, **11**, 1 (1993).
10. M.H.A. Azadi and P. Rafiei, *Adv. Drug Delivery Rev.*, **60**, 1638 (2008).
11. A. Costantini, G. Luciani, B. Silvestri, F. Tescione, and F. Branda, *J. Biomed. Mater. Res. Part B: Appl. Biomater.*, **86B**(**1**), 98 (2007).
12. M. Kiremitci and H. Cukurova, *Polymer*, **33**, 3257 (1992).
13. E. Karadağ, D. Saraydin, Y. Caldiran, and O. Güven, *Polym. Adv. Tech.*, **11**, 59 (2000).

14. T. Masuda, "Absorptivity of Water (Moisture Absorptivity and Retention of Water)," in *Gels Handbook*, Y. Osada, K. Kajiwara, T. Fushimi, O. Irasa, Y. Hirokawa, T. Matsunaga, T. Shimomura, L. Wang, and H. Ishida, Eds., Academic Press, New York, 17 (2001).
15. T. Toyoda, "Water-Swelling Rubbers," in *Gels Handbook*, Y. Osada, K. Kajiwara, T. Fushimi, O. Irasa, Y. Hirokawa, T. Matsunaga, T. Shimomura, L. Wang, and H. Ishida, Eds., Academic Press, New York, 295 (2001).
16. Y. Osada, K. Kajiwara, T. Fushimi, O. Irasa, Y. Hirokawa, T. Matsunaga, T. Shimomura, L. Wang, and H. Ishida, "Artificial Snow," in *Gels Handbook*, Y. Osada, K. Kajiwara, T. Fushimi, O. Irasa, Y. Hirokawa, T. Matsunaga, T. Shimomura, L. Wang, and H. Ishida, Eds., Academic Press, New York, 491 (2001).
17. H.-W. Jacobi, T. Annor, and E. Quansah, *J. Photochem. Photobiol. A*, **179**, 330 (2006).
18. T. Shimura and T. Namba, "Preparation and Application of High-Performance Superabsobent Polymers," in *Superabsorbent Polymers: Science and Technology*; ACS Symposium Series # 573, F.L. Buchholz and N.A. Peppas, Eds., The American Chemical Society, Washington, DÇ112 (1994).
19. J.C.M. Bordado and J.F.P. Gomes, *Int. J. Environ. Stud.*, **64**(**2**), 243 (2007).
20. T.L. Staples, D.E. Henton, and F.L. Buchholz, "Chemistry of Superabsorbent Polyacrylates," in *Modern Superabsorbent Polymer Technology*, F.L. Buchholz and A.T. Graham, Eds., Wiley-VCH, New York, 55 (1998).
21. P. Li, N.H. Kim, D. Hui, K.Y. Rhee, and J.H. Lee, *Appl. Clay Sci.*, **46**, 414 (2009).
22. K. Haraguchi, *Curr. Opin. Solid State Mater. Sci.*, **11**, 47 (2007).
23. D. Foungfung, S. Phattanarudee, N. Seetapan, and S. Kiatkamjornwong, *Polym. Adv. Tech.* (2009), DOI: 10.1002/pat.1559.
24. M. Taniguchi, K. Kato, A. Shimauchi, X. Ping, K. Fujita, T. Tanaka, Y. Tarui, and E. Hirasawa, *J. Biosci. Bioeng.*, **99**(**2**), 130 (2005).
25. D. Depan, A.P. Kumar, and R.P. Singh, *Acta Biomater.*, **5**, 93 (2009).
26. A. Li and A. Wang, *Eur. Polym. J.*, **41**, 1630 (2005).
27. J. Zhang, H. Chen, and A. Wang, *Eur. Polym. J.*, **42**, 101 (2006).
28. J. Zhang, Q. Wang, and A. Wang, *Carbohydr. Polym.*, **68**, 367 (2007).
29. S. Sharma and S. Komarneni, *Appl. Clay Sci.*, **42**, 553 (2009).
30. X. Huang, S. Xu, M. Zhong, J. Wang, S. Feng, and R. Shi, *Appl. Clay Sci.*, **42**, 455 (2009).
31. J. Wu, J. Lin, M. Zhou, and C. Wei, *Macromol. Rapid Commun.*, **21**, 1032 (2000).
32. W. Wang and A. Wang., *Carbohydr. Polym.*, **77**(**4**), 891 (2009).
33. U.Y. Kim, "Recent Developments in High Water Absorbing Polymers and Applications", in *The Proceedings of the International Conference on Recent Developments in Petrochemical and Polymer Technologies*, 6–1, December 12–16, 1989, Chulalongkorn University Press, Bangkok, Thailand.
34. H.F. Mark, N.M. Bikales, C.G. Overberger, and G. Mengel, *Encyclopedia of Polymer Science and Engineering*, *2nd ed.*, Wiley, New York, *Vol. 7*, 783 (1989).
35. A. Pourjavadi, F. Seidi, and R. Soleyman, *J. Appl. Polym. Sci.*, **108**(**5**), 3281 (2008).
36. F.L. Buchholz, *J. Chem. Ed.*, **73**, 512 (1996).
37. B. Silvestri, G. Luciani, A. Costantini, F. Tescione, F. Branda, and A. Pezzella, *J. Biomed. Mater. Res. Part B: Appl. Biomater.*, **89**, 369 (2009).
38. X. Shi, S. Xu, J. Lin, S. Feng, and J. Wang, *Mater. Lett.*, **63**(**2**), 527 (2009).
39. H. Schott, *J. Macromol. Sci. Phys.*, **31**(**1**), 1 (1992).
40. J. Baselga, M.A. Llorente, J.L. Nieto, and I.F.P. Hernández-Fuentes, *Eur. Polym. J.* **24**, 161 (1988).
41. N. Seetapan, J. Wongsawaeng, and S. Kiatkamjornwong, *Polym. Adv. Tech.* (2010), DOI: 10.1002/pat.1658.
42. N. Uyanik and C. Erbil, *Eur. Polym. J.*, **36**, 2651 (2000).
43. M. Pulat and H. Eksi, *J. Appl. Polym. Sci.*, **102**, 5994 (2006).
44. M.J. Ramazani-Harandi, M.J. Zohuriaan-Mehr, A.A. Yousefi, A. Ershad-Langroudi, and K. Kabiri, *Polym. Test.*, **25**, 470 (2006).
45. J. Qin, U.S. Pat. 6,998,367 B2 (2006).
46. D. Saraydin and Y. Caldiran, *Polym. Bull.*, **46**(**1**), 91 (2001).
47. N. Martinez-Vázquez, R. del, C. Antonio-Cruz, A. Álvarez-Castillo, A.M. Mendoza-Martinez, and A.B. Morales-Cepeda, *Rev. Mex. Ingenieria Quim.*, **6**(**3**), 337 (2007).
48. W. Saelow, S. Kiatkamjornwong, T. Watanabe, and Y. Hoshino, *J. Imaging Soc. Jpn.*, **38**(**4**), 310 (1999).
49. C. Poomtien, S. Kiatkamjornwong, and Y. Hoshino, *Part. Sci. Technol.*, **16**(**4**), 295 (1999).

Carbohydrate Polymers 82 (2010) 1124–1135

Contents lists available at ScienceDirect

Carbohydrate Polymers

journal homepage: www.elsevier.com/locate/carbpol

Modified chitosan pretreatment of polyester fabric for printing by ink jet ink

Supaporn Noppakundilograt[a], Punthorn Buranagul[a], Wilaiporn Graisuwan[b], Chawan Koopipat[a], Suda Kiatkamjornwong[a,*]

[a] Department of Imaging and Printing Technology, Faculty of Science, Chulalongkorn University, Phyathai Road, Bangkok, 10330, Thailand
[b] Program of Petrochemistry, Faculty of Science, Chulalongkorn University, Phyathai Road, Bangkok, 10330, Thailand

ARTICLE INFO

Article history:
Received 24 April 2010
Received in revised form 14 June 2010
Accepted 22 June 2010
Available online 26 June 2010

Keywords:
Chitosan
Glycine
N-[(4-dimethyl aminobenzyl)imino] chitosan
N-[(2-hydroxy-3-trimethylammonium)propyl] chitosan chloride
Color properties
Outline sharpness
Stiffness

ABSTRACT

The present research deals with the use of pretreatment solutions of chitosan (CH), N-[(4-dimethyl aminobenzyl)imino] chitosan (DBIC), N-[(2-hydroxy-3-trimethylammonium)propyl] chitosan chloride (HTACC), glycine (Gly), and a mixture of CH and Gly, for padding polyester fabrics prior to printing with a set of seven-color pigmented water-based ink jet inks. After padding the fabrics with the above cationic pretreatments, they were printed with a piezo-electric drop-on-demand jet printer. CH, DBIC and HTACC were characterized by IR and NMR spectroscopy. The zeta potentials of the pretreatment solutions, the inks and the fabrics were measured. The *K*/*S* values, color gamut, tone reproduction, outline sharpness, and the surface appearance of the fabrics were characterized. Statistical evaluation of the significance of the results was performed. Among the pretreatments, the HTACC at 0.1% (w/v) yielded fabrics with the highest *K*/*S* values, widest color gamut and gamut volume, more color saturation with good tonal reproduction, and the sharpest and smoothest outline of printed character, and a smooth fabric surface with less stiffness. The proposed ionic interactions between the protonated amino groups of CH and the anionic portion of the encapsulated ink pigments, and van der Waals and hydrophobic interactions between the polyester and the pigments are likely reasons for these enhanced properties of the printed fabrics.

© 2010 Elsevier Ltd. All rights reserved.

1. Introduction

The pretreatment of fabrics with a suitable agent is a requirement in textile-ink jet printing because the deposited pretreatment chemical on the fabric surface limits excessive ink spreading and controls ink migration and penetration into the fabric fibers, and yet allows the ink to dry after the ink has been jetted (applied) onto the fabric surface. This interaction of the pretreatment agent and the jet ink results in an increase in color gamut, sharpness and other properties of the printed fabric (Hakeim, El-Gabry, & Abou-Okeil, 2008; Leelajariyakul, Noguchi, & Kiatkamjornwong, 2008; Phattanarudee, Chakvattanatham, & Kiatkamjornwong, 2009; Wang et al., 2007; Yuen, Ku, Kan, & Choi, 2007).

Polyester, one of the more popular textile fabrics, needs dyeing and printing to provide the color and pattern ranges required by customers and hence the higher add-on value. Although polyester fabric is hydrophobic, it has a negative zeta potential value (Espinosa-Jiménez, Padilla-Weigand, Ontiveros-Ortega, Ramos-Tejada, & Perea-Carpio, 2003). Thus, a prospective pretreatment agent with positive charges should be adsorbed onto the polyester fabric due to the requirement of an ionic interaction in enhancing the color and other properties (Samu, Moulee, & Kumar, 1999). Some types of cationic pretreatment agents have been reported to be able to increase the printed polyester color strength (*K*/*S*) by as much as 36% with ink jet printing when compared with the untreated polyester fabric (Wang et al., 2007).

Chitosan (CH) is widely used as a pretreatment reagent for synthetic polymers due to its green environmental advantages, easy to use and relatively low cost yet abundant supply. Indeed, CH has been extensively used for the dyeing and finishing of various textile fabrics, where the pretreatment of fabrics with CH produced a high color yield, good shrink resistance and provided some degree of antimicrobial activity (Abou-Okeil & Hakeim, 2005; Hakeim, Abou-Okeil, Abdou, & Waly, 2005; Julia, Pascual, & Erra, 2000). In textile-ink jet printing, CH has generally been used as a pretreatment agent for silk fabrics to expand the color gamut and to improve the crock fastness of the printed fabric (Chakvattanatham, Phattanarudee, & Kiatkamjornwong, 2010; Phattanarudee et al., 2009; Yuen, Ku, & Kan, 2008), whilst CH modified with dimethyl aminobenzaldehyde (DBIC) affected the color gamut of the printed polyester (Hakeim et al., 2008). CH is dissolved in acetic acid where upon its amino groups are protonated to form quaternary ammo-

* Corresponding author. Tel.: +66 2 218 5587; fax: +66 2 255 3021.
E-mail addresses: supaporn.n@chula.ac.th (S. Noppakundilograt), puntune@hotmail.com (P. Buranagul), porn_grai@yahoo.com (W. Graisuwan), chawan.k@chula.ac.th (C. Koopipat), ksuda@chula.ac.th (S. Kiatkamjornwong).

0144-8617/$ – see front matter © 2010 Elsevier Ltd. All rights reserved.
doi:10.1016/j.carbpol.2010.06.040

nium ions, which interact with anionic dyes through electrostatic attraction (Jocic et al., 2005). CH-padded fabrics result in a higher level of pigment adsorption onto the pretreated fabric surface compared to that of uncoated fabrics, and also gave a high color quality on the surface (Chakvattanatham et al., 2010; Phattanarudee et al., 2009).

Unfortunately, the retained acetic acid (from the CH) of the pretreated cotton fabric yields reduced color gamut, compared with the untreated one, and the acrid odor is retained in the printed fabrics after the post-treatment (Yuen et al., 2007), whilst CH also increases the stiffness of the fabrics (Phattanarudee et al., 2009). To solve these problems, the water-soluble CH derivatives with highly positive charges, O-acrylamidomethyl-N-[(2-hydroxy-3-trimethylammonium)propyl] chitosan chloride (NMA-HTACC) and N-[(2-hydroxy-3-trimethyl ammonium)propyl] chitosan chloride (HTACC), were synthesized (Kim, Lee, Lee, & Park, 2003; Lim & Hudson, 2004a, 2004b). Previously, the use of NMA-HTACC was reported to increase the color yield in the dyeing of cotton fabrics, whilst HTACC generated antimicrobial activity in the textile (Seong, Whang, & Ko, 2000).

The aim of this research was to modify CH to a cationic form with better solubility. To this end, CH with two different molecular weights and deacetylation degrees were modified to HTACC and DBIC, respectively, so as to improve the pretreatment properties of CH. Due to the solubility of CH in acid, the low average molecular weight CH was used for direct pretreatment and the synthesis of DBIC. The synthesized HTACC and DBIC were then used as pretreatment agents for polyester fabrics, color printed with an ink jet ink. The effects of fabric pretreatment with HTACC, DBIC, CH, Glycine (Gly) and a mixture of CH and Gly were investigated in depth for the color appearance yield in terms of color gamut and gamut volume, color strength and tone reproduction of the subsequently ink jet printed fabrics. In addition, the outline sharpness and evenness of density of the positive and negative characters of the printed polyester fabrics were also investigated along with the stiffness of the printed fabrics.

2. Experimental

2.1. Materials

A plain weave polyester fabric, constructed of 182 ends/in. (warp) × 87 picks/in. (weft) with a basic weight of 127 g m^{-2}, was used. Triton X-100, a non-ionic surfactant, was supplied by Merck (Frankfurt, Germany). CH flakes of 57,000 g/mol of average molecular weight and 85% deacetylation degrees (DD) was used for the synthesis of N-[(4-dimethyl aminobenzyl)imino] chitosan (DBIC) due to its lower water solubility while CH flakes of 100,000 g/mol of average molecular weight and 95% DD was used to synthesize N-[(2-hydroxy-3-trimethylammonium)propyl] chitosan chloride (HTACC) due to its higher water solubility. Both types of CH were purchased from Seafresh Industry Public Co., Ltd. (Bangkok, Thailand). Gly (98.5% pure) was purchased from Ajax Finechem (Seven Hills, NSW, Australia). N,N′-dimethyl aminobenzaldehyde was purchased from Asia Pacific Specialty Chemical Ltd. (Seven Hills, NSW, Australia). Glycidyl trimethylammonium chloride (GTMAC) was purchased from Sigma–Aldrich (St. Louis, MO). A commercial set of seven-color, pigmented water-based jet inks (Epson Ultrachrome^{TM} Ink), supplied from Seiko Epson Corporation (Suwa, Nagano, Japan), was used for printing the fabrics. Based on the manufacturer's claims, the pigment dispersions were treated by polymeric dispersant and polymer encapsulation to give an average particle size of the encapsulated pigment of approximately 100 nm.

2.2. Synthesis of the modified chitosans

2.2.1. N-[(4-dimethyl aminobenzyl)imino] chitosan (DBIC)

DBIC was prepared based on the method of Hakeim et al. (2008). CH (5 g, average molecular weight = 57,000 g/mol and 85% DD) and dimethyl aminobenzaldehyde (9.3 g) were mixed in 150 mL methanol for 10 h. The product was filtered through a 100-mesh aluminum screen sieve, washed with 300 ml of a 1:1 (v/v) ratio of mixed methanol–acetone solution and then dried overnight at room temperature. The intense yellowish dried product obtained was then characterized by IR spectroscopy (Spectrum One, PerkinElmer Life and Analytical Sciences Inc, MA). The synthetic route is shown in Scheme 1.

2.2.2. N-[(2-hydroxy-3-trimethylammonium)propyl] chitosan chloride (HTACC)

The synthesis of HTACC was modified from that of Seong et al. (2000). In brief, 0.50 g of CH (average molecular weight = 100,000 g/mol with DD = 95%) was dissolved in 25 cm^3 of 1% (v/v) aqueous acetic acid. Then 0.9 g of GTMAC was slowly added into the CH solution whilst maintaining the reaction temperature at 70 °C during the mixing and over the subsequent 24 h. The solution was then poured in a dialysis tubing cellulose membrane (average flat width of 76 mm, Sigma, St. Louis, MO) for dialysis for 5 days against 1000 cm^3 of deionized water, changed every day. The white colored product obtained was freeze dried in a freeze drier (Labconco, MO), and aliquots were then characterized by IR spectroscopy (Spectrum GX, PerkinElmer Life and Analytical Sciences Inc, MA.) and NMR spectrometry (Advance 300 MHZ NMR Spectrometer, Bruker, Switzerland). The reaction is shown in Scheme 2.

2.2.3. Preparation of pretreatment solutions

The pretreatment agents of the unmodified CH, having 0.1, 1, 2, 3 and 4% (w/v), were prepared by stirring in 2% (v/v) of acetic acid until the CH (57,000 g/mol) was dissolved. Gly concentrations, from

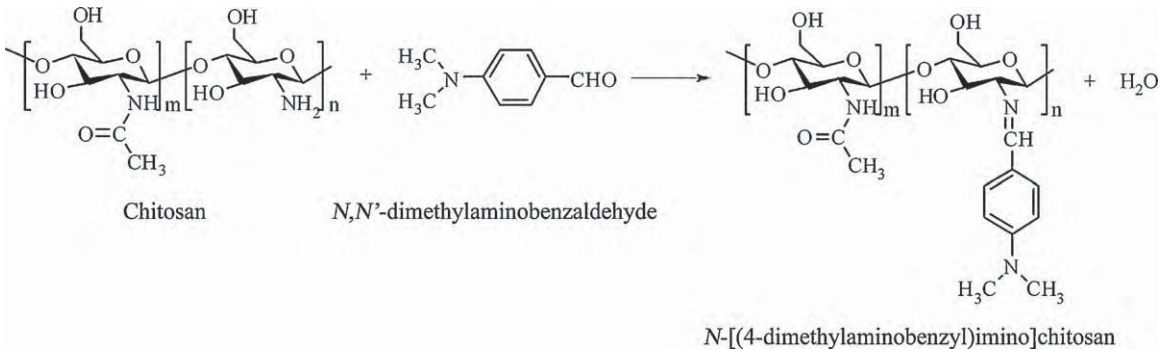

Scheme 1. Synthesis route of N-[(4-dimethyl aminobenzyl)imino] chitosan from chitosan.

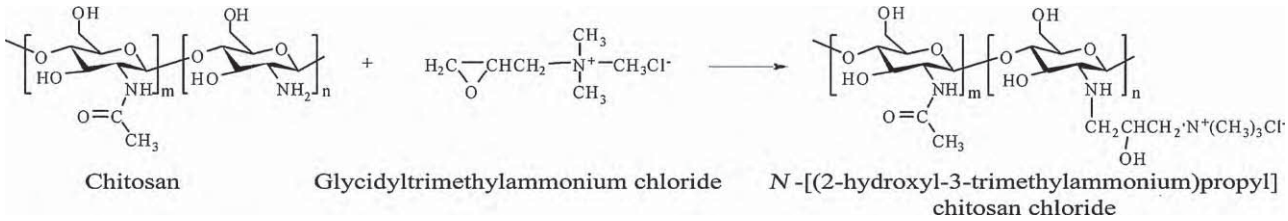

Scheme 2. Synthesis route of N-[(2-hydroxy-3-trimethylammonium)propyl] chitosan chloride (HTACC) from chitosan.

5 to 15% (w/v) in deionized water (Elga Deionizer, LA1, Elga Labwater, UK), were prepared. Likewise, 15% (w/v) of Gly was mixed with 1% (w/v) of CH to give a mixed pretreatment solution. The solutions of the two modified CH (HTACC and DBIC) at a concentration of 0.1% (w/v) were prepared by dissolving 0.25 g HTACC in deionized water in a 250 cm^3 volumetric flask, whereas 0.25 g of DBIC was dissolved in 250 cm^3 of 2% (v/v) acetic acid.

2.2.4. Purity of the polyester fabric

Purity of the polyester fabric was evaluated by testing the presence of starch and poly(vinyl alcohol) by iodine in potassium iodide solution by observing the development of purple color. Carboxyl methyl cellulose (CMC) was examined by mixed solution of ferric chloride and potassium thiosulfate which was followed by dropping solution of potassium ferrocyanide. The presence of CMC can develop a purple color on the fabric surface (Livengood, 1983). The optical brightener may interfere the color data therefore the fabric was viewed in an MEDA light color viewing booth under ultraviolet irradiation where the presence of visible fluorescent light shall be detected.

2.2.5. Zeta potential measurement

The ink jet inks, pretreatment solutions, polyester fabric and the pretreated polyester fabrics were all measured for zeta potential using a Nano-ZS, Zeta potential Analyzer (Malvern Instruments Ltd., UK) in a disposable U-shaped cell with each wall accommodating one small piece of a Cu electrode. The zeta potential of the untreated polyester fabric and the pretreated polyester fabrics were measured by first preparing a fabric suspension by pulling out the fibers from the piece of fabric and then cutting the fibers into small pieces of approximately 0.05 cm long. They were then soaked in deionized water for 24 h. The suspension obtained was used for measuring the zeta potential of the pretreated fabrics.

2.2.6. Fabric pretreatment

The polyester fabrics were cleaned with Triton X-100, rinsed in distilled water and dried at room temperature. The cleaned polyester fabrics (23 cm × 32 cm) were then padded with the above mentioned pretreatment solutions using a padding machine (PB-1, Copower Technology Co., Ltd., Taiwan) with a 70% wet pick up. The pretreated fabrics were then dried in an oven (M-3, Copower Technology Co., Ltd., Taiwan) at 80 °C for 5 min and cured at 110 °C for 2 min.

2.2.7. Ink jet printing and post-treatment

The untreated and pretreated polyester fabrics were printed with a set of seven-color, pigmented ink jet inks (cyan, light cyan, magenta, light magenta, yellow, black and light black colors), using commercially available water-based inks on a piezo-electric drop-on-demand type ink jet printer (Epson Stylus Photo 2100, Seiko Epson Corporation, Nagano, Japan). A color test chart, composed of 294 color patches, several lines and characters, was used for investigating the quality of the printed polyester fabrics. Post-treatment of the printed fabric was performed by steaming at 100 °C for 5 min in a steamer (HTS-3, Copower Technology Co., Ltd., Taiwan).

2.2.8. Color gamut evaluation

The color test chart of each printed fabric was measured in tristimulus values using an X-Rite spectrophotometer (SP62, X-Rite Inc., MI) with an illuminant D50, the CIE 1931 2° observer in a specular light excluded mode. The tristimulus values (X, Y, Z) were transformed to chromaticity coordinates (x, y, z) for creating a color gamut in a two-dimensional color space. The L^*, a^* and b^* color values were used to calculate a gamut volume in a three-dimensional space by SHIPP program (Fair, 1997; Putthimai, 2003). In the same manner, the L^* vs. C^* space was also created by measuring the sample lightness and chroma in the CIE $L^*C^*H^*$ spaces.

2.2.9. Color strength (K/S) measurement

The color strength of inks was determined based on the Kubelka–Munk equation, and expressed as a K/S value, fluctuating from the maximum absorption wavelength of each color within the visible spectrum. The percentage of reflectance was measured by the same spectrophotometer with a specular light excluded condition. The K/S value was calculated according to Eq. (1) (James, 1997):

$$\frac{K}{S} = \frac{(1 - R_\infty)^2}{2R_\infty} \quad (1)$$

where K is the absorption coefficient of the printed color on the surface, S is the scattering coefficient caused by the colored substrate, and R_∞ is reflectance of the colored sample at an infinite opacity. Evaluation of the significance level of K/S values of the pretreated fabrics compared with the untreated fabric was performed by one-way analysis of variance (ANOVA) with the least square difference (LSD) tests used for post hoc evaluations of differences between groups in Statistical Package for the Social Science (SPSS) version 14.0 software, at a confidence level of 95.0% ($\alpha = 0.05$).

2.2.10. Tone reproduction measurement

The tone reproduction was evaluated by plotting the optical density versus the percentage of the dot area. The optical density was measured by a densitometer (R730, IHARA Electronic Ind. Co., Ltd., Nagoya, Japan).

2.2.11. Outline sharpness and contrast assessment

The printed outline sharpness on the fabrics was measured by optical microscopy (PM10-AD, Olympus Corporation, Tokyo, Japan) with a 4× magnification of 10-point printed positive and negative "E" characters. The black and white line strips printed on the fabrics at the applied spatial frequencies of 0.5, 1 and 2 lines mm^{-1} in the two directions (weft and warp) of the polyester fabric of the bar target were measured by a microdensitometer (Konica, PDM-7, Tokyo, Japan). The scanning aperture was set at a width of 20 μm and a reflection mode of 500 μm, and data were then acquired at 20 data points per second to give a total scanning of 400 data points. The densities in each sample were measured and normalized to the untreated fabrics. The contrast at each frequency was calculated from Eq. (2):

$$\text{Contrast}(\omega) = D_{\max}(\omega) - D_{\min}(\omega) \quad (2)$$

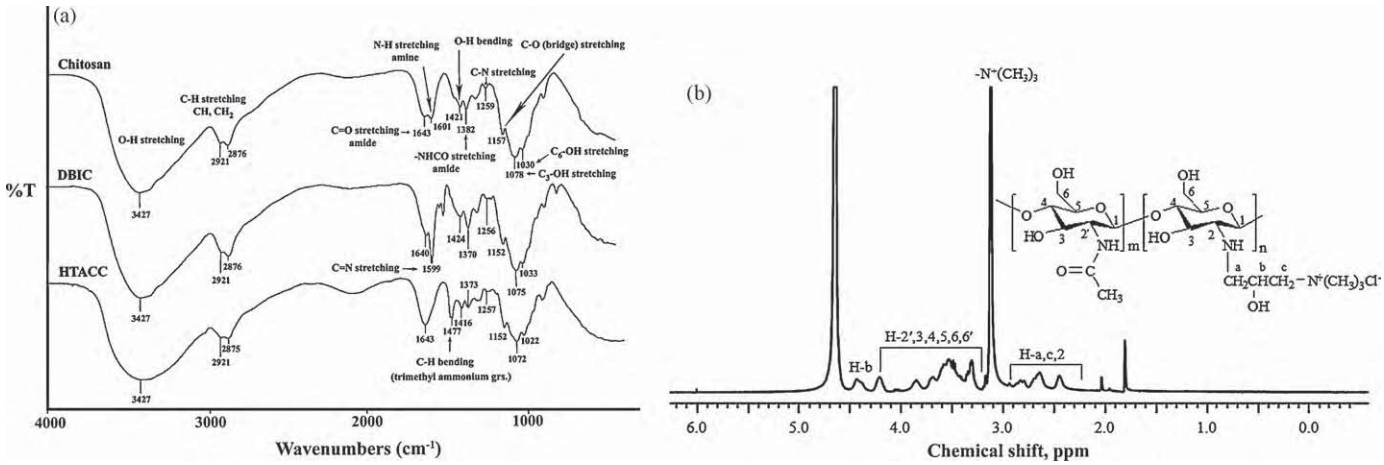

Fig. 1. Confirmation of modified chitosans: (a) IR spectra of chitosan, DBIC and HTACC; (b) ^{1}H NMR spectra of HTACC (solvent: D_2O, 25 °C).

where D_{max} and D_{min} are average maximum and minimum densities, respectively, and ω is the spatial frequency. Plots of the densities against the measured frequencies in both the weft and warp fabric directions were constructed. However, calculation of the contrast in the warp direction could not be measured because of the problems in measuring both the densities.

2.2.12. Surface appearance of the pretreated polyester fabrics

The surface of the pretreated polyester fabrics was examined by scanning electron microscopy on a Spectrum One (PerkinElmer Life and Analytical Sciences, Inc., MA) at a magnification of 2000×.

2.2.13. Stiffness of the treated fabrics

The stiffness of the fibers was measured in terms of the bending length by following the JISI 1096:1999 stiffness 145° cantilever method (Stiffness Method A, 1999). Pieces of each fabric, sized 2 cm × 15 cm, were measured and the average bending length in the warp and weft directions, obtained from five measurements, were expressed as the average stiffness. The bending length of the fabrics treated with the selected loadings of the pretreatments were then compared with that for the untreated fabrics, within the same pretreatment agent at various levels, and at the same selected loadings of the five pretreatment agents. The significance of the test was performed by one-way analysis of variance (ANOVA) with the least square difference (LSD) tests being used for post hoc evaluations of differences between groups in Statistical Package for the Social Science (SPSS) version 14.0 software, at a confidence level of 95.0% ($\alpha = 0.05$).

2.2.14. Color fastness to washing and rubbing

The effects of the pretreatment agents on color fastness to washing and to rubbing of the fabrics were investigated based on ISO 105-C10:2006 (E), and AATCC TM 8, respectively.

3. Results and discussion

3.1. Characterization of the fabric and the modified chitosans

Under the test conditions mentioned above, it showed that the polyester fabrics were free from starch, poly(vinyl alcohol), and CMC, because the mixed solution of iodine and potassium iodide for starch and poly(vinyl alcohol) did not give the purple color, and a mixed solution of ferric chloride and potassium thiosulfate for CMC did not produce the purple color on the fabric surface either. It was also found that the polyester fabric was free from optical brightener, because the visible fluorescent light was not observed on the exposed surface under ultraviolet irradiation.

The IR spectra of the unmodified CH and the two modified CHs (DBIC and HTACC) are given in Fig. 1(a). That for CH shows the overlapped peaks of N–H stretching and O–H stretching at 3427 cm^{-1} and O–H bending at 1421 cm^{-1} which indicates the presence of hydroxyl groups (Sun, Zhou, Xie, & Mao, 2007). The weak absorption peaks at 2921 and 2876 cm^{-1} are assigned to the C–H stretching (Huacai, Wan, & Dengke, 2006). The strong characteristic peaks of CH at 1643, 1601, 1382 and 1259 cm^{-1} are assigned to the C=O stretching, N–H bending and –NHCO stretching of the amide (Zhang, Wang, & Wang, 2007), and C–N stretching (Singh, Sharmaa, Tripathi, & Sanghib, 2009), respectively. In addition, the weak characteristic peaks at 1157, 1078 and 1030 cm^{-1} are ascribed to the stretching of the C–O bridge (Huacai et al., 2006; Mun et al., 2008) and the C_3–OH and C_6–OH groups (Zhang et al., 2007), respectively.

The CH amine N–H bending at 1601 cm^{-1} in the IR spectrum of DBIC is absent, but rather the spectrum displays a strong absorption peak at 1599 cm^{-1} corresponding to the C=N stretching of DBIC (Hakeim et al., 2008). This confirms that DBIC was synthesized by the reaction between the amino groups of CH and the aldehyde groups of dimethyl aminobenzaldehyde to become the imino groups (C=N) in DBIC.

The IR spectrum of HTACC reveals that the characteristic amine N–H bending peak at 1601 cm^{-1} is absent, but rather reveals the presence of the peak at 1477 cm^{-1} assigned for the C–H bending of the trimethylammonium groups (Lim & Hudson, 2004a). In addition, the N–H bending of primary amine groups is absent due to changes to the secondary amine. The peak at 3400 cm^{-1} was somewhat broadened, caused by the overlapping of the O–H group with the N–H stretching. A weak and broad band at 2200–2000 cm^{-1} was observed, potentially assigned to a combination of the asymmetrical $N(CH_3)_3^+$ bending vibration and to the torsional oscillation of the $N(CH_3)_3^+$ group.

The ^{1}H NMR spectrum of HTACC in Fig. 1(b) shows the integrations of the trimethyl ammonium group equals to 1, and the integration of the Hs at the positions 2′, 3, 4, 5, 6 and 6′ equal to 0.8. The degree of substitution (DS) of GTMAC in HTACC was calculated from Eq. (3):

$$\%DS = \left\{ \frac{\text{integral of the } N^+(CH_3)_3/9}{(\text{integral of the H-2', 3, 4, 5, 6, 6'/6}) \times (95/100)} \right\} \times 100 \quad (3)$$

where %DD is the degree of deacetylation (95/100). From the results, it confirms that HTACC contained 87.7% DS. The calculated

Table 1
Zeta potentials of the materials used.

Type of material	Zeta potential, ζ (mV)
Ink jet inks	
Cyan	−43.1
Magenta	−56.5
Yellow	−34.7
Black	−36.7
Pre-treating solutions	
1% (w/v) CH	+83.4
15% (w/v) Gly	+24.7
1% (w/v) CH + 15% (w/v) Gly	+65.1
0.1% (w/v) DIBC	+73.2
0.1% (w/v) HTACC	+36.6
Fabrics	
Untreated fabric	−22.6
Treated fabric with 1% (w/v) CH	−21.6
Treated fabric with 15% (w/v) Gly	−26.4
Treated fabric with 1% (w/v) CH + 15% (w/v) Gly	−28.8
Treated fabric with 0.1% (w/v) DIBC	−24.6
Treated fabric with 0.1% (w/v) HTACC	−23.1

average molecular weight of HTACC based on the above mentioned data is 165,000 g/mol with an aqueous solution pH of 6.8.

3.2. Zeta potential measurement

The zeta potentials of all four base ink colors were found to be negatively charged, with the magenta color having the highest negative value and the yellow color the lowest, but still relatively high (Table 1). To the best of our knowledge, the pigments of Epson inks are encapsulated by a type of crosslinked polymer to prevent coagulation. It implies that the encapsulated pigmented inks had anionic functional groups (generated negative charges), consistent with their good dispersion stability. Similarly, the polyester fabric also had a negative zeta potential, although of a lower magnitude but still sufficient to likely prevent agglomeration of the particles. For the pretreatment solutions, all of them had positive zeta potentials with CH having the highest value, some 2.3-fold higher than HTACC, whilst Gly had the lowest zeta potential. However, all can be considered to highly likely be stable in an aqueous state. Nevertheless, when the fabrics had been padded with the pretreatment solutions, all the zeta potentials of the treated fabrics became negative at around 22–29 mV, which can be considered to be less stable in terms of agglomeration and aggregation. It is clear that the fabric has a dominant effect because the analyzer measured the entire bulk solution of the substrate with thus only a relatively small (by mass) influence from the deposited thin film from the pretreatment agent. One may assume that at least a minute amount of the pretreatment solution and thus agent could be absorbed on the surface and a larger amount penetrated into the polyester fabric, leaving a very thin layer on the fabric surface.

3.3. Effects of the pretreatment agents

3.3.1. Color strength

The ink jet inks are transparent due to the inherent nature of the pigments used. The CH solutions in acetic acid (CH having average molecular weight of 57,000 g/mol) were slightly yellow to yellowish brown and so made the background yellowish. The CH having average molecular weight of 100,000 g/mol can dissolve slightly in acetic acid, therefore, CH with average molecular weight of 57,000 g/mol was used as a representative for the fabric treatment. The background color of the fabric interfered with the printed ink color, resulting in inappropriate color assessments. The color value so measured is basically the combined data of both the background color and the ink color. The background color of the fabric was, therefore, used as a reference for all the measured color values so as to obtain the real color yield of the ink and the resultant effect of the pretreatment agent and the ink.

The color strength (K/S) of the fabrics subjected to the various pretreatment solutions is summarized in Table 2. Theoretically, all of the pretreated fabrics gave generally the higher K/S values than the untreated fabrics. For the CH-treated fabrics, lower K/S values were obtained for cyan, magenta and yellow inks at all CH loadings compared to the untreated fabric. Only the black ink showed a numerically, but not statistically significantly, increased K/S level at three out of the five CH loadings, that is not for those at 2 and 4% (w/v) CH which had lower K/S values. In contrast to CH, compared to the untreated fabric, the K/S values were higher for cyan, yellow and black inks for all Gly loadings tested, whereas for magenta the K/S values were higher than the untreated fabric at 5% (w/v) Gly, but decreased with increasing Gly loadings to equal to and lower than the untreated fabric at 10 and 15% (w/v) Gly, respectively. However, when the mixed pretreatment of 1% (w/v) of CH with 15% (w/v) of Gly was used, the K/S values were all lower than that for the untreated fabric and were not as high as those of the pure Gly or CH at the same respective loading levels, except for the yellow ink which was higher than that for 1% (w/v) CH alone. However, none of these numerical differences in the K/S values relative to the untreated fabric were statistically significant except for those at 1% (w/v) CH for cyan color, 15% (w/v) Gly and the 15% (w/v) Gly mixed with 1% (w/v) CH for cyan, black and magenta colors.

Pretreatment of the fabric with DBIC also gave lower K/S values than the untreated fabric for all four inks. In contrast, pretreatment of the fabric with HTACC gave a remarkable and the highest improvement in the K/S values with the concentration of HTACC

Table 2
The color strength (K/S) and gamut volume of untreated and pretreated polyester fabrics.

Polyester fabrics		K/S at λ_{max}				
Pretreatment	Concentration (%, w/v)	Cyan 620 nm	Magenta 540 nm	Yellow 400 nm	Black 400 nm	Gamut volume
Untreated	–	2.53	4.79	5.38	3.61	6859
CH-treated	0.1	2.61	3.54	5.11	4.25	6967
	1	1.77	3.25	2.78	4.40	7535
	2	1.54	2.56	3.05	2.93	6820
	3	2.12	3.21	3.37	5.74	6961
	4	1.57	2.47	5.20	2.40	7205
Gly treated	5	3.57	5.07	6.77	3.77	7557
	10	3.04	4.80	7.00	8.50	7703
	15	2.90	4.19	6.26	7.57	7846
CH + Gly treated	1 + 15	1.67	3.10	4.56	2.61	6277
DBIC treated	0.1	2.28	4.48	4.2	3.02	7219
HTACC treated	0.1	8.74	14.15	29.14	30.40	12950

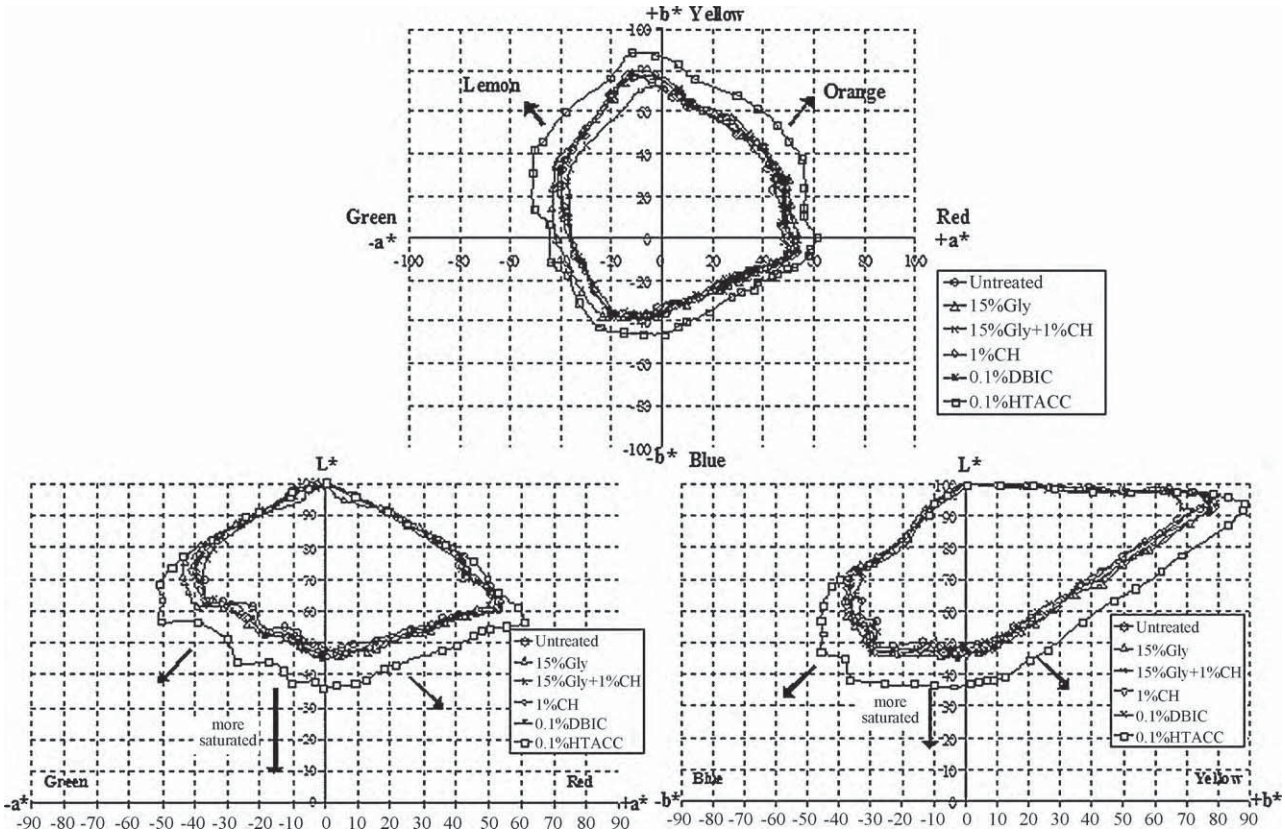

Fig. 2. Color gamuts of the printed fabrics after various pretreatments expressed as a^*b^* for the red-green color vs. yellow-blue color; L^*a^* for lightness vs. red-green color; L^*b^* for lightness vs. yellow-blue color. Data are the mean values, derived from 3 independent repeats.

as low as 0.1% (w/v). Indeed, HTACC pretreatment increased the *K*/*S* values of the cyan, magenta, yellow and black inks by some 5-, 4-, 9- and 11-fold, respectively, above that of the untreated fabric. These numerical increases in *K*/*S* values were statistically significant ($p < 0.05$).

3.3.2. Color gamut and gamut volume

A more meaningful presentation of color is the color gamut in the CIE $L^*a^*b^*$ and $L^*C^*H^*$ system because a more complete color information can be obtained. The color gamut produced by the pretreatment solutions is given in Fig. 2, in which the CIE a^*b^*, L^*a^* and L^*b^* gamuts are shown separately. In all the three gamuts, the 0.1% (w/v) HTACC pretreatment clearly gave the widest gamut followed by 15% (w/v) Gly, while the rest of the pretreatment solutions were only slightly different from each other and the untreated reference fabric. The HTACC treatment produced a far more saturated lemon and orange color, as shown in the CIE a^*b^* gamut, a saturated green and red color, as shown in the L^*a^* gamut, and saturated blue and yellow colors, as seen in the L^*b^* gamut. Moreover, the calculated gamut volumes of the untreated and treated fabrics are summarized in Table 2. One can see that increasing the pretreatment solution increased the gamut volume of the printed colors whereas only 0.1% (w/v) of HTACC padded fabric produced the highest gamut volume. Interestingly, the *K*/*S* values and the size of gamut volume were not really related in every case, as seen in the case of 0.1 and 1% (w/v) treatment by CH (Table 2). This is due to the fact that the *K*/*S* was calculated from colors of the cyan, magenta, yellow and black inks, whereas the gamut volume was calculated from all colors produced in the color sphere. Thus, the gamut volume is a better tool for comparison of the effect of pretreatment of the fabric on the color yield from subsequent printing because it represents the colors that are actually seen.

3.3.3. Tone reproduction

Tone reproduction represents the reproduced optical density with respect to the dot area in a continuous range. The higher the density, the more saturated the printed fabric becomes. Fig. 3(a) shows the tone reproduction of the pretreated fabrics, revealing that different sloped tone reproduction plots were observed for each of the different pretreated fabrics. The tonal densities of the fabrics pretreated with CH, Gly, the CH–Gly mixture and DBIC were all relatively close at the lower dot areas but they gave relatively higher tone densities at the higher dot areas. Very interestingly, the HTACC pretreated fabrics revealed a steadily increasing tonal density for the whole range of dot areas, with a much higher optical density when the dot areas were higher than 40%.

3.3.4. Chroma or color saturation

The components of color appearance are represented by L^* (lightness), C^* (chroma) and H^* (hue angle), and so an L^*C^* plot is another method to observe the extent of color saturation after printing on fabrics pretreated with the different solutions. In this representation, the higher the C^* value is, the greater the color saturation becomes. Most of the pretreated fabrics gave higher color saturations at all lightness, even at the low lightness areas (Fig. 3(b)). Pretreatment brings out a higher color saturation, as indicated by the scattering of the points in the L^*C^* plot. Basically, an ideal color production is judged by the evenly and widely scattering of the points at all lightness and chroma values, i.e., from the low to high values of both axes. With a wide scattering of the points on the L^* and C^* plot, a better tone reproduction with more details can be obtained.

When considering the CH pretreated fabrics, the color saturation was slightly increased as the CH concentrations increased. In the Gly pretreated fabrics, the color saturation increased gradu-

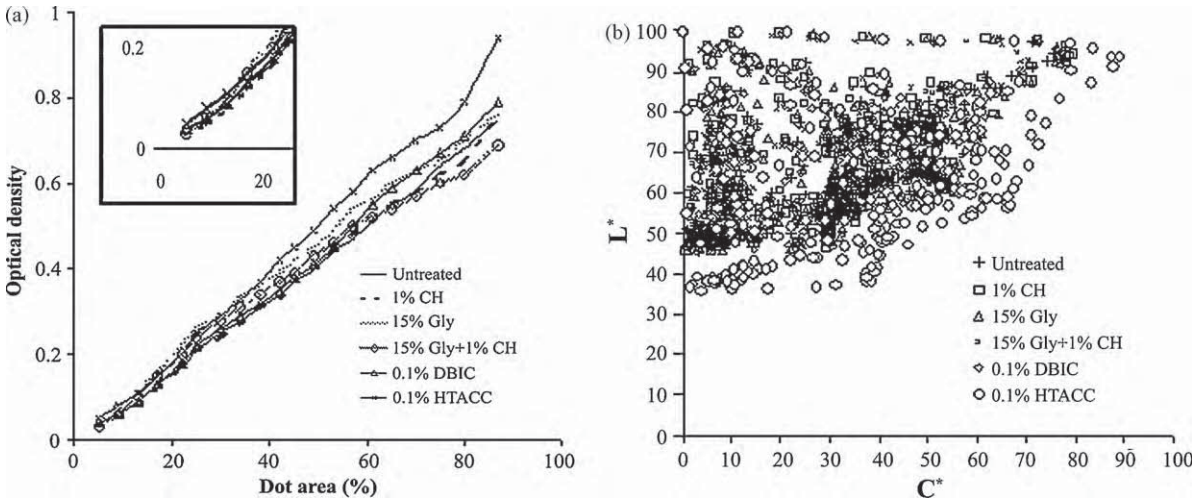

Fig. 3. Color yield: (a) The L^*C^* boundary of the printed fabrics with various pretreatments; (b) tone reproduction (shown as a plot of dot area against optical density) of the printed fabrics with various pretreatments. Data are the mean values, derived from 3 independent repeats.

ally with increasing Gly concentrations up to a maximum at 15% (w/v) Gly. However, when a 1% (w/v) CH and 15% (w/v) Gly mixture was used, the color saturation obtained was lower, being at the same level as that observed with the 1% (w/v) CH pretreated fabric samples. In contrast, when the HTACC was used, higher color saturation was found in the HTACC pretreatment compared to that found with DBIC pretreatment at the same concentration. Indeed, the 0.1% (w/v) DBIC treatment resulted in similar color saturation as that of fabrics pretreated with 1% (w/v) CH.

The extent of the interaction depends on the pretreatment agent concentration, the molecular weight, degree of deacetylation, the location of remaining acetyl units and the local environment, as influenced by the pH, the molecular size of the colorant (Jocic et al., 2005; Leelajariyakul et al., 2008; Phattanarudee et al., 2009), and physical phenomena of surface properties. The major contributor towards the higher *K*/*S* values and wider color gamut can be obtained by the adsorption onto the modified CHs, or onto Gly, of the polymer treated pigment molecules under the environmental conditions. It is now realized that chemisorption, such as ion-exchange, electrostatic attractions and so forth, is the most prevalent mechanism, with the pH being the main factor affecting adsorption (Crini & Badot, 2008; Jocic et al., 2005; Pillai, Paul, & Sharma, 2009). Under acidic conditions, the amino groups of CH are protonated to positively charged amine ions ($-NH_3^+$) that can electrostatically interact with the negative charge of the polymer encapsulated pigmented inks. It has been experimentally confirmed that the printed fabric color is enhanced under such acidic conditions. Furthermore, Jocic et al. (2005) elucidated the possible ionic states and interactions between wool, CH, CH-treated wool and dye, in an aqueous solution at either pH 4.2 or pH 6.5. This led to the postulation about the possible interactions between the polyester and the negative charge of the polymer encapsulated pigmented ink in the present case. Only one terminal end of the hydroxyl group per polyester molecule can be hydrogen bonded with the oxygen atom of the acetyl group of the adsorbed CH or the modified CH, or through van der Waals and hydrophobic interactions (Polyester/CH). Similar van der Waals and hydrophobic interactions between the polyester and the pigmented ink dispersion are also possible (Jocic et al., 2005).

Gly, a small amino acid molecule, has an isoelectric point (PI) at 5.97, the point or pH at which Gly will be centered between the pK_a of the two ionizable groups, the amino group and the carboxylic acid group. Therefore, electrostatic interactions between the protonated amino groups ($-NH_3^+$) with the negative charge of polymer encapsulated pigmented ink are also possible at a pH of less than 5.97.

When Gly was mixed with CH in an acidic condition (pH < PI), the additional protonation of H^+ to the amino group of Gly was, at first, expected because the solution pH was lower than the isoelectric point and thus Gly should be in the protonated form. Unfortunately, the opposite result was obtained in that for the mixed Gly and CH pretreatment, a lower pH yielded fabric prints with lower *K*/*S* values and a narrower color gamut. This could be caused by the fact that the acid (H^+) used for dissolving CH might protonate the carboxyl group of Gly instead.

For the DBIC pretreatment solution, there are two nitrogen atoms per glucosamine unit, and so the *K*/*S* values and color gamut were thus larger than those of the untreated fabric and the CH-treated fabrics.

Introducing a quaternary ammonium group has long been known to enhance the solubility of CH. The conjugation of glycidyltrimethylammonium chloride (GTMAC) to CH produces a CH derivative, HTACC, a water-soluble polymer at all pH values. Therefore, having two nitrogen atoms, one secondary amino group and one quaternary ammonium group, the HTACC pretreatment can synergistically produce higher *K*/*S* values of each color, a higher gamut volume and a better color saturation when compared with the low effectiveness of the primary amino group of CH alone in neutral or dilute acid solutions.

The stable positive charges may interact with the negative charge of the polymer encapsulated pigmented ink via amidation or electrostatic interaction. The much higher *K*/*S* values and the larger color gamut boundary and volume induced by the HTACC pretreatment can be further caused by the ease of site accessibility due to the longer side chain. It is anticipated that this long side chain can allow both chemisorption and physical surface adsorption of the pigmented inks to take place. The protonated CH and HTACC can provide a rapid surface adsorption followed by diffusion and chemisorption of the modified pigment molecules in the CH network via electrostatic interactions (Bahmani, East, & Holme, 2000). Furthermore, HTACC has been reported to generate antibacterial activity to cellulosic fibers (Seong et al., 2000), which is another advantage to use HTACC in textiles.

3.3.5. Outline sharpness and contrast assessment

The outline sharpness of the printed character "E" visualized and then as measured by the optical microscopy, is illustrated for the positive characters in Fig. 4(a)–(f) and negative characters in

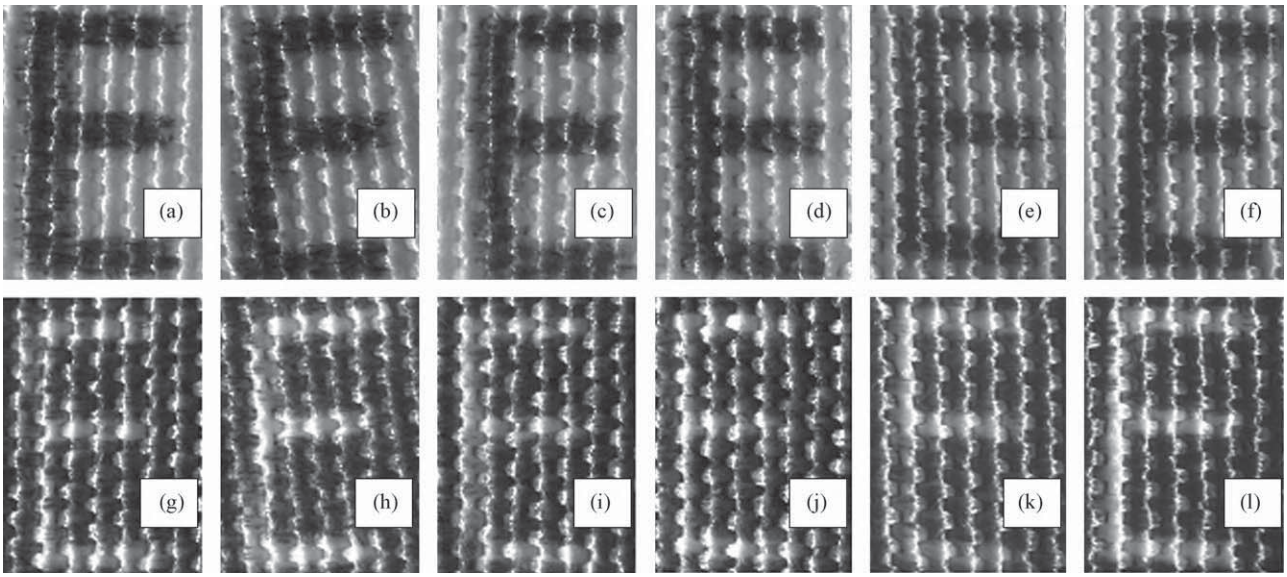

Fig. 4. Outline sharpness and printed character quality of the "E" on fabrics with various pretreatments: Positive character: (a) the untreated fabric, and the fabrics pretreated with (b) 1% (w/v) CH, (c) 15% (w/v) glycine, (d) mixture of 1% (w/v) CH and 15% (w/v) glycine, (e) 0.1% (w/v) DBIC and (f) 0.1% (w/v) HTACC; negative character: (g) the untreated fabric, and the fabrics pretreated with (h) 1% (w/v) CH, (i) 15% (w/v) glycine, (j) mixture of 1% (w/v) CH and 15% (w/v) glycine, (k) 0.1% (w/v) DBIC and (l) 0.1% (w/v) HTACC.

Fig. 4(g)–(l), printed on polyester fabrics after various pretreatments. In principle, the good printed qualities of characters are sharpness, even ink deposition and legibility. The sizes of the positive characters (Fig. 4(a)–(f)) are larger and shaper than those of the negative characters (Fig. 4(g)–(l)). Ink spreading in both vertical and horizontal directions was observed in the untreated fabric (Fig. 4(a) and (g)) and all the CH-treated fabrics (Fig. 4(b) and (h)). The edges of the positive characters were not so ragged but the negative characters were more ragged and unevenly printed. The printed positive characters and negative characters on 0.1% (w/v) DBIC pretreated fabrics in Fig. 4(e) and (k) or 0.1% (w/v) HTACC pretreated fabric in Fig. 4(f) and (l) gave a much better legibility with sharper edges, more evenly printed color densities and a higher contrast between the letter and the background than those of the untreated fabric. One obvious point was also seen in the blurred "E" characters (Fig. 4(c) and (i)) on the Gly pretreated fabrics, due to the lower viscosity resulting from the small molecular size of Gly. This observation is even more obvious in the negative characters (Fig. 4(i)).

The data of the treatments disclose that the contrast transfer function (CTF) in the warp direction is higher than those in the weft direction. The trace lines of micro-density vs. distance in pixel, and their contrast calculated from the average micro-density in the weft direction are revealed in Table 3. The contrast in the warp direction cannot be calculated due to the configuration of the fiber and thus no data could be presented. One should bear in mind that the densities of the fabrics were bared. From these results, the 0.1% (w/v) HTACC pretreated fabric gave the highest contrast, followed by the 0.1% (w/v) DBIC pretreatment, whilst fabric pretreated with the mixed 15% (w/v) Gly and 1% (w/v) CH gave the lowest contrast. All the measured samples rendered a decreasing contrast with increasing spatial frequencies at each resolution. Therefore, among all the pretreatments, the fabrics treated with 0.1% (w/v) HTACC gave the highest smoother trace lines and resolution especially at the frequency of 2 lines per mm (data are not shown here). Two possible attributes to the above observations are the extent of ink absorption, spreading and fixation. The lower ink absorption produced a higher ink density and better contrast, while the better color fixation controls an adequate ink penetration and limited ink spreading to result in the fine and smooth edges of the characters.

3.3.6. Surface appearance and stiffness of the pretreated polyester fabrics

Fig. 5 shows the surface appearance of the untreated polyester fabrics and the various treated polyester fabrics. The untreated polyester fabric, as depicted in Fig. 5(a) is not smooth and has minute and shallow channels distributed widely on the fiber. When it was treated with 1% (w/v) of CH, the channels were reduced because the CH solution could fill up the channels. With higher CH concentrations, at 2, 3 and 4% (w/v), an uneven and rough layer of CH was deposited on the fiber surfaces which made the fibers become distorted (micrographs are not shown here). This behavior may induce stiffness to the fabrics. When an excessive amount of 15% (w/v) Gly was padded, small specks, agglomerates and layers of the pretreatment Gly were deposited widely on the fiber, as shown in Fig. 5(b). The fibers became smoother and less swollen when the mixed CH and Gly solution was padded (Fig. 5(c)). The stiffness of the fabric at this level of padding was hard to hand touch. The CH and Gly pretreated fabrics were not soft to hand touch because the fabric stiffness was increased appreciably. On the other hand, the fabrics padded with 0.1% (w/v) of DBIC or 0.1% (w/v) of HTACC (Fig. 5(e) and (f), respectively) had a smooth surface texture somewhat similar to that of the untreated fabric. For softness to hand touch, the 0.1% (w/v) DBIC or 0.1% (w/v) HTACC pretreatment gave a relatively similar stiffness as that for the untreated fabric regardless of the high molecular weight of HTACC. Based on Crutzen (1995) model of ditallowdimethyl ammonium chloride deposition on cotton, this model was adopted to explain the similar softening result of the high molecular weight HTACC. The long side chain of N-(2-hydroxyl-3-trimethylammonium)propyl chloride attached at the nitrogen atom of the amine occupied more spaces on the fabric. The combined effects of adsorption and the softening power of quaternaries enable the fabric to behave somewhat like the cationic softener treated fabric.

Fig. 6 shows the extent of the bending length of the printed fabrics in the warp and weft directions for the fabrics pretreated with the different solutions. The stiffness of the untreated warp direction was higher because it is naturally stronger than that of the weft direction, due to having more incorporated fibers (182 ends in.$^{-1}$ for the warp fiber vs. 87 picks in.$^{-1}$ for the weft). When 0.1% (w/v) CH, 0.1% (w/v) HTACC and 0.1% (w/v) DBIC were used to treat the

Table 3
Print contrast in the weft direction of polyester fabrics printed by ink jet inks after pretreatment with the indicated solutions.

Type of fabrics	Traces of micro-density vs. distance (pixel)	Contrast of the printed fabrics at the applied spatial frequency (lines per mm)		
		0.5	1	2
Untreated	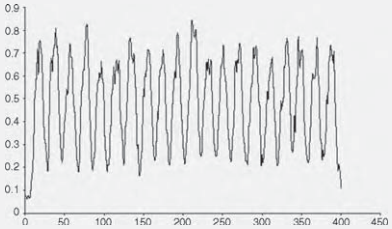	0.69	0.58	0.53
0.1% (w/v) CH	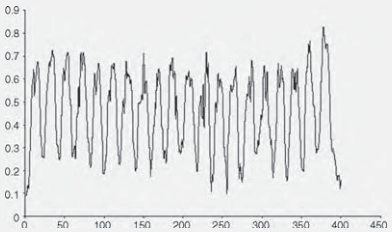	0.57	0.51	0.47
1% (w/v) CH	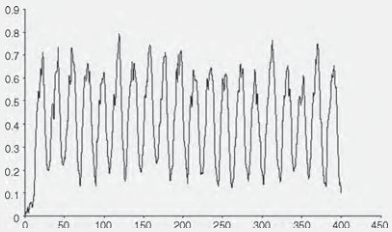	0.63	0.60	0.51
2% (w/v) CH	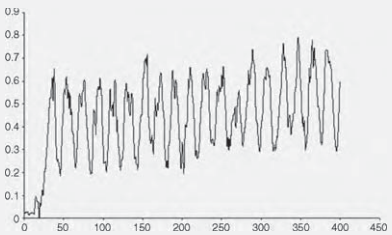	0.59	0.52	0.36
3% (w/v) CH	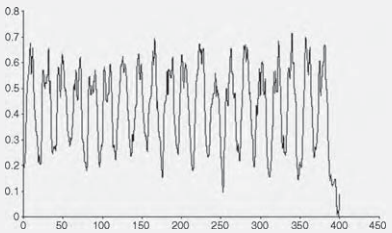	0.55	0.48	0.37
4% (w/v) CH	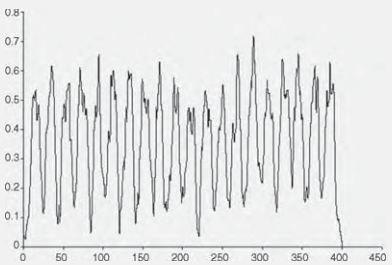	0.57	0.52	0.44
0.1% (w/v) DBIC	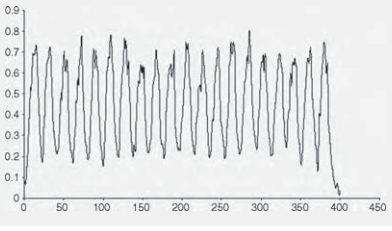	0.69	0.69	0.51

Table 3 (*Continued*)

Type of fabrics	Traces of micro-density vs. distance (pixel)	Contrast of the printed fabrics at the applied spatial frequency (lines per mm)		
		0.5	1	2
0.1% (w/v) HTACC	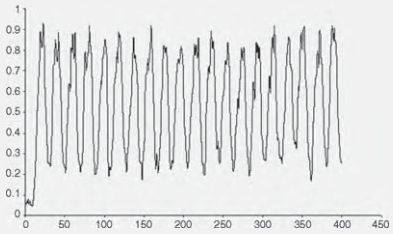	0.85	0.80	0.62
5% (w/v) Gly	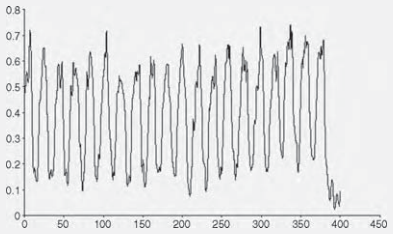	0.65	0.60	0.48
10% (w/v) Gly	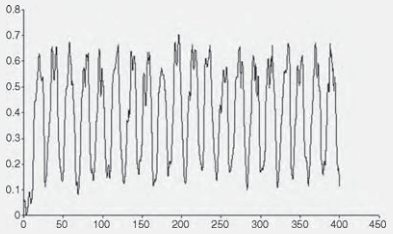	0.60	0.53	0.48
15% (w/v) Gly	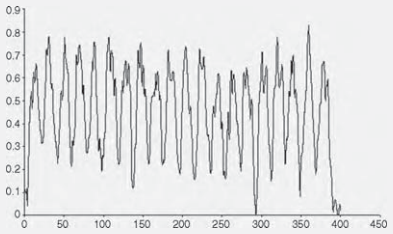	0.70	0.58	0.48
15% (w/v) Gly + 1% (w/v) CH	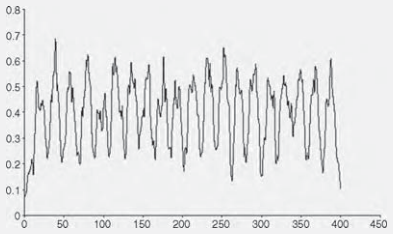	0.50	0.44	0.35

fabrics prior to printing, the stiffness in the warp direction in each pretreated fabric increased, which was influenced by the strength of the warp fibers and the pretreatment solution ($p \ll 0.05$). The HTACC pretreated fabric gave significantly lower fabric stiffness. The stiffness of the weft direction in the untreated and treated fabrics showed a similar trend as those seen for the warp direction. In contrast, when more concentrated pretreatment solutions were used, the stiffness in the weft direction increased rapidly. This is because the pretreatment solutions were absorbed easily by the fibers in the weak weft fibers due to the lower fiber density at 87 picks in.$^{-1}$ in this direction. Increasing the pretreatment of both chitosan solutions from 0.1 to 4% (w/v), and Gly solutions from 5 to 15% (w/v) significantly increased the stiffness in both the warp and the weft fiber directions, but with a greater increase in the weft fiber direction. When the fabrics were pretreated with the mixture of 1% (w/v) CH and 15% (w/v) Gly, the stiffness increased markedly and this was statistically significant ($p \ll 0.05$). The greater the stiffness of the fabrics, the less comfortable they became. It is also anticipated that the electrostatic interaction between the positive charges of the pretreatment agents and the negative charge of the polyester surface and the inks might be the major contribution to the increase in fabric stiffness. Therefore, there is a trade-off in the amount of pretreatment solution on the required printing property vs. the fabric performance properties. In the present case, HTACC is a good candidate as a pretreatment agent because only 0.1% (w/v) is required to obtain a satisfactory color strength, which does not yield too high a fabric stiffness and also has the advantage of potentially adding antibacterial activity, as reported elsewhere (Seong et al., 2000).

3.3.7. *Effect of pretreatment agent on color fastness to washing and rubbing*

Based on the ISO 105-C10:2006 (E) for evaluating color fastness to washing, and AATCC TM 8 for color fastness to rubbing, the results presented below are based on the five levels of evaluation that 5 stands for excellent, 4 for good, 3 for fair, 2 for poor, and 1

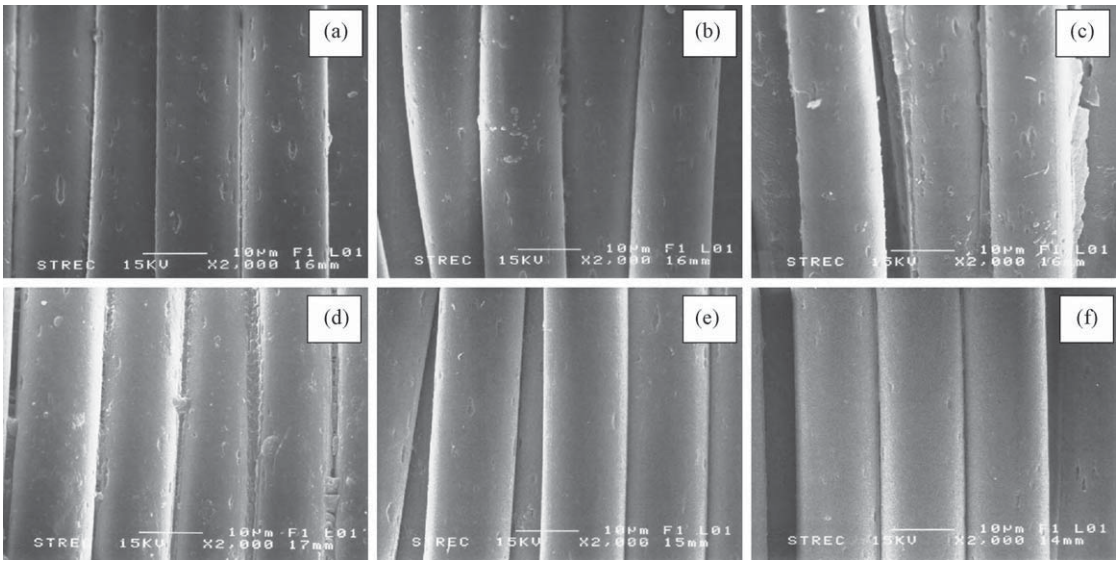

Fig. 5. Surface appearances of (a) the untreated fabric, and the fabrics pretreated with (b) 1% (w/v) CH, (c) 15% (w/v) glycine, (d) mixture of 1% (w/v) CH and 15% (w/v) glycine, (e) 0.1% (w/v) DBIC and (f) 0.1% (w/v) HTACC.

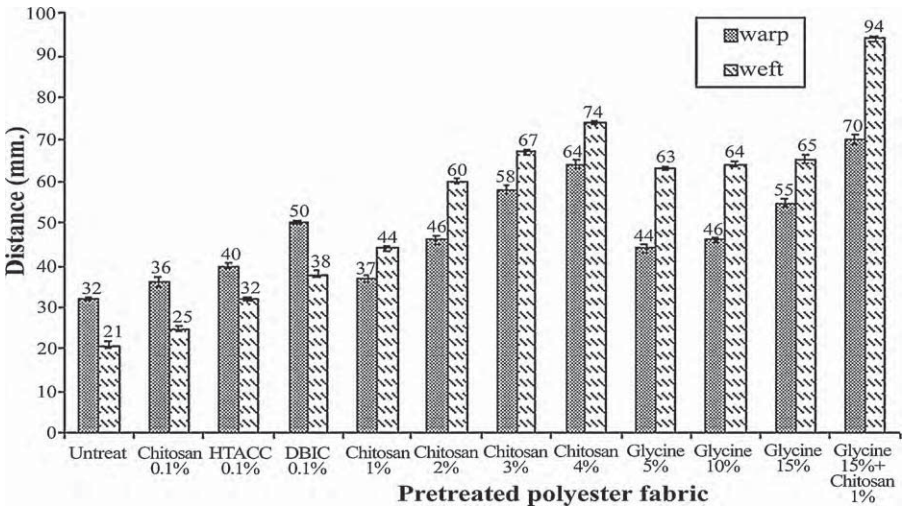

Fig. 6. Stiffness of the printed fibers of (a) untreated fabrics, weft direction, (b) untreated fabrics, warp direction, (c) treated with 0.1% (w/v) HTACC, weft direction and (d) treated with 0.1% (w/v) HTACC, warp direction. (Data are shown as the mean values ± 1 SD, derived from five independent repeats.)

for very poor:

Treatment	Color fastness level	Dry fastness level	Wet fastness level
Untreated	1	3–3.5	2.5
CH, Gly, DBIC	2	3–4	2.5–3, 2–3, 1.5–2.5
HTACC	3–4	3–4	2.5
Gly–CH mixture	3–4	3–4	2.5–3.5

The pretreated fabrics gave the higher color fastness to washing than the untreated one. The HTACC gave better color fastness to washing of the printed polyester fabric which might be contributed by HTACC as an interlayer between the ink and the fabric. Similar result was also observed for the Gly–CH mixture pretreated fabric. Color fastnesses to wet rubbing for all fabrics with all pretreatments are lower than those for dry rubbing. This could be caused by the weakness of the swollen film in the wet condition which can be easily rubbed off. One can also see that Gly–CH mixture pretreatment having the higher stiffness contributes somewhat the better color fastness to both dry and wet rubbings. It may be then said that the higher flexural modulus is also another contribution to rubbing. Both HTACC and DBIC pretreatments gave the lower color fastness to wet rubbing because they are relatively hydrophilic in nature with low flexural modulus and the pretreated films are weak in water and under rubbing.

With a very smooth interface adhesion for the ink and substrate, the only forces holding the substrate and pretreatment agent together are the interfacial attractive forces. Internal stresses act to reduce adhesion and less external force is required to disrupt the adhesive bond. As film formation proceeds, T_g rises and free volume is reduced; the film becomes fixed in unstable conformations, and internal stress increases. Stresses also result from volume expansions, such as swelling of films by exposure to high humidity or water immersion. Thus delaminating of the printed ink film under rubbing can occur easily.

4. Conclusions

The use of CH, Gly, and the two modified CHs (DBIC and HTACC) as the pretreatment reagents of polyester fabrics prior to ink jet printing indicated that these pretreated fabrics produced a much

better color quality than the untreated fabrics, but that the extent of this improvement largely depended on the type and concentration of the pretreatment solutions. Although polyester is a hydrophobic fabric, it had a negative zeta potential implying that it has negative charges on its surface. The important properties of the *K*/*S* value, color gamut and gamut volume, color saturation, tone reproduction, outline sharpness and surface appearance were evaluated. Overall, HTACC pretreatment gave overwhelming excellent properties over the rest of the pretreatments. Only 0.1% (w/v) of HTACC was required to provide a high color gamut and color saturation, good tone reproduction and outline sharpness, smooth surface and less fabric stiffness. Nevertheless, Gly could also be used as a pretreatment agent for good color reproduction, but it is not as good for outline sharpness because it produced rather poor outline sharpness and low contrast print, due to its high spreading caused by the low solution viscosity. Based on the numerical observation and statistical evaluation, the pretreatment agents gave better qualities than the untreated fabric and their efficiency can be ranked as follows for (i) color properties: HTACC $\gg$ Gly > CH $\approx$ DBIC > Gly–CH mixture (15% and 1% (w/v), respectively); (ii) for outline sharpness: HTACC > CH $\approx$ DBIC $\approx$ Gly–CH mixture (15% and 1% (w/v), respectively); and (iii) less stiffness: HTACC < DBIC < Gly < CH < Gly–CH mixture (15% and 1% (w/v), respectively); (iv) color fastness to washing: HTACC $\approx$ Gly–CH mixture > CH > gly $\approx$ DBIC; (v) color fastness to rubbing: Gly–CH mixture > gly $\approx$ CH > HTACC > DBIC.

Acknowledgements

The authors would like to acknowledge the research grant support by the National Research Council of Thailand under contract number GRB_19_51_23_03 and the Research Team Aids coded RTA5080004 for their financial support. Deep gratitude also goes to the Polymer Research Laboratory of the Department of Imaging and Printing Technology, Chulalongkorn University, for providing research facilities. The authors are indebted to the Department of Textile Chemical Engineering, the Faculty of Textile Industries, Rajamangala University of Technology, KrungThep, for permission to use their padding machine and steamer. Many thanks go to Assistant Professor Voravee, P. Hoven, Ph.D. for useful comments on the manuscript, to Publication Counseling Unit of the Research Affairs, Faculty of Science, Chulalongkorn University for language editing.

References

Abou-Okeil, A., & Hakeim, O. A. (2005). Effect of metal ion binding of chitosan on the printability of pretreated wool fabric. *Coloration Technology*, *121*, 41–44.

Bahmani, S. A., East, G. C., & Holme, I. (2000). The application of chitosan in pigment printing. *Coloration Technology*, *116*, 94–99.

Chakvattanatham, K., Phattanarudee, S., & Kiatkamjornwong, S. (2010). Anionically surface-modified pigment/binder ink jet inks for silk fabric printing. *Pigment & Resin Technology*, *39*(6).

Crini, G., & Badot, P. M. (2008). Application of chitosan, a natural aminopolysaccharide, for dye removal from aqueous solutions by adsorption processes using batch studies: A review of recent literature. *Progress in Polymer Science*, *33*, 399–447.

Crutzen, A. M. (1995). Study of the ditallowdimethylammonium chloride interaction with cellulose. *Journal of the American Oil Chemists' Society*, *72*, 137–143.

Espinosa-Jiménez, M., Padilla-Weigand, R., Ontiveros-Ortega, A., Ramos-Tejada, M. M., & Perea-Carpio, M. R. (2003). Interpretation of colloidal dyeing of polyester fabrics pretreated with ethyl xanthogenate in terms of zeta potential and surface free energy balance. *Journal of Colloid and Interface Science*, *265*, 227–233.

Fair, M. D. (1997). *Colorimetry in color appearance models*. MA: Addison-Wesley–Longman., p. 61.

Hakeim, O. A., Abou-Okeil, A., Abdou, L. A. W., & Waly, A. (2005). The influence of chitosan and some of its depolymerized grades on natural color printing. *Journal of Applied Polymer Science*, *97*, 559–563.

Hakeim, O. A., El-Gabry, L., & Abou-Okeil, A. (2008). Rendering synthetic fabrics acid printable using chitosan and binder. *Journal of Applied Polymer Science*, *108*, 2122–2127.

Huacai, G., Wan, P., & Dengke, L. (2006). Graft copolymerization of chitosan with acrylic acid under microwave irradiation and its water absorbency. *Carbohydrate Polymers*, *66*, 372–378.

James, H. N. (1997). In M. Roderick (Ed.), *Color physics for industry* (p. 296). West Yorkshire, England: Society of Dyers and Colourists.

Jocic, D., VÎlchez, S., Topalovic, T., Navarro, A., Jovancic, P., Julià, M. R., et al. (2005). Chitosan/acid dye interactions in wool dyeing system. *Carbohydrate Polymers*, *60*, 51–59.

Julia, M. R., Pascual, E., & Erra, P. (2000). Influence of the molecular mass of chitosan on shrink-resistance and dyeing properties of chitosan treated wool. *Coloration Technology*, *116*, 62–67.

Kim, J. Y., Lee, J. K., Lee, T. S., & Park, W. H. (2003). Synthesis of chitooligosaccharide derivative with quaternary ammonium group and its antimicrobial activity against *Streptococcus mutans*. *International Journal of Biological Macromolecules*, *32*, 23–27.

Leelajariyakul, S., Noguchi, N., & Kiatkamjornwong, S. (2008). Surface-modified and micro-encapsulated pigmented inks for ink jet printing on textile fabrics. *Progress in Organic Coatings*, *62*, 145–161.

Lim, S. H., & Hudson, S. M. (2004a). Application of a fibre-reactive chitosan derivative to cotton fabric as a zero-salt dyeing auxiliary. *Coloration Technology*, *120*, 108–113.

Lim, S. H., & Hudson, S. M. (2004b). Structure of the O-polysaccharide of *Citrobacter youngae* O1 containing an α-D-ribofuranosyl group. *Carbohydrate Research*, *339*, 313–325.

Livengood, C. D. (1983). Spot tests for identification of warp sizes on fabric. *Textile Industries*, *September*, 114–116.

Mun, G. A., Nurkeeva, Z. S., Dergunov, S. A., Nama, I. K., Maimakov, T. P., Shaikhutdinov, E. M., et al. (2008). Studies on graft copolymerization of 2-hydroxyethyl acrylate onto chitosan. *Reactive and Functional Polymer*, *68*, 389–395.

Phattanarudee, S., Chakvattanatham, K., & Kiatkamjornwong, S. (2009). Pretreatment of silk fabric surface with amino compounds for ink jet printing. *Progress in Organic Coatings*, *64*, 405–418.

Pillai, C. K. S., Paul, W., & Sharma, C. P. (2009). Chitin and chitosan polymers: Chemistry, solubility and fiber formation. *Progress in Polymer Science*, *34*, 641–678.

Putthimai, P. (2003). *Appendix B, in print qualities of screen and ink jet printings on cotton fabrics* (p. 105, ISBN 974-17-194-9). Masters Thesis, Chulalongkorn University.

Samu, R., Moulee, A., & Kumar, V. G. (1999). Effect of charge and hydrophobicity on adsorption of modified starches on polyester. *Journal of Colloid and Interface Science*, *220*, 260–268.

Seong, H., Whang, H. S., & Ko, S. (2000). Synthesis of a quaternary ammonium derivative of chito-oligosaccharide as antimicrobial agent for cellulosic fibers. *Journal of Applied Polymer Science*, *76*, 2009–2015.

Singh, V., Sharmaa, A. K., Tripathi, D. N., & Sanghib, R. (2009). Poly(methylmethacrylate) grafted chitosan: An efficient adsorbent for anionic azo dyes. *Journal of Hazardous Materials*, *161*, 955–966.

Stiffness Method A. (1999). JIS published standard. *JIS L*, 1096.

Sun, T., Zhou, D., Xie, J., & Mao, F. (2007). Preparation of chitosan oligomers and their antioxidant activity. *European Food Research and Technology*, *225*, 451–456.

Wang, C., Wu, G., Fang, K., Tian, A., Zhang, X., Fu, S., et al. (2007). Cationic pretreatment for improving image quality of inkjet printing on polyester fabrics. In *Proceedings of NIP23 and digital fabrication* Anchorage, United States of America, (2nd ed., pp. 500–503).

Yuen, C. W., Ku, S. K., & Kan, C. (2008). Use of a biomaterial as a thickener for textile ink-jet printing. *Journal of Applied Polymer Science*, *107*, 1057–1065.

Yuen, C. W. M., Ku, S. K. A., Kan, C. W., & Choi, P. S. R. (2007). Enhancing textile ink-jet printing with chitosan. *Coloration Technology*, *123*, 267–270.

Zhang, J., Wang, Q., & Wang, A. (2007). Synthesis and characterization of chitosan-g-poly(acrylic acid)/attapulgite superabsorbent composites. *Carbohydrate Polymers*, *68*, 367–374.

Anionically surface-modified pigment/binder ink jet inks for silk fabric printing

K. Chakvattanatham, S. Phattanarudee and S. Kiatkamjornwong
Imaging Technology Research Unit, Department of Imaging and Printing Technology, Faculty of Science, Chulalongkorn University, Bangkok, Thailand

Abstract

Purpose – The purpose of this paper is to prepare anionically surface-modified organic pigment/binder ink jet inks for printing on chitosan-pre-treated silk fabrics.

Design/methodology/approach – Anionically surface-modified organic pigment/binder ink jet inks were prepared in four colours (cyan, magenta, yellow and black). The pigment-to-binder ratio was controlled at 1:6.4 for the cyan, magenta and yellow inks, and 1:3.4 for the black ink. Ink formulations (by weight) were assembled and mixed as follows: 8 per cent pigment dispersion, 10 per cent diethylene glycol, 12 per cent glycerol, 5 per cent urea, 10 per cent polyacrylate emulsion binder and 55 per cent deionised water. They were characterised in terms of their particle size, zeta-potential, particle morphology, viscosity, surface tension and pH. The inks were printed onto silk or the chitosan pre-treated silk fabrics using a piezo-type ink jet printer. The fabrics were then heat cured and analysed for the effect of chitosan pre-treatment on colour gamut, wash fastness and crock fastness.

Findings – The formulated ink jet inks yielded an acceptably good ink jetting reliability, one-year stability and printability. The chitosan pre-treated silk fabrics gave a wider colour gamut and colour saturation than the non-treated one. Crock fastness and wash fastness of the chitosan pre-treated fabrics were relatively better than those of non-treated fabrics.

Research limitations/implications – The surface-modified pigments are transparent and thus their inks printed on the chitosan pre-treated fabrics produced slightly low K/S values of cyan, magenta, yellow, and black colours because the limited chitosan concentration in the pre-treatment is controlled by its solubility in acidic solution. The higher loading of chitosan pre-treatment gave higher K/S values and a stiffer touch of the fabrics.

Practical implications – The water-based pigmented inks having the sulphonate group on the pigment surface can be printed on the fabric surface pre-treated with chitosan molecules which have the protonated amino groups to give good colour appearance. It is anticipated that this type of ink can be applied to any textile surface which has been pre-treated with the protonated chitosan.

Originality/value – The modified organic pigments having the sulphonate group on their surface can be used to produce novel water-based ink jet inks which can print on the chitosan pre-treated silk fabric. Ionic interactions between the sulphonate group of the pigment and protonated amino groups of chitosan in conjunction with polyacrylate binder enhance colour strength, widen colour gamut and chroma, and produce good adhesion for fabric operational properties such as wash fastness and crock fastness.

Keywords Inks, Colour fastness, Silk, Pigments, Ink jet printers

Paper type Research paper

Introduction

Organic pigments that are used in ink formulations for fabric printing need to be surface modified if they are to be suitable for printing and application. Limitations on the pigments in this context usually relate to the colour gamut, the stability of the ink, the nature of the continuous medium and the drying time. In applications, various problems, such as in the development of a concentration gradient, the blocking of jets, inconsistency in colour and the low optical density of the resultant prints, are of a major concern (Fu, 2006). The pigment dispersion needs to demonstrate colloid stability with a limited and controllable particle growth in size with time, the size remaining less than 150 nm. The formulated ink must have a low viscosity and a high surface tension. There is a need, therefore, to consider both the thermal and long-term shelf life stabilities of the inks coupled with the need for colour purity (Leelajariyakul *et al.*, 2008). The stability of the pigment dispersion within the ink depends on particle separation forces (type and magnitude), whereby the separated distance can be maintained by stabilising groups that are adsorbed to polymer surface via steric and/or electrostatic forces. These stabilising groups can be covalently attached to the pigment surface in ways that ensure that the functional groups, such as carboxylic or sulphonic acid groups are available on the pigment surface (Belmont, 1994; Johnson and Belmont, 1997).

Like other fabrics, silk, which is directly printed by ink jet printing, does not provide high-quality printing because the surface of the silk fabric is not smooth. A pre-treatment

The current issue and full text archive of this journal is available at **www.emeraldinsight.com/0369-9420.htm**

Pigment & Resin Technology
39/6 (2010) 327–341
© Emerald Group Publishing Limited [ISSN 0369-9420]
[DOI 10.1108/03699421011085821]

This research was supported by a Senior Scholar Research Grant Number RTA4780004 from the Thailand Research Fund. The research facilities, provided by the Polymer Imaging Laboratory of Chulalongkorn University's Imaging and Printing Technology Department, are highly appreciated. The authors are grateful to Professor J.T. Guthrie for his valuable suggestions in paper improvement. Material donations from Cabot (Tokyo) and Shin Nakamura are highly acknowledged.

process to limit the excessive spreading of the ink is necessary before ink jet textile printing because the fabric is porous, soft and pliable. The treating system helps to smooth out the fabric surface and ink absorption becomes more uniform (Phattanarudee *et al.*, 2009). The functional groups provided by the pre-treatment compounds are designed to absorb additional ink, resulting in a better deposition of ink on the fabric surface or a higher ink holdout (Bajaj, 2002).

The majority of interest in textile and printing has been involved with cotton (Bahmani *et al.*, 2000; Oktem, 2003) or synthetic textiles as the substrate- and dye-based ink jet inks (Yuen *et al.*, 2007) have been used. The limited research into the use of the ink jet colouration of silk is a suppressing factor. The major objectives of the current research were to use the anionic, surface-modified pigments/binders to formulate four pigmented ink jet inks and to investigate those parameters that were considered to be of relevance to their printing on pre-treated silk fabrics.

Experimental

Materials

Preparation of pigmented ink jet inks

The pigmented ink jet inks that were used in the study are listed in Table I with the surface-modified pigments being supplied by Cabot Corporation, Billerica, Massachusetts, USA (Jason, 2004). The four pigments used were a cyan pigment, IJX^{TM} 253 C, modified from C.I. Pigment Blue 15:4; a magenta pigment, IJX^{TM}266D, modified from C.I. Pigment Red 122; a yellow pigment, IJX^{TM}273B, modified from C.I. Pigment Yellow 74 (Johnson and Belmont, 1997; Johnson *et al.*, 2002); and a black pigment, CAB-O-Jet 200, modified from C.I. Pigment Black 7 (Belmont, 1994; Belmont *et al.*, 1996a, b). The pigments were provided as an aqueous dispersion. The relevant structures of the pigments are shown in Figure 1, whilst the properties of the surface-modified pigment dispersions are given in Table I.

Methods

Each pigmented ink formulation was assembled as follows (total composition by per cent volume): 8 per cent pigment dispersion, 10 per cent diethylene glycol, 12 per cent glycerol, 5 per cent urea, 10 per cent polyacrylate emulsion binder and 55 per cent deionised water. The pigment/binder ratios were prepared at 1:6.4 for the cyan, magenta and yellow inks, and 1:3.4 for the black ink (Leelajariyakul *et al.*, 2008; Phattanarudee *et al.*, 2009). The polymer binder for the anionically surface-modified pigment dispersions was a polyacrylate emulsion, Vanatex S-711 polyacrylate binder (Shin Nakamura, Wakayama, Japan), added at 10 per cent w/v of dispersion in 63 per cent w/v de-ionised water. The mean diameter of the polymer particles was 116 nm. The Vanatex S-711 contained non-ionic surfactant at 48.5 per cent w/v. The viscosity was 1,000 mPa s at a shear-strain rate of 320 s^{-1} at 25°C. The pH of the dispersion was 5. The glass transition temperature of Vanatex S-711 was 1.2°C. Urea, a good hydrotropic agent, which works as an anti-hydrogen bonding additive was used to improve the stability and to provide the required reduced viscosity and clogging problems that are inherent in on-demand piezo nozzle-jetting devices.

Each component was added individually to the total system. Diluted NaOH solution was added to the ink in order to adjust the pH to within the desired range of 7-9. After mixing, the inks were filtered through a cellulose acetate filter (pore size 0.45 μm, Sartorius Stedim Biotech GmbH, Göettingen, Germany) to remove all coarse particles and so the risk of their clogging the orifices of the ink jet printer was reduced.

Characterisation of pigmented ink jet inks

The pigment dispersion was dried on a glass support, and the resulting film was dried and ground. The dried powder was subjected to Fourier transform infrared (FTIR) measurement (Perkin Elmer System 2000, UK). The pH of the ink was adjusted to the suitable range for printing (pH meter, pH Tester 20, Oaklon, Eutech instruments, Vernon Hills, Illinois, USA) at room temperature. A Brookfield viscometer (DV III, programmable rheometer, Stoughton, Massachusetts, USA) was used to measure the viscosity of the pigment dispersion and of the formulated inks, at 25°C. A particle size distribution analyser (Malvern laser scattering analyser, model Mastersizer S, long bed Ver. 2.11, Worcestershire, UK) was used for the particle size analyses of the pigment dispersions and of the formulated inks. The particle size distributions of the ink formulations were measured after various storage periods (one day, one, ten and 12 months) to confirm the stability of the inks. The surface tension of each ink preparation was measured using a surface tensiometer (K8, Kruss, Hamburg, Germany) by the DuNouy Ring method at room temperature (25°C). The morphology and particle sizes of dried samples of the pigment dispersions were viewed by transmission electron microscopy (TEM) (JEOL, JEM-2100, Tokyo, Japan). The ink samples, after one year of storage, were diluted and applied to a glass substrate. The solvent was removed by evaporation and the resultant dried ink samples were then observed by scanning electron microscopy (SEM) (JSM 6400, JEOL, Tokyo, Japan) and TEM. The inks were diluted using deionised water and their zeta-potential was measured by nanosizing Zetasizer (Nano Series, Malvern Instruments Ltd, UK). The charge on pigment surface was evaluated at 25°C.

Table I Properties of ink ingredients from the surface-modified pigment dispersions

Chemicals	Colour index of pigments used	Chemical class	Average particle size (nm)	Solid content (%(w/w))	Viscosity[a] (mPa s)	Zeta-potential (mV)
Cyan: C (IJX 253 C)	Pigment Blue 15:3	Phthalocyanine	91	9.45	1.37	−55
Magenta: M (IJX 266D)	Pigment Red 122	Dimethyl quinacridone	105	9.96	1.70	−57
Yellow: Y (IJX 273B)	Pigment Yellow 74	Monoazo; acetoacetyl	105	9.66	1.43	−52
Black: K (CAB-O-JET200)	Pigment Black 7	Carbon black	69	18.65	3.10	−64
Vanatex S-711-Polyacrylate emulsion			116	50.7	1,000	−38

Note: [a]The viscosity was measured at shear-strain rate of 330 s^{-1} at 25°C

Figure 1 FTIR spectra of the surface-modified pigments

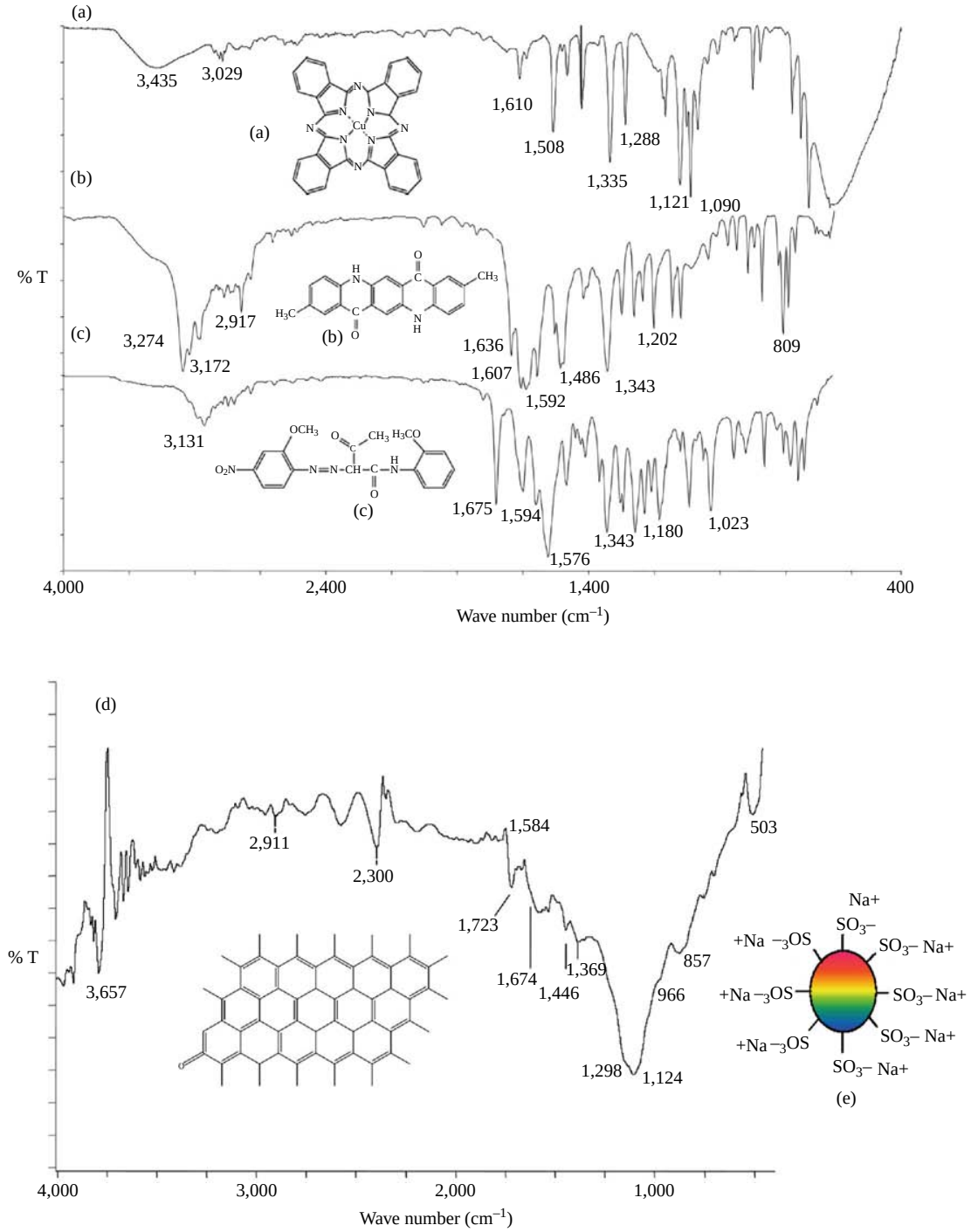

Notes: Spectrum (a) a cyan colour modified from C.I. Pigment Blue 15:4; spectrum (b) a magenta colour modified from C.I. Pigment Red 122; spectrum (c) a yellow colour modified from C.I. Pigment Yellow 74; spectrum (d) a carbon black modified from C.I. Pigment Black 7; and scheme (e) a surface-modified pigment in an electrical double layer for the above pigment

Preparation of the silk fabrics

A plain weave silk fabric, constructed with 73 ends per inch × 62 picks per inch, with a basic weight of 0.11 kg m^{-2}, was used. The fabric was cut into rectangles of 22 cm × 31 cm. Then, the samples were bleached using dilute (0.2 per cent w/v) hydrogen peroxide, at pH 10.5 and a temperature of 100°C, for 1 h. The bleaching formulation was composed of hydrogen peroxide (2 g l^{-1}, reagent grade, ≥98 per cent, anhydrous Sigma-Aldrich, Pte. Ltd, Singapore), sodium carbonate (10 g l^{-1}, American Chemical Society (ACS) reagent, anhydrous, 99.95-100.05 per cent dry basis, Sigma-Aldrich, Pte. Ltd, Singapore) and deionised water and then used at

a 1:50 (v/v) ratio of silk fabric: bleaching solution. The bleached fabrics were washed with deionised water several times to remove the remaining oxidizing agent and then dried at 50°C for 4 h.

Preparation of the chitosan-containing pre-treatment solutions

The three chitosan powders, FL-80, FM-80 and FM-40, had an average molar mass of 120, 370 and 850 kg mol^{-1}, respectively, with an *N*-deacetylation degree of 88, 87 and 88 per cent, respectively, and were obtained from the Koyo Chemical Co. Ltd (Japan). Each of the three chitosan types were prepared at 0.25, 0.5, 1 and 2 per cent w/v in a 1 per cent w/v aqueous solution of acetic acid (ACS reagent, ≥99.7 per cent, Sigma-Aldrich, Singapore) by heating at 60°C until a homogeneous solution was obtained, except that 2 per cent w/v solution could not be made for FM-40 because it could not dissolve at room temperature. The highest concentration of the pre-treatment solution gave difficulty to apply on the fabric because of both the limited solubility capacity and the stickiness of the chitosan solution when it was used for padding on the fabric.

Pretreatment of the fabrics

The bleached silk fabrics were each padded with the pre-treating solutions at 100 per cent pick up in a padding machine (Tsuji Dyeing Machine Mfg, Osaka, Japan). The fabrics were later steamed, pre-treated at 80°C for 5 min and fixed at 110°C for 2 min in an oven (Rapid Labortex Corporation, Taiwan). After the pre-treatment, the silk fabrics were characterised by FTIR-attenuated total reflectance (ATR) spectroscopy (Spectrum One, Perkin Elmer, UK), to confirm the existence of the pre-treatments on the silk fabrics. Likewise, all of the ink colours printed on the silk fabrics were characterised by FTIR spectroscopy to observe the functional groups of the inks and the fabrics.

Printing on the fabric

Each silk fabric was supported on a flat plastic sheet using double-sided adhesive tape to give stable dimensions to the fabric in the media-feeding path for the ink jet printer. The samples were printed with the in-house formulated ink jet inks using an Epson Stylus™ C65 printer (Epson (Thailand), Bangkok, Thailand), at a resolution of 5,760 × 1,440 optimised dpi. After printing, each printed silk sample was steamed at 100°C for 5 min to fix the printed inks.

Evaluation of the printed fabric

Colour gamut

The colour test chart of each of the printed fabrics was evaluated according to CIE $L^*a^*b^*$ colour space (Commission International I'Eclairage), determined using a spectrophotometer (GretagMacbeth Spectrolino, 45/0, X-rite, Incorporated, Regensdorf, Switzerland), with an illuminant D50 and the 2° observer, based on the CIE 1931 system (Berns, 2000). The L^* axis runs from top to bottom with a maximum of 100 representing a perfect reflecting diffuser. The minimum value for L^* is zero, which represents black. The a^* and b^* axes have no specific numerical limits. Positive and negative values for a^* represent a red and green colours, respectively, whilst the same for b^* represents a yellow and blue colours, respectively. The equations for CIE 1976 L^* a^* b^* (CIELAB) colour space are presented elsewhere (Berns, 2000).

Wash fastness

The treatment of the fabric before and after the printing process is an important aspect of the ability to ensure a good fastness property. Thus, the printed silk fabrics (non-treated and chitosan pre-treated) were soaked in 5 per cent w/v NaCl (ACS reagent, ≥99.7 per cent, Sigma-Aldrich, Singapore) and then steamed for 5 min to fix and stabilise the inks on the fabrics. Wash fastness evaluations were carried out according to ISO 105-C06 (1994). Thus, in each case, a sample (100 × 40 mm) in contact with the specified adjacent fabric was washed, rinsed and dried. Each printed fabric, together with its attached multifibre strip, was washed at 40°C for 30 min in liquor containing 4 g of standard detergent (SDC, ISO 105, without optical brightener) per 1 l of water at a liquor volume of 150 ml. The adjacent multifibre fabric (DW) contained wool, acrylic, polyester, polyamide, bleached cotton and cellulose diacetate fabrics. Any change in the colour of the adjacent fabric was compared using the grey scale for staining in accordance with ISO 105-A03 (1993). The colour difference in the printed fabrics, from before and after washings, was also reported in terms of the colour strength (K/S) and the relative colour strength, as derived in equations (1) and (2), from which the K/S ratio and the relative colour strength were calculated:

$$\text{Colour strength, } K/S = \frac{(1-R)^2}{2R} \quad (1)$$

$$\text{Relative colour strength} = \frac{(K/S)_{\text{after washing}}}{(K/S)_{\text{before washing}}} \quad (2)$$

Here, R = the reflectance of printed silk fabric in the range of the highest absorption, based on ISO 105-C06 (1994). The fabrics were printed as a solid pattern in the four colours (cyan, magenta, yellow and black). The printed fabrics, before and after the washing treatment, were evaluated using a spectrophotometer (X-rite, SP62, d/8, X – Rite Asia Pacific Ltd, Quarry Bay, Hong Kong). The reflectance of samples was measured five times in different areas to determine the K/S-values. An averaged value was then calculated.

Crock fastness

The crock fastness of the printed fabric was evaluated using the AATCC Crockmeter (Atlas Electric Devices Corporation, Chicago, Illinois, USA) and AATCC Test Method 8-2001 (2002). The amount of colour that was transferred from the printed surface to the other tested surfaces, during a controlled rubbing process, was judged using a grey-scale chart (Grey Scale for Staining or the Chromatic Transference Scale). Each printed sample was rubbed with a standard white cotton fabric in ten back-and-forth motions, under both dry and wet conditions. The amount of colour transferred to the cotton fabrics was graded in a range from 1 to 5, in an increasing order of rub fastness.

Results and discussion

Quality of the pigmented ink jet inks

Figure 1 shows the IR spectra of the surface-modified organic pigments: C.I. Pigment Blue 15:4 (spectrum (a)), C.I. Pigment Yellow 74 (spectrum (b)), C.I. Pigment Red 122 (spectrum (c)) and C.I. Pigment Black 7 (spectrum (d)), which all have strongly electrolytic sulphonate groups on their pigment surface, whilst the black pigment (spectrum (d)) has in

addition the weakly electrolytic carboxylic acid, hydroxyl and ketonic carbonyl groups on its surface which did not influence the behaviour of the sulphonic acid group. These weakly electrolytic groups were generated during the production of carbon black. For the four pigments, the IR peaks give evidence for the presence of the sulphonate groups as follows: the peaks at around 1,369-1,288 cm^{-1} are assigned to the asymmetrical stretching of —S—O, 1,124-1,090 cm^{-1} for the S═O stretching, and 1,023-809 cm^{-1} for —S—O symmetric stretching of the $-SO_3^-$ group. The peaks at 1,610, 1,607, 1,594-1,592, and 1,486 cm^{-1} are the —C═C— stretching of the aromatic rings in the pigments. The peak at 1,508 cm^{-1} in spectrum (a) of Figure 1 relates to the C═N stretching of the phthalocyanine blue pigment. That at 3,274 cm^{-1} in spectrum (b) of Figure 1 relates to the N═H stretching of the quinacridone red pigment, whilst that at 1,576 cm^{-1} in spectrum (c) of Figure 1 relates to the N═N stretching of the monoazo yellow pigment. The peaks at 1,636 and 1,675 cm^{-1} relate to the C═O stretching of the magenta pigment in spectrum (b) of Figure 1, and the yellow pigment in spectrum (c) of Figure 1, respectively. More peaks are seen in the spectrum of the carbon black pigment in spectrum (d) of Figure 1, where the sharp peak at 1,723 cm^{-1} indicates the C═O stretching from the carboxylic acid group and the peaks at 1,674 cm^{-1} indicate the presence of the ketone carbonyl group, that at 1,446 cm^{-1} the presence of the anionic carboxylate groups, COO^-, and finally the small peak at 3,657 cm^{-1} relates to the O—H stretching of carbon black. A schematic drawing of Figure 1(e) represents the pigment surface that was modified by Cabot's diazonium attachment chemistry (Belmont, 1994) to give the sulphonate groups. Here, the sphere is the CI pigment having the attached functional groups on the surface which are surrounded by the positive counter ions.

Zeta-potential measurements were used to confirm the nature of the negatively charged, surface-modified pigments in all of the pigment dispersions and pigmented inks. The black pigment dispersion had the highest zeta-potential (− 64 mV, Table I), as did the black ink (− 50.9 mV, Table II). It should be noted that all of the four pigments were surface modified with sulphonate groups. However, only the black ink pigment systems contained the OH and COOH groups, albeit it at only a relatively low density. We deduce that the attached functional groups on the surface, surrounded by the positive counter ions, are in a suitable continuous medium, for example, in a colloidal state with one electrical double layer, as shown schematically in schematic drawing of Figure 1(e). The negatively charged pigment surface, together with the components of the continuous aqueous medium, stabilises the inks in a colloidal state.

The presence of the sulphonate and/or carboxylate groups gives an electrostatic repulsive force between the particles, fulfilling the so-called self-dispersing property in a water-based vehicle, without the need for additional dispersing agents because all the pigment concentrates contained a 4.85 per cent final concentration of non-ionic surfactant.

The sulphonate group-containing pigments, as stronger electrolytes, have a better water solubility than that of the carboxylate anion-containing pigments. It has been reported that the print performance of the black inks having —COOH groups (Cab-O-jet 300), as defined by their optical density and water fastness, was superior to those containing $-SO_3H$ groups (Cab-O-jet 200) (Belmont, 1994; Johnson and Belmont, 1997).

Particle size and stability

The prepared inks (cyan, magenta, yellow and black colours) had pH values in the range of 8-9. The particle sizes of the inks were measured after filtration to check for the presence of oversized ink particles. This was because larger particles could clog the orifice of the printer during ink jet printing. The four inks had different average particle sizes with the black ink having the smallest average particle size at 60 nm and the cyan ink the largest size at 105 nm. The pigments in the magenta and yellow inks were in-between with average particle sizes within the range of 79 nm (Figure 2).

The pigmentary species that were present in the formulated inks had very narrow particle size distributions. Figure 2 shows the stability of the inks in terms of the particle size distributions of the inks following ten months and one year of storage. The particle sizes of the cyan and yellow inks remained fairly constant over the year, whilst the magenta and black inks contained a minute fraction of larger particles in the size range of 100-120 μm and 8-100 μm, respectively, after ten months to one year of storage. Analysis of the ink particles by TEM and SEM (Figure 3) revealed that the particle sizes of the pigments in the dried cyan and yellow inks were still less than 120 nm. However, the majority of the pigments in the magenta and black inks had larger particles, at around 300 and 200 nm, respectively. The smaller the primary particle size is the greater is the tendency towards aggregation or agglomeration. The oversized particles were created by the low level of aggregation that involved only a small amount of polymer binder. All of the oversized pigments were removed by filtration, causing the inks to become suitable for ink jet application as shown by the fact that the particle size remained unchanged over ten months. The jetting of these inks was smooth during printing and, in addition, very little, if any cleaning of the print head nozzles was required.

The zeta-potential gives a useful guide to the strength of the repulsive force that operates between the colloidal particles of the ink, and the strongly negative charges (− 43 to − 51 mV) observed for all the inks (Table II) suggest that they are likely to be stable in solution and not aggregate. This strong

Table II Ink properties of the four pigmented inkjet ink colours

Inks	Viscosity (mPa s)	Surface tension (mN m^{-1})	Density (g cm^{-3})	Zeta-potential (mV)	Solid content (%)
Cyan	2.4	44 ± 2	1.04	− 48	28
Magenta	2.5	44 ± 1	1.05	− 43	28
Yellow	2.5	45 ± 1	1.05	− 43	28
Black	2.5	43 ± 0	1.05	− 51	29

Note: Data are shown as the mean ± 1 (SD) and are derived from three replicates

Figure 2 The particle size and their distributions for the ink jet printing inks after storage for the indicated times

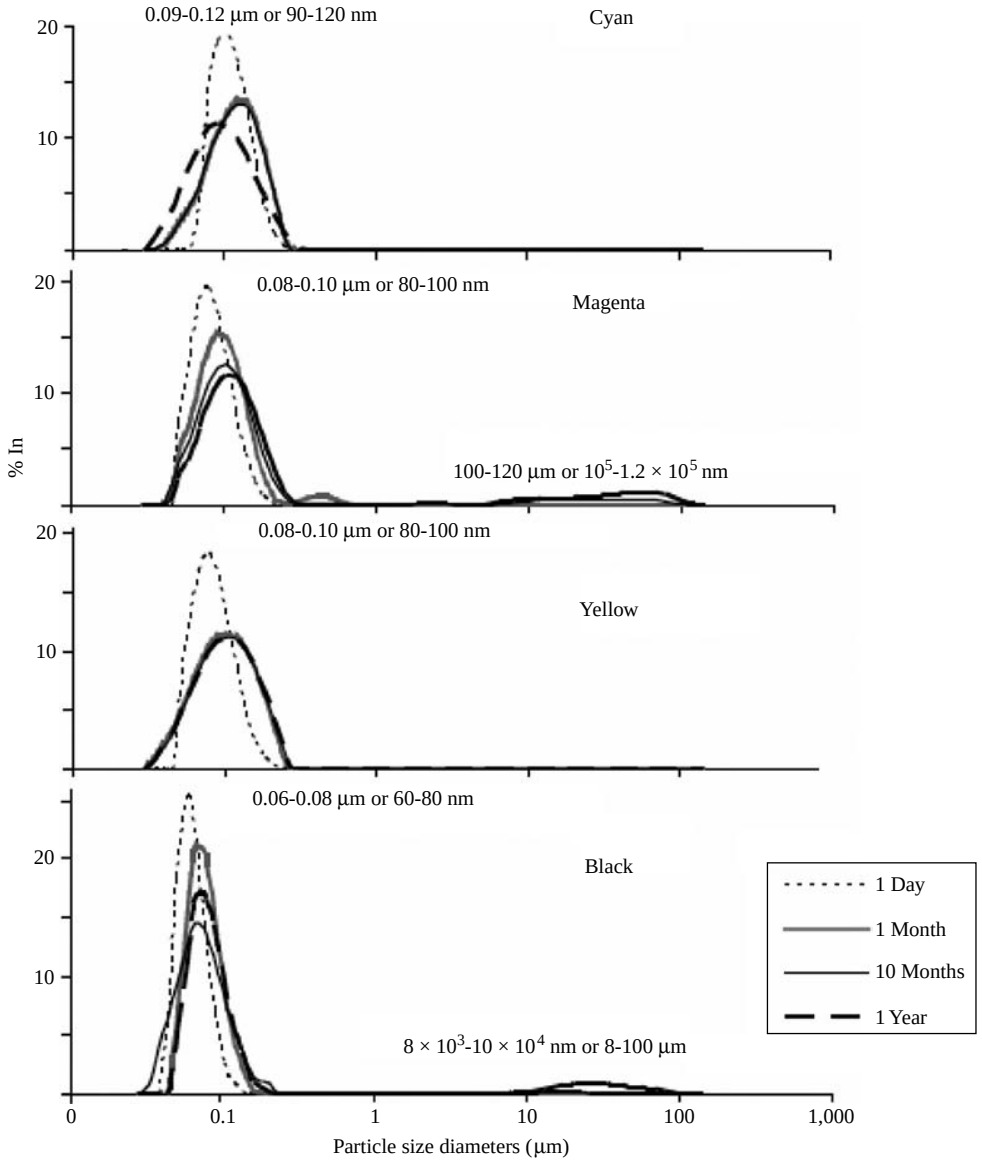

negative zeta-potential is due to the sulphonate or carboxylate groups on the pigment surface (Jason, 2004). Indeed, the other ink properties (Table II) are not contrary to the notion that these inks are suitable for use in a textile ink jet printing system.

Rheological features

Typically, the viscosity of an ink jet ink is approximately 1-5 mPa s. Above this range, the ink becomes too viscous to flow through the nozzle or pass through the orifice, resulting in a clogging problem during drop ejection. The viscosity of all of the prepared inks was measured at room temperature (25°C), where typical Newtonian flow behaviour was observed at the appropriate shear-strain rate, giving viscosity values of approximately 2.5 mPa s for all the inks. Thus, these low-viscosity inks could be printed by the ink jet printing method, using piezo technology, since the piezo print head uses a high shear force in jetting the ink.

When the inks were deposited on the silk surface, the ink bulk fluid (non-coloured medium) was absorbed by the wetting, spreading, penetration and evaporation processes that all took place simultaneously, allowing penetration into the medium. The non-volatile ink components in the medium provided the basis for many cohesive networks to be developed resulting in adhesion or mechanical entrapment on the silk surface.

Characterisation of the pre-treated fabrics and the printed silk fabrics

Chitosan has amino groups that are similar to those on the silk fabrics. Viscosity of the padding of chitosan solutions in Figure 4(a) increases with molecular mass at the fixed concentration, 0.5 per cent w/v and increasing the chitosan

Figure 3 TEM of (a) cyan, (b) magenta, (c) yellow and (d) black pigment dispersions; TEM for (e) cyan and (g) yellow inks; and SEM for (f) magenta and (h) black inks after one-year storage

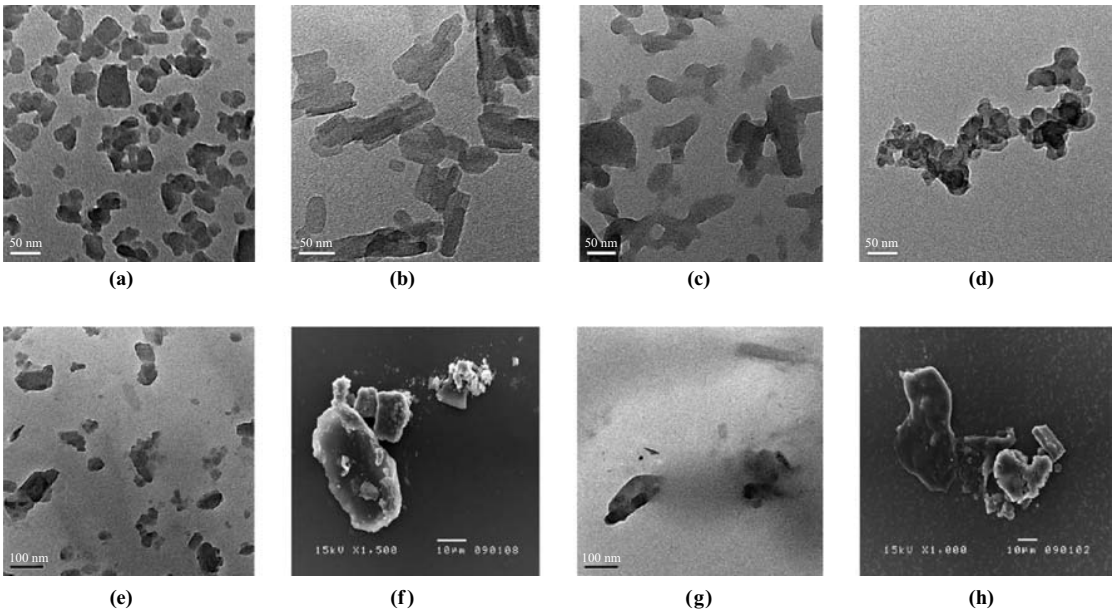

Figure 4 Viscosity of the chitosan solutions

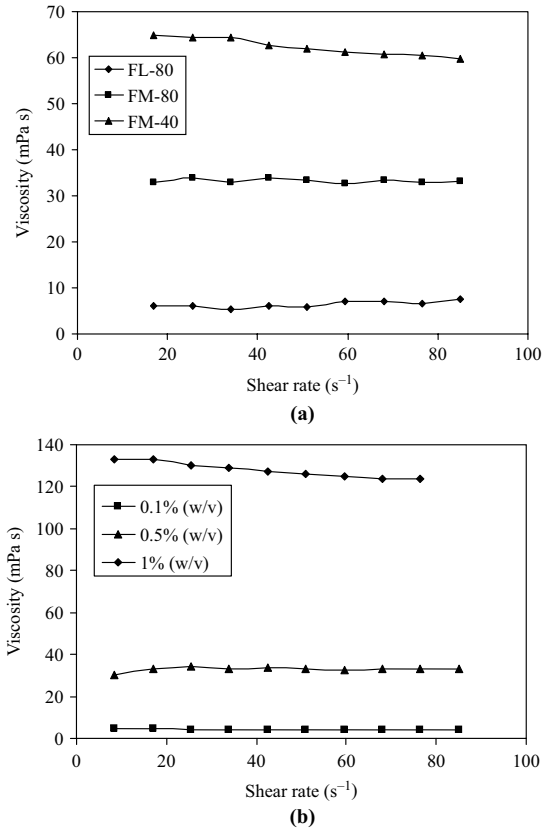

Notes: (a) Types of chitosan used at 0.5 per cent w/v and (b) FM-80 at various loadings at 25°C; data are shown as the mean ±1 (SD) and are derived from three replicates

concentration (FM-80) increases the viscosity of the padding solution (Figure 4(b)). Spectrum (a) of Figure 5 shows IR peaks of the non-treated silk fabric. In spectrum (b) of Figure 5 for chitosan-treated silk, a sharp strong NH_3^+ stretching band in the 3,278-2,901 cm^{-1} region resulting from superimposed O—H and NH_3^+ stretching band are stronger than those in spectrum (a). The stronger peaks in spectrum (b) at 1,050-989 cm^{-1} are assigned for the symmetric C—O—C stretching of chitosan. The asymmetric N—H stretching at 1,617-1,510 cm^{-1} and more weakly near

Figure 5 FTIR-ATR spectra of (a) the non-treated silk and (b) chitosan-treated silk

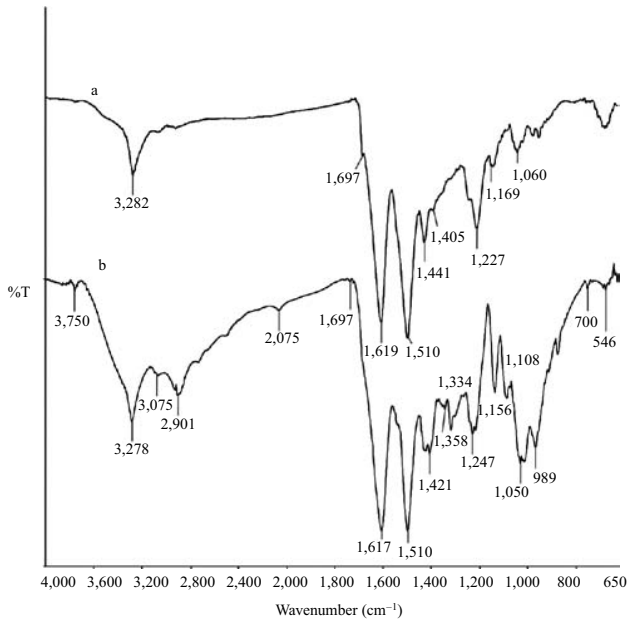

1,441-1,405 cm^{-1} are the asymmetrical and symmetrical $C(^{-}O)_2$ stretching of the carboxylate ion group (Silverstein *et al.*, 1991). This indicates that chitosan has been incorporated on the fabric. Therefore, the addition of chitosan to the silk introduces synergistic effects to be generated on colour gamut.

With the same degree of deacetylation (87-88 per cent), the three types of chitosan that were used in this work did not display any different chemical properties, for example with the IR spectra of silk fabric padded with the two types of chitosan, FM-80 and FM-40 (Figure 6). Moreover, the ink jet ink-printed silk fabrics that had previously been padded with chitosan solutions gave similar chemical surface properties, as shown by their IR spectra (Figure 7). Hydrogen peroxide bleaching of the fabric is to remove surface sericin and other waxy materials resulting in a clean and white surface for better wetting, adhesion and image permanency. Interactions between the ink and the substrate cannot be easily detected by simple spectroscopic methods because of the substrate dominance in comparison with the chitosan-treating solution. Thus, the dual objectives of developing improvements in the printing process with improvements in the colour-related properties were achieved initially. Further investigation of the extent of colour gamut expansion could provide an indication of the synergistic effects provided by the inks and the chitosan pre-treatment solution.

Effect of pre-treatment of the printed fabrics on operational properties

Colour gamut

For the three different types of chitosan, and across all the tested ranges of chitosan concentrations used, the colour gamuts (a^*-b^*, L^*-a^*, L^*-b^* and $L^*a^*b^*$) of the pre-treated fabrics were overall greater, i.e. a larger gamut volume was attained than those printed colours applied to the non-treated

Figure 6 FTIR spectra of chitosan-padded bleached silk fabrics

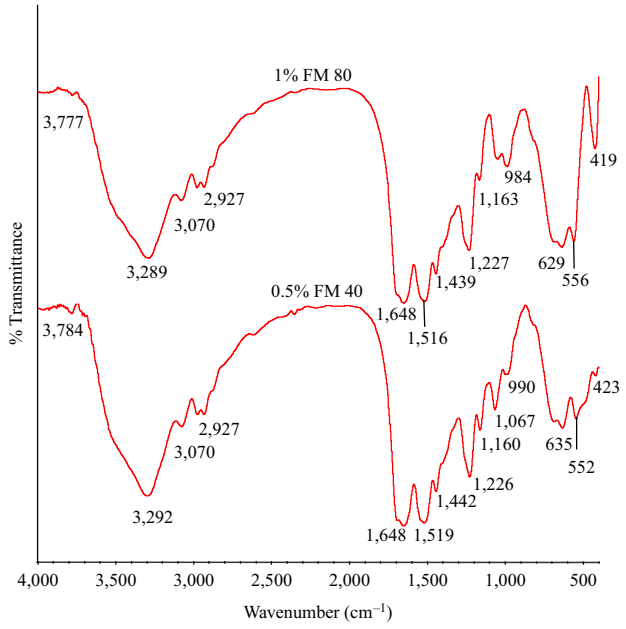

Note: The upper line with 1 per cent w/v FM-80 solution and the lower line with 0.5 per cent w/v FM-40 solution

Figure 7 FTIR spectra of the four-coloured ink jet ink printed fabrics and the substrate material

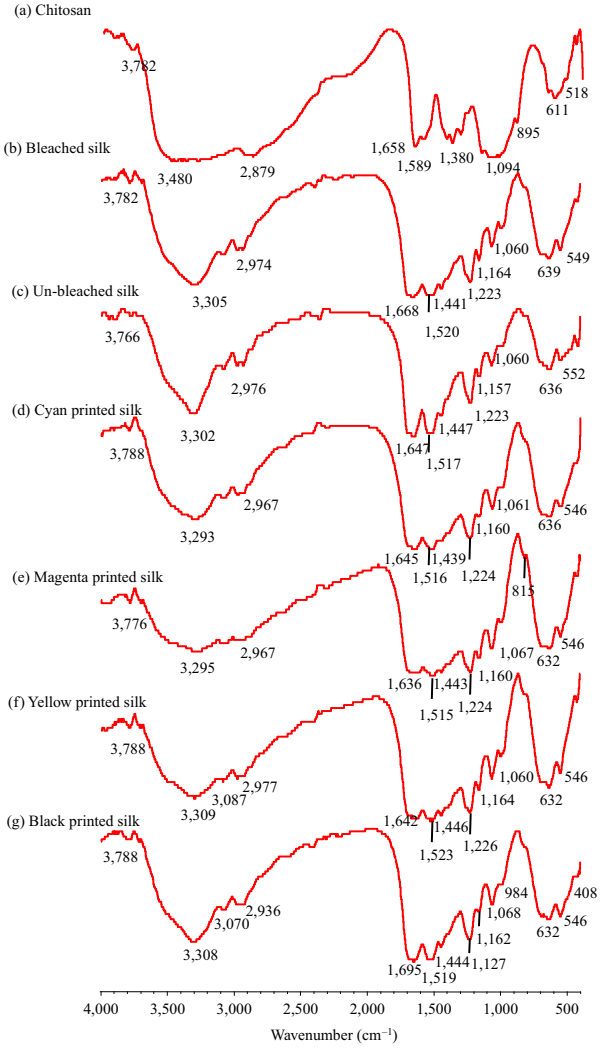

fabrics as shown in Figures 8-11. Likewise, lightness of the pre-treated fabrics was lower than those of non-treated ones (Figures 9-11), i.e. more colour saturation. Once the pigment was dispersed in water, the nanoparticles become interactive with the non-treated silk fibres, through hydrogen bonding and dipole-dipole interactions through the sulphonate or the carboxylic groups which are completely anionic under alkaline conditions. In addition, the alkalinity causes the silk fibres to swell, making them more accessible to the diffusion of the adsorbed nanoparticulate pigments from the surface towards the interior of the fibres.

Increasing the pre-treatment solution concentration for each of the three different molecular weight chitosans, resulted in a wider colour space where the chroma of the cyan colours, at many hue angles, became significantly saturated. A similar trend was also observed with the magenta colours but to a smaller extent. The colour strength of the fabrics printed following with the chitosan pre-treatments increased consistently, the chitosan concentration in the pre-treatment was increased. Amongst the three molecular weight

Figure 8 a*-b* diagrams of the non-treated silk and the silk pre-treated with chitosan of different molecular weights and loadings

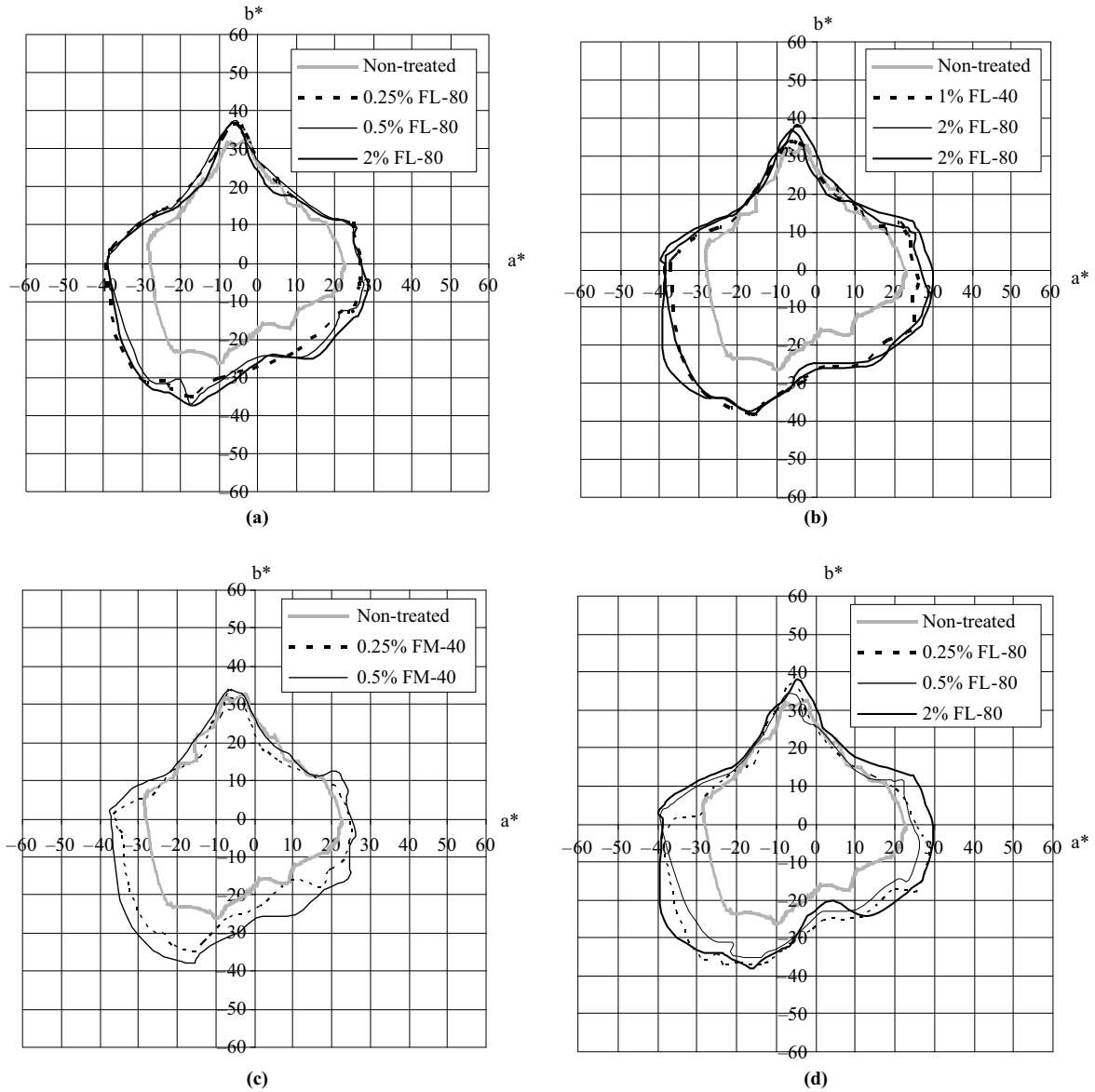

chitosans tested, the pre-treatment solution containing the medium molecular weight chitosan (FM-80), prepared at the highest concentration (2 per cent w/v), gave the largest colour gamut (the combined $L^*a^*b^*$ in Figure 11). This finding correlates well with its highest solution viscosity (Figure 4). Chitosan pre-treatment improves the colour gamut of the printing inks because the chitosan molecule contains amino groups ($-NH_2$) that are protonated ($-NH_3^+$) under acidic conditions and can electrostatically interact with the sulphonate or carboxylate groups on the pigment surfaces, even at a low chitosan concentration (Jocic *et al.*, 2005). Thus, the pre-treatment solutions provide the silk fabric with additional cationic functional groups that enhance the absorption of more ink on to the fabric surface. A colour gamut expansion on the treated fabric surfaces is related to the increases in the chroma (Figure 8). The function of the pre-treatment is to block ink penetration and to give retention of ink on the pre-treated surface. One of the chief concerns with treating silk fabric with chitosan is the increased stiffness of the treated fabrics (Leelajariyakul *et al.*, 2008; Phattanarudee *et al.*, 2009), and so it is desirable to use the smallest amount of chitosan in the pretreatment solution as possible to fulfil the need for a specific purpose.

Wash fastness

The inks contained the S-711 acrylic binder with its T_g of -31°C. This binder is designed to form a flexible film on the silk surface, giving the required properties to the fabric. The effect of the chitosan pre-treatment of silk on their wash fastness following printing was determined by following the K/S of the coloured fabrics, measured before and after the washings. The K/S values of the treated fabrics before and

Figure 9 L*-a* diagrams of the non-treated silk and the silk pre-treated with chitosan of different molecular weights and loadings

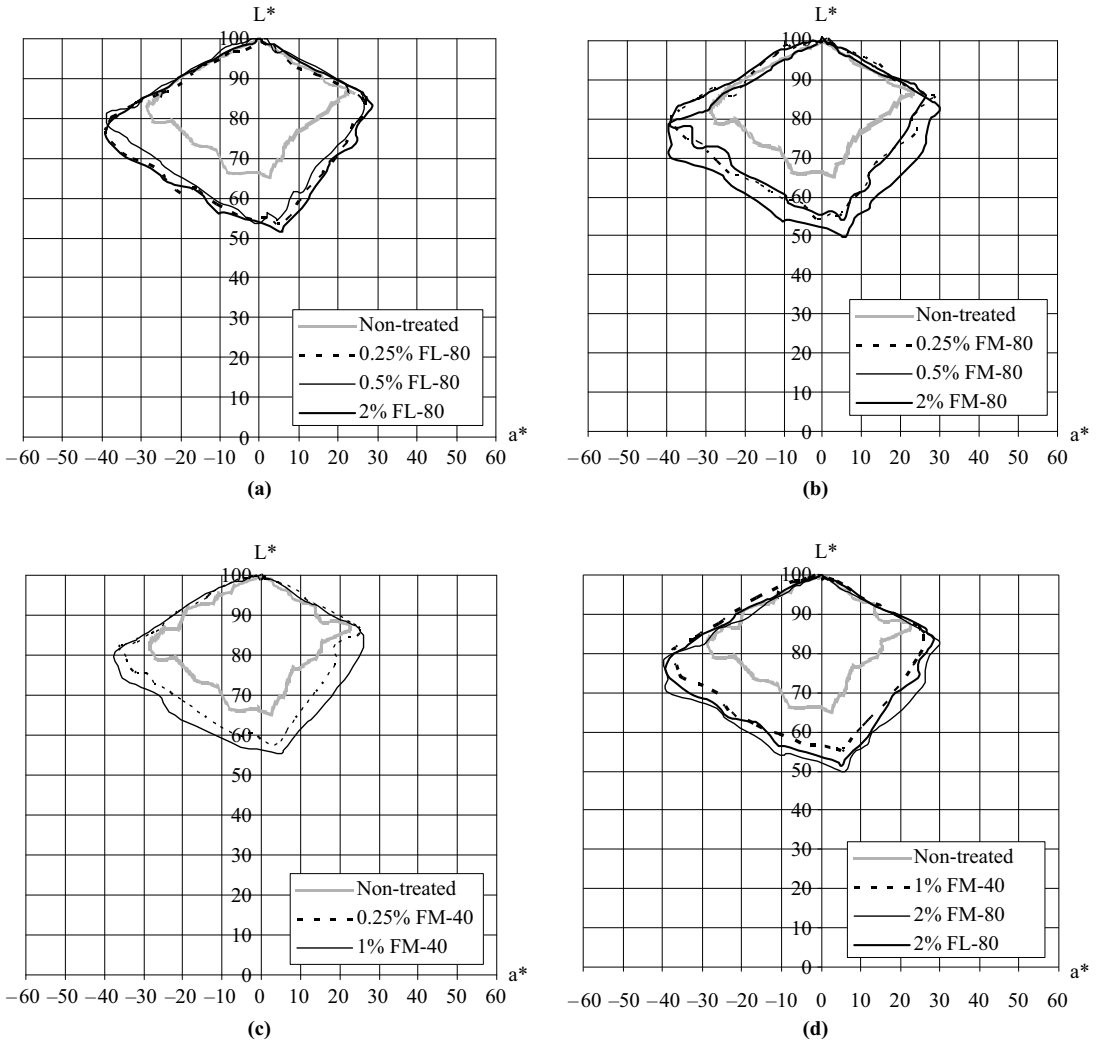

after washing were in unchanged range (0.4-0.5) for cyan and magenta inks, whereas the ranges of 1-1.3 and 1.7-2.5 were found in the yellow and black inks, respectively, depending on the treatment levels. The wash fastness of the printed fabrics was thus excellent for all of the pre-treatments (Table III), and the relative colour strength of the printed silk fabrics after washing is summarized in Table IV where a very small change in the K/S before and after washing, across all of the pre-treatments, was observed. Also, the pre-treatments moderately improved the wash fastness. The relative colour strength of the non-treated fabric was 0.82 for all colours, and the treated ones in the range of 0.9-1.2 for the cyan, magenta, yellow, and black inks, depending on the chitosan molecular weights and solution concentration. The chitosan pre-treatment of silk fabric thus enhanced the wash fastness properties. Comparing between the different chitosans used in the pre-treatments, the chitosan molecular weight and concentration had a slight effect on the wash fastness and colour gamut. At 2 per cent w/v of FL-80 and 1 per cent w/v of FM-80 and FM-40, all of the K/S values increased, especially for the black ink, when compared with the results on the coloured non-treated fabrics.

The amino group in chitosan has a pKa value of about 6.5. Thus, chitosan is positively charged and soluble in acidic to neutral solutions with a charge density that is dependent on the pH and on the percentage of deacetylation that the chitosan contains. The amino groups are protonated to (NH_3^+ (a nucleophilic group) under slightly acidic pH conditions allowing ionic (electrostatic) interactions with electrophilic centres, such as carboxylate ($—COO^-$) or sulphonate ($—SO_3^-$) groups. The proposed electronic interaction is shown in Figure 12. A large pigment molecule with a correspondingly large surface area will provide a large number of potential reactive sites, such as the N—H, O—H or C═O groups. Thus, hydrogen-bonding interactions can occur to increase the strength of the binding over that of only the electrostatic interactions (Crini and Badot, 2008). All of these interactions, whether electrostatic, polar or H bonding, between the colorant and silk fabric, produce printed silks with an excellent wash fastness (Provost *et al.*, 2009). Here, the cationic amino moiety increases the absorption potential of these negatively charged inks via an ionic bonding mechanism (Noguchi and Shirota, 2006; Li and Sun, 2007), since the amino groups in the pre-treating agent and the amino groups in

Figure 10 L*-b* diagrams of the non-treated silk and the silk pre-treated with chitosan of different molecular weights and loadings

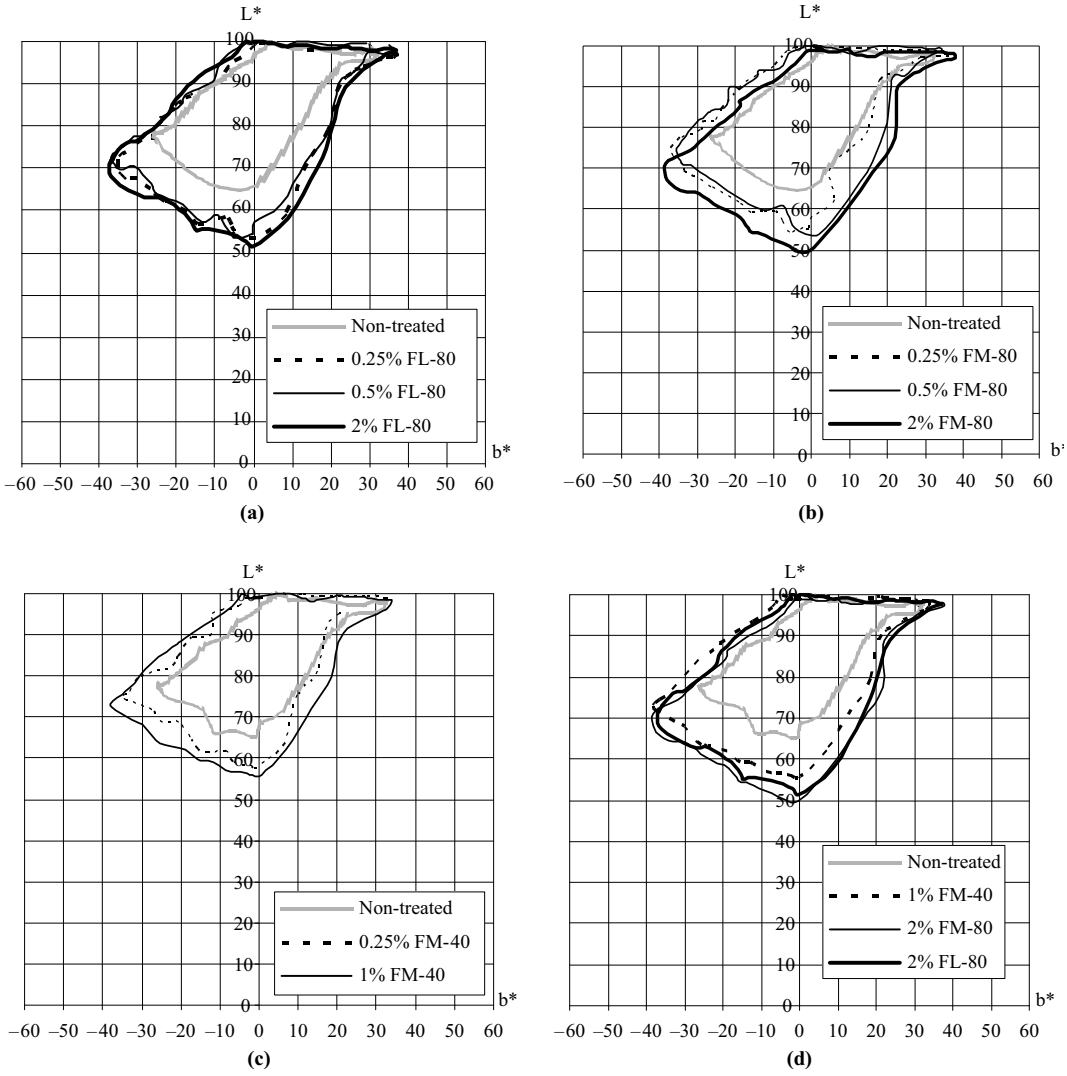

the silk are both protonated and can interact with the anionically surface-modified pigment particles, resulting in an increased interaction, increased ink binding and, consequently, an increase in the K/S values.

Carbon black pigments can contain hydrophilic carboxylic groups and hydroxyl groups from the production process (spectrum (d) in Figure 1). Such pigments can be additionally surface modified by the use of diazonium salts that contain the sulphonate functional group (Belmont, 1994). Thus, the carbon black pigments can be better dispersed under acidic conditions. It is known that carbon black is one of the most difficult-to-disperse pigments. Therefore, additional effective functional groups on the surface provide opportunity for the better development of superior black inks. The calculated K/S values, coupled with visual assessment, support the contention that these inks easily meet the appropriate performance criteria in that the visual ink density and the associated adhesion are both acceptable. The solid content of 50.7 per cent w/w of the Vanatex S-711 in the inks plays a very important role in the ability of the ink to interact with the padded chitosan on the silk fabric, i.e. holding more ink on the surface. This would be expected to increase the colour gamut and the wash fastness.

Crock fastness

From the data given in Table V, it is clear that the non- and pre-treated printed silk fabrics provide the required minimal level of a good dry/wet crock fastness, at levels of 4-5. This is because the inks contained the binder (S-711 acrylic polymer) whose film is flexible (T_g of $-31°C$) at room temperature and can withstand the rubbing processing. The chitosan pre-treatment slightly improved the fabric dry/wet crock fastness (at the 4/5 level). In dry conditions, chitosan loadings from pre-treatment with 0.25 and 0.5 per cent w/v solutions did not affect the dry rub resistance. However, a decline in the rub resistance (at the 4 level) was found under wet conditions, presumably due to a water-acid effect. For all of the chitosan pre-treatments, the dry crock fastness results were better than those of the wet crock fastness. The wet crock fastness was slightly decreased when the chitosan loading solution was more than 0.5 per cent w/v, but was essentially the same for the three different molar mass chitosans evaluated here (Leelajariyakul *et al.*, 2008). The crock and the wash fastness

Figure 11 L*a*b* of the untreated silk and the treated silk pre-treated with chitosan of different molecular weights and loadings

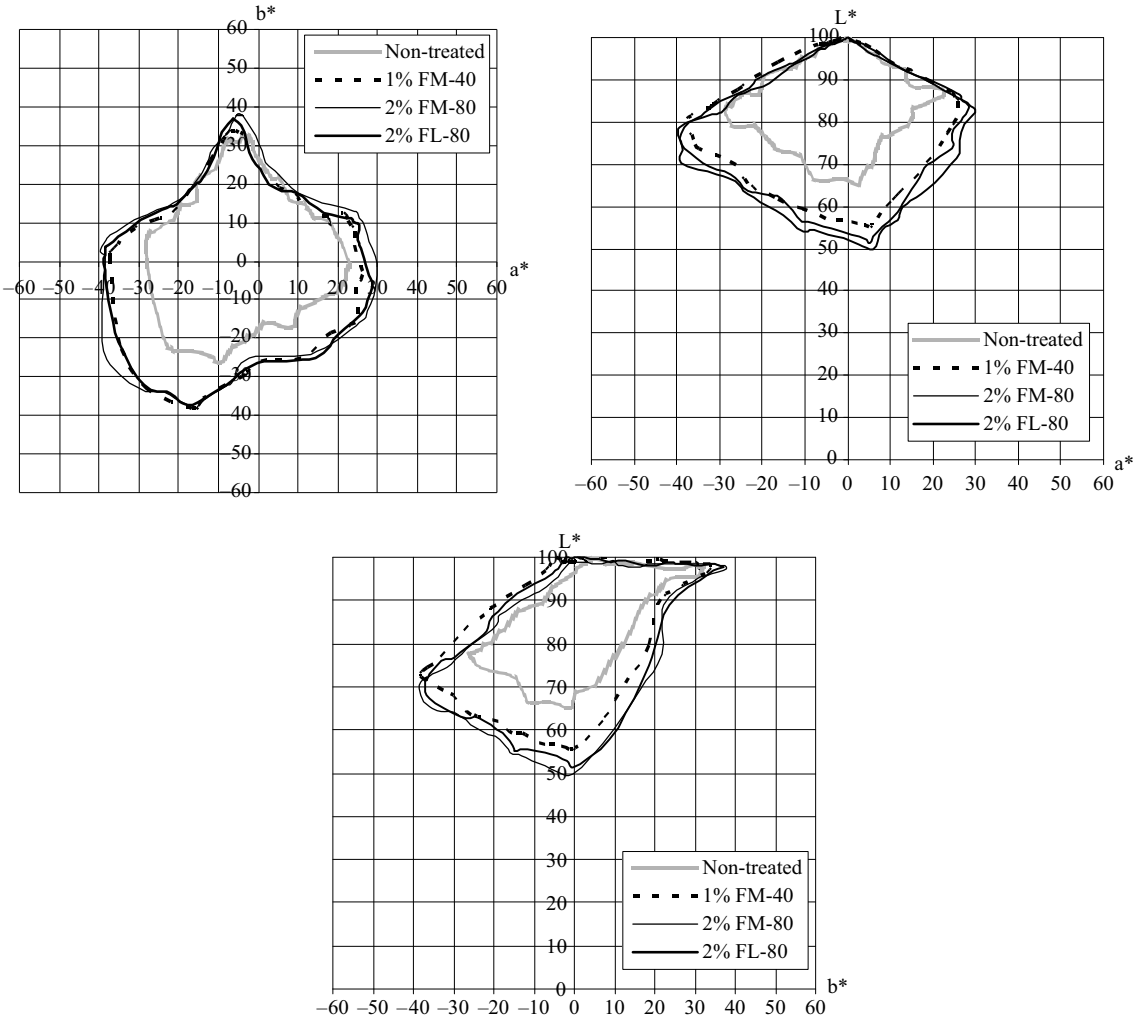

Table III K/S of the printed silk fabrics before and after washing

Condition of fabric treatment		K/S of the printed silk with the inks							
		Cyan		Magenta		Yellow		Black	
		Before washing	After washing	Before washing	After washing	Before washing	After washing	Before washing	After washing
Non-treated		0.42 ± 0.00	0.38 ± 0.01	0.45 ± 0.03	0.41 ± 0.02	1.18 ± 0.05	0.96 ± 0.07	1.41 ± 0.01	1.26 ± 0.04
Chitosan[a] (FL-80)	0.25	0.38 ± 0.04	0.40 ± 0.06	0.39 ± 0.02	0.40 ± 0.02	1.10 ± 0.04	1.08 ± 0.08	1.73 ± 0.03	1.75 ± 0.03
(%(w/v))	2	0.48 ± 0.04	0.47 ± 0.02	0.45 ± 0.03	0.45 ± 0.02	1.30 ± 0.01	1.28 ± 0.02	2.18 ± 0.04	2.24 ± 0.05
Chitosan[b] (FM-80)	0.25	0.4 ± 0.02	0.41 ± 0.02	0.37 ± 0.01	0.38 ± 0.01	0.99 ± 0.04	0.96 ± 0.03	2.54 ± 0.19	2.45 ± 0.06
(%(w/v))	1	0.45 ± 0.01	0.47 ± 0.03	0.47 ± 0.02	0.48 ± 0.01	1.29 ± 0.05	1.27 ± 0.06	2.20 ± 0.07	2.20 ± 0.02
	2	0.56 ± 0.06	0.55 ± 0.06	0.53 ± 0.01	0.51 ± 0.01	1.26 ± 0.09	1.23 ± 0.09	2.19 ± 0.14	2.15 ± 0.09
Chitosan[c] (FM-40)	0.25	0.42 ± 0.02	0.44 ± 0.02	0.41 ± 0.01	0.44 ± 0.02	1.14 ± 0.01	1.14 ± 0.04	1.92 ± 0.03	1.93 ± 0.04
(%(w/v))	1	0.45 ± 0.03	0.43 ± 0.02	0.45 ± 0.03	0.42 ± 0.03	1.34 ± 0.04	1.28 ± 0.05	2.54 ± 0.19	2.42 ± 0.24

Notes: [a]MW $= 1.2 \times 10^5$ g mol^{-1}; [b]MW $= 3.7 \times 10^5$ g mol^{-1}; [c]MW $= 8.5 \times 10^5$ g mol^{-1}; all have an 87-88% degree of *N*-deacetylation; data are shown as the mean ± 1 (SD) and are derived from three replicates

Table IV Relative colour strength of the printed silk fabrics after washing

Condition of treatment		Average of relative colour strength			
		Cyan	Magenta	Yellow	Black
Non-treated		0.82 ± 0.01	0.90 ± 0.00	0.81 ± 0.03	0.82 ± 0.02
Chitosan[a] (FL-80) (%(w/v))	0.25	1.04 ± 0.04	1.04 ± 0.01	0.98 ± 0.03	1.22 ± 0.00
	2	0.99 ± 0.03	1.00 ± 0.02	0.98 ± 0.02	1.23 ± 0.00
Chitosan[b] (FM-80) (%(w/v))	0.25	1.03 ± 0.03	1.03 ± 0.00	0.98 ± 0.01	0.98 ± 0.07
	1	1.03 ± 0.03	1.03 ± 0.01	1.04 ± 0.01	1.03 ± 0.02
	2	0.98 ± 0.00	0.96 ± 0.00	0.98 ± 0.01	0.98 ± 0.02
Chitosan[c] (FM-40) (%(w/v))	0.25	1.06 ± 0.01	1.06 ± 0.01	1.00 ± 0.02	1.01 ± 0.01
	1	0.95 ± 0.00	0.93 ± 0.00	0.96 ± 0.01	0.95 ± 0.03

Notes: [a]MW $= 1.2 \times 10^5$ g mol^{-1}; [b]MW $= 3.7 \times 10^5$ g mol^{-1}; [c]MW $= 8.5 \times 10^5$ g mol^{-1}; all have an 87-88% degree of *N*-deacetylation; data are shown as the mean ±1 (SD) and are derived from three replicates

Figure 12 Proposed scheme for the chitosan pre-treating agent and anionic pigment interactions

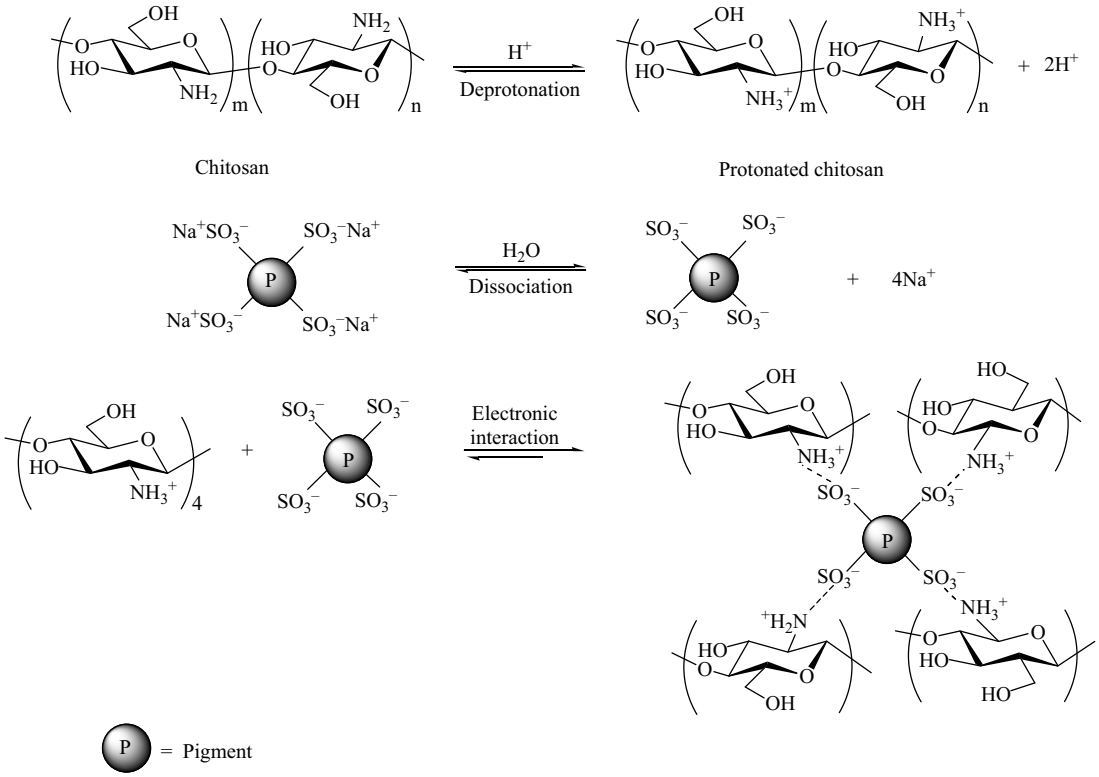

are both governed by the strength of adhesion and by the interfacial bonding between the pigment particles/ink binder/pre-treated fabric surfaces.

Conclusion

Anionically surface-modified organic pigment dispersions were used to prepare four coloured polyacrylate binder-based ink jet inks within the pH range of 8-9. These inks exhibited Newtonian flow in which the viscosity at 25°C remained constant at 2.5 mPa s under a 330 s^{-1} shear-strain rate. The surface tension of the inks was approximately 44 mN m^{-1} at 25°C, and the average particle sizes were approximately 100 nm. The zeta-potential of the inks was strongly negative, in the range of −42 to −51 mV, and they were stable for over ten months (for the magenta and black inks) or one year (for the cyan and yellow inks), as confirmed by SEM and TEM micrographs. The inks were shown to be suitable for printing by the piezo ink jet method on both non-treated and chitosan pre-treated silk fabrics. The anionically surface-modified pigmented ink interacted with the protonated amino groups of chitosan giving improved ink deposition and fixation on the fabric surface. The colour gamuts of the treated fabrics were wider with the chroma of the cyan colour being the most improved followed by that of the magenta colour. The chitosan pre-treatment produced the better crock fastness and wash fastness of the printed fabrics than the non-treated ones.

Table V Crock fastness of the non-treated and chitosan pre-treated silk fabrics

	Crock fastness							
	Dry stage				Wet stage			
Condition of treatment	C	M	Y	K	C	M	Y	K
Non-treated	4	4	4/5	4	4	4	4	4
Chitosan (FL-80) (%(w/v))	0.25	4/5	4/5	4	4/5	4/5	4/5	4
	0.5	4/5	4/5	4	4/5	4/5	4/5	4
	1	4	4	4	4/5	4	4	3/4
	2	4	4	4	4/5	4	4	3/4
Chitosan (FM-80) (%(w/v))	0.25	4/5	4	5	4/5	4/5	4/5	4
	0.5	4/5	4/5	4	4/5	4/5	4/5	4
	1	4/5	4/5	4	4/5	4/5	4	3/4
	2	4/5	4/5	4	4/5	4	4	3/4
Chitosan (FM-40) (%(w/v))	0.25	4/5	4/5	4	4/5	4/5	4/5	4
	0.5	4/5	4/5	4	4/5	4/5	4/5	4
	1	4/5	4/5	4	4/5	4/5	4/5	4

Note: 1, 2, 3, 4 and 5 are the rating levels for poor, fair, fairly good, good and excellent, respectively

References

AATCC Crockmeter Method 8-2001 (2002), *American Association of Textile Chemists and Colorists Technical Manual*, AATCC, Research Triangle Park, NC, pp. 17-19.

Bahmani, S.A., East, G.C. and Holme, I. (2000), "The application of chitosan in pigment printing", *Journal of the Society of Dyers Colorists*, Vol. 116 No. 3, pp. 94-9.

Bajaj, P. (2002), "Finishing of textile materials", *Journal of Applied Polymer Science*, Vol. 83 No. 3, pp. 631-59.

Belmont, J.A. (1994), "Process for preparing carbon materials with diazonium salts and resultant carbon products", US Patent 5,554,739, Application Date: 15 December.

Belmont, J.A., Johnson, J.E. and Adams, C.E. (1996a), "Aqueous inks and coatings containing modified carbon products", WO 96/18696A, 20 June.

Belmont, J.A., Johnson, J.E. and Adams, C.E. (1996b), "Ink jet ink formulations containing carbon black products", US Patent 5,571,311, 5 November 1996.

Berns, R.S. (2000), *Principles of Color Technology*, 3rd ed., Wiley, New York, NY.

Crini, G. and Badot, P.M. (2008), "Application of chitosan, a natural aminopolysaccharide, for dye removal from aqueous solution by adsorption process using batch studies: a review of recent literature", *Progress in Polymer Science*, Vol. 33 No. 4, pp. 399-447.

Fu, S. (2006) in Ujiie, H. (Ed.), *Pigmented Ink Formulation, Digital Printing of Textile*, Woodhead Publishing, Cambridge, pp. 220-30.

ISO 105-A03 (1993), "Textiles – tests for color fastness – part A03: grey scale for assessing staining", ISO 105-A03:1993.

ISO 105-C06 (1994), "Textiles – tests for color fastness – part C06: color fastness to domestic and commercial laundering", ISO 105-C06:1994.

Jason, H. (2004), "Surface modified pigments for ink jet ink application", available at: www.cabot.corp.com (accessed 8 November 2008).

Jocic, D., Vilchez, S., Topalovic, T., Nzvarro, A., Jovancic, P., Julia, M.R. and Erra, P. (2005), "Chitosan/acid dye interactions in wool dyeing system", *Carbohydrate Polymers*, Vol. 60 No. 1, pp. 51-9.

Johnson, J.E. and Belmont, J.A. (1997), "Modified colored pigments and ink jet inks, inks, and coatings containing modified colored pigments", US Patent 5,922,118, application date: 9 June.

Johnson, J.E., Nanying, B. and Galloway, C.P. (2002), "Modified pigments having improved dispersing properties", US Patent 6,478,863, application date: 12 November.

Leelajariyakul, S., Noguchi, H. and Kiatkamjornwong, S. (2008), "Surface-modified and micro-encapsulated pigmented inks for ink jet printing on textile fabrics", *Progress in Organic Coatings*, Vol. 62 No. 2, pp. 145-61.

Li, D. and Sun, G. (2007), "Coloration of textiles with self-dispersible carbon black nanoparticles", *Dyes and Pigments*, Vol. 72 No. 2, pp. 144-9.

Noguchi, H. and Shirota, K. (2006), "Formulation of aqueous ink jet ink", in Ujiie, E. (Ed.), *Digital Printing of Textile*, Woodhead Publishing, Cambridge, pp. 233-51.

Oktem, T. (2003), "Surface treatment of cotton fabrics with chitosan", *Coloration Technology*, Vol. 199 No. 4, pp. 241-6.

Phattanarudee, S., Chakvattanatham, K. and Kiatkamjornwong, S. (2009), "Pretreatment of silk fabric surface with amino compounds for ink jet printing", *Progress in Organic Coating*, Vol. 64 No. 4, pp. 405-18.

Provost, J., Freche, M., Hees, U., Kluge, M. and Weiser, J. (2009), "Ink-textile interactions in ink jet printing – the role of pretreatments", available at: www.users.ecs.soton.ac.uk (accessed 1 January 2009).

Silverstein, R.M., Bassler, G.C. and Morrill, T.C. (1991), *Spectrometric Identification of Organic Compounds*, 5th ed., Wiley, Singapore, pp. 123-8.

Yuen, C.W.M., Ku, S.K.A., Kan, C.W. and Choi, P.S.R. (2007), "Enhancing textile ink-jet printing with chitosan", *Coloration Technology*, Vol. 123 No. 4, pp. 267-70.

About the authors

K. Chakvattanatham is currently a Technical Supervisor at Standard Can Company, Samutprakan, Thailand. She works in R&D and Customer Service Department and is involved in quality control assessment of packaging for food and paints. She obtained her BSc degree in Industrial Chemistry from King Mongkut's Institute of Technology Ladkrabang, and her MSc degree in Printing Technology from the Department of Imaging and Printing Technology, Faculty of Science, Chulalongkorn University, in 2006. Her research expertise is in ink jet ink printing.

S. Phattanarudee is an Instructor at the Department of Imaging and Printing Technology of Chulalongkorn University, Bangkok, Thailand. She obtained her BSc degree in Materials Science from Chulalongkorn University, and her MSc and PhD degrees in Polymer Science and Engineering in 2003 from Lehigh University, Bethlehem, Pennsylvania, USA. Her research areas are emulsion polymerization and coatings.

S. Kiatkamjornwong is currently a Full Professor of Polymer Science and Engineering at the Department of Imaging and Printing Technology, Faculty of Science, Chulalongkorn University, Bangkok, Thailand. She obtained her BSc and MSc degrees in Chemistry and Physical Chemistry, respectively, from the Faculty of Science, Chulalongkorn University, and her PhD degree in Polymer Science and Engineering from Lehigh University, Bethlehem, Pennsylvania, USA, in 1983. Her research interests are in the areas of superabsorbent polymers, imbiber beads, modification of green polymers, digital printing and environment in polymers and printing. S. Kiatkamjornwong is the corresponding author and can be contacted at: ksuda@chula.ac.th

To purchase reprints of this article please e-mail: **reprints@emeraldinsight.com**
Or visit our web site for further details: **www.emeraldinsight.com/reprints**

วารสารราชบัณฑิตยสถาน

วารสารราย ๓ เดือน

ที่ปรึกษา

ศาสตราจารย์ ดร.ปัญญา บริสุทธิ์ *นายกราชบัณฑิตยสถาน*

ดร.โสภา ชูพิกุลชัย ชปีลมันน์ *อุปนายกราชบัณฑิตยสถาน*

ประธานคณะบรรณาธิการ

รองศาสตราจารย์อัศนีย์ ชูอรุณ *ราชบัณฑิต*

คณะบรรณาธิการ

รองศาสตราจารย์ ดร.ชยันต์ พิเชียรสุนทร *ราชบัณฑิต*

ศาสตราจารย์ ดร.มงคล เดชนครินทร์ *ราชบัณฑิต*

ศาสตราจารย์ ดร.ณัชชา พันธุ์เจริญ *ภาคีสมาชิก*

รองศาสตราจารย์ ดร.นิตยา กาญจนะวรรณ *ภาคีสมาชิก*

รองศาสตราจารย์ ดร.ผลิน ภู่จรูญ *ภาคีสมาชิก*

รองศาสตราจารย์มาลิทัต พรหมทัตตเวที *ภาคีสมาชิก*

รองศาสตราจารย์ ดร.วรวุฒิ หิรัญรักษ์ *ภาคีสมาชิก*

ศาสตราจารย์ ดร.สมชาย วงศ์วิเศษ *ภาคีสมาชิก*

นางสาวกนกวลี ชูชัยยะ *เลขาธิการราชบัณฑิตยสถาน*

นายประภาส แก้วสวรรค์ *ฝ่ายประสานงาน*

นางสาวศยามล แสงมณี *ฝ่ายประสานงาน*

นางสาวสมทรง ศกุนตนาค *ฝ่ายประสานงาน*

กองบรรณาธิการ

นางสาวสุปัญญา ชมจินดา *ผู้อำนวยการกองวิทยาศาสตร์*

นางณัฐมาตย์ มูสิกะเจริญ *นักวรรณศิลป์ชำนาญการ*

นายพรรษา ไทรงาม *นักวรรณศิลป์ชำนาญการ*

นางสาวรัตติกาล ศรีอำไพ *นักวรรณศิลป์ชำนาญการ*

นางสาวอารี พลดี *นักวรรณศิลป์ชำนาญการ*

นางสาวลักขณาวรรณ อนันธวัช *นักวรรณศิลป์ปฏิบัติการ*

ผู้จัดการ

นางนัยนา วราอัศวปติ *เลขานุการกรม*

The Journal of the Royal Institute of Thailand

Quarterly Journal

ADVISORY BOARD

Panya Borisutdhi	*President of the Royal Institute*
Sobha Chupikulchai Spielmann	*Vice-President of the Royal Institute*

EDITOR-IN-CHIEF

Asanee Chooarun	*FRI*

EDITORIAL BOARD

Chayan Picheansoonthon	*FRI*
Mongkol Dejnakarintra	*FRI*
Malithat Promathatavedi	*AFRI*
Natchar Pancharoen	*AFRI*
Nitaya Kanchanawan	*AFRI*
Palin Phoocharoon	*AFRI*
Somchai Wongwises	*AFRI*
Vorawoot Hirunruk	*AFRI*
Kanokwalee Chuchaiya	*Secretary-General*
Prapas Kaewsawan	*Coordinator*
Sayamol Sangmanee	*Coordinator*
Somsong Sakuntanak	*Coordinator*

DEPARTMENTAL STAFF

Supanya Chomchinda	*Director of Science Division*
Aree Poldee	*Literateur, Professional Level*
Nutthamard Musikacharoen	*Literateur, Professional Level*
Phansa Sai-ngam	*Literateur, Professional Level*
Rattikal Sriamphai	*Literateur, Professional Level*
Luckanawan Anantavat	*Literateur, Practitioner Level*

MANAGER

Naiyana Vara-asvapati	*Secretary*

วารสารราชบัณฑิตยสถาน
The Journal of the Royal Institute of Thailand

ปีที่ ๓๕ ฉบับที่ ๑ มกราคม-มีนาคม ๒๕๕๓ Volume 35 Number 1 January-March 2010

พรปีใหม่	๑	**NEW YEAR'S GREETINGS**
ประธานคณะบรรณาธิการแถลง	๒	**EDITOR-IN-CHIEF'S NOTE**
สำนักธรรมศาสตร์และการเมือง		**THE ACADEMY OF MORAL AND POLITICAL SCIENCES**
มนุษยนิยมแนวปรัชญาจีน *สิทธิ์ บุตรอินทร์*	๓	**The Chinese Humanism** *Siddhi Butr-Indr*
อัตถิภาวนิยม จิตวิทยาอัตถิภาวะ และการดำรงอยู่ของมนุษย์ในปัจจุบัน *นพมาศ อุ้งพระ*	๒๙	**Existentialism, Existential Psychology and Current Human Existence** *Nopamas Oungphra*
การก้าวเข้าสู่เศรษฐกิจคาร์บอนต่ำด้วยการซื้อขายคาร์บอนเครดิต *วรวุฒิ หิรัญรักษ์*	๕๐	**Moving toward Low Carbon Economy through Carbon Credit Trading** *Vorawoot Hirunruk*
สำนักวิทยาศาสตร์		**THE ACADEMY OF SCIENCE**
การใช้สารละลายเคมีปรับปรุงคุณภาพของดอกไม้หลังการเก็บเกี่ยว *สายชล เกตุษา*	๘๐	**Usage of Preservative Solutions Improves Quality of Cut Flowers** *Saichol Ketsa*

ปีที่ ๓๕ ฉบับที่ ๑ มกราคม-มีนาคม ๒๕๕๓ Volume 35 Number 1 January-March 2010

การพัฒนาแหล่งพลังงานทดแทนเพื่อผลิตไฟฟ้าในประเทศ *ปรีดา วิบูลย์สวัสดิ์* *วุฒิ พันธุมนาวิน*	๙๒	**Alternative Energy Sources for Electrical Power Development of Thailand** *Prida Wibulswas* *Vutthi Bhanthumnavin*
ระบบการจัดการพลังงานในอุตสาหกรรม *ศิริจันทร์ ทองประเสริฐ* *มานิจ ทองประเสริฐ*	๙๙	**Energy Management System in Industry** *Sirichan Thongprasert* *Manit Thongprasert*
การวัด Bidirectional Reflectance Distribution Function และการจำลองแบบการสะท้อนของผ้าไหม *สุดา เกียรติกำจรวงศ์* *บุญยเกียรติ ฉายเทพประสิทธิ์* *ชวาล คูร์พิพัฒน์*	๑๐๙	**Measurement of Bidirectional Reflectance Distribution Function and Reflectance Modeling of Silk Fabrics** *Suda Kiatkamjornwong* *Boonyakiat Chaitepprasith* *Chawan Koopipat*
สำนักศิลปกรรม		**THE ACADEMY OF ARTS**
ภาษารักของฌอร์ฌ ซ็อง *จินตนา ดำรงค์เลิศ*	๑๑๘	**George Sand's Language of Love** *Chintana Damronglerd*
ตำนานเดี่ยวขิมเพลงลาวแพนทางของ หลวงประดิษฐไพเราะ (ศร ศิลปบรรเลง) *ชนก สาคริก*	๑๒๗	**The History of the Khim Solo of Lao Phaen: Luang Praditpairoh (Sorn Silapabanleng) Version** *Chanok Sakrik*
ลักษณะคำประพันธ์ของบทละครเรื่องโรเมโอและจูเลียต พระราชนิพนธ์ในพระบาทสมเด็จพระมงกุฎเกล้าเจ้าอยู่หัว *โชษิตา มณีใส*	๑๓๗	**The Versification of *Romeo and Juliet* written by King Rama VI** *Chosita Maneesai*

ปีที่ ๓๕ ฉบับที่ ๑ มกราคม-มีนาคม ๒๕๕๓ Volume 35 Number 1 January-March 2010

ปกิณกะ

MISCELLANEOUS

รูปปั้นอาถรรพ์ใน La Vénus d' Ille ของปรอสแปร์ เมรีเม
จุฑารัตน์ เบญจฤทธิ์
๑๕๕

A Cursed Statue in *La Vénus d' Ille* of Prospère Mérimée
Judharat Bencharit

ปฏิทินฮิจเราะห์ในประเทศไทย
ลอย ชุนพงษ์ทอง
๑๖๕

The Hijrah Calendar of Thailand
Loy Chunpongtong

นีลส์ โบร์
สุทัศน์ ยกส้าน
๑๗๓

Niels Bohr
Suthat Yoksan

การวัด Bidirectional Reflectance Distribution Function และการจำลองแบบการสะท้อนแสงของผ้าไหม*

สุดา เกียรติกำจรวงศ์**
ภาคีสมาชิก สำนักวิทยาศาสตร์ราชบัณฑิตยสถาน
บุญยเกียรติ ฉายเทพประสิทธิ์**
ชวาล คูร์พิพัฒน์**

บทคัดย่อ

ผ้าไหมเป็นสิ่งทอที่มีความมันวาวมากกว่าสิ่งทอประเภทอื่น เนื่องจากผ้าไหมมีลักษณะการสะท้อนแสงที่มีความเฉพาะตัว ดังนั้น งานวิจัยนี้จึงศึกษาลักษณะการสะท้อนแสงของผ้าไหม โดยวัดค่าบีอาร์ดีเอฟ (BRDF, Bidirectional Reflectance Distribution Function) และนำเสนอแบบจำลองการสะท้อนแสงของพื้นผิวผ้าไหมที่คำนึงถึงการสะท้อนของแสงฟุ้งและแสงกล้า โดยใช้วิธีการหาค่าความผิดพลาดกำลังสองน้อยสุด (least-square error) หาความสัมพันธ์ระหว่างค่าที่วัดกับแบบจำลอง เมื่อทดสอบแบบจำลองที่ได้พบว่า แบบจำลองที่นำเสนอนี้มีความสัมพันธ์กับบีอาร์ดีเอฟที่วัดได้ของผ้าไหมมากกว่าแบบจำลองการสะท้อนแสงที่มีอยู่ทั่วไป ได้แก่ แบบจำลองการสะท้อนแสงของฟอง แบบจำลองการสะท้อนแสงของโอเรนและนายาร์ และแบบจำลองการสะท้อนแสงของทอร์แรนซ์และสแปร์โรว์ ผู้วิจัยสามารถพยากรณ์ค่าการสะท้อนแสง วิเคราะห์ และอธิบายลักษณะการสะท้อนแสงของผ้าไหมได้จากแบบจำลองที่นำเสนอนี้

คำสำคัญ : **บีอาร์ดีเอฟ, ผ้าไหม, แบบจำลองการสะท้อนแสง**

คำนำ

ในยุคดิจิทัลที่การค้าขายในอินเทอร์เน็ตได้รับความนิยมอย่างกว้างขวาง ความสวยงามและเหมือนจริงของสินค้าที่เป็นผ้าไหม หรือผลิตภัณฑ์อื่นจากผ้าไหมเป็นสิ่งที่มีผลต่อการตัดสินใจซื้อของผู้บริโภค ความมันวาว (gloss) เป็นปัจจัยด้านคุณรูปที่สำคัญอย่างหนึ่งที่เกิดจากสมบัติการสะท้อนแสงของผ้าไหม และมุมของแสงที่ตกกระทบและมุมมอง พื้นผิววัตถุใด ๆ สามารถเกิดการสะท้อนแสงใน ๓ ลักษณะ คือ การสะท้อนแสงแบบฟุ้ง (diffuse reflection) การสะท้อนแสงแบบกล้า (specular reflection) และการสะท้อนแสงแบบผสมระหว่างแสงฟุ้งกับแสงกล้า (mixed reflection) [Wyszecki and Stiles, 2000] ดังรูปที่ ๑

รูปที่ ๑ ลักษณะการสะท้อนแสงแบบฟุ้ง แบบกล้า และแบบผสม

ปรกติพื้นผิววัตถุส่วนใหญ่มีการสะท้อนแสงแบบผสม วัตถุที่มีความมันวาวมากจะสะท้อนแสงกล้าออกมามาก วัตถุที่มีผิวด้านหรือผิวไม่เรียบจะสะท้อนแสงฟุ้งออกมามาก ลักษณะการสะท้อนแสงเหล่านี้ ทำให้มีผู้สร้างแบบจำลองการสะท้อนแสงของพื้นผิว

* บทความนี้ปรับปรุงจากการบรรยายผลงานทางวิชาการในที่ประชุมสำนักวิทยาศาสตร์ เมื่อวันที่ ๑๗ กุมภาพันธ์ พ.ศ. ๒๕๕๓

** ภาควิชาวิทยาศาสตร์ทางภาพถ่ายและเทคโนโลยีทางการพิมพ์ คณะวิทยาศาสตร์ จุฬาลงกรณ์มหาวิทยาลัย ถนนพญาไท แขวงวังใหม่ เขตปทุมวัน กรุงเทพฯ ๑๐๓๓๐

วัตถุขึ้นมา เพื่อใช้พยากรณ์ค่าการสะท้อนแสงของพื้นผิววัตถุและได้นำไปใช้ในโปรแกรมสำหรับสร้างภาพสามมิติในคอมพิวเตอร์ เช่น ภาพแบบจำลองสินค้า ภาพการ์ตูนแอนิเมชัน ภาพยนตร์ ความเหมือนจริงของรูปที่สร้างขึ้นด้วยโปรแกรมเหล่านี้ขึ้นอยู่กับความสามารถในการจำลองค่าการสะท้อนแสงของแบบจำลอง แบบจำลองชนิดหนึ่งอาจเหมาะกับวัตถุที่มีลักษณะผิวอย่างหนึ่ง แต่อาจไม่เหมาะกับวัตถุที่มีพื้นผิวแตกต่างออกไป

Bidirectional Reflectance Distribution Function (BRDF) เป็นฟังก์ชันการสะท้อนแสงในทิศทางต่าง ๆ ของพื้นผิววัตถุ เมื่อเปลี่ยนมุมตกกระทบของแสงแบบจำลอง โดยทั่วไปกำหนดให้การสะท้อนแสงรวมเป็นผลรวมระหว่างการสะท้อนแสงแบบฟุ้งกับการสะท้อนแสงแบบกล้า ซึ่งมีตัวแปรเป็นมุมตกกระทบและมุมรับภาพ [Dana et al., 1999] ดังรูปที่ ๒

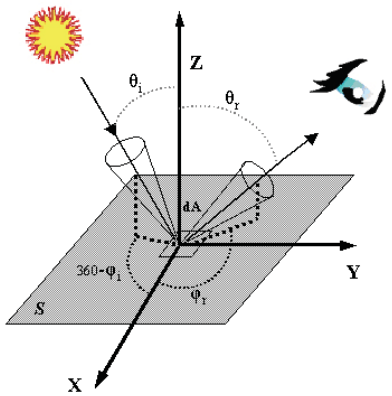

รูปที่ ๒ BRDF ของพื้นผิววัตถุใด ๆ

สมการรูปแบบทั่วไปของ BRDF สามารถเขียนได้ดังสมการที่ ๑

$$L_r = k_d L_d + k_s L_s \qquad (๑)$$

โดยที่

L_r คือ การสะท้อนแสงของวัตถุ

L_d คือ การสะท้อนแสงแบบฟุ้ง (diffuse reflection)

L_s คือ การสะท้อนแสงแบบกล้า (specular reflection)

k_d คือ สัมประสิทธิ์ของการสะท้อนแสงแบบฟุ้ง (diffuse components reflection coefficient)

k_s คือ สัมประสิทธิ์ของการสะท้อนแสงแบบแสงกล้า (specular components reflection coefficient)

$k_d + k_s = ๑$

แบบจำลองการสะท้อนแสงของพื้นผิววัตถุมีอยู่ด้วยกันหลายแบบ ซึ่งสามารถพยากรณ์การสะท้อนแสงแบบฟุ้งและแบบกล้าที่แตกต่างกัน แบบจำลองพื้นฐานที่มองพื้นผิววัตถุมีการสะท้อนแสงฟุ้งแบบอุดมคติคือ แบบจำลองการสะท้อนแสงแบบแลมเบอร์เทียน (Lambertian reflection model) [Dana et al., 1999] ส่วนแบบจำลองการสะท้อนแสงของโอเรนและนายาร์ (Oren and Nayar reflection model) [Oren and Nayar, 1995] สามารถพยากรณ์การสะท้อนแสงแบบฟุ้งได้แม่นยำมาก เพราะรวมลักษณะความขรุขระของพื้นผิววัสดุไว้ในแบบจำลองด้วย แบบจำลองที่พยากรณ์การสะท้อนแสงแบบกล้า ได้แก่ แบบจำลองของทอร์แรนซ์และสแปร์โรว์ [Torrance and Sparrow], แบบจำลองการสะท้อนแสงของคุก-ทอร์แรนซ์ (Cook-Torrance reflection model) [Dana et al., 1999] และแบบจำลองการสะท้อนแสงของบลินน์ (Blinn reflection model) [Blinn, 1977] แบบจำลองแต่ละแบบได้คำนึงถึงปริมาณแสงสะท้อนแบบกล้าที่รวมปัจจัยด้านความขรุขระของพื้นผิวเอาไว้ด้วย และแบบจำลองที่เหมาะสมสำหรับพยากรณ์การสะท้อนแสงแบบผสม ก็คือ แบบจำลองการสะท้อนแสงของฟอง (Phong reflection model) [Phong, 1975] ซึ่งเหมาะสมกับพื้นผิวเรียบ ๆ เช่น พลาสติก ในขณะที่แบบจำลองการสะท้อนแสงของวาร์ด (Ward reflection model) [Ward, 1992] และแอชิกมิน-เชอร์ลีย์ (Ashikmin-Shirley reflection model) [Ashikmin and Shirley, 2000] ได้ปรับปรุงแบบจำลองการสะท้อนแสงของฟอง (Phong) ให้เหมาะสมมากขึ้นกับลักษณะพื้นผิวที่หลากหลายและไม่สม่ำเสมอ แต่แบบจำลองที่กล่าวมาข้างต้นยังไม่มีแบบใดที่สร้างขึ้นเพื่อใช้กับการสะท้อนแสงของพื้นผิวผ้าไหมโดยเฉพาะ ดังนั้น งานวิจัยนี้จึงศึกษาลักษณะการสะท้อนแสงของพื้นผิวผ้าไหม โดยการวัดค่าบีอาร์ดีเอฟและนำค่าที่วัดได้มาสร้างเป็นแบบจำลองการสะท้อนแสงที่สัมพันธ์กับค่าการสะท้อนแสงของพื้นผิวผ้าไหม

อุปกรณ์และวิธีการ

การทดลองนี้ได้ใช้ผ้าไหมสีขาวที่ทอด้วยลายขัด ๓ ตัวอย่าง ผ้าไหมตัวอย่างที่ ๑ ใช้เส้นไหม ๒ เส้นในการทอและเส้นไหมมาจากร้านไหมไทยคอลเล็กชัน ผ้าไหมตัวอย่างที่ ๒ และตัวอย่างที่ ๓ ใช้เส้นไหม ๒ และ ๔ เส้นในการทอและเส้นไหมมาจากร้านจิม ทอมป์สัน ซึ่งมีลักษณะพื้นผิวตามรูปที่ ๓ ถึง รูปที่ ๕ ตามลำดับ งานวิจัยนี้ได้แบ่งการทดลองออกเป็น ๒ ขั้นตอน ได้แก่ การทดลองตอนที่ ๑ เป็นการวัดค่าบีอาร์ดีเอฟของผ้าไหมทั้ง ๓ ตัวอย่าง ด้วยเครื่องโกนิโอสเปกโทรโฟโตมิเตอร์ (ยี่ห้อ มุราคามิ รุ่น จีเอสพี-๒๕ ประเทศญี่ปุ่น) ซึ่งได้วัดค่าที่ศูนย์การวิจัยฟรอนเทียร์เมดิคัลเอนจิเนียริง (Research Center for Frontier Medical Engineering) แห่งมหาวิทยาลัยชิบะ ประเทศญี่ปุ่น โดยใช้มุมของแหล่งกำเนิดแสง ที่ ๐, -๑๕, -๓๐, -๔๕, -๖๐ และ -๗๕ องศา และใช้มุมรับภาพที่ -๗๕, -๖๐, -๔๕, -๓๐, -๑๕, ๐, ๑๕, ๓๐, ๔๕, ๖๐ และ ๗๕ องศา ตามลำดับ แล้วจึงนำค่าบีอาร์ดีเอฟที่ วัดได้มาเขียนกราฟเชิงขั้ว เพื่อทำให้สามารถวิเคราะห์ลักษณะการสะท้อนแสงของพื้นผิวผ้าไหม พร้อมทั้งสามารถหาลักษณะเฉพาะตัวของการสะท้อนแสงของผ้าไหมได้ ผู้วิจัยได้ทดลองตอนที่ ๒ ซึ่งเป็นการนำเสนอแบบจำลองการสะท้อนแสงของพื้นผิวผ้าไหม โดยได้ปรับปรุงจากแบบจำลองการสะท้อนแสงของฟอง และทดสอบแบบจำลองด้วยการหาความผิดพลาดที่น้อยที่สุดจากการเปรียบเทียบค่าที่คำนวณได้จากแบบจำลองการสะท้อนแสงที่นำเสนอกับค่าบีอาร์ดีเอฟที่วัดได้จากผ้าไหม และความผิดพลาดจากการเปรียบเทียบค่าที่คำนวณได้จากแบบจำลองการสะท้อนแสงที่ใช้อยู่โดยทั่วไป ได้แก่ แบบจำลองการสะท้อนแสงของฟอง แบบจำลองการสะท้อนแสงของโอเรนและนายาร์ แบบจำลองการสะท้อนแสงของวาร์ด และแบบจำลองการสะท้อนแสงของแอชิกมินและเชอร์ลีย์ เริ่มแรกผู้วิจัยได้หาค่าคงตัวในแบบจำลองต่าง ๆ ที่สัมพันธ์กับลักษณะการสะท้อนแสงของผ้าไหม โดยใช้วิธีหาค่าความผิดพลาดกำลังสองน้อยสุด (least-square error) จึงคำนวณค่าการสะท้อนแสงจากแบบจำลองที่มีค่าคงตัวครบ แล้วจึงนำค่าที่คำนวณได้มาเปรียบเทียบหาความผิดพลาดกับค่าการสะท้อนแสงจากผ้าไหม โดยใช้วิธีการหาค่ารากที่สองของกำลังสองเฉลี่ย (root-mean-square error) เพื่อหาแบบจำลองการสะท้อนแสงที่สัมพันธ์กับค่าการสะท้อนแสงของผ้าไหมมากที่สุด

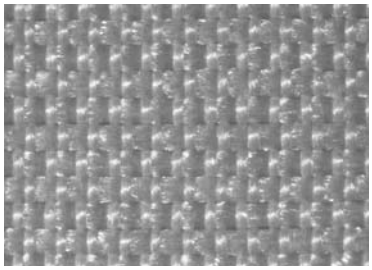

รูปที่ ๓
ลักษณะพื้นผิวของผ้าไหม
ตัวอย่างที่ ๑

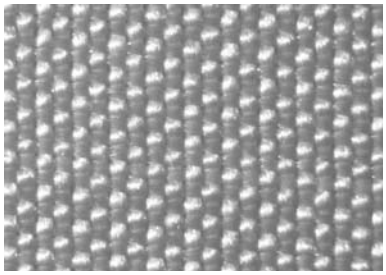

รูปที่ ๔
ลักษณะพื้นผิวของผ้าไหม
ตัวอย่างที่ ๒

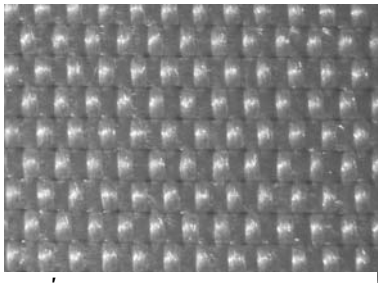

รูปที่ ๕
ลักษณะพื้นผิวของผ้าไหม
ตัวอย่างที่ ๓

ผลการทดลองและวิจารณ์

ตอนที่ ๑ การวัดค่าบีอาร์ดีเอฟของผ้าไหม

ค่าบีอาร์ดีเอฟของผ้าไหมสีขาว ๓ ตัวอย่าง สามารถเขียนเส้นโค้งในระบบพิกัดเชิงขั้ว ได้ตามรูปที่ ๖-๑๑ โดยใช้มุมของแหล่งกำเนิดแสง ๐, -๑๕, -๓๐, -๔๕, -๖๐ และ -๗๕ องศา ตามลำดับ เส้นโค้งทั้ง ๖ เส้นนี้ เส้นสีแดง (+) คือ ค่าบีอาร์ดีเอฟของผ้าไหมตัวอย่างที่ ๑ เส้นสีเขียว (*) คือ ค่าบีอาร์ดีเอฟของผ้าไหมตัวอย่างที่ ๒ และเส้นสีน้ำเงิน (o) คือ ค่าบีอาร์ดีเอฟของผ้าไหมตัวอย่างที่ ๓

เส้นโค้งของค่าบีอาร์ดีเอฟของผ้าไหมแสดงให้เห็นลักษณะการสะท้อนแสงของพื้นผิวผ้าไหมซึ่งแสงกระจายตัวออกรอบทิศทาง และเป็นสมบัติของการสะท้อนแสงแบบฟุ้ง การกระจายตัวของค่าการสะท้อนแสงยังมีแนวโน้มที่เบ้ในทิศทางเดียวกันกับทิศทางของแหล่งกำเนิดแสง แสดงให้เห็นว่า ค่าการสะท้อนแสงกระจายตัวไปหนาแน่นในทิศทางตรงข้ามกับทิศทางของแหล่งกำเนิดแสง ซึ่งเป็นทิศทางของแสงสะท้อนแบบกล้า ดังนั้น จึงสรุปได้ว่า แสงที่สะท้อนออกจากพื้นผิวของผ้าไหมมีการสะท้อนแสงแบบผสม

อย่างไรก็ตาม เมื่อพิจารณาเส้นโค้งบีอาร์ดีเอฟของพื้นผิวผ้าไหมในส่วนที่เป็นแสงฟุ้ง พบว่าเป็นการสะท้อนแบบฟุ้งที่ไม่เป็นอุดมคติ เพราะแสงสะท้อนมีความเข้มไม่เท่ากันในแต่ละทิศทาง และเมื่อพิจารณาในส่วนที่เป็นแสงกล้า จะพบว่า มุมของแสงสะท้อนที่มีความเข้มสูงสุดไม่เป็นมุมตรงข้ามกับมุมของแหล่งกำเนิดแสง แต่เกิดการเลื่อนตัวไปในทิศทางอื่น ซึ่งแสดงให้เห็นว่า แสงที่สะท้อนจากพื้นผิวผ้าไหมเกิด off-specular

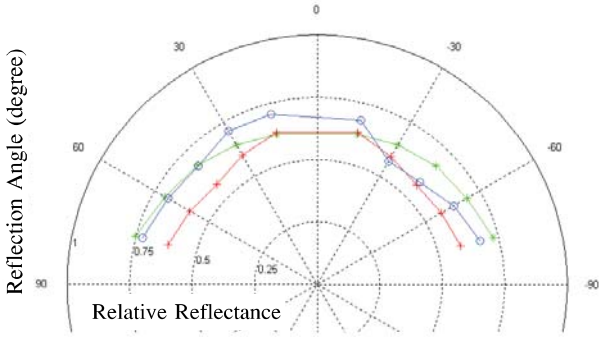

รูปที่ ๖ ค่าบีอาร์ดีเอฟของผ้าไหมตัวอย่างที่ ๑(+) ตัวอย่างที่ ๒(*) และตัวอย่างที่ ๓(o) เมื่อใช้มุมตกกระทบ ๐ องศา

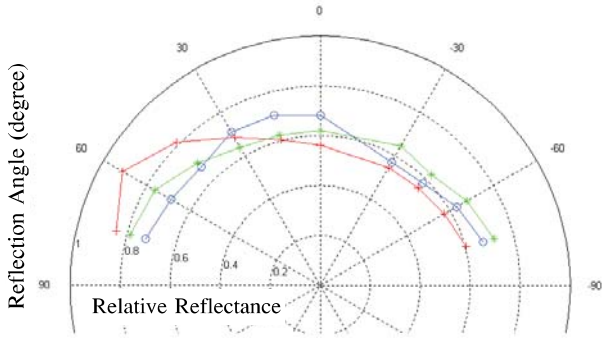

รูปที่ ๗ ค่าบีอาร์ดีเอฟของผ้าไหมตัวอย่างที่ ๑(+) ตัวอย่างที่ ๒(*) และตัวอย่างที่ ๓(o) เมื่อใช้มุมตกกระทบ -๑๕ องศา

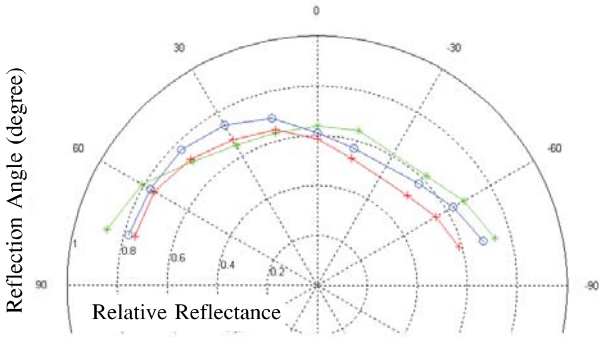

รูปที่ ๘ ค่าบีอาร์ดีเอฟของผ้าไหมตัวอย่างที่ ๑(+) ตัวอย่างที่ ๒(*) และตัวอย่างที่ ๓(o) เมื่อใช้มุมตกกระทบ -๓๐ องศา

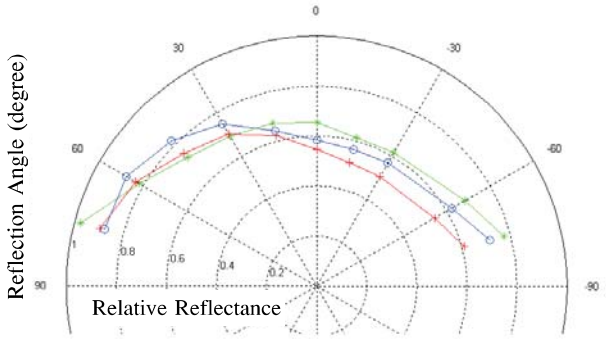

รูปที่ ๙ ค่าบีอาร์ดีเอฟของผ้าไหมตัวอย่างที่ ๑(+) ตัวอย่างที่ ๒(*) และตัวอย่างที่ ๓(o) เมื่อใช้มุมตกกระทบ -๔๕ องศา

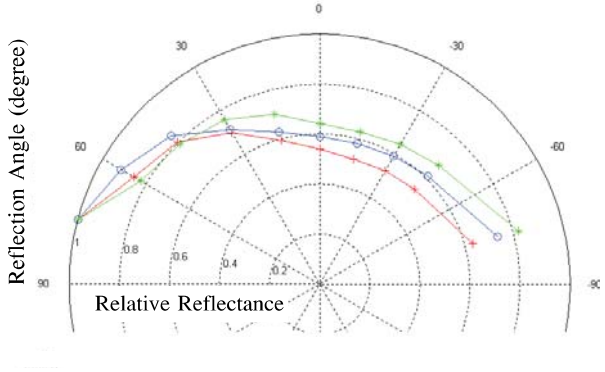

รูปที่ ๑๐ ค่าบีอาร์ดีเอฟของผ้าไหมตัวอย่างที่ ๑(+) ตัวอย่างที่ ๒(*) และตัวอย่างที่ ๓(o) เมื่อใช้มุมตกกระทบ -๖๐ องศา

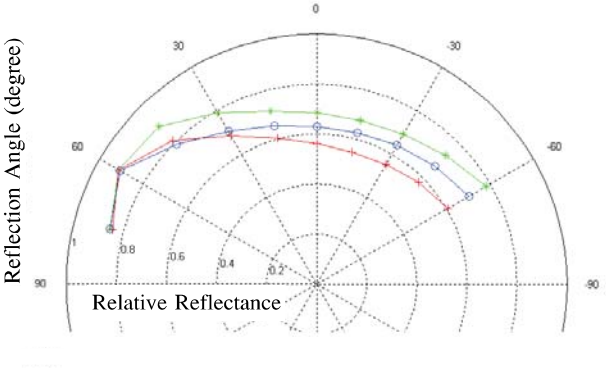

รูปที่ ๑๑ ค่าบีอาร์ดีเอฟของผ้าไหมตัวอย่างที่ ๑(+) ตัวอย่างที่ ๒(*) และตัวอย่างที่ ๓(o) เมื่อใช้มุมตกกระทบ -๗๕ องศา

ตอนที่ ๒ การเสนอแบบจำลองการสะท้อนแสงและการทดสอบแบบจำลอง

เนื่องจากสมบัติการสะท้อนแสงของผ้าไหมเป็นการสะท้อนแสงแบบผสม ผู้วิจัยจึงได้ปรับปรุงแบบจำลองการสะท้อนแสงของฟอง ในส่วนที่เป็นการสะท้อนแสงแบบฟุ้งและแบบกล้า โดยเพิ่มพารามิเตอร์ α และ β เพื่อปรับความกว้างของกรวยแสง และเพิ่มพารามิเตอร์ θ_{off} และ ϕ_{off} สำหรับปรับมุมสะท้อนแสงแบบ off-specular ดังแสดงในสมการที่ ๒

$$L(\theta_i,\theta_r,\phi_i,\phi_r) = k_d \cos^{\alpha}(\theta_r,\phi_r) + k_s \cos^{\beta}[\theta_r + (\theta_i - \theta_{off}), \phi_r + (\phi_i - \phi_{off})] \quad (๒)$$

โดยที่

L คือ ค่าการสะท้อนแสงของผ้าไหม

k_d คือ สัมประสิทธิ์ความเข้มแสงของแสงฟุ้ง

k_s คือ สัมประสิทธิ์ความเข้มแสงของแสงกล้า

α คือ ค่าควบคุมความกว้างของกรวยแสงฟุ้ง (diffuse lobe)

β คือ ค่าควบคุมความกว้างของกรวยแสงกล้า (specular lobe)

θ_r คือ มุมรับภาพในแนวมุมเงย (elevation)

θ_i คือ มุมของแหล่งกำเนิดแสงในแนวมุมเงย (elevation)

θ_{off} คือ มุม off-specular ในแนวมุมเงย (elevation)

ϕ_r คือ มุมรับภาพในแนวมุมกวาด (azimuth)

ϕ_i คือ มุมของแหล่งกำเนิดแสงในแนวมุมกวาด (azimuth)

ϕ_{off} คือ มุม off-specular ในแนวมุมกวาด (azimuth)

ผู้วิจัยได้ทดสอบแบบจำลองโดยนำค่าบีอาร์ดีเอฟที่คำนวณจากแบบจำลองการสะท้อนแสงต่าง ๆ ที่กล่าวมาข้างต้น มาเปรียบเทียบกับค่าบีอาร์ดีเอฟที่วัดจากผ้าไหม แล้วคำนวณหาความผิดพลาดโดยใช้วิธีหารากที่สองของกำลังสองเฉลี่ย (RMS) ซึ่งแสดงผลในตารางที่ ๑

เมื่อพิจารณาผลจากตารางที่ ๑ แล้วจะเห็นว่า แบบจำลองการสะท้อนแสงที่นำเสนอนี้ให้ความผิดพลาดน้อยกว่าแบบจำลองอื่น เช่น ผ้าไหมตัวอย่างที่ ๓ ใช้มุมของแหล่งกำเนิดแสง -๖๐ องศา มีค่า RMS ของแบบจำลองที่เสนออยู่ที่ ๐.๐๒๑๔ แบบจำลองของฟองมีค่าอยู่ที่ ๐.๐๙๑๘ แบบจำลองของโอเรนและนายาร์อยู่ที่ ๐.๑๖๑๐ แบบจำลองของวาร์ด อยู่ที่ ๐.๑๐๓๖ และแบบจำลองของแอชิกมิน อยู่ที่ ๐.๐๘๔๓ ซึ่งแสดงว่า ค่าบีอาร์ดีเอฟที่ได้จากแบบจำลองการสะท้อนแสงที่นำเสนอนี้สัมพันธ์กับค่าบีอาร์ดีเอฟของผ้าไหมมากกว่าแบบจำลองการ

สะท้อนแสงอื่น และเมื่อนำมาเขียนเส้นโค้งเชิงขั้วจะเห็นว่า เส้นโค้งของค่าบีอาร์ดีเอฟที่ได้จากแบบจำลองที่นำเสนอนี้ใกล้เคียงกับเส้นโค้งของบีอาร์ดีเอฟที่วัดจากผ้าไหม มากกว่าเส้นโค้งของค่าบีอาร์ดีเอฟจากแบบจำลองอื่น ดังแสดงใน รูปที่ ๑๒-๑๖

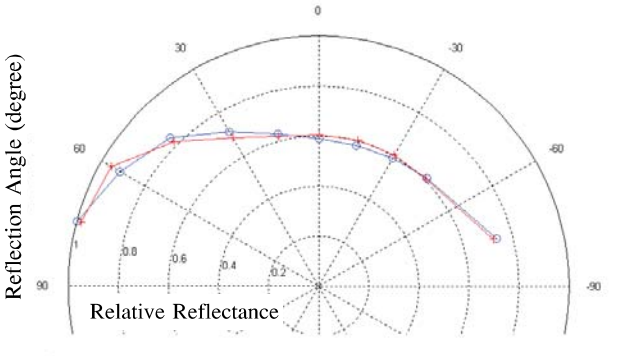

รูปที่ ๑๒ เส้นโค้งเปรียบเทียบระหว่างค่าการสะท้อนแสงที่วัดจากผ้าไหม(o) กับค่าการสะท้อนแสงที่คำนวณจากแบบจำลองที่นำเสนอของผ้าไหมตัวอย่างที่ ๓ ที่มุมตกกระทบ -๖๐ องศา

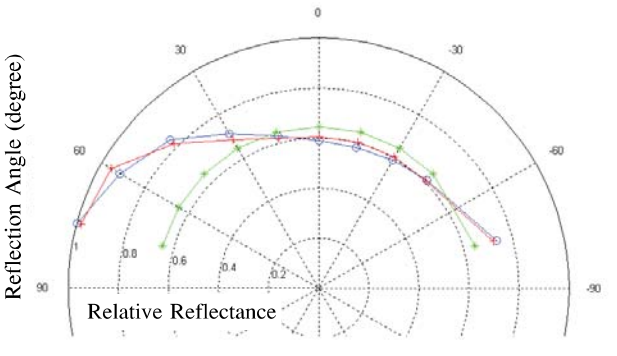

รูปที่ ๑๓ เส้นโค้งเปรียบเทียบระหว่างค่าการสะท้อนแสงที่วัดจากผ้าไหม (o) กับค่าการสะท้อนแสงที่คำนวณจากแบบจำลองที่นำเสนอ (+) และแบบจำลองฟอง (*) ของผ้าไหมตัวอย่างที่ ๓ ที่มุมตกกระทบ -๖๐ องศา

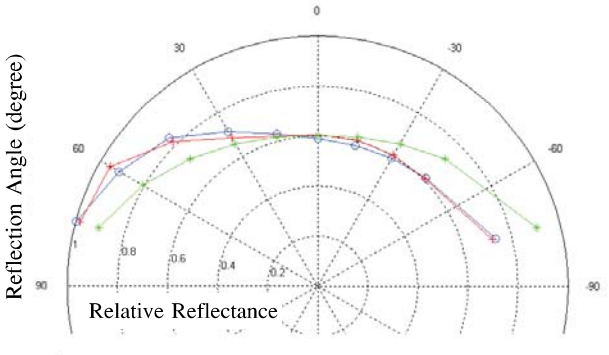

รูปที่ ๑๔ เส้นโค้งเปรียบเทียบระหว่างค่าการสะท้อนแสงที่วัดจากผ้าไหม (o) กับค่าการสะท้อนแสงที่คำนวณจากแบบจำลองที่นำเสนอ (+) และ แบบจำลองโอเรนและนายาร์ (*) ของผ้าไหมตัวอย่างที่ ๓ ที่มุมตกกระทบ -๖๐ องศา

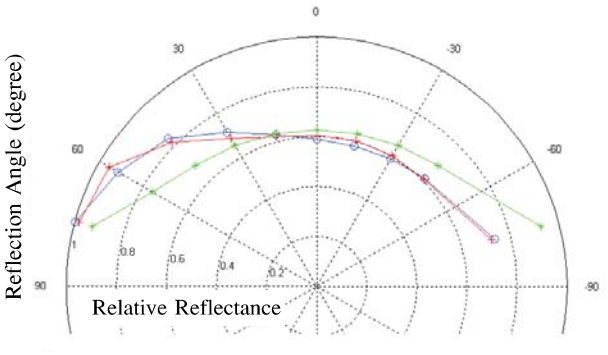

รูปที่ ๑๕ เส้นโค้งเปรียบเทียบระหว่างค่าการสะท้อนแสงที่วัดจากผ้าไหม (o) กับค่าการสะท้อนแสงที่คำนวณจากแบบจำลองที่นำเสนอ (+) และแบบจำลองวาร์ด (*) ของผ้าไหมตัวอย่างที่ ๓ ที่มุมตกกระทบ -๖๐ องศา

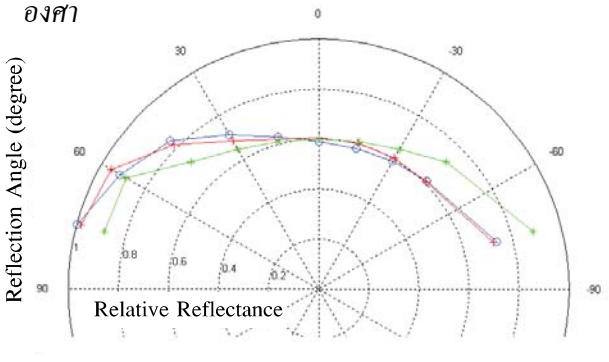

รูปที่ ๑๖ เส้นโค้งเปรียบเทียบระหว่างค่าการสะท้อนแสงที่วัดจากผ้าไหม (o) กับค่าการสะท้อนแสงที่คำนวณจากแบบจำลองที่นำเสนอ (+) และ แบบจำลองแอชิกมินและเชอร์ลีย์ (*) ของผ้าไหมตัวอย่างที่ ๓ ที่มุมตกกระทบ -๖๐ องศา

ตารางที่ ๑ ค่า RMS ของค่าการสะท้อนแสงจากแบบจำลองต่าง ๆ

ตัวอย่างที่	มุมตกกระทบ (องศา)	ค่า RMS ของ				
		แบบจำลองที่นำเสนอ	แบบจำลองของฟอง	แบบจำลองของโอเรนและนายาร์	แบบจำลองของวาร์ด	แบบจำลองของแอชิกมินและเชอร์ลีย์
๑	๐	๐.๐๑๕๓	๐.๐๒๒๓	๐.๐๒๒๕	๐.๐๒๒๕	๐.๐๒๒๘
	-๑๕	๐.๑๐๑๒	๐.๑๑๖๗	๐.๑๔๒๔	๐.๑๒๕๓	๐.๑๒๗๔
	-๓๐	๐.๐๑๖๘	๐.๐๘๒๔	๐.๐๕๐๖	๐.๐๘๖๘	๐.๐๘๒๒
	-๔๕	๐.๐๒๕๖	๐.๑๑๐๐	๐.๑๓๑๔	๐.๑๑๖๓	๐.๑๐๖๗
	-๖๐	๐.๐๓๘๐	๐.๑๑๖๑	๐.๑๕๕๔	๐.๑๒๔๓	๐.๑๑๑๒
	-๗๕	๐.๐๑๕๔	๐.๐๕๒๗	๐.๑๓๑๕	๐.๐๕๗๕	๐.๑๐๐๘
๒	๐	๐.๐๔๐๕	๐.๐๐๗๓	๐.๐๔๐๕	๐.๐๒๘๓	๐.๐๔๐๕
	-๑๕	๐.๐๓๐๗	๐.๐๒๕๖	๐.๐๘๗๖	๐.๐๔๑๕	๐.๐๕๔๐
	-๓๐	๐.๐๑๐๐	๐.๐๔๘๗	๐.๑๑๖๕	๐.๐๖๐๕	๐.๐๖๕๔
	-๔๕	๐.๐๒๓๕	๐.๐๖๑๕	๐.๑๒๕๔	๐.๐๖๔๓	๐.๐๗๖๕
	-๖๐	๐.๐๓๕๕	๐.๐๕๗๗	๐.๑๕๐๔	๐.๐๖๕๖	๐.๐๖๒๒
	-๗๕	๐.๐๒๑๗	๐.๐๕๖๖	๐.๑๕๑๖	๐.๐๖๕๘	๐.๐๘๓๕
๓	๐	๐.๐๔๘๓	๐.๐๐๕๘	๐.๐๔๕๕	๐.๐๔๘๐	๐.๐๔๕๔
	-๑๕	๐.๐๔๔๔	๐.๐๔๕๐	๐.๐๗๑๓	๐.๐๔๘๐	๐.๐๕๐๓
	-๓๐	๐.๐๑๐๕	๐.๐๗๐๗	๐.๑๐๕๗	๐.๐๗๒๘	๐.๐๖๘๕
	-๔๕	๐.๐๑๔๘	๐.๐๕๑๒	๐.๑๓๐๓	๐.๑๐๔๔	๐.๐๘๓๑
	-๖๐	๐.๐๒๑๔	๐.๐๕๑๘	๐.๑๖๑๐	๐.๑๐๓๖	๐.๐๘๔๓
	-๗๕	๐.๐๑๘๘	๐.๐๕๕๖	๐.๑๑๘๓	๐.๐๖๕๘	๐.๐๕๔๕

สรุป

งานวิจัยนี้ได้วัดและวิเคราะห์ลักษณะการสะท้อนแสงของพื้นผิวผ้าไหม พบว่า ผ้าไหมมีการสะท้อนแสงแบบผสม และมีสมบัติพิเศษที่สะท้อนแสงกล้าแบบ off-specular ผู้วิจัยได้สร้างแบบจำลองสำหรับทดสอบการสะท้อนแสงของผ้าไหมขึ้น โดยปรับปรุงจากแบบจำลองการสะท้อนแสงของฟองและได้เปรียบเทียบกับแบบจำลองอื่น ๆ อย่างไรก็ตาม แบบจำลองที่นำเสนอนี้ได้มาจากการวัดบีอาร์ดีเอฟเท่านั้น ดังนั้น การศึกษาเรื่องอิทธิพลของโครงสร้างผ้าไหมสมบัติเฉพาะของเส้นด้ายไหม จะช่วยให้สร้างแบบจำลองการสะท้อนแสงได้ถูกต้องและแม่นยำมากยิ่งขึ้น ซึ่งเป็นงานวิจัยในแนวลึกต่อไป

กิตติกรรมประกาศ

คณะผู้นิพนธ์ขอขอบพระคุณฝ่ายวิชาการ สำนักงานกองทุนสนับสนุนการวิจัย (สกว.) และสำนักงานคณะกรรมการการอุดมศึกษา (สกอ.) ที่ให้การสนับสนุนการวิจัยเรื่องนี้ ผ่านโครงการวิจัยเมธีวิจัยอาวุโส สกว. รหัสโครงการ RTA๕๐๘๐๐๐๔ นอกจากนี้ คณะวิจัยขอบคุณศูนย์การวิจัยฟรอนเทียร์เมดิคัลเอนจิเนียริง (Research Center for Frontier Medical Engineering) แห่งมหาวิทยาลัยชิบะ ประเทศญี่ปุ่น ที่เอื้อเฟื้อให้ใช้อุปกรณ์วิจัย ขอบพระคุณภาควิชาวิทยาศาสตร์ทางภาพถ่ายและเทคโนโลยีทางการพิมพ์ คณะวิทยาศาสตร์ จุฬาลงกรณ์มหาวิทยาลัย ที่เอื้อเฟื้อค่าใช้จ่ายและค่าเดินทางระหว่างประเทศ ซึ่งทำให้สามารถทำงานวิจัยบางส่วนที่ประเทศญี่ปุ่น

เอกสารอ้างอิง

Ashikmin, M., and Shirley, P. 2000. Anisotropic Phong BRDF Model. Journal of Graphic Tools, 5(2):25-32.

Blinn, J.F. 1977. Models of Light Reflection for Computer Synthesized Pictures. International Conference on Computer Graphics and Interactive Techniques, Proceedings of the 4th annual conference on Computer Graphics and Interactive Techniques, pp. 192-198.

Dana, K.J., Ginneken, B.V., Nayar, S.K. and Koenderink, J.J. 1999. Reflectance and Texture of Real-World Surfaces. ACM Transactions on Graphics, 18(1):1-34.

Oren, M., and Nayar, S.K. 1995. Generalization of Lambert's Reflectance Model. Computer Vision, 14(3):227-251.

Phong, B.T. 1975. Illumination for Computer Generated Pictures. Communications of the ACM, 18(6):311-317.

Torrance, K.E. and Sparrow, E.M. 1967. Theory for off-specular Reflection from Roughened Surface. Optical Society of America, 57(9):1105-1114.

Ward, G.J. 1992. Measuring and Modeling Anisotropic Reflection. Computer Graphics, 26(2):265-272.

Wyszecki, G., and Stiles, W.S. 2000. Color Science. 2nd ed., Wilky Classic, pp. 51-52.

Abstract

Measurement of Bidirectional Reflectance Distribution Function and Reflectance Modeling of Silk Fabrics

Suda Kiatkamjornwong

Associate Fellow of the Academy of Science, The Royal Institute, Thailand

Department of Imaging and Printing Technology, Faculty of Science, Chulalongkorn University, Bangkok 10330, Thailand

Boonyakiat Chaitepprasith,

Chawan Koopipat

Department of Imaging and Printing Technology, Faculty of Science, Chulalongkorn University, Bangkok 10330, Thailand

Silk fabric is a fabric in which its gloss is perceived differently in comparison with other fabrics due to its specific reflectance. This research measured a Bidirectional Reflectance Distribution Function (BRDF) of three types of silk fabric having different weaving styles in conjunction with reflectance characteristics. Besides the measured BRDFs of the silk fabrics, its reflection model was then proposed. The proposed reflection model incorporates a specular reflection lobe and diffuse reflection lobe. The proposed model and the measured BRDFs of the three silk fabrics were fitted by the least-square error method. The measured BRDFs of the silk fabric were also fitted with Phong reflection model, Oren-Nayar reflection model and Torrance-Sparrow reflection. It was found that the proposed model fitted better with the measured BRDF than did the general models of Phong-reflection, Oren-Nayar reflection, and Torrance-reflection. The proposed model can thus be used to approximate, analyze and elucidate the characteristics of light reflection of the three silk fabrics.

Key words **: BRDF, silk fabrics, reflection model**

บทความที่ Under revision

หรือ Under review

SYNTHESES, CHARACTERIZATION AND ANTIBACTERIAL ACTIVITY OF CHITOSAN GRAFTED HYDROGELS AND ASSOCIATED MICA-CONTAINING NANOCOMPOSITE HYDROGELS

Journal:	*Journal of Applied Polymer Science*
Manuscript ID:	Draft
Wiley - Manuscript type:	Research Article
Keywords:	swelling, hydrogels, nanocomposites, organoclay, biocompatibility

SCHOLARONE™
Manuscripts

For Review

SYNTHESES, CHARACTERIZATION AND ANTIBACTERIAL ACTIVITY OF CHITOSAN GRAFTED HYDROGELS AND ASSOCIATED MICA-CONTAINING NANOCOMPOSITE HYDROGELS

Supaporn Noppakundilograt[1], Kittichai Sonjaipanich[2], Nuttha Thongchul[3] and Suda Kiatkamjornwong[1*]

[1]Department of Printing and Imaging Technology, Faculty of Science, Chulalongkorn University, Bangkok, 10330, Thailand. [1]E-mail: *supaporn.n@chula.ac.th*; [*1]corresponding author; [1*]e-mail: *ksuda@chula.ac.th*; Tel.: +66-2218-5587.

[2]Program of Petrochemistry and Polymer Science, Faculty of Science, Chulalongkorn University, Bangkok, 10330, Thailand. [2]E-mail: kittichai_sonjai@hotmail.com.

[3]Institute of Biotechnology and Genetic Engineering, Chulalongkorn University, Bangkok, 10330, Thailand. [3]E-mail: Nuttha.T@chula.ac.th.

For Peer Review

SYNTHESES, CHARACTERIZATION AND ANTIBACTERIAL ACTIVITY OF CHITOSAN GRAFTED HYDROGELS AND ASSOCIATED MICA-CONTAINING NANOCOMPOSITE HYDROGELS

Abstract

Chitosan (CS) grafted poly[(acrylic acid)-*co*-(2-hydroxyethyl methacrylate)] (CS-*g*-poly(AA-co-HEMA)) at different molar ratios of AA and HEMA, and the associated nanocomposite hydrogels of CS-*g*-poly(AA-*co*-HEMA)/mica were synthesized by radical copolymerization. The grafting positions at the amino or hydroxyl groups in the CS were identified by Fourier transform infrared spectroscopy. CS-*g*-poly(AA-*co*-HEMA) hydrogels were intercalated in the mica and the amount of hydrogel insertion did not affect the spacing of the silicate layers in mica. The higher mica loadings produced a rougher surface of the nanocomposite hydrogel. The water absorbency of the CS-*g*-poly(AA-*co*-HEMA)/mica nanocomposite hydrogels decreased with increasing levels of mica loading to a lower level than those of the CS-*g*-poly(AA-*co*-HEMA) hydrogels. Both CS-*g*-poly(AA) and CS-*g*-poly(AA-*co*-HEMA)/mica nanocomposite hydrogels exhibited a higher antiproliferative activity against *Staphylococcus aureus* than did the neat CS hydrogel with CS-*g*-poly(AA) revealing a very pronounced minimum inhibition concentration (MIC) of 1.56 mg ml^{-1}. The extent of mica loading in the CS-*g*- poly(AA-*co*-HEMA) nanocomposite hydrogels did not affect the MIC (12.5 mg ml^{-1}).

Keywords: Chitosan; Acrylic acid; 2-hydroxyethyl methacrylate; Mica; Nanocomposite hydrogel; Antibacterial property

For Peer Review

1. Introduction

Hydrogels are slightly crosslinked hydrophilic polymers that can swell and absorb at least 15 times of their dry weight. The relative density of hydrophilic groups and the degree of crosslinking of the hydrogel are the two main factors that affect the water absorbency of a hydrogel.[1] Chitosan (CS) has found wide applications in the biomedical field, as well as other fields, because of its interesting biological properties, such as biocompatibility, biodegradability, hemostatic activity and bacteriostatic effects. Recently, CS-based hydrogels have been extensively researched and used in a wide field of applications because of their biocompatibility, biodegradability, non-toxicity and antibacterial activity,[2] as well as that CS is a plentiful, renewable and relatively cheap material. The hydrogels derived from CS grafted with hydrophilic vinyl monomers, such as acrylic acid (AA) or itaconic acid (IA), showed an increased water absorbency compared to CS alone.[3-5] The 2-hydroxyethyl methacrylate (HEMA) monomer has long been used in biomedical applications because it improves the graft copolymer biocompatibility.[6] HEMA monomer is harmful in the dental application if it does not completely polymerize, because it induces DNA damage, apoptosis and cell-cycle delay by the production of reactive oxygen species. However, it was found that the presence of antioxidant and/or CS can decrease the genotoxicity of HEMA monomer.[7,8] CS-*g*-poly(AA-*co*-HEMA) was reported to exhibit good cytocompatibility and hemocompatibility and thus possesses a high potential as an application for wound dressing.[3] Suitable wound dressings normally possess an antibacterial activity for protecting the wound from infection, and have a water absorbency of around 25 - 32 times their dry weight so as to be able to remove secretion or pus from the wound.[9] Bacterial infection is one of the main factors for the development of chronic wounds. Infected wounds may cause trauma and higher

For Peer Review

treatment costs. Pathogens frequently associated with wound infections include *Staphylococcus aureus (S. aureus*), *Enterococcus* sp., *Escherichia coli*, *Pseudomonas aeruginosa*, *Enterobacter* sp., *Proteus mirabilis*, *Klebsiella pneumonia*, *Streptococcus* sp., and *Candida albicans*. *S. aureus* is the most commonly found human pathogens which cause wound infections, boils, pustules and other human skin infections.[10] Infection by *S. aureus* is accounted for about 20% frequency of occurrence in burns, wounds, and surgical sites. Due to the above mentioned, any developed wound dressing materials should therefore possess an inhibitory effect on the most frequently found *S. aureus* in wounds.

Generally, the gel strength of a bio-absorbent is naturally rather weak and this unfortunately limits its useful applications. To improve the gel strength, thermal and inherently antibacterial properties of CS and/or grafted CS, clay minerals, such as montmorillonite,[11] rectorite[12,13] and sepiolite,[14] have been used as a filler incorporated into the CS to produce CS/nanocomposite hydrogels. Wang et al. [15] found that the antibacterial activity against *S. aureus* of CS/rectorite nanocomposite film was better than that of the neat CS film. This result agreed with the research reporting that clay minerals alone did not destroy bacteria, but they could adsorb and kill bacteria when the antimicrobial materials were intercalated into silicate layers.[16]

Mica is a clay mineral known as a 2: 1 phyllosilicate and its general formula is $AM_{2-3}T_4O_{10}X_2$, where A is usually Na, K or Ca. The M can be Fe, Al and Mg; T is Si and/or Al and X is (OH), O, Cl and F.[17] It is composed of two-dimensional layers of an edge-shared octahedral sheet that is fused to form two tetrahedrals by the shared oxygen ions of one octahedral sheet and two tetrahedral sheets.[18] Mica showed the antimicrobial activity, but it has a tendency of cytotoxicity with a larger platelet size than that of montmorillonite.[19] Nanosilicate platelet of montmorillonite has a low

For Peer Review

cytotoxicity with antibacterial activity.[19,20] However, only a few research reports on CS/mica nanocomposite hydrogels are available, leaving its potential suitability for many applications, including as a wound dressing material, unknown. Therefore, the synthesis and characterization of grafted CS/mica nanocomposite hydrogels was the main aim of this research. The effects of the reaction parameters on the morphology, water absorption and antibacterial activities of the resultant hydrogels were investigated.

2. Experimental

2.1 Materials

CS with a viscosity average molecular weight of 57,000 g mol^{-1} and an 85% deacetylation degree was purchased from Seafresh Industry Public Co., Ltd. (Bangkok, Thailand). Industrial grade AA and HEMA monomers were kindly supplied by Thai Mitsui Specialty Chemicals Co., Ltd. (Bangkok, Thailand). *N, N'*-Methylenebisacrylamide (*N*-MBA) crosslinker and *N, N, N', N'*-tetramethylethylenediamine (TEMED) co-initiator were purchased from Fluka (Buchs, Switzerland). Ammonium persulphate (APS), purchased from Ajax (Australia), was used as the initiator. Swelling mica was purchased from Wako Pure Chemical Industries, Ltd. (Osaka, Japan). Deionized water, used as the reaction medium, was obtained from an Elga Deionizer (Model LA611, Marlow international, Bucks, U.K.). Sodium ampicillin (drug grade) was purchased from T.P. Drug Laboratories (Bangkok, Thailand). *Staphylococus aureus* (*S. aureus*) isolate from textile wastewater was provided by the National Center for Genetic Engineering and Biotechnology (NSTDA, Pathum thani, Thailand). Mueller-Hinton Broth (MHB) and Mueller-Hinton Agar (MHA), used for the growth of *S. aureus* were from Difco, New Jersey, USA.

For Peer Review

2.2 Syntheses

2.2.1 Synthesis of grafted CS hydrogels

CS (1 g) was added into 30 ml of 2% w v^{-1} acetic acid solution in a 500-ml four-necked round-bottom flask with a mechanical stirrer (Ika RW 28, IKA® Werke GmbH & Co. KG, Staufen Germany), assembled with a half-moon shaped Teflon blade paddle and a condenser. The mixture was stirred for 30 min at room temperature and then heated at 60 ± 2°C under nitrogen gas which was fed constantly through the gas inlet at 10 ml min^{-1} for 30 min. APS (0.01-0.15 g) was then added and stirred for 10 min, followed by the sequential addition of either AA or HEMA or both and *N*-MBA (0.01 - 0.15 g) to the desired final concentration and stirred for 5 min. Finally, TEMED was added (0.01 - 0.4 g) to the mixture and stirred at 250 rpm for another 60 min. The reaction was then cooled down to room temperature and adjusted to pH 8 by 1 M sodium hydroxide solution. The product was dewatered with acetone, cut into pieces of approximately 1 x 1 cm square and dried in an oven at 50°C for 24 h. The dried product was extracted with an excess amount of methanol in a Soxhlet apparatus for 24 h to remove the unreacted components and obtain the CS grafted polymer (e.g. CS-*g*-poly(AA-*co*-HEMA)). The extracted product was dried in the oven at 50°C for 24 h, milled and sieved through a 100 mesh sieve to obtain the hydrogel particles in the range of 50 - 100 mesh (200 - 400 micrometers).

2.2.2 Synthesis of CS-g-poly(AA-co-HEMA)/mica nanocomposite hydrogels

The desired amount of mica was dispersed in the mixture of AA and HEMA monomers for 60 min by stirring at 250 rpm with a magnetic stirrer. CS (1 g) was dissolved in 30 ml of 2% v v^{-1} solution of acetic acid, and then added into a 500-ml four-necked round-bottomed reaction flask equipped with the mechanical stirrer and a

For Peer Review

condenser. The reactor was then immersed in a temperature controlled water bath, stirred at 250 rpm under a constant nitrogen gas fed through the gas inlet tube for 30 min before APS (0.1 g) was added and stirred for 10 min. The well-dispersed mica suspension was added into the solution of CS and APS, stirred at 250 rpm and heated to 60 ± 2°C under the nitrogen gas circulation for 30 min before *N*-MBA (0.1 g) was then added and stirred for 5 min. Finally, TEMED (0.4 g) was added and stirred for another 60 min. The polymerization product was cooled down and the product was obtained by the same procedure as described above for the grafted CS hydrogels.

2.3 Grafting ratio and efficiency of the grafted CS hydrogels by acid hydrolysis

The grafted CS hydrogel (0.5 g) was dissolved in 50 ml of 1 M HCl in a 125-ml Erlenmeyer flask which was assembled with a condenser and refluxed at 120°C for 2 h. After the acid hydrolysis, the remaining solid (grafted copolymer) was filtered, dried and weighed. The filtrate was neutralized to pH 7 by 1 M sodium hydroxide solution and then precipitated by ethanol. The precipitate was filtered and dried at room temperature for 24 h to obtain its dry weight. Finally, the filtrate from the precipitation step was evaporated to remove the residual solvent. The white solid was dried at room temperature and weighed. The remaining solid and precipitate after acid hydrolysis were investigated for functional groups by Fourier Transform Infrared Spectroscopy (FT-IR; model Tensor 27, Billerica, USA) using KBr pellets. The grafting ratio, grafting efficiency and homopolymer content were calculated from Equations (1) - (3):[21-23]

$$\%\ grafting\ efficiency = \frac{Weight\ of\ remaining\ solid\ after\ acid\ hydrolysis \times 100}{Weight\ of\ homopolymer + Weight\ of\ grafted\ copolymer} \quad (1)$$

$$\%\ grafting\ ratio = \frac{Weight\ of\ remaining\ solid\ after\ acid\ hydrolysis \times 100}{Weight\ of\ precipitate\ from\ ethanol} \quad (2)$$

For Peer Review

$$\% \text{ homopolymer} = \text{Weight of grafted CS hydrogel before Soxhlet extraction - weight of grafted CS hydrogel after Soxhlet extraction} \quad (3)$$

2.4 Identification of functional groups of grafted CS hydrogels and CS-g-poly(AA-co-HEMA)/mica nanocomposite hydrogels

The functional groups of mica, the grafted CS hydrogels and grafted CS-*g*-poly(AA-*co*-HEMA)/mica nanocomposite hydrogels were characterized by FT-IR.

2.5 Characterization of the grafted CS hydrogels and CS-g-poly(AA-co-HEMA)/mica nanocomposite hydrogels

The surface morphologies of the mica, and the grafted CS and grafted CS/mica nanocomposite hydrogels were photographed on a scanning electron microscope (SEM, model JSM-5410LV, Tokyo, Japan) without prior cross sectioning. Each sample was fixed on an aluminum stub and coated with gold. X-ray diffraction (XRD) patterns of the samples were recorded using Bruker AXS (model D8 Discover, Bruker AXS Munich, Germany) with Cu radiation, voltage of 40 kV, a current of 40 mA and scanned from 1 - 35° with a scanning rate of 0.02° min^{-1}. The transmission electron micrographs (TEM) were taken on JOEL (JEM-2100, Jeol Ltd., Tokyo, Japan).

2.6 The effect of the reagent contents on water absorbency of grafted CS hydrogels and CS-g-poly(AA-co-HEMA)/mica nanocomposite hydrogels

For Peer Review

The water absorbencies of the grafted CS hydrogel and the grafted CS-*g*-poly(AA-*co*-HEMA)/mica nanocomposite hydrogels were carried out with distilled water at room temperature in a closed system to minimize water evaporation. Distilled water (200 ml) was added to 0.1 g of the dry grafted hydrogels or the nanocomposite hydrogels. The hydrogel was swollen to equilibrium for 24 h and the swollen gel was then filtered through a 100-mesh aluminum screen sieve for 2 h. The water absorbency was determined for at least three replications for each synthesized product by Equation (4):

$$Water\ absorbency\ (Q) = \frac{(W_s - W_d)}{W_d} \quad (4)$$

where W_s is the weight of swollen hydrogels or nanocomposite hydrogels (g) and W_d is the weight of the dry hydrogels or nanocomposite hydrogels (g).

2.7 Antibacterial activity

2.7.1 Turbidity method

The CS, CS-*g*-poly(AA), CS-*g*-poly(HEMA) and CS-*g*-poly(AA-*co*-HEMA) hydrogels, and the CS-*g*-poly(AA-*co*-HEMA)/mica nanocomposite hydrogels, each weighing 250 mg, and distilled water were sterilized by UV radiation for 1 h prior to the test.

The diluted stock culture of *S. aureus* was adjusted to 0.5 units by sterile deionized water. The *S. aureus* suspension (2.5 ml) was inoculated into 47.5 ml of sterile Mueller-Hinton Broth (MHB) in a 250 ml sterile Erlenmeyer flask. For each hydrogel type, the sterile sample (250 mg) was then added to the *S. aureus* suspension in MHB media and incubated at 37°C while being shaken at 250 rpm. At every two hours a 50 ml aliquot was harvested and the swollen gel removed by filtration through

For Peer Review

filter paper no. 1 (Schleicher & Schuell, Whatman, Kent, U.K.) prior to measuring the $OD_{610\ nm}$ of the filtrate as a measure of the growth of *S. aureus* using a spectrophotometer (Spectronic 21, Bausch & Lomb Inc., Rochester, New York, U.S.A). The OD results of the growth with or without the hydrogel were plotted versus time to obtain the bacterial growth profiles. The culture time at which the antibacterial activity of the grafted CS hydrogel was found to be maximal by the optical density measurement was used to evaluate the total replication competent (viable) bacterial number using the total plate count method (see section 2.7.2. below) so as to calculate the mean colony-forming units per milliliter (CFU ml^{-1}), and from this the relative degree of inhibition of bacterial proliferation can be obtained.

2.7.2 Total plate count method

The six and eight hour old *S. aureus* cultures in MHB were diluted with sterile deionized water to 10^8 - 10^9 CFU ml^{-1} and then 100 µl aliquots of each diluted *S. aureus* suspension were spread on each MHB plate. The plates were incubated for 24 h at 37°C where upon the number of viable bacteria was counted. Mean CFU ml^{-1} and the relative inhibition were calculated by Equations (5) and (6), respectively. The negative control was the sterilized *S. aureus* cultured in MHB.

$$CFU/ml = \left(\frac{mean\ numbers\ of\ counted\ colonies}{amount\ of\ dilute\ S.aureus\ for\ spread\ plate\ (ml)} \right) \times dilution\ factor \quad (5)$$

$$Relative\ inhibition = 100 - \left(\frac{CFU/ml\ of\ the\ sample}{CFU/ml\ of\ negative\ control} \right) \times 100 \quad (6)$$

For Peer Review

2.7.3 Minimum inhibition concentration (MIC)

The antibacterial activity was determined in terms of the minimum inhibition concentration (MIC). The diluted stock culture of *S. aureus* was adjusted to 0.5 A_{610} units by sterile deionized water and 100 µl was inoculated into 4.9 ml of sterile MHB in a 10 ml test tube. The hydrogels, each evaluated at the five concentrations of 0, 3.12, 6.25, 12.5 and 25 mg ml^{-1}, were added to the 0.01 A_{610} unit suspensions of *S. aureus* (see above) in sterile MHB. The cultures were then incubated at 37°C with shaking at 120 rpm for 24 h. The mean CFU ml^{-1} of each sample tested were measured by the total plate count method as above and the experiment was performed in triplicate. The MIC was thus determined from the derived CFU ml^{-1} and statistical significance (ANOVA) was accepted at the 99% significant level or $\alpha = 0.01$.

3. Results and discussion

3.1 Characterization of the grafted hydrogels

3.1.1 Grafted CS hydrogels

The spectrum of the CS hydrogel (Figure 1(a)) shows the characteristic amino group peaks at 3428 cm^{-1} for N-H stretching, 1640 cm^{-1} for the C=O stretching of amide I,[24] 1594 cm^{-1} for the N-H bending of amide II, 1381 cm^{-1} for the -NHCO stretching of amide II[25] and 1253 cm^{-1} for C-N stretching.[26] The characteristic peaks of the saccharide structure in CS exhibit at 1152 cm^{-1} for the bridge O stretching,[23,27] and 1085 cm^{-1} and 1031 cm^{-1} for the C_3-OH and C_6-OH stretching, respectively.[25] In addition, the absorption peak at 1420 cm^{-1} is the O-H and C-H vibration which indicates the presence of a hydroxyl group.[24] The peak of C-H stretching appears at 2921 and 2864 cm^{-1}.[27]

For Peer Review

The CS-*g*-poly(AA) hydrogel spectrum (Figure 1(b)) shows a new absorption peak at 1724 cm^{-1} assigned to C=O stretching of the carboxyl group from the grafted poly(AA) part,[27] which was shifted from the peak at 1713 cm^{-1} of the carboxyl group of poly(AA). In addition, the new absorption peaks at 1563 cm^{-1} and 1402 cm^{-1} are ascribed to asymmetric and symmetric stretching of the carboxylate anion of poly(AA) in the CS-*g*-poly(AA) hydrogel.[3] The absorption peak at 1594 cm^{-1}, assigned to N-H bending of CS, disappeared in the CS-*g*-poly(AA) hydrogel. Thus, the NH_2 group is grafted in the CS backbone.[28] Moreover, the characteristic peaks of the saccharide structure of CS in the CS-*g*-poly(AA) hydrogel was shifted to 1065 cm^{-1} and 1019 cm^{-1} (C_3-OH and C_6-OH stretching) and the peak of O-H bending at 1420 cm^{-1} disappeared (Figure 1(b)). From these results, the poly(AA) chains were confirmed to be grafted at both the NH_2 and OH sites on the CS backbone.

The CS-*g*-poly(HEMA) spectrum (Figure 1(c)) shows an absorption peak at 1730 cm^{-1}, assigned to C=O asymmetric stretching, which indicates the presence of the ester carbonyl group of poly(HEMA),[3] and a new absorption peak at 746 cm^{-1} that is attributed to the CH_2 rocking of the poly(HEMA) moiety.[29] The absorption peak of N-H stretching of CS also disappeared. Thus, the NH_2 group of CS had been reacted in the graft polymerization.[28] The characteristic peaks of the saccharide structure of CS in the CS-*g*-poly(HEMA) hydrogel were shifted to 1069 cm^{-1} and 1021 cm^{-1} (C_3-OH and C_6-OH stretching) and the CS O-H bending peak at 1420 cm^{-1} disappeared. Thus, the poly(HEMA) was grafted at both NH_2 and OH sites on the CS backbone as well.

The CS-*g*-poly(AA-*co*-HEMA) hydrogel spectrum (Figure 1(d)) shows the absorption peak at 1722 cm^{-1} that is assigned to the C=O asymmetric stretching and so indicates the presence of the ester carbonyl group of the poly(HEMA) moiety,[3] and

For Peer Review

a new absorption peak at 753 cm^{-1} that is attributed to the CH_2 rocking of the poly(HEMA) moiety.[29] In addition, it also shows peaks at 1585 cm^{-1} (C=O asymmetric stretching) and 1402 cm^{-1} (C=O symmetric stretching) of the carboxylate anion in the poly(AA) moiety.[3] Moreover, the characteristic peaks of the saccharide structure of CS in the CS-*g*-poly(AA-*co*-HEMA) hydrogel (Figure 1(d)) shifted to 1074 and 1021 cm^{-1} (C_3-OH and C_6-OH stretching) and the peak of O-H bending at 1420 cm^{-1} (Figure 1(a)) disappeared (Figure 1(d)). Thus, poly(AA-*co*-HEMA) was also grafted at both the NH_2 and OH sites on the CS backbone.

3.1.2 CS-g-poly(AA-co-HEMA)/mica nanocomposite hydrogels

The FT-IR spectrum of mica is shown in Figure 1(e). It shows a peak of O-H stretching at 3600 - 3400 cm^{-1} that indicates the presence of the hydroxyl group. The absorption peaks at 2924 and 2852 cm^{-1} are attributed to the C-H stretching of the organic part and indicate that the mica used is synthetic mica. It also shows the absorption peaks of H-O-H bending of water at 1637 and 1620 cm^{-1},[30] and Si-O and Al-O stretching peaks at 1016 and 473 cm^{-1}.[31]

The FT-IR spectra of CS-*g*-poly(AA-*co*-HEMA)/mica nanocomposite hydrogels, containing mica at 7, 10 or 15% w w^{-1} of the monomer, are shown in Figure 1(f-h), respectively. In comparison with the spectra of mica (Figure 1(e)), the characteristic peaks of CS are shifted to 1636 and 1389 cm^{-1}, whilst the characteristic peaks of poly(AA-*co*-HEMA) are also shifted to 1724, 1572, 1404 and 754 cm^{-1}. In addition, new absorption peaks appear at 473, 469 and 467 cm^{-1} (Figure 1(f–h), respectively), all of which are attributed to the Al-O stretching of mica. The intensity of the absorption peak at 1016 cm^{-1} (Si-O stretching) increased with increasing mica loadings in the CS-*g*-poly(AA-*co*-HEMA)/mica nanocomposite hydrogels, which

For Peer Review

indicates the existence of mica in the CS-*g*-poly(AA-*co*-HEMA) nanocomposite hydrogel. Based on these FT-IR data, the AA or HEMA group is grafted at the OH group of the C-6 position and/or the amino group of CS. The FT-IR peaks in the spectra further confirmed that CS-*g*-poly(AA-*co*-HEMA)/mica nanocomposite hydrogels with various loadings of mica were successfully synthesized.

3.2 The grafting performance of grafted CS hydrogels

Analysis of the acid hydrolysis suggests the grafting ratio of the CS-*g*-poly(AA) hydrogel (87%) is lower than that of the CS-*g*-poly(AA-*co*-HEMA) (269%) and CS-*g*-poly(HEMA) hydrogels (343%). However, the grafting ratios of CS-*g*-poly(AA-*co*-HEMA) and CS-*g*-poly(HEMA) hydrogels were calculated from the weight differences because a poly(HEMA) C=O peak at 1710 and 1722 cm^{-1} is still observed. Thus, at least some poly(HEMA) is still incorporated in the precipitate after acid hydrolysis, it means that the acid hydrolysis of the CS-g-poly(HEMA) was not completed. In comparison with the amount of CS, a greater amount of HEMA was used and so HEMA can generate an interpenetrate polymer network (IPN) hydrogel[32] on the CS backbone. This result reflects the high grafting ratio as expected. The grafting efficiency of CS-*g*-poly(AA), CS-*g*-poly(AA-*co*-HEMA) and CS-*g*-poly(HEMA) hydrogels is 93, 94 and 96%, respectively. The amount of homopolymer normally generated during graft polymerization and the homopolymer chains could form the IPN chains. Therefore, the amount of homopolymer cannot be derived directly just from the Soxhlet extraction and acid hydrolysis. Therefore, the amounts of free poly(AA), poly(AA-*co*-HEMA) and poly(HEMA) found are only 3, 5 and 3%, respectively, which are considered to be quite small, and would probably have been incorporated as the IPN in the polymeric hydrogels.

For Peer Review

3.3 Surface morphology

The surface morphologies of the CS, mica, CS-*g*-poly(AA-*co*-HEMA) hydrogel and CS-*g*-poly(AA-*co*-HEMA)/mica nanocomposite hydrogels with 5 to 15% (w w^{-1} of the monomer) mica loadings are shown as the representative SEM micrographs in Figure 2. The relatively smooth surface of the CS hydrogel and the flat sheets of mica at approximately 1 - 3 micrometers along with their aggregated state is clearly visible (Figure 2(a,b)). The surface of the CS-*g*-poly(AA) hydrogel (see Figure 2(c)) exhibits the larger porous structure in many areas than those of CS-*g*-poly(HEMA) (see Figure 2(d)) and CS-*g*-poly(AA-*co*-HEMA) hydrogel (see Figure 2(e,f)). The surface morphology of the CS-*g*-poly(HEMA) hydrogel shows a gel network surrounded by a wide spread of uniformly distributed micro-pores and this is especially regular on the surface of the CS-*g*-poly(AA-*co*-HEMA) hydrogel (Figure 2(d)). The CS-*g*-poly(AA-*co*-HEMA) hydrogel surface exhibits further a nano-porous structure (Figure 2(e,f)).

The internal morphologies of the CS-*g*-poly(AA-*co*-HEMA)/mica nanocomposites containing 5 - 15% w w^{-1} mica of the monomer (Figure 2(g-j)) are slightly different from those of the mica-free CS-*g*-poly(AA-*co*-HEMA). It is seen that the higher the mica loading, the more the surface roughness increased and that the mica flakes are imbibed in the inner areas of the gel. When the mica loadings were high, they were agglomerated, aggregated, resided, deposited and covered the whole polymer surface. Based on these results, CS-*g*-poly(AA-*co*-HEMA)/mica nanocomposite hydrogels are confirmed to have been successfully synthesized. One must state that no residual HEMA was retained in the resulting hydrogels because no indication of the double bonds peaks was found in the IR spectra because many extractions of the unused materials were made in solvent.

For Peer Review

3.4 XRD and TEM analyses

The XRD pattern of the CS hydrogel (Figure 3(a)) shows the 2-theta of CS at 10.53° and 19.93°, which corresponds to the hydrated crystals of low crystallinity of the form I and crystallinity of the form II, respectively.[33,34] The XRD pattern of CS-*g*-poly(AA), CS-*g*-poly(HEMA) and CS-*g*-poly(AA-*co*-HEMA) exhibit the broader and weaker peaks at 20.19, 18.49 and 20.31°, respectively, whereas the 2-theta at 10.53° of all these three CS grafted hydrogels disappeared. These indicated that the crystallinity of the grafted CS was dramatically decreased. Changes in the intensity of the peaks at approximately 20° relate to different packing of the chains and/or different hydrogen bonding networks in the grafted CS.[35] Thus, the introduction of AA and/or HEMA chains onto the surface of the CS causes the breakdown of its crystallinity. These results confirmed that the grafting of polymer onto the CS chain occurred.[33,34,36] The XRD patterns of mica revealed 2-theta values of 7.13 and 9.22° that correspond to a basal spacing of 13.58 and 9.58 Å, respectively. The XRD patterns of the CS-*g*-poly(AA-*co*-HEMA)/mica nanocomposite hydrogel reveal that the 2-theta value of mica in the nanocomposite hydrogels were shifted towards a lower angle (6.27°) and that the interlayer spacing of mica increased by 1.7 Å compared with that of the swelling mica. This confirms that intercalation had taken place and that the CS-*g*-poly(AA-*co*-HEMA)/mica nanocomposite hydrogels are intercalated composites with more spacing in the silicate layers.[37] In addition, it also shows that increasing the mica loadings from 5 to 15% (w w^{-1} based on the weight of monomer) does not affect the intercalated structure of the CS-*g*-poly(AA-*co*-HEMA)/mica nanocomposite hydrogels but rather they exhibit the same basal spacing. These results agree well with the previous report of Wang and coworkers.[12]

For Peer Review

Representative TEM micrographs of the CS-*g*-poly(AA-*co*-HEMA)/mica nanocomposite hydrogels with mica loadings of 5, 7, 10 and 15% w w^{-1} of the monomer are shown in Figure 4. The dark lines in Figure 4 belong to the mica structure and the bright area is the grafted chitosan matrix. All the TEM micrographs of nanocomposite hydrogels revealed that the distance between the two adjacent dark lines, the spacing of the two silicate layers, results in an intercalated structure. Indeed, parts of the silicate layer can be seen in Figure 4(a-d). The results of the TEM analysis are consistent with the XRD data (Figure 3), and support that CS-*g*-poly(AA-*co*-HEMA)/mica nanocomposite hydrogels have an intercalated structure and no significant if any level of an exfoliated structure.

3.5 Equilibrium water absorbency

3.5.1 Effect of monomer type (AA or HEMA) on the properties of the grafted CS hydrogels

The equilibrium water absorbency of CS alone was rather low but was significantly affected by the copolymerization with AA, but not with HEMA (Table 1). CS-*g*-poly(AA) had ten-fold higher water absorbency, whereas the water absorbency of the CS-*g*-poly(HEMA) was not significantly different to that for CS alone (Table 1). The water absorbency of the CS-*g*-poly(AA-*co*-HEMA) decreased ~1.2- and 3.2-fold as the AA: HEMA ratios decreased from 3:1 to 1:1 and 1:3, respectively (Table 1). That the water absorbency of CS-*g*-poly(AA-*co*-HEMA) increased as the content of AA increased is due to the increase in the density of hydrophilic groups from the carboxylic acid contents,[38] which then provides a greater repulsion of the anionic portion allowing for the expansion of the polymer chains. This also then explains the increased water absorbency of the CS-*g*-poly(AA)

For Peer Review

hydrogels over that of the CS hydrogels. On the other hand, CS-*g*-poly(HEMA) had very low water absorbency because HEMA is not as polar as AA but rather has a rather rigid chain due to the methacrylate substituent group. The longer chain of the poly(HEMA) hydrogel thus is likely to have resulted in more molecular entanglements that limited the chain expansion[39] and caused the water absorbency of the CS-*g*-poly(HEMA) hydrogel to decrease. Thus, although CS-*g*-poly(HEMA) would be unlikely to be beneficial to intercalate with mica, the HEMA moiety is more compatible with human cells than the other types of monomer moieties.

3.5.2 Effect of mica loading

The equilibrium water absorbency of the CS-*g*-poly(AA-*co*-HEMA) hydrogel at a 1:1 AA: HEMA molar ratio was ~5.4- and 5-fold higher than that of CS or CS-*g*-poly(HEMA), respectively, but almost half that of the CS-*g*-poly(AA) hydrogel (Table 1). The addition of mica at 5, 7 or 10% (w w^{-1} of monomer) caused a 1.2-fold drop in the equilibrium water absorbency from that seen with the mica-free CS-*g*-poly(AA-*co*-HEMA) hydrogel, but did not vary significantly between the three different mica loading levels (Table 1). In contrast, when the mica loading was increased to 15% w w^{-1} of monomer, the water absorbency was significantly decreased a further 1.3-fold compared to that seen with the 5 – 10% w w^{-1} mica loaded CS-*g*-poly(AA-*co*-HEMA), or 1.54-fold less than that for the mica-free CS-*g*-poly(AA-*co*-HEMA). This is because the polymer chains were inserted into the spacing between the silicate layers of mica and so the polymer chains were restricted in these limited spaces and so less able to expand. Another reason could be the degree of rigidity of the nanocomposite hydrogel that is induced by the mica. This also supports the notion that the structure of this nanocomposite hydrogel was intercalated.

For Peer Review

3.6 Antibacterial activity

Particle sizes of the CS, CS-*g*-poly(AA-*co*-HEMA) hydrogels and CS-*g*-poly(AA-*co*-HEMA)/mica nanocomposite hydrogel were in the range of 200 - 400 μm by the sieve size 50-100 mesh which is anticipated to have an important effect on the bacterial growth inhibitio.[40] This was therefore evaluated using a co-culture of *S. aureus* with each hydrogel type and evaluating the bacterial growth relative to the control culture by measuring the culture turbidity by absorbance (after removal of the hydrogel by filtration), and by total plate counts of replication competent ("viable") cells, over a 24 h time period.

3.6.1 Turbidity method

This well used method assumes that the turbidity of a medium solution increases solely due to the increase in the number of bacterial cells. Although this method is easy to perform the bacteria sample must be in a liquid suspension state, and typically it can only be used to detect bacteria in the range of 10^6 to 10^7 bacteria ml^{-1}. Moreover, the measurement of bacterial growth in the lag phase is less accurate and is an indirect measurement that needs a calibration curve, where a direct measurement of bacterial counts must be performed.

The preliminary results of the antibacterial activity testing of the CS-*g*-poly(AA-*co*-HEMA) hydrogel, evaluated by measuring the optical density at 610 nm every 2 h and compared with the negative control (containing only the medium and the gram-positive *S. aureus*), revealed three phases in the growth cycle (Figure 5). The lag phases of S. aureus growth in the negative control and in the presence of CS-g-poly(AA-co-HEMA) hydrogel were similar, lasting for 4 h. Then, during the exponential phase, the growth rate of *S. aureus* grown in MHB containing the CS-*g*-

For Peer Review

poly(AA-*co*-HEMA) hydrogel was lower than that of the negative control during the first 2 h of growth (4 - 6 h of total culture time), but then this growth rate decreased in the control culture from after 6 h up to reaching the start of the stationary phase (12 h), whereas the growth rate did not slow down in the cultures with CS-*g*-poly(AA-*co*-HEMA) until 10 - 12 h of total culture time, by which time the total bacterial number (as culture optical density) was slightly higher (1.5-fold) than in the control culture. From 12 – 24 h of total culture time, *S. aureus* in both conditions remained in stationary phase. Thus, the presence of the CS-*g*-poly(AA-*co*-HEMA) hydrogel appeared to render a slower early exponential growth rate of *S. aureus* (or to delay it) but did not reduce the final bacterial density reached after 12 – 24 h in the stationary phase. Since we did not count the viable bacteria that are attached to the gel, or wash them out from the gel, then the CS-grafted hydrogels may not be inhibitory at all but rather the bacteria grow attached to the gel surface and so are not in suspension first and only in suspension subsequently after the gel surface is full swollen and thus has the apparent delayed kinetics appearance.

3.6.2 The total Plate count method

The antibacterial activities of sterile sodium ampicillin (positive control), CS and grafted CS hydrogels against *S. aureus* were determined by the total plate count method. The mean CFU ml^{-1} and the relative inhibition of CS and grafted CS hydrogels are summarized in Table 2. The relative inhibition observed with the CS hydrogel was 2.9-fold greater at 6 h of culture time (early log phase) than that after 8 h of culture (the late log phase). When the CS was grafted with poly(AA), the antibacterial activity was significantly improved 1.53- and 4.23-fold after both 6 and 8 h of culture at 93 and 89% relative inhibition, respectively, because of the

For Peer Review

hydrophilicity of poly(AA),[41] and the biological activity of the free amino groups at the C-2 position of the native CS.[42] The higher antibacterial activities of the CS-*g*-poly(AA) hydrogel can be caused by the interaction between the negative charges on the bacteria surface with the positive surface of the CS-*g*-poly(AA). The more positively charged hydrogels could promote bacterial adhesion onto the hydrogel surface and reduce the remaining amount in the free suspension, resulting in a decrease in the bacteria colonies in the liquid medium. It is relevant to note here that the amount (molar ratio) of the AA or HEMA monomers that were grafted onto the CS is almost the same for the three different grafted CS derivatives studied here.

It was anticipated that the pores on the CS-*g*-poly(AA) hydrogel surface would improve the ability to capture bacteria. Although, the relative inhibition of the CS-*g*-poly(AA-*co*-HEMA) hydrogel would be higher than that of CS, because of the hydrophilicity resulting from the carboxyl group of poly(AA), the surface of the CS-*g*-poly(AA-*co*-HEMA) hydrogel is much rougher than the ungrafted CS hydrogel surface, which may increase bacterial adhesion sites and result in a higher antibacterial activity in the CS-*g*-poly(AA-*co*-HEMA) hydrogel than that of the CS. However, the relative inhibition of the CS-*g*-poly(AA-*co*-HEMA) hydrogel was found to actually be 1.35- and 3.3-fold lower than that of the CH-*g*-poly(AA) hydrogel in the early (6 h) and late (8 h) log phases, respectively. This is likely to be due to the decreased hydrophilicity of the HEMA moiety.[41] Thus, graft copolymerization of CS with a 1:1 molar ratio of AA: HEMA can delay (or inhibit) the growth of *S. aureus* in the early exponential phase.

The antibacterial activity of the CS-*g*-poly(AA-*co*-HEMA)/mica nanocomposite hydrogels are summarized in Table 2. The relative inhibition of CS-*g*-poly(AA-*co*-HEMA)/mica nanocomposite hydrogels having mica loadings at 7 and

For Peer Review

10% w w^{-1} of the monomer was slightly higher (1.3- and 1.11-fold) at a culture time of 6 h than that of the CS and CS-*g*-poly(AA-*co*-HEMA) hydrogel, respectively. This finding is in agreement with those reported by Wang et al..[15] However, CS-*g*-poly(AA-*co*-HEMA) exhibited higher relative inhibition against *S. aureus* growth by 1.2- and 1.1-fold comparing with 10 and 7% w w^{-1} mica loading, respectively, at 8 h of culture. Increasing the mica loading to 15% w w^{-1} of the monomer significantly decreased the apparent antibacterial activity 2.03- and 2.13-fold of that seen with no mica addition, and 2.25- and 1.9-fold of that seen with a 7% w w^{-1} mica loading after 6 and 8 h of culture, respectively. This result agreed quite well with Meng et al.,[16] finding that CS intercalated mica hydrogels could kill more bacteria than the neat CS or the clay minerals.

Nanocomposite hydrogels can generate a larger surface area to absorb more bacterial colonies and so give a greater chance to increase the antibacterial activity through interactions between the positive charges of the CS hydrogel and the negative charges on the cytoplasmic cell membrane of the bacteria.[15,42] In addition, *S. aureus* does not have an outer membrane to prevent the influx of foreign molecules[42] and so it can be inhibited more easily. However, the higher mica loading at 15% w w^{-1} of the monomer revealed a significantly decreased level of relative inhibition of *S. aureus* growth. This might be because the higher mica content screens and prevents the polymer chains from adhering with the bacteria to trigger the antibacterial activity.

3.6.3 Minimum inhibition concentration (MIC)

The MIC obtained for the CS-*g*-poly(AA) at 1.56 mg ml^{-1} against the 0.01 A_{610} Units of *S. aureus* cultured in MHB for 24 h (i.e. to the late stationary phase) at room temperature was 16- and >16-fold better than that of CS and CS-*g*-poly(HEMA),

For Peer Review

respectively (Table 3). These MICs agree with that of viable counts and relative inhibition of *S. aureus* in the log phase of growth (Table 1). The extent of the water absorbency and acidity of the hydrogels plays influencing roles as described in the total plate count method for the MIC result. The more the hydrogel expanded, the higher the number of colonies of *S. aureus* that could be trapped and inhibited through the diffusion effect by water in the hydrogel. The higher acidic moiety of the CS-*g*-poly(AA) hydrogels, which carry a higher positive charge, may enhance the inhibitory effect with CS. It is worth noting that the presence of the COO^- group in the poly(AA) containing hydrogels (CS-*g*-poly(AA) and CS-*g*-poly(AA-*co*-HEMA)) becomes a major driving force for bacterial adhesion in the positively charged CS. AA in the feed is a key factor governing the antibacterial property in the resulting hydrogel and nanocomposites hydrogels. The high MIC value for the CS-*g*-poly(HEMA) was potentially caused by the proposed semi-IPN structure and the rigid conformation of poly(HEMA) chains grafted onto the CS backbones.

Surprisingly, the CS-*g*-poly(AA-*co*-HEMA)/mica nanocomposite hydrogels with mica loadings of 5, 7, 10 and 15% w w^{-1} of the monomer had the same MIC values as each other and as that for the CS-*g*-poly(AA-*co*-HEMA) hydrogel (Table 3). This correlates with the almost constant water absorbency observed for the CS-*g*-poly(AA-*co*-HEMA) and the CS-*g*-poly(AA-*co*-HEMA)/mica nanocomposite hydrogels regardless of the mica loadings but relatively lower water absorbency at 15% w/w. Likewise, a much higher concentration of CS (25 mg ml^{-1}) or CS-*g*-poly(HEMA) (>25 mg ml^{-1}) or CS-*g*-poly(AA-*co*-HEMA)/mica nanocomposite hydrogels (12.5 mg ml^{-1}) is required for inhibiting *S. aureus* after 24 h of incubation.

Typical SEM micrographs of *S. aureus* cells cultured for 24 h in the MHB media alone (negative control), and in the various grafted CS copolymer and CS-*g*-

For Peer Review

poly(AA-*co*-HEMA)/mica nanocomposite hydrogels are shown in Figure 6. Since the positive control in the total plate count did not produce any viable cells, then the positive control in MIC was not performed. The normal roundish-shapes of *S. aureus* cells were evident when cultured in the MHB media alone and also as adhered on the surface of mica (Figure 6(a,b), respectively). However, the cell walls of some of the *S. aureus* in or on the CS-*g*-poly(HEMA) and CS-g-poly(AA-*co*-HEMA) hydrogels after culture for 24 h were destroyed to give open cells (Figure 6(c) as shown in Figure 6(d)). Moreover, of the *S. aureus* cells that were adsorbed and immobilized on the surface and in the pores of the CS-*g*-poly(AA-*co*-HEMA)/mica nanocomposite hydrogels, some had distorted shapes and were destroyed to give fractured cell walls and these were randomly distributed in the hydrogel matrix (Figure 6(e-h)).

Although the water absorbency of the nanocomposite hydrogels was relatively lower than that of the grafted CS hydrogel, the hydrogels had larger surface area to absorb more bacterial colonies.[15] With this compensation, the MIC values of nanocomposite hydrogels are not different from that of the grafted CS hydrogel. Thus, CS-*g*-poly(AA-*co*-HEMA) hydrogel or CS-*g*-poly(AA-*co*-HEMA)/mica nanocomposite hydrogels were at an equilibrium condition and gave similar MIC values.

The MIC values and SEM micrographs support that the mica content in the grafted CS hydrogel did not influence the antibacterial activity. On the other hand, the different results from the plate count method are caused by the absorbance assays undertaken in the mid- and late-log phases of growth at 6 and 8 h, respectively, whilst the MIC was evaluated at a late stationary phase (24 h). The different culture times could have resulted in different cell numbers due to different chances of cell adsorption by the nanocomposite hydrogels, as well as growth and death rates

For Peer Review

4. Conclusion

CS was used to graft with AA and/or HEMA to give the grafted-CS hydrogels. CS-*g*-poly(AA-*co*-HEMA)/mica nanocomposite hydrogels were synthesized at different mica loadings and all hydrogels were characterized by FT-IR spectroscopy, SEM, XRD, TEM and equilibrium water absorbency. FT-IR spectroscopy indicated that the CS was grafted at the NH_2 and OH sites on the CS backbone. The water absorbency of the CS-*g*-poly(AA) hydrogel was the highest whilst those of CS and CS-*g*-poly(HEMA) were the lowest. The CS-*g*-poly(AA-*co*-HEMA)/mica nanocomposite hydrogels had an intercalated structure, as revealed by XRD and TEM analyses.

At the fixed 1:1 molar ratio of AA: HEMA, the extent of water absorbency of the nanocomposite hydrogels was constant at 5, 7 and 10% (w w^{-1} of the monomer) mica loading but slightly decreased at 15% w w^{-1} mica loading. The CS-*g*-poly(AA) hydrogel can inhibit the early-to-mid-log phase growth of *S. aureus* up to 93% with a MIC value as low as 1.56 mg ml^{-1}. For the CS-*g*-poly(AA-*co*-HEMA)/mica nanocomposite hydrogels, the relative inhibition was very similar (at ~81%) with mica loadings of 5, 7 and 10% w w^{-1} of the monomer, but abruptly decreased at a 15% w w^{-1} mica loading. Regardless of the mica loading levels in the CS-*g*-poly(AA-*co*-HEMA)/mica nanocomposite hydrogels, the MIC value at the late stationary phase was constant at 12.5 mg ml^{-1}. The CS-*g*-poly(HEMA) had a greater MIC (>25 mg ml^{-1}) than CS (25 mg ml^{-1}). Several possible explanations for the different inhibitory activities against *S. aureus* are discussed, but await further research for clarification.

For Peer Review

Acknowledgements

The authors would like to acknowledge the financial support from the Thailand Research Fund under the Research Team Aided Program Contract no. RTA5080004. Partial financial support from the Graduate School, Chulalongkorn University is acknowledged. The provision of research facilities by the Imaging Polymer Laboratory of Chulalongkorn University's Department of Imaging and Printing Technology, Faculty of Science is highly appreciated. English edition by the Publication Counselor Unit of the Research Division, Faculty of Science, Chulalongkorn University, and fruitful suggestion provided by Dr. Robert Butcher are highly appreciated.

For Peer Review

References

1. Devine, D. M.; Higginbotham, C. L. Eur Polym J 2005, 41, 1272.
2. Rinaudo, M. Prog Polym Sci 2006, 31, 603.
3. Dos Santos, K. S. C. R.; Coelho, J. F. J.; Ferreira, P.; Pinto, I.; Lorenzetti, S.G., Ferreira, E. I.; Higa, O. Z.; Gil, M. H. Int J Pharm 2006, 310, 37.
4. Mahdavinia, G. R.; Pourjavadi, A.; Hosseinzadeh, H.; Zohuriaan, M. J. Eur Polym J 2004, 40, 1399.
5. Jalal Zohuriaan-Mehr, M. Iran Polym J 2005, 14, 235.
6. Carenza, M. Int J Radiat Appl Instrum C Radiat Phys Chem 1992, 39, 485.
7. Schweikl, H.; Hartmann, A.; Hiller, K-A.; Spagnuolo, G.; Bolay, C.; Brockhoff, G.; Schmalz, G. Dent Mater 2007, 23, 688.
8. Pawlowska, E.; Poplawski, T.; Ksiazek, D.; Szczepanska, J., Blasiak, J. Mutation Res 2010, 696, 122.

9. Tanodekaew, S.; Prasitsilp, M.; Swasdison, S.; Thavornyutikarn, B.; Pothsree, T.; Pateepasen, R. Biomaterials 2004, 25, 1453.

10. Sahu, K.; Verma, Y.; Sharma, M.; Rao, K. D.; Gupta, P. K. Skin Res Tech 2010, 16, 428.

11. Tang, C.; Chen, N.; Zhang, Q.; Wang, K.; Fu, Q.; Zhang, X. Polym Degrad Stabil 2009, 94, 124.

12. Wang, X.; Du, Y.; Luo, J.; Yang, J.; Wang, X.; Shi, X.; Hu, Y. Polymer 2006, 47, 6738.

13. Wang, X.; Du, Y.; Luo, J.; Yang, J.; Wang, W.; Kennedy, J. F. Carbohydr Polym 2009, 77, 449.

14. Xie, Y.; Wang, A.; Liu, G. Polym Compos 2010, 3, 89.

15. Wang, X.; Du, Y.; Luo, J.; Lin, B.; Kennedy, J. F. Carbohydr Polym 2007, 69, 41.

16. Meng, N.; Zhou, N.; Zhang, S.; Shen, J. Appl Clay Sci 2009, 42, 667.

17. Bozhilov, K. N.; Xu, Z.; Dobrzhinetskaya, L. F.; Jin, Z-M.; Green II, H. W. Lithos 2009, 109, 304.

18. Tjong, S. C. Synthesis and structure-property characteristics of clay-polymer Nanocomposites, Nanocrystalline Materials; Oxford: Elsevier, 2006; Chapter 10; p. 311.

19. Hsu, S.; Tseng, H.; Hung, H.; Wang, M.; Hung, C.; Li, P.; Lin, J. Appl Mater Interfaces 2009, 1(11), 2556.

20. Li, P.; Wei, J.; Chiu, Y.; Su, H.; Peng, F.; Lin, J. Appl Mater Interfaces 2010, 2, 1608.

21. Patil, D. R., Fanta, G. F. J Appl Polym Sci 1993, 47, 1765.

22. Lanthong, P.; Nuisin, R.; Kiatkamjornwong, S. Carbohydr Polym 2006, 66, 229.

For Peer Review

23. Mun, G. A.; Nurkeeva, Z. S.; Dergunov, S. A.; Nama, I. K.; Maimakov, T.P.; Shaikhutdinov, E. M.; Lee, S. C.; Park, K. React Funct Polym 2008, 68, 389.

24. Sun, T.; Zhou, D.; Xie, J.; Mao, F. Eur Food Res Technol 2007, 225, 451.

25. Zhang, J.; Wang, Q.; Wang, A. Carbohydr Polym 2007, 68, 367.

26. Singha, V.; Sharmaa, A. K.; Tripathi, D. N.; Sanghib, R. J Hazard Mater 2009, 161, 955.

27. Huacai, G.; Wan, P.; Dengke, L. Carbohydr Polym 2006, 66, 372.

28. Mishra, D. K.; Tripathy, J.; Srivastava, A.; Mishra, M. M.; Behari, K. Carbohydr Polym 2008, 74, 632.

29. Casimiroa, M. H.; Botelho, M. L.; Leal, J. P.; Gil, M. H. Radiat Phys Chem 2005, 72, 731.

30. Semenzato, S.; Lorenzetti, A.; Modesti, M.; Ugel, E.; Hrelja, D.; Besco, S.; Michelin, R. A.; Sassi, A.; Facchin, G.; Zorzi, F.; Bertani, R. Appl Clay Sci 2009, 44, 35.

31. Dai, H.; Li, H.; Wang, F. Surf Coat Technol 2006, 201, 2859.

32. Bayramoğlu, G.; Arica, M. Y. Colloids Surf A 2002, 202, 41.

33. Wang, J. P.; Chen, Y. Z.; Zhang, S. J.; Yu, H. Q. Bioresour Technol 2008, 99, 3397.

34. Luckachan, G. E.; Pillai, C. K. S. Carbohydr Polym 2006, 64, 254.

35. Kittur, F. S.; Kumar, A. B. V.; Tharanathan, R. N. Carbohydr Res 2003, 338, 1283.

36. Krishna Rao, K. S. V.; Chung, I.; Ha, C. S. React Funct Polym 2008, 68, 943.

37. Sivudu, K. S.; Thomas, S.; Shailaja, D. Appl Clay Sci 2007, 37, 185.

38. Sperling, L. H. Introduction to Physical Polymer Sciences. 4th ed.; New York: John Wiley & Sons, 2006; p. 477.

For Peer Review

39. Zhou, Y.; Yang, D.; Gao, X.; Chen, X.; Xu, Q.; Lu, F.; Nie, J. Carbohydr Polym 2009, 75, 293.

40. Mohan, Y. M.; Lee, K.; Premkumar, T.; Geckeler, K. E. Polymer 2007, 48, 158.

41. Oh, S. T.; Han, S. H.; Ha, C. S.; Cho, W. J. J Appl Polym Sci 1996, 59, 1871.

42. Je, J.; Kim, S. J Agric Food Chem 2006, 54, 6629.

For Peer Review

Table 1. The water absorbency of hydrogels derived from CS, AA and /or HEMA grafted-CS copolymers and CS-g-poly(AA-*co*-HEMA)/mica nanocomposites.

Polymer	AA: HEMA (mol ratio)	Mica (w w^{-1} of monomer)	Water absorbency (g g^{-1})[1]
CS	--	--	10 ± 2
CS-*g*-poly(AA)	--	--	101 ± 4
CS-*g*-poly(HEMA)	--	--	11 ± 1
CS-*g*-poly(AA-*co*-HEMA)	3:1	--	64 ± 2
	1:1	--	54 ± 3
	1:3	--	20 ± 2
	1:1	5	45 ± 3
	1:1	7	44 ± 1
	1:1	10	46 ± 2
	1:1	15	35 ± 5

[1]Data are shown as the mean ± 1 SD and are derived from 5 repeats. Means within the column are significantly different ($p<0.05$).

For Peer Review

Table 2. Total plate counts (replication competent cells) and the relative inhibition of growth of *S. aureus* in the presence of sodium ampicillin and the hydrogels of CS, AA and/or HEMA grafted-CS copolymers and CS-*g*-poly(AA-*co*-HEMA)/mica nanocomposites with various mica loadings.

Sample type	Mica (% w w^{-1})	6 h culture time		8 h culture time	
		CFU ml^{-1} (x 10^9)[1]	Relative inhibition (%)	CFU ml^{-1} (x 10^9)[1]	Relative inhibition (%)
Negative control[2]	--	6.95 ± 1.51	-	8.15 ± 1.25	-
Positive control[3]	--	0	100	0	100
CS[4]	--	2.7 ± 0.25	61	6.4 ± 1.68	21
CS-*g*-poly(AA)[4]	--	0.52 ± 0.48	93	0.91 ± 0.85	89
CS-*g*-poly(HEMA)[4]	--	2.18 ± 0.28	69	5.95 ± 1.25	27
CS-g-poly(AA-*co*-HEMA)[4]	--	1.90 ± 0.19	73	2.92 ± 0.07	64
CS-*g*-poly(AA-*co*-HEMA)[4]	7	1.4 ± 0.37	81	3.6 ± 0.55	57
CS-*g*-poly(AA-*co*-HEMA)[4]	10	1.5 ± 0.34	81	3.9 ± 0.31	54
CS-*g*-poly(AA-*co*-HEMA)[4]	15	5.0 ± 1.68	36	5.9 ± 2.4	30

[1]CFU ml^{-1} is shown as the mean ± 1 SD and are derived from 6 repeats. Means within a column or across a row are significantly different ($p<0.05$).

[2]Negative control contains only the MHB medium and *S. aureus*.

[3]Positive control contains 250 mg of the sodium ampicillin, MHB medium and *S. aureus*.

[4]All hydrogel samples were co-cultured with *S. aureus* in MHB media at 250 mg ml^{-1}.

For Peer Review

Table 3. Minimum inhibition concentration of hydrogels derived from CS, AA and/or HEMA grafted-CS copolymers and CS-*g*-poly(AA-*co*-HEMA)/mica nanocomposites with various mica loadings.

Sample test	Mica (% w w^{-1})	CFU ml^{-1} (x 10^8)[1]	MIC (mg ml^{-1})[2]
Negative control[3]	-	18 ± 1.0	-
CS[4]	--	10 ± 0.6	25
CS-*g*-poly(AA)[4]	--	3.0 ± 0.4	1.56
CS-*g*-poly(HEMA)[4]	--	6.6 ± 3.5	> 25
CS-*g*-poly(AA-*co*-HEMA)[4]	--	1.2 ± 0.5	12.5
CS-*g*-poly(AA-*co*-HEMA)[4]	5	1.1 ± 0.4	12.5
CS-*g*-poly(AA-*co*-HEMA)[4]	7	5.1 ± 0.6	12.5
CS-*g*-poly(AA-*co*-HEMA)[4]	10	4.6 ± 0.4	12.5
CS-*g*-poly(AA-*co*-HEMA)[4]	15	4.9 ± 4.9	12.5

[1]CFU ml^{-1} is shown as the mean ± 1 SD and is derived from 3 repeats. Means within the column are significantly different ($p<0.05$).

[2]MIC are shown as mg ml^{-1} for a 2% (v v^{-1}) seeding of a late log phase culture of *S. aureus* in MHB media and evaluated at late stationary phase (24 hr of culture).

[3]Negative control contains only the MHB medium and *S. aureus*.

[4]All hydrogel samples were co-cultured with *S. aureus* in MHB media at 250 mg ml^{-1}.

For Peer Review

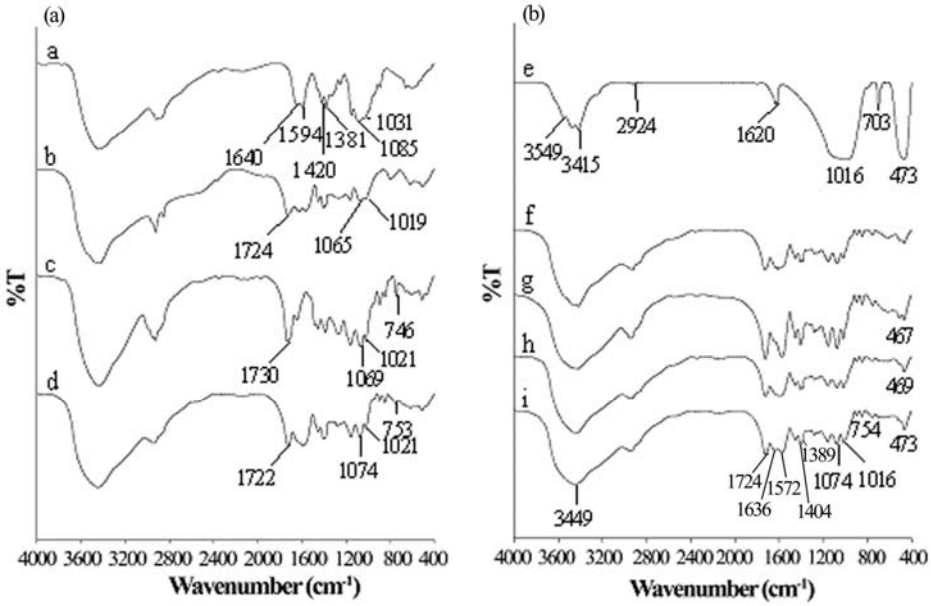

Figure 1

Representative FT-IR spectra of (A): (a) CS, and (b) CS-g-poly(AA), (c) CS-g-poly(HEMA) and (d) CS-g-poly(AA-co-HEMA) hydrogels, the last being synthesized with an AA: HEMA, N-MBA: CH, APS: CH and TEMED: CH molar ratios of 1, 0.11, 0.07 and 0.58, respectively; (B): (e) mica, and CS-g-poly(AA-co-HEMA)/mica nanocomposite hydrogels with mica loadings of: (f) 5%, (g) 7%, (h) 10% and (i) 15% w w-1 based on the monomer.
104x72mm (600 x 600 DPI)

eview

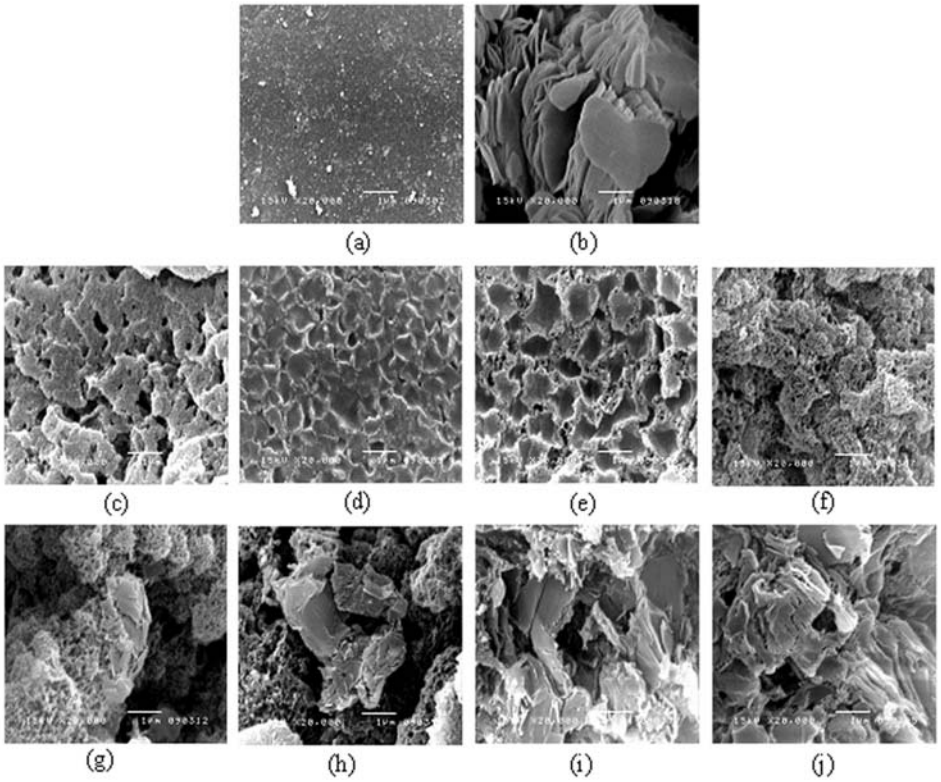

Figure 2

Representative SEM micrographs of (a) CS, (b) mica, (c) CS-g-poly(AA), (d) CS-g-poly(HEMA), (e, f) CS-g-poly(AA-co-HEMA), and CS-g-poly(AA-co-HEMA)/mica composite hydrogels synthesized with mica loading levels of (g) 5%, (h) 7%, (i) 10% and (j) 15% w w-1 of the monomer.
158x140mm (400 x 400 DPI)

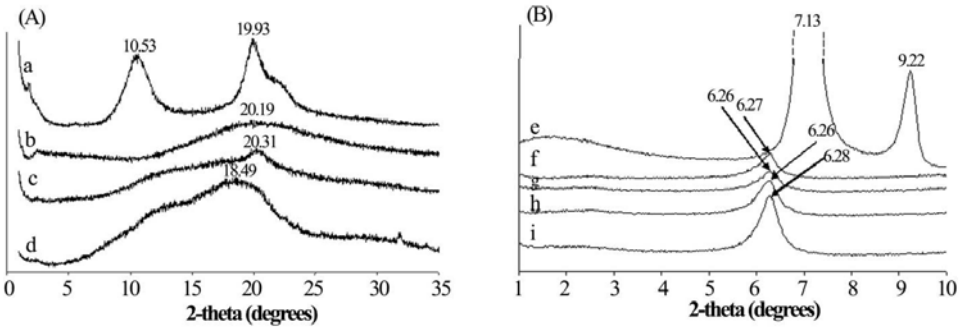

Figure 3

Representative XRD patterns of hydrogels synthesized from (A): (a) CS, (b) CS-g-poly(AA) synthesized with 1 g CS, 54 mmol AA, and N-MBA, APS and TEMED at 10%, 10% and 40% w w-1 of CS, respectively, (c) CS-g-poly(AA-co-HEMA) and (d) CS-g-poly(HEMA); (B): (e) mica, and CS-g-poly(AA-co-HEMA)/mica nanocomposite hydrogels synthesized with mica loadings of (f) 5%, (g) 7%, (h) 10% and (i) 15% w w-1 based on the monomer, 1 g CS, an AA: HEMA molar ratio of 1:1, and N-MBA, APS and TEMED at 10%, 10% and 40% w w-1 of CS, respectively.
60x24mm (600 x 600 DPI)

eer Review

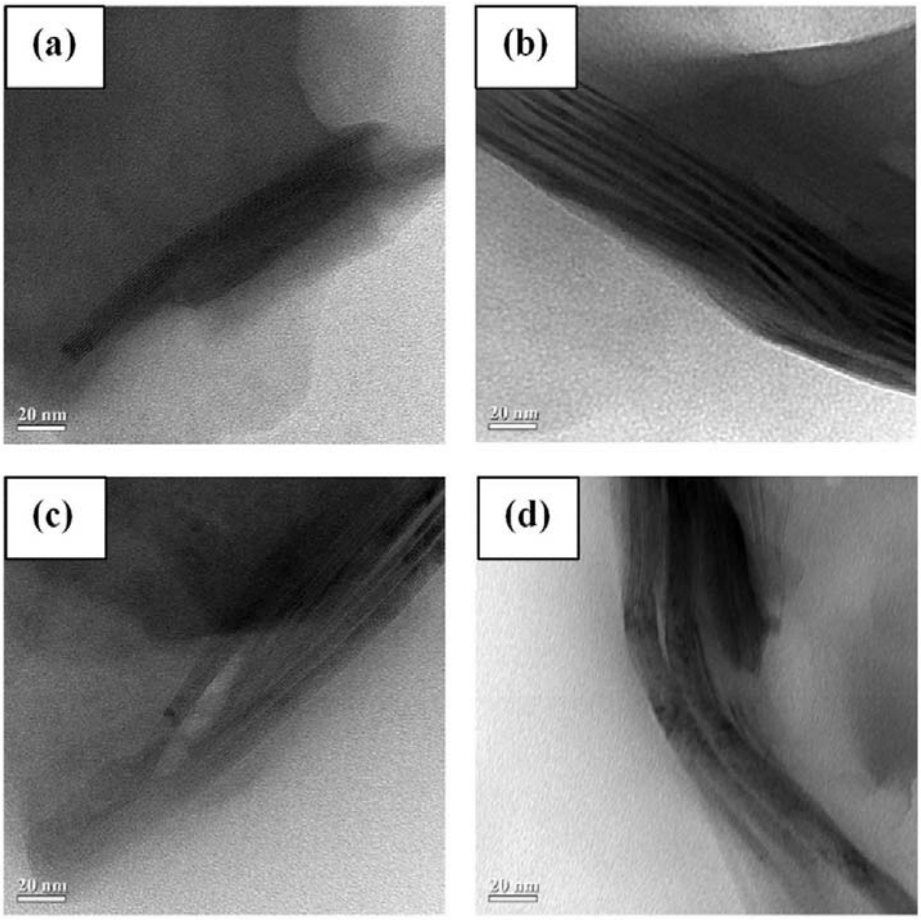

Figure 4

Representative TEM micrographs of CS-g-poly(AA-co-HEMA)/mica composite hydrogels synthesized with mica loadings of (a) 5%, (b) 7%, (c) 10% and (d) 15% w w-1 based on the monomer.
104x115mm (300 x 300 DPI)

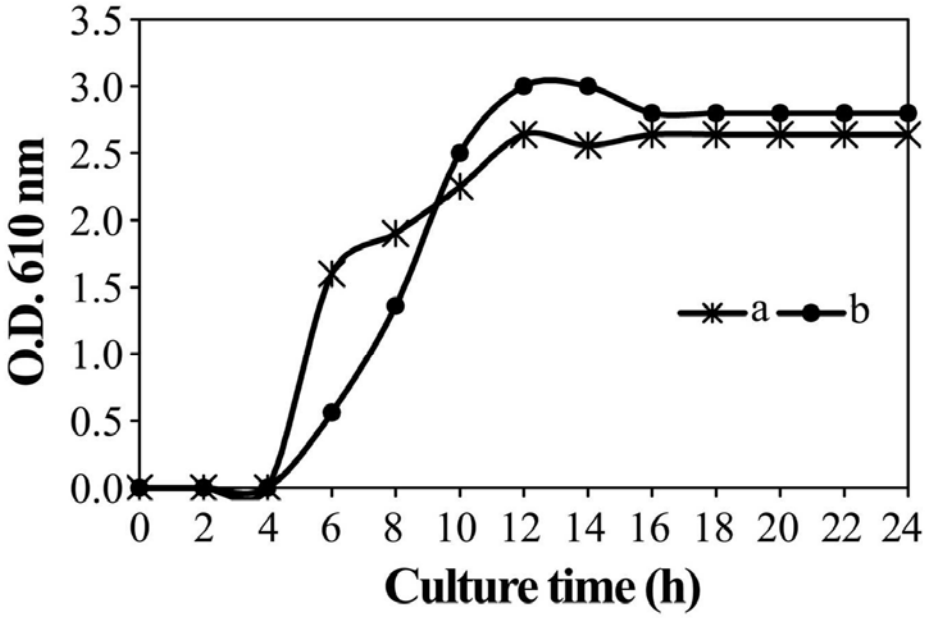

Figure 5

The optical density at 610 nm of S. aureus cultured in HMB media at various culture times with (a) the negative control, or 250 mg ml-1of (b) CS-g-poly(AA-co-HEMA) hydrogel prepared with 1 g CS, a AA: HEMA molar ratio of 1:1, and N-MBA, APS and TEMED at 10%, 10% and 40% w w-1 of CS, respectively, with polymerization performed at 250 pm and 60 °C for 60 min.
59x45mm (600 x 600 DPI)

view

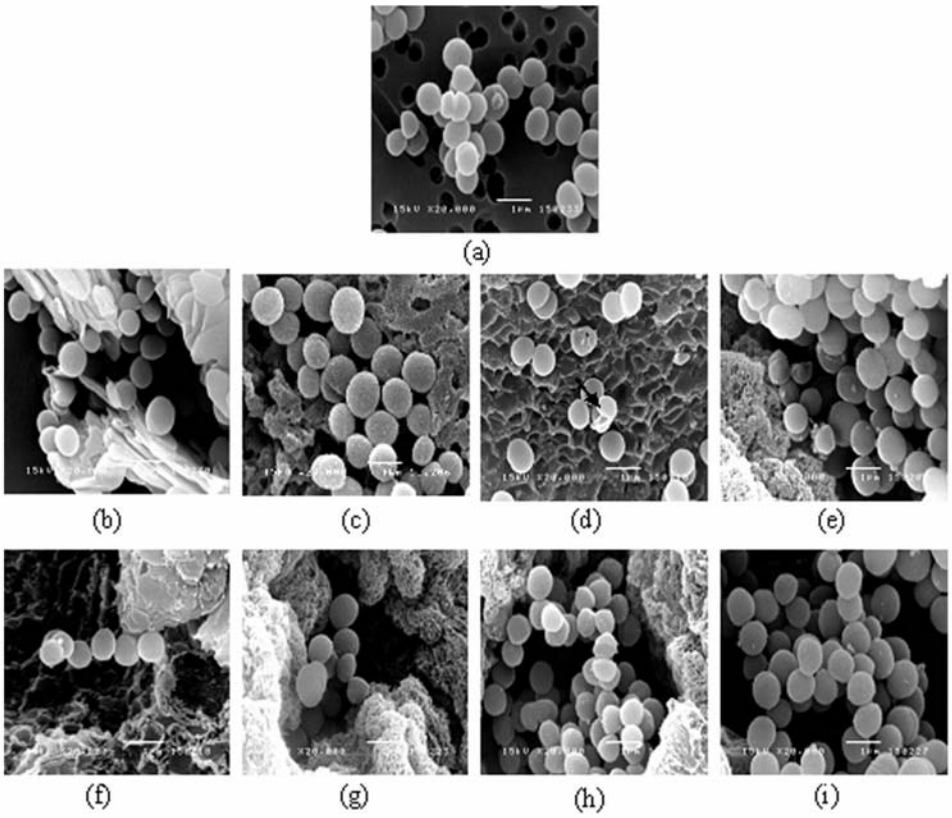

Figure 6

Representative SEM micrographs of S. aureus after co-culture for 24 h with (a) negative control, (b) mica, (c) CS-g-poly(AA), (d) CS-g-poly(HEMA), (e) CS-g-poly(AA-co-PHEMA) and CS-g-poly(AA-co-PHEMA)/mica nanocomposites with mica loadings of: (f) 5%, (g) 7%, (h) 10% and (i) 15% w w-1 based on the monomer. The arrow in (d) highlights a damaged cell.
152x142mm (600 x 600 DPI)

KAPOK I: CHARACTERISTCS OF KAPOK FIBER AS A POTENTIAL PULP SOURCE FOR PAPERMAKING

Somporn Chaiarrekij,* Apiporn Apirakchaiskul, Kuntinee Suvarnakich, and Suda Kiatkamjornwong

The potential use of kapok fiber for pulping and papermaking has been investigated. The kapok fibers were cooked using the optimal dosage of sodium hydroxide determined from the experiments. Then, the pulp was refined twice using a disc refiner with a disc gap of 1/100 inch and this kapok pulp was mixed with commercial hardwood pulp and/or softwood pulp at different blend ratios to make papers. Addition of the kapok pulp to the mixed pulps improved the tensile and burst strengths of the sheets but decreased the tear resistance and elongation. Brightness and opacity of the sheets were also dropped with the addition of kapok pulp to the mixed pulps. Water repellency of the sheets prepared from the kapok pulp mixed with the commercial pulps was also improved. These results indicate that kapok fiber can be a quality pulp source for papermaking, especially for packaging paper.

Keywords: Kapok fiber; Properties; Raw material; Papermaking

*Contact information: Department of Imaging and Printing Technology, Faculty of Science, Chulalongkorn University, Phayathai Road, Bangkok, 10330 Thailand; *Corresponding author: Huaja@hotmail.com*

INTRODUCTION

The kapok tree, *Ceiba pentandra (L.)* Gaertn. (Malvales: Malvaceae), formerly Bombacaceae family, is cultivated widely in Southeast Asia, as well as other parts of East Asia and Africa. The kapok fiber is an agricultural product obtained from the fruits of the kapok tree (Tang et al. 2008; Qiuling and Lin 2009). Kapok fibers have a hollow structure with a thin fiber wall and large lumen (Hong et al. 2005; Lim and Huang 2007). The diameter including the fiber wall is 16.5 ± 2.4 μm. The lumen diameter is 14.5 ± 2.4 μm and the fiber length is 25 ± 5 μm (Huang and Lim 2006). Kapok fibers are fluffy, light-weight and too inelastic to be spun, and so are good for stuffing beds, pillows and cushions. Chemical compositions of kapok fiber were differently reported by two groups of researchers. The first one mentioned that kapok fiber is chemically composed of 64% cellulose, 13% lignin and 23% pentosan on a weight basis (Kobayashi et al. 1977) while the other stated that it comprises of 35% cellulose, 21.5% lignin, 22% xylan and 13% of acetyl groups on a weight basis (Hori et al. 2000). Besides all those mentioned chemical compositions, they also contain a waxy cutin on the fiber surface which makes them water repellent and oil absorbent. Thus, they are also useful in oil removal applications (Hori et al. 2000; Khan et al. 2004; Huang and Lim 2006; Rengasamy et al. 2011).

There are few reports on utilizing blended kapok fibers for papermaking, such as, the blend of 75:25 (w/w) kapok fibers: bamboo pulp was treated with detergent and

sodium hydroxide before being used to produce paper (Malab et al. 2001). In this case, the combination of the two non-wood fibers significantly reduced the volume of the bamboo pulp, and the amounts of chemical reagents and energy consumption, without adversely affecting the paper strength properties. Another study has indicated that kapok fibers could potentially be pulped to produce paper (Chaiarrekij et al. 2008), but this claim has not been established and any products have not been further characterized. However, it has been observed that paper sheets made from kapok pulp seemed to demonstrate superior water resistant behavior even without any sizing agents being added.

Consequently, the optimum set of pulping conditions for the kapok fibers to give the best strength properties was investigated. This optimal set of pulping conditions was then employed to produce kapok pulp. The influence of kapok pulp on paper properties when the kapok pulp was mixed with commercial hardwood pulp and softwood pulp was also determined. The hypothesis being tested was that kapok pulp might increase the strength properties of the hybrid paper prepared from mixtures of kapok pulp with conventional commercial softwood pulp and/or hardwood pulp. It was thought that as well as providing better strength, paper made of kapok pulp might possess superior water resistance, which is generally required for a packaging paper.

EXPERIMENTAL

Materials

Before pulping, the kapok fibers (sourced from the north eastern part of Thailand) were washed, cleaned, and immersed in water for three weeks prior to manually squeezing out the excess water and cutting to 3-5 cm in length. The moisture content was determined using the moisture balance (FD-600, Kett Electric Laboratory, Japan). The commercial softwood (SW) pulp from Pine and hardwood (HW) pulp from Eucalyptus were obtained from the Crofton Pulp & Paper Mill, Canada and the Phoenix Pulp & Paper Public Co., Ltd, Thailand, respectively.

Methods

The experiment was divided into 2 parts. The first part was about determination of optimal pulping condition for kapok fiber, while the second part was about examining the effects of kapok pulp addition to commercial softwood and hardwood pulps on the properties of the resultant pulp and paper.

Determination of optimal pulping condition for kapok fiber

Kapok fibers were separately pulped using 10, 15, 20, and 25% (w/w) NaOH, based on the oven-dried pulp weight. The liquor-to-wood ratio was 17:1. The pulping was carried out in an autoclave digester, (UEC-2017A, Universal Engineering, India) with an initial digesting temperature at 40 °C. The pulp matrix was then gradually heated to 120 °C over 30 min. Pulping was proceeded at this temperature for another 120 min. The pulp was then extensively washed with tap water to remove the alkalinity from the pulp by controlling with a pH meter (Hanna HI 98128, Hanna Instrument, U.S.A.).

Kapok pulps were refined twice through a disc refiner, using a 1/100 inch disc gap (Andritz Sprout, U.S.A.). The degree of refining was determined following the Canadian Standard Freeness (CSF) standard, using a freeness tester (CF/A, Regmed, Brazil) according to TAPPI Standard Method T227 om-04. Kapok pulps were disintegrated in a standard disintegrator (Formax T-100, Adirondack, U.S.A.) for 100,000 revolutions in hot water (80 °C) to remove latency. The average length of 5,000 fibers per sample was automatically determined using a fiber quality analyzer (FQA, Optest, Canada) according to the TAPPI Standard Method T271 om-98 using the following equations.

The arithmetic average length of individual fibers (L) is calculated from equation (1):

$$L = \frac{\Sigma n_i l_i}{\Sigma n_i} \quad (1)$$

The length-weighted average length of the fibers (L_l) is calculated from equation (2):

$$L_l = \frac{\Sigma n_i l_i^2}{\Sigma n_i l_i} \quad (2)$$

The weight-weighted average length of the fibers (L_w) is calculated from equation (3):

$$L_w = \frac{\Sigma n_i l_i^3}{\Sigma n_i l_i^2} \quad (3)$$

where the number of fibers (n_i) is the number of fibers in each class of length (l_i).

The chemical composition of each pulp was determined using TAPPI Standard Method T222 om-98 for lignin determination, TAPPI Standard Method T203 cm-99 for alpha cellulose (α-cellulose) determination, and Browning's method for holocellulose determination (Browning 1963). The amount of hemicellulose was calculated from the difference between the holocellulose content and the alpha cellulose content.

Kapok pulp was also made into 60 g/m^2 handsheets on a Rapid-Köthen sheet former (RK-2A KWT, PTI, Austria) according to the ISO Standard Method 5269-2. The brightness and opacity of the handsheets were measured using an optical tester (Color Touch PC, Technidyne, U.S.A.), based on ISO Standard Methods 2470 and 2471, respectively. The tensile, burst, tear, and zero-span tensile strengths were measured using a tensile strength tester (Strograph E-S, Toyo Seiki, Japan), a burst strength tester

(SE002P, Lorentzen & Wettre, Sweden), a tear strength tester (Protear, Thwing-Albert, U.S.A.), and a modified tensile strength tester (Pendulum Tensile Strength Tester with special clamps adjustable to zero, Toyo Seiki, Japan), according to TAPPI Standard Method T494 om-01, T403 om-02, T414 om-04 and T231 cm-96, respectively. The contact angle of water in contact with surface of handsheet was automatically measured using the Pocket Goniometer PG-3 (Fibro System, Sweden) by capturing and processing the water droplet images. The dynamic mode was used to measure the rate of change of the contact angle as a function of time. The test was done following TAPPI standard T558 om-06.

The effects of the addition of kapok pulp to commercial softwood pulp and hardwood pulps on the properties of the resultant paper samples

Kapok pulp produced by using the set of optimal conditions previously described was bleached using 3% (w/w) aqueous hydrogen peroxide at a 1.5% consistency and 80 °C for 120 min. The product was disintegrated using a disintegrator (Formax T-100, Adirondack Machine, U.S.A.) for 100,000 revolutions in hot water (80 °C) to remove latency. Each commercial pulp was beaten in a valley beater (UEC-2018A, Universal Engineering, India) in which 360 g of the oven-dried pulp in 23 L of water was accommodated, according to TAPPI Standard method T200 sp-01. The softwood pulp and hardwood pulp were separately beaten to meet the Canadian Standard Freeness of 350 mL and 300 mL, respectively. Then, the bleached kapok pulp was mixed with the commercial beaten hardwood pulp, softwood pulp and mixed pulp (25:75 (w/w) softwood: hardwood) to make handsheets. These procedures of papermaking and paper characterization were repeated in the manner as described.

Statistical analysis

Parametric data were analyzed using the analysis of variance (ANOVA). In all cases, a p-value smaller than or equal to 0.05 was accepted as being a statistically significant difference. For all of the experiments, three replicates were performed.

RESULTS AND DISCUSSION

Determination of Optimal Pulping Condition

Chemical composition of kapok pulp

The effects of the sodium hydroxide solution on the chemical composition of the kapok pulp are summarized in Table 1. Analysis of the chemical composition of the pulps showed that an increased amount of sodium hydroxide in cooking liquor resulted in lower percentages of lignin, higher percentages of holocellulose and alpha cellulose, with lower percentages of hemicellulose. It should be noted that holocellulose is composed of alpha cellulose and hemicellulose. This finding was to be expected, since sodium hydroxide solution dissolves lignin. Carbohydrates, especially hemicellulose, can also be easily destroyed by sodium hydroxide, leaving a higher ratio of alpha cellulose behind. Since all of the P-values of the chemical compositions were lower than 0.05, the effects of sodium

hydroxide solution on kapok pulp chemical compositions were thus statistically significant.

Table 1. Effects of Sodium Hydroxide Concentration on the Chemical Composition of the Kapok Pulp

Pulp Chemical Composition	NaOH Dosage (% w/w)				
	10	15	20	25	P-value
Lignin (%)	19.20	18.27	17.57	17.53	0.0109*
Holocellulose (%)	76.12	76.53	78.49	78.50	0.0005*
Alpha cellulose (%)	65.63	69.87	69.65	69.96	0.0002*
Hemicellulose (%)	10.49	6.66	8.84	8.54	0.0007*
* Statistically significant since P-value is lower than 0.05					

Kapok pulp and fiber characteristics

The effects of sodium hydroxide treatment level on pulp yield, freeness and the average fiber length, characterized in terms of arithmetic, length-weighted, and weight-weighted criteria are summarized in Table 2, along with the percentage of fines.

Table 2. Pulp and Fiber Characteristics of the Kapok Pulp after Soda Pulping

Pulp and Fiber Properties	NaOH Dosage (% w/w)			
	10	15	20	25
Pulp yield (%)	62.40	51.25	44.69	40.46
Freeness (CSF, mL)	401	362	296	277
Average fiber length-Arithmetic (mm)	0.91	0.91	0.83	0.81
Average fiber length-Length weighted (mm)	1.51	1.49	1.32	1.28
Average fiber length-Weight weighted (mm)	2.26	2.17	1.93	1.83
Fines (%)	21.5	21.6	22.7	23.7

The results in Table 2 indicate that high sodium hydroxide concentration could also result in a lower pulp yield because of the removal of lignin and extractives. Also, high sodium hydroxide dosage could lead to carbohydrate degradation, especially with the hemicellulose, due to a peeling reaction. This might also contribute to the lower pulp yield.

Table 2 shows that increasing the concentration of sodium hydroxide significantly decreased the degree of the pulp freeness. Thus, there was a decrease in the pulp's drainage capacity. This was probably due to an increasing amount of fines which would have a significantly greater surface area than fibers for water absorption. Also relevant are the removal of hydrophobic lignin, the dissolution of hemicellulose and possibly the saponification of the cutin wax by the alkali with "solvation" of the cellulose. The latter two possibilities were supported by the results from contact angle studies in which the contact angle with water decreased when the amount of alkali was increased (Fig. 1).

Figure 1 also shows that the handsheets in the dry state (at a zero contact time) had the greater water contact angles. However, after contact with the water, the contact angles decreased due to wetting, absorption, penetration, and spreading of the water under the influence of the cellulosic hydrophilic interactions.

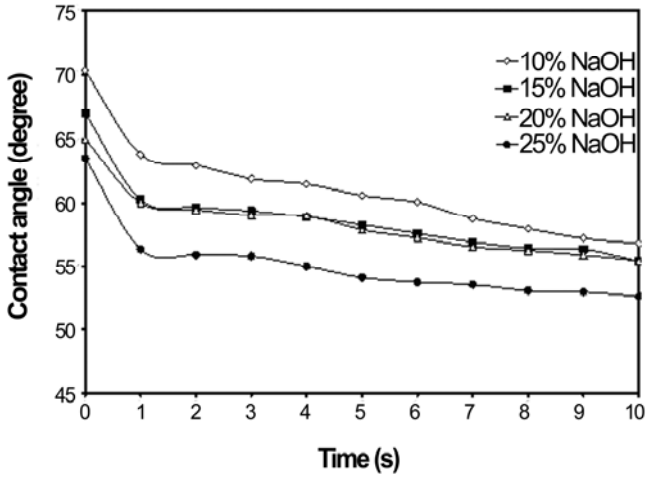

Fig. 1. The effects of different sodium hydroxide concentrations on water contact angles of the kapok fiber sheets.

It should be noted that weight weighted average fiber length is one of the average fiber length values, but it emphasizes more on the content of long fibers as compared to the length weighted fiber length and the arithmetic average fiber length, respectively. When the amount of sodium hydroxide increased, the average fiber length significantly decreased, whilst the fines content was increased (Table 2). This was likely to have occurred because the fibers were damaged by a peeling reaction under the strong alkali conditions leading to carbohydrate degradation (Sjöström 1993). Thus, the greater the amount of carbohydrate that was degraded by the alkali, the lower would be the mean fiber length and the greater would be the amount of fiber fines.

Kapok handsheet properties

The effects of the sodium hydroxide solution on the kapok handsheet properties are summarized in Table 3.

Table 3. Effects of Sodium Hydroxide Concentration on the Kapok Handsheet Properties

Pulp and Paper Properties	NaOH Dosage (% w/w)				
	10	15	20	25	P-value
Apparent density (g/cm^3)	0.68	0.80	0.82	0.88	0.1264
ISO opacity (%)	97.9	97.5	97.4	97.0	0.0235*
ISO brightness (%)	21.3	19.1	18.6	18.1	0.1917
Tensile index (N m/g)	80.3	100.4	111.5	101.3	0.0002*
Elongation (%)	1.75	2.01	2.10	2.05	0.0335*
Burst index (kPa m^2/g)	4.44	5.73	5.96	5.98	0.0348*
Tear index (mN m^2/g)	1.78	1.68	1.60	1.59	0.4005
Zero span tensile index (N m/g)	59.5	58.2	56.7	55.9	0.9801
* Statistically significant since P-value is lower than 0.05					

Increasing the amount of sodium hydroxide solution led to an increase in the apparent density of the sheets which was defined as handsheet grammage divided by

handsheet thickness, but a lower opacity (Table 3). Such effects are likely to be due to the role of sodium hydroxide solution in breaking up lignin molecules within the fiber cell wall. As the hydrophobic lignin was removed, the fiber surface became more hydrophilic, encouraging fiber swelling and conformability. This would result in a more compacted sheet that in turn, which could lead to fewer air-to-fiber interfaces and a lower opacity. In addition, the increasing content of fines and the greater amount of fiber contact areas would help to improve fiber bonding, leading to denser sheets, as indicated by the higher apparent density. Shorter fibers and a greater amount of fines also provided a basis for more effective filling of existing voids, which might also have contributed to lower opacity of the sheet. However, the effect of sodium hydroxide solutions on the apparent density appeared in this case to be statistically insignificant while its effect on opacity was statistically significant.

Pulp brightness would be expected to increase when greater amounts of sodium hydroxide solution were used, since more lignin would be removed. However, the observed trend was the opposite of this expectation, as indicated by the statistical evaluation (Table 3). However, greater concentrations of sodium hydroxide solution might reduce pulp brightness through an alkali darkening reaction, resulting in structural changes of the chromophoric groups in the residual lignin. These groups could also absorb light and thus cause the brightness of the pulp to decrease. An additional plausible explanation might be that the sodium hydroxide solution mediated the removal of lignin and caused greater sheet compactness with a resultant reduced level of light scattering of the sheet, whilst the greater amount of fines might also lead to sheet compactness.

The tensile index defines the tensile strength of paper. It is the tensile strength divided by the grammage. The burst index defines the burst strength of the paper and is equal to the burst strength divided by the grammage. Fiber bonding is highly likely to affect the tensile strength and burst strength. Increasing sodium hydroxide dosage provided higher tensile and burst strengths due to increasing fiber bonding, since lignin was removed and fibers became more conformable (Table 3). Increased fiber bonding caused by the greater sodium hydroxide dosage also led to the higher elongation. However, it should be noticed that using too high dosage of sodium hydroxide was detrimental to tensile and burst strengths as a result of carbohydrate degradation by peeling reaction at a strong alkali condition. The effects of the sodium hydroxide concentration in cooking liquor on the tensile index, the elongation and the burst index were statistically significant.

The tear index, the tear resistance value divided by the grammage, defines the tear resistance of the paper. Tear resistance is affected by many factors, such as the intrinsic fiber strength, the fiber length, and fiber bonding. The most important factor for well-bonded sheets is the fiber strength. The zero span tensile index is defined by the zero-span tensile strength divided by the grammage. Generally, zero span tensile index is a function of both the intrinsic fiber strength and the fiber bonding; however, the intrinsic fiber strength is a major contributing factor. The tear index decreased when the sodium hydroxide concentration increased (Table 3). The same observation was found for the zero span tensile index. This effect could be caused by the peeling reaction that destroys endwise, the chains of cellulose and hemicellulose and by the alkaline hydrolysis that leads to a drop in the degree of polymerization of the fibers (Shatalov and Pereira 2005).

The decrease in tear resistance might also be caused by the shorter fiber length and the greater amount of fines that are created. However, the effects of sodium hydroxide dosage on the tear and zero span tensile index values were so small that they were statistically insignificant.

Overall, the optimum condition for kapok fiber pulping was that of the cooking liquor containing 20% (w/w) of sodium hydroxide, which gave the maximum tensile properties as discussed. Thus, kapok pulp that was prepared using a 20% (w/w) sodium hydroxide dosage was used in subsequent experiments. However, the pulp was bleached before being mixed with commercial pulps.

Effects of Kapok Pulp Addition to Commercial Softwood and Hardwood Pulps on the Properties of the Resultant Pulp and Paper

Fiber length distributions of kapok, softwood and hardwood pulps

The fiber length distributions of the kapok pulp that was produced using the cooking liquor of 20% (w/w) sodium hydroxide and the commercial softwood pulp and hardwood pulp are shown in Fig. 2.

The kapok pulp had an intermediate amount of short fibers that was less than that of the hardwood pulps. The softwood pulp gave the lowest short fiber content. The kapok pulp was also intermediate in the amount of both medium and long fibers. These were lower than that from the hardwood pulp. The softwood pulp contained the greater amount of long fibers.

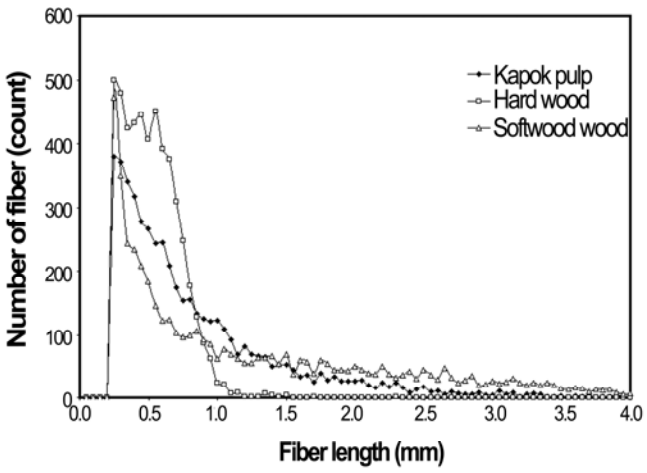

Fig. 2. Fiber length distributions of the kapok, hardwood and softwood pulps.

Fiber length, fines content and zero span tensile index of kapok, softwood and hardwood pulps

Fiber length, fines content and zero span tensile index of kapok, softwood and hardwood pulps are compared and illustrated in Table 4.

Table 4. Fiber Length, Fines Content and Zero Span Tensile Index of Kapok and the Commercial Pulps

Pulp Properties	Pulp Types		
	Kapok	Softwood (SW)	Hardwood (HW)
Average fiber length-Arithmetic (mm)	0.83	1.25	0.50
Fines (%)	22.7	43.2	34.0
Zero span tensile index (N m/g)	56.7	82.6	44.2

After being refined to the freeness of 300 mL as shown in Table 4, the average fiber length of the kapok pulp (0.834 mm) was between those of the softwood pulp (1.253 mm) and hardwood pulp (0.496 mm). The kapok pulp also had the lowest level of fines, followed by the hardwood pulp and softwood pulp, respectively.

As shown in Table 4, the sheets made from the softwood and hardwood pulps had the greatest and least zero-span tensile index at 82.6 and 44.2 N m/g, respectively. That made from kapok pulp was 56.7 N m/g. Since kapok fiber was brittle, this led to the lower zero span tensile index of kapok pulp.

Apparent density

The apparent densities of the sheets that were prepared from different ratios of the kapok pulp to the commercial softwood (SW), hardwood (HW) and softwood-hardwood mixed pulps, are shown in Fig. 3.

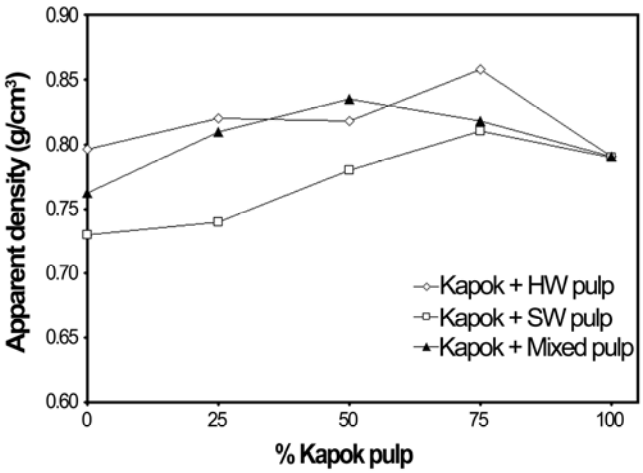

Fig. 3. Apparent density of the sheets made from kapok pulp mixed with the commercial hardwood (HW) pulp and softwood (SW) pulp at the indicated percentages.

The sheets made from the hardwood pulp had a greater apparent density than those containing either the softwood pulp or the kapok pulp. That is because the shorter fibers of the hardwood pulp fill the voids and pores in the sheet structure, making the sheets more compact. The inclusion of kapok pulp increased the apparent density of the sheets in all of the pulp mixtures. This could be because the kapok fibers have very thin cell wall, being easily collapsed, making more compact sheets. However, sheets derived

from the pure kapok pulp were not greater in apparent density, as seen by the fact that the kapok fibers become easily entangled. Thus, pure kapok sheets gave poor sheet formation and an irregular sheet surface.

Tensile index and burst index

The sheets made from kapok pulp gave the highest tensile index (Fig. 4). This could be because the kapok fibers were long and the lumens were easily collapsed when forming paper, producing highly bonded regions and denser sheets with a resulting superior sheet tensile index.

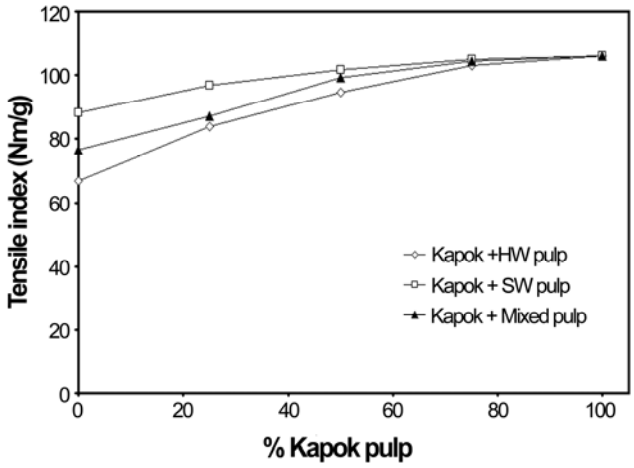

Fig. 4. Tensile index of the sheets made from kapok pulp mixed with the commercial hardwood (HW) pulp and softwood (SW) pulp at the indicated percentages.

The sheets made from the hardwood pulp produced the lowest tensile index. Those made from a 75:25 (w/w) blend of the hardwood: softwood pulps had a medium tensile index. Those made from the pure softwood pulp gave the greatest tensile index. With respect to kapok-commercial pulp mixtures, as the ratio of kapok pulp increased, the tensile index also increased (Fig. 4). However, the results were more prominent when the kapok pulp was mixed with the hardwood pulp than with the softwood pulp.

The sheets derived from the pure kapok pulp gave the highest burst index, the values being somewhat similar to those of the sheets made from the softwood pulp (Fig. 5). This is because both kapok fiber and the softwood fiber are long and have extensive contact areas that are available for fiber bonding. The sheets made from the hardwood pulp had the lowest burst index. This is because the hardwood pulp contained a greater amount of short fibers, resulting in poor bonding. As the ratio of the kapok pulp in mixtures with the hardwood pulp or the 75:25 ratios (w/w) of hardwood pulp: softwood pulp increased, the burst indexes of the resultant paper significantly increased, because fiber bonding was greatly improved.

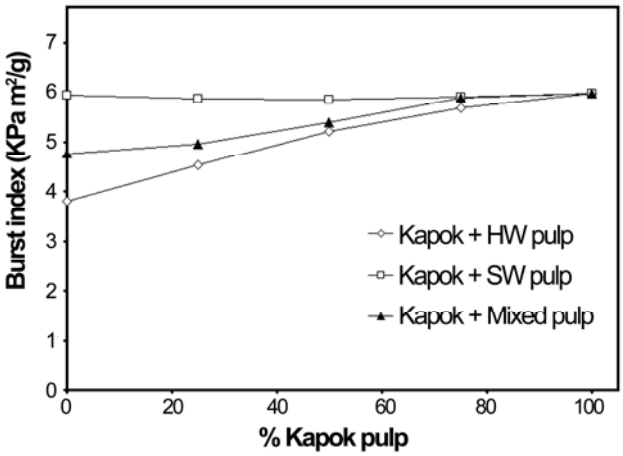

Fig. 5. Burst index of the sheets made from kapok pulp mixed with the commercial hardwood (HW) pulp and softwood (SW) pulp at the indicated percentages.

Tear index and elongation

One of the key characteristics of kapok fibers is their brittleness. Thus, the sheets made from the kapok pulp had the lowest tear index relative to those made from the commercial softwood pulp, the hardwood pulp, and the softwood-hardwood mixed pulp. For kapok-commercial pulp mixtures at different ratios, it was clearly observed that as the ratio of kapok pulp increased, the tear index significantly decreased (Fig. 6).

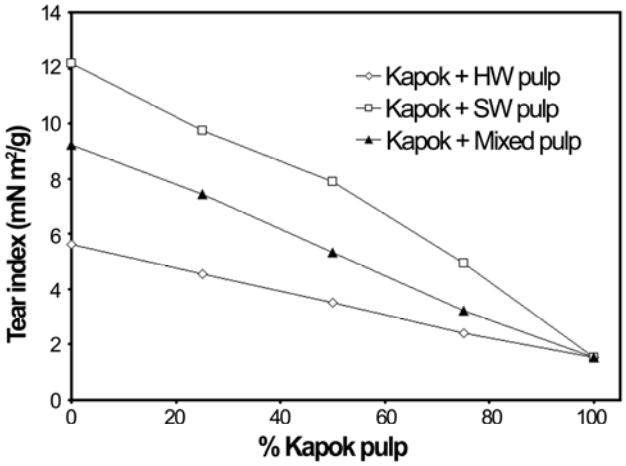

Fig. 6. Tear index of the sheets made from kapok pulp mixed with the commercial hardwood (HW) pulp and softwood (SW) pulp at the indicated percentages.

The elongation of the sheets that were prepared from different ratios of the kapok pulp is compared in Fig. 7. Sheets made from kapok pulp had the lowest elongation. This is because the key characteristics of kapok fibers are their brittleness and inelasticity, which might reduce the elongation of the sheets when a load was applied. Thus, as the

ratio of the kapok pulp was increased, the elongation significantly decreased in all pulp mixtures.

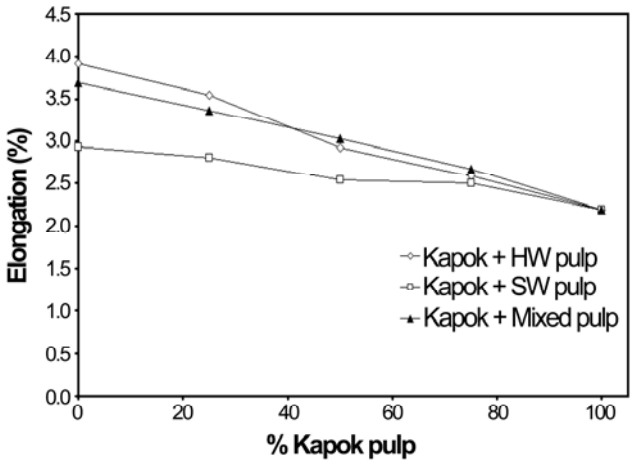

Fig. 7. Elongation of the sheets made from kapok pulp mixed with the commercial hardwood (HW) pulp and softwood (SW) pulp at the indicated percentages.

Water contact angle

The water contact angles of the sheets made from kapok pulp mixed with the commercial softwood pulp and hardwood pulp are shown in Fig. 8. As seen in Fig. 8, K 100 represented handsheets made from 100% kapok pulp. HW100 indicated handsheets made from 100% hardwood pulp while SW100 illustrated handsheets made from 100% softwood pulp. M100 designated handsheets made from mixed pulp (25:75 (w/w) softwood pulp: hardwood pulp). Handsheets prepared from kapok pulp mixed with hardwood, softwood and mixed pulps with different percentages characterized by K: HW, K: SW and K: M with the percentage indicated in parenthesis.

The results indicated that as the time of contact increased, the water contact angles decreased because of absorption and penetration of the water droplets into the sheet. Those made from 100% kapok pulp gave the greatest values for the water contact angle. This effect was due to the unique characteristics of the kapok fibers having a wax coating on the surface. Although the kapok fibers were pulped, some of the wax was still present. When mixed with the commercial pulps (softwood, hardwood and mixed pulps), as the ratio (w/w) of the kapok pulps increased, the water contact angle values increased.

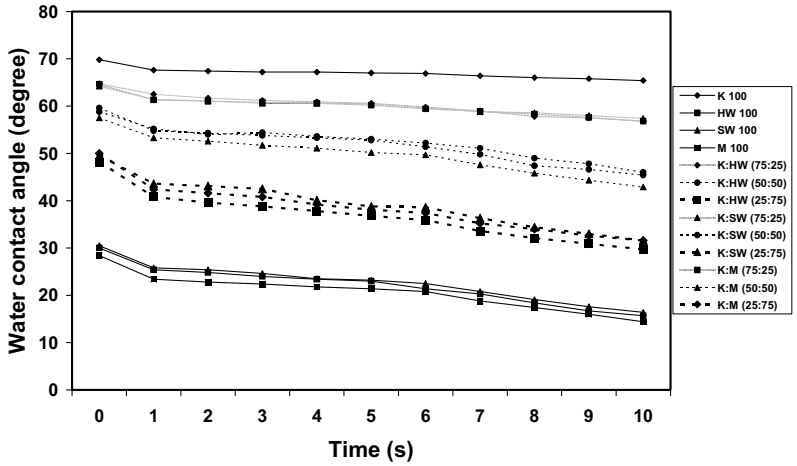

Fig. 8. Water contact angles of the sheets from the kapok (K) pulp mixed with the commercial hardwood (HW) pulp, softwood (SW) pulp and mixed (M) pulp at the indicated percentages.

CONCLUSIONS

1. When kapok pulp was mixed with the commercial softwood pulp and/or hardwood pulp, the tensile and burst strengths of the blended sheets increased but with the lower tear resistance and elongation due to the excellent tensile strength and brittleness of kapok pulp.
2. Brightness and opacity of the blended sheets decreased when higher amounts of kapok pulp were added in the pulp mixture due to the yellowness of the kapok pulp.
3. Handsheets containing kapok pulp gave greater water contact angles due to the hydrophobic nature of kapok fibers.
4. Thus, kapok pulp can potentially be mixed with the commercial softwood pulp and/or hardwood pulp to produce commercial packaging paper when the strength and light weight characteristics are required.

ACKNOWLEDGMENTS

This research was financially supported by a Research Team Aid Grant from the Thailand Research Fund and Commission of Higher Education under the contract number RTA5080004. The authors would like to thank the Department of Imaging and Printing Technology of Chulalongkorn University, and the Product and Technology Development Center of Siam Cement Group Paper Company Limited for providing relevant research facilities.

REFERENCES CITED

Browning, B. L. (1963). *Methods in Wood Chemistry*, Interscience Publishers, New York.

Chaiarrekij, S., Wongsaisuwan, U., and Watchanakit, S. (2008). "Papermaking from Kapok fiber," *Thai Petty Patent, 4279*, June 13, 2008.

Hong, X., Wei-dong, Y., and Mei-wu, S. (2005). "Structure and Performances of the Kapok Fiber," *Journal of Textile Research* 26(4), 4-6.

Hori, K., Flavier, M. E., Kuga, S., Lam, T. B. T., and Liyama, K. (2000). "Excellent oil absorbent kapok [*Ceiba pentandra (L.) Gaertn*.] fiber: Fiber structure, chemical characteristics, and application," *J. Wood Sci.* 46(5), 401-404.

Huang, X. F., and Lim, T. T. (2006). "The performance and mechanism of hydrophobic–oleophilic kapok filter for oil/water separation," *Desalination* 190(1-3), 295-307.

Khan, E., Virojnagud, W., and Ratpukdi, T. (2004). "Use of biomass sorbents for oil removal from gas station runoff," *Chemosphere* 57, 681-689.

Kobayashi, Y., Matsuo, R., and Nishiyama, M. (1977). "Method for adsorption of oils," *Japanese Patent*, 52,138,081, November, 17, 1977.

Lim, T.-T., and Huang, X. (2007). "Evaluation of Kapok (*Ceiba pentandra* (L.) Gaertn.) as a Natural Hollow Hydrophobic-Oleophilic Fibrous Sorbent for Oil Spill Cleanup," *Chemosphere* 66, 955-963.

Malab, S. C., Agrupis, S., Cabalar, L., and Ballesteros, R. (2001). "Paper sheets from bamboo and kapok," *PCARRD Press Release* No.153, December, 14, 2001.

Qiuling, C., and Lin, W. (2009). "Structure and Property Contrast of Kapok Fibre and Cotton Fibre," *Contton Textile Technology* 37(11), 668-670.

Rengasamy, R.S., Dipayan, D., and Karan, P.C. (2011). "Study of Oil Sorption Behavior of Filled and Structured Fiber Assemblies Made from Polypropylene, Kapok and Milkweed Fibers," *Journal of Hazardous Materials* 186(1), 526-532.

Shatalov, A. A., and Pereira, H. (2005). "Kinetics of polysaccharide degradation during ethanol–alkali delignification of giant reed-Part 1. cellulose and xylan," *Carbohydr. Polym.* 59(4), 435-442.

Sjöström, E. (1993). *Wood Chemistry-Fundamentals and Applications*, 2nd ed., Academic Press, San Diego.

Tang, A.-m., Sun, Z.-h., Fu, X., Zi, M., Zhang, H.-w., Chen, G., and Lin, Y. (2008). "Chemical and Structural Characteristics of Kapok Fibers," *Zhongguo Zaozhi Xuebao/Translations of China Pulp and Paper* 23(3), 1-5.

Article resubmitted: July 31, 2011;

Elsevier Editorial System(tm) for Journal of Chromatography A
Manuscript Draft

Manuscript Number:

Title: Comparative study of the mesostructure of natural and synthetic polyisoprene by SEC-MALS and AF4-MALS

Article Type: Full Length Article

Keywords: Field flow fractionation; size exclusion chromatography; polyisoprene; multi angle light scattering; rubber

Corresponding Author: Mr. Stéphane Dubascoux,

Corresponding Author's Institution: Montpellier SupAgro

First Author: Stéphane Dubascoux

Order of Authors: Stéphane Dubascoux; Chalao Thepchalerm; Eric Dubreucq; Suwaluk Wisunthorn; Laurent Vaysse; Suda Kiatkamjornwong; Charoen Nakason; Frédéric Bonfils

Suggested Reviewers: Stepan Podzimek
stepan.podzimek@synpo.cz
expert in AF4 and polymer science

Bruno Grassl
bruno.grassl@univ-pau.fr
expert in polymer science

Yacine Hemar
y.hemar@auckland.ac.nz
expert in physico-chemistry of colloidal system

Opposed Reviewers:

Montpellier SupAgro

CENTRE INTERNATIONAL D'ETUDES SUPERIEURES EN SCIENCES AGRONOMIQUES

DEPARTEMENT DES SCIENCES POUR LES AGRO-BIOPROCEDES

UMR INGENIERIE DES AGROPOLYMERES ET TECHNOLOGIES EMERGENTES
(UMR 1208 IATE, CIRAD-INRA-MONTPELLIER SUPAGRO-UM2)

République Française

Dr. Stéphane Dubascoux
Tel : +33 (0) 499613016
Email : stephane.dubascoux@supagro.inra.fr

Montpellier, 05th July 2011

Cover letter

Dear Managing Editor,

Please find enclosed the submission of our regular research paper entitled: "*Comparative study of the mesostructure of natural and synthetic polyisoprene by SEC-MALS and AF4-MALS*". In this article, we present the first original results about natural and synthetic rubber characterization by asymmetrical flow field flow fractionation (AF4). Mesostructure evaluation by AF4 is compared with that obtained with size exclusion chromatography.

Up to now, there is a real lack of information concerning natural rubber mesosctructure and more precisely about the presence and the nature of microaggregates (gel content) among the linear polyisoprene chains. AF4 allows assessing simultaneously both the distribution of polyisoprene chains and gel content. Results obtained allow to validate the AF4 fractionation (compared to SEC results) and to consider the gel part of polyisoprene samples.

For these reasons, we think that our article matches with the topic of your journal and is appropriate for publication in journal of chromatography A.

Sincerely yours,

The authors: Stephane Dubascoux, Chalao Thepchalerm, Eric Dubreucq, Suwaluk Wisunthorn, Laurent Vaysse, Suda Kiatkamjornwong, Charoen Nakason, Frederic Bonfils

*Manuscript
Click here to view linked References

Comparative study of the mesostructure of natural and synthetic polyisoprene by SEC-MALS and AF4-MALS.

Stephane Dubascoux*[1], Chalao Thepchalerm[1,2,6], Eric Dubreucq[1], Suwaluk Wisunthorn[3], Laurent Vaysse[4], Suda Kiatkamjornwong[5], Charoen Nakason[2], Frederic Bonfils*[6]

[1] *Montpellier SupAgro, UMR IATE 1208, 2 Place Viala, 34060 Montpellier, France*

[2] *Center of Excellence in Natural Rubber Technology, Faculty of Science & Technology, Prince of Songkla University, Pattani campus, Thailand*

[3] *Faculty of Science and Industrial Chemistry, Prince of Songkla University, Surat Thani campus, Thailand*

[4] *CIRAD, UMR IATE 1208, KU-CIRAD laboratory, Agroindustry building 3, 7th Floor, Kasetsart University, Bangkok 10900, Thailand*

[5] *Faculty of Science, Chulalongkorn University, Bangkok, Thailand*

[6] *CIRAD, UMR IATE 1208, 2 Place Viala, 34060 Montpellier, France*

Abstract

This paper presents results from the first analyses of the mesostructure of natural rubber (NR) by asymmetrical flow field flow fractionation (AF4). The results are compared with those obtained by size exclusion chromatography (SEC) in terms of average molar masses, radius of gyration and insoluble part (or gel quantity). Comparable results were obtained for the sample not containing gel. Conversely, for samples with gel, significant differences were found due to the presence of microaggregates. In fact, contrary to SEC, AF4 fractionation enables partial fractionation of polyisoprene chains and microaggregates in a single run without preliminary treatment. The results presented here also highlight the special structure (very compact spheres) of microaggregates in NR compared to chemical crosslinked microaggregates in synthetic polyisoprene. The advantages and drawbacks of both techniques for analysing NR samples are also discussed.

Introduction

For natural rubber (NR), as for numerous biopolymers, it is rather simplistic to speak about macromolecular structure. Indeed, biopolymers often exhibit a complex associative structure, a mixture of macromolecular chains, microaggregates and macroaggregates [1,2]. Because of that, the term mesoscopic structure or mesostructure, which includes both macromolecular structure and aggregate characterization, is increasingly being used. Although NR mesostructure has been studied for many years, the origins of its unique properties are not yet fully clear. Recently, Kim *et al*. [3,4] revisited the mesostructure of NR. Kim *et al*. [3,4] analysed NR samples with SEC-MALS and showed that the soluble part injected into a SEC system contained very few branched macromolecules, contrary to earlier published studies [5-7]. Kim *et al*. [3,4] showed that the soluble part of NR in solution in tetrahydrofuran (THF) was composed of a mixture of linear chains and assumed compact microaggregates ($R_g \approx$ 110-130 nm). They showed that to more effectively ascertain the mesostructure of NR, as is the case with most polymers, a MALS detector coupled with SEC is required to avoid a misunderstanding of the structure. From a mechanistic point of view, many mechanisms have been proposed to explain the associative structure of NR [8-11]. The most recent proposal is Tanaka's group scheme involving a protein and a phospholipid at each end of the poly(*cis*-1,4-isoprene) chain. These two reactive end chains would appear to be involved in what they called the "naturally occurring network" of NR [12,13].

Today, many tools are available for macromolecule analysis. Of these techniques, size exclusion chromatography (SEC) and field flow fractionation (FFF) are tools of choice to fractionate macromolecules according to their sizes. SEC is beyond doubt the most popular and developed technique for polymer separation. However, a recent study has also highlighted some difficulties for NR separation with SEC coupled with a multi-angle light scattering (MALS) detector because of an abnormal elution phenomenon [3]. This abnormal elution is

due to co-elution of microaggregates with short chains. Kim *et al*. [3] showed that the abnormal elution occurring with NR could be overcome by treating the SEC columns with an ionic surfactant. After treatment, it was possible to separate these compact microaggregates from linear random coil polyisoprene chains [3]. However, it is difficult to be sure whether or not all microaggregates elute and the procedure is rather cumbersome. The solution to this SEC limitation for NR sample analysis might be the use of techniques based on field flow fractionation. Recent reviews have demonstrated the potentiality of FFF in various fields, such as polymer science [14], biomolecule characterization [15], nanoparticles [16] or the environment [17]. Moreover, FFF could easily be coupled on-line with different detectors, such as a refractive index detector, an ultra-violet detector, a light scattering or inductively coupled plasma mass spectrometer [18]. Recently, Messaud *et al*. [14] emphasized the fact that field flow fractionation techniques can provide effective simultaneous separation of polymer and microgel. The most popular FFF techniques used for polymer fractionation are thermal flow field flow fractionation (Th-FFF) and Flow Field Flow Fractionation (Fl-FFF or F4) [14]. The main difference between these two sub-techniques is the field used for the fractionation. Fractionation takes place in a channel and the field is a thermal gradient for Th-FFF, while it is a crossflow stream carried through an ultrafiltration membrane in the case of Fl-FFF [19]. Up to now, only Th-FFF has been used for NR characterization [20-23]. However, during Th-FFF, macromolecules are separated according to their size and their chemical composition. Thus, heterogeneity in the chemical composition of a given polymer can complicate the determination of macromolecular structure. Asymmetrical Fl-FFF (AsFl-FFF or AF4) is Fl-FFF where the channel is semi-permeable and asymmetric, involving less sample dilution [19]). Natural rubber has been analysed by Th-FFF using either the polyisoprene calibration curve [20,22,23] or a multi-angular light scattering detector (MALS) [21]. Lee and Molnar [23] compared the analysis of natural rubber by Th-FFF and SEC. They

used a calibration curve made with linear standards poly(*cis*-1,4-isoprene). The analysed NR samples (RSS1 type) had a number-average molar mass (M_n) of about 0.8 million g.mol^{-1} and a weight-average molar mass (M_w) of about 29 million g.mol^{-1}, M_w being three times higher than that given by SEC. Lee and Molnar **[23]** showed that the high molar masses and microgels disappeared after mastication of a NR sample in an extruder. The range of molar masses found was between 10,000 and 10 million g.mol^{-1} (non-masticated RSS). Filtration of the solution through filters with 5 µm pores led to a shift in the fractogram towards lower retention times. This phenomenon was observed for non-masticated rubber but not for masticated rubber. This shift to lower molar masses was attributed to the removal and/or degradation of microgels (or ultra-high molar mass species). They quantified the gel rate (as a % of total rubber, w/w) in the NR samples by Th-FFF and found slightly lower values (RSS 13%, masticated RSS 0%) than with their conventional method – i.e. filtration through a 125 µm wire mesh after 24 h in toluene (RSS 15%, masticated RSS 0%). Fulton and Groves **[21]** analysed two synthetic polyisoprenes (IR305, Natsyn2200), a polybutadiene (Europrene BR40) and a natural rubber (SMR5L) in cyclohexane by Th-FFF-MALS without any filtration. They showed that the IR305 sample was essentially linear with no gel, as confirmed later by Kim *et al.* **[3]** by SEC-MALS, contrary to the Natsyn2200 sample, which had a 25% gel rate and was branched for molar masses above 5.10^5 g.mol^{-1}. While there was no steric effect in the separation process for the two synthetic polyisoprenes, they observed such an effect for the polybutadiene and the NR samples. As a consequence of this phenomenon, very large entities eluted together with the smaller molecules. Bang *et al.* **[24]** used AF4 to characterize and determine the molar mass distribution of styrene–butadiene rubber.

This paper presents the first study of synthetic and natural polyisoprene fractionation by AF4 coupled with MALS in an organic solvent (tetrahydrofuran). The peak shape is discussed and the results in terms of average molar masses, radius of gyration and gel content are compared

105 with those obtained by SEC-MALS. The comparison of AF4-MALS with SEC-MALS also
106 made it possible to evaluate the discrepancies between the two techniques for analysing NR
107 samples.
108

Material & methods

Samples

In order to compare SEC and AF4 results on synthetic polyisoprene and natural rubber (NR), four samples were chosen for their differences in mesostructure. The two synthetic poly(*cis*-1,4-isoprenes) were Kraton IR 307 (Kraton polymer, Houston, USA) and Nippol 2200 (Zeon Corporation, Louisville, USA). The main difference between these two synthetic polyisoprenes is the gel rate: no gel in the IR307 sample and presence of microgel in Nippol 2200. The two natural rubbers, M160 and M121, were TSR5CV (Technically Specified Rubber with a Constant Viscosity) made from monoclonal *Hevea brasiliensis* latex. The preparation of the samples was described previously **[25]**.

In order to reach a sample concentration of 1 $mg.mL^{-1}$, 30 ± 5 mg of the samples was dissolved in about 30 mL of HPLC grade tetrahydrofuran (THF, VWR, West Chester, USA) stabilized with 2,6-di-tert-butyl-4-methylphenol – BHT – (Sigma Aldrich, Saint Louis, USA) at 250 $mg.L^{-1}$. The flasks were precisely weighed (± 0.01 mg) before and after filling with THF to determine the exact concentration of the solutions. The solvent (THF + BHT) was filtered at 0.1 µm before use. Each sample was analysed in triplicate to evaluate measurement repeatability. All solutions were stored in the dark in a water bath at 30°C for 7 days and gently shaken at 30 rpm (rotational agitator REAX 2, Heidolph, Schwabach, Germany) for 1 hour each day for optimum dissolution. Before injection, the macrogel and part of the microgels were removed from all the solutions by filtration at a 1 µm cutoff with Acrodisc glass filters (Pall, Port Washington, USA) to avoid both clogging of the column during SEC analysis and a steric effect (resulting in inverse elution) on AF4 fractionation **[21]**.

Two monodisperse polystyrene standards at 200 and 1460 kDa from Polymer Standard Service (PSS, Mainz, Germany) were used to assess the quality of the separation/fractionation and detector response for each SEC/AF4 injection series.

134

135 ***AF4 experiments***

136 The AF4 system was a Postnova AF2000 MT series (Postnova Analytics GmbH, Landsberg,
137 Germany) equipped with a channel adapted for organic solvents and a 350 µm spacer. The
138 membrane was made of cellulose material treated for compatibility with organic solvents with
139 a cut-off of 5 kDa (Postnova Analytics GmbH, Landsberg, Germany). The temperature
140 setpoint of the AF4 oven containing the channel was 45°C. The detector flow was kept
141 constant at 0.65 $mL.min^{-1}$. The focusing step consisted of a flow delivered by the injection
142 port of about 0.2 $mL.min^{-1}$ with a crossflow of 1 $mL.min^{-1}$ for 6 minutes. Then, a 1 min
143 transition time was applied to avoid a major pressure drop during the switch from the focus
144 step to the elution step. The programme to decrease the linear crossflow during the elution
145 step was as follows:

146

147 ***Table 1***

148

149 An autosampler (PN 5300 model, Postnova Analytics GmbH) was used to carry out the
150 100 µL sample injections.
151 Detection was carried out with a 7-angle multi-angle light scattering detector (PN 3070
152 model, Postnova Analytics GmbH) in line with a refractive index detector (2414 model,
153 Waters Corporation, Milford, USA). The data gathered were processed with AF2000 software
154 (Postnova Analytics GmbH) after blank subtraction for the DRI signal (used as a
155 concentration detector) and according to the Berry model with 2^{nd} order polynomial
156 formalism. In fact, it has been shown that this formalism is well adapted for entities with a
157 radius up to 50 nm **[26]**. As the refractive index detector signal changes during transition steps
158 due to the AF4 functioning principle, five blank (mobile phase) injections were carried out in

each injection series. The refractive index detector signal from the blank injections was subtracted for each sample injected.

For one series, each sample triplicate was injected once. Two series were carried out (i.e. a total of 6 injections was carried out for each sample) with different operators in order to evaluate the reproducibility of the analysis. Prior to each series of injections, the membrane was replaced and the detector was recalibrated.

SEC experiments

The SEC system was based on an on-line ERC 3112 degaser (ERC, Saitama, Japan), a Waters 515 pump (Waters Corporation, Milford, USA) and 3 MIXED-A columns in series: 2 styragel columns (porosity 20 µm, 300 mm × 7.5 mm I.D.) from Waters and 1 PLgel column (porosity 20 µm, 300 mm × 7.5 mm I.D.) from Varian (Varian, Walnut Creek, USA). All the columns were kept in an oven at 45°C. The detectors were an 18-angle multi-angle light scattering detector (Dawn DSP model, Wyatt Technology, Santa Barbara, USA) and a refractive index detector (Optilab rEX model, Wyatt Technology). Data from angles 5 to 16 were collected and processed with Astra software version 5.3.1 (Wyatt Technology) according to the Berry method with a 2^{nd} order polynomial model. Similarly to the AF4 injection series, each sample triplicate was injected once. Two series were carried out (i.e. a total of 6 injections carried out for each sample).

Theory/calculation

Light scattering theory

For the Berry method with a 2nd order polynomial fit, $[Kc/\Delta R(\theta)]^{1/2}$ is plotted against $\sin^2(\theta/2)$. According to the light scattering theory, this plot makes it possible to determine M_{wi} and R_{gi} for each slice of the fractogram from AF4 or the chromatogram from SEC, respectively, according to equation 1.

$$\left[\frac{Kc}{\Delta R(\theta)}\right]_i^{1/2} = \left[\frac{1}{M_{wi}} + \frac{16\pi^2}{3_0^2}\frac{\langle R_g^2\rangle_i}{M_{wi}}\sin^2\left(\frac{\theta}{2}\right)\right]^{1/2} \quad \textit{Equation 1}$$

where $\mathbf{K}$ is an optical constant
c is the solute concentration (in $g.mL^{-1}$)
θ is the scattering angle
$\Delta R(\theta)$ is the excess Rayleigh ratio, the ratio of scattered and incident light intensity
M_{wi} is the weight-average molar mass of the solute
λ_0 is the wavelength of the laser beam in a vacuum (in nm)
R_g is the gyration radius of the solute (nm)

The optical constant $\mathbf{K}$ is given by equation 2.

$$K = \frac{4\pi^2 n_0^2}{N_{A0}^2}\left(\frac{dn}{dc}\right)^2 \quad \textit{Equation 2}$$

where n_0 is the refractive index of the solvent
N_A is Avogadro's number
$\left(\frac{dn}{dc}\right)$ is the differential refractive index increment of the polymer in the solvent used

For detailed information about the light scattering theory, refer to **[27,28]**.

Molar mass and radius definitions

The different molar masses calculated and presented are defined as:

$$M_n = \frac{\sum_i N_i M_i}{\sum_i N_i} \qquad M_w = \frac{\sum_i N_i M_i^2}{\sum_i N_i M_i} \qquad M_z = \frac{\sum_i N_i M_i^3}{\sum_i N_i M_i^2} \quad \textit{Equation 3, 4 \& 5}$$

Where N_i is the number of polymers with molecular weight M_i

The radius of gyration ($<R_g>$ or R_z) or root mean square radius (r.m.s) is defined for a non-rigid particle as:

$$< R_g >= \frac{\sum_i c_i M_i \langle R_g^2 \rangle_i}{\sum_i c_i M_i} \quad \textit{Equation 6}$$

Gel content calculation

In order to evaluate the amount of gel retained by the 1 µm filter, the whole peak from the concentration detector (refractive index detector) observed in SEC or AF4 separation was integrated using 0.13 as the value of $^{dn}/_{dc}$ [29]. This gel content was called the "filtrate gel on 1 µm" or $Gel_{>1\mu}$. In previous papers this quantity of aggregates (macro and micro) was called "total gel". However, as shown by Kim *et al*. [3] and as we will see later in this paper, a not insubstantial quantity of microaggregates passes through the 1 µm filter. As a consequence, the real total gel (G_T) is:

$$G_T = Gel_{>1\mu} + Gel_{<1\mu} \quad \textit{Equation 7}$$

$Gel_{<1\mu}$ is the quantity of microaggregates with a size smaller than 1 µm. $Gel_{<1\mu}$ cannot be determined by SEC-MALS, except by treating the columns with tetrabutylammonium bromide (TBABr) as shown previously [3]. This procedure is rather cumbersome, whereas it will be shown that $Gel_{<1\mu}$ can easily be estimated using AF4 analysis of NR samples. Indeed, by knowing the initial concentration of the sample before filtration, it is possible to determine from the fractogram (DRI signal) the concentration of the two populations in solution after filtration: polyisoprene chains and microaggregates smaller than 1 µm.

Thus:

$$Gel_{>1\mu m} = \frac{C_1 \times 100}{C_0} \quad \textit{Equation 8}$$

$$Gel_{<1\mu m} = \frac{C_2 \times 100}{C_0} \quad \textit{Equation 9}$$

Where C_0 is the initial concentration of the analysed sample, C_1 the concentration of the analysed sample passing through the 1 µm filter (polyisoprene chains + microaggregates) and C_2 the concentration of only the microaggregates passing through the 1 µm filter. C_1 can be determined either by SEC or AF4 by integrating the whole peak of the concentration detector (DRI). C_2 can be calculated only by AF4 integrating the part of the DRI peak containing microaggregates.

Results & Discussion

Qualitative description of fractograms

SEC-MALS profiles for the different samples are presented in Figure 1. M_w variations started with a linear decrease corresponding to a normal elution from large chains to small chains but displayed a deviation of the slope of this curve for samples containing gel (i.e. Nippol, M121 and M160, figure 1B, C & D). As described in the introduction and as previously detailed **[3]**, SEC separation of rubber generally presents this abnormal elution due to co-elution of delayed large macromolecules, assumed to be microaggregates ($GEL_{<1\mu}$), with the small chains of poly(*cis*-1,4-isoprene). This particular elution was highlighted when either a change or an inversion of the slope presenting the variation in weight-average molar mass versus elution volume occurred. Regarding the detectors, the differential refractive index (DRI) signal during the SEC elution profile corresponded to a main Gaussian peak (with slight back-tailing) for Nippol and M121, and to a bimodal molar mass distribution for the IR307 and M160 samples. The LS signal was more unimodal with back-tailing varying depending on the sample.

Figure 1

Unlike SEC, AF4 fractionated the macromolecules from small to large ones and the peak shapes appeared quite different. For poly(*cis*-1,4-isoprene) with gel (i.e. Nippol 2200, M160 and M121), the shape of the LS fractograms did not correspond to a Gaussian peak. The fractograms displayed a long front tailing, (i.e. a long and low signal increase) and an abrupt increase in the LS signal from 25 to 30 min (corresponding to a crossflow ranging from 0.5 to

0.3 $mL.min^{-1}$) (Figure 2). For the IR307 sample, the fractogram exhibited a clearly less pronounced increase in the LS signal (Figure 2A). As the IR307 sample did not contain gel, unlike the Nippol 2200 sample, this abrupt increase in the signal was due to microaggregates, as observed by Andersson *et al.* **[30]** for AF4 analysis of ethylhydroxyethyl cellulose. For the refractive index detector signal, the behaviour was unfamiliar, with a first peak close to void volume (elution starting at 7 min), corresponding to small chains, followed by either a slight increase in the concentration signal (for IR 307), or a decrease (for Nippol 2200), or quite a constant signal up to the end of the peak (for the two natural samples) (Figure 2). With both the DRI and LS detectors, the fractograms gave a continuous elution whatever the entities eluting, be they random coil or compact microaggregates (sphere-like). However, the evolution of the molar masses (M_{wi}) in line with the elution time was not linear from a qualitative viewpoint (Figure 2). For the IR307 sample, Figure 2A shows a change in slope for an elution time of 17-18 min ($M_{wi} \approx 600$ kg mol^{-1}). A clear decrease in the variability of the measured R_{gi} was observed from this elution time (t_e = 17-18 min) (Figure 2). Indeed, for the first 18 minutes of the fractogram, R_{gi} values were very dispersed whatever the samples analysed using Berry 2 formalism (Figure 2), compared to SEC-MALS. This high dispersion of R_{gi} may have occurred because the concentrations of the injected solutions were too low (≈ 1 $mg.mL^{-1}$) for LS detection or because there was a lack of resolution for small molecule fractionation under our AF4 conditions. This initial slope change in M_{wi} was observed for other samples at times that varied depending on the sample (from 13 up to 17 min). With the Nippol sample, a second marked change appeared in the M_{wi} slope at an elution time of about 31 min (Figure 2B). This abrupt slope change was accompanied by a dramatic increase in the LS signal due to huge entities eluting ($250 < R_{gi} < 1000$ nm). This second change in the M_{wi} slope in line with the elution time was not visible for the other synthetic polyisoprene

(IR307), but was visible to a lesser extent for the two NR samples (M121 and M160) at an elution time of about 26-27 min (Figure 2C & D).

Figure 2

The M_{wi} AF4 profile for IR 307 confirmed the presence of only one population of chains with a M_{wi} ranging from 60,000 g.mol^{-1} to 5 million g.mol^{-1} (Figure 2A). Conversely, the Nippol AF4 profile clearly showed the presence of 2 distinct populations (Figure 2B). The first population was composed of isolated polyisoprene chains and the second one (starting at 32 min) was composed of microaggregates with sizes under 1 µm (Gel$<_{1\mu}$) with a drastic increase in the M_{wi} slope. For the two NR samples (M121 and M160) (Figure 2C and 2D), the M_{wi} profiles were quite different from that for Nippol. Isolated polyisoprene chains seemed to elute first up to about 27 min. After this elution time, the M_{wi} profile exhibited an increase in slope (from 27 to about 35 min), reaching a quasi-plateau (from 35 min). This behaviour suggests that this population was quite monodisperse. These two parts could be attributed to co-elution of isolated polyisoprene chains and Gel$<_{1\mu}$ in the first case and Gel$<_{1\mu}$ only for the plateau.

Large differences were observed for the $M_{wi}=f(V_e)$ and $R_{gi}=f(V_e)$ slopes, the sizes (R_{gi}) and the molar masses (M_{wi}) of the second populations for Nippol compared to the two natural polyisoprene samples (Figure 2). These results tend to confirm that the gel was not intrinsically the same for natural and synthetic polyisoprene. Indeed for NR, the radius for the Gel$<_{1\mu}$ was about 150 nm for a molar mass close to 15 million g.mol^{-1} whereas for Nippol for the same molar mass the radius was about 240 nm (i.e. 60% higher), as illustrated in Figure 3. Moreover, there was no "plateau effect" for Nippol compared to the NR samples. Thus, with a lower R_{gi} for the same M_{wi}, the microaggregates in the NR samples seemed more compact

316 than in the Nippol synthetic polyisoprene. However, some of the difference observed in the
317 slopes may have been due to an underestimation of M_{wi} for the microaggregates of the NR
318 samples. Indeed, it cannot be ruled out that the dn/dc of NR microoaggregates is not constant.
319 Changes in the non-isoprene composition (lipids and/or proteins) of microaggregates cannot
320 be excluded. A change in the proportion of non-isoprene compounds versus polyisoprene in
321 the microaggregates could lead to a change in the dn/dc and so in the M_{wi} determined.
322
323 ***Figure 3***
324
325 One of the main difficulties encountered with AF4 fractionation is to define a correct and
326 unbiased integration range. For our data, the integration range for average molar mass and
327 radius of gyration assessment was started when the M_{wi} and R_{gi} signals were stabilized (out of
328 void peak influence) and stopped just before the end of the peak (shown as the red box in
329 figure 4 for M160, for example). This choice of integration area was made in order to have
330 results including almost all the peak surface and to avoid a decrease in repeatability for the
331 AF4 results due to pre- and post-peak radius and mass dispersion and heterogeneity because
332 of a low LS signal. This method was applied for the AF4 signals from IR307, M160 and
333 M121. On the other hand, the treatment for Nippol 2200 was different. Indeed, the variation in
334 M_{wi} in the second part of Nippol 2200 fractionation was quite high due to the presence of
335 microaggregates with ultra high molar masses (over 10^{10} g mol^{-1}). Moreover, this final M_w
336 increase was quite noisy and unrepeatable, probably due to the low associated RID signal. In
337 fact, as presented in table 2 for example, increasing the Nippol 2200 integration range (from
338 9.5 - 35 min to 9.5 - 40 min), drastically increased the average molar masses, but also the
339 standard deviation. Lastly, a 7% increase in RID integration area (hence in quantity) led to an
340 increase of 4 orders of magnitude for the M_w and resulted in an increase in the standard

deviation from 25% to 71%. Consequently, for Nippol, the integration range was shortened,compared to the other samples, to avoid excessive variability in the results.

Table 2

In order to quantify aggregates exceeding 1 µm ($Gel_{>1\mu}$) (estimation of C_1 in eq. 9), the whole peak was integrated (green box in figure 4). The quantity of microaggregates smaller than 1 µm ($Gel_{<1\mu}$) (estimation of C_2 in eq. 10) was calculated according to a third integration range (the blue box in figure 4) starting from the middle of the zone we considered as a mixture of polyisoprene chains and microaggregates (data $R_g=f(V_e)$) up to the end of the peak.

Figure 4

<u>Comparison of data between SEC-MALS and AF4-MALS</u>

Average molar masses

M_n, M_w and M_z were calculated from the SEC and AF4 results for each sample. The results are presented in Figure 5.

Figure 5

The number average molar mass M_n did not present significant differences whether determined by SEC or AF4 (Figure 5). The ratio of M_n obtained by AF4 to that obtained by SEC was ranged between 0.85 and 1.0. Unlike M_n, M_w and M_z were different, with a higher M_w and M_z obtained for AF4. As described previously, these larger M_w and M_z can be

366 explained by the presence of large microaggregates not observed with SEC. This observation
367 is confirmed by the fact that for IR 307 (poly(*cis*-1,4-isoprene) without gel), M_w and M_z
368 exhibited no significant difference between SEC and AF4 results. The difference between
369 AF4 and SEC in terms of average molar masses was, as expected, higher for M_z than for M_w.
370 The M_w ratios ($M_{w\text{-}AF4}$:$M_{w\text{-}SEC}$) ranged from 1.0 to 4.3 (for IR 307 and M121 respectively)
371 whereas the M_z ratios ($M_{z\text{-}AF4}$:$M_{z\text{-}SEC}$) ranged from 1.0 to 18.6 (for IR 307 and Nippol
372 respectively). For the three average molar masses considered (i.e. M_n, M_w or M_z), the AF4
373 results showed greater heterogeneity than for the SEC results, with high standard deviations.
374 This lower reproducibility and repeatability was mainly due to the difficulty in defining the
375 integration range, as previously explained, but also to the substantial variability generated by
376 the refractive index detector baseline position. Indeed, the AF4 principle resulted in some
377 noise, deviations and jumps in the DRI baseline and thus to some doubts / uncertainties on the
378 baseline position, despite the blank subtraction. The large M_z difference (from AF4 to SEC)
379 and RSD for Nippol was due to the large amount of microaggregates with ultra high molar
380 masses and to the poor repeatability in the high mass range, as explained later on.
381
382 ***Determination of gel rates***
383 The gel rates in the samples were calculated after SEC and AF4 analysis. $Gel_{>1\mu}$ was
384 calculated for both the SEC and AF4 analyses whereas $Gel_{<1\mu}$ was only calculated after AF4
385 analysis. Figure 6 presents the $Gel_{>1\mu}$ rate after SEC and AF4 analyses. For the IR 307 and
386 Nippol samples, the $Gel_{>1\mu}$ rate did not display any significant difference (no gel for IR307
387 and average $Gel_{>1\mu}$ slightly higher for Nippol with AF4). For the two NR samples, only M160
388 exhibited a significant difference in the $Gel_{>1\mu}$ rate between SEC and AF4 determination
389 (23.8% for SEC and 17.2% for AF4). For M121, the lack of significant difference was due to
390 the high variance of the AF4 result. The $Gel_{<1\mu}$ calculation was estimated at 9.5% for Nippol,

27% for M160 and 29% for M121 (no $Gel_{<1\mu}$ for IR 307). These large quantities of $Gel_{<1\mu}$ explained the large differences observed for M_w and M_z in the NR samples and the Nippol sample (higher M_w and M_z for AF4 analyses compared to SEC). However, as a result of such a large quantity of $Gel_{<1\mu}$ for the NR samples, assumed to be "lost" in not insubstantial proportions in SEC, the $Gel_{>1\mu}$ rate should have been much lower with AF4 compared to SEC for Nippol, M160 and M121. The slight difference observed between AF4 and SEC for the $Gel_{>1\mu}$ rate could be explained either by the large measurement variability for AF4, or by an overestimated $Gel_{>1\mu}$ calculation in AF4 analysis (potentially due to concentration peak area determination and therefore to blank subtractions). For the $Gel_{<1\mu}$ calculation, Kim *et al*. **[3]** obtained $Gel_{<1\mu}$ values close to 10% (calculated by SEC after ionic surfactant treatment of the columns) for NR samples similar to M160 and M121, meaning a difference with our $Gel_{<1\mu}$ values of about 15%.

Figure 6

<u>Comparison of radii of gyration</u>

As for the average molar masses, the R_g values obtained with AF4 were higher than those obtained with SEC, except for the IR307 sample, whose R_g was the same for both separation techniques (see table 3). Nevertheless, the differences in R_g obtained with the two techniques were less pronounced than for M_z. This was due to the narrower radius of gyration size range observed (typically varying from 20 to 200 nm) compared to the 10^2 - 10^3 order of magnitudes for the masses over the whole fractionation (up to 10^5 for Nippol). The variation in R_{gi} depending on the elution time with AF4 displayed a similar behaviour to that for M_{wi} (Figure 2). As the variation in R_{gi} was less significant than for M_{wi}, it implies that the material was becoming increasingly compact (greater increase for masses than for radii) towards the

416 end of the elution, especially for the second population, as previously illustrated in figure 3.
417 This observation confirms the presence of compact microaggregates highlighted by Kim *et al.*
418 **[3]**.
419
420 ***Table 3***
421

Conclusions

This work demonstrates the ability of AF4 to fractionate natural and synthetic poly(*cis*-1,4-isoprene). Distinct populations (characterized by a clear slope change in M_{wi} variation) corresponding to isolated polyisoprene chains and microaggregates smaller than 1 µm ($Gel_{<1\mu}$) were detected. Average molar masses were determined and compared with those obtained by SEC. Similar M_n values were obtained but large differences were observed for M_w and M_z. These differences could be explained by a microgel population observed in AF4 but not during SEC separation. Moreover, microaggregates in the NR samples exhibited quite a different structure, appearing more compact than the microaggregates in the Nippol synthetic polyisoprene. Some problems (difficulties in defining the baseline, DRI signal jumps, etc.) due to the use of DRI with AF4 were encountered, in particular for gel rate determination. It seems obvious that some analytical developments are needed to optimize fractionation, increase the resolution for small polyisoprene chains and enable better reproducibility. However, these results are promising and microgel ($Gel_{<1\mu}$) can be considered for further individual studies and physico-chemical characterization.

Acknowledgements

The authors gratefully thank Emilie Croizat and Christine Char for their valuable contribution to this project. A4F-MALS and SEC-MALS analyses were carried out on the LipPol-Green platform (http://www.supagro.fr/plantlippol-green/). We kindly thank CIRAD DRS and Agropolis fondation (http:// http://www.agropolis-fondation.fr) for financial support, and the Hubert Curien Programme for funding Miss Chalao Thepchalerm's scholarship.

References

[1] Hongsheng Liua, Fengwei Xiea, Long Yua, Ling Chena, L. Li, Prog. Polym. Sci. 34 (2009) 1348.

[2] L. Vaysse, F. Bonfils, P. Thaler, J. Sainte Beuve, in D.R. Höfer (Editor), Sustainable Solutions for Energy Generation, Royal Society of Chemistry, Cambridge, 2009, p. 335.

[3] C. Kim, M. Morel, J. Sainte Beuve, A. Collet, S. Guilbert, F. Bonfils, J. Chromatogr. A 1213 (2008) 181.

[4] C. Kim, J. Sainte Beuve, S. Guilbert, F. Bonfils, Eur. Polym. J. 45 (2009) 2249.

[5] Angulo-Sanchez JL, Caballero-Mata P, Rubber Chem. Technol. 54 (1981) 34.

[6] K.N.G. Fuller, W.S. Fulton, Polymer 31 (1990) 609.

[7] J. Tangpakdee, Y. Tanaka, J. Rubber Res. 1 (1998) 14.

[8] S.N. Gan, J. Membrane Sci., Pure Applied Chemistry A33 (1996) 1939.

[9] J. Tangpakdee Sakdapipanich, T. Kowitteerawut, K. Suchiva, Y. Tanaka, Rubber Chem. Technol. 72 (1999) 712.

[10] F. Ngolemasango, E. Ehabe, C. Aymard, J. Sainte-Beuve, B. Nkouonkam, F. Bonfils, Polym. Int. 52 (2003) 1365.

[11] Y. Tanaka, L. Tarachiwin, Rubber Chem. Technol. 82 (2009) 283.

[12] S. Amnuaypornsri, J. Sakdapipanich, S. Toki, B.S. Hsiao, N. Ichikawa, Y. Tanaka, Rubber Chem. Technol. 81 (2008) 753.

[13] J. Carretero–Gonzalez, T. A. Ezquerra, S. Amnuaypornsri, S. Toki, R. Verdejo, A. Sanz, J. Sakdapipanich, B.S. Hsiaod, M.A. Lopez–Manchadoa, Soft Matter 6 (2010) 3636.

[14] F.A. Messaud, R.D. Sanderson, J.R. Runyon, T. Otte, H. Pasch, S.K.R. Williams, Prog. Polym. Sci. 34 (2009) 351.

[15] R. Qureshi, W. Kok, Anal. Bioanal. Chem. 399 (2011) 1401.

[16] G. Lespes, J. Gigault, Anal. Chim. Acta 692 (2011) 26.

[17] L.J. Gimbert, K.N. Andrew, P.M. Haygarth, P.J. Worsflod, Trends Anal. Chem. 22 (2003) 615.

[18] S. Dubascoux, I. Le Hecho, M. Hassellov, F. Von der Kammer, M.P. Gautier, G. Lespes, J. Anal. At. Spectrom. 25 (2010) 613.

[19] M.E. Schimpf, K.D. Caldwell, G.J. C., Field Flow Fractionation Handbook, Wiley Interscience, 2000.

[20] W.-S. Kim, C.H. Eum, A. Molnar, J.-S. Yu, S. Lee, Analyst 131 (2006) 429.

[21] W.G. Fulton, SA, J. Nat. Rubber Res. 12 (1997) 154.

[22] S. Lee, C. Eum, A. Plepys, B. Korean Chem. Soc. 21 (2000) 69.

[23] S. Lee, A. Molnar, Macromolecules 28 (1995) 6354.

[24] D.Y. Bang, D.Y. Shin, S. Lee, M.H. Moon, J Chromatogr. A 1147 (2007) 200.

[25] C. Kim, M. Morel, J. Sainte Beuve, S. Guilbert, F. Bonfils, Polym. Eng. Sci. 50 (2010) 240.

[26] M. Andersson, B. Wittgren, K.-G. Wahlund, Polymer 46 (2003) 4279.

[27] I. Teraoka, Polymer Solutions: An Introduction to Physical Properties, New York, 2002.

[28] P.J. Wyatt, Anal. Chim. Acta 272 (1993) 1.

[29] C. Kim, A. Deratani, F. Bonfils, J. Liq. Chromatogr. Relat. Technol. 33 (2010) 37.

[30] M. Andersson, B. Wittgren, K.G. Wahlund, Anal. Chem. 73 (2001) 4852.

Figure 1

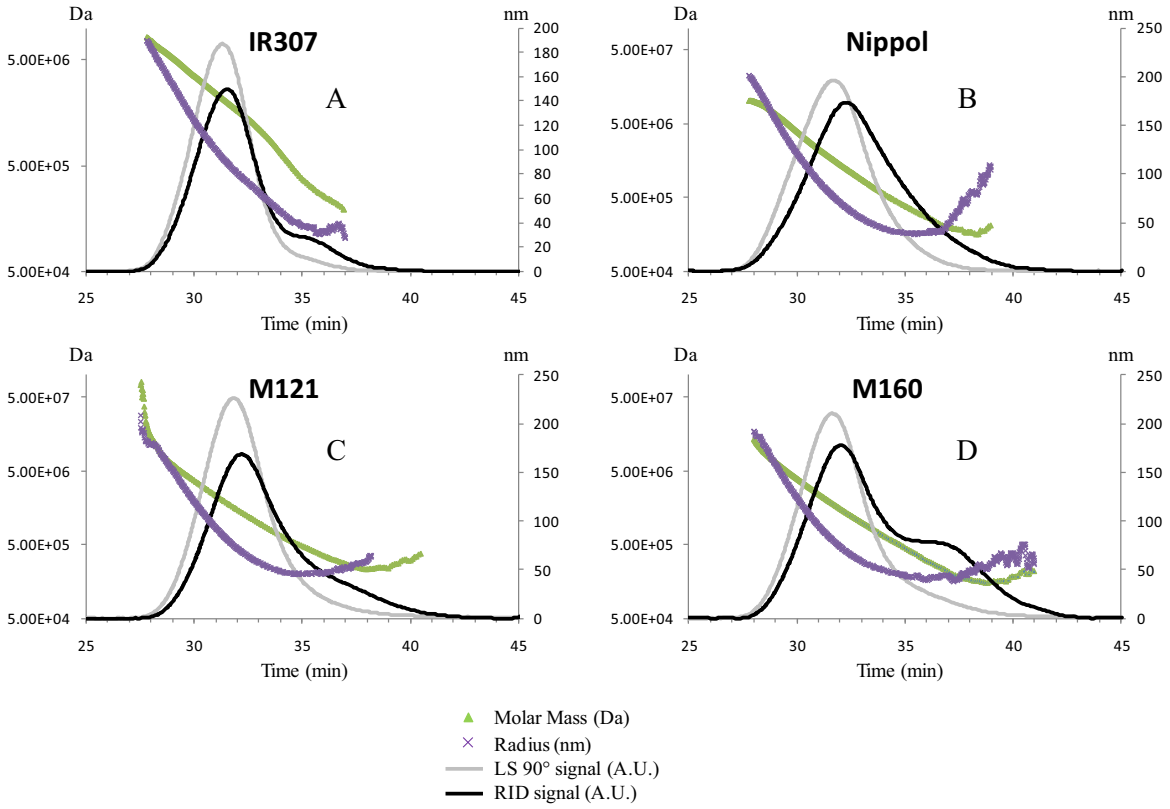

Figure 1: Chromatograms (from the RID and LS detector at 90°) and variation in R_g and M_i depending on the elution time during SEC analysis

Figure 2

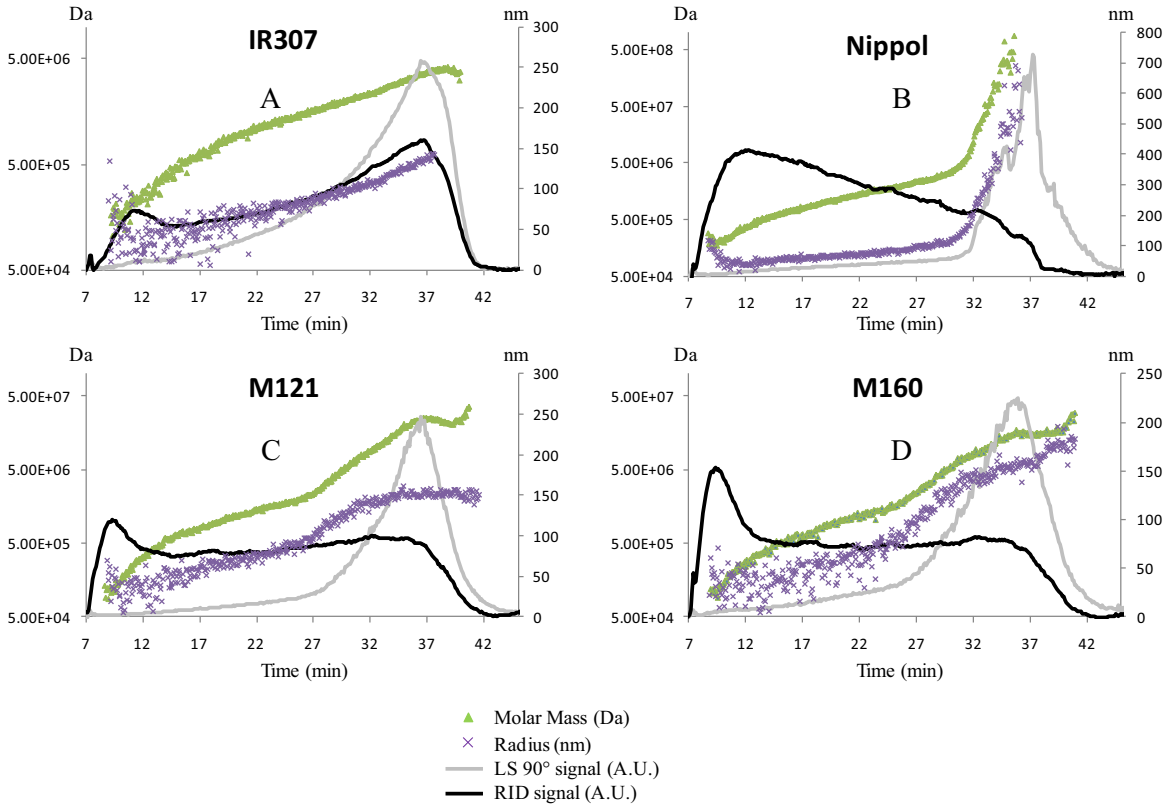

Figure 2: Fractograms (from the RID and LS detector at 90°) and variation in R_g and M_i depending on the elution time during AF4 analysis

Figure 3

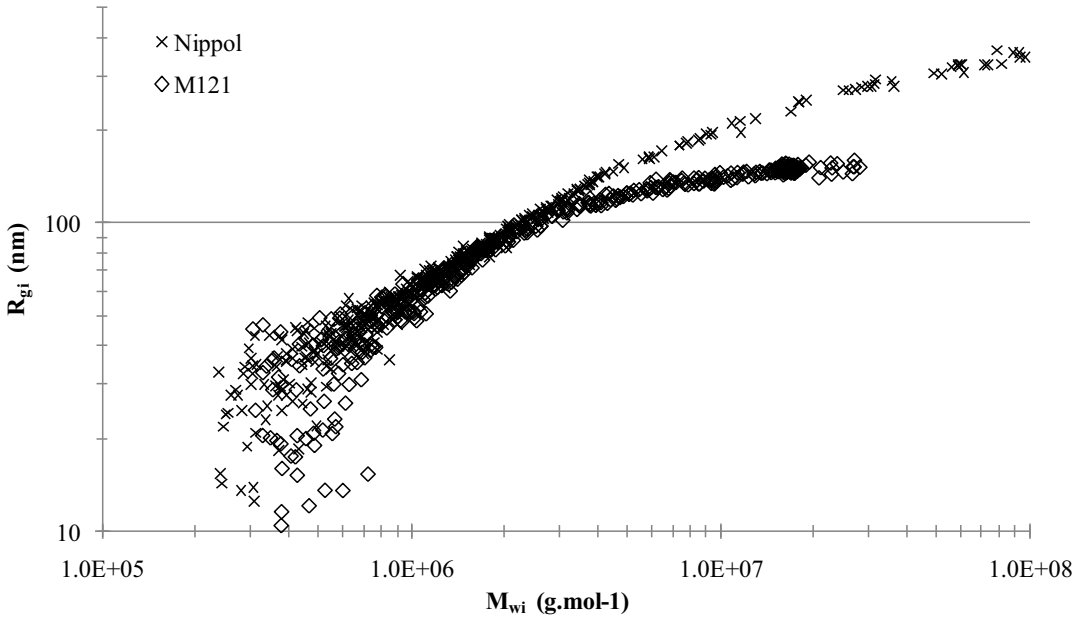

Figure 3: Variation of the radius of gyration (R_{gi}) depending on molar masses (M_{wi}) for the Nippol 2200 and M121 samples.

Figure 4

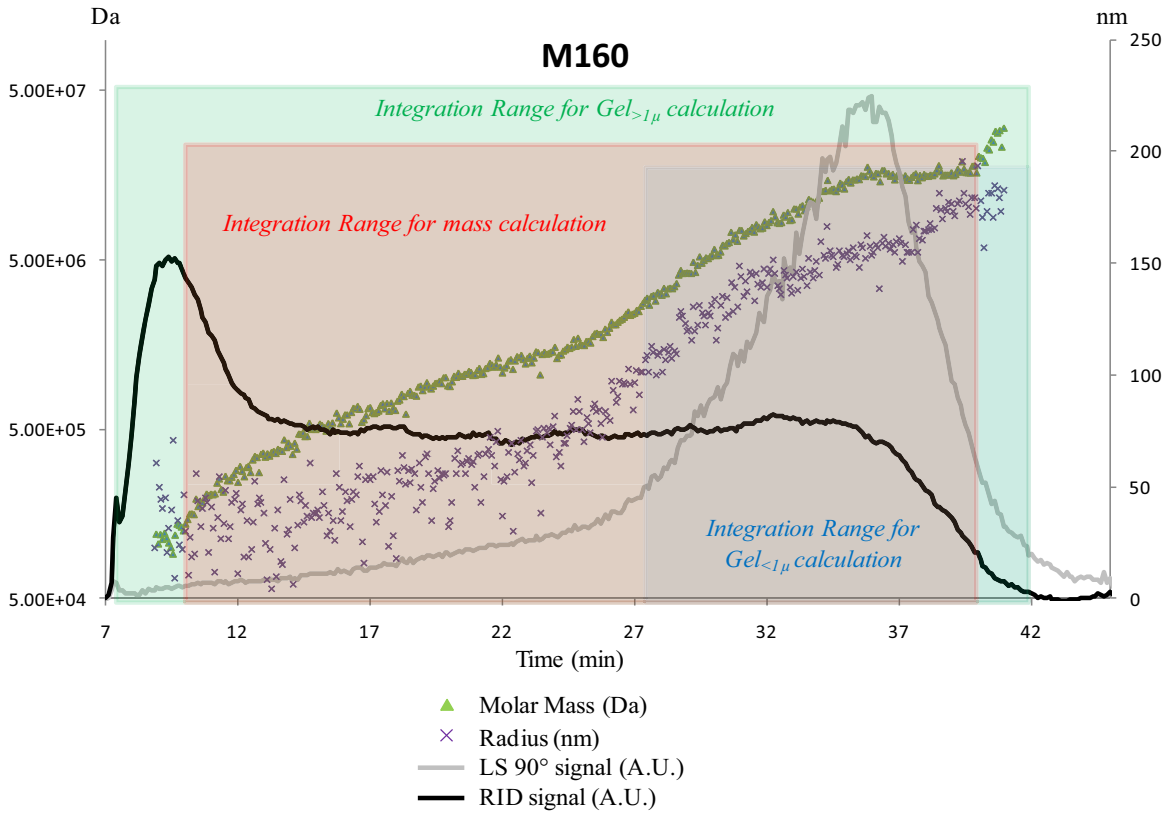

Figure 4: Determination of the AF4 integration range for the M160 sample

Figure 5

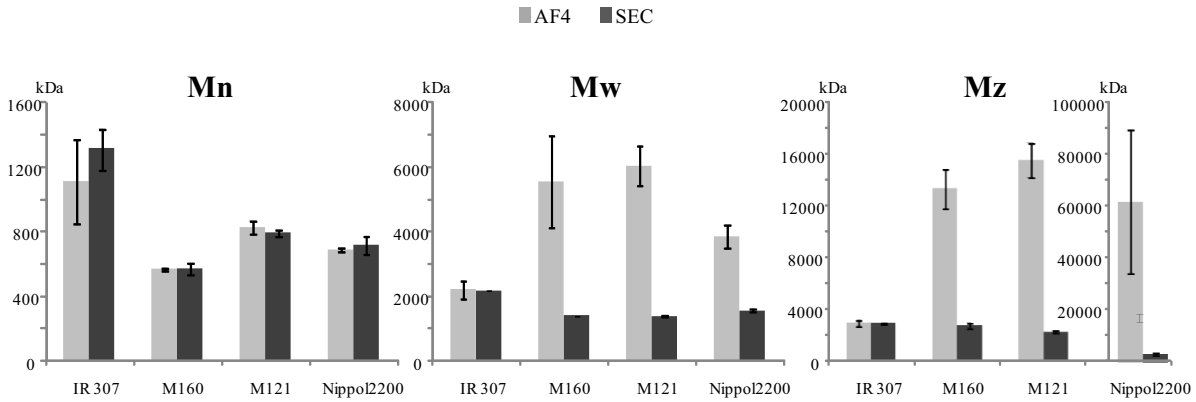

Figure 5: Comparison of masses obtained by SEC and AF4

Figure 6

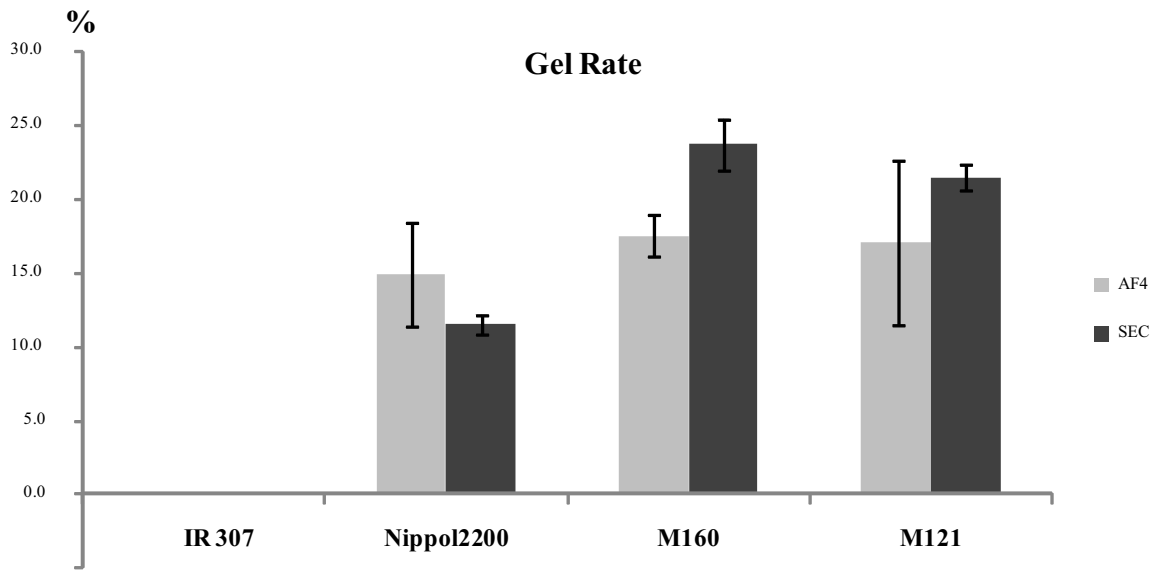

Figure 6: Comparison of filtrate gel on 1 µm ($Gel_{>1\mu}$) rate calculated by AF4 and SEC

Tables 1

Step	***Duration (min)***	***Crossflow ($mL.min^{-1}$)***	***Type of rate***
1	*1.5*	*1*	*Constant*
2	*30*	*From 1 to 0.08*	*Linear*
3	*9*	*0.08*	*Constant*
4	*7*	*0*	*Constant*

Table 1: AF4 crossflow programme during elution

Tables 2

	integration start	integration end	M_n (Da)	RSD	M_w (Da)	RSD	M_z (Da)	RSD
Nippol 2200	9.5 min	35 min	6.95E+05	4%	3.61E+06	25%	4.24E+07	62%
	9.5 min	40 min	7.48E+05	4%	9.36E+10	71%	1.40E+14	81%

Integration : +7% of surface area

Table 2: Nippol 2200 mass calculation (M_n, M_w and M_z with respective RSD from one AF4 series) with different integration ranges

		R_g (nm)	SD (nm) (1)	CV (1)
IR307	AF4	*115.8*	*3.8*	*4.0%*
	SEC	*112.1*	*1.4*	*1.3%*
Nippol	AF4	*249.9*	*28.8*	*28.8%*
	SEC	*108.5*	*4.2*	*3.9%*
M160	AF4	*136.5*	*7.0*	*4.3%*
	SEC	*102.8*	*2.3*	*2.2%*
M121	AF4	*133.5*	*7.8*	*3.4%*
	SEC	*92.5*	*2.4*	*2.6%*

(1) SD: standard deviation, CV: coefficient of variation ((SD/mean) x 100)

Table 3: R_g determined by AF4 and SEC

Elsevier Editorial System(tm) for Colloids and Surfaces B: Biointerfaces
Manuscript Draft

Manuscript Number:

Title: Surface-quaternized chitosan particles as an alternative and effective organic antibacterial filler

Article Type: Full Length Article

Keywords: chitosan; particle; heterogeneous quaternization; minimum inhibitory concentration.

Corresponding Author: Dr. Voravee Hoven, Ph.D.

Corresponding Author's Institution: Chulalongkorn University

First Author: Oraphan Wiarachai, MS

Order of Authors: Oraphan Wiarachai, MS; Nuttha Thongchul, PhD; Suda Kiatkamjornwong, PhD; Voravee Hoven, Ph.D.

Abstract: Taking advantage of the large surface area that is covered with permanent positive charges of quaternary ammonium entities, this research aimed to develop environmentally friendly, organic antibacterial fillers from quaternized chitosan particles that may be applicable for biomedical devices, health and textile industries. The particles were formulated by ionic crosslinking of chitosan with tripolyphosphate followed by quaternization that was conducted under heterogeneous condition via either direct methylation or reductive N-alkylation with a selected aldehyde followed by methylation. Sub-micron, spherical, and positively charged quaternized chitosan particles were formed, as determined by 1H-NMR, FT-IR, PCS, and TEM analysis. Antibacterial activity tests performed by viable cell counts suggested that all quaternized chitosan particles exhibited superior antibacterial activity against the model Gram-positive bacteria, S.aureus, as compared to the native chitosan particles at neutral pH. Only some quaternized chitosan particles, especially those having a high charge density and bearing large alkyl substituent groups, were capable of suppressing the growth of the model Gram-negative bacteria, E. coli. The inhibitory efficiency of the quaternized chitosan particles was quantified in terms of the minimum inhibitory concentration (MIC).

June 12, 2011

Dear Sir/Madam:

I would like to send a manuscript, entitled **"Surface-quaternized chitosan particles as an alternative and effective organic antibacterial filler"** to be considered for publication as a full paper in **Colloids and Surfaces B: Biointerfaces**. On behalf of all authors, namely, Oraphan Wiarachai, Nuttha Thongchul, Suda Kiatkamjornwong, Voravee P. Hoven, I hereby confirm that this manuscript or its contents in some other form has not been published previously by any of the authors and/or is not under consideration for publication in another journal at the time of the submission.

This work introduces surface-quaternized chitosan particles as an effective, environmentally friendly, organic antibacterial filler that may be incorporated into materials that require antibacterial activity. Based on the minimum inhibitory concentration, it was found that some surface-quaternized chitosan particles are more effective in inhibiting the bacterial growth than the quaternized chitosan solution. The fact that the heterogeneous quaternization used for the preparation of surface-quaternized chitosan particles can simply be done without the requirement for tedious purification process opens up an opportunity to produce such effective antibacterial filler at a large scale and that is very beneficial from industrial perspective.

The authors believe that the content of this contribution would be of interest to **Colloids and Surfaces B: Biointerfaces** audiences. Should there be any further information which may be required or if any problems arise, please contact me at the address shown below.

Sincerely yours,

Vp. Hoven

Voravee P. Hoven, Ph.D.
Corresponding Author

Organic Synthesis Research Unit, Department of Chemistry, Faculty of Science, Chulalongkorn University
Phayathai Road, Patumwan, Bangkok 10330, THAILAND
Telephone +(662) 218-7626-7 ext 102, Facsimile +(662) 218-7598
e-mail: vipavee.p@chula.ac.th

*Graphical Abstract

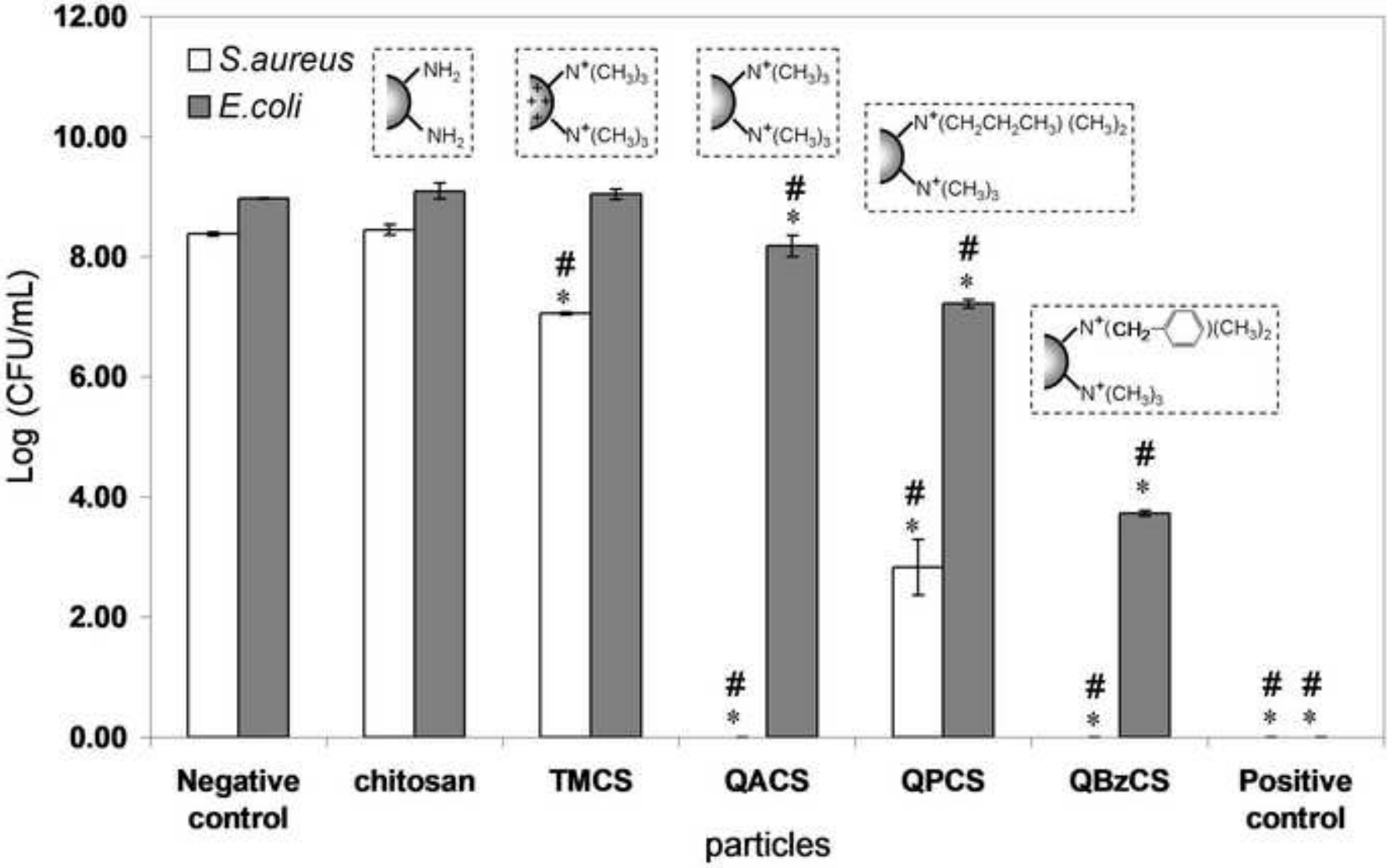

[*p < 0.01 (compared with the negative control), #p < 0.01 (compared with the chitosan particles)]

Research highlights

- Quaternized chitosan particles prepared by heterogeneous quaternization exhibited significantly higher antibacterial activity against *S. aureus* (Gram positive bacteria) and *E. coli* (Gram negative bacteria) than the particles prepared by homogeneous quaternization.
- Only some quaternized chitosan particles, especially those having a high charge density and bearing a large alkyl substituent, were capable of suppressing the growth of *E. coli*, the Gram-negative bacteria.

*Manuscript
Click here to view linked References

Surface-quaternized chitosan particles as an alternative and effective organic antibacterial filler

Oraphan Wiarachai[a,b], Nuttha Thongchul[c], Suda Kiatkamjornwong[d], Voravee P. Hoven[e*]

[a] *Program in Petrochemistry and Polymer Science, Faculty of Science, Chulalongkorn University, Phayathai Road, Pathumwan, Bangkok 10330, Thailand*

[b] *Center for Petroleum, Petrochemicals, and Advanced Materials, Chulalongkorn University, Phayathai Road, Pathumwan, Bangkok 10330, Thailand*

[c] *Institute of Biotechnology and Genetic Engineering, Chulalongkorn University, Phayathai Road, Pathumwan, Bangkok 10330, Thailand*

[d] *Department of Imaging and Printing Technology, Faculty of Science, Chulalongkorn University, Phayathai Road, Pathumwan, Bangkok 10330, Thailand*

[e] *Organic Synthesis Research Unit, Department of Chemistry, Faculty of Science, Chulalongkorn University, Phayathai Road, Pathumwan, Bangkok 10330, Thailand*

* Corresponding author. Tel: +66-2218-7626-7 ext 102; fax: +66-2218-7598

E-mail address: vipavee.p@chula.ac.th.

ABSTRACT

Taking advantage of the large surface area that is covered with permanent positive charges of quaternary ammonium entities, this research aimed to develop environmentally friendly, organic antibacterial fillers from quaternized chitosan particles that may be applicable for biomedical devices, health and textile industries. The particles were formulated by ionic crosslinking of chitosan with tripolyphosphate followed by quaternization that was conducted under heterogeneous condition via either direct methylation or reductive *N*-alkylation with a selected aldehyde followed by methylation. Sub-micron, spherical, and positively charged quaternized chitosan particles were formed, as determined by ^{1}H-NMR, FT-IR, PCS, and TEM analysis. Antibacterial activity tests performed by viable cell counts suggested that all quaternized chitosan particles exhibited superior antibacterial activity against the model Gram-positive bacteria, *S.aureus*, as compared to the native chitosan particles at neutral pH. Only some quaternized chitosan particles, especially those having a high charge density and bearing large alkyl substituent groups, were capable of suppressing the growth of the model Gram-negative bacteria, *E. coli*. The inhibitory efficiency of the quaternized chitosan particles was quantified in terms of the minimum inhibitory concentration (MIC).

Keywords: chitosan; particle; heterogeneous quaternization; minimum inhibitory concentration

1. Introduction

Incorporation of antibacterial fillers is an efficient approach to introduce antibacterial activity to materials. There are many types of filler that can be incorporated into the materials to induce their antibacterial activity such as antibiotic [1], nitric oxide [2], halogen species [3, 4] , biocide [5] and heavy metal [6-8]. From several types of antibacterial fillers, heavy metal in the form of silver nanoparticles (AgNPs), are well recognized to exhibit an effective antibacterial activity and are widely used in many applications such as medical devices [9], paint [10], coating [11] and textiles [12]. Recently, it has been reported that the AgNPs could affect human tissues from diverse routes of exposure including the respiratory system, skin, and gastrointestinal tract [13]. It has been proposed that AgNPs may interact with thiol groups of proteins and enzymes within mammalian cells, some of which are key components in the antioxidant defense mechanism of the cell. Inhibition of this mechanism would then result in an increase in the concentration of reactive oxygen species that can alter or damage the function of the cells. Also, it has been found that the AgNPs can be released from commercial clothing (socks) into the wash water [14], and so could increase the risk of environmental contamination. Therefore, it is highly desirable if the antibacterial fillers can be developed from natural, nontoxic and environmentally friendly material.

Chitosan is a natural biopolymer derived from the deacetylation of chitin, an abundantly available biopolymer found in the exoskeletons of insects, the shell of crustaceans, and fungal cell walls. It is nontoxic, biodegradable, biocompatible and possesses antibacterial properties [15]. In fact, the potential of chitosan particles as an effective antibacterial agent/filler has been realized and continuously reported. Early work by Qi and co-workers demonstrated that chitosan in the form of nanoparticles exerted a higher antibacterial activity against *E. coli, S. choleraesis, S. typhimurium, and S. aureus* than chitosan solution, and it was proposed that the greater surface area of the particles provided a

more intimate contact with the surface of bacterial cells [16]. Ye and co-workers, on the other hand, have shown that cotton fabrics coated with core-shell particles, having poly(*n*-butyl acrylate) as the core and chitosan as the shell, exhibited an excellent antibacterial activity against *S. aureus* with a reduction in viable bacteria numbers of more than 99% [17].

In general, chitosan would exhibit its antibacterial activity only in acidic medium, due to the poor solubility of chitosan above its pKa (pH 6.5). Quaternization of the amino groups to introduce permanent positively charged quaternary ammonium groups has been recognized as a potential way to enhance the antibacterial activity of chitosan over a broader pH range. The reaction can simultaneously introduce the permanent positive charge and hydrophobicity, the two parameters that are believed to affect the antibacterial activity [18-20]. Synthetic routes and applications of quaternized derivatives of chitosan have been recently reviewed and published [21, 22], whilst the application of quaternized chitosan particles has been reported. For example, particles fabricated from chitosan that was formerly quaternized by hexyl bromide were incorporated as bactericidal fillers in poly(methyl methacrylate) bone cement and tested against *S. aureus* and *S. epidermidis* under a neutral pH environment [23].

In order to promote ionic interactions with the negatively charged components of the bacterial cell membrane, the incorporation of metal ions [24-26] or cationic polymer [27] into chitosan particles has also been recently reported as an alternative approach. Qi and co-workers have suggested that the antibacterial activity can be enhanced by incorporating Cu^{2+} into chitosan particles [25]. Later, Du and co-workers have shown that chitosan particles loaded with various metal ion such as Ag^{+}, Cu^{2+}, Zn^{2+}, Mn^{2+}, Fe^{2+}, exhibited higher antibacterial effect against *E. coli*, *S. choleraesuis*, and *S. aureus* than chitosan particles [24, 26]. In addition, Inphonlek and coworkers have found that core-shell nanoparticles having poly(methyl methacrylate) core coated with polyethyleneimine, and chitosan-mixed-

polyethyleneimine shells exhibited higher antibacterial activity against *S. aureus* and *E. coli* than chitosan nanoparticles [27].

Here in this research, we attempt to develop an environmentally friendly, organic antibacterial filler from chitosan particles. The permanent positive charges in the form of quaternary ammonium groups were introduced to the surface of pre-fabricated chitosan particles under heterogeneous condition via direct methylation or reductive *N*-alkylation using two different aldehydes, propionaldehyde and benzaldehyde, followed by methylation with methyl iodide. This method has the advantage that it can be performed conveniently in the absence of tedious purification process that is generally required for homogeneous quaternization. The success of this type of method for enhancing antibacterial activity especially in a neutral pH environment has been previously reported for the chitosan films [28]. And the fact that the addition of cationic metal species or polymers is no longer necessary truly simplifies the fabrication method.

2. Materials and methods

2.1. Materials

Chitosan flake (DAC 85%, M_V = 45,000 Da) was purchased from Seafresh Chitosan (Lab) Co., Ltd (Thailand). Propionaldehyde, methyl iodide (CH_3I), sodium borohydride ($NaBH_4$), sodium chloride (NaCl), sodium hydroxide (NaOH), sodium iodide (NaI) and tripolyphosphate (TPP) were purchased from Fluka (Switzerland). Acetic acid, benzaldehyde, ethanol (EtOH), and methanol (MeOH) were purchased from Merck (Germany). Dialysis membrane (cut-off molecular weight of 12,400 g/mol) was purchased from Sigma (USA). All reagents and materials were of analytical grade and used without further purification. *E. coli* and *S. aureus* were provided by National Center for Genetic Engineering and Biotechnology (BIOTEC), Thailand. Mueller-Hinton agar (MHA) and Mueller-Hinton broth (MHB) were

purchased from Difco (USA). Mueller Hinton agar plates were supplied by Department of Medical Science, Ministry of Public Health, Thailand. Ultrapure distilled water was obtained after purification using a Millipore Milli-Q system (USA) that involves reverse osmosis, ion exchange, and a filtration step.

2.1. Preparation of surface-quaternized chitosan particles

Chitosan particles were prepared using TPP as a crosslinking agent according to the published procedure by Qi *et al.* [16] Preparation of quaternized *N*-alkyl chitosan particles were done following the method of Vallapa *et al.* [28]. In brief, an anhydrous methanol solution of a selected aldehyde (10 mL) having a desired concentration was added into a flask containing chitosan particles (0.03 g). After stirring for a given time at ambient temperature (~ 28-30^{o}C), $NaBH_4$ (0.3 g, 0.8 mol) was added into the reaction mixture and the solution was stirred for 24 h. The resulting *N*-alkyl chitosan particles were then isolated by centrifugation at 12,000 rpm for 30 min. The supernatant was discarded and the particles were centrifugally washed as above with methanol three times and then dried *in vacuo*. An anhydrous methanol solution (10 mL) containing NaI (0.30 g, 2 mmol) and NaOH (0.13 g, 3 mmol) was then added into a flask containing chitosan or *N*-alkyl chitosan particles (0.03 g) and CH_3I was then added via syringe. The reaction mixture was stirred at 50°C for a given time. The particles were isolated and purified as above mentioned.

2.2. Characterization of surface-quaternized chitosan particles

Fourier Transform-Infrared (FT-IR) spectra were collected using a Nicolet Impact 410 FT-IR spectrometer. All samples were prepared as KBr pellets. All ^{1}H NMR spectra were recorded in a 1% (v/v) solution of CF_3COOH/D_2O or D_2O using a Varian model Mercury-400 nuclear magnetic resonance spectrometer (USA) operating at 400 MHz. Chemical shifts

(δ) are reported in parts per million (ppm) relative to tetramethylsilane (TMS) or using the residual protonated solvent signal as a reference. The size and the morphology of all particles were examined by transmission electron microscope (TEM, Model JEM-2100, Japan) with the average diameter calculated using Semafore software and reported from the measurement of 100 randomly selected particles. The ζ-potential values of the particles were determined using a Nanosizer Nano-ZS (Malvern Instruments, UK) at 25^{o}C with a scattering angle of 173^{o}. All data are displayed as the mean $\pm$ one standard deviation and are derived from at least three independent experiments. The data were calculated using the Helmholtz-Smoluchowski equation.

2.8. Evaluation of antibacterial activity

All glasswares used for the tests were sterilized in an autoclave at 121°C for 15 min prior to use. All particles were sterilized by exposing to UV radiation for 60 min prior to the tests. The antibacterial test was performed according to a modified method of Qi *et al*. [16]. Chitosan and quaternized chitosan particles (2.5 mg) were added to 5 mL of MHB in test tubes and aseptically inoculated with 50 μL of the freshly prepared bacterial suspension in distilled water (OD_{600} = 0.5). The pH of the broth was about 7.4. The negative and positive controls were a broth solution alone and a broth solution with ampicillin (50 mg/mL), respectively. After mixing, broth cultures were incubated at 37°C in a shaking incubator (Model G-25, New Brunswick Scientific Co., Inc., USA), at 110 rpm for 24 h. Then, 100 μL of the bacterial solution was removed and 10-fold serially diluted down to 10^{6}-fold the original level. A 100 μL aliquots of each diluted bacterial suspension was then spreaded onto the MHA plates for total plate counting. After incubating at 37°C for 18 h, the number of colonies, and thus replication competent bacteria, were then counted as a measure of the

assumed viable number of bacteria. The results after correction for the dilution factor were expressed as mean colony forming units per volume (CFU/mL).

To determine the minimum inhibitory concentration (MIC) of all particles, the particles were first suspended in 5 mL of MHB and two-fold serial dilutions prepared. Each set of serial dilutions was then inoculated under aseptic conditions with 50 μL of the freshly prepared bacterial suspension in distilled water (OD_{600} = 0.5). After incubating at 37°C for 24 h, the total plate count enumeration of the CFU/mL was evaluated as described above. The lowest concentration of the particles that inhibited the growth of bacteria was considered as the minimum inhibitory concentration (MIC).

All tests of antibacterial activity were performed in triplicate per sample, upon at least three independent samples and expressed as mean ± standard deviation (SD). Statistical analysis was performed using the Statistical Package for the Social Science (SPSS) version 17.0 software. Statistical comparisons made by One-Way Analysis of Variance (ANOVA) with the Least Square Difference (LSD) tests were used for post hoc evaluations of differences between groups. The threshold level for accepting statistical significance was set at $p < 0.01$.

3. Results and Discussion

3.1. Preparation and characterization of surface-quaternized chitosan particles

Chitosan particles were first fabricated by ionic crosslinking between positively charged chitosan and negatively charged TPP. The process was conducted at ambient temperature in the absence of any surfactant or oil phase. The resulting chitosan particles appeared as fine white powder after drying and were insoluble in water, dilute acidic and alkali solutions. As outlined in Scheme 1, chitosan particles were then surface-modified by heterogeneous reductive *N*-alkylation with selected aldehyde, namely propionaldehyde and

benzaldehyde which yielded *N*-propyl chitosan particles and *N*-benzyl chitosan particles, respectively. Subsequent methylation with CH_3I thus formed quaternized *N*-propyl chitosan (QPCS) particles and quaternized *N*-benzyl chitosan (QBzCS) particles, respectively. Furthermore, the quaternization (Scheme 1) was also conducted directly on chitosan particles by methylation with CH_3I and gave quaternary ammonium-containing chitosan (QACS) particles as products. The optimized conditions for the preparation of each surface-quaternized chitosan particles via heterogeneous quaternization, so as to yield the highest degree of quaternization in terms of reaction time and reagent concentration were empirically identified (Table S1, Supplementary Material) based on the results from water contact angle and ζ-potential measurements following the criteria as previously described [28]. Another type of quaternized particles designated as *N,N,N*-trimethylchitosan (TMCS) particles were prepared for comparison. Although the quaternary ammonium entity (trimethyl, $-N(CH_3)_3$) of the TMCS particles is similar to that of the QACS particles, the TMCS particles were prepared differently by ionic gelation of *N,N,N*-trimethylchitosan synthesized homogeneously from chitosan according to the method reported by Sieval *et al*. [29]. In other words, TMCS particles should not only bear positive quaternary ammonium groups at the particles' surface which is the case for the QACS particles, but also inside the particles.

Chemical functionalities of all quaternized chitosan particles were first identified by FT-IR analysis. As shown in Fig. 1, absorption peaks at 1650 and 1544 cm^{-1} can be assigned to the C=O stretching (Amide I) and N-H bending (Amide II) of the glucosamine unit of chitosan, respectively. The decrement of the N-H bending signal at 1544 cm^{-1} and the appearance of the C-H deformation signal in a range of 1470-1460 cm^{-1} in the spectra of all quaternized chitosan particles implied that the amino groups were functionalized by alkyl substituents introduced by either reductive *N*-alkylation/methylation or direct methylation. Nonetheless, the C-H deformation peak belonging to the TMCS particles was obviously weak

as opposed to those observed for other particles implying that there was smaller content of quaternary ammonium groups in the TMCS particles.

The degree of success in the quaternization of chitosan particles was also confirmed by ^{1}H NMR analysis. As illustrated in Fig.2, the multiplet in the range of δ3.3 - 4.4 ppm comes from the six carbon atoms at the 2', 3, 4, 5, 6, and 6' positions, while the two singlets at δ1.9 and δ2.9 ppm are due to the methyl protons from the acetyl groups (position A) and at the 2 position of *N*-acetyl glucosamine unit, respectively. For the QPCS and QBzCS particles, it should be emphasized that not all of the amino groups of chitosan were alkylated in the first step of reductive *N*-alkylation. As a consequence, the signals of the methyl protons appearing in Fig.2(d-e) would come from methyl groups attached to both alkylated and non-alkylated amino functionalities. The signal at δ3.1-3.3, δ3.0, and δ2.7 ppm can be assigned to the methyl protons of the trisubstituted (-$N^{+}(C\underline{H}_3)_3$ or $NR^{+}(C\underline{H}_3)_2$, position B), disubstituted (-$N(C\underline{H}_3)_2$ or -$NR(C\underline{H}_3)$, position C) and monosubstituted (-$NH(C\underline{H}_3)$, position D) amino groups, respectively. The trace signals of methylene protons (δ1.0 ppm) and methyl protons (δ0.85 ppm) observed on the spectrum of QPCS particles (Fig.2(e)) can be used as additional evidences confirming the attachment of propyl groups at the amino moieties of chitosan in the step of reductive *N*-alkylation. For the QBzCS particles (Fig.2(f)), the signals of aromatic protons at δ7.4 ppm together with the benzylic protons at 1.0 ppm could be used to verify the attachment of benzyl groups at the amino positions of chitosan.

Based on the ^{1}H NMR analysis, the degree of quaternization (%DQ) can also be estimated. To simplify the calculation, it was assumed that the majority of quaternary ammonium groups existed in the form of -$N^{+}(C\underline{H}_3)_3$ and only a few were present in the form of $NR^{+}(C\underline{H}_3)_2$. This assumption is based on the fact that the non-alkylated or free amino groups (-NH_2) left after the *N*-reductive alkylation step are less bulkier than the alkylated amino group (-NHR) and should thus be more accessible for nucleophilic substitution of CH_3I. Such

characteristics should favor the formation of $-N^{+}(C\underline{H}_3)_3$ as opposed to that of the $NR^{+}(C\underline{H}_3)_2$. The %DQ can thus be calculated from the relative ratio between the integration of the nine protons from the three methyl groups of the quaternized *N*-alkyl chitosan at the position δ3.1-3.3 ppm and the peak integration of the six protons of chitosan (δ3.3-4.4 ppm). Accordingly, the calculated %DQ value based on the content of $N^{+}(C\underline{H}_3)_3$ was 2.1, 7.1, 4.2, and 5.7 % for TMCS, QACS, QPCS, and QBzCS particles, respectively. It should be taken into account that the quaternized chitosan particles were not completely soluble in the CF_3COOH/D_2O, the solvent used for NMR analysis. As a result, the %DQ values obtained from ^{1}H NMR analysis are not capable of reflecting the actual degree of surface quaternization, they can only be used as a qualitative measure of the extent of surface substitution. The fact that %DQ of TMCS particles was the lowest agrees quite well with the data formerly described based on FT-IR analysis (Fig.1).

TEM analysis revealed that all particles were quite spherical in shape and had average diameters in a sub-micron range of 260 -490 nm (Fig. 3). The dimension of QACS particles was quite comparable to that of the TMCS particles implying that the preparation method did not have significant impact on the particle size and morphology. On the other hand, the size of chitosan particles seemed to be greater when being modified by a larger alkyl substituent (propyl, benzyl) which came from the aldehyde used in the reductive *N*-alkylation step. The charge characteristic of the quaternized chitosan particles was determined by photon correlation spectroscopy (PCS). As shown in Fig. 3, all particles prepared by heterogeneous quaternization via reductive *N*-alkylation followed by methylation (QPCS and QBzCS particles) or direct methylation (QACS particles) exhibited greater zeta potential values than those of chitosan and TMC particles. Indeed, comparing TMCS and QACS particles, it seems that the heterogeneous quaternization approach was more efficient in enhancing positive charges of the chitosan particles than the homogeneous one. This may stem from the fact that some positive charges of

TMC were neutralized following ionic crosslinking with the negatively charged TPP upon the particle formation. In accord with this notion is that the TMCS particles formed by the crosslinking of TMC and TPP were not completely soluble in CF_3COOH/D_2O. As a result, the %DQ of TMC particles (2.1%) was much lower than that of the originally synthesized TMC (%DQ = 11.8%) indicating the consumption of the positive charges during crosslinking. Unlike the TMCS particles, the introduction of trimethyl groups to chitosan particles via direct methylation to yield the QACS particles was performed after the particle formation. Thus, the positive charge density generated thereafter was not depleted by the crosslinking. A similar explanation can be applied for the QPCS and QBzCS particles, where again the quaternization was applied after the particle formation. Interestingly, the presence of the larger alkyl substituents (propyl and benzyl) somewhat promoted the subsequent methylation accounting for why the ζ-potential was raised above +35 eV for both the QPCS and QBzCS particles. It is postulated that the more hydrophobic environment created by the propyl and benzyl substituents may increase a chance of CH_3I, a small organic molecule of low polarity, to reach the amino active sites of chitosan chain during methylation. Previous work has also demonstrated that the degree of surface quaternization can be tailored by adjusting the CH_3I concentration used in the methylation step [28].

3.2 Antibacterial efficacy of surface-quaternized chitosan particles

The antibacterial activity of surface-quaternized chitosan particles were tested against the representative Gram-positive and Gram-negative bacteria, *S. aureus* and *E. coli*, respectively, and reported as the total number of replication competent (viable) cells as mean colony forming units per volume (CFU/mL). In the case of *S. aureus*, all quaternized chitosan particles, TMCS, QACS, QPCS and QBzCS particles, exhibited significantly higher antibacterial ratio (> 95%) than the chitosan particles at pH 7.4 (Fig. 4), supporting that the

introduction of the positive charges via quaternization can effectively improve the antibacterial activity of chitosan particles especially in neutral media. In contrast, the antibacterial action of chitosan particles cannot be detected given that their viable counts closely resembled those of the negative control. This outcome is in line with our previous observation on chitosan film implying that chitosan particles would exhibit its potential in suppressing the bacterial growth only when they are in acidic media in which they are positively charged [28]. This also further suggested that the chelation of the amino groups of chitosan as proposed by others [30, 31] is definitely not the major mechanism that controls the antibacterial activity at this particular condition. These evidences support that the superior antibacterial activities of some quaternized chitosan particles, especially QPCS and QBzCS particles, to the chitosan particles are mainly due to their higher charge density in near neutral pH condition than the latter (See Fig. 3 for ζ-potential data). Overall, this trend is in accordance with previously observed data reported by Qi and coworkers [16], who proposed that the positively charged chitosan particles should interact favorably with negatively charged cell membranes, causing an increase in membrane permeability and eventually rupture and leakage of intracellular components. This proposed mechanism is particularly reasonable in the case of the Gram-positive bacteria, such as *S. aureus* since their outer membrane consists of negatively charged teichoic acid, that is believed to be responsible for the electrostatic binding with the positively charged particles.

Although the TMCS particles exhibited a slightly lower ζ-potential than the chitosan particles, they still inhibited the growth of *S. aureus*, potentially suggesting that the inhibition did not solely rely on the contact-inhibitory mechanism which should be charge density-dependent, but may also be influenced by the charge inside the particles or the ability to dissolve in the media considering that TMC is water soluble and not all of the TMC molecules were crosslinked by TPP during the particle formation. In fact, this release-inhibitory

mechanism involving surface leaching of soluble chitosan and/or its quaternized derivatives has been recently proposed by Fernandez-Saiz and co-workers [32] and also in our earlier work on the surface-quaternized chitosan films [28]. Similar explanations may also be applied in the case of QACS particles whose charge density (ζ-potential = +29.3 mV) was slightly higher than those of both chitosan particles (ζ-potential = +27.1 mV) and TMCS particles (ζ-potential = +23.2 mV). Having the same type of quaternary ammonium groups (-$N(CH_3)_3$), the QACS particles exhibited better antibacterial action against *S. aureus* than the TMCS particles indicating that the heterogeneous quaternization was potentially a more effective route to promote the antibacterial activity of chitosan particles than the homogeneous one. This is extremely important considering that the higher charge density can be achieved via heterogeneous route without sacrificing the positive charges to the crosslinking process. The lowering of the ζ-potential upon ionotropic crosslinking of TMC by TPP has also been reported by Sadeghi and co-workers [33]. It is also conceivable that the uncrosslinked surface-modified quaternized layer on the surface of QACS particles may leach out easier than the quaternary entities trapped or crosslinked by TPP inside and/or on the surface of TMCS particles.

The trend observed for the representative Gram-negative bacteria, *E. coli* is quite different from that seen with the Gram-positive *S. aureus* described above. In comparison with the negative control and chitosan particles, the quaternized chitosan particles with only slightly higher charge density, namely TMCS, and QACS particles, did not possess significant antibacterial activity against *E. coli* (Fig. 4). QACS particles exhibited % antibacterial activity of 82.9% whereas the detrimental action of TMCS cannot be detected. On the other hand, the quaternized chitosan particles with larger alkyl groups having higher charge density, namely QPCS and QBzCS particles, exerted much higher antibacterial action against the *E. coli.* With a similar ζ-potential, the QBzCS particles displays a greater inhibitory action than the QPCS particles which is reasonable considering that the uppermost

layer of the outer membrane of *E. coli* contains lipopolysaccharide that should interact favorably with hydrophobic entities of the particles. In addition, the fact that QACS film was reported to exhibit much lower % antibacterial activity against *S. aureus* (26%antibacterial ratio) and *E.coli* (29% antibacterial ratio) [28], in comparison with the QACS particles apparently suggests that the antibacterial efficacy can be magnified by the enhanced surface area of the particles.

Comparatively, as outlined in Fig. 4, it was found that *E. coli* had a greater resistance to quaternized chitosan particles than the *S. aureus*. This can be explained by three reasons. Firstly, the absence of an outer membrane and the presence of negatively charged teichoic acid within a thick peptidoglycan layer (20-80 nm) on the surface of *S. aureus* should make them more attractive to the positively charged, quaternized chitosan particles and more specific to be damaged by positively charged molecules than *E. coli*. Secondly, the presence of a number of small channels of porins within the outer membrane of *E. coli* may help block the entrance of the particles into the bacterial cell, making them more difficult to inhibit than *S. aureus*. Finally, the smaller dimension of *S. aureus* (sphere, i.d. ~ 0.5-1 μm) may partly account for more intimate contact with the quaternized chitosan particles, making the antibacterial activity more effective than the *E. coli* (rod, 0.3-1.0 × 1.0-6.0 μm) .

Minimum inhibitory concentration (MIC) is the lowest concentration of an antimicrobial agent that can inhibit the growth of the target microorganism. From a practical perspective, this value is a key indication of the inhibitory efficiency of the substance against the microorganism. In this study, the MIC values of chitosan, TMCS, QACS, and QBzCS particles were evaluated by viable cell counting methods. The MIC values for each type of particle were identified by comparing the viable cell counts (log (CFU/mL)) between the suspension having the designated particles and the negative control). Results for all quaternized chitosan particles are displayed in Table 1. The fact that the concentration of as

high as 1000 mg/mL was neccessary for chitosan particles to express their inhibitory power explained why no inhibitory action was detected when previously tested with 0.5 mg/mL or 500 μg/mL chitosan particles (Fig.4). To start suppressing the growth of *E. coli* by chitosan particles demanded a concentration as high as 2000 μg/mL. These results support the previous assumption that *E. coli* is more tolerant than *S. aureus*. However, using the same growth media for bacteria, MHB, much lower MIC values of 234 and 117 μg/mL against *S. aureus* and *E. coli*, respectively have been reported for the chitosan particles also prepared by ionotropic crosslinking by TPP [24]. It is suspected that this difference may be a result of their particles having a much smaller size (~54 nm) and so possess a greater available surface area than ours (~320 nm). Therefore, a significantly lower quantity of chitosan particles was required in their case. In contrast, Sadeghi and co-workers [33] reported a two-fold higher MIC value for the TPP-crosslinked chitosan particles against *S. aureus*. This is reasonable given that their particles had a comparable size (~250 nm) to ours but with less ζ- potential (+15.9 eV).

As anticipated, the QACS particles with lower MIC were more potent in prohibiting bacterial growth than the TMCS particles. This MIC value (62.5 μg/mL) was apparently lower than those reported for TMC solutions with various degree of quaternization (%DQ) [33, 34] indicating their superior antibacterial efficacy. This outcome truly indicated the potential of heterogeneous route for the preparation of quaternized chitosan particles as opposed to the conventional homogeneous one which is obviously suffered from the drawback of a deteriorated antibacterial activity because the particles have to be formed after quaternization. The data demonstrated by Sadeghi and co-workers (also shown in Table 1) can be used as a good example [33]. The variation in experimental parameters such as molecular weight and degree of deacetylation of chitosan, %DQ, growth media, pH, initial bacteria concentration, bacterial source, method used for determination of the antibacterial

activity (i.e. optical density (OD), total plate counts for viable cells) should be taken into account when comparing the results. Eventhough a greater quantity of QPCS and QBzCS particles was required to start their detrimental effect on both bacterial strains as compared with the QACS particles, their antibacterial action was more effective when the quantity of all particles were as equal to or above the MIC values of the QPCS and QBzCS particles. This can be evidenced from the data shown in Fig.4 (tested with 500 μg/mL particles). Interestingly, the MIC values of both QACS and QBzCS particles were independent on the bacterial strain.

4. Conclusions

Quaternized chitosan particles having different alkyl substitutents can be successfully prepared by heterogeneous direct methylation or reductive *N*-alkylation/methylation as verified by ^{1}H NMR and FT-IR analyses. The particles were spherical in shape, having an average diameter in a range of 230-490 nm and carried positive charges with ζ-potential ranging from +23.2 to +46.8 mV. As determined by viable count method, it was found that all quaternized chitosan particles exhibited higher antibacterial activity against *S. aureus* (Gram positive bacteria) than the chitosan particles in neutral media. It is believed that the electrostatic binding between the positive charges on the particles and the negatively charged teichoic acid on the outer membrane of *S. aureus* was responsible for their superior antibacterial activity. In contrast, only the QPCS and QBzCS particles, which have a high charge density and relatively large alkyl groups, were capable of suppressing the growth of *E. coli* (Gram-negative bacteria). The fact that *E. coli* had greater resistance to all quaternized chitosan particles than the *S. aureus* may be explained as a result of their difference in shape and outer membrane properties. The minimum inhibitory concentration (MIC) data led to two important conclusive remarks: (1) the antibacterial efficiency of each particle was dose-

dependent and (2) having the same alkyl substituent as TMCS particles, QACS particles were a more potent antibacterial material indicating that the heterogeneous quaternization was a more effective method than the homogeneous one. The results obtained from this research suggested that the surface-quaternized chitosan particles may potentially be used as effective antibacterial fillers for biomedical applications.

Acknowledgments

This research was financially supported by Research Team Promotion Grant from the Thailand Research Fund (RTA50800004). The authors appreciated a language editing service provided by Dr. Robert Butcher, the Publication Counselling Unit (PCU), Faculty of Science, Chulalongkorn University.

References

[1] M. Changez, V. Koul, A. K. Dinda, Efficacy of antibiotics-loaded interpenetrating network (IPNs) hydrogel based on poly(acrylic acid) and gelatin for treatment of experimental osteomyelitis: in vivo study, Biomaterials 26 (2005) 2095-2104.

[2] B. J. Nablo, A. R. Rothrock, M. H. Schoenfisch, Nitric oxide-releasing sol-gels as antibacterial coatings for orthopedic implants, Biomaterials 26 (2005) 917-924.

[3] Y. Y. Sun, G. Sun, Novel refreshable *N*-halamine polymeric biocides: *N*-chlorination of aromatic polyamides, Ind. Eng. Chem. Res. 43 (2004) 5015-5020.

[4] Y. Sun, G. Sun, Synthesis, characterization, and antibacterial activities of novel *N*-halamine polymer beads prepared by suspension copolymerization, Macromolecules 35 (2002) 8909-8912.

[5] S. M. Iconomopoulou, G. A. Voyiatzis, The effect of the molecular orientation on the release of antimicrobial substances from uniaxially drawn polymer matrixes, J. Control. Release 103 (2005) 451-464.

[6] N. Cioffi, L. Torsi, N. Ditaranto, G. Tantillo, L. Ghibelli, L. Sabbatini, T. Bleve-Zacheo, M. D'Alessio, P. G. Zambonin, E. Traversa, Copper nanoparticle/polymer composites with antifungal and bacteriostatic properties, Chem. Mater. 17 (2005) 5255-5262.

[7] M. Rai, A. Yadav, A. Gade, Silver nanoparticles as a new generation of antimicrobials, Biotechnol. Adv. 27 (2009) 76-83.

[8] V. K. Sharma, R. A. Yngard, Y. Lin, Silver nanoparticles: Green synthesis and their antimicrobial activities, Adv. Colloid Interf. 145 (2009) 83-96.

[9] F. Furno, K. S. Morley, B. Wong, B. L. Sharp, P. L. Arnold, S. M. Howdle, R. Bayston, P. D. Brown, P. D. Winship, H. J. Reid, Silver nanoparticles and polymeric medical devices: A new approach to prevention of infection, J. Antimicrob. Chemoth. 54 (2004) 1019-1024.

[10] A. Kumar, P. K. Vemula, P. M. Ajayan, G. John, Silver-nanoparticle-embedded antimicrobial paints based on vegetable oil, Nat. Mate. 7 (2008) 236-241.

[11] M. Wagener, Antimicrobial coatings, Polym. Paint Colour J. 196 (2006) 34-37.

[12] N. Duran, P. D. Marcato, G. I. H. De Souza, O. L. Alves, E. Esposito, Antibacterial effect of silver nanoparticles produced by fungal process on textile fabrics and their effluent treatment, J. Biomed. Nanotechnol. 3 (2007) 203-208.

[13] X. Chen, H. J. Schluesener, Nanosilver: A nanoproduct in medical application, Toxicol. Lett. 176 (2008) 1-12.

[14] T. M. Benn, P. Westerhoff, Nanoparticle silver released into water from commercially available sock fabrics, Environ. Sci. Technol. 42 (2008) 4133-4139.

[15] M. N. V. R. Kumar, R. A. A. Muzzarelli, C. Muzzarelli, H. Sashiwa, A. J. Domb, Chitosan chemistry and pharmaceutical perspectives, Chem. Rev. 104 (2004) 6017-6084.

[16] L. F. Qi, Z. R. Xu, X. Jiang, C. H. Hu, X. F. Zou, Preparation and antibacterial activity of chitosan nanoparticles, Carbohyd. Res. 339 (2004) 2693-2700.

[17] W. J. Ye, M. F. Leung, J. Xin, T. L. Kwong, D. K. L. Lee, P. Li, Novel core-shell particles with poly(*n*-butyl acrylate) cores and chitosan shells as an antibacterial coating for textiles, Polymer 46 (2005) 10538-10543.

[18] X. L. Ye, X. G. Li, L. J. Yuan, L. H. Ge, B. S. Zhang, S. B. Zhou, Interaction of houttuyfonate homologues with the cell membrane of gram-positive and gram-negative bacteria, Colloid Surf. A-Physicochem. Eng. Asp. 301 (2007) 412-418.

[19] M. E. I. Badawy, Structure and antimicrobial activity relationship of quaternary *N*-alkyl chitosan derivatives against some plant pathogens, J. Appl. Polym. Sci. 117 (2010) 960-969.

[20] C. H. Kim, K. S. Choi, Synthesis and antibacterial activity of quaternized chitosan derivatives having different methylene spacers, J. Ind. Eng. Chem. 8 (2002) 71-76.

[21] W. Sajomsang, Synthetic methods and applications of chitosan containing pyridylmethyl moiety and its quaternized derivatives: A review, Carbohyd. Polym. 80 (2010) 631-647.

[22] V. K. Mourya, N. N. Inamdar, Trimethyl chitosan and its applications in drug delivery, J. Mater. Sci.-Mater. Med. 20 (2009) 1057-1079.

[23] Z. L. Shi, K. G. Neoh, E. T. Kang, W. Wang, Antibacterial and mechanical properties of bone cement impregnated with chitosan nanoparticles, Biomaterials 27 (2006) 2440-2449.

[24] W. L. Du, S. S. Niu, Y. L. Xu, Z. R. Xu, C. L. Fan, Antibacterial activity of chitosan tripolyphosphate nanoparticles loaded with various metal ions, Carbohyd. Polym. 75 (2009) 385-389.

[25] L. F. Qi, Z. R. Xu, X. Jiang, Y. Li, M. Q. Wang, Cytotoxic activities of chitosan nanoparticles and copper-loaded nanoparticles, Bioorg. Med. Chem. Lett. 15 (2005) 1397-1399.

[26] W. L. Du, Y. L. Xu, Z. R. Xu, C. L. Fan, Preparation, characterization and antibacterial properties against *E. coli* K88 of chitosan nanoparticle loaded copper ions, Nanotechnology 19 (2008) 085707.

[27] S. Inphonlek, N. Pimpha, P. Sunintaboon, Synthesis of poly(methyl methacrylate) core/chitosan-mixed-polyethyleneimine shell nanoparticles and their antibacterial property, Colloid Surf. B-Biointerfaces 77 (2010) 219-226.

[28] N. Vallapa, O. Wiarachai, N. Thongchul, J. S. Pan, V. Tangpasuthadol, S. Kiatkamjornwong, V. P. Hoven, Enhancing antibacterial activity of chitosan surface by heterogeneous quaternization, Carbohyd. Polym. 83 (2011) 868-875.

[29] A. B. Sieval, M. Thanou, A. F. Kotze, J. C. Verhoef, J. Brussee, H. E. Junginger, Preparation and NMR characterization of highly substituted *N*-trimethyl chitosan chloride, Carbohyd. Polym. 36 (1998) 157-165.

[30] M. Kong, X. G. Chen, C. S. Liu, C. G. Liu, X. H. Meng, L. J. Yu, Antibacterial mechanism of chitosan microspheres in a solid dispersing system against *E. coli*, Colloid Surf. B-Biointerfaces 65 (2008) 197-202.

[31] R. G. Cuero, G. Osuji, A. Washington, *N*-Carboxymethylchitosan inhibition of aflatoxin production: Role of zinc, Biotechnol. Lett. 13 (1991) 441-444.

[32] P. Fernandez-Saiz, J. M. Lagaron, M. J. Ocio, Optimization of the biocide properties of chitosan for its application in the design of active films of interest in the food area, Food Hydrocolloids 23 (2009) 913-921.

[33] A. M. M. Sadeghi, F. A. Dorkoosh, M. R. Avadi, P. Saadat, M. Rafiee-Tehrani, H. E. Junginger, Preparation, characterization and antibacterial activities of chitosan, *N*-trimethyl chitosan (TMC) and *N*-diethylmethyl chitosan (DEMC) nanoparticles loaded with insulin using both the ionotropic gelation and polyelectrolyte complexation methods, Int. J. Pharm. 355 (2008) 299-306.

[34] W. Sajomsang, P. Gonil, S. Saesoo, Synthesis and antibacterial activity of methylated *N*-(4-*N,N*-dimethylaminocinnamyl) chitosan chloride, Eur. Polym. J. 45 (2009) 2319-2328.

List of Figure and Scheme Captions

Scheme 1 Preparation of surface-quaternized chitosan particles by reductive *N*-alkylation/methylation (top row) and direct methylation (bottom row).

Fig. 1. FT-IR spectra of (a) chitosan particles, (b) TMCS particles, (c) QACS particles, (d) QPCS particles, and (e) QBzCS particles.

Fig. 2. ^{1}H-NMR spectra of (a) chitosan particles, (b) TMCS particles, (c) QACS particles, (d) QPCS particles, and (f) QBzCS particles.

Fig. 3. Representative TEM micrographs (x 12,000), average particles sizes and ζ- potentials of chitosan and quaternized chitosan particles. Micrographs shown are representative of at least 10 such fields of view per sample and 3 independent samples.

Fig. 4. Total replication competent (viable) cell counts of *S. aureus* and *E. coli* in suspension after incubation with different chitosan particles (0.5 mg/mL) for 24 h. Statistical significance with $p < 0.01$ of the viable count is compared with the negative control (*) and the chitosan particles *(#*). Below in the table is the corresponding antibacterial ratio.

Figure(s)
Click here to download high resolution image

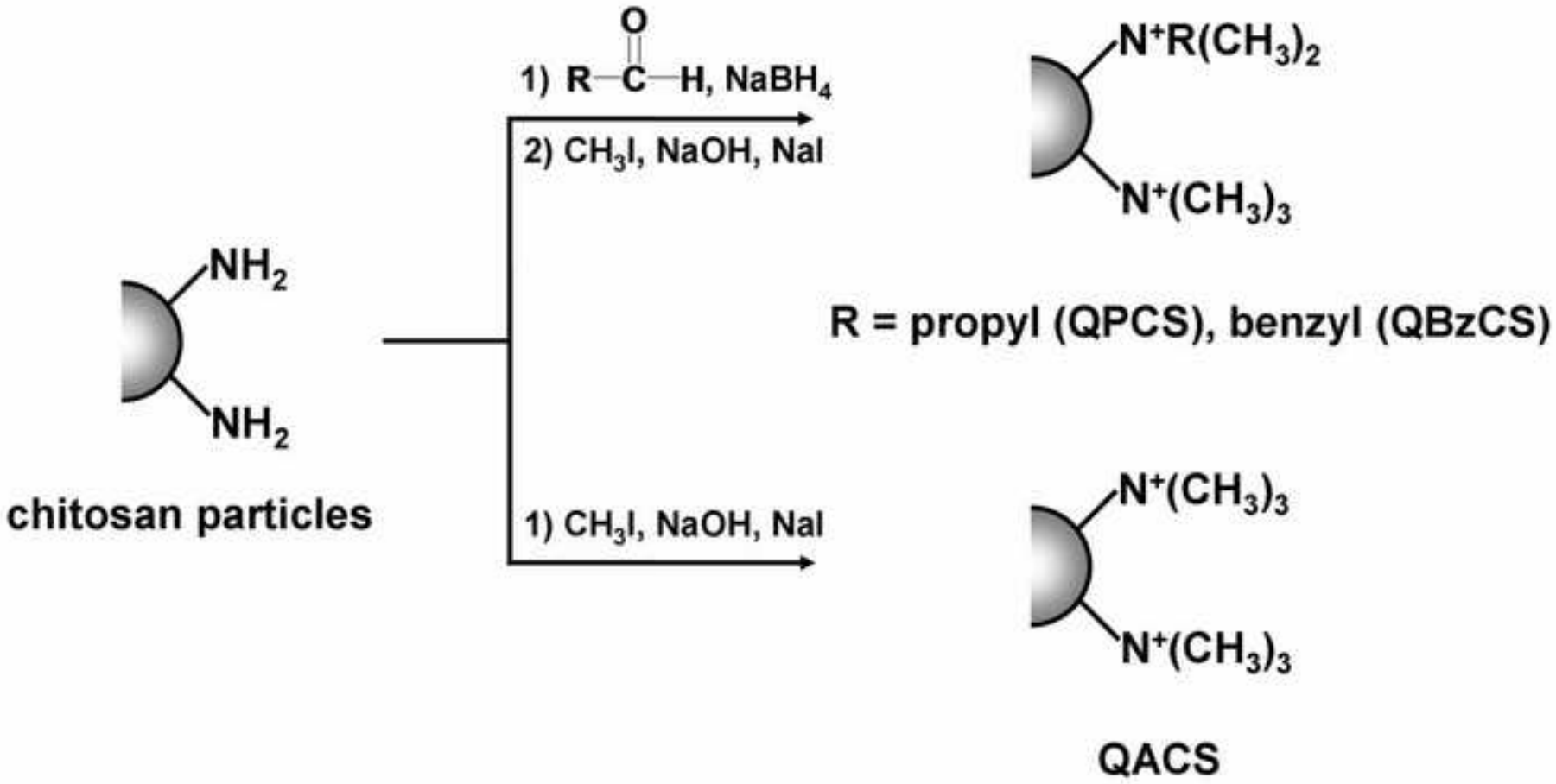

Figure(s)

Click here to download high resolution image

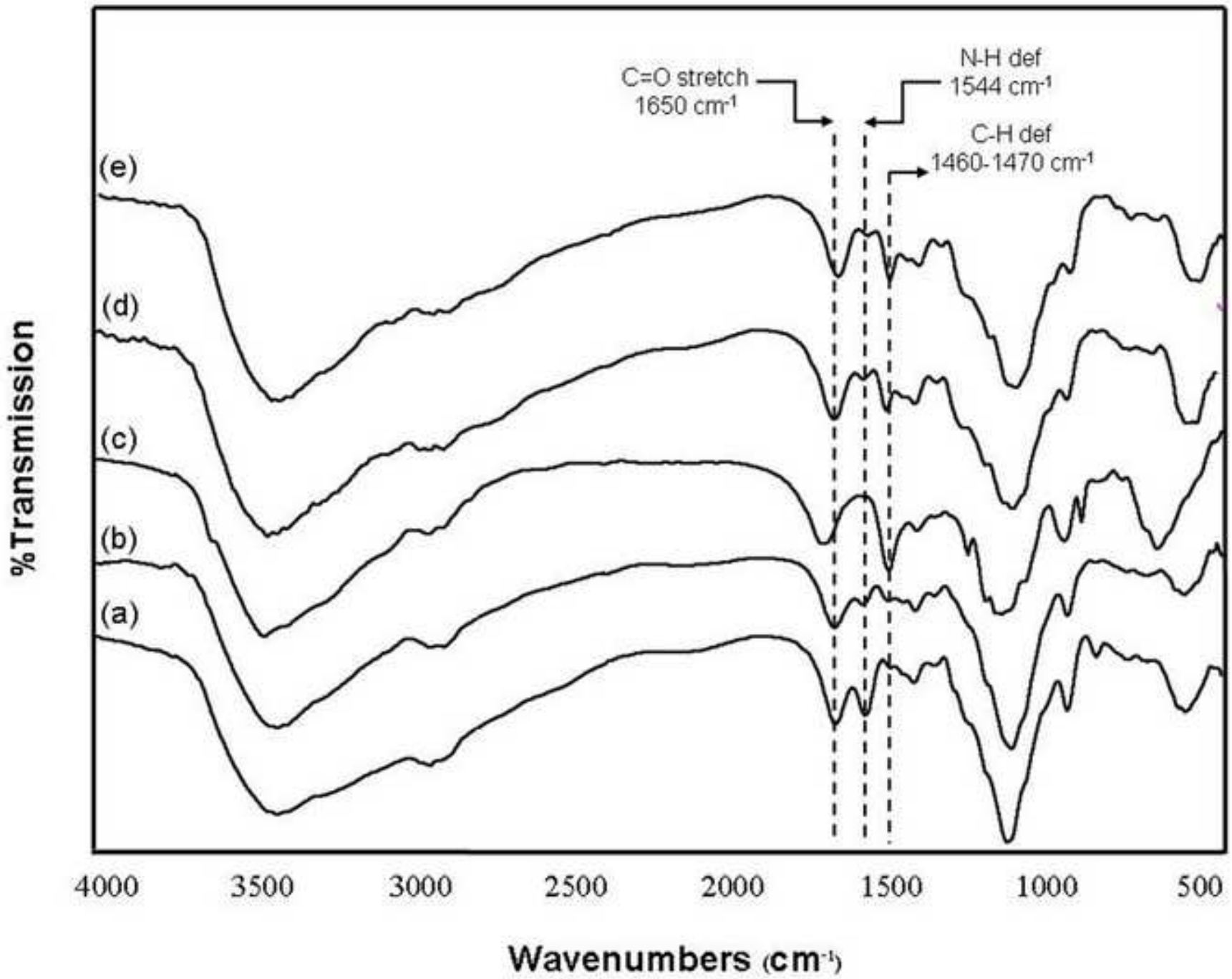

Figure(s)

Click here to download high resolution image

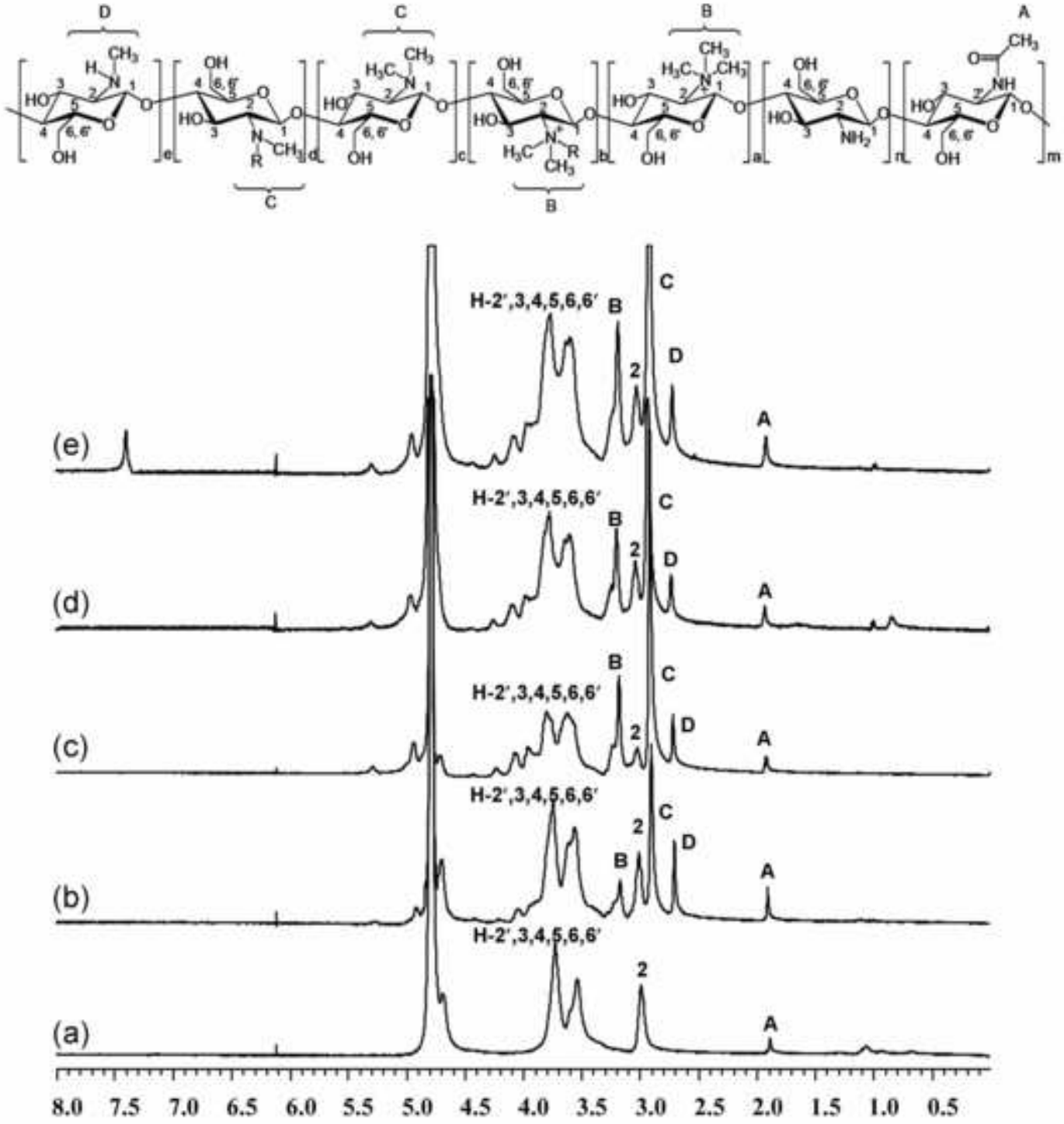

Figure(s)

Click here to download high resolution image

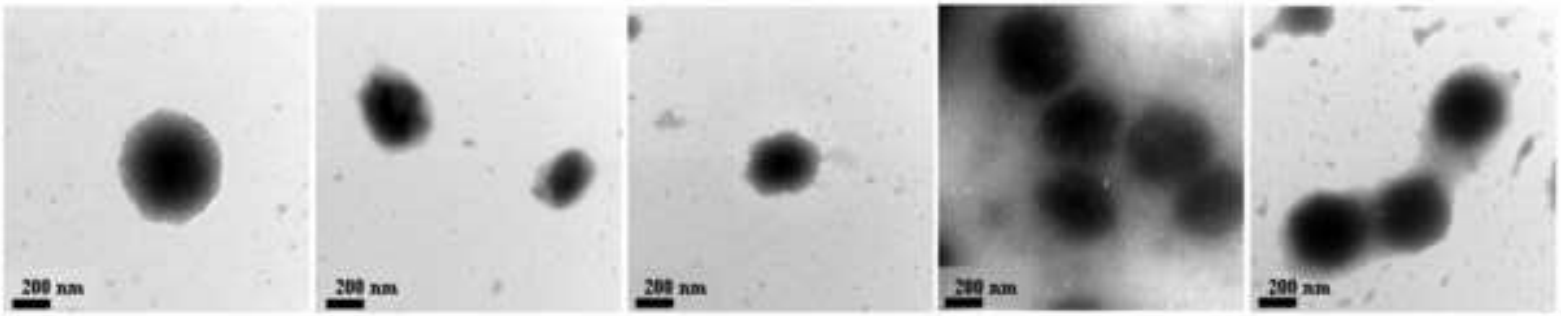

	chitosan	TMCS	QACS	QPCS	QBzCS
size (nm)	320 ± 160	290 ± 210	260 ± 90	440 ± 120	490 ± 210
ζ-potential (mV)	+27.1	+23.2	+29.3	+45.9	+46.8

Figure(s)

Click here to download high resolution image

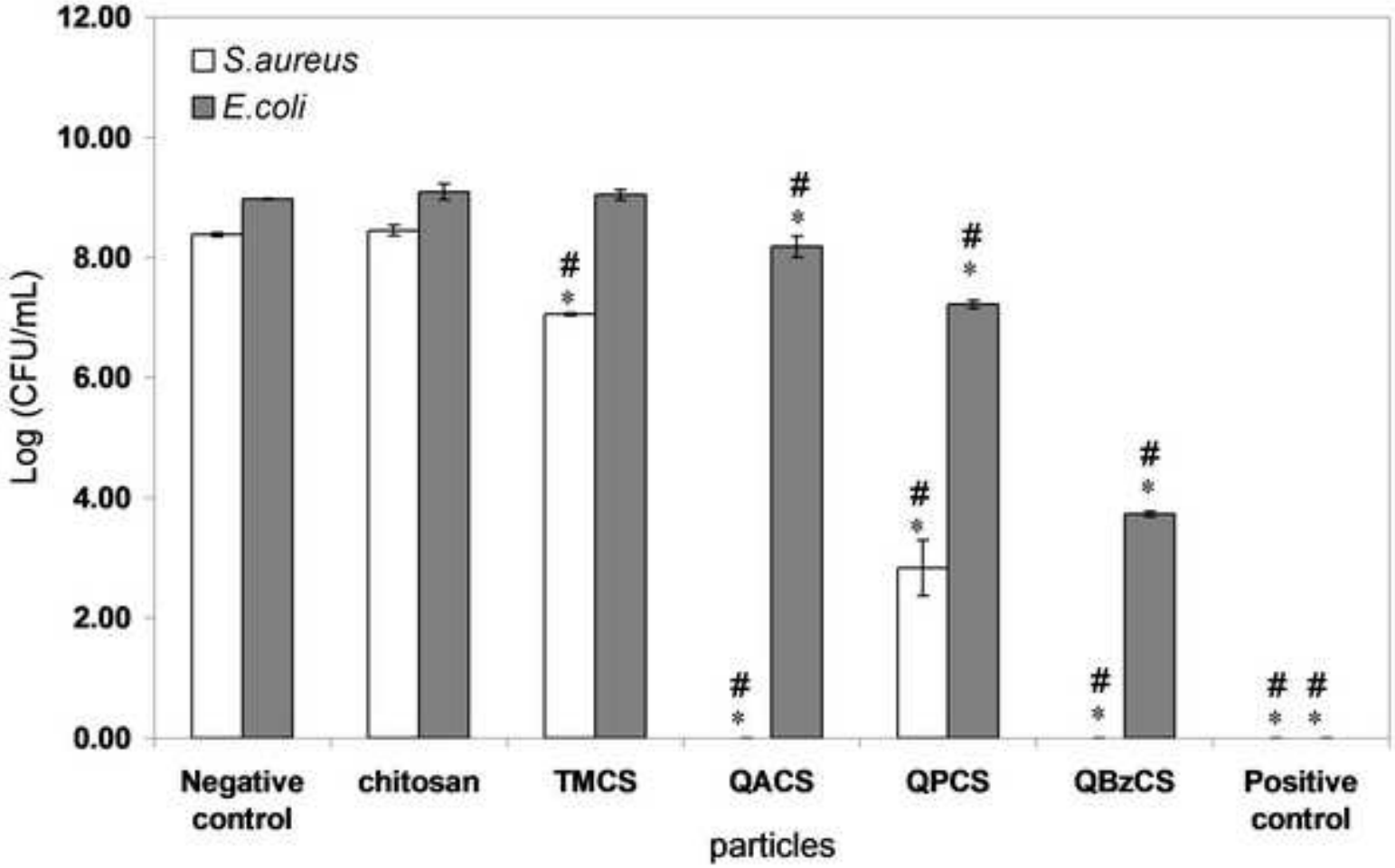

	% Antibacterial ratio						
S. aureus	0.0	ND	95.3	100.0	99.9	100.0	100.0
E. coli	0.0	ND	ND	82.9	98.2	99.9	100.0

ND (Not Detected)

Table(s)

Table 1. MIC values of chitosan and quaternized chitosan particles prepared in this work against *S. aureus* and *E. coli* in comparison with those of chitosan particles and quaternized chitosan both in the form of solution and particles as reported in the literatures

Materials	MIC (μg/mL)	
	S. aureus	*E. coli*
chitosan particles; size = 320 ± 160 nm [TS]	1000	2000
chitosan particles; size = 54 nm [24]	234	117
chitosan particles; size = 250 nm [33]	2000	N/A
TMCS particles; size = 290 ± 210 nm [TS]	250	125
QACS particles; size = 260 ± 90 nm [TS]	62.5	62.5
TMC particles; size = 215 nm [33]	500	N/A
TMC solution; 55±5%DQ [33]	250	N/A
TMC solution; MW = 120 kDa, 64%DQ [34]	125	250
TMC solution; MW = 200 kDa, 28%DQ [34]	500	1000
QPCS particles; size = 440 ± 120 nm [TS]	125	250
QBzCS particles; size = 490 ± 210 nm [TS]	125	125

[TS] = this study; N/A = not available

Supplementary Material

Click here to download Supplementary Material: Wiarachai_CSB_Supplementary_Final.doc

Polymer International

Improvement of tensile modulus and tear strength of natural rubber dipped films by vinylated silica generated in situ

Journal:	*Polymer International*
Manuscript ID:	PI-11-0382
Wiley - Manuscript type:	Original Article
Date Submitted by the Author:	06-Jun-2011
Complete List of Authors:	Rachanark, Navagan; Chulalongkorn University, Program of Petrochemistry and Polymer Science Tangpasuthadol, Varawut; Chulalongkorn University, Chemistry Kiatkamjornwong, Suda; Chulalongkorn University, Department of Imaging and Printing Technology
Key Words:	composite, silica, sol-gel process, natural rubber

For Review

SCHOLARONE™
Manuscripts

submitted to 'Polymer International'

Improvement of tensile modulus and tear strength of natural rubber dipped films by vinylated silica generated in situ

Navagan Rachanark, Varawut Tangpasuthadol*, Suda Kiatkamjornwong

Vinylated silicas were generated in natural rubber latex. The silica-rubber vulcanizates showed high tensile modulus and tear strength, possibly due to vinyl group participation in the sulfur curing of rubber.

For Peer Review

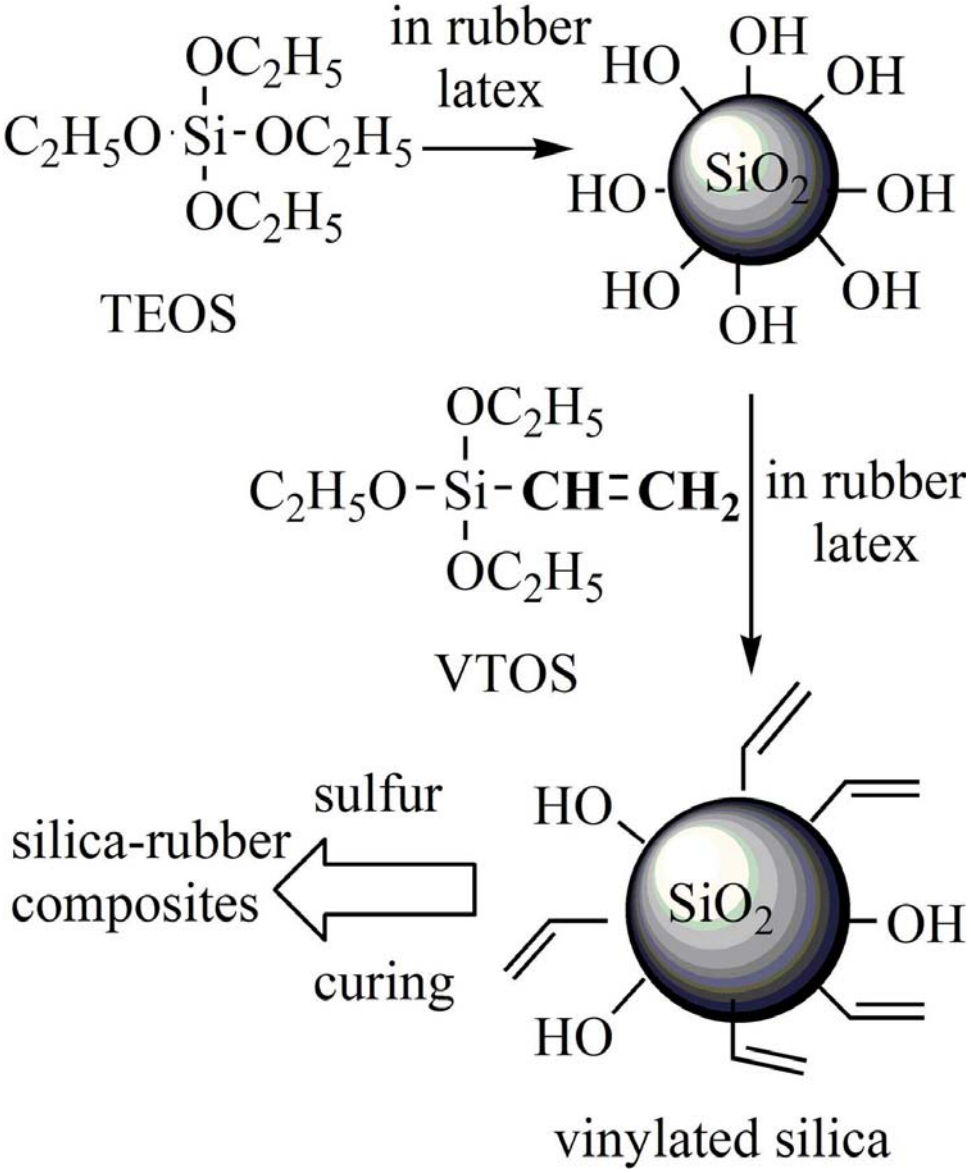

59x71mm (600 x 600 DPI)

submitted to 'Polymer International'

Improvement of tensile modulus and tear strength of natural rubber dipped films by vinylated silica generated in situ

Navagan Rachanark[1], Varawut Tangpasuthadol[2,*], Suda Kiatkamjornwong[3]

[1]Program of Petrochemistry and Polymer Science, Faculty of Science, Chulalongkorn University, Bangkok, Thailand 10330

[2]Organic Synthesis Research Unit, Department of Chemistry, Faculty of Science, Chulalongkorn University, Bangkok, Thailand 10330

[3]Department of Imaging and Printing Technology, Faculty of Science, Chulalongkorn University, Bangkok, Thailand 10330

*Corresponding author: Tel. 66-2218-7626, Fax. 66-2218-7598

E-mail address: varawut.t@chula.ac.th

Email: navagan@hotmail.com, suda.k@chula.ac.th

For Peer Review

Abstract

Alkylated silica particles were generated in dipped natural rubber films by sol-gel process of tetraethoxysilane (TEOS) and alkyltrialkoxysilane that were mixed with rubber latex before dipping process. Vinyltriethoxysilane (VTOS), ethyltriethoxysilane (ETOS), and methacryloxypropyltrimethoxysilane (MPS) were three alkyltrialkoxysilanes investigated as surface-treating reagents for the silica formed in the system. After heating the mixed alkaline latex at 80°C, the conversions from the silane to silica were in the range of 38-77% by mole of the total added silanes, depending on the size and polarity of the alkyl group in the silane. By TEM, the *in situ* silica particles were observed around rubber particles in the latex. Among the three

silanes, only the addition of VTOS in the TEOS-mixed latex led to significantly increases of tensile modulus and tear strength of the vulcanized films as compared to the addition of TEOS alone, possibly due to the participation of vinyl groups in the curing process.

Keywords: composite; silica; sol-gel process; natural rubber

For Peer Review

Introduction

Natural rubber (NR) latex is used to produce thin film products such as gloves and condoms, which require high elongation and excellent resilience. Nevertheless, NR has some weak characteristics, such as low tensile strength and modulus. A conventional technique to reinforce NR products is to physically mix fine silica powder with solid rubber or to mix aqueous slurry of silica with NR latex.[1] However, in the mixing process, silica particles tend to aggregate and agglomerate due to intermolecular hydrogen bonding between the hydroxyl groups on the silica surface. This often results in poor particle dispersion in the rubber matrix and high viscosity during mixing.[2] Silica can also adsorb or react with curing agents and accelerators on its surface which results in the reduction of curing efficiency.[3]

A method for overcome these problem is to generate silica particles right in the NR matrix. *In situ* silica formation is achieved by the sol–gel process of a silica precursor, such as tetraethoxysilane (TEOS), within the rubber matrix. There have been many reports on the *in situ* silica formation methods in solid rubber sheet,[3,4] rubber solution,[5,6] and rubber latex.[7-10] However, the use of TEOS alone as the silica precursor results in silica with polar hydroxyl groups on its surface. These polar groups potentially cause incompatibility between silica and rubber. One way to reduce the number of hydroxyl groups on the silica surface was to utilize alkyltrialkoxysilane to form 'alkylated' silica. The alkyltrialkoxysilane is a compound that carries three alkoxy groups and an alkyl substituent. The three alkoxy arms are required for bonding with silica, while the alkyl substituent is designated for *bonding* or *interacting* with the rubber matrix. They were regularly used under the name 'coupling agent' in rubber processing industry to chemically modify silica powder, in order to improve the filler

For Peer Review

dispersion and prevent adsorption of curing agents on the silica surface. Some functional groups such as alkyl, phenyl, amine, and vinyl groups can be introduced by selecting the right choice of alkyltrialkoxysilanes.[11,12]

The mixing of TEOS and alkyltrialkoxysilanes in NR latex for the preparation of *in situ* silica reinforced rubber vulcanizates were reported recently. The composite containing *in situ* silica had higher tensile modulus and tear strength than the composite prepared by conventionally mixing with silica powder.[9] A combination of bis-(3-triethoxysilylpropyl)tetrasulfide (TESPT) and TEOS that was mixed with the latex was shown to improve the mechanical properties and sulfur curing rates during milling and compression process.[7] Triethoxysilanes carring either vinyl, ethyl, and iso-butyl group were reportedly used to generate silica in sulfur-cured NR sheets obtained by melt-compression process.[9] Among them, vinyltriethoxysilanes was the most promising silane that was able to enhance the tensile modulus and resistance to tear of the rubber vulcanizates.

In this work, the focus was to utilize a mixed silane system in the reinforcement of natural rubber films that were prepared by 'latex-dipping' process. TEOS was used in combination with either VTOS or methacryloxypropylmethoxysilane (MPS) to prepare *in situ* silica having carbon-carbon double bonds on the particle surface. ETOS was also used in the film preparation for the purpose of investigating the role of C=C double bond in the reinforcement capability of the resulting silica. The structures of TEOS, VTOS, ETOS, and MPS are shown in Fig. 1. It was hypothesized that the *in situ* 'vinylated' silica particles can improve the dispersibility and mechanical properties of the NR/silica dipped films.

For Peer Review

Experimental

Materials

Concentrated natural rubber latex with 60% weight content of dry rubber (DRC) incorporated 0.7% NH_3 was purchased from the Rubber Research Institute of Thailand. Liquid dispersion of vulcanizing agents was donated from Polymer Innovation Co., Ltd., Nonthaburi, Thailand. Tetraethoxysilane (TEOS, >98%), vinyltriethoxysilane (VTOS, >98%), ethyltriethoxysilane (ETOS, >97%), methacryloxypropyltrimethoxysilane (MPS, >98%) were purchased from Aldrich, Germany.

Preparation of pre-vulcanized NR latex

The concentrated NR latex was diluted with 0.7% v/v ammonia solution to obtain 30% DRC latex. It was then mixed with the dispersion of vulcanizing agents formulated as shown in Table 1. Then a predetermined amount of TEOS was added to the latex compound with stirring. After maturated at room temperature for 24 hr, a predetermined amount of VTOS, ETOS, or MPS was mixed with the latex mixture as listed in Table 2. The homogeneous milky mixture of silane-latex was maturated for an additional 24 hr before it was used in the dipping process. During the maturation period, the reaction of silane slowly took place in the presence of water and base in the latex. The total amount of alkoxysilanes added into the latex was limited to 30 phr, because the latex tended to be unstable if a higher amount of the silanes was added.

For Peer Review

Table 1 Composition of vulcanization reagents in the form of dispersed liquid used in the latex dipping process

Ingredients	Amount (phr[a])
Natural rubber	100
Sulfur	2.5
ZMBT[b]	0.5
ZDEC[c]	1.5
ZnO[d]	2.0

[a] part per hundred part of rubber by weight, [b]zinc salt of 2-mercaptobenzothiazole, [c]zinc-diethyldithiocarbamate, [d]zinc oxide

Table 2 Variation of alkoxysilane amounts mixed into NR latex for *in situ* silica-NR composites preparation

Entry	Silane amount (phr)			
	TEOS	VTOS	ETOS	MPS
VNR	-	-	-	-
30T	30	-	-	-
25T	25	-	-	-
25T5V	25	5	-	-
20T10V	20	10	-	-
25T5E	25	-	5	-
20T10E	20	-	10	-
25T5M	25	-	-	5
20T10M	20	-	-	10

For Peer Review

Dipping process

In situ silica-NR vulcanized films were prepared by dipping glass cylinders (pre-dipped in $Ca(NO_3)_2$ solution, 40 mm in diameter) in the prepared latex-silane-vulcanizing agent mixtures. The coated former was then heated in an oven at 80°C for 24 hr to initiate the vulcanization and sol-gel process of the added silanes. On average, the film thickness obtained was 0.15 mm.

Determination of silica content in the *in situ* silica-NR dipped films

The silica content was determined by cutting the NR/silica dipped films into small pieces (~50 mg). After an exact weight was determined, the sample was heated at 850°C for 15 min in an oven. The weight of the remaining ash was calculated for the silica content in the composite by equations 1 and the conversion of the alkyltrialkoxysilane to silica was calculated using equation 2,

$$\text{Silica Content (phr)} = 100\ (W_1/W_2) \quad (1)$$

$$\text{Conversion (\%)} = 100\ (W_3/W_4) \quad (2)$$

where, W_1 is the weight of silica in the sample, W_2 is the weight of the organic rubber, W_3 is the obtained amount of the *in situ* generated silica in the sample, and W_4 is the theoretical amount of silica generated from the added amount of alkoxysilane in the latex. The calculation of W_4 was based on the chemical equation shown in Fig. 2 by assuming a quantitative conversion of TEOS and alkyltriethoxysilane to silica and alkylated silica, respectively. The results reported were averaged from three specimens.

Microscopic Analysis

For Peer Review

A scanning electron microscope (JOEL JSM-6480LV SEM) was used to analyze silica distribution in the NR matrix at 15 keV. The analysis was performed on the fractured surface of silica-NR dipped films prepared by breaking the film specimens while it was immersed in liquid nitrogen. Energy dispersive X-ray spectrometric (EDX) detector was carried out at an elevation angle of 35° in order to determine atomic types on the analyzed surface. A transmission electron microscope (JOEL JEM-2100) was used to examine the morphology of rubber and silica particles in the latex mixed with the silane precursors. The silane-latex mixture was diluted with distilled water to obtain a DRC of 0.75%. The substrate was stained by exposure to RuO_4 vapor before TEM analysis.

Mechanical properties

Tensile properties were measured with an H10KS universal testing machine (Hounsfield, Redhill, UK), according to JIS K6251-8 at a grip length of 10 mm, and a crosshead speed of 500 mm/min. Each data point was an average value obtained from four replicates of specimens. Tear properties were measured using a Hounsfield H10KS universal testing machine, following ASTM D624-91. The die C-cut specimens were tested at a gauge length of 70 mm and a crosshead speed of 500 mm/min. The values reported for each sample were averaged from three specimens.

Tension set measurement

All dipped film samples were cut into the size of 5×60 mm. Two lines about 10 mm apart were marked at the center of the sample strip. The sample was extended until the distance between the two lines was twice that of the original length, and was held for 10 min. After that, the sample was allowed to retract for 10 min. The final distance

For Peer Review

between the two lines was then measured. All measurements were made by using a vernier caliper. The tension set was calculated using equation 3 where L_i and L_f were the initial and final distances between the two lines.

$$\text{Tension set (\%)} = ((L_f - L_i)/L_i) \times 100 \quad (3)$$

Results and Discussions

Silica content and percentage conversion of silanes to silica

Earlier, we reported a cross-condensation of TEOS and alkyltrialkoxysilanes that were mixed together in the NR latex to form 'alkylated' silicas *in situ*.[9] In this work, TEOS was first mixed into the latex in order to form the silica particles during the maturation period. Then one of the alkyltrialkoxysilanes was added so that it could condense with the pre-formed silica, resulting in silica particles with selected alkyl groups (R) on the surface (Fig. 3).

The amounts of silicas formed in the rubber matrix are listed in Table 3. The conversion of TEOS to silica in the silica-NR dipped film was the highest at 77%, resulting in 6.7 phr of silica. Although the sol-gel process of the silane took place preferably in an alkaline latex, the conversion obtained here for TEOS was somewhat lower than our previous reports of >90%.[7-9] In those reports, the concentration of NR latex was 60% DRC but in this work the latex was diluted to 30% to suit the dipping process. The diluted latex contained a large amount of water, possibly suppressing the chemical equilibrium back to silicic acid, and thus reducing the silicon dioxide network formation. At various ratios of TEOS and alkyltrialkoxysilanes (Table 3), the degree of silane-to-silica conversions in the rubber vulcanizates decreased when the relative amount of alkyltrialkoxysilane was increased. This was because each of the selected

For Peer Review

alkyltrialkoxysilanes contained only three hydrolysable siloxane arms as compared to four siloxanes in the structure of TEOS. In addition, the degree of silane-to-silica conversion was also affected by the structure and polarity of the alkyl substituent in the silanes used, i.e. TEOS-VTOS > TEOS-ETOS > TEOS-MPS. In highly polar aqueous medium, a polar and small alkyl group on the silane molecule should allow higher access of water and another silanol group (-Si-OH) at condensation site than does the non-polar and bulky substituent. In this case, the vinyl group (in VTOS) is more polarized than the ethyl (in ETOS), the mixed VTOS-TEOS silanes therefore results in a higher conversion than the ETOS-TEOS. In the case of MPS, the methacryloxypropyl group is long and bulky. It therefore partially inhibits the sol-gel process, resulting in slightly lower silica formation than does the VTOS system. This result is in fact in good agreement with our earlier finding.[9]

Table 3 Silica content and degree of conversion from alkoxysilane to silica in rubber.

Entry	Silica content (phr)	Conversion (%)
30T	6.7 ± 0.3	77 ± 3.0
25T	5.1 ± 0.1	70 ± 1.0
25T5V	5.6 ± 0.3	61 ± 3.5
20T10V	5.2 ± 0.1	52 ± 0.6
25T5E	5.0 ± 0.2	54 ± 2.2
20T10E	4.8 ± 0.2	48 ± 2.2
25T5M	5.2 ± 0.4	48 ± 3.2
20T10M	4.9 ± 0.1	38 ± 0.8

For Peer Review

Moreover it was believed that the alkoxysilane precursors could evaporate from the mixed latex during the dipping and drying steps. To overcome the loss of starting silane reagents, the silane-mixed latex was maturated (or stored) at room temperature for 1-2 days in order to allow partial sol-gel process to take place. This hypothesis was tested with results shown in Fig. 4, in which the degree of conversion was determined after one and two days of maturation. Without the maturation, the conversion of TEOS to silica in the rubber matrix was only 25% but increased dramatically to almost 80% (or about 7 phr) after one day of storage at room temperature.

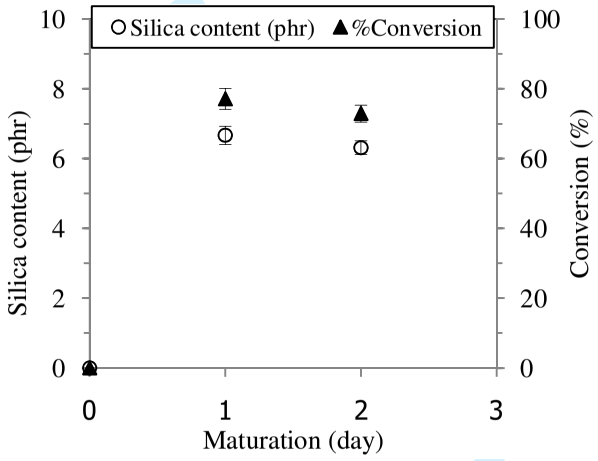

Figure 4 Changes of silica content and degree of conversion of TEOS (30 phr) mixed in the NR latex (30% DRC) as a function of latex maturation time

Morphology of *the in situ* silica and NR

The image from transmission electron microscope (TEM) was used to locate the silica particles in the rubber latex (Fig. 5). Analysis of the ruthenium-stained latex sample showed that the shape of NR particles appeared to be spherical with size ranging from 0.1-1 μm (Fig. 5a). The *in situ* generated silica were observed as dark irregular-shaped

particles, with the size of about 100 nm or less, surrounding the rubber particle in the latex compound mixed with TEOS (Fig. 5b), TEOS-VTOS (Fig. 5c), and TEOS-MPS (Fig. 5d).

The distribution of silica particles in the fractured surface of the composite films was analyzed by scanning electron microscope (SEM) (Fig. 6). The silica formed in the vulcanizate was visualized as aggregates among ZnO particles, an activator used in the vulcanization process (Fig. 6a). The identity of silicon atoms was confirmed by its characteristic peak at 1.7 keV in the EDX spectrum, while the ZnO was identified by the signal at 1.0 keV (Fig. 6b).

Comparison of the characteristic of *in situ*-formed silica generated from the mixed silanes was made as shown in Fig. 7. The silica particles of all precursor types form aggregates with sizes ranging from <1 to several μm and are dispersed throughout the rubber matrix. The particles obtained appear to be quite similar in terms of size and shapes, regardless of its precursor type.

Mechanical properties

In order to investigate the effect of alkyltrialkoxysilane types on the tensile properties of the *in situ* silica-NR dipped films, four rubber samples filled with approximately equal amounts of *in situ* generated silica (5.0 ± 0.4 phr) were prepared and named as 25T, 20T10V, 20T10E, and 20T10M. Their analyses for modulus value at 300% & 500% elongation and tensile strength at break were performed in comparison with the silica-free vulcanized film (VNR) as shown in Fig. 8. The modulus at 500% elongation of the 20T10V was significantly higher than the others. The use of mixed TEOS-ETOS and TEOS-MPS were slightly less effective in reinforcing the rubber film than using TEOS-

For Peer Review

VTOS or only TEOS. It seemed that MPS, also containing the vinyl group, was not as efficient as a reinforced precursor as VTOS for the dipped system.

The elongations at break of these selected vulcanizates, with or without the *in situ* silica, were between 630-690% (Fig. 9). No relation between the ultimate elongation and the type of silane precursor was observed. Tear testing of all NR/silica composites was performed on cast rubber sheets (~0.6 mm thick) that were prepared from the same latex compound as used for the dipping process. From the results shown in Fig. 10, only two samples, 20T10V and 20T10E, had significantly higher tear strength than did the VNR. The highest tear strength belonged to 20T10V.

From the tensile and tear test results of the *in situ* silica-NR vulcanizates, the vinyl group in VTOS that was mixed with TEOS in the ratio of 1:2 (VTOS:TEOS) plays an important role in the mechanical properties of the rubber films. The vinyl group on the *in situ* generated vinylated silica can most likely take part in the sulfur vulcanization process. In other words, the sulfur crosslinking takes place not only among the isoprene units of NR chains but possibly also with the vinylated silica particles. Unfortunately using a spectroscopic method such as IR to detect the disappearance of vinyl group after sulfur cure step would be inconclusive, since the NR matrix also contains a large number of double bonds. Nevertheless this type of participation was reported in other works, such as the preparation of wood fiber/PE and PP composites, in which the vinyl group was reportedly bonded with polyolefin backbone via radical grafting while the ethoxy silyl group on the other end of VTOS reacted with the hydroxyl groups of cellulose structure.[13,14]

For Peer Review

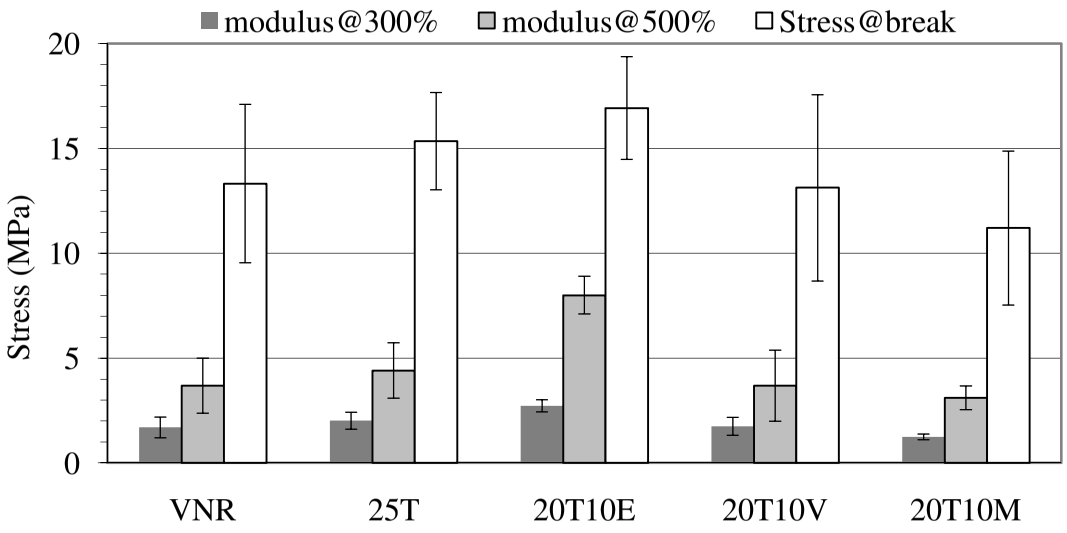

Figure 8 Modulus at 300&500% elongation and tensile strength of the dipped NR films filled with *in situ* silica generated by various types of alkoxysilane precursor, compared with silica-free dipped film (VNR).

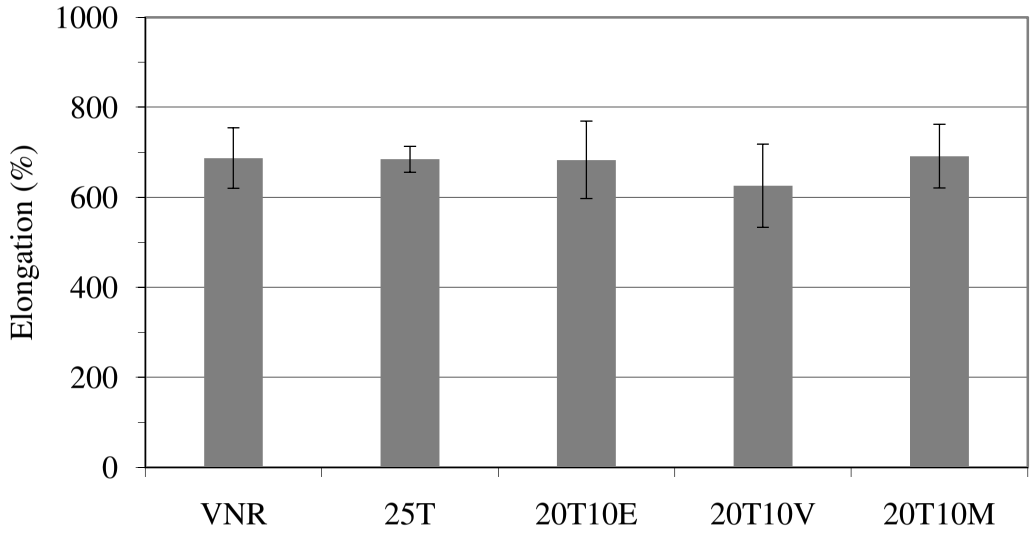

Figure 9 Elongation at break of the dipped NR films filled with *in situ* silica generated by various types of alkoxysilane precursor, compared with silica-free dipped film (VNR).

For Peer

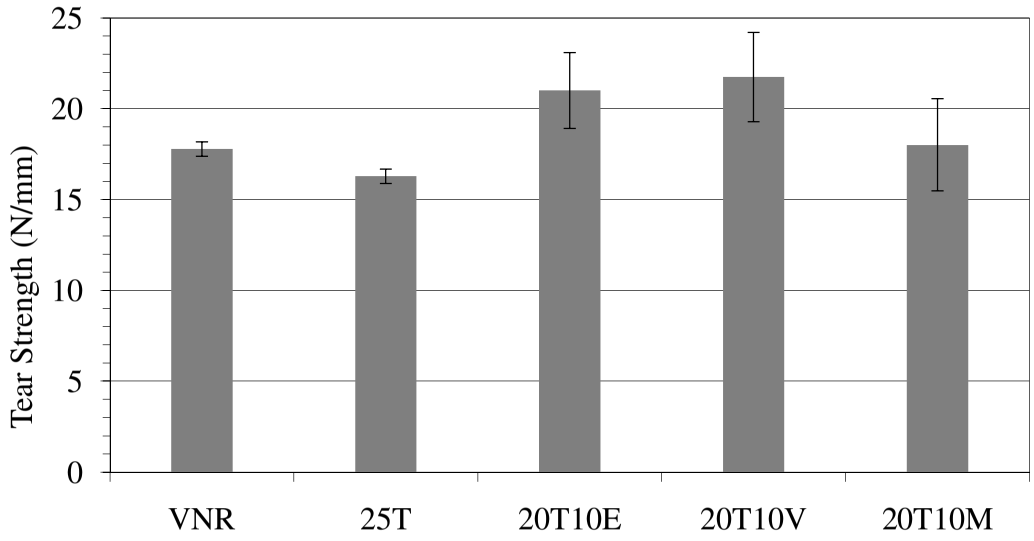

Figure 10 Tear strength of the vulcanized cast NR sheets filled with *in situ* silica generated by various types of alkoxysilane precursor, compared with silica-free sheets (VNR).

Figure 11 shows the results of tension set study. The tension set parameter, reflects the elasticity of rubber. It is the extent to which vulcanized rubber is permanently deformed after the film is stretched for a certain length and time. Here the tension set percentages of all *in situ* NR/silica dipped films were between 2.3 to 4.3%. No difference between the *in situ* silica-reinforced and non-reinforced samples was observed. The use of TEOS and other alkyltrialkoxysilanes to generate silica in the dipped film did not significantly affect to the tension set.

For Peer Review

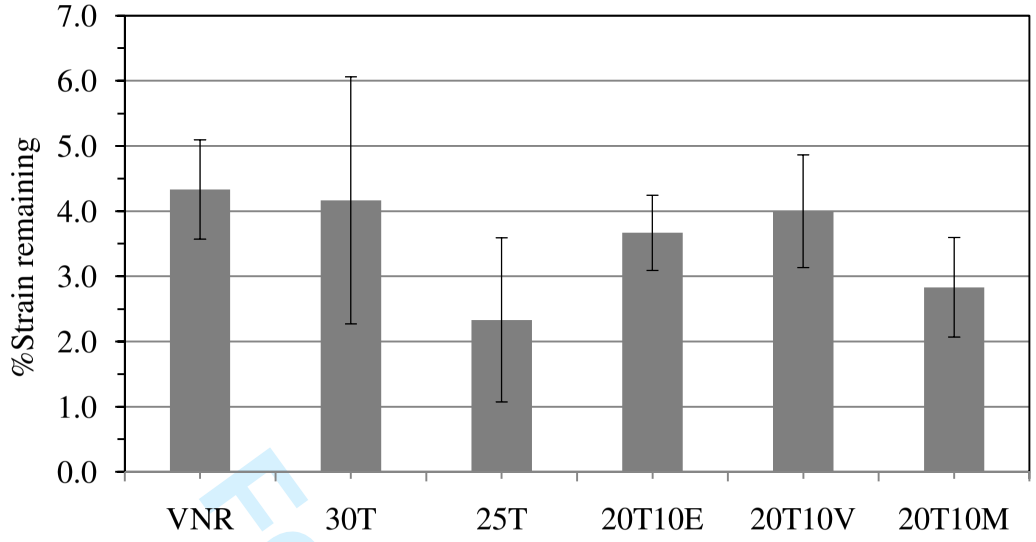

Figure 11 Result of tension set study of the dipped rubber films filled with *in situ* silica generated by various types of alkoxysilane precursor, compared with silica-free dipped rubber film (VNR).

For Peer Review

Conclusion

Silicas with different alkyl groups were successfully generated in the vulcanized dipped NR films by the use of TEOS/alkyltriethoxysilane as precursors. Maturation of the silane-latex mixture for at 2 days was required in order to obtain high degree of silane-to-silica conversion. A single heating step was used to initiate sulfur-vulcanization of the rubber films as well as silica formation in the rubber matrix. By TEM, the *in situ* silica particles were observed around the NR particle. The size of silica particle was less than 100 nm, but it did not depend on the silane types. The SEM images and EDX analysis confirmed that the *in situ* silica particles were fairly dispersed inside the rubber matrix. The use of vinyl containing alkoxysilane to treat the surface of *in situ*-formed silica resulted in the vulcanizate that possessed higher tensile modulus than the other silanes. Based on the mechanical testing results, we believed that the unsaturation

nature of the C=C double bond on the *in situ* formed silica could involve in the sulfur vulcanization process of the NR.

Acknowledgement

The research funding provided by Research Team Assistance Grant under Contract Number RTA5080004 from the Thailand Research Fund was highly acknowledged. Many thanks also go to Chemical Innovation Co., Ltd., Thailand, for mechanical testing facilities.

For Peer Review

REFERENCES

1. Mathew S, Varghese S, Rajammal G and Thomas PC, *J Appl Polym Sci* **104**: 58-65 (2007).
2. Castellano M, Conzatti L, Codta G, Falqui L, Turturro A, Valenti B and Negroni F, *Polymer* **46**: 695-703 (2005).
3. Kohjiya S and Ikeda Y, *Rubber Chem Technol* **73**: 534-550 (2000).
4. Ikeda Y, Poompradub S, Morita Y and Kohjiya S, *J Sol-Gel Sci Technol* **45**: 299-306 (2008).
5. Poompradub S, Chaichua B, Kanchanaamporn C, Boosalee T and Prasassarakich P, *Kgk-Kaut Gummi Kunst* **61**: 152-155 (2008).
6. Chaichua B, Prasassarakich P and Poompradub S, *J Sol-Gel Sci Technol* **52**: 219-227 (2009).
7. Tangpasuthadol V, Intasiri A, Nantivanich D, Niyompanich N and Kiatkamjornwong S, *J Appl Polym Sci* **109**: 424-433 (2008).
8. Satraphan P, Intasiri A, Tangpasuthadol V and Kiatkamjornwong S, *Polym Adv Technol* **20**: 473-486 (2009).
9. Siramanont J, Tangpasuthadol V, Intasiri A, Na-Ranong N and Kiatkamjornwong S, *Polym Eng Sci* **49**: 1099-1106 (2009).
10. Watcharakul N, Poompradub S and Prasassarakich P, *J Sol-Gel Sci Technol* **58**: 407-418 (2011).
11. Hsiue GH, Chen JK and Liu YL, *J Appl Polym Sci* **76**: 1609-1618 (2000).
12. Chen G, Zhou S, Gu G, Yang H and Wu L, *J Colloid Interface Sci* **281**: 339-350 (2005).

For Peer Review

13. Bengtsson M and Oksman K, *Compos Sci Technol* **66**: 2177-2186 (2006).

14. Xie Y, Hill CAS, Xiao Z, Militz H and Mai C, *Composites Part A* **41**: 806-819 (2010).

For Peer Review

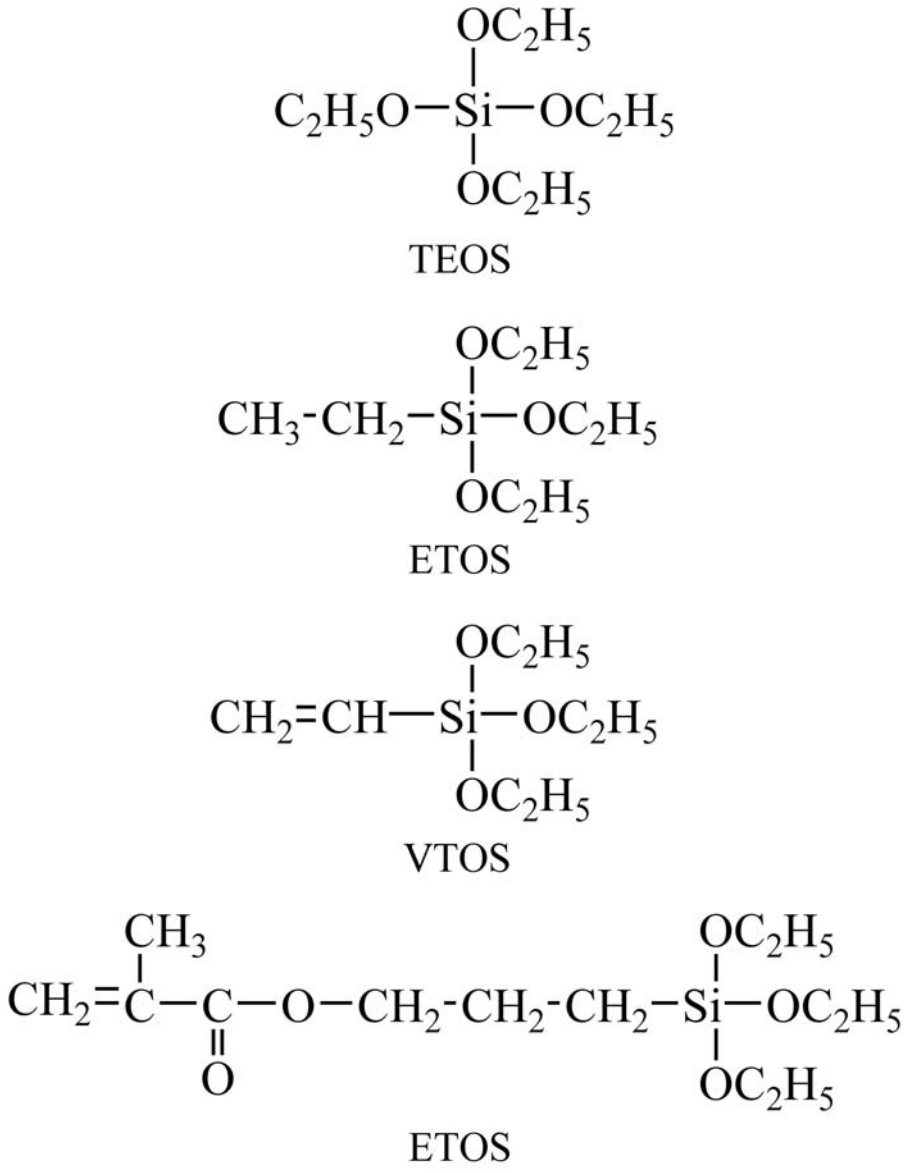

Figure 1 Structures of tetraethoxysilane (TEOS), ethyltriethoxysilane (ETOS), vinyltriethoxysilane (VTOS), and methacryloxypropyltrimethoxysilane (MPS).
118x154mm (600 x 600 DPI)

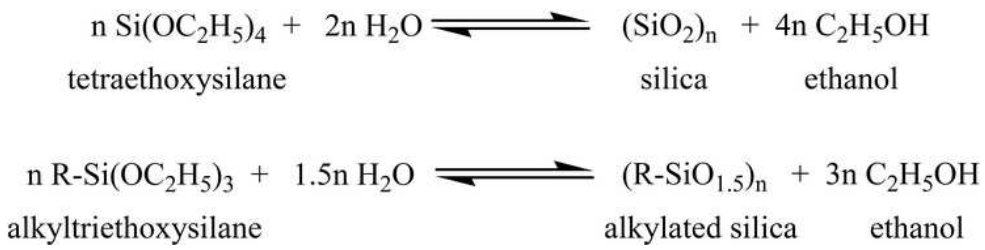

Figure 2 Chemical equations of the conversion of TEOS to silica (top) and alkyltriethoxysilane to alkylated silica (bottom).
31x7mm (600 x 600 DPI)

For Peer Review

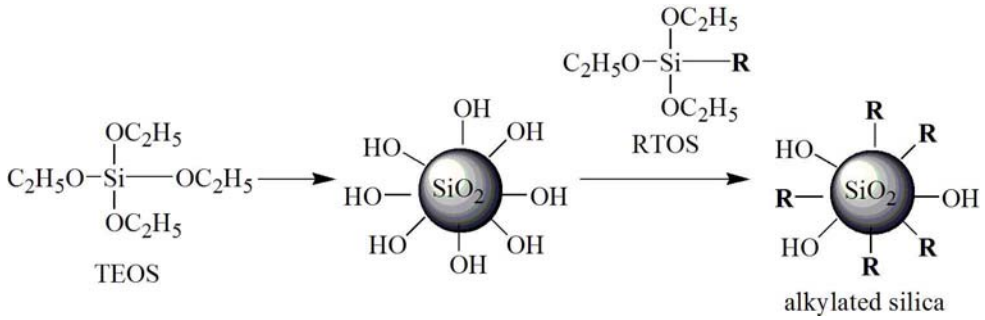

Figure 3 Cross-condensation of alkyltrialkoxysilane (RTOS) and a silica particle from tetraethoxysilane (TEOS) precursor.
128x41mm (300 x 300 DPI)

For Peer Review

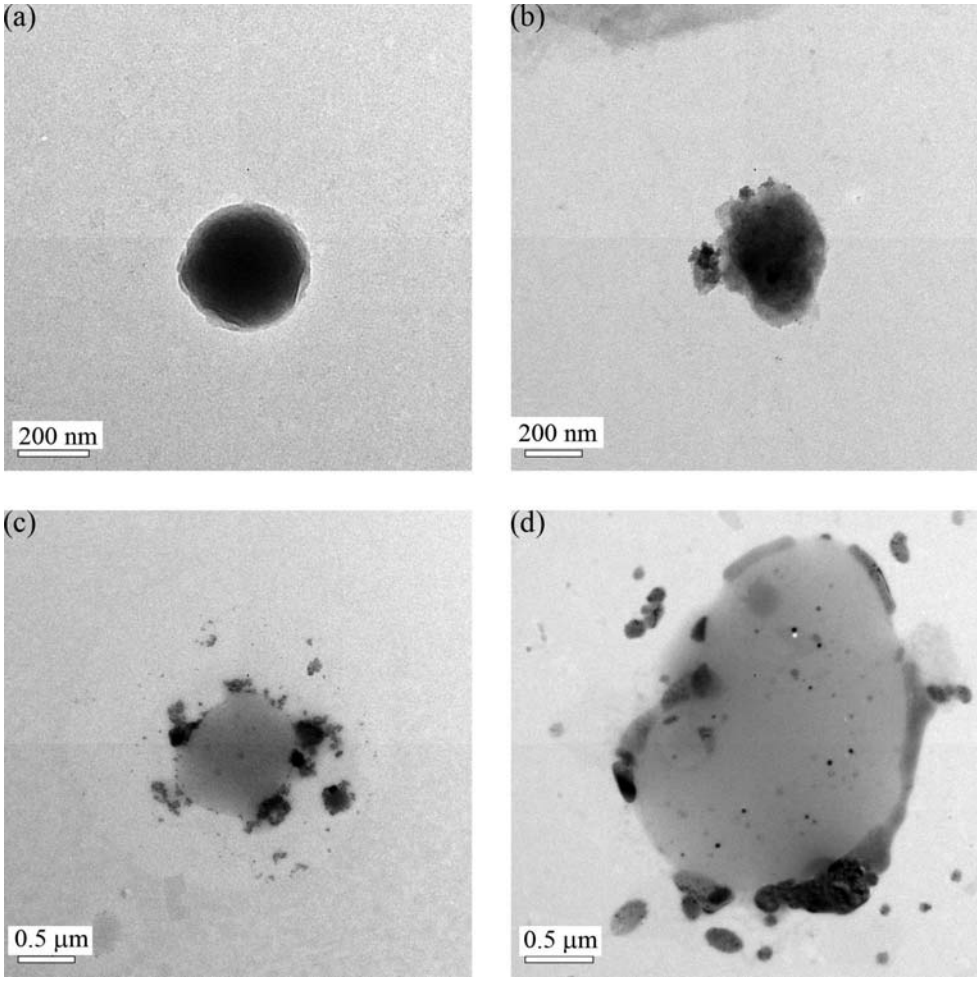

Figure 5 The TEM image of NR particle in (a)non-modified latex in comparison the images obtained from the latex that was mixed with (b)TEOS, (c)TEOS-VTOS, and (d) TEOS-MPS. The in situ-formed silica particles were seen as the dark spots surrounding the rubber core.
158x158mm (300 x 300 DPI)

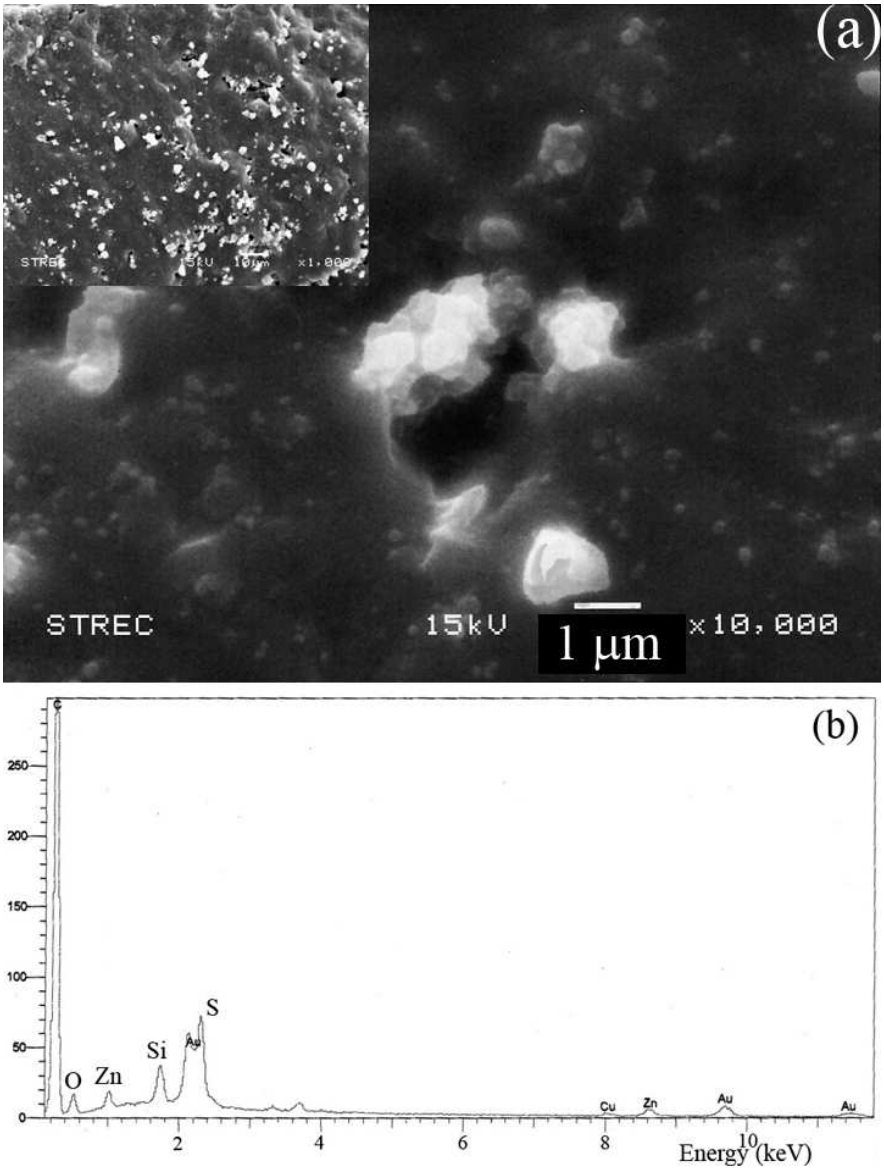

Figure 6 (a)The inset figure (1,000×) shows the distribution of in situ-formed silica obtained from the fractured surface of silica-NR vulcanizates (sample: 30T; 6.7 phr silica). The main image (10,000×) shows close-up detail of the silica aggregates. (b)The EDX spectrum of the shown area in the main image displays a series of elements, including Zn and Si.
60x81mm (300 x 300 DPI)

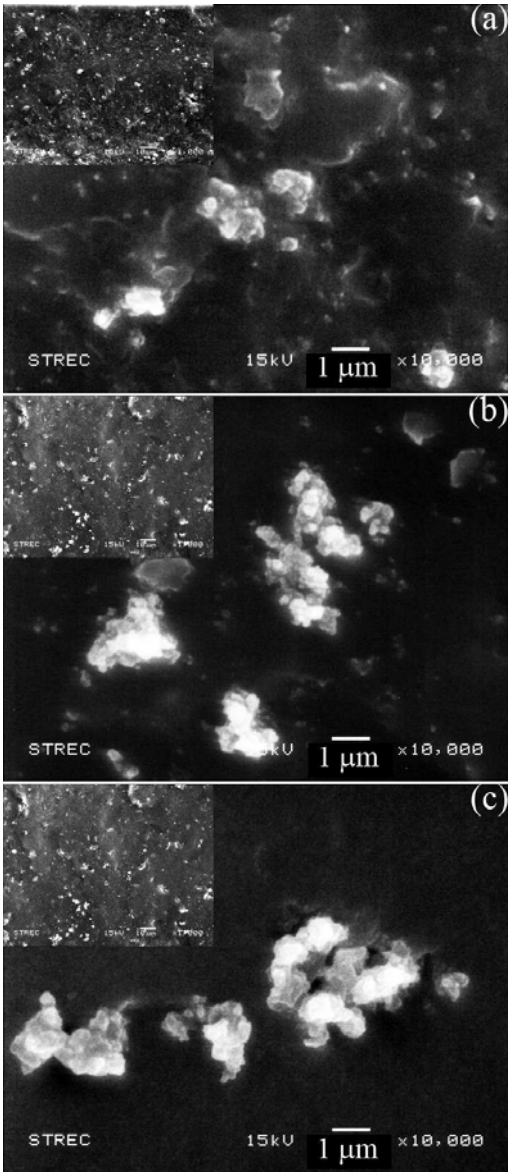

Figure 7 The SEM images show the distribution of in situ-formed silica (inset; 1,000×) and detailed silica aggregates (main; 10,000×) obtained from the fractured surface of silica-NR vulcanized films of (a)20T10V (silica: 5.2 phr), (b)20T10E (silica: 4.8 phr), and (c)20T10M (silica: 4.9 phr).
60x140mm (300 x 300 DPI)

Draft

Multilayer Film Assembled from Charged Derivatives of Chitosan: Physical Characteristics and Biological Responses

Wilaiporn Graisuwan[1,2], Cheeraporn Ananthanawat[3], Oraphan Wiarachai[1,2], Songchan Puthong[4], Suphan Soogarun[5], Suda Kiatkamjornwong[6], Voravee P. Hoven[7]*

[1] Program in Petrochemistry and Polymer Science, Faculty of Science, Chulalongkorn University, Phayathai Road, Pathumwan, Bangkok 10330, Thailand

[2] Center for Petroleum, Petrochemicals, and Advanced Materials, Chulalongkorn University, Phayathai Road, Pathumwan, Bangkok 10330, Thailand

[3] Program in Macromolecular Science, Faculty of Science, Chulalongkorn University, Phayathai Road, Pathumwan, Bangkok 10330, Thailand

[4] The Institute of Biotechnology and Genetic Engineering, Chulalongkorn University, Phayathai Road, Pathumwan, Bangkok 10330, Thailand

[5] Department of Clinical Microscopy, Faculty of Allied Health Sciences, Chulalongkorn University, Phayathai Road, Pathumwan, Bangkok 10330, Thailand

[6] Department of Imaging and Printing Technology, Faculty of Science, Chulalongkorn University, Phayathai Road, Pathumwan, Bangkok 10330, Thailand

[7] Organic Synthesis Research Unit, Department of Chemistry, Faculty of Science, Chulalongkorn University, Phayathai Road, Pathumwan, Bangkok 10330, Thailand

RECEIVED DATE (to be automatically inserted after your manuscript is accepted if required according to the journal that you are submitting your paper to)

TITLE RUNNING HEAD. Multilayer film of charged chitosan

*To whom correspondence should be addressed. Tel: +66-2218-7627 ext 102. Fax: +66-2218-7598. E-mail: vipavee.p@chula.ac.th

ABSTRACT. Polyelectrolyte multilayer films were assembled from charged derivatives of chitosan: *N*-[(2-hydroxyl-3-trimethylammonium)propyl]chitosan chloride (HTACC), *N*-succinyl chitosan (SCC), and *N*-sulfofurfuryl chitosan (SFC) and selected oppositely charged polyelectrolytes which are poly(acrylic acid) (PAA) and poly(allylamine hydrochloride) (PAH) successfully deposited on the surface-treated poly(ethylene terephthalate) (treated PET) substrates by alternate layer-by-layer adsorption. The assembly process was monitored by quartz crystal microbalance with dissipation (QCM-D). Stratification of the multilayer films was demonstrated by water contact angle data. The coverage of the assembled films was characterized by AFM. Biological responses of the assembled films were assessed in terms of *in vitro* cell adhesion and proliferation of fibroblasts, antibacterial activity, and protein adsorption. The *in vitro* cells study showed slightly alternating trend depending on the outermost layer. The multilayer film containing HTACC exhibited greater antibacterial activity against *E. coli* and *S. aureus* than the treated PET substrate and the control. The blood compatibility study suggested that (PAH/SFC) can reduce protein adsorption.

KEYWORDS. Charged derivative, Chitosan, Muitlayer film, Layer-by-layer, Cytocompatibility, Antibacterial activity, Antithrombogenicity

Introduction

The layer-by-layer (LBL) assembly technique,[1] typically based on the alternating adsorption of oppositely charged polyelectrolytes, has been widely employed for the modification of biomaterial surfaces in order to render them bioactive, adhesive or non-adhesive for cells or specific microorganisms so that they can be used for biomedical applications. This versatile strategy, involving building up of thin multilayer film, is mostly driven by electrostatic interactions between a charged polyelectrolyte and an oppositely charged surface. The first adsorbed layer of polyelectrolyte from aqueous solution leads to the surface charge reversal and enables second adsorption of an oppositely charged polyelectrolyte. The process is simple and can be adapted for any type of substrate as long as the surface charge is present without the limitation of substrate topology. In principle, the thickness of the multilayer film can be varied as a function of adsorption variables as well as the number of deposition. Most importantly, the surface properties of the supported films are determined by the outermost layer that is last deposited.

Chitosan is considered as one of the most attractive natural polyelectrolyte often used for generating biocompatible surfaces via multilayer assembly. It is the partially deacetylated form of chitin, the second-most abundant natural polymer, mainly harvested from the exoskeleton of insects, marine crustaceans and fungal cell walls. Its favorable physico-chemical and biological characteristics such as biocompatible,[2] biodegradable,[3,4] non-toxic,[5] and antibacterial activity[6] makes chitosan suitable for many bio-related applications. Besides, charged derivatives of chitosan exhibit diversified bioactivities. Quaternary ammonium chitosan, a positively charged derivative possesses superior antimicrobial activity[7,8]. Succinyl chitosan, a negatively charged derivative, has favorable properties such as low toxicity and long-term retention in the body so it

was applied as a drug carrier.[9] Sulfonated chitosan, another negatively charged derivative, on the other hand, is antithrombogenic.[10-12]

Several researches have been reported on the formation of polyion complex multilayer films between chitosan and a number of anionic polyelectrolytes. Serizawa, *et al.*[13,14] have revealed the alternating anti-vs procoagulation activity of ultrathin polymer films prepared from dextran sulfate and chitosan by the layer-by-layer assembly technique against human blood. Zhu, *et al.*[15] assembled the multilayer films of poly(styrene sulfonate, sodium salt) (PSS) and chitosan to improve cytocompatibility of the poly(L-lactic acid) surface. Cai, *et al.*[16] constructed a multilayer film using chitosan and gelatin on titanium in order to improve their biocompatibility. Fu, *et al.*[17] generated multilayer films from heparin (anti-adhesive agent) and chitosan (antibacterial agent) on aminolyzed PET films. It was found that the multilayer films not only reduced the bacterial adhesion but also kill the bacteria adhered onto the surface. This desirable feature renders the multilayer film a powerful anti-infection coating for cardiovascular devices. Liu, *et al.*[18] modified a surface of poly(ethylene terephthalate) (PET) by hydrolysis and built up multilayer films by alternative adsorption of chitosan and chondroitin sulfate. The *in vitro* cell culture revealed that the adherence of endothelial cells was enhanced on the multilayer-deposit PET film with their preserved function.

In our previous publication,[19] we have demonstrated that the multilayer films can be successfully assembled from charged derivatives of chitosan (CHI), *N*-sulfofurfuryl chitosan (SFC) and *N*-[(2-hydroxyl-3-trimethylammonium)propyl]chitosan chloride (HTACC) on the plasma-treated PET. Alternate bioactivity of the multilayer assembly of three pairs of polycation/polyanion: CHI/poly(styrene sulfonate sodium salt) (CHI/PSS), poly(allylamine hydrochloride)/SFC (PAH/SFC), and HTACC/poly(acrylic acid) (HTACC/PAA) were realized

by testing against four proteins having different size and charge characteristic which are albumin, fibrinogen, γ-globulin, and lysozyme.

In the present study, we explore further on the insight into the physical characteristics of the multilayer films assembled from those charged derivatives that have been reported earlier (SFC and HTACC) as well as an additional negatively charged derivative, *N*-succinyl chitosan (SCC). For the first time, the internal structure, water content, and viscoelastic properties of the multilayer films were assessed by quartz crystal microbalance with dissipation mode (QCM-D). Three pairs of oppositely charged polyelectrolytes were investigated: HTACC/PAA, PAH/SCC, and PAH/SFC (Figure 1). Biological responses of selected multilayer systems were tested against fibroblast cells, bacteria, plasma proteins, and platelets. The consequence of this study should provide fundamental information that should be very useful for further development of these charged derivatives of chitosan for biomedical applications.

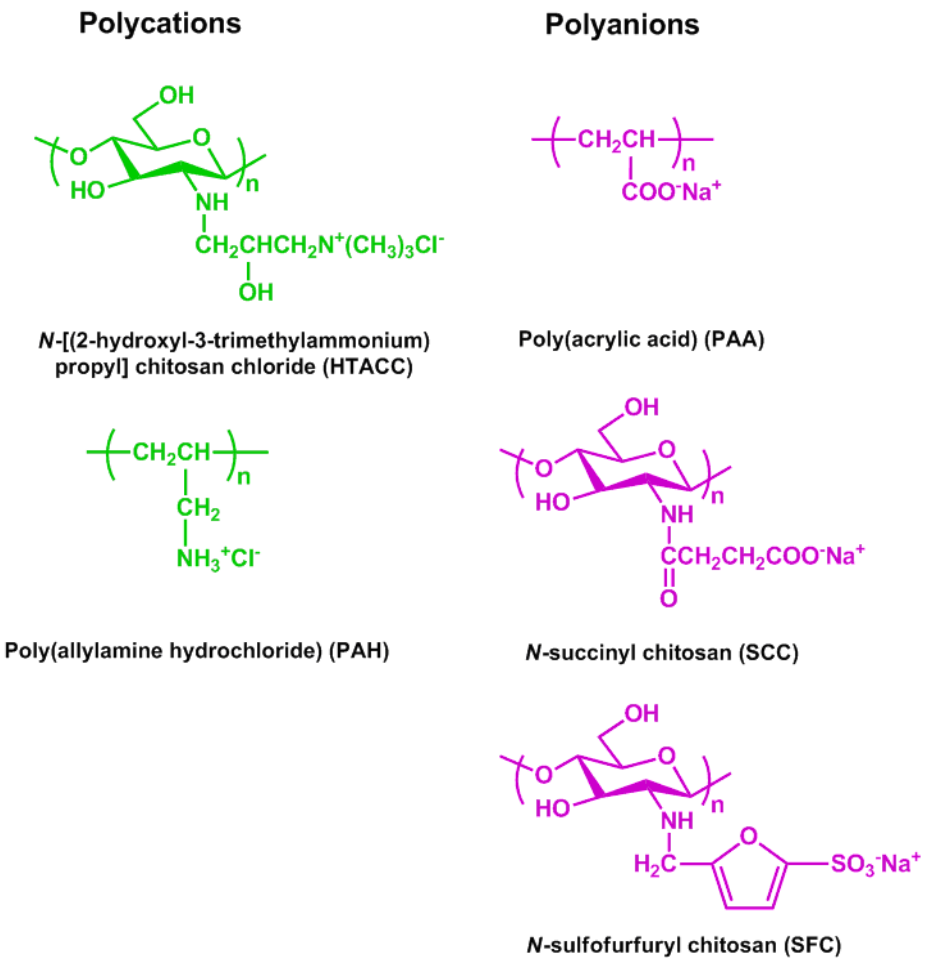

Figure 1. Polycations and polyanions used for multilayer assembly.

Experimental Section

Materials. Chitosan flakes (DAC of 95%, M_w = 100,000 g·mol^{-1}) were obtained from Seafresh Chitosan (Lab) Co., Ltd. (Thailand). Succinic anhydride (SA) was purchased from May&Baker (England). 5-Formyl-2-furan-sulfonic acid, sodium salt (FFSA), poly(allylamine hydrochloride) (PAH), M_w = 70,000 g·mol^{-1}, phosphate buffered saline (PBS), glycine, and a bicinchoninic acid assay kit (QuantiPro^{TM} BCA assay) were supplied by Sigma-Aldrich (USA). Heparin (HEP), M_w = 4,000-6,000 g ·mol^{-1} was purchased from Fluka (USA). Triethanolamine, sodium borohydride

($NaBH_4$), glycidyltrimethylammonium chloride (GTMAC), and poly(acrylic acid) (PAA), M_w = 60,000 $g \cdot mol^{-1}$ were purchased from Fluka (Switzerland). Plasma-treated poly(ethylene terephthalate) films (i.d. = 14 mm) were supplied by Wako Pure Chemical Industry, Ltd. (Japan). Fibroblast L929 cells were purchased from American Type Culture Collection (ATCC) (USA). Fetal bovine serum (FBS) and RPMI medium 1640 were purchased from InVitromex (USA). Penicillin was purchased from General Drugs House Co.,Ltd. Streptomycin was purchased from M&H manufactureing Co.,Ltd. (Thailand). *E. coli* and *S. aureus* were provided by National Center for Genetic Engineering and Biotechnology (BIOTEC), Thailand. Mueller-Hinton agar (MHA) and Mueller-Hinton broth (MHB) were purchased from Difco (USA). Mueller Hinton agar plate was supplied by Department of Medical Science, Ministry of Public Health, Thailand. The chemicals were of analytical grade and used as received without further purification. Ultrapure distilled water (Milli-Q water) was obtained after purification using a Millipore Milli-Q system (USA) that involves reverse osmosis, ion exchange and a filtration step. *N*-[(2-hydroxyl-3-trimethylammonium)propyl] chitosan chloride (HTACC), *N*-sulfofurfuryl chitosan (SFC), and *N*-succinyl chitosan (SCC) were synthesized according to the method modified from that of Seong *et al.*[7] Amiji.[10] and Aoki *et al.*,[20] respectively. Detailed experimental procedures and chemical characteristics of all derivatives characterized by FT-IR spectrometer (Nicolet, model Impact 410, USA) and ^1H NMR spectrometer (Varian, model Mercury-400, USA) are available in Supporting Information Section.

Multilayer Assembly. Plasma-treated PET substrates were immersed in a solution of 1 M NaOH (aq) at 60°C for 1 h. After incubated for a given time, the substrates were taken out, washed with 0.1 M HCl (aq) for 10 min to rinse off NaOH. Finally, the substrates were rinsed thoroughly with Milli-Q water and air-dried at ambient temperature to obtain the surface-hydrolyzed PET films. After surface hydrolysis, the treated PET substrates were subjected to

multilayer assembly by sequentially dipping in a polycation solution (2 mg/mL of PAH, or 2 mg/mL of HTACC) and a polyanion solution (1 mg/mL of SCC, 2 mg/mL of SFC, or 2 mg/mL of PAA) for 20 min interval. The optimal concentration of each polyelectrolyte was identified by conventional QCM measurements as previously described.[19] All polyelectrolytes were not buffered. For most of the experiments, the salt concentration of 0.1 M NaCl (aq) was added in both solutions. The pH of the solution was adjusted by using 0.1 HCl (aq) or 0.1 NaOH (aq). The substrates were rinsed thoroughly with Milli-Q water between each dipping and after the final adsorption. Three pairs of polyelectrolyte self-assemblies were fabricated: at pH 7 for HTACC/PAA and PAH/SCC, and at pH 8 for PAH/SFC.

Characterization of Deposited Multilayer Film. A contact angle goniometer model 100-00 equipped with a Gilmont syringe and a 24-gauge flat-tipped needle (Ramé-Hart, Inc., USA) was used for the determination of water contact angles. A droplet of Milli-Q water was placed on the tested surface by bringing the surface into contact with a droplet suspended from a needle on the syringe. The measurements were carried out in air at ambient temperature. The reported angle is an average of 5 measurements on different areas of each sample. The structure and morphology of the multilayer films were examined by atomic force microscopy (AFM). AFM images were recorded with a Scanning Probe Microscope; model NanoScope®IV, Veeco, USA. Measurements were performed in air at ambient temperature using a tapping mode. Silicon nitride tips with a resonance frequency of 267-298 kHz and a spring constant 20-80 N/m were used.

Analysis by Quartz Crystal Microbalance. The apparatus and the quartz crystals used for QCM measurements were obtained from Maxtek, Inc. (USA). An AT-cut quartz crystal with a fundamental resonance frequency of 5 MHz, model SC-501-1 was used. The plating crystal (1

inch in diameter) was covered by evaporated gold on both faces. The frequency shift of the gold-coated QCM plate was monitored by a Maxtek plating monitor (model PM-710) coupled with an MPS-550 sensor probe. The Data-Log Software (Maxtek) was used for data acquisition and monitoring. For QCM measurements with dissipation mode (QCM-D), a Q-Sense D300 (Q-Sense, Götenborg, Sweden) fitted with a Q-sense axial flow chamber was used for real-time simultaneous measurement of frequency and dissipation changes. An AT-cut piezoelectric crystal coated with gold electrodes on its two faces having a fundamental resonance frequency of 5 MHz (Q-Sense AB, Götenborg, Sweden) was excited at its fundamental frequency (n=1) as well as at the third, fifth, and seventh overtones (n = 3, 5, and 7, respectively) corresponding to 15, 25, and 35 MHz, respectively. The gold-coated QCM plate was cleaned by soaking in piranha solution (3:1 H_2SO_4:30% H_2O_2) for 5 min, rinsing thoroughly with Milli-Q water and drying with a light stream of nitrogen gas prior to use. The surface modification of the gold-coated QCM plate was carried out by immersion in an ethanolic solution containing 1:1 (v/v) of 10 mM 11-mercaptoundecanoic acid and 10 mM 11-mercapto-1-undecanol at ambient temperature. After 24 h, the plate was rinsed with ethanol and dried with a light stream of nitrogen gas. For the QCM measurements in the conventional mode, one side of the gold-coated QCM plate was covered with a designated polyelectrolyte solution for a desired period of time, rinsed with Milli-Q water, dried with a light stream of nitrogen gas after each step of deposition and then the resonance frequency was measured in air. For the QCM-D measurements in real-time, one side of the gold-coated quartz crystal was kept in permanent contact with a designated polyelectrolyte solution and the frequency change was recorded continuously at ambient temperature.

Cell Adhesion and Proliferation Tests. The Fibroblast L929 cells were cultured in RPMI 1640 medium supplemented with 5% fetal bovine serum (FBS), penicillin (100,000 U/L) and

streptomycin (100 mg/mL). They were incubated at 37°C in atmosphere containing 5% CO_2 where the culture medium was changed every 3 days. Both the treated PET substrates with and without multilayer films were sterilized by soaking in 70% ethanol in water for 30 min and washed twice with RPMI medium 1640. The substrates were then transferred to cover the bottom of 96-well tissue culture polystyrene (TCPS) plate. Three replicated samples were used for each condition. Approximately $5x10^3$ of L929 cells in 0.2 mL culture medium were pipetted into each well containing the substrates as well as blank wells made of tissue culture polystyrene (TCPS) as a control and then incubated under 5% CO_2 at 37°C. MTT assay was used to investigate cell adhesion and proliferation. After 12 h of incubation, the culture medium was removed to discard the unattached cell and the 0.2 mL fresh culture medium was pipetted into each well followed by 10 μL of 0.5 mg/mL MTT/normal saline solution. After incubation for 4 h, the supernatant solution was removed and 150 μL of DMSO was pipetted into each well to dissolve the purple crystals of formazan. Next, 25 μL of 0.1 M glycine (pH 10.5) was added. The optical density of the solution was measured using a microplate reader (MK II, Titertek Multiskan MCC/340, Finland) at the wavelength at 540 nm.

Antibacterial Activity Test. The antibacterial activity of the multilayer film of HTACC/PAA assembled on the treated PET substrates against the Gram-positive bacteria, *S. aureus* and Gram-negative bacteria, *E. coli* was assessed by viable cell-counting method. The treated PET substrates carrying multilayer films were sterilized by exposing to UV irradiation for 1 h prior to the tests. The substrates were placed one per well of a 24-well plate containing 2 mL Mueller-Hinton broth (MHB). Then 12 μL of bacterial suspension in distilled water (OD_{600} = 0.1) was pipetted into each well and the plate incubated in a shaking incubator (Model G-25, New Brunswick Scientific Co., Inc., USA) at 37°C, 110 rpm, for 24 h. A 100 μL of each of the

bacterial suspensions was then transferred from each well and then diluted 10^4 times and 100 μL of this diluted bacterial suspension was then spread onto Mueller-Hinton agar (MHB). After incubating at 37°C for 24 h, the number of colonies, and thus replication competent bacteria were then counted as a measure of assumed viability. The results, after correction for the dilution factor, were expressed as the mean number of colony forming units per volume (CFU/mL). All tests of antibacterial activity were performed in triplicate per sample and upon at least three independent samples.

Preparation of Platelet-rich Plasma (PRP) and Platelet-poor Plasma (PPP). Human whole blood (100 mL) from a healthy volunteer was collected into a sterile plastic syringe and mixed with 3.8 %(wt/v) sodium citrate in PBS (1 mL:10 mL blood). To obtain the platelet-rich plasma (PRP) for *in vitro* static platelet adhesion testing,[21,22] the human whole blood was centrifuged at 1,200 rpm for 10 min. After centrifugation, the red blood cells and platelets were separated into 2 layers. The PRP as yellowish solution (top layer) was carefully withdrawn via micropipette. Subsequently, a portion of PRP was taken and then centrifuged at 2,000 rpm for 15 min to obtain the platelet-poor plasma (PPP) to be used for protein adsorption test.[21,22]

Determination of the Total Amount of Adsorbed Human Plasma Protein. The multilayer films of PAH/SFC and PAH/HEP assembled on the treated PET substrates were placed into 24-well tissue culture plate containing deionized water and hydrated overnight to reach an equilibrium hydration before experiment. Triplicate samples were used (n = 3). Each sample was removed from deionized water and suspended into the well containing 1.0 mL of PPP and incubated at 37°C for 3 h. After incubation, the samples were removed from PPP and followed by rinsing twice with PBS to remove any loosely attached protein. The adsorbed protein on the

sample surface was detached by soaking each sample in 1.0 mL of 1 %(wt/v) aqueous solution of sodium dodecyl sulfate (SDS) for 30 min. A 100 μL of SDS solution which socked each sample was pipetted into 96-well tissue culture plate. The solution was then mixed with 100 μL of BCA working solution in each well and followed by incubation the well-plate at 37°C for 2 h. The absorbance of the solution was measured at 562 nm by UV microplate reader (Microtiter plate reader; Model Sunrise, Tecan Austria GmbH). The amount of protein adsorbed on the samples was calculated from the protein concentration in SDS solution. The data were express as mean ±standard deviation (S.D). A protein analysis kit based on the bicinchoninic acid (BCA) method was used to determine the concentration of the protein dissolved in the SDS solution.

Evaluation of Platelet Adhesion. The multilayer films of PAH/SFC and PAH/HEP assembled on the treated PET substrates were put into the 24-well TCPS and hydrated overnight in PBS. After PBS was removed, the samples were immersed in 1 mL of freshly prepared PRP and incubated at 37°C for 1 h. After incubation, samples were gently rinsed with PBS to remove loosely adherent platelets from the surface and then treated with 2.5% glutaraldehyde in PBS to fix the platelets adhered to the surfaces for 1 h at ambient temperature. Finally, the samples were washed again with PBS and then subsequently dehydrated with gradient immersion of ethanol/water solutions (50, 60, 70, 80, 90, 95, and 100 vol.-%) for 10 min each and dried *in vacuo* overnight. The substrates were then sputter-coated with gold for the scanning electron microscope characterization (JEOL Model JSM-5410LV, Japan).

Statistical Analysis. Statistical analysis of cell adhesion/proliferation tests, antibacterial activity test, and protein adsorption are expressed as the means±standard deviations (S.D.) of a representative of three similar experiments carried out in triplicate. Statistical analysis was

performed using the Statistical Package for the Social Science (SPSS) version 14.0 software. Statistical comparisons made by One-Way Analysis of Variance (ANOVA) with the Least Square Difference (LSD) tests were used for post hoc evaluations of differences between groups. The threshold level for accepting statistical significance was set at $p < 0.05$.

Results and Discussion

Physical Characteristics of Multilayer Assembly. QCM is an effective tool to investigate the growth of multilayer film. It is an ultrasensitive mass sensor, consisting of a piezoelectric quartz crystal sandwiched between a pair of electrodes. When a suitable RF voltage is applied across the electrodes, the quartz crystal oscillates at its resonant frequency; a small layer added to the electrodes induces a decrease in resonant frequency ($\triangle F$). If a rigid layer is deposited on one or both sides of the electrodes, the resonant frequency will decrease proportionally to the mass of the absorbed layer according to the Sauerbrey equation: [23]

$$\Delta F = \frac{-2F_0^2 \Delta m}{A(\rho_q \mu_q)^{1/2}} \qquad (1)$$

In Equation (1), ΔF = measured frequency shift, F_0 = fundamental frequency of the crystal, Δm = mass change per unit area, A = piezoelectrically active area, ρ_q = density of quartz (2.648 g/cm^3), and μ_q = shear modulus of quartz (2.947×10^6 N/cm^2). Typically, the relationship between the frequency shift and the adsorbed mass per unit area (Δm) is linear obeying the Sauerbrey equation, Equation (2):

$$\Delta m = -C\Delta F/n \quad (2)$$

where C is the mass sensitivity constant (17.7 ng·cm^{-2} Hz^{-1} at 5 MHz), and n is the overtone number. In addition, dissipation can be characterized by the dissipation factor D, which is defined by Equation (3):

$$D = \frac{E_{dissipated}}{2\pi E_{stored}} \quad (3)$$

where $E_{dissipated}$ is the energy dissipated during one oscillation and E_{stored} is the total energy stored in the oscillating system. With the QCM-D measurements, the change in dissipation factor, $\Delta D = D\text{-}D_0$ is deduced, where D_0 is the dissipation factor of the pure crystal in solvent before adsorption and D is the dissipation factor after adsorption.

In this research, QCM analysis was conducted on a thiol-modified gold-coated QCM plate containing an equal composition of COOH and OH groups which is used as a model for treated PET substrates which were later subjected to multilayer assembly and determination of biological responses. Its water contact angle of 55° being close to that of the treated PET substrate (53°) suggests that it can satisfactorily mimic the treated PET substrate. Figure 2 displays the evolution of the normalized frequency changes ($\Delta F/n$) on the 3rd, 5th, and 7th overtone numbers and the corresponding changes in energy dissipation on the 3rd overtone number versus time of three multilayer systems as measured by QCM-D. At time (t) = 0 min, a stable baseline starting with 0.1 M NaCl was first established prior to adsorption of polyelectrolyte. At t = 5 min, a polycation (HTACC or PAH) solution was injected into the measurement chamber and allowed to adsorb for

5 min before the rinsing step began. After rinsing with 0.1 M NaCl for 5 min, at t = 15 min, the polyanion (PAA, SCC, or SFC) solution was then introduced followed by the same rinsing procedure. The adsorption and rinsing cycles were repeated until 10 individual layers of the polyelectrolyte were deposited. The change in frequency (ΔF) and dissipation (ΔD) throughout the building-up process were continuously observed indicating the stepwise deposition of the polyelectrolyte molecules to the QCM substrate. The fact that the $\Delta F/n$ of all three overtones can be superimposed throughout the whole range investigated strongly indicates that the assembled films are relatively rigid, not viscoelastic and that the adsorbed mass can be calculated from the observed frequency shift following Sauerbrey relationship.

For the HTACC/PAA system, an increase in ΔD and a decrease in $\Delta F/n$ were apparently more dramatic in the step of HTACC deposition (odd layer) as opposed to those in the step of PAA adsorption (even layer) suggesting that the HTACC layer was less rigid and perhaps greater in thickness than the its negatively charged counterpart, PAA. To explain such scenario, it is conceivable to take the comparative charge density of the HTACC and PAA into consideration. With 78% degree of substitution (%DS) of positively charged quaternary ammonium entities ($N(CH_3)_3^+$), HTACC should be less charged than PAA, a weak polyelectrolyte having a pKa of 4.3[24] at pH 7. Therefore, HTACC can adopt less extended conformations at the interface with a higher proportion of loops and tails than PAA. Not only can that bring in more HTACC chains to adsorb and yielded a thicker layer than did the PAA, but such coil-like conformation should also be able to trap more water molecules within its structure. These two reasons are believed to be responsible for the substantial difference in the decrease in $\Delta F/n$ and the increase in ΔD upon the adsorption between HTACC and PAA. It was not totally unexpected to observe a collapse of the entire multilayer film towards the interface upon the adsorption PAA. Its greater charge density as compared with HTACC makes the interpenetration and complexation/crosslinking between

the oppositely charged polyelectrolytes resulting in intrinsic charge compensation at the interface much more efficient. The stiffening of the adsorbed multilayer together with the preferably extended conformation led to a thinner layer of PAA having presumably less coupled water within its structure.

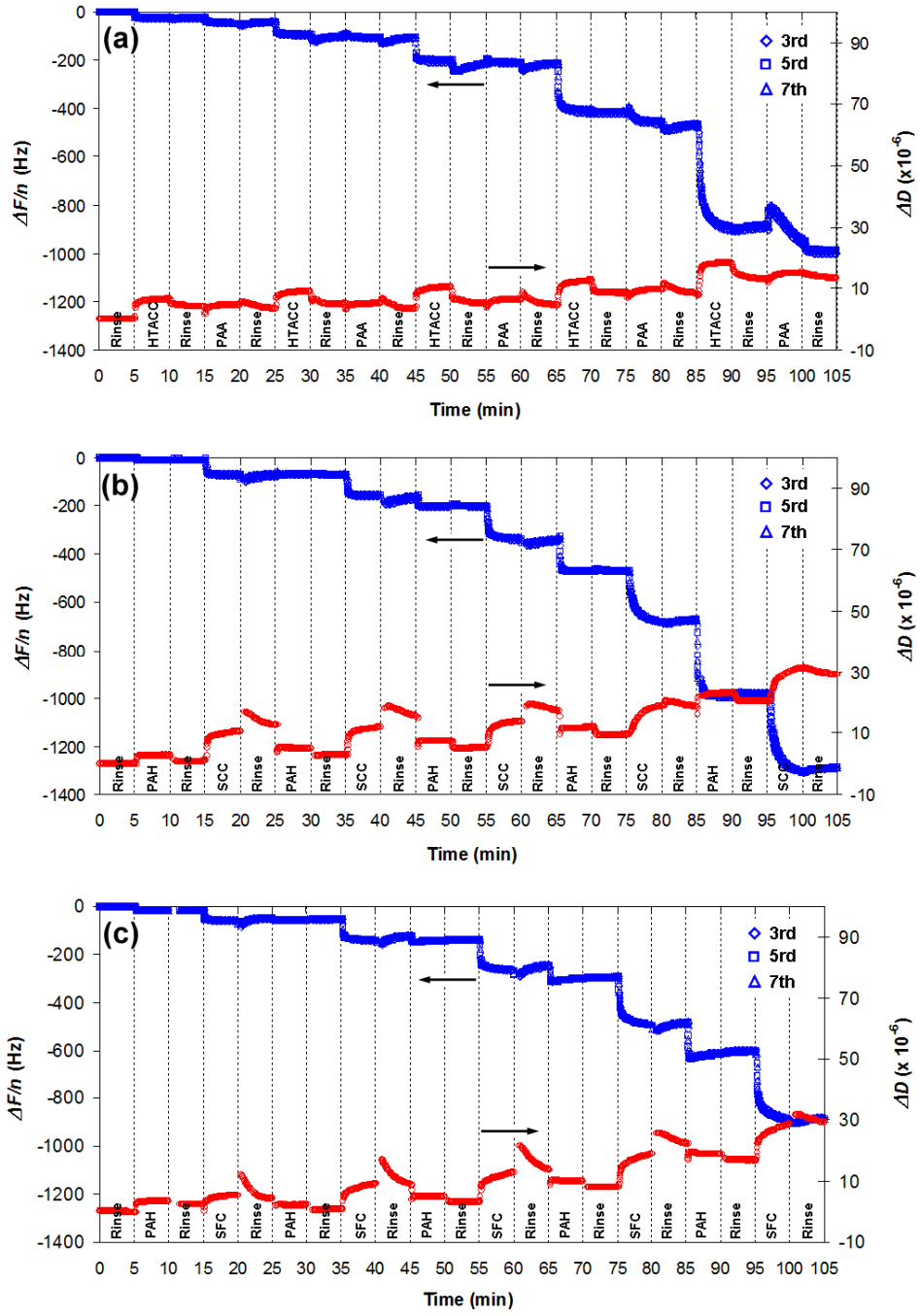

Figure 2. The change in normalized frequency ($\Delta F/n$) on the 3rd, 5th, and 7th overtones and the energy dissipation change (ΔD) on the 3rd overtone as a function of time upon consecutive adsorption of polyelectrolytes for 3 multilayer systems: (a) HTACC/PAA, (b) PAH/SCC, and (c) PAH/SFC.

The odd-even effect in terms of $\Delta F/n$ and ΔD variation was also evidenced on other two multilayer films, PAH/SCC and PAH/SFC, both of which were assembled from the same cationic polyelectrolyte, PAH (Figure 2 (b) and (c)). The explanation based on the charge density should also be valid. As a consequence of the incomplete substitution of negatively charged entities at the NH_2 position on the chitosan backbones, SCC with 44% DS (of *N*-succinyl groups) and SFC with 68%DS (*N*-sulfofurfuryl groups) should be less charged than PAH, a weak polyelectrolyte having a p*Ka* of 9.67.[25] At pH 7-8 at which PAH/SCC and PAH/SFC multilayer films were assembled, 98-99% of $-NH_3^+$ of PAH remained undissociated. This is the reason why an increase in ΔD and a decrease in $\Delta F/n$ were appreciably much greater in the step of SCC and SFC deposition (even layer) than those in the step of PAH adsorption (odd layer) suggesting that the SCC and SFC layers were thicker and presumably more water-rich than their positively charged counterpart, PAH. The higher charge density of the PAH facilitated interfacial crosslinking between the oppositely charged polyelectrolytes and so thus imparted the collapse of the film upon its deposition. This suggests that the properties of multilayer thin film depend on which the adsorbed layer in the outermost layer. Evidently, it can be concluded that all three multilayer films have a relatively compact, rigid internal structure and the differences in the observed dissipation are determined by the interfacial properties of the last deposited layer.

The water content of each individual layer for all three multilayer systems can be estimated from the mass per unit area for dry films (m_d) and wet film (m_w) following Equation (4): [26] It should be emphasized that m_d and m_w were calculated based on the assumed density of the dry films (1.2 g/cm^3)[27] by Sauerbrey equation from ΔF obtained from QCM and QCM-D measurements, respectively.

$$\% \text{ water content} = \frac{m_w - m_d}{m_w} \times 100 \qquad (4)$$

According to the results shown in Figure 3, the water contents of all three multilayer pairs are relatively high with all values being above 60%. The alternating trend of the water content between the odd and even layer was only observed at initial stage of assembly process (up to 4-7 layers). The water contents tended to level out at 85-90% between 7-10 deposited layers. Together in the same figure, the dried adsorbed mass determined by QCM was plotted to demonstrate that the odd-even effect of $\Delta F/n$ and ΔD variation analyzed by QCM-D as previously shown in Figure 2 and the m_w displayed in Figure S1 (Supporting Information) at the early stage of deposition was very much influenced by the different content of associated water within each individual layer between the odd and even layer. Once the assembly process was well established (from 5 layers onward), the odd-even fluctuation of both $\Delta F/n$ and ΔD was no longer governed by the entrapped water, but mainly dictated by the varied amount of the adsorbed polyelectrolyte which is dependent on its charge density and conformation

It is not unprecedented to see an exponential growth of deposited mass and thickness (Figure S2 in Supporting Information) in the investigated range for all three multilayer systems. Schlenoff and Dubas[28] described this initial nonlinear growth regime as a result of excess charge profile being truncated by the impenetrable multilayer. Ladam and co-workers[29], on the other hand, suggested that there are polyelectrolyte chains diffusing into and out of the film during the buildup process. It was proposed that free polyelectrolyte chains within the multilayer film diffuse out to form complexes with the oppositely charged polyelectrolytes at the surface upon the change of the bulk solution to one with polyelectrolytes of opposite charge. And that would

promote the adsorption of more material on the surface in each adsorption step than that should be expected from the regular charge compensation.

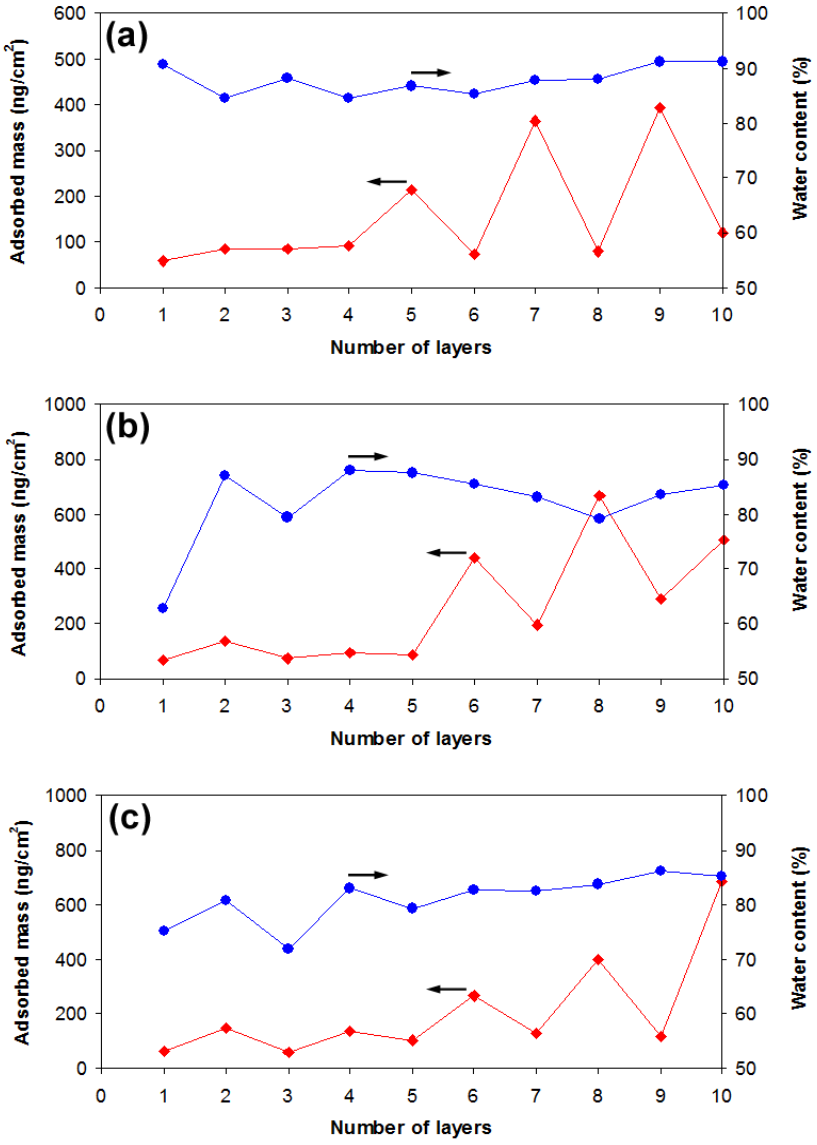

Figure 3. Water content (•) and mass per unit area for dry films (m_d) determined by QCM (◆) as a function of layer number for 3 multilayer systems: (a) HTACC/PAA, (b) PAH/SCC, and (c) PAH/SFC

Surface Coverage and Wettability of the Multilayer Films. In this research, the plasma-treated PET plates, commercially available and commonly used polymeric materials for biomedical and biomaterials applications, were employed as substrates for multilayer assembly. After the treatment by basic hydrolysis, the treated PET substrate with a water contact angle of 53° and carboxyl group density of 1.46 x 10^{-8} mol/cm^2 as estimated by Toluidine blue O assay were obtained.[19] The coverage of the deposited multilayer films was monitored by AFM analysis. Upon basic hydrolysis, the treated PET substrate became rougher as can be evidenced from the root-mean-square roughness (R_{rms}) being increased from 1.76 to 7.68 nm (micrographs not shown). As illustrated in Figure 4, the surfaces became apparently smoother after the deposition of HTACC/PAA multilayer. A similar trend was also observed for the system of PAH/SCC, except that the roughness of the even layer (having SCC as the outermost layer) seemed to be rougher than their adjacent odd layer (having PAH as the outermost layer). In contrast, the assembled PAH/SFC film became increasingly rougher upon the growth of the multilayer film implying that the defects or aggregates generated during the deposition of the first layers have been accumulated in the consecutive layer. The adsorbed polyelectrolyte that was expected to fill previously formed valleys on the surface and smoothened the film, in turn made the film rougher. This may be explained as a consequence of the loosely bound polyelectrolyte form complexes upon partial or total desorption and deposited back into the assembled layer during the adsorption process. Apparently, the interdigitation was less perfect in this particular case. The fact that the surface roughness of the film having the chitosan derivative (HTACC, SCC or SFC) as the top layer were always greater than that having its oppositely charged polyelectrolyte (PAA or PAH) as the top layer agree quite well with the QCM data which previously indicated that all chitosan derivatives with their lower charge density than their counterparts adsorbed in the less extended and more loop-like conformations and yield thicker

individual layer. And that can be the origin of the odd-even topographic variation. Nonetheless, it can be assumed that the assembled films grow homogeneously when the size of the roughness and the pores is far larger than molecular sizes of polyelectrolytes and smaller than the average thickness of a single bilayer. (Table S1 in Supporting Information)

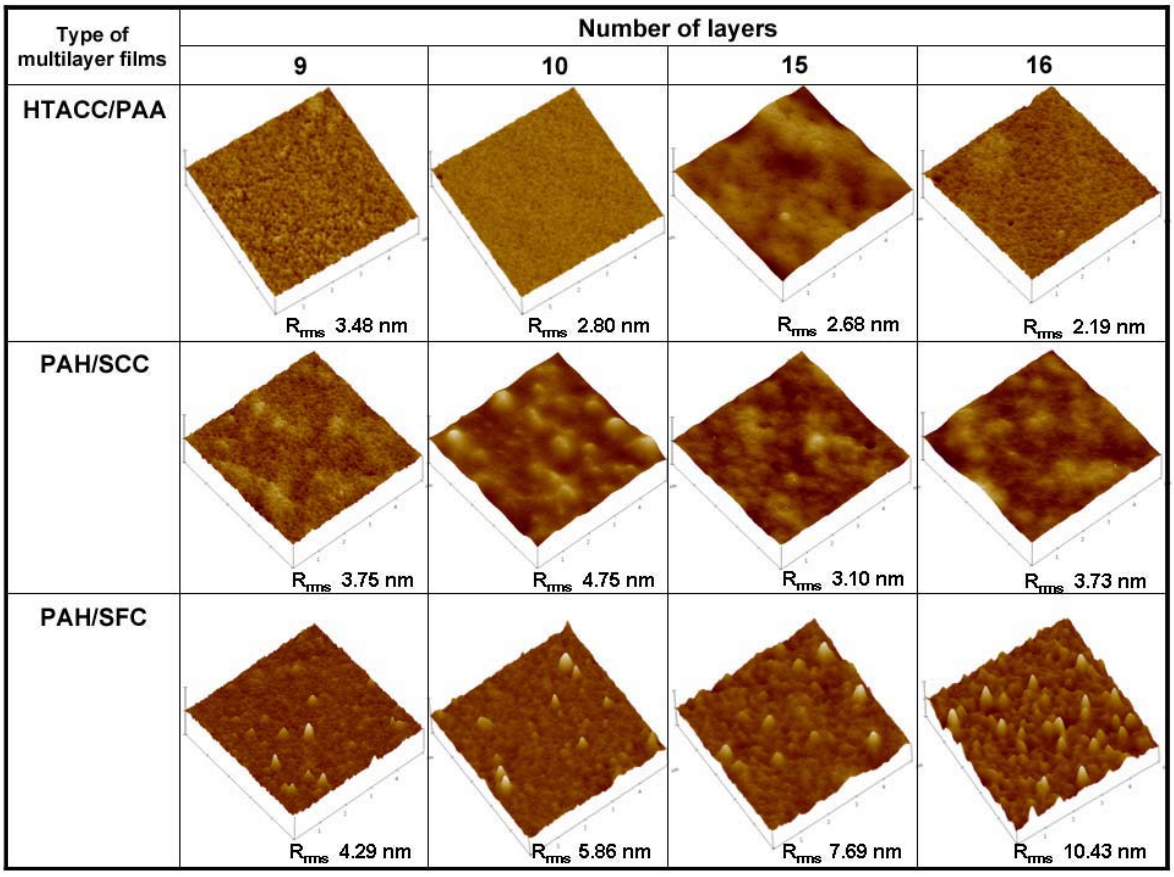

Figure 4. AFM images (5x5 μm^2) of treated PET substrates with three multilayer systems: HTACC/PAA, PAH/SCC, and PAH/SFC. The value listed under each micrograph is the corresponding root-mean-square roughness ($R_{rms.}$) for each micrograph.

The wettability of the multilayer film was probed by water contact angle measurements. The results depicted in Figure 5 suggested that the assembled film was stratified. And the films

having the odd number of deposited layer and positively charged was more hydrophobic than those having an even number of deposited layer and negatively charged. The odd-even wetting behavior coincides with the fact that each individual layer based on QCM analysis (half of the bilayer thickness shown in Table S1) is thicker than the sampling depth of contact angle measurement (a few Å) so that the wettability of the multilayer film is strongly determined by the last layer deposited and the influence of the underlying layers was not observed.

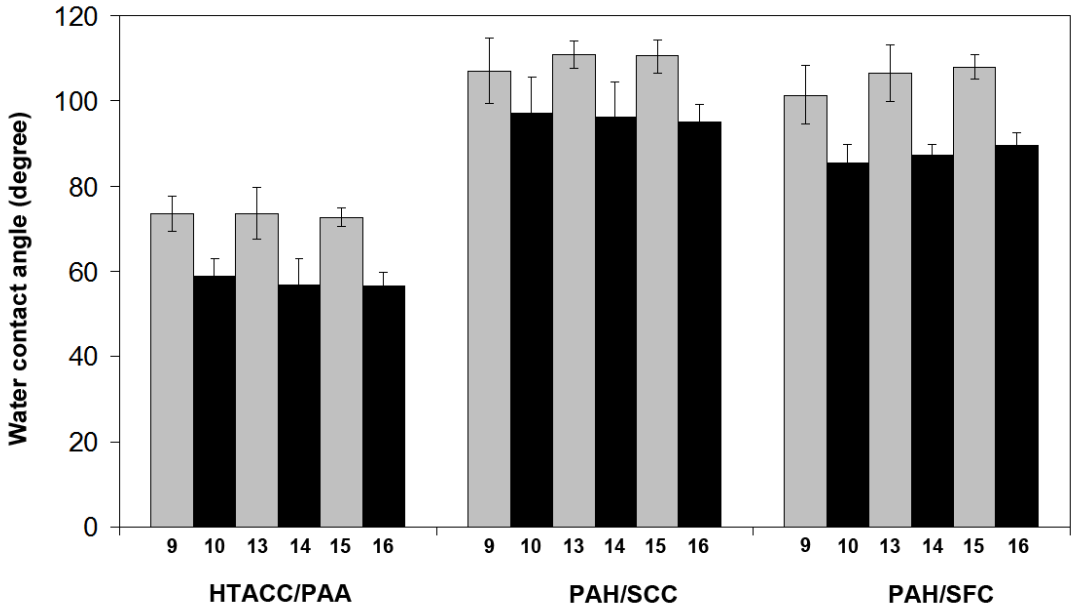

Figure 5. Water contact angle of multilayer films assembled on treated PET substrates. The number appearing on the horizontal scale represents the number of depositions.

Cell Adhesion and Proliferation. The *in vitro* cytocompatibility of three multilayer systems, on the treated PET substrates was carried out against L929 fibroblasts. To investigate the mitochondrial functions of the cultured L929, reduction of MTT reagent was used as an assay to measure mitochondrial redox activity. MTT reagent is a pale yellow substance that is reduced to a dark blue formazan product when incubating with viable cells by mitochondrial succinate

dehydrogenase in complex II, which plays a critical role in both oxidative phosphorylation and tricarboxylic acid cycle. Therefore, the production of formazan can reflect the level of cell viability. The results shown in Figure 6 are reported in terms of the cell adhesion (after 12 h incubation) and proliferation ratio (after 48 and 96 h incubations) with relative to TCPS. The number appearing on the horizontal scale represented the number of deposition. If the number of layer is odd, the charge of the outermost layer is positive. If the number of layer is even, the charge of the outermost layer is negative.

Considering the HTACC/PAA system, the multilayer film having the even number of layer with PAA as the top layer seems to be more favorable for both cell adhesion and proliferation than those having the odd number of layer with HTACC as the top layer. The effectiveness of PAA in promoting positive cellular responses is equivalent to the TCPS which was used as a positive control. It is generally known that the cell membrane possesses negative charges. The opposite charges of HTACC should lead to a strong attraction with the cells and causes detrimental influence on the cells. The effect is more pronounced after 4 days of incubation. It has been previously reported that HTACC exhibit potent antibacterial activity.[7,8] And this may be the reason why it is not a favorable substrate for promoting cell growth and maintaining cell viability.

As opposed to the system of HTACC/PAA, the PAH/SCC multilayer films exhibit the opposite tendency. After 2 and 4 days of incubation, a significant improvement of cell adhesion was observed, especially when the number of layer was equal to 15 and PAH was the top layer. Unlike HTACC, PAH is a weak synthetic polyelectrolyte that has been found to enhance early cell adhesion in the multilayer system of (PSS/PAH)[30] when it is the outermost layer of the film. The fact that SCC bears some negative charge, which is the same charge as the cell membrane, can explain why it is unfavorable for cell attachment. Evidently, the hydrophilic nature is not

enough to counteract the charge repulsion. However, the same explanation cannot be applied with PAA. A similar trend was observed in the case of PAH/SFC system. In particular, the 9-layer multilayer film with PAH as the outermost layer gave significantly higher in both cell adhesion and proliferation than the treated PET substrate. The charge repulsion may also account for the inferior cellular responses of the multilayer films having SFC as the top layer. The cellular responses seem to be worse as a larger number of layers were deposited. There may be some influence from the increased roughness (See AFM data).

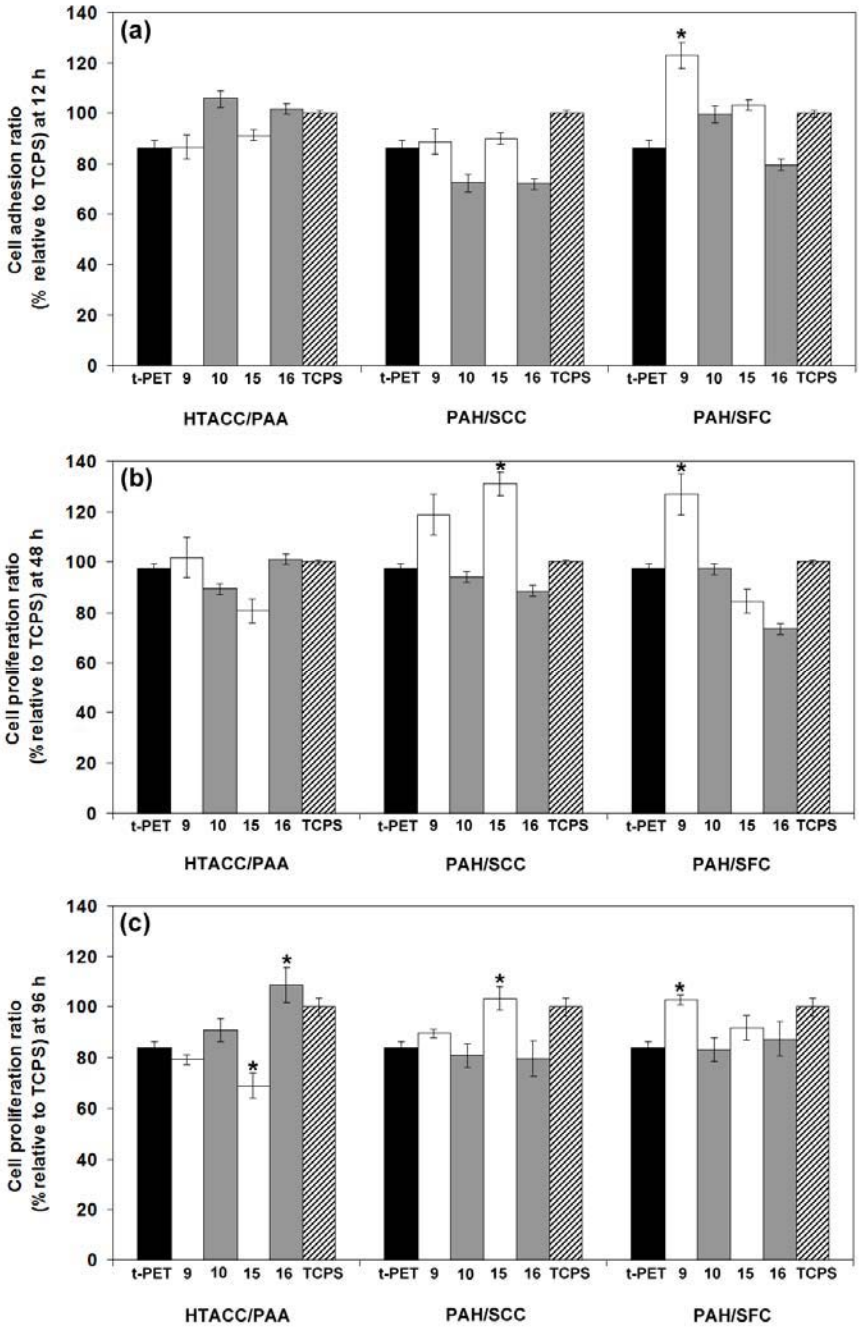

Figure 6. Responses of L929 cells (% relative to TCPS) with a seeding density of 5.0×10^3 cells/well on treated PET substrates with three multilayer systems in terms of (a) cell adhesion ratios at 12 h and cell proliferation ratios at (b) 48 and (c) 96 h. Statistical significance with $p < 0.05$ is compared with the control (t-PET) (*).

Antibacterial activity of the HTACC/PAA Multilayer Film. HTACC has been known to deliver desirable antibacterial activity when used in the soluble form[31,32] and chemically grafted or coated on materials.[7] Here, we anticipate that a similar antibacterial action can also be achieved when HTACC is deposited as assembled layers on any substrates. In this research, the antibacterial activity of the HTACC/PAA multilayer deposited on the treated PET substrate was tested against the Gram-positive and Gram-negative representative bacteria, *S. aureus* and *E. coli*, respectively, in terms of the total number of replication competent (viable) cells as mean colony forming units per volume (CFU/mL). The tested results are displayed in Figure 7 in which the number appearing on the horizontal scale represents the number of depositions. If the number of layers is odd (9 and 15), HTACC was the last layer deposit. If the number of layers is even (10 and 16), PAA was the last layer deposit. In the case of *S.aureus,* the detrimental effect was detected for the HTACC/PAA multilayer films having 15 and 16 layers. The former seemed to possess greater activity than the latter considering its %antibacterial ratio reached 70.5% as opposed to 57.8% of the latter. This can be expected taking into account that the surface of *S. aureus* consists of negatively charged teichoic acid within a thick peptidoglycan layer and lacks of an outer membrane. Such characteristic should render the bacterial cell more attractive to and easier to be damaged through the contact-inhibitory mechanism when exposed to the positively charged 15-layer film than the negatively charged 16-layer film.

In contrast, the damaging impact on *E.coli* was observed on the multilayer film having at least10 layers with only a slight odd-even effect was observed between the multilayer film having 15 and 16 deposited layers. The lower antibacterial potency of the multilayer film against *E.coli* than that against *S. aureus* may be explained as a result of the different bacterial membrane structures. Unlike *S. aureus*, *E. coli* has a double protective layer: the outer lipopolysaccharide layer embedded with a number of small channels of porins and the inner peptidoglycan layer (7-8

nm). The fact that it does not contain the negatively charged entities that can electrostatically interact with HTACC makes it less sensitive to be destroyed by positively charged molecules like HTACC. Although HTACC was not the top layer of the 16-layer HTACC/PAA film, the substrate exhibits favorable cellular responses (See Figure 6), it can introduce a reasonable antibacterial property (~50% antibacterial ratio) against both bacterial strains to the multilayer film. This is a desirable characteristic for biomaterials applications given that the film supported cell attachment and proliferation and at the same time appreciably prevented bacterial growth. Also, it should be emphasized that HTACC can be used as an effective material for antibacterial coating especially against bacterial strains having negatively charged cell membrane, *S. aureus* in this particular case.

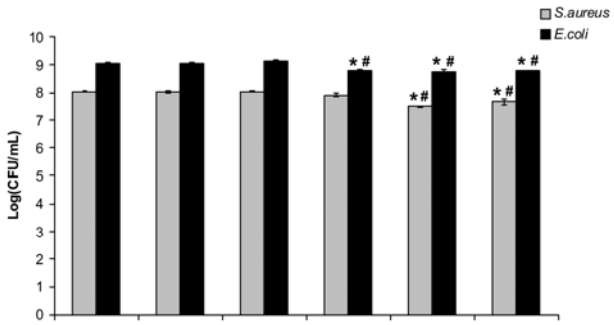

% Antibacterial ratio						
S. aureus	0.0	3.7	ND	20.6	70.5	56.9
E. coli	0.0	1.7	ND	46.3	48.6	45.7

ND = Not Detected

Figure 7. Total replication competent (viable) cell counts of bacteria grown for 24 h in media alone (control) or in the presence of treated PET substrate (t-PET) and multilayer film of HTACC/PAA assembled on treated PET substrate. The number appearing on the horizontal scale represents the number of depositions. Statistical significance with $p < 0.05$ of the viable count is compared with the control (*) and t-PET (#). Below in the table is the corresponding antibacterial ratio.

Antithrombogenic Properties of the PAH/SFC Multilayer Film. It has been previously demonstrated that SFC in a soluble or a surface-coated form expresses antithrombogenic property[10,11,33] a necessary feature for the development of materials to be used in contact with blood. This can be derived from the presence of sulfonic acid groups in its structure, the same negatively charged moieties present in heparin (HEP), a well-known and widely used anti-blood coagulation polymeric material. In principle, when a material is in contact with blood, a surface-induced thrombosis is initiated by adsorption of plasma proteins, followed by the adhesion and activation of platelets.[21] Herein, for the first time, the anticoagulating characteristic of SFC in the assembled form (PAH/SFC) was assessed in terms of amount of adsorbed plasma protein/surface area (mean±S.D.) and platelet adhesion of which results are illustrated together in Figure 8. The investigation was done in comparison with the multilayer films assembled from HEP and the same cationic polyelectrolyte, PAH.

As anticipated, the amount of adsorbed protein on the multilayer film having the odd number of layer with PAH as the top layer (9-layer and 15-layer) was greater than those having the even number of layer with SFC and HEP as the top layer (10-layer and 16-layer). It is generally known that under normal physiological condition at pH 7.4, the human serum carries negative charge due to the presence of albumin, its major protein component having the isoelectric point of 4.8.[22] Thus, the plasma proteins can favorably interact with cationic polyelectrolyte, PAH with a p*Ka* of 9.67[25] in this particular case, mainly through electrostatic interactions. On the other hand, the amount of adsorbed protein was approximately 31-33% and 48-62 % reduced on the assembled films terminating with SFC and HEP (the 10-layer and 16-layer), respectively when compared with that on the treated PET surface. This can be described as a result of the electrostatic repulsion between the negatively charged entities in the SFC and HEP layer and the plasma proteins. It should be emphasized that the negative charges in HEP do not only come from the

sulfonate groups (in the form of $–NHSO_3^-$), but also from the sulfate groups ($–CH_2OSO_3^-$ and OSO_3^-) and carboxylate groups (COO^-). Thereby, there are two negative entities in each repeat unit of HEP. Unlike HEP, SFC used in this investigation only bears 68% of negatively charged sulfonate groups substituted on the chitosan backbone. This is the reason why the ability of the films terminating with SFC in preventing plasma protein adsorption is inferior to that terminating with HEP. It should be noted that the level of antithromboginicity was varied as a function %DS of sulfofurfuryl groups on chitosan backbone in SFC. Upon mixing with 5 mL of whole blood for 15 min, 0.2 mg of SFC having 68%DS (dissolved in 0.85% NaCl(aq)) showed the lowest degree of partial blood coagulation as opposed to the SFC derivative having lower %DS. The real time coagulation of whole blood mixed with SFC having %DS of 68 and 55 can be viewed from Video S1 and S2 in Supporting Information, respectively. In contrast, the blood coagulation of whole blood mixed with the same amount of HEP (Video S3) was entirely suppressed whereas the blood became totally clotted within 3 min of mixing with chitosan (Video S4).

The results from static platelet adhesion assay (Figure 8) are in excellent agreement with the protein adsorption test. Aggregation of adherent platelets at partially activated stage having extensions of pseudopods were apparent on the substrates with high amount of adsorbed plasma proteins such as the treated PET substrate alone or the treated PET substrates with the 9-layer assembled PAH/SFC film. Fewer numbers of platelets adhered with insignificant degree of activation on the assembled PAH/SFC films terminated with SFC (10-layer and 16-layer) than those adhered on the PAH/SFC films terminated with PAH (9-layer and 15-layer). The alternating trend of platelet adhesion was also observed on the assembled PAH/HEP films confirming that the anticoagulant property is surface-dependent with the 16-layer assembled PAH/HEP showing an absolute anti-platelet adhesion. Although SFC is not as effective as HEP in suppressing plasma protein adsorption and platelet adhesion, its anticoagulating property is at

a satisfactory level given that its negative charge density is much less than HEP so that it can be considered as an alternative, nature-derived antithrombogenic material, being capable of forming assembled layer on materials to be used in blood-contacting applications.

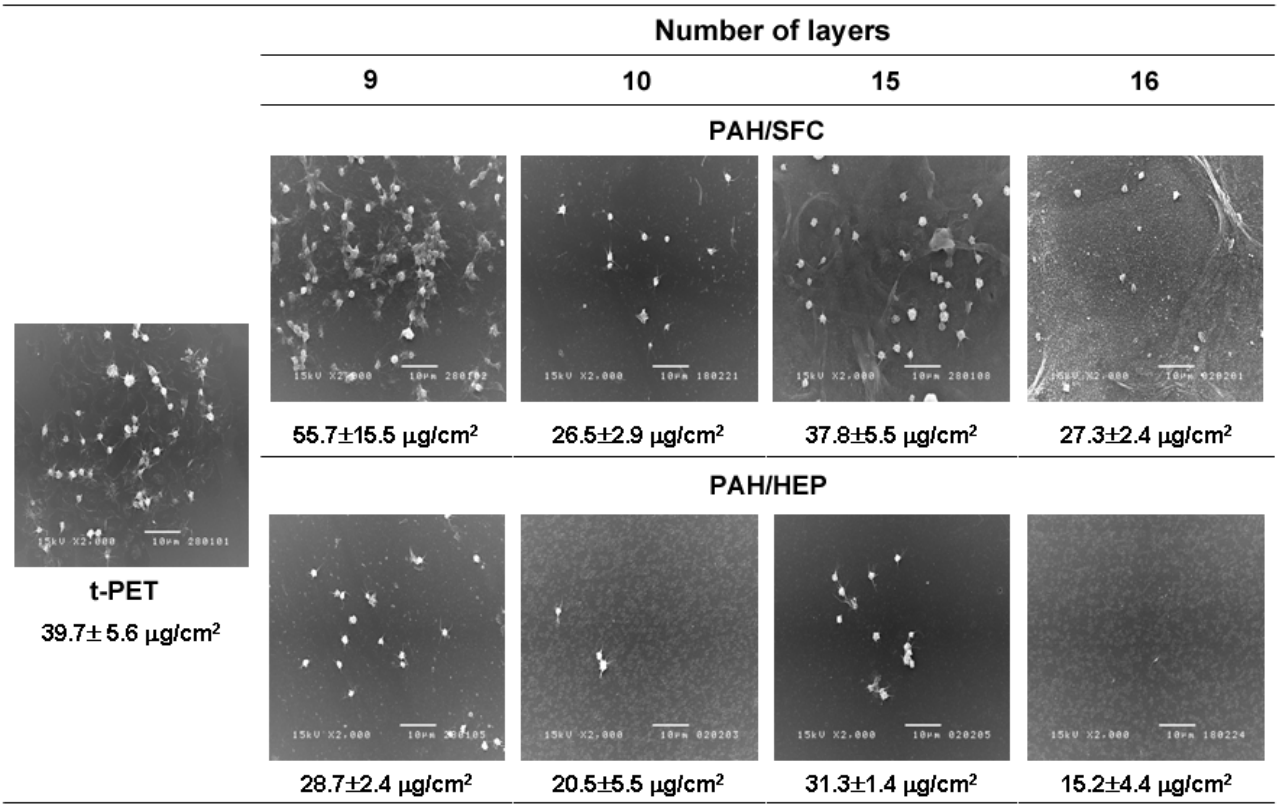

Figure 8. Representative SEM micrographs of treated PET substrates with multilayer systems after exposure to PRP for 1 h. Micrographs shown are representative of at least 10 such fields of view per sample and 3 independent samples. Below each micrograph is the corresponding amount of plasma protein adsorption ($\mu g/cm^2$) after the substrates were exposed to PPP for 3 h.

Conclusion

QCM analysis suggested that multilayer films of these 3 pairs of polyelectrolytes: (HTACC/PAA), (PAH/SCC) and (PAH/SFC) have been successfully formed by alternate layer-

by-layer adsorption. The stratification of the multilayer films deposited on the plasma-treated poly(ethylene terephthalate) (treated PET) substrates was verified by water contact angle measurements, respectively. As characterized by AFM, the multilayer films can homogeneously cover the substrate and have the ability to smooth-out a rough surface of the treated PET substrates. The *in vitro* cell adhesion and proliferation of fibroblasts showed that the degree of cytocompatibility of the multilayer films depends strongly on the polyelectrolyte used for the assembly process and the last layer deposited. The antibacterial activity of (HTACC/PAA) showed that the multilayer film is able to inhibit the growth of *E. coli* and *S.aureus* which was consistent to cell study. The results from blood compatibility indicated that the (PAH/SFC) multilayer film terminating with SFC can reduce protein adsorption. All above results of this study demonstrated that multilayer film assembled from charged derivatives of chitosan are potential candidates for biomedical applications.

Acknowledgment. This research is financially supported by a Research Team Promotion Grant, the Thailand Research Fund (RTA4780004 and RTA5080004). The authors are indebted to Dr.Xiaodi Su of Institute of Materials Research and Engineering, Singapore for providing a QCM-D facility.

References

(1) Decher, G. *Science* **1997**, *277*, 1232-1237.

(2) Shahidi, F.; Arachchi, J. K. V.; Jeon, Y.-J. *Trends Food Sci. Technol.* **1999**, *10*, 37-51.

(3) Sashiwa H, S. H., Shigemasa Y, Ogawa R, Tokura S. *Int. J. Biol. Macromol.* **1990**, *12*, 295-296.

(4) Shigemasa, Y.; Saito, K.; Sashiwa, H.; Saimoto, H. *Int. J. Biol. Macromol.* **1994**, *16*, 43-49.

(5) Iwasaki, N.; Yamane, S. T.; Majima, T.; Kasahara, Y.; Minami, A.; Harada, K.; Nonaka, S.; Maekawa, N.; Tamura, H.; Tokura, S.; Shiono, M.; Monde, K.; Nishimura, S. I. *Biomacromolecules* **2004**, *5*, 828-833.

(6) Rabea, E. I.; Badawy, M. E. T.; Stevens, C. V.; Smagghe, G.; Steurbaut, W. *Biomacromolecules* **2003**, *4*, 1457-1465.

(7) Seong, H. S.; Whang, H. S.; Ko, S. W. J. *Appl. Polym. Sci.* **2000**, *76*, 2009-2015.

(8) Lim, S. H.; Hudson, S. M. *Carbohydr. Res.* **2004**, *339*, 313-319.

(9) Kato, Y.; Onishi, H.; Machida, Y. *Biomaterials* **2004**, *25*, 907-915.

(10) Amiji, M. M. *Colloids Surf. B* **1998**, *10*, 263-271.

(11) Jayakumar, R.; Nwe, N.; Tokura, S.; Tamura, H. *Int. J. Biol. Macromol.* **2007**, *40*, 175-181.

(12) Vongchan, P.; Sajomsang, W.; Subyen, D.; Kongtawelert, P. *Carbohydr. Res.* **2002**, *337*, 1239-1242.

(13) Serizawa, T.; Yamaguchi, M.; Matsuyama, T.; Akashi, M. *Biomacromolecules* **2000**, *1*, 306-309.

(14) Serizawa, T.; Yamaguchi, M.; Akashi, M. *Biomacromolecules* **2002**, *3*, 724-731.

(15) Zhu, Y. B.; Gao, C. Y.; He, T.; Liu, X. Y.; Shen, J. C. *Biomacromolecules* **2003**, *4*, 446-452.

(16) Cai, K.; Rechtenbach, A.; Hao, J.; Bossert, J.; Jandt, K. D. *Biomaterials* **2005**, *26*, 5960-5971.

(17) Fu, J.; Ji, J.; Yuan, W.; Shen, J. *Biomaterials* **2005**, *26*, 6684-6692.

(18) Liu, Y.; He, T.; Gao, C. *Colloids Surf. B* **2005**, *46*, 117-126.

(19) Channasanon, S.; Graisuwan, W.; Kiatkamjornwong, S.; Hoven, V. P. *J. Colloid Interface Sci.* **2007**, *316*, 331-343.

(20) Aoki, N.; Nishikawa, M.; Hattori, K. *Carbohydr. Polym.* **2003**, *52*, 219-223.

(21) Hoven, V. P.; Chombanpaew, K.; Iwasaki, Y.; Tasakorn, P. *J. Appl. Polym. Sci.* **2009**, *112*, 208-217.

(22) Lin, W.-C.; Liu, T.-Y.; Yang, M.-C. *Biomaterials* **2004**, *25*, 1947-1957.

(23) Sauerbrey, G. *Zeitschrift fuer Physik* **1959**, *155*, 206-222.

(24) Notley, S. M.; Eriksson, M.; Wågberg, L. *J. Colloid Interface Sci.* **2005**, *292*, 29-37.

(25) Yu, Y.; Wang, F.; Shi, W. Q.; Wang, L. Y.; Wang, W. B.; Shen, J. C. *Chin. Sci. Bull.* **2008**, *53*, 22-26.

(26) Garg, A.; Heflin, J. R.; Gibson, H. W.; Davis, R. M. *Langmuir* **2008**, *24*, 10887-10894.

(27) Lvov, Y.; Ariga, K.; Onda, M.; Ichinose, I.; Kunitake, T. *Colloids Surf. A* **1999**, *146*, 337-346.

(28) Schlenoff, J. B.; Dubas, S. T. *Macromolecules* **2001**, *34*, 592-598.

(29) Ladam, G.; Gergely, C.; Senger, B.; Decher, G.; Voegel, J. C.; Schaaf, P.; Cuisinier, F. J. G. *Biomacromolecules* **2000**, *1*, 674-687.

(30) Boura, C.; Menu, P.; Payan, E.; Picart, C.; Voegel, J. C.; Muller, S.; Stoltz, J. F. *Biomaterials* **2003**, *24*, 3521-3530.

(31) Kim, J. Y.; Lee, J. K.; Lee, T. S.; Park, W. H. Int. *J. Biol. Macromol.* **2003**, *32*, 23-27.

(32) Liu, C. X.; Zhang, D. R.; He, Y.; Zhao, X. S.; Bai, R. *J. Membr. Sci.* **2010**, *346*, 121-130.

(33) Sagnella, S.; Mai-Ngam, K. *Colloids Surf. B* **2005**, *42*, 147-155.

Graphic for Table of Contents

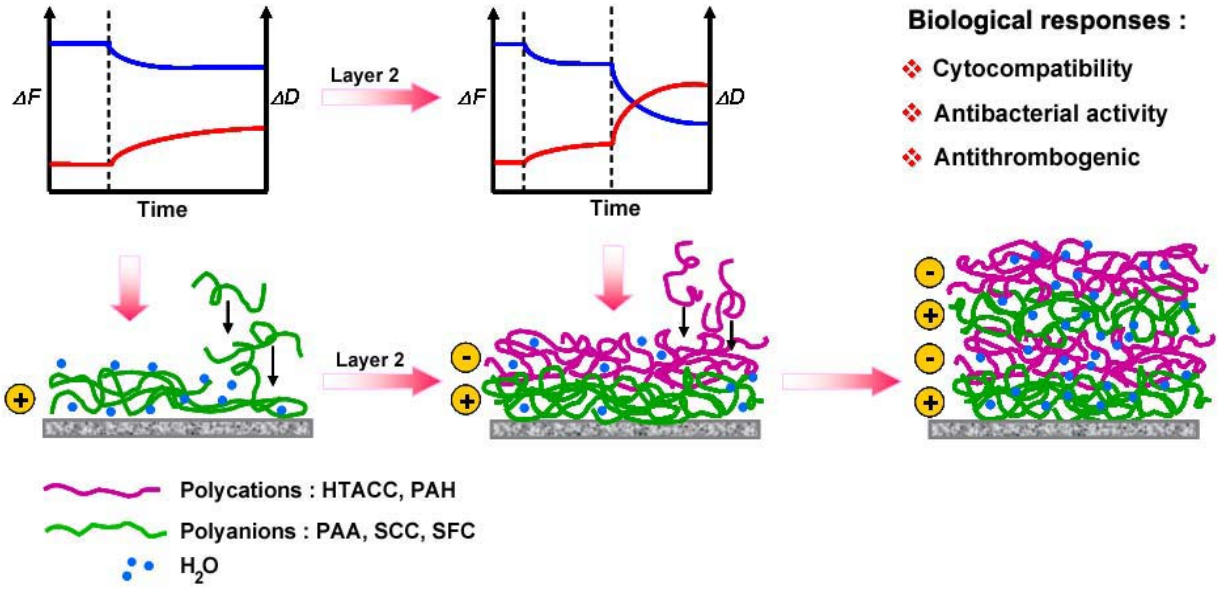

Supporting Information

Multilayer Thin Film Assembled from Charged Derivatives of Chitosan: Physical Characteristics and Biological Responses

Wilaiporn Graisuwan, Cheeraporn Ananthanawat, Oraphan Wiarachai, Songchan Puthong, Suphan Soogarun, Suda Kiatkamjornwong, Voravee P. Hoven

Page

2 Synthesis and Characterization of Charged Derivatives of Chitosan

4 **Figure S1.** The mass per unit area for wet films (m_d) determined by QCM-D as a function of layer number for 3 multilayer systems

5 **Figure S2.** Thickness of multilayer film assembled on the thiol-modified gold-coated QCM plate, obtained from QCM analysis as a function of the number of depositions.

6 **Table S1.** Average frequency shift and thickness of deposited multilayer film analyzed by QCM measurements using conventional mode.

Synthesis and Characterization of Charged Derivatives of Chitosan

***N*-[(2-hydroxyl-3-trimethylammonium)propyl] chitosan chloride (HTACC).** Chitosan flakes (0.50 g, 1 equiv. of NH_2) were dissolved in 1 vol. % (v/v) aqueous acetic acid (25 mL) to prepare a 2.0 % (w/v) chitosan solution. GTMAC (1.82 g, 4 equiv.) was added. The reaction was performed at 70°C for 24 h. After the reaction, the solution was poured into the dialysis tubing and dialyzed in deionized water for 5 days and then the solution was lyophilized to obtain a cotton-like white material.

IR (KBr): ν = 1,598 cm^{-1} (N-H bending of amino groups of chitosan), and 1,480 cm^{-1} (C-H bending of methyl groups of quaternary ammonium groups)

^{1}H NMR (D_2O): δ = 2.6 ppm (-NHC$\underline{H}_2$-), 3.1 ppm (N^+-(C$\underline{H}_3$)$_3Cl^-$), 4.4 ppm (-NHCH$_2$C$\underline{H}$-), and 3.3-4.3 ppm (m, $H^{2'}$,H^3, H^4, H^5, H^6, and $H^{6'}$). Degree of substitution of HTACC calculated from ^{1}H NMR data was 78%

***N*-sulfofurfuryl chitosan (SFC).** Chitosan flakes (0.50 g, 1 equiv. of NH_2) were dissolved in 1 % (v/v) aqueous acetic acid (25 mL) to prepare a 2.0 % (w/v) solution. Methanol (10 mL) containing 1.0 % (w/v) triethanolamine was slowly added to the chitosan solution. The mixture was stirred for 6 h at ambient temperature. FFSA (2.38 g, 4 equiv.) was slowly added to the chitosan slurry. The reaction was allowed to proceed for 24 h at ambient temperature. As the reaction continued, the Schiff's base thus formed was reduced by a slow addition of sodium borohydride ($NaBH_4$) (0.70 g, 6 equiv.). After the reduction for 6 h, the Schiff's base slowly dissolved to form a viscous solution. After the reaction, the solution was poured into the dialysis tubing and dialyzed in deionized water for 5 days and then the solution was lyophilized to obtain a cotton-like white material.

IR (KBr): ν = 1,237 cm^{-1} (O=S-O stretching of the sulfonate salt), and 1,040 cm^{-1} (S=O stretching of sulfonic acid)

^{1}H NMR (D_2O): δ = 4.4 ppm (-NHC$\underline{H}_2$-), 3.3-4.1 ppm ($H^{2'}$, H^3, H^4, H^5, H^6, and $H^{6'}$), and 6.3-6.7 ppm (=C$\underline{H}_2$C$\underline{H}_2$=). Degree of substitution of SFC calculated from ^{1}H NMR data was 68%.

***N*-succinyl chitosan (SCC).** Chitosan flakes (0.50 g, 1 equiv. of NH_2) were dissolved in 1 % (v/v) aqueous acetic acid solution (25 mL) to prepare a 2.0 % (w/v) chitosan solution. The chitosan solution was diluted with 40 mL of methanol. SA (1.20 g, 4 equiv.) dissolved in a minimum amount of acetone, was then added to the chitosan solution. The mixture was

vigorously stirred for 2 h at ambient temperature. The obtained viscous solution was diluted with 50 mL of water and the pH of the solution was adjusted to 10 using 2 M NaOH solution. After dialysis for 5 days, the solution was lyophilized to obtain a cotton-like white material.

IR (KBr): ν = 1,650 cm^{-1} (amide I, increase from chitosan), 1,560 cm^{-1} (amide II, increase from chitosan), and 1,598 (N-H bending of amino groups of chitosan, decrease from chitosan)

^{1}H NMR (CF_3COOH/D_2O): δ = 2.2-2.5 ppm (-NHCOC$\underline{H_2}$C$\underline{H_2}$-), and 3.0-3.8 ppm (m, $H^{2'}$, H^3, H^4, H^5, H^6, and $H^{6'}$). Degree of substitution of SFC calculated from ^{1}H NMR data was 44%.

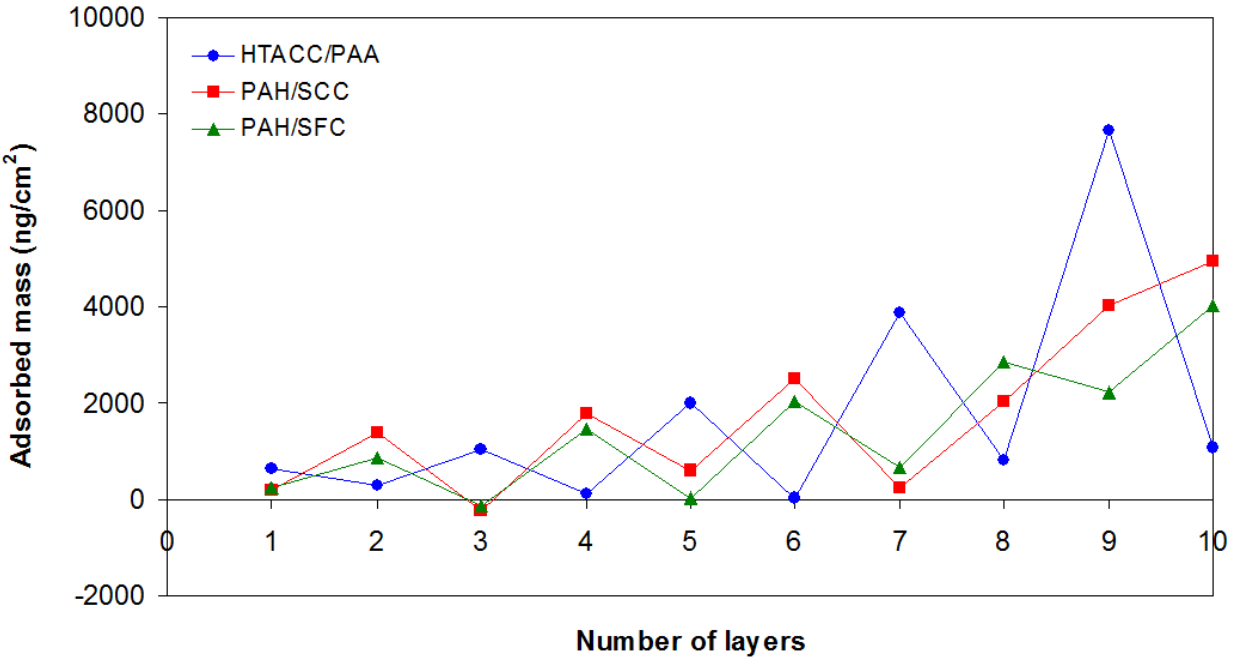

Figure S1. The mass per unit area for wet films (m_d) determined by QCM-D as a function of layer number for 3 multilayer systems

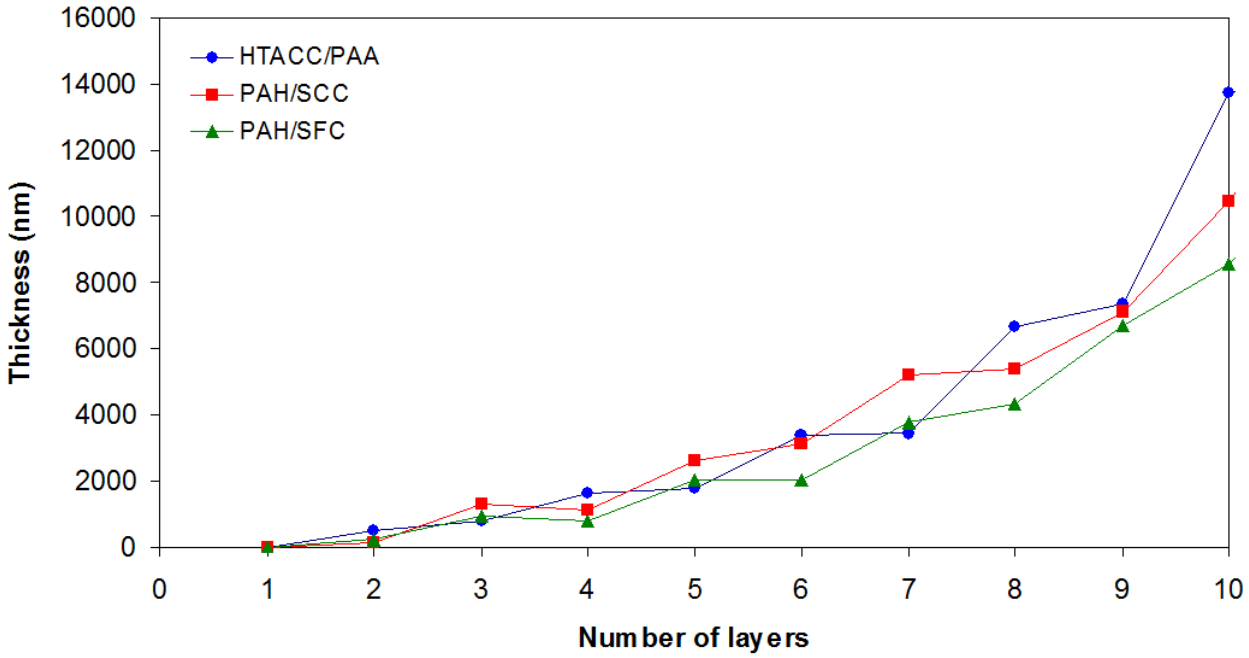

Figure S2. Thickness of multilayer film assembled on the thiol-modified gold-coated QCM plate, obtained from QCM analysis as a function of the number of depositions.

Table S1. Average frequency shift and thickness of deposited multilayer film analyzed by QCM measurements using conventional mode**.**

Multilayer system	Average ΔF_{odd} (Hz)	Bilayer thickness, $d_{b,odd}$ (nm)	Average ΔF_{even} (Hz)	Bilayer thickness, $d_{b,even}$ (nm)
HTACC/PAA	81.3	11.9	85.5	12.6
PAH/SCC	142.5	20.9	148.3	21.8
PAH/SFC	81.0	11.9	118.5	17.4

All VDO clips listed below are attached as separated files

Video S1. Real time monitoring for coagulating property of 5 mL whole blood in a closed test tube upon mixing for 15 min with 0.2 mg of SFC having 68%DS, dissolved in 0.85% NaCl(aq).

Video S2. Real time monitoring for coagulating property of 5 mL whole blood in a closed test tube upon mixing for 15 min with 0.2 mg of SFC having 60%DS, dissolved in 0.85% NaCl(aq)**.**

Video S3. Real time monitoring for coagulating property of 5 mL whole blood in a closed test tube upon mixing for 15 min with 0.2 mg of SFC having 55%DS, dissolved in 0.85% NaCl(aq).

Video S4. Real time monitoring for coagulating property of 5 mL whole blood in a closed test tube upon mixing for 15 min with 0.2 mg of HEP, dissolved in 0.85% NaCl(aq).

Video S5. Real time monitoring for coagulating property of 5 mL whole blood in a closed test tube upon mixing for 15 min with 0.2 mg of chitosan, dissolved in 0.85% NaCl(aq).

Draft Manuscript

Kapok II: PRETREATMENT OF KAPOK FIBERS FOR PULPING AND PAPERMAKING

Somporn Chaiarrekij[a*] Thippawan Hommaivai[b], Kuntinee Suvarnakich[a], and Suda Kiatkamjornwong[a]**

[a]Department of Imaging and Printing Technology, Faculty of Science, Chulalongkorn University, 254 Phayathai Road, Bangkok 10330, Thailand.
*Tel: +662 218 5572; e-mail: huaja@hotmail.com
**Tel: +662 218 5587; Fax: +662 255 3021; e-mail: ksuda@chula.ac.th

[b]Pulp and Paper Technology Program, Faculty of Science, Chulalongkorn University, 254 Phayathai Road, Bangkok 10330, Thailand.

Abstract

Kapok fibers are naturally coated with wax and cutin which renders them hydrophobic. To obtain fibers that are suitable for pulping, they must first be immersed in tap water for up to three to four weeks which is very time consuming. This research then investigated the effects of fiber pretreatment with sodium hydroxide (NaOH) or lipase for varied immersion times before it was subjected to soda pulping, in comparison with the control fibers that were pretreated by immersion in tap water for 3 weeks. For chemical pretreatment, two doses of NaOH (5 and 10% (w/w) based on the O.D. kapok fiber weight) were used with three immersion times (1, 2 and 3 weeks). For biological pretreatment, a commercial lipase with the enzyme activity of 100 KLU/g with the dosages of 0.25 and 0.5% (w/w) based on O.D. kapok fiber weight was used for three immersion times (1, 3 and 5 hours) of the fibers. After soda pulping and latency removal of the kapok fibers, the pulp and their sheets formed (60 g/m^2) from each pretreatment were characterized for the pulping efficiency, and physical and optical properties. It was found that both alkali and lipase pretreatments provided the pulp with the lower lignin content but higher opacity. However, higher tensile and burst strengths were obtained when the pulp was pretreated with NaOH while higher tear resistance was acquired with lipase pretreatment.

Key words: Lipase, Pulping, Paper making, Chemical pretreatment, Biological pretreatment

Introduction

In a previous study of the pulping of kapok fibers for papermaking, it was concluded that kapok fiber can be a quality pulp source for papermaking, especially for strengthening tensile strength of paper (Apirakchaiskul, 2008). However, the idea of using kapok fibers as one of the new potential fiber sources for the demands of the pulp and paper industries is intimidated by the inherent difficulty in soaking the hydrophobic kapok fibers prior to processing them to soda pulping. Indeed, wetting kapok fibers is not easy and practically takes around three weeks for kapok fibers to get wet after being immersed in plain tap water. This is due to the waxy cutin on the fiber surface that provides strong water repellency. So, the pretreatment of kapok fibers before soda pulping is required in order to remove the surface waxy material, and this might also increase the soda pulping efficiency of kapok fibers. In turn, this would make the process more economically and ecologically viable with a lower chemical consumption and/or shorter immersing time and pulping time of kapok fibers.

Fiber pretreatment involves modification of the fibers before the pulping process, and can be divided into two broad types. The first is chemical pretreatment, which utilizes chemicals, typically alkali, such as NaOH or potassium hydroxide (KOH), to digest or soften the material (woodchips or, as in this case, fibers) and to open the fiber surface so that

pulping becomes easier and more efficient. The second broad approach is that of biological pretreatment, which uses micro-organisms or enzymes to digest the woodchips or fibers before processing them by the pulping process. Enzymes that have been used in this method include cellulases, hemicellulases, xylanases, pectinase and cutinase. These micro-organisms and enzymes may react with waxy fiber surface, cellulose, hemicellulose and lignin, including the lignin-carbohydrate complex. This causes the opening of more fiber surfaces to the aqueous environment and therefore provides a better reaction between the fibers and cooking chemicals during the pulping processes.

For biopulping, the fungus *C. subvermispora* has been applied to spruce woodchips for two weeks before processing them in a refiner to produce the mechanical pulp (Scott *et al*., 1998). The bio-pretreatment of these woodchips provided an energy saving of 24 to 38% during the refining process. Moreover, the bio-treated pulp had a higher strength than that of the control pulp, as indicated by the higher tensile, burst and tear indexes. Although the pulp brightness obtained from the bio-treated pulp was lower than the control pulp, it could, if required, be improved by pulp bleaching. Wax elimination from the surface of cotton fibers was also evaluated using a mixture of mechanical and biological action with cutinase and pectinase (Agrawal *et al*., 2008). The temperature required for wax elimination decreased from 100 °C, when NaOH was used, to 50 °C, when pectinase was used. In addition, using pectinase with cutinase was able to further reduce the required temperature to 30 °C and the reaction time to 15 min.

In this work, chemical pretreatment using NaOH for kapok fibers was evaluated, along with the biological pretreatment of kapok fibers using lipase. The objectives of the present work are to investigate the effects of these chemical and biological pretreatments on the soda pulping efficiency of the kapok fibers; to determine the optimum condition of each chemical and biological pretreatment of the kapok fibers; and to compare the results from the optimum condition of the chemical pretreatment with those from the biological pretreatment.

Experimental

The kapok fibers sourced in Thailand were subjected to chemical or biological pretreatment. Both pretreated fibers were then pulped by the soda process and analyzed with respect to the control pulp. The control pulp in all cases was derived by replacing the pretreatment stage with simply immersing the fibers in tap water for three weeks. Three replicates were done for all control and pretreated pulps.

Pretreatment of kapok fibers

500 g of Kapok fibers were pretreated by either immersion in tap water for three weeks (control) or chemical (NaOH) or biological (lipase enzyme) pretreatment. For the chemical pretreatment, the kapok fibers were treated with NaOH at 5% or 10% (w/w, based on the oven dried (O.D). kapok fiber weight) in 13 L of tap water for 1, 2 and 3 weeks. For the biological pretreatment, kapok fibers were pretreated with the Lipolase 100L, the commercial enzyme from Novozymes having the enzyme activity of 100 KLU/g (KLU stands for kilo lipase unit) at two different dosages (0.25% and 0.50% w/w, based on O.D. fiber weight) in 13 L of tap water and three times (1, 3 and 5 hours). After the pretreatment, the kapok fibers were washed prior to squeezing out the excess water and cut to 3-5 cm in length before being processed by soda pulping.

Soda pulping of kapok fibers

Kapok fibers with and without the pretreatments were separately pulped using NaOH at 20% (w/w, based on O.D. kapok fiber weight). The liquor-to-wood ratio (L: W) was 17:1 (v/w). The pulping was carried out in an autoclave digester, (UEC-2017A, Universal Engineering, India) with an initial digesting temperature at 40 °C. The pulp matrix was then gradually heated to 120 °C over 30 min. The pulping was proceeded at this temperature for

another 120 min. The pulp was then extensively washed with tap water to remove the excess alkali from the pulp by controlling with a pH meter (Hanna HI 98128, Hanna Instrument, U.S.A.). The net pulp yield and residual alkaline level were then determined.

Kapok pulp at 5% pulp consistency (w/w) was refined twice through a disc refiner, using a 1/100 inch disc gap (Andritz Sprout, U.S.A.). Then, refined kapok pulp was disintegrated at 1.5% pulp consistency (w/w) in a standard disintegrator (Formax T-100, Adirondack, U.S.A.) for 50,000 revolutions in hot water (80 °C) to remove latency.

Evaluation of pulp and paper properties

The chemical composition of each pulp was determined using TAPPI Standard Method T222 om-98 for lignin determination, TAPPI Standard Method T203 cm-99 for alpha cellulose (α-cellulose) determination, and Browning's method for holocellulose determination (Browning, 1963). The amount of hemicellulose was calculated from the difference between the holocellulose content and the alpha cellulose content.

Kappa number, an indication of lignin content in the pulp, was analyzed according to TAPPI Standard Method T236 om-99. Kapok pulp drainage was also determined following the Canadian Standard Freeness (CSF) standard, using a freeness tester (CF/A, Regmed, Brazil) according to TAPPI Standard Method T227 om-04. Kapok pulp was also made into 60 g/m^2 handsheets on a Rapid-Köthen sheet former (RK-2A KWT, PTI, Austria) according to the ISO Standard Method 5269-2. The brightness and opacity of the handsheets were measured using an optical tester (Color Touch PC, Technidyne, U.S.A.), based on ISO Standard Methods 2470 and 2471, respectively. The tensile, burst and tear strengths were measured using a tensile strength tester (Strograph E-S, Toyo Seiki, Japan), a burst strength tester (SE002P, Lorentzen & Wettre, Sweden), and a tear strength tester (Protear, Thwing-Albert, U.S.A, according to TAPPI Standard Method T494 om-01, T403 om-02, and T414 om-04, respectively.

Results and discussion

Chemical pretreatment of the fibers

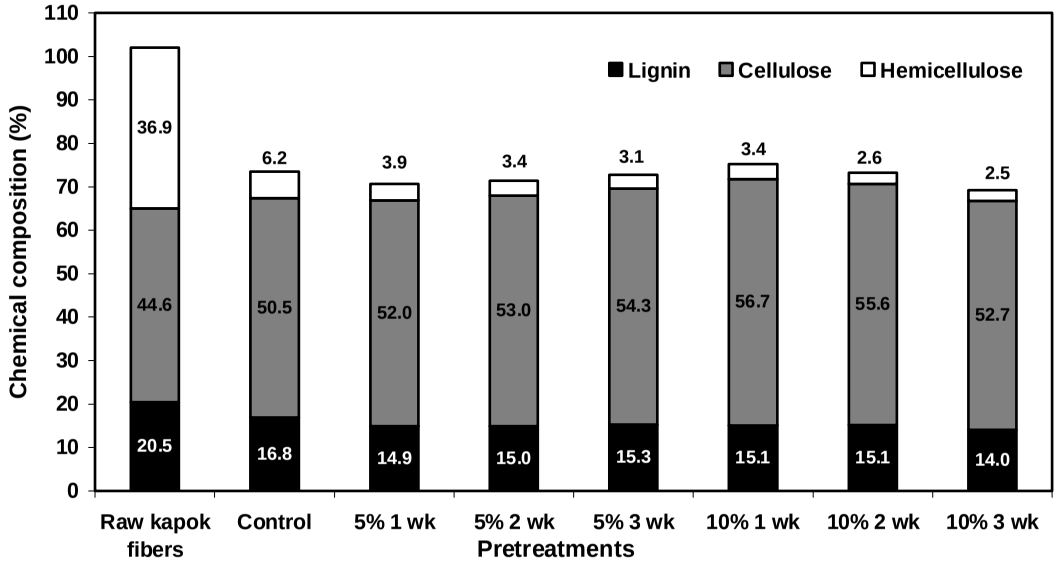

Figure 1. Effects of chemical pretreatment on chemical composition of kapok pulp.

As shown in Figure 1, the analysis of the pulp chemical composition indicated that the alkali pretreated samples had the lower lignin contents than the control pulp since NaOH dissolved the lignin. In addition, NaOH pretreatment was observed to produce a lower hemicellulose content but a higher cellulose content than the control pulp because NaOH partly dissolved the hemicellulose in the pulp leaving the cellulose content mostly intact. It was also noticed that hemicellulose content decreased with the higher dosage and longer alkali pretreatment time. However, cellulose content potentially increased with the higher alkali dosage while the effect of alkali pretreatment time on cellulose content was apparently indistinguishable. The effects of alkali pretreatment dosages and times seemingly have no different impacts on the lignin content of the alkali pretreated pulp except for the extreme case that used the highest alkali dosage with the highest pretreatment time which inevitably provided the lowest lignin content.

Table 1. Effects of chemical pretreatment on pulp yield, residual alkali, and kappa number

Pretreatment condition		Pulp yield (%)	Residual alkali (%)	Kappa number
NaOH dosage (%)	Number of weeks			
0 (Control)	3	76.02 ± 1.79	2.00 ± 0.59	108 ± 2
5	1	73.71 ± 0.06	2.90 ± 0.14	99 ± 2
	2	75.02 ± 2.25	3.50 ± 0.14	98 ± 2
	3	76.00 ± 2.06	3.60 ± 0.28	98 ± 1
10	1	78.20 ± 1.06	4.00 ± 0.00	116 ± 2
	2	76.08 ± 0.41	4.60 ± 0.28	130 ± 3
	3	72.66 ± 7.17	5.80 ± 0.28	132 ± 5

The control experiment as indicated by 0% NaOH dosage was for immersing kapok fibers in tap water for 3 weeks.

The results tabulated in Table 1 indicate that the alkali dosage and pretreatment time used in this study seemed to have a small effect on pulp yield. However, the residual alkali increased with the higher NaOH concentration and longer pretreatment time. The residual alkali levels imply that the alkali consumption during the soda pulping was lower with the alkali pretreated samples than the control. Thus, there was probably less chance for carbohydrate degradation during the pulping leading to the pulp yields comparable to that of the control.

The Kappa numbers of the NaOH pretreated pulp were lower than that of the control pulp only when the lower dosage (5% w/w) of NaOH was used. In contrast, the kappa numbers increased significantly with the higher NaOH pretreatment concentration (10% w/w) and with the longer pretreatment times at this higher dose. Perhaps the presence of cutin interferes with the permanganate oxidation of lignin. At the higher NaOH concentration for the longer pretreatment times, the cutin could be much easier to dissolve during the subsequent soda pulping stage, which might markedly disrupt the permanganate oxidation of lignin.

The results from Table 2 illustrate that the effects of NaOH dosage and pretreatment time on the density were indistinguishable. Opacity typically increased with increasing NaOH dosage and reacting time, the only exception being that seen for the pretreatment with 5% (w/w) alkali for three weeks (Table 2). This might probably cause by the alkali pretreatment which led to the higher fines contents of the pulp and thus could increase light scattering of these handsheets. However, NaOH pretreatment seemed to initially lower the brightness at

the short pretreatment times, and then increase it with the longer treatment times or higher NaOH concentrations. This might be due to the alkali induced darkening effect to render the pulp yellow. Nevertheless, increasing the pretreatment time produced a brighter pulp, which was caused by the result of more wax removed from the fiber surface and so the cooking liquor could penetrate into and react better with more fibers. Thus, more lignin was removed and the pulp became brighter.

Table 2. Effects of chemical pretreatment on density, brightness and opacity

Pretreatment condition		Density (g/m^3)	Brightness (%)	Opacity (%)
NaOH dosage (%)	Number of weeks			
0	3	0.72 ± 0.03	21.3 ± 0.5	81.2 ± 1.0
5	1	0.73 ± 0.05	21.0 ± 0.4	85.8 ± 0.6
	2	0.78 ± 0.04	20.9 ± 0.2	86.1 ± 1.5
	3	0.78 ± 0.05	21.5 ± 0.4	81.2 ± 0.4
10	1	0.72 ± 0.04	20.0 ± 0.5	86.5 ± 1.1
	2	0.79 ± 0.04	21.2 ± 0.5	88.8 ± 1.0
	3	0.76 ± 0.05	22.5 ± 0.5	91.4 ± 0.7

The control experiment as indicated by 0% NaOH dosage was for immersing kapok fibers in water for 3 weeks.

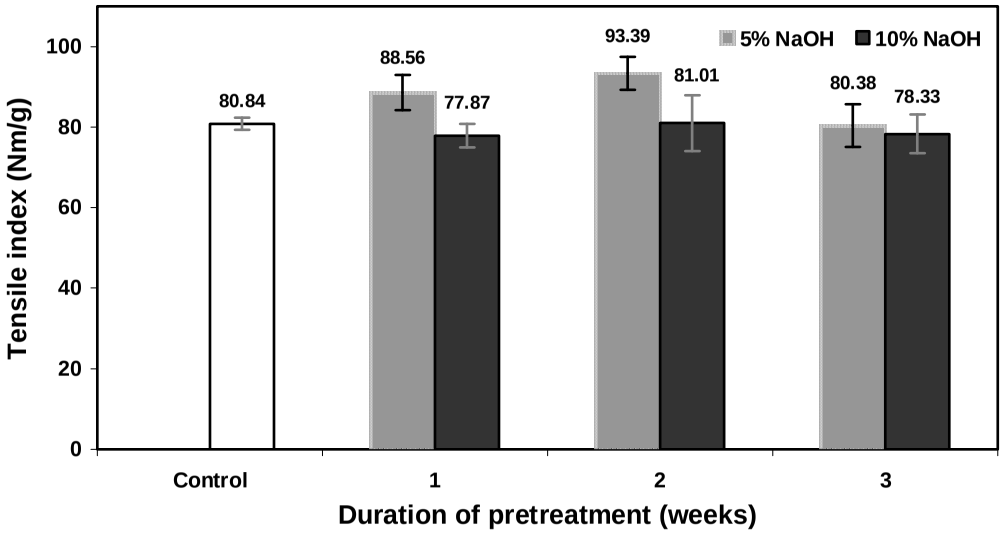

Figure 2. Effects of chemical pretreatment on tensile index.

As shown in Figures 2 and 3, after the pretreatment with the lower concentration of NaOH, the pulp displayed the highest tensile index and burst index, higher than those derived from the control pulp. However, the effects of the NaOH pretreatment time on the tensile index and burst index were somewhat variable but important. The pulp became stronger when it was pretreated with NaOH for two weeks yet three weeks of the pretreatment was detrimental to both the tensile and burst strengths, reducing them to essentially the same level as the control pulp. This could be because NaOH aided in not only removing the fiber surface wax but also attacked the lignin leading to a better fiber bonding in the sheets, at least when pretreated at the optimal NaOH concentration and time. Also, the NaOH led to a higher

cellulose content which might in turn helped increase the fiber strength. However, when too high a NaOH dose was used for a long time, the tensile and burst strengths declined, and this is likely to be due to carbohydrate degradation by the peeling reaction under a strong alkali condition.

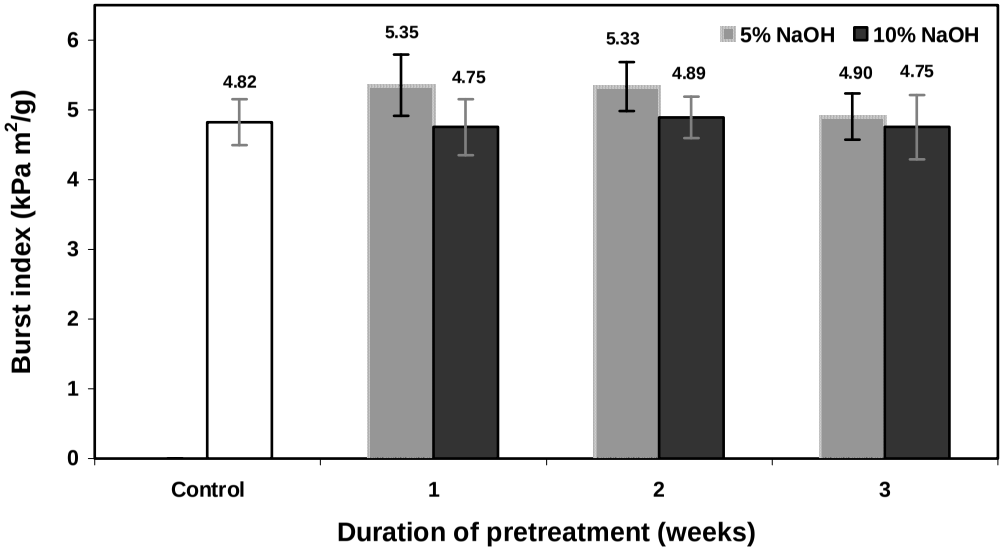

Figure 3. Effects of chemical pretreatment on burst index.

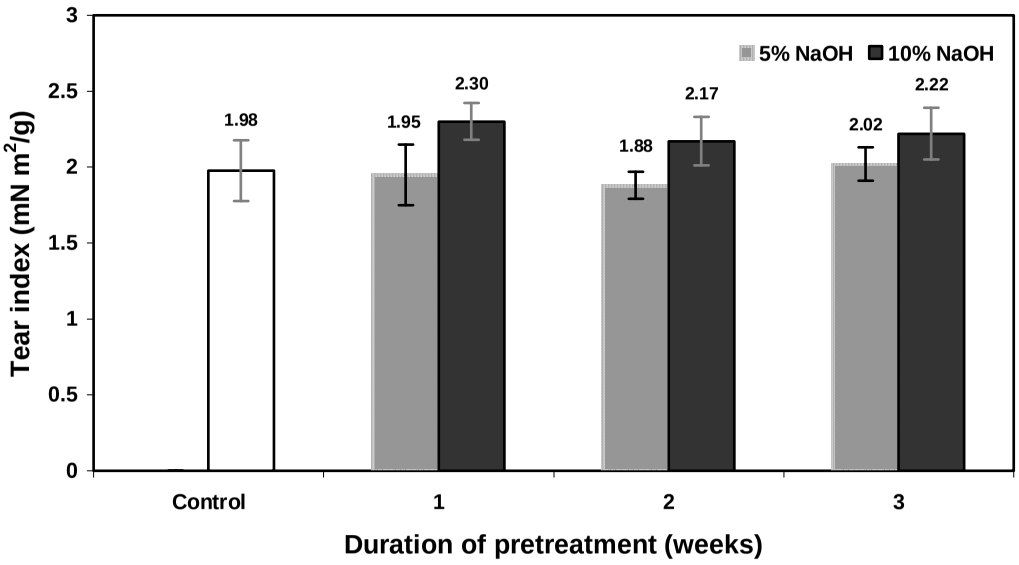

Figure 4. Effects of chemical pretreatment on tear index.

The pulp pretreated with the higher concentration (10% w/w) of NaOH potentially provided a higher tear index (Figure 4), which is opposite to the cases for the tensile and burst indexes. Generally, in contrast to tensile and burst strengths, tear resistance depends mostly on the strength of individual fibers rather than the strength of inter-fiber bonding. The higher NaOH concentration produced pulp with the higher cellulose content but the lower

hemicellulose contents (Figure 1), which might increase the fiber strength and then tear strength of the pulp as a whole.

Based on the overall results, pretreatment of the kapok fibers with NaOH at 5% (w/w) for two weeks was selected as the optimal condition. Under these pretreatment conditions, the kapok pulp provided the highest tensile strength with the lowest kappa number. Burst and tear strengths were acceptable and it also gave a suitable residual alkali level which was in the optimal range for pulping.

Biological pretreatment of the fibers

Pretreatment of the kapok fibers with lipase beneficially resulted in a lower lignin content than that seen in the control pulp, whilst the lignin content was further reduced with the higher lipase dose (Figure 5). Likewise, the hollocellulose contents were lower in pulp pretreated with any lipase dose than that seen in the control, suggesting that the lipase had reacted with the wax at the kapok fiber surface. This might then cause the fiber surface to open more and allow greater access to NaOH during the soda pulping. That the resulting holocellulose and especially alpha cellulose of the lipase pretreated pulps were lower implies that the cellulose was attacked more than was the hemicellulose after the lipase pretreatment. It was also noticed that the effects of the pretreatment time on the chemical composition were more evident only in the case of higher dosage of lipase as indicated by the lower lignin and cellulose contents but the higher hemicellulose content with the longer pretreatment time.

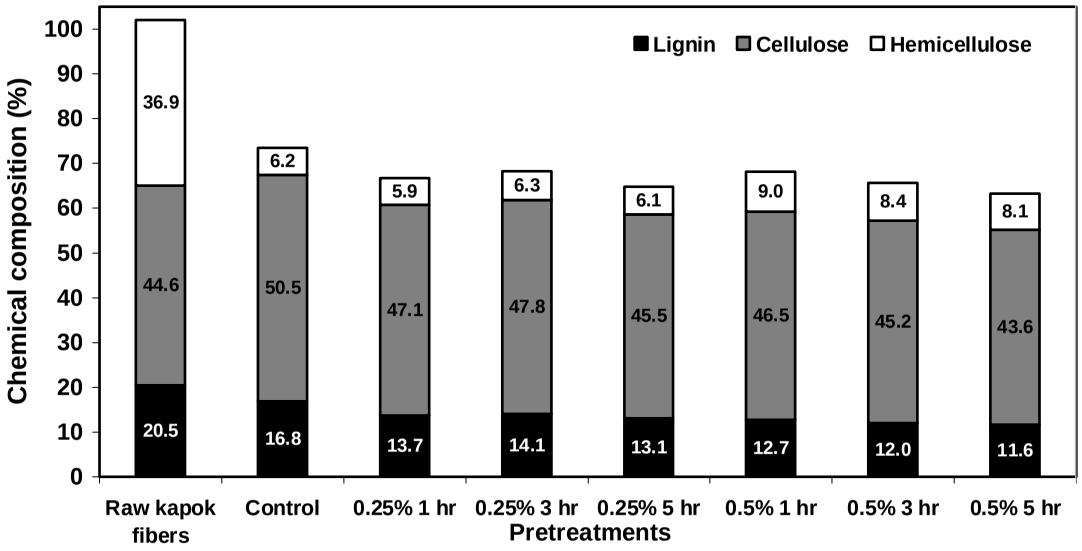

Figure 5. Effects of lipase pretreatment on chemical composition of kapok pulp.

Table 3 reveals that the lipase pretreated pulps gave a lower pulp yield than that of the control pulp, and the yield decreased with a higher enzyme dosage and pretreatment times. The residual alkali content was lower in the lipase-pretreated samples and was minimal after two-hour exposure. This also implied that the alkali consumption during the soda pulping stage was higher following the lipase pretreatment. The lipase pretreated pulp also produced a slightly lower kappa number, compared to that of the control, at the low lipase dose; but at the higher lipase dose, it was lower than the control only after a three-hour exposure. The kappa number and pulp yields obtained indicated that lipase eventually reacted with cutin at

the fiber surface and caused the surface to open for the alkali to react with the kapok fibers more easily in the pulping stage.

It should also be noted that the lipase enzyme pretreated pulp gave a lower pulp yield and residual alkali content than did the NaOH pretreated pulp (Tables 1 and 3). Thus, the enzyme pretreatment provided a better accessibility of the kapok fibers for the NaOH in the pulping reaction than did the NaOH pretreatment.

Table 3. Effects of lipase pretreatment on pulp yield, residual alkali, and kappa number

Pretreatment condition		Pulp yield (%)	Residual alkali (%)	Kappa number
Lipase dosage (%)	Number of hours			
0 (Control)	504	76.02 ± 1.79	2.00 ± 0.59	108 ± 2
0.25	1	70.52 ± 1.04	1.60 ± 0.57	106 ± 0
	3	72.10 ± 0.12	0.80 ± 0.00	105 ± 2
	5	68.73 ± 1.70	1.05 ± 0.07	107 ± 0
0.50	1	71.59 ± 1.70	1.20 ± 0.00	108 ± 3
	3	69.22 ± 1.07	0.90 ± 0.14	108 ± 3
	5	66.92 ± 1.68	1.25 ± 0.07	105 ± 3

The control experiment as indicated by 0% NaOH dosage was for immersing kapok fibers in tap water for 3 weeks

Table 4. Effects of lipase pretreatment on density, brightness and opacity

Pretreatment condition		Density (g/m^3)	Brightness (%)	Opacity (%)
Lipase dosage (%)	Number of hours			
0	504	0.72 ± 0.03	21.3 ± 0.5	81.2 ± 1.0
0.25	1	0.68 ± 0.03	22.7 ± 0.7	87.7 ± 1.1
	3	0.67 ± 0.04	22.2 ± 0.7	87.1 ± 1.2
	5	0.71 ± 0.02	22.8 ± 0.7	88.3 ± 1.4
0.50	1	0.65 ± 0.02	22.2 ± 0.8	88.9 ± 1.3
	3	0.70 ± 0.03	23.0 ± 0.7	87.6 ± 1.3
	5	0.70 ± 0.03	22.3 ± 0.6	85.4 ± 1.9

The control experiment as indicated by 0% NaOH dosage was for immersing kapok fibers in tap water for 3 weeks

Lipase pretreatment hardly impacted sheet density but provided the pulp with a higher brightness and opacity as compared to the control pulp (Table 4). Higher brightness of lipase pretreated pulp was caused by a higher level of lignin removal while higher opacity might probably be caused by higher fines contents which then increased the light scattering coefficients of these handsheets. This might implied that lipase pretreatment improved accessibility of the kapok fibers for NaOH in pulping reaction. However, the effects of enzyme dosage and treatment time on density, brightness and opacity seemed to be very small.

When comparing the effects of the lipase pretreatment on the density, brightness and opacity to those of the NaOH pretreatment, it was found that both pretreatments provided

essentially the same effects on the density and opacity, but the lipase pretreatment potentially produced a higher brightness level.

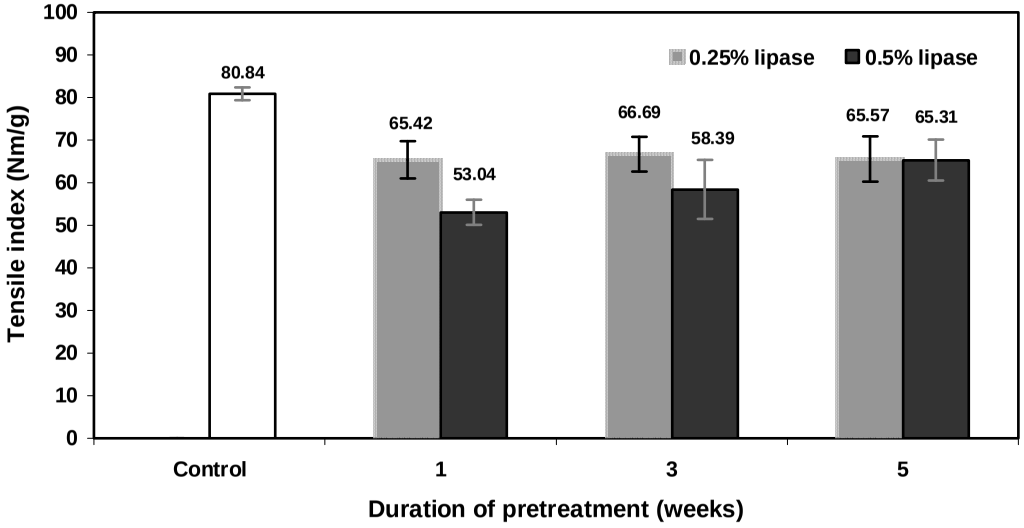

Figure 6. Effects of lipase pretreatment time on tensile index.

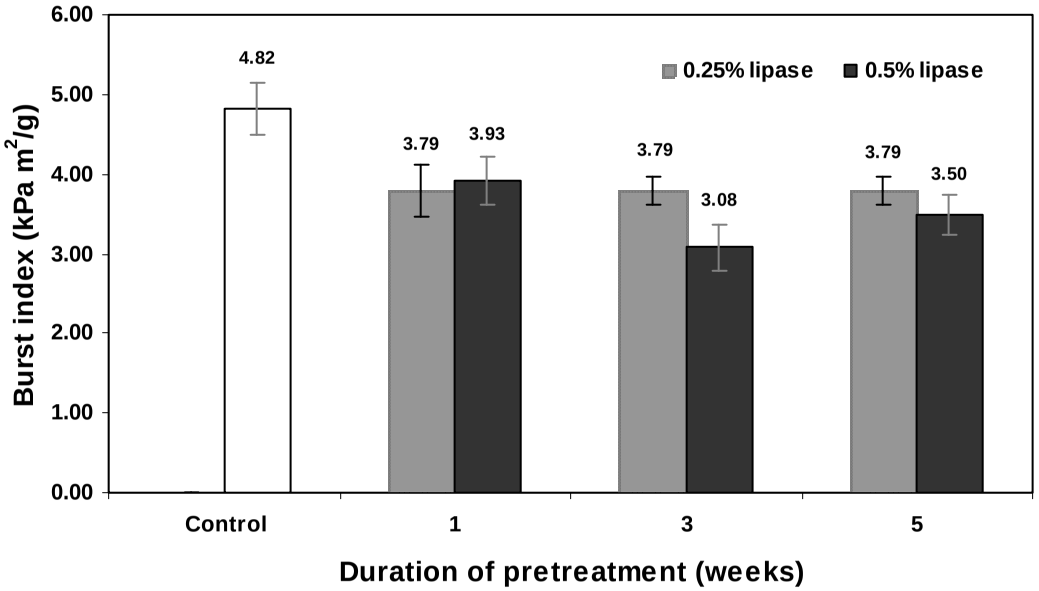

Figure 7. Effects of lipase pretreatment time on burst index.

The tensile and burst strengths of all lipase pretreated pulp were lower than those of the control pulp (Figures 6 and 7). This could be because the cellulose content was lower whilst the hemicellulose content was higher for the lipase pretreated pulp (Figure 5). Thus, the individual fiber strength of the enzyme pretreated pulp might be diminished due to the lower cellulose content and this might decrease the tensile and burst indexes. It should also be noted that these tensile and burst strength of lipase pretreated pulp typically decreased with pretreatment at the higher lipase dose, while effects of the longest enzyme treatment time on the tensile and burst index.

The lipase pretreated pulp gave lower tensile and burst strengths than that of the NaOH pretreated pulp (Figures 2 and 3 compared to Figures 6 and 7), which emphasizes that the enzyme pretreatment could provide a better accessibility of the NaOH into the kapok fibers in the pulping stage than did the NaOH pretreatment.

Unlike the tensile and burst indexes, the tear index of the lipase pretreated pulp was surprisingly higher than that of the control pulp, and this was more markedly at the higher lipase dose, although the preincubation time at both lipase doses seemed irrelevant (Figure 8).

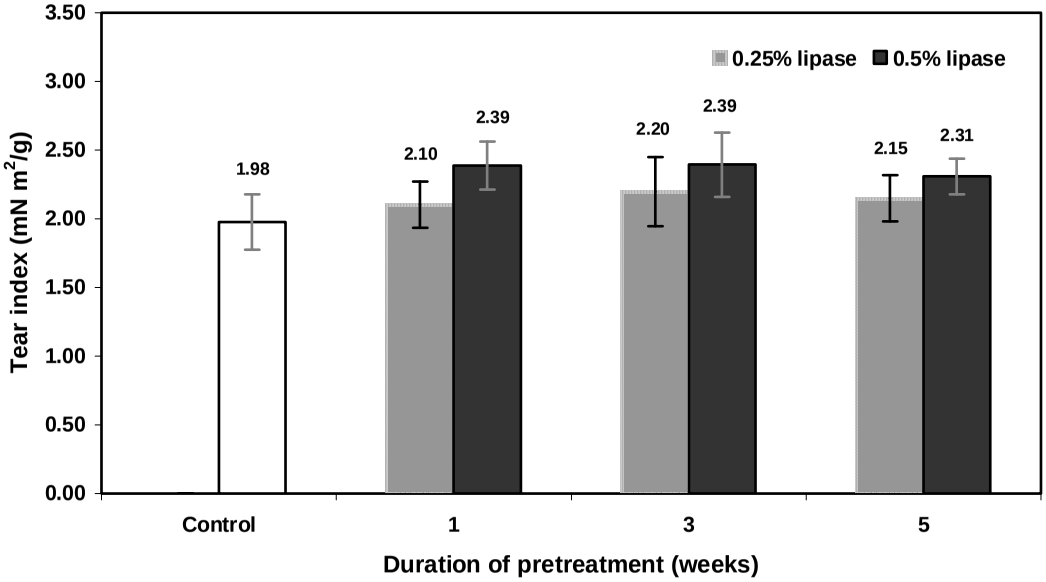

Figure 8. Effects of lipase pretreatment on tear index.

Based on the overall results, the biological pretreatment with a lipase dosage of 0.25% (w/w), based on the O.D. fiber weight, for three hours was selected as the optimal condition, since at this condition the kapok pulp provided the highest tensile strength and pulp yield with the lowest kappa number and residual alkali content.

Overall comparison between the chemical and biological pretreatments

Based on the results obtained from both the NaOH and lipase pretreatments in comparison with respective control pulp, the pulp and paper properties obtained at the optimal conditions for each of the pretreatments are summarized in Table 5. The optimal conditions for the alkali pretreatment was NaOH at 5% (w/w) based on the O.D. fiber weight for two weeks, whilst those for the lipase pretreatment was a lipase dose at 0.25% (w/w) based on O.D. fiber weight, for three hours.

The benefits of both chemical and biological pretreatments are the lower kappa number and higher opacity obtained compared to that of the control pulp. Perhaps the pretreated kapok pulp has more opened structures and more fines content which could lead to the higher light scattering and opacity.

The advantages of using the alkali pretreatment are better tensile and burst indexes. The residual alkali content of the chemical pretreatment was also higher than that of the control and lipase enzyme pretreated pulps, which implied that the alkali content in the pulping reaction can be decreased in future work. The lower kappa number also indicated that the cooking liquor could penetrate through the kapok fibers and react with a greater proportion of the total number of reaction sites.

The advantages of utilizing the lipase pretreatment were the lower kappa number with the higher tear index, brightness and opacity. Finally, it was recommended that mechanical or physical parameters such as a proper mixing and suitable reaction temperature for the lipase enzyme, which were not evaluated and optimized here, might be selectively employed for the biological pretreatment in order to increase the rate of enzyme reaction at the kapok fiber surface.

Table 5. Comparison of the control, alkali (chemical) and lipase (biological) pretreatments of kapok fibers

Pulp and paper properties	Control	NaOH pretreatment	Lipase pretreatment
Lignin (%)	16.8 ± 0.3	15.0 ± 0.2	14.1 ± 0.2
Cellulose (%)	50.5 ± 0.0	53.0 ± 0.2	47.8 ± 1.0
Hemicellulose (%)	6.2 ± 0.2	3.4 ± 0.0	6.3 ± 0.9
Pulp yield (%)	76.02 ± 1.79	75.02 ± 2.25	72.10 ± 0.12
Residual alkali (%)	2.00 ± 0.59	3.50 ± 0.14	0.80 ± 0.00
Kappa number	108 ± 2	98 ± 2	105 ± 2
Tensile index (N m/g)	80.8 ± 1.5	93.4 ± 4.1	66.7 ± 4.0
Burst index (kPa m^2/g)	4.82 ± 0.33	5.33 ± 0.35	3.79 ± 0.18
Tear index (mN m^2/g)	1.98 ± 0.20	1.88 ± 0.09	2.20 ± 0.25
Density (g/m^3)	0.72 ± 0.03	0.78 ± 0.04	0.67 ± 0.04
Brightness (%)	21.3 ± 0.5	20.9 ± 0.2	22.2 ± 0.7
Opacity (%)	81.2 ± 1.0	86.1 ± 1.5	87.1 ± 1.2

The control experiment as indicated by 0% NaOH dosage was for immersing kapok fibers in water for 3 weeks

Conclusions

Chemical (NaOH) and biological (lipase enzymatic) pretreatment of kapok fibers were shown to be beneficial to the soda pulping of kapok fibers, because the immersing time and NaOH consumption could be reduced. The pretreated pulp also had a lower kappa number and higher opacity. The chemical pretreatment with NaOH should be employed when increases in tensile and burst index are demanded, whilst the biological pretreatment with lipase is more attractive when the tear resistance of sheets is desired. Combining both chemical and biological pretreatments is also supposition since both treatments can provide beneficially synergistic effects to the soda pulping of kapok fibers.

Acknowledgements

This research is fully financially supported by the Research Team Aided Grant from the Thailand Research Fund and the Commission of Higher Education under the Contract number RTA5080004. Some research facilities provided by the Product and Technology Development Center of Siam Cement Group Paper Company Limited are also gratefully appreciated.

References

Apirakchaiskul, A., "The Use of Kapok Fiber to Improve Strength of Paper", M.S. Thesis, Department of Imaging and Printing Technology, Faculty of Science, Chulalongkorn University, 2008.

Scott, G.M., Akhtar, M., Lentz, M.J., Kirk, T.K., and Swaney, R., "New Technology for Papermaking: Commercializing Biopulping", TAPPI Journal, 81(11), 1998, 220-225.

Zhang, W., Okubayashi, S., and Bechtoid, T., "Fibrillation Tendency of Cellulosic Fibers-Part 3. Effects of Alkali Pretreatment of Lyocell Fiber", Carbohydrate Polymers, 59(2), 2005, 173-179.

Browning, B. L. (1963). *Methods in Wood Chemistry*, Interscience Publishers, New York.

Comments to Archan Somporn: More corrections are needed. Suda

Draft Manuscript

Colloids and Surfaces A: Physicochemicals and Engineering Aspects

Manuscript Number:

Title: Microencapsulation of menthol by crosslinked chitosan via porous glass membrane emulsification technique and their controlled release properties

Article Type: Research Paper

Keywords: Microcapsules; chitosan; menthol; SPG membrane emulsification; encapsulation

Abstract: Chitosan encapsulated menthol microcapsules were successfully prepared by the oil-in-water emulsion process using Shirasu porous glass (SPG) membrane emulsification technique. The SPG membrane with a membrane pore size of 5.2 μm was found to be suitable for a high viscosity dispersion phase containing light mineral oil. The effect of operating pressure, the amount of menthol loading and crosslinking time on the size and size distribution of microcapsules were systemically investigated. The size of the menthol-loaded chitosan microcapsules was strongly dependent on the mean pore size of the SPG membrane and the amount of menthol loading in the dispersion phase. The average diameter of emulsion droplets of 28.3 μm with a coefficient of variation of 24.7% was obtained. Increasing the menthol loading in the dispersion phase from 5 to 10 wt% of chitosan decreased the emulsion droplets with a broad droplet size distribution. The crosslinked microcapsule size and size distribution of the o/w emulsion droplets decreased with increasing crosslinking time. The mechanism of menthol release was a diffusion control which depended on the proportion of amino group in chitosan-to-tripolyphosphate and crosslinking time.

Microencapsulation of menthol by crosslinked chitosan via porous glass membrane emulsification technique and their controlled release properties

Roongkan Nuisin[a)], Jaruwan Krongsin[b)], Supaporn Noppakundilograt[c)], Suda Kiatkamjornwong[c)*]

[a)] Department of Environmental Science, Faculty of Science, Chulalongkorn University, Bangkok 10330, Thailand

[b)] Multidisciplinary Program of Petrochemistry and Polymer Science, Faculty of Science, Chulalongkorn University, Bangkok 10330, Thailand

[c)] Department of Imaging and Printing Technology, Faculty of Science, Chulalongkorn University, Bangkok 10330, Thailand

Short running title: Microencapsulation of menthol by crosslinked chitosan via porous glass membrane

[*]Corresponding author

Suda Kiatkamjornwong
Address: Department of Imaging and Printing Technology, Faculty of Science, Chulalongkorn University, Bangkok 10330, Thailand
Telephone: +66-02-218-5587
E-mail: ksuda@Chula.ac.th

Abstract

Chitosan encapsulated menthol microcapsules were successfully prepared by the oil-in-water emulsion process using Shirasu porous glass (SPG) membrane emulsification technique. The SPG membrane with a membrane pore size of 5.2 μm was found to be suitable for a high viscosity dispersion phase containing light mineral oil. The effect of operation pressure, the amount of menthol loading and crosslinking time on the size and size distribution of microcapsules were systemically investigated. The size of the menthol-loaded chitosan microcapsules was strongly dependent on the mean pore size of the SPG membrane and the amount of menthol loading in the dispersion phase. The average diameter of emulsion droplets of 28.3 μm with a coefficient of variation of 24.7% was obtained. Increasing the menthol loading in the dispersion phase from 5 to 10 wt% of chitosan decreased the emulsion droplets with a broad droplet size distribution. The size and size distribution of o/w crosslinked microcapsules decreased with increasing crosslinking time.

Keywords: Microcapsules; chitosan; menthol; SPG membrane emulsification; homogenizing

1. Introduction

Menthol is a cyclic terpene alcohol with three asymmetric carbon atoms. Among the optical isomers, menthol is the one that occurs most widely in nature and it is endowed with the peculiar property to be a fragrance and flavor compound. For this reason, it is widely used as flavoring for toothpaste, oral hygiene and personal care products [1]. Menthol is generally available in the form of crystals or granules with a melting point of 41–43°C. However, its high volatility and whisker growth are the very important problems concerning its applications and shelf life. The microencapsulation method is an accountable and appropriate technique to solve these problems [2]. Chitosan is derivatized by deacetylation of chitin. Chitosan has been used in many applications because of its biocompatibility, biodegradability, non-toxicity and antibacterial activity [3]. Chitosan can form microcapsules by various methods such as spray drying, emulsification/solvent evaporation, ionotropic gelation, coacervation techniques, and so on. It can prevent loss of volatile flavors, and enhance stability of the flavor core materials [2]. The capsule is kept stable during the release time. However, the size of the microcapsules prepared by these methods is difficult to control, and the size distribution is thus very broad [4].

In conventional emulsification devices, such as high-pressure homogenizer, mechanical stirring, and rotor-stator systems, these methods produce rather polydisperse emulsions and consume high energy [5]. A membrane emulsification system produces emulsions by permeating a dispersed phase into a continuous phase through a membrane having a uniform pore diameter. The membrane emulsification method makes it possible to produce monodisperse emulsions and consume less energy [6, 7]. The most commonly used microporous membrane for the emulsification is a Shirasu Porous Glass (SPG) membrane. The SPG membrane is made from SiO_2–Al_2O_3, with a very narrow pore size distribution. It was fabricated by Nakashima and Shimizu [8] via a series of sophisticated heat treatments,

an induced phase separation created a bi-continuous structure of $CaO\text{-}B_2O_3$, and $SiO_2–Al_2O_3$. Commercially, the pore sizes ranging from 0.1 to 18.0 μm have been available. The SPG membrane is inherently hydrophilic and it is much easier to get the monodisperse oil-in-water (o/w) emulsions than water-in-oil emulsion (w/o) due to the presence of negatively charged silanol groups on the surface [9]. Kiatkamjornwong et al. [10] had successfully prepared the microcapsules of chitosan (0.5–40 μm in diameter) by the conventional stirring method in which chitosan is the shell of microcapsules encapsulating the core material of menthol. The size distribution of the conventional method is rather polydisperse and thus a better technique of porous glass membrane emulsification can remedy the large size distribution to a narrow size distribution of microcapsules.

In this study, the SPG membrane emulsification method was applied to prepare menthol-loaded sodium tripolyphosphate crosslinked chitosan microcapsules. The effects of membrane pore size, the amount of menthol loading and crosslinking time were investigated on the microcapsule size and size distribution. Release kinetics of menthol from microcapsules correspondence to crosslinking time, concentration, and molar ratio of amino and tripolyphosphate were studied.

2. Experimental

2.1 Materials

Chitosan (Sea fresh Chitosan Lab Co., Ltd., Bangkok, Thailand) with a degree of deacetylation of 95% with a viscosity-average molecular weight ($\overline{M}_v$) of 100,000 g/ mol was used as received. Sodium tripolyphosphate (TPP, Merck, Hohenbrunn, Germany) was used as a crosslinker. Light mineral oil (Hopewell International Co., Ltd., Thailand) was used as an oil phase. Menthol with a molecular weight of 156.27 g/mol (Hong Huat Co., Ltd., Thailand) was used as an encapsulating material. Poly(oxyethylene-2-stearyl ether) (Brij 72,

Greensville Co., Ltd., Thailand) was used as an oil-soluble surfactant. Sodium dodecyl sulfate (SDS, Merck, Germany) and cetyl stearyl alcohol (Kao Co., Ltd., Thailand) were used as a surfactant and a co-surfactant, respectively. Poly(vinyl alcohol), PVA-220, (Kuraray Co., Ltd., Japan) with 87-89% of hydrolysis degree was used as a stabilizer.

2.2 Apparatus

A miniature kit for emulsification with an SPG module was purchased from Kiyomoto Co., Ltd (Japan). A tubular porous glass membrane with the size of 2 cm length and 1 cm diameter was installed in the module. The dispersed phase (oil phase) was stored in a Teflon vessel (20 ml) which was connected to nitrogen gas inlet, the continuous phase (water phase) containing a mixture of SDS and PVA in a 250-ml beaker was stirred at 300 rpm with a magnetic bar to prevent creaming of the droplets. With an optimum pressure of nitrogen gas, the dispersed phase can permeate through the uniform pores of the membrane into the continuous phase to form droplets. The droplets were then stabilized by the PVA and SDS dissolved in the continuous phase.

2.3 Preparation of chitosan microcapsules

The procedures of preparing oil-in-water emulsion of chitosan/menthol microcapsules were manufactured as follows: continuous phase was composed of 50.0 g of deionized water, 0.05 g of sodium dodecyl sulfate, then pour 1w/v% chitosan solution in acetic acid 1v/v%. Oil phase consist of 5.0 g of mineral oil, the solution were then mix using high speed homogenizer at 6000, 10000, 14000 and 16000 rpm for 30-120 minutes. The mixture was continuous stirred at 400 rpm to prevent the coagulation.

2.3.1Preparation of chitosan microcapsules via SPG emulsification

The SPG membrane with an average pore size of 1.4 and 5.2 μm was used for the emulsification. The preparative condition for the emulsification is shown in Table 1. The

SPG membrane was pre-wetted in the aqueous phase. Menthol was dissolved in a mixture of light mineral oil, surfactant and co-surfactant by heating up to 40-43°C and was used as a dispersed phase. The aqueous phase where PVA and SDS had been dissolved was used as a continuous phase. The oil phase permeated through the uniform pores of the SPG membrane by the pressure of nitrogen gas into the aqueous phase to form the o/w emulsion. Sodium tripolyphosphate (TPP) solution was slowly dropped into the o/w emulsion to crosslink the chitosan droplets by stirring at 200 rpm for 1 to 5 h. Finally, the chitosan microcapsules were collected and washed repeatedly two times with petroleum ether and acetone by centrifugation at 3000 rpm, and then the microcapsules were freeze dried. A pressure used was slightly above the critical pressure. In this study, the ranges of the permeation pressures at 48.9 to 88.8 kPa for the 1.4 μm pore size, and 14.1 to 67.0 kPa for the 5.2 μm membrane pore size were used.

Insert Table 1

2.3.2 Preparation of chitosan microcapsules via double emulsion methods

Primary and secondary emulsions in a ratio of 1:1 were mixed and stirred in mild condition of 200 rpm for 1 hr. Sodium tripolyphosphate (TPP) with various concentration of 1, 5, 10, and 15% was dropped into the mixture as crosslinkng agent. Varying amount of amino group of chitosan to TPP of 2:1, 4:1, 6:1, and 8:1, the mixtures were then stirred at 400 rpm using different time interval of 30, 60, 90, and 120 minutes. The pH was adjusted to 3, 5, 7, and 9 using acetic acid and sodium hydroxide solution. A simple flowchart for the preparation of chitosan microcapsules by the double emulsion is shown in Fig. 1.

Insert Figure 1

2.4. Characterization of chitosan microcapsules

2.4.1. Measurement of size distribution of the droplets

Droplets before and after the crosslinking were observed with an optical microscope. Diameters of approximately 150 droplets were measured to calculate the average diameter. The number average diameter ($\overline{d_e}$) was calculated according to eq. (1). The coefficient of variation (CV) was determined using the formula in eq. (2).

$$\bar{d}_e = \Sigma_{i=1}^{n} d_i / N \quad (1)$$

$$CV = \left(\sum_{i=1}^{n} \frac{(d_i - \bar{d}_e)^2}{N} \right)^{1/2} \Big/ \bar{d}_e \quad (2)$$

where, d_i is the diameter of each droplet, N is total number of the droplets measured, and $\overline{d_e}$ is the number average diameter of the droplets.

2.4.2 Observation of morphology of the microparticles

Morphology of the emulsion microparticles was observed using an optical microscope (model BH2, Olympus Optical Co., Ltd, Tokyo, Japan).

2.4.3 Controlled release study

The 5 ml of prepared chitosan microcapsules were transferred to 15 ml test tube and centrifuged at 3000 rpm for 30 minutes. The creamy layer was separated from aqueous layer, and then transferred to vacuum oven at 30°C for 12 hr. The encapsulation efficiency was calculated as shown in eq.3. Release profiles were calculated in term menthol release (%) with time as shown in eq. 4. All samples were assayed in triplicate for 60 hr.

$$\text{Encapsulation efficiency} = \frac{W_m - W_0}{W_m} \times 100 \quad (3)$$

$$\text{Release } (\psi) = \left[\frac{W_m - W_m(t)}{W_m - W_0} \right] \times 100 \quad (4)$$

where, W_m is the weight of dried microcapsule after vapor evaporation, $W_{(t)}$ is the weight of microcapsules in a 40°C oven at time t (hr). The samples were weight at different time interval of 1, 3, 5, 7, 12, 24, 48, and 60 hr. The W_o is the weight of microcapsules after menthol evaporated in a 120°C [11, 12].

2.5 Release kinetic studies of menthol from microcapsules

The release profile of menthol from chitosan microcapsules was studied using the release (%) calculated from eq. 4. The release data of microcapsules were analyzed following mathematical models: Zero-order kinetic; first-order kinetic; Higuchi equation (square-root of time equation) [13]; Baker-Lonsdale equation; Hixson-Crowell; and Ritger-Peppas equation [14], as shown in Table 2. Linear regression value has been used for calculation the correlation coefficient (R^2) in order to predict the release behavior from microcapsules.

Insert Table 2

3. Results and discussion

3.1. Effect of the pore size of membrane on the droplet size and size distribution

The SPG membranes with the average pore diameter of 1.4, and 5.2 μm were used to prepare the o/w emulsion. The uniform emulsion droplets were prepared, and the average diameter ($\overline{d_e}$) of 10.2 and 19.6 μm for the membrane pore sizes of 1.4 and 5.2 μm obtained. It was found that the diameter of droplets in the o/w emulsion was approximately 8 and 4 times the diameters of membrane pore. The dispersed phase containing light mineral oil without menthol as an additive was difficult to permeate through the SPG membrane pore size of 1.4 μm. The possible cause was occurred from the high viscosity of light mineral oil. Furthermore, due to the high molecular weight of PVA stabilizer used, the PVA molecules were covered onto the membrane surface and plugged the pores, the oil phase was thus

retained and could not be permeated. As a resulted, the SPG membrane pore size of 5.2 μm was used for further studied.

3.2. Effect of the amount of menthol loading on droplet size and size distribution

The menthol dissolved in the dispersed phase affected the o/w emulsion. The permeation pressure decreased from 7.4 kPa to 2.5 kPa and 0.6 kPa when increasing the amount of menthol from 0 to 5 and 10 wt%, respectively. The hydrophilic in the disperse phase increased with increasing the amount of menthol loading in disperse phase. The hydroxyl group of menthol enhances the hydrophilicity of the oil phase, thus to permeate it easily through the hydrophilic pore wall of the SPG membrane. The permeation pressure was then decreased. Optical micrographs and the histogram of size distribution of the droplets in oil phase at different amounts of menthol loadings are shown in Fig. 2. Without the menthol, an average diameter of emulsion droplets of 28.3 μm with the CV of 24.7% was obtained. When the amounts of menthol loading in the disperse phase increased from 5 to 10 wt%, the average diameters of emulsion droplets decreased from 24.2 to 16.8 μm with the CV of the droplets increased from 34.4 to 57.6%. The size distributions expressed as histograms in Figure 2 a-c) indicate that more menthol loading in the dispersed phase produced the smaller size droplets in the range of 10 μm. This effect is caused by the increases in hydrophilicity of the hydroxyl groups when increasing the menthol loadings.

Insert Fig. 2

Insert Fig.2a, Fig 2b, Fig 2c

3.3. Effect of crosslinking time on the size and size distribution

Chitosan as the shell of o/w emulsion droplets was crosslinked with TPP solution. TPP was dissociated into OH^- and $P_3O_{10}^{5-}$ anions. The positively charged amino group of chitosan reacted with $P_3O_{10}^{5-}$ anions to form crosslinking bonds [15]. The crosslinked microcapsule

sizes of the o/w emulsion droplets decreased from 47.4 to 27.6 μm with increasing crosslinking time (Fig. 3) due to the increase of crosslink density of chitosan-TPP matrix [16]. The less crosslinking time of 1 h could not form the small droplet size for the subsequence process in this research. Very interestingly, the longer crosslinking time gave the narrow size distribution.

Insert Fig. 3

3.4Preparation of microcapsules via conventional homogenizing method

The preparation of o/w emulsion with narrow size distribution by SPG emulsification technique is that the o/w emulsion should be stable with a narrow emulsion droplets size distribution. Since, the oil phase composed of chitosan with different amount of menthol, a hydrophilic properties was reviewed. Therefore, it is necessary to find a condition where a large amount of chitosan can be maintained and performed microcapsules. The ultrasonic homogenizer was used with high homogenizing rate. The effects of homogenizing speed, time, and chitosan concentration were studied.

3.4.1 Effect of homogenizing speed

Chitosan microcapsules with broad coefficient of variation of 55.9% were obtained using the lower homogenizing speed of 6000 rpm. Increasing the homogenizing speed from 14000 to 16000 rpm, the microcapsules with CV of 38.9 and 39.7%, were obtained, respectively. However, the homogenizing speed at 10000 rpm was found the lowest CV% of 31.5. The phase separation of emulsion was observed at the beginning of emulsification process approximately within 1 hr after the homogenizing process. As shown in Table 3, the homogenizing speed of 10000 rpm was selected for further study since the emulsion droplets in size of 39.1±12.3 μm.

Insert Table 3

3.4.2 Effect of homogenizing time

Chitosan microcapsules was prepared and used as a secondary emulsion for combination with a primary emulsion obtained via SPG emulsification process. The homogenizing speed of homogenizer was used at 10000 rpm. The effect of homogenizing time of 30, 60, 90, and 120 second were studied. As shown in Table 4, the emulsion droplets with coefficient of variation of 30.8 and 34.8% were obtained with homogenizing time of 30 and 60 second, respectively. The broad droplets size distribution was reviewed comparison with using the homogenizing time of 60 and 120 second. The coefficient of variation of 24.8 and 24.6% was calculated. The short period of homogenizing time, the droplets disruption with less stability occurred. The micelles formation was unstable. The oil droplets distribution related to the stirring time that affected to the micelles of oils in water phase was reviewed [10]. An increasing in stirring time from 90 to 120 minute, an emulsion droplets size was increased from 39.8±9.9 to 41.2±10.1 μm. The stirring time of 90 second were then selected for further studies.

Insert Table 4

3.4.3 Effect of chitosan concentration

Preparation of chitosan microcapsules was prepared with various concentration of chitosan in acetic acid solution. As shown in Table 5, the amount of chitosan was varied from 1, 1.5, and 2.0 w/v% of acetic acid. It was found that the emulsion droplets of chitosan in size of 17.9±8.1, 17.0±6.3, and 16.7±6.9 μm was obtained, respectively. The 1.5 w/v% chitosan solution in acetic acid was considered as a suitable concentration for further experiment since the viscosity is concerned for emulsification processing [17].

Insert Table 5

3.5 Preparation of menthol encapsulated chitosan microcapsule

Menthol encapsulated microcapsules was prepared via double emulsion method. The emulsions from SPG emulsification using SPG membrane pore size of 5.2 μm as a primary, and high-speed homogenizer at 14,000 rpm for 90 minutes as secondary emulsion was prepared. The miscibility of two emulsions was studied in terms of size and encapsulation efficiency. In this experiment, the primary emulsion of 24.2±8.3 μm was mild stirred with secondary emulsion of 17.0±6.3 μm, and left for 1 hr. The emulsion droplets in size of 31.0±8.5 μm was obtained and the narrow coefficient of variation observed as shown in Table 6. It was found that the small size of secondary emulsion was diffused and absorbed into the primary emulsion, the swelling droplets obtained with narrow size distribution. The mechanism is followed the non-destructive swelling [18]. Since, the less thermodynamics stability of secondary emulsion tend to migrate to the more stable droplets of primary emulsions, the absorption were then occurred.

Insert Table 6

3.5.1 Effect of pH on size and size distribution of microcapsules

The effects of pH adjusted solution onto size and size distribution of swollen microcapsules was studied. The pH in ranges of 5 to 7 was preferred for the use of microcapsules in further application as an additive in leave-on conditioners. The pH values of 3.6, 5.0, 7.0, and 8.9 were studied. As shown in Fig. 4, the droplets size of microcapsules tend to decreased with increasing coefficient of variation at pH of 3.6 (Figure 4a, and 4b). The affects of microcapsules degradation may results from the non-crosslinked chitosan molecules dissolved from microcapsule at low pH. The pH of 5.0, 7.0, and 8.9 in emulsions were adjusted using sodium hydroxide. The menthol encapsulated chitosan microcapsules in size of 26.8, 28.6, and 28.0 μm were obtained, respectively. The narrow emulsion size

distribution as increasing pH was reviewed. The coefficient of variation of 20.6, 23.7, and 30% was calculated. Then, the workable pH for microcapsules in further uses was considered in ranges of 5 to 7.

Insert Figure 4a

Insert Figure 4b

3.6 Efficiency of encapsulation and controlled release of menthol from microcapsule

The efficiency of encapsulation and controlled release of menthol from microcapsules were studied as follows:

3.6.1 Effects of crosslinking time

Menthol encapsulated chitosan microcapsules were prepared via double emulsion, 5 w/w% sodium tripolyphosphate (TPP) as crosslinking agent. The crosslinking time was varied for 30, 60, 90, and 120 min. The encapsulation efficiency profiles of microcapsules were graphically presented in Figure 5. The results revealed that the menthol encapsulated in chitosan microcapsules was increased with increasing crosslinked time. The order of menthol encapsulated in microcapsules was 9.9±0.1, 35.6±0.1, 35.5±1.0 and 36.1±0.3% when the crosslinking time of 30, 60, 90 and 120 min, respectively. The encapsulation pattern indicated that the menthol was released and controlled by the thickness of microcapsule wall. The ionic interaction between a negatively charged counterion of tripolyphosphate and a positively charged amino group of chitosan was an important role on degree of crosslinking [16]. Encapsulation efficiency of menthol in microcapsules was retained when the longer period of crosslinking time was applied. The release of menthol was very slow which could be due to the thickness of chitosan wall. Figure 6 shows release behavior of menthol from chitosan microcapsules prepared with TPP solution as ionic crosslinking agent at various crosslinking times.

Insert Fig. 5

Insert Fig. 6

3.6.2 Effects of crosslinking concentrations

Figure 7 shows release behavior of menthol from chitosan microcapsules prepared with tripolyphosphate solution at various concentrations. As previously described, the amount of crosslinking agent influenced the ionic-crosslinking density of TPP-chitosan. As shown in Figure 7, the encapsulation efficiency of menthol was improved by the increasing amount of TPP concentration. The amount of TPP solution of 1, 5, 10, and 15 w/w% was applied, the encapsulation efficiency values of 14.8±7.8, 36.1±0.3, 38.1±1.7 and 37.7±3.3% were obtained. The higher the amounts of TPP is, the thicker the microcapsule walls became. Figure 8 shows the effect of the TPP as the crosslinking agent on the release behavior of menthol. There was a release 95% of menthol at 60 hr in 1 w/w% TPP-chitosan microcapsules. The amount of TPP of 5, 10, and 15 w/w%, the amount of menthol releasing from microcapsules were 46.1±1.5, 43.8±2.3, and 38.3±2.5, respectively. The higher concentration of TPP, the lower amount of menthol released from chitosan microcapsules. It depends on the crosslinking density of TPP-chitosan.

Insert Fig. 7

Insert Fig. 8

3.6.3 Effects of molar ratio of amino group in chitosan to tripolyphosphate

Encapsulation efficiency increases with increasing the molar ratio of amino group in chitosan to TPP, as shown in Figure 9. The effects of molar ratio of amino group in chitosan to tripolyphosphate of 2:1, 4:1, 6:1, and 8:1 to encapsulated efficiency of menthol was carried out. Chitosan microcapsules with encapsulated efficiency of 47.5±3.5, 52.7±0.5, 67.0±1.5 and 69.2±1.3% was obtained, respectively. In Figure 10, the comparative releasing

profile of menthol from chitosan microcapsules decreased with increasing amount of molar ration of amino group to TPP. The menthol diffusion was reduced after 12 hours. It was found that the amount of menthol releasing of 34.0±2.0, 22.9±2.9, 18.4±2.9 and 16.2±2.8% obtained when the molar ratio of amino group-to-TPP of 2:1, 4:1, 6:1, and 8:1, respectively. The slope of releasing profiles for all molar ratio of amino and tripolyphosphate increased at the initial stage and declined after 60 hr. From the graph, the release rate of menthol could find slows down when the molar ratio of amino and tripolyphosphate increases. The chitosan wall membrane almost completely seals up when increasing degree of crosslinked.

Insert Fig. 9

Insert Fig. 10

3.7 Release kinetics studies of menthol from microcapsules

The release kinetics of menthol from various conditions based upon crosslinking time, crosslink concentration, and molar ratio of amino and tripolyphosphate was determined by comparing their respective co-relation coefficients. Various models and equations of zero order, first order, Higuchi, Hixson-Crowell, Baker-Lonsdale, and Ritger-Peppas [19, 20] have been used after linearization to predict mechanisms of menthol release. Ritger-Peppas plots were found to be the highest linearity with correlation coefficient greater than that of the other kinetics as shown in Fig. 11a-c. The results indicating that the menthol release mechanism from these chitosan microcapsules was diffusion controlled with diffusion index (n) calculated from slope. In Table 7, the n values revealed that the releasing menthol was found from spherical capsules. The diffusion index n was ≤ 0.43, which indicates a Fickian diffusion, and $0.43 \leq n \leq 1.00$ indicates a non-Fickian [19]. The value of "n" in Ritger-Peppas is approximately 0.5, which implies that the menthol follows non-Fickian transport.

The resulted demonstrated that the transportation of menthol was controlled by crosslink density [21]. The crosslinking density increases, the value of *n* was increased.

Insert Fig. 11

Insert Table 7

4. Conclusion

Chitosan as the wall membrane material, menthol as volatile core material microcapsules were prepared using high speed homogenizer and SPG membrane emulsification techniques. The effects of membrane pore size, the amount of menthol loadings and crosslinking time were affected to size and size distribution of droplets. The uniform-sized chitosan microcapsules can also be prepared when the membrane pore size used was 5.2 μm; the higher amount of menthol gave the smaller mean diameter of the emulsion droplets with narrow size distribution. The longer crosslinking time, the smaller microcapsules with a narrow size distribution was produced. The emulsion droplets with average size of 31.0±8.5 μm and coefficient of variation of 27.4% were obtained. The suitable pH for microcapsules stability was found at pH in range of 5 to 7. To control release of menthol by changing manufacturing conditions of crosslinking time, amount of tripolyphosphate, and molar ratio of amino group in chitosan to tripolyphosphate were studied. The resulted indicated that encapsulation efficiency and release properties of menthol were depended on the crosslinking time, amount of tripolyphosphate, and molar ratio of amino group to tripolyphosphate. The menthol release curve shows an exponential release normally at a higher rate in the beginning. Non-Fickian diffusion was described behavior of menthol release from microcapsules. The diffusion patterns were found to be dependent on the crosslinking density.

Acknowledgements

The authors thank the Thailand Research Fund for funding the research under the Senior Scholarly Consolidation Grant no. RTA5080004. Research facilities from the Department of Imaging and Printing Technology are highly appreciated.

References

[1] N. Galeotti, L. Di Cesare Mannelli, G. Mazzanti, A. Bartolini, C. Ghelardini, Menthol: a natural analgesic compound. Neurosci. Lett. 322 (2002) 145–148.

[2] A. Soottitantawat, K. Takayama, K. Okamura, D. Muranaka, H. Yoshii, T. Furuta, M. Ohkawara, P. Linko, Microencapsulation of l-menthol by spray drying and its release characteristics. Innovat. Food Sci. Emerg. Tech. 6 (2005) 163–170.

[3] M. Rinaudo, Chitin and chitosan: Properties and applications. Prog. Polym. Sci. 31 (2006) 603–632.

[4] W. Wei, L.Y. Wang, L. Yuan, X.D. Yang, Z.G. Su, G.H. Ma, Bioprocess of uniform-sized crosslinked chitosan microspheres in rats following oral administration. Eur. J. Pharm. Biopharm. 69 (2008) 878–886.

[5] G.T. Vladisavljevic, H. Schubert, Preparation and analysis of oil-in-water emulsions with a narrow droplet size distribution using Shirasu-porous-glass (SPG) membranes. Desalination 144 (2002) 167–l72.

[6] M. Yasuno, M. Nakajima, S. Iwamoto, T. Maruyama, S. Sugiura, I. Kobayashi, A. Shono, K. Satoh, Visualization and characterization of SPG membrane emulsification. J. Membr. Sci. 210 (2002) 29–37.

[7] S.M. Joscelyne, G. Trägårdh, Membrane emulsification – a literature review. J. Membr, Sci. 169 (2000), 107–117.

[8] T. Nakashima, M. Shimizu, Porous glass from calcium alumino boro-silicate glass. Ceramics 21 (1986), 408.

[9] G.T. Vladisavljevic, I. Kobayashi, M. Nakajima, R.A. Williams, M. Shimizu, T. Nakashima, Shirasu Porous Glass membrane emulsification: Characterization of membrane structure by high-resolution X-ray microtomography and microscopic observation of droplet formation in real time. J. Membr. Sci. 302 (2007) 243–253.

[10] S. Kiatkamjornwong, S. Phansomboon, V. Hoven, Chitosan microencapsulation of menthol and its controlled release, The Journal of the Royal Institute of Thailand 34 (2009) 337–371.

[11] C.P. Chang, T.K. Leung, S.M. Lin, C.C. Hsu, Release properties on gelatin-gum Arabic microcapsules containing camphor oil with added polystyrene. Colloids Surf. B Biointerfaces 50 (2006) 136–140.

[12] W.C. Hsieh, C.P. Chang, Y.L. Gao, Controlled release properties of chitosan encapsulated volatile citronella oil microcapsules by thermal treatments. Colloids Surf. B Biointerfaces 53 (2006) 209–214.

[13] T. Higuchi, Mechanism of sustained-action medication. Theoritical analysis of rate of release of solid drugs disperse in solid matrices. J. Pharm. Sci. 52 (1963) 1145–1149.

[14] R.W. Korsmeyer, R. Gurny, E. Doelker, P. Buri, N.A. Peppas, Mechanisms of solute release from porous hydrophilic polymers. Inter. J. Pharm. 15 (1983) 25–35.

[15] F.M. Hsieh, C. Huang, T.F. Lin, Y.M. Chen, J.C. Lin, Study of sodium Tripolyphosphate-crosslinked chitosan beads entrapped with *Pseudomonas putida* for phenol degradation, Process Biochem. 43 (2008) 83–92.

[16] J.A. Ko, H.J. Park, S.J. Hwang, J.B. Park, J.S. Lee, Preparation and characterization of chitosan microparticles intended for controlled drug delivery. Inter. J. Pharm. 249 (2002) 165–174.

[17] L.Y. Wang, G.H. Ma, Z.G. Su, Preparation of uniform sized chitosan microspheres by membrane emulsification technique and application as a carrier of protein drug. J. Control. Release 106 (2005) 62–75.

[18] G.H. Ma, M. Nagai, S. Omi, Synthesis of uniform microspheres with higher content of 2-hydroxyethyl methacrylate by employing SPG emulsification Technique followed by swelling process of droplets. J. Appl. Polym. Sci. 66 (1997) 1325–1341.

[19] P.L. Ritger, N.A. Peppas, A simple equation for description of solute release I. Fickian and non-Fickian release from non-swellable devices in the form of slabs, spheres, cylinders or discs. J. Control. Release 5 (1987) 23–36.

[20] K. Shi, Y. Jiang, M. Zhang, Y. Wang, F. Cui, Tocopheryl succinate-based lipid nanospheres for paclitaxel delivery: Preparation, characters, and in vitro release kinetics. Drug Delivery 17(1) (2010) 1–10.

[21] R.V. Kulkarni, B.S. Mangond, S. Mutalik, B. Sa, Interpenetrating polymer network microcapsules of gellan gum and egg albumin entrapped with diltiazem–resin complex for controlled release application. Carbohydr. Polym. 83 (2011) 1001–1007.

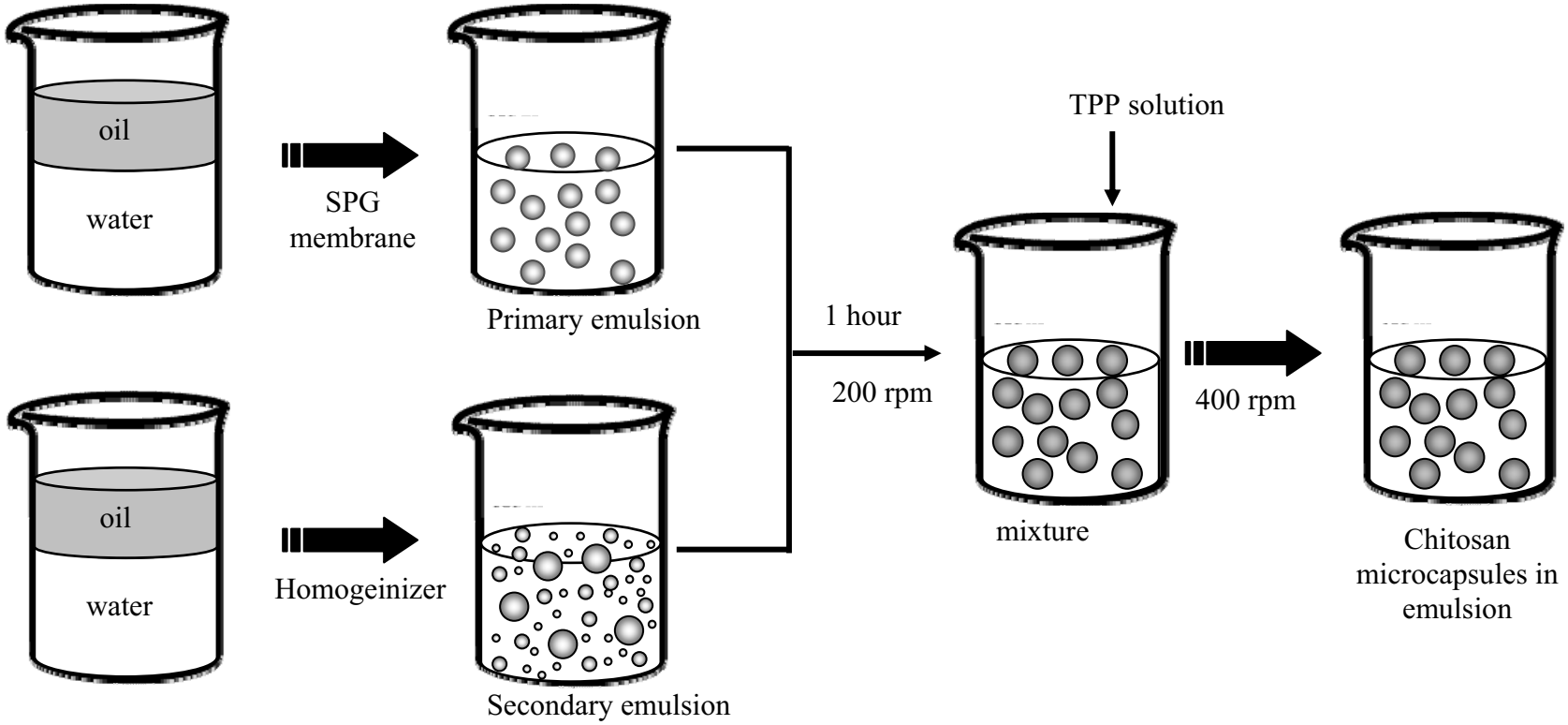

Figure 1 Flowchart for preparation of chitosan microcapsules by double emulsification

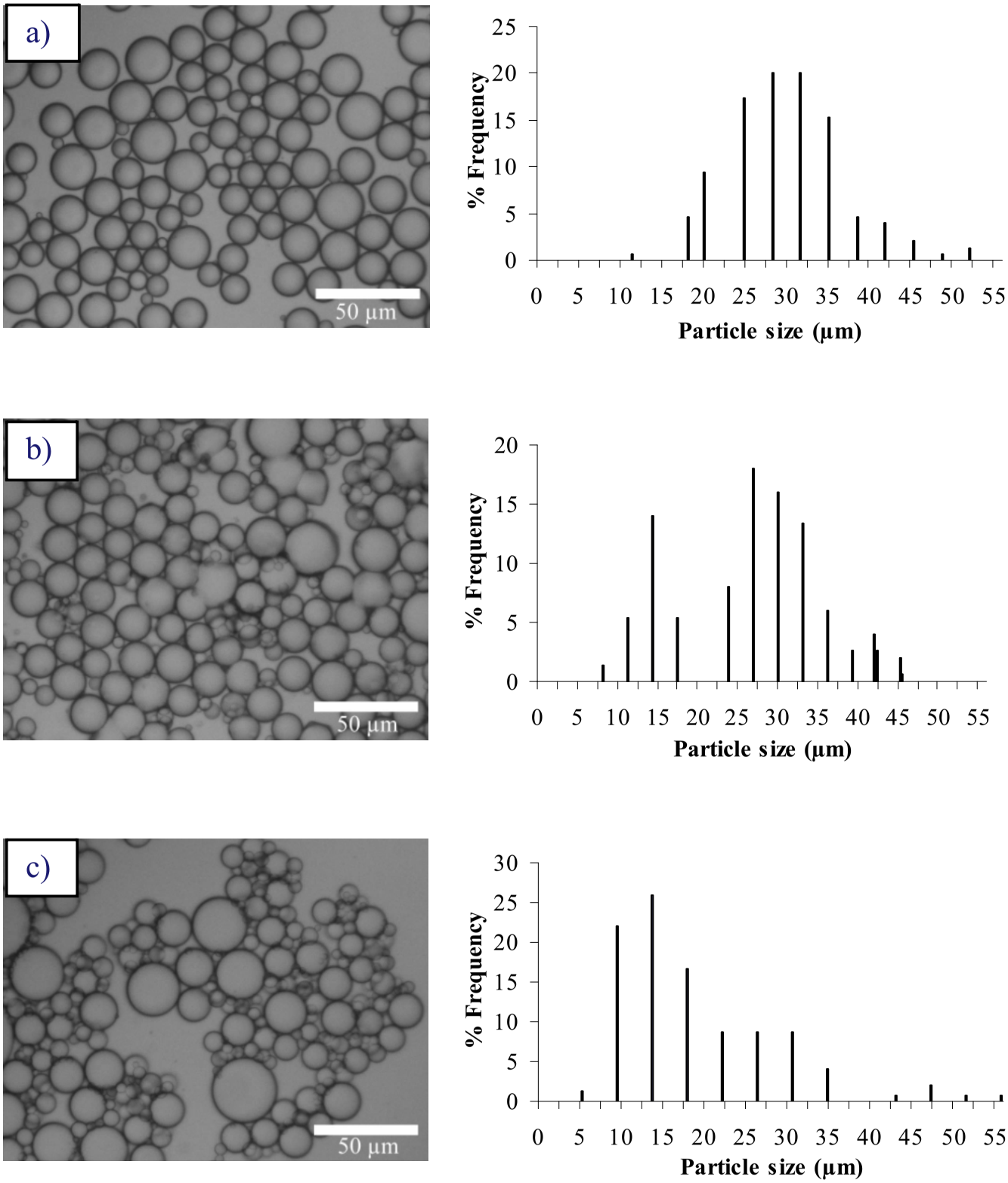

Figure 2 Optical micrographs (left) and histograms of the size distribution (right) of o/w emulsion with different amounts of menthol loadings for a) without menthol, b) 5 wt% menthol, c) 10 wt% menthol

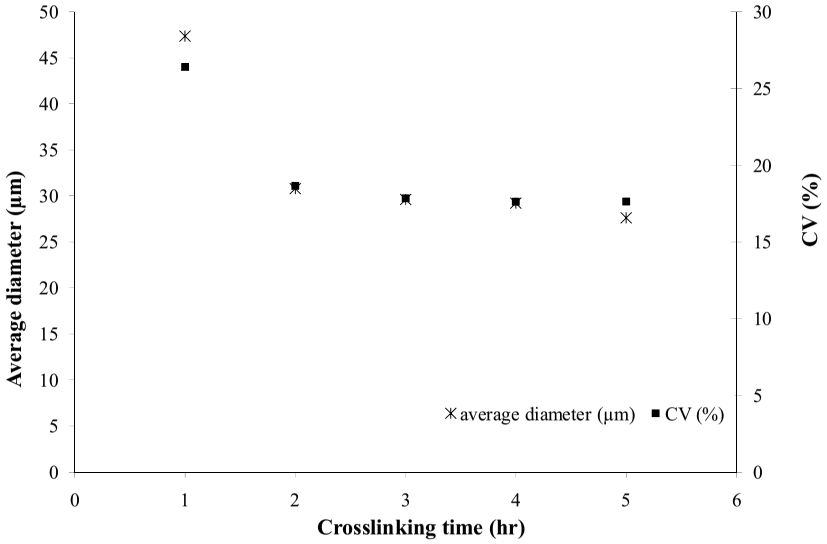

Figure 3 Relationship between the crosslinking time, the average size and the coefficient of variation

a) size

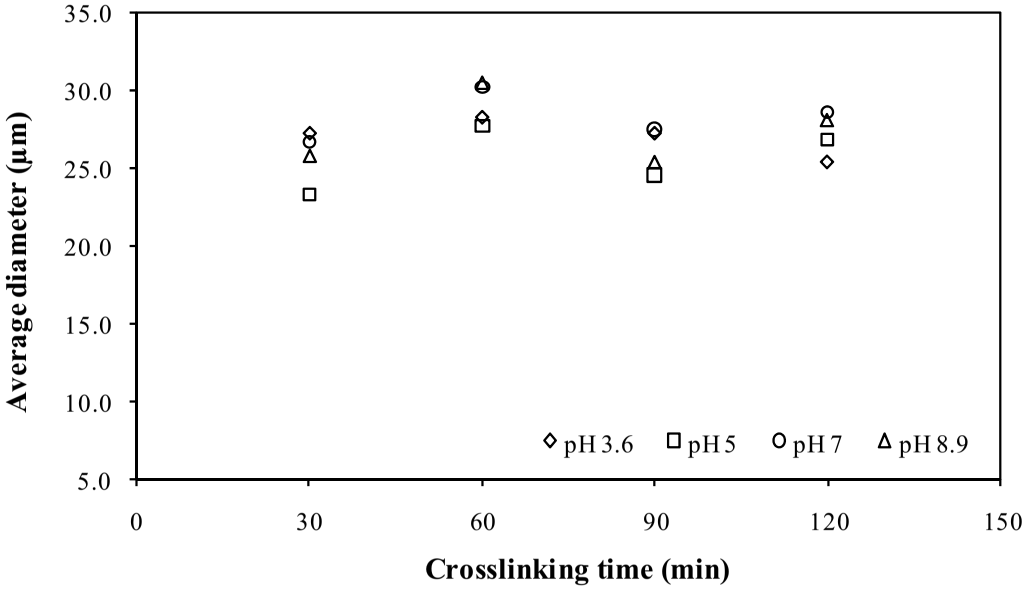

Figure 4 Relationship of microcapsules with different pHs: a) size, b) coefficient of variation

b) coefficient of variation

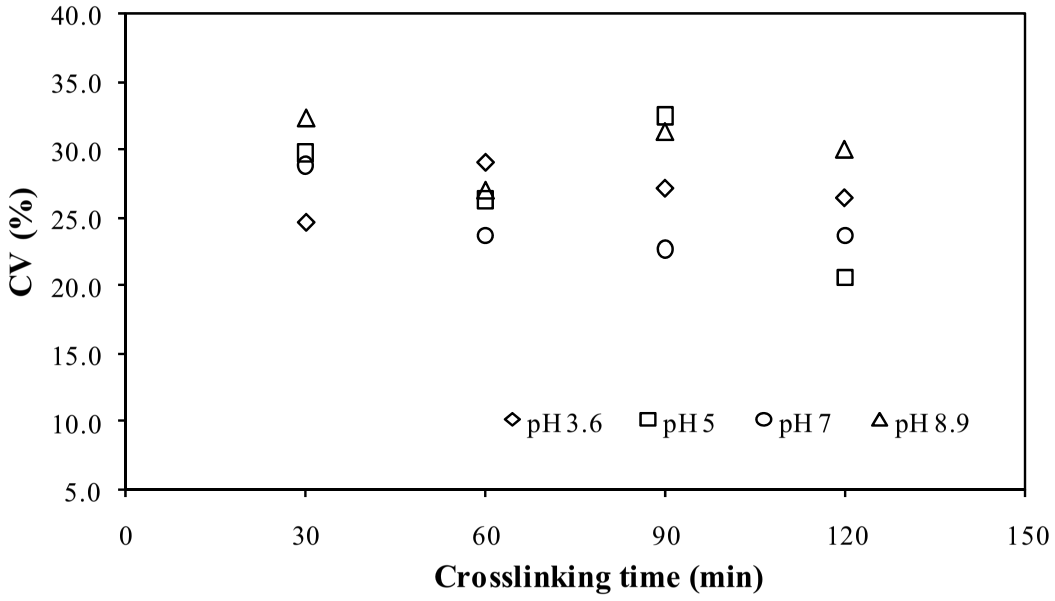

Figure 4 Coefficient of variation Vs. crosslinking time at various pHs

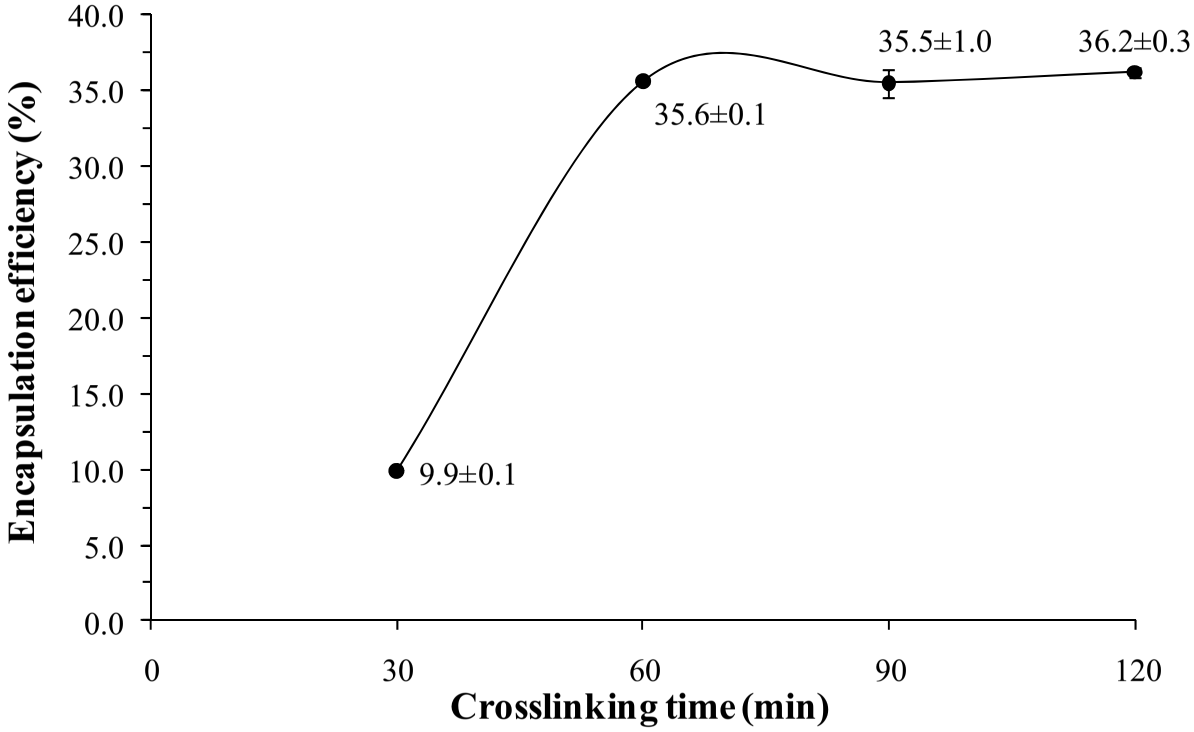

Figure 5 Encapsulation efficiency curves of menthol at 72 hr with various crosslinking times with 5w/w% of TPP, and molar ratio of amino group in chitosan to TPP of 1:1.

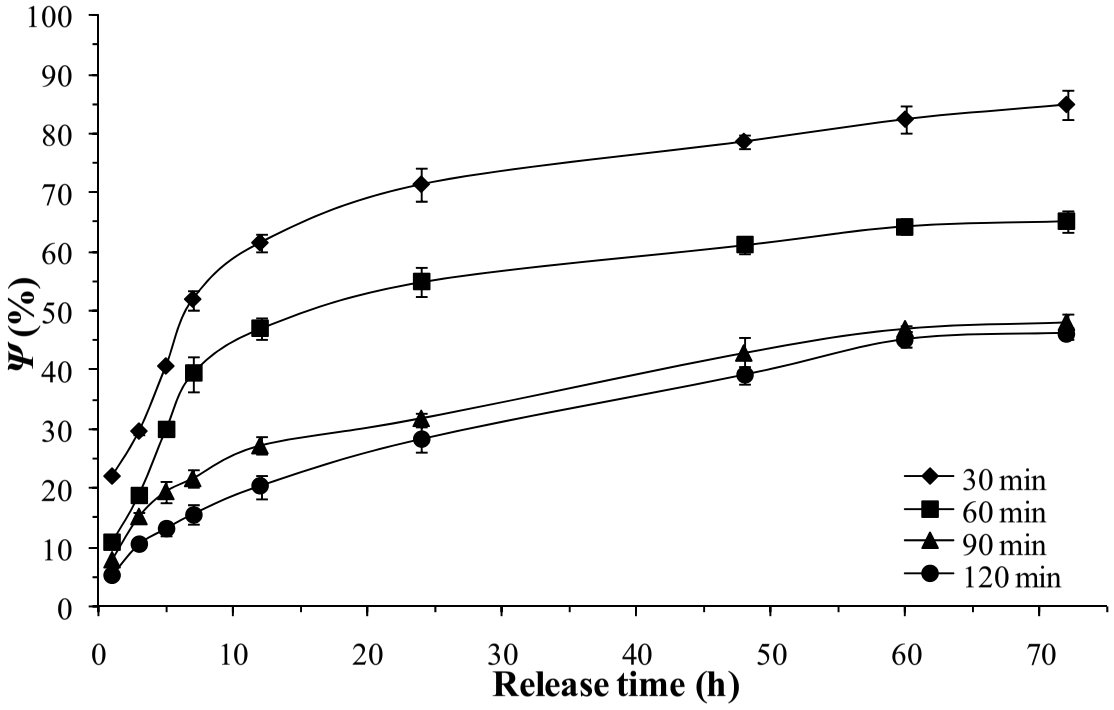

Figure 6 Comparative curves of menthol at 72-hr release, the chitosan amino group-to-TPP mole ratio of 1:1 at various crosslinking times

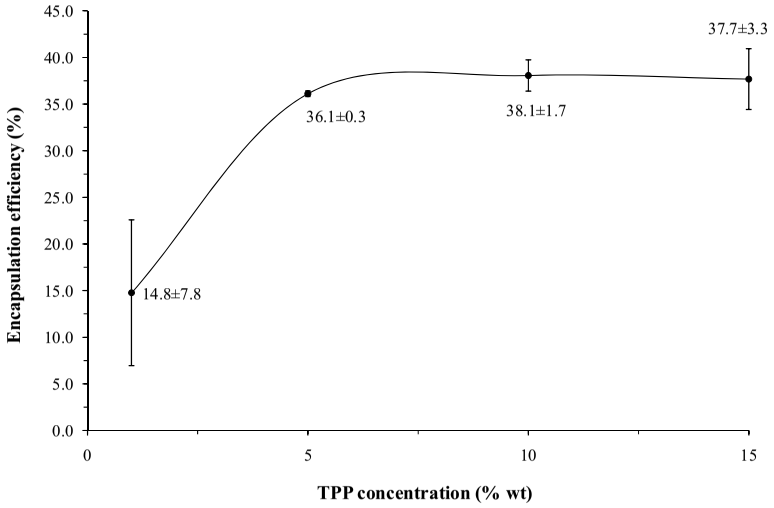

Figure 7 Menthol releasing curve at 72 hr with various TPP concentrations

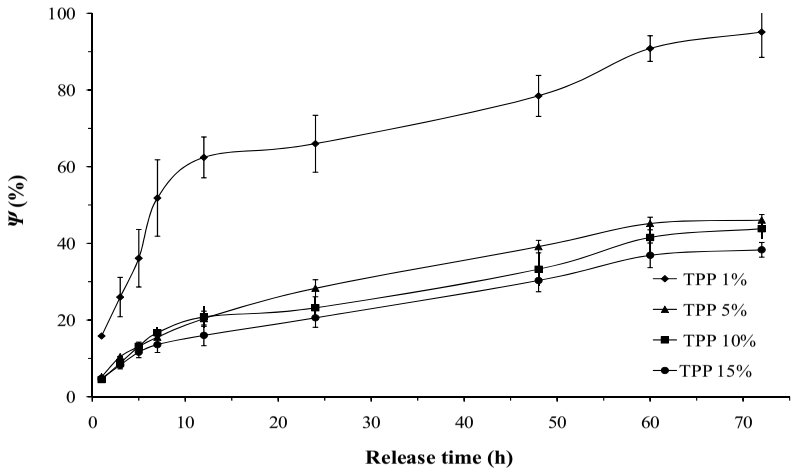

Figure 8 Menthol release curves as a function of TPP concentrations at the crosslinking time of 120 min.

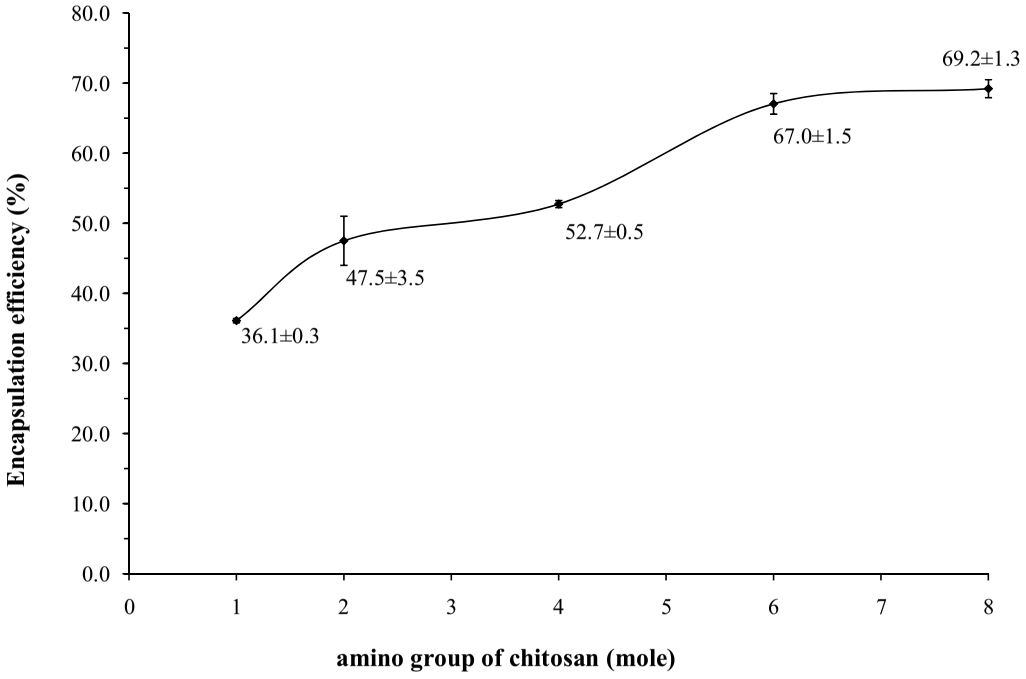

Figure 9 Encapsulation efficiency curve of menthol at 72 hr at various molar ratios of amino group in chitosan, 5 w/w% TPP at a crosslinking time at 120 min.

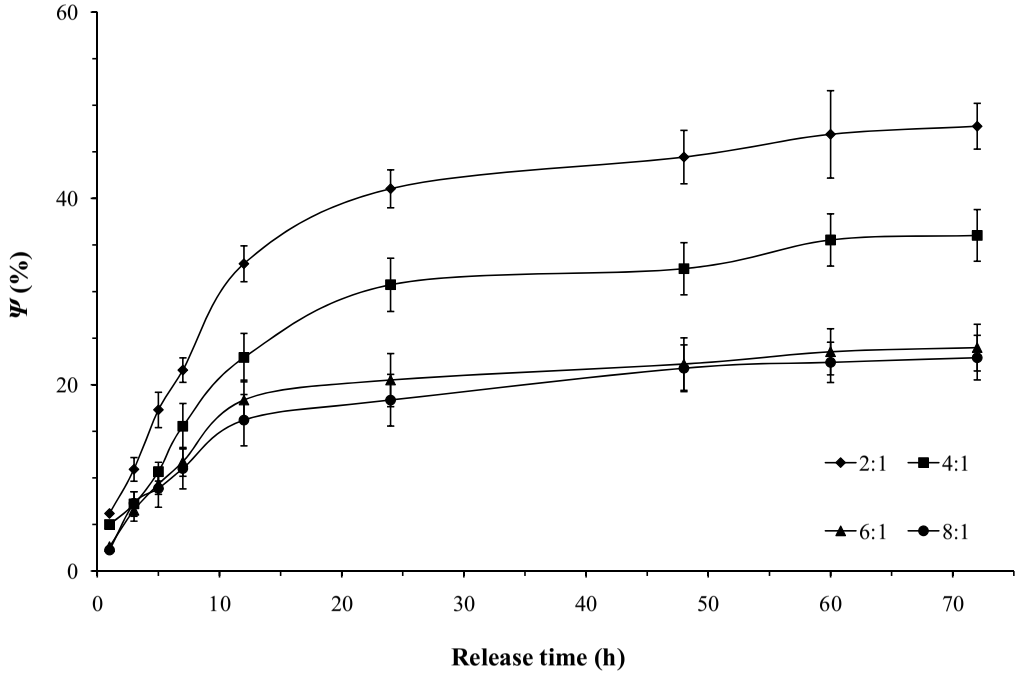

Figure 10 Effect of release time at the function of molar ratios of amino group in chitosan to TPP with 120 min crosslinking time

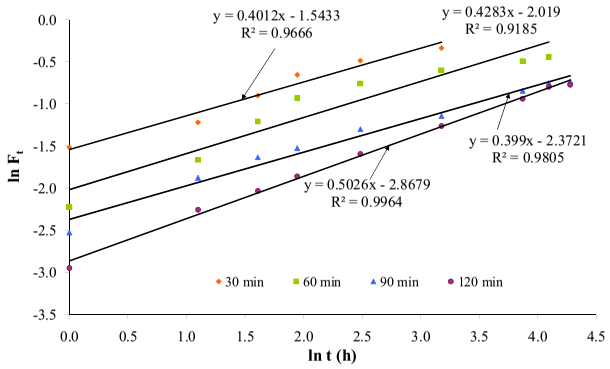

a) crosslinking time

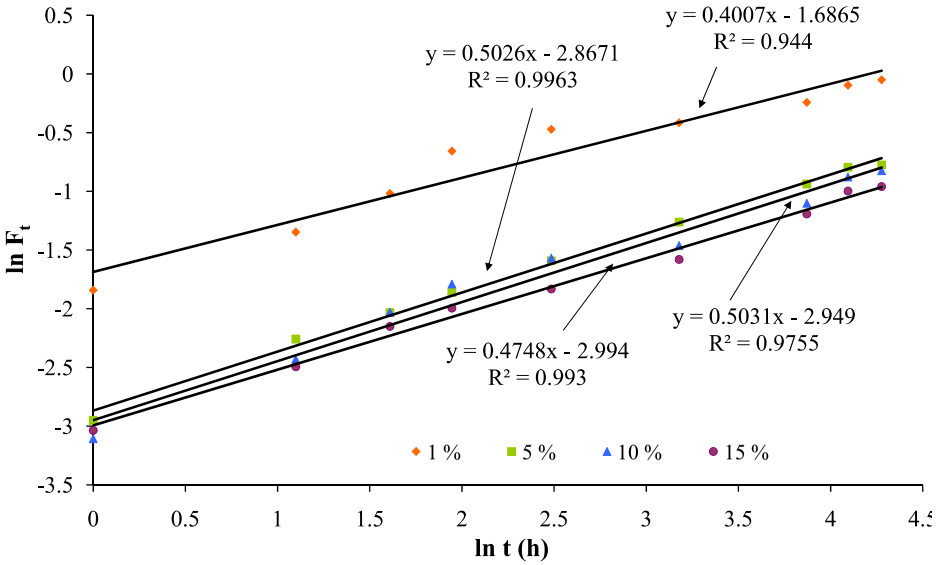

b) concentration of TPP

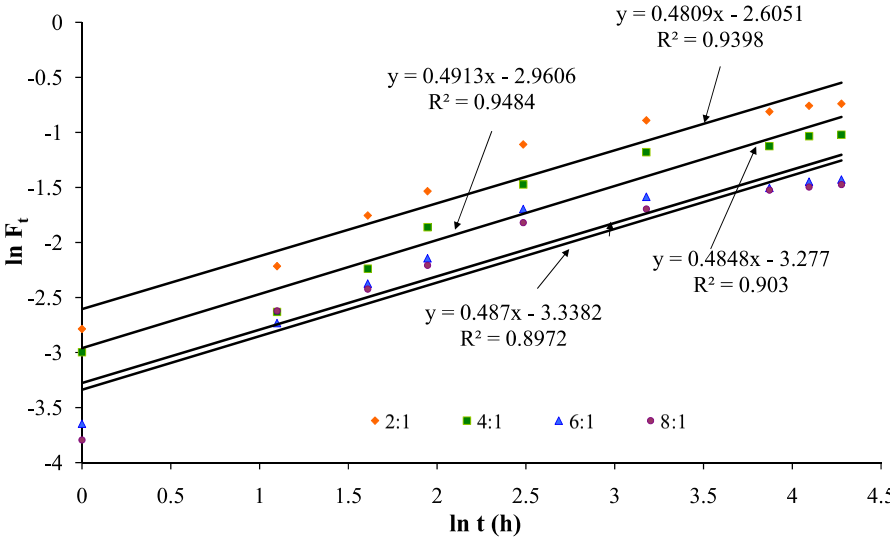

c) molar ratio of an amino group to TPP

Figure 11 Linear regression of Ritger-Peppas models for release kinetics of menthol; a) crosslinking time, b) concentration of TPP, and c) molar ratio of an amino group to TPP

Table 1 A recipe for the o/w emulsion

Component	Weight (g)
Continuous phase	
water	220
chitosan solution (1% w/v in 1 M acetic acid)	20
PVA	3.0
SDS	1.5
Disperse phase	
light mineral oil	20
menthol	0.5-2.0
Brij 72	0.5
cetyl-stearyl alcohol	0.5

Table 2 The o/w emulsion droplets (without menthol) obtained by two pore size membranes

Particle property	pore size (μm)	
	1.4	5.2
Number average diameter, $\overline{d_e}$ (μm)	10.2	19.6
CV (%)	10.1	11.5

Table 3 Size and size distribution of emulsion with different homogenizing speeds

Run no.[a]	Speed (rpm)	$\overline{d_e}$ (μm) ±SD	CV (%)
D001	6000	62.6±34.9	55.9
D002	10000	39.1±12.3	31.5
D003	14000	20.2±7.9	38.9
D004	16000	30.5±12.1	39.7

[a] Chitosan solution 1 w/v% of 2 M acetic acid, the amount of chitosan was 10.0 g.

Table 4 Size and size distribution with various homogenizing times

Run no.	Time (second)	$\overline{d_e}$ ±SD (μm)	CV (%)
T30	30	38.7±11.9	30.8
T60	60	38.7±13.5	34.8
T90	90	39.8±9.9	24.8
T120	120	41.2±10.1	24.6

Table 5 Size and size distribution of microcapsules with various chitosan concentrations

Run no.	Chitosan concentration (%w/v)	$\overline{d_e}$ ±SD (μm)	CV (%)
CH1	1.0	17.9±8.1	45.6
CH1.5	1.5	17.0±6.3	37.1
CH2	2.0	16.7±6.9	41.0

Table 6 Size and size distribution of emulsion droplets prepared with double emulsion method

Conditions	$\overline{d_e}$ ±SD (μm)	CV (%)
Primary emulsion	24.2±8.3	34.4
Secondary emulsion	17.0±6.3	37.1
Double emulsion	31.0±8.5	27.4

Primary emulsion was prepared using homogenizing speed at 14,000 rpm for 90 minutes.
Secondary emulsion using SPG pore size having 5.2 micrometers.

Table 7 Mathematical models for controlled release kinetics understudy

Model	Equations	X	y
Zero-order	$Q_t = Q_0 + k_0 t$	Q_t	t
First order	$\log Q_t = \log Q_0 + kt/2.303$	$\log Q_t$	t
Higuchi	$Q_t = k_H t^{1/2}$	Q_t	$t^{1/2}$
Baker-Lonsdale	$3/2[1-(1-F_t)^{2/3}]-F_t = kt$	$3/2[1-(1-F_t)^{2/3}]-F_t$	t
Hixson-Crowell	$(1-F_t)^{1/3} = 1-kt$	$(1-F_t)^{1/3}$	t
Ritger-Peppas	$\text{Ln } F_t = \ln k + n \ln t$	$\ln F_t$	ln t

Table 8 Release exponent (k), diffusion index (n), and correlation coefficient (R^2) from the linear regression using Ritger-Peppas model with $\ln F_t = k + n \ln t$

Condition	k	R^2	n
Crosslinking time (min)			
30	-1.5433	0.9666	0.4020
60	-2.0190	0.9185	0.4283
90	-2.3721	0.9805	0.3990
120	-2.8679	0.9964	0.5026
Concentration of TPP (%)			
1	-1.6865	0.9440	0.4007
5	-2.8671	0.9963	0.5026
10	-2.9490	0.9755	0.5031
15	-2.9940	0.9930	0.4748
Molar ratio of CS:TPP			
2:1	-2.6051	0.9398	0.4809
4:1	-2.9606	0.9484	0.4913
6:1	-3.2770	0.9030	0.4848
8:1	-3.3382	0.8972	0.4874

Draft Manuscript

Synthesis and Characterization of Water Swellable Natural Rubber Composites

Charoen Nakason[1]*, Yeampon Nakaramontee [1], Azizon Kaesaman[1], Wiyong Kangwansukpamonkon, and Suda Kiatkamjornwong[2]**

[1]Center of Excellence in Natural Rubber Technology, Department of Rubber Technology and Polymer Science, Faculty of Science and Technology, Prince of Songkla University, Pattani, 94000, Thailand;

*[1]*e-mail:ncharoen@bunga.pn.psu.ac.th*

[2]Multidisciplinary Program of Petrochemistry and Polymer Science, Department of Imaging and Printing Technology, Faculty of Science, Chulalongkorn University, Bangkok, 10330, Thailand;

*[2]**e-mail: ksuda@chula.ac.th*

Synthesis and Characterization of Water Swellable Natural Rubber Composites

ABSTRACT

A superabsorbent polymer (SAP) based on cassava starch-*g*-polyacrylamide (CSt-*g*-PAM) was prepared by a reactive batch processing using a specially designed batch reactor. SAP composites (SAPCs) were prepared from the CSt-g-PAM by blending with 20 phr of bentonite clay to increase the water absorbency of the SAP from 605 g/g up to 730 g/g for the SAPC. Water swellable natural rubber (WSNR) was then prepared by blending high-ammonia natural rubber (HANR) latex, or dry blending either epoxidized natural rubber (ENR) or maleated natural rubber (MNR) with the SAPC, coupled with poly(ethylene oxide) (PEO) and/or trimethylol propane trimethacrylate (TMPTMA). The curing, mechanical and morphological properties and the water absorbency of the different WSNRs were characterized. The WSNRs with both 10 phr PEO and 2 phr TMPTMA gave a higher mechanical strength and water absorbency. Increasing the PEO loadings to 20 or 40 phr rendered a higher absorbency but with a lower mechanical strength. A higher scorch time and cure time with a lower crosslinking density and cure rate index were found in the MNR based WSNRs compared with the WSNRs derived from the unmodified NR or ENR. The ENR base WSNR exhibited the highest water absorbency with lower mechanical strength compared with the unmodified NR base WSNR.

Keywords: Water swellable natural rubber, Superabsorbent polymer composite, Poly(ethylene oxide), Trimethylol propane trimethacrylate coupling agent.

INTRODUCTION

Superabsorbent polymers (SAPs) have been synthesized by modifying the molecular structure of cassava starch (CSt), and thus has gained in interest since such CSt based SAPs are claimed to be biodegradable products [Nakason, Wohmang, Kaesaman & Kiatkamjornwong, 2010; Lanthong, Nuisin & Kiatkamjornwong, 2006]. In contrast, most of the current SAPs are synthetic polymers that have a poor biodegradability that then leads to environmental problems upon their disposal. The development of starch-based SAPs could potentially be used to solve this problem. Potential applications of starch-based SAPs are fairly diverse and include, amongst others, personal care products, fire-fighting gels and agricultural uses [Willette & Finkenstadt, 2006]. Starch-based SAPs are developed by grafting starch with unsaturated hydrophilic monomers, such as acrylic acid (AA), acrylamide (AM) [Nakason, Wohmang, Kaesaman & Kiatkamjornwong, 2010; Lanthong, Nuisin & Kiatkamjornwong, 2006; Willette & Finkenstadt, 2006; Athawale & Lele, 1998; Karadage, Uzum & Saraydin, 2005; Lostafa, 1995] and ε-caprolactone [Chen, Ni, Bian, Qiu, Zhang & Chen, 2005], by a chemical initiated radical chain copolymerization [Athawale & Lele, 2000; Chen, Park & Park, 1999], or by using γ-ray irradiation [Kiatkamjornwong, Mongkolsawat & Sonsuk, 2002]. A reactive extrusion process has been used to prepare starch-based graft copolymers [Carr, Kim, Yoon & Stanley, 1992; Yoon, Carr & Bagley, 1992]. Starch-*g*-polyacrylamide (St-g-PAM) has been successfully prepared using a co-rotating twin screw extruder [Willette & Finkenstadt, 2003, Finkenstadt & Willette, 2005], but the maximum water absorbency capacity of the St-g-SAPs obtained using this process was relatively low at only approximately 300 times their dry weight [Carr, Kim, Yoon & Stanley, 1992]. However, our previous work based on the reactive blending process [Nakason,

Wohmang, Kaesaman & Kiatkamjornwong, 2010] with a specially designed batch reactor gave St-g-SAPs with a higher maximum water absorbency capacity at ~ 730 times their dry weight.

In recent years, the development of water swellable (natural) rubbers (WS(N)Rs) has been developed. WS(N)Rs are functional polymers that expand their volume up to more than 1.5 times their original weight by absorbing surrounding water. They can be used as a sealing material or in calking applications, preventing water leakage from pipes or blocking connections in civil constructions, such as subways and subsea tunnels [Park & Kim, 2001].

Any given WS(N)R is typically prepared by dispersing SAP particles in common hydrophobic rubbers, such as chloroprene rubber [Wang, Li & Chen, 1999; Liu, Ding, Zhou & Chen, 2006], chlorohydrin rubber [Zhang, Zhang, Wang, Liu, Liu & Chen, 1999; Zhang, Zhang, Wang, Liu, Liu & Chen, 2000] and NR [Park & Kim, 2001, Wang, Zhang, Dong, Chen & Tan, 2002]. This special type of rubber possesses not only the properties of general rubber, such as a high mechanical strength, set and resilience properties, but also has high water absorbency. These properties are due to the presence of the crosslinking network in the rubber and water absorbing material.

A specially designed batch reactor was used to prepare St-*g*-PAM based SAPs via reactive processing, based on the optimum conditions found in Nakason *et al.* [2010]. In this work, SAP composites (SAPCs) of the St-*g*-PAM mixed with bentonite clay were prepared and later blended with NR and other important ingredients. That is, each WSNR was prepared by mixing SAPC particles with the NR, poly(ethylene oxide) (PEO) and trimethylol propane trimethacrylate (TMPTMA). Each ingredient was then compounded and cured by the sulfur vulcanization system. The effects of the addition of SAPC, PEO and TMPTMA on the water absorbency, curing, mechanical

and morphological properties of the resulting WSNR compound and vulcanizate were then investigated.

2. EXPERIMENTAL

2.1 Materials

High ammonia (HA) NR latex having a dried rubber content of approximately 60% was manufactured by Yala Latex, Co., Ltd (Yala, Thailand). Epoxidized natural rubber (ENN)) with 25% mol epoxide (i.e., Epoxyprene 25 (ENR-25)) was manufactured by Muang Mai Guthrie Public Co., Ltd. (Surathani, Thailand). Maleated natural rubber (MNR) was prepared in-house by blending the rubber air-dried sheet (manufactured by Khuan Pun Tae Farmer Co-operation, Phattaluang, Thailand) with 8 phr of maleic anhydride at 150 °C using an internal mixer (Brabender Plasticorder, model PLE331, Brabender OHG Duisburg, Germany) at a rotor speed of 60 rpm. Details of the preparation and characterization procedures of MNR are described by Nakason and Saiwari [2008].

CSt, used as a polymer substrate, was obtained from Siam Starch (1966) Co., Ltd., Rayong, Thailand. AM, used as a grafting monomer, and *N, N'*-methylenebisacrylamide, used as a crosslinker were from Fluka (Buchs, Switzerland). Potassium persulfate, used as a free radical initiator, was obtained from Asia Pacific Specialty Chemicals Ltd., (Seven Hills, Australia). Hydroquinone, used as a free radical scavenger, was from Merck (Darmstadt, Germany). Sodium lauryl sulfate was prepared in-house by reacting lauric acid (Imperial Industrial Chemicals (Thailand) Ltd.) with sodium hydroxide (BDH, England). For the preparation of SAPCs, bentonite clay, grade SAC-1, was from Thai Nippon Chemical Industry, Co., Ltd., (Samut Sakhon, Thailand), and TMPTMA, used as a coupling agent for functional

groups, was obtained from Behn Meyer Chemical Co., Ltd, Rayong, Thailand. PEO was from Alkox E-30, Meisei Chemical Works, Ltd., Kyoto, Japan, and was used to enhance the water absorbing properties of the rubber. Zinc oxide (white seal) and stearic acid, used as the activators in the sulfur vulcanization system, were supplied by Metoxide Thailand Co., Ltd. (Pathumthani, Thailand) and Imperial Industry Chemical Co., Ltd. (Pathumthani, Thailand), respectively. *N*-tert-butyl-2-benzothiazyl sulphenamide (TBBS), used as an accelerator, was manufactured by Flexsys America L.P. (Reliance Technochem Co., Ltd., Bangkok, Thailand). Sulfur, used as a curing agent, was manufactured by Ajax Chemical Co., Ltd. (Auckland, New Zealand).

Figure 1 A illustrates Infrared spectra of the major raw materials (a) poly(ethylene oxide), (b) starch-*g*-polyacrylmide and bentonite 20 phr, and (c) TMPTMA. The neat natural rubber peaks (not shown here) contained the following peaks: 3224 cm^{-1} (w), ν_{O-H} OH (moisture in the rubber); 3037 cm^{-1} (s) $\nu_{=C-H}$; 2960, 2916 and 2850 cm^{-1}, ν_{-C-H}; 1661 cm^{-1}, $\nu_{C=C}$; 1447 and 1375 cm^{-1}, ρ_{C-H}; 833 cm^{-1} ν_{C-H} on cis C=C of polyisoprene, or $\delta_{=C-H}$ polyisoprene. For the neat PEO, the following peaks were found. 3450 cm^{-1}, ν_{-OH} (hydration of PEO); 2889 cm^{-1}, ν_{-CH}; 1632 cm^{-1}, $\nu_{-C=O;}$ 1467 cm^{-1}, $\delta_{asH-C-H}$; 1360 cm^{-1}, δ_{sH-C-H}; 1149 cm^{-1}, ν_{C-O-C}; 916, 842 cm^{-1}, ρ_{CH_2} (guache) (Manoratne, Rajapake &Dissanayake, 2006; Zain & Arof, 1998). For the neat TMPTMA, 2980, 2920, 2900 cm^{-1}, ν_{CH} (ali); 1870 cm^{-1}, $\nu_{as\ C=O}$ (w); 1720 cm^{-1}, $\nu_{as\ C=O}$ (s); 1640 cm^{-1}, $\nu_{C=C}$ (m); 1480 cm^{-1}, δ_{C-H}.

2.2 Preparation of Cassava Starch-Graft-Polyacrylamide Superabsorbents (CSt-PAM SAPs) and Associated Composites (SAPCs) by Reactive Blending

CSt-PAM was prepared by reactive batch processing using a specially designed batch reactor, with the preparation and characterization as described before [1]. The SAPC loaded with 20 phr of bentonite clay was prepared from the CSt-PAM according to the described procedures [1].

2.3 Preparation of WSNR

The HA concentrated NR latex was first mixed with the SAPC loaded with 20 phr bentonite clay and 2% (w/w) of SDS surfactant for 1 h at room temperature, and then the mixture was aged for another 24 h to allow it to reach equilibrium. The mixture was then cast into 10 x 10 cm thin films and dried at room temperature for 24 h followed by in a hot air oven for another 24 h at 40 °C. The ENR and MNR derived WSNRs or called modified WSNRs were produced by a dry blending process with the internal mixer at 40 °C and a rotor speed of 60 rpm, with the formulation and mixing schedule shown in Table 1.

2.4 Influence of PEO and TMPTMA loadings on properties of WSNRs

WSNR composites from the CSt-PAM SAP loaded with 20 phr bentonite clay were prepared according to the procedure described in section 2.3. Each dried composite was mixed at 50 °C using the internal mixer (capacity of 80 cm^3) at a rotor speed of 60 rpm following the formulations shown in Table 2. In this work, the properties of the WSNR composites and also with the addition of PEO with or without the coaddition of TMPTMA were investigated.

2.5 Water absorbency

Each WSNR composite (0.1 - 0.5 g) was immersed in distilled water (250 mL) for 24 h at ambient temperature (25 - 30 ºC) to reach equilibrium swelling. The residual water was removed by filtration through an 80-mesh stainless steel screen with the WSNR composite left on the screen for at least 1 h to drain off the unabsorbed water. During this period, the screen was gently shaken with a declining angle of 15 - 20º to ensure that most of the unabsorbed water was separated. The water absorbency was determined by weighing the fully swollen WSNR and its dried composite as follows:

$$Water\ absorbency\ (g/g) = \frac{(W_1 - W_0)}{W_0} \quad (1)$$

where W_0 is the weight of the dried WSNR and W_1 is the weight of the swollen WSNR. In this work, the water absorbency of the WSNR composites before vulcanization (rubber compound) and after vulcanization (rubber vulcanizate) was carried out.

2.6 Cure characterization

A rotorless rheometer (Rheo Tech MD+, Tech Pro, Inc., from Cuyahoya Falls, U.S.A.) was used to determine the curing characteristics of the rubber composites at 160 °C with 1° arc and 60 min. The optimum cure time (tc_{90}) and scorch time (t_{s1}), the minimum and maximum torque (M_L and M_H, respectively), and delta torque (M_H - M_L) were determined from the curing curves. Cure rate index (CRI) was measured based on ASTM D5289 and the formula for the calculation is shown below.

$$CRI = 100/t_{c90}\text{-}t_{s1} \quad (2)$$

where t_{s1} is the time required to increase one unit torque from the minimum torque, t_{90} is the time required to reach 90% of the total cure.

Vulcanizates with a thickness of approximately 550 ± 50 μm were then prepared by compression molding at 160 °C according to the determined optimum cure time (tc_{90}). The mechanical, morphological and water absorbency properties of the composite vulcanizates were investigated.

2.7 Infrared Spectroscopic Analysis

The existence of the functional groups of the rubber samples and raw materials was investigated by Fourier Transform Infrared Spectroscopy (FT-IR; System 2000, Perkin Elmer, U.S.A.). The dried sample and KBr powder were mixed, ground, pressed, and then subjected to the FT-IR spectrometry.

2.8 Microstructure studies

Scanning electron microscopy (SEM) (model JSM-6510LA, Jeol Ltd., Akishima, Japan) was used to characterize microstructures of the cryogenic fractured surfaces of the WSNR composites. The samples were coated with a thin layer of gold under vacuum before characterization.

2.9 Thermal properties analysis

Thermal behavior of the WSNR composite at different PEO contents was investigated using differential scanning calorimetry (DSC) (Mettler Toledo DSC823e/400, USA) and thermogravimetric analysis (TGA) (Mettler Toledo). In the case of DSC, the powder sample sealed into the aluminum pan was heated up at the rate of 10 °C min^{-1} from -50 to 100 °C. During the heating, nitrogen gas (N_2) was

flowed into the furnace at a flow rate of 20 cm^3 min^{-1} for 5 min. In TGA, the samples were put inside alumina pans hanged in the heating furnace. The weight of remaining material was recorded while the furnace was heating from 25 °C to 500 °C at a rate of 10 °C min^{-1}. Oxygen (O_2) was fed into the furnace at 20 cm^3 min^{-1} as a purge gas.

2.10 X-ray diffraction analysis

X-ray diffraction measurements of WSNR composite at different PEO contents were carried out using an X-Ray Diffractometer: Bruker AXS Germany (Model D8 Advance with the target and wavelength (CuK_{∞} radiation, λ = 0.15406 nm, 40 kV, 30 mA). The X-ray diffraction (XRD) patterns were recorded from 5° to 80° with an increment of 0.02 degree in a 2θ mode at a scanning rate of 1° min^{-1}. The dried composite powder was mounted on a sample holder with smooth double-sided adhesive tape.

2.11 Mechanical properties

Dumbbell shaped specimens were prepared from a sheet of the rubber vulcanizates by die cutting according to ASTM die type C. The stress-strain behavior of the vulcanizates was then investigated using a universal tensile testing machine (Hounsfield Tensometer, model H 10KS, Hounsfield Test Equipment Co., Ltd, Surrey, U.K.) at a speed of 500 mm/min and an initial gauge length of 25 mm, according to ASTM D412. The tensile strength and elongation at break were then determined based on the stress-strain behavior.

3. RESULTS AND DISCUSSION

3.1 IR studies

The materials derived were investigated for IR spectroscopic information to look for some interaction. Figure 1 B illustrates the peaks of the unmodified NR synthesized with bentonite-modified SAP and compounded with PEO with/without TMPTMA, the additional peaks are found as follows.

Sample A [NR+bentonite]: one can see the peak at 3318 cm^{-1} ν(-OH) of Si-OH group; the peak at 1646 cm^{-1} for deformation vibration of the interlayer water in the clay; the peak at 1263 cm^{-1} ρ_s(-Si-CH_3), peaks at 1100 cm^{-1} ν(-Si-O) in-plane, and 1030 cm^{-1} ν(-Si-O) out-of-plane (Alabarse, Conceição, Balzaretti, Schenato & Xavier, 2011; Paluszkiewicz, Holtzer & Bobrowski, 2008; Madejova, Janek, Komadel, Herbert & Moog, 2002; Özcan & Özcan, 2004).

Sample B ([NR+ bentonite + PEO (10 phr)]: the additional peak at 3318 cm^{-1} ν(-OH) of Si-OH group; 873 cm^{-1} ρ(Al-Fe-OH) bentonite.

Sample C [NR+ bentonite + PEO (10 phr) + TMPTMA (2 phr)]: the additional peaks were found as follows: 3318 cm^{-1} ν(-OH) of Si-OH group; 1725 cm^{-1} ν(C=O) TMPTMA, and 1145 cm^{-1} ν(C-O-C) PEO.

Sample D [NR+ bentonite + PEO (20 phr) + TMPTMA (2 phr)]: additional peaks were found: 3318 cm^{-1} ν(-OH) of Si-OH group; 1725 cm^{-1} ν(C=O) TMPTMA; 1637 cm-1 ν(C=O) PEO; 1342 cm^{-1} $\delta_s CH_2$ PEO; and 1143 cm^{-1} ν(C-O-C) PEO.

Sample E [NR+ bentonite + PEO (40 phr) + TMPTMA (2 phr)]: additional peaks were found: 3318 cm^{-1} ν(-OH) of Si-OH group; 1725 cm^{-1} ν(C=O) TMPTMA;

1360 cm^{-1} $\delta_S(CH_2)$ PEO; 1145 cm-1 ν(-C-O-C) PEO; 916, 842 cm^{-1}, ρ_{CH_2} (guache) (Manoratne, Rajapake &Dissanayake, 2006; Zain & Arof, 1998).

Sample F [ENR+ bentonite + PEO (10 phr) + TMPTMA (2 phr)]: 3318 cm^{-1} ν(-OH) of Si-OH group; 1725 cm^{-1} ν(C=O) TMPTMA; 1539 cm^{-1}???; 1342 and 1360 cm^{-1} δ_s CH_2 PEO; 1144 cm^{-1} ν(C-O-C) PEO; 962, 946 and 873 cm^{-1} ν(oxirane ring) epoxide (Zong-Qiang, He-Ping, Qi-Fang & Guang, 2008; Yoksan,2008)

Sample G [MNR+ bentonite + PEO (10 phr) + TMPTMA (2 phr)]:)]: 3318 cm^{-1} ν(-OH) of Si-OH group; 1793 cm^{-1} ν(C=O) succinic anhydride rings; 1723 cm^{-1} ν(C=O) succinic acid (hydrolysis of succinic anhydride ring); 1146 cm^{-1}, ν(C-O-C) PEO; 872 cm^{-1} ν(oxirane ring) maleic anhydride (Saelao & Phinyocheep, 2004; Nakason, Kaesaman & Supasanthitikul, 2004; Vicente, Campos, Bordado & Ribeiro, 2008).

3.1 Influence of PEO and TMPTMA on Curing Properties

The curing curves of the WSNR composites and those with the addition of PEO with and without the co-addition of TMPTMA reveal that all of the composites have a curing equilibrium state (the plateau curves), with equilibrium being obtained with 20 min (Figure 2). Furthermore, the NR-based composites alone (i.e. without PEO and TMPTMA) showed the longest delayed action at the beginning of the curing with the longest scorch time of 4.0 min (Table 3). Incorporation of 10 phr PEO produced a significantly shorter scorch time (1.43-fold) of the composites due to reactivity of PEO with polar functinal groups in the composite system. Moreover, co-incorporation of 2 phr TMPTMA with the PEO induced only a slight reduction in the scorch time compared with the one without PEO and TMPTMA, and much less than

with the addition of the same content (10 phr) of PEO alone. This is attributed to the fact that, besides the role of crosslinking agent, TMPTMA could react with the TBBS accelerator and delay the scorching of the materials while a shorter scorch time resulted from the incorporation of the PEO. In this scenario then, these two effects overshadow and compensate each other with a net unchanged scorch time. Basically, the addition of zinc oxide (ZnO) as an activator for the sulfur vulcanization of rubbers enhances the vulcanization efficiency and vulcanizate properties and reduces the vulcanization time. The co-addition of 2 phr TMPTA and 10 phr PEO reduced the scorch time by 1.11-fold compared to that with no addition, but to a lower extent than the addition of 10 phr PEO alone (Table 3). Moreover, the incorporation of 10 phr PEO and 2 phr TMPTMA also slightly decreased the crosslinked density (M_H - M_L) and the cure rate index (CRI), by significantly decreasing both the minimum and the maximum torque, of the rubber composites.

3.2 Influence of PEO and TMPTMA on Water Absorbency

Figure 3 illustrates the water absorbency capabilities of the WSNR composites and vulcanizates, either alone or with the addition of 10 phr PEO with or without the coaddition of 2 phr TMPTMA. With each given blend system, the WSNR composite compounds exhibited a higher water absorbency (e.g. 2.6-fold to 4.7-fold higher at two days of immersion) than that of the corresponding vulcanizate at all time points. This is attributed to the crosslinked structure that is formed in the rubber vulcanizates and provides a lower free volume for water to enter into the bulk of the rubber. As a result of the hydrophilic nature of PEO, its incorporation at 10 phr rendered a higher water absorbency capacity of the products. Furthermore, the PEO contributed to a better dispersion of the SAP and SAPC in the rubber matrix. The highest water

absorbency was obtained in the WSNR containing both 10 phr PEO and 2 phr TMPTMA. The hydrophilic nature of both PEO and TMPTMA has the capability to form a strong hydrophilic network with NR, SAP, PEO and SAPC to generate the highest water absorbency.

Three PEO loadings (10, 20 and 40 phr) at a fixed concentration of 2 phr TMPTMA used to prepare WSNR composite compounds and their associated vulcanizates are shown in Figure 4. The water absorbency capabilities of these vulcanized and unvulcanized WSNR composites differed, where as expected, at each given loading of PEO, the water absorbency capabilities of the unvulcanized composite compounds were higher than those of the corresponding vulcanizates at all time points of water immersion (e.g. from 1.4-fold to 2.6-fold after two days immersion). The water absorbency of the unvulcanized composite compounds with and without PEO differed, showing a slightly decreasing trend with increasing immersion times of longer than 6 days in the absence of PEO, but remained constant (10 phr PEO) or continued to increase (20 & 40 phr PEO) after six days of immersion. Probably the SAP was prone to be eluted from the composite compounds into the water phase due to lack of interaction between the different phases of the composite compounds. Certainly, increasing the PEO loading to 20 and 40 phr increased the water absorbency at each time point of water immersion and lead to increasing water absorbency with increasing water immersion times. A corresponding trend, but with a lower magnitude, was observed for the water absorbency in the vulcanizates. This suggested a stronger network because of the interaction between the polar functional groups and the reactive groups of different components in the composites. The WSNR composite vulcanizates showed the highest water absorbency capacity of 530% (w/w) at a PEO loading of 40 phr after 14 days of water immersion.

3.3 Influence of PEO and TMPTMA on Mechanical Properties

The tensile strength and elongation at break of WSNR composite vulcanizates decreased and increased slightly, respectively, with increasing water immersion time (Table 4). This suggests that a certain portion of the water sensitive SAP or SAPC still present in the composites is not damaged by a long-term immersion in water, and so the strength of these materials can potentially be used in damping conditions. It was also noted that the inclusion of 10 phr PEO to the vulcanizates significantly (1.24-fold to 1.1-fold at 0 to 14 days immersion time, respectively) increased the elongation at break but had only a marginal affect on the tensile strength due to the presence of the crosslinked network that is capable of a higher elongation. In contrast, the co-addition of 2 phr TMPTMA with 10 phr PEO to the WSNR composite vulcanizates and compounds resulted in the highest tensile strength properties, but essentially the same elongation at break values (Table 4). The WSNR with PEO or with PEO plus TMPTMA showed the same trend of a decreasing tensile strength with increasing water immersion time and an opposite but weaker trend for the elongation at break.

The influence of the PEO loading levels on the tensile strength and elongation at break of the WSNR composite vulcanizates is shown in Table 4, respectively. As expected, for all four PEO loadings (0, 10, 20 and 20 phr), increasing the water immersion time rendered a decreasing trend of the tensile strength, which is attributed to the swelled hydrophilic components of the WSNR composites. At any given immersion time larger than 2 days, the composite loaded with 10 phr PEO exhibited the highest tensile strength and that with a PEO of 40 phr exhibited the lowest strength. The tensile strength of the WSNR composites with different PEO loadings could then be ranked as follows: 10 phr > 0 phr > 20 phr > 40 phr. The WSNR composite vulcanizate loaded with 10 phr PEO is presumed to have the appropriate

371 amount to react and interact between the different components. Wang et al [1999]
372 found that when increasing the amount of PEO in the blends, it could not only
373 decrease the intermolecular forces of the NR phase functioning as a plasticizer, but
374 also produced more flaws in the rubber phase and also increase the low crosslinking
375 density moieties. The mechanical properties thus decreased in which they found
376 coincided with the decreases in crosslinking density.

377 The elongation at break (Table 4) is increased by incorporation of PEO into
378 the WSNR composite vulcanizate at all three levels examined (10, 20 and 40 phr vs. 0
379 phr), but to essentially the same extent for all three PEO inclusion levels at any water
380 immersion time. However, the WSNR composite vulcanizates without PEO exhibited
381 the lowest extension capability. It is likely that the swelling network of PEO could
382 lubricate the WSNR composite system to gain more extensibility. These properties
383 then mean that these WSNR composite vulcanizates can likely be used for sealing and
384 caulking applications.

385

386 ***3.4 Influence of PEO and TMPTMA on Morphological Properties***

387 SEM micrographs of the WSNR composite vulcanizates with PEO loadings at
388 20 and 40 phr before and after immersion in water for 14 days show clear differences
389 in morphologies in Figure 5a and 5c and Figure 5b and 5d, respectively. The white
390 particulates and agglomerates of SAP, SAPC, PEO and ZnO are clearly observed as
391 particulate in nature before immersing in water (Figure 5a and 5b), but after
392 immersion in water for 14 days, a large number of holes were seen while the white
393 particulates or agglomerates had disappeared (Figure 5c and 5d). The higher (40 phr)
394 PEO loaded WSNR composite vulcanizates (Figure 5 d) had larger holes in the
395 surface after a long time immersion in water, suggesting that some of the PEO, SAP

396 and SAPC, the hydrophilic nature materials, were removed from the composites. This
397 appearance could be related to the inferior mechanical strength of the WSNR
398 composites (Table 4).
399
400 ***3.5 Thermal properties analysis***
401 Figure 6A shows the DSC curves of WSNR composites with different
402 contents of PEO in which the WSNR composite without PEO exhibited no peak while
403 two transition peaks at approximately −12 °C and 38 °C were observed when the PEO
404 contents were 20 and 40 phr, respectively. The first peaks may be caused by PEO
405 which was well-dispersed and interacted with the WSNR composites whereas the
406 second peak might be caused by the phase separation due to the excess PEO content.
407 The intensity of PEO peaks at 38 °C increased with increasing amounts of PEO
408 loading in the WSNR composite (Figure 6A (c, d)). This result indicates that the
409 crystallization of PEO in the WSNR composite is strictly confined.
410 Thermal stability is an ability of a material to maintain its physical properties
411 when being exposed to high temperatures. The TGA curves in Figure 6B show that
412 the neat PEO in curve (a) is the most thermally stable material, whereas the WSNR
413 composites having higher PEO content (Figure 6B (c, d)) are more stable materials
414 than the WSNR composite without PEO (Figure 5B (b)). This is additional evidence
415 that the PEO crystalline phases were dispersed in the polymer matrix in the XRD
416 work to be discussed below.
417
418 ***3.5 Effect of PEO amount loaded in unmodified*** WSNR ***on mechanical properties***
419 The XRD patterns of bentonite, PEO and SAP (all starting materials for
420 preparing WSNR), unmodified WSNR composites in the different contents of PEO,

421 and the modified NR are graphically represented in Figure 6. The XRD pattern of
422 bentonite was found at 6.02° with a d-spacing value of 14.7 Å, while those of PEO at
423 19.6° and 23.7° had the d-spacing values of 4.5 and 3.8Å. The starch-*g*-PAM had
424 only one intense peak at 22.1° with a d-spacing of 4.0Å. Table X illustrates the
425 effect of PEO and TMPTMA loadings on XRD pattern. The XRD pattern of WSNR
426 composite without PEO (Figure 7 (a)) showed a strong peak at $2\theta = 9.54°$ which
427 involves that the layers of bentonite were partially exfoliated in the polymer matrix.
428 The absence of diffraction peaks for WSNR composite with PEO 10 phr (Figure 7
429 (b)) suggests that the bentonite clay has been totally exfoliated and dispersed in the
430 polymer matrix to form a nanocomposite structure. The WSNR composites with
431 various contents of PEO (Figure 7 (c, d)) produced the peaks at approximately $2\theta =$
432 19.2° and 23.3° correspond to the 011 and 210 planes of the crystalline structure of
433 PEO in the polymer composite [Wang, Li & Chen, 1999]. The intensity of the
434 characteristic PEO peaks increased more intensely with increasing amounts of PEO
435 loadings in the WSNR composite, in comparison with the WSNR composite with less
436 PEO loadings (Figure 7 (b, c)). Thus, mechanical properties of the swollen rubber
437 samples decreased with an increase in the amount of PEO as mentioned above due to
438 increases in the absorbed water.
439
440 ***3.6 Influence of NR Type on Curing Properties.***
441 The curing curves of the WSNR composites derived from three different types
442 of rubber bases (NR, ENR and MNR) revealed that the unmodified NR and the ENR
443 exhibited broadly similar curing characteristics (Figure 8) and a broadly similar
444 scorch time (Table 4). Likewise, the curing curves revealed they reached an
445 equilibrium state by about 10 min for NR to 20 min for ENR. In contrast, the curing

446 curve of the MNR containing WSNR compound exhibited a very slow and delayed
447 action, not beginning to cure until after some 10 min and then proceeding slowly such
448 that equilibrium was still not attained after 60 min, a characteristic marching curve,
449 where only a slight increase in the torque with increasing time was observed. In
450 addition, the MNR compounds exhibited a significantly longer scorch time (3.3- and
451 3.83-fold) and cure time (3.19- and 4.46-fold) than did the ENR and NR vulcanizates,
452 respectively, together with the lowest cure rate index (2.92- and 5.71-fold) and
453 crosslinked density (2.53- and 2.17-fold, respectfully) (Table 3). This effect is induced
454 by the remaining maleic anhydride, and maleic acid from the reaction with moisture,
455 which then react with the TBBS accelerator. As a direct consequence there is
456 insufficient TBBS accelerator left for the vulcanization process leading to the inferior
457 curing characteristics. Also seen in Figure 8 and Table 4 is that the ENR compound
458 exhibited the longest cure time and the lowest cure rate index compared with the
459 unmodified NR compound. However, the ENR compound gave the highest
460 crosslinked density. This could be caused by the chemical interaction from the polar
461 functional groups in ENR molecules with the blend components, and the coupling
462 reaction among the blend components with TMPTMA.
463
464 ***3.7 Influence of the NR Type on Water Absorbency***
465 The water absorbency of the WSNR composite compounds and vulcanizates
466 derived from NR, ENR and MNR show marked differences (Figure 9). In all cases
467 the water absorbency of the WSNR composites increased with increasing immersion
468 time and were still increasing after 14 days of water immersion (the longest time point
469 assayed), although this was less marked for the vulcanized samples than the
470 unvulcanized ones. The modified NR (i.e., ENR and MNR) showed a markedly

471 higher (from 2.8- and 3.4-fold to 2.0- and 2.5-fold higher for ENR and MNR at two
472 and 14 days immersion, respectively) water absorbency of the WSNR composite
473 compounds (unvulcanized) than NR. Indeed, ENR showed the highest water
474 absorbency followed by MNR and the unmodified NR showed by far the lowest water
475 absorbency and this trend was maintained over the entire 14 days of water immersion.
476 This is attributed to the stronger chemical interactions and bonding between the
477 modified NR, PEO and SAPC that are assisted by the TMPTMA. However, note that
478 although the vulcanizates showed the same trend of water absorbency and the same
479 ranked order of ENR > MNR > NR, a lower level of water could enter into the
480 crossliked structure of the vulcanizates and the difference in magnitude between the
481 three different rubber types was less marked than in the non-vulcanized samples.
482 Thus, the water absorbency of the ENR based WSNR vulcanizate showed the highest
483 value with the maximum value at approximately 600 wt% for the vulcanizate.
484

485 ***3.8 Influence of type of natural rubber on Mechanical properties***

486 The tensile strength and elongation at break of the WSNR vulcanizates derived
487 from the NR, ENR and MNR show clear differences (Table 6). As with the higher
488 water absorbency, the WSNR of ENR and MNR showed a dramatic reduction in the
489 tensile strength. It is possible that some NR molecules might be degraded during the
490 modifying process. Additionally, a number of polar functional groups along the chain
491 of NR that form weak linkages, such as –C-O, and -O-O-, are removed in the
492 modification process. The elongation at break of the WSNR vulcanizates increased
493 slightly with increasing immersion time, but the ENR- and MNR-based WSNR
494 vulcanizates yielded lower elongation at break values that were still within the range

of good extensibility of the rubber vulcanizates. Therefore, it is concluded that the ENR and MNR base WSNR vulcanizates exhibited a superior water absorbency but

One can see that the peak intensity at 873 cm^{-1} in (e) and (f) for the inclusion of 10 phr PEO decreased sharply which is in agreement with the XRD and thermal properties. As mentioned by Wang et al (1999) that increases in PEO content had a significant effect on the crystallinity of the vulcanized rubber, i.e., the PEO contents higher than 10 phr are not used in the process and cause increases in water absorption which reduce tensile strength.

CONCLUSION

SAPs of CSt-*g*-PAM were prepared by a reactive batch process using a specially designed batch reactor. The SAPCs were then prepared with the addition of 20 phr bentonite clay to the SAP mixture. WSNRs were prepared by blending HANR latex, or dry blending of ENR or MNR, with the SAPC alone or with the addition of various loadings of PEO with or without the co-addition of 2 phr TMPTMA. The WSNR compounds and vulcanizates with PEO and TMPTMA gave the highest mechanical strength and water absorbency. A PEO loading of 10 phr gave the highest mechanical strength and water absorbency compared with the WSNR without PEO. Increasing the PEO loading increased the water absorbency and lowered the mechanical strength, with the lowest tensile strength being observed at a 40 phr PEO loading. The curing behavior of the WSNR depended on the NR type. The highest scorch time and cure time with the lowest crosslinked density and cure rate index were obtained in the MNR based WSNR, whilst the ENR based WSNR exhibited the highest water absorbency but with a lower mechanical strength than that of the WSNR made from the unmodified NR.

ACKNOWLEDGEMENTS

The authors are indebted to the Thailand Research Fund for funding the research project under the Research Team Aid (Grant no. RTA5080004). Sincere thanks and appreciation are given to the Prince of Songkla University (Pattani Campus) and Chulalongkorn University for provision of the research facilities. Language editing from Publication Consultation Unit of the Research Division, Faculty of Science, Chulalongkorn University, is acknowledged.

REFERENCES

Alabarse, F. G.; Conceição, R. V.; Balzaretti, N. M.; Schenato, F.; Xavier, A. M. (2011). In-situ FTIR analyses of bentonite under high-pressure. *Applied Clay Science 51*, 202-208.

Athawale, V.D, Lele, V. (1998). Graft copolymerization onto starch. II. Grafting of acrylic acid and preparation of its hydrogels. *Carbohyd. Polym.*, **35**, 21.

Athawale, V.D., Lele, *V.* (2000). Thermal Studies on Granular Maize Starch and its Graft Copolymers with Vinyl Monomers. *Starch/Starke*, **52**, 205.

Carr, M. E., Kim, S., Yoon, K. J., & Stanley, K. D. (1992). Graft polymerization of cationic methacrylate, acrylamide, and acrylonitrile monomers onto starch by reactive extrusion. *Cereal Chem*, **69**, 70–75.

Chen, J., Park, H., and Park, K. (1999). Synthesis of superporous hydrogels: hydrogels with fast swelling and superabsorbent properties, *J Biomed Mater Res*, **44**, 53.

Chen, L., Ni, Y., Bian, X., Qiu, X., Zhang, X., Chen, X. A novel approach to grafting polymerization of ε-caprolactone onto starch granules (2005). *Carbohyd. Poly*m., **60**, 103.

545 Finkenstadt, V.L., Wilett, J.L. (2005). Reactive Extrusion of Starch-Polyacrylamide
546 Graft Copolymers: Effects of Monomer/Starch Ratio and Moisture Content
547 Karadag, E; Uzum, OB; Saraydin, D. (2005). Water uptake in chemically crosslinked
548 poly(acrylamide-*co*-crotonic acid) hydrogels, *Mater Design*, **26 (4)**, 265–270.
549 Kiatkamjornwong, S., Mongkolsawat, K., Sonsuk, M. (2002). Synthesis and property
550 characterization of cassava starch grafted poly[acrylamide-*co*-(maleic acid)]
551 superabsorbent via γ-irradiation *Polymer*, **43**, 3915.
552 Lanthong, P., Nuisin, R., Kiatkamjornwong, S. (2006). Graft copolymerization,
553 characterization, and degradation of cassava starch-*g*-acrylamide/itaconic acid
554 superabsorbents *Carbohyd. Polym.* **66**, 229.
555 Liu, C., Ding, J., Zhou, L., Chen, S. (2006). Mechanical properties, water-swelling
556 behavior, and morphology of water-swellable rubber prepared using
557 crosslinkedsodium polyacrylate *J. Appl. Polym. Sci.*, **102**, 1489**.**
558 Madejova, J., Janek, M.; Komadel, P., Herbert, H.-J., Moog, H. C. (2002) FTIR
559 analyses of water in MX-80 bentonite compacted from high salinity salt solution
560 systems. *Applied Clay Science 20*, 255- 271.
561 Manoratne, C. H.; Rajapakse, R. M. G.; Dissanayake, M. A. K. L. (2006). Ionic
562 Conductivity of Poly(ethylene oxide) (PEO)-Montmorillonite (MMT)
563 Nanocomposites Prepared by Intercalation from Aqueous Medium.
564 *International Journal of Electrochemcal Science, 1*, 32-46.
565 Mostafa, K.H.M. (1995). Graft polymerization of acrylic acid onto starch using
566 potassium permanganate acid (redox system) *J. Appl. Polym. Sci.*, **56**, 263.
567 Nakason, C., Saiwari, S. (2008). Effect of Grafted Maleic Anhydride Content
568 Recyclability of Dynamically Cured Maleated Natural Rubber/Polypropylene
569 Blends.*J. Appl. Polym. Sci.*, **110,** 4071.

570 Nakason, C., Wohmang, T., Kaesaman, A., Kiatkamjornwong, S. (2010). Preparation
571 of cassava starch-graft-polyacrylamide superabsorbents and associated
572 composites by reactive blending *Carbohyd. Polym.*, **81,** 348.

573 Özcan, A. S., Özcan, A. (2004). Adsorption of acid dyes from aqueous solutions onto
574 acid-activated bentonite. *Journal of Colloid and Interface Science 276*, 39-46.

575 Paluszkiewicz, C., Holtzer, M., Bobrowski, A. (2008). FTIR analysis of bentonite in
576 moulding sands. *Journal of Molecular Structure 880*, 109-114.

577 Park, J.H., Kim, D. (2001). Preparation and characterization of water-swellable
578 natural rubbers *J. Appl. Polym. Sci.*, **80**,115.

579 Wang, C., Zhang, G., Dong, Y., Chen, X., Tan, H. (2002). Study on a water-
580 swellable rubber compatibilized by amphiphilic block polymer based on
581 poly(ethylene oxide) and poly(butyl acrylate). *J. Appl. Polym. Sci.*, **86**, 3120
582 (2002).

583 Wang, G., Li, M., Chen, X. (1999). Effects of fillers on mechanical properties of a
584 water swellable rubber *J. Appl. Polym. Sci.* **72**, 577.

585 Willet, J.L., Finkenstadt, V.L. (2003). Preparation of starch-graft-polyacrylamide
586 copolymers by reactive extrusion, *Polym. Eng. Sci*, **43**, 1666.

587 Willette, J.L., Finkenstadt, V.L. (2006). Reactive Extrusion of Starch–Polyacrylamide
588 Graft Copolymers Using Various Starches. *J. Polym. Environ*, **14**, 125.

589 Yoksan, R. (2008). Epoxidized Natural Rubber for Adhesive Applications. *Kasetsart*
590 *Journal: Natural Science 42*, 325 - 332.

591 Yoon, D. J., Carr, M. E., & Bagley, E. B. (1992). Reactive extrusion vs. batch
592 preparation of starch-*g*-polyacrylonitrile. *J. Appl. Polym. Sci.,* **45**, 1093–1100.

593 Zain, N. M.; Arof, A. K. (1998). Structural and electrical properties of poly (ethylene
594 oxide)-cadmium sulphate complexes. *Materials Science and Engineering: B 52*,
595 40-46.

596 Zhang, G., Zhang, Z., Xie, F., Hu, X., Luo, X. Chen, X. (2000). Chlorohydrin water
597 swellable rubber compatibilized by an amphiphilic graft copolymer. I. Synthesis
598 and characterization of compatibilizer PVA-*g*-PBA *J. Appl. Polym. Sci.*, **75**,
599 977.
600 Zhang, Z., Zhang, G., Li, D., Liu, Z., Chen, X. (1999). Chlorohydrin water-swellable
601 rubber compatibilized by an amphiphilic graft copolymer. II. Effects of PVA-*g*-
602 PBA and CPA on water-swelling behaviors, *J. Appl. Polym. Sc.i*, **74**, 3145.
603 Zhang, Z., Zhang, G., Wang, C., Liu, D., Liu, Z., Chen, X. (2001). Chlorohydrin
604 water-swellable rubber compatibilized by an amphiphilic graft copolymer. III.
605 Effects of PEG and PSA on water-swelling behavior, *J. Appl. Polym. Sci.*, **79**,
606 2509
607 Zong-Qiang, Z.; He-Ping, Y.; Qi-Fang, W.; Guang, L. (2008). Effects of Coagulation
608 Processes on Properties of Epoxidized Natural Rubber. *Journal of Applied*
609 *Polymer Science 109*, 1944-1949.

Unterschrift

Ort, Datum

ที่ ศธ 0527.01/ว 1742

มหาวิทยาลัยนเรศวร
ตำบลท่าโพธิ์ อำเภอเมืองพิษณุโลก
จังหวัดพิษณุโลก 65000

18 กุมภาพันธ์ 2551

เรื่อง ตอบรับการนำเสนอผลงานทางวิชาการ “นเรศวรวิจัย” ครั้งที่ 4

เรียน นายอภิพร อภิรักษ์ชัยสกุล

ตามที่ท่านสมัครเข้าร่วมนำเสนอผลงานวิจัยในการประชุมทางวิชาการ “นเรศวรวิจัย” ครั้งที่ 4 : การบริหารนวัตกรรม ในระหว่างวันที่ 28-29 กรกฎาคม 2551 ณ คณะวิทยาศาสตร์ มหาวิทยาลัยนเรศวร จังหวัดพิษณุโลก โดยท่านเข้าร่วมนำเสนอผลงานประเภท Postor Presentation ในหัวข้อเรื่อง “การใช้เส้นใยนุ่นในการปรับปรุงสมบัติกระดาษ” นั้น

คณะกรรมการจัดงานได้ตรวจสอบผลงานของท่านเป็นที่เรียบร้อยแล้ว และขอแจ้งให้ทราบว่าผลงานวิจัยของท่านได้รับการคัดเลือกให้นำเสนอในการประชุมทางวิชาการ “นเรศวรวิจัย” ครั้งที่ 4

ทั้งนี้ ขอให้ตรวจสอบกำหนดการนำเสนอและรายละเอียดการเตรียมข้อมูลการนำเสนอทางเว็บไซต์ << http://irda.research.nu.ac.th/ns4/ >> ตั้งแต่วันที่ 15 มิถุนายน 2551 เป็นต้น

จึงเรียนมาเพื่อโปรดทราบ

ขอแสดงความนับถือ

(ผู้ช่วยศาสตราจารย์ ดร.วิบูลย์ วัฒนาธร)
รองอธิการบดีฝ่ายวิจัยและประกันคุณภาพ ปฏิบัติราชการแทน
อธิการบดีมหาวิทยาลัยนเรศวร

สถาบันบริหารการวิจัยและพัฒนา
โทร.0-5526-1000-4 ต่อ 1647
โทรสาร. 0-5526-1107

เอกสารแจ้งรายละเอียดของการเข้าร่วมการประชุมทางวิชาการ

“นเรศวรวิจัย” ครั้งที่ 4 : การบริหารนวัตกรรม

วันที่ 28-29 กรกฎาคม 2550 ณ คณะวิทยาศาสตร์ มหาวิทยาลัยนเรศวร จังหวัดพิษณุโลก

★ ★ ★ ★ ★ ★ ★ ★ ★ ★ ★ ★ ★ ★ ★ ★

คำชี้แจง โปรดแสดงเอกสารฉบับนี้กับเจ้าหน้าที่รับลงทะเบียนหน้างาน

ส่วนที่ 1 ข้อมูลพื้นฐาน

รหัสเข้างาน	**นำเสนอ** : << ...รหัส...>>	**เข้าชมผลงาน** : << ..ลำดับ...>>
หมายเลขประจำตัวประชาชน	3419900170491	
ชื่อ-สกุล	นายอภิพร อภิรักษ์ชัยสกุล	
สังกัดหน่วยงาน	จุฬาลงกรณ์มหาวิทยาลัย	
โทรศัพท์(มือถือ)	0817991749	
E-mail	peat2000@hotmail.com	

ข้อมูลสำหรับออกใบเสร็จ

ได้รับเงินจาก	.
หน่วยงาน	.
ที่อยู่	542/35 หมู่บ้านกลางเมืองรัชดา 3 ซอยสหการประมูล ถนนประชาอุทิศ เขตวังทองหลาง กรุงเทพ 10310
จำนวนเงิน	1500 *(ถ้าเลือก 1 ชำระ 1,200 บาท , ถ้าเลือก 2 ชำระ 1,500 บาท)*

ส่วนที่ 2 การเข้าร่วมงานเลี้ยง

เข้าร่วมงานเลี้ยง

ประเภท ปกติ

ส่วนที่ 3 ผลงานวิจัย

เรื่องที่ 1	ประเภท	Postor Presentation
	เรื่อง	การใช้เส้นใยนุ่นในการปรับปรุงสมบัติกระดาษ
	กลุ่ม	กลุ่มวิทยาศาสตร์และเทคโนโลยี
	ตีพิมพ์	Abstact ,Proceeding
เรื่องที่ 2 (ถ้ามี)	ประเภท	<<Oral Presentation / Poster Presentation>>
	เรื่อง	<< ชื่องานวิจัย>>
	กลุ่ม	<<กลุ่ม>>
	ตีพิมพ์	<<การตีพิมพ์>>
เรื่องที่ 3 (ถ้ามี)	ประเภท	<<Oral Presentation / Poster Presentation>>
	เรื่อง	<< ชื่องานวิจัย>>
	กลุ่ม	<<กลุ่ม>>
	ตีพิมพ์	<<การตีพิมพ์>>

การใช้เส้นใยนุ่นในการปรับปรุงสมบัติกระดาษ

อภิพร อภิรักษ์ชัยสกุล* กุนทินี สุวรรณกิจ สมพร ชัยอารีย์กิจ สุดา เกียรติกำจรวงศ์

The Use of Kapok Fiber to Improve Paper Properties

Apiporn Apirakchaiskul, Kuntinee Suvarnakich, Somporn Chaiarrekij,
Suda Kiatkamjornwong

ภาควิชาวิทยาศาสตร์ทางภาพถ่ายและเทคโนโลยีทางการพิมพ์ คณะวิทยาศาสตร์ จุฬาลงกรณ์มหาวิทยาลัย ถนนพญาไท เขตปทุมวัน กรุงเทพ 10330
Department of Photographic Science and Printing Technology, Faculty of Science, Chulalongkorn University, Phayathai road., Pathumwan, Bangkok 10330
Corresponding author. E-mail: peat2000@hotmail.com

บทคัดย่อ

สมบัติของเส้นใยนุ่นมีศักยภาพที่จะเป็นวัตถุดิบเพื่อทดแทนเส้นใยจากต้นไม้ในการผลิตกระดาษ เส้นใยนุ่นมีความยาวเส้นใย 25-30 มิลลิเมตร และมีผนังเส้นใยที่บาง เมื่อนำมาใช้ในกระบวนการผลิตกระดาษน่าจะช่วยเพิ่มความแข็งแรงของกระดาษได้ งานวิจัยนี้เป็นการศึกษาหาภาวะการผลิตเยื่อที่เหมาะสมจากเส้นใยนุ่นเพื่อใช้ในการผลิตกระดาษ และศึกษาอิทธิพลของเยื่อนุ่นที่มีต่อสมบัติกระดาษเมื่อนำเยื่อนุ่นไปผสมกับเยื่อใยสั้นทางการค้า การทดลองเริ่มจากนำเส้นใยนุ่นมาแช่น้ำเป็นเวลา 3 สัปดาห์ ผลิตเยื่อด้วยกระบวนการโซดา โดยใช้โซเดียมไฮดรอกไซด์ร้อยละ 10, 15, 20, และ 25 ของน้ำหนักเยื่อแห้ง ใช้อัตราส่วนสารละลายต่อน้ำหนักแห้งของนุ่นเท่ากับ 17 ต่อ 1 ต้มเยื่อที่อุณหภูมิ 120 องศาเซลเซียส เป็นเวลา 2 ชั่วโมง นำเยื่อที่ได้มาบดด้วยเครื่องบดเยื่อแบบจานบด (Disc Refiner) โดยบดที่ระยะระหว่างจานบดเท่ากับ 10/1000 นิ้ว จำนวน 2 รอบ นำเยื่อมาตีกระจาย 100,000 รอบ และขึ้นแผ่นกระดาษโดยให้มีน้ำหนักมาตรฐานเท่ากับ 60 กรัมต่อตารางเมตร จากการทดลองพบว่า เมื่อใช้ปริมาณของโซเดียมไฮดรอกไซด์เพิ่มขึ้น ทำให้ค่าสภาพระบายได้ของเยื่อลดลง แต่ความหนาแน่น ความเรียบ ดรรชนีความแข็งแรงต่อแรงดึง และดรรชนีความแข็งแรงต่อแรงดันทะลุของกระดาษสูงขึ้น ภาวะที่เหมาะสมในการทำเยื่อคือ ใช้โซเดียมไฮดรอกไซด์ร้อยละ 20 ของน้ำหนักเยื่อแห้ง เพราะให้ดรรชนีความแข็งแรงต่อแรงดึงสูงสุด เยื่อนุ่นมีการกระจายตัวของความยาวเส้นใยค่อนไปทางเยื่อใยยาว การนำเยื่อนุ่นมาผสมกับเยื่อใยสั้นทางการค้าจะช่วยเพิ่มความแข็งแรงต่อแรงดึง ความแข็งแรงต่อแรงดันทะลุ และช่วยเพิ่มความต้านทานน้ำของกระดาษได้

คำสำคัญ : นุ่น การผลิตเยื่อแบบโซดา สมบัติกระดาษ

Abstract

Kapok fiber has a potential to substitute or use with other fibers from wood. With the fiber length of 25-30 mm and a thin fiber wall, kapok fiber might be able to increase strength of paper prepared by mixed commercial pulp and kapok pulp. This research was thus aimed to find the optimal pulping condition for kapok fiber and investigate the influence of kapok pulp on paper properties when handsheets were prepared by the mixture of kapok pulp and commercial hardwood pulp with different ratios. Kapok fibers were immersed in water for 3 weeks then pulped by a soda process using different sodium hydroxide (NaOH) dosages (10, 15, 20, and 25% based on oven dry pulp weight). The fibers were pulped with a liquor-to-wood ratio of 17:1 with the temperature of 120 °C for 2 hours. Then, the kapok pulp was refined twice by a disc refiner with a 10/1000 inch disc gap and disintegrated at 100,000 revolutions. The handsheets having a basis weight of 60 g/m^2 were made, and optical and physical properties were examined. The results indicated that higher sodium hydroxide dosage decreased pulp freeness but increased apparent density, smoothness, tensile index and burst index. The optimal dosage of sodium hydroxide was 20% based on the oven dry pulp weight since the highest strength as indicated by tensile index was obtained. The kapok pulp in this research had the fiber length distribution close to the one from softwood pulp than that from hardwood pulp. It was also found that tensile strength, burst strength and water repellency increased by using kapok pulp mixed with the commercial hardwood pulp.

Key words: Kapok Soda pulping Paper properties

บทนำ

วัสดุที่นำมาผลิตกระดาษส่วนใหญ่มาจากลำต้นของต้นไม้ ซึ่งอาจเป็นการตัดไม้ทำลายป่า แม้ในปัจจุบันจะมีการปลูกป่าทดแทนหรือทำฟาร์มต้นไม้ แต่ก็อาจกระทบกระเทือนต่อระบบนิเวศน์และดินของพื้นที่บริเวณนั้นได้ จึงได้มีความพยายามที่จะนำพืชเส้นใยที่ไม่ได้มาจากลำต้นของต้นไม้มาใช้ทดแทน นุ่นเป็นพืชเส้นใยชนิดหนึ่งที่พบได้ในทุกภาคของประเทศไทย โดยมีการนำนุ่นมาใช้เป็นไส้หมอนและที่นอนเพื่อเพิ่มความนุ่ม อย่างไรก็ตาม ปัจจุบันการใช้เส้นใยนุ่นลดน้อยลง เนื่องจากมีเส้นใยสังเคราะห์เข้ามาแทนที่ รวมถึงยังมีนุ่นที่เหลือทิ้งจากหมอนและที่นอนเก่า งานวิจัยนี้จึงมุ่งที่จะนำนุ่นที่เหลือใช้ รวมถึงนุ่นที่ผ่านการใช้งานแล้วมาเพิ่มมูลค่า โดยนำมาใช้เป็นวัตถุดิบในการผลิตกระดาษ จากงานวิจัยของ Lim และคณะ (Lim & Huang, 2007) ได้ศึกษาการนำเส้นใยนุ่นมาใช้ในการดูดซึมน้ำมัน พบว่าเส้นใยนุ่นมีความต้านการซึมน้ำแต่ดูดซึมน้ำมันได้ดี งานวิจัยของอุทุมพร และคณะ (Wongsaisuwan & Watchanakit, 2007) ได้ศึกษาการทำกระดาษจากเส้นใยนุ่น พบว่าเส้นใยนุ่นสามารถนำมาทำกระดาษได้

เส้นใยนุ่นมีลักษณะยาวรี ผนังบางและเรียบ ลักษณะของตัวเส้นใยค่อนข้างเปราะ มีเส้นผ่านศูนย์กลางรวมผนังเส้นใยประมาณ 16.5±2.4 ไมโครเมตร มีช่องว่างกลางเส้นใย (Lumen) ประมาณ 14.5±2.4 ไมโครเมตร และมีความยาวเส้นใยประมาณ 25–30 มิลลิเมตร (Lim & Huang, 2007) เนื่องด้วยเส้นใยนุ่นมีเส้นใยที่ยาว และมีผนังเส้นใยที่บาง จึงมีแนวคิดว่าเมื่อนำมาผลิตเป็นเยื่อเพื่อผสมกับเยื่อทางการค้า น่าจะช่วยเพิ่มความแข็งแรงให้กับกระดาษ รวมถึงน่าจะช่วยเพิ่มสมบัติความต้านทานน้ำให้แก่กระดาษได้ เนื่องจากเส้นใยนุ่นมีลักษณะต้านทานการซึมน้ำได้ดี

กระดาษที่ใช้กันทั่วไปมีส่วนผสมของเยื่อใยสั้นและเยื่อใยยาว โดยเยื่อใยยาวช่วยเพิ่มสมบัติด้านความแข็งแรง ในขณะที่เยื่อใยสั้นช่วยเพิ่มความเรียบแก่กระดาษ เยื่อใยสั้นสามารถผลิตได้ในประเทศไทย ในขณะที่เยื่อใยยาวต้องมีการนำเข้าจากต่างประเทศ เนื่องจากเส้นใยนุ่นมีเส้นใยที่ยาว เมื่อนำมาผลิตเป็นเยื่อจึงน่าจะทดแทนการนำเข้าเยื่อใยยาวจากต่างประเทศได้ งานวิจัยนี้เป็นการหาภาวะที่เหมาะสมในการผลิตเยื่อจากเส้นใยนุ่น และศึกษาสมบัติกระดาษที่ได้จากการนำเยื่อนุ่นมาผสมกับเยื่อใยสั้นทางการค้า ผลที่ได้นอกจากจะเป็นการเสนอพืชเส้นใยชนิดใหม่เพื่อใช้ในกระบวนการผลิตกระดาษแล้ว ยังอาจจะเป็นทางเลือกในการนำวัสดุเหลือใช้ มาทดแทนการนำเข้าของเยื่อใยยาวจากต่างประเทศได้

วัสดุอุปกรณ์และวิธีการทดลอง

<u>ตอนที่ 1</u> : การหาภาวะการผลิตเยื่อที่เหมาะสม (หาปริมาณโซเดียมไฮดรอกไซด์ที่เหมาะสม)

นำเส้นใยนุ่นที่ผ่านการแช่น้ำเป็นเวลา 3 สัปดาห์ มาบีบน้ำออกและตัดเป็นชิ้นขนาดประมาณ 3–5 เซนติเมตร จากนั้นนำมาผลิตให้เป็นเยื่อด้วยกระบวนการโซดา คือ ต้มเยื่อโดยใช้โซเดียมไฮดรอกไซด์ (NaOH) ในการทดลองมีการใช้โซเดียมไฮดรอกไซด์ในปริมาณต่าง ๆ เพื่อหาค่าที่เหมาะสม โดยใช้โซเดียมไฮดรอกไซด์ร้อยละ 10, 15, 20, และ 25 ของน้ำหนักเยื่อแห้ง ใช้ค่าอัตราส่วนสารละลายต่อน้ำหนักแห้งของนุ่น (Liquor-to-wood ratio) เท่ากับ 17 ต่อ 1 ต้มเยื่อโดยใช้เครื่อง Autoclave digester ที่อุณหภูมิ 120 องศาเซลเซียส เป็นเวลา 120 นาที นำเยื่อที่ผลิตได้มาล้างให้สะอาดและตัดเป็นชิ้นขนาด 3–5 เซนติเมตร และนำเยื่อที่ผ่านการคัดแล้วมาบดโดยใช้เครื่องบดแบบจาน (Disc refiner) ซึ่งใช้ระยะระหว่างจานบดที่ 10/1000 นิ้ว บดเป็นจำนวน 2 รอบ นำเยื่อที่บดได้มาตีกระจายที่ 100,000 รอบ ก่อนที่จะนำเยื่อมาขึ้นแผ่นกระดาษให้มีน้ำหนักมาตรฐาน 60 กรัมต่อตารางเมตร

<u>ตอนที่ 2</u> : การศึกษาสมบัติของกระดาษเมื่อนำเยื่อนุ่นมาผสมกับเยื่อใยสั้นทางการค้า

นำเยื่อที่ได้จากการทดลองตอนที่ 1 ซึ่งให้สมบัติของกระดาษที่ดีที่สุดมาฟอกด้วยไฮโดรเจนเปอร์ออกไซด์ (H_2O_2) โดยใช้ความเข้มข้นของไฮโดรเจนเปอร์ออกไซด์ร้อยละ 3 ของน้ำหนักเยื่อแห้ง ใส่โซเดียมซิลิเกต (Na_2SiO_3) ร้อยละ 0.75 ของปริมาตรรวม ทำการฟอกเยื่อที่อุณหภูมิ 80 องศาเซลเซียส เป็นเวลา 120 นาที จากนั้นนำเยื่อที่ฟอกแล้วมาตีกระจายที่ 100,000 รอบ และนำมาผสมกับเยื่อใยสั้นทางการค้า (Phenix Pulp & Paper mill,

Thailand) โดยใช้อัตราส่วนนุ่นต่อเยื่อทางการค้าเท่ากับ 0:100, 25:75, 50:50, 75:25, และ 100:0 นำเยื่อผสมมาขึ้นแผ่นกระดาษโดยให้มีน้ำหนักมาตรฐานเท่ากับ 60 กรัมต่อตารางเมตร

นำเยื่อและแผ่นกระดาษที่ได้มาทำการทดสอบสมบัติต่าง ๆ โดยค่าสภาพระบายได้ (Freeness) ของเยื่อจะวัดแบบ Canadian Standard Method ตามมาตรฐาน TAPPI T-227 โดยทำการวัด 2 ตัวอย่างและนำมาหาค่าเฉลี่ย ส่วนสมบัติอื่น ๆ ของแผ่นกระดาษนั้นทำการวัดโดยใช้แผ่นกระดาษจำนวน 6 ตัวอย่าง สมบัติที่ทดสอบมีดังนี้ ความเรียบ (Smoothness) ของแผ่นกระดาษจะวัดแบบ Bekk ตามมาตรฐาน TAPPI T-479 ความขาวสว่าง (Brightness) วัดตามมาตรฐาน ISO-2470 ความทึบแสง (Opacity) วัดตามมาตรฐาน ISO-2471 ค่าดรรชนีความแข็งแรงต่อแรงดึง (Tensile index) วัดตามมาตรฐาน TAPPI T-494 ค่าดรรชนีความแข็งแรงต่อแรงดันทะลุ (Burst index) วัดตามมาตรฐาน TAPPI T-403 และการกระจายตัวของความยาวเส้นใย (Fiber length distribution) เป็นค่าเฉลี่ยจากเส้นใยจำนวน 4,000 เส้น และวัดโดยใช้เครื่อง HiRes FQA-Fiber quality analyzer

ผลการศึกษา

ผลการทดลองตอนที่ 1

ตารางที่ 1 สมบัติกระดาษจากเยื่อนุ่นที่ผลิตโดยใช้ความเข้มข้นของโซเดียมไฮดรอกไซด์แตกต่างกัน

Properties	Sodium hydroxide (NaOH) concentration (%)			
	10%	15%	20%	25%
Freeness (CSF, mL)	447	398	302	285
Apparent Density (g/cm^3)	0.60	0.78	0.80	0.86
Bottom Smoothness (s)	2.83	6.33	7.51	8.04
Top Smoothness (s)	5.27	10.05	10.59	12.28
Brightness (%)	22.63	19.76	19.40	18.42
Opacity (%)	98.13	97.47	97.48	96.91
Tensile index (Nm/g)	79.43	99.52	112.89	102.48
Burst index (kPa m^2/g)	3.94	5.79	5.91	5.96

จากตารางที่ 1 เมื่อผลิตเยื่อโดยใช้ความเข้มข้นของโซเดียมไฮดรอกไซด์สูงขึ้น ส่งผลให้ค่าสภาพระบายได้ของเยื่อ และค่าความขาวสว่างลดลง อย่างไรก็ตามสมบัติด้านความหนาแน่น ความเรียบ ดรรชนีความแข็งแรงต่อแรงดึง และดรรชนีความแข็งแรงต่อแรงดันทะลุ กลับมีแนวโน้มเพิ่มสูงขึ้น ปริมาณโซเดียมไฮดรอกไซด์ที่ใช้ในการทดลองนี้มีผลต่อความทึบแสงน้อยมาก ผลที่ได้จากการทดลองตอนที่ 1 แสดงให้เห็นว่าปริมาณของโซเดียมไฮดรอกไซด์ที่เหมาะสมในการผลิตเยื่อนุ่นมีค่าเท่ากับร้อยละ 20 ของน้ำหนักเยื่อแห้ง ดังนั้นเยื่อนุ่นที่ใช้ในการทดลองตอนที่ 2 จึงเป็นเยื่อนุ่นที่ผลิตโดยใช้โซเดียมไฮดรอกไซด์ในการต้มเยื่อร้อยละ 20

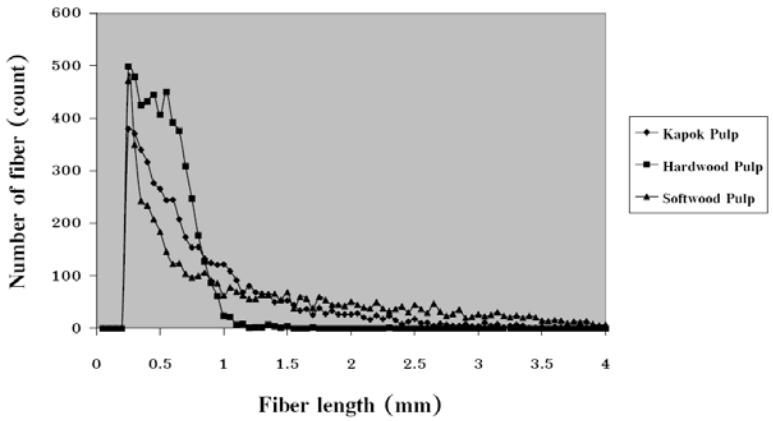

รูปที่ 1 การกระจายตัวของความยาวเส้นใยเปรียบเทียบระหว่างเยื่อนุ่น เยื่อใยสั้น และเยื่อใยยาว (เมื่อผลิตเยื่อนุ่นด้วย NaOH 20%)

รูปที่ 1 เป็นการเปรียบเทียบการกระจายตัวของความยาวเส้นใยของเยื่อใยสั้น เยื่อใยยาว และเยื่อนุ่น ที่ผ่านการบดเยื่อจนได้ค่าสภาพระบายได้ประมาณ 300 มิลลิลิตร (ภาวะการผลิตเยื่อนุ่นโดยใช้โซเดียมไฮดรอกไซด์ร้อยละ 20) จะเห็นได้ว่าเยื่อใยสั้นจะมีการกระจายตัวของเส้นใยอยู่ในช่วงความยาวประมาณ 0.3–1 มิลลิเมตร สำหรับเยื่อนุ่นและเยื่อใยยาวจะมีการกระจายตัว 0.3–4 มิลลิเมตร โดยลักษณะการกระจายตัวของเยื่อนุ่นมีแนวโน้มใกล้เคียงกับเยื่อใยยาว

ตารางที่ 2 สมบัติด้านความแข็งแรงของกระดาษที่ผลิตจากเยื่อนุ่น เยื่อใยสั้น และเยื่อใยยาว (เมื่อผลิตเยื่อนุ่นด้วย NaOH 20%)

Strength properties	Type of pulp		
	Kapok	Hardwood	Softwood
Tensile index (Nm/g)	105.84	66.87	91.36
Burst index (kPa m^2/g)	6.05	3.75	5.75

จากตารางที่ 2 จะเห็นได้ว่าเยื่อนุ่นที่ผลิตได้มีค่าดรรชนีความแข็งแรงต่อแรงดึง และค่าดรรชนีความแข็งแรงต่อแรงดันทะลุสูงกว่าเยื่อใยสั้นและเยื่อใยยาว

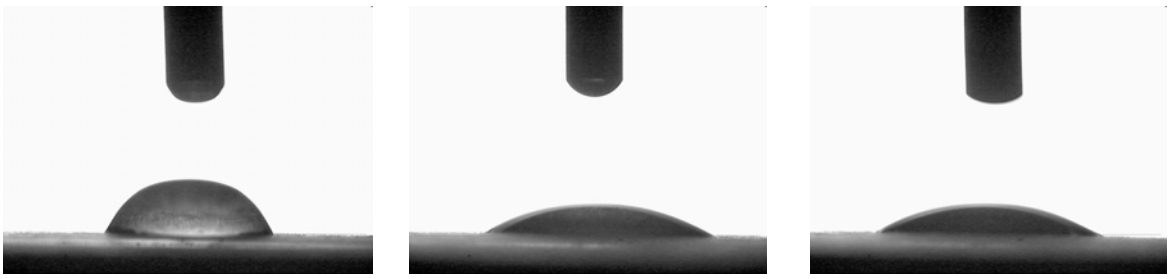

รูปที่ 2 รูปหยดน้ำบนแผ่นกระดาษที่ผลิตจากเยื่อนุ่น เยื่อใยสั้น และเยื่อใยยาว (เมื่อผลิตเยื่อนุ่นด้วย NaOH 20%)

รูปที่ 2 แสดงผลของหยดน้ำบนกระดาษที่ผลิตจากเยื่อนุ่น เยื่อใยสั้น และเยื่อใยยาว จะเห็นได้ว่ากระดาษที่ผลิตจากเยื่อนุ่นมีมุมสัมผัสของน้ำสูงกว่า แสดงว่ากระดาษที่ผลิตจากเยื่อนุ่นมีความสามารถในการต้านการซึมน้ำได้ดีกว่า

ผลการทดลองตอนที่ 2

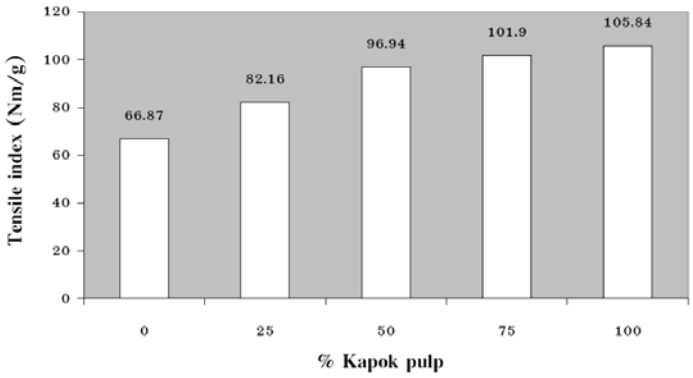

รูปที่ 3 ดรรชนีความแข็งแรงต่อแรงดึงของกระดาษที่ผลิตจากเยื่อผสมระหว่างเยื่อนุ่นและเยื่อใยสั้นในปริมาณต่าง ๆ กัน

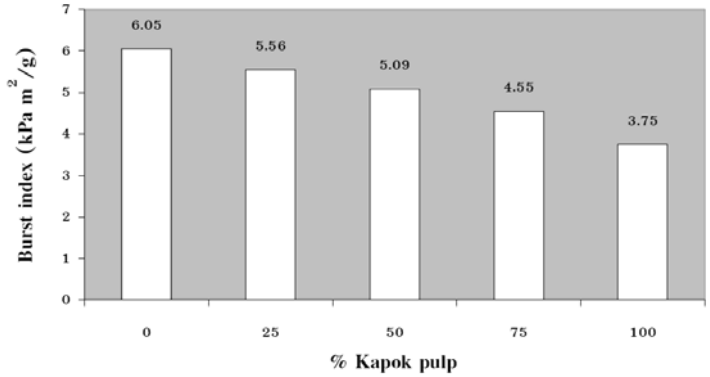

รูปที่ 4 ดรรชนีความแข็งแรงต่อแรงดันทะลุของกระดาษที่ผลิตจากเยื่อผสมระหว่างเยื่อนุ่นและเยื่อใยสั้นในปริมาณต่าง ๆ กัน

จากรูปที่ 3 และ 4 พบว่า เมื่อใช้เยื่อนุ่นผสมในสัดส่วนที่มากขึ้น ส่งผลให้ค่าดรรชนีความแข็งแรงต่อแรงดึงและค่าดรรชนีความแข็งแรงต่อแรงดันทะลุเพิ่มสูงขึ้น แสดงว่าการผสมเยื่อนุ่นลงในแผ่นกระดาษจะทำให้แผ่นกระดาษที่ได้มีความแข็งแรงมากขึ้น

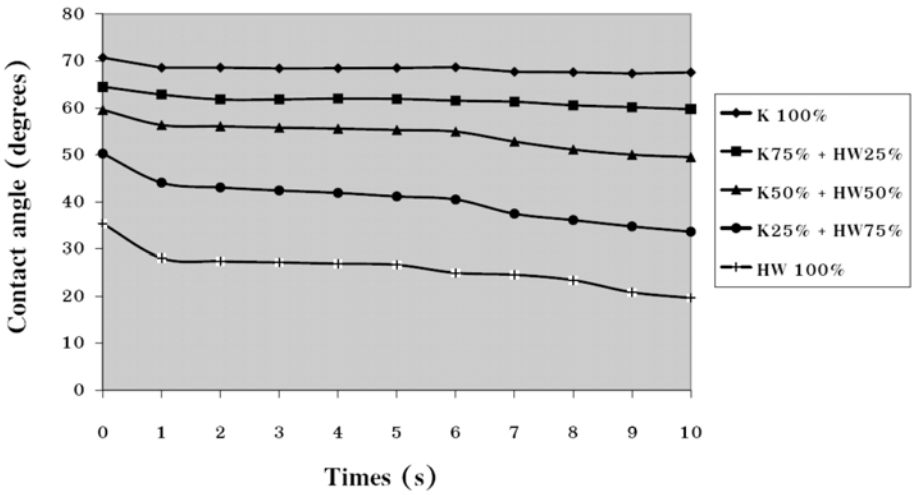

รูปที่ 5 ค่ามุมสัมผัสของน้ำบนกระดาษที่ผลิตจากเยื่อผสมระหว่างเยื่อนุ่นและเยื่อใยสั้นในปริมาณต่าง ๆ กัน
(K= kapok และ HW = hardwood)

จากรูปที่ 5 กระดาษที่ผลิตจากเยื่อใยสั้นที่มีสัดส่วนเยื่อนุ่นผสมเพิ่มมากขึ้น ค่ามุมสัมผัสของน้ำจะเพิ่มสูงขึ้น แสดงว่า การผสมเยื่อนุ่นลงในกระดาษทำให้กระดาษมีความต้านทานการซึมน้ำเพิ่มขึ้น

อภิปรายผลการศึกษา

ผลการทดลองจากตอนที่ 1 ชี้ให้เห็นว่าเมื่อผลิตเยื่อโดยใช้ความเข้มข้นของโซเดียมไฮดรอกไซด์สูงขึ้น ค่าสภาพระบายได้ของเยื่อจะลดลง ทั้งนี้อาจเนื่องมาจากปริมาณโซเดียมไฮดรอกไซด์ที่เพิ่มขึ้น ทำให้สามารถกำจัดลิกนินออกได้มากขึ้น เส้นใยจึงเป็นอิสระและมีพื้นที่ผิวในการอุ้มน้ำเพิ่มขึ้น ค่าสภาพระบายได้จึงลดลง การใช้ปริมาณโซเดียมไฮดรอกไซด์ที่สูงขึ้น ยังส่งผลให้ค่าความหนาแน่นและความแข็งแรงของกระดาษเพิ่มสูงขึ้น เป็นเพราะว่าลิกนินถูกกำจัดออกมากขึ้น เส้นใยเดี่ยว ๆ จึงสามารถสร้างพันธะต่อกันได้ดีขึ้น ทำให้กระดาษแน่นและแข็งแรงขึ้น อย่างไรก็ตามเป็นที่น่าสังเกตว่า เมื่อใช้ปริมาณด่างสูงจนเกินไปเช่นในกรณีของการใช้โซเดียมไฮดรอกไซด์ร้อยละ 25 ของน้ำหนักเยื่อแห้ง กลับส่งผลให้ความแข็งแรงต่อแรงดึงลดลง ทั้งนี้อาจเป็นเพราะเซลลูโลสและเฮมิเซลลูโลส ซึ่งเป็นองค์ประกอบหลักของเส้นใยถูกทำลาย โดยปฏิกิริยาที่เรียกว่า Peeling reaction นอกจากนี้การใช้ปริมาณด่างที่สูงขึ้นยังมีแนวโน้มทำให้ค่าความขาวสว่างลดน้อยลง ทั้งนี้เป็นเพราะการใช้ปริมาณโซเดียมไฮดรอกไซด์ที่มากเกินไป จะทำให้เยื่อเกิดสีคล้ำขึ้นจากปฏิกิริยาที่เรียกว่า Alkali darkening ผลการทดลองยังชี้ให้เห็นว่า ปริมาณโซเดียมไฮดรอกไซด์ที่ใช้ในการทดลองนี้ มีผลต่อความทึบแสงของกระดาษน้อยมาก

จากผลการทดลองตอนที่ 1 ทำให้สรุปได้ว่า ค่าปริมาณโซเดียมไฮดรอกไซด์ที่เหมาะสมสำหรับการผลิตเยื่อนุ่นในงานวิจัยนี้คือ ร้อยละ 20 ของน้ำหนักเยื่อแห้ง เนื่องจากเป็นค่าที่ให้สมบัติของเยื่อนุ่นที่ผลิตได้เหมาะสมที่สุด ดังนั้นจึงใช้ค่านี้ในการผลิตเยื่อนุ่นสำหรับการทดลองในตอนที่ 2 ต่อไป

จากการทดลองตอนที่ 2 พบว่า การใช้เยื่อนุ่นมาผสมกับเยื่อใยสั้นทางการค้าเพื่อผลิตกระดาษ ทำให้กระดาษที่ได้มีค่าความต้านทานการซึมน้ำสูงขึ้น เมื่อใช้ปริมาณเยื่อนุ่นเพิ่มขึ้น ทั้งนี้เนื่องมาจากเส้นใยนุ่นมีสมบัติความต้านทานการซึมน้ำสูงกว่าเยื่อใยสั้นและเยื่อใยยาว ลักษณะเฉพาะของเส้นใยนุ่นคือ การมี Cutin waxes เคลือบที่ผิวเส้นใยทำให้มีสมบัติการต้านการซึมของน้ำ กระบวนการผลิตเยื่อแม้มีการขจัดแวกซ์ออก แต่ก็ยังเหลืออยู่บนผิวของเส้นใย เมื่อนำเยื่อนุ่นไปผลิตกระดาษ จึงส่งผลให้กระดาษมีความไม่ชอบน้ำ การใช้เยื่อนุ่นผสมในอัตราส่วนที่มากขึ้นยังทำให้กระดาษที่ผลิตได้มีความแข็งแรงเพิ่มขึ้น ทั้งนี้เนื่องจากเส้นใยนุ่นมีการกระจายตัวของความยาวเส้นใยค่อนข้างใกล้เคียงกับเยื่อใยยาว จึงส่งผลให้กระดาษที่ผลิตได้จากเยื่อผสมมีความแข็งแรงมากขึ้น เนื่องจากมีสัดส่วนของเส้นใยยาวมากขึ้น และเส้นใยนุ่นมีผนังบาง ทำให้เมื่อนำมาทำกระดาษ จะเกิดการยุบตัวของช่องว่างภายในเส้นใย ทำให้เส้นใยแนบชิดและสร้างพันธะกันได้ดีกว่า ส่งผลให้ความแข็งแรงของกระดาษสูงขึ้น

สรุปผลการศึกษา

เส้นใยนุ่นสามารถนำมาใช้ผลิตเป็นกระดาษได้ ปริมาณโซเดียมไฮดรอกไซด์ที่ใช้ในการต้มเยื่อส่งผลต่อสมบัติของเยื่อและกระดาษที่ผลิตได้จากเส้นใยนุ่น กล่าวคือเมื่อใช้ปริมาณของโซเดียมไฮดรอกไซด์เพิ่มขึ้น ค่าความหนาแน่น และความแข็งแรงของกระดาษจะเพิ่มขึ้น ในขณะที่ค่าสภาพระบายได้และความขาวสว่างมีแนวโน้มลดลง ภาวะในการผลิตเยื่อนุ่นที่เหมาะสมสำหรับงานวิจัยนี้คือใช้ปริมาณโซเดียมไฮดรอกไซด์ร้อยละ 20 ของน้ำหนักเยื่อแห้ง เมื่อนำเส้นใยนุ่นมาผสมกับเยื่อใยสั้นทางการค้าเพื่อผลิตเป็นกระดาษพบว่า การใช้ปริมาณเยื่อนุ่นเพิ่มขึ้นทำให้กระดาษที่ผลิตได้มีความแข็งแรง และความต้านทานการซึมน้ำเพิ่มขึ้น

กิตติกรรมประกาศ

คณะผู้วิจัยขอขอบพระคุณในความสนับสนุนด้านเงินทุนจากโครงการเมธีวิจัยอาวุโส สกว.-สกอ. (สำนักงานกองทุนสนับสนุนการวิจัย – สำนักงานคณะกรรมการการอุดมศึกษา) รหัสโครงการ RTA508004 และผู้อำนวยการศูนย์พัฒนาผลิตภัณฑ์และเทคโนโลยี บริษัท เอสซีจี เปเปอร์ จำกัด (มหาชน) รวมถึงคุณสามารถ ขำทวี ผู้เชี่ยวชาญ

ทางด้านไม้และเยื่อ จากศูนย์พัฒนาผลิตภัณฑ์และเทคโนโลยี บริษัท เอสซีจี เปเปอร์ จำกัด (มหาชน) ที่ได้สละเวลาอันมีค่าให้ความช่วยเหลือ และให้คำปรึกษาในงานวิจัย

เอกสารอ้างอิง

Lim, T.T. & Huang, X.F. (2007). Evaluation of hydrophobicity/oleophilicity of kapok and its performance in oily water filtration: Comparison of raw and solvent-treated fibers. *Industrial Crops and Products*, 26, 125-134.

Lim, T.T. & Huang, X.F. (2007). Evaluation of kapok (*Ceiba pentandra* (L.) Gaertn.) as a natural hollow hydrophobic–oleophilic fibrous sorbent for oil spill cleanup. *Chemosphere*, 66, 957.

Wongsaisuwan, U., & Watchanakit, S. (2007). *Pulping of kapok*. Senior Project in Photographic Science and Printing Technology, Faculty of Science, Chulalongkorn University.

เอกสารแจ้งรายละเอียดของการเข้าร่วมการประชุมทางวิชาการ

“นเรศวรวิจัย” ครั้งที่ 4 : การบริหารนวัตกรรม

วันที่ 28-29 กรกฎาคม 2550 ณ คณะวิทยาศาสตร์ มหาวิทยาลัยนเรศวร จังหวัดพิษณุโลก

★ ★ ★ ★ ★ ★ ★ ★ ★ ★ ★ ★ ★ ★ ★ ★

คำชี้แจง โปรดแสดงเอกสารฉบับนี้กับเจ้าหน้าที่รับลงทะเบียนหน้างาน

ส่วนที่ 1 ข้อมูลพื้นฐาน

รหัสเข้างาน	**นำเสนอ** : << ...รหัส...>>	**เข้าชมผลงาน** : << ..ลำดับ...>>
หมายเลขประจำตัวประชาชน	3419900170491	
ชื่อ-สกุล	นายอภิพร อภิรักษ์ชัยสกุล	
สังกัดหน่วยงาน	จุฬาลงกรณ์มหาวิทยาลัย	
โทรศัพท์(มือถือ)	0817991749	
E-mail	peat2000@hotmail.com	

ข้อมูลสำหรับออกใบเสร็จ

ได้รับเงินจาก	.
หน่วยงาน	.
ที่อยู่	542/35 หมู่บ้านกลางเมืองรัชดา 3 ซอยสหการประมูล ถนนประชาอุทิศ เขตวังทองหลาง กรุงเทพ 10310
จำนวนเงิน	1500 *(ถ้าเลือก 1 ชำระ 1,200 บาท , ถ้าเลือก 2 ชำระ 1,500 บาท)*

ส่วนที่ 2 การเข้าร่วมงานเลี้ยง

เข้าร่วมงานเลี้ยง

ประเภท ปกติ

ส่วนที่ 3 ผลงานวิจัย

เรื่องที่ 1	ประเภท	Postor Presentation
	เรื่อง	การใช้เส้นใยนุ่นในการปรับปรุงสมบัติกระดาษ
	กลุ่ม	กลุ่มวิทยาศาสตร์และเทคโนโลยี
	ตีพิมพ์	Abstact ,Proceeding
เรื่องที่ 2 (ถ้ามี)	ประเภท	<<Oral Presentation / Poster Presentation>>
	เรื่อง	<< ชื่องานวิจัย>>
	กลุ่ม	<<กลุ่ม>>
	ตีพิมพ์	<<การตีพิมพ์>>
เรื่องที่ 3 (ถ้ามี)	ประเภท	<<Oral Presentation / Poster Presentation>>
	เรื่อง	<< ชื่องานวิจัย>>
	กลุ่ม	<<กลุ่ม>>
	ตีพิมพ์	<<การตีพิมพ์>>

การเกิดและความเข้ากันได้ทางชีวภาพของมัลติเลเยอร์ฟิล์มประกอบจากอนุพันธ์ที่มีประจุของไคโทซาน

Formation and biocompatibility of multilayer films assembled from charged derivatives of chitosan

Wilaiporn Graisuwan[1], Songchan Puthong[2], Suda Kiatkamjornwong[3], Voravee P. Hoven[4*]

[1]*Program of Petrochemistry and Polymer Science,* [2]*Institute of Biotechnology and Genetic Engineering,*
[3]*Department of Photoimaging and Printing,* [4]*Organic Synthesis Research Unit, Department of Chemistry,*
Faculty of Science, Chulalongkorn University, Bangkok, Thailand
Tel: +66-2218-7627, Fax: +66-2218-7598, E-mail address: vipavee.p@chula.ac.th

---

บทคัดย่อ : สังเคราะห์อนุพันธ์ที่มีประจุของไคโทซาน 3 ชนิด คือ เอ็น-[(2-ไฮดรอกซิล-3-ไตรเมทิลแอมโมเนียม)โพรพิว]ไคโทซานคลอไรด์, เอ็น-ซักซินิลไคโทซาน และเอ็น-ซัลโฟเฟอร์ฟูริลไคโทซาน เตรียมมัลติเลเยอร์ฟิล์มของอนุพันธ์ที่มีประจุของไคโทซานโดยวิธีการดูดซับแบบประกอบชั้นต่อชั้นได้ ติดตามกระบวนการประกอบเป็นฟิล์มด้วยควอตซ์คริสทัลไมโครบาลานซ์, การวัดมุมสัมผัสของน้ำ, อะตอมมิกฟอร์ซไมโครสโกปีและเอทีอาร์เอฟทีไออาร์สเปกโทรสโกปี จากการทดสอบการตอบสนองทางชีวภาพของมัลติเลเยอร์ฟิล์มที่มีต่อการยึดเกาะและการเพิ่มจำนวนของเซลล์ไฟโบรบลาสต์ในหลอดทดลอง แสดงแนวโน้มแบบสลับเล็กน้อยขึ้นกับฟิล์มชั้นนอกสุด

Abstract: Three charged derivatives of chitosan, *N*-[(2-hydroxyl-3-trimethylammonium) propyl] chitosan chloride (HTACC), *N*-succinyl chitosan (SCC), and *N*-sulfofurfuryl chitosan (SFC) were synthesized. Multilayer films of charged derivatives of chitosan were fabricated by alternate layer-by-layer assembly. The layer-by-layer deposition process was monitored by quartz crystal microbalance (QCM), water contact angle measurement, atomic force microscopy (AFM), and ATR-FTIR spectroscopy. Biological responses of the assembled films assessed by *in vitro* cell adhesion and proliferation of fibroblasts showed slight alternating trend depending on the outermost layer.

Introduction: Charged derivatives of chitosan are categorized as polyelectrolytes which are capable of forming supported multilayer film by the layer-by-layer assembly. This technique has been developed over the past several years as a powerful and versatile method for surface modification of materials. The thickness of multilayer film can be varied as a function of adsorption variables as well as the number of deposition. Most importantly, the surface properties of supported film are determined by the outermost layer that is last deposited. In this respect, a concept of building multilayer film from charged derivatives of chitosan is emerged as an attractive tool for controlling biocompatibility of materials which would satisfy the advanced applications in nanotechnology and biotechnology.

Materials and Methods: Chitosan (95% DD, M_w = 100,000) was obtained from Seafresh Chitosan (Lab). Poly(allylamine hydrochloride) (PAH), M_w = 70,000 was purchased from Aldrich. Poly(acrylic acid) (PAA), M_w = 60,000 was purchased from Fluka. Plasma-treated poly(ethylene terephthalate) films were purchased from Wako Pure Chemical Industry. HTACC was prepared by reacting 2.0 % w/v chitosan solution (1 equiv. of NH_2) with glycidyltrimethylammonium chloride (GTMAC) (4 equiv.) at 70 ºC for 3 h [1]. HTACC was precipitated from an acetone/ethanol (1:1, v/v) mixture, washed and dried under vacuum. SCC was prepared by reacting 2.0 %w/v chitosan solution (1 equiv. of NH_2) with succinic anhydride (SA) (4 equiv.) in methanol at room temperature for 2 h [2]. The pH of the solution was adjusted to 10 using 2 M NaOH solution. After dialysis for 5 days, the solution was freeze-dried to obtain a cotton-like white material. SFC was prepared by reacting 2.0 % w/v chitosan solution (1 equiv. of NH_2) with 5-formyl-2-furansulfonic acid, sodium salt (FFSA) (2 equiv.) in acetic acid/methanol (1:1, v/v) mixture containing 1% w/v triethanolamine at room temperature for 18 h [3]. SFC was obtained after reduction with $NaBH_4$, precipitation in methanol and drying under vacuum. HTACC, SCC, and SFC structures were investigated by ^{1}H NMR and FTIR. The alternating layers were assembled by sequential dipping the plasma-treated PET substrates in a polycation solution (2 mg/mL of PAH, or 2 mg/mL of HTACC) and a polyanion solution (1 mg/mL of SCC, 2 mg/mL of SFC, or 2 mg/mL of PAA). All solutions contained 0.5 M NaCl. Three pairs of polyelectrolyte assemblies were fabricated: at pH 7 for HTACC-PAA and PAH-SCC, and at pH 8 for PAH-SFC. To monitor the stepwise deposition of each pair of polycation-polyanion by QCM, the same procedure was also applied on 5 Hz quartz crystal coated with gold and chemically modified by a mixture of

11-mercaptoundecanoic acid and 10 mM 11-mercapto-1-undecanol. *In vitro* cell adhesion and proliferation ratios of Fibroblast L929 were determined using MTT assay.

Results and Discussion: The conventional mode of QCM measurements was used to follow the multilayer formation on the thiol-modified gold-coated QCM plate by monitoring frequency change as a function of the number of depositions. It should be underlined that this substrate containing a mixed composition of COOH and OH groups represents a model of treated PET substrates, later used for cytocompatibility test. Progressive increases in QCM frequency shift with the number of deposition steps (Fig.1) evidently indicated a stepwise deposition of all three systems. The QCM measurements in air using the conventional mode allow the thickness to be directly calculated from Sauerbrey equation [4]. An average thickness of the bilayer is 25.9, 25.7, and 24.6 nm for HTACC-PAA, PAH-SCC, and PAH-SFC multilayer films, respectively. As a result of the incomplete substitution of HTACC, SCC, and SFC (78%, 44%, and 64%, respectively) at the NH_2 group of chitosan, the adsorption of each charged derivative of chitosan on oppositely charged layer and vice versa were therefore driven by both electrostatic interactions and H-bonding. Besides the train conformation, the adsorbed polyelectrolytes were also in the forms of loop, tail, or coil, making the adsorbed layer relatively thick.

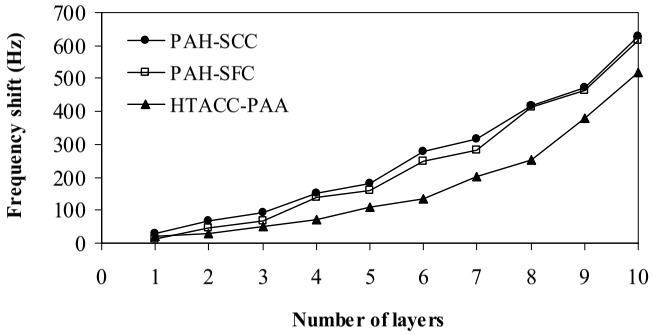

Fig.1. Frequency shift (Hz) due to multilayer assembly on thiol-modified gold-coated QCM plate.

The coverage and functional groups of the multilayer films on the treated PET substrate were verified by ATR-FTIR analysis. Fig.2 reveals the presence of signals corresponding to the desired functionalities of the multilayer films. The presence of new signals that are characteristic peaks of polyelectrolytes in all samples implied that the thickness of the multilayer films reached the detection limit of ATR-FTIR technique. This result was consistent with the QCM data.

The coverage of the deposited multilayer films can be revealed from topographic images obtained by AFM analysis (picture not shown). According to the root-mean-square roughness ($R_{r.m.s.}$) values of the HTACC-PAA and PAH-SCC multilayer systems, the surfaces became smoother after the deposition of 9-16 layers. In the case of PAH-SFC multilayer system, the treated PET substrate was smoother after the deposition of 9 layers. The surface, however, became gradually rougher as the number of layer increased from 9 to 16.

Water contact angle data confirmed that the assembled film was stratified (Fig.3). According to the calculation based on QCM analysis, each individual layer is apparently thicker than the sampling depth of contact angle measurement (a few Å) so that the wettability of the multilayer film should be strongly dictated by the last layer deposited and the influence of the underlying layers should not be observed.

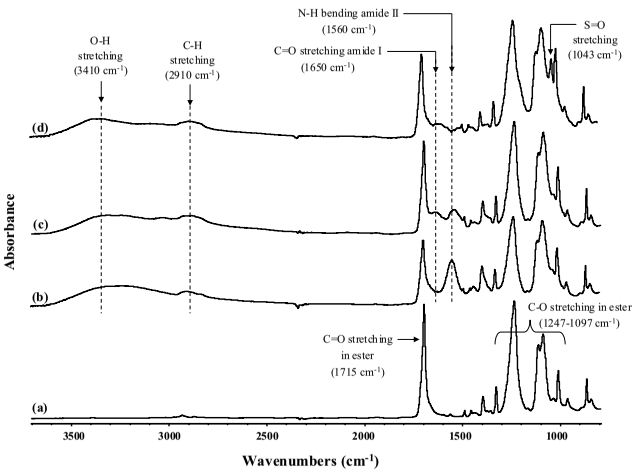

Fig.2. ATR-FTIR spectra of treated PET substrates: (a) after pre-treatment and with multilayer films of (b) $(HTACC\text{-}PAA)_8$, (c) $(PAH\text{-}SCC)_8$, and (d) $(PAH\text{-}SFC)_8$.

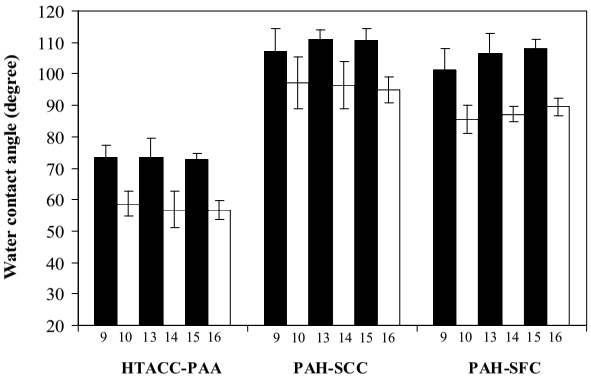

Fig.3. Water contact angle of multilayer films assembled on treated PET substrates.

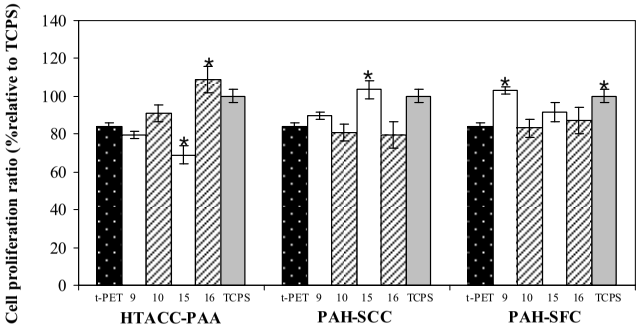

Fig.4. Cell proliferation ratios (% relative to TCPS) of L929 cells at 4 days with a seeding density of 5.0 x 10^3 cells/well on treated PET substrates with three multilayer systems: HTACC-PAA, PAH-SCC, PAH-SFC, and TCPS. Error bars represent mean ± SD for n = 3. *$P < 0.05$ (compared to t-PET)

The *in vitro* cytocompatibility of three multilayer systems on the treated PET substrates was carried out against L929 fibroblasts. Considering the HTACC-PAA system, the multilayer film having the even number of layer with PAA as the top layer seems to be more favorable for both cell adhesion (picture not shown) and proliferation than those having the odd number of layer with HTACC as the top layer. It is generally known that the cell membrane possesses negative charges. The opposite charges of HTACC should lead to a strong attraction with the cells and inhibit the cell growth. The effect is more pronounced after 4 days of incubation (Fig.4). This is in accordance with the work previously reported on the ability to inhibit the bacterial growth of HTACC when used as antibacterial agent in fibers [1,5]. As opposed to the system of HTACC-PAA, the PAH-SCC multilayer films exhibit the opposite tendency. After 2 (picture not shown) and 4 days of incubation, a significant improvement of cell adhesion was observed, especially when the number of layer was equal to 15 and PAH was the top layer. Unlike HTACC, PAH is a weak synthetic polyelectrolyte that has been found to enhance early cell adhesion in the multilayer system of PSS/PAH [6] when it is the outermost layer of the film. The fact that SCC bears some negative charge, which is the same charge as the cell membrane, can explain why it is unfavorable for cell attachment. However, the same explanation cannot be applied with PAA. A similar trend was observed in the case of PAH-SFC system. In particular, the 9-layer multilayer film with PAH as the outermost layer gave significantly higher in both cell adhesion and proliferation than the treated PET substrate. The charge repulsion may also account for the inferior cellular responses of the multilayer films having SFC as the top layer.

Conclusion: Charged derivatives of chitosan, *N*-[(2-hydroxyl-3-trimethylammonium)propyl] chitosan chloride (HTACC), *N*-succinyl chitosan (SCC), and *N*-sulfofurfuryl chitosan (SFC) are capable of forming multilayer film by the layer-by-layer assembly technique. The QCM and water contact angle results verified the progressive buildup the multilayer films by alternate deposition of polyelectrolytes. The coverage of the assembled films was characterized by ATR-FTIR and AFM analyses. *In vitro* cell adhesion and proliferation showed that the degree of cytocompatibility of the multilayer films depends strongly on the polyelectrolyte used for the assembly process and the last layer deposited. The results also suggest that these three charged derivatives of chitosan are potential candidates for biomedical applications.

Acknowledgment: This research is financially supported by a Research Team Promotion Grant, the Thailand Research Fund (RTA4780004 and RTA5080004). The authors are very grateful to Associate Professor Sanong Ekgasit of the Sensor Research Unit, Department of Chemistry, Faculty of Science, Chulalongkorn University for use of ATR-FTIR facility.

References:

[1] Seong, HS, Whang, HS, Ko, SW. (2000) Synthesis of a quaternary ammonium derivative of chito-oligosaccharide as antimicrobial agent for cellulosic fibers. *Journal of Applied Polymer Science,* 76, 2009-2015.

[2] Aoki, N, Nishikawa, M, Hattori, K. (2003) Synthesis of chitosan derivatives bearing cyclodextrin and adsorption of *p*-nonylphenol and bisphenol A. *Carbohydrate Polymers,* 52, 219-223.

[3] Amiji, MM. (1998) Platelet adhesion and activation on an amphoteric chitosan derivative bearing sulfonate groups. *Colloids and Surfaces B: Biointerfaces,* 10, 263-271.

[4] Sauerbrey, G. (1959) Use of quartz crystal vibrator for weighting thin films on a microbalance. *Zeitschrift fur Physik,* 155, 206-222.

[5] Lim, SH, Hudson, SM. (2004) Synthesis and antimicrobial activity of a water-soluble chitosan derivative with a fiber-reactive group. *Carbohydrate Research,* 339, 313-319.

[6] Boura, C, Menu, P, Payan, E, Picart, C, Voegel, JC, Muller, S, Stoltz, JF. (2003) Endothelial cells grown on thin polyelectrolyte multilayered films: an evaluation of a new versatile surface modification. *Biomaterials*, 24, 3521-3530.

Local organizing committee, NTS 2008

Chair	:	S. Songsivilai, NANOTEC/NSTDA, Thailand
Co-Chair	:	T. Pornsinsirirak, NANOTEC/NSTDA, Thailand
		N. Tanpipat, NANOTEC/NSTDA, Thailand
Advisor	:	P. Angkasith, CMU, Thailand
		P. Bhandhubanyong, MTEC/NSTDA, Thailand
		S. Chotipanich, MOST, Thailand
		K. Greigarn, Board of MTEC., Thailand
		S. Irandoust, AIT, Thailand
		V. KapilaKanchana, KU, Thailand
		S. Kiranandana, CU, Thailand
		K. Kiranandana, NSTDA, Thailand
		P. Matangkasombut, MU, Thailand
		S. Sakolchai, KKU, Thailand
		B. Siribumrungsukha, PSU, Thailand
		P. Siriruchatapong, NECTEC/NSTDA, Thailand
		K. Sukondhasingha, NANOTEC, Thailand
		V. Tandaechanurat, THAITEXTILE, Thailand
		M. Tanticharoen, BIOTEC/NSTDA, Thailand
		W. Tanthapanichakoon, SCG
		C. Tengamnuay, GREATERPHARMA, Thailand
		C. Thebtaranonth, TMC/NSTDA, Thailand
		Y. Thebtaranonth, BIOTEC/NSTDA, Thailand
		K. Tiraseth, KMITL, Thailand
		W. Udomkichadecha MTEC/NSTDA, Thailand
		P. Vidtayasuk, DIP, Thailand
		D. Worarith, BB, Thailand
Committee	:	V. Amornkitbamrung, KKU, Thailand
		J. Dutta, AIT, Thailand
		J. Limtrakul, KU, Thailand
		N. Mangkorntong, CMU, Thailand
		J. Nookaew, KMITL, Thailand
		T. Osotchan, MU, Thailand
		S. Panyakeow, CU, Thailand
		C. Silawatshananai, NANOTEC/NSTDA
		P. Vanichapichart, PSU, Thailand
Secretariat	:	S. Teparkum, NANOTEC/NSTDA

PREPARATION AND DYE REMOVAL EFFICIENCY STUDY USING NANO TiO_2/POLY[ACRYLAMIDE-*CO*-(ACRYLIC ACID)] COMPOSITE

***Walasinee JITBUNPOT*[1], *Suda KIATKAMJORNWONG*[2] *and Wiyong KANGWANSUPAMONKON*[3]**

[1]*Program of Petrochemistry and Polymer Science, Faculty of Science, Chulalongkorn University, Phyathai Road, Bangkok 10330, Thailand. E-mail address: yoghurt55@hotmail.com*

[2]*Department of Imaging and Printing Technology, Faculty of Science, Chulalongkorn University, Phyathai Road, Bangkok 10330, Thailand. E-mail address: ksuda@chula.ac.th*

[3]*National Nanotechnology Center, National Science and Technology Development Agency; 130 Thailand Science Park, Paholyothin Road, Klong 1, Klong Luang, Pathumthani 12120, Thailand. E-mail address: wiyong@nanotec.or.th*

Keywords: *Hydrogel composite, TiO_2, Photocatalytic degradation, Water absorbency, Dye removal*

INTRODUCTION

Hydrogel polymer is ionic polymer networks containing ionizable pendent groups such as -OH, -CONH-, -$CONH_2$, -COOH and -SO_3H. These networks can swell hundreds to thousands times their original weight depending on nature of the ionic functional groups. Hydrogel poymer has been used with widespread applications in different fields. The removal of color from textile wastewaters is a major environmental problem because of the difficulty of treating such water by conventional methods. These adsorbents were prepared from the reaction of acrylamide and acrylic acid. The ability of poly(AAm-co-AAc) hydrogels to adsorb cationic dyes from methylene blue solution. Methylene blue has wide applications, which include coloring paper, temporary hair colorant, dyeing cottons, and wools. Although not strongly hazardous, it can cause some harmful effects, such as heartbeat increase, vomiting, shock, cyanosis, jaundice, quadriplegia, and tissue necrosis in human. In recent years, heterogeneous photocatalytic technique is a new horizon for removal of dyes. TiO2 is used as effective, inexpensive and nontoxic semiconductor photocatalysts for degradation of textile dyes. The only drawback is the separation of nano-sized TiO_2 from reaction solution is rather difficult. In this research, syntheses of hydrogel composites containing TiO_2 shall be carried out because they have many advantages, such as low cost and easy separation from reaction solutions.

EXPERIMENTAL

MATERIAL

Acrylamide (AAm, commercial grade) and acrylic acid (AAc, commercial grade) were obtained from Siam Chemical Industry, Thailand. *N,N'*-methylenebisacrylamide (MBA, Fluka, analytical grade) was used as a crosslinking agent. TiO_2 (P-25, Degussa Corporation, commercial grade) was used as a photcatalyst. Ammonium persulfate (APS, Merck, analytical grade)/*N,N,N'N'*-tetramethylenediamine (TEMED, Aldrich, analytical grade) a redox initiator was used for radical polymerization reaction. Methanol (MeOH, BDH, commercial grade) was used for dehydrating water from the gel. Basic blue 9 (Methylene blue having C.I 52015, a light blue dye powder) from Dystar Thai Co. Ltd. was used as received. All other chemicals were used without further purification.

SYNTHESIS OF POLY(AAM-CO-AAC) AND TiO_2/POLY(AAM-CO-AAC) COMPOSITES

The solution of monomers was placed into the four-necked round bottomed flask, equipped with a mechanical stirrer set at 200 rpm and an inlet tube for feeding nitrogen gas. The reaction temperature was controlled at 60 °C. NMBA of 5% mol by weight of the monomer was added into the reaction flask and the reaction was stirred for 10 min. The solution of TiO_2 was sonicated for 5 min; the monomer solution was added into the reaction flask which was stirred for 10 min. Then APS 0.5% mole by weight was added. After stirring for 5 min, the mixture was added with 0.5 mL of TEMED coinitiator. Solution polymerization continued for 30 min. The resulting polymer was dewatered with methanol, cut into small pieces, dried at 50 °C for 24 h in a vacuum oven to a constant weight and then milled before characterization. The water absorbency and percent dye removal were determined. All conditions used in the polymerization reaction are shown in Table 1.

Table 1 Polymerization conditions of TiO_2/poly(AAm-*co*-AAc) composites

Ingredients	Amount
- Mole ratio of AAm : AAc (% mole by monomer)	100 : 0, 50 : 50, 0 : 100
- TiO_2 (% wt)	5, 10, 15, 20
- NMBA (% mole)	5, 10, 20
- APS (% mole)	0.5, 1, 1.5
- TEMED (mL)	0.5
- Reaction temperature (°C)	60
- Agitation speed (rpm)	200
- Reaction time (min)	30

Water absorbency and photocatalytic degradation of methylene blue

Equilibrium water absorbencies (Q) were carried out with distilled water at room temperature. Distilled water (200 ml) was added to 0.1 g of the dry hydrogels and it was allowed to equilibrium swelling for 24 h. Then, the swollen hydrogel was filtered with through a 100-mesh sieve aluminum screen for 30 min at ambient temperature. The gel was dried in a vacuum oven until a constant weight was obtained. The Q value is calculated by Equation (1) as follows:

$$(Q) = \frac{A - B}{B} \quad (1)$$

where *A* is the weight of the hydrogel polymer after complete water absorption, and B is the weight of the hydrogel polymer before water absorption.

Photocatalytic degradation of methylene blue

Photocatalytic degradation of methylene blue was studied by using 0.2 g of TiO_2/poly(AAm-*co*-AAc) hydrogel composite and a control containing poly(AAm-*co*-AAc) without TiO_2 were each poured into 200 mL solution of 5 ppm methylene blue. It was kept at room temp for 24 h. After the equilibrium adsorption, the unadsorbed dye solution was removed by filtration. The swollen hydrogels were placed in a quartz cuvette and it was ready for UV light irradiation by a UV lamp at the wavelength of 365 nm and radiation intensity of 1 mW cm^{-2}. Hydrogel composite samples were measured spectrophotometrically at the wavelength of 308 nm at time intervals 0 - 40 min. The % Dye removal of methylene blue in hydrogel was calculated by Equation (2).

$$\%\,Dye\ removal = \frac{C_0 - C_1}{C_0} \times 100 \quad (2)$$

Where C_0 and C_1 are the concentration of methylene blue at 308 nm in adsorption equilibrium hydrogel before and after irradiation, respectively.

RESULTS AND DISCUSSION

The water absorbency of poly(AAm-*co*-AAc) synthesized with various mole ratios of AAm: AAc was shown in Figure 1(a). The addition of acrylic acid increased electrostatic repulsive force of carboxylate anions in the polymer chains. The highest water absorbency was found at AAm-to-AAc ratio of 0/100 due to the sole effect of the carboxylate groups. When the crosslink concentrations increased, the increased crosslinking density of the polymer was also shown in Figure 1(b). This results in a decrease in repulsion forces among the chains and leads to a decrease in water absorbency. The effect of initiator concentrations on the water absorbency was shown in Figure 1(c). At the higher initiator concentration, the water absorbency decreased because of too many radicals generation, resulting in the short polymer chains that cannot swell to larger extent due to a small number of the carboxylate group.

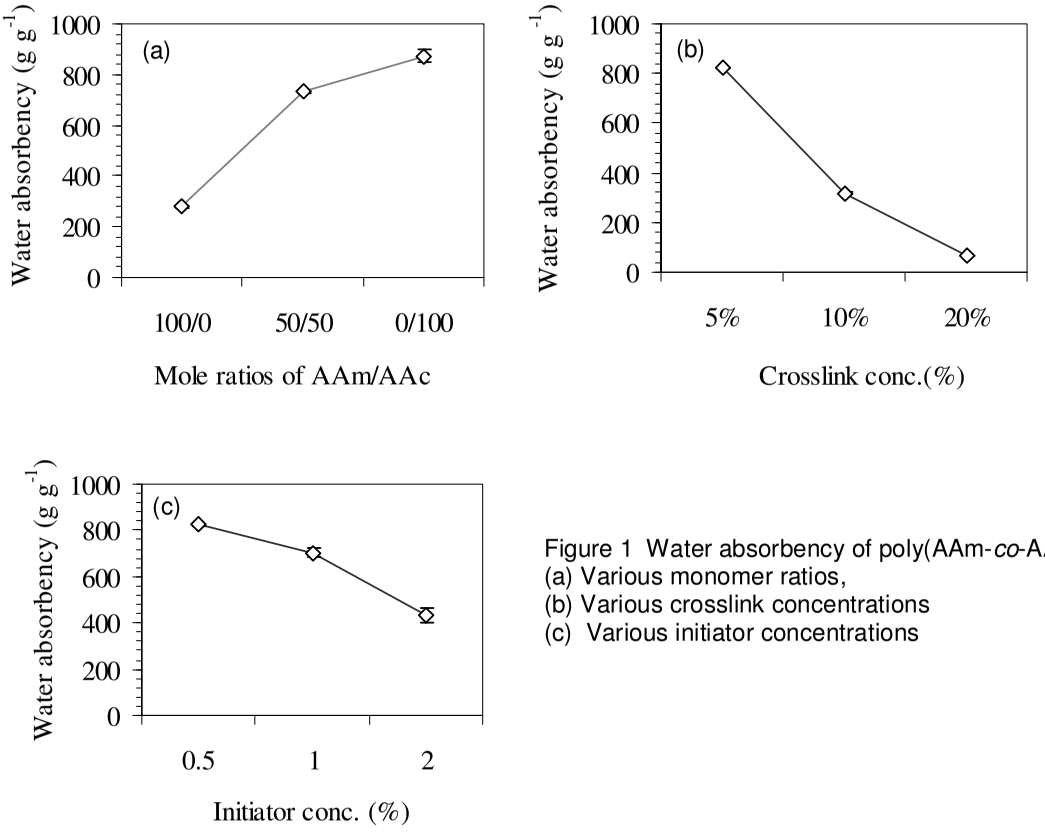

Figure 1 Water absorbency of poly(AAm-*co*-AAc) at
(a) Various monomer ratios,
(b) Various crosslink concentrations
(c) Various initiator concentrations

In order to elucidate the effect of photocatalytic degradation of methylene blue by UV irradiation at wavelength 365 nm and UV light intensity at 1 mW cm^{-2}. The light intensity of UV lamp was measured by a UVP radiometer (UVP, USA) at 254 nm and 365 nm. Figure 2(a) and (b) demonstrate the enhancement of methylene blue photodegradation in the presence of TiO_2/poly(AAm-*co*-AAc) composites. In the presence of TiO_2/poly(AAm-*co*-AAc) composites, about 91% of dye degraded in an irradiation time of 40 min at room temperature. This was contrasted with 3% degradation for UV irradiation without TiO_2. There were no change in dye degradation, when poly(AAm-*co*-AAc) and TiO_2/poly(AAm-*co*-AAc) composites were used in darkness.

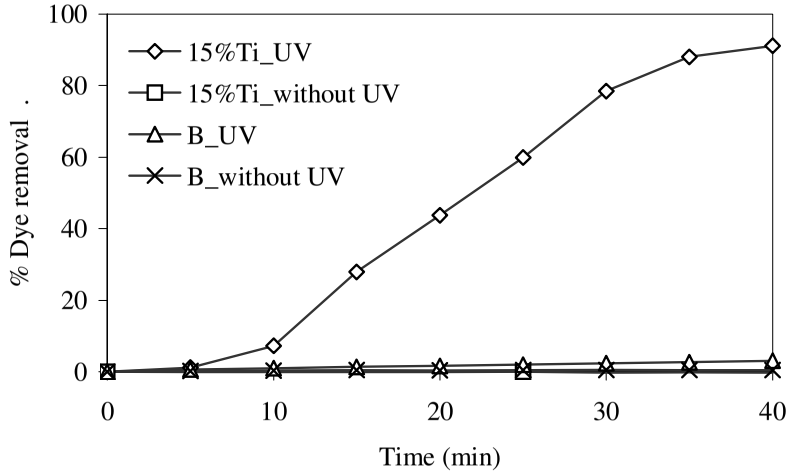

Figure 2(a) Effect of UV light and different photocatalyst on photocatalytic degradation of methylene blue

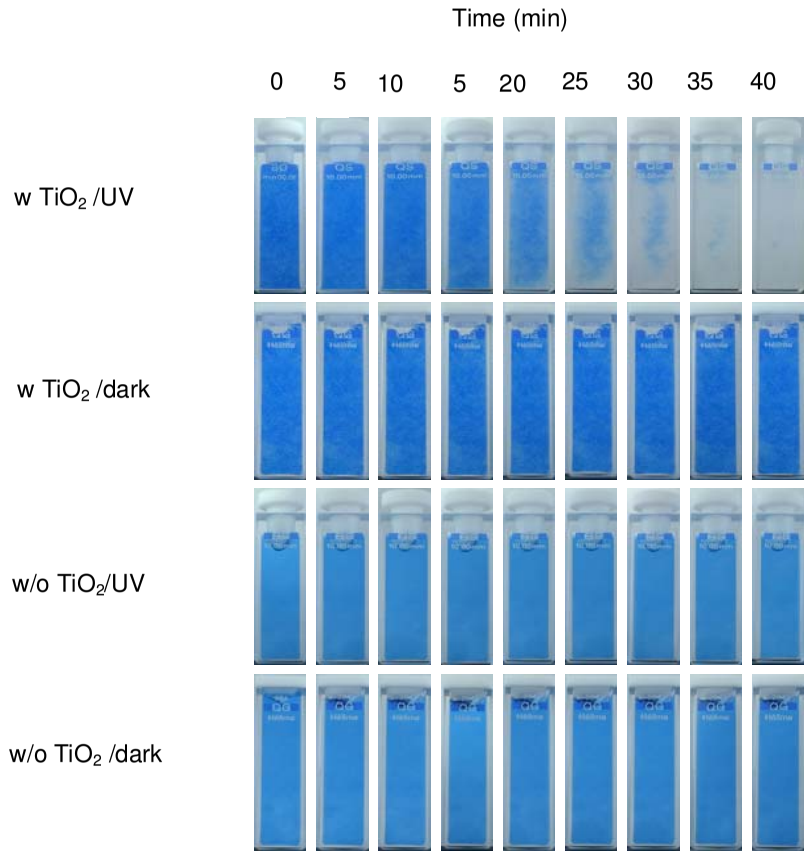

Figure 2(b) Removal of methylene blue dye in water with the hydrogel composites under various conditions

Figure 3 (a) and (b) show the morphologies of TiO_2/poly(AAm-*co*-AAc) composites before and after irradiation, respectively. The TiO_2/poly(AAm-*co*-AAc) composites becomes a blue color after equilibrium adsorption methylene blue solution shown figure 3(a), indicating that methylene blue solution penetrated inside the TiO_2/poly(AAm-*co*-AAc) composites. It is obvious that blue color of TiO_2/poly(AAm-*co*-AAc) composites have been disappeared completely after being irradiated at UV light for 1.30 h by UV irradiation at wavelength 365 nm and UV light intensity at 1 mW cm^{-2}. The light intensity of UV lamp was measured by a UVP radiometer (UVP, USA) at 254 nm and 365 nm., as seen in Figure 2(b).

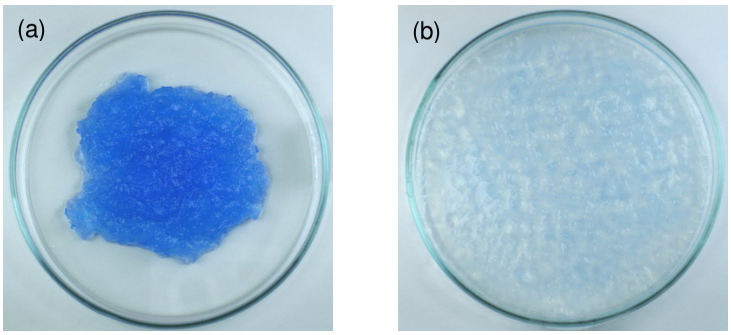

Figure 3 (a) and (b) The morphologies of TiO_2/poly(AAm-*co*-AAc) composites

The result of % Dye removal by variation of amount of TiO_2 in hydrogel was shown in Figure 4. This figure indicates that the dye removal efficiency increases with increasing TiO_2 concentration until about 15 %wt of TiO_2 concentration and then decreases moderately. The reason of this observation is thought to be that TiO_2 is a good photocatalytic degradation agent, when the TiO_2 amount in the polymer is increased, the active sites of the catalysts followed by the photocatalytic degradation. However, TiO_2 nano-particles are prone to conglomerate, especial in the concentration beyond 15% and consequently, the active sites of the catalysts decreased and be degraded moderately.

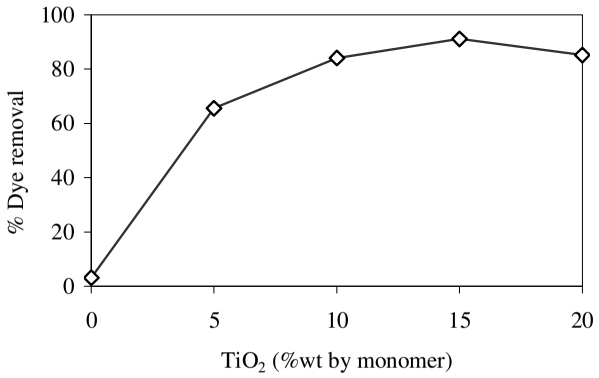

Figure 4 Variation of color removal with the amount of TiO_2 in hydrogel

CONCLUSIONS

Poly[acrylamide-*co*-(acrylic acid)] (poly(AAm-*co*-AAc)) and TiO_2/poly(AAm-*co*-AAc) composite hydrogels were prepared by an aqueous solution polymerization method. The TiO_2/poly(AAm-*co*-AAc) composite has favorable adsorption ability for methylene blue solution. Higher photocatalytic efficiency for degradation of methylene blue solution is synergistically enhanced under UV irradiation.

ACKNOWLEDGMENTS

This research is financially supported by a Research Team Consolidation Grant, the Thailand Research Fund – Higher Education Commission (RTA5080004), Professor Suda Kiatkamjornwong as the project head. The authors are very grateful to Department of Imaging and Printing Technology, Faculty of Science, Chulalongkorn University, and National Nanotechnology Center, National Science and Technology Development Agency for use of research facilities.

REFERENCES

Nikolaos, A.P. and R.K. Atul; “Preparation structure and diffusional behavior of hydrogels in controlled release,” *Advanced Drug Delivery Review*, **11**,1-35 (1993)

Solpan, D., S. Duran and M. Torun; “Removal of cationic dyes by poly(acrylamide-co-acrylic acid) hydrogels in aqueous solutions,” Radiation Physics and Chemistry, **77**, 447-452 (2008)

Yi, J-Z. and L-M. Zhang; “Removal of methylene blue dye from aqueous solution by adsorption onto sodium humate/polyacrylamide/clay hybrid hydrogels,” *Bioresource Technology*, **99**, 2182-2186 (2008)

การสังเคราะห์ไคโทซานกราฟต์พอลิอะคริลิกแอซิด-โค-2-ไฮดรอกซีเอทิลเมทาคริเลตไฮโดรเจลสำหรับฤทธิ์ต้านแบคทีเรีย

SYNTHESIS OF GRAFTED CHITOSAN POLY[(ACRYLIC ACID)-*CO*-(2-HYDROXYETHYL METHACRYLATE)] HYDROGELS FOR ANTIBACTERIAL ACTIVITY

กิตติชัย สนใจพาณิชย์[1], สุภาภรณ์ นพคุณดิลกรัตน์[2], ณัฏฐา ทองจุล[3], สุดา เกียรติกำจรวงศ์[2*]

Kittichai Sonjaipanich[1], Supaporn Noppakundilograt[2], Nuttha Thongchul[3], Suda Kiatkamjornwong[2*]

[1]Program of Petrochemistry and Polymer Science, Faculty of Science, Chulalongkorn University, Bangkok 10330, Thailand, e-mail: *kittichai_sonjai@hotmail.com*.

[2]Department of Printing and Imaging Technology, Faculty of Science, Chulalongkorn University, Bangkok 10330, Thailand. [2]e-mail: *supaporn.n@chula.ac.th*; [*2]corresponding author, e-mail address: *ksuda@chula.ac.th*; *ksuda@sc.chula.ac.th*, Tel: +66-2218-5587

[3]Institute of Biotechnology and Genetic Engineering, Chulalongkorn University, Bangkok 10330, Thailand. [3]e-mail address: *Nuttha.T@chula.ac.th*

บทคัดย่อ: สังเคราะห์ไคโทซานกราฟต์พอลิอะคริลิกแอซิด-โค-2-ไฮดรอกซีเอทิลเมทาคริเลต โดยกระบวนการพอลิเมอไรเซชันแบบสารละลาย โดยใช้อะคริลิกแอซิดและ 2-ไฮดรอกซีเอทิลเมทาคริเลตเป็นคู่มอนอเมอร์ แอมโมเนียมเปอร์ซัลเฟตเป็นสารเริ่มปฏิกิริยา เอ็น, เอ็น, เอ็น', เอ็น'-เททระเมทิลเอทิลีนไดแอมีนเป็นสารเริ่มปฏิกิริยาร่วม และเอ็น, เอ็น'-เมทิลีนบิสอะคริลาไมด์เป็นสารเชื่อมขวาง ตรวจสอบหมู่ฟังก์ชันของไคโทซานกราฟต์พอลิอะคริลิกแอซิด-โค-2-ไฮดรอกซีเอทิลเมทาคริเลต ด้วยเทคนิคอินฟราเรดสเปกโทรสโกปี ศึกษาผลของอัตราส่วนมอนอเมอร์ของอะคริลิกแอซิด/2-ไฮดรอกซีเอทิลเมทาคริเลตต่อค่าการดูดซึมน้ำ และทดสอบฤทธิ์ต้านแบคทีเรีย *Staphylococcus aureus* (*S. aureus*) พบว่าค่าการดูดซึมน้ำของกราฟต์ไฮโดรเจลไคโทซานเพิ่มขึ้น เมื่ออัตราส่วนของมอนอเมอร์เพิ่มขึ้นและกราฟต์ไฮโดรเจลไคโทซานมีสมบัติการต้านแบคทีเรียโดยยับยั้งการเติบโตของ *S. aureus* ส่งผลให้อัตราการเจริญในช่วงเลขชี้กำลัง (Exponential) ช้าลง

Abstract: Grafted chitosan poly[(acrylic acid)-*co*-(2-hydroxyethyl methacrylate)], CH-*g*-poly(AA-*co*-HEMA), was synthesized by solution polymerization in which acrylic acid (AA) and 2-hydroxy ethylmethacrylate (HEMA), ammonium persulfate (APS)/N, N, N', N'-tetramethylethylenediamine (TEMED) and N, N',-methylenebisacrylamide (N-MBA) were used as a pair of monomers, a redox initiator couple and a crosslinking agent, respectively. Existences of functional groups of CH-*g*-poly(AA-*co*-HEMA) were characterized by FTIR spectrum. Effects of the monomer ratio of AA/HEMA on water absorbency and antibacterial activity of the grafted chitosan were investigated. The water absorbency of grafted chitosan was found to increase when the monomer ratio of AA/HEMA increased and grafted chitosan provides antibacterial activity by inhibiting the growth rate of *S. aureus* resulted from the decrease in growth rate during the exponential phase.

Introduction: Chitosan as shown in Figure 1 is derived by deacetylation of chitin. Chitosan has been used in many applications because of its biocompatibility, biodegradability, non-toxicity and antibacterial activity [1]. Drawback of chitosan usage for bio-absorber applications is its low water absorbency. Graft polymerization of chitosan with hydrophilic vinyl monomer is one solution to solve the limited water absorption of chitosan [2-4]. Chitosan grafted with hydrophilic AA monomer becomes a highly hydrophilic material because the grafted polymer can absorb a large amount of water with respect to its dried weight. HEMA monomer has been used in biomedical applications such as drug delivery, contact lenses and also used as co-monomer for improving biocompatibility [5]. The materials for wound dressing should have the water absorbency at around 25-32 times its dried weight in order to remove secretion or pus from wound [6]. In addition, they should have the antibacterial activity for protecting the wound from infection. Thus, hydrogel can be applied to wound dressing material. *S. aureus* (Figure 2) is a gram-positive anaerobic bacterium and causes a wide range of diseases in human. It is the main microorganism to cause wound infections, boils, pustules, and other human skin infections. In this research, CH-*g*-poly(AA-*co*-HEMA) hydrogels were synthesized. The effects of AA/HEMA ratio on water absorbency and the antibacterial activity of grafted chitosan against *S. aureus* were investigated.

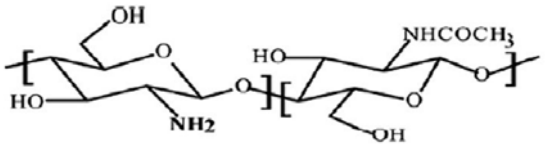

Figure 1 Structure of chitosan

Figure 2 *S. aureus* (from www.google.com)

Methodology: Chitosan (Seafresh Industry Public Co., Ltd., Thailand) was dissolved in 30 ml of 2% w/v acetic acid solution in a 500-cm^3 four-necked round-bottom flask. It was then equipped with a mechanical stirrer assembled with a half-moon shaped Teflon blade agitator and the mixture was stirred at room temperature until a clear solution was obtained. It was then heated at 60^{o}C under nitrogen atmosphere. APS (Ajax, Australia) was then added and stirred. AA, HEMA (Thai Mitsui Specialty Chemicals Co., Ltd., Thailand), and N-MBA (Fluka, Switzerland) were sequentially added and stirred. Finally, TEMED (Fluka, Switzerland) was added. The mixture was stirred for 60 min to complete the graft copolymerization. The reaction was cooled down to room temperature and neutralized to pH 8 by 1 M sodium hydroxide solution. The reaction product was dewatered with acetone, dried in a vacuum oven at 50^{o}C for 24 h and milled to classify particle size. Synthetic conditions of CH-*g*-poly(AA-*co*-HEMA) hydrogels are presented in Table 1.

Table 1 Synthetic condition of the grafted chitosan hydrogels

Reagents	Synthetic conditions		
	1	2	3
Chitosan (g)	1	1	1
AA (mmol)	54	27	13.5
HEMA (mmol)	-	27	40.5
APS (g)	0.1	0.1	0.1
N-MBA (g)	0.1	0.1	0.1
TEMED (ml)	0.52	0.52	0.52

The synthesized products were characterized by Fourier Transform Infrared Spectroscopy (System 2000, Perkin Elmer, U.S.A.). The water absorbencies of the grafted chitosan particles were carried out with distilled water at room temperature in a closed system to minimize water evaporation. Distilled water (200 cm^3) was added to 0.1 g of the dry product. It was allowed to swell for 24 h. Then, the swollen gel was filtered through a 100-mesh aluminum screen sieve for 2 h. The water absorbency was determined three replications for each synthesized product and calculated from Equation (1) [7]:

$$Water\ absorbency\ (Q) = (W_s - W_d)/W_d \quad (1)$$

where W_d = the weight of dry products (g), and W_s = the weight of the swollen gel (g).

Antibacterial activity of CH-*g*-poly(AA-*co*-HEMA) hydrogel against *S. aureus* was evaluated by turbidity method using 5 mg of the grafted chitosan/ml of Mueller Hinton Broth (Difco, U.S.A.) as a culture medium. After *S. aureus* had been cultured in the medium, the turbidity of the culture was measured by reading an optical density at 610 nm [8].

Results, Discussion and Conclusion: The FTIR spectra of chitosan, poly(AA-*co*-HEMA) and CH-*g*-poly(AA-*co*-HEMA) hydrogel are shown in Figure 3. The spectrum (a) of chitosan shows absorption peaks at 1653, 1595, 1381, 1256 and 1089 cm^{-1} assigned to C=O stretching of amide I, -NH stretching of amine, -NHCO stretching of amide, -CN stretching and C_3-OH stretching, respectively [9]. The spectrum (b) of poly(AA-*co*-HEMA) hydrogel shows a peak at 1714 cm^{-1} of C=O stretching and the peaks at 1162, 1080 cm^{-1} of C-O-C stretching which indicates the presence of the ester group of poly(HEMA). In addition, it also shows peaks at 1568 (C=O asymmetric stretching) and 1406 cm^{-1} (C=O symmetric stretching) of the carboxylate anion in poly(AA) moiety [4]. The spectrum (c) of CH-*g*-poly(AA-*co*-HEMA) hydrogel shows a new peak at 1723 cm^{-1} of C=O stretching of the ester group which indicates the evidence of grafting. It also shows the peaks at 1571 (C=O asymmetric stretching) and 1400 cm^{-1} (C=O symmetric stretching) of the carboxylate anion in poly(AA) moiety. A peak of C=O stretching of the ester group of poly(AA-*co*-HEMA) (1714 cm^{-1}) overlapped with a new peak at 1723 cm^{-1}. From the FTIR spectra of (a to c), it confirmed that the synthesized product was CH-*g*-poly(AA-*co*-HEMA) hydrogel.

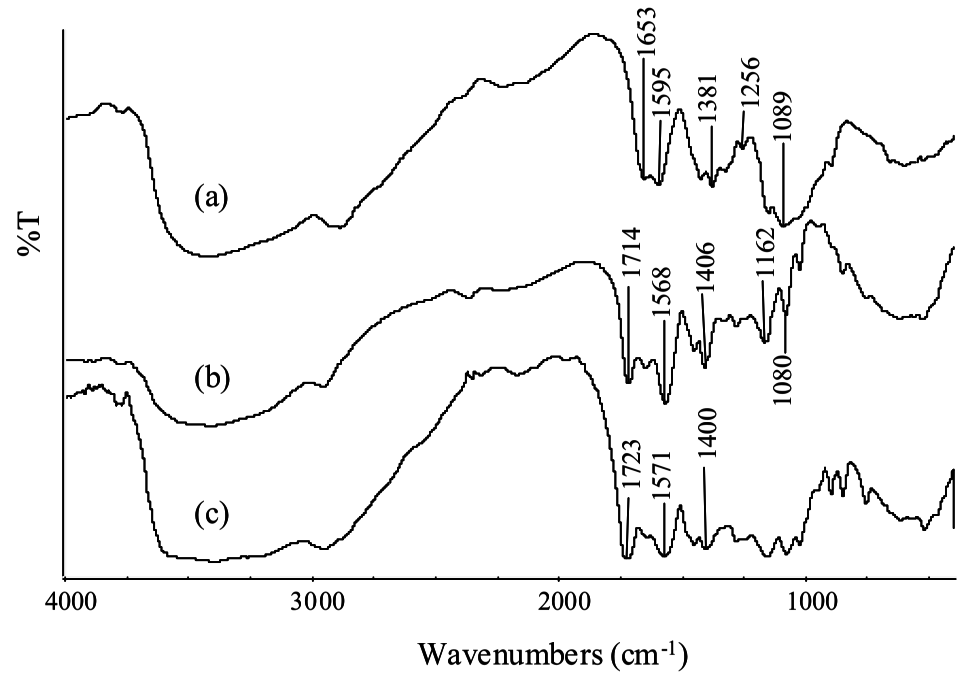

Figure 3 FTIR spectra of (a) chitosan, (b) poly(AA-*co*-HEMA) hydrogel, and (c) CH-*g*-poly(AA-*co*-HEMA) hydrogel

The water absorbencies of chitosan and CH-*g*-poly(AA-*co*-HEMA) hydrogel are shown in Figure 4. The water absorbency increases when the amount of AA increases due to increasing carboxylic acid content leading to the chain expansion. The higher the repulsion of anion portion, the greater the polymer chain expansion, thus, its water absorbency increases.

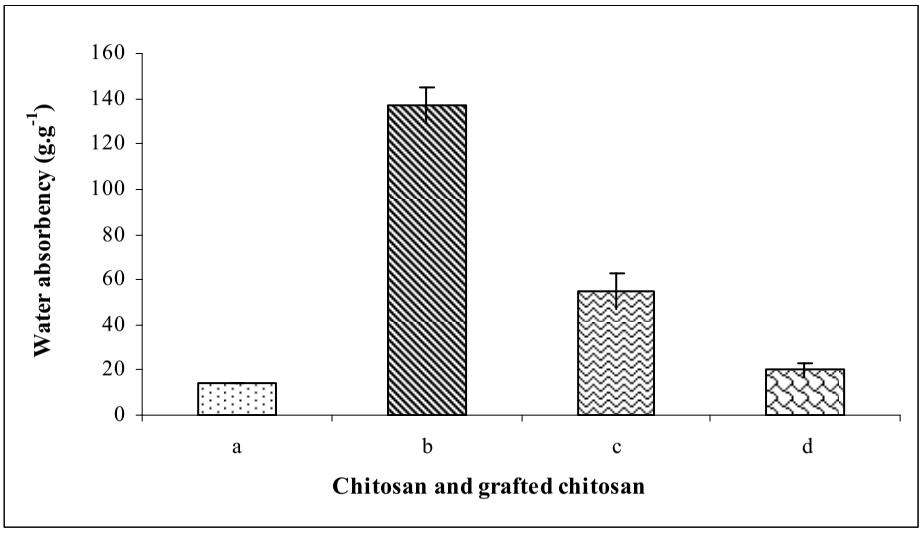

Figure 4 Water absorbency of (a) chitosan, and CH-*g*-poly(AA-*co*-HEMA) hydrogels for AA-to-HEMA ratios (mmol/mmol) in (b) 54/0, (c) 27/27 and (d) 13.5/40.5

The antibacterial activity obtained from the hydrogel was determined (Figure 5). Three phases in a growth cycle were observed. The lag phases of *S. aureus* grown in Mueller Hinton Broth (MHB) and in MHB in the presence of hydrogel were similar in term of time (4h). During the exponential phase, the growth rate of *S. aureus* grown in MHB containing hydrogel was lower than that of the cells grown in MHB during 4-6 h. The cells in both conditions entered the stationary phase after 12 h. At the culture time of 6-8 h, CH-*g*-poly(AA-*co*-HEMA) hydrogel rendered a slow growth rate of *S. aureus* because the grafted chitosan hydrogel inhibited the growth of *S. aureus*. They were confirmed by $O.D._{610nm}$ at 6-8 h of CH-*g*-poly(AA-*co*-HEMA) hydrogel which was less than that of a negative control. Therefore, the CH-*g*-poly(AA-*co*-HEMA) hydrogel with the AA-to-HEMA ratio (mmol/mmol) of 1/1 (27/27) could inhibit the growth rate of *S. aureus* in the exponential phase.

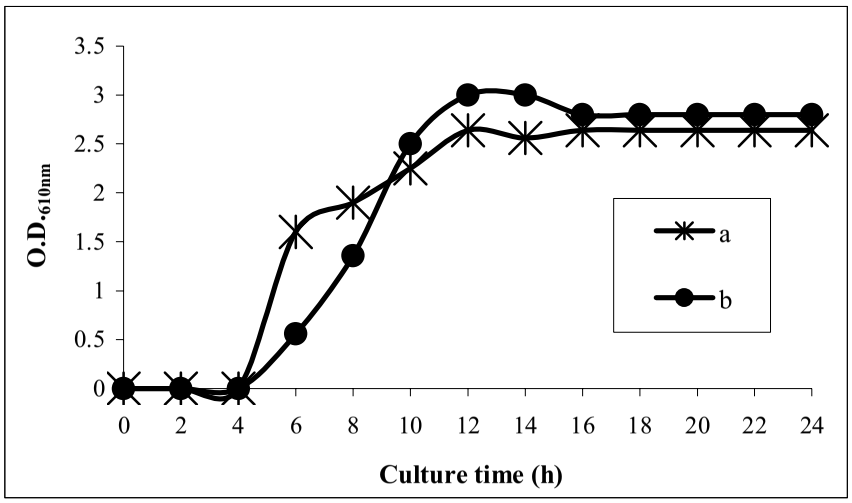

Figure 5 The optical density at 610 nm versus culture time of (a) the negative control, and (b) the CH-*g*-poly(AA-*co*-HEMA) hydrogel

In conclusion, FTIR spectrum of CH-*g*-poly(AA-*co*-HEMA) hydrogel indicated the existence of poly(AA-*co*-HEMA) chains grafted on the chitosan chain. The water absorbency of chitosan was improved by grafting copolymerization with AA and HEMA. Water absorbency of the CH-*g*-poly(AA-*co*-HEMA) hydrogels is governed by the increasing amount of AA monomer. The CH-*g*-poly(AA-*co*-HEMA) hydrogel can inhibit the growth of *S. aureus* by decreasing the growth rate during the exponential phase.

Acknowledgements: This research is supported by the Research Team Promotion Grant from the Thailand Research Fund – Commission for Higher Education under the contract number RTA5080004.

Keywords: grafted chitosan, water absorbency, antibacterial activity

References:

1. Rinaudo M. Chitin and chitosan: properties and applications. *Progress in Polymer Science*, 31 (2006): 603-632.
2. Jalal Zohuriaan-Mehr M. Advances in chitin and chitosan modification through graft copolymerization: comprehensive review. *Iranian Polymer Journal*, 14 (2005):235–265.

3. Mahdavinia G.R., Pourjavadi A., Hosseinzadeh H., and Zohuriaan M.J. Modified chitosan 4. Superabsorbent hydrogels from poly[(acrylic acid)-*co*-acrylamide] grafted chitosan with salt- and pH-responsiveness properties. *European Polymer Journal*, 40 (2004): 1399-1407.
4. Dos Santos K.S.C. R., Coelho J. F. J., Ferreira P., Pinto I., Lorenzetti S.G., Ferreira E.I., Higa O. Z., and Gil M. H. Synthesis and characterization of membranes obtained by graft copolymerization of 2-hydroxyethyl methacrylate and acrylic acid onto chitosan. *International Journal of Pharmaceutics*, 310 (2006): 37-45.
5. Carenza M. Recent achievements in the use of radiation polymerization and grafting for biomedical applications. *International Journal of Radiation Applications and Instrumentation. Part C. Radiation Physics and Chemistry*, 39 (1992): 485–493.
6. Tanodekaew S., Prasitsilp M., Swasdison S., Thavornyutikarn B., Pothsree T., and Pateepasen R. Preparation of acrylic grafted chitin for wound dressing application. *Biomaterials*, 25 (2004): 1453-1460.
7. Lee WF, Chen YC. Preparation of reactive mineral powders used for poly(sodium acrylate) composite superabsorbent. *Journal of Applied Polymer Science.* 97(3) (2005): 855–860.
8. Li Y., Chen XG, Liu N., Liu CS, Liu CG, Meng XH, Yu LJ, Kenendy JF. Physicochemical characterization and antibacterial property of chitosan acetates. *Carbohydrate Polymers*, 67 (2007): 227–232.
9. Zhang J., Wang Q., and Wang A. Synthesis and characterization of chitosan-*g*-poly(acrylic acid)/attapulgite superabsorbent composites. *Carbohydrate Polymers*, 68 (2007): 367–374.

การปรับสภาพพื้นผิวผ้าพอลิเอสเทอร์ก่อนพิมพ์ด้วยสารละลายไคโทซานเพื่อการพิมพ์อิงก์เจ็ต

PRETREATMENT OF POLYESTER FABRIC SURFACE WITH CHITOSAN SOLUTION FOR INK JET PRINTING

ปัญฑ์ธร บูรณะกูล, สุภาภรณ์ นพคุณดิลกรัตน์*, สุดา เกียรติกำจรวงศ์**

Punthorn Buranagul, Supaporn Noppakundilograt*, Suda Kiatkamjornwong**

[1]Program of Printing and Imaging Technology, Faculty of Science, Chulalongkorn University, Bangkok 10330, Thailand, e-mail: puntune@hotmail.com. *corresponding author, e-mail: supaporn.n@chula.ac.th;**e-mail address: ksuda@chula.ac.th; ksuda@sc.chula.ac.th

บทคัดย่อ: งานวิจัยนี้ศึกษาผลของสารละลายไคโตซานซึ่งเป็นสารละลายปรับสภาพพื้นผิวผ้าพอลิเอสเทอร์ก่อนการพิมพ์อิงก์เจ็ต พิมพ์ผ้าพอลิเอสเทอร์ที่ไม่ปรับสภาพและผ้าที่ผ่านการปรับสภาพพื้นผิวด้วยสารละลายไคโตซานความเข้มข้นต่าง ๆ ด้วยหมึกทางการค้าเจ็ดสีประเภทสารสีฐานน้ำ แล้วนำไปอบไอน้ำ วัดขอบเขตสีของผ้าที่พิมพ์ได้ด้วยระบบสีซีไออีและวัดการผลิตสี ผลการทดลองพบว่า ผ้าที่ผ่านการปรับสภาพพื้นผิวด้วยสารละลายไคโตซาน มีขอบเขตสีกว้างกว่าผ้าที่ไม่ผ่านการปรับสภาพ นอกจากนี้ สารละลายไคโตซานยังมีผลต่อการผลิตสีและสีที่ผลิตได้ดีที่สุดอยู่ในช่วงสีเหลืองสว่าง

Abstract: This research was aimed to study the effect of chitosan solution as a pre-treating solution for padding polyester fabric before ink jet printing. The non-padded and padded fabrics with various concentrations of chitosan were printed with a commercial set of seven-color, pigmented water-based ink, and they were streamed afterwards. The printed fabrics were evaluated for color gamut with the CIE color system and color reproduction. The results show that the padded fabrics with chitosan solutions have a bigger color gamut than that of the non-treated polyester fabric. Moreover, chitosan solutions give a larger color reproduction with a dominance of bright yellow.

Introduction: Ink jet printing has been extensive studied as a new technology for textile printing due to its advantages over conventional printing, such as low required ink volumes, direct printing from computer and unique print-designs for individual desire. The quality of the printed fabric by ink jet printing depends on weave structure and composition of the fabric. Thus, printed quality of fabric, such as color gamut, tone reproduction, and physical appearance can be improved by using a suitable treating agent for the fabric surface.

Chitosan as shown in Figure 1 [1] is derived by deacetylation of chitin. Chitosan has been used in many applications due to its biodegradable and non-toxic [2]. In textile industries, chitosan is used in dyeing and finishing processes to improve

dyeability and wash fastness of cotton, wool and polyester [3, 4]. Poly(ethylene terephthalate) (PET) is the most widely used as polyester fiber. Polyester fabric is strong and wrinkle-resistant [5]. Its hydrophobic nature is disadvantaged to dyeing, finishing and printing. It was found that the non-treated polyester fabric has a negative zeta potential value [6]. In a pre-treatment process of polyester fabric, the suitable pretreating agent with positive charges is adsorbed on the fabric due to ionic interaction [7].

Wongwikorn and Kieatcharoenwit [8] found that chitosan improved color gamut of the silk fabrics pretreated for ink jet printing. Thus, it is interesting to investigate the effect of chitosan treatment on qualities of the printed polyester fabric.

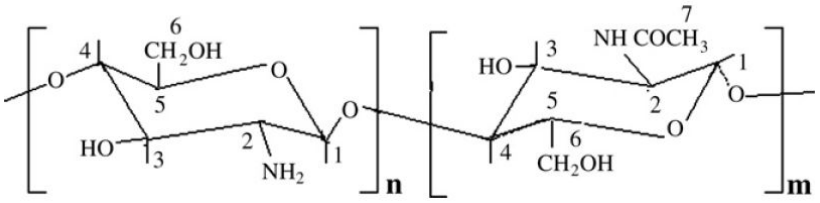

Figure 1 Structure of chitosan

Methodology: The pretreating solutions of chitosan (Seafresh Industry Public Co., Ltd., Thailand) MW 57 kD, 85% deacetylation degree were prepared at 1, 2, 3 and 4% w/v. The polyester fabrics were each padded with the pretreating solution by a padding method. The surface morphologies of non-treated and treated fabrics were investigated using a scanning electron microscope (SEM, model JSM-6400, Japan) without cross section. The treated fabric was printed using Epson Stylus Photo R2100 printer with a commercial set of seven-color pigmented, water-based ink. Color gamut and color reproduction of the printed fabrics were measured by a spectrophotometer (X-Rite SP62). The sharpness of the negative and positive fonts was investigated by an optical microscope (Olympus model PM 10-AD, Japan).

Results, Discussion and Conclusion: The untreated polyester fabric micrographs in Figure 2 (a) shows small and shallow holes on surface of each fiber. After polyester fabric has been treated with 1 % w/v of chitosan, the micrographs shows a smoother surface due to chitosan coverage on the small pores as shown in Figure 2 (b).

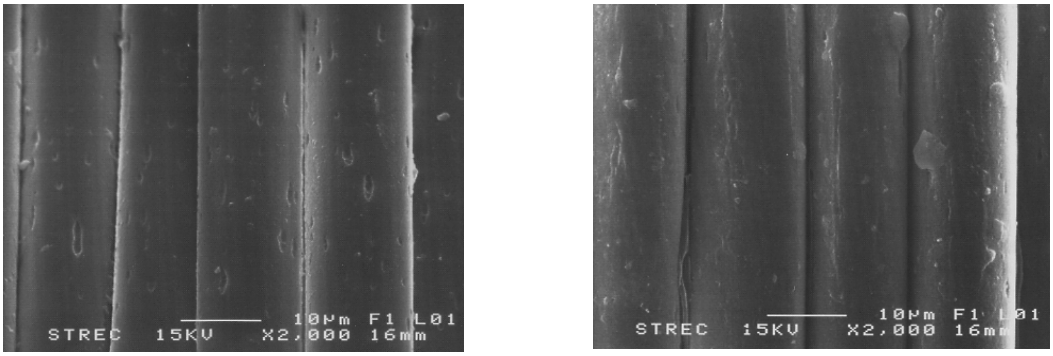

Figure 2 SEM micrographs of untreated fabric (a), treated fabric (b)

Color gamut of the pigmented ink jet inks printed on the same polyester fabric was not changed by steaming as shown in Figure 3. Thus, the color gamut measurement after steaming showed a color difference after removal of excess pigmented ink jet inks on the fabrics.

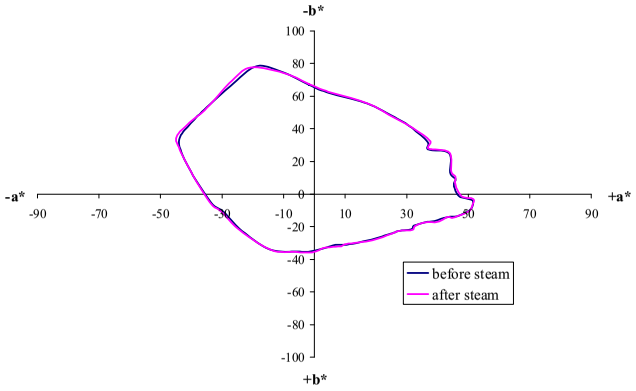

Figure 3 Color gamut of the printed polyester fabric before and after steaming

The treated fabrics with chitosan gave a bigger color gamut than that of the untreated polyester fabric, and the former gave the maximum gamut in reddish yellow region. The chitosan concentration did not affect color gamut as shown in Figure 4.

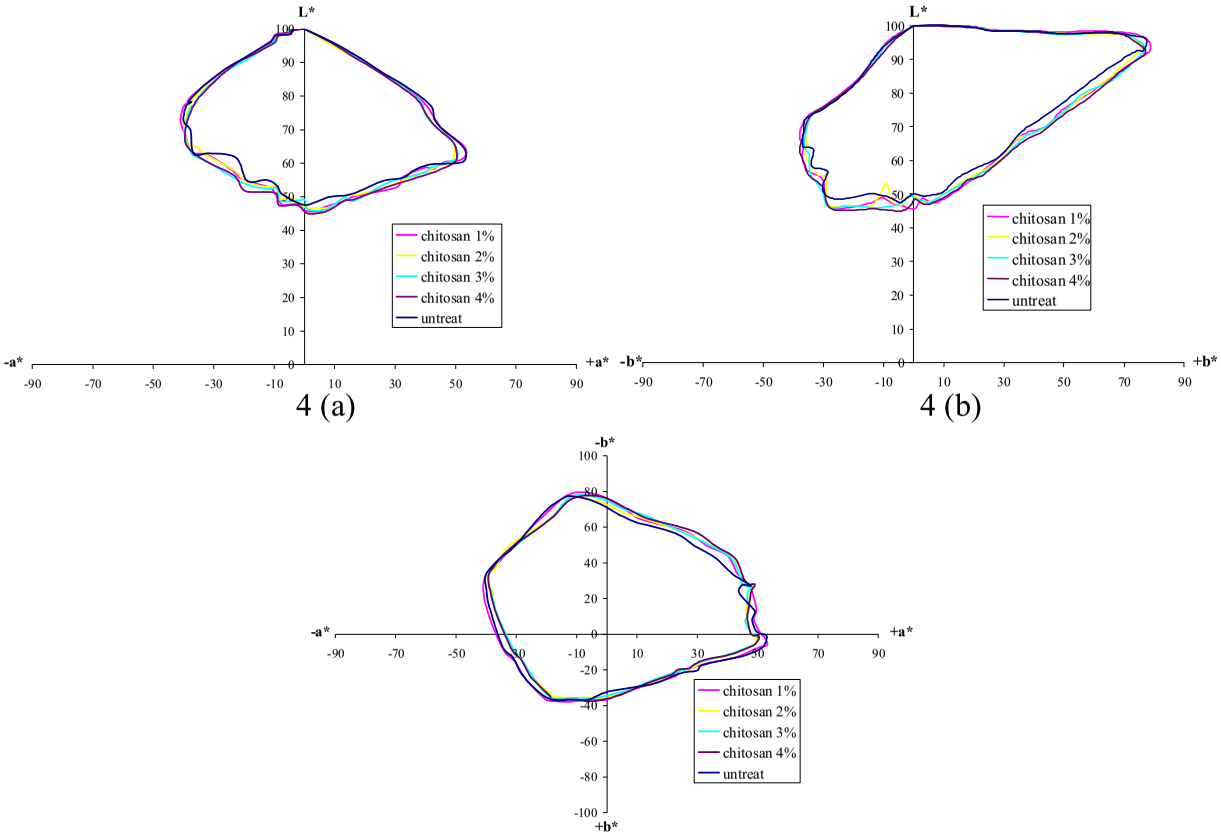

Figure 4 Color gamut of the untreated and the treated polyester fabrics in a plot of (a) L* and a*, (b) L* and b* (b), (c) a* and b*

Color reproduction of the treated polyester fabric is showed in Table 1. The fabrics pretreated with 1, 2, 3 and 4%w/v of chitosan gave ΔE_{max} in bright yellow color at code L2. The higher the ΔE_{max} is, the greater the color change becomes. All concentrations of chitosan produced the similar ΔE_{max} value. It indicates that the concentration of chitosan does not affect color reproduction of the treated polyester fabric.

Table 1 Effect of chitosan content on color reproduction of the treated polyester fabric at code L2

chitosan content (%w/v)	ΔE_{max}	ΔE_{min}	$\Delta E_{average}$	$L^*_{\Delta Emax}$	$C_{\Delta Emax}$	$h_{\Delta Emax}$
1	10.01	0.21	2.28	99.85	10.01	104.36
2	10.51	0.25	2.6	100	10.51	103.83
3	11.05	0.26	2.66	99.95	11.05	104.25
4	10.63	0.17	3.04	99.81	10.63	103.37

The negative and positive fonts on the printed treated polyester fabric are sharper than that of the untreated fabric because the adsorption of chitosan on polyester fiber (Figure 2 (b)) reduces the ink spreading and bleeding on the polyester fabric as shown in Figures 5 and 6, respectively.

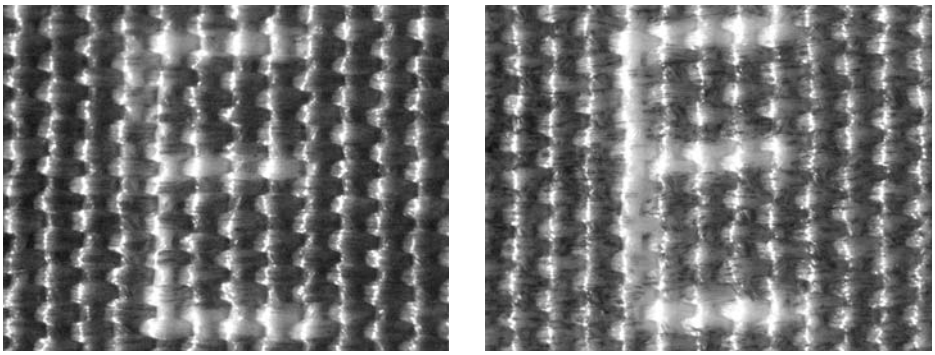

(a) (b)

Figure 5 Sharpness of the negative fonts at 10 point on (a) the untreated polyester fabric, and (b) the treated polyester fabric with 4% w/v of chitosan

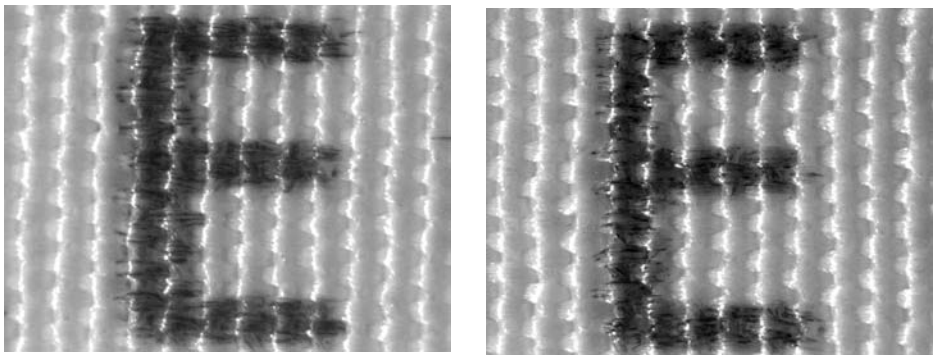

(a) (b)

Figure 6 Sharpness of the positive fonts at 10 point on (a) the untreated polyester fabric, and (b) the treated polyester fabric with 4% w/v of chitosan

Chitosan can be used as a pre-treating agent for polyester fabric for ink jet printing by improving the reddish yellow region with dominant color in bright yellow. Moreover, the sharpness of negative and positive fonts on the treated polyester fabrics is improved.

Acknowledgements: This research is supported by NRCT Fund. Research facility from the Imaging Polymer laboratory in the Department of Imaging and Printing Technology, Faculty of Science, Chulalongkorn University, and Faculty of Textile Industry, Rajamangala University of Technology Krungthep is gratefully acknowledged.

Keywords: Chitosan, Polyester, Ink jet printing

References:

1. Huang, K-S. Wu, W-J., Chen, J-B., Lian, H-S. Application of low-molecular-weight chitosan in durable press finishing. *Carbohydrate Polymers*, 73 (2008): 254 – 260.
2. Rinaudo M. Chitin and chitosan: properties and applications. *Progress in Polymer Science*, 31 (2006): 603 – 632.
3. Gupta, D., Haile, A. Multifunctional properties of cotton fabric treated with chitosan and carboxymethyl chitosan. *Carbohydrate Polymers,* 69 (2007): 164 – 171.
4. Hakeim, O.A., El-Gabry, L., Abou-Okeil, A. Rendering synthetic fabrics acid printable using chitosan and binder, Journal of Applied Polymer Science, 108 (2008): 2122 – 2127.
5. East, A.J. Synthetic fibres: nylon, polyester, acrylic, polyolefin, New York: Woodhead Publishing, 2005, p 95.
6. Espinosa-Jiménez, M., Padilla-Weigand, R., Ontiveros-Ortega, A., Ramos-Tejada, M.M., and Perea-Carpio, R., Interpretation of colloidal dyeing of polyester fabrics pretreated with ethyl xanthogenate in terms of zeta potential and surface free energy balance. *Journal Colloid and Interface Science.* 265 (2003): 227– 233.
7. Samu, R., Moulee, A., and Kumar, V. G., Effect of Charge and Hydrophobicity on Adsorption of Modified Starches on Polyester. *Journal Colloid and Interface Science.* 220 (1999): 260 – 268.
8. Wongwikkorn, P., Kieatcharoenwit, J., Kasadesinchai, N., Noppakundilograt, S., Kiatkamjornwong, S. Pretreatment of Thai silk fabric surface with chitosan and amino acid for inkjet printing. Abstract of the 14th Science and Technology Annual Academic Meeting, 16 –17 March 2006, p. pt-21.

ประสิทธิภาพการกำจัดสีเมทิลีนบลูด้วยวัสดุเชิงประกอบพอลิอะคริลาไมด์-*โค*-อะคริลิกแอซิด/อนุภาคไทเทเนียมไดออกไซด์

REMOVAL EFFICIENCY OF METHYLENE BLUE DYE USING TiO_2/POLY[ACRYLAMIDE-*CO*-(ACRYLIC ACID)] COMPOSITES

วลาสินี จิตรบรรพต[1], วิยงค์ กังวานศุภมงคล[2], สุดา เกียรติกำจรวงศ์[3]

Walasinee Jitbunpot[1], Wiyong Kangwansupamonkon[2], Suda Kiatkamjornwong[3]

[1]*Program of Petrochemistry and Polymer Science, Faculty of Science, Chulalongkorn University, Phyathai Road, Bangkok 10330, Thailand e-mail: yoghurt55@hotmail.com*

[2]*National Nanotechnology Center, National Science and Technology Development Agency; 130 Thailand Science Park, Paholyothin Road, Klong 1, Klong Luang, Pathumthani 12120, Thailand e-mail: wiyong@nanotec.or.th*

[3]*Department of Imaging and Printing Technology, Faculty of Science, Chulalongkorn University, Phyathai Road, Bangkok 10330, Thailand, e-mail: ksuda@chula.ac.th*

บทคัดย่อ: ได้สังเคราะห์พอลิอะคริลาไมด์-*โค*-อะคริลิกแอซิด และสารเชิงประกอบพอลิอะคริลาไมด์-*โค*-กรดอะคริลิกที่มีอนุภาคของไทเทเนียมไดออกไซด์โดยปฏิกิริยาพอลิเมอไรเซชันแบบสารละลาย ศึกษาผลของอัตราส่วนโดยโมลของพอลิอะคริลาไมด์-*โค*-อะคริลิกแอซิด และความเข้มข้นสารเชื่อมขวางต่อค่าการดูดซึมน้ำ พบว่า ค่าการดูดซึมน้ำเพิ่มขึ้น เมื่อเพิ่มความเข้มข้นอะคริลิกแอซิดและลดปริมาณความเข้มข้นสารเชื่อมขวาง ศึกษาประสิทธิภาพการกำจัดสีย้อมด้วยเครื่อง UV-visible spectrophotometer ของสารเชิงประกอบไฮโดรเจล ที่เวลา 2 ชั่วโมง สามารถกำจัดสีเมทิลีนบลูได้มากกว่า ร้อยละ 70 จากการศึกษาด้วย GPC พบว่า น้ำหนักโมเลกุลของพอลิเมอร์โซ่ตรงที่เตรียมจากระบบเดียวกันในสภาวะที่มีไทเทเนียมไดออกไซด์ไม่มีการเปลี่ยนแปลงทั้งที่ได้รับรังสีอัลตราไวโอเลตและในที่มืด แสดงว่าสารเชิงประกอบโครเจลแตกสลายได้ช้าหรือไม่เกิดการแตกสลายในสภาวะที่มีรังสีอัลตราไวโอเลต ที่เวลา 4 ชั่วโมง ดังนั้น จึงมีความเป็นไปได้ที่จะนำสารเชิงประกอบไฮโดรเจลที่ผ่านการดูดซับและแตกสลายสีย้อมแล้วกลับมาใช้ใหม่ได้อีก

Abstract: Poly[acrylamide-*co*-(acrylic acid)] (Poly(AAm-*co*-AAc)) and TiO_2/Poly(AAm-*co*-AAc) composites were synthesized by an aqueous solution polymerization method. The effects of acrylamide-to-acrylic acid mole ratios and concentrations of *N*-MBA were investigated on water absorbency. It was found that water absorbency increases with increasing acrylic acid concentration and decreasing *N*-MBA concentration. Then the efficiency of dye removal was studied by UV-visible spectrophotometer. It was observed that more than 70% of methylene blue dye in the aqueous solution was decolorized with TiO_2/Poly(AAm-*co*-AAc) composites for 2 h of UV radiation. From the GPC result, it was found that molecular weights of the linear polymer with TiO_2 prepared by the same condition were not changed in the absence and presence of the UV radiation. It showed that this hydrogel composite is idly degraded or even hard to degrade under the UV radiation in 4 h. We noted that this hydrogel composite could be separated and reused.

Introduction: Hydrogel polymer is ionic polymer networks containing ionizable pendent groups such as -OH, -CONH-, $-CONH_2$, -COOH and $-SO_3H$ [1]. These networks can swell hundreds to thousands times their original weight depending on nature of the ionic functional groups. These materials are used in a wide range of applications such as infant diapers to absorb body fluids, drug delivery, especially hydrogels can absorb and retain ionic dyes such as methylene blue from wastewater from textile, food, beverage and printing industries [2]. In recent years, heterogeneous photocatalytic technique is a new horizon for removal of dyes. TiO_2 is the most extensively used photocatalyst; the separation of nano-sized TiO_2 from reaction solution is rather difficult. In this research, syntheses of hydrogel composites containing TiO_2 shall be carried out because they have many advantages, such as low cost and easy to separate from reaction solutions.

Methodology: Synthesis of poly(AAm-*co*-AAc) and TiO_2/poly(AAm-*co*-AAc) composites

The solution of mixed monomers was placed into a four-necked round-bottomed flask, equipped with a mechanical stirrer set at 200 rpm and an inlet tube for feeding nitrogen gas. The reaction temperature was controlled at 60 °C. *N*-MBA, TiO_2, APS and TEMED were added into the reaction mixture, respectively, and the reaction was stirred for 30 min. The resulting polymer was dewatered with methanol, cut into small pieces, and then dried in a vacuum oven at 50 °C for 24 h.

Water absorbency and photocatalytic degradation of methylene blue

Equilibrium water absorbencies (Q) were carried out with distilled water at room temperature. Distilled water (200 ml) was added to 0.1 g of the dry hydrogels and it was allowed to equilibrium swelling for 24 h. Then, the swollen hydrogel was filtered with through a 100-mesh sieve aluminum screen for 30 min at ambient temperature. The gel was dried in a vacuum oven until a constant weight was obtained. The Q value is calculated by Equation (1) as follows:

$$(Q) = \frac{A - B}{B} \quad (1)$$

where A is the weight of the hydrogel polymer after complete water absorption, and B is the weight of the hydrogel polymer before water absorption.

Photocatalytic degradation of methylene blue

One g of TiO_2/poly(AAm-*co*-AAc) hydrogel composite was poured in a 400-mL beaker containing 5 ppm methylene blue solution and kept at room temperature for 24 h. After the equilibrium adsorption, the unadsorbed dye solution was removed by filtration. Approximately 80 g of the swollen TiO_2/Poly(AAm-*co*-AAc) hydrogel composite was saturated with the dye which was placed on a glass plate for UV light irradiation by the UV lamp (30 W) at the wavelength of 254 nm for one sample, and without UV light irradiation for another sample. Eight g of the hydrogel composite sample was collected at time intervals of 0, 30, 60, 120, 180, and 240 min after the UV irradiation.

Results, Discussion and Conclusion: The water absorbency of poly(AAm-*co*-AAc) synthesized with various mole ratios of AAm: AAc and crosslink agent concentrations are shown in Figure 1. The addition of acrylic acid increased electrostatic repulsive force of carboxylate anions in the polymer chains. The highest water absorbency was found at AAm-to-AAc ratio of 0/100 due to the sole effect of the carboxylate groups. When the crosslinker concentrations increased, the crosslinking density of the polymer also increased. This would result in a decrease in repulsion force among the chains and leads to a decrease in water absorbency.

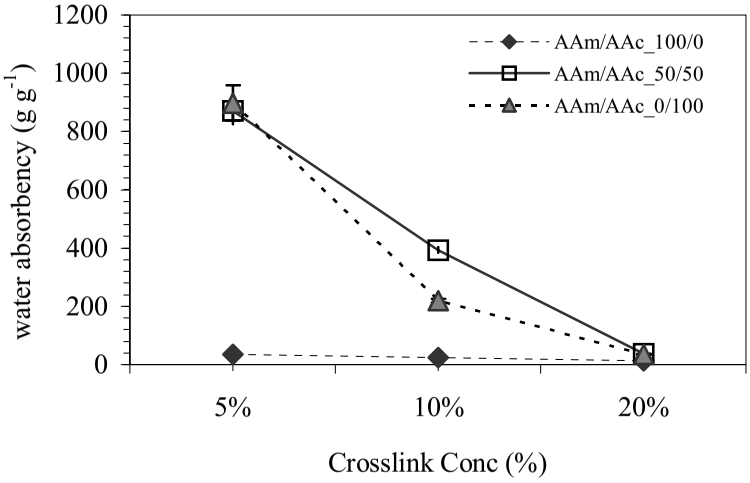

Figure 1 Water absorbency of poly(AAm-*co*-AAc) at various monomer ratios

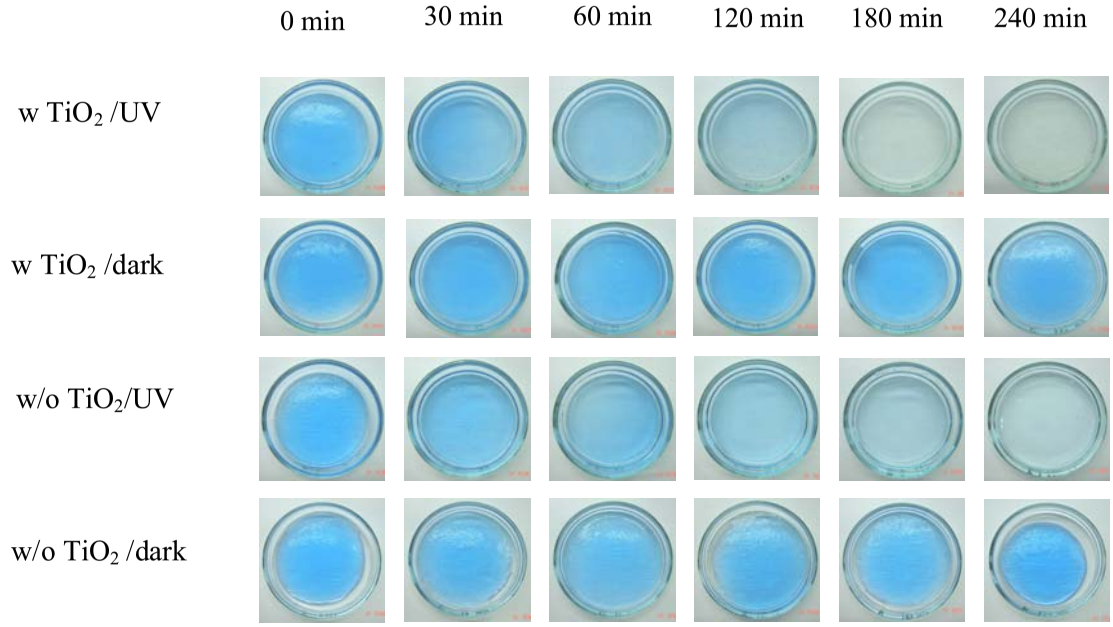

Figure 2 Removal of methylene blue dye in water with the hydrogel composites under various conditions

The result for photocatalytic degradation of 5 ppm of methylene blue dye was carried out by UV irradiation at wavelength 254 nm and lamp power of 30 W is shown in Figure 2. It indicates that under both TiO_2 and UV irradiation, 78% of the dye was degraded at the irradiation time of 2 h while only 53% degradation was found for UV irradiation without TiO_2. In the absence of TiO_2 and UV radiation, only 2% dye degradation was found while 6% was found in the presence of TiO_2 only. Thus both UV light and TiO_2 are indeed necessary for the effective destruction of methylene blue. In conclusion, the TiO_2 hydrogel nanocomposites have higher efficiency in degrading the dye under UV irradiation.

References:

1. Nikolaos, A.P., and Atul, R.K., 1993. Preparation structure and diffusional behavior of hydrogels in controlled release. *Advanced Drug Delivery Review*. 11, 1-35.
2. Yi, J-Z., Zhang, L-M., 2008. Removal of methylene blue dye from aqueous solution by adsorption onto sodium humate/ polyacrylamide/clay hybrid hydrogels. *Bioresource Technology*. 99, 2182-2186.

Keywords: *Hydrogel composite, TiO_2, Photocatalytic degradation, Water absorbency*, *Dye removal*

Acknowledgements

This research is financially supported by a Research Team Consolidation Grant, the Thailand Research Fund – Higher Education Commission (RTA5080004), Professor Suda Kiatkamjornwong as the project head. The authors are very grateful to Department of Imaging and Printing Technology, Faculty of Science, Chulalongkorn University, and National Nanotechnology Center, National Science and Technology Development Agency for use of research facilities.

CONTENTS

PLENARY SPEECHES

The Future of Print and the Digital Printing Revolution……*Stephen P. Hoover and George A. Gibson* (001)
Challenge to Digital Imaging“ Past, Present and Future ”…….....*Shinpei Ikenoue* (005)
The Past, Present and Future of Display Technology……*Hee Dong Park* (008)
Hardcopy Technologies and the Carbon Footprint……*Koji Hirakura* (009)
History and Outlook of Industrial Inkjet Printing……...*Werner Zapka* (010)
The Evolution of UV Photopolymerization in Global Industrial Manufacturing Markets and the Promising Outlook for the Future of the Technology……..*A.D.P. Harbourne* (013)
Mobile Image Capture, Consumption, and Applications…….
……*Qian Lin, Suk Hwan Lim, Kevin Matherson, Jerry Liu, Daniel Tretter* (016)

ORAL PRESENTATION SESSION

Track A: Digital Imaging and the Related Technologies

Keynote Speech

High Resolution Technologies of Digital Imaging and its Achievements in Remote Sensing……
…….....*Lei Yan, Yunfei Lu* (020)

Keynote Speech

The Transformation of Commercial Printing by Digital Printing Process……..*Eric Hanson* (024)

Invited Speech

Green Rendering for Printing…….....
.....*Zhigang Fan, Michael Furst, and Warren Kleiman* (027)
Performance Evaluation of Rollers for Charging, Development and Transfer in Electrophotography.
…….....…….....*Ming-Kai Tse and Inan Chen* (031)
Colour Management for Cholesteric Displays: Creation and Usage of ICC Colour Profiles……..
…….....*Gregory High, Phil Green, David Coates, and Chris Hughes* (035)
Liquid Crystals -their High Potential in FET Applications…….
…….....*Hiroaki Iino, Kyohei Nakano, and Jun-ichi Hanna* (039)
Morphological Image Analysis for Analysis for Automated Surface Quality Inspection of Moving Steel Plates……..... *Dadong Wang, Ke Xu, and Jinwu Xu* (042)
Real-time Enhancing Method for Night Scene of Vehicular Camera Based on Multi- scale Retinex
….....*Wang-Jun Kyung, Ho-Gun Ha, Cheol-Hee Lee, and Yeong-Ho Ha*(046)
An Image Processing Pipeline for Mobile Document Capture…….....
…….....…….....…….....*Jian Fan, Qian Lin, and Jerry Liu* (050)

A Novel Tamil Character Recognition Using Chain Code Method……
……*S.Selvakumar Raja and Mala John* (054)
Exact Representation of Glyph Contours and Its Application in Text Vectorization……
……*Tao He, Jie Feng, and Bingfeng Zhou* (058)
Forensic Application of Spectral Imaging: Fingerprint Detection Using Visible Absorption and Luminescence……..*Wei Huang, Guiqiang Wang, Xiaojing Xu, Tao Yu, and Zhicheng Yang* (062)
Preparation and Characterization of Microcapsules with Compact Wall Structure for Electrophoretic Displays……..*Runying Dai, Peipei Yin, Sheng Liu, Gang Wu, and Hongzheng Chen* (066)
Color Balance Method for Digital Orthographic Maps Based on Neural Network……..
……*Zhaohui Cao and Shi Ruizhi* (069)
The Research on the Anti-counterfeiting Technology Using Moire Based on Conventional Printing…
……*Taolin Ma, Xiang Li, and Lei Liu* (072)
Accelerated Gemological Image Analysis for Opal Grading……
…*Dadong Wang, Leanne Bischof,Bryan Dai,Ryan Lagerstrom, Graham Hornabrook,and Peter Sutton* (076)
Continuous Tone Image with Phthalate Derivatives-based Three Primary Color Electrochromic Cell..
……*Yuichi Watanabe, Satomi Tanaka, Kazuki Nakamura, and Norihisa Kobayashi* (080)
Textile Inkjet Print Quality of Polymer Pretreatment on Cotton…….....
……*Yutthana Lila, and Juntira Komasatitaya* (082)
Research on the Coating's Aging Performance of the Ink-jet Printing Paper……..
……*Gang Chen, Zhiqiang Fang, Jiajun Zhen, Yanliang Wu, and Guangxue Chen* (086)
Numerical Simulation of Dielectric Barrier Discharges in Electrophotography…….....
……*Napoleon Leoni, and Bhooshan Paradkar* (090)
Creation of Luminescent Eu(III) Complex with Remarkably Sharp Emission Band for Achieving Novel Lasing Medium……*Kazuki Nakamura, Yasuchika Hasegawa, and Norihisa Kobayashi* (094)
Modeling BRDF of Silk Fabric by Modifying Phong Reflection Model……..
……*Chawan Koopipat, Boonyakiat Chaitepprasith, and Suda Kiatkamjornwong* (098)
Adjective, Color, and Strength…….....*Mengtsung Tai, Tsung-Yu Hao, and Li-Yi Ma* (102)
3-Dimentional Imaging Technique Based on 2-Dimentional Plane…….
……*Ruizhi Shi, Jing An, Xiao Zhou , Yanlin Wang* (106)
World's First Charge Roller System Implemented in High-End Digital Commercial Printing Engine..
Omer Gila,Michael H.Lee, Seongsik Chang,Bill Holland, Eric Hanson,Boaz Tagansky ,and Gadi Oron (110)
Research on Color Uniformity of Tiled Multiple Projectors Display System…….
……..*Zhen Liu, and Mingwei Yu* (114)
A Vehicle License Plate Recognition Algorithm Using Bilateral Filter and Wavelet Transform……...
……...*Yao Li, Yan Hou, Zhenhua Chai, Hang Yang, Minying Zhang, Qi Li, and Samuel H. Chang* (118)
An Environmentally Benign General Deinking Approach……
…….....*Hou T. Ng, Manoj K. Bhattacharyya, Laurie S. Mittelstadt, and Eric G. Hanson* (122)
A Method for Calculating Similarity among Glyphs Using Cross Correlation……...
……*Tao He, Jie Feng, Bingfeng Zhou, Zhigang Fan, and Francis Kapo Tse* (126)
Novel Digital Media with Electronic Inks…….....
….....*Zhang-Lin Zhou, Jong-Souk Yeo, Jeff Mabeck,GreggCombs,Dick Henze, and Tim Koch* (130)

Modeling BRDF of Silk Fabric by Modifying Phong Reflection Model

*Chawan Koopipat, Boonyakiat Chaitepprasith and Suda Kiatkamjornwong**
Department of Imaging and Printing Technology
Faculty of Science, Chulalongkorn University
Bangkok, Thailand

Abstract

The optical quality of silk fabric is mainly considered on its color and gloss. In this study, the BRDF (bidirectional reflectance distribution function) of silk fabrics was measured by a gonio- spectrophotometer. The measured BRDFs were analyzed in terms of diffuse and specular components. It was observed that silk fabric tends to reflect the diffuse component according to Phong reflection model. However, the specular component has off-specular characteristic. We modified Phong reflection model and proposed a new model by taking off-specular reflection of silk fabric into consideration. Then, the proposed model was evaluated and compared to Phong, Oren-Nayar, Ward and Ashikmin-Shirley reflection models. It is found that BRDF calculated by the proposed model had been fitted to the measured BRDF better than the other models.

.

Introduction

In e-commerce and internet shopping, the appearance of products on monitors has influences on the customer purchasing decision. For the silk fabric or product made from silk, gloss is an important factor that affects the optical quality of such products. Gloss is the property of a material surface that involves mixed reflection and is responsible for a mirror-like appearance of a surface [1]. The possibility of reflection of a surface can be diffuse reflection, specular reflection or mixed reflection as shown in Figure 1.

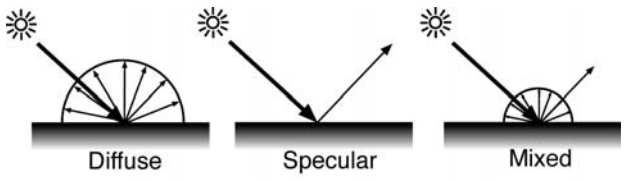

Figure 1. Three types of reflection from a surface

Most materials have mixed reflection, as well as silk fabric. The more quantity of specular reflection, the more glossiness will be observed. In contrast, the more quantity of diffuse reflection the more matte appearance will be observed. To present a 3D image of a product on a monitor, a good model is needed to render image reflectance and thereafter its appearance. There are many reflection models that can predict or estimate the reflectance of a surface. Some models are suitable of a shiny surface [2], some are for matte surface [3], [4] and some are for mixed surface [5]-[8]. For silk fabric, there is no specific model for this type of surface, therefore, this paper measured the BRDF (bidirectional reflectance distribution function) of silk fabric, analyzed and proposed a model for silk fabric. Finally, the performance of proposed model to predict the reflectance of silk fabric was compared to Phong, Oren-Nayar, Ward and Ashikmin refection models.

BRDF of Silk Fabric

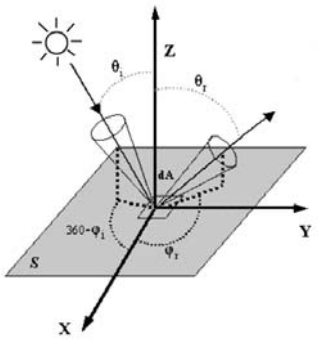

Figure 2. Schematic diagram of BRDF

BRDF describes the reflectance of a surface as a function of illumination geometry and viewing geometry as shown in Figure 2.

In order to measure BRDF of silk fabric, we used a goino-spectrophotometer (Murakami GP 100) to measure the three types of silk fabric as shown in Figure 3. All silk fabrics are bleached to become white color from different manufacturers. In this study we fixed the azimuth angle of the light source and viewing angle, therefore, only zenith angles were varied. The incident angles were 0, -15, -30, -45 -60, -75 degrees and the viewing angles were -75, -60, -45 -30, -15, 0, 15, 30, 45, 60, 75 degrees for each incident angle, respectively. Therefore, the total of 66 measurements of each silk fabric was made.

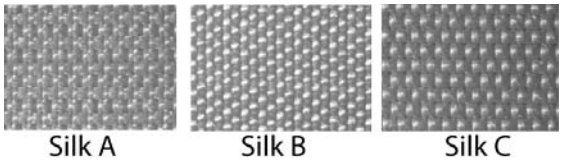

Figure 3. Silk fabrics used in this study

The measured reflectances were plotted in the polar coordinate for each of incident angle and type of fabric. Figures 4-9 show the measured reflectance of silks A, B and C at different incident angles.

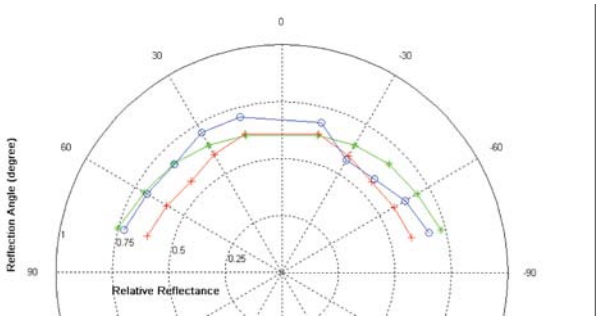

Figure 4. BRDF of silk fabric A(+), B(*) and C(o) at 0 ° incident angle

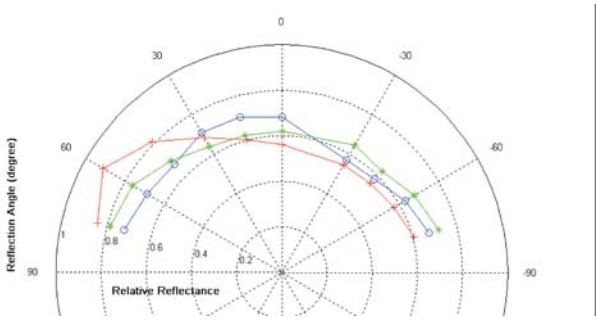

Figure 5. BRDF of silk fabric A(+), B(*) and C(o) at -15 ° incident angle

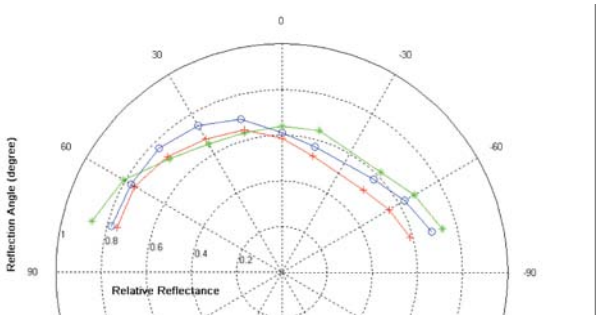

Figure 6. BRDF of silk fabric A(+), B(*) and C(o) at -30 ° incident angle

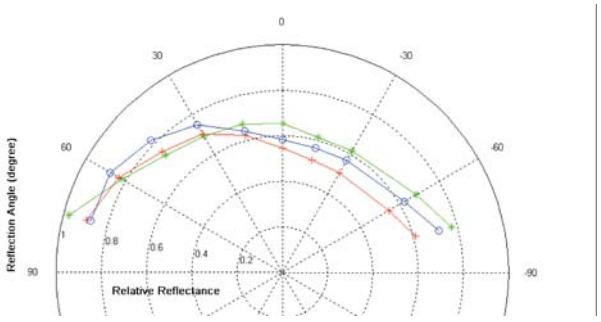

Figure 7. BRDF of silk fabric A(+), B(*) and C(o) at -45 ° incident angle

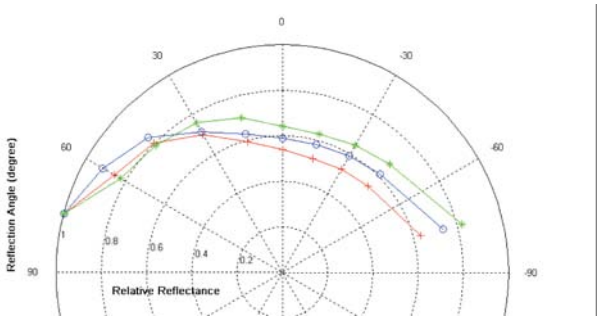

Figure 8. BRDF of silk fabric A(+), B(*) and C(o) at -60 ° incident angle

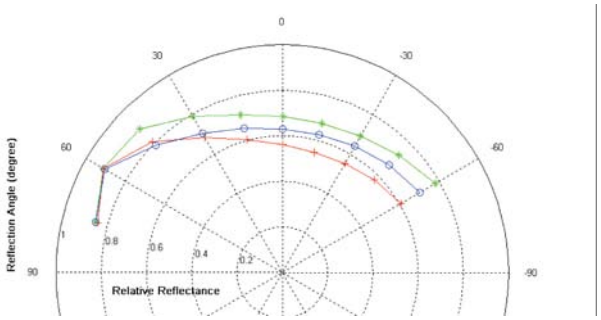

Figure 9. BRDF of silk fabric A(+), B(*) and C(o) at -75° incident angle

From these measured results, it is observed that silk fabric has the mixed reflectance. All silk fabrics have a similar reflection characteristic, that is, specular reflection is not so strong in the opposite angle of the incident light; therefore, the diffuse component is a major influence of its appearance. The specular component has an off-specular characteristic. The maximum off-specular reflection appeared at -15 degrees while the minimum appeared at 0 degree for all silk fabrics.

Modified Phong Reflection Model

To find a model for predicting the reflectance of a surface, a physical model is preferred if all parameters are known. The models consider many aspects of light path and also the micro facets of a surface. These make

the models much more complex and computation cost is high. The empirical model, such as Phong reflection model, is of interest in our study. It is based on a dichromatic model that is the total reflectance which is the sum of diffuse component and specular component. In addition, from our observation, the reflectance from silk fabric has off-specular property; therefore we modified the Phong reflection model by adding α and β to take into account for the reflectance lobe of diffuse and specular component respectively. The θ_{off} and $\phi_{o\phi}$ are the angle that compensate for the off-specular angle of reflected light in zenith and azimuth as shown in equation (1)

$$L(\theta_i,\theta_r,\phi_i,\phi_r) = k_d \cos^{\alpha}(\theta_r,\phi_r) + k_s \cos^{\beta}[\theta_r + (\theta_i - \theta_{off}),\phi_r + (\phi_i - \phi_{off})] \quad (1)$$

where L is the reflectance of silk fabric, k_d is the coefficient for diffuse component, k_s is the coefficient for specular component, θ_i and θ_r are zenith incident and viewing angles, ϕ_i and ϕ_r are azimuth incident and viewing angle respectively.

Evaluation of the proposed model

To evaluate the proposed model, we compared it with other reflection models, such as, Phong. Oren-Nayar, Ward and Ashikmin reflection models. The experiments were carried out by using the models to calculate reflectance by adjusting the model parameters to get the lowest rms error of the measured BRDF. The results are shown in Table 1.

Table 1. RMS between measured BRDF and reflection model

Fabric	Incident angle	measured RMS from the reflection models				
		proposed	Phong	Oren-Nayar	Ward	Ashikmin
A	0	**0.0153**	0.0223	0.0229	0.0229	0.0228
	-15	**0.1012**	0.1167	0.1424	0.1253	0.1274
	-30	**0.0168**	0.0824	0.0906	0.0868	0.0822
	-45	**0.0296**	0.1100	0.1314	0.1163	0.1067
	-60	**0.0380**	0.1161	0.1594	0.1243	0.1112
	-75	**0.0154**	0.0927	0.1319	0.0979	0.1008
B	0	0.0409	**0.0073**	0.0409	0.0283	0.0405
	-15	0.0307	**0.0296**	0.0876	0.0415	0.0540
	-30	**0.0100**	0.0487	0.1165	0.0609	0.0694
	-45	**0.0235**	0.0615	0.1294	0.0643	0.0765
	-60	**0.0355**	0.0577	0.1504	0.0656	0.0622
	-75	**0.0217**	0.0566	0.1516	0.0658	0.0835
C	0	0.0483	**0.0058**	0.0499	0.0480	0.0494
	-15	**0.0444**	0.0490	0.0713	0.0480	0.0503
	-30	**0.0109**	0.0707	0.1057	0.0728	0.0685
	-45	**0.0148**	0.0912	0.1303	0.1044	0.0831
	-60	**0.0214**	0.0918	0.1610	0.1036	0.0843
	-75	**0.0188**	0.0556	0.1183	0.0658	0.0949

Table 1 shows the RMS error of the model and the measured BRDF. Our proposed model can fit the measured reflectance better than the other models. In addition, Figures 10-14 show the comparison of measured BRDF and the proposed model in polar coordinate.

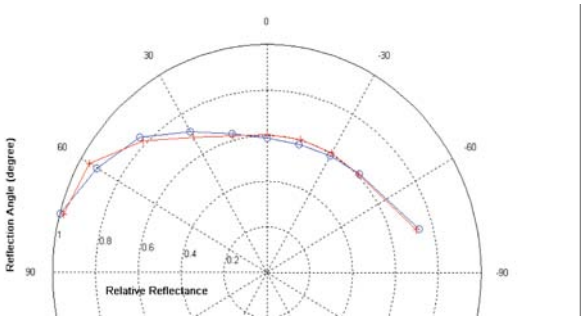

Figure 10. Comparison between measured BRDF(o) and BRDF calculated from proposed model(+) on silk fabric 3 at -60 ° incident angle

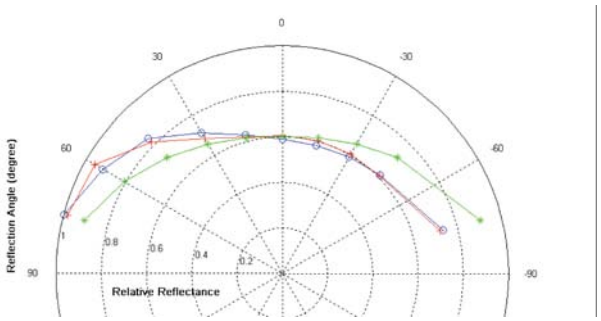

Figure 11. Comparison between measured BRDF(o), BRDF calculated from proposed model(+) and Phong model(*) on silk fabric 3 at -60 ° incident angle

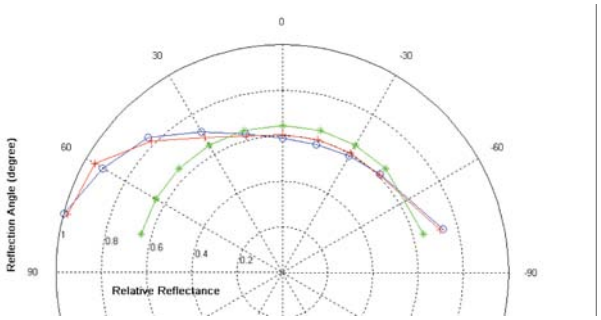

Figure 12. Comparison between measured BRDF(o), BRDF calculated from proposed model(+) and Oren-Nayar model(*) on silk fabric 3 at -60° incident angle

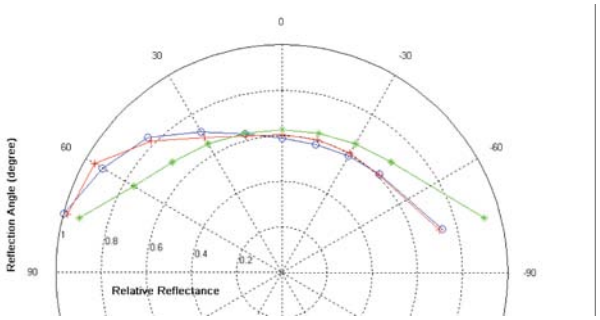

Figure 13. Comparison between measured BRDF(o), BRDF calculated from proposed model(+) and Ward model(*) on silk fabric 3 at -60 ° incident angle

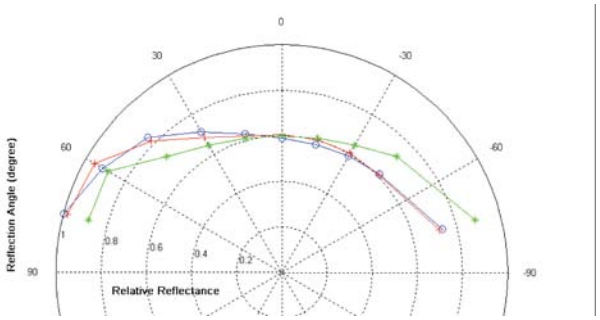

Figure 14. Comparison between measured BRDF(o), BRDF calculated from proposed model(+) and Ashikmin model(*) on silk fabric 3 at -60° incident angle

Conclusion

This research measured and analyzed the BRDF of silk fabric. The result showed that the silk fabric illustrates the mixed reflection in which the diffuse component is much greater than the specular component and has Lambertian-behavior like. The specular component also included the off-specular characteristic. Phong reflection model was modified to fit with the measured BRDF and this proposed model was compared to the existing reflection model. The obtained results showed that the proposed model can better fit to the measured BRDF of the silk fabric investigated.

Acknowledgements

We would like to give our grateful to Prof. Dr. Yoichi Miyake of Research Center for Frontier Medical Engineering, Chiba University, Japan for providing the gonio-spectrophotometer for the measurement of this research. This research is granted by The Thailand Research Fund under the Contract number RTA5080004.

References

1. Wyszecki, G., and Stiles, W.S., Color Science. 2nd edition, John Wiley & Son, pg. 51-52. (1982)
2. Torrance, K. E. and Sparrow, E.M. Theory for off-specular Reflection from Roughened Surface. Optical Society of America, 57(9), Pg.1105-1114. (1967)
3 Oren, M., and Nayar, S.K., Generalization of Lambert's Reflectance Model. Computer Vision, 14(3), Pg. 227-251. (1995)
4. Dana, K.J., Ginneken, B.V., Nayar, S.K. and Koenderink, J.J., Reflectance and Texture of Real-World Surfaces. ACM Transactions on Graphics, 18(1), Pg 1-34. (1999)
5. Blinn, J.F., Models of Light Reflection for Computer Synthesized Pictures., Proceedings of the 4th annual conference on Computer Graphics and Interactive Techniques, Pg. 192-198. (1977)
6. Phong, B.T., Illumination for Computer Generated Pictures. Communications of the ACM, 18(6), Pg. 311-317. (1975)
7. Ashikmin, M., and Shirley, P., Anisotropic Phong BRDF Model. Journal of Graphic Tools, 5(2), Pg. 25-32. (2000).
8. Ward, G.J., Measuring and Modeling Anisotropic Reflection. Computer Graphics, 26(2), Pg. 265-272. (1992)

.

Biography

Chawan Koopipat received his B.Sc degree in Photographic Science and Printing Technology from Chulalongkorn University, Thailand in 1989, and MPhil (Printing Technology) from West Herts College, UK in 1996. He received Ph.D. degree (Image Information Processing) from Chiba University, Japan in 2002. He is currently an assistant professor in imaging science at Department of Imaging and Printing Technology, Faculty of Science Chulalongkorn University, Thailand. He researches in the area of printing quality evaluation especially in ink jet printing on fabric. He is currently a researcher under Prof. Dr. Suda Kiatkamjornwong project (Senior Scholar Research Fellowship) granted by The Thailand Research Fund.

1st Polymer Conference of Thailand

October 7-8, 2010
Convention Center, Chulabhorn Research Institute, Bangkok

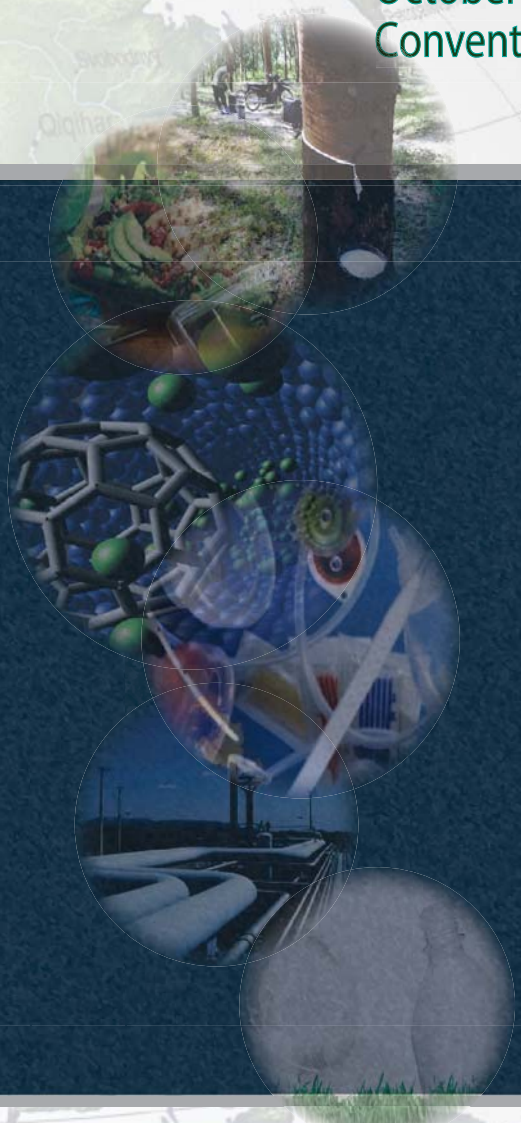

PROCEEDINGS

Organized by :

Sponsored by :

1st POLYMER CONFERENCE OF THAILAND

PCT-1

Organized by

The Polymer Society of Thailand (PST)

Sponsored by

Platinum

PTT Chemical Public Company Limited

Gold

- SCG Chemicals Company Limited
- National Science and Technology Development Agency (NSTDA)
  National Metal and Materials Technology Center (MTEC)
- National Nanotechnology Center (NANOTEC)

Silver

- Thai Plastic and Chemicals Public Company Limited
- PTT Phenol Company Limited

BACKGROUND OF PCT-1

The Polymer Society of Thailand (PST) was founded in 1999 to be a center for connecting people who are working on or interested in polymers from academic, industrial, and governmental sectors in Thailand. PST has also been representing the Thai polymer community in the international arena. Among the activities organized by PST are conferences, seminars, workshops, and short courses.

In recent years, the number of polymer scientists, technologists, and engineers in Thailand has increased dramatically to more than one thousand personnels. Rarely that a scientific conference devoted exclusively to all fields of polymer science, technology, and engineering was organized in Thailand. Therefore PST has aimed to host The 1st Polymer Conference of Thailand (PCT-1) to provide a forum for meeting and sharing of research results and ideas among the Thai polymer community and also with international polymer experts. We hope that the PCT will prove to be a major platform for facilitating academic and technical development of polymers in Thailand.

The aims of PCT-1 are,

1. To bring together academic personnel, students, researchers in university, government institutes and industrial sectors, to share their experiences and knowledge relating to polymer science, technology and engineering.

2. To promote networking and the establishment of new collaboration among polymer scientists and interested persons or groups in both academic and industrial sectors in order to push forward the development of polymer science and technology in Thailand.

MESSAGE FROM PRESIDENT

PCT-1

One of the important roles of the Polymer Society of Thailand (PST) is to promote the development of polymer science, technology and engineering in Thailand. Such development is believed to be important since the polymer and petrochemical industries in Thailand are growing rapidly and are contributing very importantly to the economy of the country.

In 2007, the Polymer Society of Thailand, in collaboration with the Graduate Program in Polymer Science and Technology, Mahidol University, organized the 1st Polymer Graduate Conference of Thailand (PGCT-1), to provide a meeting place for polymer graduate students in Thailand to present and exchange their research results. The 2nd PGCT was organized by the Petrochemistry and Polymer Science Program, Chulalongkorn University in 2009. Both PGCTs were proved to be successful events. However, it was felt that the Thai polymer community needed a bigger forum for exchanging information, ideas and experiences among polymer scientists, technologists and engineers from both the public and private sectors as the number of the people involved with polymers in the country steadily grows. Furthermore, there is an increasing need for closer collaborations between researchers from universities and government institutes and industrial companies in order to achieve research results which have greater impacts for the country.

For this reason, the 1st Polymer Conference of Thailand (PCT-1) is organized with cooperation and supports from various graduate schools in polymer science and technology of major universities and also some large petrochemical companies. It is hoped that the PCT will develop into an annual meeting for PCT members and other interested parties of the Thai polymer community, similar to those that have taken place in other advanced countries such as in the USA, Europe and Asia.

Finally, I would like to express my sincere thanks to members of the organizing committee who have put in hard work and strenuous efforts in organizing the PCT-1. I also would like to express my deep appreciation to the sponsors of the PCT-1, including PTT Chemicals Public Co., Ltd., SCG Chemicals Co., Ltd., National Science and Technology Development Agency (NSTDA), National Metal and Materials Technology Center (MTEC), National Nanotechnology Center (NANOTEC), Thai Plastic and Chemicals Public Co., Ltd., and PTT Phenol Co., Ltd. for their understandings and supports which will make the PCT-1 a successful event.

Dr. Krisda Suchiva
Chairman of the PCT-1 Organizing Committee
President of the Polymer Society of Thailand

COMMITTEE

PCT-1

Advisory Committee

1. Dr. Jintana Siripitayananon	Department of Chemistry, Chiang Mai University
2. Dr. Jantrawan Pumchoosak	Department of Industrial Chemistry, Chiang Mai University
3. Dr. Nuanphan Chantarasiri	Department of Chemistry, Chulalongkorn University
4. Dr. Sirithan Bulpakdi	Department of Materials Science, Chulalongkorn University
5. Dr. Pranut Potiyaraj	Metallurgy and Materials Science Research Institute, Chulalongkorn University
6. Dr. Pomthong Malakul Na Ayudhaya	The Petroleum and Petrochemical College, Chulalongkorn University
7. Dr. Patiphan Juijerm	Department of Materials Engineering, Kasetsart University
8. Dr. Amnat Permsubscul	Department of Chemistry, King Mongkut's Institute of Technology Ladkrabang
9. Dr. Sirisart Ouajai	Department of Industrial Chemistry, King Mongkut's University of Technology North Bangkok
10. Dr. Boonnak Sukhummek	Department of Chemistry, King Mongkut's University of Technology Thonburi
11. Prof. Siriwat Wongsiri	School of Science, Mae Fah Luang University
12. Dr. Pranee Phinyocheep	Department of Chemistry, Mahidol University
13. Dr. Sa-ad Riyajan	Department of Materials Science and Technology, Prince of Songkla University (Hat Yai)
14. Dr. Nattapong Nithi-Uthai	Department of Rubber Technology and Polymer Science, Prince of Songkla University (Pattani)
15. Dr. Narongchai O-Charoen	Department of Materials and Metallurgical, Rajamangala University of Technology Thanyaburi
16. Natee Srisawat	Department of Textile Engineering, Rajamangala University of Technology Thanyaburi
17. Dr. Niti Yongvanich	Department of Materials Science and Engineering, Silpakorn University
18. Dr. Nitinat Suppakarn	School of Polymer Engineering, Suranaree University of Technology
19. Seranee Srisuk	Department of Textile Science and Technology, Thammasat University
20. Dr. Wanchart Preechatiwong	Department of Materials Science and Engineering, Walailak University
21. Dr.Wilaiporn Chetanachan	The Siam Cement Public Co., Ltd.
22. Dr. Chaya Jantavasu	PTT Chemical Public Co., Ltd.
23. Jackra Swasdiburi	BST Latex Co., Ltd.
24. Banja Junhasavasdikul	Chemical Innovation Co., Ltd.

Chairman

Dr. Krisda Suchiva	Department of Chemistry, Mahidol University National Metal and Materials Technology Center (MTEC) (President of the Polymer Society of Thailand)

Scientific Committee

1. Prof. Suda Kiatkamjornwong	Department of Imaging and Printing Technology, Chulalongkorn University
2. Dr. Suwabun Chirachanchai	The Petroleum and Petrochemical College, Chulalongkorn University
3 . Dr. Krisda Suchiva	Department of Chemistry, Mahidol University National Metal and Materials Technology Center (MTEC)
4. Dr. Pranee Phinyocheep	Department of Chemistry, Mahidol University
5 . Dr. Taweechai Amornsakchai	Department of Chemistry, Mahidol University
6 . Dr. Robert Molloy	Department of Chemistry, Chiang Mai University
7. Dr. Charoen Nakason	Faculty of Science and Technology Prince of Songkla University (Pattani)
8. Dr. Asira Fuongfuchat	National Metal and Materials Technology Center (MTEC)

Budgeting Committee

1. Dr. Chaiyoot Changsarn	Faculty of Engineering, Rajamangala University of Technology Thanyaburi
2. Dr. Surat Areerat	Department of Chemical Engineering, King Mongkut's Institute of Technology Ladkrabang

Exhibition Committee

1. Dr. Ittipol Jangchud	Department of Chemistry, King Mongkut's Institute of Technology Ladkrabang
2. Dr. Jitladda Sakdapipanich	Department of Chemistry, Mahidol University
3. Dr. Pajaera Patanathabutr	Department of Materials Science and Engineering, Silpakorn University
4. Dr. Pasaree Laokijcharoen	National Metal and Materials Technology Center (MTEC)

Public Relation Committee

1. Dr. Kanoktip Boonkerd	Department of Materials Science, Chulalongkorn University
2. Dr. Toemsak Srikhirin	Department of Physics, Mahidol University
3. Dr.Sommai Pivsa-Art	Faculty of Science and Technology, Rajamangala University of Technology Thanyaburi

Secretariat

1. Dr.Varawut Tangpasuthadol	Department of Chemistry, Chulalongkorn University
2. Dr. Surapich Loykulnant	National Metal and Materials Technology Center (MTEC)
3. Dr. Warayuth Sajomsang	National Nanotechnology Center (NANOTEC)
4. Nittranant Saingam	The Polymer Society of Thailand

Microencapsulation of Menthol by Crosslinked Chitosan Via Porous Glass Membrane Emulsification Technique

Jaruwan Krongsin[1], Supaporn Noppakundilograt[2], Roongkan Nuisin[3] and Suda Kiatkamjornwong[2*]

[1]Multidisciplinary Program of Petrochemistry and Polymer Science, Faculty of Science, Chulalongkorn University, Bangkok 10330, Thailand, [1]e-mail: ja033.su@hotmail.com

[2]Department of Imaging and Printing Technology, Faculty of Science, Chulalongkorn University, Bangkok 10330, Thailand, [2]e-mail: supaporn.n@Chula.ac.th; [2]*e-mail: ksuda@Chula.ac.th

[3]Department of General Science, Faculty of Science, Chulalongkorn University, Bangkok 10330, Thailand, [3]E-mail: Roongkan.n@Chula.ac.th

Abstract

Chitosan encapsulated menthol microcapsules were successfully prepared by the oil-in-water emulsion process using Shirasu porous glass (SPG) membrane emulsification technique. The SPG membrane with a membrane pore size of 5.2 μm was found to be suitable for a high viscosity dispersion phase containing light mineral oil. The effect of operation pressure, the amount of menthol loading and crosslinking time on the size and size distribution of microcapsules were systemically investigated. The size of the menthol-loaded chitosan microcapsules was strongly dependent on the mean pore size of the SPG membrane and the amount of menthol loading in the dispersion phase. The average diameter of emulsion droplets of 28.3 μm with a coefficient of variation of 24.7% was obtained. Increasing the menthol loading in the dispersion phase from 5 to 10 wt% of chitosan decreased the emulsion droplets with a broad droplet size distribution. The crosslinked microcapsules size and size distribution of o/w emulsion droplets decreased with increasing crosslinking time.

Keywords: Microcapsules; Chitosan; Menthol; SPG membrane emulsification

1. Introduction

Menthol is a cyclic terpene alcohol with three asymmetric carbon atoms. Among the optical isomers, menthol is the one that occurs most widely in nature and it is endowed with the peculiar property to be a fragrance and flavor compound. For this reason, it is widely used as flavoring for toothpaste, oral hygiene and personal care products [1]. Menthol is generally available in the form of crystals or granules with a melting point of 41–43 °C. However, its high volatility and whisker growth are the very important problems concerning its applications and shelf life. The microencapsulation method is an accountable and appropriate technique to solve these problems [2].

Chitosan is derivatized by deacetylation of chitin. Chitosan has been used in many applications because of its biocompatibility, biodegradability, non-toxicity and antibacterial activity [3]. Chitosan can form microcapsules by various methods such as spray drying, emulsification/ solvent evaporation, ionotropic gelation, coacervation techniques, and so on. It can prevent loss of volatile flavors, and enhance stability of the flavor core materials [2]. The size of the microcapsules prepared by these methods is difficult to control, and the size distribution is thus very broad [4].

In conventional emulsification devices, such as high-pressure homogenizer, mechanical stirring, and rotor-stator systems, these methods produce rather polydisperse emulsions and consume high energy [5]. A membrane emulsification system produces emulsions by permeating a dispersed phase into a continuous phase through a membrane having a uniform pore diameter. The

membrane emulsification method makes it possible to produce monodisperse emulsions and consume less energy [6, 7]. The most commonly used microporous membrane for the emulsification is a Shirasu Porous Glass (SPG) membrane. The SPG membrane is made from SiO_2–Al_2O_3, with a very narrow pore size distribution. It was fabricated by Nakashima et al. [8] via a series of sophisticated heat treatments, an induced phase separation created a bi-continuous structure of CaO-B_2O_3, and SiO_2–Al_2O_3. Commercially, the pore sizes ranging from 0.1 to 18.0 μm have been available. The SPG membrane is inherently hydrophilic and it is much easier to get the monodisperse oil-in-water (o/w) emulsions than water-in-oil emulsion (w/o) due to the presence of negatively charged silanol groups on the surface [9].

Kiatkamjornwong et al. [10] had successfully prepared the microcapsules of chitosan (0.5-40 μm in diameter) by the conventional stirring method in which chitosan is the shell of microcapsules encapsulating the core material of menthol. The size distribution of the conventional method is rather polydisperse and thus a better technique of porous glass membrane emulsification can remedy the large size distribution to a narrow size distribution of microcapsules.

In this study, the SPG membrane emulsification method was applied to prepare menthol-loaded TPP crosslinked chitosan microcapsules. The effects of membrane pore size, the amount of menthol loading and crosslinking time were investigated on the microcapsule size and size distribution.

2. Experimental procedures

2.1. Materials

Chitosan (Sea fresh Chitosan Lab Co., Ltd., Bangkok, Thailand) with a degree of deacetylation of 95% with a viscosity-average molecular weight ($\overline{M}_v$) of 100,000 g/ mol was used as received. Sodium tripolyphosphate (TPP, Merck, Hohenbrunn, Germany) was used as a crosslinker. Light mineral oil (Hopewell International Co., Ltd., Thailand) was used as an oil phase. Menthol with a molecular weight of 156.27 g/mol (Hong Huat Co., Ltd., Thailand) was used as an encapsulating material. Poly(oxyethylene-2-stearyl ether) (Brij 72, Greensville Co., Ltd., Thailand) was used as an oil-soluble surfactant. Sodium dodecyl sulfate (SDS, Merck, Germany) and cetyl stearyl alcohol (Kao Co., Ltd., Thailand) were used as a surfactant and a co-surfactant, respectively. Poly(vinyl alcohol), PVA-220, (Kuraray Co., Ltd., Japan) with 87-89% of hydrolysis degree was used as a stabilizer.

Table 1 A recipe for the o/w emulsion

Component	Weight (g)
Continuous phase	
water	220
chitosan solution(1% w/v)	20
PVA	3.0
SDS	1.5
Disperse phase	
light mineral oil	20
menthol	0.5-2.0
brij 72	0.5
cetyl-stearyl alcohol	0.5

2.2. Apparatus

A miniature kit for emulsification with an SPG module was purchased from Kiyomoto Co., Ltd (Japan). A tubular porous glass membrane with the size of 2 cm length and 1 cm diameter was installed in the module. The dispersed phase (oil phase) was stored in a Teflon vessel (20 ml) which was connected to nitrogen gas inlet, the continuous phase (water phase) containing a mixture of SDS and PVA in a 250-ml beaker was stirred at 300 rpm with a magnetic bar to prevent creaming of the droplets. With an optimum pressure of nitrogen gas, the dispersed phase can permeate through the uniform pores of the membrane into the continuous phase to form droplets. The droplets were then stabilized by the PVA and SDS dissolved in the continuous phase.

2.3. Preparation of chitosan microcapsules

The SPG membrane with an average pore size of 1.4 and 5.2 μm was used for the emulsification. The preparative condition for the emulsification is shown in Table 1. The SPG membrane was pre-wetted in the aqueous phase. Menthol was dissolved in a mixture of light mineral oil, surfactant and co-surfactant by heating up to 40-43 °C and was used as a dispersed phase. The aqueous phase where PVA and SDS had been dissolved

was used as a continuous phase. The oil phase permeated through the uniform pores of the SPG membrane by the pressure of nitrogen gas into the aqueous phase to form the o/w emulsion. TPP solution (5 wt%) was slowly dropped into

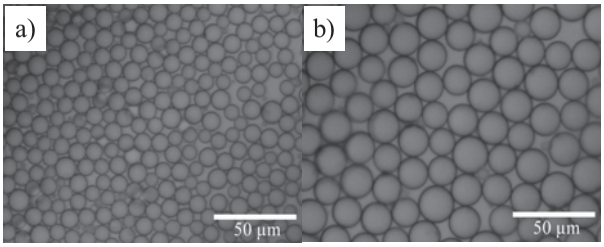

Figure 1. Optical micrographs of the o/w emulsion (without menthol) prepared by the SPG membrane emulsification with different pore sizes

the o/w emulsion to crosslink the chitosan droplets by stirring at 200 rpm for 1 to 5 h. Finally, the chitosan microcapsules were collected and washed repeatedly two times with petroleum ether and acetone by centrifugation at 3000 rpm, and then the microcapsules were freeze dried.

A pressure used was slightly above the critical pressure. In this study, the ranges of the permeation pressures at 48.9 to 88.8 kPa for the 1.4 μm pore size, and 14.1 to 67.0 kPa for the 5.2 μm membrane pore size were used.

2.4. Characterization of chitosan microcapsules

2.4.1. Optical microscopic observation

Droplets before and after the crosslinking were observed with an optical microscope. Diameters of approximately 150 droplets were measured to calculate the average diameter. The number average diameter ($\overline{d_e}$) was calculated according to eq. (1). The coefficient of variation (CV) was determined using the formula in eq. (2).

$$\overline{d}_e = \sum_{i=1}^{n} d_i \Big/ N \quad (1)$$

$$\%CV = \left(\sum_{i=1}^{n} \frac{\left(d_i - \overline{d}_e\right)^2}{N} \right)^{1/2} \Big/ \overline{d}_e \times 100 \quad (2)$$

where d_i is the diameter of each droplet, N is total number of the droplets measured, and $\overline{d_e}$ is the number average diameter of the droplets.

3. Results and discussion

3.1. Effect of the pore size of membrane on the droplet size and size distribution

The SPG membranes with the average pore diameter of 1.4, and 5.2 μm were used to prepare the o/w emulsion. The uniform emulsion droplets were prepared as shown in the microphotograph in Fig. 1. The average diameter ($\overline{d_e}$) of 10.2 and 19.6 μm for the membrane pore sizes of 1.4 and 5.2 μm were obtained, respectively. It was found that the diameter of droplets in the o/w emulsion was approximately 8 and 4 times the diameters of membrane pore. The dispersed phase containing light mineral oil without menthol as an additive was difficult to permeate through the SPG membrane pore size of 1.4 μm. The possible cause was from the high viscosity of light mineral oil. Furthermore, due to the high molecular weight of PVA stabilizer used, the PVA molecules were covered onto the membrane surface and plugged the pores, the oil phase was thus retained and could not be permeated.

Table 2 The o/w emulsion droplets (without menthol) obtained by different pore size membranes

property	pore size (μm)	
	1.4	5.2
Number average diameter, $\overline{d_e}$ (μm)	10.2	19.6
CV (%)	10.1	11.5

3.2. Effect of the amount of menthol loading on droplet size and size distribution

The menthol dissolved in the dispersed phase affected the o/w emulsion. The permeation pressure decreased from 7.4 kPa to 2.5 kPa and 0.6 kPa when increasing the amount of menthol from 0 to 5 and 10 wt%, respectively. The hydrophilic in the disperse phase increased with increasing the amount of menthol loading in disperse phase. The hydroxyl group of menthol enhances the hydrophilicity of the oil phase, thus to

permeate it easily through the hydrophilic pore wall of the SPG membrane. The permeation pressure was then decreased. Optical micrographs and the histogram of size distribution of the droplets in oil phase at different amounts of menthol loadings are shown in Fig. 2. Without the menthol, an average diameter of emulsion droplets of 28.3 µm with the CV of 24.7% was obtained. When the amounts of menthol loading in the disperse phase increased from 5 to 10 wt%, the average diameters of emulsion droplets decreased from 24.2 to 16.8 µm with the CV of the droplets increased from 34.4 to 57.6%, respectively. The size distributions of histogramsin Fig. 2. a)-c) indicate that more menthol loading in the dispersed phase produced the smaller size droplets in the range of 10 µm. This effect is caused by the increases in hydrophilicity of the hydroxyl groups when increasing the menthol loadings.

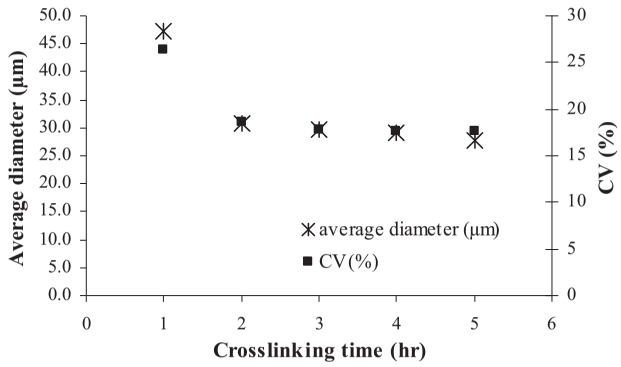

Figure 3. Relationship between the crosslinking time and the average size and the coefficient of variation (5 wt% menthol and 1% w/v chitosan solution)

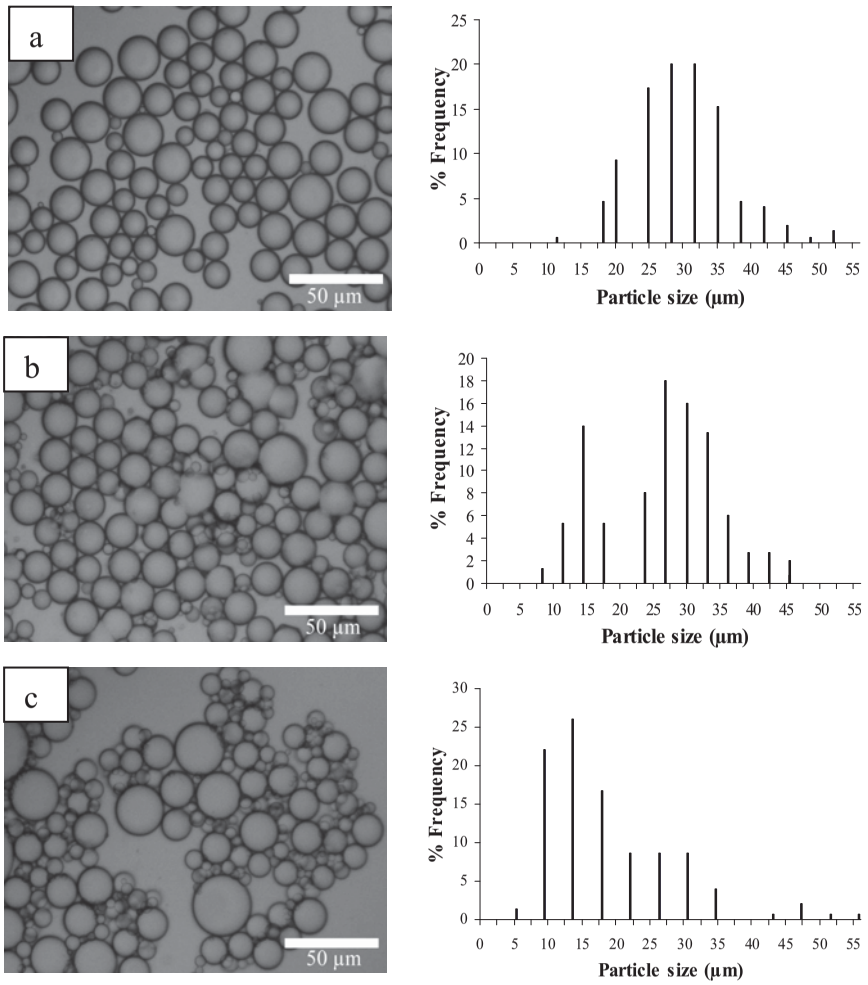

Figure 2. Optical micrographs (left) and histograms of the size distribution (right) of o/w emulsion with different amounts of menthol loadings when a) without menthol, b) 5 wt% menthol, c)10 wt% menthol

3.3. Effect of crosslinking time on the size and size distribution

Chitosan as the shell of o/w emulsion droplets was crosslinked with TPP solution. TPP was dissociated into OH^- and $P_3O_{10}^{5-}$ anions. The positively charged amino group of chitosan reacted with $P_3O_{10}^{5-}$ anions to form crosslinking bonds [11]. The crosslinked microcapsule sizes of the o/w emulsion droplets decreased from 47.4 to 27.6 μm with increasing crosslinking time from 1 to 5 hr are show in Fig. 3, due to the increase of crosslink density of chitosan-TPP matrix [12]. The less crosslinking time of 1 h could not form the small droplet size for the subsequence process in this research. Very interestingly, the longer crosslinking time gave the narrow size distribution.

4. Conclusion

Chitosan encapsulated menthol microcapsules using the SPG membrane emulsification technique were prepared. The effects of membrane pore size, the amount of menthol loadings and crosslinking time affected the size and size distribution of the droplets. The uniform-sized chitosan microcapsules can also be prepared when the membrane pore size used was 5.2 μm; the higher amount of menthol gave the smaller mean diameter of the emulsion droplets with narrow size distribution. The longer crosslinking time produced the smaller microcapsules with a narrow size distribution.

Acknowledgements

The authors thank the Thailand Research Fund for funding the research under the Senior Scholarly Consolidation Grant no. RTA5080004.

References

[1] Galeotti, N., Di Cesare Mannelli, L., Mazzanti, G., Bartolini, A., Ghelardini, C., 2002. Menthol: a natural analgesic compound. *Neuroscience Letters*, 322, 145–148.

[2] Soottitantawat, A., Takayama, K., Okamura, K., Muranaka, D., Yoshii, H., Furuta, Takeshi., Ohkawara, M., Linko, P., 2005. Microencapsulation of l-menthol by spray drying and its release characteristics. *Innovative Food Science and Emerging Technologies*, 6, 163– 170.

[3] Rinaudo, M., 2006. Chitin and chitosan: Properties and applications. *Progress in Polymer Science*, 31, 603–632.

[4] Wei, W., Wang, L.Y., Yuan, L., Yang, X.D., Su, Z.G., Ma, G.H., 2008. Bioprocess of uniform-sized crosslinked chitosan microspheres in rats following oral administration. *European Journal of Pharmaceutics and Biopharmaceutics*, 69, 878–886.

[5] Vladisavljevic, G. T., Schubert, H., 2002. Preparation and analysis of oil-in-water emulsions with a narrow droplet size distribution using Shirasu-porous-glass (SPG) membranes. *Desalination*, 144, 167-l72.

[6] Yasuno, M., Nakajima, M., Iwamoto, S., Maruyama, T., Sugiura, S., Kobayashi, I., Shono, A., Satoh, K., 2002. Visualization and characterization of SPG membrane emulsification. *Journal of Membrane Science*, 210, 29-37.

[7] Joscelyne, S.M., Trägårdh, G., 2000. Membrane emulsification – a literature review. *Journal of Membrane Science*, 169, 107–117.

[8] Nakashima, T., Shimizu, M., 1986. Porous glass from calcium alumino boro-silicate glass. *Ceramics*, 21, 408.

[9] Vladisavljevic, G.T., Kobayashi, I., Nakajima, M., Williams, R.A., Shimizu, M., Nakashima, T., 2007. Shirasu Porous Glass membrane emulsification: Characterization of membrane structure by high-resolution X-ray microtomography and microscopic observation of droplet formation in real time. *Journal of Membrane Science*, 302, 243–253.

[10] Kiatkamjornwong, S., Phansomboon, S., Hoven, V., 2009. Chitosan microencapsulation of menthol and its controlled release, *The Journal of the Royal Institute of Thailand*, 34, 337-371.

[11] Hsieh, F. M.; Huang, C.; Lin, T. F.; Chen, Y. M.; Lin, J. C., 2008. Study of sodium tripolyphosphate-crosslinked chitosan beads entrapped with *Pseudomonas putida* for phenol degradation, *Process Biochemistry*, 43, 83–92.

[12] Ko, J.A., Park, H.J., Hwang, S.J., Park, J.B., Lee, J.S., 2002. Preparation and characterization of chitosan microparticles intended for controlled drug delivery. International Journal of Pharmaceutics 249, 165-174.

1st Polymer Conference of Thailand

October 7-8, 2010
Convention Center, Chulabhorn Research Institute, Bangkok

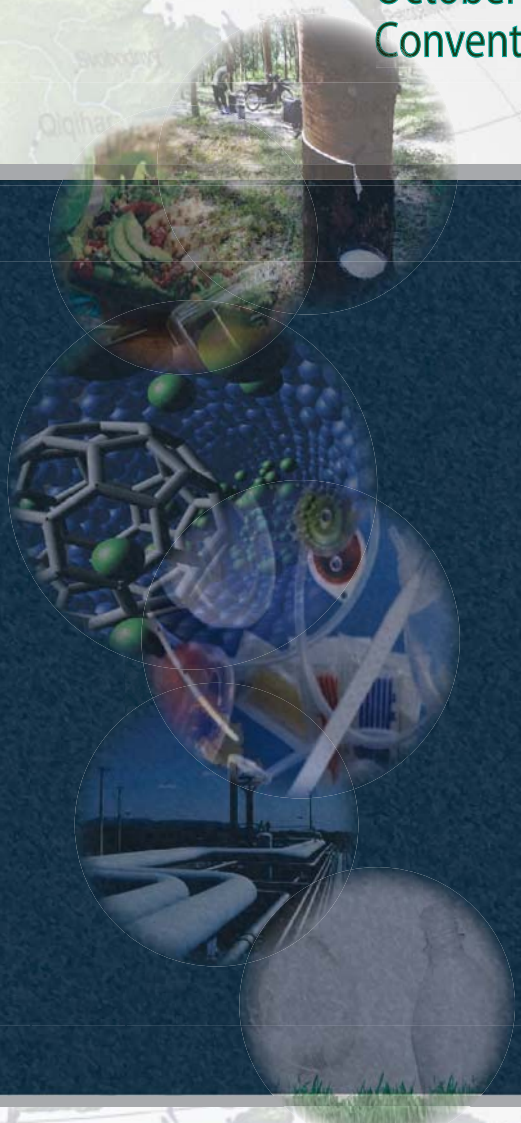

PROCEEDINGS

Organized by :

Sponsored by :

1st POLYMER CONFERENCE OF THAILAND

PCT-1

Organized by

The Polymer Society of Thailand (PST)

Sponsored by

Platinum

PTT Chemical Public Company Limited

Gold

- SCG Chemicals Company Limited
- National Science and Technology Development Agency (NSTDA)
  National Metal and Materials Technology Center (MTEC)
- National Nanotechnology Center (NANOTEC)

Silver

- Thai Plastic and Chemicals Public Company Limited
- PTT Phenol Company Limited

BACKGROUND OF PCT-1

The Polymer Society of Thailand (PST) was founded in 1999 to be a center for connecting people who are working on or interested in polymers from academic, industrial, and governmental sectors in Thailand. PST has also been representing the Thai polymer community in the international arena. Among the activities organized by PST are conferences, seminars, workshops, and short courses.

In recent years, the number of polymer scientists, technologists, and engineers in Thailand has increased dramatically to more than one thousand personnels. Rarely that a scientific conference devoted exclusively to all fields of polymer science, technology, and engineering was organized in Thailand. Therefore PST has aimed to host The 1st Polymer Conference of Thailand (PCT-1) to provide a forum for meeting and sharing of research results and ideas among the Thai polymer community and also with international polymer experts. We hope that the PCT will prove to be a major platform for facilitating academic and technical development of polymers in Thailand.

The aims of PCT-1 are,

1. To bring together academic personnel, students, researchers in university, government institutes and industrial sectors, to share their experiences and knowledge relating to polymer science, technology and engineering.

2. To promote networking and the establishment of new collaboration among polymer scientists and interested persons or groups in both academic and industrial sectors in order to push forward the development of polymer science and technology in Thailand.

MESSAGE FROM PRESIDENT

PCT-1

One of the important roles of the Polymer Society of Thailand (PST) is to promote the development of polymer science, technology and engineering in Thailand. Such development is believed to be important since the polymer and petrochemical industries in Thailand are growing rapidly and are contributing very importantly to the economy of the country.

In 2007, the Polymer Society of Thailand, in collaboration with the Graduate Program in Polymer Science and Technology, Mahidol University, organized the 1st Polymer Graduate Conference of Thailand (PGCT-1), to provide a meeting place for polymer graduate students in Thailand to present and exchange their research results. The 2nd PGCT was organized by the Petrochemistry and Polymer Science Program, Chulalongkorn University in 2009. Both PGCTs were proved to be successful events. However, it was felt that the Thai polymer community needed a bigger forum for exchanging information, ideas and experiences among polymer scientists, technologists and engineers from both the public and private sectors as the number of the people involved with polymers in the country steadily grows. Furthermore, there is an increasing need for closer collaborations between researchers from universities and government institutes and industrial companies in order to achieve research results which have greater impacts for the country.

For this reason, the 1st Polymer Conference of Thailand (PCT-1) is organized with cooperation and supports from various graduate schools in polymer science and technology of major universities and also some large petrochemical companies. It is hoped that the PCT will develop into an annual meeting for PCT members and other interested parties of the Thai polymer community, similar to those that have taken place in other advanced countries such as in the USA, Europe and Asia.

Finally, I would like to express my sincere thanks to members of the organizing committee who have put in hard work and strenuous efforts in organizing the PCT-1. I also would like to express my deep appreciation to the sponsors of the PCT-1, including PTT Chemicals Public Co., Ltd., SCG Chemicals Co., Ltd., National Science and Technology Development Agency (NSTDA), National Metal and Materials Technology Center (MTEC), National Nanotechnology Center (NANOTEC), Thai Plastic and Chemicals Public Co., Ltd., and PTT Phenol Co., Ltd. for their understandings and supports which will make the PCT-1 a successful event.

Dr. Krisda Suchiva
Chairman of the PCT-1 Organizing Committee
President of the Polymer Society of Thailand

COMMITTEE

PCT-1

Advisory Committee

1. Dr. Jintana Siripitayananon	Department of Chemistry, Chiang Mai University
2. Dr. Jantrawan Pumchoosak	Department of Industrial Chemistry, Chiang Mai University
3. Dr. Nuanphan Chantarasiri	Department of Chemistry, Chulalongkorn University
4. Dr. Sirithan Bulpakdi	Department of Materials Science, Chulalongkorn University
5. Dr. Pranut Potiyaraj	Metallurgy and Materials Science Research Institute, Chulalongkorn University
6. Dr. Pomthong Malakul Na Ayudhaya	The Petroleum and Petrochemical College, Chulalongkorn University
7. Dr. Patiphan Juijerm	Department of Materials Engineering, Kasetsart University
8. Dr. Amnat Permsubscul	Department of Chemistry, King Mongkut's Institute of Technology Ladkrabang
9. Dr. Sirisart Ouajai	Department of Industrial Chemistry, King Mongkut's University of Technology North Bangkok
10. Dr. Boonnak Sukhummek	Department of Chemistry, King Mongkut's University of Technology Thonburi
11. Prof. Siriwat Wongsiri	School of Science, Mae Fah Luang University
12. Dr. Pranee Phinyocheep	Department of Chemistry, Mahidol University
13. Dr. Sa-ad Riyajan	Department of Materials Science and Technology, Prince of Songkla University (Hat Yai)
14. Dr. Nattapong Nithi-Uthai	Department of Rubber Technology and Polymer Science, Prince of Songkla University (Pattani)
15. Dr. Narongchai O-Charoen	Department of Materials and Metallurgical, Rajamangala University of Technology Thanyaburi
16. Natee Srisawat	Department of Textile Engineering, Rajamangala University of Technology Thanyaburi
17. Dr. Niti Yongvanich	Department of Materials Science and Engineering, Silpakorn University
18. Dr. Nitinat Suppakarn	School of Polymer Engineering, Suranaree University of Technology
19. Seranee Srisuk	Department of Textile Science and Technology, Thammasat University
20. Dr. Wanchart Preechatiwong	Department of Materials Science and Engineering, Walailak University
21. Dr.Wilaiporn Chetanachan	The Siam Cement Public Co., Ltd.
22. Dr. Chaya Jantavasu	PTT Chemical Public Co., Ltd.
23. Jackra Swasdiburi	BST Latex Co., Ltd.
24. Banja Junhasavasdikul	Chemical Innovation Co., Ltd.

Chairman

Dr. Krisda Suchiva	Department of Chemistry, Mahidol University National Metal and Materials Technology Center (MTEC) (President of the Polymer Society of Thailand)

Scientific Committee

1. Prof. Suda Kiatkamjornwong	Department of Imaging and Printing Technology, Chulalongkorn University
2. Dr. Suwabun Chirachanchai	The Petroleum and Petrochemical College, Chulalongkorn University
3 . Dr. Krisda Suchiva	Department of Chemistry, Mahidol University National Metal and Materials Technology Center (MTEC)
4. Dr. Pranee Phinyocheep	Department of Chemistry, Mahidol University
5 . Dr. Taweechai Amornsakchai	Department of Chemistry, Mahidol University
6 . Dr. Robert Molloy	Department of Chemistry, Chiang Mai University
7. Dr. Charoen Nakason	Faculty of Science and Technology Prince of Songkla University (Pattani)
8. Dr. Asira Fuongfuchat	National Metal and Materials Technology Center (MTEC)

Budgeting Committee

1. Dr. Chaiyoot Changsarn	Faculty of Engineering, Rajamangala University of Technology Thanyaburi
2. Dr. Surat Areerat	Department of Chemical Engineering, King Mongkut's Institute of Technology Ladkrabang

Exhibition Committee

1. Dr. Ittipol Jangchud	Department of Chemistry, King Mongkut's Institute of Technology Ladkrabang
2. Dr. Jitladda Sakdapipanich	Department of Chemistry, Mahidol University
3. Dr. Pajaera Patanathabutr	Department of Materials Science and Engineering, Silpakorn University
4. Dr. Pasaree Laokijcharoen	National Metal and Materials Technology Center (MTEC)

Public Relation Committee

1. Dr. Kanoktip Boonkerd	Department of Materials Science, Chulalongkorn University
2. Dr. Toemsak Srikhirin	Department of Physics, Mahidol University
3. Dr.Sommai Pivsa-Art	Faculty of Science and Technology, Rajamangala University of Technology Thanyaburi

Secretariat

1. Dr.Varawut Tangpasuthadol	Department of Chemistry, Chulalongkorn University
2. Dr. Surapich Loykulnant	National Metal and Materials Technology Center (MTEC)
3. Dr. Warayuth Sajomsang	National Nanotechnology Center (NANOTEC)
4. Nittranant Saingam	The Polymer Society of Thailand

Synthesis and Characterization of Prolonged-Dissolution NPK Fertilizer Hydrogel

Nhatthaya Pheatcharat[1], Supaporn Noppakundilograt[2] and Suda Kiatkamjornwong [3]*

[1] Program of Petrochemical and Polymer Science, Faculty of Science, Chulalongkorn University, Bangkok 10330, E-mail: myomy_secret@hotmail.com

[2,3] Department of Imaging and Printing Technology, Faculty of Science, Chulalongkorn University, Bangkok 10330

[2]E-mail: supaporn.n@chula.ac.th

*Corresponding author, E-mail address: ksuda@chula.ac.th, ksuda@sc.chula.ac.th.

Abstract

A novel three-layered NPK fertilizer hydrogel was prepared by dipping the fertilizer granules in poly(vinyl alcohol) (PVA) solution and followed by chitosan solution and crosslinked via vapor deposition by glutaraldehyde solution in a 2.9-L closed chamber. The crosslinked layer was grafted with acrylamide (AM) and acrylic acid (AA) mixtures by inverse suspension polymerization. Water dissolution times of the fertilizer hydrogel were investigated. The fertilizer hydrogel so prepared has the core NPK fertilizer granule with the subsequent layers of PVA, crosslinked chitosan, and the grafted poly[(AM-*co*-AA)]. The crosslinked chitosan layer protects NPK fertilizer from dissolution. The doubly-coated fertilizer granules comprising PVA and crosslinked chitosan layers gave the longest water dissolution time. The existences of functional groups of the crosslinked chitosan and the grafted fertilizer hydrogel were confirmed by FTIR technique. Water absorbency of the fertilizer hydrogel increases with increasing AA contents.

Keywords: NPK fertilizer, Poly(vinyl alcohol), Chitosan, Glutaraldehyde, Fertilizer hydrogel

1. Introduction

The fertilizer and water are the vital factors for producing agricultural crops and products. Generally, normal fertilizers comprising 40-70% of nitrogen salt, 80-90% of phosphorus salt, and 50-70% of potassium salt are fast soluble in water and loss its nutrients to the surrounding environment because plants cannot absorb total soluble salts within very short times. These not only cause problems in economics, agriculture, and horticulture but also serious problems of environment pollution. One method of reducing fertilizer nutrient losses involves the usage of slow or controlled-release fertilizers. Coated fertilizers are physically prepared by coating granules of conventional fertilizers with various materials that reduce their dissolution rate [1]. It is generally known that the coating solution must possess a lower surface tension than that of the substrate to be coated; in other words, the substrate to be coated must have the higher surface energy [2].

Chitosan (CH) is an aminopolysaccharide produced from chitin. It has been widely used in pharmaceutical, biomedical, agricultural, horticultural fields and water treatment applications because of its biodegradability, non-toxicity, biocompatibility and antibacterial activity. CH has both reactive amino and hydroxyl groups that can react with many reagents to modify or improve its properties under mild reaction conditions [1, 3, 4].

Poly(vinyl alcohol), PVA, is a water-soluble synthetic polymer due to its hydroxyl groups. Moreover, PVA also has good physical and chemical properties in film-forming ability. It has been used in many applications, such as controlled drug delivery system, membrane preparation, recycling of polymers and packaging [5], because it is non-toxicity and environmentally friendly. The chemical structures of CH and PVA are shown in Figure 1 [6]. Many coating polymers have been reported for coating on fertilizers but

PVA has not yet been disclosed as a film former for this material.

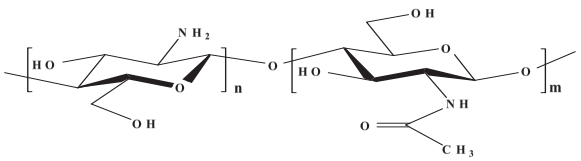

Chitosan (CH)
(n ≥ 50)

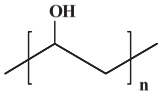

Poly(vinyl alcohol)
(PVA)

Figure 1. Chemical structures of CH and PVA

Glutaraldehyde (GA) consists of two aldehyde groups (-CHO) which can react with the amino groups (-NH_2) and hydroxyl groups (OH) in chitosan and PVA [6]. Fang et al. [7] found that GA could crosslink CH via a Schiff base reaction to give the link of the -C=N- bond.

Hydrogel are three-dimensional hydrophilic polymer networks, which has high water absorbency [8]. Wu and Liu [3] prepared control release fertilizer hydrogel through 2 steps of reactions: (1) coating fertilizer with CH, (2) synthesis of hydrogel as an outer layer of the CH-coated fertilizer by suspension polymerization after which water absorbency of the hydrogel at 1.5 h immersion in water was measured.

In this research, a novel NPK fertilizer hydrogel was prepared. The coating conditions of PVA and CH, and the crosslinking condition of CH and GA were examined. The effect of monomer ratio on water absorbency of NPK fertilizer hydrogel was investigated. The functional groups of NPK fertilizer hydrogel were characterized by FTIR technique.

2. Experimental

2.1. Materials

The industrial grade poly(vinyl alcohol) (PVA) with 100,000 g/mol of molecular weight (MW) with a degree of hydrolysis of 86-89% and a degree of polymerization 2400 was kindly supplied from Thai Mitsui Specialty Chemicals Co., LTD. (Bangkok Thailand). Chitosan (CH) with 100,000 and 200,000 g/mol of MW with a degree of deacetylation of 95% was purchased from Seafresh Chitosan (Lab) Co., Ltd. (Bangkok, Thailand). Acrylamide (AM) was supplied from Siam Chemical Industry Co., Ltd. (Bangkok, Thailand). The industrial grade acrylic acid (AA) was provided by Thai Mitsui Specialty Chemicals Co., Ltd. (Bangkok Thailand). *N, N'*-methylenebisacrylamide (*N*-MBA) and *N, N, N', N'*-tetramethylethylene diamine (TEMED) (both were analytical grade) were purchased from Fluka (Buchs, Switzerland). The analytical grade ammonium persulfate (APS) was purchased from Ajax (Seven Hills, Australia)]. Deionized water (Elga Deionizer, Model LA611, UK) was used for coating, synthesis and water absorbency experiments.

2.2 Surface tension of CH and surface energy of PVA film

Surface tension of CH was measured by the Du Nuoy Ring tensiometry and surface energy of the PVA film was measured through water and methylene iodide contact angles and the surface energy was calculated by Equation (1).

$$\gamma_{lv}(\cos\theta+1) = 2\left[(\gamma^d_l \gamma^d_s)^{1/2} + (\gamma^p_l \gamma^p_s)^{1/2}\right] \qquad (1)$$

where θ = contact angle; γ_{lv} = surface tension of liquid; γ^d_l = surface tension of non polar contribution of the liquid; γ^d_s = surface energy of non polar contribution of the solid; γ^p_l = surface tension of polar contribution of the liquid; γ^p_s = surface energy of polar contribution of the solid.

The total surface energy is the sum of the two contributions of surface energy as shown in Equation (2):

$$\gamma = \gamma^p + \gamma^d \qquad (2)$$

where γ is total surface free energy while γ^d is the dispersion component of total surface free energy and γ^p is the polar force component of total surface free energy.

2.3 Coating of PVA and CH on fertilizer granules

The NPK fertilizer granules were immersed into a beaker having 7% PVA solution and the granules were dried at room temperature to obtain PVA-coated fertilizer granules. The PVA-coated fertilizer granules were then immersed in 2% (w/v) CH solution (dissolved in 2% (v/v) acetic acid solution) and dried at room temperature for 4 h. Finally, the PVA-coated granules and CH-coated NPK compound fertilizer granules were obtained. Water dissolution times of the original NPK fertilizer granules, PVA-coated fertilizer granules, and PVA-coated/CH-coated fertilizer granules were investigated.

2.4 Crosslinking of CH-coated layer of fertilizer

The PVA-coated fertilizer granules and CH-coated NPK compound fertilizer granules were placed on an aluminum sieve over a Petri dish containing 2 ml of 50% GA aqueous solution in a closed system of a 2.9 L-chamber for 4 days. The double layers of PVA and crosslinked CH-coated fertilizer granules were thus obtained.

2.5 Preparation of hydrogel-coated layer of fertilizer.

The fertilizer hydrogel was prepared by inverse suspension polymerization. For the synthesis of copolymers, the specified amounts of sorbitan oleate, sorbitan (Z)-mono-9-octadecenoate (Span 80) and cyclohexane were added into a 4-necked flask equipped with a mechanical stirrer, a condenser, and a dropping funnel which were stirred at 180 rpm under nitrogen atmosphere. The double layers of PVA and CH-coated fertilizer granules were added into the flask and a fixed amount of APS initiator was dropped into the flask and stirred with 180 rpm for 15 min. The mixed solution of AM, AA and N-MBA solution was then added into the flask and the temperature was raised to 70 $^{\circ}$C in a temperature-controlled water bath and stirred for 45 min. The mixture was filtered to remove the un-reacted reagents and dried at 50 $^{\circ}$C in an oven to obtain the final product (double layers of PVA and CH-coated fertilizer hydrogel).

2.6 Identification of the functional groups of fertilizer by FTIR technique

The functional groups of PVA and crosslinked CH-coated fertilizer granules and the hydrogel outer layer of fertilizer hydrogel were identified by Fourier Transform Infrared spectroscopy (FTIR, System 2000, Perkin Elmer, U.S.A.) with a KBr pellet technique. The hydrogel layer of the fertilizer hydrogel was peeled off, cut, ground and mixed with KBr and FTIR spectra was investigated.

2.7 Water absorbency of the fertilizer hydrogel

A dry fertilizer hydrogel weighing 1 g was immersed into 200 cm^3 of deionized water and allowed to swell at room temperature for 1.5, 15, 24 and 48 h. The swollen fertilizer hydrogel were separated from the unabsorbed water by filtering through a 100-mesh sieve aluminum screen for 2 h. The swollen fertilizer hydrogel were weighed and the water absorbency (g g^{-1}) was calculated by Equation (3):

$$W_A = (W_s - W_d)/W_d \quad (3)$$

where W_A is the water absorbency in a weight ratio of the dried fertilizer hydrogel. W_d is the weight of dry fertilizer hydrogel (g) and W_s is the weight of the swollen fertilizer hydrogel (g).

3. **Results and discussion**

3.1 Surface tension of CH solution and surface energy of PVA film

Table 1 Surface tension of CH and surface energy of PVA film

Material	Surface tension (mN/m)	Surface energy (mN/m)
Chitosan		
100,000 g/mol	56.4±1	-
200,000 g/mol	61.0±1	-
De-ionized water	71±1	-
PVA film	-	66.7±1

Table 1 shows that the different molecular weights of CH solution give different surface tensions. The surface tensions of 100,000 and 200,000 g/mol CH solution are 56.4±1 and 61.0±1 mN/m, respectively. The surface

tension of deionized water is 71 mN/m. The PVA film has the surface energy of 66.7±1 mN/m. Therefore, Chitosan solution at both particular molecular weights and concentrations can be used as a coating solution on the PVA film because it can wet the PVA film. However, chitosan with the molecular weight of 100,000 g/mol is not suitable for coating fertilizer granules because it lets more water penetrate into the fertilizer. Thus, chitosan with the molecular weight of 200,000 g/mol was used in this research.

3.2 Coating of PVA and CH on the fertilizer granules

The water soluble fertilizer granules were coated two times with PVA and CH. The photographs of various fertilizer granules are shown in Figure 2. Effect of the coated fertilizer layer on water dissolution is shown in Table 2.

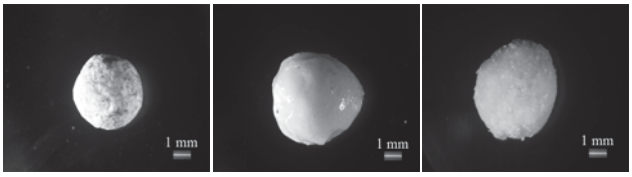

Figure 2. The photographs of fertilizer granules: (a) the uncoated fertilizer granule, (b) PVA-coated fertilizer granule and (c) PVA- and CH-coated fertilizer granule

In Figure 2, it was found that the PVA-coated fertilizer granule was bigger than the original fertilizer granule. The PVA coated layer was whiter with smoother surface. The sizes of PVA- and CH-coated fertilizer granules were similar compared with that of the PVA-coated fertilizer granule, but the surface of CH-coated layer as the outer layer was whiter but rougher.

Table 2 Water soluble time of fertilizers

Type of fertilizer	Water soluble time (min)
Un-coated	12±2
PVA-coated	54±3
PVA and CH-coated	74±3
PVA, X-linked CH/GA coated	138±2

The water dissolution of fertilizer granule varied depending on the type of coated layer (Table 2). The original fertilizer granule dissolved fastest in water,

whereas the doubly coated (PVA-coated layer and crosslinked CH-coated layer) fertilizer granule dissolved least and slowest in water. Thus, the crosslinked CH-coated layer prevented penetration of water into the fertilizer granules. This confirms that coating of the fertilizer granules with different coating layers was achieved.

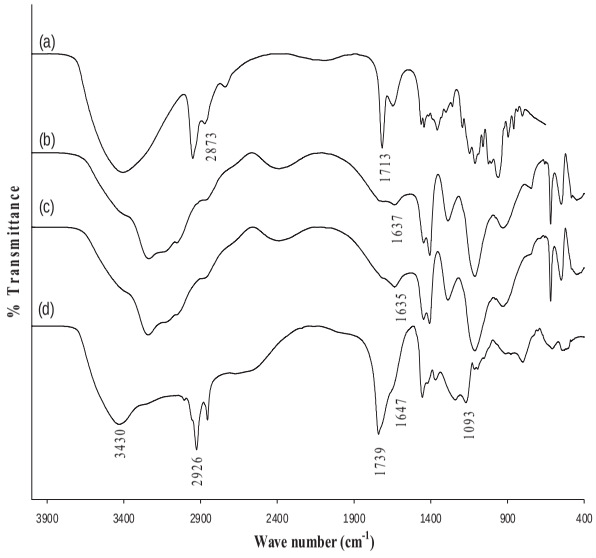

Figure 3. FTIR spectra of (a) glutaraldehyde solution (b) PVA and CH-coated fertilizer (c) PVA-coated fertilizer and crosslinked CH-coated fertilizer and (d) the outer layer of poly[(AM-*co*-AA)] hydrogel

The infrared spectra of glutaraldehyde solution and 2 types of the coated fertilizer are shown in Figure 3. It shows the characteristic peaks of glutaraldehyde at 2873 and 1713 cm^{-1}, assigning to –C-H stretching of aldehyde group and –C=O stretching of aldehyde, respectively (Figure 3(a)). It is found that the peak of –N-H bending (amide) of CH at 1637 cm^{-1}in Figure 3(b) disappeared in Figure 3(c). The stronger intensity of the peak at 1635 cm^{-1} in Figure 3(c) corresponding to -C=N- bending of cosslinked bond between amino group of CH and C=O of glutaraldehyde [6]. This confirms that the outer layer of CH-coated fertilizer could be crosslinked by glutaraldehyde vapor.

3.3 Identification of the functional groups of hydrogel outer layer by FTIR technique

The spectrum of the hydrogel outer layer (poly[(AM-*co*-AA)]) is shown in Figure 3(d). It exhibits the peaks at 3430, 2926, 1647 cm^{-1}, corresponding to the -N-H stretching, -C-H stretching and -C=O stretching of acrylamide moiety. It also gives the peaks at 1739 and 1093 cm^{-1}, assigning to the stretching of -C=O and -CO-O- stretching of acrylic acid moiety. This result confirms that the outer coating material was poly[(AM-*co*-AA)] [2].

3.4 Effect of the AM-to-AA monomer ratios on water absorbency of fertilizer hydrogel

The effect of AA content on water absorbency at 1.5 h [3] of PVA-coated fertilizer and crosslinked CH-coated fertilizer hydrogel is shown in Figure 4. The water absorbency slightly increases with increasing AA content due to incorporating of more hydrophilic moiety. The higher the hydrophilicity, the greater the expansion of hydrogel becomes, leading to higher water absorbency [8]. A small increase in water absorbency was observed after a short time of water immersion, because the hydrogel at the outer-coated layer of fertilizer was swollen and became larger compared with the whole coated fertilizer granule.

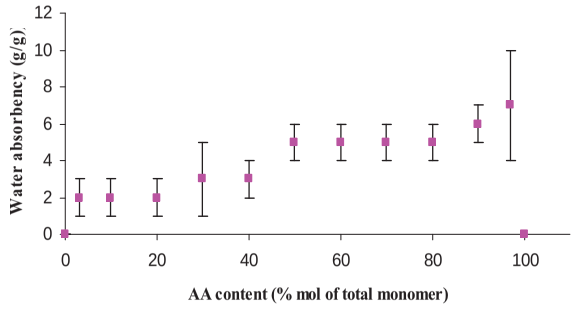

Figure 4. The effect of AM-to-AA monomer ratio on water absorbency of PVA-coated and crosslinked CH-coated fertilizer hydrogel at room temperature after 1.5 h of water immersion

3.5 The swelling of PVA-coated fertilizer and crosslinked CH-coated fertilizer hydrogel

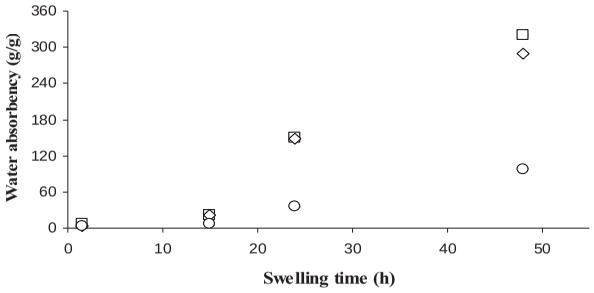

Figure 5. Effect of swelling time on water absorbency at room temperature of PVA-coated fertilizer and crosslinked CH-coated fertilizer hydrogel by varying the AM-to-AA monomer mole ratios at: 3:97 ( ), 6:94 (◇), and 8:92 (○) at room temperature for 1.5, 15, 24 and 48 h of swelling

The swelling of PVA-coated fertilizer and crosslinked CH-coated fertilizer hydrogel at various swelling times is shown in Figure 5. When increasing the swelling time to 48 h, water absorbency increases. This is because hydrogel absorbs water slowly, and cannot reach the equilibrium water absorbency within 48 h. The water absorbency of fertilizer hydrogel synthesized with AA content of 97 (% mol of total monomer) was 320±2 g g^{-1} at 48 h of immersion in water.

4. Conclusion

A novel NPK fertilizer hydrogel was successfully prepared. The fertilizer hydrogel has a three-layered structure. The core is the water-soluble NPK fertilizer granule. The first layer is the PVA-coated layer. The second layer is the crosslinked CH-coated layer and the third layer (outer layer) is poly[(AM-*co*-AA)] hydrogel. The dissolution time of the fertilizer could be prolonged by a sequential coating with PVA and crosslinking CH layer by vapor deposition of GA. The thicker the coated layer, the slower the water dissolution of the fertilizer becomes. The hydrogel on the crosslinked CH-coated fertilizer was achieved by inverse suspension polymerization of AM and AA. The water absorbency of the fertilizer hydrogel so modified increases with

increasing acrylic acid content as a function of swelling time.

Acknowledgements

The authors gratefully acknowledge the financial support from the Thailand Research Fund under the Research Team Aided Program Contract no. RTA5080004. Research facilities provided by the Imaging Polymer Laboratory of Chulalongkorn University's Department of Imaging and Printing Technology, Faculty of Science are gratefully acknowledged.

References

[1] Wu, L., Liu, M. Z., Preparation and characterization of cellulose acetate-coated compound fertilizer with controlled-release and water-retention, *Polymer for Advanced Technologies*, **2008**, 19, 785-792.

[2] Kiatkamjornwong, S., Noppakundilograt, S., Imaging Chemistry Laboratory, Chulalongkorn University Publishing, Bangkok, **2008**, pp.1, 26-50.

[3] Wu, L., Liu, M. Z., Preparation and properties of chitosan-coated NPK compound fertilizer with controlled-release and water-retention, *Carbohydrate Polymers*, **2008**, 72, 240-247.

[4] Wu, L., Liu, M. Z., Liang, R., Preparation and properties of a double-coated slow-release NPK compound fertilizer with superabsorbent and water-retention, *Bioresource Technology,* **2008**, 547-554.

[5] Bahrami, S. B., Kordestani, S. S., Mirzadeh, H., Mansoori, P., Poly(vinyl alcohol)-Chitosan Blends: Preparation, Mechanical and Physical properties, *Iranian Polymer Journal*, **2003**, 12 (2), 139-146

[6] Svang-Ariyaskul, A., Huang, R. Y. M., Douglas, P. L., Pal, R., Feng, X., Chen, P., Liu, L., Blended chitosan and polyvinyl alcohol membranes for the pervaporation dehydration of isopropanol, *Journal of* [7] Fang, F., Yu, L., Binyuan, Z., Keao, H., In vitro Biomineralization of glutaraldehyde crosslinked Chitosan/Glutamic acid film, *Journal of Wuhan University of Technology-Mater. Science Education*, **2009**, 24(1), 9-14.

[8] Mahdavinia, G. R., Mousavi, S. B., Karimi, F., Marandi, G. B., Garabaghi, H., Shahabvand, S., Synthesis of porous poly(acrylamide) hydrogel using calcium carbonate and its application for slow release of potassium nitrate, *Express Polymer Letter*, **2009**, 3, 279-285.

[9] Hennink, W. E., Nostrum, C. F. V., Novel crosslinking methods to design hydrogels, *Advanced Drug Delivery Reviews,* **2002**, 54, 13-36.

1st Polymer Conference of Thailand

October 7-8, 2010
Convention Center, Chulabhorn Research Institute, Bangkok

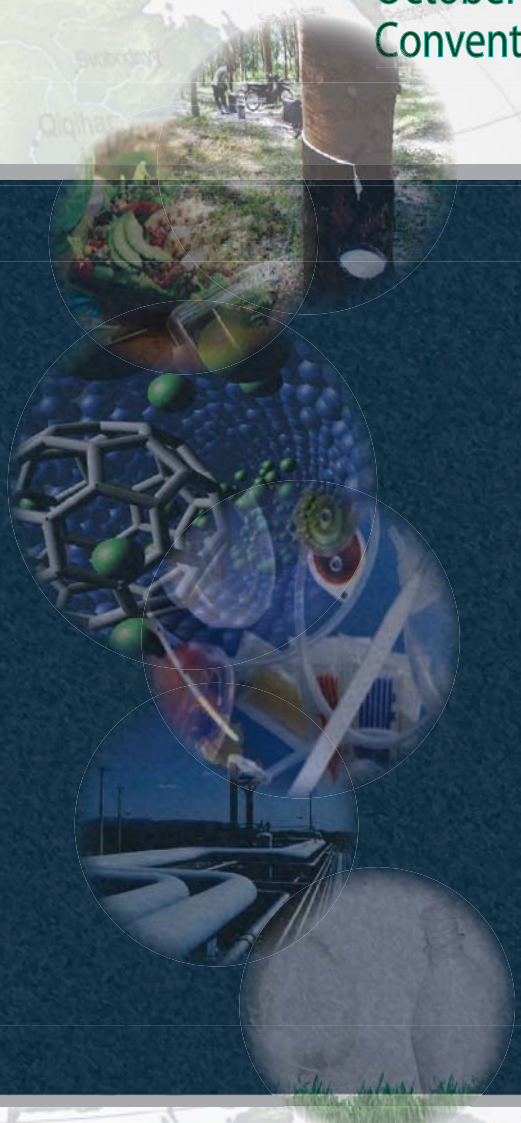

PROCEEDINGS

Organized by :

Sponsored by :

1st POLYMER CONFERENCE OF THAILAND

PCT-1

Organized by

The Polymer Society of Thailand (PST)

Sponsored by

Platinum

PTT Chemical Public Company Limited

Gold

- SCG Chemicals Company Limited
- National Science and Technology Development Agency (NSTDA)
  National Metal and Materials Technology Center (MTEC)
- National Nanotechnology Center (NANOTEC)

Silver

- Thai Plastic and Chemicals Public Company Limited
- PTT Phenol Company Limited

BACKGROUND OF PCT-1

The Polymer Society of Thailand (PST) was founded in 1999 to be a center for connecting people who are working on or interested in polymers from academic, industrial, and governmental sectors in Thailand. PST has also been representing the Thai polymer community in the international arena. Among the activities organized by PST are conferences, seminars, workshops, and short courses.

In recent years, the number of polymer scientists, technologists, and engineers in Thailand has increased dramatically to more than one thousand personnels. Rarely that a scientific conference devoted exclusively to all fields of polymer science, technology, and engineering was organized in Thailand. Therefore PST has aimed to host The 1st Polymer Conference of Thailand (PCT-1) to provide a forum for meeting and sharing of research results and ideas among the Thai polymer community and also with international polymer experts. We hope that the PCT will prove to be a major platform for facilitating academic and technical development of polymers in Thailand.

The aims of PCT-1 are,

1. To bring together academic personnel, students, researchers in university, government institutes and industrial sectors, to share their experiences and knowledge relating to polymer science, technology and engineering.

2. To promote networking and the establishment of new collaboration among polymer scientists and interested persons or groups in both academic and industrial sectors in order to push forward the development of polymer science and technology in Thailand.

MESSAGE FROM PRESIDENT

PCT-1

One of the important roles of the Polymer Society of Thailand (PST) is to promote the development of polymer science, technology and engineering in Thailand. Such development is believed to be important since the polymer and petrochemical industries in Thailand are growing rapidly and are contributing very importantly to the economy of the country.

In 2007, the Polymer Society of Thailand, in collaboration with the Graduate Program in Polymer Science and Technology, Mahidol University, organized the 1st Polymer Graduate Conference of Thailand (PGCT-1), to provide a meeting place for polymer graduate students in Thailand to present and exchange their research results. The 2nd PGCT was organized by the Petrochemistry and Polymer Science Program, Chulalongkorn University in 2009. Both PGCTs were proved to be successful events. However, it was felt that the Thai polymer community needed a bigger forum for exchanging information, ideas and experiences among polymer scientists, technologists and engineers from both the public and private sectors as the number of the people involved with polymers in the country steadily grows. Furthermore, there is an increasing need for closer collaborations between researchers from universities and government institutes and industrial companies in order to achieve research results which have greater impacts for the country.

For this reason, the 1st Polymer Conference of Thailand (PCT-1) is organized with cooperation and supports from various graduate schools in polymer science and technology of major universities and also some large petrochemical companies. It is hoped that the PCT will develop into an annual meeting for PCT members and other interested parties of the Thai polymer community, similar to those that have taken place in other advanced countries such as in the USA, Europe and Asia.

Finally, I would like to express my sincere thanks to members of the organizing committee who have put in hard work and strenuous efforts in organizing the PCT-1. I also would like to express my deep appreciation to the sponsors of the PCT-1, including PTT Chemicals Public Co., Ltd., SCG Chemicals Co., Ltd., National Science and Technology Development Agency (NSTDA), National Metal and Materials Technology Center (MTEC), National Nanotechnology Center (NANOTEC), Thai Plastic and Chemicals Public Co., Ltd., and PTT Phenol Co., Ltd. for their understandings and supports which will make the PCT-1 a successful event.

Dr. Krisda Suchiva
Chairman of the PCT-1 Organizing Committee
President of the Polymer Society of Thailand

COMMITTEE

PCT-1

Advisory Committee

1. Dr. Jintana Siripitayananon	Department of Chemistry, Chiang Mai University
2. Dr. Jantrawan Pumchoosak	Department of Industrial Chemistry, Chiang Mai University
3. Dr. Nuanphan Chantarasiri	Department of Chemistry, Chulalongkorn University
4. Dr. Sirithan Bulpakdi	Department of Materials Science, Chulalongkorn University
5. Dr. Pranut Potiyaraj	Metallurgy and Materials Science Research Institute, Chulalongkorn University
6. Dr. Pomthong Malakul Na Ayudhaya	The Petroleum and Petrochemical College, Chulalongkorn University
7. Dr. Patiphan Juijerm	Department of Materials Engineering, Kasetsart University
8. Dr. Amnat Permsubscul	Department of Chemistry, King Mongkut's Institute of Technology Ladkrabang
9. Dr. Sirisart Ouajai	Department of Industrial Chemistry, King Mongkut's University of Technology North Bangkok
10. Dr. Boonnak Sukhummek	Department of Chemistry, King Mongkut's University of Technology Thonburi
11. Prof. Siriwat Wongsiri	School of Science, Mae Fah Luang University
12. Dr. Pranee Phinyocheep	Department of Chemistry, Mahidol University
13. Dr. Sa-ad Riyajan	Department of Materials Science and Technology, Prince of Songkla University (Hat Yai)
14. Dr. Nattapong Nithi-Uthai	Department of Rubber Technology and Polymer Science, Prince of Songkla University (Pattani)
15. Dr. Narongchai O-Charoen	Department of Materials and Metallurgical, Rajamangala University of Technology Thanyaburi
16. Natee Srisawat	Department of Textile Engineering, Rajamangala University of Technology Thanyaburi
17. Dr. Niti Yongvanich	Department of Materials Science and Engineering, Silpakorn University
18. Dr. Nitinat Suppakarn	School of Polymer Engineering, Suranaree University of Technology
19. Seranee Srisuk	Department of Textile Science and Technology, Thammasat University
20. Dr. Wanchart Preechatiwong	Department of Materials Science and Engineering, Walailak University
21. Dr.Wilaiporn Chetanachan	The Siam Cement Public Co., Ltd.
22. Dr. Chaya Jantavasu	PTT Chemical Public Co., Ltd.
23. Jackra Swasdiburi	BST Latex Co., Ltd.
24. Banja Junhasavasdikul	Chemical Innovation Co., Ltd.

Chairman

Dr. Krisda Suchiva	Department of Chemistry, Mahidol University National Metal and Materials Technology Center (MTEC) (President of the Polymer Society of Thailand)

Scientific Committee

1. Prof. Suda Kiatkamjornwong	Department of Imaging and Printing Technology, Chulalongkorn University
2. Dr. Suwabun Chirachanchai	The Petroleum and Petrochemical College, Chulalongkorn University
3 . Dr. Krisda Suchiva	Department of Chemistry, Mahidol University National Metal and Materials Technology Center (MTEC)
4. Dr. Pranee Phinyocheep	Department of Chemistry, Mahidol University
5 . Dr. Taweechai Amornsakchai	Department of Chemistry, Mahidol University
6 . Dr. Robert Molloy	Department of Chemistry, Chiang Mai University
7. Dr. Charoen Nakason	Faculty of Science and Technology Prince of Songkla University (Pattani)
8. Dr. Asira Fuongfuchat	National Metal and Materials Technology Center (MTEC)

Budgeting Committee

1. Dr. Chaiyoot Changsarn	Faculty of Engineering, Rajamangala University of Technology Thanyaburi
2. Dr. Surat Areerat	Department of Chemical Engineering, King Mongkut's Institute of Technology Ladkrabang

Exhibition Committee

1. Dr. Ittipol Jangchud	Department of Chemistry, King Mongkut's Institute of Technology Ladkrabang
2. Dr. Jitladda Sakdapipanich	Department of Chemistry, Mahidol University
3. Dr. Pajaera Patanathabutr	Department of Materials Science and Engineering, Silpakorn University
4. Dr. Pasaree Laokijcharoen	National Metal and Materials Technology Center (MTEC)

Public Relation Committee

1. Dr. Kanoktip Boonkerd	Department of Materials Science, Chulalongkorn University
2. Dr. Toemsak Srikhirin	Department of Physics, Mahidol University
3. Dr.Sommai Pivsa-Art	Faculty of Science and Technology, Rajamangala University of Technology Thanyaburi

Secretariat

1. Dr.Varawut Tangpasuthadol	Department of Chemistry, Chulalongkorn University
2. Dr. Surapich Loykulnant	National Metal and Materials Technology Center (MTEC)
3. Dr. Warayuth Sajomsang	National Nanotechnology Center (NANOTEC)
4. Nittranant Saingam	The Polymer Society of Thailand

Alkali Pretreatment of Kapok Fibers for Pulping and Papermaking

Thippawan Hommaivai[1], Kuntinee Suvarnakich[2], Somporn Chaiarrekij[2] and Suda Kiatkamjornwong[2*]

[1]Pulp and Paper Technology Program, Faculty of Science, Chulalongkorn University, Bangkok 10330

Phone 0-89889-6525, Fax. 0-2255-3021, E-mail: aa_aom2@hotmail.com

[2]Department of Imaging and Printing Technology, Faculty of Science, Chulalongkorn University, Bangkok 10330

Phone 0-2218-5581, Fax. 0-2255-3021, E-mail: ksuda@Chula.ac.th

Abstract

Kapok fiber can be one of the potential fiber sources for papermaking because paper containing kapok pulp provided excellent tensile strength and burst strength. However, wetting kapok fibers as an essential part of pulping process was problematic. Due to the waxy cutin on the kapok fiber surface making kapok fibers hardly dampened, kapok fibers needed to be immersed in water for at least 3 weeks before being processed through soda pulping. Therefore, to make soda pulping of kapok fibers to be more practical and efficient, immersing time of kapok fibers before soda pulping needed to be cut down. It was hypothesized that the waxy cutin coating kapok fiber surface might be removed by alkali pretreatment. So, the objective of this research was to study the effects of alkali pretreatment in terms of sodium hydroxide dosages and immersing times on soda pulping efficiency of kapok fibers. The pretreatment of kapok fibers was achieved by immerging kapok fibers in 13 L of two dosages of sodium hydroxide (5% and 10% of sodium hydroxide based on oven dried (O.D.) fiber weight) and three immersing times (1, 2 and 3 weeks). After the pretreatment, kapok fibers were pulped using soda process with 20% of sodium hydroxide based on O.D. fiber weight at 120 °C for 2 hours. The results obtained from all these alkali pretreatments of kapok fibers were then compared to those obtained from the control experiment without alkali pretreatment by immersing it in water for 3 weeks before soda pulping. It was found that the sodium hydroxide pretreatment of kapok fibers did not affect pulp yield. Kappa numbers of the 5% sodium hydroxide pre-treated pulps were lower than kappa number of the controlled pulp. Alkali pretreatment could save more pulping chemical than that of the control experiment as indicated by higher residual alkali after soda pulping. In addition, more pulping chemical could be saved if higher dosages of sodium hydroxide and longer immersing time were employed for alkali pretreatment because residual alkali was further increased. Kapok paper made from the alkali pre-treated pulp provided higher tensile strength and burst strength than kapok paper made from the controlled pulp. Among the alkali pretreated pulp, it was discovered that 5% sodium hydroxide pretreatment offered the stronger kapok paper than the 10% sodium hydroxide pretreatment while the immersing time of 1 to 2 weeks provided the stronger kapok paper than did the 3 weeks immersion.

Keywords: Kapok, Pretreatment, Sodium hydroxide, Soda pulping, Immersing time

1. Introduction

Paper consumption in Thailand is increasing. Normally, printing/writing paper is made from the mixture of hardwood (short fiber) pulp and softwood (long fiber) pulp. Hardwood pulp can be produced locally whereas softwood pulp needs to be imported from abroad. Thus, to find a new fiber source, especially to compensate for the shortage of softwood pulp in Thailand, is a significant motivation. Kapok (*Ceiba pentandra*) abundantly found in Thailand can be an attractive fiber source since it provides long fiber and has fiber characteristics relatively similar to those of softwood trees. Kapok research in Thailand indicated that kapok could be used to make paper [1]. In addition, in the work where kapok pulp was mixed with commercial hardwood pulp, it was found that paper strength became

higher with the increasing amount of kapok pulp added in the pulp mixture [2]. Thus, it was possible to replace long fibers in papermaking with the kapok fibers. Generally, kapok fiber consists of 64% cellulose, 13% lignin, 23% pentosan, and some small amount of cutin on the fiber surface [3]. This cutin makes kapok fiber become hydrophobic and hardly dampened. Because of this hydrophobicity, kapok fibers needed to be immersed in water for three weeks before being processed through soda pulping. Therefore, this research aimed to reduce the immersing time of kapok fibers by chemical pretreatment prior to soda pulping. The effects of chemical pretreatment on kapok pulp and paper properties were investigated as well. Avinash et al [4] studied the pretreatment of lyocell fabrics with sodium hydroxide (NaOH) which concentration was 120 g/l or potassium hydroxide (KOH) of 250 g/l and found that alkali pretreatment partially dissolved fibers but did not have significant effects on carboxyl content and crystallinity as compared to the control experiment. Penetration of alkali chemicals into the fiber seemed to occur at only the outer surface of the fiber rather than in the center hole of the fiber (lumen). Zhang et al [5] investigated the pretreatment of lyocell fabrics with sodium hydroxide, potassium hydroxide, lithium hydroxide (LiOH) and trimethyl ammonium hydroxide (TMAH). It was discovered that fibers pretreated by NaOH and KOH became more swollen but less fibrillated. They also had a higher water retention value (WRV) but a lower weight loss as compared to fibers pretreated by LiOH and TMAH.

2. Experimental and method

The experiment was divided into 2 parts. The first part involved the investigation of the effects of sodium hydroxide dosages and latency removal on properties of kapok pulp and paper and to find the optimal dosage of sodium hydroxide for being used in the next part. The second part concerned the study the effects of NaOH pretreatment on pulp and paper properties of kapok after soda pulping.

The first experimental part was started by immersing kapok fibers from Nakhonpathom province in water for 3 weeks. Then, kapok fibers were squeezed out the excess water and cut to 2-3 cm long pieces. Soda pulping of kapok fibers was carried out in autoclave digester (UEC-2017A, Universal Engineering, India) with various dosages of sodium hydroxide expressed as % active alkali of 10, 15, 20, 25 and 30% based on oven dried (O.D.) pulp weight. Pulping was done at 120˚C for 2 hours using liquor to wood ratio of 17:1. After pulping, kapok pulp was thoroughly washed and centrifuged. Pulp yield was calculated. Kappa number, an indicator of residual lignin in pulp, was also determined following TAPPI standard T236 cm-85. Black liquor after soda pulping was sampled from each pulping condition to analyze for residual alkali according to SCAN standard N33:94.

Next, washed kapok pulp was refined by the disc refiner (Andritz Sprout, U.S.A.) using 10/1000 inch disc gap for two passes refining. Refining was done at about 5% pulp consistency. Then, kapok pulp was sampled and disintegrated using a disintegrator (Formax T-100, Adirondack, U.S.A.) for 50,000 revolutions in hot water (80 ^{o}C) in order to remove latency. Average fiber length and fines content of both latency-removed and latency-retained kapok pulps were determined using a fiber quality analyzer (FQA, Optest, Canada). The total number of fibers counted was 5000. Also, 60 g/m^2 handsheets were made from both pulps according to ISO 5269-2 standard. The strength properties of handsheets were then determined as follows: tensile strength according to TAPPI standard T494 om-96 and bursting strength according to TAPPI standard T403 om-97.

For the second experimental part, kapok fibers were pre-treated by immersing in 13L of two different sodium hydroxide solutions (5% and 10% of sodium hydroxide based on oven dried (O.D.) fiber weight) at three different immersing times (1, 2 and 3 weeks). After the alkali pretreatment, kapok fibers were washed and cut to 2-3 cm long pieces. Then, soda pulping of kapok fibers was carried out using the optimal dosage of sodium hydroxide determined from the first part and with the

same pulping condition used in the first part. Then, kapok pulp was refined and latency removal was achieved using the same conditions as indicated in the first part. Next, average fiber length and fines content of kapok pulp were analyzed. The 60 g/m^2 handsheets were also made. Properties of kapok pulp and handsheets were finally examined.

3. Results and discussion

3.1 Effects of sodium hydroxide dosages and latency removal

Table 1 Effects of active alkali on pulp properties of kapok fiber

% Active alkali	Pulp properties		
	Pulp yield (%)	Kappa number	Residual alkali (g/L)
10	81	111	0.0
15	77	111	0.3
20	67	121	2.4
25	70	111	5.3
30	74	115	7.4

The effects of different dosages of sodium hydroxide used in pulping on properties of kapok pulp such as pulp yield, kappa number and residual alkali are shown in Table 1. Pulp yield potentially decreased when NaOH dosage increased due to more lignin and extractives removal. High NaOH concentration could also induce carbohydrate degradation especially the degradation of hemicellulose due to the peeling reaction. Kappa number which is an indication of the lignin content in measures the consumption of potassium permanganate by pulp samples. Generally, when NaOH concentration in pulping was increased, kappa number should be decreased since more lignin was dissolved. However, the results in Table 1 did not show the expected trend. It might be possible that other substances presented in the pulp might consume permanganate. Residual alkali indicates the amount of excess NaOH present in the system after the pulping. No residual alkali of 10% NaOH was observed since it was completely consumed. Then, residual alkali increased with increasing NaOH dosage in pulping.

Table 2 Effects of active alkali on strength properties of kapok handsheets

% active alkali	Tensile index (N m/g)		Burst index (kPa m^2/g)	
	Before latency removal	After latency removal	Before latency removal	After latency removal
10	68.50	75.32	4.72	5.03
15	81.58	80.65	5.17	5.68
20	81.03	84.66	4.90	5.28
25	81.55	82.99	5.30	5.58
30	74.86	81.65	5.56	5.74

Table 2 shows the effects of NaOH dosages and latency removal on the tensile index and burst index. Tensile index defines as tensile strength divided by handsheet grammage. Burst index defines as burst strength divided by handsheet grammage. It was found that tensile index and burst index had a tendency to increase when NaOH dosage was higher. This might be because fiber bonding was improved due to a better separation of individual fiber at higher NaOH dosage. However, too high the NaOH dosage was detrimental to pulp strength because the fibers were damaged by the peeling reaction under the strongly alkaline conditions leading to carbohydrate degradation [6]. Tensile and burst strengths could be further improved by latency removal because fibers were stretched as indicated by increasing fiber length (LWW) as shown in Table 3. This could lead to the better fiber bonding.

As illustrated in Table 3, NaOH dosage did not significantly affect fiber length and fines content of kapok pulp. Nevertheless, it could be noted that fiber length was higher after latency removal. This was likely due to fiber stretching.

Based on the overall results from the first part, 20% NaOH was thus chosen to be further used in the second part because 20% NaOH dosage provided the pulp with the highest tensile strength. Besides, residual alkali was justified for the case of 20% NaOH since alkali depletion in pulping could cause undesirable lignin condensation. Thus, there should be some amount of alkali left in the system after pulping is done. Also, with the benefits of latency removal indicated by better strength properties and higher fiber length of kapok pulp,

all pulps in the second part were then processed through latency removal after soda pulping.

Table 3 Effects of active alkali on weight-weighted average fiber length (LWW) and fines content of kapok pulp

% active alkali	LWW (mm)		Fines (%)	
	Before latency removal	After latency removal	Before latency removal	After latency removal
10	2.13	2.26	23.57	22.03
15	2.15	2.33	21.44	20.40
20	2.04	2.08	25.17	24.22
25	2.25	2.52	20.70	20.60
30	2.34	2.50	21.52	21.01

3.2 Effects of NaOH pretreatment

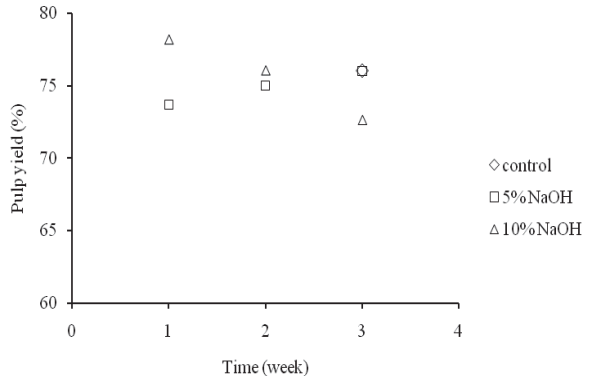

Figure 1. Effects of alkali pretreatment on pulp yield. "Control" represents kapok fibers which were immersed in water for 3 weeks without pretreatment

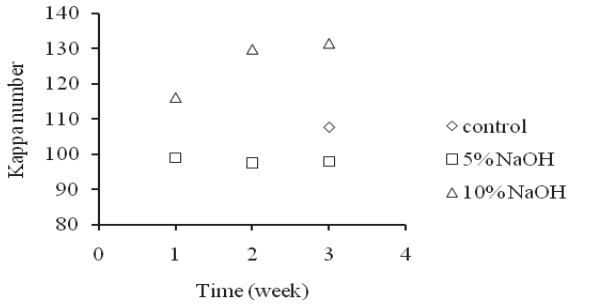

Figure 2. Effects of alkali pretreatment on kappa number. "Control" represents kapok fibers which were immersed in water for 3 weeks without pretreatment

NaOH concentration and alkali immersing time had no evident effects on pulp yield (Figure 1). The results from Figure 1 also demonstrate that pulp yields of alkali pre-treated kapok fibers were about the same as in the control case.

Figure 2 shows that kappa numbers of the pulps from the 5% NaOH pretreatment were lower than that of the control case but surprisingly higher than those of 10% NaOH pretreatment. With the higher NaOH concentration, kappa number should have become lower since more cutin was expected to be removed with the higher dosage of NaOH, allowing more cooking chemicals to penetrate into the fibers during pulping and dissolving more lignin. However, in this case, it might probably be similar to the results obtained from the first part, that other substances might be released more when the higher concentration of NaOH was employed during pretreatment. These might consume more permanganate concentration. It was also discovered that the effects of alkali pretreatment time on kappa number were more obvious in the case of the lower NaOH concentration than in the case of the higher NaOH concentration.

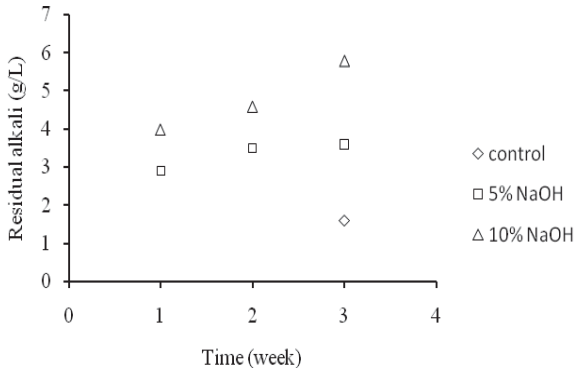

Figure 3. Effects of alkali pretreatment on residual alkali. Control represents kapok fibers which were immersed in water for 3 weeks instead

As expected, residual alkali increased with increasing NaOH concentration and pretreatment times. The increase of residual alkali may possibly result from the excess of NaOH during pretreatment and this might reduce alkali consumption during pulping (Figure 3).

Table 4 Effects of alkali pretreatment on weight-weighted average fiber length (LWW) and fines percentage of kapok pulp

NaOH dosage (%)	LWW (mm) at week			Fine (%) at week		
	1	2	3	1	2	3
0	-	-	2.59	-	-	22.48
5	2.33	2.11	2.35	21.28	22.42	24.19
10	2.34	2.28	2.17	22.22	23.48	25.38

The results shown in Table 4 reveal that alkali pretreatment resulted in the lower fiber length and the higher fines content as compared to the control case. The higher dosage of alkali and the longer pretreatment time potentially decreased fiber length and increased fines content due to carbohydrate degradation by the peeling reaction under a strong alkaline condition.

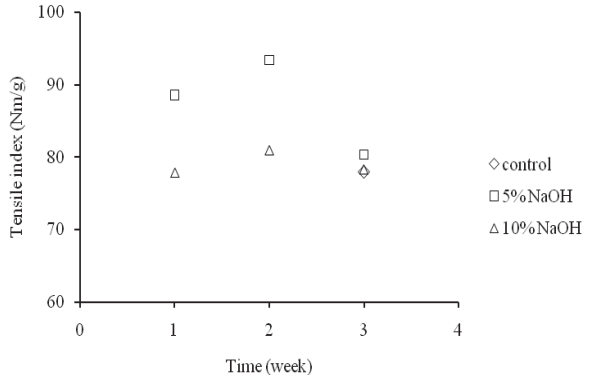

Figure 4. Effects of alkali pretreatment on tensile index. "Control" represents kapok fibers which were immersed in water for 3 weeks without pretreatment

There were no significant differences in tensile indices between control and 10% NaOH pretreatment, while the tensile index of 5% NaOH pretreatment was highest (Figure 4). Increasing NaOH concentration provided the lower tensile strength due to carbohydrate degradation by the peeling reaction at a strong alkaline condition. This might lead to poor fiber bonding and lower tensile strength. The longer pretreatment time seemed to be beneficial to tensile index due to more lignin removal and better fiber bonding. However, too long the alkali pretreatment time was detrimental to tensile index because of carbohydrate degradation. It was also noticed that tensile index reached the maximum at 5% NaOH pretreatment and 2 weeks of pretreatment time.

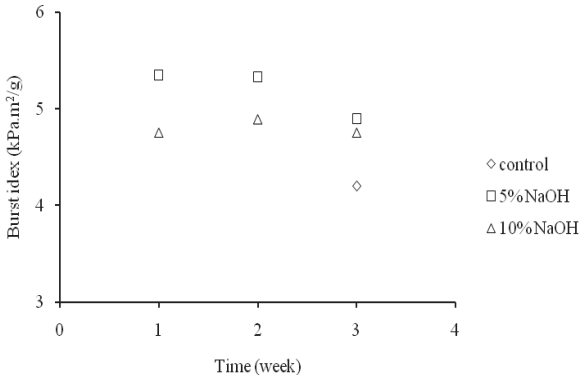

Figure 5. Effects of alkali pretreatment on burst index. "Control" represents kapok fibers which were immersed in water for 3 weeks without pretreatment

As indicated in Figure 5, the effects of alkali pretreatment on burst index showed the same trend as in the case of tensile index due to the reasons previously described in the case of tensile index. From Figure 5, burst index reached a maximum at 5% NaOH pretreatment with one week pretreatment time.

Based on the overall results from the second part, the optimal alkali pretreatment condition was 5% NaOH dosage and 1 to 2 weeks immersing time since it offered pulp with the highest tensile and burst strengths.

4. Conclusions

Alkali pretreatment of kapok fibers did not affect the pulp yield. Instead, more pulping chemical could be saved by alkali pretreatment as indicated by higher residual alkali after soda pulping. In addition, kapok handsheets made from the alkali pre-treated pulp provided the better tensile and burst strengths than those prepared from the controlled pulp. The 5% sodium hydroxide pretreatment offered the stronger kapok paper than the 10% sodium hydroxide pretreatment while the immersing time of 1 to 2 weeks provided the stronger kapok paper than did the 3 weeks immersion.

Acknowledgments

This research was financially supported by a Research Team Assistance Grant from the Thailand Research Fund and Higher Education Commission (RTA5080004). Some research facilities provided by the Product and Technology Development Center of Siam Cement Group Paper Company Limited were also gratefully acknowledged. The authors appreciate highly the facility and research equipment provided by the Department of Imaging and Printing Technology of the Faculty of Science, Chulalongkorn University.

References

[1] Chaiarrekij, S., Wongsaisuwan, U., and Watchanakit, S. Pulping of Kapok. Thai Petty Patent no.4279, **2008**.

[2] Apirakchaiskul, A., "The Use of Kapok Fiber to Improve Strength of Paper", M.S. Thesis, Dept. of Imaging and Printing Technology, Faculty of Science, Chulalongkorn University, **2008**.

[3] Lim,T.T., and Huang, X., "Evaluation of Kapok *(Ceiba pentandra (L.) Gaertn.)* as a Natural Hollow Hydrophobic–Oleophilic Fibrous Sorbent for Oil Spill Cleanup", *Chemosphere*, 66 (5), **2007**, 955–963.

[4] Manian, A.P., Abu-Rous, M., Lenninger, M., Roeder, T., Schuster, C.K., and Bechtold, T., "The Influence of Alkali Pretreatment in Lyocell Resin Finishing - Fiber Structure", *Carbohydrate Polymer*, 71 (4), **2008**, 664-671.

[5] Zhang, W., Okubayashi, S., and Bechtoid, T., "Fibrillation Tendency of Cellulosic Fibers - Part 3. Effects of Alkali Pretreatment of Lyocell Fiber", *Carbohydrate Polymers*, 59 (2), **2005**, 173-179.

[6] Sjöström, E., "Wood Chemistry - Fundamentals and Applications", 2nd edition, Academic Press, San Diego, **1993**, pp. 63, 149.

1st Polymer Conference of Thailand

October 7-8, 2010
Convention Center, Chulabhorn Research Institute, Bangkok

PROCEEDINGS

Organized by :

Sponsored by :

1st POLYMER CONFERENCE OF THAILAND

PCT-1

Organized by

The Polymer Society of Thailand (PST)

Sponsored by

Platinum

PTT Chemical Public Company Limited

Gold

- SCG Chemicals Company Limited
- National Science and Technology Development Agency (NSTDA)
  National Metal and Materials Technology Center (MTEC)
- National Nanotechnology Center (NANOTEC)

Silver

- Thai Plastic and Chemicals Public Company Limited
- PTT Phenol Company Limited

BACKGROUND OF PCT-1

The Polymer Society of Thailand (PST) was founded in 1999 to be a center for connecting people who are working on or interested in polymers from academic, industrial, and governmental sectors in Thailand. PST has also been representing the Thai polymer community in the international arena. Among the activities organized by PST are conferences, seminars, workshops, and short courses.

In recent years, the number of polymer scientists, technologists, and engineers in Thailand has increased dramatically to more than one thousand personnels. Rarely that a scientific conference devoted exclusively to all fields of polymer science, technology, and engineering was organized in Thailand. Therefore PST has aimed to host The 1st Polymer Conference of Thailand (PCT-1) to provide a forum for meeting and sharing of research results and ideas among the Thai polymer community and also with international polymer experts. We hope that the PCT will prove to be a major platform for facilitating academic and technical development of polymers in Thailand.

The aims of PCT-1 are,

1. To bring together academic personnel, students, researchers in university, government institutes and industrial sectors, to share their experiences and knowledge relating to polymer science, technology and engineering.

2. To promote networking and the establishment of new collaboration among polymer scientists and interested persons or groups in both academic and industrial sectors in order to push forward the development of polymer science and technology in Thailand.

MESSAGE FROM PRESIDENT

PCT-1

One of the important roles of the Polymer Society of Thailand (PST) is to promote the development of polymer science, technology and engineering in Thailand. Such development is believed to be important since the polymer and petrochemical industries in Thailand are growing rapidly and are contributing very importantly to the economy of the country.

In 2007, the Polymer Society of Thailand, in collaboration with the Graduate Program in Polymer Science and Technology, Mahidol University, organized the 1st Polymer Graduate Conference of Thailand (PGCT-1), to provide a meeting place for polymer graduate students in Thailand to present and exchange their research results. The 2nd PGCT was organized by the Petrochemistry and Polymer Science Program, Chulalongkorn University in 2009. Both PGCTs were proved to be successful events. However, it was felt that the Thai polymer community needed a bigger forum for exchanging information, ideas and experiences among polymer scientists, technologists and engineers from both the public and private sectors as the number of the people involved with polymers in the country steadily grows. Furthermore, there is an increasing need for closer collaborations between researchers from universities and government institutes and industrial companies in order to achieve research results which have greater impacts for the country.

For this reason, the 1st Polymer Conference of Thailand (PCT-1) is organized with cooperation and supports from various graduate schools in polymer science and technology of major universities and also some large petrochemical companies. It is hoped that the PCT will develop into an annual meeting for PCT members and other interested parties of the Thai polymer community, similar to those that have taken place in other advanced countries such as in the USA, Europe and Asia.

Finally, I would like to express my sincere thanks to members of the organizing committee who have put in hard work and strenuous efforts in organizing the PCT-1. I also would like to express my deep appreciation to the sponsors of the PCT-1, including PTT Chemicals Public Co., Ltd., SCG Chemicals Co., Ltd., National Science and Technology Development Agency (NSTDA), National Metal and Materials Technology Center (MTEC), National Nanotechnology Center (NANOTEC), Thai Plastic and Chemicals Public Co., Ltd., and PTT Phenol Co., Ltd. for their understandings and supports which will make the PCT-1 a successful event.

Dr. Krisda Suchiva
Chairman of the PCT-1 Organizing Committee
President of the Polymer Society of Thailand

COMMITTEE

PCT-1

Advisory Committee

1. Dr. Jintana Siripitayananon	Department of Chemistry, Chiang Mai University
2. Dr. Jantrawan Pumchoosak	Department of Industrial Chemistry, Chiang Mai University
3. Dr. Nuanphan Chantarasiri	Department of Chemistry, Chulalongkorn University
4. Dr. Sirithan Bulpakdi	Department of Materials Science, Chulalongkorn University
5. Dr. Pranut Potiyaraj	Metallurgy and Materials Science Research Institute, Chulalongkorn University
6. Dr. Pomthong Malakul Na Ayudhaya	The Petroleum and Petrochemical College, Chulalongkorn University
7. Dr. Patiphan Juijerm	Department of Materials Engineering, Kasetsart University
8. Dr. Amnat Permsubscul	Department of Chemistry, King Mongkut's Institute of Technology Ladkrabang
9. Dr. Sirisart Ouajai	Department of Industrial Chemistry, King Mongkut's University of Technology North Bangkok
10. Dr. Boonnak Sukhummek	Department of Chemistry, King Mongkut's University of Technology Thonburi
11. Prof. Siriwat Wongsiri	School of Science, Mae Fah Luang University
12. Dr. Pranee Phinyocheep	Department of Chemistry, Mahidol University
13. Dr. Sa-ad Riyajan	Department of Materials Science and Technology, Prince of Songkla University (Hat Yai)
14. Dr. Nattapong Nithi-Uthai	Department of Rubber Technology and Polymer Science, Prince of Songkla University (Pattani)
15. Dr. Narongchai O-Charoen	Department of Materials and Metallurgical, Rajamangala University of Technology Thanyaburi
16. Natee Srisawat	Department of Textile Engineering, Rajamangala University of Technology Thanyaburi
17. Dr. Niti Yongvanich	Department of Materials Science and Engineering, Silpakorn University
18. Dr. Nitinat Suppakarn	School of Polymer Engineering, Suranaree University of Technology
19. Seranee Srisuk	Department of Textile Science and Technology, Thammasat University
20. Dr. Wanchart Preechatiwong	Department of Materials Science and Engineering, Walailak University
21. Dr.Wilaiporn Chetanachan	The Siam Cement Public Co., Ltd.
22. Dr. Chaya Jantavasu	PTT Chemical Public Co., Ltd.
23. Jackra Swasdiburi	BST Latex Co., Ltd.
24. Banja Junhasavasdikul	Chemical Innovation Co., Ltd.

Chairman

Dr. Krisda Suchiva	Department of Chemistry, Mahidol University National Metal and Materials Technology Center (MTEC) (President of the Polymer Society of Thailand)

Scientific Committee

1. Prof. Suda Kiatkamjornwong	Department of Imaging and Printing Technology, Chulalongkorn University
2. Dr. Suwabun Chirachanchai	The Petroleum and Petrochemical College, Chulalongkorn University
3 . Dr. Krisda Suchiva	Department of Chemistry, Mahidol University National Metal and Materials Technology Center (MTEC)
4. Dr. Pranee Phinyocheep	Department of Chemistry, Mahidol University
5 . Dr. Taweechai Amornsakchai	Department of Chemistry, Mahidol University
6 . Dr. Robert Molloy	Department of Chemistry, Chiang Mai University
7. Dr. Charoen Nakason	Faculty of Science and Technology Prince of Songkla University (Pattani)
8. Dr. Asira Fuongfuchat	National Metal and Materials Technology Center (MTEC)

Budgeting Committee

1. Dr. Chaiyoot Changsarn	Faculty of Engineering, Rajamangala University of Technology Thanyaburi
2. Dr. Surat Areerat	Department of Chemical Engineering, King Mongkut's Institute of Technology Ladkrabang

Exhibition Committee

1. Dr. Ittipol Jangchud	Department of Chemistry, King Mongkut's Institute of Technology Ladkrabang
2. Dr. Jitladda Sakdapipanich	Department of Chemistry, Mahidol University
3. Dr. Pajaera Patanathabutr	Department of Materials Science and Engineering, Silpakorn University
4. Dr. Pasaree Laokijcharoen	National Metal and Materials Technology Center (MTEC)

Public Relation Committee

1. Dr. Kanoktip Boonkerd	Department of Materials Science, Chulalongkorn University
2. Dr. Toemsak Srikhirin	Department of Physics, Mahidol University
3. Dr.Sommai Pivsa-Art	Faculty of Science and Technology, Rajamangala University of Technology Thanyaburi

Secretariat

1. Dr.Varawut Tangpasuthadol	Department of Chemistry, Chulalongkorn University
2. Dr. Surapich Loykulnant	National Metal and Materials Technology Center (MTEC)
3. Dr. Warayuth Sajomsang	National Nanotechnology Center (NANOTEC)
4. Nittranant Saingam	The Polymer Society of Thailand

Synthesis and Characterization of Hydrogel from Collagen Grafted Poly[(acrylic acid)-*co*-(methacrylic acid)]

Sopinya Choopromkaw[1], Supaporn Noppakundilograt[2] and Suda Kiatkamjornwong[2*]

[1]Program of Petrochemistry and Polymer Science, Faculty of Science, Chulalongkorn University, Bangkok 10330, Thailand
E-mail: choopromkaw_s@hotmail.com.

[2]Department of Imaging and Printing Technology, Faculty of Science, Chulalongkorn University, Bangkok 10330, Thailand
phone +66-2218-5569, E-mail: supaporn.n@chula.ac.th

[2*]Corresponding author, Phone +66-2218-5587, E-mail: ksuda@chula.ac.th, ksuda@sc.chula.ac.th.

Abstract

Collagen grafted poly[(acrylic acid)-*co*-(methacrylic acid)] hydrogels were synthesized by solution polymerization. Acrylic acid (AA) and methacrylic acid (MAA), ammonium persulfate (APS), *N, N, N', N'*-tetramethylethylenediamine (TEMED), and *N, N'*-methylenebisacrylamide (MBA) were used as a pair of monomer, an initiator, a co-initiator, and a crosslinking agent, respectively. The presence of functional groups of the grafted collagen hydrogel was examined by FTIR technique. Too high or low content of APS did not provide the grafted collagen hydrogel with good gel property and adequate water absorbency. The optimal ratio of AA-to-MAA was 86:14 by mol. Water absorbency of the grafted collagen hydrogel increased with increasing the AA content.

Keywords: Hydrogel, Hydrolyzed collagen, Grafted collagen, Acrylic acid, Methacrylic acid

1. Introduction

Hydrogel is lightly crosslinked hydrophilic polymer networks which can absorb water or biological fluids up to ten times its dry weight. The presence of crosslinked network renders hydrogel expand and swell in water without dissolution, while hydrophilic groups, such as the -COOH, $-SO_3H$ in hydrogel assist in high water absorbency [1]. Hydrogel has been used in many applications, such as, disposable diapers, agriculture, cosmetics and biomedical engineering [2]. Although hydrogel synthesized from synthetic monomers or polymers provides excellent water absorbency its toxicity and non-biodegradability induce environmental problems. This is one limitation for applications for drug delivery systems and consumer products. Recently, researchers have focused on employing natural polymers, such as, starch [1], gelatin [3], chitosan [4] and protein [5] to produce natural-based hydrogels for medical and pharmaceutical applications because of their biocompatibility, biodegradability, renewability and non-toxicity. Natural-based hydrogels can be synthesized by grafting vinylic monomers onto the backbones of natural polymer in the presence of crosslinking agent. In nature, collagen is found exclusively in animals. It is the main component of connective tissue and the most abundant protein in mammals, making up about 25% to 35% of the whole-body protein content. Collagen has a unique triple-helix configuration of three polypeptide subunits [6, 7]. Generally, proteins, such as, collagen, keratin, gelatin, soy protein, are high molecular weight polymers and difficult to dissolve in aqueous solutions. Thus, hydrolyzed collagen with lower molecular weight is generally used for hydrogel synthesis due to its water solubility [8].

Acrylic acid (AA) and methacrylic acid (MAA) are unsaturated carboxylic acid, consisting of a vinyl group connected directly to a carboxyl group. Hydrogels composing of AA or MAA provide high water absorbency, pH sensitive [9] and thermal sensitive properties due to hydrophilicity of the carboxyl groups [10]. Pourjavadi and Kurdtabar [11] reported that the hydrolyzed collagen grafted poly[(acrylamide)-*co*-(acrylic acid)] had a high

water absorbency value of 600 g g^{-1}. However, there is still no report of the synthesized collagen grafted poly[(acrylic acid)-*co*-(methacrylic acid)] hydrogels (collagen-*g*-poly(AA-*co*-MAA) hydrogel). In this research, collagen-*g*-poly(AA-*co*-MAA) hydrogels were synthesized by solution polymerization. The effects of APS initiator on hydrogel formation and of the ratio of AA-to-MAA monomer on water absorbency were investigated.

2. Experimental

2.1 Materials

Hydrolyzed collagen was kindly supplied from Udomkorn Engineering Co., Ltd. (Bangkok, Thailand). The industrial grade acrylic acid (AA) and methacrylic acid (MAA) were provided from Thai Mitsui Specialty Chemicals Co., LTD. (Bangkok, Thailand). *N,N'*-methylenebisacrylamide (*N*-MBA) and *N,N,N',N'*-tetramethylethylenediamine (TEMED) (both are analytical grade) were purchased from Fluka (Buchs, Switzerland) and used as a crosslinking agent and a co-initiator, respectively. Ammonium persulfate (APS) (analytical grade) was purchased from Ajax (Seven Hills, Australia) and was used as an initiator. Deionized water (Elga Deionizer, Model LA611, UK.) was used for the synthesis and the water absorbency experiment.

2.2 Synthesis of collagen-*g*-poly(AA-*co*-MAA) hydrogel

Hydrolyzed collagen was dissolved in 25 ml deionized water in a 500-cm^3 four-necked round-bottom flask equipped with a mechanical stirrer assembled with a half moon-shaped Teflon blade paddle and the mixture was stirred for 10 min at 80°C in a temperature controlled water bath under nitrogen atmosphere. APS was added and stirred for 5 min. AA, MAA and *N*-MBA were sequentially added and stirred for 5 min and TEMED was finally added. The mixture was stirred for 60 min to complete the graft copolymerization. The reaction was cool down to room temperature and dewatered with acetone. The product was dried in an oven at 50°C for 24 h. The dry product was milled and sieved through a 100-mesh sieve.

The synthetic conditions of collagen-*g*-poly(AA-*co*-MAA) hydrogel for evaluating the effects of APS on hydrogel formation and the AA-to-MAA ratio on water absorbency are shown in Table 1.

Table 1 Synthetic conditions of collagen-*g*-poly(AA-*co*-MAA) hydrogel

Ingredient/content	Quantity (% mole)
APS (%mole)*	0.1, 0.025, 0.05
AA-to-MAA ratios (%mole)**	100:0, 90:10, 80:20, 70:30, 60:40, 50:50, 40:60, 30:70, 20:80, 10:90, 0:100, 88:12, 86:14, 84:16, 82:18, 76:24

*Hydrogel synthesized with a collagen-to-monomer weight ratio of 1:8; AA-to-MAA mole ratio at 70:30; 0.1% mole each of *N*-MBA and TEMED based on the monomers, and 50 ml deionized water.

**Hydrogel synthesized with a collagen-to-monomer weight ratio at 1:8; 0.05% mole of APS based on the monomer; 0.1% mole each of N-MBA and TEMED based on the monomer, and 50 ml deionized water.

2.3 Characterization

2.3.1 Identification of functional groups of the collagen-*g*-poly(AA-*co*-MAA) hydrogel

The functional groups of collagen-*g*-poly(AA-*co*-MAA) hydrogel were examined by Fourier Transform Infrared Spectroscopy (FTIR, Spectrum one, Perkin Elmer, U.S.A.) using a KBr pellet technique.

2.3.2 Effect of the monomer ratio on equilibrium water absorbency

The equilibrium water absorbency of collagen-*g*-poly(AA-*co*-MAA) hydrogel was carried out in deionized water at room temperature. The dry grafted collagen hydrogel weighing 0.1 g was allowed to swell in the 200 cm^3 of deionized water for 24 h. The fully swollen hydrogel was then separated from the unabsorbed water by filtering through a 100-mesh sieve aluminum screen for 2 h. The swollen hydrogel was weighed and the

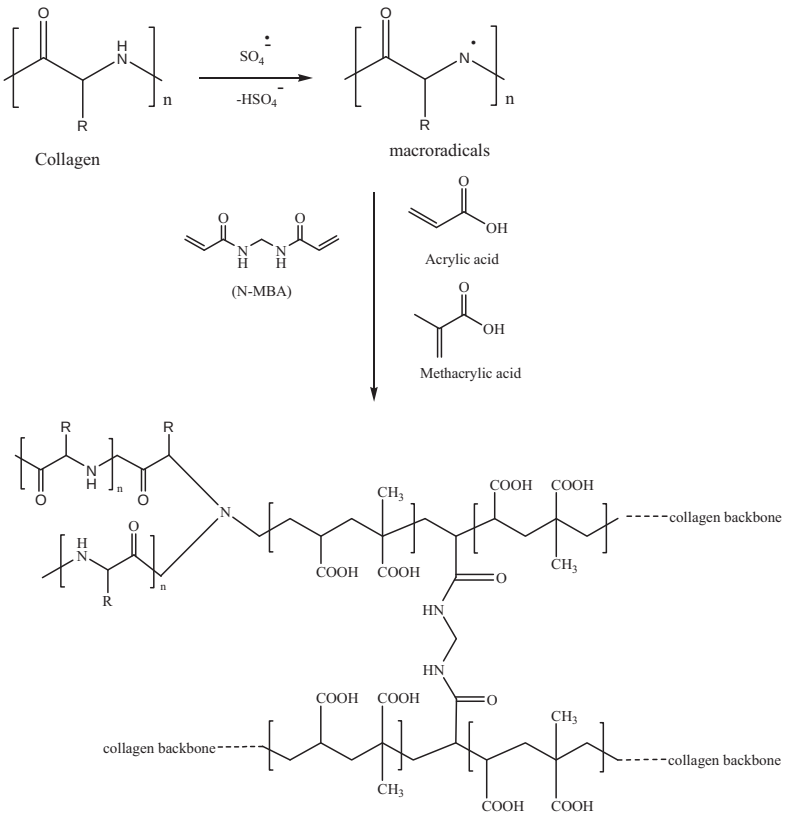

Scheme 1. Proposed mechanistic pathway for synthesis of the collagen-*g*-poly(AA-*co*-MAA) hydrogel based on Pourjavadi and Kurdtabar [11]

equilibrium water absorbency (g g^{-1}) was calculated by Equation (1):

$$\textit{Equilibrium water absorbency } (Q) = (W_s - W_d)/W_d \quad (1)$$

where W_d is the weight of dry grafted collagen hydrogel (g), and W_s is the weight of the swollen hydrogel (g).

3. Results and discussion

3.1 Effect of APS on collagen-*g*-poly(AA-*co*-MAA) hydrogel formation

The APS content imposes a significant effect on the formation of hydrogel. The photographs of synthesized hydrogels with various APS contents are shown in Figure 1. It is found that the synthesized products with APS content of 0.1 and 0.025% mole of monomers are white latex (Figure 1(a) and (b)) and could not be dewatered with acetone, because they are soluble in acetone. Thus, the dry collagen-*g*-poly(AA-*co*-MAA) hydrogel could not be synthesized by these conditions. This is because when too high content of APS (0.1% mole of the monomer) was used in the graft copolymerization, an abundance of radicals was generated resulting in the formation of too many short polymer chains and might produce a latex-form product. Likewise when a low contents of APS (0.025% mole of the monomer) was used in the graft copolymerization, a few radicals were generated leading to many short polymer chains. Thus, the synthesized products from these APS contents had the similar physical property, i.e., cannot be dewatered and solidified.

In contrast, when the grafted collagen hydrogel was synthesized with the APS content of 0.05% mole of the monomers, the product is the white solid (Figure 1(c)) which could be dewatered with acetone to obtain dry collagen-*g*-poly(AA-*co*-MAA) hydrogel with the water absorbency of 136 ± 13 g g^{-1}. At the optimal content of APS (0.05% mole of the monomers), adequate amounts

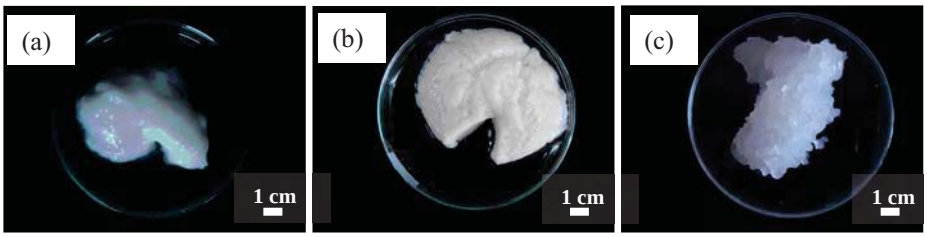

Figure 1. The photographs of synthesized hydrogels at various APS contents: (a) 0.1, (b) 0.025, and (c) 0.05% mole of the monomers

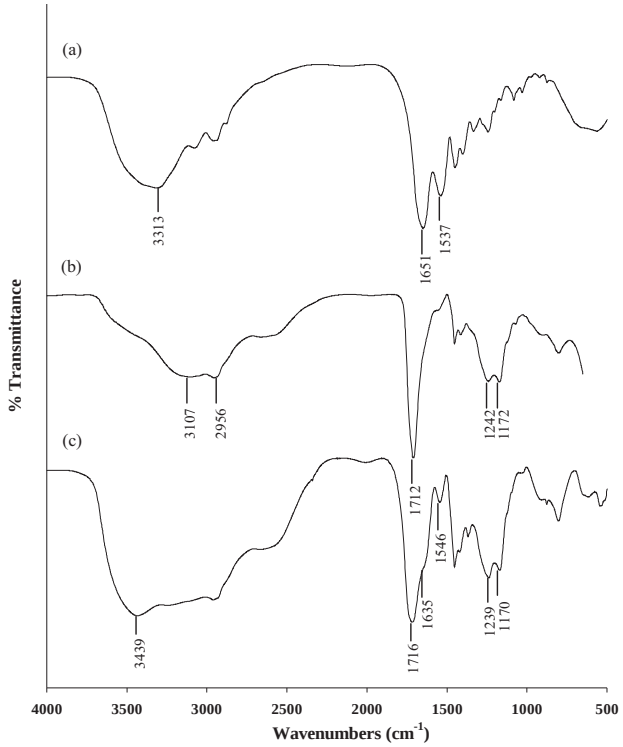

Figure 2. FTIR spectra of: (a) hydrolyzed collagen (b) poly(AA-*co*-MAA) and (c) collagen-*g*-poly(AA-*co*-MAA) hydrogel

of primary radicals generated could produce the flexible three dimensional network of hydrogel structures. The resulting water absorbency was thus obtained. The concentrations of APS, TEMED, and *N*-MBA were fixed at 0.05, 0.1 and 0.1% mol of the monomers, respectively, for studying the effect of AA-to-MAA ratio on water absorbency of the hydrogel.

The mechanism of graft copolymerization of AA and MAA monomers onto collagen backbones in the presence of APS and *N*-MBA has been proposed as shown in Scheme 1 [11]. At the first step, APS is decomposed by thermal initiation at 80^{o}C to produce the sulfate anion-radical. The anion-radical abstracts a hydrogen radical from one of the functional groups in collagen backbone, such as COOH, SH, OH, and NH_2, to form macroradicals to initiate acrylic acid and/or methacrylic acid at the carbon-carbon double bond to result in a graft copolymer. In the presence of *N*-MBA, the crosslinking reaction took place to produce the flexible three dimensional network of the hydrogel.

3.2 Identification of the functional groups of collagen-*g*-poly(AA-*co*-MAA) hydrogel by FTIR technique

The FTIR spectra of hydrolyzed collagen, poly(AA-*co*-MAA) and collagen-*g*-poly(AA-*co*-MAA) hydrogel are shown in Figure 2. The spectrum of hydrolyzed collagen (Figure 2(a)) shows the overlapped peaks at 3313 cm^{-1} of –NH stretching and –OH stretching

[12]. It also shows the peaks at 1651 and 1537 cm^{-1} assigning to C=O stretching of amide I and –NH bending of amide group, respectively. The spectrum of poly(AA-*co*-MAA) hydrogel (Figure 2(b)) shows peaks at 3107, 2956 and 1712 cm^{-1} corresponding to –OH stretching of carboxylic acid, C–H stretching and C=O stretching of carboxylic acid, respectively [13]. The absorption peaks at 1242 and 1172 cm^{-1} corresponding to C–O stretching [15]. Spectrum (c) of the synthesized product (Figure 2(c)) shows the strong absorption peak at 1716 cm^{-1}, shifted from 1712 cm^{-1}, assigning to C=O stretching of carboxylic acid of poly(AA-*co*-MAA) moiety. In addition, the absorption peaks of C–O stretching in poly(AA-*co*-MAA) moiety also shifted from 1242 to 1239 cm^{-1} and from 1172 to 1170 cm^{-1}. Moreover, it shows the medium intensity peak at 1635 cm^{-1} of C=O stretching of amide I. The spectrum (c) of the synthesized product also reveals that the peak of –NH bending of amide group in hydrolyzed collagen moiety has less intensity and shifts from 1537 to 1546 cm^{-1} compared with original collagen. This indicates that collagen-*g*-poly(AA-*co*-MAA) hydrogel was successfully synthesized by the grafting reaction between the amino group (–NH) of collagen and the vinyl group (C=C) of AA and/or MAA monomers via free radical copolymerization (Scheme 1). The results confirmed that the synthesized product was collagen-*g*-poly(AA-*co*-MAA) hydrogel.

3.3 Effect of AA-to-MAA ratio on water absorbency

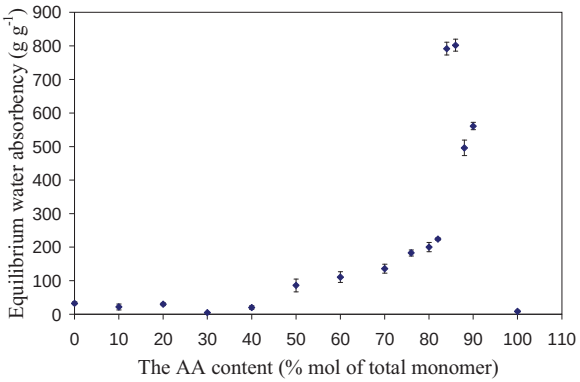

Figure 3. Equilibrium water absorbency of collagen-*g*-poly(AA-*co*-MAA) hydrogel as a function of comonomer contents

The equilibrium water absorbency of collagen-*g*-poly(AA-*co*-MAA) hydrogel increases from 33 ± 4 g g^{-1} to 802 ± 18 g g^{-1} with increasing the AA content from 0 to 86% mol of total monomers. However, when the AA content increases from 86 to 100% mol of total monomers, the water absorbency decreases from 802 g g^{-1} to 9 g g^{-1} as shown in Figure 3. Increasing AA content (0 to 86% mol of total monomers) also can cause water absorbency to increase due to increases in hydrophilicity of the collagen-*g*-poly(AA-*co*-MAA) hydrogel by increasing levels of the carboxylate anions. The higher the repulsion force between carboxylate groups in the crosslinked collagen-*g*-poly(AA-*co*-MAA) hydrogel, the greater the water absorbency becomes. However, when the AA content increases from 86 to 100% mol of total monomers, the water absorbency decreases. This may cause by the low or weak gel strength in swelling leading to losses of gel particles during filtering through a 100-mesh sieve aluminum screen. Thus, the optimal ratio of AA-to-MAA was 86:14 by mol.

4. Conclusion

The synthesis of collagen-*g*-poly(AA-*co*-MAA) hydrogel was carried out by solution polymerization. The content of APS affected the hydrogel formation. The equilibrium water absorbency of collagen-*g*-poly(AA-*co*-MAA) hydrogel increases with increasing the AA content not greater than 86% mol. The optimal ratio of AA-to-MAA was 86:14 by mol.

Acknowledgements

The authors gratefully acknowledge the financial support from the Thailand Research Fund under the Research Team Aid Program Contract no. RTA5080004. Research facilities provided by the Imaging Polymer Laboratory of Chulalongkorn University's Department of Imaging and Printing Technology, Faculty of Science are gratefully acknowledged

References

[1] Kiatkamjornwong S., Chomsaksakul W. and Sonsuk M. Radiation modification of water absorption of cassava starch by acrylic acid/acrylamide. *Radiation Physics and Chemistry*, 59 (2000): 413-427.

[2] Pourjavadi A., Ayyari M. and Amini-Fazl M.S. Taguchi optimized synthesis of collagen-*g*-poly(acrylic acid)/kaolin composite superabsorbent hydrogel. *European Polymer Journal*, 44 (2008): 1209-1216.

[3] Changeza M., Burugapallia K., Koula V. and Choudhary V. The effect of composition of poly(acrylic acid)–gelatin hydrogel on gentamicin sulphate release: in vitro. *Biomaterials*, 24 (2003): 527–536.

[4] Mahdavinia G.R., Pourjavadi A., Hosseinzardeh H. and Zohuriaan M.J. Modified chitosan 4. Superabsorbent hydrogel from poly(acrylic acid-co-acrylamide) grafted chitosan with salt- and pH-responsiveness properties. *European Polymer Journals*, 40 (2004): 1399-1407.

[5] Hwang D.C. and Damodaran S. Chemical modification strategies for synthesis of protein-based hydrogel. *Journal of Agricultural and Food Chemistry*, 44 (1996): 751-758.

[6] Friess W. Collagen-biomaterial for drug delivery. *European Journal of Pharmaceutics and Biopharmaceutics*, 45 (1998): 113-136.

[7] Gelsea K., Poschlb E. and Aignera T. Collagens-structure, function, and biosynthesis. *Advanced Drug Delivery Reviews*, 55 (2003): 1531–1546.

[8] Pourjavadi A., Kurdtabar M., Mahdavinia G.R. and Hosseinzadeh H. Synthesis and superswelling behavior of a novel protein-based superabsorbent hydrogel. *Polyme Bulletin*, 57 (2006): 813-824.

[9] Nho Y.-C., Park S.-E., Kim H.-H., and Hwang T.-S. Oral delivery of insulin using pH-sensitive hydrogels based on poly(vinyl alcohol) grafted with acrylic acid/methacrylic acid by radiation. *Nuclear Instruments and Methods in Physics Research B*, 236 (2005), 283-288.

[10] Adnadjevic B. and Jovanovic J. A comparative study of isothermal drug release from poly(acrylic acid) and poly[(acrylic acid)-*co*-(methacrylic acid)] hydrogel. *Colloid and Surfaces B: Biointerfaces*, 69 (2009), 31-42.

[11] Pourjavadi A. and Kurdtabar M. Collagen-based highly porous hydrogel without any porogen: Synthesis and characteristics. *European Polymer Journal*, 43 (2007): 877-889.

[12] Sionkowska A. Effect of solar radiation on collagen and chitosan films. *Journal of Photochemistry and Photobiology B: Biology*, 82 (2006): 9-15.

[13] Heng L.Y. and Hall E.A.H. Methacrylic-acrylic polymers in ion-selective membranes: achieving the right polymer recipe. *Analytica Chimica Acta*, 403 (2000): 77-89.

[14] Amornsit M. and Petsom A. In Principles and Techniques of Instrumental Analysis. ChulaPress: Bangkok. (2008) pp. 170-176.

[15] Sciarratta V., Vohrer U., Hegemann D., Muller M. and Oehr C. Plasma functionalization of polypropylene with acrylic acid. *Surface and Coatings Technology*, 174 –175 (2003): 805–81.

Surface Modification of Electrospun Chitosan Nanofiber

W. Tiawtrakoonwat,[1] P. Supaphol,[2] W. Kangwansupamonkon[3] and S. Kiatkamjornwong[4*]

[1] Program of Petrochemistry and Polymer Science, Faculty of Science, Chulalongkorn University, Bangkok 10330

[2] The Petroleum and Petrochemical College and The Center for Petroleum, Petrochemicals and Advanced Materials, Chulalongkorn University, Bangkok 10300

[3] National Nanotechnology Center, National Science and Technology Development Agency, Pathumthani 12120

[4] Department of Imaging and Printing, Faculty of Science, Chulalongkorn University, Bangkok 10330

[*] Corresponding Author: k.suda@sc.chula.ac.th

Abstract: In the present contribution, chitosan with a degree of deacetylation of 95% in its blend with poly(ethylene oxide) (PEO) was fabricated into nanofibrous membranes by electrospinning. The introduction of PEO was to facilitate the fiber formation. The spinning solution was 6.7% w/v chitosan and 0.3% w/v PEO in 70:30 v/v trifluoroacetic acid/dichloromethane. The obtained fibers were smooth without the presence of beads, as confirmed by scanning electron microscopy (SEM). The diameters of the individual fibers were 272 ± 56 nm. The surface of the obtained chitosan fibers was modified with *N*-(2-hydroxyl) propyl-3-trimethyl ammonium chloride (HTAC) with an aim of making the chitosan nanofibrous membranes into a quaternary ammonium salt. The reaction was characterized by Fourier-transformed infrared spectroscopy (FTIR) and degree of swelling.

Introduction

Chitosan or poly-*β*-(1-4)-D-glucosamine, a deacetylated derivative of chitin, is one of the most widely used biomaterial for wound dressings and scaffolding materials in regenerative medicine. This is made possible because of its biocompatibility, non-toxicity, biodegradable and antibacterial activity. However, its antibacterial activity is limited to acidic conditions, because of its inherently poor solubility at a pH above 6.5 [1]. The antibacterial activity of chitosan arises from the protonation of the amino groups upon its dissolution in an acid. Many studies purpose that the interaction of polycationic chitosan with negatively charged surface of bacteria results in the loss of membrane permeability, cell leakage and cell death [2]. Comparing with chitosan, chitosan derivatives that bear quaternary amino groups are more effective against bacteria in a much wider pH range, obviously a result of the permanent positive charges that they carry [3].

Recently, fibers with diameters in sub-micron ranges can be facilely prepared, usually in the form of fibrous membranes, by a process known as electrospinning. Due to the highly porous nature of the membranes, they are suitable to be used as wound dressings and carriers for transdermal/topical delivery of active agents [4-6]. However, electrospinning of chitosan is limited by its poor solubility and its polyelectrolytic nature upon dissolving in an acid aqueous solution. The successful electrospinning of pure chitosan fibers has been reported from its solution in 90% aqueous acetic acid [7], trifluoroacetic acid (TFA), and a co-solvent system of TFA and dichloromethane (DCM) [8-10]. The direct electrospinning of a quaternary ammonium salt of chitosan is even more difficult, because of the repulsive forces among the permanent charged moieties. This can be alleviated through the blending of it with an electrospinnable polymer template, such as poly(vinyl alcohol)[4] and poly(vinyl pyrrolidone)[5].

The goal of the present research work is to prepare electrospun fibrous membranes from the chitosan solutions in a TFA and DCM co-solvent system, followed by modification of the surface amino groups with glycidyltrimethylammonium chloride (GTMAC) to give *N*-[(2-hydroxyl-3-trimethylammonium) propyl] chitosan chloride (HTAC) as shown in Figure 1. The potential use of the HTAC-modified chitosan nanofibrous membranes as anti-bacterial non-woven fabrics shall be investigated in future work.

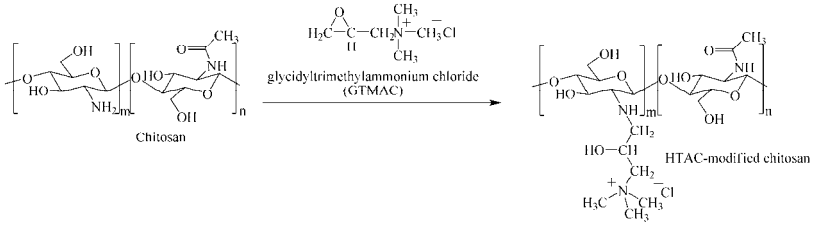

Figure 1. Modification of chitosan with GTMAC (Seong *et al*)[6].

Experimental Details

Materials

Chitosan (CS) powder (degree of deacethylation of 95%), TFA (CF_3COOH, 98% purity) and GTMAC (analytical grade) were purchased from Fluka (Germany). Acetic acid, ethanol and DCM were purchased from Lab-Scan Analytical Science (Ireland). PEO with an average molecular weight of 600,000 Da and glutaraldehyde were purchased from Sigma-Aldrich (USA).

Preparation of the spinning solution

The spinning solution of 7% w/v CS/PEO solution was prepared by dissolving specific amounts of CS and PEO at various weight ratios in a co-solvent system of TFA and DCM at a volumetric ratio of 70:30.

Fabrication of electrospun chitosan membranes

Chitosan fibrous membranes were prepared by electrospinning the CS/PEO solution at room temperature [10]. Briefly, the solution was loaded in a glass syringe (20 mL) with a stainless steel needle having a gauge size of 20. The positive electrode of a high voltage power supply (BMEI, China) was connected to the metal capillary by copper wires. The applied voltage and the tip-to-collector distance were fixed at 25 kV and 12 cm, respectively. The obtained fibrous membranes had been dried *in vacuo* at ambient temperature for 24 h prior to being cross-linked with glutaraldehyde vapor in a desiccator for 6 h at ambient temperature. After the cross-linking, the membranes were finally dried *in vacuo* for 24 h. The cross-linked membranes were neutralized further in 5 M Na_2CO_3 aqueous solution for 3 h, washed several times with deionized (DI) water and finally dried at ambient temperature for 24 h [10].

Synthesis of HTAC-modified chitosan fibrous membranes

HTAC-modified chitosan fibrous membranes were was synthesized according to an established method as outlined in Figure 1. Briefly, four pieces of CS/PEO fiber mats (6 cm by 3 cm) were placed in 40 mL of DI water and GTMAC. The CS:GTMAC mole ratio was 1:4. The reaction was carried out at 70 °C. The modified CS/PEO fibrous membranes were washed with DI water and ethanol was added to remove the unreacted GTMAC. The membranes were dried *in vacuo* at ambient temperature for 1 d.

Characterization

Morphologies of the neat and the modified CS/PEO fibrous membranes were investigated by scanning electron microscopy (SEM, JEOL JSM-5200, Japan). The fiber mats were coated with gold (JEOL JFC-1100E sputtering device, Japan) for 3 min prior to the SEM observation. Fourier-transform infrared spectroscopy (FTIR, Nicolet Nexus 671, UK) and the degree of swelling were used to confirm the success of the modification reaction.

The degree of swelling was determined gravimetrically. Each specimen, after being submerged in DI water for 1 h, was sandwiched between a pair of tissue papers. A flat metal sheet (500 g) was placed on top of the specimen to remove excessive amount of water. The degree of swelling (α) was then calculated according to the following equation:

$$\alpha = \frac{\text{wt of swollen fibers - wt of dry fibers}}{\text{wt of dry fibers}} \times 100 \qquad (1)$$

where α is the degree of swelling (%) and wt stands for the weight.

Results and Discussion

SEM was used to investigate morphologies of the obtained fibrous matrices. Representative images are shown in Figure 2. The diameters of the neat CS fibers varied rather widely, with the presence of beaded segments as well as discrete beads distributing throughout (Figure 2a). PEO was selected as a suitable nonionogenic partner for the preparation of electrospun chitosan fibers. Clearly, the morphologies of the obtained CS/PEO fibers were strongly influenced by the weight compositions of the two polymers in the spinning solutions. At the CS:PEO ratio of 6.9:0.1 w/w, the jet did not come out from the opening of the needle as a continuous stream, as discrete drops of the solution were occasionally observed on the collective screen, despite the rather smooth fiber surface shown in the SEM image (Figure 2b). The electrospinnability of the solution improved greatly at the CS:PEO ratio of 6.8:0.2 w/w (Figure 2c). However, the beads disappeared completely at the CS:PEO ratio of 6.7:0.3 w/w (Figure 2d). Further increase in the PEO content within the solutions to 0.4 and 0.5 % w/v helped facilitate the electrospinning even more so. Analysis of the diametric distribution of the obtained fibers reveals marked increase in the fiber diameters from 148 ± 41 nm of the neat CS fibers to 234 ± 41 nm of the 6.9:0.1 w/w CS/PEO fibers and finally to 624 ± 106 nm of the 6.5:0.5 w/w CS/PEO fibers (Figure 3).

The 6.7:0.3 w/w CS/PEO fiber mats were chosen for further investigation. The fiber mats were further cross-linked with glutaraldehyde (GT) vapor to limit the dissolution of the materials in water. The dissolution in water arises from the aqueous solubility of both the CS-TFA salts [10] and the PEO. When the CS/PEO fiber mats had been cross-linked with GT vapor, the materials retained their fibrous character during the HTAC modification. In addition, the disappearance of the IR transmittance peak at 1587 cm^{-1} (Figure 4) of the cross-linked CS/PEO fiber mat suggested the loss of the free amino groups [11].

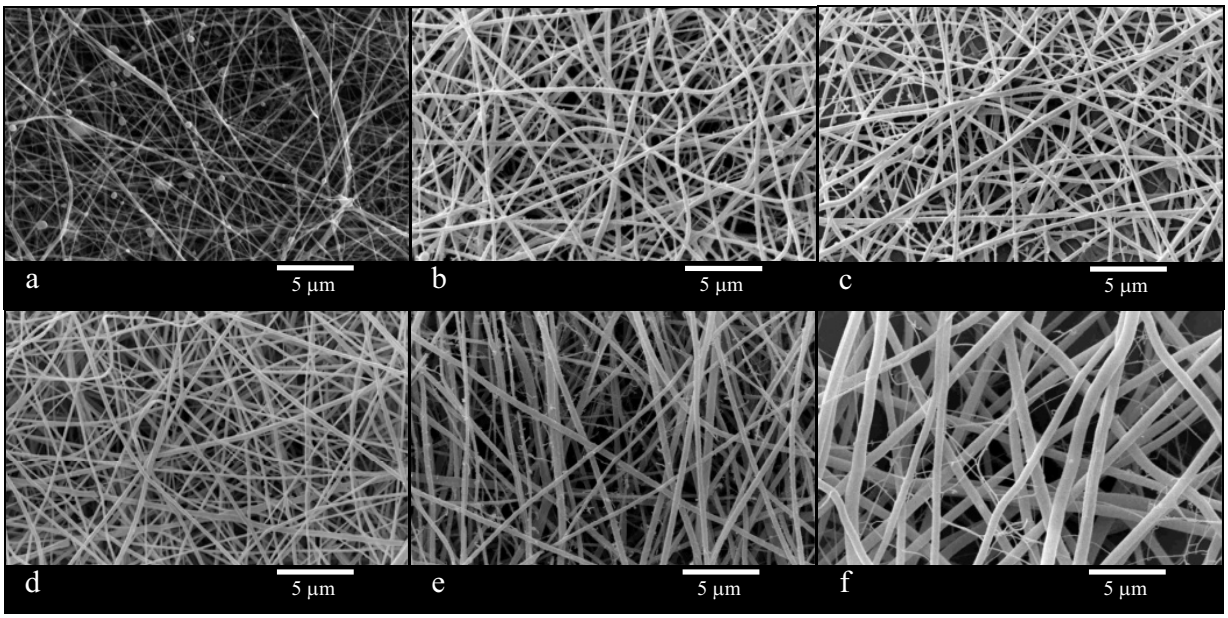

Figure 2. Effect of composition of CS/PEO spinning solution on the morphology of the obtained fibers (CS:PEO weight ratio): (a) 7:0; (b) 6.9:0.1; (c) 6.8:0.2; (d) 6.7:0.3; (e) 6.6:0.4;(f) 6.5:0.5.

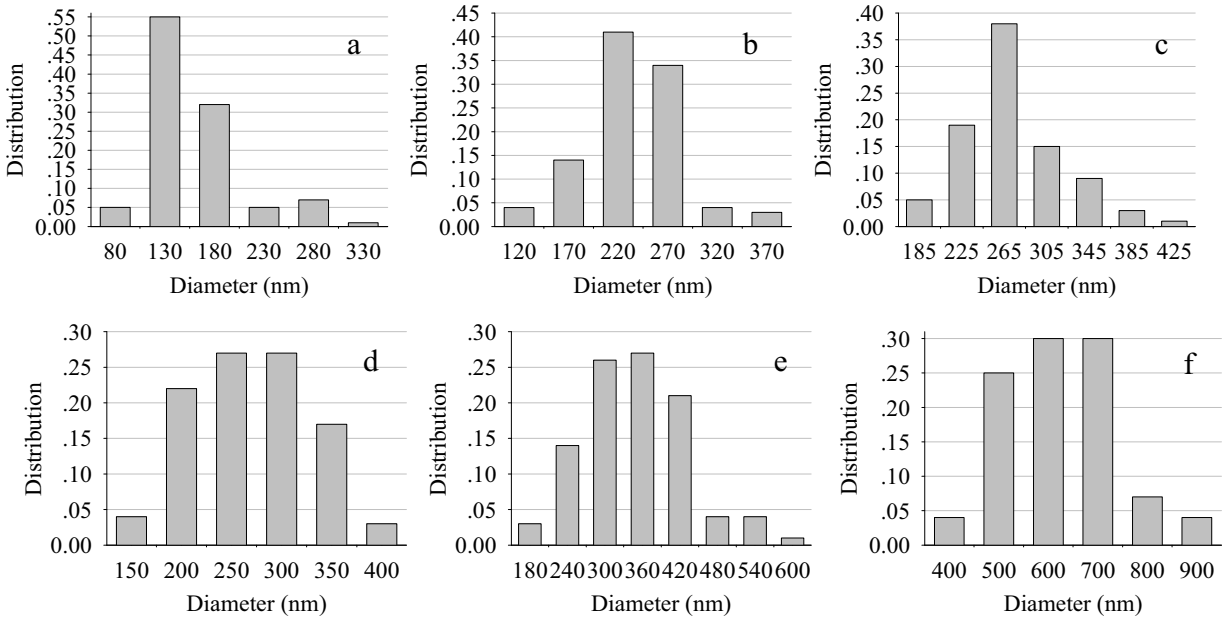

Figure 3. Diametric distribution of the obtained CS/PEO fibers (CS:PEO weight ratio): (a) 7:0; (b) 6.9:0.1; (c) 6.8:0.2; (d) 6.7:0.3; (e) 6.6:0.4;(f) 6.5:0.5.

Seong et al. [6] supposed that the HTAC was synthesized from the reaction between GTMAC and the amino groups of CS, as shown in Figure 1. Under acidic condition, GTMAC reacted mainly with the amino groups, while, under alkaline condition, GTMAC did so with the hydroxyl groups. Figure 4 shows the FTIR spectra of the neat CS, CS/PEO fibers, crosslink CS/PEO fibers, and the modified CS/PEO fibers. Characteristic peaks of CS at 3400 cm^{-1} are for –OH stretching, 1653 and 1569 cm^{-1} for -NH_2 stretching and bending. The characteristic transmittance peaks of the chitosan fiber were observed at 1675 and 1530 cm^{-1},

corresponding to the stretching of the protonated amino ($-NH_3^+$) groups. The large band around 1675 cm^{-1} and three absorption bands around 845-720 cm^{-1} showed the presence of trifluoroacetic acid in CS/PEO fibers as amine salts [10, 12]. In the FTIR spectra of HATC-modified CS/PEO fibers, the amino peak at 1530 cm^{-1} disappeared and a new peak at 1487 cm^{-1} appeared to be the methyl band of GTMAC.

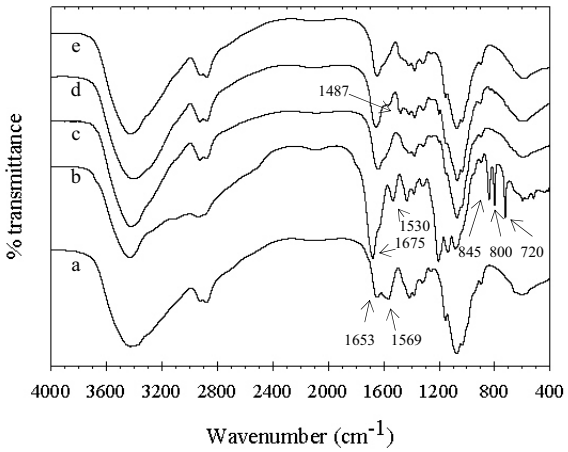

Figure 4. FT-IR spectra of (a) CS, (b) CS/PEO fibers, (c) cross-linked CS/PEO fibers, (d) the product from 8 h-reaction of GTMAC with non-neutralized CS/PEO fibers, and (e) the product from 8 h-reaction of GTMAC with neutralized CS/PEO fibers.

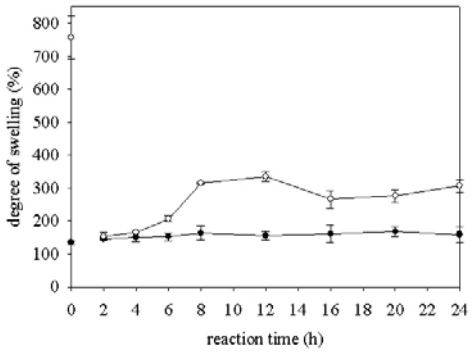

Figure 5. Degree of swelling of the products from reaction of GTMAC with (○) non-neutralized and (●) neutralized CS/PEO fibers, respectively.

Degree of swelling of the product from the reaction of GTMAC with the neutralized CS/PEO fiber was almost constant as shown in Figure 5 (●). The surface modified-HTAC was incomplete due to an improvement in the packing ability of chitosan; intermolecular hydrogen interaction between chitosan molecules improved the molecular packing after neutralization [10]. In reaction of GTMAC with the non-neutralized CS/PEO fibers, the HTAC-modified CS/PEO fibers were prepared to confirm the decreasing degree of swelling from 753% (pre-modified surface) to 153% (post-modified surface after the 2 h reaction). Protonated ammonium groups from the electrospinning process reacted with GTMAC and the hydrophilicity was decreased. When increasing the reaction time, the hydrophilicity of HTAC-modified CS/PEO fibers increased.

Conclusions

To be able to electrospin chitosan, a solvent blend of trifluoroacetic acid and dichloromethane at the 70:30 ratio was used to dissolve chitosan and promote spinnability. Addition of a small amount of poly(ethylene oxide) increased the chitosan viscosity and reduces beads on the fiber surface. The average diameters of the fiber mats was 272±56 nm. This research shows that though the glutaraldehyde crosslinked CS/PEO fibers surface, the quaternary ammonium salt of chitosan can be achieved. FTIR and degree of swelling (%) investigation confirmed the success of the reaction.

Acknowledgements

This research is supported by RTA5080004 from the Thailand Research Fund. Many thanks go to the Nanotechnology National Center and Petroleum and Petrochemistry College for research facilities.

References

[1] J. Cho, J. Grant, M.P. Miller, and C. Allen, *Biomacromolecules*, **7**(2006), pp. 2845–2855
[2] C.H. Kim, J.W. Choi, H.J. Chun, and K.S. Choi, *Polym. Bull.*, **38**(1997), pp. 387-393
[3] K. Desai, K. Kit, Jiajie. Li, and S. Zivanovic, *Biomacromolecules*, **9**(2008), pp. 1000-1006
[4] M. Ignatova, K. Starbova, N. Markova, N. Manolova, and I. Rashkov, *Carbohydr. Res.*, **341**(2006), pp. 2098-2107
[5] M. Ignatova, N. Manolova, and I. Rashkov, *Eur. Polym. J.*, **43**(2007), pp. 1112-1122
[6] H. Seong, H. S. Whang, and S. Ko, *J. Appl. Polym. Sci.*, **76**(2000), pp. 2009-2015
[7] X. Geng, O. H. Kwon, and J. Jang, *Biomaterials*, **26**(2005), pp. 5427-5432
[8] K. Ohkawa, D. Cha, H. Kim, A. Nishida, and H. Yamamoto, *Macromol. Rapid Commun.*, **25**(2004), pp. 1600-1605
[9] K. Ohkawa, K. Minato, G. Kumagai, S. Hayashi, and H. Yamamoto, *Biomacromolecules*, **7**(2006), pp. 3291-3294
[10] S. Sangsanoh and P. Supaphol, *Biomacromolecules*, **7**(2006), pp. 2710-2714
[11] C. Tual, E. Espuche, M. Escoubes, A. Domard, *J. Polym. Sci., Part B: Polym. Phys.*, **38**(2000), pp. 1521–1529
[12] M. Hasegawa, A. Isogai, F. Onabe, M. Usuda, *J. Appl. Polym. Sci.* **45**(1992), pp. 1857-1863

Together for Hevea and Natural Rubber Research
The Third Annual Seminar of HRPP: May 10th, 2011
Prince of Songkla University, Surat Thani Campus
Conference's abstracts

Characterization of Natural Rubber Mesostructure by Size-Exclusion Chromatography (SEC) and Asymmetric Flow Field-Flow Fractionation (AF4) Coupled with an Online Multi-Angle Light Scattering Detector (MALS)

Chalao Thepchalerm[1,5], Stephane Dubascoux*[1], Eric Dubreucq[1], Suwaluk Wisunthorn[2], Laurent Vaysse[3], Suda Kiatkamjornwong[4], Charoen Nakason[5], Frederic Bonfils*[1]

1. UMR IATE 1208, CIRAD, INRA, Montpellier SupAgro, UMII, Montpellier, France

2. Faculty of Science and Industrial Technology, Prince of Songkla University, Surat Thani Campus, Thailand

3. UMR IATE 1208, CIRAD, INRA, Montpellier SupAgro, UMII, Kasetsart University, Bangkok, Thailand

4. Faculty of Science, Chulalongkorn University, Bangkok, Thailand

5. Center of Excellence in Natural Rubber Technology, Prince of Songkla University, Pattani campus, Thailand

Abstract

The mesostructure of natural rubber defined as complex aggregates between macromolecules. This structure can destroyed when dissolved in a conventional solvent of polyisoprene. However, in many cases, a proportion of natural rubber remains insoluble in those solvents referred as the gel phase (Vaysse *et al.*, 2009).

Kim *et al.* (2008) was the first to characterize the macromolecular structure of *Hevea brasiliensis* NR by size-exclusion chromatography coupled with an online multi-angle light scattering detector (SEC-MALS). However, SEC–MALS characterization is limited by upper molecular weight exclusion limits, sample adsorption to the stationary phase, and shear degradation at high pressures and flow rates (Messaud *et al.*, 2009). Nowadays, Field-flow fractionation (FFF) is a rapidly emerging technique which can fractionate a wide range of analytes. Moreover, no studies by FFF on the structure of NR have been reported to date.

This study was storage latex in ambient temperature with difference time (t_0, t_{90}, and t_{180}). The compositions of latex were separated by centrifugation. The bottom fraction of centrifuged latex shown more instability with increasing storage time but less than Rapeepun's work. Field latex (FL), Field latex adding sodium azide (FL+N), and cream fraction of centrifuged latex (CL) were collected to prepared film and small ADS. The solutions of these samples were analyzed by SEC-MALS. It was found that the solution of FL+N film shown macrogel in the bigger size than FL, while the solution of CL was disappears macrogel. However, percentage of gel of t_0 and t_{90} sample was not shown the same trend with appeared macrogel. The comparison of FL, FL+N, and CL molar mass shown that sodium azide affect on decreasing molar mass for film but not for sheet, while the centrifuged latex has lower molar mass than field latex.

These samples were not analyzed by AF4 yet because it is going on the study of suitable conditions for analyze natural rubber by AF4-MALS. There are 4 samples to use in this study; M160 and M121 are constant viscosity *Hevea brasiliensis* natural rubbers, IR307 and Nippol2200 is synthetic rubber. The basically results of comparison between SEC-MALS and AF4-MALS results found that similar M_n values but differences in M_w and M_z values especially for natural rubber. These could be explained by the observed microgel in AF4 but not during SEC separation. Moreover, there are some troubles to solve; such as baseline adjustment, integration limits, and blank subtractions, for better reducibility.

Keywords: *Hevea brasiliensis*; Mesostructure; Size Exclusion chromatography; Asymmetric Flow Field-Flow Fractionation

ICIPT PROGRAM

17 August 2011

18.00 – 20.00 pre-registration and reception drink **(Peking Room)**

18 August 2011 (Kingthong Room)

8.30-8.40 Opening speech

Time	Session I: Printing and Materials **Chairman:** Dr. Hiromichi Noguchi Prof.Dr.Suda Kiatkamjornwong	Speakers	Institutes
8.40-9.20	Review of non impact printing technologies focusing on toner based printing technologies **(Keynote lecture)**	Prof.Dr. Yasushi Hoshino	Nippon Institute of Technology
9.20-9.40	Development of New-True Process-less Thermal CtP plate	Mr. Takanori Mori	Fujifilm Corporation
9.40-10.00	**Break**		
10.00-10.20	Properties and printability of petroleum-based and bio-based biodegradable blend film	Assoc.Prof.Dr. Suchapa Netpradit	King Mongkut's University of Technology Thonburi
10.20-10.40	Effects of plasticizers on properties and printability of carboxymethyl cellulose film from durian rind	Dr. Krittika Tanprasert	King Mongkut's University of Technology Thonburi
10.40-11.10	Method for identifying, analyzing and preserving colours of Thai mural paintings	Asst.Prof.Dr.Pitchayada Ketmake	Chulalongkorn University
	Session II: Image Processing **Chairman**: Prof. Dr. Yasushi Kiyoki Asst.Prof.Dr.Chawan Koopipat		
11.10-11.30	New noise reduction technique for document reading using localized color space	Mr. Hidekazu Sekizawa	Kanagawa Institute of Technology
11.30-12.00	Embedding watermarking into real object image data using QR-code and optical watermarking technique	Dr. Yasunori Ishikawa	Kanagawa Institute of Technology
12.00-12.10	Embedding words in photographs – a study of legibility	Dr. Ayako Hoshino	Independent

12.00-13.30	**Lunch**		
13.30-13.50	The usability of respiratory protective device on instruction with images	Dr. Sakol Teeravarunyou	King Mongkut's University of Technology Thonburi
13.50-14.10	A study of snakes parameter setting as a GA application	Prof.Dr. Takehiko Tomikawa	Kanagawa Institute of Technology
14.10-14.30	Automatic tone mapping for high dynamic range image	Ms.Areerat Pathomchaiwal	Chulalongkorn University
14.30-14.50	**Break**		
14.50-15.10	Current research on electronic paper	Prof.Dr. Makoto Omodani	Tokai University
	Session III: Environment **Chairman:** Assoc.Prof.Dr.Suchapa Netpradit Dr.Krittika Tanprasert		
15.10-15.30	Phytoremediation of volatile organic compounds and wastewater in printing industry **(Invited lecture)**	Dr.Paitip Thiravetyan	King Mongkut's University of Technology Thonburi
15.30-15.50	EcoPrint of book publishing in Thailand	Assoc.Prof.Dr. Aran Hansuebsai	Chulalongkorn University
15.50-17.10	**Special session: Interactive presentation** 3 minutes each		

19.00 – 21.30 Welcome dinner -Chinese Cuisine (Prakuy Petch Room)

19 August 2011 (Kingthong Room)

Time	Session IV: Printing and Materials (cont.) **Chairman:** Prof.Dr.Toshifumi Satoh Dr.Pichit Kajondecha	Speakers	Institutes
9.00-9.40	Next generation of inkjet ink & substrates **(Keynote lecture)**	Dr. Hiromichi Noguchi	Chulalongkorn University
9.40-10.00	Effects of ink formulation containing surface-modified pigmented jet inks on jettability	Prof. Dr. Suda Kiatkamjornwong	Chulalongkorn University
10.00-10.20	Use of Kapok pulp to improve properties of recycled paper	Ms. Somporn Chaiareekij	Chulalongkorn University
10.20-10.40	**Break**		

	Session V: Premedia and Design **Chairman:** Prof. Dr.Yasushi Hoshino Asst.Prof.Dr.Pitchayada Ketmake		
10.40-11.00	"*Kansei*" multimedia computing systems for realizing international and cross-cultural research environments **(Keynote lecture)**	Prof.Dr. Yasushi Kiyoki	Keio University
11.00-11.20	Generation of image perceived as floating using concave Fresnel mirror **(Keynote lecture)**	Prof.Dr. Kazuhisa Yanaka	Kanagawa Institute of Technology
11.20-11.40	Physics and physiologically based skin color image analysis and synthesis **(Invited lecture)**	Assoc.Prof.Dr. Norimichi Tsumura	Chiba University
11.40-12.00	Prediction of visually perceived location of virtual objects using observer's reaching motion--Influence of reaching distance on precision and accuracy	Mr.Keigo Takazawa	Kanagawa Institute of Technology
12.00-13.30	**Lunch**		
13.30-14.30	**Poster session**		
	Session VI: Frontier and Innovation in Printing Industry **Chairman**: Assoc. Prof. Dr. Aran Hansuebsai		
14.30-15.00	Change of our industry means change of our business models	Mr.Volker Illert	Illert Project
15.00-15.20	Innovation of printing inks for food packaging and environmental friendly society	Ms. Yong Siew Chin	Siegwerk
15.20-15.40	**Break**		
15.40-16.00	New role of paper industry towards environmental issues	Mr. Satya Swarup Nanda	Double A Research center
16.00-16.20	Next generation of colour measurement tool	Mr. Noriaki Matsubara	Konica Minolta Sensing
16.20-16.40	How does new media challenge print media?	Mr.Kajorn Bhirakit	Adobe Community Professional
16.40-16.50	**Closing ceremony**		

List of posters

Printing and materials

P1 Color research on wall painting of each dynasty period of Thailand *(Ms. Kanakarn Ruxpaitoon, Chiba University)*

P2 Fully printable powder electroluminescent device *(Ms.Yukiho Hoshino, Tokyo Polytechnic University)*

P3 High-color-rendering powder electroluminescent device (*Mr.Yusuke Noguchi, Tokyo Polytechnic University*)

P4 Effect of drying technique on chitosan-cassava starch film and applying film with fresh rose apple and jujube fruit (*Ms.Julaluk Jarujutarat, Siam University*)

P5 Optimum thickness and dye concentration condition of wax-based electrophoretic thin media (*Mr.Takeshi Hasekawa, Nippon Institute of Technology*)

P6 Effects of chitosan and glycine pretreatment on polyester fabric printed by ink jet ink (*Punthorn, Rajamangala, University of Technology Krungthep*)

P7 Effects of gas plasma treated polyester fabric on color qualities printed by water-based pigmented inkjet ink (*Porntapin Pransilp, Chulalongkorn University*)

P8 Printing Properties of Water-based Pigmented Inkjet Inks on the Oxygen-plasma Modified Polylactide Sheets (Warinpong Jittiwattanapong, Chulalongkorn University)

P9 Development of the packing gauge for cylinder with bearer on printing machine (*Mr. Pitagpong Boonprasom, Siam University*)

P10 Parameter affecting soft proof efficiency (*Assoc.Prof.Dr. Suchapa Netpradit, King Mongkut's University of Technology Thonburi*)

P11 Effect of rheological behaviour on ink flying (*Ms. Chinnamas Garnjanapokin, Note Printing Works, Bank of Thailand)*

P12 Influence of fumigation processes on photographic images and their stability in long-term preservation (*Ms.Takako Yamaguchi, Tokyo Metropolitan Museum of Photography*)

P13 Toner charging characteristics dependence on different types of carriers (*Mr.Disna Jayampathi, Nippon Institute of Technology*)

P14 A consideration of resist coating based on inkjet technology *(Prof.Dr. Kazuhisa Matsuo, Fukuoka Institute of Technology)*

P15 Specific photo acid-generating reaction of oxime by 222nm excimer UV irradiation *(Mr. Hiroki Hata, Chiba University)*

P16 Molecular association of dialkyl-heterocoerdianthrones and application to photo functional solubilizer *(Mr. Masaya Ninoyu, Chiba University)*

P17 Multi-functional photoampholyte compounds generators *(Mr. Yusuke Sato, Chiba University)*

P18 Template-free chemical synthesis of conducting polycarbazole nanowires *(Mr. Takuya Tokuda, Chiba University)*

P19 Photo-polymerization system using volume-expansion cationic polymerizable monomer for holographic recording material *(Mr. Tatsuki Yamaguchi, Chiba University)*

Image Processing

P21 Technique for capturing image containing invisible depth information about an object (*Ms. Sae Isaka, Kanagawa Institute of Technology*)

P22 Evaluation of dynamic range of digital still camera by natural scene simulation box (*Ms. Tithimanan Srimongkon, Chulalongkorn University*)

P23 Attraction degree control by image enhancement (*Mr. Takuya Matsumoto, Nippon Institute of Technology)*

P24 Subjective evaluation of gaze-based tone mapping operators for HDR images (*Mr. Takuya Yamauchi, Chiba University)*

P25 Evaluating specular appearance subjectively for multiple observations using projector-camera system *(Ms. Mayu Yokoya, Chiba University)*

P26 Appearance simulation system of hardcopy based on Gonio-spectral reflection *(Ms. Rui Takano, Chiba University)*

P27 Observation of horizontal distribution of city aerosols by using polarization Lidar System (*Mr. Sun Yijie, Chiba University*)

P28 UAV on-board CP-SAR Image Processing System using one FPGA Board with 2GB DDR 3 DRAM (*Mr. Koshi Oishi, Chiba University)*

P29 Simultaneous tracking and recognition of hand gestures using particle filter *(Mr. Ryuta Fukuoka, Chiba University)*

Effects of Chitosan and Glycine Pretreatment on Polyester Fabric Printed by Ink Jet Ink

Punthorn Buranagul[1, 2], Supaporn Noppakundilograt[1], Suda Kiatkamjornwong[1*]
[1]Department of Imaging and Printing Technology,
Faculty of Science, Chulalongkorn University, Phyathai Road, Bangkok, 10330
****e-mail: ksuda@chula.ac.th***
[2]Program of Printing Technology, Faculty of Science and Technology, Rajamangala University of Technology Krungthep,
2 Nanglinchee Road, Tungmahamek, Sathorn, Bangkok 10120

Abstract

The effects of pretreatment solutions of chitosan (CS) and glycine (Gly) on polyester fabric and their printing results were investigated. The polyester fabrics were padded with CS (4% w/v) or Gly (5% w/v) solution prior to printing with a set of seven-color pigmented water-based jet inks from a piezo-electric jet printer. Hydrophobicity/hydrophilicity of the untreated and treated polyester fabrics was measured by wicking test. K/S values and color difference of the polyester printed fabrics were investigated. The printed fabric with Gly pretreatment had the higher K/S values and color difference than those with CS pretreatment due to its interaction with color inks. Gly increased hydrophilicity of the treated polyester fabric, while CS markedly decreased the hydrophilicity. The higher hydrophilicity of the treated polyester fabric is, the greater the wetting of the treated polyester fabric becomes. Gly pretreatment solution gave the higher K/S values and color difference of the printed polyester fabric.

Keywords: Chitosan, Glycine, Polyester fabric, Ink jet printing

Introduction

Polyester fabric is hydrophobic. Thus, it has a limitation for dyeing and printing with water-based ink. However, it has a negative zeta potential value [1]. The pretreatment of polyester fabric with a suitable agent is the technique to enhance its printed quality. Wang *et al.* [2] found that the positive charges of pretreatment reagent could enhance the color and other properties of the polyester fabric with ink jet printing. Chitosan (CS) is extensively used as a pretreatment reagent for various textile fabrics. The CS pretreatment fabric had high color gamut [3-5]. In this research, the effects of fabric pretreatment with Gly and CS were investigated in the color difference and color strength of the subsequently ink jet printed fabrics. In addition, the interactions of Gly and CS with inks and polyester fabric were also investigated.

Experimental

Materials

A plain weave polyester fabric, constructed of 182 ends/in. (warp) × 87 picks/in. (weft) with a basic weight of 127 g m^{-2}, was used. Triton X-100, a non-ionic surfactant, was supplied by Merck (Frankfurt, Germany). CS flakes of 57,000 g/mol of average molecular weight and 85% deacetylation degrees (DD) was purchased from Seafresh Industry Public Co., Ltd. (Bangkok, Thailand). Gly (98.5% pure) was purchased from Ajax Finechem (Seven Hills, NSW, Australia). A commercial set of seven-color, pigmented water-based jet inks (Epson UltrachromeTM Ink), supplied from Seiko Epson Corporation (Suwa, Nagano, Japan), was used for printing the fabrics.

Preparation of pretreatment solutions

The pretreatment solution of CS, 4% w/v, was prepared by stirring in 2% v/v of acetic acid until dissolved. Gly, 5% w/v, was dissolved in de-ionized water (Elga Deionizer, LA1, Elga Labwater, UK).

Zeta potential measurement

The ink jet inks, CS and Gly pretreatment solutions, polyester fabric and the pretreated polyester fabrics were all measured for zeta potential using a Nano-ZS, Zeta Potential Analyzer (Malvern Instruments Ltd., UK) in a disposable U-shaped cell with each wall that accommodates one small piece of a Cu electrode.

Fabric pretreatment and ink jet printing

The cleaned polyester fabrics were then padded with CS, 4% w/v, or Gly, 5% w/v, solution using a padding machine (PB-1, Copower Technology Co., Ltd., Taiwan) with a 70% wet pick up. The treated fabrics were then dried in an oven (M-3, Copower Technology Co., Ltd., Taiwan) at 80°C for 5 min and cured at 110°C for 2 min.

A color test chart was printed on the untreated and treated polyester fabrics with a set of seven-color, water-

based pigmented ink jet inks from an ink jet printer (Epson Stylus Photo 2100, Seiko Epson Corporation, Nagano, Japan). The printed fabric was steamed at 100˚C for 5 min in a steamer (HTS-3, Copower Technology Co., Ltd., Taiwan).

Wicking test

Polyester fabric samples were cut into two sets of fiber directions, namely warp direction and weft direction. The fluids used for measuring the hydrophilicity and hydrophobicity of polyester fabrics were the distilled water (W) and 2-octanol (O), respectively. Each fabric strip (25-mm wide and 305-mm long) was positioned vertically over a beaker containing distilled water or 2-octanol and the end of the fabric strip was immersed in the fluid. The wicking rate was measured in terms of the height of fluid achieved in polyester fabric strip after 5 min immersion. The wicking ratio (W/O) was used as an indicator of the hydrophilicity vs. hydrophobicity of the polyester fabrics.

Interaction of pretreatment solution with color inks

The interaction of pretreatment solution with color inks was investigated by UV-Visible Spectrophotometry. Each color inks 0.03% w/v of 10 ml was prepared and mixed with CS 4% w/v or Gly 5% w/v solution of 0.5 ml and stood for 24 h. The mixed solutions were centrifuged with 3000 rpm for 20 min at 25˚C. The upper solution was collected and then measured its absorption with UV-Visible Spectrophotometer model HP-8453 (HewLett Packard, Germany).

Color strength (K/S) measurement

The color strength of inks was determined based on the Kubelka–Munk equation, and expressed as a K/S value. The percentage of reflectance was measured by spectrophotometer with a specular light excluded condition. The K/S value was calculated according to Eq. (1) [6]:

$$K/S = (1 - R_\infty)^2/2R_\infty \quad (1)$$

where K is the absorption coefficient of the printed color on the surface, S is the scattering coefficient caused by the colored substrate, and R_∞ is reflectance of the colored sample at an infinite opacity. The significance level of K/S values of the pretreated fabrics compared with the untreated fabric was performed by one way analysis of variance (ANOVA) with the least square difference (LSD) tests used for post hoc evaluations of differences between groups in Statistical Package for the Social Science (SPSS) version 14.0 software, at a confidence level of 95.0% (α= 0.05).

Color difference

Color difference of color patches in a test chart between the untreated and treated polyester fabric was determined based on CIE color difference and calculated according to Eq. (2) [7]:

$$\Delta E = \sqrt{\Delta L^{*2} + \Delta a^{*2} + \Delta b^{*2}} \quad (2)$$

where ΔE is color difference of the printed color on the surface, L is the lightness where a* and b* are the red-green and yellow-green values, respectively.

Result and discussions

Zeta potential measurement

The zeta potentials of all four color inks were found to be negatively charged as shown in Table 1. The magenta color ink had the highest negative value and the yellow color ink the lowest one, but still relatively high (-34.7 mV). The pigments of Epson inks are encapsulated by a type of crosslinked polymer to prevent coagulation. It implies that the encapsulated pigmented inks had anionic functional groups, consistent with their good dispersion stability. CS solution had the 3.4-fold higher of positive zeta potentials value than Gly solution.

Table 1. Zeta potentials of the color inks and pretreatment solutions

Type of material	Zeta potential, ζ (mV)
Cyan ink	−43.1
Magenta ink	−56.5
Yellow ink	−34.7
Black ink	−36.7
Chitosan solution	+83.4
Glycine solution	+24.7

Effects of the pretreatment agents

Hydrophilicity of polyester fabrics

Wicking ratios (W/O) of the untreated and treated fabrics are shown in Table 2. The order of higher wicking ratios can be ranked as follows: Gly treated fabric (0.91) > untreated polyester fabric (0.72) > CS treated polyester fabric (0.42). The higher W/O value is, the higher hydrophilicity of fabric becomes. It indicated that Gly increased hydrophilicity, whereas CS decreased hydrophilicity of the treated polyester fabric.

Table 2. Wicking rate of the untreated and treated fabrics with CS or Gly pretreatment solutions

Type of fabrics	Testing reagents	Warp distances (P)	Weft distances (F)	P/F	W/O_{avg}
Untreated	W	4.2	5.1	0.82	0.72
	O	5.6	7.4	0.75	
CS treated	W	2.8	3.1	0.88	0.42
	O	6.1	7.9	0.77	
Gly treated	W	4.5	4.4	1.03	0.91
	O	6.4	6.9	0.92	

Interaction of pretreatment solution with color inks

The absorption of upper portion solution of each pretreatment solution mixed with any individual color ink was shown in Figures 1-4. It was found that the mixed solution of Gly pretreatment solution with all color inks had the significantly lower absorbance than that of CS pretreatment solution**.**

Gly, a small amino acid molecule, has an isoelectric point (PI) at 5.97. At a pH of less than 5.97 Gly is in a form of the protonated amino group ($-NH_3^+$) and can interact with the negative charge of polymer encapsulated pigment in ink leading to precipitation of Gly-pigment adduct. Thus, the upper portion solution had lower absorbance because of the less pigment remained in the solution. CS, a long chain polymer, was also in a form of the protonated amino groups with some hindrance due to its molecular size resulting in a lower interaction with encapsulated pigment even though it had a relatively high positive charge. This confirms that Gly rendered a higher interaction with the encapsulated pigment in the color inks.

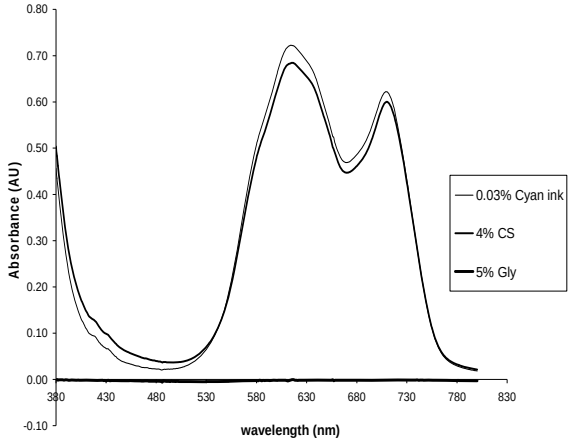

Figure 1. Absorption spectra of the upper portion solution of mixed cyan ink with CS or Gly pretreatment solution

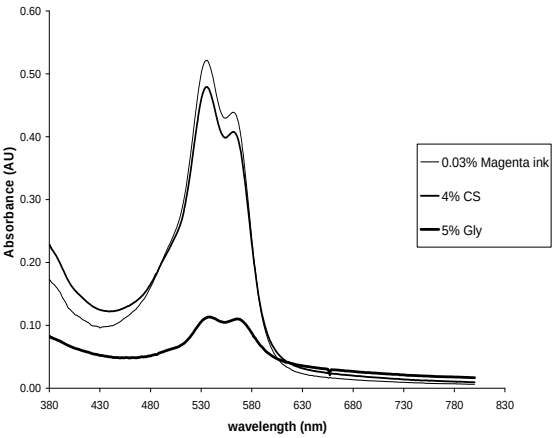

Figure 2. Absorption spectra of the upper portion solution of mixed magenta ink with CS or Gly pretreatment solution

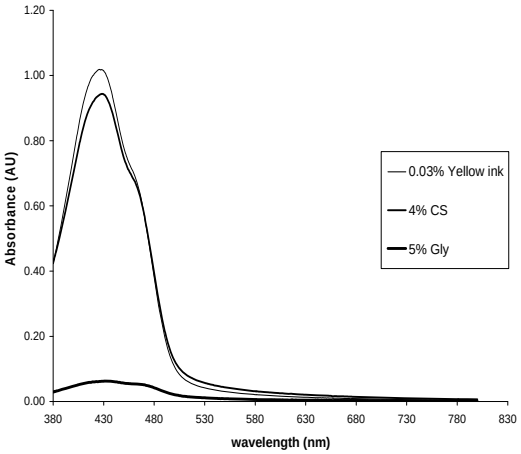

Figure 3. Absorption spectra of the upper portion solution of mixed yellow ink with CS or Gly pretreatment solution

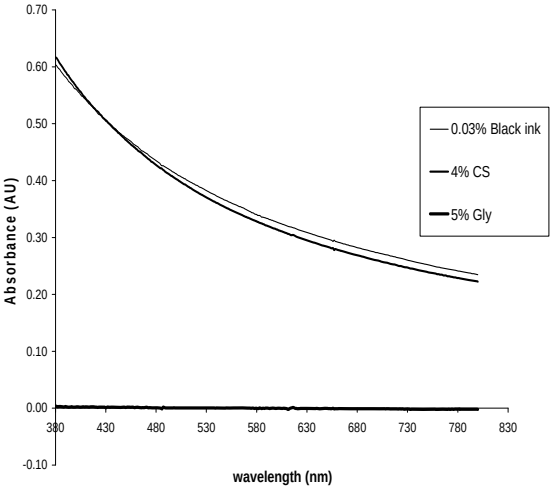

Figure 4. Absorption spectra of the upper portion solution of mixed black ink with CS or Gly pretreatment solution

Color strength

The color strength (K/S) of the fabrics subjected to CS and Gly pretreatment solutions is summarized in Table 3. Gly treated fabrics gave the higher K/S values than did the untreated fabrics. For the CS treated fabrics, the lower K/S values were obtained for the four ink colors compared to the untreated fabric and Gly treated fabrics. This was caused by the CS treated fabric to produce the lower hydrophilicity; a lower ink wetting was thus found than that of Gly treated surface.

Moreover, the lower interaction of CS with each pigment in color inks led to less pigment adherence on the surface of the printed CS treated fabric.

Table 3. Color strength (K/S) of the untreated and pretreated polyester fabrics

Polyester fabrics	K/S at λ_{max}			
	Cyan 620 nm	Magenta 540 nm	Yellow 400 nm	Black 400 nm
Untreated	2.53	4.79	5.38	3.61
CS 4% w/v treated	1.57	2.47	5.2	2.4
Gly 5% w/v treated	3.57	5.07	6.77	3.77

Color difference

The color difference of the untreated and treated fabrics with CS or Gly pretreatment solutions is summarized in Table 4. It shows that both CS and Gly treated fabrics had a higher color value than that of the untreated polyester fabric. Gly increased the blue, green, cyan and magenta inks with the higher color difference than that of CS. The reasons were explained in color strength section. This confirmed that the protonated CS and Gly could be used as the pretreatment solution for polyester fabrics printing by ink jet technique to achieve the good color quality of printed fabrics.

Conclusions

CS and Gly improved color quality of the printed fabrics than the untreated fabric. Gly pretreatment gave the higher K/S value and color difference over the CS pretreatment due to its higher wetting and better interaction with the encapsulated pigment in the inks.

References

1. M. Espinosa-Jimenez, R. Padilla-Weigand, A. Ontiveros-Ortega, M.M. Ramos-Tejada, and M.R. Perea-Carpio, J. Colloid Interface Sci., 265, 227 (2003).
2. C. Wang, G. Wu, K. Fang, A. Tian, X. Zhang, S. Fu, Cationic pretreatment for improving image quality of inkjet printing on polyester fabrics. In Proc. NIP23, pg. 500 (2007).
3. K. Chakvattanatham, S. Phattanarudee, S., and S. Kiatkamjornwong, Pigment & Resin Technol., 39(6), 327 (2010).
4. S. Phattanarudee, K. Chakvattanatham, and S. Kiatkamjornwong, Prog. Organic Coat, 64, 405 (2009).
5. C.W. Yuen, S.K. Ku, and C.J. Kan, Appl. Polym. Sci., 107, 1057 (2008).
6. H.N. James, In M. Roderick (Ed.), Colour physics for industry Society of Dyers and Colourists, West Yorkshire, England, 1997, pp. 296.
7. B. Rigg, In M. Roderick (Ed.), Colour Physics for Industry, Society of Dyers and Colourists, West Yorkshire, England, 1997, pp. 111.

Acknowledgements

The authors would like to acknowledge the research grant support by the National Research Council of Thailand under contract number GRB 19 51 23 03 and the Research Team Aids coded RTA5080004 for their financial support. Deep gratitude also goes to the Polymer Research Laboratory of the Department of Imaging and Printing Technology, Chulalongkorn University, for providing research facilities. The authors are indebted to the Department of Textile Chemical Engineering, the Faculty of Textile Industries, Rajamangala University of Technology, KrungThep, for permission to use their padding machine and steamer.

Biography

Punthorn Buranagul received her B.Sc. degree in Printing and Imaging Technology in 2003 and M.Sc. degree in Imaging Technology in 2009 from the Faculty of Science, Chulalongkorn University. She worked as a lecturer at the Printing Technology Division, Faculty of Science and Technology, Rajamangala University of Technology Krungthep in 2010. Her research interests are in the area of printing and printing material. Her e-mail address is punthorn.b@rmutk.ac.th.

Supaporn Noppakundilograt is an Assistant Professor of Photographic Science and Printing Technology at the Department of Imaging and Printing Technology, Faculty of Science, Chulalongkorn University, Bangkok, Thailand. She obtained her B.Sc. and M.Sc. degrees in Chemistry and Organic Chemistry, respectively, from the Faculty of Science, Chulalongkorn University, and her PhD degree in Photo-functional Materials Science from Chiba University, Chiba, Japan in 2002. Her research areas are superabsorbent polymers, photopolymer, printing ink, and surface treatment of textile. Recently, her research interests are modification of green polymers for superabsorbent polymers and printing materials. Her e-mail address is supaporn.n@chula.ac.th.

Suda Kiatkamjornwong is currently a Full Professor (PC11 or A 1) of Polymer Science and Engineering at the Department of Imaging and Printing Technology, Faculty of Science, Chulalongkorn University, Bangkok, Thailand. She obtained her B.Sc. and M.Sc. degrees in Chemistry and Physical Chemistry, respectively, from the Faculty of Science, Chulalongkorn University, and her PhD degree in Polymer Science and Engineering from Lehigh University, Bethlehem, Pennsylvania, USA, in 1983. Her research interests are in the areas of superabsorbent polymers, imbiber beads, modification of green polymers, digital printing and environment in polymers and printing. Suda Kiatkamjornwong is the corresponding author of this article and can be contacted at ksuda@chula.ac.th.

Effects of Ink Formulation Containing Surface-Modified Pigmented Jet Inks on Jettability

Pichet Thanapongjongruay[1], Hiromichi Noguchi[1, 2], Suda Kiatkamjornwong[1]*
[1]Department of Imaging and Printing Technology, Faculty of Science, Chulalongkorn University, Bangkok 10330, Thailand; Phone: +66 2 218 5587, Fax: + 66 2 255 3021,
**e-mail:ksuda@chula.ac.th*
[2]2-19-10, Shimoyugi, Hachioji-shi, Tokyo, Japan,
Phone 81-426-74-7084, Fax: 81-426-74-7084.

Abstract

Six surface-modified pigmented inkjet inks comprising black, cyan, magenta, yellow, light cyan, and light magenta colors were prepared with a pigment-to-binder ratio of 1:2. Styrene-acrylic acid emulsion was used as a binder. Fluid system composed of diethylene glycol and glycerol was examined by varying their ratios to adjust the ink viscosity. Overall particle size of pigment and polymer emulsion was controlled within the range of 100 to 300 nm. Surface tensions were varied by surfactant concentration. The range of viscosity and surface tension affecting the jettability were investigated. Good jettability range was found in a viscosity-surface tension operation window in each series of ink formulation 5 which could produce the complete test patterns.

Key words*: Ink formulation, surface modified pigment, viscosity, surface tension, ink jet ink, jetting*

Introduction

Viscosity and surface tension of ink are the important parameters in the design of ink because they aid droplet formation through nozzles in a controlled manner for any given inkjet technology. Many approaches have been used to develop pigment-based inks as pigments are substrate independent and can be applied on most printing substrates. Pigment appears to be the most suitable candidate to achieve performance benefits. With increasing environmental pressure on dye-based colorant systems and with improvements in pigment applications, it is expected that there will be a rapid growth in pigment-based colorant systems. Pigment dispersion is a very important factor because particle sizes in the range of 20 to 200 nm are preferred for inkjet inks for reliable performance through nozzle since the pigment dispersion and the rest of the ingredients in the ink jet ink formulation serve to position the pigment particles to the right place on the substrate through a given print head in order to generate beautiful images, or to bind the pigment particles to the substrate so that the image can last a long time with respect to different types of resistance.

A proprietary technology to modify pigment surfaces by attaching various ionic functional groups such as sulphonate ($-SO_3^-$), carboxylate ($-COO^-$) or quaternary ammonium ($-R_4N^+$) to impart electrostatic stabilization and desired physicochemical properties to aqueous pigment dispersions were developed [1] which eliminated the need of conventional dispersants. The technology was first utilized for surface modification of carbon black pigments which resulted in commercial products such as CAB-O-JET® 200 and CAB-O-JET® 300 black pigment dispersions. Surface treatment of pigment with its own derivatives has been very successful in ink applications. A novel color pigment dispersion set for aqueous inkjet ink applications that comprised of surface modified copper phthalocyanine blue pigment (IJX™ 253, PB 15:4), Quinacridone red pigment (IJX™ 266, PR 122) and monoazo yellow pigment (IJX™ 273, PY 74) was developed [1] using Cabot surface modification technology. It was demonstrated that surface modification of color pigments with ionic groups provides stable dispersions with favorable physical characteristics for the formulations of aqueous inkjet inks. Yu and Gottberg [2] investigated surface modified carbon black pigments by potentiometric titration found to be effective in understanding the stability of pigment dispersions. The effect of ionic strength, inkjet ink components and nature of surface functional groups were studied and could be related to the pigment stability. Daplyn and Lin [3] reported preparations of three different pigment dispersions and formulations of inkjet inks from the prepared dispersions. The ink formulations comprised 2% pigment dispersion, 15% thermal curing binder, 5% ethylene glycol, 5% isopropyl alcohol and 73% water. The ink formulations were evaluated for their suitability for jet printing on textile fabrics. Results of this study showed that ink formulation containing a surface modified pigment (Cabot Magenta IJX 266) was most suitable for inkjet printing. This was attributed to the pigments smaller particle size, lower viscosity and stability to the freeze-thaw cycles and pH changes. Kiatkamjornwong *et al*. [4] prepared the pigmented inkjet inks composed of 4%wt of each pigment dispersion (cyan, magenta, yellow and black), 10%wt

diethylene glycol, 15%wt glycerin, 16.5%wt acrylic binder with a pigment to binder ratio of 1:2 and deionized water. The pH of the inks was adjusted to 9.0 using sodium hydroxide. The particle size distribution and viscosity of inkjet inks were slightly increased during ambient storage of two months. Leelajariyakul *et al*. [5] studied the effect of pigment dispersion techniques such as surface modification and micro-encapsulation on inkjet printing of silk fabric. The properties of both types of inks were: viscosity 3.5– 5 mPa s, surface tension 38– 45 mN m^{-1} and particle size 220– 230 nm which gave a good ink jetting. The particle size and viscosity of both types of ink stored at ambient room temperature for 12 weeks increased by 2–15% and 20– 40%, respectively. The surface modified pigmented inks provided high optical density, good tone reproduction, better color gamut and gamut volume on both untreated and pre-treated silk fabrics.

Experimental

Preparation of pigmented inkjet inks

Table 1 describes the detailed information of pigment dispersion and binder and the pigmented inkjet formulations as shown in Table 2.

The pigment-to-binder ratio was fixed at 1:2, which is a typically selective ratio used in a general inkjet formulation [5] and the formulated ink viscosity was adjusted and compared with those of Epson inks. The proportion of diethylene glycol and glycerol was adjusted for monitoring the ink viscosity. Binder (Printofix 710), urea and surfactant (Surfynol 104) were added individually to avoid any unfavorable inhomogeneity in the solution. Then, a dilute NaOH solution (10% w v^{-1}) was added to the ink in order to adjust the pH in the range of 7 to 9. After mixing, the inks were filtered through a cellulose acetate filter (pore size 0.45 μm) to prevent any coarse particles from clogging the orifices of the printer. The formulated inks were diluted with deionized water before measuring the zeta potential by Zeta nanosizer (Zeta nanosizer ZS model Zen 3600, Malvern Instrument Ltd., England). The charges on the pigment surfaces were evaluated at 25°C.

Table 1 Properties of pigment dispersions and binder

Materials	Chemical properties			Physical properties			
	Color Index of pigment	Chemical class of pigment	Pigment concentration (wt. %)	pH	Viscosity (mPa s)	Mean particle size (nm)	Zeta potential (mV)
Cyan : C (CAB-O-JET® 250C)	PB 15:4	Copper phthalocyanine	10.03	6.11	2.40	98.7 ± 41.2	-54.6
Magenta : M (CAB-O-JET® 260M)	PR 122	Quinacridone	9.98	4.05	2.47	132.7 ± 47.7	-53.2
Yellow : Y (CAB-O-JET® 270Y)	PY 74	Monoazo	10.09	7.24	2.36	190.1 ± 89.0	-50. 7
Black : Bk (CAB-O-JET® 200)	PBk 7	Carbon black	20.44	7.29	3.88	154.6 ± 64. 9	-55.1
Printofix binder 710	-	Styrene-Acrylate copolymer	40.00	6.14	43.2	235.5 ± 71.2	-37.9

Table 2 A water-based pigmented ink formulation

Chemical	Weight (%)
Pigment dispersion (by weight)	5.00
For process colors	2.00
For light colors	
Diethylene glycol	2.5 – 10
Glycerol	1– 12
Urea	5.00
Binder (by weight)	
For process colors	10.00
For light colors	4.00
Deionized water	volume was made up to 100% weight

Properties of the pigmented inkjet inks

For developing a set of water-based pigmented inkjet ink, six color inks composed of the black, cyan, light cyan, magenta, light magenta and yellow colors were prepared and the physical properties were measured. The formulated ink viscosity was adjusted and compared with the Epson commercial ink. The concentrations of diethylene glycol and glycerol were adjusted for monitoring the right ink viscosity, and the physical properties of pH, viscosity and surface tension were measured. The jet ability of the formulated ink sets was printed with the test pattern images.

Results and discussion

Ink formulation and physical properties

The surface-modified pigments with sulphonic acid group were used for ink formulation [5]. The surface-modified pigments were made from copper phthalo-cyanine blue (C.I. Pigment Blue 15:4), quinacridone red (C.I. Pigment Red 122), monoazo yellow (C.I. Pigment Yellow 74), and carbon black (C.I. Pigment Black 7). A rheology modifier is an ingredient used to control the viscosity of the ink or more precisely the rheological profile of the ink. For the ink formulation, diethylene glycol and glycerol are performed as a rheology modifier. The proportion of diethylene glycol and glycerol was adjusted for monitoring the ink viscosity at a low shear rate. The pH, viscosity, and surface tension of the formulated inks are shown in the Tables 3–8.

Black ink formulation

The five black ink formulations in each ink formulation, which include a pigment dispersion of black (CAB-O-JET® 200): C.I. Pigment Black 7, are shown in Table 3 which presents the ink ingredients and concentrations. All inks exhibit the Newtonian fluid property, i.e., shear stress is in a linear proportion to shear rate and viscosity is constant at all shear rates. The high ratio of diethylene glycol-to-glycerol content in ink formulation 1 had the highest viscosity (4.74 mPa s) whereas the low ratio of diethylene glycol-to-glycerol content in ink formulations 3 and 4 had the lowest viscosity (3.00 and 3.27 mPa s). The viscosity of the commercial ink is similar to those of ink formulations 2–5 (3.00–3.33 mPa s). The pHs of the ink formulations 1–3 are higher because of the effect of alkaline solution added (10% w v^{-1} NaOH) and the lower pH in the ink formulations 4–5. The commercial ink (Epson T0491) has the highest pH (8.48). Surface tensions of the black inks formulations 1 and 2 are higher (44.2–44.9 mN m^{-1}) than the other ink formulations 3 – 5 and the commercial ink. The lower surface tension of ink formulations 3–5 was caused by the addition of surfactant, Surfynol 104. The commercial black ink has the lowest surfactant tension of 30 mN m^{-1}.

Cyan ink formulation

The five cyan inks in the ink formulations are shown in Table 4. The ink viscosities and pH of the cyan inks are relatively lower. The pH of the commercial ink is much higher than the cyan inks. In contrast, the ink surface tensions are in the range of 43–51 mN m^{-1}. All inks have the Newtonian fluid property. The proportion of diethylene glycol-to-glycerol ratio of 5/10 in formulation 5 is relatively high and close to that of Epson cyan ink.

Light cyan ink formulation

The five light cyan inks in the ink formulations are shown in the Table 5. The ink formulation prepared with the diethylene glycol-to-glycerol ratio of 10/15 can also produce the Newtonian fluid. The ink rheological property shows the shear-thickening behavior in the ink formulations 2, 3 and 4 at a shear rate higher than that at 150 s^{-1}.

Magenta ink formulation

The five magenta ink formulations are shown in the Table 6. One can see in Table 6 that the viscosity of the magenta ink formulation 1 is very high (7.45 mPa s). Comparison between the ink formulations 1 and 3, the high viscosity inks with shear-thinning behavior were found in the alkaline adjusted inks. All other inks showed the Newtonian fluid property. The surface tensions of the prepared inks were relatively high when comparing with that of the commercial ink.

Light magenta ink formulation

The five light magenta inks in the ink formulations are shown in Table 7. The ink viscosities of ink formulations 2 to 5 are relatively low than the standard commercial ink. The Newtonian fluid property is observed in the ink formulations 1, 2 and 5 while in the ink formulations 3 and 4 show the shear-thickening fluid. The surface tensions of all inks are very high in the non-surfactant loaded inks formulations 1 and 2, and relatively high in the ink formulations 3–5 with 0.1% w w^{-1} addition of the

surfactant while the commercial ink has the lowest surface tension of 29.7 mN m^{-1}.

Yellow ink formulation

The five yellow ink formulations are shown in the Table 8. The inks formulations 3–5 show the Newtonian fluid property. Comparison between the ink formulations 3 and 5 showed that the high viscose inks were found in the alkaline-adjusted inks formulations 1– 3. One thing is observed that the ink formulations 1 and 2 exhibit the inevitable shear thinning behavior. The non-adjusted pH inks had very low ink viscosity (at around 3). One thing is observed that the ink formulations 1 and 2 exhibit the inevitable shear thinning behavior. The non-adjusted pH inks had very low ink viscosity (around 3 mPa s). The ink formulation 5 containing the diethylene glycol-to-glycerol ratio of 1/2 had the similar viscosity with the commercial ink. The surface tensions of the inks without surfactant were very high (51–54 mN m^{-1}) while the surfactant added inks had much lower ink surface tension (43–46 mN m^{-1}).

Table 3 Chemical composition and properties of the formulated black inks

Formula	Chemical concentration (%w w^{-1})			Physical properties		
	Diethylene glycol	Glycerol	Surfactant	pH	Viscosity (mPa s)	Surface Tension (mN m^{-1})
1	10	10	-	7.25	4.74*	44.2
2	5	5	-	7.22	3.23**	44.9
3	5	5	0.1	7.27	3.05**	38.7
4	5	6	0.1	6.79	3.00**	40.6
5	5	8	0.1	6.89	3.27**	38.9
Epson T0491				8.48	3.33**	30.2

For the ink formula 1–3, the pHs were adjusted with 10% w v^{-1} NaOH; viscosity at 25 °C, spindle #S00; rotational speed, *150 s^{-1}, **220 s^{-1}.

Table 4 Chemical composition and properties of the formulated cyan inks

Formula	Chemical concentration (%w w^{-1})			Physical properties		
	Diethylene glycol	Glycerol	Surfactant	pH	Viscosity (mPa s)	Surface Tension (mN m^{-1})
1	10	10	-	7.07	3.75*	51.0
2	5	5	-	7.24	2.68**	49.8
3	10	5	0.1	7.58	3.86*	42.3
4	5	5	0.1	6.68	2.85**	44.4
5	5	10	0.1	6.76	3.33**	43.1
Epson T0492				9.45	3.17**	30.8

For the ink formula 1– 3, the pHs were adjusted with 10% w v^{-1} NaOH. Viscosity was measured at 25 °C, spindle #S00, rotational speed, *180 s^{-1}, **220 s^{-1}.

Table 5 Chemical composition and properties of the formulated light cyan inks

Formula	Chemical concentration (%w w^{-1})			Physical properties		
	Diethylene glycol	Glycerol	Surfactant	pH	Viscosity (mPa s)	Surface Tension (mN m^{-1})
1	10	10	-	7.70	2.83	50.4
2	5	5	-	7.46	2.57	51.5
3	10	10	0.1	8.33	3.01	39.9
4	10	10	0.1	6.90	2.83	42.3
5	10	15	0.1	6.99	2.81	40.1
Epson T0495				9.08	3.26	32.9

For the ink formula 1–3, the pHs were adjusted with 10% w v^{-1} NaOH. Viscosity was measured at 25 °C, spindle #S00, rotational speed 220 s^{-1}.

Table 6 Chemical composition and properties of the formulated magenta inks

Formula	Chemical concentration (%w w^{-1})			Physical properties		
	Diethylene glycol	Glycerol	Surfactant	pH	Viscosity (mPa s)	Surface Tension (mN m^{-1})
1	10	10	-	7.27	7.45*	50.9
2	5	5	-	7.10	4.22**	52.7
3	5	2.5	0.1	7.47	18.7*	43.3
4	5	2.5	0.1	6.65	3.89**	45.1
5	5	1	0.1	6.73	3.44**	42.1
Epson T0493				9.33	3.37**	34.1

For the ink formula 1–3, the pHs were adjusted with 10% w v^{-1}NaOH. Viscosity was measured at 25 °C, spindle #S00, rotational speed, *100 s^{-1}, **170 s^{-1}.

Table 7 Chemical compositions and properties of the formulated light magenta inks

Formula	Chemical concentration (%w w^{-1})			Physical properties		
	Diethylene glycol	Glycerol	Surfactant	pH	Viscosity (mPa s)	Surface Tension (mN m^{-1})
1	10	10	-	7.78	4.58	50.75
2	5	5	-	7.79	3.01	52.1
3	5	5	0.1	8.18	2.56	40.7
4	5	10	0.1	6.89	2.7	41.8
5	10	12	0.1	7.13	2.78	41.3
Epson T0496				9.05	3.13	29.7

For the ink formula 1–3, the pHs were adjusted with 10% w v^{-1}NaOH. Viscosity was measured at 25 °C, spindle # S00, rotational speed, *100 s^{-1}, **170 s^{-1}.

Table 8 Chemical composition and properties of the formulated yellow inks

Formula	Chemical concentration (%w w^{-1})			Physical properties		
	Diethylene glycol	Glycerol	Surfactant	pH	Viscosity (mPa s)	Surface Tension (mN m^{-1})
1	10	10	-	7.25	7.88*	51.5
2	5	5	-	7.32	5.85*	53.5
3	5	2.5	0.1	7.88	4.23**	42.8
4	2.5	2	0.1	6.77	2.97**	45.6
5	5	2.5	0.1	6.89	3.1**	45.5
Epson T0494				9.19	3.31**	32.9

For the ink formula 1-3, the pHs were adjusted with 10% w v^{-1}NaOH. Viscosity was measured at 25 °C, spindle #S00, rotational speed, *120 s^{-1}, **220 s^{-1}

Among all the five ink formulations, the effect of the pH on the ink viscosity was pronounced. A nonlinear relation between pH and viscosity was found. The higher ink viscosity was found in the magenta and yellow inks having the higher pHs in general. The yellow ink No.3 ink has pH = 7.88, viscosity = 4.23 mPa s while the no.1 ink has pH = 7.25, viscosity = 7.88 mPa s. In theory, increases in the ink viscosity could possibly be caused by the emulsion binder in the ink. The binder used, Printofix binder is a self-crosslinking acrylate-based copolymer dispersion with butadiene. The emulsion polymer contains the large fractions of hydrophilic (typically carboxyl-rich) monomers. This high degree of hydrophilicity means that the particulate nature of the dispersion is lost when the acidic dispersion (pH<7) is added to alkaline environment of the ink formulation (pH>7). That means, when the emulsion polymer binder is in the acidic condition, the polymer can coagulate and then precipitate. When NaOH solution was added to the emulsion inks, the emulsion polymer chains can better disentangle and disperse which allow the pigment

particles to be dispersed in the emulsion system. The resulting structures, which range from massively swollen polymer networks to polymer chain dissolved in the aqueous phase, influence the rheology of the ink formulation. Apart from the increase in the viscosity of aqueous phase due to dissolved polymer molecules, which are stiff chain at the pH of the ink formulation, polymer bridges also form between the pigment particles [6]. Because of the acrylate emulsion polymer having the pH of 6.14 and the addition of alkaline solution (10% w v^{-1}NaOH) to make the pH of the inks to be greater than 7, both conditions affect pH and viscosity of the inks, therefore, the formulations 4 and 5 were not adjusted with the alkaline solution (10% w v^{-1} NaOH) for comparison of the ink properties. The ink formulations No.1 and No. 2 gave very high viscosity in all 6 color formulations. The variables so designed generated high viscosity and reduced the extent of jettability. In the same manner, ink formulations No. 3, 4, 5 are also to be discussed about their jettability more precisely later.

Surfactant is one ingredient for delivering the pigment and the binder from the ink to substrate through the print head. The low HLB surfactant is used to lower the surface tension, so the ink can wet the nozzle capillary to establish and maintain the meniscus at the nozzle tip. The low HLB surfactant is also a major factor which determines the interaction between the ink and the substrate; therefore it controls or affects wetting, bleeding, dot-gain, dot quality and ultimately the image quality [7]. The low HLB surfactant, surfynol 104 (HLB = 5), 0.1% by weight is used to reduce the surface tension of the ink system as shown in the result with a range 39 to 46 mN m^{-1}.

Printofix 710 binder, the binder for the current inkjet ink controls the viscosity of the system and promotes droplet formation. The polymer also serves to bind the colorant and provides the adhesion to the surface. It is also responsible for other properties for ink applications. In common with other ingredients in ink, the binder must exhibit good stability upon storage and during use. The binder rheological properties influence jet break-up and high end use performance, such as good adhesion, are constrained by the low viscosity requirements of the fluid required for printer operation. When this is combined with the application of a thin film in a form of a dot, it proves to be an extremely demanding set of properties required for the polymer.

Jetting behavior

The jetting patterns of black, cyan, light cyan, magenta, light cyan and yellow colors of the ink formulations 3, 4 and 5 are shown in Figure 1. The ink formulations 3 and 4 did not produce the complete patterns for all color inks. Unlikely, the printed test patterns by ink formulation 5 produced no missing spots or lines but smooth and well-defined lines and straight borders in all six color inks.

The jetting failure of the black ink formulation was not detected for the ink viscosity and surface tension in the range 3.00 to 3.27 mPa s and 38.7 to 40.6 mN m^{-1} which possessed the Newtonian fluid. For the cyan ink formulation, the jetting failure was, however, detected in the ink formula 3 with the ink viscosity equaling to 3.86 mPa s. The printed pattern showed a nearly complete jetting pattern for the ink viscosity and surface tension in the range of 2.85– 3.33 mPa s and 43.1– 44.4 mN m^{-1}, a Newtonian fluid.

The jetting failure in the light cyan ink formulation was detected for all ink formulations except ink formulation 5. That is, the complete jetting and printed pattern was found in ink formulation 5 with the ink viscosity and surface tension, in a range of 2.81 to 3.01 mPa s and 39.9 to 42.3 mN m^{-1}, respectively, as mentioned earlier. The complete failure of the jetting and printed pattern of ink formulation 3 could be caused by the clogging resulted from the pH effect.

The jetting failure of the magenta ink was detected in ink formulations 3 and 4. The magenta ink color in ink formulation No.3 had pH = 7.47 and viscosity = 18.7 mPa s, a very high value and this causes jetting problem. Both magenta ink formulations showed the higher viscosity which made both inks an injection problem from the nozzle. The ink formulation 5 showed the complete jetting and printed pattern with an ink viscosity = 3.44 mPa s and surface tension = 42.1 mN m^{-1}, a Newtonian fluid as well.

The jetting failure of the light magenta ink formulation was detected in the ink formulation 3 and a large amount of jetting failure found also in the ink formulation 4. Both ink formulations showed the shear-thickening fluid property. The ink formulation 5 showing the complete jetting and printed pattern with the ink viscosity of 2.78 mPa s and surface tension at 41.3 mN m^{-1} was found with the Newtonian fluid property. Likewise, the jetting and printed failure pattern was detected in the yellow ink for the ink formulations 3 and 4. The jetting failure of the ink formulation 3 could possibly be caused by a flow problem of its ink. The complete jetting and printed pattern in the ink formulation 5 was obtained with the ink viscosity of 3.1 mPa s and surface tension of 45.5 mN m^{-1} with the Newtonian fluid.

Viscosity and surface tension are the controlling physical properties for drop formation. With respect to the latter, its dynamic value is important because of the very short time of flight available for chemical species to migrate to the surface of the drop. Thus its value tends to be near that of water. The static value plays a role in preventing the ink from weeping out of the print head when not jetting and the wetting the medium for good penetration. Viscosity affects jet dynamic via (1) viscous damping of the generated capillary wave, (2) the jet's velocity, which in turn changes its break-off length, and more importantly (3) the voltage window over which

stable stimulation occurs without satellite formation of ink drops.

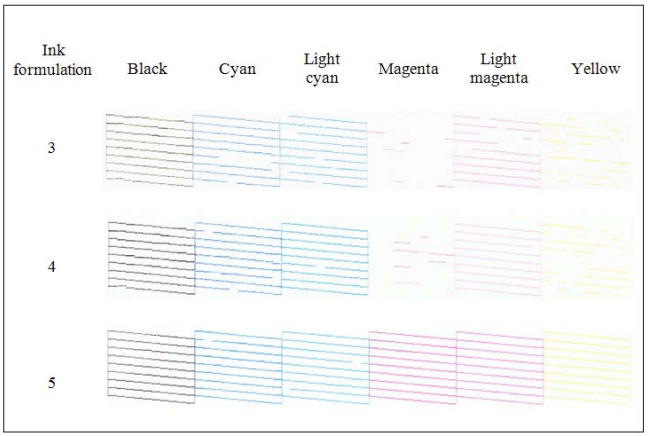

Figure 1 *The print patterns of the ink formulations*

Assessment of the jettability of inks is essential in the process of developing ink formulations and in the process of verifying suitability of inks for print-head assemblies. Currently, evaluation of jettability of inks has largely relied on testing the inks in the print-head assemblies concerned, which, whilst being a reliable method, does have its drawbacks. Thus, there is a high level of risk of the inks of poor performance properties damaging the print head. Lin and He [8] suggested that assessment of the jettability of inks through the creation of a "jettability plot" or "operation window plot" using easily measurable properties such as viscosity and surface tension of the ink. Thus, for each print-head assembly, a jettability plot can be created which contains jettable and un-jettable regions. Consequently, the assessment of the jettability of an ink can be achieved by measuring the viscosity and surface tension of the ink followed by determination of the region the viscosity/surface tension combination falls in.

The criteria used to identify the two regions are based on the results as shown in Figure 1. Figure 2 illustrates the operation window plots of ink viscosity vs. ink surface tension to determine jettable region as shown by the two oval boundaries and un-jettable region outside the two oval boundaries. The big oval is for the six experimental ink sets while the small oval is for Epson commercial ink set. One can see that within the regimes of viscosity, the commercial ink set has a narrow map while the experimental ink sets have the wide map.

Considering velocity and jettability of the ink, it is observable from the experiment that drop velocity produced by a pressurized ink-jet nozzle is expressed by two empirical constants; the fluid parameters of pressure, viscosity, and density; and the nozzle parameters. Le [9] stated formerly that the research and commercial inkjet print head eject at the rate of faster than 6000 drops s^{-1} with a measured ink channel of 0.001 inch in length and 25–30 μm in diameter. It is anticipated that at the current technology, the speed of drop ejection rate is far faster with finer droplet size in the femto scale. Even the latest piezo and thermal printing for graphic arts, the smallest size is one picoliter, they are 1000 times larger than the femto range. On the speed or frequency, the highest level is 25 KHz

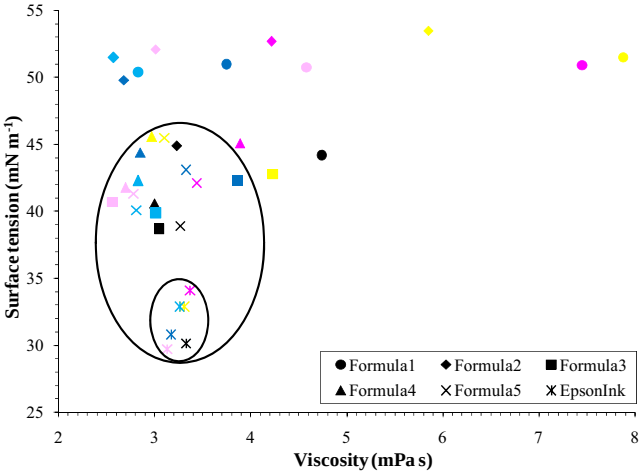

Figure 2 *Operation windows (the color legends represent the ink colors)*

Applied pressure to the drops depends primarily on the shape and size of the nozzle and on fluid viscosity. In addition, the forced oscillation to cause a separation length of a jet is related to the voltage applied to a piezoelectric crystal, to disturbance growth rate, and to velocity. This condition is applicable to "normal" liquids (those having good stream stability) in this study having viscosities between 2–4 mPa s and dynamic surface tensions between 25 and 45 mN m^{-1}. Furthermore, the stream stability of the polymer solutions depends inversely on concentration and molecular weight which is related with the polymer viscoelastic character. Jetting reliability of the present binder is stable because it has a relatively low molecular weight that shall not cause nozzle blockage due to deposition of the binder when it was forced to release solvent or diluent in the ink.

Particle sizes and Zeta potential

Viscosity and surface tension are found to be the controlling physical properties for drop formation and ejection; particle size and zeta potential are also the important factors for inkjet ink. The particle sizes of the inks must be measured after filtration to check for the oversized ink particles in a cartridge. The ink large particle sizes may clog the orifice of the printer during printing therefore filtration is a necessary requirement before printing. The six color inks have different average particle diameters depending on the types of pigments. The average particle sizes of the resulting inks and the binder are in the range of 100–300 nm and 160–300 nm, respectively. The zeta potential values of the ink

formulations are in the range of (-35) to (-50) mV in that the inks have been charged negatively resulting from the presence of the sulphonic acid group ($-SO_3^-$). Zeta-potential of acrylate/styrene copolymer emulsion binder is also negative having a value of (-38) mV. Moreover, a dispersant on the pigment surface can migrate from the pigment surface during the ink preparation as indicated by a decrease in a zeta-potential from (-35) to (-50) mV compared to the zeta-potential of pigment dispersions (-50) to (-55) mV. When the density of the ink was 1 g cm^{-3}, the square root of surface tension to viscosity ratios of the inks is relatively constant except that of magenta color. With the same ink chemistry, the penetration of the five inks is similar. In summary, the ink properties mentioned above confirm the acceptable behavior of the inkjet ink for a printing system.

Conclusion

Four surface-modified pigment dispersions were used to formulate six-color inkjet inks (black, cyan, magenta, yellow, light cyan and light magenta) with Printofix 710 binder with a pigment-to-binder ratio of 1:2. Specified amounts of diethylene glycol and glycol were used to fine tune the ink viscosity, surface tension and jettaiblity compared with Eposn ink via a test pattern images. Ink formulation 5 gave the better jettability pattern of the six inks. The formulation exhibited the Newtonian fluid property in each color. The color inks had ink viscosity in the range of 2.78–3.33 mPa s while the surface tension of the inks is in the range of 38.7–45.5 mN m^{-1}. The average ink particle size and the Zeta potential of the formulated inks are the range of 100–300 nm and (-35) to (-50) mV, respectively. The operation window plot of ink viscosity and surface tension of ink formulation indicates the jettability window which was conformed to the print patterns of all color inks in the ink formulation 5.

Acknowledgements

The authors would like to thank Graduate School of Chulalongkorn University, The Thailand Research Fund under the Contract number RTA5080004 for supporting this research; to Associate Professor Supanee Chayabura, Ph.D., for supporting the first author and providing ink preparation facility for this research. Great appreciation is due to the Department of Imaging and Printing Technology for providing the research facilities through-out the research. Sincere thanks go to the East Asiatic (Thailand) Public Co., for supporting the surface-modified pigments; to South City Petrochem Co., Ltd. for supporting Surfynol 104, and to Clariant Chemical Ltd., for supporting Printofix binder 710.

References

1. Y. Yu, and F.V. Gottberg. Surface modified color pigments for inkjet ink application. *IS&Ts NIP 16 International Conference on Digital Printing Technologies*: pp. 512–515 (2000).
2. Y. Yu, and F.V. Gottberg. Titration of Surface Modified Pigment Particles. *IS&Ts NIP 20 International Conference on Digital Printing Technologies*: pp. 769–772, (2004)
3. S. Daplyn, and L. Lin. Evaluation of pigmented ink formulations for jet printing onto textile fabrics. *Pigment & Resin Technology* 32(5): 307–318 (2003).
4. S. Kiatkamjornwong, P. Putthimai and H. Noguchi. Comparison of textile print quality between inkjet and screen printings. *Proceedings of IS&Ts NIP 19: International Conference on Digital Printing Technologies*: pp. 638–642 (2003).
5. S. Leelajariyakul, H. Noguchi and S. Kiatkamjornwong. Surface-modified and micro-encapsulated pigmented inks for inkjet printing on textile fabrics**.** *Progress in Organic Coatings* 62(2):145–161 (2008).
6. D. Urban. and K. Takamura. *Polymer dispersion and their industrial application*. Weinheim. Wiley-VCH Verlag GmbH: pp. 88–89 (2002).
7. Z. Fu Pigmented ink formulation. In H. Ujiie (ed.), *Digital printing of textiles*, Cambridge: Woodhead Publishing. pp. 218–226 (2006).
8. L. Lin. and W.A. He. Novel method for the evaluation of jettability. *IS&T's NIP24: International Conference on Digital Printing Technologies and Digital Fabrication*: p. 129 (2008).
9. H.P. Le. Progress and trends in ink-jet printing technology. In E. Hanson (ed.), *Recent progress in inkjet technologies II*, Springfield: Society of Imaging Science and Technology pp. 5 –6. (1999).

Biography

Pichet Thananpongjongruay received his Bachelors Degree in Chemistry from the Faculty of Science, Silapokorn University in 2005. While working in the Color Center, Silapokorn University, he furthered his study in Masters Degree in Imaging Technology at the Department of Imaging and Printing Technology, Faculty of Science, Chulalongkorn University in 2006 and finished the Degree in 2010. His research interest is in inkjet technology and its application to textile fabrics. Currently, he is working as a researcher in Pan Group Companies.

Hiromichi Noguchi received the Ph.D. degree from Tokyo Institute of Technology in 1976 in the research area of thermodynamics of polymer solution. He has worked on imaging materials in pigment companies and in inkjet companies for traditional printing systems and inkjet system. Noguchi has worked as a visiting professor at Chulalongkorn University since 1999 on inkjet printing technology. He works for textile inkjet

and nano-metal ink by collaborating with chemical companies in Japan and Chulalongkorn University for Thai printing industry.

Suda Kiatkamjornwong is currently a Full Professor (PC 11or A1) of Polymer Science and Engineering at the Department of Imaging and Printing Technology, at the Faculty of Science, Chulalongkorn University, Bangkok, Thailand. She obtained her B.Sc. and M.Sc. degrees in Chemistry and Physical Chemistry, respectively, from the Faculty of Science, Chulalongkorn University, and her Ph.D. degree in Polymer Science and Engineering from Lehigh University, U.S.A. in 1983. Her research interests are in the areas of superabsorbent polymers, imbiber beads, modification of green polymers, digital printing and environmental friendly polymers and printing materials. Suda Kiatkamjornwong is the corresponding author of many articles in ISI journals and can be contacted at ksuda@chula.ac.th.

Use of kapok pulp to improve properties of recycled paper

Sannipa Pattanapiyasup, Sudtatip Lekhalawan, Supanee Phiphatwitthay, Somporn Chaiarrekij* and Suda Kiatkamjornwong
Department of Imaging and Printing Technology, Faculty of Science, Chulalongkorn University, Bangkok 10330 Thailand,
****Corresponding author, E-mail: Huaja@hotmail.com***

Abstract

Using recycled paper is the one way to reduce environment problems. However, higher cycle numbers of recycling leads to reduction of paper strength; thus, improvement of recycled paper properties is very important. One way to improve strength of recycled paper is to use kapok pulp because kapok is the long fiber and a large number of kapok fibers are found in Thailand. In this study, paper was made using kapok and recycled pulp to compare with those using softwood-to-recycled pulp ratios at 100:0, 10:90, 20:80, 30:70 and 0:100. As a result, it was found that recycling up to three cycles had a small effect on paper properties. Higher amount of kapok pulp in the mixed pulp between kapok pulp and recycled pulp increased porosity, opacity, density and tensile index but decreased brightness and whiteness of handsheets. On the other hand, higher amount of softwood pulp led to higher tear index only. So, the combination and amount of pulps used is really dependent on the final paper property required.
Keywords: Recycled paper, Kapok, Softwood, Paper properties

Introduction

Waste paper recycling now becomes remarkably important due to environmental concerns, increasing paper consumption, government regulation, deforestation, fiber shortage in some countries and so on. However, the challenging part of waste paper recycling is the quality improvement of paper made from these recycled fibers since the pulp quality especially the paper strength is normally decreased after repeated recycling. Generally, the way to improve recycled pulp strength can be done by refining that pulp before making it into sheets of paper. By doing so, recycled pulp is fibrillated and this can increase the surface areas of fibers available for water absorption and bonding. Another way of improving the strength property of paper made from recycled fibers is to mix the recycled pulp with the virgin pulp. Softwood pulp can be a good candidate for this purpose since paper made from softwood pulp is generally stronger than paper made from hardwood pulp due to the higher fiber length of softwood fiber as compared to hardwood fiber. However, Thailand as one of the tropical countries usually has no softwood pulp and need to import from abroad. So, finding a new fiber source in Thailand to do this task for softwood fiber is incredibly fascinating.

Kapok fiber abundantly found in Thailand might be used as a substitute of the softwood fiber to improve the strength of recycled pulp due to its remarkably high fiber strength. In general, kapok fiber is hollow with a thin fiber wall and 8-30 mm long. Though kapok fiber has high tensile strength but it is very brittle. As such, kapok fiber is rarely used in textile industry but it is used as stuffing for pillow and mattress instead due to its light weight. Taking the advantages of its hydrophobicity, kapok fiber is also used as stuffing for life jacket as well. Also, the papermaking potential of kapok fibers was investigated by Chaiarrekij *et al*, [1]. It was found that kapok fiber can be a potential fiber source for papermaking in Thailand. Paper made from kapok pulp has high tensile and burst strengths and its moderately hydrophobic surface; kapok paper might be potentially used as a packaging paper.

This research was thus aimed to study the effects of kapok pulp on improving properties of paper made from recycled pulp and then compared them with the results obtained from using softwood pulp instead of kapok pulp. If kapok pulp seems to provide the competitive results then this might provide a good opportunity to increase the use of recycled paper in Thailand.

Experimental

The experiment was divided into 3 parts as follows:

Preparation of kapok pulp
Since kapok fibers were so difficult to be dampened, kapok fibers were first soaked in 5% (w/v) sodium hydroxide solution for 2 weeks [2]. Then, they were cut into small pieces around 1.0 cm long. These kapok fibers were then pulped at 120 °C for 2 hours using 20% (w/v)

of sodium hydroxide based on O.D. (oven dried) fiber weight. Kapok pulp was then washed and refined twice using a disc refiner with the disk gap of 10/1000 inch. Then, the refined kapok pulp was disintegrated at 80°C for 5 min to remove latency [3].

Preparation of softwood pulp

Commercial softwood pulp was soaked overnight. Then, it was beaten using a valley beater until pulp freeness reached the value of 350±50 ml.

Preparation of recycle pulp and handsheet making

Commercial A4 paper sheets from the same brand were cut into small pieces and soaked overnight. Then, these paper sheets were re-pulped at 50°C for 90 min at the speed of 500 rpm. The pulp was then divided into three parts. The first part was mixed with kapok pulp with the ratios of kapok pulp: recycled pulp of 0:100, 10:90, 20:80 and 30:70. The second part was also followed that had been done in the first part but the kapok pulp was changed to softwood pulp instead. The remaining recycled pulp was then made into handsheets and dried at 90 °C for around 6 min.

All these handsheets made from only recycled pulp was then repulped again following the same path as described earlier up to 3 cycles. For each cycle, paper was made from the mixed pulps using the ratio mentioned earlier. Finally, all these handsheets were tested for paper properties like brightness, opacity, density, porosity tensile and tear strengths and so on. The results were then compared as to examine the effects of numbers of recycling cycles. The effects of kapok and softwood pulps on paper properties were also compared.

Results and discussion

Brightness

As shown in Figure 1, the handsheets made from 100% recycled paper were the brightest while those made from 100% kapok pulp had the lowest brightness. Also, the effect of recycling on brightness was so small as compared to the effects of pulp types. Clearly, the effect of kapok pulp on brightness is more pronounced than softwood pulp. Brightness was decreased more by adding kapok pulp as compared to those of the softwood pulp at the same ratio. This might be because kapok fibers are so yellowish. So, adding a higher amount of kapok can lead to lower brightness eventually.

Whiteness

Figure 2 illustrates the effects of recycling, kapok pulp and softwood pulp on whiteness. It was apparent that the results obtained from whiteness followed the same trend as in the case of brightness with the same explanation.

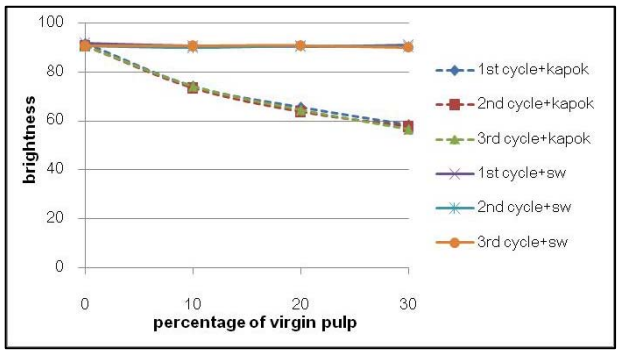

Figure 1 The Effects of Recycling, Kapok Pulp and Softwood (SW) Pulp on Brightness (Kapok and SW pulps have 19.15 and 84.31% brightness, respectively.)

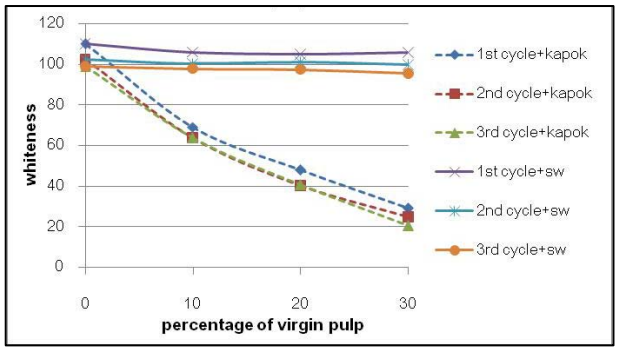

Figure 2 The Effects of Recycling, Kapok Pulp and Softwood (SW) Pulp on Whiteness (Kapok and SW have 72.62 and - 83.44%, respectively.)

Opacity

Opacity of the handsheets made from 100% recycled pulp was the highest and was higher than those made from kapok and softwood pulps, respectively (Figure 3). The effect of numbers of recycling on opacity was small as compared to the effects of pulp type and percentage. Unlikely, increasing amount of kapok pulp in the pulp mixture provided the handsheets with higher opacity while the opposite results were obtained from the softwood pulp. Opacity could be lower when longer fibers like softwood and kapok pulps were added into the pulp mixture since the surface areas for light scattering were smaller. This could be clearly seen for the case of softwood pulp. When the kapok pulp was added, yellow-

ness of the pulp seemed to overcome the effects on its length and this led to lower opacity.

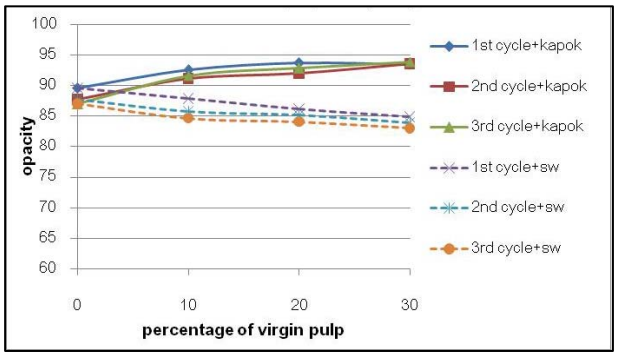

Figure 3 The Effects of Recycling, Kapok Pulp and Softwood (SW) Pulp on Opacity (Kapok and SW pulps have 69.19 and 82.05%, respectively.)

It can be seen from Figure 4 that the paper made from 100% softwood pulp had the highest density while that from 100% kapok pulp had the lowest density. Although both pulps contained long fiber which should contribute to the higher density due to more contact areas for inter-fiber bonding, kapok fibers were then entangled and provided a poor paper formation. This might be the reason for the low density of 100% kapok handsheets. However, the effect of recycling on density was quite small as compared to the effects of pulp type and the amount of pulp added. The more kapok or softwood pulp was added, the denser the handsheet became. This might be because the better fiber bonding was obtained by adding long fibers into the short fibers of 100% recycled pulp.

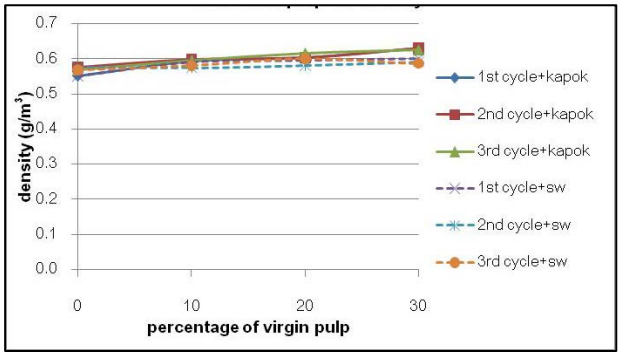

Figure 4 The Effects of Recycling, Kapok Pulp and Softwood (SW) Pulp on Density (Kapok and SW pulps have 0.525 and 0.627g/m³.)

Porosity

As can be seen from Figure 5, it was clear that recycled fibers produced the paper with the lowest porosity because these short fibers would fill up the voids or pores in the handsheets. Kapok pulp provided handsheets with lowest porosity as compared to softwood pulp probably because of its longer fiber length. Recycling paper up to 3 cycles did not have a strong impact on porosity while the pulp type and the amount added affected the porosity. Since kapok pulp itself had the lowest porosity, the paper containing kapok fiber had much higher porosity than that containing softwood pulp at the same ratio.

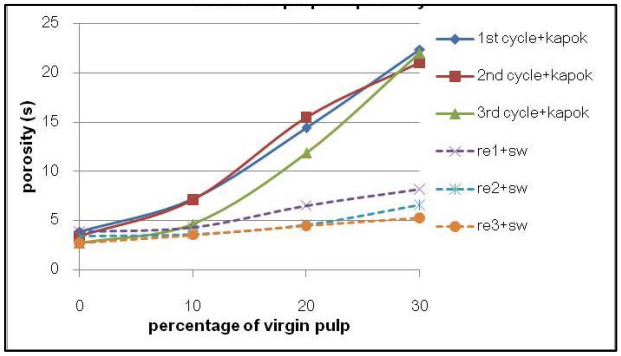

Figure 5 The Effects of Recycling, Kapok Pulp and Softwood (SW) Pulp on Porosity (Kapok and SW pulps have 38.2 and 24.4 s, respectively.)

Tensile index

Tensile index is defined as tensile strength divided by grammage. The results from Figure 6 indicate that paper made from 100% kapok pulp was strongest as depicted by its highest tensile index due to its outstanding fiber strength. Paper made from 100% recycled pulp was weakest as expected since fibers were destroyed during the recycling process. Also, the numbers of recycling cycles had a small impact on tensile index. Both kapok and softwood pulps seemed to improve the tensile strength of recycle paper but the effects of kapok pulp is more powerful than softwood pulp in term of increasing tensile strength of papers.

Tear index

The effects of number of recycling and pulp type on tear index are shown in Figure 7. Tear index is defined as tear resistance divided by grammage. It was clear that the number of recycling had no effect on tear index. Paper made from only softwood fibers had a highest tear index while the tear index of paper made from 100% kapok pulp was close to those from the recycled pulp. The lowest tear index was found when 100% recycled fibers was used to make the paper. Adding the kapok fibers in the recycled pulp did not provide any benefit in terms of tear index improvement; however, tear index was slightly improved when softwood pulp was added into the recycled pulp.

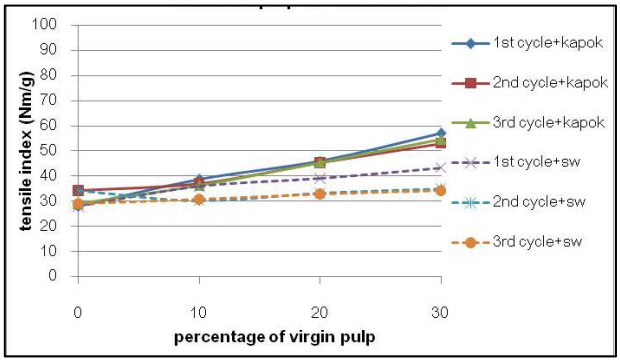

Figure 6. The Effects of Recycling, Kapok Pulp and Softwood (SW) Pulp on Tensile Index (Kapok and SW pulps have 86.35 and 51.85 N m/g, respectively.)

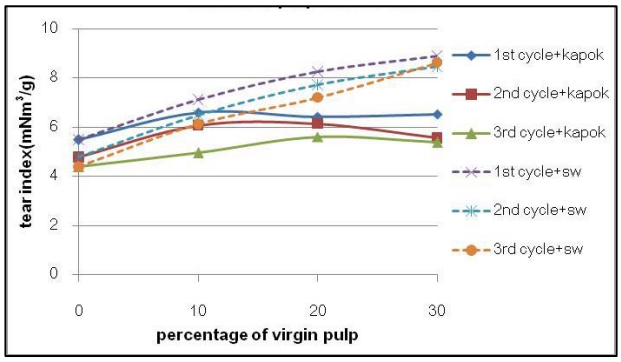

Figure 7 The Effects of Recycling, Kapok Pulp and Softwood (SW) Pulp on Tear Index (Kapok and SW pulps have 6.622 and 53.037 mN m^3/g, respectively.)

Conclusion

Recycling seemed to have a small impact on paper properties. However, only up to three cycles of recycling were evaluated in this study. If the number of recycles increases, the effects of recycling might be possibly detected. Increasing amount of the kapok pulp used with the recycled pulp brought about higher porosity, opacity, density and tensile index but lower brightness and whiteness of the handsheets. Using higher amount of softwood pulp led to higher tear index only. So, using the kapok pulp or softwood pulp or both with the proper amount of the pulp is definitely dependent on the final paper property required.

Acknowledgements

Financial support from the Thailand Research Fund (Research code: RTA5080004) is very grateful. Some research facilities provided by the Product and Development Center of the SGC Paper Public Company Limited were also thankful. Many thanks are due to the Department of Imaging Science and Technology for full support of research facilities.

References

1) Chaiarrekij, S., Wongsaisuwan, U., and Watchanakij, S., "Paper Making from Kapok Fibers", Thailand Petty Patent Number: 4279. Issued date: June 13 (2008).
2) E. Sjöström. *Wood Chemistry-Fundamentals and Applications*, 2nd ed., Academic Press, San Diego (1993).
3) S. Chaiarrekij, A. Apirakchaiskul, K. Suvarnakich, and S. Kiatkamjornwong. Kapok I: Properties Investigation of Kapok Fiber as a Potential Pulp Source for Papermaking, BioResources, in press.

Biography

Sannipa Pattanapiyasup, Sudtatip Lekhalawan and Supanee Phiphatwitthay were senior students at the Department of Imaging and Printing Technology, Faculty of Science, Chulalongkorn University, Bangkok, Thailand when they conducted this research. They won the first Place Hitachi Trophy in Applied Science and Technology given at the Science Forum 2011, Faculty of Science, Chulalongkorn University on March 11, 2011. They just recently got their B.Sc. degrees in Imaging and Printing Technology, Faculty of Science, Chulalongkorn University. Ms. Pattanapiyasup is planning to continue her study in MBA program in the USA this year while Ms. Phiphatwitthay will continue her M.Sc. degree in the Pulp and Paper Technology Program at Asian Institute of Technology (AIT) this coming August 2011.

Somporn Chaiarrekij is currently a faculty member at the Department of Imaging and Printing Technology, Faculty of Science, Chulalongkorn University, Bangkok, Thailand. She got her B.Sc. degree in Photographic Science and Printing Technology from Faculty of Science, Chulalongkorn University and M.Sc. degree in Paper Science and Engineering from Western Michigan University, USA. Her research interests are in the areas of waste paper recycling and deinking.

Suda Kiatkamjornwong is currently a full Professor (PC 11) of Polymer Science and Engineering at the Department of Imaging and Printing Technology, Faculty of Science, Chulalongkorn University, Bangkok, Thailand. She obtained her B.Sc. and M.Sc. degrees in Chemistry and Physical Chemistry, respectively, from the Faculty of Science, Chulalongkorn University, and her Ph.D. degree in Polymer Science and Engineering from Lehigh University, USA, in 1983. Her research interests are in the areas of superabsorbent polymers, imbiber beads, modification of green polymers, digital

printing and environment in polymers and printing. Suda Kiatkamjornwong is the corresponding author of many articles in ISI journals and can be contacted at ksuda@chula.ac.th.

สิทธิบัตร

สถาบันทรัพย์สินทางปัญญาแห่งจุฬาลงกรณ์มหาวิทยาลัย
Chulalongkorn University Intellectual Property Institute

สิงหาคม 2553

เรื่อง ขอผ่อนผันการส่งเอกสารประกอบคำขอรับสิทธิบัตร ครั้งที่ 1

เรียน ผู้อำนวยการสำนักสิทธิบัตร

ด้วยสถาบันทรัพย์สินทางปัญญาแห่งจุฬาลงกรณ์มหาวิทยาลัยได้รับมอบหมายจากจุฬาลงกรณ์มหาวิทยาลัย สำนักงานกองทุนสนับสนุนการวิจัย และสำนักงานพัฒนาวิทยาศาสตร์และเทคโนโลยีแห่งชาติ ให้ดำเนินการยื่นคำขอรับสิทธิบัตร เรื่อง "พอลิเมอร์คอมพอสิตดูดซึมน้ำมากที่แตกสลายได้ด้วยตนเองโดยการกระตุ้นด้วยรังสีอัลตราไวโอเลต และกรรมวิธีการผลิตพอลิเมอร์ดังกล่าว" โดยมีข้าพเจ้านายมงคล แก้วมหา ตัวแทนสิทธิบัตร เลขที่ 1453 เป็นผู้ดำเนินการ ซึ่งขณะนี้อยู่ระหว่างดำเนินการให้ผู้ที่เกี่ยวข้องลงนามในสัญญาโอนสิทธิในการขอรับสิทธิบัตร และหนังสือมอบอำนาจ ซึ่งจำเป็นที่จะต้องใช้ระยะเวลาหนึ่งในการดำเนินการ แต่เนื่องจากการประดิษฐ์นี้ ทางผู้ประดิษฐ์มีความประสงค์ที่จะเผยแพร่ผลงานวิจัย ซึ่งหากมีการนำไปเผยแพร่ผลงานก่อนที่จะได้มีการยื่นคำขอรับสิทธิบัตร ข้าพเจ้าเกรงว่าจะมีผลต่อการพิจารณารับจดทะเบียนของคำขอรับสิทธิบัตรฉบับนี้ได้

ด้วยเหตุผลดังกล่าวข้างต้น ข้าพเจ้าจึงเรียนมาเพื่อโปรดพิจารณาอนุมัติผ่อนผันการยื่นเอกสารประกอบคำขอรับสิทธิบัตรพร้อมกับคำขอรับสิทธิบัตรด้วย จักขอบพระคุณยิ่ง

ขอแสดงความนับถือ

(นายมงคล แก้วมหา)
ผู้รับมอบอำนาจ
ตัวแทนสิทธิบัตร เลขที่ 1453

อาคารจัตุรัสจามจุรี ชั้น 12 ยูนิต 13 ถนนพญาไท เขตปทุมวัน กรุงเทพฯ 10330 โทรศัพท์ 0-2160-5340-1 โทรสาร 0-2160-5343
Chamchuri Square Building 12nd Floor, 13th Unit, Phyathai Road, Bangkok 10330
Tel +66(0)-21605340-1 Fax +66 (0)-2160-5343

คำขอรับสิทธิบัตร/อนุสิทธิบัตร

☑ การประดิษฐ์
☐ การออกแบบผลิตภัณฑ์
☐ อนุสิทธิบัตร

ข้าพเจ้าผู้ลงลายมือชื่อในคำขอรับสิทธิบัตร/อนุสิทธิบัตรนี้ ขอรับสิทธิบัตร/อนุสิทธิบัตร ตามพระราชบัญญัติสิทธิบัตร พ.ศ. 2522 แก้ไขเพิ่มเติมโดยพระราชบัญญัติสิทธิบัตร (ฉบับที่ 2) พ.ศ 2535 และพระราชบัญญัติสิทธิบัตร (ฉบับที่ 3) พ.ศ 2542

สำหรับเจ้าหน้าที่	
วันรับคำขอ 2 ... 2553 วันยื่นคำขอ	เลขที่คำขอ 1301001473
สัญลักษณ์จำแนกการประดิษฐ์ระหว่างประเทศ	
ใช้กับแบบผลิตภัณฑ์ ประเภทผลิตภัณฑ์	
วันประกาศโฆษณา	เลขที่ประกาศโฆษณา
วันออกสิทธิบัตร/อนุสิทธิบัตร	เลขที่สิทธิบัตร/อนุสิทธิบัตร
ลายมือชื่อเจ้าหน้าที่	

1.ชื่อที่แสดงถึงการประดิษฐ์/การออกแบบผลิตภัณฑ์
พอลิเมอร์คอมพอสิตดูดซึมน้ำมากที่แตกสลายได้ด้วยตนเองโดยการกระตุ้นด้วยรังสีอัลตราไวโอเลต และกรรมวิธีการผลิตพอลิเมอร์ดังกล่าว

2.คำขอรับสิทธิบัตรการออกแบบผลิตภัณฑ์นี้เป็นคำขอสำหรับแบบผลิตภัณฑ์อย่างเดียวกันและเป็นคำขอลำดับที่
ในจำนวน คำขอ ที่ยื่นในคราวเดียวกัน

3.ผู้ขอรับสิทธิบัตร/อนุสิทธิบัตร และที่อยู่ (เลขที่ ถนน ประเทศ) ดูที่หน้า 3	3.1 สัญชาติ
	3.2 โทรศัพท์
	3.3 โทรสาร
	3.4 อีเมล์

4.สิทธิในการขอรับสิทธิบัตร/อนุสิทธิบัตร
☐ ผู้ประดิษฐ์/ผู้ออกแบบ ☑ ผู้รับโอน ☐ ผู้ขอรับสิทธิโดยเหตุอื่น

5.ตัวแทน(ถ้ามี)/ที่อยู่ (เลขที่ ถนน จังหวัด รหัสไปรษณีย์) นายมงคล แก้วมหา สถาบันทรัพย์สินทางปัญญาแห่งจุฬาลงกรณ์มหาวิทยาลัย อาคารจัตุรัสจามจุรี ชั้น 12 ยูนิต 13 ถนนพญาไท แขวงปทุมวัน เขตปทุมวัน กรุงเทพฯ 10330	5.1 ตัวแทนเลขที่ 1453
	5.2 โทรศัพท์ 0-2160-5340-2
	5.3 โทรสาร 0-2160-5343
	5.4 อีเมล์

6.ผู้ประดิษฐ์/ผู้ออกแบบผลิตภัณฑ์ และที่อยู่ (เลขที่ ถนน ประเทศ)
ดูที่หน้า 3

7. คำขอรับสิทธิบัตร/อนุสิทธิบัตรนี้แยกจากหรือเกี่ยวข้องกับคำขอเดิม
ผู้ขอรับสิทธิบัตร/อนุสิทธิบัตร ขอให้ถือว่าได้ยื่นคำขอรับสิทธิบัตร/อนุสิทธิบัตรนี้ ในวันเดียวกับคำขอรับสิทธิบัตร
เลขที่ วันยื่น เพราะคำขอรับสิทธิบัตร/อนุสิทธิบัตรนี้แยกจากหรือเกี่ยวข้องกับคำขอเดิมเพราะ
☐ คำขอเดิมมีการประดิษฐ์หลายอย่าง ☐ ถูกคัดค้านเนื่องจากผู้ขอไม่มีสิทธิ ☐ ขอเปลี่ยนแปลงประเภทของสิทธิ

หมายเหตุ ในกรณีที่ไม่อาจระบุรายละเอียดได้ครบถ้วน ให้จัดทำเป็นเอกสารแนบท้ายแบบพิมพ์นี้โดยระบุหมายเลขกำกับข้อและหัวข้อที่แสดงรายละเอียดเพิ่มเติมดังกล่าวด้วย

8.การยื่นคำขอนอกราชอาณาจักร

วันยื่นคำขอ	เลขที่คำขอ	ประเทศ	สัญลักษณ์จำแนกการประดิษฐ์ระหว่างประเทศ	สถานะคำขอ
8.1				
8.2				
8.3				

8.4 ☐ ผู้ขอรับสิทธิบัตร/อนุสิทธิบัตรขอสิทธิให้ถือว่าได้ยื่นคำขอนี้ในวันที่ได้ยื่นคำขอรับสิทธิบัตร/อนุสิทธิบัตรในต่างประเทศเป็นครั้งแรกโดย
☐ ได้ยื่นเอกสารหลักฐานพร้อมคำขอนี้ ☐ ขอยื่นเอกสารหลักฐานหลังจากวันยื่นคำขอนี้

9.การแสดงการประดิษฐ์ หรือการออกแบบผลิตภัณฑ์ ผู้ขอรับสิทธิบัตร/อนุสิทธิบัตรได้แสดงการประดิษฐ์ที่หน่วยงานของรัฐเป็นผู้จัด
วันแสดง วันเปิดงานแสดง ผู้จัด

10.การประดิษฐ์เกี่ยวกับจุลชีพ

10.1 เลขทะเบียนฝากเก็บ	10.2 วันที่ฝากเก็บ	10.3 สถาบันฝากเก็บ/ประเทศ

11.ผู้ขอรับสิทธิบัตร/อนุสิทธิบัตร ขอยื่นเอกสารภาษาต่างประเทศก่อนในวันยื่นคำขอนี้ และจะจัดยื่นคำขอรับสิทธิบัตร/อนุสิทธิบัตรนี้ที่จัดทำเป็นภาษาไทยภายใน 90 วัน นับจากวันยื่นคำขอนี้ โดยขอยื่นเป็นภาษา
☐ อังกฤษ ☐ ฝรั่งเศส ☐ เยอรมัน ☐ ญี่ปุ่น ☐ อื่นๆ

12.ผู้ขอรับสิทธิบัตร/อนุสิทธิบัตร ขอให้อธิบดีประกาศโฆษณาคำขอรับสิทธิบัตร หรือรับจดทะเบียน และประกาศโฆษณาอนุสิทธิบัตรนี้ หลังจากวันที่ เดือน พ.ศ
☐ ผู้ขอรับสิทธิบัตร/อนุสิทธิบัตรขอให้ใช้รูปเขียนหมายเลข ในการประกาศโฆษณา

13.คำขอรับสิทธิบัตร/อนุสิทธิบัตรนี้ประกอบด้วย
ก. แบบพิมพ์คำขอ 3 หน้า
ข. รายละเอียดการประดิษฐ์ หรือคำพรรณนาแบบผลิตภัณฑ์ 8 หน้า
ค. ข้อถือสิทธิ 2 หน้า
ง. รูปเขียน 4 รูป 3 หน้า
จ. ภาพแสดงแบบผลิตภัณฑ์
☐ รูปเขียน รูป หน้า
☐ ภาพถ่าย รูป หน้า
ฉ. บทสรุปการประดิษฐ์ 1 หน้า

14.เอกสารประกอบคำขอ
☐ เอกสารแสดงสิทธิในการขอรับสิทธิบัตร/อนุสิทธิบัตร
☐ หนังสือรับรองการแสดงการประดิษฐ์/การออกแบบผลิตภัณฑ์
☐ หนังสือมอบอำนาจ
☐ เอกสารรายละเอียดเกี่ยวกับจุลชีพ
☐ เอกสารการขอนับวันยื่นคำขอในต่างประเทศเป็นวันยื่นคำขอในประเทศไทย
☐ เอกสารขอเปลี่ยนแปลงประเภทของสิทธิ
☐ เอกสารอื่น ๆ

15. ข้าพเจ้าขอรับรองว่า
☑ การประดิษฐ์นี้ไม่เคยยื่นขอรับสิทธิบัตร/ อนุสิทธิบัตรมาก่อน
☐ การประดิษฐ์นี้ได้พัฒนาปรับปรุงมาจาก.....

16.ลายมือชื่อ (☐ ผู้ขอรับสิทธิบัตร / อนุสิทธิบัตร; ☑ ตัวแทน)
นายมงคล แก้วมหา

หมายเหตุ บุคคลใดยื่นขอรับสิทธิบัตรการประดิษฐ์หรือการออกแบบผลิตภัณฑ์ หรืออนุสิทธิบัตร โดยการแสดงข้อความอันเป็นเท็จแก่พนักงานเจ้าหน้าที่ เพื่อให้ได้ไปซึ่งสิทธิบัตรหรืออนุสิทธิบัตร ต้องระวางโทษจำคุกไม่เกินหกเดือน หรือปรับไม่เกินห้าพันบาท หรือทั้งจำทั้งปรับ

3. ผู้ขอรับสิทธิบัตร/อนุสิทธิบัตร และที่อยู่ (เลขที่ ถนน ประเทศ)

จุฬาลงกรณ์มหาวิทยาลัย

อยู่ที่ เลขที่ 254 ถนนพญาไท แขวงวังใหม่ เขตปทุมวัน กรุงเทพฯ 10330

3.1 สัญชาติ ไทย 3.2 โทรศัพท์ 0-2160-5340-2 3.3 โทรสาร 0-2160-5343

สำนักงานกองทุนสนับสนุนการวิจัย

อยู่ที่ ชั้น 14 อาคาร เอส เอ็ม ทาวเวอร์ เลขที่ 979/17-21 ถนนพหลโยธิน แขวงสามเสนใน เขตพญาไท กรุงเทพฯ 10400

3.1 สัญชาติ ไทย 3.2 โทรศัพท์ 0-2278-8200 3.3 โทรสาร 0-2298-0476

สำนักงานพัฒนาวิทยาศาสตร์และเทคโนโลยีแห่งชาติ

อยู่ที่ 111 อุทยานวิทยาศาสตร์ประเทศไทย ถนนพหลโยธิน ตำบลคลองหนึ่ง อำเภอคลองหลวง จังหวัดปทุมธานี 12120

3.1 สัญชาติ ไทย 3.2 โทรศัพท์ 0-2564-7000 3.3 โทรสาร 0-2564-7001-5

6. ผู้ประดิษฐ์/ผู้ออกแบบผลิตภัณฑ์ และที่อยู่ (เลขที่ ถนน ประเทศ)

นางสาวสุดา เกียรติกำจรวงศ์ และ นางสาววลาสินี จิตรบรรพต

อยู่ที่ คณะวิทยาศาสตร์ จุฬาลงกรณ์มหาวิทยาลัย ถนนพญาไท แขวงวังใหม่ เขตปทุมวัน กรุงเทพฯ 10330

นางสาวกนิษฐา บุญภาวาณิชกุล และ นายวิยงค์ กังวานศุภมงคล

อยู่ที่ สำนักงานพัฒนาวิทยาศาสตร์และเทคโนโลยีแห่งชาติ 111 อุทยานวิทยาศาสตร์ประเทศไทย ถนนพหลโยธิน ตำบลคลองหนึ่ง อำเภอคลองหลวง จังหวัดปทุมธานี 12120

รายละเอียดการประดิษฐ์

ชื่อที่แสดงถึงการประดิษฐ์

พอลิเมอร์คอมพอสิตดูดซึมน้ำมากที่แตกสลายได้ด้วยตนเองโดยการกระตุ้นด้วยรังสีอัลตราไวโอเลต และกรรมวิธีการผลิตพอลิเมอร์ดังกล่าว

สาขาวิทยาการที่เกี่ยวข้องกับการประดิษฐ์

การประดิษฐ์นี้อยู่ในสาขาวัสดุศาสตร์ ในส่วนที่เกี่ยวข้องกับพอลิเมอร์ดูดซึมน้ำมาก โดยเฉพาะอย่างยิ่งเกี่ยวข้องกับพอลิเมอร์คอมพอสิตดูดซึมน้ำมากที่สามารถแตกสลายตัวเองได้โดยอาศัยการกระตุ้นด้วยรังสีอัลตราไวโอเลต

ภูมิหลังของศิลปะหรือวิทยาการที่เกี่ยวข้อง

ปัจจุบันพอลิเมอร์ดูดซึมน้ำมาก (Superabsorbent Polymers, SAPs) หรือไฮโดรเจล (hydrogel) เป็นที่สนใจในอุตสาหกรรมหลาย ๆ ด้าน เนื่องจากมีความสามารถในการดูดซึมน้ำได้สูง พอลิเมอร์ดูดซึมน้ำมากมีสมบัติในการบวมน้ำ และสามารถกักเก็บน้ำไว้ในโครงสร้างได้มากกว่า 20 เท่าของน้ำหนักพอลิเมอร์แห้งและไม่ละลายน้ำ

พอลิเมอร์ดูดซึมน้ำมากสามารถนำไปใช้ประโยชน์ได้ในหลาย ๆ ด้าน เช่น ทางการเกษตรกรรม การทำสวนประดับ พอลิเมอร์จะช่วยในการปรับปรุงคุณภาพดิน โดยเพิ่มความสามารถในการกักเก็บน้ำ และปล่อยน้ำสู่ดิน และรากของพืช ซึ่งจะเป็นการรักษาสมดุลของความชื้นในดิน และยังช่วยกักเก็บสารอาหารของพืชซึ่งละลายในเจลพอลิเมอร์ ทางด้านอุตสาหกรรม พอลิเมอร์ดูดซึมน้ำมากสามารถนำมาใช้ในการทำผลิตภัณฑ์เพื่อสุขอนามัย ผ้าอ้อมเด็ก ผ้าอ้อมผู้สูงวัย ผ้าอ้อมผู้ป่วย และกระดาษชำระ เป็นต้น ทางด้านการแพทย์ ได้นำพอลิเมอร์ดูดซึมน้ำมากมาทำผ้าพันแผล (wound dressing) หรือใช้เป็นสารควบคุมอัตราการปล่อยยาสำหรับผู้ป่วย ทางด้านอาหาร สามารถนำพอลิเมอร์ดูดซึมน้ำมากมาใช้เป็นสารป้องกันการรั่วซึมของของเหลวในภาชนะบรรจุอาหาร ส่วนทางด้านวิศวกรรมการก่อสร้าง พอลิเมอร์ดูดซึมน้ำสามารถใช้เป็นสารช่วยกักเก็บน้ำในคอนกรีต นอกจากนี้ ยังนำพอลิเมอร์ดูดซึมน้ำมากมาใช้ในงานด้านอื่น ๆ อีก เช่น เรซินแลกเปลี่ยนไอออน สารดับเพลิง หิมะเทียม หมึกพิมพ์ มีพอลิเมอร์หลายชนิดที่ได้ถูกนำมาใช้ในการสังเคราะห์พอลิเมอร์ดูดซึมน้ำมาก เช่น พอลิอะคริลาไมด์ (polyacrylamide) พอลิอะคริลิกแอซิด [poly(acrylic acid)] พอลิโซเดียมอะคริเลต [poly(sodium acrylate)] และพอลิไวนิลไพร์โรลิโดน [poly(vinyl pyrrolidone)] ส่วนใหญ่ของพอลิเมอร์เหล่านี้เป็นผลิตภัณฑ์จากปิโตรเคมีที่จะต้องใช้ระยะเวลายาวนานหลายร้อยปีในการแตกสลาย หรือ ไม่สามารถแตกสลายได้เองตามธรรมชาติ ประกอบกับปัจจุบันมีแนวโน้มการใช้พอลิเมอร์ดูดซึมน้ำมากเพิ่มขึ้นอย่างชัดเจน เนื่องจากพอลิเมอร์ดูดซึมน้ำมากมีสมบัติเด่น และเป็นองค์ประกอบอยู่ในวัสดุหลากหลายประเภท

การใช้งานที่เพิ่มขึ้นและการที่ใช้เวลาในการแตกสลายนาน จึงก่อให้เกิดขยะตลอดจนปัญหาทางด้านสิ่งแวดล้อมตามมา จากความตระหนักถึงปัญหาสิ่งแวดล้อมโลก หลายประเทศจึงมีความตื่นตัวและพยายามหาทางแก้ไขพัฒนาวัสดุต่าง ๆ ที่สามารถแตกสลายได้เองตามธรรมชาติ

การประดิษฐ์นี้ ได้นำอนุภาคไททาเนียมไดออกไซด์ระดับนาโนเมตรมาใช้กับพอลิเมอร์ดูดซึมน้ำมาก โดยผ่านกรรมวิธีการผลิตได้เป็นพอลิเมอร์คอมพอสิตดูดซึมน้ำมาก (Superabsorbent Polymer Composites, SAPCs) ที่สามารถดูดซับสีย้อมสิ่งทอและสามารถแตกสลายทั้งสีย้อมและตนเองได้ โดยอาศัยการกระตุ้นด้วยรังสีอัลตราไวโอเลต

พอลิเมอร์คอมพอสิตดูดซึมน้ำมากที่ได้จากกรรมวิธีการผลิตตามการประดิษฐ์นี้ เมื่อถูกกระตุ้นด้วยรังสีอัลตราไวโอเลตจากแหล่งกำเนิดรังสี หรือจากดวงอาทิตย์ที่มากพอ จะเกิดการเปลี่ยนแปลงสมบัติและโครงสร้างทางเคมีจนแตกสลายในที่สุด การแตกสลายนี้เกิดขึ้นได้อย่างรวดเร็วเพียงพอที่จะไม่ทำให้เกิดการสะสมของเสียต่อภาวะแวดล้อม นอกจากนั้น พอลิเมอร์คอมพอสิตดูดซึมน้ำมากยังสามารถดูดซับ และแตกสลายสีย้อมสิ่งทอ ซึ่งก่อให้เกิดน้ำเสียหลังจากกระบวนการย้อมเสร็จสิ้น

มีเอกสารงานวิจัยจำนวนหนึ่งที่เกี่ยวข้องกับการเตรียมและใช้วัสดุพอลิเมอร์คอมพอสิตกับตัวเร่งปฏิกิริยาโดยการกระตุ้นด้วยแสงในหลายด้าน เช่น การยับยั้งเชื้อจุลินทรีย์ และการแตกสลายสีย้อมสิ่งทอ ดังนี้

เอกสารคำขอรับสิทธิบัตรประเทศไทย เลขที่คำขอ 0801001595 เกี่ยวข้องกับการเตรียมพอลิเมอร์ดูดซึมน้ำมาก (Superabsorbent Polymers, SAPs) ซึ่งประกอบด้วย ไวนิลมอนอเมอร์ที่ละลายน้ำได้, สารเชื่อมขวางสายโซ่ ทำให้พอลิเมอร์ดังกล่าวไม่ละลายน้ำ แต่บวมตัวและกักเก็บน้ำ และมีอนุภาคสังกะสีออกไซด์ระดับนาโนเมตรที่มีสมบัติเป็นตัวเร่งปฏิกิริยาแบบการกระตุ้นด้วยแสงสีขาว รังสีอัลตราไวโอเลต และแสงฟลูออเรสเซนต์ ซึ่งทำให้พอลิเมอร์ดูดซึมน้ำมากที่ได้มีสมบัติในการยับยั้งเชื้อจุลินทรีย์ชนิดก่อโรคและก่อกลิ่นได้ เนื่องจากสารดังกล่าวจะทำให้พอลิเมอร์ดูดซึมน้ำมากมีความสะอาด ปลอดเชื้อที่ก่อให้เกิดโรคและกลิ่น (กังวานศุภมงคล และคณะ สิทธิบัตรประเทศไทย *เลขที่คำขอ 0801001595*)

เอกสารงานวิจัยของ Zainal และคณะ เรื่อง "Characterization of TiO_2-chitosan/glass photocatalyst for the removal of a manoazo dye via photodegradation-adsorption process" เกี่ยวข้องกับการเตรียมวัสดุคอมพอสิตของอนุภาคไททาเนียมไดออกไซด์กับไคโทซานที่เคลือบบนแผ่นกระจก เพื่อใช้เป็นวัสดุทางเลือกในการบำบัดน้ำเสียของสีย้อมสิ่งทอ โดยอาศัยการดูดซับสีย้อมที่มีประสิทธิภาพของไคโทซานและการแตกสลายโมเลกุลของสารประกอบอินทรีย์ได้ของอนุภาคไททาเนียมไดออกไซด์ วัสดุคอมพอสิตดังกล่าวเตรียมได้จากการผสมไคโทซานน้ำหนัก 2.5 กรัม ในสารละลายผสมระหว่างกรดแอซิติก ความเข้มข้น 0.1 โมลาร์ ปริมาตร 300 มิลลิลิตร กับโซเดียมคลอไรด์ ความเข้มข้น 0.2 โมลาร์ ปริมาตร 40 มิลลิลิตร กวนเป็นเวลา 12 ชั่วโมง จน

ไคโทซานละลายหมด เติมผงอนุภาคไททาเนียมไดออกไซด์ (Degussa P-25) ปริมาณ 2.5 กรัม ลงในสารละลายที่เตรียมได้ข้างต้น เติมสารละลายกรดแอซิติกความเข้มข้น 0.1 โมลาร์ ปริมาตร 50 มิลลิเมตร กวนต่ออีกเป็นเวลา 24 ชั่วโมง นำกระจกที่ทำความสะอาดแล้วมาเคลือบด้วยสารผสมที่เตรียมได้ด้วยวิธีการจุ่ม อบแผ่นกระจกที่เคลือบแล้วในตู้อบด้วยอุณหภูมิ 100 องศาเซลเซียส เป็นเวลา 4 ชั่วโมง ศึกษาผลของจำนวนครั้งของการเคลือบจาก 1 ถึง 6 ชั้น ต่อการกำจัดสีย้อม พบว่ากำจัดสีย้อมเมทิลีนบลูได้มากถึงร้อยละ 87 แต่งานวิจัยนี้ไม่มีการศึกษาเกี่ยวกับการแตกสลายของไคโทซาน (Zainal, Z.; Hui, L.K.; Hussein, M.Z.; Abdullah, A.H. *J. Hazard. Mater.*, 2009, **164**, 138-145.)

Hafez และคณะ รายงานในเอกสารวิจัยเรื่อง "Photocatalytic efficiency of TiO_2 immobilized on PVP/AAc hydrogel membranes: A comparative study for safe disposal of wastewater of Remazol Red RB-133 textile dye" ซึ่งเกี่ยวข้องกับการเตรียมแผ่นเมมเบรนคอมพอสิตอนุภาคไททาเนียมไดออกไซด์กับโคพอลิเมอร์ไฮโดรเจลของพอลิไวนิลไพร์โรลิโดน/กรดอะคริลิกโดยวิธีการฉายรังสีแกมมา พบว่า แผ่นเมมเบรนคอมพอสิตที่เตรียมได้สามารถกำจัดสีย้อม RB-133 ได้ถึงร้อยละ 58 และยังพบอีกว่า เมมเบรนคอมพอสิตที่ใช้งานแล้ว สามารถใช้งานซ้ำได้อีก 2 – 3 ครั้ง แต่งานวิจัยนี้ก็ไม่มีการศึกษาเกี่ยวกับการแตกสลายของแผ่นเมมเบรนคอมพอสิต (Hafez, H.S.; Ali, A. El-H.; Abdel-Mottaleb, M.S.A. *Internat. J. Photoenergy*, 2005, **7**, 181-185.)

Tang และคณะ รายงานในเอกสารวิจัยเรื่อง "Preparation and photocatalytic degradability of TiO_2/polyacrylamide composite" เกี่ยวข้องกับการเตรียมพอลิเมอร์คอมพอสิตดูดซึมน้ำมาก (พอลิอะคริลาไมด์) กับอนุภาคไททาเนียมไดออกไซด์ที่มีสมบัติเป็นตัวเร่งปฏิกิริยาโดยการกระตุ้นด้วยแสงด้วยกระบวนการพอลิเมอไรเซชันแบบสารละลาย โดยมี เอ็น,เอ็น-เมทิลีนบิสอะคริลาไมด์ (*N,N*-methylenebisacrylamide) และ โพแทสเซียมเพอร์ซัลเฟต (potassium persulfate) เป็นสารเชื่อมขวางสายโซ่และตัวริเริ่มปฏิกิริยาตามลำดับ พบว่า พอลิเมอร์คอมพอสิตที่เตรียมได้สามารถแตกสลายสีย้อมเมทิลออเรนจ์ ได้เพียงร้อยละ 54 และสามารถใช้งานซ้ำได้มากกว่า 6 ครั้ง โดยในครั้งที่ 6 ยังสามารถแตกสลายสีย้อมได้ร้อยละ 47 (Tang, Q.; Lin, J.; Wu, Z.; Wu, J.; Huang, M.; Yang, Y. *Euro. Polym. J.* 2007, **43**, 2214-2220.)

งานการประดิษฐ์ของ Tang และคณะ มอนอเมอร์เริ่มต้นที่ใช้ ใช้เฉพาะอะคริลาไมด์เท่านั้น แต่การประดิษฐ์นี้ ใช้มอนเมอร์ 2 ชนิด ได้แก่ กรดอะคริลิกและอะคริลาไมด์ ในสัดส่วน 50:50 โดยโมลของมอนอเมอร์ สารริเริ่มปฏิกิริยาที่ใช้ในการประดิษฐ์นี้ คือ แอมโมเนียมเพอร์ซัลเฟต ร่วมกับสารริเริ่มปฏิกิริยาร่วม คือ เอ็น เอ็น เอ็น' เอ็น'-เททระเมทิลเอทิลีนไดแอมีน (*N,N,N',N'*-Tetramethylethylenediamine) และในการประดิษฐ์นี้ พอลิเมอร์คอมพอสิตที่เตรียมได้สามารถแตกสลายตัวได้โดยตนเอง ส่วนงานของ Tang และคณะ ไม่มีการกล่าวถึง งานของ Tang และคณะ พบว่า พอลิเมอร์คอมพอสิตที่เตรียมได้สามารถใช้ซ้ำได้ แต่การประดิษฐ์นี้ ค้นพบว่า

พอลิเมอร์คอมพอสิตที่เตรียมได้สามารถแตกสลายตัวเองได้ ซึ่งไม่เหมือนกับงานของ Tang และคณะ แต่ถือได้ว่าเป็นข้อดีกว่าอีกประการหนึ่งในการจัดการด้านสิ่งแวดล้อม

งานวิจัยข้างต้นเป็นงานวิจัยที่นำพอลิเมอร์ดูดซึมน้ำมาก หรือพอลิเมอร์คอมพอสิตดูดซึมน้ำมากมาดูดซับสีย้อมในหลากหลายประเภท นำวัสดุที่ผ่านการดูดซับสีย้อมสิ่งทอแล้วมาฉายรังสีภายใต้รังสีอัลตราไวโอเลต เพื่อแตกสลายสีย้อมของสิ่งทอออกจากตัวพอลิเมอร์ดูดซึมน้ำมาก แต่ยังไม่มีงานวิจัยใดที่รายงานความสามารถในการแตกสลายสีย้อมของสิ่งทอพร้อมทั้งสามารถแตกสลายตนเองได้ โดยอาศัยการกระตุ้นด้วยรังสีอัลตราไวโอเลต

พอลิเมอร์คอมพอสิตดูดซึมน้ำมากที่ได้จากการประดิษฐ์นี้ จากการทดสอบการแตกสลายสีย้อมของสิ่งทอ พบว่า สีย้อมของสิ่งทอที่ถูกดูดซับด้วยพอลิเมอร์คอมพอสิตดูดซึมน้ำมากนั้น ถูกแตกสลายได้หมดภายใต้รังสีอัลตราไวโอเลตที่ความเข้มแสง 1 – 2 มิลลิวัตต์ เป็นเวลา 20 – 40 นาที นอกจากนั้น เมื่อฉายรังสีอัลตราไวโอเลตที่ความเข้มแสงเดิมต่อไปเป็นระยะเวลา 24 ชั่วโมง พบว่า พอลิเมอร์คอมพอสิตดูดซึมน้ำมากถูกแตกสลายกลายเป็นของเหลวใส จนเหลือเพียงอนุภาคไททาเนียมไดออกไซด์ในปริมาณน้อยมาก ซึ่งมาจากการเติมในกรรมวิธีการผลิตพอลิเมอร์คอมพอสิตดูดซึมน้ำมาก พอลิเมอร์คอมพอสิตดูดซึมน้ำมากที่ได้จากการประดิษฐ์นี้จัดเป็นวัสดุสีเขียวที่สามารถช่วยลดปัญหาสิ่งแวดล้อม และเป็นวัสดุที่สามารถนำมาใช้กับอุตสาหกรรมได้หลากหลายประเภท เนื่องจากมีความสามารถในการแตกสลายตัวเองได้ภายใต้รังสีอัลตราไวโอเลตในระยะเวลาสั้น

สำหรับการเตรียมพอลิเมอร์คอมพอสิตดูดซึมน้ำมาก สามารถเตรียมได้โดยผ่านกระบวนการพอลิเมอไรเซชันแบบอนุมูลอิสระแบบสารละลาย ในกระบวนการเตรียมแบบสารละลายนั้น สารเคมีทุกชนิดในระบบ ได้แก่ มอนอเมอร์ ตัวริเริ่มปฏิกิริยา และตัวริเริ่มปฏิกิริยาร่วม สารเชื่อมขวางสายโซ่พอลิเมอร์ละลายอยู่ในวัฏภาคน้ำ และเมื่อปฏิกิริยาพอลิเมอไรเซชันดำเนินไป จะได้พอลิเมอร์ดูดซึมน้ำมากหรือไฮโดรเจลที่มีลักษณะเป็นก้อนวุ้นหรือเจลใสๆ หรือเป็นของเหลวที่มีความหนืดสูง จึงตกตะกอนก้อนเจลที่ได้เป็นก้อนแข็งและบดให้มีขนาดเล็กต่อไป

ไททาเนียมไดออกไซด์ หรือ ไททาเนีย (titania) มีสูตรโมเลกุล คือ TiO_2 เป็นสารกึ่งตัวนำในรูปผลึกของ anatase และเป็นตัวเร่งปฏิกิริยาโดยการกระตุ้นด้วยแสง (photocatalyst) หรือกล่าวง่าย ๆ ว่า เป็นสารที่สามารถถูกเร่งปฏิกิริยาได้ด้วยรังสีอัลตราไวโอเลต ซึ่งมีการศึกษาเป็นเวลานานถึงความสามารถในการกำจัดทั้งสารอินทรีย์และสารอนินทรีย์ในน้ำ อากาศ และสิ่งมีชีวิต หลักการพื้นฐานของเทคนิคการเร่งปฏิกิริยาด้วยการกระตุ้นด้วยแสงนั้น เริ่มจากรังสีอัลตราไวโอเลตที่มีความยาวคลื่นช่วง 300 – 400 นาโนเมตร (Near ultraviolet) ไปกระตุ้นอิเล็กตรอนที่แถบเวเลนซ์ (valence-band) ของอนุภาคไททาเนียมไดออกไซด์ซึ่งเป็นสารประกอบกึ่งตัวนำ จึงสามารถทำปฏิกิริยากับโมเลกุลน้ำที่ผิวและเหนี่ยวนำให้เกิดเป็นสารอนุมูลอิสระที่มีพลังออกซิไดส์สูงมาก เช่น ไฮดรอกซิลแรดิเคิล ($OH^{\cdot}$, hydroxyl radicals) และซูเปอร์ออกไซด์แรดิ

เคิล ($O_2^{\cdot}$, superoxide radicals) ซึ่งอนุมูลอิสระเหล่านี้มีประสิทธิภาพในการกำจัดสารอินทรีย์ต่าง ๆ โดยทำให้เกิดการแตกสลายเป็นน้ำและคาร์บอนไดออกไซด์ในที่สุด ด้วยสมบัติตามที่ได้กล่าวมา จึงได้มีการนำไททาเนียมไดออกไซด์ไปใช้งานหลากหลายรูปแบบ เช่น เพื่อการบำบัดน้ำเสีย เพื่อเพิ่มการยับยั้งเชื้อแบคทีเรียให้กับวัสดุ ผลการวิจัยส่วนมากยืนยันว่า ไททาเนียมไดออกไซด์เป็นตัวเร่งปฏิกิริยาแบบกระตุ้นด้วยรังสีที่มีประสิทธิภาพดี เพราะมีสมบัติที่ไม่ถูกรังสีทำลาย ไม่เป็นสารพิษและไม่ละลาย ทำให้สามารถนำกลับมาใช้ใหม่ได้

การประดิษฐ์นี้ จึงมุ่งเน้นที่จะพัฒนาพอลิเมอร์คอมพอสิตดูดซึมน้ำมากที่มีองค์ประกอบของอนุภาคไททาเนียมไดออกไซด์ระดับนาโนเมตร ให้มีสมบัติในการแตกสลายสีย้อมสิ่งทอพร้อมทั้งสามารถแตกสลายพอลิเมอร์ตัวเองได้ โดยอาศัยการกระตุ้นด้วยรังสีอัลตราไวโอเลต สามารถนำมาใช้กับอุตสาหกรรมได้หลากหลาย อีกทั้งยังช่วยลดปัญหาทางด้านสิ่งแวดล้อมได้ เนื่องจากมีความสามารถในการแตกสลายตัวเองได้ภายใต้รังสีอัลตราไวโอเลตในระยะเวลาสั้น

ลักษณะและความมุ่งหมายของการประดิษฐ์

การประดิษฐ์นี้เกี่ยวข้องกับพอลิเมอร์คอมพอสิตดูดซึมน้ำมากที่สามารถแตกสลายสีย้อมประเภทสีเบสิกพร้อมทั้งสามารถย่อยสลายตัวเองได้ โดยอาศัยการกระตุ้นด้วยรังสีอัลตราไวโอเลต ซึ่งพอลิเมอร์คอมพอสิตดูดซึมน้ำมากดังกล่าว ประกอบด้วย ไวนิลมอนอเมอร์ที่ละลายน้ำได้, สารเชื่อมขวางสายโซ่พอลิเมอร์, สารริเริ่มปฏิกิริยา, สารริเริ่มปฏิกิริยาร่วม, น้ำ ซึ่งเป็นตัวทำละลาย และอนุภาคไททาเนียมไดออกไซด์ระดับนาโนเมตรที่มีสมบัติเป็นตัวเร่งปฏิกิริยาโดยการกระตุ้นด้วยแสง วัตถุประสงค์ของการประดิษฐ์นี้มุ่งเน้นที่จะพัฒนาพอลิเมอร์ดูดซึมน้ำมากให้มีความสามารถในการย่อยสลายสีย้อมประเภทสีเบสิกพร้อมทั้งสามารถย่อยสลายตัวเองได้ โดยอาศัยการกระตุ้นด้วยรังสีอัลตราไวโอเลต และใช้เวลาในการย่อยสลายสั้น เนื่องจากวัตถุดิบเริ่มต้นที่ใช้ในกรรมวิธีการผลิต จัดเป็นผลิตภัณฑ์ที่ได้จากปิโตรเคมี ซึ่งปกติใช้ระยะเวลาหลายร้อยปีในการแตกสลาย และมีผลกระทบต่อสิ่งแวดล้อม เกิดปัญหาด้านมลภาวะตามมา การประดิษฐ์นี้ จึงได้นำอนุภาคไททาเนียมไดออกไซด์ระดับนาโนเมตรมาใช้งานร่วมกับพอลิเมอร์ดูดซึมน้ำมาก จึงน่าจะเป็นแนวทางหนึ่งในการช่วยลดปัญหาด้านสิ่งแวดล้อมได้ ซึ่งจะมีประโยชน์ทั้งในด้านธุรกิจ สังคม และสิ่งแวดล้อม อีกทั้งสามารถตอบสนองความต้องการของผู้บริโภคอีกด้วย

คำอธิบายรูปเขียนโดยย่อ

รูปที่ 1 ภาพถ่ายจุลทรรศน์อิเล็กตรอนแบบส่องกราดของ (ก) อนุภาคไททาเนียมไดออกไซด์ (ข) พอลิเมอร์ดูดซึมน้ำมากที่ไม่มีอนุภาคไททาเนียมไดออกไซด์ (ค) คอมพอสิตพอลิเมอร์ดูดซึมน้ำมากที่มีอนุภาคไททาเนียมไดออกไซด์ร้อยละ 15 เทียบกับน้ำหนักมอนอเมอร์ และ

(ง) คอมพอสิตพอลิเมอร์ดูดซึมน้ำมากที่มีอนุภาคไททาเนียมไดออกไซด์ร้อยละ 20 เทียบกับน้ำหนักมอนอเมอร์ (กำลังขยาย 15,000 เท่า)

รูปที่ 2 แผนภูมิแบบเส้นแสดงความสัมพันธ์ของร้อยละการกำจัดสีย้อมของสิ่งทอ ณ เวลาต่าง ๆ ของอนุภาคไททาเนียมไดออกไซด์ พอลิเมอร์ดูดซึมน้ำมากที่ไม่มีอนุภาคไททาเนียมไดออกไซด์ และพอลิเมอร์ดูดซึมน้ำมากที่มีอนุภาคไททาเนียมไดออกไซด์ ภายใต้สภาวะมืด

รูปที่ 3 แผนภูมิแบบเส้นแสดงความสัมพันธ์ของร้อยละการกำจัดสีย้อมสิ่งทอ ณ เวลาต่าง ๆ ของอนุภาคไททาเนียมไดออกไซด์ พอลิเมอร์ดูดซึมน้ำมากที่ไม่มีอนุภาคไททาเนียมไดออกไซด์ และคอมพอสิตของพอลิเมอร์ดูดซึมน้ำมากที่มีอนุภาคไททาเนียมไดออกไซด์ ภายใต้การกระตุ้นด้วยรังสีอัตราไวโอเลต

รูปที่ 4 กราฟแสดงความสัมพันธ์ระหว่างค่ามอดุลัสสะสมและมอดุลัสสูญเสียกับความถี่ของการกวาดของพอลิเมอร์ดูดซึมน้ำมาก รูป (ก) ไม่มีอนุภาคไททาเนียมไดออกไซด์ และรูป (ข) มีอนุภาคไททาเนียมไดออกไซด์ เมื่อได้รับการฉายรังสีอัลตราไวโอเลต เป็นเวลา 0, 8 และ 24 ชั่วโมง ตามลำดับ

การเปิดเผยการประดิษฐ์โดยสมบูรณ์

กรรมวิธีการผลิตพอลิเมอร์คอมพอสิตดูดซึมน้ำมากที่สามารถแตกสลายสีย้อมสิ่งทอพร้อมทั้งสามารถแตกสลายตัวเองได้ โดยอาศัยการกระตุ้นด้วยรังสีอัลตราไวโอเลต ตามการประดิษฐ์นี้ อาศัยหลักการทางนาโนเทคโนโลยีและสมบัติของอนุภาคไททาเนียมไดออกไซด์ระดับนาโนเมตร ในการทำให้เกิดการเปลี่ยนแปลงสมบัติ และโครงสร้างทางเคมี จนวัสดุแตกสลายไปได้เมื่อได้รับการกระตุ้นด้วยรังสีอัลตราไวโอเลต การประดิษฐ์นี้เกี่ยวข้องกับพอลิเมอร์ดูดซึมน้ำมากหรือไฮโดรเจล (hydrogel) ซึ่งประกอบด้วย สารผสมของมอนอเมอร์ กรดอะคริลิกและอะคริลาไมด์ จัดเป็นไวนิลมอนอเมอร์ชนิดละลายน้ำได้ สารเชื่อมขวางสายโซ่พอลิเมอร์ ทำให้พอลิเมอร์ดังกล่าวสามารถบวมตัวและกักเก็บน้ำ สารละลาย ไว้ภายในได้หลายเท่าตัวเมื่อเปรียบเทียบกับน้ำหนักแห้งเริ่มต้น และมีอนุภาคไททาเนียมไดออกไซด์ระดับนาโนเมตรที่มีสมบัติเป็นตัวเร่งปฏิกิริยาด้วยการกระตุ้นด้วยแสง ซึ่งทำให้พอลิเมอร์คอมพอสิตดูดซึมน้ำมากที่ได้มีสมบัติในการแตกสลายของสีย้อมสิ่งทอพร้อมทั้งสามารถแตกสลายตัวเองได้ โดยอาศัยการกระตุ้นด้วยรังสีอัลตราไวโอเลต เนื่องจากสารดังกล่าวจะทำให้พอลิเมอร์คอมพอสิตดูดซึมน้ำมากมีสมบัติในการแตกสลายได้ ทำให้สามารถช่วยลดปัญหาด้านสิ่งแวดล้อม ดังนั้น วัตถุประสงค์ของการประดิษฐ์นี้มุ่งเน้นที่จะพัฒนาพอลิเมอร์ดูดซึมน้ำมากให้มีสมบัติในการแตกสลายสีย้อมของสิ่งทอพร้อมทั้งสามารถแตกสลายตัวเองได้ โดยอาศัยการกระตุ้นด้วยรังสีอัลตราไวโอเลต เพื่อนำไปใช้ในอุตสาหกรรมหลากหลายประเภทที่เกี่ยวข้อง อีกทั้งยังมีประโยชน์ต่อสังคม และสิ่งแวดล้อมด้วย

พอลิเมอร์คอมพอสิตดูดซึมน้ำมากที่มีสมบัติในการแตกสลายสีย้อมของสิ่งทอพร้อมทั้งสามารถแตกสลายตัวเองได้ โดยอาศัยการกระตุ้นด้วยรังสีอัลตราไวโอเลต ตามการประดิษฐ์นี้ประกอบด้วย สารผสมของมอนอเมอร์กรดอะคริลิกและอะคริลาไมด์ ที่อัตราส่วนร้อยละ 50 ต่อ 50 โดยโมลของมอนอเมอร์ สารริเริ่มปฏิกิริยา เช่น แอมโมเนียมเพอร์ซัลเฟต (ammonium persulfate) ร้อยละ 0.2 – 1.0 โดยน้ำหนักของมอนอเมอร์ สารเชื่อมขวางสายโซ่พอลิเมอร์ ได้แก่ เอ็น, เอ็น- เมทิลีนบิสอะคริลาไมด์(*N,N*-methylenebisacrylamide) ร้อยละ 2 – 10 โดยน้ำหนักของมอนอเมอร์, สารริเริ่มปฏิกิริยาร่วม ได้แก่ เอ็น เอ็น เอ็น' เอ็น'-เททระเมทิลเอทิลีนไดแอมีน (*N,N,N',N'*-Tetramethylethylenediamine) ร้อยละ 0.01 – 0.1 โดยน้ำหนักของมอนอเมอร์ อนุภาคไททาเนียมไดออกไซด์ระดับนาโนเมตรที่มีสมบัติเป็นตัวเร่งปฏิกิริยาโดยการกระตุ้นด้วยรังสี ร้อยละ 5 – 20 โดยน้ำหนักของมอนอเมอร์ และน้ำ ร้อยละ 80 – 95 โดยน้ำหนักทั้งหมด

สำหรับกรรมวิธีในการผลิตพอลิเมอร์คอมพอสิตดูดซึมน้ำมาก มีขั้นตอนดังนี้

- การผสมของมอนอเมอร์กรดอะคริลิกและอะคริลาไมด์ที่ละลายน้ำได้ กวนผสมในน้ำให้เป็นเนื้อเดียวกัน เติมสารเชื่อมขวางสายโซ่พอลิเมอร์ กวนต่อจนสารผสมกลายเป็นเนื้อเดียวกัน เติมอนุภาคไททาเนียมไดออกไซด์ และกวนผสมตั้งไว้เป็นเวลา 10 – 20 นาที เติมสารริเริ่มปฏิกิริยา กวนตั้งไว้เป็นเวลา 5 – 20 นาที แล้วเติมสารริเริ่มปฏิกิริยาร่วม และกวนให้เข้าเป็นเนื้อเดียวกันด้วยเครื่องกวนที่ความเร็วรอบกวน 100 – 300 รอบต่อนาที ที่อุณหภูมิ 50 – 70 องศาเซลเซียส เป็นเวลา 20 – 60 นาที
- การแยกมอนอเมอร์ที่ไม่เกิดปฏิกิริยาและการดึงน้ำออกจากตัวพอลิเมอร์ด้วยการตกตะกอนในตัวทำละลายอินทรีย์ประเภทนอนโซลเวนต์ (non-solvent) เช่น เมทิลแอลกอฮอล์ หรือเอทิลแอลกอฮอล์ และกวนต่ออีกเป็นเวลา 10 – 20 นาที นำพอลิเมอร์ที่ได้ไปอบที่อุณหภูมิ 50 – 70 องศาเซลเซียส เป็นเวลา 24 ชั่วโมงหรือจนแห้งสนิท จึงนำมาบดให้เป็นผงละเอียด

อนุภาคไททาเนียมไดออกไซด์ที่ใช้ในกรรมวิธีการผลิต เป็นอนุภาคไททาเนียมไดออกไซด์ระดับนาโนเมตรที่ผ่านการทำให้กระจายตัวได้ดีขึ้นด้วยคลื่นเสียงความถี่สูง เป็นเวลา 5 – 20 นาที

จากรูปที่ 1 ซึ่งแสดงภาพถ่ายจุลทรรศน์อิเล็กตรอนแบบส่องกราดของ (ก) อนุภาคไททาเนียมไดออกไซด์ (ข) พอลิเมอร์ดูดซึมน้ำมากที่ไม่มีอนุภาคไททาเนียมไดออกไซด์ (ค) พอลิเมอร์คอมพอสิตดูดซึมน้ำมากที่มีอนุภาคไททาเนียมไดออกไซด์ร้อยละ 15 เทียบกับน้ำหนักมอนอเมอร์ และ (ง) พอลิเมอร์คอมพอสิตดูดซึมน้ำมากที่มีอนุภาคไททาเนียมไดออกไซด์ร้อยละ 20 เทียบกับน้ำหนักมอนอเมอร์ (ที่กำลังขยาย 15,000 เท่า) พบว่า มีอนุภาคไททาเนียมไดออกไซด์

อยู่ภายในโครงสร้างของพอลิเมอร์คอมพอสิตดูดซึมน้ำมากและมีปริมาณเพิ่มขึ้นเมื่อเพิ่มร้อยละของอนุภาคไททาเนียมไดออกไซด์เริ่มต้นจากร้อยละ 15 – 20

จากผลการทดสอบประสิทธิภาพการแตกสลายของสีย้อมสิ่งทอที่ถูกดูดซับด้วยพอลิเมอร์คอมพอสิตดูดซึมน้ำมากโดยอาศัยการกระตุ้นด้วยรังสีอัลตราไวโอเลต ที่ความเข้มของรังสี 1 มิลลิวัตต์ ต่อตารางเซนติเมตร ดังแสดงในรูปที่ 2 พบว่า มีเฉพาะพอลิเมอร์คอมพอสิตดูดซึมน้ำมากเท่านั้นที่สามารถแตกสลายสีย้อมสิ่งทอได้ เมื่อได้รับการกระตุ้นด้วยรังสีอัลตราไวโอเลต และสีย้อมจะถูกแตกสลายหมดภายในเวลาไม่เกิน 40 นาที

รูปที่ 3 แสดงความสามารถในการดูดซับหรือกำจัดสีย้อมสิ่งทอของอนุภาคไททาเนียมไดออกไซด์ พอลิเมอร์ดูดซึมน้ำมาก และพอลิเมอร์คอมพอสิตดูดซึมน้ำมากในภาวะที่ไม่มีแสงหรือในที่มืด พบว่า ทั้งพอลิเมอร์ดูดซึมน้ำมากและพอลิเมอร์คอมพอสิตดูดซึมน้ำมาก สามารถดูดซับ หรือกำจัดสีย้อมของสิ่งทอได้ใกล้เคียงกันและมากถึงร้อยละ 87 ในเวลาไม่ถึง 20 นาที ขณะที่อนุภาคไททาเนียมไดออกไซด์เพียงอย่างเดียวสามารถดูดซับ หรือกำจัดสีย้อมสิ่งทอได้เพียงร้อยละ 15 เท่านั้น

รูปที่ 4 แสดงความสามารถในการแตกสลายสีย้อมในสิ่งทอด้วยอนุภาคไททาเนียมไดออกไซด์ พอลิเมอร์ดูดซึมน้ำมาก และพอลิเมอร์คอมพอสิตดูดซึมน้ำมาก ในภาวะที่ได้รับการฉายรังสีอัลตราไวโอเลต พบว่า พอลิเมอร์ดูดซึมน้ำมาก และอนุภาคไททาเนียมไดออกไซด์มีความสามารถในการแตกสลายสีย้อมของสิ่งทอเพียงร้อยละ 3 และ 45 ขณะที่กรณีของพอลิเมอร์คอมพอสิตดูดซึมน้ำมากสามารถแตกสลายสีย้อมสิ่งทอได้มากถึงร้อยละ 91

นอกจากนั้น เมื่อพอลิเมอร์คอมพอสิตดูดซึมน้ำมากได้รับการฉายรังสีอัลตราไวโอเลตเป็นเวลา 8 - 24 ชั่วโมง พบว่า พอลิเมอร์คอมพอสิตดูดซึมน้ำมากจะถูกแตกสลายกลายเป็นของเหลวใส จนเหลือเพียงอนุภาคของไททาเนียมไดออกไซด์ในปริมาณน้อยมากซึ่งมาจากการเติมลงไปในขั้นตอนการเตรียมพอลิเมอร์คอมพอสิตดูดซึมน้ำมากตอนเริ่มต้น จากการศึกษาด้วยเครื่องรีโอมิเตอร์ (rheometer) ในรูปที่ 4 ได้กราฟความสัมพันธ์ระหว่างค่ามอดุลัสสะสมและมอดุลัสสูญเสียกับความถี่ของการกวาดในพอลิเมอร์ดูดซึมน้ำมาก พอลิเมอร์คอมพอสิตดูดซึมน้ำมากซึ่งมีอนุภาคไททาเนียมไดออกไซด์ที่ได้รับการฉายรังสีอัลตราไวโอเลต 8 ชั่วโมง มีค่ามอดุลัสสูญเสียมากกว่า หรือเหลวมากกว่าในกรณีของพอลิเมอร์ดูดซึมน้ำมากที่ไม่มีอนุภาคไททาเนียมไดออกไซด์

วิธีการในการประดิษฐ์ที่ดีที่สุด

เหมือนกับที่ได้กล่าวมาแล้วในหัวข้อการเปิดเผยการประดิษฐ์โดยสมบูรณ์

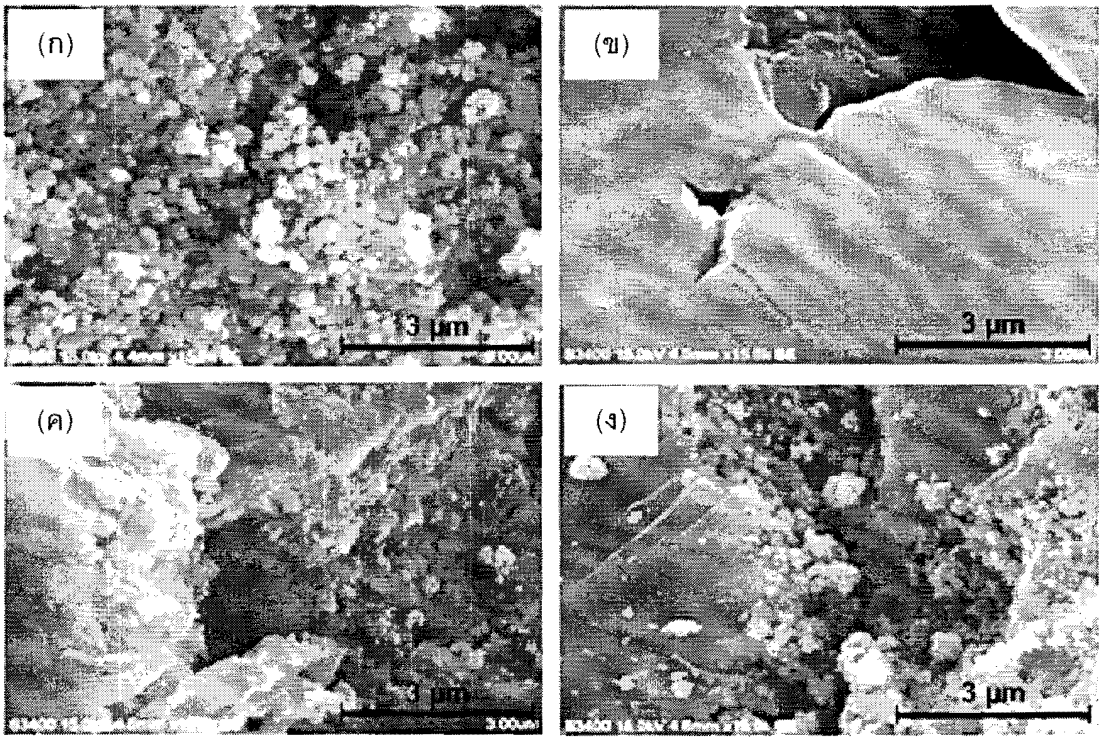

รูปที่ 1

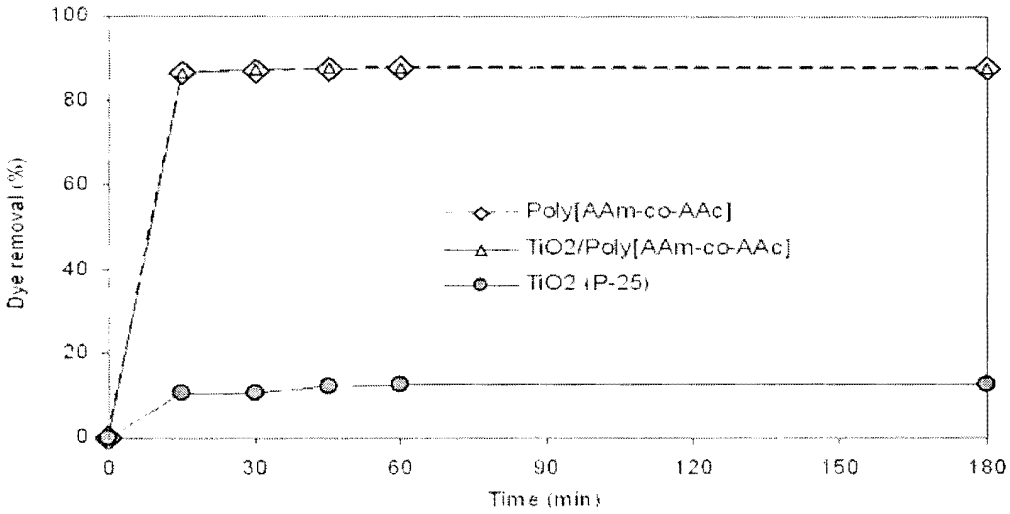
100
80
60
40
20
0
Dye removal (%)
0
30
60
90
120
150
180
Time (min)
Poly[AAm-co-AAc]
TiO2/Poly[AAm-co-AAc]
TiO2 (P-25)

รูปที่ 2

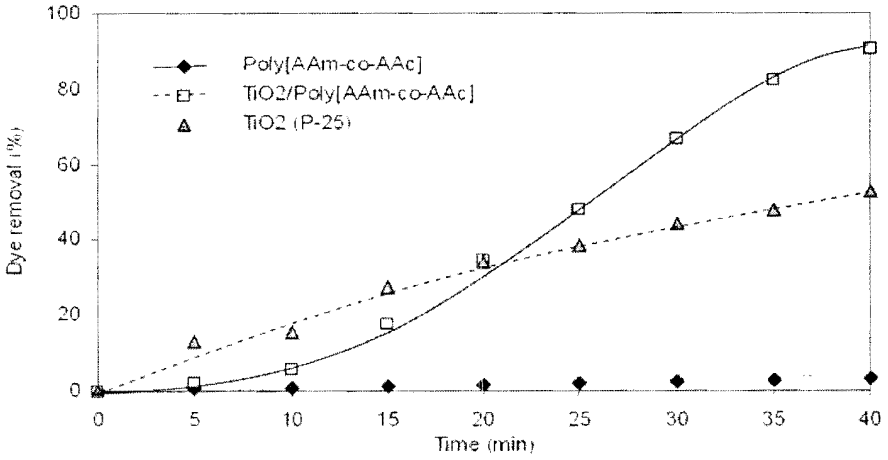
100
80
60
40
20
0
Dye removal (%)
0
5
10
15
20
25
30
35
40
Time (min)
Poly[AAm-co-AAc]
TiO2/Poly[AAm-co-AAc]
TiO2 (P-25)

รูปที่ 3

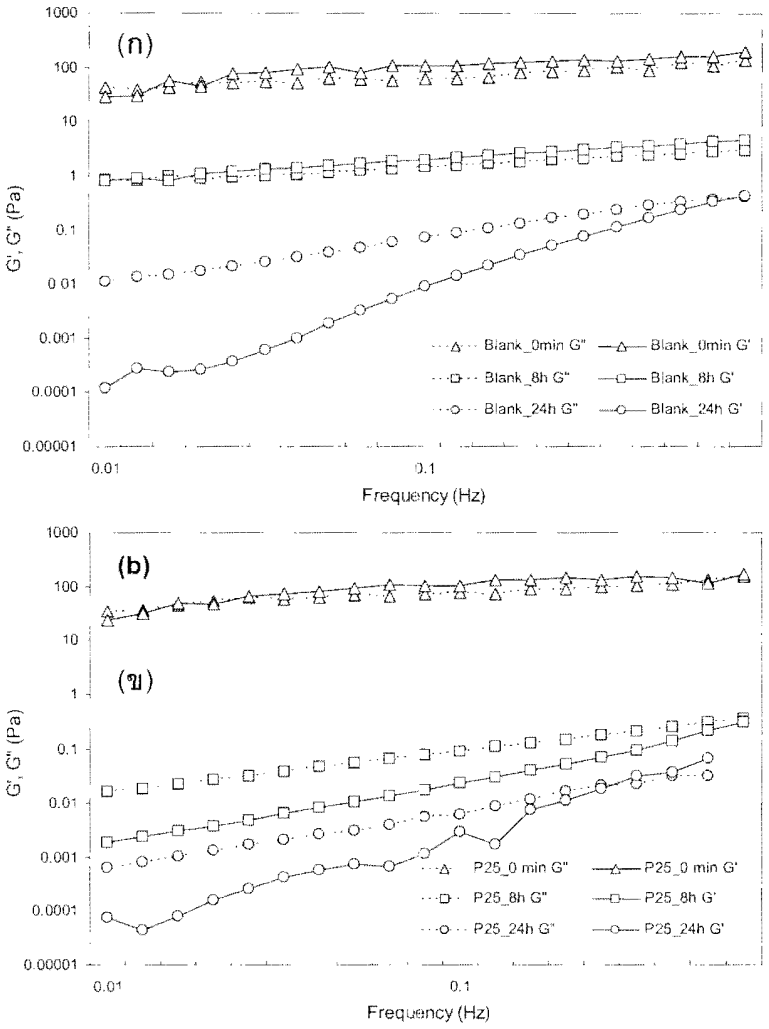
(ก)
1000
100
10
1
0.1
0.01
0.001
0.0001
0.00001
G', G" (Pa)
0.01
0.1
Frequency (Hz)
Blank_0min G"
Blank_0min G'
Blank_8h G"
Blank_8h G'
Blank_24h G"
Blank_24h G'
(b)
(ข)
P25_0 min G"
P25_0 min G'
P25_8h G"
P25_8h G'
P25_24h G"
P25_24h G'

รูปที่ 4

ข้อถือสิทธิ

1. พอลิเมอร์คอมพอสิตดูดซึมน้ำมาก ซึ่งประกอบด้วย

- มอนอมอเมอร์ กรดอะคริลิก และ อะคริลาไมด์
- สารริเริ่มปฏิกิริยา
- สารริเริ่มปฏิกิริยาร่วม
- สารเชื่อมขวางสายโซ่พอลิเมอร์
- อนุภาคไททาเนียมไดออกไซด์ ระดับนาโนเมตร และ
- น้ำ

2. พอลิเมอร์คอมพอสิตดูดซึมน้ำมากตามข้อถือสิทธิ 1 ที่ซึ่งประกอบด้วย

- มอนอเมอร์ กรดอะคริลิก และ อะคริลาไมด์ ที่อัตราส่วนร้อยละ 50 ต่อ 50 โดยโมลของมอนอเมอร์
- สารริเริ่มปฏิกิริยา ร้อยละ 0.2 – 1.0 โดยน้ำหนักของมอนอเมอร์
- สารริเริ่มปฏิกิริยาร่วม ร้อยละ 0.01 – 0.1 โดยน้ำหนักของมอนอเมอร์
- สารเชื่อมขวางสายโซ่พอลิเมอร์ ร้อยละ 2 – 10 โดยน้ำหนักของมอนอเมอร์
- อนุภาคไททาเนียมไดออกไซด์ระดับนาโนเมตร ร้อยละ 5 – 20 โดยน้ำหนักของมอนอเมอร์ และ
- น้ำ ร้อยละ 80 – 95 โดยน้ำหนักทั้งหมด

3. พอลิเมอร์คอมพอสิตดูดซึมน้ำมากตามข้อถือสิทธิ 1 ที่ซึ่งสารริเริ่มปฏิกิริยาร่วมดังกล่าว คือ สารประกอบเอ็น เอ็น เอ็น' เอ็น'-เททระเมทิลเอทิลีนไดแอมีน (*N,N,N',N'*-tetramethylethylene-diamine)

4. พอลิเมอร์คอมพอสิตดูดซึมน้ำมากตามข้อถือสิทธิ 1 ที่ซึ่งสารเชื่อมขวางสายโซ่พอลิเมอร์ดังกล่าว คือ เอ็น,เอ็น-เมทิลีนบิสอะคริลาไมด์ (*N,N*-methylenebisacrylamide)

5. กรรมวิธีการผลิตพอลิเมอร์คอมพอสิตดูดซึมน้ำมากตามข้อถือสิทธิ 1 ถึง 4 ข้อใดข้อหนึ่ง ซึ่งประกอบด้วยขั้นตอนดังนี้ คือ

- การผสมของมอนอเมอร์กรดอะคริลิก และ มอนอเมอร์อะคริลาไมด์ ที่อัตราส่วนร้อยละ 50 ต่อ 50 โดยโมลของมอนอเมอร์ กวนผสมในน้ำให้เป็นเนื้อเดียวกัน เติมสารเชื่อมขวางสายโซ่พอลิเมอร์ ร้อยละ 2 – 10 โดยน้ำหนักของมอนอเมอร์ และกวนต่อจนสารผสมกลายเป็นเนื้อเดียวกัน เติมอนุภาคไททาเนียมไดออกไซด์ระดับนาโนเมตร ในปริมาณร้อยละ 5 – 20 โดยน้ำหนักของมอนอเมอร์ กวนผสมตั้งไว้เป็นเวลา 10 – 20 นาที เติมสารริเริ่มปฏิกิริยาร้อยละ 0.2 – 1.0 โดยน้ำหนักของมอนอเมอร์ กวนตั้งไว้เป็นเวลา 5 – 20 นาที เติมสารริเริ่มปฏิกิริยาร่วม ร้อยละ 0.01 – 0.1 โดยน้ำหนักของมอนอเมอร์ และกวนให้เข้าเป็นเนื้อเดียวกันด้วยเครื่องกวน

ที่ความเร็วรอบกวน 100 – 300 รอบต่อนาที ที่อุณหภูมิ 50 – 70 องศาเซลเซียส เป็นเวลา 20 – 60 นาที

- การแยกมอนอเมอร์ที่ไม่เกิดปฏิกิริยาและการดึงน้ำออกจากตัวพอลิเมอร์ด้วยการตกตะกอนในตัวทำละลายอินทรีย์ประเภทนอนโซลเวนต์ (non-solvent) และกวนต่ออีกเป็นเวลา 10 – 20 นาที นำพอลิเมอร์ที่ได้ไปอบที่อุณหภูมิ 50 – 70 องศาเซลเซียส เป็นเวลา 24 ชั่วโมงหรือจนแห้งสนิท

6. กรรมวิธีการผลิตพอลิเมอร์คอมพอสิตดูดซึมน้ำมากตามข้อถือสิทธิ 5 ที่ซึ่งอนุภาคไททาเนียมไดออกไซด์ระดับนาโนเมตรตามที่กล่าวแล้ว เป็นอนุภาคไททาเนียมไดออกไซด์ระดับนาโนเมตรที่ผ่านการทำให้กระจายตัวได้ดีขึ้นด้วยคลื่นเสียงความถี่สูง เป็นเวลา 5 – 20 นาที

บทสรุปการประดิษฐ์

การประดิษฐ์นี้เกี่ยวข้องกับพอลิเมอร์คอมพอสิตดูดซึมน้ำมากที่สามารถแตกสลายสีย้อมประเภทสีเบสิกพร้อมทั้งสามารถย่อยสลายตัวเองได้ โดยอาศัยการกระตุ้นด้วยรังสีอัลตราไวโอเลต ซึ่งพอลิเมอร์คอมพอสิตดูดซึมน้ำมากดังกล่าว ประกอบด้วย ไวนิลมอนอเมอร์ที่ละลายน้ำได้, สารเชื่อมขวางสายโซ่พอลิเมอร์, สารริเริ่มปฏิกิริยา, สารริเริ่มปฏิกิริยาร่วม, น้ำ ซึ่งเป็นตัวทำละลาย และอนุภาคไททาเนียมไดออกไซด์ระดับนาโนเมตรที่มีสมบัติเป็นตัวเร่งปฏิกิริยาโดยการกระตุ้นด้วยแสง

สถาบันทรัพย์สินทางปัญญาแห่งจุฬาลงกรณ์มหาวิทยาลัย

Chulalongkorn University Intellectual Property Institute

กุมภาพันธ์ 2554

เรื่อง ขอผ่อนผันการส่งเอกสารประกอบคำขอรับสิทธิบัตร ครั้งที่ 1

1101000203

เรียน ผู้อำนวยการสำนักสิทธิบัตร

ด้วยสถาบันทรัพย์สินทางปัญญาแห่งจุฬาลงกรณ์มหาวิทยาลัยได้รับมอบหมายจากจุฬาลงกรณ์มหาวิทยาลัย สำนักงานกองทุนสนับสนุนการวิจัย และสำนักงานพัฒนาวิทยาศาสตร์และเทคโนโลยีแห่งชาติ ให้ดำเนินการยื่นคำขอรับสิทธิบัตร เรื่อง "เจลอิมัลชันวัสดุเชิงประกอบพอลิเมอร์ดูดซึมน้ำมากและเจลอิมัลชันพอลิเมอร์ดูดซึมน้ำมากที่มีสมบัติหน่วงการติดไฟ" โดยมีข้าพเจ้านายมงคล แก้วมหา ตัวแทนสิทธิบัตร เลขที่ 1453 เป็นผู้ดำเนินการ ซึ่งขณะนี้อยู่ระหว่างดำเนินการให้ผู้ที่เกี่ยวข้องลงนามในสัญญาโอนสิทธิในการขอรับสิทธิบัตรและหนังสือมอบอำนาจ ซึ่งจำเป็นที่จะต้องใช้ระยะเวลาหนึ่งในการดำเนินการ แต่เนื่องจากการประดิษฐ์นี้ทางผู้ประดิษฐ์มีความประสงค์ที่จะเผยแพร่ผลงานวิจัย ซึ่งหากมีการนำไปเผยแพร่ผลงานก่อนที่จะได้มีการยื่นคำขอรับสิทธิบัตร ข้าพเจ้าเกรงว่าจะมีผลต่อการพิจารณารับจดทะเบียนของคำขอรับสิทธิบัตรฉบับนี้ได้

ด้วยเหตุผลดังกล่าวข้างต้น ข้าพเจ้าจึงเรียนมาเพื่อโปรดพิจารณาอนุมัติผ่อนผันการยื่นเอกสารประกอบคำขอรับสิทธิบัตรพร้อมกับคำขอรับสิทธิบัตรด้วย จักขอบพระคุณยิ่ง

ขอแสดงความนับถือ

(นายมงคล แก้วมหา)

ผู้รับมอบอำนาจ

ตัวแทนสิทธิบัตร เลขที่ 1453

อาคารจัตุรัสจามจุรี ชั้น 12 ยูนิต 13 ถนนพญาไท เขตปทุมวัน กรุงเทพฯ 10330 โทรศัพท์ 0-2160-5340-1 โทรสาร 0-2160-5343

Chamchuri Square Building 12nd Floor, 13th Unit, Phyathai Road, Bangkok 10330

Tel +66(0)-21605340-1 Fax +66 (0)-2160-5343

คำขอรับสิทธิบัตร/อนุสิทธิบัตร

☑ การประดิษฐ์
☐ การออกแบบผลิตภัณฑ์
☐ อนุสิทธิบัตร

ข้าพเจ้าผู้ลงลายมือชื่อในคำขอรับสิทธิบัตร/อนุสิทธิบัตรนี้ ขอรับสิทธิบัตร/อนุสิทธิบัตร ตามพระราชบัญญัติสิทธิบัตร พ.ศ. 2522 แก้ไขเพิ่มเติมโดยพระราชบัญญัติสิทธิบัตร (ฉบับที่ 2) พ.ศ 2535 และพระราชบัญญัติสิทธิบัตร (ฉบับที่ 3) พ.ศ 2542

สำหรับเจ้าหน้าที่

วันรับคำขอ 15 ก.ย. 2554	เลขที่คำขอ 1101000208
วันยื่นคำขอ	

สัญลักษณ์จำแนกการประดิษฐ์ระหว่างประเทศ

ใช้กับแบบผลิตภัณฑ์
ประเภทผลิตภัณฑ์

วันประกาศโฆษณา	เลขที่ประกาศโฆษณา

วันออกสิทธิบัตร/อนุสิทธิบัตร	เลขที่สิทธิบัตร/อนุสิทธิบัตร

ลายมือชื่อเจ้าหน้าที่

1.ชื่อที่แสดงถึงการประดิษฐ์/การออกแบบผลิตภัณฑ์
เจลอิมัลชันวัสดุเชิงประกอบพอลิเมอร์ดูดซึมน้ำมากและเจลอิมัลชันพอลิเมอร์ดูดซึมน้ำมากที่มีสมบัติหน่วงการติดไฟ

2.คำขอรับสิทธิบัตรการออกแบบผลิตภัณฑ์นี้เป็นคำขอสำหรับแบบผลิตภัณฑ์อย่างเดียวกันและเป็นคำขอลำดับที่
ในจำนวน คำขอ ที่ยื่นในคราวเดียวกัน

3.ผู้ขอรับสิทธิบัตร/อนุสิทธิบัตร และที่อยู่ (เลขที่ ถนน ประเทศ)	
ดูที่หน้า 3	3.1 สัญชาติ
	3.2 โทรศัพท์
	3.3 โทรสาร
	3.4 อีเมล์

4.สิทธิในการขอรับสิทธิบัตร/อนุสิทธิบัตร
☐ ผู้ประดิษฐ์/ผู้ออกแบบ ☑ ผู้รับโอน ☐ ผู้ขอรับสิทธิโดยเหตุอื่น

5.ตัวแทน(ถ้ามี)/ที่อยู่ (เลขที่ ถนน จังหวัด รหัสไปรษณีย์)	
นายมงคล แก้วมหา สถาบันทรัพย์สินทางปัญญาแห่งจุฬาลงกรณ์มหาวิทยาลัย อาคารจัตุรัสจามจุรี ชั้น 12 ยูนิต 13 ถนนพญาไท แขวงปทุมวัน เขตปทุมวัน กรุงเทพฯ 10330	5.1 ตัวแทนเลขที่ 1453
	5.2 โทรศัพท์ 0-2160-5340-2
	5.3 โทรสาร 0-2160-5343
	5.4 อีเมล์

6.ผู้ประดิษฐ์/ผู้ออกแบบผลิตภัณฑ์ และที่อยู่ (เลขที่ ถนน ประเทศ)
ดูที่หน้า 3

7. คำขอรับสิทธิบัตร/อนุสิทธิบัตรนี้แยกจากหรือเกี่ยวข้องกับคำขอเดิม
ผู้ขอรับสิทธิบัตร/อนุสิทธิบัตร ขอให้ถือว่าได้ยื่นคำขอรับสิทธิบัตร/อนุสิทธิบัตรนี้ ในวันเดียวกับคำขอรับสิทธิบัตร
เลขที่ วันยื่น เพราะคำขอรับสิทธิบัตร/อนุสิทธิบัตรนี้แยกจากหรือเกี่ยวข้องกับคำขอเดิมเพราะ
☐ คำขอเดิมมีการประดิษฐ์หลายอย่าง ☐ ถูกคัดค้านเนื่องจากผู้ขอไม่มีสิทธิ ☐ ขอเปลี่ยนแปลงประเภทของสิทธิ

หมายเหตุ ในกรณีที่ไม่อาจระบุรายละเอียดได้ครบถ้วน ให้จัดทำเป็นเอกสารแนบท้ายแบบพิมพ์นี้โดยระบุหมายเลขกำกับข้อและหัวข้อที่แสดงรายละเอียดเพิ่มเติมดังกล่าวด้วย

8.การยื่นคำขอนอกราชอาณาจักร

วันยื่นคำขอ	เลขที่คำขอ	ประเทศ	สัญลักษณ์จำแนกการประดิษฐ์ระหว่างประเทศ	สถานะคำขอ
8.1				
8.2				
8.3				

8.4 ☐ ผู้ขอรับสิทธิบัตร/อนุสิทธิบัตรขอสิทธิให้ถือว่าได้ยื่นคำขอนี้ในวันที่ได้ยื่นคำขอรับสิทธิบัตร/อนุสิทธิบัตรในต่างประเทศเป็นครั้งแรกโดย
☐ ได้ยื่นเอกสารหลักฐานพร้อมคำขอนี้ ☐ ขอยื่นเอกสารหลักฐานหลังจากวันยื่นคำขอนี้

9.การแสดงการประดิษฐ์ หรือการออกแบบผลิตภัณฑ์ ผู้ขอรับสิทธิบัตร/อนุสิทธิบัตรได้แสดงการประดิษฐ์ที่หน่วยงานของรัฐเป็นผู้จัด
วันแสดง วันเปิดงานแสดง ผู้จัด

10.การประดิษฐ์เกี่ยวกับจุลชีพ

10.1 เลขทะเบียนฝากเก็บ	10.2 วันที่ฝากเก็บ	10.3 สถาบันฝากเก็บ/ประเทศ

11.ผู้ขอรับสิทธิบัตร/อนุสิทธิบัตร ขอยื่นเอกสารภาษาต่างประเทศก่อนในวันยื่นคำขอนี้ และจะจัดยื่นคำขอรับสิทธิบัตร/อนุสิทธิบัตรนี้ที่จัดทำเป็นภาษาไทยภายใน 90 วัน นับจากวันยื่นคำขอนี้ โดยขอยื่นเป็นภาษา
☐ อังกฤษ ☐ ฝรั่งเศส ☐ เยอรมัน ☐ ญี่ปุ่น ☐ อื่นๆ

12.ผู้ขอรับสิทธิบัตร/อนุสิทธิบัตร ขอให้อธิบดีประกาศโฆษณาคำขอรับสิทธิบัตร หรือรับจดทะเบียน และประกาศโฆษณาอนุสิทธิบัตรนี้ หลังจากวันที่ เดือน พ.ศ
☐ ผู้ขอรับสิทธิบัตร/อนุสิทธิบัตรขอให้ใช้รูปเขียนหมายเลข ในการประกาศโฆษณา

13.คำขอรับสิทธิบัตร/อนุสิทธิบัตรนี้ประกอบด้วย
ก. แบบพิมพ์คำขอ 3 หน้า
ข. รายละเอียดการประดิษฐ์ หรือคำพรรณนาแบบผลิตภัณฑ์ 7 หน้า
ค. ข้อถือสิทธิ 2 หน้า
ง. รูปเขียน รูป หน้า
จ. ภาพแสดงแบบผลิตภัณฑ์
☐ รูปเขียน รูป หน้า
☐ ภาพถ่าย รูป หน้า
ฉ. บทสรุปการประดิษฐ์ 1 หน้า

14.เอกสารประกอบคำขอ
☐ เอกสารแสดงสิทธิในการขอรับสิทธิบัตร/อนุสิทธิบัตร
☐ หนังสือรับรองการแสดงการประดิษฐ์/การออกแบบผลิตภัณฑ์
☐ หนังสือมอบอำนาจ
☐ เอกสารรายละเอียดเกี่ยวกับจุลชีพ
☐ เอกสารการขอนับวันยื่นคำขอในต่างประเทศเป็นวันยื่นคำขอในประเทศไทย
☐ เอกสารขอเปลี่ยนแปลงประเภทของสิทธิ
☐ เอกสารอื่น ๆ

15. ข้าพเจ้าขอรับรองว่า
☑ การประดิษฐ์นี้ไม่เคยยื่นขอรับสิทธิบัตร/ อนุสิทธิบัตรมาก่อน
☐ การประดิษฐ์นี้ได้พัฒนาปรับปรุงมาจาก.....

16.ลายมือชื่อ (☐ ผู้ขอรับสิทธิบัตร / อนุสิทธิบัตร; ☑ ตัวแทน)
นายมงคล แก้วมหา มงคล แก้วมหา

หมายเหตุ บุคคลใดยื่นขอรับสิทธิบัตรการประดิษฐ์หรือการออกแบบผลิตภัณฑ์ หรืออนุสิทธิบัตร โดยการแสดงข้อความอันเป็นเท็จแก่พนักงานเจ้าหน้าที่ เพื่อให้ได้ไปซึ่งสิทธิบัตรหรืออนุสิทธิบัตร ต้องระวางโทษจำคุกไม่เกินหกเดือน หรือปรับไม่เกินห้าพันบาท หรือทั้งจำทั้งปรับ

3. ผู้ขอรับสิทธิบัตร/อนุสิทธิบัตร และที่อยู่ (เลขที่ ถนน ประเทศ)

จุฬาลงกรณ์มหาวิทยาลัย

อยู่ที่ เลขที่ 254 ถนนพญาไท แขวงวังใหม่ เขตปทุมวัน กรุงเทพฯ 10330

3.1 สัญชาติ ไทย 3.2 โทรศัพท์ 0-2160-5340-2 3.3 โทรสาร 0-2160-5343

สำนักงานกองทุนสนับสนุนการวิจัย

อยู่ที่ ชั้น 14 อาคาร เอส เอ็ม ทาวเวอร์ เลขที่ 979/17-21 ถนนพหลโยธิน แขวงสามเสนใน เขตพญาไท กรุงเทพฯ 10400

3.1 สัญชาติ ไทย 3.2 โทรศัพท์ 0-2278-8200 3.3 โทรสาร 0-2298-0476

สำนักงานพัฒนาวิทยาศาสตร์และเทคโนโลยีแห่งชาติ

อยู่ที่ 111 อุทยานวิทยาศาสตร์ประเทศไทย ถนนพหลโยธิน ตำบลคลองหนึ่ง อำเภอคลองหลวง จังหวัดปทุมธานี 12120

3.1 สัญชาติ ไทย 3.2 โทรศัพท์ 0-2564-7000 3.3 โทรสาร 0-2564-7001-5

6. ผู้ประดิษฐ์/ผู้ออกแบบผลิตภัณฑ์ และที่อยู่ (เลขที่ ถนน ประเทศ)

นางสาวสุดา เกียรติกำจรวงศ์ และ นายณัฐวุฒ ลิ้มประยูร

อยู่ที่ คณะวิทยาศาสตร์ จุฬาลงกรณ์มหาวิทยาลัย ถนนพญาไท แขวงวังใหม่ เขตปทุมวัน กรุงเทพฯ 10330

นางนิสภา ศีตะปันย์

อยู่ที่ ศูนย์เทคโนโลยีโลหะและวัสดุแห่งชาติ สำนักงานพัฒนาวิทยาศาสตร์และเทคโนโลยีแห่งชาติ 111 อุทยานวิทยาศาสตร์ประเทศไทย ถนนพหลโยธิน ตำบลคลองหนึ่ง อำเภอคลองหลวง จังหวัดปทุมธานี 12120

รายละเอียดการประดิษฐ์

ชื่อที่แสดงถึงการประดิษฐ์

เจลอิมัลชันวัสดุเชิงประกอบพอลิเมอร์ดูดซึมน้ำมากและเจลอิมัลชันพอลิเมอร์ดูดซึมน้ำมากที่มีสมบัติหน่วงการติดไฟ

สาขาวิทยาการที่เกี่ยวข้องกับการประดิษฐ์

สาขาพอลิเมอร์ในส่วนที่เกี่ยวข้องกับการพัฒนาเจลอิมัลชันจากวัสดุเชิงประกอบพอลิเมอร์ดูดซึมน้ำมากและเจลอิมัลชันจากพอลิเมอร์ดูดซึมน้ำมากสำหรับการนำไปใช้งานเพื่อหน่วงการติดไฟที่มีอุณหภูมิสูง เช่น ไฟป่า

ภูมิหลังของศิลปะหรือวิทยาการที่เกี่ยวข้อง

พอลิเมอร์ดูดซึมน้ำมาก (superabsorbent polymers, SAPs) คือ พอลิเมอร์เชื่อมขวางที่สามารถดูดซึมและกักเก็บน้ำ สารละลายเกลือ หรือของเหลวในร่างกายได้ในปริมาณมากอาจถึงพันเท่าของน้ำหนักพอลิเมอร์แห้ง และสามารถปลดปล่อยน้ำที่เก็บไว้ออกมาภายใต้อิทธิพลของสิ่งกระตุ้น เนื่องจากโครงสร้างประกอบไปด้วยหมู่ฟังก์ชันที่ชอบน้ำ พอลิเมอร์ประเภทนี้จะไม่ละลายในตัวทำละลาย เนื่องจากมีโครงสร้างเชื่อมขวางอยู่ภายใน การที่พอลิเมอร์ดูดซึมน้ำมากมีหมู่ฟังก์ชันเป็นหมู่ที่มีไอออนที่สามารถแตกตัวได้ในน้ำ (ionic groups) เป็นองค์ประกอบ ช่วยให้ความสามารถในการดูดซึมน้ำมากขึ้นเมื่อเทียบกับพอลิเมอร์ดูดซึมน้ำมากที่ไม่มีหมู่ฟังก์ชันที่แตกตัวได้ เนื่องจากการผลักกันระหว่างประจุของหมู่ฟังก์ชันที่แตกตัวได้ส่งผลให้โครงสร้างร่างแหขยายตัวมากขึ้น มอนอเมอร์ประเภทไวนิลที่มีหมู่ฟังก์ชันแตกตัวได้ ได้แก่ อะคริลิกแอซิด อิทาโคนิกแอซิด เกลือของ 2-อะคริลามิโด-2-เมทิลโพรเพนซัลโฟนิกแอซิด ได้นำมาใช้เพื่อสังเคราะห์พอลิเมอร์ดูดซึมน้ำมาก มักนิยมสังเคราะห์เป็นพอลิเมอร์ร่วมกับพอลิเมอร์ที่ไม่มีหมู่ฟังก์ชันที่แตกตัวได้ เช่น อะคริลาไมด์ จากลักษณะดังกล่าวทำให้มีการนำพอลิเมอร์ดูดซึมน้ำมากไปใช้งานกันอย่างกว้างขวาง เช่น ในอุตสาหกรรมผ้าอ้อม ผ้าอนามัย อุตสาหกรรมเกษตร เครื่องสำอาง แผ่นดูดซึม และสำหรับการนำไปใช้งานเพื่อหน่วงการลุกลามของไฟ โดยเฉพาะไฟป่า ซึ่งมักมีอุณหภูมิสูง เกิดในบริเวณกว้าง ทำให้การควบคุมเป็นไปด้วยความยากลำบาก

ปกติ การดับไฟที่ลุกลามนั้น นิยมใช้น้ำฉีดไปที่วัตถุที่ติดไฟเพื่อลดอุณหภูมิให้ต่ำกว่าอุณหภูมิที่สามารถติดไฟได้ แต่ข้อเสีย คือ ปริมาณน้ำส่วนมากจะระเหยกลายเป็นไอเมื่อน้ำไปสัมผัสกับวัตถุที่กำลังลุกไหม้ นอกจากนี้ น้ำส่วนหนึ่งก็มักจะไหลตกลงมาอยู่ที่พื้นโดยไม่ได้ถูกดูดซึมไว้ในโครงสร้างของวัตถุที่กำลังติดไฟ ทำให้เป็นการสูญเสียน้ำในปริมาณมากที่ไม่ได้ใช้ประโยชน์ ยังพบว่าน้ำปริมาณน้อยกว่าร้อยละ 10 ถูกดูดซึมไว้ในวัตถุที่กำลังลุกไหม้และมีประสิทธิภาพในการดับไฟ และข้อเสียอีกอย่างคือ น้ำปริมาณที่ถูกดูดซึมไว้ในวัตถุที่กำลังลุกไหม้นั้นมีประสิทธิภาพในการดับไฟ

อย่างจำกัด กล่าวคือ โครงสร้างของวัตถุที่ติดไฟส่วนใหญ่นั้นสามารถดูดซึมน้ำในปริมาณจำกัด ส่งผลให้น้ำที่ถูกดูดซึมน้ำระเหยไปอย่างรวดเร็วเมื่อได้รับความร้อนสูงเนื่องจากความร้อนจากไฟไหม้ ดังนั้น วิธีการดับไฟด้วยน้ำจึงต้องใช้น้ำในปริมาณมากฉีดไปที่วัตถุที่กำลังลุกไหม้อย่างต่อเนื่อง เพื่อป้องกันการลุกลามของไฟ และเพื่อดับไฟให้ได้ในที่สุด

ดังนั้น วัสดุที่สามารถช่วยควบคุมหรือหน่วงการลุกลามของไฟโดยเฉพาะไฟป่าจึงได้รับความสนใจมาก วัสดุชนิดนี้ต้องมีการดูดซึมความชื้นไว้ภายในตัววัสดุในตอนที่ยังไม่ได้เกิดไฟป่า ทนความร้อนได้สูง สามารถปลดปล่อยความชื้นได้ในขณะที่รับความร้อน และวัสดุนี้ไม่ลุกไหม้ติดไฟได้ง่าย จากสมบัติที่ต้องการนี้ จึงมีการนำพอลิเมอร์ดูดซึมน้ำมาก (SAP) มาประยุกต์สำหรับการนำไปใช้ดังกล่าว กลไกการหน่วงการลุกลามของไฟ คือ การทำให้พื้นผิวของวัตถุที่ติดไฟเย็นลง และลดปริมาณของแก๊สออกซิเจนที่ผิวของวัตถุที่ติดไฟ ส่งผลให้ไฟดับเอง อนุภาค SAP ที่บวมตัวในน้ำสามารถเกาะติดกับพื้นผิววัตถุได้ดีเมื่อเทียบกับการใช้น้ำ ดังตัวอย่างสิทธิบัตร US 5190110 ใช้ SAP ที่เตรียมจากพอลิเมอร์ร่วมของกรดอะคริลิกกระจายตัวในน้ำ และสิทธิบัตร US 5849210 ใช้ SAP ที่เตรียมจากพอลิเมอร์ร่วมของกรดอะคริลิกและเกลือโซเดียมอะคริเลตมาบวมตัวในน้ำ ความสามารถในการบวมตัวในน้ำของ SAP ที่ใช้อย่างน้อย 50 เท่าของน้ำหนักแห้ง ทำให้สารแขวนลอยที่ได้มีความหนืดสูงเพียงพอที่จะเกาะติดกับพื้นผิวของวัตถุในแนวตั้ง หรือวัตถุที่มีความชัน

สิทธิบัตร US 7670513 B2 กล่าวถึงการใช้สารแขวนลอยของอนุภาค SAP สารให้สี (colorant) และสารทึบ (opacifying agent) ในน้ำสำหรับใช้ป้องกัน และ/หรือหน่วงการลุกลามของไฟป่า สีที่นำมาใช้เพื่อทำให้สามารถทราบได้ว่า พื้นที่ใดได้รับการฉีด หรือ aerial dropping สารแขวนลอยของน้ำดังกล่าวแล้ว และสารทึบที่ใช้เพื่อเพิ่มประสิทธิภาพในการมองเห็นของสารให้สี สารทึบที่นิยมใช้ได้แก่ แคลเซียมคาร์บอเนต อิมัลชัน หรือลาเท็กซ์ของพอลิเมอร์เอกพันธุ์ หรือพอลิเมอร์ร่วมสังเคราะห์ เช่น พอลิเมอร์ร่วมของสไตรีน-บิวทาไดอีน-สไตรีน แป้ง พอลิสไตรีน พอลิไวนิลแอลกอฮอล์ นอกจากนี้ อาจมีการเติมสารเพิ่มความหนืด สารเพิ่มการกระจายตัว เพื่อเพิ่มความเสถียรของอนุภาค SAP ที่แขวนลอยในน้ำ

เอกสารประกาศโฆษณาคำขอรับสิทธิบัตร US 2009/0151963 A1 เตรียมอิมัลชันของอนุภาค SAP ในน้ำมันพืช อิมัลชันที่เตรียมได้จะมีสมบัติเป็นเจลที่มีความหนืดสูงเพียงพอที่จะเกาะติดกับพื้นผิวทั้งในแนวตั้ง และแนวนอน อนุภาค SAP ที่ใช้เป็นอนุภาคพอลิเมอร์ชอบน้ำ เช่น เกลือของกรดอะคริลิก และเทอร์พอลิเมอร์ของเกลืออะคริเลต อะคริลาไมด์ และเกลือของ 2-อะคริลามิโด-2-เมทิลโพรเพนซัลโฟนิกแอซิด สารลดแรงตึงผิวที่ใช้ในการเตรียมอิมัลชันมีค่า hydrophilic/lipophilic balance (HLB) สูงกว่า 9.5 และมีการเติมสารช่วยแขวนลอย (suspending agent) เช่น fume silica ลงไปด้วยเพื่อช่วยเพิ่มความเสถียรให้เจลอิมัลชัน

อย่างไรก็ตาม พอลิเมอร์ดูดซึมน้ำมากที่ได้กล่าวอ้างไว้ในสิทธิบัตรและเอกสารประกาศโฆษณาคำขอรับสิทธิบัตรที่กล่าวแล้วข้างต้นไม่ได้มีการผสมสารหน่วงไฟลงไปด้วย จึงไม่สามารถ

ทนความร้อนได้ดีในช่วงอุณหภูมิที่เกิดไฟป่า อีกทั้งเป็นสารอินทรีย์ จึงสามารถสลายตัวและปลดปล่อยน้ำที่ดูดซึมไว้อย่างรวดเร็วที่อุณหภูมิต่ำกว่าอุณหภูมิที่เกิดไฟป่า ดังนั้น จึงมีสมบัติไม่เหมาะสมกับการนำไปใช้ควบคุมการลุกลามของไฟป่า

ลักษณะและความมุ่งหมายของการประดิษฐ์

เพื่อแก้ไขปัญหาที่ได้กล่าวไว้ในภูมิหลังของศิลปะหรือวิทยาการที่เกี่ยวข้อง การประดิษฐ์นี้จึงได้สังเคราะห์และพัฒนาเจลอิมัลชันจากพอลิเมอร์ดูดซึมน้ำมากที่มีความสามารถในการดูดซึมน้ำในปริมาณมาก ทนความร้อน และหน่วงการติดไฟ เพื่อให้มีสมบัติเหมาะสมกับการนำไปใช้ในการควบคุมการลุกลามของไฟป่า โดยการประดิษฐ์นี้สังเคราะห์พอลิเมอร์ดูดซึมน้ำมากจากมอนอเมอร์ร่วมคือ อะคริลาไมด์ และ 2-อะคริลามิโด-2-เมทิลโพรเพนโซเดียมซัลโฟเนต ซึ่งจะช่วยเพิ่มการดูดซึมน้ำของพอลิเมอร์ดูดซึมน้ำมากให้มากขึ้น เนื่องจากในการนำไปใช้งานจริงจำเป็นต้องใช้น้ำที่มีอยู่ในบริเวณพื้นที่ที่เกิดไฟป่า ซึ่งอาจเป็นน้ำกระด้างที่มีเกลือประจุบวกในปริมาณมาก นอกจากนี้ ยังเพิ่มความสามารถในการทนความร้อนและหน่วงการติดไฟโดยเติมไมกา ซึ่งเป็นเคลย์ชนิดหนึ่งเพื่อเพิ่มความเสถียรเชิงความร้อน เติมซิงก์บอเรตซึ่งเป็นสารหน่วงการติดไฟชนิดไร้สารฮาโลเจนซึ่งเป็นสารพิษ เติมเมลามีนลงไปในปฏิกิริยาการสังเคราะห์พอลิเมอร์ดูดซึมน้ำมาก ทำให้ได้วัสดุเชิงประกอบพอลิเมอร์ดูดซึมน้ำมากขนาดนาโนเมตร นำมาเตรียมเป็นเจลอิมัลชันที่มีสัดส่วนของอนุภาคแห้งของวัสดุเชิงประกอบพอลิเมอร์ดูดซึมน้ำมากขนาดนาโนเมตร ต่อน้ำมันพืช ต่อสารลดแรงตึงผิว และต่อน้ำ ในสัดส่วนร้อยละ 2 : 2.5 : 0.5 : 95 โดยน้ำหนัก ตามลำดับ

วัสดุเชิงประกอบพอลิเมอร์ดูดซึมน้ำมากขนาดนาโนเมตรที่เตรียมจากการผสมซิงก์บอเรตและเมลามีนในสัดส่วนร้อยละ 20 : 10 โดยน้ำหนัก เมื่อเทียบกับปริมาณมอนอเมอร์ที่ใช้สามารถหน่วงการจุดติดไฟได้นานถึง 278 วินาที ก่อนที่ชิ้นไม้ที่เคลือบด้วยอิมัลชันของวัสดุเชิงประกอบพอลิเมอร์ดูดซึมน้ำมากขนาดนาโนเมตรที่ความหนา 3 มิลลิเมตรจะติดไฟ เมื่อเทียบกับชิ้นไม้ที่เคลือบด้วยพอลิเมอร์ดูดซึมน้ำมากที่ความหนา 3 มิลลิเมตร จะลุกติดไฟเมื่อเวลาผ่านไป 125 วินาที และชิ้นไม้ที่ไม่ได้เคลือบซึ่งจะติดไฟที่เวลา 13 วินาที หลังจากสัมผัสกับเปลวไฟที่อุณหภูมิ 885 องศาเซลเซียส

การเปิดเผยการประดิษฐ์โดยสมบูรณ์

เจลอิมัลชันวัสดุเชิงประกอบพอลิเมอร์ดูดซึมน้ำมากขนาดนาโนเมตรที่มีสมบัติหน่วงไฟตามการประดิษฐ์นี้เกี่ยวข้องกับพอลิเมอร์ดูดซึมน้ำมากที่มีสมบัติในการควบคุม และหน่วงการลุกลามของไฟที่มีอุณหภูมิสูง เช่น ไฟป่า พอลิเมอร์สามารถดูดซึมน้ำไว้ภายในในปริมาณมาก ทนความร้อนได้สูง สามารถปลดปล่อยความชื้นได้ในขณะได้รับความร้อน และไม่ลุกติดไฟ วัสดุเชิงประกอบพอลิเมอร์ดูดซึมน้ำมากขนาดนาโนเมตรนี้มีองค์ประกอบสำคัญ คือ

- พอลิ(อะคริลาไมด์-*โค*-2-อะคริลามิโด-2-เมทิลโพรเพนโซเดียมซัลโฟเนต) ที่สัดส่วนร้อยละโดยโมล 98 : 2 ถึง 15 : 85 ตามลำดับ โดยเฉพาะอย่างยิ่ง 20 : 80 ถึง 15 : 85

- สารหน่วงไฟ ได้แก่ ไมกา ซิงก์บอเรต และเมลามีน ในปริมาณร้อยละ 5-30 โดยน้ำหนักเมื่อเทียบกับน้ำหนักมอนอเมอร์

พอลิเมอร์ดูดซึมน้ำมากของพอลิ(อะคริลาไมด์-*โค*-2-อะคริลามิโด-2-เมทิลโพรเพนโซเดียมซัลโฟเนต) สังเคราะห์จากกระบวนการเกิดพอลิเมอร์แบบเชื่อมขวางด้วยอนุมูลอิสระ โดยใช้แอมโมเนียมเพอร์ซัลเฟต, เอ็น เอ็น เอ็น′ เอ็น′- เททระเมทิลเอทิลีนไดแอมีน และเอ็น เอ็น′-เมทิลีนบิสอะคริลาไมด์ เป็นสารริเริ่มปฏิกิริยา สารริเริ่มปฏิกิริยาร่วม และสารเชื่อมขวาง ตามลำดับ โดยปริมาณของมอนอเมอร์อะคริลาไมด์ ต่อ มอนอเมอร์ 2-อะคริลามิโด-2-เมทิลโพรเพนโซเดียมซัลโฟเนตร้อยละโดยโมล 98 : 2 ถึง 15 : 85 ตามลำดับ โดยเฉพาะอย่างยิ่ง 20 : 80 ถึง 15 : 85 ปริมาณสารริเริ่มปฏิกิริยาแอมโมเนียมเพอร์ซัลเฟต ร้อยละ 0.6-1.8 โดยโมลของมอนอเมอร์ โดยเฉพาะอย่างยิ่งร้อยละ 0.6 ปริมาณสารริเริ่มปฏิกิริยาร่วมเอ็น เอ็น เอ็น′เอ็น′- เททระเมทิลเอทิลีนไดแอมีนร้อยละ 0.6-1.8 โดยโมลของมอนอเมอร์ โดยเฉพาะอย่างยิ่งร้อยละ 0.6 ปริมาณสารเชื่อมขวางเอ็น เอ็น′-เมทิลีนบิสอะคริลาไมด์ร้อยละ 0.05-0.2 โดยโมลของมอนอเมอร์ โดยเฉพาะอย่างยิ่งร้อยละ 0.05 ปริมาณน้ำที่ใช้ในปฏิกิริยาการเกิดพอลิเมอร์อยู่ในช่วง 10-40 มิลลิลิตร

วัสดุเชิงประกอบพอลิ(อะคริลาไมด์-*โค*-2-อะคริลามิโด-2-เมทิลโพรเพนโซเดียมซัลโฟเนต) ขนาดนาโนเมตร สังเคราะห์ได้จากกระบวนการเดียวกันกับการเตรียมพอลิเมอร์ดูดซึมน้ำมากดังกล่าว โดยมีการเติมไมกา ซิงก์บอเรต และ/หรือเมลามีน ในปริมาณระหว่างร้อยละ 5-30 โดยน้ำหนักเมื่อเทียบกับน้ำหนักมอนอเมอร์ ลงไปในสารละลายของมอนอเมอร์ ก่อนปฏิกิริยาการเกิดพอลิเมอร์ โดยสารหน่วงไฟที่ใช้ดังกล่าวสามารถเติมเพียงชนิดเดียว หรือใช้ในรูปของผสม โดยเฉพาะอย่างยิ่ง ของผสมระหว่างซิงก์บอเรตร้อยละ 20 กับเมลามีนร้อยละ 10 โดยน้ำหนัก

พอลิเมอร์ดูดซึมน้ำมาก และวัสดุเชิงประกอบพอลิเมอร์ดูดซึมน้ำมากขนาดนาโนเมตร นำมาเตรียมเป็นอิมัลชันโดยการผสมอนุภาคพอลิเมอร์เข้ากับน้ำมันพืช เช่น น้ำมันปาล์ม น้ำมันถั่วเหลือง และสารลดแรงตึงผิวแบบไม่มีไอออน (nonionic surfactant) ซึ่งอาจใช้ในรูปของผสมของสารลดแรงตึงผิว เช่น ของผสมระหว่างพอลิซอร์เบต 80 (polysorbate 80) กับ ซอร์บิแทนโมโนโอลิเอต (sorbitan monooleate) ในปริมาณร้อยละ 54 ต่อ 46 โดยน้ำหนัก ตามลำดับ และค่า HLB สุทธิมีค่ามากกว่า 9.5 เพื่อให้เหมาะสมกับการนำไปใช้ในรูปของอิมัลชันของน้ำมันในน้ำ สัดส่วนโดยน้ำหนักของอนุภาคพอลิเมอร์ดูดซึมน้ำมาก ต่อ น้ำมันพืช ต่อ สารลดแรงตึงผิว มีค่า 40 ต่อ 50 ต่อ 10 เมื่อนำสารแขวนลอยของอนุภาคพอลิเมอร์ดูดซึมน้ำมากในน้ำมันไปผสมในน้ำประปาที่ปริมาณสารโดยปริมาตรในช่วงร้อยละ 1.25-5 จะมีค่าความหนืดอยู่ที่ 25-100 ถึง 0.1-1 พาสคัล วินาที ที่ค่าอัตราเฉือนต่ำและสูง ตามลำดับ

เจลอิมัลชันวัสดุเชิงประกอบพอลิเมอร์ดูดซึมน้ำมากตามการประดิษฐ์นี้ มีสัดส่วนร้อยละโดยน้ำหนักของอนุภาคแห้งวัสดุเชิงประกอบพอลิเมอร์ดูดซึมน้ำมากขนาดนาโนเมตร ต่อ น้ำมันพืช ต่อ สารลดแรงตึงผิวที่เป็นของผสมในน้ำประปา เท่ากับ 2 ต่อ 2.5 ต่อ 0.5 ต่อ 95

ในส่วนของเจลอิมัลชันพอลิเมอร์ดูดซึมน้ำมากตามการประดิษฐ์นี้ มีสัดส่วนร้อยละโดยน้ำหนักของอนุภาคแห้งพอลิเมอร์ดูดซึมน้ำมาก ต่อ น้ำมันพืช ต่อ สารลดแรงตึงผิวที่เป็นของผสมในน้ำประปา เท่ากับ 2 ต่อ 2.5 ต่อ 0.5 ต่อ 95

นำแผ่นไม้ที่เคลือบด้วยเจลอิมัลชันพอลิเมอร์ดูดซึมน้ำมาก และแผ่นไม้เคลือบเจลอิมัลชันวัสดุเชิงประกอบพอลิเมอร์ดูดซึมน้ำมากขนาดนาโนเมตร มาทดสอบความสามารถในการติดไฟเมื่อสัมผัสเปลวไฟที่อุณหภูมิ 885 องศาเซลเซียส จากเครื่อง cone calorimeter ในสภาวะบรรยากาศ (air atmosphere) โดยใช้แผ่นไม้ที่ไม่เคลือบเจลอิมัลชันเป็นตัวควบคุม

ตัวอย่างต่อไปนี้แสดงให้เห็นเพิ่มเติมถึงการประดิษฐ์ โดยมิได้มีวัตถุประสงค์ที่จะจำกัดขอบเขตของการประดิษฐ์นี้แต่อย่างใด

ตัวอย่างที่ 1 การสังเคราะห์พอลิเมอร์ดูดซึมน้ำมากของพอลิ(อะคริลาไมด์-โค-2-อะคริลามิโด-2-เมทิลโพรเพนโซเดียมซัลโฟเนต)

การสังเคราะห์พอลิเมอร์ดูดซึมน้ำมากของพอลิ(อะคริลาไมด์-*โค*-2-อะคริลามิโด-2-เมทิลโพรเพนโซเดียมซัลโฟเนต) นั้น ทำโดยการละลายอะคริลาไมด์ในน้ำปริมาตร 10 มิลลิลิตร ในขวดก้นกลม ที่ต่อด้วยแท่งกวนเชิงกล คอนเดนเซอร์ และท่อนำแก๊สไนโตรเจน เติม 2-อะคริลามิโด-2-เมทิลโพรเพนโซเดียมซัลโฟเนตลงไปในของผสม โดยสัดส่วนของอะคริลาไมด์ต่อ 2-อะคริลามิโด-2-เมทิลโพรเพนโซเดียมซัลโฟเนตเท่ากับร้อยละ 15 ต่อ 85 โดยโมล กวนมอนอเมอร์ผสมให้เข้ากันที่ 250 รอบต่อนาที ที่อุณหภูมิห้อง นาน 5 นาที เพิ่มอุณหภูมิเป็น 60 องศาเซลเซียส นำของผสมระหว่างสารริเริ่มปฏิกิริยาแอมโมเนียมเพอร์ซัลเฟต กับสารเชื่อมขวาง เอ็น เอ็น′-เมทิลีนบิสอะคริลาไมด์ที่ปริมาณร้อยละ 0.6 และ 0.05 โดยโมล เทียบกับมอนอเมอร์ตามลำดับ เติมลงไปในปฏิกิริยาและกวนนาน 5 นาที จากนั้นเติมปริมาณสารริเริ่มปฏิกิริยาร่วม เอ็น เอ็น เอ็น′ เอ็น′- เททระเมทิลเอทิลีนไดแอมีนที่ปริมาณร้อยละ 0.6 โดยโมลเทียบกับมอนอเมอร์ ลงไปในปฏิกิริยาและทำปฏิกิริยาต่อนาน 30 นาที เพื่อให้ปฏิกิริยาเกิดสมบูรณ์ นำผลผลิตที่ได้มากำจัดน้ำออกโดยล้างพอลิเมอร์ที่ได้ด้วยอะซีโทน จะได้อนุภาคพอลิเมอร์ดูดซึมน้ำมาก นำไปทำให้แห้งด้วยการอบในเตาอบที่อุณหภูมิ 50 องศาเซลเซียส นาน 24 ชั่วโมง นำพอลิเมอร์ที่ได้ไปผ่านกระบวนการสกัดใน soxhlet เพื่อกำจัดมอนอเมอร์ที่ไม่ทำปฏิกิริยาออก และอบให้แห้งเป็นเวลา 24 ชั่วโมง นำพอลิเมอร์ที่ได้มาบด และคัดขนาดอนุภาค

ด้วยตะแกรงขนาด 100 เมช พอลิเมอร์ที่ได้มีความสามารถในการดูดซึมน้ำปราศจากไอออนได้สูงถึง 1212 ± 54 กรัมต่อกรัมของน้ำหนักแห้ง

ตัวอย่างที่ 2 การสังเคราะห์วัสดุเชิงประกอบพอลิเมอร์ดูดซึมน้ำมากขนาดนาโนเมตรของพอลิ(อะคริลาไมด์-*โค*-2-อะคริลามิโด-2-เมทิลโพรเพนโซเดียมซัลโฟเนต) ซิงก์บอเรต และเมลามีน

สังเคราะห์วัสดุเชิงประกอบเหมือนตัวอย่างที่ 1 แต่ให้เติมสารหน่วงไฟที่เป็นของผสมระหว่างซิงก์บอเรตในปริมาณร้อยละ 20 กับ เมลามีนในปริมาณร้อยละ 10 โดยน้ำหนัก เมื่อเทียบกับน้ำหนักมอนอเมอร์ ลงไปในสารละลายผสมของมอนอเมอร์ทั้งสอง กวนให้เข้ากันที่อุณหภูมิห้องนาน 2 ชั่วโมง จึงเติมสารริเริ่มปฏิกิริยา สารเชื่อมขวาง และสารริเริ่มปฏิกิริยาร่วม ตามลำดับ วัสดุเชิงประกอบที่สังเคราะห์ได้มีความสามารถในการดูดซึมน้ำปราศจากไอออนได้สูงถึง 668 ± 8 กรัมต่อกรัมของน้ำหนักแห้ง

การเตรียมเจลอิมัลชันของพอลิเมอร์ดูดซึมน้ำมาก และวัสดุเชิงประกอบพอลิเมอร์ดูดซึมน้ำมากขนาดนาโนเมตร

ผสมอนุภาคแห้งของพอลิเมอร์ดูดซึมน้ำมาก หรือวัสดุเชิงประกอบพอลิเมอร์ดูดซึมน้ำมากขนาดนาโนเมตร น้ำมันพืช เช่น น้ำมันปาล์ม สารลดแรงตึงผิวที่เป็นของผสมมีสัดส่วนของพอลิซอร์เบต 80 (polysorbate 80) ต่อ ซอร์บิแทนโมโนโอลิเอต (sorbitan monoolcate) ร้อยละ 54 ต่อ 46 โดยน้ำหนัก ตามลำดับ และน้ำประปา ในสัดส่วนร้อยละ 2 ต่อ 2.5 ต่อ 0.5 ต่อ 95 โดยน้ำหนัก ตามลำดับ กวนให้เข้ากัน แล้วนำเจลอิมัลชันที่เตรียมไปเคลือบบนแผ่นไม้ (Apocynaceae, Wrightia religiosa *Benth.*) ที่มีความกว้าง x ความยาว x ความหนา เท่ากับ 100 x 100 x 3 ลูกบาศก์เซนติเมตร โดยเจลอิมัลชันที่ใช้เคลือบมีความหนา 3 มิลลิเมตร

การทดสอบความสามารถในการติดไฟของแผ่นไม้เคลือบเจลอิมัลชันพอลิเมอร์ดูดซึมน้ำมาก และแผ่นไม้เคลือบเจลอิมัลชันวัสดุเชิงประกอบพอลิเมอร์ดูดซึมน้ำมากขนาดนาโนเมตร

จากการวิเคราะห์การลุกติดไฟด้วยเครื่อง cone calorimeter ที่อุณหภูมิ 885 องศาเซลเซียส พบว่า แผ่นไม้ที่เคลือบด้วยเจลอิมัลชันพอลิเมอร์ดูดซึมน้ำมากหรือเจลอิมัลชันวัสดุเชิงประกอบพอลิเมอร์ดูดซึมน้ำมากขนาดนาโนเมตรชนิดต่าง ๆ มีความสามารถในการหน่วงไฟที่แตกต่างกันดังแสดงในตารางที่ 1 ใช้แผ่นไม้ที่ไม่ได้เคลือบเจลอิมัลชันเป็นตัวควบคุม

ตารางที่ 1 ผลการทดลองใช้งาน

ตัวอย่างแผ่นไม้	เวลาลุกติดไฟ (วินาที)	เวลาที่ใช้ในการเผาชั้นเคลือบ (วินาที)
ไม่เคลือบ (ควบคุม)	13 ± 2	-
เคลือบเจล SAP	125 ± 2	4 ± 2
เคลือบเจล SAP + ไมกา (ร้อยละ 30)	186 ± 3	84 ± 6
เคลือบเจล SAP + ซิงก์บอเรต (ร้อยละ 20)	118 ± 3	96 ± 1
เคลือบเจล SAP + เมลามีน (ร้อยละ 30)	117 ± 2	119 ± 2
เคลือบเจล SAP + ซิงก์บอเรต (ร้อยละ 20) + เมลามีน (ร้อยละ 10)	278 ± 5	60 ± 2

แผ่นไม้ควบคุมที่ไม่ได้เคลือบลุกติดไฟภายในเวลา 13 วินาที หลังจากสัมผัสกับเปลวไฟ แผ่นไม้ที่เคลือบด้วยเจลอิมัลชันสามารถหน่วงการลุกติดไฟได้ดีมาก ตัวอย่างไม้ที่เคลือบด้วยเจลอิมัลชัน SAP, SAP + ซิงก์บอเรต ร้อยละ 20 และ SAP + เมลามีน ร้อยละ 30 ลุกติดไฟที่เวลาประมาณ 125, 118 และ 117 วินาที ตามลำดับ แผ่นไม้ที่เคลือบด้วยเจลอิมัลชัน SAP + ไมกา ร้อยละ 30 และ SAP + ซิงก์บอเรต (ร้อยละ 20) + เมลามีน (ร้อยละ 10) หน่วงการติดไฟได้นาน 186 และ 278 วินาที ตามลำดับ

เมื่อเปรียบเทียบระยะเวลาที่เปลวไฟเผาไหม้ชั้นเคลือบพบว่า การเคลือบด้วยเจลอิมัลชันของวัสดุเชิงประกอบ SAP ขนาดนาโนเมตรชนิดต่าง ๆ หน่วงการติดไฟได้นานกว่าเจลอิมัลชัน SAP จนกว่าจะเผาไหม้หมด ประมาณ 60-120 วินาที เมื่อเปรียบเทียบกับเจลอิมัลชัน SAP ซึ่งหน่วงการติดไฟได้แค่ 4 วินาที ในการเผาไหม้จนหมด เนื่องจากมีไมกา ซิงก์บอเรต และเมลามีนอยู่ในวัสดุเชิงประกอบ SAP สามารถหน่วงการแพร่ผ่านของความร้อน และทำให้การเผาไหม้ช้าลง เถ้าของสารหน่วงไฟปกคลุมอยู่บนพื้นผิวของแผ่นไม้ช่วยลดปริมาณของแก๊สออกซิเจนที่พื้นผิว ทำให้หน่วงเวลาการติดไฟของแผ่นไม้ได้มากขึ้น

วิธีการในการประดิษฐ์ที่ดีที่สุด

เหมือนกับที่ได้กล่าวไว้แล้วในหัวข้อการเปิดเผยการประดิษฐ์โดยสมบูรณ์

ข้อถือสิทธิ

1. เจลอิมัลชันวัสดุเชิงประกอบพอลิเมอร์ดูดซึมน้ำมาก ที่เตรียมจากการผสมสารแขวนลอยของวัสดุเชิงประกอบพอลิเมอร์ดูดซึมน้ำมากในน้ำมันและสารลดแรงตึงผิว กับน้ำประปา ซึ่งวัสดุเชิงประกอบพอลิเมอร์ดูดซึมน้ำมากประกอบด้วย

ก. พอลิเมอร์ร่วมของพอลิอะคริลาไมด์กับพอลิ (2-อะคริลามิโด-2-เมทิลโพรเพนโซเดียมซัลโฟเนต)

ข. สารหน่วงไฟ ซึ่งเลือกจาก ไมกา ซิงก์บอเรต และ เมลามีน สารใดสารหนึ่งหรือใช้เป็นของผสม

2. เจลอิมัลชันพอลิเมอร์ดูดซึมน้ำมาก ที่เตรียมจากการผสมสารแขวนลอยของพอลิเมอร์ดูดซึมน้ำมากในน้ำมันและสารลดแรงตึงผิว กับน้ำประปา ซึ่งพอลิเมอร์ดูดซึมน้ำมากประกอบด้วย

ก. พอลิเมอร์ร่วมของพอลิอะคริลาไมด์กับพอลิ (2-อะคริลามิโด-2-เมทิลโพรเพนโซเดียมซัลโฟเนต)

3. เจลอิมัลชันตามข้อถือสิทธิ 1 หรือ 2 ที่ซึ่งพอลิเมอร์ร่วมของพอลิอะคริลาไมด์กับพอลิ (2-อะคริลามิโด-2-เมทิลโพรเพนโซเดียมซัลโฟเนต) ได้จากปฏิกิริยาการสังเคราะห์พอลิเมอร์แบบเชื่อมขวางด้วยอนุมูลอิสระ โดย

ก. สัดส่วนของอะคริลาไมด์ ต่อ 2-อะคริลามิโด-2-เมทิลโพรเพนโซเดียมซัลโฟเนต อยู่ในช่วง 98 ต่อ 2 ถึง 15 ต่อ 85 โดยโมล ตามลำดับ โดยเฉพาะอย่างยิ่ง 20 ต่อ 80 ถึง 15 ต่อ 85

ข. ปริมาณสารริเริ่มปฏิกิริยาแอมโมเนียมเพอร์ซัลเฟตอยู่ในช่วงร้อยละ 0.6-1.8 โดยโมลของมอนอเมอร์ โดยเฉพาะอย่างยิ่งร้อยละ 0.6

ค. ปริมาณสารริเริ่มปฏิกิริยาร่วมเอ็น เอ็น เอ็น′ เอ็น′-เททระเมทิลเอทิลีนไดแอมีนอยู่ในช่วงร้อยละ 0.6-1.8 โดยโมลของมอนอเมอร์ โดยเฉพาะอย่างยิ่งร้อยละ 0.6

ง. ปริมาณสารเชื่อมขวางเอ็น เอ็น′-เมทิลีนบิสอะคริลาไมด์อยู่ในช่วงร้อยละ 0.05-0.2 โดยโมลของมอนอเมอร์ โดยเฉพาะอย่างยิ่งร้อยละ 0.05

จ. ปริมาณน้ำที่ใช้ในปฏิกิริยาการเกิดพอลิเมอร์อยู่ในช่วง 10-40 มิลลิลิตร

4. เจลอิมัลชันตามข้อถือสิทธิ 1 ที่ซึ่งปริมาณของสารหน่วงไฟอยู่ในช่วงร้อยละ 5 – 30 โดยน้ำหนักเทียบกับน้ำหนักมอนอเมอร์

5. เจลอิมัลชันตามข้อถือสิทธิ 1 หรือ 4 ที่ซึ่งสารหน่วงไฟ ประกอบด้วย ของผสมระหว่างซิงก์บอเรตร้อยละ 20 กับเมลามีนร้อยละ 10 โดยน้ำหนัก

6. เจลอิมัลชันตามข้อถือสิทธิ 1 หรือ 2 ที่ซึ่งน้ำมันที่ใช้ คือ น้ำมันพืช ได้แก่ น้ำมันปาล์ม และน้ำมันถั่วเหลือง

7. เจลอิมัลชันตามข้อถือสิทธิ 1 หรือ 2 ที่ซึ่งสารลดแรงตึงผิวที่ใช้เป็นแบบไม่มีไอออน

8. เจลอิมัลชันตามข้อถือสิทธิ 7 ที่ซึ่งสารลดแรงตึงผิวแบบไม่มีไอออน สามารถใช้ในรูปของผสมของสารลดแรงตึงผิว ได้แก่ ของผสมระหว่างพอลิซอร์เบต 80 (polysorbate 80) กับ ซอร์บิแทนโมโนโอลิเอต (sorbitan monooleate) ในปริมาณร้อยละ 54 ต่อ 46 โดยน้ำหนัก ตามลำดับ

9. เจลอิมัลชันตามข้อถือสิทธิ 1 ที่ซึ่งสัดส่วนของอนุภาคแห้งวัสดุเชิงประกอบพอลิเมอร์ดูดซึมน้ำมากขนาดนาโนเมตร ต่อ น้ำมันพืช ต่อ สารลดแรงตึงผิวที่เป็นของผสมในน้ำประปา มีสัดส่วนร้อยละ 2 ต่อ 2.5 ต่อ 0.5 ต่อ 95 โดยน้ำหนัก ตามลำดับ

10. เจลอิมัลชันตามข้อถือสิทธิ 2 ที่ซึ่งสัดส่วนของอนุภาคแห้งพอลิเมอร์ดูดซึมน้ำมาก ต่อ น้ำมันพืช ต่อ สารลดแรงตึงผิวที่เป็นของผสมในน้ำประปา มีสัดส่วนร้อยละ 2 ต่อ 2.5 ต่อ 0.5 ต่อ 95 โดยน้ำหนัก ตามลำดับ

บทสรุปการประดิษฐ์

การประดิษฐ์นี้เกี่ยวข้องกับการสังเคราะห์เจลอิมัลชันวัสดุเชิงประกอบพอลิเมอร์ดูดซึมน้ำมากที่มีสมบัติหน่วงการติดไฟ โดยมีองค์ประกอบคือ พอลิเมอร์ดูดซึมน้ำมากซึ่งประกอบด้วยพอลิเมอร์ร่วมของพอลิอะคริลาไมด์กับพอลิ (2-อะคริลามิโด-2-เมทิลโพรเพนโซเดียมซัลโฟเนต) สารหน่วงไฟที่เลือกคือ ไมกา ซิงก์บอเรต และ/หรือเมลามีน ในปริมาณร้อยละ 5-30 โดยน้ำหนักของมอนอเมอร์ที่ใช้ในการสังเคราะห์พอลิเมอร์ เมื่อเคลือบเจลอิมัลชันของพอลิเมอร์ดูดซึมน้ำมากตามการประดิษฐ์นี้บนแผ่นไม้ พบว่า ชั้นเคลือบจะลุกติดไฟในเวลาประมาณ 125 วินาที ขณะที่การใช้เจลอิมัลชันของวัสดุเชิงประกอบพอลิเมอร์ดูดซึมน้ำมากตามการประดิษฐ์นี้เคลือบแผ่นไม้ พบว่าชั้นเคลือบจะลุกติดไฟที่เวลา 117-278 วินาที เมื่อเปรียบเทียบกับแผ่นไม้ที่ไม่ได้เคลือบ พบว่า แผ่นไม้ติดไฟภายในเวลา 13 นาทีหลังจากสัมผัสกับเปลวไฟที่อุณหภูมิ 885 องศาเซลเซียส

แบบฟอร์มเปิดเผยการประดิษฐ์และแสดงความจำนงขอให้จดทะเบียนสิทธิบัตร/อนุสิทธิบัตร

(Invention Disclosure Form)

NO.:.....
Receive date:.....

1. ชื่อที่แสดงถึงการประดิษฐ์ (ไทยและอังกฤษ).....
สารปรับสภาพผิวผ้าจากไคโทซานดัดแปรสำหรับผ้าพิมพ์ด้วยหมึกพิมพ์อิงก์เจ็ต
.....
Surface pretreatment from modified chitosan for textile printed by inkjet ink
.....

ลักษณะโดยย่อของการประดิษฐ์ (แนบเอกสารประกอบได้).....

สารปรับสภาพผิวผ้าไคโทซานดัดแปร เอ็น-2-ไฮดรอกซี-3-ไทรเมทิลแอมโมเนียมพรอพิลไคโทซานคลอไรด์ (*N*-[(2-hydroxyl-3-trimethylammonium) propyl] chitosan chloride, HTACC) ซึ่งประกอบด้วย

(1) ไคโทซานดัดแปร HTACC ในสัดส่วนร้อยละ 0.04-10 โดยน้ำหนักขององค์ประกอบทั้งหมดภายในสูตรสารปรับสภาพผิวผ้าจากเส้นใยธรรมชาติหรือเส้นใยธรรมชาติผสมเส้นใยสังเคราะห์

(2) น้ำในสัดส่วนร้อยละ 90-99.96 โดยน้ำหนักขององค์ประกอบทั้งหมดภายในสูตรสารปรับสภาพผิวผ้าจากเส้นใยธรรมชาติหรือเส้นใยธรรมชาติผสมเส้นใยสังเคราะห์

2. ชื่อผู้ประดิษฐ์ / ผู้ประดิษฐ์ร่วม	สัดส่วนการประดิษฐ์/ การแบ่งปันผลประโยชน์ (%)	สังกัด / ที่อยู่	โทรศัพท์ / โทรสาร / อีเมล์
นางสาวสุดา เกียรติกำจรวงศ์	35	คณะวิทยาศาสตร์ จุฬาลงกรณ์มหาวิทยาลัย	02 2185587 / ksuda@chula.ac.th
นางสาวสุภาภรณ์ นพคุณดิลกรัตน์	35	คณะวิทยาศาสตร์ จุฬาลงกรณ์มหาวิทยาลัย	02 2185569 Supaporn.n@chula.ac.th
นางสาวปัญฑ์ธร บูรณะกูล	30	10 ซอยนครลุง 13 แขวงบางไผ่ เขตบางแค กทม 10160	089 6858457 puntune@hotmail.com

3. การประดิษฐ์นี้ได้รับการสนับสนุนทางด้านการเงินจากแหล่งเงินทุนหรือร่วมวิจัยกับ องค์กร บริษัท หรือหน่วยงานใดหรือไม่

☑ ได้รับ โปรดระบุชื่อหน่วยงานที่เกี่ยวข้อง.. สำนักงานกองทุนสนับสนุนการวิจัย ☐ ไม่ได้รับ

4. ผลงานนี้เคยมีการตีพิมพ์ หรือเผยแพร่ผลงานมาก่อนหรือไม่

☐ มี โปรดระบุลักษณะการเผยแพร่..... เมื่อ..... ☑ ไม่มี

5. ศักยภาพของเทคโนโลยีในเชิงพาณิชย์ (โปรดอธิบาย แนบเอกสารประกอบได้)

ผลิตภัณฑ์หรือเทคโนโลยีที่ใกล้เคียงที่มีอยู่แล้วในตลาด... ไม่มี .....

.....

.....

ลักษณะการใช้ประโยชน์จากผลงาน (Application).....

สารละลายปรับผิวผ้าละลายในน้ำได้ ง่ายต่อการใช้งานในเวลาจุ่มรีด ผ้าที่ได้มีสีสันสดใสมาก ขอบเขตสีที่พิมพ์ได้กว้างมากขึ้น มีความเข้มของสีมากขึ้น และผ้าพิมพ์ที่ได้ไม่แข็งกระด้าง มีความนุ่มมือมากขึ้น

จุดเด่นของผลิตภัณฑ์หรือเทคโนโลยีเมื่อเปรียบเทียบกับผลิตภัณฑ์หรือเทคโนโลยีปัจจุบัน.....

สารปรับผิวผ้านี้ละลายน้ำได้ ไม่ต้องใช้กรดแก่ในการละลายเหมือนผลิตภัณฑ์ที่ขายทั่วไป ผ้าที่พิมพ์ได้ไม่มีกลิ่นเปรี้ยว ผลิตสีสันได้มากสี ขอบเขตสีกว้างและเข้มมากขึ้น

โปรดระบุชื่อบริษัทซึ่งท่านคิดว่าน่าจะมีความสนใจในเทคโนโลยีหรือสิ่งประดิษฐ์ของท่าน

บริษัท.....โทรศัพท์ (ถ้ามี).....

บริษัท.....โทรศัพท์ (ถ้ามี).....

6. การสืบค้นข้อมูลสิทธิบัตร

6.1 Keyword ที่ใช้ในการสืบค้น HTACC; Modified chitosan; Surface pretreatment; Inkjet ink.....

6.2 ผลการสืบค้นพบว่า ☐ เหมือนหรือคล้ายกับงานที่ปรากฏอยู่แล้ว ☑ ไม่เหมือนหรือคล้ายกับงานที่ปรากฏอยู่แล้ว

6.3 Website ที่ใช้ในการสืบค้น ☑ ประเทศไทย: www.ipthailand.org ☐ สหรัฐอเมริกา : www.uspto.gov

☐ ญี่ปุ่น : www.jpo.go.jp ☑ ยุโรป : http://ep.espacenet.com ☐ อื่นๆ ระบุ.....

(ในกรณีที่พบว่าเหมือนหรือคล้ายกับงานที่ปรากฏอยู่แล้ว กรุณาแนบเอกสารที่สืบค้นได้มาให้สถาบันฯ ด้วย)

7. ข้าพเจ้าขอยืนยันว่าข้อมูลดังกล่าวข้างต้นครบถ้วนและถูกต้อง

ลงนาม.....หัวหน้าโครงการ

นางสาวสุดา เกียรติกำจรวงศ์

(.....)

23 / พ.ค. / 2554

กรุณาส่งแบบฟอร์มนี้กลับมายัง

สถาบันทรัพย์สินทางปัญญาแห่งจุฬาลงกรณ์มหาวิทยาลัย

ชั้น 9 อาคารเทพทวาราวดี คณะนิติศาสตร์ จุฬาลงกรณ์มหาวิทยาลัย

โทรศัพท์: 02-2182895-96 โทรสาร: 02-2182871

คำขอรับสิทธิบัตร/~~อนุสิทธิบัตร~~

☑ การประดิษฐ์
☐ การออกแบบผลิตภัณฑ์
☐ อนุสิทธิบัตร

ข้าพเจ้าผู้ลงลายมือชื่อในคำขอรับสิทธิบัตร/~~อนุสิทธิบัตร~~นี้ ขอรับสิทธิบัตร/~~อนุสิทธิบัตร~~ ตามพระราชบัญญัติสิทธิบัตร พ.ศ 2522 แก้ไขเพิ่มเติมโดยพระราชบัญญัติสิทธิบัตร (ฉบับที่ 2) พ.ศ 2535 และ พระราชบัญญัติสิทธิบัตร (ฉบับที่ 3) พ.ศ 2542

สำหรับเจ้าหน้าที่

วันรับคำขอ 23 **พฤษภาคม** 2554	เลขที่คำขอ
วันยื่นคำขอ	
สัญลักษณ์จำแนกการประดิษฐ์ระหว่างประเทศ	
ใช้กับแบบผลิตภัณฑ์ ประเภทผลิตภัณฑ์	
วันประกาศโฆษณา	เลขที่ประกาศโฆษณา
วันออกสิทธิบัตร/อนุสิทธิบัตร	เลขที่สิทธิบัตร/อนุสิทธิบัตร
ลายมือชื่อเจ้าหน้าที่	

1.ชื่อที่แสดงถึงการประดิษฐ์/~~การออกแบบผลิตภัณฑ์~~

สารปรับสภาพผิวผ้าจากไคโทซานดัดแปรสำหรับผ้าพิมพ์ด้วยหมึกพิมพ์อิงก์เจ็ต

2.คำขอรับสิทธิบัตรการออกแบบผลิตภัณฑ์นี้เป็นคำขอสำหรับแบบผลิตภัณฑ์อย่างเดียวกันและเป็นคำขอลำดับที่
ในจำนวน คำขอ ที่ยื่นในคราวเดียวกัน

3.ผู้ขอรับสิทธิบัตร/~~อนุสิทธิบัตร~~ และที่อยู่ (เลขที่ ถนน ประเทศ) **จุฬาลงกรณ์มหาวิทยาลัย** 254 **ถนนพญาไท แขวงวังใหม่ เขตปทุมวัน กรุงเทพฯ** 10330 **(มีต่อหน้า** 3)	3.1 สัญชาติ **ไทย** 3.2 โทรศัพท์ 02-218-3590; 02-564-7000 **ต่อ** 1314-1350 3.3 โทรสาร 02-218-3589; 02-564 7008 3.4 อีเมล์ CU.prop@chula.ac.th; tlo@tmc.nstda.or.th

4.สิทธิในการขอรับสิทธิบัตร/~~อนุสิทธิบัตร~~
☐ ผู้ประดิษฐ์/ผู้ออกแบบ ☑ ผู้รับโอน ☐ ผู้ขอรับสิทธิโดยเหตุอื่น

5.ตัวแทน (ถ้ามี)/ที่อยู่ (เลขที่ ถนน จังหวัด รหัสไปรษณีย์) **สำนักงานจัดการทรัพย์สิน จุฬาลงกรณ์มหาวิทยาลัย** **254 ถนนพญาไท แขวงวังใหม่ เขตปทุมวัน กทม** 10330	5.1 ตัวแทนเลขที่ 5.2 โทรศัพท์ 02-218-3590 5.3 โทรสาร 02-218-3589 5.4 อีเมล์ CU.prop@chula.ac.th

6.ผู้ประดิษฐ์/~~ผู้ออกแบบผลิตภัณฑ์~~ และที่อยู่ (เลขที่ ถนน ประเทศ)
1. **นางสาวสุดา เกียรติกำจรวงศ์ และคณะ (มีต่อหน้า** 3)

7. คำขอรับสิทธิบัตร/อนุสิทธิบัตรนี้แยกจากหรือเกี่ยวข้องกับคำขอเดิม
ผู้ขอรับสิทธิบัตร/อนุสิทธิบัตร ขอให้ถือว่าได้ยื่นคำขอรับสิทธิบัตร/อนุสิทธิบัตรนี้ ในวันเดียวกับคำขอรับสิทธิบัตร เลขที่ วันยื่น เพราะคำขอรับสิทธิบัตร/อนุสิทธิบัตรนี้แยกจากหรือเกี่ยวข้องกับคำขอเดิมเพราะ
คำขอเดิมมีการประดิษฐ์หลายอย่าง ถูกคัดค้านเนื่องจากผู้ขอไม่มีสิทธิ ขอเปลี่ยนแปลงประเภทของสิทธิ

<u>หมายเหตุ</u> ในกรณีที่ไม่อาจระบุรายละเอียดได้ครบถ้วน ให้จัดทำเป็นเอกสารแนบท้ายแบบพิมพ์นี้โดยระบุหมายเลขกำกับข้อและหัวข้อที่แสดงรายละเอียดเพิ่มเติมดังกล่าวด้วย

8.การยื่นคำขอนอกราชอาณาจักร

วันยื่นคำขอ	เลขที่คำขอ	ประเทศ	สัญลักษณ์จำแนกการประดิษฐ์ระหว่างประเทศ	สถานะคำขอ
8.1				
8.2				
8.3				

8.4 ผู้ขอรับสิทธิบัตร/อนุสิทธิบัตรขอสิทธิให้ถือว่าได้ยื่นคำขอนี้ในวันที่ได้ยื่นคำขอรับสิทธิบัตร/อนุสิทธิบัตรในต่างประเทศเป็นครั้งแรกโดย
ได้ยื่นเอกสารหลักฐานพร้อมคำขอนี้ ขอยื่นเอกสารหลักฐานหลังจากวันยื่นคำขอนี้

9.การแสดงการประดิษฐ์ หรือการออกแบบผลิตภัณฑ์ ผู้ขอรับสิทธิบัตร/อนุสิทธิบัตรได้แสดงการประดิษฐ์ที่หน่วยงานของรัฐเป็นผู้จัด
วันแสดง วันเปิดงานแสดง ผู้จัด

10.การประดิษฐ์เกี่ยวกับจุลชีพ

10.1 เลขทะเบียนฝากเก็บ	10.2 วันที่ฝากเก็บ	10.3 สถาบันฝากเก็บ/ประเทศ

11.ผู้ขอรับสิทธิบัตร/อนุสิทธิบัตร ขอยื่นเอกสารภาษาต่างประเทศก่อนในวันยื่นคำขอนี้ และจะจัดยื่นคำขอรับสิทธิบัตร/อนุสิทธิบัตรนี้ที่จัดทำเป็นภาษาไทยภายใน 90 วัน นับจากวันยื่นคำขอนี้ โดยขอยื่นเป็นภาษา

☐ อังกฤษ ☐ ฝรั่งเศส ☐ เยอรมัน ☐ ญี่ปุ่น ☐ อื่นๆ

12.ผู้ขอรับสิทธิบัตร/อนุสิทธิบัตร ขอให้อธิบดีประกาศโฆษณาคำขอรับสิทธิบัตร หรือรับจดทะเบียน และประกาศโฆษณาอนุสิทธิบัตรนี้
หลังจากวันที่ เดือน พ.ศ
☐ ผู้ขอรับสิทธิบัตร/อนุสิทธิบัตรขอให้ใช้รูปเขียนหมายเลข ในการประกาศโฆษณา

13.คำขอรับสิทธิบัตร/~~อนุสิทธิบัตร~~นี้ประกอบด้วย

ก. แบบพิมพ์คำขอ 3 หน้า
ข. รายละเอียดการประดิษฐ์
หรือ~~คำพรรณนาแบบผลิตภัณฑ์~~ 6 หน้า
ค. ข้อถือสิทธิ 1 หน้า
ง. รูปเขียน รูป หน้า
จ. ภาพแสดงแบบผลิตภัณฑ์
☐ รูปเขียน รูป หน้า
☐ ภาพถ่าย รูป หน้า
ฉ. บทสรุปการประดิษฐ์ 1 หน้า

14.เอกสารประกอบคำขอ

☐ เอกสารแสดงสิทธิในการขอรับสิทธิบัตร/อนุสิทธิบัตร
☐ หนังสือรับรองการแสดงการประดิษฐ์/การออกแบบผลิตภัณฑ์
☐ หนังสือมอบอำนาจ
☐ เอกสารรายละเอียดเกี่ยวกับจุลชีพ
☐ เอกสารการขอนับวันยื่นคำขอในต่างประเทศเป็นวันยื่นคำขอในประเทศไทย
☐ เอกสารขอเปลี่ยนแปลงประเภทของสิทธิ
☐ เอกสารอื่น ๆ

15. ข้าพเจ้าขอรับรองว่า

☑ การประดิษฐ์นี้ไม่เคยยื่นขอรับสิทธิบัตร/~~อนุสิทธิบัตร~~มาก่อน
☐ การประดิษฐ์นี้ได้พัฒนาปรับปรุงมาจาก.....

16.ลายมือชื่อ (☐ผู้ขอรับสิทธิบัตร / อนุสิทธิบัตร; ☐ ตัวแทน)

<u>หมายเหตุ</u> บุคคลใดยื่นขอรับสิทธิบัตรการประดิษฐ์หรือการออกแบบผลิตภัณฑ์ หรืออนุสิทธิบัตร โดยการแสดงข้อความอันเป็นเท็จแก่พนักงานเจ้าหน้าที่ เพื่อให้ได้ไปซึ่งสิทธิบัตรหรืออนุสิทธิบัตร ต้องระวางโทษจำคุกไม่เกินหกเดือน หรือปรับไม่เกินห้าพันบาท หรือทั้งจำทั้งปรับ

3. ผู้ขอรับสิทธิบัตร/~~อนุสิทธิบัตร~~ และที่อยู่ (เลขที่ ถนน ประเทศ)

จุฬาลงกรณ์มหาวิทยาลัย 254 **ถนนพญาไท วังใหม่ ปทุมวัน กทม.** 10330
สำนักงานกองทุนสนับสนุนการวิจัย ถนนพหลโยธิน กรุงเทพ

6. ผู้ประดิษฐ์/ผู้ออกแบบผลิตภัณฑ์ และที่อยู่ (เลขที่ ถนน ประเทศ)

นางสาวสุดา เกียรติกำจรวงศ์
นางสาวสุภาภรณ์ นพคุณดิลกรัตน์
นางสาวปัญฑ์ธร บูรณะกูล
ภาควิชาวิทยาศาสตร์ทางภาพถ่ายและเทคโนโลยีทางการพิมพ์ คณะวิทยาศาสตร์ จุฬาลงกรณ์มหาวิทยาลัย ถนนพญาไท วังใหม่ ปทุมวัน กทม. 10330

รายละเอียดการประดิษฐ์

ชื่อที่แสดงถึงการประดิษฐ์

สารปรับสภาพผิวผ้าจากไคโทซานดัดแปรสำหรับผ้าพิมพ์ด้วยหมึกพิมพ์อิงก์เจ็ต

ลักษณะและความมุ่งหมายของการประดิษฐ์

การประดิษฐ์นี้เกี่ยวข้องกับสารปรับสภาพผิวผ้าจากไคโทซานดัดแปรสำหรับพิมพ์ผ้าด้วยระบบการพิมพ์อิงก์เจ็ต

ความมุ่งหมายของการประดิษฐ์นี้ คือ การเพิ่มมูลค่าผ้าจากเส้นใยธรรมชาติหรือเส้นใยธรรมชาติผสมเส้นใยสังเคราะห์ เช่น ผ้าไหม ผ้าฝ้าย ผ้าฝ้ายผสมพอลิเอสเตอร์ พิมพ์ด้วยระบบหมึกพิมพ์อิงก์เจ็ต การพิมพ์ผ้าโดยไม่ใช้สารปรับสภาพผิวผ้า ทำให้งานพิมพ์ผ้าด้วยหมึกพิมพ์อิงก์เจ็ตที่ได้ไม่คมชัด สีเลอะ และสีสันไม่สดใส สารปรับสภาพผิวผ้าช่วยทำให้พื้นผิวผ้าเรียบขึ้น และเกิดการยึดติดกับสารสีในหมึกพิมพ์ดีขึ้น ส่งผลให้คุณภาพของผ้าพิมพ์ที่ได้มีความคมชัด สีสันสดใส สามารถนำไปใช้เป็นผลิตภัณฑ์ต่าง ๆ ได้ เช่น เป็นภาพถ่ายที่ระลึก หรือภาพใส่กรอบประดับห้องทำงาน ออกแบบผ้าพิมพ์เป็นของชำร่วย หรือของขวัญต่าง ๆ ได้ นอกจากนี้ ไคโทซานดัดแปรที่ละลายน้ำได้สังเคราะห์จากไคโทซานที่เป็นสารจากธรรมชาติ จึงปลอดภัยต่อผู้ใช้และสิ่งแวดล้อม และพบว่า ยังมีฤทธิ์ยับยั้งแบคทีเรียที่มากกว่าไคโทซานที่ไม่ดัดแปรอีกด้วย โดยสรุป จึงดีกว่าใช้สารปรับสภาพผิวผ้าที่เป็นสารพอลิเมอร์สังเคราะห์ที่สลายตัวยาก ดังนั้น การประดิษฐ์นี้จึงเป็นทางเลือกหนึ่งสำหรับเพิ่มมูลค่าของผ้าพิมพ์ด้วยระบบอิงก์เจ็ต และลดผลกระทบกับสิ่งแวดล้อม ในเชิงพาณิชย์ สารปรับสภาพผิวผ้านี้ใช้ปริมาณน้อยมากแต่เพิ่มคุณภาพผ้าพิมพ์ได้มากอย่างชัดเจน การออกแบบลายพิมพ์ด้วยเครื่องคอมพิวเตอร์สามารถต่ออินไลน์กับเครื่องพิมพ์อิงก์เจ็ตได้ทันที พิมพ์เสร็จได้ในเวลาสั้นมาก นอกจากนี้ ยังออกแบบได้หลากหลายตามความต้องการของลูกค้า และพิมพ์ด้วยเครื่องพิมพ์อิงก์เจ็ตทั้งขนาดเล็กที่ใช้ในสำนักงานและตามบ้านเรือนทั่วไป หรือเครื่องพิมพ์ขนาดหน้ากว้างแบบอุตสาหกรรม จึงเป็นแนวทางหนึ่งในการเสริมสร้างอาชีพให้กับผู้มีงบลงทุนไม่มากนักและอุตสาหกรรมขนาดเล็กได้

สาขาวิทยาการที่เกี่ยวข้องกับการประดิษฐ์

เทคโนโลยีการเคลือบและการพิมพ์

ภูมิหลังของศิลปะหรือวิทยาการที่เกี่ยวข้อง

ระบบการพิมพ์ผ้าที่ใช้ในปัจจุบัน คือ ระบบการพิมพ์สกรีน การเตรียมแม่พิมพ์มีความยุ่งยากและใช้เวลา จึงมีการพัฒนาหาวิธีการพิมพ์แบบใหม่เพื่อให้ง่ายและสะดวกยิ่งขึ้น ระบบการพิมพ์ที่กำลังพัฒนาอย่างต่อเนื่องและน่าสนใจในการพิมพ์ผ้า คือ การพิมพ์ด้วยระบบอิงก์เจ็ต แต่ยังคงพบปัญหาสำคัญในการพิมพ์ผ้าด้วยระบบอิงก์เจ็ต นั่นคือ การยึดติดระหว่างสารให้สีกับเส้นใยของผ้าที่ไม่คงทน ให้ขอบเขตสีที่แคบ และการพิมพ์ที่ไม่คมชัด เนื่องจากผ้ามีรูพรุนและผิวผ้าไม่เรียบสม่ำเสมอ สารปรับสภาพผิวผ้าช่วยทำให้ผ้าเรียบมากขึ้น เพิ่มพื้นที่ดูดซึมหมึกพิมพ์และตรึงหมึกพิมพ์ในขอบเขตที่กำหนดได้มากขึ้น สารเคมีที่ใช้ปรับสภาพผิวผ้าทางการค้าทั่วไปเป็นสารสังเคราะห์ เช่น ซิลก์สตาร์ (silk star) หรือซันฟิกซ์ (sunfix) ซึ่งสลายตัวยากในธรรมชาติ และให้คุณภาพผ้าพิมพ์ดีไม่มากนัก ผู้ประดิษฐ์ได้เคยเตรียมสารปรับสภาพผิวผ้าจากธรรมชาติ คือ ไคโทซานและไกลซีนในกรดแอซิติก เพื่อใช้ปรับสภาพผิวผ้าแทนสารสังเคราะห์ที่ใช้ในปัจจุบัน ซึ่งให้ผ้าพิมพ์ที่มีสีสันสดใสและคมชัด การประดิษฐ์นี้เป็นการเตรียมสารปรับสภาพผิวผ้าจากไคโทซานดัดแปรที่ละลายน้ำได้ทำให้สารสีในหมึกพิมพ์ยึดติดกับเส้นใยผ้าดีขึ้น อีกทั้งยังทำให้ขอบเขตสีในการพิมพ์อิงก์เจ็ตบนผิวผ้ากว้างขึ้น ผ้าพิมพ์มีสีสันสดใสและคมชัดมากขึ้นกว่าใช้ไคโทซานและไกลซีนในกรดแอซิติก สามารถนำการประดิษฐ์นี้ไปใช้กับผ้าและพิมพ์ด้วยเครื่องพิมพ์อิงก์เจ็ตที่ใช้ตามสำนักงานหรือบ้านเรือนทั่วไป หรือเครื่องพิมพ์ขนาดใหญ่ในอุตสาหกรรม

การเปิดเผยการประดิษฐ์โดยสมบูรณ์

สารปรับสภาพผิวผ้าตามการประดิษฐ์นี้ คือ

สารปรับสภาพผิวผ้าไคโทซานดัดแปร เอ็น-2-ไฮดรอกซี-3-ไทรเมทิลแอมโมเนียมพรอพิลไคโทซานคลอไรด์ (*N*-[(2-hydroxyl-3-trimethylammonium) propyl] chitosan chloride, HTACC) ซึ่งประกอบด้วย

1. ไคโทซานดัดแปร HTACC ในสัดส่วนร้อยละ 0.04 ถึง 10 โดยน้ำหนักขององค์ประกอบทั้งหมดภายในสูตรสารปรับสภาพผิวผ้า
2. น้ำในสัดส่วนร้อยละ 90 ถึง 99.96 โดยน้ำหนักขององค์ประกอบทั้งหมดภายในสูตรสารปรับสภาพผิวผ้า

ไคโทซาน (chitosan) ที่ใช้ในการประดิษฐ์นี้มีลักษณะเป็นผงสีเหลืองอ่อน น้ำหนักโมเลกุล 100,000 กรัมต่อโมล (gm per mol) มีค่าระดับขั้นการกำจัดหมู่แอซิทิลร้อยละ 95

การประดิษฐ์นี้เลือกใช้ไคโทซานดัดแปร HTACC เนื่องจากไคโทซานดัดแปร HTACC เป็นสารที่ละลายน้ำได้และมีประจุบวก จึงสามารถจับกับสารที่มีประจุลบได้ เช่น โปรตีน สีย้อมผ้า โลหะหนัก พอลิเมอร์

สารปรับสภาพผิวผ้าตามการประดิษฐ์นี้ เหมาะสำหรับใช้กับผ้าที่เส้นใยมีหมู่แอมิโน ($-NH_2$ group) และ/หรือ หมู่ไฮดรอกซิล (–OH group) เป็นองค์ประกอบ เช่น ผ้าไหม ผ้าฝ้าย

การปรับสภาพผิวผ้า หมายถึง การทำให้ปริมาณของสารปรับสภาพพื้นผิวติดบนผ้าร้อยละ 100 โดยการจุ่มรีด (padding)

$$\text{ร้อยละของการจุ่มรีด} = \frac{(\text{น้ำหนักผ้าหลังการจุ่มรีด} - \text{น้ำหนักผ้าก่อนการจุ่มรีด}) \times 100}{\text{น้ำหนักผ้าก่อนการจุ่มรีด}}$$

นำผ้าที่จุ่มรีดไปอบให้แห้งในตู้อบที่อุณหภูมิ 80 องศาเซลเซียส เป็นเวลา 5 นาที และอบผนึกที่อุณหภูมิ 110 องศาเซลเซียส เป็นเวลา 2 นาที นำผ้าที่ได้ไปพิมพ์ด้วยเครื่องพิมพ์อิงก์เจ็ตที่ใช้หมึกพิมพ์อิงก์เจ็ตฐานน้ำชนิดสารสี พิมพ์ที่ความละเอียด 300 จุดต่อนิ้ว แล้วนำไปเข้าเครื่องอบไอน้ำเป็นเวลา 5 นาที

วัดคุณภาพงานพิมพ์ วัดสีด้วยเครื่องสเปกโทรโฟโตมิเตอร์ ความคมชัดของงานพิมพ์ การผลิตน้ำหนักสีต่อเนื่อง และการซึมเข้าหากันของหมึกพิมพ์ และคำนวณหาค่าขอบเขตสี

ตัวอย่างต่อไปนี้แสดงให้เห็นเพิ่มเติมถึงการประดิษฐ์ แต่มิได้มีวัตถุประสงค์ที่จะจำกัดขอบเขตของการประดิษฐ์นี้แต่อย่างใด

ตัวอย่าง

<u>ขั้นตอนที่ 1 การเตรียมไคโทซานดัดแปร HTACC</u>

1.1 ละลายไคโทซานน้ำหนักโมเลกุล 100,000 กรัมต่อโมล ค่าระดับการกำจัดหมู่แอซิทิลร้อยละ 95 ปริมาณ 0.5 กรัม ด้วยสารละลายกรดแอซิติกความเข้มข้นร้อยละ 2 ปริมาตร 25 มิลลิลิตร กวนสารละลายด้วยแท่งแม่เหล็ก (magnetic stirrer) ที่ความเร็วรอบ 150 รอบต่อนาที จนสารละลายเป็นเนื้อเดียวกัน

1.2 เติมสารละลายไกลซิดิลไทรเมทิลแอมโมเนียมคลอไรด์ (glycidyltrimethylammonium chloride, GTMAC) 1.8 g กวนสารละลายด้วยแท่งแม่เหล็กที่ความเร็วรอบ 150 รอบต่อนาที อุณหภูมิ 70 องศาเซลเซียส เป็นเวลา 24 ชั่วโมง

1.3 ตั้งสารละลายให้อุณหภูมิลดลงจนถึงอุณหภูมิ 27 องศาเซลเซียส เทสารละลายลงในถุงเซลลูโลสไดอะไลซีส (dialysis tubing cellulose membrane) แกว่งในน้ำกลั่นเป็นเวลา 5 วัน เปลี่ยนน้ำทุกวัน นำสารละลายที่อยู่ในถุงเซลลูโลสไดอะไลซีสไปทำให้แห้งด้วย freeze dry

ขั้นตอนที่ 2 การเตรียมสารปรับสภาพผิวผ้าไคโทซานดัดแปร HTACC

1. ชั่งไคโทซานดัดแปร HTACC 0.5 กรัม ลงในน้ำ กวนด้วยแท่งแม่เหล็กที่ความเร็ว 150 รอบต่อนาที จนละลายเป็นเนื้อเดียวกัน
2. เทสารละลายทั้งหมดลงในขวดวัดปริมาตรขนาด 500 มิลลิลิตร เติมน้ำกลั่นจนได้ปริมาตร 500 มิลลิลิตร

วิธีการจุ่มรีด ชั่งน้ำหนักผ้าที่ตัดไว้ขนาด A4 ชุบผ้าด้วยสารปรับสภาพผิวให้เปียกทั่วทั้งผืน แล้วนำไปผ่านเครื่องจุ่มรีด ตั้งระยะห่างระหว่างโมของเครื่องให้พอดี เพื่อให้ปริมาณของสารละลายติดบนผ้าร้อยละ 100 โดยคำนวณตามสมการ อบผ้าให้แห้งในตู้อบที่อุณหภูมิ 80 องศาเซลเซียส เป็นเวลา 5 นาที และอบผนึกที่อุณหภูมิ 110 องศาเซลเซียส เป็นเวลา 2 นาที

นำผ้าที่อบผนึกแล้วไปพิมพ์ด้วยเครื่องพิมพ์อิงก์เจ็ตที่ใช้หมึกพิมพ์ฐานน้ำชนิดสารสี 7 สี พิมพ์แผ่นทดสอบบนผ้าที่ความละเอียด 300 จุดต่อนิ้ว ที่มีช่องสี 294 ช่อง เพื่อวัดขอบเขตสีตามมาตรฐานของ GretagMacbeth ด้วยโปรแกรม Profile Maker 5.0 และแบบทดสอบส่วนเส้นด้วยโปรแกรม Photoshop และ Illustrator ที่ไม่มีการจัดการสี นำผ้าที่พิมพ์เสร็จไปใส่ในเครื่องอบไอน้ำเป็นเวลา 5 นาที เพื่อกำจัดสีส่วนเกินออก

วัดคุณภาพงานพิมพ์ โดยวัดขอบเขตของสีด้วยเครื่องสเปกโทรโฟโตมิเตอร์ GretagMacbeth Spectrolino บนช่องผลิตสีสำหรับวัดขอบเขตสีตามมาตรฐานของ GretagMacbeth จำนวน 294 ช่อง พบว่า ผ้าที่ปรับสภาพผิวให้ขอบเขตสีที่กว้างกว่าผ้าที่ไม่ปรับสภาพผิวในทุกช่องสี งานพิมพ์มีความคมชัดมากขึ้น ผ้าที่ปรับสภาพผิวให้ค่าความดำของหมึกพิมพ์มากขึ้น และมีลำดับขั้นน้ำหนักสีที่เด่นชัดกว่าผ้าที่ไม่ปรับสภาพผิว การซึมเข้าหากันของหมึกพิมพ์ (inter-color bleeding) วัดจากเส้นสีเหลืองที่ขยายหรือหดจากขนาด 1 มิลลิเมตร บนพื้นทึบสีดำ พบว่า เส้นสีเหลืองบนผ้าที่ปรับสภาพผิวซึมเข้าหากันน้อยกว่าผ้าที่ไม่ปรับสภาพผิว

วิธีการในการประดิษฐ์ที่ดีที่สุด

เหมือนกับที่ได้กล่าวมาแล้วในหัวข้อการเปิดเผยการประดิษฐ์โดยสมบูรณ์

ข้อถือสิทธิ

1. สารปรับสภาพผิวผ้าไคโทซานดัดแปร *เอ็น*-2-ไฮดรอกซี-3-ไทรเมทิลแอมโมเนียมพรอพิลไคโทซานคลอไรด์ (*N*-[(2-hydroxyl-3-trimethylammonium) propyl] chitosan chloride, HTACC) ซึ่งประกอบด้วย

(1). ไคโทซานดัดแปร HTACC ในสัดส่วนร้อยละ 0.04 ถึง 10 โดยน้ำหนักขององค์ประกอบทั้งหมดภายในสูตรสารปรับสภาพผิวผ้าจากเส้นใยธรรมชาติหรือเส้นใยธรรมชาติผสมเส้นใยสังเคราะห์

(2). น้ำในสัดส่วนร้อยละ 90 ถึง 99.96 โดยน้ำหนักขององค์ประกอบทั้งหมดภายในสูตรสารปรับสภาพผิวผ้าจากเส้นใยธรรมชาติหรือเส้นใยธรรมชาติผสมเส้นใยสังเคราะห์

บทสรุปการประดิษฐ์

การประดิษฐ์นี้เกี่ยวข้องกับสารปรับสภาพผิวผ้าสำหรับการพิมพ์ผ้าจากเส้นใยธรรมชาติหรือเส้นใยธรรมชาติผสมเส้นใยสังเคราะห์ด้วยระบบหมึกพิมพ์อิงก์เจ็ต ซึ่งประกอบด้วยไคโทซานดัดแปร *เอ็น*-2-ไฮดรอกซี-3-ไทรเมทิลแอมโมเนียมพรอพิลไคโทซานคลอไรด์ (*N*-[(2-hydroxyl-3-trimethylammonium) propyl] chitosan chloride, HTACC) และน้ำ ไคโทซานดัดแปร HTACC ทำหน้าที่ปรับสภาพผิวผ้า และเป็นสารยึดสารสีในหมึกพิมพ์ให้ติดกับผ้า และน้ำเป็นตัวทำละลาย

แบบฟอร์มเปิดเผยการประดิษฐ์และแสดงความจำนงขอให้จดทะเบียนสิทธิบัตร/อนุสิทธิบัตร

(Invention Disclosure Form)

NO.:.....
Receive date:.....

1. ชื่อที่แสดงถึงการประดิษฐ์ (ไทยและอังกฤษ).....

สารปรับสภาพผิวผ้าจากไคโทซานดัดแปรละลายน้ำได้สำหรับการพิมพ์อิงก์เจ็ต

Water soluble modified chitosan solution for textile surface pretreatment in inkjet printing

ลักษณะโดยย่อของการประดิษฐ์ (แนบเอกสารประกอบได้).....

1. สารปรับสภาพผิวผ้าไคโทซานในกรดมะนาว ซึ่งประกอบด้วย

(1). กรดมะนาว (citric acid monohydrate) ในสัดส่วนร้อยละ 0.5 ถึง 10 โดยน้ำหนักขององค์ประกอบทั้งหมดภายในสูตรสารปรับสภาพผิวผ้า (2). ไคโทซานในสัดส่วนร้อยละ 0.05 ถึง 7 โดยน้ำหนักขององค์ประกอบทั้งหมดภายในสูตรสารปรับสภาพผิวผ้า (3). โซเดียมคาร์บอเนต (sodium carbonate anhydrous) ในสัดส่วนร้อยละ 0.1 ถึง 5 โดยน้ำหนักขององค์ประกอบทั้งหมดภายในสูตรสารปรับสภาพผิวผ้า (4). น้ำในสัดส่วนร้อยละ 78-99.4 โดยน้ำหนักขององค์ประกอบทั้งหมดภายในสูตรสารปรับสภาพผิวผ้า

2. สารปรับสภาพผิวผ้าไคโทซานดัดแปร *เอ็น*-2-ไฮดรอกซี-3-ไทรเมทิลแอมโมเนียมพรอพิลไคโทซานคลอไรด์ (*N*-[(2-hydroxyl-3-trimethylammonium) propyl] chitosan chloride, HTACC) ซึ่งประกอบด้วย

(1). ไคโทซานดัดแปร HTACC ในสัดส่วนร้อยละ 0.04 ถึง 10 โดยน้ำหนักขององค์ประกอบทั้งหมดของภายในสูตรสารปรับสภาพผิวผ้า (2). กรดมะนาวในสัดส่วนร้อยละ 0.01 ถึง 10 โดยน้ำหนักขององค์ประกอบทั้งหมดภายในสูตรสารปรับสภาพผิวผ้า (3). น้ำในสัดส่วนร้อยละ 79 ถึง 99.95 โดยน้ำหนักขององค์ประกอบทั้งหมดภายในสูตรสารปรับสภาพผิวผ้า

3. สารปรับสภาพผิวผ้าไคโทซานดัดแปร HTACC ในกรดมะนาว ซึ่งประกอบด้วย

(1). กรดมะนาวในสัดส่วนร้อยละ 0.5 ถึง 10 โดยน้ำหนักขององค์ประกอบทั้งหมดภายในสูตรสารปรับสภาพผิวผ้า (2). ไคโทซานดัดแปร HTACC ในสัดส่วนร้อยละ 0.04 ถึง 10 โดยน้ำหนักขององค์ประกอบทั้งหมดภายในสูตรสารปรับสภาพผิวผ้า (3). โซเดียมคาร์บอเนตในสัดส่วนร้อยละ 0.1 ถึง 5 โดยน้ำหนักขององค์ประกอบทั้งหมดภายในสูตรสารปรับสภาพผิวผ้า (4). น้ำในสัดส่วนร้อยละ 74 ถึง 99.1 โดยน้ำหนักขององค์ประกอบทั้งหมดภายในสูตรสารปรับสภาพผิวผ้า

2. ชื่อผู้ประดิษฐ์ / ผู้ประดิษฐ์ร่วม	สัดส่วนการประดิษฐ์/ การแบ่งปันผลประโยชน์ (%)	สังกัด / ที่อยู่	โทรศัพท์ / โทรสาร / อีเมล์
นางสาวสุดา เกียรติกำจรวงศ์	35	คณะวิทยาศาสตร์ จุฬาลงกรณ์มหาวิทยาลัย	02 2185587 / ksuda@chula.ac.th
นางสาวสุภาภรณ์ นพคุณดิลกรัตน์	35	คณะวิทยาศาสตร์ จุฬาลงกรณ์มหาวิทยาลัย	02 2185569 Supaporn.n@chula.ac.th
นางสาวสวเนตร์ วงศ์แป้น	15	คณะวิทยาศาสตร์ จุฬาลงกรณ์มหาวิทยาลัย	
นางสาวลิตสา วงศ์ศิริทรัพย์	15	คณะวิทยาศาสตร์ จุฬาลงกรณ์มหาวิทยาลัย	

3. การประดิษฐ์นี้ได้รับการสนับสนุนทางด้านการเงินจากแหล่งเงินทุนหรือร่วมวิจัยกับ องค์กร บริษัท หรือหน่วยงานใดหรือไม่

☑ ได้รับ โปรดระบุชื่อหน่วยงานที่เกี่ยวข้อง.. สำนักงานกองทุนสนับสนุนการวิจัย ☐ ไม่ได้รับ

4. ผลงานนี้เคยมีการตีพิมพ์ หรือเผยแพร่ผลงานมาก่อนหรือไม่

☐ มี โปรดระบุลักษณะการเผยแพร่..... เมื่อ..... ☑ ไม่มี

5. ศักยภาพของเทคโนโลยีในเชิงพาณิชย์ (โปรดอธิบาย แนบเอกสารประกอบได้)

ผลิตภัณฑ์หรือเทคโนโลยีที่ใกล้เคียงที่มีอยู่แล้วในตลาด... ไม่มี .....

.....

.....

ลักษณะการใช้ประโยชน์จากผลงาน (Application).....

สารละลายปรับผิวผ้าละลายในน้ำได้ ง่ายต่อการใช้งานในเวลาจุ่มรีด ผ้าที่ได้มีสีสันสดใสมาก ขอบเขตสีที่พิมพ์ได้กว้างมากขึ้น มีความเข้มของสีมากขึ้น และผ้าพิมพ์ที่ได้ไม่แข็งกระด้าง มีความนุ่มมือมากขึ้น

จุดเด่นของผลิตภัณฑ์หรือเทคโนโลยีเมื่อเปรียบเทียบกับผลิตภัณฑ์หรือเทคโนโลยีปัจจุบัน.....

สารปรับผิวผ้านี้ละลายน้ำได้ ไม่ต้องใช้กรดแก่ในการละลายเหมือนผลิตภัณฑ์ที่ขายทั่วไป ผ้าที่พิมพ์ได้ไม่มีกลิ่นเปรี้ยว ผลิตสีสันได้มากสี ขอบเขตสีกว้างและเข้มมากขึ้น

โปรดระบุชื่อบริษัทซึ่งท่านคิดว่าน่าจะมีความสนใจในเทคโนโลยีหรือสิ่งประดิษฐ์ของท่าน

บริษัท.....โทรศัพท์ (ถ้ามี).....

บริษัท.....โทรศัพท์ (ถ้ามี).....

6. การสืบค้นข้อมูลสิทธิบัตร

6.1 Keyword ที่ใช้ในการสืบค้น superabsorbent; photocatalysis; titanium dioxide; composite

6.2 ผลการสืบค้นพบว่า ☐ เหมือนหรือคล้ายกับงานที่ปรากฏอยู่แล้ว ☑ ไม่เหมือนหรือคล้ายกับงานที่ปรากฏอยู่แล้ว

6.3 Website ที่ใช้ในการสืบค้น ☑ ประเทศไทย: www.ipthailand.org ☐ สหรัฐอเมริกา : www.uspto.gov

☐ ญี่ปุ่น : www.jpo.go.jp ☑ ยุโรป : http://ep.espacenet.com ☐ อื่นๆ ระบุ.....

(ในกรณีที่พบว่าเหมือนหรือคล้ายกับงานที่ปรากฏอยู่แล้ว กรุณาแนบเอกสารที่สืบค้นได้มาให้สถาบันฯ ด้วย)

7. ข้าพเจ้าขอยืนยันว่าข้อมูลดังกล่าวข้างต้นครบถ้วนและถูกต้อง

ลงนาม.....หัวหน้าโครงการ

นางสาวสุดา เกียรติกำจรวงศ์

(.....)

..23.../...พ.ค../..2554

กรุณาส่งแบบฟอร์มนี้กลับมายัง

สถาบันทรัพย์สินทางปัญญาแห่งจุฬาลงกรณ์มหาวิทยาลัย

ชั้น 9 อาคารเทพทวาราวดี คณะนิติศาสตร์ จุฬาลงกรณ์มหาวิทยาลัย

โทรศัพท์: 02-2182895-96 โทรสาร: 02-2182871

คำขอรับสิทธิบัตร/~~อนุสิทธิบัตร~~

☑ การประดิษฐ์
☐ การออกแบบผลิตภัณฑ์
☐ อนุสิทธิบัตร

ข้าพเจ้าผู้ลงลายมือชื่อในคำขอรับสิทธิบัตร/~~อนุสิทธิบัตร~~นี้ ขอรับสิทธิบัตร/~~อนุสิทธิบัตร~~ ตามพระราชบัญญัติสิทธิบัตร พ.ศ 2522 แก้ไขเพิ่มเติมโดยพระราชบัญญัติสิทธิบัตร (ฉบับที่ 2) พ.ศ 2535 และ พระราชบัญญัติสิทธิบัตร (ฉบับที่ 3) พ.ศ 2542

สำหรับเจ้าหน้าที่

วันรับคำขอ 23 **พฤษภาคม** 2554	เลขที่คำขอ
วันยื่นคำขอ	
สัญลักษณ์จำแนกการประดิษฐ์ระหว่างประเทศ	
ใช้กับแบบผลิตภัณฑ์ ประเภทผลิตภัณฑ์	
วันประกาศโฆษณา	เลขที่ประกาศโฆษณา
วันออกสิทธิบัตร/อนุสิทธิบัตร	เลขที่สิทธิบัตร/อนุสิทธิบัตร
ลายมือชื่อเจ้าหน้าที่	

1.ชื่อที่แสดงถึงการประดิษฐ์/~~การออกแบบผลิตภัณฑ์~~

สารปรับสภาพผิวผ้าจากไคโทซานดัดแปรละลายน้ำได้สำหรับการพิมพ์ระบบอิงก์เจ็ต

2.คำขอรับสิทธิบัตรการออกแบบผลิตภัณฑ์นี้เป็นคำขอสำหรับแบบผลิตภัณฑ์อย่างเดียวกันและเป็นคำขอลำดับที่
ในจำนวน คำขอ ที่ยื่นในคราวเดียวกัน

3.ผู้ขอรับสิทธิบัตร/~~อนุสิทธิบัตร~~ และที่อยู่ (เลขที่ ถนน ประเทศ) **จุฬาลงกรณ์มหาวิทยาลัย** 254 **ถนนพญาไท แขวงวังใหม่ เขตปทุมวัน กรุงเทพฯ** 10330 **(มีต่อหน้า** 3)	3.1 สัญชาติ **ไทย** 3.2 โทรศัพท์ 02-218-3590; 02-564-7000 **ต่อ** 1314-1350 3.3 โทรสาร 02-218-3589; 02-564 7008 3.4 อีเมล์ CU.prop@chula.ac.th; tlo@tmc.nstda.or.th

4.สิทธิในการขอรับสิทธิบัตร/~~อนุสิทธิบัตร~~
☐ ผู้ประดิษฐ์/ผู้ออกแบบ ☑ ผู้รับโอน ☐ ผู้ขอรับสิทธิโดยเหตุอื่น

5.ตัวแทน (ถ้ามี)/ที่อยู่ (เลขที่ ถนน จังหวัด รหัสไปรษณีย์) **สำนักงานจัดการทรัพย์สิน จุฬาลงกรณ์มหาวิทยาลัย** **254 ถนนพญาไท แขวงวังใหม่ เขตปทุมวัน กทม** 10330 **สำนักงานกองทุนสนับสนุนการวิจัย กรุงเทพ ฯ**	5.1 ตัวแทนเลขที่ 5.2 โทรศัพท์ 02-218-3590 5.3 โทรสาร 02-218-3589 5.4 อีเมล์ CU.prop@chula.ac.th

6.ผู้ประดิษฐ์/~~ผู้ออกแบบผลิตภัณฑ์~~ และที่อยู่ (เลขที่ ถนน ประเทศ)
1. **นางสาวสุดา เกียรติกำจรวงศ์ และคณะ (มีต่อหน้า** 3)

7. คำขอรับสิทธิบัตร/อนุสิทธิบัตรนี้แยกจากหรือเกี่ยวข้องกับคำขอเดิม
ผู้ขอรับสิทธิบัตร/อนุสิทธิบัตร ขอให้ถือว่าได้ยื่นคำขอรับสิทธิบัตร/อนุสิทธิบัตรนี้ ในวันเดียวกับคำขอรับสิทธิบัตร เลขที่ วันยื่น เพราะคำขอรับสิทธิบัตร/อนุสิทธิบัตรนี้แยกจากหรือเกี่ยวข้องกับคำขอเดิมเพราะ
คำขอเดิมมีการประดิษฐ์หลายอย่าง ถูกคัดค้านเนื่องจากผู้ขอไม่มีสิทธิ ขอเปลี่ยนแปลงประเภทของสิทธิ

<u>หมายเหตุ</u> ในกรณีที่ไม่อาจระบุรายละเอียดได้ครบถ้วน ให้จัดทำเป็นเอกสารแนบท้ายแบบพิมพ์นี้โดยระบุหมายเลขกำกับข้อและหัวข้อที่แสดงรายละเอียดเพิ่มเติมดังกล่าวด้วย

8.การยื่นคำขอนอกราชอาณาจักร

วันยื่นคำขอ	เลขที่คำขอ	ประเทศ	สัญลักษณ์จำแนกการประดิษฐ์ระหว่างประเทศ	สถานะคำขอ
8.1				
8.2				
8.3				

8.4 ผู้ขอรับสิทธิบัตร/อนุสิทธิบัตรขอสิทธิให้ถือว่าได้ยื่นคำขอนี้ในวันที่ได้ยื่นคำขอรับสิทธิบัตร/อนุสิทธิบัตรในต่างประเทศเป็นครั้งแรกโดย
ได้ยื่นเอกสารหลักฐานพร้อมคำขอนี้ ขอยื่นเอกสารหลักฐานหลังจากวันยื่นคำขอนี้

9.การแสดงการประดิษฐ์ หรือการออกแบบผลิตภัณฑ์ ผู้ขอรับสิทธิบัตร/อนุสิทธิบัตรได้แสดงการประดิษฐ์ที่หน่วยงานของรัฐเป็นผู้จัด
วันแสดง วันเปิดงานแสดง ผู้จัด

10.การประดิษฐ์เกี่ยวกับจุลชีพ

10.1 เลขทะเบียนฝากเก็บ	10.2 วันที่ฝากเก็บ	10.3 สถาบันฝากเก็บ/ประเทศ

11.ผู้ขอรับสิทธิบัตร/อนุสิทธิบัตร ขอยื่นเอกสารภาษาต่างประเทศก่อนในวันยื่นคำขอนี้ และจะจัดยื่นคำขอรับสิทธิบัตร/อนุสิทธิบัตรนี้ที่จัดทำเป็นภาษาไทยภายใน 90 วัน นับจากวันยื่นคำขอนี้ โดยขอยื่นเป็นภาษา

☐ อังกฤษ ☐ ฝรั่งเศส ☐ เยอรมัน ☐ ญี่ปุ่น ☐ อื่นๆ

12.ผู้ขอรับสิทธิบัตร/อนุสิทธิบัตร ขอให้อธิบดีประกาศโฆษณาคำขอรับสิทธิบัตร หรือรับจดทะเบียน และประกาศโฆษณาอนุสิทธิบัตรนี้
หลังจากวันที่ เดือน พ.ศ
☐ ผู้ขอรับสิทธิบัตร/อนุสิทธิบัตรขอให้ใช้รูปเขียนหมายเลข ในการประกาศโฆษณา

13.คำขอรับสิทธิบัตร/~~อนุสิทธิบัตร~~นี้ประกอบด้วย

ก. แบบพิมพ์คำขอ 3 หน้า
ข. รายละเอียดการประดิษฐ์
หรือ~~คำพรรณนาแบบผลิตภัณฑ์~~ 7 หน้า
ค. ข้อถือสิทธิ 3 หน้า
ง. รูปเขียน รูป หน้า
จ. ภาพแสดงแบบผลิตภัณฑ์
☐ รูปเขียน รูป หน้า
☐ ภาพถ่าย รูป หน้า
ฉ. บทสรุปการประดิษฐ์ 1 หน้า

14.เอกสารประกอบคำขอ

☐ เอกสารแสดงสิทธิในการขอรับสิทธิบัตร/อนุสิทธิบัตร
☐ หนังสือรับรองการแสดงการประดิษฐ์/การออกแบบผลิตภัณฑ์
☐ หนังสือมอบอำนาจ
☐ เอกสารรายละเอียดเกี่ยวกับจุลชีพ
☐ เอกสารการขอนับวันยื่นคำขอในต่างประเทศเป็นวันยื่นคำขอในประเทศไทย
☐ เอกสารขอเปลี่ยนแปลงประเภทของสิทธิ
☐ เอกสารอื่น ๆ

15. ข้าพเจ้าขอรับรองว่า

☑ การประดิษฐ์นี้ไม่เคยยื่นขอรับสิทธิบัตร/~~อนุสิทธิบัตร~~มาก่อน
☐ การประดิษฐ์นี้ได้พัฒนาปรับปรุงมาจาก.....

16.ลายมือชื่อ (☐ผู้ขอรับสิทธิบัตร / อนุสิทธิบัตร; ☐ ตัวแทน)

<u>หมายเหตุ</u> บุคคลใดยื่นขอรับสิทธิบัตรการประดิษฐ์หรือการออกแบบผลิตภัณฑ์ หรืออนุสิทธิบัตร โดยการแสดงข้อความอันเป็นเท็จแก่พนักงานเจ้าหน้าที่ เพื่อให้ได้ไปซึ่งสิทธิบัตรหรืออนุสิทธิบัตร ต้องระวางโทษจำคุกไม่เกินหกเดือน หรือปรับไม่เกินห้าพันบาท หรือทั้งจำทั้งปรับ

3. ผู้ขอรับสิทธิบัตร/~~อนุสิทธิบัตร~~ และที่อยู่ (เลขที่ ถนน ประเทศ)

จุฬาลงกรณ์มหาวิทยาลัย 254 **ถนนพญาไท วังใหม่ ปทุมวัน กทม.** 10330

สำนักงานกองทุนสนับสนุนการวิจัย ถนนพหลโยธิน กรุงเทพ ฯ

6. ผู้ประดิษฐ์/ผู้ออกแบบผลิตภัณฑ์ และที่อยู่ (เลขที่ ถนน ประเทศ)

นางสาวสุดา เกียรติกำจรวงศ์

นางสาวสุภาภรณ์ นพคุณดิลกรัตน์

นางสาวสวเนตร์ วงศ์แป้น

นางสาวลิตสา วงศ์ศิริทรัพย์

ภาควิชาวิทยาศาสตร์ทางภาพถ่ายและเทคโนโลยีทางการพิมพ์ คณะวิทยาศาสตร์ จุฬาลงกรณ์มหาวิทยาลัย ถนนพญาไท วังใหม่ ปทุมวัน กทม. 10330

รายละเอียดการประดิษฐ์

ชื่อที่แสดงถึงการประดิษฐ์

สารปรับสภาพผิวผ้าจากไคโทซานดัดแปรละลายน้ำได้สำหรับการพิมพ์ระบบอิงก์เจ็ต

ลักษณะและความมุ่งหมายของการประดิษฐ์

การประดิษฐ์นี้เกี่ยวข้องกับสารปรับสภาพผิวผ้าจากไคโทซานดัดแปรที่ละลายน้ำได้สำหรับการพิมพ์ผ้าด้วยระบบอิงก์เจ็ต

ความมุ่งหมายของการประดิษฐ์นี้ คือ การเพิ่มมูลค่าผ้าพิมพ์ระบบอิงก์เจ็ต การพิมพ์ผ้าโดยไม่ใช้สารปรับสภาพผิวผ้า ทำให้งานพิมพ์ผ้าด้วยอิงก์เจ็ตที่ได้ไม่คมชัด สีเลอะ และ สีสันไม่สดใส สารปรับสภาพผิวผ้าช่วยทำให้พื้นผิวผ้าเรียบขึ้น และเกิดการยึดติดกับสารสีในหมึกพิมพ์ดีขึ้น ส่งผลให้คุณภาพของผ้าพิมพ์ที่ได้มีความคมชัด สีสันสดใส สามารถนำไปใช้เป็นผลิตภัณฑ์ต่าง ๆ ได้มากขึ้น เช่น เป็นภาพถ่ายที่ระลึก หรือภาพใส่กรอบประดับห้องทำงาน และออกแบบผ้าพิมพ์เป็นของชำร่วย หรือของขวัญต่าง ๆ ได้ นอกจากนี้ ไคโทซานดัดแปรที่ละลายน้ำได้สังเคราะห์จากไคโทซานที่เป็นสารจากธรรมชาติ จึงปลอดภัยต่อผู้ใช้และสิ่งแวดล้อม และพบว่า ยังมีฤทธิ์ยับยั้งแบคทีเรียที่สูงกว่าไคโทซานตั้งต้นอีกด้วย โดยสรุป จึงดีกว่าใช้สารปรับสภาพผิวผ้าที่เป็นสารพอลิเมอร์สังเคราะห์ที่สลายตัวยาก ดังนั้นการประดิษฐ์นี้จึงเป็นทางเลือกหนึ่งสำหรับเพิ่มมูลค่าของผ้าพิมพ์ด้วยระบบอิงก์เจ็ต และลดผลกระทบกับสิ่งแวดล้อม ในเชิงพาณิชย์ สารปรับสภาพผิวผ้านี้ใช้ปริมาณน้อยมากแต่เพิ่มคุณภาพผ้าพิมพ์ได้อย่างชัดเจน การออกแบบลายพิมพ์ด้วยเครื่องคอมพิวเตอร์สำหรับพิมพ์อิงก์เจ็ตสามารถทำได้ในเวลารวดเร็ว นอกจากนี้ ยังออกแบบได้หลากหลายตามความต้องการของลูกค้า และพิมพ์ด้วยเครื่องพิมพ์อิงก์เจ็ตที่ใช้ในสำนักงานและตามบ้านเรือนทั่วไป จึงเป็นแนวทางหนึ่งในการเสริมสร้างอาชีพให้กับผู้มีงบประมาณลงทุนไม่มากนักได้

สาขาวิทยาการที่เกี่ยวข้องกับการประดิษฐ์

เทคโนโลยีทางการพิมพ์

ภูมิหลังของศิลปะหรือวิทยาการที่เกี่ยวข้อง

ระบบการพิมพ์ผ้าที่ใช้ในปัจจุบัน คือ ระบบการพิมพ์สกรีน การเตรียมแม่พิมพ์มีความยุ่งยากและใช้เวลา จึงมีการพัฒนาหาวิธีการพิมพ์แบบใหม่เพื่อให้ง่ายและสะดวกยิ่งขึ้น ระบบการพิมพ์ที่กำลังพัฒนาอย่างต่อเนื่องและน่าสนใจในการพิมพ์ผ้า คือ การพิมพ์ด้วยระบบอิงก์เจ็ต แต่ยังคงพบปัญหาสำคัญในการพิมพ์ผ้าด้วยระบบอิงก์เจ็ต นั่นคือ การยึดติดระหว่างสารให้สีกับเส้นใยของผ้าที่ไม่คงทน ให้

ขอบเขตสีที่แคบ และการพิมพ์ที่ไม่คมชัด เนื่องจากผ้ามีรูพรุนและไม่เรียบสม่ำเสมอ สารปรับสภาพผิวผ้าช่วยทำให้ผ้าเรียบมากขึ้น เพิ่มพื้นที่ดูดซึมหมึกพิมพ์และตรึงหมึกพิมพ์ในขอบเขตที่กำหนดได้มากขึ้น สารเคมีที่ใช้ปรับสภาพผิวผ้าทางการค้าทั่วไปเป็นสารสังเคราะห์ เช่น ซิลก์สตาร์ (silk star) หรือซันฟิกซ์ (sunfix) ซึ่งสลายตัวยากในธรรมชาติ และให้คุณภาพผ้าพิมพ์ดีขึ้นไม่มากนัก ผู้ประดิษฐ์ได้เคยเตรียมสารปรับสภาพผิวผ้าจากธรรมชาติ คือ ไคโทซานและไกลซีนในกรดแอซิติก เพื่อใช้ปรับสภาพผิวผ้าแทนสารสังเคราะห์ที่ใช้ในปัจจุบัน ซึ่งให้ผ้าพิมพ์ที่มีสีสันสดใสและคมชัด การประดิษฐ์นี้เป็นการเตรียมสารปรับสภาพผิวผ้าจากไคโทซานในกรดมะนาว และไคโทซานดัดแปรที่ละลายน้ำได้ทำให้สารสีในหมึกพิมพ์ยึดติดกับเส้นใยผ้าดีขึ้น อีกทั้งยังทำให้ขอบเขตสีในการพิมพ์อิงก์เจ็ตบนผิวผ้ากว้างขึ้น ผ้าพิมพ์มีสีสันสดใสและคมชัดมากขึ้นกว่าใช้ไคโทซานและไกลซีนในกรดแอซิติก สามารถนำการประดิษฐ์นี้ไปใช้กับผ้าและพิมพ์ด้วยเครื่องพิมพ์อิงก์เจ็ตที่ใช้ตามสำนักงานหรือบ้านเรือนทั่วไป

การเปิดเผยการประดิษฐ์โดยสมบูรณ์

สารปรับสภาพผิวผ้าตามการประดิษฐ์นี้มี 3 สูตร คือ

<u>สูตรที่ 1 สารปรับสภาพผิวผ้าไคโทซานในกรดมะนาว</u> ซึ่งประกอบด้วย

1. กรดมะนาว (citric acid monohydrate) ในสัดส่วนร้อยละ 0.5-10 โดยน้ำหนักขององค์ประกอบทั้งหมดภายในสูตรสารปรับสภาพผิวผ้า
2. ไคโทซานในสัดส่วนร้อยละ 0.05-7 โดยน้ำหนักขององค์ประกอบทั้งหมดภายในสูตรสารปรับสภาพผิวผ้า
3. โซเดียมคาร์บอเนต (sodium carbonate anhydrous) ในสัดส่วนร้อยละ 0.1-5 โดยน้ำหนักขององค์ประกอบทั้งหมดภายในสูตรสารปรับสภาพผิวผ้า
4. น้ำในสัดส่วนร้อยละ 78-99.4 โดยน้ำหนักขององค์ประกอบทั้งหมดภายในสูตรสารปรับสภาพผิวผ้า

<u>สูตรที่ 2 สารปรับสภาพผิวผ้าไคโทซานดัดแปร เอ็น-2-ไฮดรอกซี-3-ไทรเมทิลแอมโมเนียมพรอพิลไคโทซานคลอไรด์ (*N*-[(2-hydroxyl-3-trimethylammonium) propyl] chitosan chloride, HTACC)</u> ซึ่งประกอบด้วย

1. ไคโทซานดัดแปร HTACC ในสัดส่วนร้อยละ 0.04 ถึง 10 โดยน้ำหนักขององค์ประกอบทั้งหมดภายในสูตรสารปรับสภาพผิวผ้า
2. กรดมะนาวในสัดส่วนร้อยละ 0.01 ถึง 10 โดยน้ำหนักขององค์ประกอบทั้งหมดภายในสูตรสารปรับสภาพผิวผ้า

3. น้ำในสัดส่วนร้อยละ 79 ถึง 99.95 โดยน้ำหนักขององค์ประกอบทั้งหมดภายในสูตรสารปรับสภาพผิวผ้า

สูตรที่ 3 สารปรับสภาพผิวผ้าไคโทซานดัดแปร HTACC ในกรดมะนาว ซึ่งประกอบด้วย

1. กรดมะนาวในสัดส่วนร้อยละ 0.5 ถึง 10 โดยน้ำหนักขององค์ประกอบทั้งหมดภายในสูตรสารปรับสภาพผิวผ้า

2. ไคโทซานดัดแปร HTACC ในสัดส่วนร้อยละ 0.04 ถึง 10 โดยน้ำหนักขององค์ประกอบทั้งหมดภายในสูตรสารปรับสภาพผิวผ้า

3. โซเดียมคาร์บอเนตในสัดส่วนร้อยละ 0.1 ถึง 5 โดยน้ำหนักขององค์ประกอบทั้งหมดภายในสูตรสารปรับสภาพผิวผ้า

4. น้ำในสัดส่วนร้อยละ 74 ถึง 99.1 โดยน้ำหนักขององค์ประกอบทั้งหมดภายในสูตรสารปรับสภาพผิว ผ้า

ไคโทซาน (chitosan) ที่ใช้ในการประดิษฐ์นี้มีลักษณะเป็นผงสีเหลืองอ่อน น้ำหนักโมเลกุล 100,000 กรัมต่อโมล (gm per mol) มีค่าระดับขั้นการกำจัดหมู่แอซีทิลร้อยละ 95

การประดิษฐ์นี้เลือกใช้ไคโทซานและไคโทซานดัดแปร HTACC เนื่องจากไคโทซานในกรดสามารถเกิดประจุบวกได้ โดยหมู่แอมิโนจำนวนมากรับโปรตอนจากกรด ไคโทซานดัดแปร HTACC เป็นสารที่ละลายน้ำได้และมีประจุบวก จึงสามารถจับกับสารที่มีประจุลบได้ เช่น โปรตีน สีย้อมผ้า โลหะหนัก และพอลิเมอร์อื่น ๆ

สารปรับสภาพผิวผ้าตามการประดิษฐ์นี้ เหมาะสำหรับใช้กับผ้าที่เส้นใยมีหมู่แอมิโน ($-NH_2$ group) และ/หรือ หมู่ไฮดรอกซิล (–OH group) เป็นองค์ประกอบ

การปรับสภาพผิวผ้า หมายถึง การทำให้ปริมาณของสารปรับสภาพพื้นผิวติดบนผ้าร้อยละ 100 โดยการจุ่มรีด (padding)

$$\text{ร้อยละของการจุ่มรีด} = \frac{(\text{น้ำหนักผ้าหลังการจุ่มรีด} - \text{น้ำหนักผ้าก่อนการจุ่มรีด})}{\text{น้ำหนักผ้าก่อนการจุ่มรีด}} \times 100$$

นำผ้าที่จุ่มรีดไปอบให้แห้งในตู้อบที่อุณหภูมิ 80 องศาเซลเซียส เป็นเวลา 5 นาที และอบผนึกที่อุณหภูมิ 110 องศาเซลเซียส เป็นเวลา 2 นาที นำผ้าที่ได้ไปพิมพ์ด้วยเครื่องพิมพ์อิงก์เจ็ตที่ใช้หมึกพิมพ์อิงก์เจ็ตฐานน้ำชนิดสารสี พิมพ์ที่ความละเอียด 300 จุดต่อนิ้ว แล้วนำไปเข้าเครื่องอบไอน้ำเป็นเวลา 5 นาที

วัดคุณภาพงานพิมพ์ โดยวัดขอบเขตของสีด้วยเครื่องสเปกโทรโฟโตมิเตอร์ยี่ห้อ Gretag Macbeth Spectrolino ความคมชัดของงานพิมพ์ การผลิตน้ำหนักสีต่อเนื่อง และการซึมเข้าหากันของหมึกพิมพ์

ตัวอย่างต่อไปนี้แสดงให้เห็นเพิ่มเติมถึงการประดิษฐ์ แต่มิได้มีวัตถุประสงค์ที่จะจำกัดขอบเขตของการประดิษฐ์นี้แต่อย่างใด

ตัวอย่าง

ขั้นตอนที่ 1 การเตรียมไคโทซานดัดแปร HTACC

1.1 ละลายไคโทซานน้ำหนักโมเลกุล 100,000 กรัมต่อโมล ค่าระดับการกำจัดหมู่แอซีทิลร้อยละ 95 ปริมาณ 0.5 กรัม ด้วยสารละลายกรดแอซีติกความเข้มข้นร้อยละ 2 ปริมาตร 25 มิลลิลิตร กวนสารละลายด้วยแท่งแม่เหล็ก (magnetic stirrer) ที่ความเร็วรอบ 150 รอบต่อนาที จนสารละลายเป็นเนื้อเดียวกัน

1.2 เติมสารละลายไกลซิดิลไทรเมทิลแอมโมเนียมคลอไรด์ (glycidyltrimethylammonium chloride, GTMAC) 1.8 g ในสารละลายจากข้อ 1.1 กวนสารละลายด้วยแท่งแม่เหล็กที่ความเร็วรอบ 150 รอบต่อนาที อุณหภูมิ 70 องศาเซลเซียส เป็นเวลา 24 ชั่วโมง

1.3 ตั้งสารละลายให้อุณหภูมิลดลงจนถึงอุณหภูมิ 27 องศาเซลเซียส เทสารละลายลงในถุงเซลลูโลสไดอะไลซีส (dialysis tubing cellulose membrane) แกว่งในน้ำกลั่นเป็นเวลา 5 วัน เปลี่ยนน้ำทุกวัน นำสารละลายที่อยู่ในถุงเซลลูโลสไดอะไลซีสไปทำให้แห้งด้วยวิธี freeze dry

ขั้นตอนที่ 2 การเตรียมสารปรับสภาพผิวผ้าสูตรที่ 3 ไคโทซานดัดแปร HTACC ในกรดมะนาว

1. ชั่งกรดมะนาว 35 กรัม ละลายลงในน้ำกลั่น 100 กรัม
2. เติมไคโทซานดัดแปร HTACC 0.5 กรัม ลงในสารละลายกรดมะนาว กวนด้วยแท่งแม่เหล็กที่ความเร็ว 150 รอบต่อนาที จนละลายเป็นเนื้อเดียวกัน
3. เติมโซเดียมคาร์บอเนต 5.3 กรัม กวนด้วยแท่งแม่เหล็กให้ละลายเป็นเนื้อเดียวกัน
4. เทสารละลายทั้งหมดลงในขวดวัดปริมาตรขนาด 500 มิลลิลิตร เติมน้ำกลั่นจนได้ปริมาตร 500 มิลลิลิตร

วิธีการจุ่มรีด ชั่งน้ำหนักผ้าที่ตัดไว้ขนาด A4 ชุบผ้าด้วยสารปรับสภาพผิวให้เปียกทั่วทั้งผืน แล้วนำไปผ่านเครื่องจุ่มรีด ตั้งระยะห่างระหว่างโมของเครื่องให้พอดี เพื่อให้ปริมาณของสารละลายติดบนผ้าร้อยละ 100 โดยคำนวณตามสมการข้างบน อบผ้าให้แห้งในตู้อบที่อุณหภูมิ 80 องศาเซลเซียส เป็นเวลา 5 นาที และอบผนึกที่อุณหภูมิ 110 องศาเซลเซียส เป็นเวลา 2 นาที

นำผ้าที่อบผนึกแล้วไปพิมพ์ด้วยเครื่องพิมพ์อิงก์เจ็ตที่ใช้หมึกพิมพ์ฐานน้ำชนิดสารสี 7 สี พิมพ์แผ่นทดสอบบนผ้าที่ความละเอียด 300 จุดต่อนิ้ว ที่มีช่องสี 294 ช่อง สำหรับวัดขอบเขตสีตามมาตรฐานของ GretagMacbeth ด้วยโปรแกรม Profile Maker 5.0 และแบบทดสอบส่วนเส้นด้วยโปรแกรม Photoshop และ Illustrator ที่ไม่มีการจัดการสี นำผ้าที่พิมพ์เสร็จไปใส่ในเครื่องอบไอน้ำเป็นเวลา 5 นาที เพื่อกำจัดสีส่วนเกินออก

วัดคุณภาพงานพิมพ์ โดยวัดขอบเขตของสีด้วยเครื่องสเปกโทรโฟโตมิเตอร์ GretagMacbeth Spectrolino บนช่องผลิตสีสำหรับวัดขอบเขตสีตามมาตรฐานของ Gretag Macbeth จำนวน 294 ช่อง พบว่า ผ้าไหมที่ปรับสภาพผิวให้ขอบเขตสีที่กว้างกว่าผ้าที่ไม่ปรับสภาพผิวในทุกช่วงสี งานพิมพ์มีความคมชัดมากขึ้น ผ้าที่ปรับสภาพผิวให้ค่าความดำของหมึกพิมพ์มากขึ้น และมีลำดับขั้นน้ำหนักสีที่เด่นชัดกว่าผ้าที่ไม่ปรับสภาพผิว การซึมเข้าหากันของเส้นสี 2 เส้นของหมึกพิมพ์ (inter-color bleeding) วัดจากเส้นสีเหลืองที่ขยายหรือหดจากขนาด 1 มิลลิเมตร บนพื้นทึบสีดำ พบว่า เส้นสีเหลืองบนผ้าที่ปรับสภาพผิวซึมเข้าหากันน้อยกว่าผ้าที่ไม่ปรับสภาพผิว

วิธีการในการประดิษฐ์ที่ดีที่สุด

เหมือนกับที่ได้กล่าวมาแล้วในหัวข้อการเปิดเผยการประดิษฐ์โดยสมบูรณ์

ข้อถือสิทธิ

1. สารปรับสภาพผิวผ้าไคโทซานในกรดมะนาว ซึ่งประกอบด้วย

(1). กรดมะนาว (citric acid monohydrate) ในสัดส่วนร้อยละ 0.5 ถึง 10 โดยน้ำหนักขององค์ประกอบทั้งหมดภายในสูตรสารปรับสภาพผิวผ้า

(2). ไคโทซานในสัดส่วนร้อยละ 0.05 ถึง 7 โดยน้ำหนักขององค์ประกอบทั้งหมดภายในสูตรสารปรับสภาพผิวผ้า

(3). โซเดียมคาร์บอเนต (sodium carbonate anhydrous) ในสัดส่วนร้อยละ 0.1 ถึง 5 โดยน้ำหนักขององค์ประกอบทั้งหมดภายในสูตรสารปรับสภาพผิวผ้า

(4). น้ำในสัดส่วนร้อยละ 78-99.4 โดยน้ำหนักขององค์ประกอบทั้งหมดภายในสูตรสารปรับสภาพผิวผ้า

2. สารปรับสภาพผิวผ้าไคโทซานดัดแปร *เอ็น*-2-ไฮดรอกซี-3-ไทรเมทิลแอมโมเนียมพรอพิลไคโทซานคลอไรด์ (*N*-[(2-hydroxyl-3-trimethylammonium) propyl] chitosan chloride, HTACC) ซึ่งประกอบด้วย

(1). ไคโทซานดัดแปร HTACC ในสัดส่วนร้อยละ 0.04 ถึง 10 โดยน้ำหนักขององค์ประกอบทั้งหมดภายในสูตรสารปรับสภาพผิวผ้า

(2). กรดมะนาวในสัดส่วนร้อยละ 0.01 ถึง 10 โดยน้ำหนักขององค์ประกอบทั้งหมดภายในสูตรสารปรับสภาพผิวผ้า

(3). น้ำในสัดส่วนร้อยละ 79 ถึง 99.95 โดยน้ำหนักขององค์ประกอบทั้งหมดภายในสูตรสารปรับสภาพผิวผ้า

3. สารปรับสภาพผิวผ้าไคโทซานดัดแปร HTACC ในกรดมะนาว ซึ่งประกอบด้วย

(1). กรดมะนาวในสัดส่วนร้อยละ 0.5 ถึง 10 โดยน้ำหนักขององค์ประกอบทั้งหมดภายในสูตรสารปรับสภาพผิวผ้า

(2). ไคโทซานดัดแปร HTACC ในสัดส่วนร้อยละ 0.04 ถึง 10 โดยน้ำหนักขององค์ประกอบทั้งหมดภายในสูตรสารปรับสภาพผิวผ้า

(3). โซเดียมคาร์บอเนตในสัดส่วนร้อยละ 0.1 ถึง 5 โดยน้ำหนักขององค์ประกอบทั้งหมดภายในสูตรสารปรับสภาพผิวผ้า

(4). น้ำในสัดส่วนร้อยละ 74 ถึง 99.1 โดยน้ำหนักขององค์ประกอบทั้งหมดภายในสูตรสารปรับสภาพผิวผ้า

บทสรุปการประดิษฐ์

การประดิษฐ์นี้เกี่ยวข้องกับสารปรับสภาพผิวผ้าสำหรับการพิมพ์ระบบอิงก์เจ็ต 3 สูตร โดยสูตรที่ 1 ประกอบด้วยกรดมะนาว ไคโทซาน โซเดียมคาร์บอเนต และน้ำ สูตรที่ 2 ประกอบด้วย ไคโทซานดัดแปรเอ็น-2-ไฮดรอกซี-3-ไทรเมทิลแอมโมเนียมพรอพิลไคโทซานคลอไรด์ (*N*-[(2-hydroxyl-3-trimethylammonium) propyl] chitosan chloride, HTACC) และน้ำ และสูตรที่ 3 ประกอบด้วย กรดมะนาว ไคโทซานดัดแปร HTACC โซเดียมคาร์บอเนต และน้ำ ไคโทซาน หรือไคโทซานดัดแปร HTACC ทำหน้าที่ปรับสภาพผิวผ้า และเป็นสารยึดสารสีในหมึกพิมพ์ให้ติดกับผ้า กรดมะนาวนอกจากละลายไคโทซาน ยังทำให้ไคโทซานมีประจุบวกเพื่อเพิ่มการยึดกับสารสี โซเดียมคาร์บอเนตเป็นสารเร่งปฏิกิริยาและน้ำเป็นตัวทำละลาย

แบบฟอร์มเปิดเผยการประดิษฐ์และแสดงความจำนงขอให้จดทะเบียนสิทธิบัตร/อนุสิทธิบัตร

(Invention Disclosure Form)

NO.:.....
Receive date:.....

1. ชื่อที่แสดงถึงการประดิษฐ์ (ไทยและอังกฤษ).....

ปุ๋ยละลายช้าและกรรมวิธีการผลิตปุ๋ยละลายช้าดังกล่าว

Slow release fertilizers and methods to prepare the mentioned slow release fertilizers

ลักษณะโดยย่อของการประดิษฐ์ (แนบเอกสารประกอบได้).....

การประดิษฐ์นี้ จึงมุ่งเน้นที่จะผลิตปุ๋ยละลายช้าจากเม็ดปุ๋ยละลายเร็วที่นำมาเคลือบพอลิไวนิลแอลกอฮอล์ และไคโทซานเชื่อมขวาง รวมกับการสังเคราะห์ไฮโดรเจลเป็นชั้นเคลือบนอกสุดของเม็ดปุ๋ยที่ผ่านการเคลือบด้วยพอลิไวนิลแอลกอฮอล์ และไคโทซานเชื่อมขวางแล้ว ได้เม็ดปุ๋ยที่มีการปลดปล่อยธาตุอาหารพืชแบบควบคุมได้ ทำให้เม็ดปุ๋ยสามารถปลดปล่อยธาตุอาหารพืชอย่างช้า ๆ ซึ่งเป็นการชะลอการละลายน้ำของเม็ดปุ๋ย และลดการสูญเสียปุ๋ยไปโดยเปล่าประโยชน์

นำเม็ดปุ๋ยละลายเร็วมาเคลือบด้วยพอลิไวนิลแอลกอฮอล์ และเคลือบเม็ดปุ๋ยที่ผิวเคลือบแห้งแล้วอีกครั้งด้วยไคโทซานและเชื่อมขวางชั้นเคลือบไคโทซานด้วยกลูทารัลดีไฮด์ นำเม็ดปุ๋ยที่เคลือบและเชื่อมขวางชั้นเคลือบแล้ว มาสังเคราะห์ไฮโดรเจลเป็นชั้นเคลือบชั้นนอกสุด ด้วยปฏิกิริยาการเกิดพอลิเมอร์แบบแขวนลอย ได้เม็ดปุ๋ยที่มีการปลดปล่อยธาตุอาหารพืชแบบควบคุมได้ สามารถปลดปล่อยธาตุอาหารพืชอย่างน้อยภายในเวลา 30 วัน ณ อุณหภูมิห้อง ด้วยปริมาณที่พอเหมาะ ซึ่งเป็นแนวทางหนึ่งในการช่วยลดปัญหาด้านสิ่งแวดล้อม และมีประโยชน์ทั้งในด้านการเกษตร เศรษฐกิจ สังคม และสิ่งแวดล้อม อีกทั้งสามารถตอบสนองความต้องการของผู้บริโภคและพืชอีกด้วย

2. ชื่อผู้ประดิษฐ์ / ผู้ประดิษฐ์ร่วม	สัดส่วนการประดิษฐ์/ การแบ่งปันผลประโยชน์ (%)	สังกัด / ที่อยู่	โทรศัพท์ / โทรสาร / อีเมล์
นางสาวสุดา เกียรติกำจรวงศ์	35	คณะวิทยาศาสตร์ จุฬาลงกรณ์มหาวิทยาลัย	02 2185587 / ksuda@chula.ac.th
นางสาวสุภาภรณ์ นพคุณดิลกรัตน์	35	คณะวิทยาศาสตร์ จุฬาลงกรณ์มหาวิทยาลัย	02 218 8869/ Supaporn.n@chula.ac.th
นางสาวณัฏฐ์ธยาน์ เพชรรัตน์	30	9 ซอย 5 ถ. ราชดำเนิน 1 ต. ในเมือง อ. เมือง จ. กำแพงเพชร 62000	087 474 7334/ myomy_secret@hotmail.com

3. การประดิษฐ์นี้ได้รับการสนับสนุนทางด้านการเงินจากแหล่งเงินทุนหรือร่วมวิจัยกับ องค์กร บริษัท หรือหน่วยงานใดหรือไม่

☑ ได้รับ โปรดระบุชื่อหน่วยงานที่เกี่ยวข้อง สำนักงานกองทุนสนับสนุนการวิจัย ☐ ไม่ได้รับ

4. ผลงานนี้เคยมีการตีพิมพ์ หรือเผยแพร่ผลงานมาก่อนหรือไม่ จะเผยแพร่ในวารสารวิชาการในอนาคต กำลังเขียนบทความวิชาการ

☐ มี โปรดระบุลักษณะการเผยแพร่ .เมื่อ..... ☑ ไม่มี

5. ศักยภาพของเทคโนโลยีในเชิงพาณิชย์ (โปรดอธิบาย แนบเอกสารประกอบได้)

ผลิตภัณฑ์หรือเทคโนโลยีที่ใกล้เคียงที่มีอยู่แล้วในตลาด.....

เม็ดปุ๋ยละลายช้าที่วางขายในตลาด เป็นการเคลือบชั้นกาวบาง ๆ ด้วยสารอีพอกซี ไม่พบมีการเคลือบด้วยสารเคมีที่การประดิษฐ์นี้ใช้เคลือบและไม่มีชั้นไฮโดรเจลที่ช่วยควบคุมการดูดซึม การปลดปล่อยสารอาหารของปุ๋ย และการย่อยสลาย

ลักษณะการใช้ประโยชน์จากผลงาน (Application).....

เม็ดปุ๋ยที่มีชั้นเคลือบและชั้นไฮโดรเจล ช่วยควบคุมการซึมผ่านของน้ำจากสิ่งแวดล้อมเข้าไปในเม็ดปุ๋ย ทำให้เม็ดปุ๋ยละลายช้า ๆ ภายในเม็ด และซึมผ่านชั้นเคลือบอย่างช้า ๆ และสม่ำเสมอ ทำให้กรณีที่เป็นปุ๋ย เอ็น พี เค สารอาหารค่อย ๆ ออกมาด้วยอัตราที่แตกต่างกัน ทำให้พืชนำสารอาหารไปใช้ได้อย่างมีประสิทธิภาพ

จุดเด่นของผลิตภัณฑ์หรือเทคโนโลยีเมื่อเปรียบเทียบกับผลิตภัณฑ์หรือเทคโนโลยีปัจจุบัน.....

จุดเด่นคือ การนำเคลือบเม็ดปุ๋ยด้วยสารเคลือบชีวภาพที่ย่อยสลายได้ทางชีวภาพ และการนำไฮโดรเจลที่สามารถแตกสลายได้ง่ายโดยธรรมชาติมาเคลือบเป็นชั้นนอกสุดที่ควบคุมการเข้าออกของน้ำ หรือสารละลายจากสิ่งแวดล้อม และยังควบคุมการปลดปล่อยสารอาหารจากปุ๋ย

โปรดระบุชื่อบริษัทซึ่งท่านคิดว่าน่าจะมีความสนใจในเทคโนโลยีหรือสิ่งประดิษฐ์ของท่าน

บริษัท.. บริษัท เจียงไต๋ จำกัด โทรศัพท์ (ถ้ามี).....

บริษัท.....โทรศัพท์ (ถ้ามี).....

6. การสืบค้นข้อมูลสิทธิบัตร

6.1 Keyword ที่ใช้ในการสืบค้น..... Fertilizer, fertilizer hydrogel, control release

6.2 ผลการสืบค้นพบว่า ☐ เหมือนหรือคล้ายกับงานที่ปรากฏอยู่แล้ว ☑ ไม่เหมือนหรือคล้ายกับงานที่ปรากฏอยู่แล้ว

6.3 Website ที่ใช้ในการสืบค้น ☑ ประเทศไทย: www.ipthailand.org ☐ สหรัฐอเมริกา : www.uspto.gov

☐ ญี่ปุ่น : www.jpo.go.jp ☑ ยุโรป : http://ep.espacenet.com ☐ อื่นๆ ระบุ.....

(ในกรณีที่พบว่าเหมือนหรือคล้ายกับงานที่ปรากฏอยู่แล้ว กรุณาแนบเอกสารที่สืบค้นได้มาให้สถาบันฯ ด้วย)

7. ข้าพเจ้าขอยืนยันว่าข้อมูลดังกล่าวข้างต้นครบถ้วนและถูกต้อง

ลงนาม.....หัวหน้าโครงการ

(.....นางสาวสุดา เกียรติกำจรวงศ์.....)

.....2...../ มิ.ย. ...../ 2554.....

กรุณาส่งแบบฟอร์มนี้กลับมายัง

สถาบันทรัพย์สินทางปัญญาแห่งจุฬาลงกรณ์มหาวิทยาลัย
ชั้น 9 อาคารเทพทวาราวดี คณะนิติศาสตร์ จุฬาลงกรณ์มหาวิทยาลัย
โทรศัพท์: 02-2182895-96 โทรสาร: 02-2182871

คำขอรับสิทธิบัตร/~~อนุสิทธิบัตร~~

☑ การประดิษฐ์
☐ การออกแบบผลิตภัณฑ์
☐ อนุสิทธิบัตร

ข้าพเจ้าผู้ลงลายมือชื่อในคำขอรับสิทธิบัตร/~~อนุสิทธิบัตร~~นี้ ขอรับสิทธิบัตร/~~อนุสิทธิบัตร~~ ตามพระราชบัญญัติสิทธิบัตร พ.ศ 2522 แก้ไขเพิ่มเติมโดยพระราชบัญญัติสิทธิบัตร (ฉบับที่ 2) พ.ศ 2535 และ พระราชบัญญัติสิทธิบัตร (ฉบับที่ 3) พ.ศ 2542

สำหรับเจ้าหน้าที่

วันรับคำขอ **1 มิถุนายน**. 2554	เลขที่คำขอ
วันยื่นคำขอ	
สัญลักษณ์จำแนกการประดิษฐ์ระหว่างประเทศ	
ใช้กับแบบผลิตภัณฑ์ ประเภทผลิตภัณฑ์	
วันประกาศโฆษณา	เลขที่ประกาศโฆษณา
วันออกสิทธิบัตร/อนุสิทธิบัตร	เลขที่สิทธิบัตร/อนุสิทธิบัตร
ลายมือชื่อเจ้าหน้าที่	

1.ชื่อที่แสดงถึงการประดิษฐ์/~~การออกแบบผลิตภัณฑ์~~
ปุ๋ยละลายช้าและกรรมวิธีการผลิตปุ๋ยละลายช้าดังกล่าว

2.คำขอรับสิทธิบัตรการออกแบบผลิตภัณฑ์นี้เป็นคำขอสำหรับแบบผลิตภัณฑ์อย่างเดียวกันและเป็นคำขอลำดับที่
ในจำนวน คำขอ ที่ยื่นในคราวเดียวกัน

3.ผู้ขอรับสิทธิบัตร/~~อนุสิทธิบัตร~~ และที่อยู่ (เลขที่ ถนน ประเทศ) **จุฬาลงกรณ์มหาวิทยาลัย 254 ถนนพญาไท แขวงวังใหม่ เขตปทุมวัน กรุงเทพฯ** 10330 **(มีต่อหน้า** 3)	3.1 สัญชาติ **ไทย**
	3.2 โทรศัพท์ 02-218-3590; 02-564-7000 **ต่อ** 1314-1350
	3.3 โทรสาร 02-218-3589; 02-564 7008
	3.4 อีเมล์ CU.prop@chula.ac.th; tlo@tmc.nstda.or.th

4.สิทธิในการขอรับสิทธิบัตร/~~อนุสิทธิบัตร~~
☐ ผู้ประดิษฐ์/ผู้ออกแบบ ☑ ผู้รับโอน ☐ ผู้ขอรับสิทธิโดยเหตุอื่น

5.ตัวแทน (ถ้ามี)/ที่อยู่ (เลขที่ ถนน จังหวัด รหัสไปรษณีย์) **สำนักงานจัดการทรัพย์สิน จุฬาลงกรณ์มหาวิทยาลัย** **254 ถนนพญาไท แขวงวังใหม่ เขตปทุมวัน กทม** 10330	5.1 ตัวแทนเลขที่
	5.2 โทรศัพท์ 02-218-3590
	5.3 โทรสาร 02-218-3589
	5.4 อีเมล์ CU.prop@chula.ac.th

6.ผู้ประดิษฐ์/~~ผู้ออกแบบผลิตภัณฑ์~~ และที่อยู่ (เลขที่ ถนน ประเทศ)
1. **นางสาวสุดา เกียรติกำจรวงศ์** 2. **นางสาวสุภาภรณ์ นพคุณดิลกรัตน์ และ** 3. **นางสาวณัฏฐ์ธยาน์ เพชรรัตน์ ที่อยู่ จุฬาลงกรณ์มหาวิทยาลัย 254 ถนนพญาไท แขวงวังใหม่ เขตปทุมวัน กทม.** 10330

7. คำขอรับสิทธิบัตร/อนุสิทธิบัตรนี้แยกจากหรือเกี่ยวข้องกับคำขอเดิม
ผู้ขอรับสิทธิบัตร/อนุสิทธิบัตร ขอให้ถือว่าได้ยื่นคำขอรับสิทธิบัตร/อนุสิทธิบัตรนี้ ในวันเดียวกับคำขอรับสิทธิบัตร เลขที่ วันยื่น เพราะคำขอรับสิทธิบัตร/อนุสิทธิบัตรนี้แยกจากหรือเกี่ยวข้องกับคำขอเดิมเพราะ
คำขอเดิมมีการประดิษฐ์หลายอย่าง ถูกคัดค้านเนื่องจากผู้ขอไม่มีสิทธิ ขอเปลี่ยนแปลงประเภทของสิทธิ

หมายเหตุ ในกรณีที่ไม่อาจระบุรายละเอียดได้ครบถ้วน ให้จัดทำเป็นเอกสารแนบท้ายแบบพิมพ์นี้โดยระบุหมายเลขกำกับข้อและหัวข้อที่แสดงรายละเอียดเพิ่มเติมดังกล่าวด้วย

8.การยื่นคำขอนอกราชอาณาจักร

วันยื่นคำขอ	เลขที่คำขอ	ประเทศ	สัญลักษณ์จำแนกการประดิษฐ์ระหว่างประเทศ	สถานะคำขอ
8.1				
8.2				
8.3				

8.4 ผู้ขอรับสิทธิบัตร/อนุสิทธิบัตรขอสิทธิให้ถือว่าได้ยื่นคำขอนี้ในวันที่ได้ยื่นคำขอรับสิทธิบัตร/อนุสิทธิบัตรในต่างประเทศเป็นครั้งแรกโดย
ได้ยื่นเอกสารหลักฐานพร้อมคำขอนี้ ขอยื่นเอกสารหลักฐานหลังจากวันยื่นคำขอนี้

9.การแสดงการประดิษฐ์ หรือการออกแบบผลิตภัณฑ์ ผู้ขอรับสิทธิบัตร/อนุสิทธิบัตรได้แสดงการประดิษฐ์ที่หน่วยงานของรัฐเป็นผู้จัด
วันแสดง วันเปิดงานแสดง ผู้จัด

10.การประดิษฐ์เกี่ยวกับจุลชีพ

10.1 เลขทะเบียนฝากเก็บ	10.2 วันที่ฝากเก็บ	10.3 สถาบันฝากเก็บ/ประเทศ

11.ผู้ขอรับสิทธิบัตร/อนุสิทธิบัตร ขอยื่นเอกสารภาษาต่างประเทศก่อนในวันยื่นคำขอนี้ และจะจัดยื่นคำขอรับสิทธิบัตร/อนุสิทธิบัตรนี้ที่จัดทำเป็นภาษาไทยภายใน 90 วัน นับจากวันยื่นคำขอนี้ โดยขอยื่นเป็นภาษา

☐ อังกฤษ ☐ ฝรั่งเศส ☐ เยอรมัน ☐ ญี่ปุ่น ☐ อื่นๆ

12.ผู้ขอรับสิทธิบัตร/อนุสิทธิบัตร ขอให้อธิบดีประกาศโฆษณาคำขอรับสิทธิบัตร หรือรับจดทะเบียน และประกาศโฆษณาอนุสิทธิบัตรนี้
หลังจากวันที่ เดือน พ.ศ
☐ ผู้ขอรับสิทธิบัตร/อนุสิทธิบัตรขอให้ใช้รูปเขียนหมายเลข ในการประกาศโฆษณา

13.คำขอรับสิทธิบัตร/~~อนุสิทธิบัตร~~นี้ประกอบด้วย

ก. แบบพิมพ์คำขอ 3 หน้า
ข. รายละเอียดการประดิษฐ์
หรือ~~คำพรรณนาแบบผลิตภัณฑ์~~ 11 หน้า
ค. ข้อถือสิทธิ 2 หน้า
ง. รูปเขียน รูป หน้า
จ. ภาพแสดงแบบผลิตภัณฑ์
☐ รูปเขียน รูป หน้า
☐ ภาพถ่าย รูป หน้า
ฉ. บทสรุปการประดิษฐ์ 1 หน้า

14.เอกสารประกอบคำขอ

☐ เอกสารแสดงสิทธิในการขอรับสิทธิบัตร/อนุสิทธิบัตร
☐ หนังสือรับรองการแสดงการประดิษฐ์/การออกแบบผลิตภัณฑ์
☐ หนังสือมอบอำนาจ
☐ เอกสารรายละเอียดเกี่ยวกับจุลชีพ
☐ เอกสารการขอนับวันยื่นคำขอในต่างประเทศเป็นวันยื่นคำขอในประเทศไทย
☐ เอกสารขอเปลี่ยนแปลงประเภทของสิทธิ
☐ เอกสารอื่น ๆ

15. ข้าพเจ้าขอรับรองว่า

☑ การประดิษฐ์นี้ไม่เคยยื่นขอรับสิทธิบัตร/~~อนุสิทธิบัตร~~มาก่อน
☐ การประดิษฐ์นี้ได้พัฒนาปรับปรุงมาจาก.....

16.ลายมือชื่อ (☐ผู้ขอรับสิทธิบัตร / อนุสิทธิบัตร; ☐ ตัวแทน)

<u>หมายเหตุ</u> บุคคลใดยื่นขอรับสิทธิบัตรการประดิษฐ์หรือการออกแบบผลิตภัณฑ์ หรืออนุสิทธิบัตร โดยการแสดงข้อความอันเป็นเท็จแก่พนักงานเจ้าหน้าที่ เพื่อให้ได้ไปซึ่งสิทธิบัตรหรืออนุสิทธิบัตร ต้องระวางโทษจำคุกไม่เกินหกเดือน หรือปรับไม่เกินห้าพันบาท หรือทั้งจำทั้งปรับ

3. ผู้ขอรับสิทธิบัตร/อนุสิทธิบัตร และที่อยู่ (เลขที่ ถนน ประเทศ)

สำนักงานกองทุนสนับสนุนการวิจัย ชั้น 14 **เอส เอ็ม ทาวเวอร์ เลขที่** 979/17-21 **ถ.พหลโยธิน แขวงสามเสนใน เขตพญาไท กรุงเทพฯ** 10400

6. ผู้ประดิษฐ์/ผู้ออกแบบผลิตภัณฑ์ และที่อยู่ (เลขที่ ถนน ประเทศ)

รายละเอียดการประดิษฐ์

ชื่อที่แสดงถึงการประดิษฐ์

ปุ๋ยละลายช้าและกรรมวิธีการผลิตปุ๋ยละลายช้าดังกล่าว

สาขาวิทยาการที่เกี่ยวข้องกับการประดิษฐ์

การประดิษฐ์นี้อยู่ในสาขาวัสดุศาสตร์ ในส่วนที่เกี่ยวข้องกับการผลิตปุ๋ยละลายช้าที่มีพอลิเมอร์ดูดซึมน้ำมากเป็นสารผิวชั้นนอก

ภูมิหลังของศิลปะหรือวิทยาการที่เกี่ยวข้อง

ปุ๋ย คือ หนึ่งในผลิตภัณฑ์ที่สำคัญของอุตสาหกรรมทางการเกษตร ปุ๋ยในดินสามารถปล่อยธาตุอาหารที่จำเป็นให้แก่พืชเพื่อใช้เจริญเติบโต ธาตุอาหารหลักที่สำคัญ ได้แก่ ไนโตรเจน ฟอสฟอรัส และโพแทสเซียม แต่อย่างไรก็ตาม การใช้ปุ๋ยละลายเร็ว ที่ประกอบด้วยธาตุอาหารที่มีสมบัติละลายในน้ำได้ดีในปริมาณมาก ปุ๋ยส่วนใหญ่ละลายน้ำหมดไปในเวลาอันรวดเร็วโดยรากพืชสามารถดูดไปใช้ได้เพียงบางส่วนเท่านั้น ซึ่งเป็นการสิ้นเปลืองและอาจเกิดผลเสียกับดินในบริเวณที่มีธาตุอาหารพืชตกค้าง จึงมีการกำหนดขอบเขตการใช้ปุ๋ย เพื่อป้องกันผลกระทบที่อาจเกิดกับสิ่งแวดล้อม โดยทั่วไป ปุ๋ยธรรมดามีปริมาณธาตุอาหารไนโตรเจนร้อยละ 40-70 ธาตุอาหารฟอสฟอรัสร้อยละ 80-90 และธาตุอาหารโพแทสเซียมร้อยละ 50-70 นั้น จะสูญหายไปกับสิ่งแวดล้อมได้ง่าย และพืชไม่สามารถดูดธาตุอาหารเหล่านั้นได้ จึงมีการใช้ปุ๋ยละลายช้าเพื่อลดการสูญเสียธาตุอาหารดังกล่าว และเพื่อลดผลกระทบต่อสิ่งแวดล้อมให้เกิดน้อยที่สุด

ปุ๋ยละลายช้า หมายถึง ปุ๋ยเคมีบางชนิดที่มีสมบัติไม่ละลายน้ำหรือละลายน้ำได้น้อยตามธรรมชาติ แต่เมื่อใส่ปุ๋ยนี้ลงในดิน ธาตุอาหารพืชในส่วนที่ไม่ละลายน้ำเกิดการเปลี่ยนแปลงและค่อย ๆ ปล่อยธาตุอาหารออกมาในรูปที่พืชสามารถดูดใช้ได้ ขึ้นอยู่กับชนิดของปุ๋ย ขนาดและความละเอียดของเม็ดปุ๋ย ความชื้นในดิน สามารถแบ่งประเภทของปุ๋ยละลายช้าได้เป็น 2 ประเภท คือ ปุ๋ยละลายช้าตามสมบัติของปุ๋ย และปุ๋ยที่ผลิตโดยกรรมวิธีควบคุมการปล่อยธาตุอาหารพืช เช่น ปุ๋ยไฮโดรเจล (fertilizer hydrogel) ซึ่งสังเคราะห์โดยนำพอลิเมอร์ดูดซึมน้ำมาก (superabsorbent polymers, SAPs) มาเคลือบบนพื้นผิวของเม็ดปุ๋ย

ปัจจุบันพอลิเมอร์ดูดซึมน้ำมากและไฮโดรเจลเป็นที่สนใจในอุตสาหกรรมหลาย ๆ ด้าน เนื่องจากพอลิเมอร์ดูดซึมน้ำมากมีสมบัติบวมน้ำ และสามารถกักเก็บน้ำไว้ในโครงสร้างได้มากกว่า 10 เท่าของน้ำหนักพอลิเมอร์แห้งและไม่ละลายน้ำ

พอลิเมอร์ดูดซึมน้ำมากสามารถนำไปใช้ประโยชน์ได้ในหลาย ๆ ด้าน เช่น ทางเกษตรกรรม การทำสวนประดับ พอลิเมอร์ช่วยปรับปรุงคุณภาพดิน โดยเพิ่มการกักเก็บน้ำของดิน ทำให้ดินปล่อยน้ำสู่รากของพืชได้นานขึ้น เป็นการรักษาสมดุลของความชื้นในดิน และยังช่วยกักเก็บ

สารอาหารของพืชซึ่งละลายในเจลพอลิเมอร์ มีพอลิเมอร์หลายชนิดที่ได้นำมาใช้ในการสังเคราะห์พอลิเมอร์ดูดซึมน้ำมาก เช่น พอลิอะคริลาไมด์ (polyacrylamide) พอลิอะคริลิกแอซิด (polyacrylic acid) และพอลิอะคริลาไมด์-*โค*-อะคริลิกแอซิด (poly(acrylamide-*co*-acrylic acid))

มีเอกสารงานวิจัยจำนวนหนึ่งที่เกี่ยวข้องกับการเตรียมและใช้พอลิเมอร์ดูดซึมน้ำมากในการเตรียมปุ๋ยละลายช้าและควบคุมการปลดปล่อยธาตุอาหารพืช ดังนี้

Du และคณะ รายงานในเอกสารวิจัยเรื่อง “Release characteristic of nutrients from polymer-coated compound controlled release fertilizers” ศึกษาการปลดปล่อยธาตุอาหารพืชจากพอลิเมอร์ที่เคลือบเม็ดปุ๋ยคอมพาวนด์ เปรียบเทียบอุณหภูมิและความหนาของชั้นเคลือบเม็ดปุ๋ยที่อุณหภูมิ 20, 30 และ 40 องศาเซลเซียสในดิน พบว่า ที่อุณหภูมิต่ำ และความหนาของชั้นเคลือบที่มากขึ้นทำให้เม็ดปุ๋ยปลดปล่อยธาตุอาหารพืชช้าลง ในแต่ละวันปุ๋ยไนเทรตมีอัตราการปลดปล่อยที่เร็วที่สุด ตามด้วยปุ๋ยแอมโมเนียม โพแทสเซียม และฟอสเฟต โดยปลดปล่อยธาตุอาหารพืชดังกล่าวร้อยละ 1.05, 0.85, 0.67 และ 0.39 ต่อวัน ตามลำดับ ที่ความหนาของชั้นเคลือบเม็ดปุ๋ย 0.0065 เซนติเมตร (Du, C., Zhou, J., และ Shaviv, A. *Journal of Polymer Environment.* 2006, **14**, 223-230.)

Liu และคณะ รายงานในเอกสารวิจัยเรื่อง “Synthesis of a slow-release and superabsorbent nitrogen fertilizer and its properties” สังเคราะห์ปุ๋ยไนโตรเจนซูเปอร์แอบซอร์เบนต์ ผ่านปฏิกิริยาการเกิดโคพอลิเมอร์แบบสารละลาย สารตั้งต้นที่ใช้ คือ อะคริลิกแอซิด และมาเลอิกแอนไฮไดรด์ สารเชื่อมขวางเป็น *เอ็น,เอ็น’*- เมทิลีนบิสอะคริลาไมด์ มีแอมโมเนียมเปอร์ซัลเฟตและโซเดียมซัลไฟต์เป็นสารริเริ่มปฏิกิริยาการเกิดพอลิเมอร์ในภาวะที่มียูเรีย ผลการทดลองพบว่า ปริมาณที่เหมาะสมของสารเชื่อมขวาง สารริเริ่มปฏิกิริยา และมาเลอิกแอนไฮไดรด์เป็นร้อยละ 0.093, 0.17 และ 30 ตามลำดับ ระดับการทำให้เป็นกลางร้อยละ 63 เวลาในการเกิดปฏิกิริยา 2 ชั่วโมง ที่อุณหภูมิ 70 องศาเซลเซียส และ น้ำหนักยูเรียต่อน้ำหนักของอะคริลิกแอซิดเป็น 1.33 กรัม ซึ่งให้ค่าการดูดซึมน้ำมากที่สุด มีปริมาณไนโตรเจนร้อยละ 28.5 ปริมาณการดูดซึมน้ำในน้ำกลั่นและในน้ำประปาเป็น 900 และ 180 กรัมต่อน้ำหนักกรัมแห้ง ตามลำดับ (Liu, M., Liung, R., Zhan, F., Liu, Z., และ Niu, A. *Polymers for Advanced Technologies*. 2006, **17**, 430-438.)

Liu และคณะ รายงานในเอกสารวิจัยเรื่อง “Preparation of superabsorbent slow release nitrogen fertilizer by inverse suspension polymerization” สังเคราะห์ปุ๋ยไนโตรเจนซูเปอร์แอบซอร์เบนต์ด้วยปฏิกิริยาการเกิดพอลิเมอร์แบบแขวนลอย มอนอเมอร์ที่ใช้ คือ อะคริลิกแอซิด สารเชื่อมขวางเป็นเอ็น,เอ็น’- เมทิลีนบิสอะคริลาไมด์ สารริเริ่มปฏิกิริยาการเกิดพอลิเมอร์เป็นแอมโมเนียมเปอร์ซัลเฟต ไซโคลเฮกเซนเป็นตัวกลางทำกระจาย โซเดียมออกทะเดซิลฟอสเฟต (sodium octadecyl phosphate) เป็นสารช่วยแขวนลอย ในภาวะที่มียูเรีย และศึกษาผลของปริมาณสารเชื่อมขวาง สารริเริ่มปฏิกิริยา ยูเรีย เวลา อุณหภูมิ และระดับการทำให้เป็นกลาง พบว่า

ภาวะที่เหมาะสมในการสังเคราะห์ คือ ปริมาณของสารเชื่อมขวางและสารริเริ่มปฏิกิริยาร้อยละ 1.04 และ 0.08 และใช้สัดส่วนยูเรียต่ออะคริลิกแอซิดโดยน้ำหนักเป็น 1.0 เวลาเกิดปฏิกิริยา 1.5 ชั่วโมง ที่อุณหภูมิ 70 องศาเซลเซียส ระดับการทำให้เป็นกลาง(neutralization degree) ร้อยละ 60 ได้ค่าการดูดซึมน้ำมากที่สุด และยังพบอีกว่า ปุ๋ยที่สังเคราะห์ได้มีปริมาณไนโตรเจนร้อยละ 22.7 ค่าการดูดซึมน้ำ 965 กรัมต่อน้ำหนักกรัมแห้งในน้ำกลั่น และ 185 กรัมต่อน้ำหนักกรัมแห้งในน้ำประปา การปล่อยธาตุไนโตรเจนในปุ๋ยไม่เกินร้อยละ 80 ในเวลา 28 วัน (Liu, M., Liang, R., Zhan, F., Liu, Z., และ Niu, A. *Polymer international*. 2007, **56**, 729-737.)

Wu และ Liu รายงานในเอกสารวิจัยเรื่อง “Preparation and properties of cellulose acetate-coated compound fertilizer with controlled-release and water-retention” ซึ่งเกี่ยวข้องกับการเตรียมและศึกษาสมบัติของไคโทซานที่เคลือบอยู่บนปุ๋ยคอมพาวนด์เอ็นพีเค เพื่อควบคุมการปลดปล่อยธาตุอาหารพืช มอนอเมอร์ที่ใช้ คือ อะคริลิกแอซิด และ อะคริลาไมด์ สารเชื่อมขวางเป็น *เอ็น,เอ็น’*-เมทิลีนบิสอะคริลาไมด์ และสารริเริ่มปฏิกิริยาการเกิดพอลิเมอร์เป็นแอมโมเนียมเปอร์ซัลเฟต ผลิตภัณฑ์ที่ได้เป็นปุ๋ยคอมพาวนด์เอ็นพีเคที่มีไคโทซานเป็นสารเคลือบปุ๋ยชั้นใน และพอลิ(อะคริลาไมด์-*โค*-อะคริลิกแอซิด) เป็นสารเคลือบชั้นนอก พบว่า ปุ๋ยคอมพาวนด์เอ็นพีเคซูเปอร์แอบซอร์เบนต์มีปริมาณไนโตรเจน ฟอสฟอรัส และโพแทสเซียม ร้อยละ 8.06, 8.14 และ 7. 98 โดยน้ำหนัก ตามลำดับ ภาวะที่เหมาะสมในการสังเคราะห์ที่ทำให้เกิดสภาพการบวมตัวของซูเปอร์แอบซอร์เบนต์และการปลดปล่อยธาตุอาหารพืชดีที่สุดคือ ที่ระดับการทำให้เป็นกลาง ร้อยละ 70 ปริมาณสารริเริ่มปฏิกิริยา สารเชื่อมขวาง และอะคริลาไมด์มอนอเมอร์เป็นร้อยละ 0.91, 0.28 และ 20 โดยน้ำหนัก ที่อุณหภูมิ 65 องศาเซลเซียส ปุ๋ยคอมพาวนด์เอ็นพีเคซูเปอร์แอบซอร์เบนต์สามารถปลดปล่อยธาตุอาหารพืชในเวลา 30 วัน และปลดปล่อยไม่เกินร้อยละ 75 ของธาตุอาหารพืชเริ่มต้น งานวิจัยทำในปีเดียวกันได้เปลี่ยนสารเคลือบชั้นในจากไคโทซานเป็น เซลลูโลสแอซิเทต (Wu, L. and Liu, M. *Polymers for Advanced Technologies*. 2008, **19**, 785-792.)

Wu และคณะ ได้รายงานในเอกสารวิจัยเรื่อง “Preparation and properties of chitosan-coated NPK compound fertilizer with controlled-release and water-retention” สังเคราะห์และศึกษาลักษณะของเซลลูโลสแอซิเทต ที่นำมาเคลือบบนปุ๋ยคอมพาวนด์เอ็นพีเค มอนอเมอร์ที่ใช้ คือ อะคริลิกแอซิด และ อะคริลาไมด์ สารเชื่อมขวางเป็น *เอ็น,เอ็น’*-เมทิลีนบิสอะคริลาไมด์ และสารริเริ่มปฏิกิริยาการเกิดพอลิเมอร์เป็นแอมโมเนียมเปอร์ซัลเฟต ได้ซูเปอร์แอบซอร์เบนต์พอลิเมอร์ที่มีเซลลูโลสแอซิเทตเป็นสารเคลือบปุ๋ยชั้นใน และมีพอลิอะคริลาไมด์-*โค*-อะคริลิกแอซิดเป็นสารเคลือบชั้นนอก พบว่า ปุ๋ยคอมพาวนด์เอ็นพีเคซูเปอร์แอบซอร์เบนต์ที่สังเคราะห์ได้มีปริมาณไนโตรเจน ฟอสฟอรัส โพแทสเซียม แคลเซียม และแมกนีเซียม ร้อยละ 11, 6, 9, 1 และ 0.4 โดยน้ำหนัก ตามลำดับ ภาวะที่เหมาะสมในการสังเคราะห์ที่ทำให้เกิดสภาพการบวมตัวของเจลและการปลดปล่อยของธาตุอาหารพืชดีที่สุดคือ ที่ระดับการทำให้เป็นกลางของอะคริลิกแอซิดเป็น

ร้อยละ 70 ปริมาณสารริเริ่มปฏิกิริยา สารเชื่อมขวาง และอะคริลาไมด์เป็นร้อยละ 0.8, 0.12 และ 20 โดยน้ำหนัก เวลาการเกิดปฏิกิริยา 90 นาที ที่อุณหภูมิ 65 องศาเซลเซียส สามารถปลดปล่อยธาตุอาหารพืชในเวลา 30 วัน ไม่เกินร้อยละ 75 การสังเคราะห์ปุ๋ยไฮโดรเจล นอกจากลดการสูญเสียแร่ธาตุดังที่กล่าวมาแล้ว ยังเป็นการประหยัดเวลาและต้นทุนการผลิตอีกด้วย (Wu, L., และ Liu, M. *Carbohydrate Polymer*. 2008, **72**, 240-247.)

งานวิจัยข้างต้นเป็นงานที่ใช้สารเคลือบและพอลิเมอร์ดูดซึมน้ำมากมาเตรียมปุ๋ยละลายช้า แต่ยังไม่มีงานวิจัยใดใช้พอลิไวนิลแอลกอฮอล์ และไคโทซานเชื่อมขวางเคลือบเม็ดปุ๋ย รวมกับการสังเคราะห์ไฮโดรเจลเป็นชั้นเคลือบนอกสุดของเม็ดปุ๋ยที่ผ่านการเคลือบด้วยพอลิไวนิลแอลกอฮอล์และไคโทซานเชื่อมขวาง

การประดิษฐ์นี้ จึงมุ่งเน้นที่จะผลิตปุ๋ยละลายช้าจากเม็ดปุ๋ยละลายเร็วที่นำมาเคลือบพอลิไวนิลแอลกอฮอล์ และไคโทซานเชื่อมขวาง รวมกับการสังเคราะห์ไฮโดรเจลเป็นชั้นเคลือบนอกสุดของเม็ดปุ๋ยที่ผ่านการเคลือบด้วยพอลิไวนิลแอลกอฮอล์ และไคโทซานเชื่อมขวางแล้ว ได้เม็ดปุ๋ยที่มีการปลดปล่อยธาตุอาหารพืชแบบควบคุมได้ ทำให้เม็ดปุ๋ยสามารถปลดปล่อยธาตุอาหารพืชอย่างช้า ๆ ซึ่งเป็นการชะลอการละลายน้ำของเม็ดปุ๋ย และลดการสูญเสียปุ๋ยไปโดยเปล่าประโยชน์ รวมทั้งลดค่าใช้จ่ายที่สิ้นเปลื้องจากการใช้ปุ๋ยละลายเร็ว และลดผลกระทบต่อสิ่งแวดล้อมจากการใช้ปุ๋ยดังกล่าวอีกด้วย

ลักษณะและความมุ่งหมายของการประดิษฐ์

การประดิษฐ์นี้เกี่ยวข้องกับการผลิตปุ๋ยละลายช้าโดยการใช้พอลิเมอร์ดูดซึมน้ำมากมาเตรียมชั้นสารเคลือบเม็ดปุ๋ยละลายเร็วที่มีราคาถูกและหาได้ทั่วไป ให้เกิดเป็นปุ๋ยที่มีสมบัติดีขึ้นในด้านการละลายน้ำ เพื่อลดจำนวนครั้งในการใส่ปุ๋ยในดิน และให้ปุ๋ยค่อย ๆ ปลดปล่อยธาตุอาหารที่จำเป็นให้แก่พืชเพื่อใช้ในการเจริญเติบโต

วัตถุประสงค์ของการประดิษฐ์นี้มุ่งเน้นที่จะผลิตปุ๋ยละลายช้า โดยนำเม็ดปุ๋ยละลายเร็วมาเคลือบด้วยพอลิไวนิลแอลกอฮอล์ และเคลือบเม็ดปุ๋ยที่ผิวเคลือบแห้งแล้วอีกครั้งด้วยไคโทซานและเชื่อมขวางชั้นเคลือบไคโทซานด้วยกลูทารัลดีไฮด์ นำเม็ดปุ๋ยที่เคลือบและเชื่อมขวางชั้นเคลือบแล้ว มาสังเคราะห์ไฮโดรเจลเป็นชั้นเคลือบชั้นนอกสุด ด้วยปฏิกิริยาการเกิดพอลิเมอร์แบบแขวนลอย ได้เม็ดปุ๋ยที่มีการปลดปล่อยธาตุอาหารพืชแบบควบคุมได้ สามารถปลดปล่อยธาตุอาหารพืชอย่างน้อยภายในเวลา 30 วัน ซึ่งเป็นแนวทางหนึ่งในการช่วยลดปัญหาด้านสิ่งแวดล้อม และมีประโยชน์ทั้งในด้านการเกษตร เศรษฐกิจ สังคม และสิ่งแวดล้อม อีกทั้งสามารถตอบสนองความต้องการของผู้บริโภคอีกด้วย

การเปิดเผยการประดิษฐ์โดยสมบูรณ์

ปุ๋ยละลายช้าตามการประดิษฐ์นี้ ประกอบด้วย

1. ชั้นเคลือบพอลิไวนิลแอลกอฮอล์
2. ชั้นเคลือบไคโทซานเชื่อมขวาง
3. ชั้นเคลือบพอลิเมอร์ดูดซึมน้ำมาก

การเตรียมปุ๋ยละลายช้ามี 3 ขั้นตอน ดังนี้

<u>ขั้นตอนที่ 1 การเคลือบเม็ดปุ๋ยด้วยสารเคลือบพอลิไวนิลแอลกอฮอล์</u>

1. การเตรียมสารละลายพอลิไวนิลแอลกอฮอล์
   (1). พอลิไวนิลแอลกอฮอล์ร้อยละ 6-8 โดยน้ำหนักของสารเคลือบทั้งหมด
   (2). น้ำร้อยละ 92-94 โดยน้ำหนักของสารเคลือบทั้งหมด
2. การเคลือบพอลิไวนิลแอลกอฮอล์

เคลือบเม็ดปุ๋ย ด้วยสารละลายพอลิไวนิลแอลกอฮอล์ด้วยวิธีการจุ่ม หรือสเปรย์ พ่น ตากแห้งที่อุณหภูมิห้องในภาชนะบรรจุที่มีลักษณะเป็นบล็อกหลุมลึก

<u>ขั้นตอนที่ 2 การเคลือบเม็ดปุ๋ยที่เคลือบด้วยพอลิไวนิลแอลกอฮอล์แล้วด้วยสารเคลือบไคโทซานเชื่อมขวาง</u>

1. การเตรียมสารละลายไคโทซาน
   (1). ไคโทซานร้อยละ 1-3 โดยน้ำหนักของสารเคลือบทั้งหมด
   (2). กรดแอซิติกร้อยละ 1-3 โดยน้ำหนักของสารเคลือบทั้งหมด
   (3). น้ำร้อยละ 94-98 โดยน้ำหนักของสารเคลือบทั้งหมด
2. การเตรียมสารละลายเชื่อมขวาง
   (1). กลูทารัลดีไฮด์ร้อยละ 50 โดยปริมาตรของสารละลายทั้งหมด
   (2). น้ำร้อยละ 50 โดยปริมาตรของสารละลายทั้งหมด
3. การเคลือบชั้นไคโทซานเชื่อมขวาง

(1). เคลือบเม็ดปุ๋ยที่เคลือบด้วยพอลิไวนิลแอลกอฮอล์ที่ตากแห้งแล้ว ด้วยสารละลายไคโทซานด้วยวิธีการจุ่ม หรือสเปรย์ พ่น ตากแห้งที่อุณหภูมิห้อง

(2). นำสารละลายกลูทารัลดีไฮด์ใส่ในจานเพาะเชื้อขนาดเล็ก และนำไปใส่ในภาชนะแก้วปิด นำเม็ดปุ๋ยที่ผ่านการเคลือบในข้อ (1). ที่แห้งแล้ว มาวางบนตะแกรงอะลูมิเนียมที่วางอยู่ในภาชนะแก้วปิดเหนือสารละลายกลูทารัลดีไฮด์ เป็นเวลา 2-5 วัน นำมาอบให้แห้งในตู้อบที่อุณหภูมิ 50 องศาเซลเซียส

<u>ขั้นตอนที่ 3 การเตรียมเม็ดปุ๋ยละลายช้าที่มีพอลิเมอร์ดูดซึมน้ำมากเคลือบผิวชั้นนอก</u> ซึ่งชั้นเคลือบพอลิเมอร์ดูดซึมน้ำมากสังเคราะห์โดยใช้สารต่าง ๆ ดังนี้

(1). มอนอมอเมอร์ อะคริลิกแอซิด และ อะคริลาไมด์ ที่อัตราส่วนร้อยละ 97 ต่อ 3 โดยโมลของมอนอเมอร์

(2). แอมโมเนียมเปอร์ซัลเฟต (ammonium persulphate) ซึ่งเป็นสารริเริ่มปฏิกิริยาร้อยละ 0.03 – 0.24 โดยน้ำหนักของมอนอเมอร์

(3). *เอ็น,เอ็น,เอ็น',เอ็น'*-เททระเมทิลเอทิลีนไดแอมีน (*N,N,N',N'*-tetramethylethylene-diamine) ซึ่งเป็นสารริเริ่มปฏิกิริยาร่วมร้อยละ 0.03 – 4.16 โดยน้ำหนักของมอนอเมอร์

(4). *เอ็น,เอ็น*-เมทิลีนบิสอะคริลาไมด์ (*N,N*-methylenebisacrylamide) ซึ่งเป็นสารเชื่อมขวางสายโซ่พอลิเมอร์ ร้อยละ 0.005 – 0.04 โดยน้ำหนักของมอนอเมอร์

กรรมวิธีการเตรียมเม็ดปุ๋ยละลายช้าที่มีพอลิเมอร์ดูซึมน้ำมากเคลือบผิวชั้นนอก

(1). นำ Span 80 และไซโคลเฮกเซนอย่างละ 5-25 มิลลิลิตรใส่ลงในขวด 4 คอ กวนด้วยความเร็วรอบ 100-300 รอบต่อนาที จนสารละลายเป็นเนื้อเดียวกัน

(2). นำเม็ดปุ๋ยที่เคลือบชั้นในด้วยพอลิไวนิลแอลกอฮอล์และไคโทซาน 2 ชั้นที่ผ่านการเชื่อมขวางด้วยไอของสารละลายกลูทารัลดีไฮด์ มาใส่ในบีกเกอร์ที่มีสารละลายแอมโมเนียมเปอร์ซัลเฟต คน 2-5 นาที แล้วเทลงไปในสารละลายของ Span 80 และไซโคลเฮกเซน กวนด้วยความเร็วรอบ 100-300 รอบต่อนาที เป็นเวลา 5-15 นาที

(3). เติมน้ำลงในบีกเกอร์ที่มีอะคริลิกแอซิด อะคริลาไมด์ *เอ็น,เอ็น*–เมทิลีนบีสอะคริลาไมด์ คนให้เข้ากัน นำไปเทลงในขวด 4 คอ ที่มีสารละลายของ Span 80 และไซโคลเฮกเซน ซึ่งมีเม็ดปุ๋ยที่เคลือบชั้นในด้วยพอลิไวนิลแอลกอฮอล์และไคโทซานเชื่อมขวางอยู่ (ในข้อ (2).) ปรับอุณหภูมิเป็น 50-80 องศาเซลเซียส และให้เกิดปฏิกิริยาพอลิเมอไรเซชันเป็นเวลา 20-60 นาที นำไปกรองเอาสารละลายออก ได้ผลิตภัณฑ์เป็นเม็ดปุ๋ยละลายช้าที่มีไฮโดรเจลเคลือบบนพื้นผิวชั้นนอก

(4). การแยกมอนอเมอร์ที่ไม่เกิดปฏิกิริยาและการดึงน้ำออกจากชั้นเคลือบพอลิเมอร์ดูดซึมน้ำมาก ด้วยการเทเม็ดปุ๋ยละลายช้าที่สังเคราะห์ได้ลงในตัวทำละลายอินทรีย์ประเภทนอนโซลเวนต์ (non-solvent) เช่น เอทานอล หรือ แอซีโทน และกวนต่ออีกเป็นเวลา 10 – 20 นาที นำไปอบในตู้อบที่อุณหภูมิ 50 – 70 องศาเซลเซียส เป็นเวลา 24 ชั่วโมง หรือจนแห้งสนิท

ตัวอย่างต่อไปนี้แสดงให้เห็นเพิ่มเติมถึงการประดิษฐ์ แต่มิได้มีวัตถุประสงค์ที่จะจำกัดขอบเขตของการประดิษฐ์นี้แต่อย่างใด

ตัวอย่าง

<u>ขั้นตอนที่ 1 การเคลือบเม็ดปุ๋ยด้วยสารเคลือบพอลิไวนิลแอลกอฮอล์</u>

ชั่งพอลิไวนิลแอลกอฮอล์ 7 กรัม (น้ำหนักโมเลกุล 100,000 กรัม/โมล เกรดพาณิชย์ ที่มีระดับไฮโดรไลซีสร้อยละ 86-89 โดยโมล ระดับพอลิเมอไรเซชัน 2,400) ละลายในน้ำอุ่นที่มีอุณหภูมิ

50-70 องศาเซลเซียส ได้สารละลายปริมาตร 170 มิลลิลิตร นำสารละลายที่เตรียมได้ไปเคลือบเม็ดปุ๋ยด้วยวิธีการจุ่ม ตากในบล็อกหลุมให้แห้งที่อุณหภูมิห้อง

ขั้นตอนที่ 2 การเคลือบเม็ดปุ๋ยที่เคลือบด้วยพอลิไวนิลแอลกอฮอล์แล้วด้วยสารละลายเคลือบไคโทซานเชื่อมขวาง

ละลายไคโทซานน้ำหนักโมเลกุล 200,000 กรัม/โมล ที่มีร้อยละการกำจัดหมู่แอซิทิล 95 จำนวน 1 กรัม ในสารละลายกรดแอซิติก ความเข้มข้นร้อยละ 2 โดยปริมาตร ในขวดวัดปริมาตรขนาด 100 มิลลิลิตร นำสารละลายที่เตรียมได้ไปเคลือบเม็ดปุ๋ยที่เคลือบด้วยพอลิไวนิลแอลกอฮอล์ที่ตากแห้งแล้ว ด้วยวิธีการจุ่ม ตากในบล็อกหลุมให้แห้งที่อุณหภูมิห้อง

นำสารละลายกลูทารัลดีไฮด์ความเข้มข้นร้อยละ 50 โดยปริมาตร จำนวน 2 มิลลิลิตรใส่ในจานเพาะเชื้อขนาดเล็ก และนำไปใส่ในภาชนะแก้วปิดขนาด 29 ลิตร นำเม็ดปุ๋ยที่ผ่านการเคลือบด้วยพอลิไวนิลแอลกอฮอล์ที่แห้งแล้วมาเคลือบด้วยไคโทซานที่แห้งแล้ว มาวางบนตะแกรงอะลูมิเนียมที่วางอยู่เหนือสารละลายกลูทารัลดีไฮด์ เป็นเวลา 4 วัน นำมาอบให้แห้งในตู้อบ อุณหภูมิ 50 องศาเซลเซียส

หรือ นำสารละลายกลูทารัลดีไฮด์ ความเข้มข้นร้อยละ 50 โดยปริมาตร ใส่ในบีกเกอร์ นำเม็ดปุ๋ยที่ผ่านการเคลือบด้วยพอลิไวนิลแอลกอฮอล์ที่แห้งแล้วมาเคลือบด้วยไคโทซานที่แห้งแล้วมาจุ่มลงในสารละลายกลูทารัลดีไฮด์ เป็นเวลา 15-40 นาที นำมาอบให้แห้งในตู้อบ อุณหภูมิ 50 องศาเซลเซียส

ขั้นตอนที่ 3 การเตรียมเม็ดปุ๋ยละลายช้าที่มีพอลิเมอร์ดูซึมน้ำมากเคลือบผิวชั้นนอก

(1). นำ Span 80 และไซโคลเฮกเซนอย่างละ 15 มิลลิลิตรใส่ลงในขวด 4 คอ กวนด้วยความเร็วรอบ 250 รอบต่อนาที จนสารละลายเป็นเนื้อเดียวกัน

(2). นำเม็ดปุ๋ยที่เคลือบชั้นในด้วยพอลิไวนิลแอลกอฮอล์และไคโทซาน 2 ชั้นที่ผ่านการเชื่อมขวางด้วยไอของสารละลายกลูทารัลดีไฮด์ มาใส่ในบีกเกอร์ที่มีแอมโมเนียมเปอร์ซัลเฟต 0.08 กรัม คน 2-5 นาที แล้วเทลงไปในสารละลายของ Span 80 และไซโคลเฮกเซน กวนด้วยความเร็วรอบ 250 รอบต่อนาที เป็นเวลา 10 นาที

(3). เติมน้ำลงในบีกเกอร์ที่มีอะคริลิกแอซิด 18.5 กรัม อะคริลาไมด์ 0.6 กรัม *เอ็น,เอ็น*–เมทิลีนบีสอะคริลาไมด์ 0.004 กรัม คนให้เข้ากัน นำไปเทลงในขวด 4 คอ ที่มีสารละลายของ Span 80 และไซโคลเฮกเซน ซึ่งมีเม็ดปุ๋ยที่เคลือบชั้นในด้วยพอลิไวนิลแอลกอฮอล์และไคโทซานเชื่อมขวางอยู่ (ในข้อ (2).) ปรับอุณหภูมิเป็น 70 องศาเซลเซียส และให้เกิดปฏิกิริยาพอลิเมอไรเซชันเป็นเวลา 60 นาที นำไปกรองเอาสารละลายออก ได้ผลิตภัณฑ์เป็นเม็ดปุ๋ยละลายช้าที่มีไฮโดรเจลเคลือบบนพื้นผิวชั้นนอก

(4). เทเม็ดปุ๋ยละลายช้าที่สังเคราะห์ได้ลงในแอซีโทน และกวนต่ออีกเป็นเวลา 10 – 20 นาที นำไปอบในตู้อบที่อุณหภูมิ 50 องศาเซลเซียส เป็นเวลา 24 ชั่วโมง หรือจนแห้งสนิท

ปุ๋ยละลายช้าที่ผลิตได้ปลดปล่อยธาตุอาหารไนโตรเจน ฟอสฟอรัส และโพแทสเซียมร้อยละ 21.1±12, 18.3±3 และ 7.4±3.5 ในวันที่ 1 และ 83.9±18, 62.3±12และ 36.2±15 ในวันที่ 30 ของการแช่น้ำ ตามลำดับ

วิธีการในการประดิษฐ์ที่ดีที่สุด

เหมือนกับที่ได้กล่าวมาแล้วในหัวข้อการเปิดเผยการประดิษฐ์โดยสมบูรณ์

ข้อถือสิทธิ

1. ปุ๋ยละลายช้าซึ่งประกอบด้วย

(1). ชั้นเคลือบพอลิไวนิลแอลกอฮอล์

(2). ชั้นเคลือบไคโทซานเชื่อมขวาง

(3). ชั้นเคลือบพอลิเมอร์ดูดซึมน้ำมาก

2. ชั้นเคลือบพอลิไวนิลแอลกอฮอล์ตามข้อถือสิทธิที่ 1 ซึ่งสารละลายพอลิไวนิลแอลกอฮอล์ที่ใช้ประกอบด้วย

(1). พอลิไวนิลแอลกอฮอล์ร้อยละ 6-8 โดยน้ำหนักของสารเคลือบทั้งหมด

(2). น้ำร้อยละ 92-94 โดยน้ำหนักของสารเคลือบทั้งหมด

3. ชั้นเคลือบพอลิไวนิลแอลกอฮอล์ตามข้อถือสิทธิที่ 1 ซึ่งมีวิธีการเคลือบดังนี้

เคลือบเม็ดปุ๋ย ด้วยสารละลายพอลิไวนิลแอลกอฮอล์ตามข้อถือสิทธิที่ 2 ด้วยวิธีการจุ่มหรือสเปรย์พ่น ตากแห้งที่อุณหภูมิห้อง ในภาชนะบรรจุที่มีลักษณะเป็นบล็อกหลุมลึก

4. ชั้นเคลือบไคโทซานเชื่อมขวางตามข้อถือสิทธิที่ 1 ซึ่งสารละลายไคโทซานที่ใช้ประกอบด้วย

(1). ไคโทซานร้อยละ 1-3 โดยน้ำหนักของสารเคลือบทั้งหมด

(2). กรดแอซีติกร้อยละ 1-3 โดยน้ำหนักของสารเคลือบทั้งหมด

(3). น้ำร้อยละ 94-98 โดยน้ำหนักของสารเคลือบทั้งหมด

5. ชั้นเคลือบไคโทซานเชื่อมขวางตามข้อถือสิทธิที่ 1 ซึ่งสารละลายเชื่อมขวางที่ใช้ประกอบด้วย

(1). กลูทารัลดีไฮด์ร้อยละ 50 โดยปริมาตรของสารละลายทั้งหมด

(2). น้ำร้อยละ 50 โดยปริมาตรของสารละลายทั้งหมด

6. ชั้นเคลือบไคโทซานเชื่อมขวางตามข้อถือสิทธิที่ 1 ซึ่งมีวิธีการเคลือบดังนี้

เคลือบเม็ดปุ๋ยที่เคลือบด้วยพอลิไวนิลแอลกอฮอล์ที่ตากแห้งแล้ว ด้วยสารละลายไคโทซานตามข้อถือสิทธิที่ 4 ด้วยวิธีการจุ่มหรือสเปรย์พ่น ตากแห้งที่อุณหภูมิห้อง

7. ชั้นเคลือบไคโทซานเชื่อมขวางตามข้อถือสิทธิที่ 1 ซึ่งมีวิธีการเชื่อมขวางดังนี้

(1). นำสารละลายกลูทารัลดีไฮด์ตามข้อถือสิทธิที่ 5 ใส่ในจานเพาะเชื้อขนาดเล็ก และนำไปใส่ในภาชนะแก้วปิดขนาด นำเม็ดปุ๋ยที่ผ่านการเคลือบตามข้อถือสิทธิที่ 6 ที่แห้งแล้ว มาวางบนตระแกรงอะลูมิเนียมที่วางอยู่ในภาชนะแก้วปิดเหนือสารละลายกลูทารัลดีไฮด์ เป็นเวลา 2-5 วัน นำมาอบให้แห้งในตู้อบ อุณหภูมิ 50 องศาเซลเซียส

หรือ (2). นำสารละลายกลูทารัลดีไฮด์ตามข้อถือสิทธิที่ 5 ใส่ในบีกเกอร์ นำเม็ดปุ๋ยที่ผ่านการเคลือบตามข้อถือสิทธิที่ 6 ที่แห้งแล้ว มาจุ่มลงในสารละลายกลูทารัลดีไฮด์ เป็นเวลา 15-40 นาที นำมาอบให้แห้งในตู้อบ อุณหภูมิ 50 องศาเซลเซียส

8. ชั้นเคลือบพอลิเมอร์ดูดซึมน้ำมากตามข้อถือสิทธิที่ 1 ซึ่งประกอบด้วย

(1). มอนอมอเมอร์ อะคริลิกแอซิด และ อะคริลาไมด์ ที่อัตราส่วนร้อยละ 97 ต่อ 3 โดยโมลของมอนอเมอร์

(2). สารริเริ่มปฏิกิริยาร้อยละ 0.03 – 0.24 โดยน้ำหนักของมอนอเมอร์

(3). สารริเริ่มปฏิกิริยาร่วมร้อยละ 0.03 – 4.16 โดยน้ำหนักของมอนอเมอร์

(4). สารเชื่อมขวางสายโซ่พอลิเมอร์ ร้อยละ 0.005 – 0.04 โดยน้ำหนักของมอนอเมอร์

9. ชั้นเคลือบพอลิเมอร์ดูดซึมน้ำมากตามข้อถือสิทธิที่ 1 และ 8 ซึ่งสารริเริ่มปฏิกิริยาดังกล่าว คือ แอมโมเนียมเปอร์ซัลเฟต (ammonium persulphate)

10. ชั้นเคลือบพอลิเมอร์ดูดซึมน้ำมากตามข้อถือสิทธิที่ 1 และ 8 ซึ่งสารริเริ่มปฏิกิริยาร่วมดังกล่าว คือ *เอ็น,เอ็น,เอ็น',เอ็น'*-เททระเมทิลเอทิลีนไดแอมีน (*N,N,N',N'*-tetramethylethylene- diamine)

11. ชั้นเคลือบพอลิเมอร์ดูดซึมน้ำมากตามข้อถือสิทธิที่ 1 และ 8 ซึ่งสารเชื่อมขวางสายโซ่พอลิเมอร์ดังกล่าว คือ *เอ็น,เอ็น*-เมทิลีนบิสอะคริลาไมด์ (*N,N*-methylenebisacrylamide)

12. กรรมวิธีการผลิตปุ๋ยละลายช้าตามข้อถือสิทธิที่ 1 ถึง 11 ข้อใดข้อหนึ่ง ซึ่งประกอบด้วยขั้นตอนดังนี้ คือ

(1). นำ Span 80 และไซโคลเฮกเซนอย่างละ 5-25 มิลลิลิตรใส่ลงในขวด 4 คอ กวนด้วยความเร็วรอบ 100-300 รอบต่อนาที จนสารละลายเป็นเนื้อเดียวกัน

(2). นำเม็ดปุ๋ยที่เคลือบชั้นในด้วยพอลิไวนิลแอลกอฮอล์และไคโทซาน 2 ชั้นที่ผ่านการเชื่อมขวางด้วยไอของสารละลายกลูทารัลดีไฮด์ตามข้อถือสิทธิที่ 7 มาใส่ในบีกเกอร์ที่มีสารละลายแอมโมเนียมเปอร์ซัลเฟต คน 2-5 นาที แล้วเทลงไปในสารละลายของ Span 80 และไซโคลเฮกเซน กวนด้วยความเร็วรอบ 100-300 รอบต่อนาที เป็นเวลา 5-15 นาที

(3). เติมน้ำลงในบีกเกอร์ที่มีอะคริลิกแอซิด อะคริลาไมด์ *เอ็น,เอ็น*–เมทิลีนบีสอะคริลาไมด์ คนให้เข้ากัน นำไปเทลงในขวด 4 คอ ที่มีสารละลายของ Span 80 และไซโคลเฮกเซน ซึ่งมีเม็ดปุ๋ยที่เคลือบชั้นในด้วยพอลิไวนิลแอลกอฮอล์และไคโทซานเชื่อมขวางอยู่ (ในข้อ (2).) ปรับอุณหภูมิเป็น 50-80 องศาเซลเซียส และให้เกิดปฏิกิริยาพอลิเมอไรเซชันเป็นเวลา 20-60 นาที นำไปกรองเอาสารละลายออก ได้ผลิตภัณฑ์เป็นเม็ดปุ๋ยละลายช้าที่มีไฮโดรเจลเคลือบบนพื้นผิวชั้นนอก

(4). การแยกมอนอเมอร์ที่ไม่เกิดปฏิกิริยาและการดึงน้ำออกจากชั้นเคลือบพอลิเมอร์ดูดซึมน้ำมาก ด้วยการเทเม็ดปุ๋ยละลายช้าที่สังเคราะห์ได้ลงในตัวทำละลายอินทรีย์ประเภทนอนโซลเวนต์ (non-solvent) เช่น เอทานอล หรือ แอซีโทน และกวนต่ออีกเป็นเวลา 10 – 20 นาที นำไปอบในตู้อบที่อุณหภูมิ 50 – 70 องศาเซลเซียส เป็นเวลา 24 ชั่วโมง หรือจนแห้งสนิท

บทสรุปการประดิษฐ์

การประดิษฐ์นี้เกี่ยวข้องกับการผลิตปุ๋ยละลายช้า ซึ่งประกอบด้วย (1). ชั้นเคลือบพอลิไวนิลแอลกอฮอล์ (2). ชั้นเคลือบไคโทซานเชื่อมขวาง และ (3). ชั้นเคลือบพอลิเมอร์ดูดซึมน้ำมาก ซึ่งใช้อะคริลิกแอซิด และ อะคริลาไมด์เป็นมอนอเมอร์ แอมโมเนียมเปอร์ซัลเฟตเป็นสารริเริ่มปฏิกิริยา *เอ็น,เอ็น,เอ็น',เอ็น'*-เททระเมทิลเอทิลีนไดแอมีนเป็นสารริเริ่มปฏิกิริยาร่วม และ*เอ็น,เอ็น*-เมทิลีนบิสอะคริลาไมด์เป็นสารเชื่อมขวางสายโซ่พอลิเมอร์ น้ำเป็นตัวทำละลาย

freepatentsonline
all the inventions of mankind

SEARCH:
FIND
GO TO ADVANCED SEARCH

LOGIN:
Login
Create Free Account

HOME | SEARCH PATENTS | FOR INVENTORS | FOR ATTORNEYS | IP SERVICES | HELP

Synthesis of acrylamide-co-(itaconic acid) superabsorbent polymers and associated silica superabsorbent polymer composites.

Abstract: Superabsorbent polymers (SAPs) were synthesized from acrylamide (AM) and itaconic acid (IA) via a cross-linking polymerization. SAP composites (SAPCs) were formed by the incorporation of silica with three particle sizes into the polymerization to increase the gel strength of SAPs. Effects of AM: IA molar ratios, silica types and concentrations on water absorbency, absorbency rate and absorbency under loadings (AUL) of the composites were investigated. The highest water absorbency of the SAP is 233 [+ or -] 8 g [g.sup.-1] at an AM: IA molar ratio of 97:3 with absorbency of 149 [+ or -] 2 g [g.sup.-1] within 15 min. The highest AUL of the SAPC with 0.5%-2.0% w [w.sub.-1] silica is 13 g [g.sup.-1] by 1.93 x [10.sup.3] Pa load. A pseudo-second-order kinetics for water absorbency was found in both SAPs and in situ SAPCs. In situ SAPCs and the mechanically mixed SAPCs in vertical and horizontal direction yielded similar water absorbency values. POLYM. ENG. SCP., 51:764-775, 2011.

[C] 2011 Society of Plastics Engineers

Article Type: Report

Subject: Silica (Usage)
Polymeric composites (Production processes)
Polymeric composites (Composition)
Polymeric composites (Chemical properties)
Chemical synthesis (Methods)

Authors: Seetapan, Nispa
Srisithipantakul, Natsiri
Kiatkamjornwong, Suda

Pub Date: 04/01/2011

Publication: **Name**: Polymer Engineering and Science **Publisher**: Society of Plastics Engineers, Inc. **Audience**: Academic **Format**: Magazine/Journal **Subject**: Engineering and manufacturing industries; Science and technology **Copyright**: COPYRIGHT 2011 Society of Plastics Engineers, Inc.
ISSN: 0032-3888

Issue: **Date**: April, 2011 **Source Volume**: 51 **Source Issue**: 4

Topic: **Event Code**: 320 Manufacturing processes

Product: **Product Code**: 1443000 Silica & Silica Sand; 2819532 Silicon Dioxide **NAICS Code**: 212322 Industrial Sand Mining; 325188 All Other Basic Inorganic Chemical Manufacturing **SIC Code**: 1446 Industrial sand

Geographic: **Geographic Scope**: Thailand **Geographic Code**: 9THAI Thailand

Accession Number: 253927194

Full Text: INTRODUCTION

Superabsorbent polymers (SAPs) and their associated SAP composites (SAPCs) have drawn much interest since the early 1970s. During that period, Fanta et al. investigated graft copolymerization of vinyl acrylate or acrylonitrile onto starch and other polysaccharides, which yielded products that could absorb from several hundred to several thousand times their own weight in water and also had a high water holding capacity under pressure, also known as absorbency under load (AUL) [1], and thus the name "superabsorbent polymer" was adopted. Research and development into SAPs have focused on their extraordinarily high-water absorbency and applications. Indeed, over 80% of SAPs have found extensive commercial applications as sorbents in personal care products, such as infant diapers [2], feminine hygiene products, and incontinence products [3]. Not only that, but also many new applications have already been investigated through such active research and development, Leading to the successful application of SAPs in new fields, such as matrices for enzyme immobilization [4, 5], bio-sorbents in preparative chromatography [6], materials for agricultural mulches and fertilizers [7, 8], matrices for controlled release devices [9], drug delivery [10], bioactive scaffolds for bone engineering [11], bio-separation [12], moisture retention in soil [13, 14], SAPCs as a sealing material [15], debris flow control, artificial snow [16, 17], a gel actuator [18], and fire fighting [19]. The desired features of superabsorbents are a high swelling capacity, high swelling rate, and a greater strength of the swollen gel. The majority of the reported superabsorbents comprise of only the first mentioned feature, i.e., a high absorbency, but there are few studies concerning improvements of the absorbency rate and gel strength. Absorbent particles are conventionally strengthened through surface crosslinking [20]. Traditionally, an inorganic component is used as a filling material for the purpose of improving the material properties and reducing the product cost. The addition of inorganic powder (usually <5% w [w.sup.-1]) to a SAP provides a method for increasing the gel strength [21-23]. The utility of the inorganic nanoparticles as additives to enhance the polymer performance has been increased. Such inorganic materials for the preparation of SAPCs can be laponite [21], kaolin [24], montmorillonite [22, 25], attapulgite [26-28], mica [23, 29], bentonite [30], sercite [31], or rectorite [32] to form the layered silicate structures.

A novel SAPC based upon starch-g-AM/mineral powder, with a water absorbency of about 4000 times its own weight, was synthesized by a graft-copolymerization reaction of AM, potato starch, and mineral ultrafine powder, followed by hydrolysis with sodium hydroxide [33]. The SAPCs doped with kaolinite powder possessed a higher water absorbency than those doped with bentonite or sercite powder, since the kaolinite powder can moderately disperse in the water and crosslink with the AM and starch. Moreover, the collaborative absorbent effect of--CO[NH.sub.2], --COONa, and--COOH groups has been found to be superior to that of a single--CO[NH.sub.2], --COONa, or--COOH group. The ultrafine mineral powder as a crosslinking point plays an important role in the formation of a network structure in SAPCs. Incorporation of kaolin into hydrogel SAPCs caused a reduced equilibrium swelling and swelling rate to as low as 17-31% and 19-29% (w [w.sup.-1]), respectively, but resulted in an enhanced gel strength by as much as 21-35% above that of the corresponding SAP as a control [34]. Grafted sodium carboxymethylcllulose (CMC) - silica gel SAPC with a water absorbency capacity as high as 4000 g [g.sup.-1] in distilled water has been reported [35]. Super porous hydrogel composites with the inclusion of modified cellulose gum or an internally cross-linked form of CMC typically gave a significant improvement in the properties of super porous hydrogels, such as a high mechanical strength and a high swelling ratio. Indeed, the inclusion of a suitable composite material typically increases the physical crosslinking density and so provides a high strength and prevents the polymer chains from collapsing during air drying [36]. The in situ sol-gel method used to prepare bioactive hydrogels [11, 37, 38] is considered to be quite expensive for industrial use. Therefore, the use of amorphous silica powder to form the non-layered silica SAPCs is a cheaper way for industries to manufacture personal care products. On the other hand, the mechanical mixing of

layered silica SAPCs is a cheaper way for industries to manufacture personal care products. On the other hand, the mechanical mixing of SAP with silicate powder can be another economical way to prepare SAPCs.

In this research, poly[acrylamide-co-(itaconic acid)]/silica composites as potential SAPCs were made by in situ solution polymerization with three different sizes of silica. The SAPCs with a high water absorbency rate and capacities were compared with the SAPCs prepared by mechanical mixing between the P(AM-IA) SAP and silica powder of the same composition.

EXPERIMENTAL PROCEDURES

Materials and Methods

Acrylamide (AM, Siam Chemicals, Bangkok, Thailand), itaconic acid (IA, Merck, Hohenbrunn, Germany), N, N'-methylenebisacrylamide (N-MBA, Fluka, Buchs, Switzerland), ammonium persulfate (APS, Merck, Hohenbrunn, Germany), N,N,N',N'-tetramethylethylenediamine (TEMED, Fluka, Buchs, Switzerland), and silica (Si[O.sub.2], J.J-Degussa-Huts, Thailand) were used. The three types of silica used in this research, and their properties, are shown in Table 1 and their IR spectra are given in Fig. 1.

[FIGURE 1 OMITTED]

Polymerization

A 100-[cm.sup.3] mixture of AM: IA of 100:0, 99:1, 98:2, and 97:3 (by % molar ratios) was supplemented with 0.5% w [w.sup.-1] N-MBA crosslinker, the initiator couple of APS (1.0% w [w.sup.-1]) and TEMED (0.20 [cm.sup.3]), and then poured into a 500-[cm.sup.3] four-necked round-bottomed flask equipped with a mechanical stirrer (Ika-Ruhrwerke RW20, Staufen, Germany), a spiral condenser and a thermometer. The polymerization reaction was allowed to proceed at 45[degrees]C in a water bath (WBU 45 Memmert, Schwabach, West Germany) under a nitrogen gas atmosphere for 30 min with stirring at 250 rpm The resulting polymer was dehydrated with methanol, cut into small pieces of half a centimeter in diameter, dried in a vacuum oven (Hotpack, USA) for 24 h to a constant weight, and then milled. The obtained copolymer powders were then investigated for their water absorbency capacity. The monomer AM: IA molar ratio from which the synthesized P(AM-IA) copolymer possessed the highest water absorbency was then selected to prepare the P(AM-IA)/silica SAPC.

To prepare the SAPCs, three types of silica, namely Aerosil 90, Aerosil 200, and Aerosil 300, each at four different concentrations of 0.1, 0.2, 0.5, and 2% w [w.sup.-1], were added in situ with the other ingredients in the polymerization process as shown in Table 2.

Characterization of the Copolymers

Identification of the Functional Groups of the Synthesized Copolymers. The functional groups of the copolymers were investigated by Fourier transform infrared spectroscopy (FTTR model Nicolet Impact 410) using a KBr pellet method with 32 scans and 4 [cm.sup.-1] resolution. The interface software (Nicolet Omnic) was connected to the Nicolet FTIR in a data acquisition system.

Surface Morphology of the Synthesized Copolymers. The surface morphology of the copolymers was investigated using scanning electron microscopy (SEM, model JSM-6400, Japan) without cross-sectioning. The thickness of gold coated on the copolymer was 25 nm, and SEM was operated with a 15 kV accelerating voltage. The elemental analyses of the SEM micrographs were investigated by energy dispersive X-ray spectrometry (EDXS).

Equilibrium Water Absorbency

In deionized Water. Deionized water (150 g) was added to 0.1 g of the dry copolymer (A) in a 250 [cm.sup.3] glass beaker covered with a lid and it was allowed to swell for 30 min. The completely swollen copolymer gel was filtered through 100-mesh aluminum sieve screen for 3 h and the remaining swollen copolymer gel was weighed (B). The water absorbency (g [g.sup.-1] of the dry copolymer) was calculated by Eq. 1 shown below:

Water absorbency of copolymer (g[g.sup.-1]) = (B - A)/A (1)

Absorbency Under Load (AUL). Deionized water (25 [cm.sup.3]) was placed in a Petri dish. A 0.16 g (A) aliquot of the dry copolymer was carefully scattered onto the filter screen of the test device (a flexiglass cylinder of 26 mm diameter, 35 mm height, and a 100 mesh stainless steel cloth in the bottom). A piston assembly, including an additional weight to achieve a load of 0.28 psi (1.93 X [10.sup.3] Pa) was placed on the top of the dry copolymer. After weighing the assembly device (B), it was placed on the Petri dish, and absorbency was allowed to proceed for 1 h after which time the entire device was reweighed (C). Similar experiments were carried out for a load of 0.70 psi (4.83 X [10.sup.3] Pa). The AUL (g [g.sub.-1]) was calculated by Eq. 2:

AUL(g[g.sup.-1]) = (C - B)/A (2)

Swelling Kinetics of the SAPs and SAPCs. Deionized water of 1000 [cm.sup.3] was placed in a 2-[dm.sup.3] beaker. The dry copolymer of 0.1 g was sealed in a teabag and placed in a beaker where it was allowed to swell for 15 min. The soaked teabag was removed from the beaker and the swollen copolymer was weighed after excess water on the bag was blotted out on filter paper. Similar experiments were carried out but for gel swelling times of 15, 45, 105, 225, 1125, and 1605 min. Schott's equation [39], as shown in Eq. 3, is used to describe a well-known pseudo second-order absorbency kinetics equation and was used in these studies to test for pseudo second-order absorbency kinetics of water absorbency by the SAPs and SAPCs. Since:

t/[Q.sub.t] = t/[Q.sub.[infinity]] + 1/k[Q.sub.[infinity].sup.2], (3)

where [Q.sub.t] and [Q.sub.[varies]] are the absorbencies at time t and infinite time for full swelling and k is the absorbency coefficient which describes the rate constant of swelling, then by plotting t/[Q.sub.t] vs. t, [Q.sub.[varies]] and k can be calculated.

The Level of Retained Silica in the P(AM-IA) Gel. A 1.00 g (A) aliquot of the dry copolymer was placed in a 100 [cm.sub.3] porcelain crucible on a hot plate and heated at 100[degrees]C for 45 min before being placed in a muffle furnace (Vulcan 3-550 PD) at 600[degrees]C for 90 min until all the powder became white. The crucible was removed from the furnace and cool. The white powder was weighed (B), and the amount of retained silica in the gel was calculated by Eq. 4:

Silica retained in the gel = (B - A)/A (4)

SAPCs by Mechanical Mixing. A 0.2 g aliquot of the dried P(AM-IA) copolymer powder having a mesh size of not larger than 100 and the specified amount of silica were mixed in the bottle by a home-made mixing rotator with a controllable speed at 600 rpm for 30 min for horizontal mixing (HM). For the vertical mixing (VM), the mixture was shaken with a speed of 100 rpm in a rolling type mixer (MS1 Mini shaker, IKA-Work, Inc, Wilmington). After mixing (either HM or VM), the sample was transferred for the water absorbency experiment. The types of silica and copolymer used for the mixing are shown in Table 2.

RESULTS AND DISCUSSION

The assignments of the FTIR spectra of the three silicas are shown in Fig. 1. All three types of silica (Aerosil 90, Aerosil 200, and Aerosil 300) gave the similar IR peaks with a medium OH stretching peak at 3444-3441 c[m.sup.-1], a weak C=O stretching peak at 1630 [cm.sup.-1], a strong peak at 1112 - 1103 [cm.sup.-1] for Si--O--Si bending, a medium peak at 811-810 [cm.sup.-1] for Si--OH and a sharp peak at 474 - 170 [cm.sup.-1] for Si--O--Si bending. Table 1 shows that their BET surface areas and average primary particle sizes are significantly different.

The peaks of P(AM) (Fig. 2a), P(AM)/Aerosil 90 silica SAPC (Fig. 2b, P(AM-IA) (Fig. 3a) and P(AM-IA)/Aerosil 90 silica SAPC (Fig. 3b) indicated that silica was attached onto both the AM and IA moieties via covalent bonding. All copolymers showed the strong peak at 3450 - 3440 c [m.sup.-1] for the N–H stretching overlapping with the OH–stretching, the medium peak at 2939 - 2936 [cm.sup.-1] for the C–H stretching, the medium peak at about 1650 [cm.sup.-1] of the C=O stretching for amide I, the peak at 1415 - 1452 [cm.sup.-1] for the C–H bending of amide, and the medium peak at 1112-1120 c[m.sup.-1] for the N–H (amide II) bending. Besides the aforementioned peaks, the Si–O–Si sharp peak of Aerosil 90 silica at 470 [cm.sup.-1] was shifted to 448 [cm.sup.-1] in the P(AM)/Aerosil 90 silica (Fig. 2b) and to 447 [cm.sup.-1] in the P(AM-TA)/Aerosil 90 silica SAPCs (Fig. 3b). Other SAPCs with either Aerosil 200 or Aerosil 300 silica addition demonstrated the similar spectra (not shown here) as the Aerosil 90 silica-co-polymer composites.

[FIGURE 2 OMITTED]

[FIGURE 3 OMITTED]

The existence of silica particles in the SAPCs was confirmed by SEM micrographs (see Fig. 4). PAM and P(AM-IA) copolymers have a rough morphology (Fig. 4a and b), while the micrograph of P(AM-IA)/Aerosil 90 silica composite shows a similar morphology but with large agglomerates of white particles of silica trapped on the rough surface of polymer matrix (Fig. 4c). EDXS analysis of P(AM-IA) and P(AM-IA)/Aerosil 90 silica composite (Fig. 4d and e) indicates that besides common elements such as carbon and oxygen found in both copolymers, the presence of silicon element was also detected in the prepared copolymer composite at the energy peak at 1.75 keV. Therefore, data from SEM-EDXS confirmed that the silica particles were retained within the SAPCs.

[FIGURE 4 OMITTED]

Effect of I laconic Acid Concentration

The Water Absorbency of the Synthesized Copolymer. The water absorbency of the copolymers synthesized in situ by solution polymerization with three concentrations (0, 1, 2, and 3% molar ratio) of IA is shown in Table 3. Because the reactivity ratios [r.sub.1] and [r.sub.2] values for AM/N-MBA are 0.64 and 1.77, respectively, the PAM was thus rigid due to more effective crosslinking density to cause the low water absorbency [40]. The effective crosslinking density is defined as the number of moles of elastically effective crosslinks per unit volume of polymer. Therefore, an increase of hydrophilic monomer (IA) in the SAPs enhances the swelling capability and, hence, decreases the effective crosslinking density. This statement has been investigated by several researches. Our previous investigation, for example, found that SAPs with high water absorbency were accompanied by low gel strength and the calculated low value of effective cross-linking density [41]. The water absorbency increases with increasing concentrations of the hydrophilic and ionic functional groups of IA, in good agreement with the previous findings by Uyanik and Erbil [42] and Pulat and Eksi [43], who reported that increasing IA concentrations in copolymer structures decreases the effective crosslinking densities of the polymer networks. As IA cannot form superabsorbent polymers by itself, an excessive amount of IA in the monomer mixture made it more difficult to form a copolymer gel. Thus, here we could show the results of IA concentrations up to only 3% (molar ratio). The degree of swelling of the synthesized P(AM-IA) copolymers mainly depends on the repulsive forces between the hydrophilic pendants (amide and carboxylic groups) in their structures. For AM/IA copolymer, IA was reported to be more reactive than AM ([r.sub.IA] > [r.sub.AM]) [42]. Therefore, IA molecules are used up via a crosslinking reaction with N-MBA before AM monomer, even if AM feed concentrations are higher. In the present case, the structure of the copolymer should contain more units of the uncrosslinked PAM moiety than crosslinked IA units owing to a higher AM concentration and higher reactivity of N-MBA. The synthesized copolymer must have an optimum ratio of AM-to-IA to balance hydrophilic or ionic functional groups and chain flexibility to produce the copolymer with the highest water absorbency capacity. The copolymer synthesized by an AM: IA molar ratio of 97:3 can absorb deionized water to as high as 233 [+ or -] 8 g [g.sup.-1] (Table 3). However, the AUL values were nearly constant at 11 - 12 g [g.sup.-1] and 12 - 14 g [g.sup.-1] for a load of 0.28 psi (1.93 X 10 (3) Pa) and 0.70 psi (4.83 X 10 (3) Pa), respectively, regardless of the IA concentration. Thus, the AUL was essentially constant regardless of the loads and the concentration of the hydrophilic or ionic functional groups and chain flexibility.

The AUL is a measure of the ability of an SAP to absorb a liquid while the SAP is under an application of load or restraining force. The value of AUL is altered proportionally to the strength of the swollen gel, thus, AUL is often reported in the technical data sheets and patent articles in order to quantify the gel strength suitable for a particular application such as diapers for baby and adult [44, 45].

In free swelling (without an application of external load), the presence of ionic charges along polymer chains significantly increases the swelling of SAPs due to an increase in electrostatic repulsive forces between charged sites on the carboxylate anions (in case of IA) upon their complete dissociation and thus leads to a more extended configuration, as seen in Table 3 that the copolymer system of 3% mole of IA yielded the water absorbency of around 233 g [g.sup.-1], while the water absorbency of the P(AM) SAP was about 51 g [g.sup.-1].

However, under an application of load, the swelling ability of SAP is decreased with respect to the load-free absorbency (see Table 3) as a result of the restricted mobility of polymer chain. Therefore, the diffusion of a liquid into the SAP particle is counterbalanced by the external pressure applied on the SAP particles. As a result, our data imply that the extended conformations of the main chain, especially in SAP containing ionic charges, are prohibited under an application of load. Therefore, the observed AUL value was insignificantly altered irrespective of the applied loads and the concentration of ionic groups within the SAP.

The Swelling Kinetics of the Synthesized Copolymers. In practical applications, not only is a higher absorbency capacity required for the absorbent, but also a high swelling rate. The swelling kinetics of hydrogels have been characterized as occurring in two stages; an initial first order (Fickian diffusion model) stage followed by a later second order (Schott model) stage. In the initial stage, the swelling of hydrogel in water is governed by a first order diffusion process which involves migration of water to fill the spaces between polymer chains. The Fick model is thus valid for the initial swell stage where the fractional swelling value ([Q.sub.1]/[Q.sub.[varies]]) is less than or equal to 0.6 [46]. The Schott model is used for longer swelling times when the density of the hydrogel has increased. At this second order swelling, the swelling kinetic is not controlled by diffusion, but by the relaxation of the polymer chains [39, 47]. The evaluated swelling kinetics of the P(AM-IA) copolymer, synthesized by in situ solution polymerization of various concentrations (0, 1, 2, and 3% molar ratios) of IA revealed that the higher the IA concentration, the larger the water absorbency became (Fig. 5a). In other words, the P(AM) SAP gave the lowest water absorbency and the 97:3 (molar ratio) P(AM-IA) SAP gave the highest water absorbency (233 [+ or -] 8 g [g.sup.-1]) due to the hydrophilic nature of the carboxylic acid of the IA monomer. The 97:3 (molar ratio) P(AM-IA) SAP could absorb deionized water up to 149 [+ or -] 2 g [g.sup.-1] of the dry copolymer within 15 min and reached the highest absorbency within 200 min. A plot of t/[Q.sub.t] vs. t reveals that all the absorbency data almost perfectly fit in a linear line with small positive intercepts and high [r.sup.2] values, in support of pseudo-second order kinetics (Fig. 5b). The fitting equation and the [r.sup.2] value are reported in Table 4. Indeed, the experimentally determined water absorbency values fit the theoretically determined values from the Schott model (Eq. 3) supporting pseudo-second order kinetics for the swelling behavior of the P(AM-IA) SAPs (Table 4). In comparison to the P(AM) SAP, the presence of IA in the hydrogel lowered the swelling rate constant (k), although the k value at a 3% molar ratio of IA was higher than that for 1 and 2% IA but still less than that seen in the P(AM) SAP (Table 4). Likewise, the first order kinetics model also tested (not shown here) does not give a good straight line but gives low regression values.

[FIGURE 5 OMITTED]

Effect of Silica

Type and Concentration of Silica on the Water Absorbency of SAPCs. The incorporation of each type of silica (Aerosil 90, 200, and 300) into the 97:3 (molar ratio) P(AM-IA) copolymer to form P(AM-IA)/silica composites reduced the water absorbency of the SAPC in a dose dependent manner, reaching a level of some 15-20% lower at 2% w [w.sup.-1] silica than that seen without silica, 0% (see Fig. 6). In addition, there was a dependency upon the type of silica, with the larger silica particles yielding a SAPC with lower water absorbency at the same nominal silica concentration. For example, compared to that at 0% silica, the water absorbency was decreased from 233 [+ or -] 8 g [g.sup.-1] to 199 [+ or -] 4, 193 [+ or -] 6, and 188 [+ or -] 1 g [g.sup.-1], a reduction of 15, 17, and 20%, with the incorporation of Aerosil 90, Aerosil 200, and Aerosil 300 at 2%: w [w.sup.-l], respectively. This is to be expected since water absorbency is related to the higher hydrophilic properties of the hydrophilic chain and the silica particle size, as shown in Table 1, the BET surface areas of the three silicas differ significantly. As to the dose-dependent effect, the silica particles present in SAPs act as crosslinking points [5], and so more crosslinking points are available with the increased

addition of Si[O.sub.2] in addition to the W-MBA crosslinking agent. Although more hydrogen bonding takes place between the hydrophilic silanol group on the silica, water absorbency through this bonding may increase the rigidity of the chain. Since the surface physical-chemical properties are the same, and so do not differentially affect the water absorbency of the SAPCs, their surface areas and average primary particle size are, therefore, the important attributes controlling the extent of water absorbency.

[FIGURE 6 OMITTED]

Type of Silica and Silica Content on the Swelling Kinetics. The swelling kinetics of the SAPCs, synthesized from a 97:3 molar ratio of AM:IA with in situ incorporation of 2.0% w [w.sup.-l] of silica were essentially the same for all three types of silica (Fig. 7a) and showed pseudo second-order absorbency kinetics regardless of the presence of silica and its concentration (Fig. 7b). The high quality of linear curve fitting is represented by the value of [r.sup.2] equal to 1 (Table 5). Again the experimental water absorbency values were very close to those derived theoretically from the Schott model of pseudo second-order kinetics (Table 5). In the presence of 2.0% w [w.sup.-1] silica, the resulting 97:3 molar ratio P(AM-IA)/silica SAPC could absorb water at the very similar values of 121 [+ or -] 8, 119 [+ or -] 8, and 118 [+ or -] 8 g [g.sup.-1] of the dry polymer within 15 min for Aerosil 90, Aerosil 200, and Aerosil 300, respectively. The dependence of swelling time on the equilibrium swelling rate arises because the mass of liquid absorbed during the swelling, so that the rate increases until constant at the absorbency time longer than 300 min. The water swelling rate depends on the equilibrium swelling capacity of the polymer. The swelling absorbency values of the 97:3 P(AM-IA)/silica SAPCs with Aerosil 90, Aerosil 200, and Aerosil 300 are not much different to each other but decreased with increasing concentrations of silica (Table 6). As mentioned before, the line silica particles act as additional crosslinking junctions and so the crosslink density increased with increasing silica levels, leading to a decreased swelling.

[FIGURE 7 OMITTED]

The swelling kinetics of the P(AM-IA)/silica SAPCs, synthesized from a 97:3 molar ratio of AM: IA with four contents of Aerosil 90, are shown in Fig. 8a, and replotted as t/[Q.sub.t] vs. t in Fig. 8b. As mentioned earlier, all the t/[Q.sub.t] vs. t plots are linear and fit well with the calculated values using the Schott's pseudo second-order absorbency kinetics model (Table 7). The incorporation of silica causes a dose-dependent decrease in the water absorbency, but the rate constant of swelling (k) was accelerated by increasing silica contents, due to the increasing level of crosslinking density within the SAPCs.

[FIGURE 8 OMITTED]

In view of the second-order absorbency kinetics observed in a later time course (Figs. 5, 7, and 8), one can describe the absorbency behavior as follows. When the P(AM-IA) SAP or P(AM-IA)/silica SAPC contacts with the excess amount of water, diffusion takes place which is governed by a first-order process on a short time scale (Fick model), and then subsequently the rate of swelling at long swelling times is not governed by the diffusion, but rather is mainly controlled by stress relaxation of the amorphous regions of the polymer network which follows a pseudo second-order kinetics control (Scott model).

The Effect of the Type of Silica and its Content on the Water AUL of the Synthesized Copolymers. The water AUL (1.93 X [10.sup.3] Pa and 4.83 x [10.sup.3] Pa) of the P(AM-IA)/silica SAPCs, synthesized from a 97:3 molar ratio of AM: IA in the presence of the three silica types (Aerosol 90, 200, and 300) and four contents (0.1, 0.2, 0.5, and 2% w [w.sup.-1]) of silica is shown in Table 6. The AULs at 1.93 X [10.sup.3] Pa and 4.83 x [10.sup.3] Pa for the 97:3 P(AM-IA) SAP were very similar at 12 g [g.sup.-1] 11 g [g.sup.-1] and, respectively (Table 3), and were not significantly changed by the addition of silica, type or concentration, with all tested P(AM-IA)/silica SAPCs having an AUL of 11-13 g [g.sup.-1] at both evaluated loads.

In general, silica has been used to help improve the gel strength so as to provide a higher AUL to swollen gels with an otherwise reduced water absorbency. The swelling in the present work was observed to decrease slightly with increasing contents of silica in the P(AM-IA)/silica composite. The additional amounts of silica probably act as nonreactive filler dispersed in the network. It may be attributed to the fact that fine silica particles act as additional junctions. Therefore, silica imposes effects on gel strength or AUL improvement, in that the higher the silica concentration, the higher the gel strength becomes.

Besides the crosslinking reaction, these characteristics may be attributed to the fact that the fine silica particles act as additional junctions for grafting reaction on their surface to increase the SAPC density. Increasing silica contents led to increased gel strength, although the water absorbency value of the SAPCs with different silica types (particle sizes) is not different at all. Increasing the water absorbency was achieved by a lower crosslinking reaction, AUL decreased because the swollen particles easily deformed and clumped together under load, liquid supplying voids or spaces were closed. If this is the case, then to increase the AUL, a second polymerization on the surface with a small amount of additional crosslinking density may be needed.

The Retained Silica in the Gel

The actual amount of silica that is incorporated into the 97:3 P(AM-IA)/silica SAPC was evaluated by the difference in silica contents between those in the initial pre-polymerization and the final products after the polymerization (Table 8). The amounts of silica retained in the SAPCs are lower than the added amounts of silica added, i.e., the whole amount of silica is not incorporated into the polymer network, but rather only some 86-95% is retained. This is not linearly dependent upon the silica content in the polymerization reaction and, although their average primary particle sizes are significantly different, the interaction between SAPCs and the three different silica types cannot be differentiated. The retention of silica within the SAPCs is in agreement with the IR spectra (see Fig. 3) and the SEM-EDXS data (see Fig. 4).

Effect of Mechanical Mixing on Water Absorbency of SAPCs'

Since it is possible to mix or blend the SAP with the silica particles as an organic and inorganic composite, it is of interest if the resulting composite will perform similarly to the in situ polymerized SAPCs. That is, the performance of the silica-filled SAPC can match that the in situ silica SAPC arises because the silica can leak out from the composite. Then, its strength might be somewhat lower compared to the in situ polymerized SAPCs.

Effect of the Mixing Method

The VM motion uses an eccentric motion in the vertical direction with a constant speed of 100 rpm while the HM method uses a constant rotation speed of 600 rpm in the horizontal direction. To this are added the SAP particles with silica powder, and dispersion of the components in the cylindrical bottle is accomplished by rotating the bottle and its contents about the horizontal axis of the cylindrical bottle at a rate sufficient to lift the silica particles to one side and then cause them to roll, slide and tumble or cascade to the lower side. At this speed, the rotation movement is the cascade manner. When the HM rotation of SAP and silica particles in the cylindrical bottle takes place, some parts of the particles contact with the cylindrical wall in the diameter direction of the roller movement, contact sites of the SAPs for silica particles decrease when the movement of the cylindrical bottle is continued. In the VM motion, both the SAPs and silica particles move up and down along the length of the cylindrical bottle. Therefore, the contact sites of the SAPs and silica particles in the VM direction are higher than the HM motion leading to the larger probability of silica particles in adhering to the SAP surface. The adsorption of silica is strengthened by hydrogen bonding between hydroxyl groups on silica surface and carboxylic and amine groups on P(AM-IA) SAP. Based on the mixing mechanism and speed, the Aerosil 300 having larger surface area (BET surface area of 300 [+ or -] 30 [m.sup.2] [g.sup.-1] and 7 nm particle size) adsorbed on SAP particles more than the Aerosil 90 silica did (BET surface area of 90 [+ or -] 15 [m.sup.2] [g.sup.-1] and 20 nm particle size). As a result Aerosil 300-SAPC should provide the lower water absorbency since the adsorbed silica might interrupt the diffusion or the binding of water into the SAP particle. However, the results in Table 9 indicated that both the mixing direction and types of the investigated silica particles did not significantly alter the water absorbency of the SAPC comparative to the in situ SAPC polymerization.

When the mixture of SAPs and silica particles is mixed by an eccentric rotation (VM), they move up and down along the length of the cylindrical bottle. Therefore, the mixing force is controlled by a centrifugal acceleration, [alpha], as shown in Eq. 5 [48, 49]:

[alpha] = ([r.sub.b] + [r.sub.c])[[omega].sup.2] (5)

where [r.sub.b] is the radius of the glass bottle, [r.sub.e] is the eccentric radius, and [omega] is the rotation angular velocity. According to the theory of the elasticity contact between spheres [48], the contact area S increases as indicated in Eq. 6:

S[alpha][F.sup.2/3] (6)

where F is the force worked on the spheres. The Aerosil 300 silica has a stronger force to hold silica particles on the surface of the SAP due to its larger surface area and smaller size. Thus, the SAPs and Aerosil 300 can physically interact, aggregate, or agglomerate together more strongly than those of Aerosil 90.

It is necessary to mention that SAPs at various AM:IA ratios without silica were also mixed horizontally or vertically as for a control purpose at the same condition for the SAPCs. The mixing force given to SAPs actually helps only disperse the particle agglomeration and imposes a slight effect on water absorbency as shown in Table 9. Regardless of the dependence of the mixing time on the SAPs-silica contact, the HM rotation rate is higher than the VM rotation and, therefore, the force between the SAP and silica particles by HM rotation increases rapidly. The mixing force between the SAP and silica particles can be divided into three regions: elastic, plastic and destructive. In the low mixing force region, the contact between SAPs and silica particles is supposed to be elastic, in good approximation, and after the mixing, the shapes of SAPs and silica do not change. Over the elastic force range, some plastic region can be observed, and if the force becomes greater than plastic region, SAP destruction may arise.

The results in Table 9 indicate that all the SAPs having various silica types and contents mixed under VM or HM motions are linear and it can be concluded that their mixing forces are elastic because the water absorbency values are in a linear trend. The extent of water absorbency of the in situ SAPCs containing a 97:3 molar AM: IA ratio with various silica contents used in comparison with the mechanical mixing SAPCs at the same monomer ratio are similar with only a small deviation in most cases.

The Role of Silica in SAPCs

The preparation of SAPs needs to have a crosslinking agent to control the gel properties. However, when a crosslinking agent, such as N-MBA, is used, the water absorbency decreased. To control the desirable level of water absorbency through the chemical crosslinking reaction, a well-designed recipe and reaction condition must be strictly controlled. Inorganic particulate filler with a hydrophilic surface, such as silica, is normally recommended for incorporation during the polymerization of SAPs as another crosslinking site or grafting site for the in situ prepared SAPCs or mechanical mixing of SAPs and silica to give SAPCs. As shown above, the silica particles can be embedded in the polymer to give a better overall strength. Moreover, the presence of silica in the SAPCs reduces the load-free water absorbency very slightly. Data from the water AUL, however, were not significantly different between the SAP and SAPCs due to the aforementioned discussion. When the SAPCs are assembled as a baby diaper or famine napkins, the absorbed fluid is still held within the superabsorbent network and silica also helps the polymer to flow easily from the sack and can improve fluid permeability of the hydrated SAPs. In this work, we tuned the combination between the chemical crosslinking reaction by N-MBA and the minimum silica incorporation to obtain the desirable water absorbency behavior.

CONCLUSIONS

The P(AM-IA) SAPs prepared by in situ solution polymerization produced a high level of water absorbency and a much lower AUL water absorbency. Increasing the IA concentration in the SAPs significantly increased the water absorbency. In situ polymerized SAPCs containing various molar ratios of AM: IA and incorporating three types of silica particles at various contents were synthesized. The water absorbency of SAPCs was lower than those of SAPs, the extent of which depended on the amount of silica incorporated. However, the AUL of SAPs and SAPCs at a 97:3 molar ratio of AM: IA was almost unchanged regardless of the type and amount of silica added. The amounts of silica retained in the SAPCs of the three silica types and contents were in the range of 88-95% by weight. Water absorbency kinetics of the P(AM-IA) SAPs or the P(AM-IA)/silica SAPCs obeys Langmuir absorbency isotherm with a pseudo second-order absorbency phenomenon. Horizontal or vertical mixed SAPs with two types of silica at 0.1, 0.5, and 2% by weight did not give significant differences in water absorbency. In addition, the levels of water absorbency of the mechanically mixed SAPCs did not significantly vary from the levels obtained from the in situ SAPCs. Therefore, the obtained results indicated that in order to prepare SAP with improved mechanical properties via the addition of silica particles, one could avoid the complicated in situ polymerization reaction in the presence of the silica particles by mechanical mixing the neat SAP with silica particles to obtain the associated SAPC.

ACKNOWLEDGMENTS

The authors thank Publication Counseling Unit (PCU) for the language check and some useful suggestion.

REFERENCES

(1.) F.L. Buchholz, "Preparation and Structure of Polyacrylate," in Absorbent Polymer Technology, L. Brannon-Peppas and R.S. Harland, Eds., Amsterdam, Elsevier Science, 23 (1990).

(2.) K. Kosemund, H. Schlatter, J.L. Ochsenhirt, E.L. Krause, D.S. Marsman, and G.N. Erasala, Regul. Toxicol. Pharmacol., 53(2), 81 (2008).

(3.) F. Masuda, "Trends in the Development of Superabsorbent Polymers for Diaper," in Superabsorbent Polymers: Science and Technology; ACS Symposium Series # 573, F.L. Buchholz and N.A. Peppas, Eds., The American Chemical Society, Washington, DC, 88 (1994).

(4.) R. Chandra and R. Rustgi, Prog. Polym. Sci., 23, 1273 (1998).

(5.) M.J. Ham and Y.H. Kim, Polym. Eng. Sci., 48, 2439 (2008).

(6.) S. Dalal, S. Raghava, and M.N. Gupta, Biochem. Eng. J., 42, 301 (2008).

(7.) R. Liang, M. Liu, and L. Wu, React. Funct. Polym., 67, 769 (2007).

(8.) R.E. Sojka, D.L. Bjorneberg, J.A. Entry, R.D. Lentz, and W.J. Orts. Adv. Agronomy, 92, 75 (2007).

(9.) A. P. Nikolaos and R.K. Atul, Adv. Drug Delivery Rev., 11, 1 (1993).

(10.) M.H.A. Azadi and P. Rafiei, Adv. Drug Delivery Rev., 60, 1638 (2008).

(11.) A. Costantini, G. Luciani, B. Silvestri, F. Tescione, and F. Branda, J. Biomed. Mater. Res. Part B: Appl. Biomater., 86B(1), 98 (2007).

(12.) M. Kiremitci and H. Cukurova, Polymer, 33, 3257 (1992).

(13.) E. Karadag, D. Saraydin, Y. Caldiran, and O. Guven, Polym. Adv. Tech., 11, 59 (2000).

(14.) T. Masuda, "Absorptivity of Water (Moisture Absorptivity and Retention of Water)," in Gels Handbook, Y. Osada, K. Kajiwara, T. Fushimi, O. Irasa, Y. Hirokawa, T. Matsunaga, T. Shimomura, L. Wang, and H. Ishida, Eds., Academic Press, New York, 17 (2001).

(15.) T. Toyoda, "Water-Swelling Rubbers," in Gels Handbook, Y. Osada, K. Kajiwara, T. Fushimi, O. Irasa, Y. Hirokawa, T. Matsunaga, T. Shimomura, L. Wang, and H. Ishida, Eds., Academic Press, New York, 295 (2001).

Shimomura, L. Wang, and H. Ishida, Eds., Academic Press, New York, 295 (2001).

(16.) Y. Osada, K. Kajiwara, T. Fushimi, O. Irasa, Y. Hirokawa, T. Matsunaga, T. Shimomura, L. Wang, and H. Ishida, "Artificial Snow," in Gels Handbook, Y. Osada, K. Kajiwara, T. Fushimi, O. Irasa, Y. Hirokawa, T. Matsunaga, T. Shimomura, L. Wang, and H. Ishida, Eds., Academic Press, New York, 491 (2001).

(17.) H.-W. Jacobi, T. Annor, and E. Quansah, J. Photochem. Photobiol. A, 179, 330 (2006).

(18.) T. Shimura and T. Namba, "Preparation and Application of High-Performance Superabsobent Polymers," in Superabsorbent polymers: Science and Technology; ACS Symposium Series # 573, F.L. Buchholz and N.A. Peppas, Eds., The American Chemical Society, Washington, DC112 (1994).

(19.) J.C.M. Bordado and J.F.P. Gomes, Int. J. Environ. Stud., 64(2), 243 (2007).

(20.) T.L. Staples, D.E. Henton, and F.L. Buchholz, "Chemistry of Superabsorbent Polyacrylates," in Modern Superabsorbent Polymer Technology, F.L. Buchholz and A.T. Graham, Eds., Wiley-VCH, New York, 55 (1998).

(21.) P. Li, N.H. Kim, D. Hui, K.Y. Rhee, and J.H. Lee, Appl. Clay Sci., 46, 414 (2009).

(22.) K. Haraguchi, Curr. Opin. Solid State Mater. Sci., 11, 47 (2007).

(23.) D. Foungfung, S. Phattanarudee, N. Seetapan, and S. Kiatkamjornwong, Polym. Adv. Tech. (2009), DOI: 10.1002/pat.1559.

(24.) M. Taniguchi, K. Kato, A. Shimauchi, X. Ping, K. Fujita, T. Tanaka, Y. Tarui, and E. Hirasawa, J. Biosci. Bioeng., 99(2), 130 (2005).

(25.) D. Depan, A.P. Kumar, and R.P. Singh, Acta Biomater., 5, 93 (2009).

(26.) A. Li and A. Wang, Eur. Polym. J., 41, 1630 (2005).

(27.) J. Zhang, H. Chen, and A. Wang, Eur. Polym. J., 42, 101 (2006).

(28.) J. Zhang, Q. Wang, and A. Wang, Carbohydr. Polym., 68, 367 (2007).

(29.) S. Sharma and S. Komarneni, Appl. Clay Sci., 42, 553 (2009).

(30.) X. Huang, S. Xu, M. Zhong, J. Wang, S. Feng, and R. Shi, Appl. Clay Sci., 42, 455 (2009).

(31.) J. Wu, J. Lin, M. Zhou, and C. Wei, Macromol. Rapid Commun., 21, 1032 (2000).

(32.) W. Wang and A. Wang., Carbohydr. Polym., 77(4), 891 (2009).

(33.) U.Y. Kim, "Recent Developments in High Water Absorbing Polymers and Applications", in The Proceedings of the International Conference on Recent Developments in Petrochemical and Polymer Technologies, 6-1, December 12-16, 1989, Chulalongkorn University Press, Bangkok, Thailand.

(34.) H.F. Mark, N.M. Bikales, C.G. Overberger, and G. Mengel, Encyclopedia of Polymer Science and Engineering, 2nd ed., Wiley, New York, Vol. 7, 783 (1989).

(35.) A. Pourjavadi, F. Seidi, and R. Soleyman, J. Appl. Polym. Sci., 108(5), 3281 (2008).

(36.) F.L. Buchholz, J. Chem. Ed., 73, 512 (1996).

(37.) B. Silvestri, G. Luciani, A. Costantini, F. Tescione, F. Branda, and A. Pezzella, J. Biomed. Mater. Res. Part B: Appl. Biomater., 89, 369 (2009).

(38.) X. Shi, S. Xu, J. Lin, S. Feng, and J. Wang, Mater. Lett., 63(2), 527 (2009).

(39.) H. Schott, J. Macromol. Sci. Phys., 31(1), 1 (1992).

(40.) J. Baselga, M.A. Llorente, J.L. Nieto, and I.F.P. Hernandez-Fuentes, Eur. Polym. J. 24, 161 (1988).

(41.) N. Seetapan, J. Wongsawaeng, and S. Kiatkamjornwong, Polym. Adv. Tech. (2010), DOI: 10.1002/pat.1658.

(42.) N. Uyanik and C. Erbil, Eur. Polym. J., 36, 2651 (2000).

(43.) M. Pulat and H. Eksi, J. Appl. Polym. Sci., 102, 5994 (2006).

(44.) M.J. Ramazani-Harandi, M.J. Zohuriaan-Mehr, A.A. Yousefi, A. Ershad-Langroudi, and K. Kabiri, Polym. Test., 25, 470 (2006).

(45.) J. Qin, U.S. Pat. 6,998,367 B2 (2006).

(46.) D. Saraydin and Y. Caldiran, Polym. Bull., 46(1), 91 (2001).

(47.) N. Martinez-Vazquez, R. del, C. Antonio-Cruz, A. Alvarez-Castillo, A.M. Mendoza-Martinez, and A.B. Morales-Cepeda, Rev. Mex. Ingenieria Quim., 6(3), 337 (2007).

(48.) W. Saelow, S. Kiatkamjornwong, T. Watanabe, and Y. Hoshino, J. Imaging Soc. Jpn., 38(4), 310 (1999).

(49.) C. Poomtien, S. Kiatkamjornwong, and Y. Hoshino, Part. Sci. Technol., 16(4), 295 (1999).

Nispa Seetapan, (1) Natsiri Srisithipantakul, (2) Suda Kiatkamjornwong (3)

(1) National Metal and Materials Technology Center, National Science and Technology Development Agency, Pathumthani 12120, Thailand

(2) Faculty of Science, Chulalongkorn University, Bangkok 10330, Thailand

(3) Program of Petrochemistry and Polymer Science, Faculty of Science, Chulalongkorn University, Bangkok 10330, Thailand

Correspondence to: Suda Kiatkamjornwong; e-mail: ksuda@chula.ac.th

Contract grant sponsor: Thailand Research Fund; contract grant number: RTA5080004; contract grant sponsor: Imaging Polymer Laboratory of the Faculty of Science's Department of Imaging and Printing Technology, Chulalongkorn University.

DOI 10.1002/pen.21882

Published online in Wiley Online Library (wileyonlinelibrary.com).

[C] 2010 Society of Plastics Engineers

TABLE 1. Silica types and their physical properties.

Physical properties	Aerosil 90	Aerosil 200	Aerosil 300
BET surface area, ([m.sup.2] [g.sup.-1])	90 [+ or -] 15	200 [+ or -] 25	300 [+ or -] 30
Average primary particle size, (nm)	20	12	7
pH	3.7-4.7	3.7-4.7	3.7-4.7
Si[O.sub.2] (% w [w.sup.-1])	>99.8	>99.8	>99.8
[AI.sub.2][O.sub.3] (% w [w.sup.-1])	<0.05	<0.05	<0.05
[Fe.sub.2][O.sub.3] (% w [w.sup.-1])	<0.003	<0.003	<0.003
HCI (% w [w.sup.-1])	<0.025	<0.025	<0.025

TABLE 2. Basic formulation for the preparation of P(AM-IA) SAPs and P(AM-IA)/silica SAPCs.

Ingredient	In situ polymerization method	Mechanical mixing method
AM/IA (mole/mole)	100/0, 99/1, 98/2, 97/3	100/0, 99/1, 98/2, 97/3
Aerosil 90 silica (w [w.sup.-1])	0.1, 0.2, 0.5, 2.0	0.1, 0.5, 2.0
Aerosil 200 silica (w [w.sup.-1])	0.1, 0.2, 0.5, 2.0	--
Aerosil 300 silica (w [w.sup.-1])	0.1, 0.2, 0.5, 2.0	0.1, 0.5, 2.0
N-MBA (w [w.sup.-1])	0.5	0.5
APS (w [w.sup.-1])	1.0	1.0
TEMED ([cm.sup.3])	0.2	0.2
Horizontal mixing (rpm)	600	600
Vertical mixing (rpm)	100	100

TABLE 3. Effect of itaconic acid concentration (molar ratio) on the water absorbency of the P(AM-IA) SAP.

	Water absorbency under load (AUL [Pa]) of		
Itaconic acid concentration (% molar ratio)	0	1.93 x [10.sup.3]	4.83 x [10.sup.3]
0	51 [+ or -] 2	14	12
1	157 [+ or -] 9	14	12
2	191 [+ or -] 6	13	11
3	233 [+ or -] 8	12	11

APS, 1.0% w [w.sup.-1]; N-MBA, 0.5% w [w.sup.-1] at 45[degrees]C, 250 rpm, 30 min.

TABLE 4. Equilibrium water absorbency ([Q.sub.[infinity]]) and rate

constant of swelling of P(AM-IA) SAPs prepared from various IA contents.

IA content (% molar)	[Q.sub.[infinity]] (Schott model)	K ([min.sup.-1])	[Q.sub.[infinity]] (experimental)
0	62	6.14e-3	51 [+ or -] 2
1	156	2.53e-4	157 [+ or -] 9
2	182	2.27e-4	191 [+ or -] 6
3	238	5.44e-4	233 [+ or -] 8

IA content (% molar)	Fitting second order kinetic equation	[r.sup.2]
0	y = 0.0161x + 0.0422	0.9894
1	y = 0.0064x + 0.162	0.9996
2	y = 0.0055x + 0.1333	0.9997
3	y = 0.0042x + 0.0324	1

TABLE 5. Equilibrium water absorbency ([Q.sub.[infinity]] and rate constant of swelling (k): of SAPCs prepared from P(AM-IA)/2% w w [w.sup.1] silica (97:3 molar ratio of AM: IA), with the indicated different types of silica particles.

System	[Q.sub.[infinity]] (Schott model)	k ([min.sup.-1])	[Q.sub.[infinity]] (experimental)
No silica	238	5.44e-4	233 [+ or -] 8
Aerosil 90	189	9.03e-4	188 [+ or -] 6
Aerosil 200	185	3.14e-4	184 [+ or -] 2
Aerosil 300	182	6.53e-4	183 [+ or -] 4

System	Fitting second order kinetic equation	[r.sup.2]
No silica	y = 0.0042x + 0.0324	1
Aerosil 90	y = 0.0053x + 0.0311	1
Aerosil 200	y = 0.0054x + 0.0928	0.9994
Aerosil 300	y = 0.0055x + 0.0463	1

TABLE 7. Equilibrium water absorbency ([Q.sub.[infinity]]) and rate constant of swelling (k): of SAPCs prepared from P(AM-IA)/Aerosil 90 silica (97:3 molar ratio of AM: IA) with the incorporation of the indicated final Aerosil 90 concentration.

Aerosil 90 (w [w.sup.-1])	([Q.sub.[infinity]] (Schott model)	k ([min.sup.-1])	[Q.sub.[infinity]] (experimental)
0	238	5.44e-4	233 [++or--] 8
0.1	238	5.78e-4	235 [++or--] 6
0.2	227	7.53e-4	227 [++or--] 1
0.5	213	8.09e-4	214 [++or--] 6
2	189	9.39e-4	188 [++or--] 6

Aerosil 90 (w [w.sup.-1])	Fitting second order kinetic equation	[R.sup.2]
0	y = 0.0042x + 0.0324	1
0.1	y = 0.0042x + 0.0305	1
0.2	y = 0.0044x + 0.0257	1
0.5	y = 0.0047x + 0.0273	1
2	y = 0.0053x + 0.0299	1

TABLE 6. Effect of silica types and concentrations on the water absorbency of SAPCs (97:3 molar ratio of AM:IA).

	Water absorbency (g [g.sup.-1]) under loads (Pa) of		
	0		
Concentration or silica (% w [w.sup.-1])	Aerosil 90	Aerosil 200	Aerosil 300
0.1	228 [+ or -] 1	228 [+ or -] 7	225 [+ or -] 2
0.2	220 [+ or -] 1	218 [+ or -] 2	216 [+ or -] 3
0.5	218 [+ or -] 1	210 [+ or -] 5	208 [+ or -] 5
2.0	199 [+ or -] 4	193 [+ or -] 6	188 [+ or -] 1

Water absorbency (g [g.sup.-1]) under loads (Pa) of

	1.93 x [10.sup.3]			4.83 X [10.sup.3]		
Concentration or silica (% w [w.sup.-1])	Aerosil 90	Aerosil 200	Aerosil 300	Aerosil 90	Aerosil 200	Aerosil 300
0.1	12	12	12	11	11	11
0.2	12	12	13	11	11	12
0.5	13	13	13	12	12	12
2.0	13	13	13	12	12	12

TABLE 8. The silica retained in the gel at various silica concentrations.

Type of Aerosil	Silica concentration added in polymerization (% w [w.sup.-1])	Silica concentration after sintering (% w [w.sup.-])	Silica concentration retained in the gel (% w [w.sup.-1])
Aerosil 90	0.1	0.09	90
	0.2	0.19	95
	0.5	0.44	88
	2.0	1.79	90
Aerosil 200	2.0	1.85	93
Aerosil 300	2.0	1.71	86

TABLE 9. Mechanical mixing of the superabsorbent copolymer with silica by horizontal mixing or vertical mixing.
Water absorbency (g [g.sup.-1]) of SAPCs from AM/IA (mol %)

100/0

Silica surface area ([m.sup.2] [g.sup.-1])	Silica content (% w)	In situ	VM	HM
90	0	51 [+ or -] 2	35 [+ or -] 1	35 [+ or -] 1
	0.1	--	36 [+ or -] 2	19 [+ or -] 2
	0.5	--	37 [+ or -] 5	20 [+ or -] 3
	2.0	--	34 [+ or -] 0	21 [+ or -] 3
300	0	51 [+ or -] 2	35 [+ or -] 1	35 [+ or -] 1
	0.1	--	41 [+ or -] 2	37 [+ or -] 1
	0.5	--	40 [+ or -] 1	40 [+ or -] 1
	2.0	--	40 [+ or -] 2	42 [+ or -] 2

99/1

Silica surface area ([m.sup.2] [g.sup.-1])	Silica content (% w)	In situ	VM	HM
90	0	157 [+ or -] 9	144 [+ or -] 8	144 [+ or -] 8
	0.1	--	177 [+ or -] 7	182 [+ or -] 41
	0.5	--	165 [+ or -] 2	183 [+ or -] 24
	2.0	--	189 [+ or -] 35	136 [+ or -] 19
300	0	157 [+ or -] 9	144 [+ or -] 8	144 [+ or -] 8
	0.1	--	147 [+ or -] 19	151 [+ or -] 6
	0.5	--	143 [+ or -] 8	132 [+ or -] 12
	2.0	--	141 [+ or -] 19	135 [+ or -] 3

98/2

Silica surface area ([m.sup.2] [g.sup.-1])	Silica content (% w)	In situ	VM	HM
90	0	191 [+ or -] 6	201 [+ or -] 5	201 [+ or -] 5
	0.1	--	178 [+ or -] 9	174 [+ or -] 9
	0.5	--	155 [+ or -] 7	176 [+ or -] 11
	2.0	--	165 [+ or -] 19	164 [+ or -] 6
300	0	191 [+ or -] 6	201 [+ or -] 5	201 [+ or -] 5
	0.1	--	191 [+ or -] 6	213 [+ or -] 51
	0.5	--	198 [+ or -] 14	208 [+ or -] 5
	2.0	--	193 [+ or -] 6	205 [+ or -] 2

97/3

Silica	Silica	In situ	VM	HM

surface area ([m.sup.2] [g.sup.-1])	content (% w)			
90	0	233 [+ or -] 8	225 [+ or -] 4	225 [+ or -] 4
	0.1	228 [+ or -] 1	239 [+ or -] 29	228 [+ or -] 17
	0.5	218 [+ or -] 1	250 [+ or -] 13	340 [+ or -] 63
	2.0	199 [+ or -] 4	225 [+ or -] 22	228 [+ or -] 8
300	0	233 [+ or -] 8	225 [+ or -] 4	225 [+ or -] 4
	0.1	225 [+ or -] 2	166 [+ or -] 5	220 [+ or -] 48
	0.5	208 [+ or -] 2	209 [+ or -] 23	195 [+ or -] 23
	2.0	188 [+ or -] 1	201 [+ or -] 3	212 [+ or -] 5

0.2 g sample, mixing time = 30 rain, vertical mixing (VM) at 100 rpm and horizontal mixing (HM) at 600 rpm, "--" for do not measure.

Gale Copyright: Copyright 2011 Gale, Cengage Learning. All rights reserved.

Previous Article: Drawing and ultimate tensile properties of modified polyamide 6 fibers.

Next Article: Synthesis of Y-shaped Poly(N,N-dimethylamino-2-ethyl methacrylate) and Poly(trimethylene carbonate) ...

Copyright 2004-2011 FreePatentsOnline.com. All rights reserved. Privacy Policy & Terms of Use.

Home | Search Patents | IP Services | Help | Contact us | Advertise on this Site

SYNTHESES, CHARACTERIZATION AND ANTIBACTERIAL ACTIVITY OF CHITOSAN GRAFTED HYDROGELS AND ASSOCIATED MICA-CONTAINING NANOCOMPOSITE HYDROGELS

Journal:	*Journal of Applied Polymer Science*
Manuscript ID:	Draft
Wiley - Manuscript type:	Research Article
Keywords:	swelling, hydrogels, nanocomposites, organoclay, biocompatibility

SCHOLARONE™
Manuscripts

For Review

SYNTHESES, CHARACTERIZATION AND ANTIBACTERIAL ACTIVITY OF CHITOSAN GRAFTED HYDROGELS AND ASSOCIATED MICA-CONTAINING NANOCOMPOSITE HYDROGELS

Supaporn Noppakundilograt[1], Kittichai Sonjaipanich[2], Nuttha Thongchul[3] and Suda Kiatkamjornwong[1*]

[1]Department of Printing and Imaging Technology, Faculty of Science, Chulalongkorn University, Bangkok, 10330, Thailand. [1]E-mail: *supaporn.n@chula.ac.th*; [*1]corresponding author; [1*]e-mail: *ksuda@chula.ac.th*; Tel.: +66-2218-5587.

[2]Program of Petrochemistry and Polymer Science, Faculty of Science, Chulalongkorn University, Bangkok, 10330, Thailand. [2]E-mail: kittichai_sonjai@hotmail.com.

[3]Institute of Biotechnology and Genetic Engineering, Chulalongkorn University, Bangkok, 10330, Thailand. [3]E-mail: Nuttha.T@chula.ac.th.

For Peer Review

SYNTHESES, CHARACTERIZATION AND ANTIBACTERIAL ACTIVITY OF CHITOSAN GRAFTED HYDROGELS AND ASSOCIATED MICA-CONTAINING NANOCOMPOSITE HYDROGELS

Abstract

Chitosan (CS) grafted poly[(acrylic acid)-*co*-(2-hydroxyethyl methacrylate)] (CS-*g*-poly(AA-co-HEMA)) at different molar ratios of AA and HEMA, and the associated nanocomposite hydrogels of CS-*g*-poly(AA-*co*-HEMA)/mica were synthesized by radical copolymerization. The grafting positions at the amino or hydroxyl groups in the CS were identified by Fourier transform infrared spectroscopy. CS-*g*-poly(AA-*co*-HEMA) hydrogels were intercalated in the mica and the amount of hydrogel insertion did not affect the spacing of the silicate layers in mica. The higher mica loadings produced a rougher surface of the nanocomposite hydrogel. The water absorbency of the CS-*g*-poly(AA-*co*-HEMA)/mica nanocomposite hydrogels decreased with increasing levels of mica loading to a lower level than those of the CS-*g*-poly(AA-*co*-HEMA) hydrogels. Both CS-*g*-poly(AA) and CS-*g*-poly(AA-*co*-HEMA)/mica nanocomposite hydrogels exhibited a higher antiproliferative activity against *Staphylococcus aureus* than did the neat CS hydrogel with CS-*g*-poly(AA) revealing a very pronounced minimum inhibition concentration (MIC) of 1.56 mg ml^{-1}. The extent of mica loading in the CS-*g*- poly(AA-*co*-HEMA) nanocomposite hydrogels did not affect the MIC (12.5 mg ml^{-1}).

Keywords: Chitosan; Acrylic acid; 2-hydroxyethyl methacrylate; Mica; Nanocomposite hydrogel; Antibacterial property

For Peer Review

1. Introduction

Hydrogels are slightly crosslinked hydrophilic polymers that can swell and absorb at least 15 times of their dry weight. The relative density of hydrophilic groups and the degree of crosslinking of the hydrogel are the two main factors that affect the water absorbency of a hydrogel.[1] Chitosan (CS) has found wide applications in the biomedical field, as well as other fields, because of its interesting biological properties, such as biocompatibility, biodegradability, hemostatic activity and bacteriostatic effects. Recently, CS-based hydrogels have been extensively researched and used in a wide field of applications because of their biocompatibility, biodegradability, non-toxicity and antibacterial activity,[2] as well as that CS is a plentiful, renewable and relatively cheap material. The hydrogels derived from CS grafted with hydrophilic vinyl monomers, such as acrylic acid (AA) or itaconic acid (IA), showed an increased water absorbency compared to CS alone.[3-5] The 2-hydroxyethyl methacrylate (HEMA) monomer has long been used in biomedical applications because it improves the graft copolymer biocompatibility.[6] HEMA monomer is harmful in the dental application if it does not completely polymerize, because it induces DNA damage, apoptosis and cell-cycle delay by the production of reactive oxygen species. However, it was found that the presence of antioxidant and/or CS can decrease the genotoxicity of HEMA monomer.[7,8] CS-*g*-poly(AA-*co*-HEMA) was reported to exhibit good cytocompatibility and hemocompatibility and thus possesses a high potential as an application for wound dressing.[3] Suitable wound dressings normally possess an antibacterial activity for protecting the wound from infection, and have a water absorbency of around 25 - 32 times their dry weight so as to be able to remove secretion or pus from the wound.[9] Bacterial infection is one of the main factors for the development of chronic wounds. Infected wounds may cause trauma and higher

For Peer Review

treatment costs. Pathogens frequently associated with wound infections include *Staphylococcus aureus (S. aureus*), *Enterococcus* sp., *Escherichia coli*, *Pseudomonas aeruginosa*, *Enterobacter* sp., *Proteus mirabilis*, *Klebsiella pneumonia*, *Streptococcus* sp., and *Candida albicans*. *S. aureus* is the most commonly found human pathogens which cause wound infections, boils, pustules and other human skin infections.[10] Infection by *S. aureus* is accounted for about 20% frequency of occurrence in burns, wounds, and surgical sites. Due to the above mentioned, any developed wound dressing materials should therefore possess an inhibitory effect on the most frequently found *S. aureus* in wounds.

Generally, the gel strength of a bio-absorbent is naturally rather weak and this unfortunately limits its useful applications. To improve the gel strength, thermal and inherently antibacterial properties of CS and/or grafted CS, clay minerals, such as montmorillonite,[11] rectorite[12,13] and sepiolite,[14] have been used as a filler incorporated into the CS to produce CS/nanocomposite hydrogels. Wang et al. [15] found that the antibacterial activity against *S. aureus* of CS/rectorite nanocomposite film was better than that of the neat CS film. This result agreed with the research reporting that clay minerals alone did not destroy bacteria, but they could adsorb and kill bacteria when the antimicrobial materials were intercalated into silicate layers.[16]

Mica is a clay mineral known as a 2: 1 phyllosilicate and its general formula is $AM_{2-3}T_4O_{10}X_2$, where A is usually Na, K or Ca. The M can be Fe, Al and Mg; T is Si and/or Al and X is (OH), O, Cl and F.[17] It is composed of two-dimensional layers of an edge-shared octahedral sheet that is fused to form two tetrahedrals by the shared oxygen ions of one octahedral sheet and two tetrahedral sheets.[18] Mica showed the antimicrobial activity, but it has a tendency of cytotoxicity with a larger platelet size than that of montmorillonite.[19] Nanosilicate platelet of montmorillonite has a low

For Peer Review

cytotoxicity with antibacterial activity.[19,20] However, only a few research reports on CS/mica nanocomposite hydrogels are available, leaving its potential suitability for many applications, including as a wound dressing material, unknown. Therefore, the synthesis and characterization of grafted CS/mica nanocomposite hydrogels was the main aim of this research. The effects of the reaction parameters on the morphology, water absorption and antibacterial activities of the resultant hydrogels were investigated.

2. Experimental

2.1 Materials

CS with a viscosity average molecular weight of 57,000 g mol^{-1} and an 85% deacetylation degree was purchased from Seafresh Industry Public Co., Ltd. (Bangkok, Thailand). Industrial grade AA and HEMA monomers were kindly supplied by Thai Mitsui Specialty Chemicals Co., Ltd. (Bangkok, Thailand). *N, N'*-Methylenebisacrylamide (*N*-MBA) crosslinker and *N, N, N', N'*-tetramethylethylenediamine (TEMED) co-initiator were purchased from Fluka (Buchs, Switzerland). Ammonium persulphate (APS), purchased from Ajax (Australia), was used as the initiator. Swelling mica was purchased from Wako Pure Chemical Industries, Ltd. (Osaka, Japan). Deionized water, used as the reaction medium, was obtained from an Elga Deionizer (Model LA611, Marlow international, Bucks, U.K.). Sodium ampicillin (drug grade) was purchased from T.P. Drug Laboratories (Bangkok, Thailand). *Staphylococus aureus* (*S. aureus*) isolate from textile wastewater was provided by the National Center for Genetic Engineering and Biotechnology (NSTDA, Pathum thani, Thailand). Mueller-Hinton Broth (MHB) and Mueller-Hinton Agar (MHA), used for the growth of *S. aureus* were from Difco, New Jersey, USA.

For Peer Review

2.2 Syntheses

2.2.1 Synthesis of grafted CS hydrogels

CS (1 g) was added into 30 ml of 2% w v^{-1} acetic acid solution in a 500-ml four-necked round-bottom flask with a mechanical stirrer (Ika RW 28, IKA® Werke GmbH & Co. KG, Staufen Germany), assembled with a half-moon shaped Teflon blade paddle and a condenser. The mixture was stirred for 30 min at room temperature and then heated at 60 ± 2°C under nitrogen gas which was fed constantly through the gas inlet at 10 ml min^{-1} for 30 min. APS (0.01-0.15 g) was then added and stirred for 10 min, followed by the sequential addition of either AA or HEMA or both and *N*-MBA (0.01 - 0.15 g) to the desired final concentration and stirred for 5 min. Finally, TEMED was added (0.01 - 0.4 g) to the mixture and stirred at 250 rpm for another 60 min. The reaction was then cooled down to room temperature and adjusted to pH 8 by 1 M sodium hydroxide solution. The product was dewatered with acetone, cut into pieces of approximately 1 x 1 cm square and dried in an oven at 50°C for 24 h. The dried product was extracted with an excess amount of methanol in a Soxhlet apparatus for 24 h to remove the unreacted components and obtain the CS grafted polymer (e.g. CS-*g*-poly(AA-*co*-HEMA)). The extracted product was dried in the oven at 50°C for 24 h, milled and sieved through a 100 mesh sieve to obtain the hydrogel particles in the range of 50 - 100 mesh (200 - 400 micrometers).

2.2.2 Synthesis of CS-g-poly(AA-co-HEMA)/mica nanocomposite hydrogels

The desired amount of mica was dispersed in the mixture of AA and HEMA monomers for 60 min by stirring at 250 rpm with a magnetic stirrer. CS (1 g) was dissolved in 30 ml of 2% v v^{-1} solution of acetic acid, and then added into a 500-ml four-necked round-bottomed reaction flask equipped with the mechanical stirrer and a

For Peer Review

condenser. The reactor was then immersed in a temperature controlled water bath, stirred at 250 rpm under a constant nitrogen gas fed through the gas inlet tube for 30 min before APS (0.1 g) was added and stirred for 10 min. The well-dispersed mica suspension was added into the solution of CS and APS, stirred at 250 rpm and heated to 60 ± 2°C under the nitrogen gas circulation for 30 min before *N*-MBA (0.1 g) was then added and stirred for 5 min. Finally, TEMED (0.4 g) was added and stirred for another 60 min. The polymerization product was cooled down and the product was obtained by the same procedure as described above for the grafted CS hydrogels.

2.3 Grafting ratio and efficiency of the grafted CS hydrogels by acid hydrolysis

The grafted CS hydrogel (0.5 g) was dissolved in 50 ml of 1 M HCl in a 125-ml Erlenmeyer flask which was assembled with a condenser and refluxed at 120°C for 2 h. After the acid hydrolysis, the remaining solid (grafted copolymer) was filtered, dried and weighed. The filtrate was neutralized to pH 7 by 1 M sodium hydroxide solution and then precipitated by ethanol. The precipitate was filtered and dried at room temperature for 24 h to obtain its dry weight. Finally, the filtrate from the precipitation step was evaporated to remove the residual solvent. The white solid was dried at room temperature and weighed. The remaining solid and precipitate after acid hydrolysis were investigated for functional groups by Fourier Transform Infrared Spectroscopy (FT-IR; model Tensor 27, Billerica, USA) using KBr pellets. The grafting ratio, grafting efficiency and homopolymer content were calculated from Equations (1) - (3):[21-23]

$$\%\ grafting\ efficiency = \frac{Weight\ of\ remaining\ solid\ after\ acid\ hydrolysis \times 100}{Weight\ of\ homopolymer + Weight\ of\ grafted\ copolymer} \quad (1)$$

$$\%\ grafting\ ratio = \frac{Weight\ of\ remaining\ solid\ after\ acid\ hydrolysis \times 100}{Weight\ of\ precipitate\ from\ ethanol} \quad (2)$$

For Peer Review

$$\% \text{ homopolymer} = \text{Weight of grafted CS hydrogel before Soxhlet extraction - weight of grafted CS hydrogel after Soxhlet extraction} \quad (3)$$

2.4 Identification of functional groups of grafted CS hydrogels and CS-g-poly(AA-co-HEMA)/mica nanocomposite hydrogels

The functional groups of mica, the grafted CS hydrogels and grafted CS-*g*-poly(AA-*co*-HEMA)/mica nanocomposite hydrogels were characterized by FT-IR.

2.5 Characterization of the grafted CS hydrogels and CS-g-poly(AA-co-HEMA)/mica nanocomposite hydrogels

The surface morphologies of the mica, and the grafted CS and grafted CS/mica nanocomposite hydrogels were photographed on a scanning electron microscope (SEM, model JSM-5410LV, Tokyo, Japan) without prior cross sectioning. Each sample was fixed on an aluminum stub and coated with gold. X-ray diffraction (XRD) patterns of the samples were recorded using Bruker AXS (model D8 Discover, Bruker AXS Munich, Germany) with Cu radiation, voltage of 40 kV, a current of 40 mA and scanned from 1 - 35° with a scanning rate of 0.02° min^{-1}. The transmission electron micrographs (TEM) were taken on JOEL (JEM-2100, Jeol Ltd., Tokyo, Japan).

2.6 The effect of the reagent contents on water absorbency of grafted CS hydrogels and CS-g-poly(AA-co-HEMA)/mica nanocomposite hydrogels

For Peer Review

The water absorbencies of the grafted CS hydrogel and the grafted CS-*g*-poly(AA-*co*-HEMA)/mica nanocomposite hydrogels were carried out with distilled water at room temperature in a closed system to minimize water evaporation. Distilled water (200 ml) was added to 0.1 g of the dry grafted hydrogels or the nanocomposite hydrogels. The hydrogel was swollen to equilibrium for 24 h and the swollen gel was then filtered through a 100-mesh aluminum screen sieve for 2 h. The water absorbency was determined for at least three replications for each synthesized product by Equation (4):

$$Water\ absorbency\ (Q) \quad = \quad \frac{(W_s - W_d)}{W_d} \qquad (4)$$

where W_s is the weight of swollen hydrogels or nanocomposite hydrogels (g) and W_d is the weight of the dry hydrogels or nanocomposite hydrogels (g).

2.7 Antibacterial activity

2.7.1 Turbidity method

The CS, CS-*g*-poly(AA), CS-*g*-poly(HEMA) and CS-*g*-poly(AA-*co*-HEMA) hydrogels, and the CS-*g*-poly(AA-*co*-HEMA)/mica nanocomposite hydrogels, each weighing 250 mg, and distilled water were sterilized by UV radiation for 1 h prior to the test.

The diluted stock culture of *S. aureus* was adjusted to 0.5 units by sterile deionized water. The *S. aureus* suspension (2.5 ml) was inoculated into 47.5 ml of sterile Mueller-Hinton Broth (MHB) in a 250 ml sterile Erlenmeyer flask. For each hydrogel type, the sterile sample (250 mg) was then added to the *S. aureus* suspension in MHB media and incubated at 37°C while being shaken at 250 rpm. At every two hours a 50 ml aliquot was harvested and the swollen gel removed by filtration through

For Peer Review

filter paper no. 1 (Schleicher & Schuell, Whatman, Kent, U.K.) prior to measuring the $OD_{610\ nm}$ of the filtrate as a measure of the growth of *S. aureus* using a spectrophotometer (Spectronic 21, Bausch & Lomb Inc., Rochester, New York, U.S.A). The OD results of the growth with or without the hydrogel were plotted versus time to obtain the bacterial growth profiles. The culture time at which the antibacterial activity of the grafted CS hydrogel was found to be maximal by the optical density measurement was used to evaluate the total replication competent (viable) bacterial number using the total plate count method (see section 2.7.2. below) so as to calculate the mean colony-forming units per milliliter (CFU ml^{-1}), and from this the relative degree of inhibition of bacterial proliferation can be obtained.

2.7.2 Total plate count method

The six and eight hour old *S. aureus* cultures in MHB were diluted with sterile deionized water to 10^8 - 10^9 CFU ml^{-1} and then 100 µl aliquots of each diluted *S. aureus* suspension were spread on each MHB plate. The plates were incubated for 24 h at 37°C where upon the number of viable bacteria was counted. Mean CFU ml^{-1} and the relative inhibition were calculated by Equations (5) and (6), respectively. The negative control was the sterilized *S. aureus* cultured in MHB.

$$CFU/ml = \left(\frac{mean\ numbers\ of\ counted\ colonies}{amount\ of\ dilute\ S.aureus\ for\ spread\ plate\ (ml)} \right) \times dilution\ factor \quad (5)$$

$$Relative\ inhibition = 100 - \left(\frac{CFU/ml\ of\ the\ sample}{CFU/ml\ of\ negative\ control} \right) \times 100 \quad (6)$$

For Peer Review

2.7.3 Minimum inhibition concentration (MIC)

The antibacterial activity was determined in terms of the minimum inhibition concentration (MIC). The diluted stock culture of *S. aureus* was adjusted to 0.5 A_{610} units by sterile deionized water and 100 µl was inoculated into 4.9 ml of sterile MHB in a 10 ml test tube. The hydrogels, each evaluated at the five concentrations of 0, 3.12, 6.25, 12.5 and 25 mg ml^{-1}, were added to the 0.01 A_{610} unit suspensions of *S. aureus* (see above) in sterile MHB. The cultures were then incubated at 37°C with shaking at 120 rpm for 24 h. The mean CFU ml^{-1} of each sample tested were measured by the total plate count method as above and the experiment was performed in triplicate. The MIC was thus determined from the derived CFU ml^{-1} and statistical significance (ANOVA) was accepted at the 99% significant level or $\alpha = 0.01$.

3. Results and discussion

3.1 Characterization of the grafted hydrogels

3.1.1 Grafted CS hydrogels

The spectrum of the CS hydrogel (Figure 1(a)) shows the characteristic amino group peaks at 3428 cm^{-1} for N-H stretching, 1640 cm^{-1} for the C=O stretching of amide I,[24] 1594 cm^{-1} for the N-H bending of amide II, 1381 cm^{-1} for the -NHCO stretching of amide II[25] and 1253 cm^{-1} for C-N stretching.[26] The characteristic peaks of the saccharide structure in CS exhibit at 1152 cm^{-1} for the bridge O stretching,[23,27] and 1085 cm^{-1} and 1031 cm^{-1} for the C_3-OH and C_6-OH stretching, respectively.[25] In addition, the absorption peak at 1420 cm^{-1} is the O-H and C-H vibration which indicates the presence of a hydroxyl group.[24] The peak of C-H stretching appears at 2921 and 2864 cm^{-1}.[27]

For Peer Review

The CS-*g*-poly(AA) hydrogel spectrum (Figure 1(b)) shows a new absorption peak at 1724 cm^{-1} assigned to C=O stretching of the carboxyl group from the grafted poly(AA) part,[27] which was shifted from the peak at 1713 cm^{-1} of the carboxyl group of poly(AA). In addition, the new absorption peaks at 1563 cm^{-1} and 1402 cm^{-1} are ascribed to asymmetric and symmetric stretching of the carboxylate anion of poly(AA) in the CS-*g*-poly(AA) hydrogel.[3] The absorption peak at 1594 cm^{-1}, assigned to N-H bending of CS, disappeared in the CS-*g*-poly(AA) hydrogel. Thus, the NH_2 group is grafted in the CS backbone.[28] Moreover, the characteristic peaks of the saccharide structure of CS in the CS-*g*-poly(AA) hydrogel was shifted to 1065 cm^{-1} and 1019 cm^{-1} (C_3-OH and C_6-OH stretching) and the peak of O-H bending at 1420 cm^{-1} disappeared (Figure 1(b)). From these results, the poly(AA) chains were confirmed to be grafted at both the NH_2 and OH sites on the CS backbone.

The CS-*g*-poly(HEMA) spectrum (Figure 1(c)) shows an absorption peak at 1730 cm^{-1}, assigned to C=O asymmetric stretching, which indicates the presence of the ester carbonyl group of poly(HEMA),[3] and a new absorption peak at 746 cm^{-1} that is attributed to the CH_2 rocking of the poly(HEMA) moiety.[29] The absorption peak of N-H stretching of CS also disappeared. Thus, the NH_2 group of CS had been reacted in the graft polymerization.[28] The characteristic peaks of the saccharide structure of CS in the CS-*g*-poly(HEMA) hydrogel were shifted to 1069 cm^{-1} and 1021 cm^{-1} (C_3-OH and C_6-OH stretching) and the CS O-H bending peak at 1420 cm^{-1} disappeared. Thus, the poly(HEMA) was grafted at both NH_2 and OH sites on the CS backbone as well.

The CS-*g*-poly(AA-*co*-HEMA) hydrogel spectrum (Figure 1(d)) shows the absorption peak at 1722 cm^{-1} that is assigned to the C=O asymmetric stretching and so indicates the presence of the ester carbonyl group of the poly(HEMA) moiety,[3] and

For Peer Review

a new absorption peak at 753 cm^{-1} that is attributed to the CH_2 rocking of the poly(HEMA) moiety.[29] In addition, it also shows peaks at 1585 cm^{-1} (C=O asymmetric stretching) and 1402 cm^{-1} (C=O symmetric stretching) of the carboxylate anion in the poly(AA) moiety.[3] Moreover, the characteristic peaks of the saccharide structure of CS in the CS-*g*-poly(AA-*co*-HEMA) hydrogel (Figure 1(d)) shifted to 1074 and 1021 cm^{-1} (C_3-OH and C_6-OH stretching) and the peak of O-H bending at 1420 cm^{-1} (Figure 1(a)) disappeared (Figure 1(d)). Thus, poly(AA-*co*-HEMA) was also grafted at both the NH_2 and OH sites on the CS backbone.

3.1.2 CS-g-poly(AA-co-HEMA)/mica nanocomposite hydrogels

The FT-IR spectrum of mica is shown in Figure 1(e). It shows a peak of O-H stretching at 3600 - 3400 cm^{-1} that indicates the presence of the hydroxyl group. The absorption peaks at 2924 and 2852 cm^{-1} are attributed to the C-H stretching of the organic part and indicate that the mica used is synthetic mica. It also shows the absorption peaks of H-O-H bending of water at 1637 and 1620 cm^{-1},[30] and Si-O and Al-O stretching peaks at 1016 and 473 cm^{-1}.[31]

The FT-IR spectra of CS-*g*-poly(AA-*co*-HEMA)/mica nanocomposite hydrogels, containing mica at 7, 10 or 15% w w^{-1} of the monomer, are shown in Figure 1(f-h), respectively. In comparison with the spectra of mica (Figure 1(e)), the characteristic peaks of CS are shifted to 1636 and 1389 cm^{-1}, whilst the characteristic peaks of poly(AA-*co*-HEMA) are also shifted to 1724, 1572, 1404 and 754 cm^{-1}. In addition, new absorption peaks appear at 473, 469 and 467 cm^{-1} (Figure 1(f–h), respectively), all of which are attributed to the Al-O stretching of mica. The intensity of the absorption peak at 1016 cm^{-1} (Si-O stretching) increased with increasing mica loadings in the CS-*g*-poly(AA-*co*-HEMA)/mica nanocomposite hydrogels, which

For Peer Review

indicates the existence of mica in the CS-*g*-poly(AA-*co*-HEMA) nanocomposite hydrogel. Based on these FT-IR data, the AA or HEMA group is grafted at the OH group of the C-6 position and/or the amino group of CS. The FT-IR peaks in the spectra further confirmed that CS-*g*-poly(AA-*co*-HEMA)/mica nanocomposite hydrogels with various loadings of mica were successfully synthesized.

3.2 The grafting performance of grafted CS hydrogels

Analysis of the acid hydrolysis suggests the grafting ratio of the CS-*g*-poly(AA) hydrogel (87%) is lower than that of the CS-*g*-poly(AA-*co*-HEMA) (269%) and CS-*g*-poly(HEMA) hydrogels (343%). However, the grafting ratios of CS-*g*-poly(AA-*co*-HEMA) and CS-*g*-poly(HEMA) hydrogels were calculated from the weight differences because a poly(HEMA) C=O peak at 1710 and 1722 cm^{-1} is still observed. Thus, at least some poly(HEMA) is still incorporated in the precipitate after acid hydrolysis, it means that the acid hydrolysis of the CS-g-poly(HEMA) was not completed. In comparison with the amount of CS, a greater amount of HEMA was used and so HEMA can generate an interpenetrate polymer network (IPN) hydrogel[32] on the CS backbone. This result reflects the high grafting ratio as expected. The grafting efficiency of CS-*g*-poly(AA), CS-*g*-poly(AA-*co*-HEMA) and CS-*g*-poly(HEMA) hydrogels is 93, 94 and 96%, respectively. The amount of homopolymer normally generated during graft polymerization and the homopolymer chains could form the IPN chains. Therefore, the amount of homopolymer cannot be derived directly just from the Soxhlet extraction and acid hydrolysis. Therefore, the amounts of free poly(AA), poly(AA-*co*-HEMA) and poly(HEMA) found are only 3, 5 and 3%, respectively, which are considered to be quite small, and would probably have been incorporated as the IPN in the polymeric hydrogels.

For Peer Review

3.3 Surface morphology

The surface morphologies of the CS, mica, CS-*g*-poly(AA-*co*-HEMA) hydrogel and CS-*g*-poly(AA-*co*-HEMA)/mica nanocomposite hydrogels with 5 to 15% (w w^{-1} of the monomer) mica loadings are shown as the representative SEM micrographs in Figure 2. The relatively smooth surface of the CS hydrogel and the flat sheets of mica at approximately 1 - 3 micrometers along with their aggregated state is clearly visible (Figure 2(a,b)). The surface of the CS-*g*-poly(AA) hydrogel (see Figure 2(c)) exhibits the larger porous structure in many areas than those of CS-*g*-poly(HEMA) (see Figure 2(d)) and CS-*g*-poly(AA-*co*-HEMA) hydrogel (see Figure 2(e,f)). The surface morphology of the CS-*g*-poly(HEMA) hydrogel shows a gel network surrounded by a wide spread of uniformly distributed micro-pores and this is especially regular on the surface of the CS-*g*-poly(AA-*co*-HEMA) hydrogel (Figure 2(d)). The CS-*g*-poly(AA-*co*-HEMA) hydrogel surface exhibits further a nano-porous structure (Figure 2(e,f)).

The internal morphologies of the CS-*g*-poly(AA-*co*-HEMA)/mica nanocomposites containing 5 - 15% w w^{-1} mica of the monomer (Figure 2(g-j)) are slightly different from those of the mica-free CS-*g*-poly(AA-*co*-HEMA). It is seen that the higher the mica loading, the more the surface roughness increased and that the mica flakes are imbibed in the inner areas of the gel. When the mica loadings were high, they were agglomerated, aggregated, resided, deposited and covered the whole polymer surface. Based on these results, CS-*g*-poly(AA-*co*-HEMA)/mica nanocomposite hydrogels are confirmed to have been successfully synthesized. One must state that no residual HEMA was retained in the resulting hydrogels because no indication of the double bonds peaks was found in the IR spectra because many extractions of the unused materials were made in solvent.

For Peer Review

3.4 XRD and TEM analyses

The XRD pattern of the CS hydrogel (Figure 3(a)) shows the 2-theta of CS at 10.53° and 19.93°, which corresponds to the hydrated crystals of low crystallinity of the form I and crystallinity of the form II, respectively.[33,34] The XRD pattern of CS-*g*-poly(AA), CS-*g*-poly(HEMA) and CS-*g*-poly(AA-*co*-HEMA) exhibit the broader and weaker peaks at 20.19, 18.49 and 20.31°, respectively, whereas the 2-theta at 10.53° of all these three CS grafted hydrogels disappeared. These indicated that the crystallinity of the grafted CS was dramatically decreased. Changes in the intensity of the peaks at approximately 20° relate to different packing of the chains and/or different hydrogen bonding networks in the grafted CS.[35] Thus, the introduction of AA and/or HEMA chains onto the surface of the CS causes the breakdown of its crystallinity. These results confirmed that the grafting of polymer onto the CS chain occurred.[33,34,36] The XRD patterns of mica revealed 2-theta values of 7.13 and 9.22° that correspond to a basal spacing of 13.58 and 9.58 Å, respectively. The XRD patterns of the CS-*g*-poly(AA-*co*-HEMA)/mica nanocomposite hydrogel reveal that the 2-theta value of mica in the nanocomposite hydrogels were shifted towards a lower angle (6.27°) and that the interlayer spacing of mica increased by 1.7 Å compared with that of the swelling mica. This confirms that intercalation had taken place and that the CS-*g*-poly(AA-*co*-HEMA)/mica nanocomposite hydrogels are intercalated composites with more spacing in the silicate layers.[37] In addition, it also shows that increasing the mica loadings from 5 to 15% (w w^{-1} based on the weight of monomer) does not affect the intercalated structure of the CS-*g*-poly(AA-*co*-HEMA)/mica nanocomposite hydrogels but rather they exhibit the same basal spacing. These results agree well with the previous report of Wang and coworkers.[12]

For Peer Review

Representative TEM micrographs of the CS-*g*-poly(AA-*co*-HEMA)/mica nanocomposite hydrogels with mica loadings of 5, 7, 10 and 15% w w^{-1} of the monomer are shown in Figure 4. The dark lines in Figure 4 belong to the mica structure and the bright area is the grafted chitosan matrix. All the TEM micrographs of nanocomposite hydrogels revealed that the distance between the two adjacent dark lines, the spacing of the two silicate layers, results in an intercalated structure. Indeed, parts of the silicate layer can be seen in Figure 4(a-d). The results of the TEM analysis are consistent with the XRD data (Figure 3), and support that CS-*g*-poly(AA-*co*-HEMA)/mica nanocomposite hydrogels have an intercalated structure and no significant if any level of an exfoliated structure.

3.5 Equilibrium water absorbency

3.5.1 Effect of monomer type (AA or HEMA) on the properties of the grafted CS hydrogels

The equilibrium water absorbency of CS alone was rather low but was significantly affected by the copolymerization with AA, but not with HEMA (Table 1). CS-*g*-poly(AA) had ten-fold higher water absorbency, whereas the water absorbency of the CS-*g*-poly(HEMA) was not significantly different to that for CS alone (Table 1). The water absorbency of the CS-*g*-poly(AA-*co*-HEMA) decreased ~1.2- and 3.2-fold as the AA: HEMA ratios decreased from 3:1 to 1:1 and 1:3, respectively (Table 1). That the water absorbency of CS-*g*-poly(AA-*co*-HEMA) increased as the content of AA increased is due to the increase in the density of hydrophilic groups from the carboxylic acid contents,[38] which then provides a greater repulsion of the anionic portion allowing for the expansion of the polymer chains. This also then explains the increased water absorbency of the CS-*g*-poly(AA)

For Peer Review

hydrogels over that of the CS hydrogels. On the other hand, CS-*g*-poly(HEMA) had very low water absorbency because HEMA is not as polar as AA but rather has a rather rigid chain due to the methacrylate substituent group. The longer chain of the poly(HEMA) hydrogel thus is likely to have resulted in more molecular entanglements that limited the chain expansion[39] and caused the water absorbency of the CS-*g*-poly(HEMA) hydrogel to decrease. Thus, although CS-*g*-poly(HEMA) would be unlikely to be beneficial to intercalate with mica, the HEMA moiety is more compatible with human cells than the other types of monomer moieties.

3.5.2 Effect of mica loading

The equilibrium water absorbency of the CS-*g*-poly(AA-*co*-HEMA) hydrogel at a 1:1 AA: HEMA molar ratio was ~5.4- and 5-fold higher than that of CS or CS-*g*-poly(HEMA), respectively, but almost half that of the CS-*g*-poly(AA) hydrogel (Table 1). The addition of mica at 5, 7 or 10% (w w^{-1} of monomer) caused a 1.2-fold drop in the equilibrium water absorbency from that seen with the mica-free CS-*g*-poly(AA-*co*-HEMA) hydrogel, but did not vary significantly between the three different mica loading levels (Table 1). In contrast, when the mica loading was increased to 15% w w^{-1} of monomer, the water absorbency was significantly decreased a further 1.3-fold compared to that seen with the 5 – 10% w w^{-1} mica loaded CS-*g*-poly(AA-*co*-HEMA), or 1.54-fold less than that for the mica-free CS-*g*-poly(AA-*co*-HEMA). This is because the polymer chains were inserted into the spacing between the silicate layers of mica and so the polymer chains were restricted in these limited spaces and so less able to expand. Another reason could be the degree of rigidity of the nanocomposite hydrogel that is induced by the mica. This also supports the notion that the structure of this nanocomposite hydrogel was intercalated.

For Peer Review

3.6 Antibacterial activity

Particle sizes of the CS, CS-*g*-poly(AA-*co*-HEMA) hydrogels and CS-*g*-poly(AA-*co*-HEMA)/mica nanocomposite hydrogel were in the range of 200 - 400 μm by the sieve size 50-100 mesh which is anticipated to have an important effect on the bacterial growth inhibitio.[40] This was therefore evaluated using a co-culture of *S. aureus* with each hydrogel type and evaluating the bacterial growth relative to the control culture by measuring the culture turbidity by absorbance (after removal of the hydrogel by filtration), and by total plate counts of replication competent ("viable") cells, over a 24 h time period.

3.6.1 Turbidity method

This well used method assumes that the turbidity of a medium solution increases solely due to the increase in the number of bacterial cells. Although this method is easy to perform the bacteria sample must be in a liquid suspension state, and typically it can only be used to detect bacteria in the range of 10^6 to 10^7 bacteria ml^{-1}. Moreover, the measurement of bacterial growth in the lag phase is less accurate and is an indirect measurement that needs a calibration curve, where a direct measurement of bacterial counts must be performed.

The preliminary results of the antibacterial activity testing of the CS-*g*-poly(AA-*co*-HEMA) hydrogel, evaluated by measuring the optical density at 610 nm every 2 h and compared with the negative control (containing only the medium and the gram-positive *S. aureus*), revealed three phases in the growth cycle (Figure 5). The lag phases of S. aureus growth in the negative control and in the presence of CS-g-poly(AA-co-HEMA) hydrogel were similar, lasting for 4 h. Then, during the exponential phase, the growth rate of *S. aureus* grown in MHB containing the CS-*g*-

For Peer Review

poly(AA-*co*-HEMA) hydrogel was lower than that of the negative control during the first 2 h of growth (4 - 6 h of total culture time), but then this growth rate decreased in the control culture from after 6 h up to reaching the start of the stationary phase (12 h), whereas the growth rate did not slow down in the cultures with CS-*g*-poly(AA-*co*-HEMA) until 10 - 12 h of total culture time, by which time the total bacterial number (as culture optical density) was slightly higher (1.5-fold) than in the control culture. From 12 – 24 h of total culture time, *S. aureus* in both conditions remained in stationary phase. Thus, the presence of the CS-*g*-poly(AA-*co*-HEMA) hydrogel appeared to render a slower early exponential growth rate of *S. aureus* (or to delay it) but did not reduce the final bacterial density reached after 12 – 24 h in the stationary phase. Since we did not count the viable bacteria that are attached to the gel, or wash them out from the gel, then the CS-grafted hydrogels may not be inhibitory at all but rather the bacteria grow attached to the gel surface and so are not in suspension first and only in suspension subsequently after the gel surface is full swollen and thus has the apparent delayed kinetics appearance.

3.6.2 The total Plate count method

The antibacterial activities of sterile sodium ampicillin (positive control), CS and grafted CS hydrogels against *S. aureus* were determined by the total plate count method. The mean CFU ml^{-1} and the relative inhibition of CS and grafted CS hydrogels are summarized in Table 2. The relative inhibition observed with the CS hydrogel was 2.9-fold greater at 6 h of culture time (early log phase) than that after 8 h of culture (the late log phase). When the CS was grafted with poly(AA), the antibacterial activity was significantly improved 1.53- and 4.23-fold after both 6 and 8 h of culture at 93 and 89% relative inhibition, respectively, because of the

For Peer Review

hydrophilicity of poly(AA),[41] and the biological activity of the free amino groups at the C-2 position of the native CS.[42] The higher antibacterial activities of the CS-*g*-poly(AA) hydrogel can be caused by the interaction between the negative charges on the bacteria surface with the positive surface of the CS-*g*-poly(AA). The more positively charged hydrogels could promote bacterial adhesion onto the hydrogel surface and reduce the remaining amount in the free suspension, resulting in a decrease in the bacteria colonies in the liquid medium. It is relevant to note here that the amount (molar ratio) of the AA or HEMA monomers that were grafted onto the CS is almost the same for the three different grafted CS derivatives studied here.

It was anticipated that the pores on the CS-*g*-poly(AA) hydrogel surface would improve the ability to capture bacteria. Although, the relative inhibition of the CS-*g*-poly(AA-*co*-HEMA) hydrogel would be higher than that of CS, because of the hydrophilicity resulting from the carboxyl group of poly(AA), the surface of the CS-*g*-poly(AA-*co*-HEMA) hydrogel is much rougher than the ungrafted CS hydrogel surface, which may increase bacterial adhesion sites and result in a higher antibacterial activity in the CS-*g*-poly(AA-*co*-HEMA) hydrogel than that of the CS. However, the relative inhibition of the CS-*g*-poly(AA-*co*-HEMA) hydrogel was found to actually be 1.35- and 3.3-fold lower than that of the CH-*g*-poly(AA) hydrogel in the early (6 h) and late (8 h) log phases, respectively. This is likely to be due to the decreased hydrophilicity of the HEMA moiety.[41] Thus, graft copolymerization of CS with a 1:1 molar ratio of AA: HEMA can delay (or inhibit) the growth of *S. aureus* in the early exponential phase.

The antibacterial activity of the CS-*g*-poly(AA-*co*-HEMA)/mica nanocomposite hydrogels are summarized in Table 2. The relative inhibition of CS-*g*-poly(AA-*co*-HEMA)/mica nanocomposite hydrogels having mica loadings at 7 and

For Peer Review

10% w w^{-1} of the monomer was slightly higher (1.3- and 1.11-fold) at a culture time of 6 h than that of the CS and CS-*g*-poly(AA-*co*-HEMA) hydrogel, respectively. This finding is in agreement with those reported by Wang et al..[15] However, CS-*g*-poly(AA-*co*-HEMA) exhibited higher relative inhibition against *S. aureus* growth by 1.2- and 1.1-fold comparing with 10 and 7% w w^{-1} mica loading, respectively, at 8 h of culture. Increasing the mica loading to 15% w w^{-1} of the monomer significantly decreased the apparent antibacterial activity 2.03- and 2.13-fold of that seen with no mica addition, and 2.25- and 1.9-fold of that seen with a 7% w w^{-1} mica loading after 6 and 8 h of culture, respectively. This result agreed quite well with Meng et al.,[16] finding that CS intercalated mica hydrogels could kill more bacteria than the neat CS or the clay minerals.

Nanocomposite hydrogels can generate a larger surface area to absorb more bacterial colonies and so give a greater chance to increase the antibacterial activity through interactions between the positive charges of the CS hydrogel and the negative charges on the cytoplasmic cell membrane of the bacteria.[15,42] In addition, *S. aureus* does not have an outer membrane to prevent the influx of foreign molecules[42] and so it can be inhibited more easily. However, the higher mica loading at 15% w w^{-1} of the monomer revealed a significantly decreased level of relative inhibition of *S. aureus* growth. This might be because the higher mica content screens and prevents the polymer chains from adhering with the bacteria to trigger the antibacterial activity.

3.6.3 Minimum inhibition concentration (MIC)

The MIC obtained for the CS-*g*-poly(AA) at 1.56 mg ml^{-1} against the 0.01 A_{610} Units of *S. aureus* cultured in MHB for 24 h (i.e. to the late stationary phase) at room temperature was 16- and >16-fold better than that of CS and CS-*g*-poly(HEMA),

For Peer Review

respectively (Table 3). These MICs agree with that of viable counts and relative inhibition of *S. aureus* in the log phase of growth (Table 1). The extent of the water absorbency and acidity of the hydrogels plays influencing roles as described in the total plate count method for the MIC result. The more the hydrogel expanded, the higher the number of colonies of *S. aureus* that could be trapped and inhibited through the diffusion effect by water in the hydrogel. The higher acidic moiety of the CS-*g*-poly(AA) hydrogels, which carry a higher positive charge, may enhance the inhibitory effect with CS. It is worth noting that the presence of the COO^- group in the poly(AA) containing hydrogels (CS-*g*-poly(AA) and CS-*g*-poly(AA-*co*-HEMA)) becomes a major driving force for bacterial adhesion in the positively charged CS. AA in the feed is a key factor governing the antibacterial property in the resulting hydrogel and nanocomposites hydrogels. The high MIC value for the CS-*g*-poly(HEMA) was potentially caused by the proposed semi-IPN structure and the rigid conformation of poly(HEMA) chains grafted onto the CS backbones.

Surprisingly, the CS-*g*-poly(AA-*co*-HEMA)/mica nanocomposite hydrogels with mica loadings of 5, 7, 10 and 15% w w^{-1} of the monomer had the same MIC values as each other and as that for the CS-*g*-poly(AA-*co*-HEMA) hydrogel (Table 3). This correlates with the almost constant water absorbency observed for the CS-*g*-poly(AA-*co*-HEMA) and the CS-*g*-poly(AA-*co*-HEMA)/mica nanocomposite hydrogels regardless of the mica loadings but relatively lower water absorbency at 15% w/w. Likewise, a much higher concentration of CS (25 mg ml^{-1}) or CS-*g*-poly(HEMA) (>25 mg ml^{-1}) or CS-*g*-poly(AA-*co*-HEMA)/mica nanocomposite hydrogels (12.5 mg ml^{-1}) is required for inhibiting *S. aureus* after 24 h of incubation.

Typical SEM micrographs of *S. aureus* cells cultured for 24 h in the MHB media alone (negative control), and in the various grafted CS copolymer and CS-*g*-

For Peer Review

poly(AA-*co*-HEMA)/mica nanocomposite hydrogels are shown in Figure 6. Since the positive control in the total plate count did not produce any viable cells, then the positive control in MIC was not performed. The normal roundish-shapes of *S. aureus* cells were evident when cultured in the MHB media alone and also as adhered on the surface of mica (Figure 6(a,b), respectively). However, the cell walls of some of the *S. aureus* in or on the CS-*g*-poly(HEMA) and CS-g-poly(AA-*co*-HEMA) hydrogels after culture for 24 h were destroyed to give open cells (Figure 6(c) as shown in Figure 6(d)). Moreover, of the *S. aureus* cells that were adsorbed and immobilized on the surface and in the pores of the CS-*g*-poly(AA-*co*-HEMA)/mica nanocomposite hydrogels, some had distorted shapes and were destroyed to give fractured cell walls and these were randomly distributed in the hydrogel matrix (Figure 6(e-h)).

Although the water absorbency of the nanocomposite hydrogels was relatively lower than that of the grafted CS hydrogel, the hydrogels had larger surface area to absorb more bacterial colonies.[15] With this compensation, the MIC values of nanocomposite hydrogels are not different from that of the grafted CS hydrogel. Thus, CS-*g*-poly(AA-*co*-HEMA) hydrogel or CS-*g*-poly(AA-*co*-HEMA)/mica nanocomposite hydrogels were at an equilibrium condition and gave similar MIC values.

The MIC values and SEM micrographs support that the mica content in the grafted CS hydrogel did not influence the antibacterial activity. On the other hand, the different results from the plate count method are caused by the absorbance assays undertaken in the mid- and late-log phases of growth at 6 and 8 h, respectively, whilst the MIC was evaluated at a late stationary phase (24 h). The different culture times could have resulted in different cell numbers due to different chances of cell adsorption by the nanocomposite hydrogels, as well as growth and death rates

For Peer Review

4. Conclusion

CS was used to graft with AA and/or HEMA to give the grafted-CS hydrogels. CS-*g*-poly(AA-*co*-HEMA)/mica nanocomposite hydrogels were synthesized at different mica loadings and all hydrogels were characterized by FT-IR spectroscopy, SEM, XRD, TEM and equilibrium water absorbency. FT-IR spectroscopy indicated that the CS was grafted at the NH_2 and OH sites on the CS backbone. The water absorbency of the CS-*g*-poly(AA) hydrogel was the highest whilst those of CS and CS-*g*-poly(HEMA) were the lowest. The CS-*g*-poly(AA-*co*-HEMA)/mica nanocomposite hydrogels had an intercalated structure, as revealed by XRD and TEM analyses.

At the fixed 1:1 molar ratio of AA: HEMA, the extent of water absorbency of the nanocomposite hydrogels was constant at 5, 7 and 10% (w w^{-1} of the monomer) mica loading but slightly decreased at 15% w w^{-1} mica loading. The CS-*g*-poly(AA) hydrogel can inhibit the early-to-mid-log phase growth of *S. aureus* up to 93% with a MIC value as low as 1.56 mg ml^{-1}. For the CS-*g*-poly(AA-*co*-HEMA)/mica nanocomposite hydrogels, the relative inhibition was very similar (at ~81%) with mica loadings of 5, 7 and 10% w w^{-1} of the monomer, but abruptly decreased at a 15% w w^{-1} mica loading. Regardless of the mica loading levels in the CS-*g*-poly(AA-*co*-HEMA)/mica nanocomposite hydrogels, the MIC value at the late stationary phase was constant at 12.5 mg ml^{-1}. The CS-*g*-poly(HEMA) had a greater MIC (>25 mg ml^{-1}) than CS (25 mg ml^{-1}). Several possible explanations for the different inhibitory activities against *S. aureus* are discussed, but await further research for clarification.

For Peer Review

Acknowledgements

The authors would like to acknowledge the financial support from the Thailand Research Fund under the Research Team Aided Program Contract no. RTA5080004. Partial financial support from the Graduate School, Chulalongkorn University is acknowledged. The provision of research facilities by the Imaging Polymer Laboratory of Chulalongkorn University's Department of Imaging and Printing Technology, Faculty of Science is highly appreciated. English edition by the Publication Counselor Unit of the Research Division, Faculty of Science, Chulalongkorn University, and fruitful suggestion provided by Dr. Robert Butcher are highly appreciated.

For Peer Review

References

1. Devine, D. M.; Higginbotham, C. L. Eur Polym J 2005, 41, 1272.
2. Rinaudo, M. Prog Polym Sci 2006, 31, 603.
3. Dos Santos, K. S. C. R.; Coelho, J. F. J.; Ferreira, P.; Pinto, I.; Lorenzetti, S.G., Ferreira, E. I.; Higa, O. Z.; Gil, M. H. Int J Pharm 2006, 310, 37.
4. Mahdavinia, G. R.; Pourjavadi, A.; Hosseinzadeh, H.; Zohuriaan, M. J. Eur Polym J 2004, 40, 1399.
5. Jalal Zohuriaan-Mehr, M. Iran Polym J 2005, 14, 235.
6. Carenza, M. Int J Radiat Appl Instrum C Radiat Phys Chem 1992, 39, 485.
7. Schweikl, H.; Hartmann, A.; Hiller, K-A.; Spagnuolo, G.; Bolay, C.; Brockhoff, G.; Schmalz, G. Dent Mater 2007, 23, 688.
8. Pawlowska, E.; Poplawski, T.; Ksiazek, D.; Szczepanska, J., Blasiak, J. Mutation Res 2010, 696, 122.

9. Tanodekaew, S.; Prasitsilp, M.; Swasdison, S.; Thavornyutikarn, B.; Pothsree, T.; Pateepasen, R. Biomaterials 2004, 25, 1453.

10. Sahu, K.; Verma, Y.; Sharma, M.; Rao, K. D.; Gupta, P. K. Skin Res Tech 2010, 16, 428.

11. Tang, C.; Chen, N.; Zhang, Q.; Wang, K.; Fu, Q.; Zhang, X. Polym Degrad Stabil 2009, 94, 124.

12. Wang, X.; Du, Y.; Luo, J.; Yang, J.; Wang, X.; Shi, X.; Hu, Y. Polymer 2006, 47, 6738.

13. Wang, X.; Du, Y.; Luo, J.; Yang, J.; Wang, W.; Kennedy, J. F. Carbohydr Polym 2009, 77, 449.

14. Xie, Y.; Wang, A.; Liu, G. Polym Compos 2010, 3, 89.

15. Wang, X.; Du, Y.; Luo, J.; Lin, B.; Kennedy, J. F. Carbohydr Polym 2007, 69, 41.

16. Meng, N.; Zhou, N.; Zhang, S.; Shen, J. Appl Clay Sci 2009, 42, 667.

17. Bozhilov, K. N.; Xu, Z.; Dobrzhinetskaya, L. F.; Jin, Z-M.; Green II, H. W. Lithos 2009, 109, 304.

18. Tjong, S. C. Synthesis and structure-property characteristics of clay-polymer Nanocomposites, Nanocrystalline Materials; Oxford: Elsevier, 2006; Chapter 10; p. 311.

19. Hsu, S.; Tseng, H.; Hung, H.; Wang, M.; Hung, C.; Li, P.; Lin, J. Appl Mater Interfaces 2009, 1(11), 2556.

20. Li, P.; Wei, J.; Chiu, Y.; Su, H.; Peng, F.; Lin, J. Appl Mater Interfaces 2010, 2, 1608.

21. Patil, D. R., Fanta, G. F. J Appl Polym Sci 1993, 47, 1765.

22. Lanthong, P.; Nuisin, R.; Kiatkamjornwong, S. Carbohydr Polym 2006, 66, 229.

For Peer Review

23. Mun, G. A.; Nurkeeva, Z. S.; Dergunov, S. A.; Nama, I. K.; Maimakov, T.P.; Shaikhutdinov, E. M.; Lee, S. C.; Park, K. React Funct Polym 2008, 68, 389.

24. Sun, T.; Zhou, D.; Xie, J.; Mao, F. Eur Food Res Technol 2007, 225, 451.

25. Zhang, J.; Wang, Q.; Wang, A. Carbohydr Polym 2007, 68, 367.

26. Singha, V.; Sharmaa, A. K.; Tripathi, D. N.; Sanghib, R. J Hazard Mater 2009, 161, 955.

27. Huacai, G.; Wan, P.; Dengke, L. Carbohydr Polym 2006, 66, 372.

28. Mishra, D. K.; Tripathy, J.; Srivastava, A.; Mishra, M. M.; Behari, K. Carbohydr Polym 2008, 74, 632.

29. Casimiroa, M. H.; Botelho, M. L.; Leal, J. P.; Gil, M. H. Radiat Phys Chem 2005, 72, 731.

30. Semenzato, S.; Lorenzetti, A.; Modesti, M.; Ugel, E.; Hrelja, D.; Besco, S.; Michelin, R. A.; Sassi, A.; Facchin, G.; Zorzi, F.; Bertani, R. Appl Clay Sci 2009, 44, 35.

31. Dai, H.; Li, H.; Wang, F. Surf Coat Technol 2006, 201, 2859.

32. Bayramoğlu, G.; Arica, M. Y. Colloids Surf A 2002, 202, 41.

33. Wang, J. P.; Chen, Y. Z.; Zhang, S. J.; Yu, H. Q. Bioresour Technol 2008, 99, 3397.

34. Luckachan, G. E.; Pillai, C. K. S. Carbohydr Polym 2006, 64, 254.

35. Kittur, F. S.; Kumar, A. B. V.; Tharanathan, R. N. Carbohydr Res 2003, 338, 1283.

36. Krishna Rao, K. S. V.; Chung, I.; Ha, C. S. React Funct Polym 2008, 68, 943.

37. Sivudu, K. S.; Thomas, S.; Shailaja, D. Appl Clay Sci 2007, 37, 185.

38. Sperling, L. H. Introduction to Physical Polymer Sciences. 4th ed.; New York: John Wiley & Sons, 2006; p. 477.

For Peer Review

39. Zhou, Y.; Yang, D.; Gao, X.; Chen, X.; Xu, Q.; Lu, F.; Nie, J. Carbohydr Polym 2009, 75, 293.

40. Mohan, Y. M.; Lee, K.; Premkumar, T.; Geckeler, K. E. Polymer 2007, 48, 158.

41. Oh, S. T.; Han, S. H.; Ha, C. S.; Cho, W. J. J Appl Polym Sci 1996, 59, 1871.

42. Je, J.; Kim, S. J Agric Food Chem 2006, 54, 6629.

For Peer Review

Table 1. The water absorbency of hydrogels derived from CS, AA and /or HEMA grafted-CS copolymers and CS-g-poly(AA-*co*-HEMA)/mica nanocomposites.

Polymer	AA: HEMA (mol ratio)	Mica (w w^{-1} of monomer)	Water absorbency (g g^{-1})[1]
CS	--	--	10 ± 2
CS-*g*-poly(AA)	--	--	101 ± 4
CS-*g*-poly(HEMA)	--	--	11 ± 1
CS-*g*-poly(AA-*co*-HEMA)	3:1	--	64 ± 2
	1:1	--	54 ± 3
	1:3	--	20 ± 2
	1:1	5	45 ± 3
	1:1	7	44 ± 1
	1:1	10	46 ± 2
	1:1	15	35 ± 5

[1]Data are shown as the mean ± 1 SD and are derived from 5 repeats. Means within the column are significantly different ($p<0.05$).

For Peer Review

Table 2. Total plate counts (replication competent cells) and the relative inhibition of growth of *S. aureus* in the presence of sodium ampicillin and the hydrogels of CS, AA and/or HEMA grafted-CS copolymers and CS-*g*-poly(AA-*co*-HEMA)/mica nanocomposites with various mica loadings.

Sample type	Mica (% w w^{-1})	6 h culture time		8 h culture time	
		CFU ml^{-1} (x 10^9)[1]	Relative inhibition (%)	CFU ml^{-1} (x 10^9)[1]	Relative inhibition (%)
Negative control[2]	--	6.95 ± 1.51	-	8.15 ± 1.25	-
Positive control[3]	--	0	100	0	100
CS[4]	--	2.7 ± 0.25	61	6.4 ± 1.68	21
CS-*g*-poly(AA)[4]	--	0.52 ± 0.48	93	0.91 ± 0.85	89
CS-*g*-poly(HEMA)[4]	--	2.18 ± 0.28	69	5.95 ± 1.25	27
CS-g-poly(AA-*co*-HEMA)[4]	--	1.90 ± 0.19	73	2.92 ± 0.07	64
CS-*g*-poly(AA-*co*-HEMA)[4]	7	1.4 ± 0.37	81	3.6 ± 0.55	57
CS-*g*-poly(AA-*co*-HEMA)[4]	10	1.5 ± 0.34	81	3.9 ± 0.31	54
CS-*g*-poly(AA-*co*-HEMA)[4]	15	5.0 ± 1.68	36	5.9 ± 2.4	30

[1]CFU ml^{-1} is shown as the mean ± 1 SD and are derived from 6 repeats. Means within a column or across a row are significantly different ($p<0.05$).

[2]Negative control contains only the MHB medium and *S. aureus*.

[3]Positive control contains 250 mg of the sodium ampicillin, MHB medium and *S. aureus*.

[4]All hydrogel samples were co-cultured with *S. aureus* in MHB media at 250 mg ml^{-1}.

For Peer Review

Table 3. Minimum inhibition concentration of hydrogels derived from CS, AA and/or HEMA grafted-CS copolymers and CS-*g*-poly(AA-*co*-HEMA)/mica nanocomposites with various mica loadings.

Sample test	Mica (% w w^{-1})	CFU ml^{-1} (x 10^8)[1]	MIC (mg ml^{-1})[2]
Negative control[3]	-	18 ± 1.0	-
CS[4]	--	10 ± 0.6	25
CS-*g*-poly(AA)[4]	--	3.0 ± 0.4	1.56
CS-*g*-poly(HEMA)[4]	--	6.6 ± 3.5	> 25
CS-*g*-poly(AA-*co*-HEMA)[4]	--	1.2 ± 0.5	12.5
CS-*g*-poly(AA-*co*-HEMA)[4]	5	1.1 ± 0.4	12.5
CS-*g*-poly(AA-*co*-HEMA)[4]	7	5.1 ± 0.6	12.5
CS-*g*-poly(AA-*co*-HEMA)[4]	10	4.6 ± 0.4	12.5
CS-*g*-poly(AA-*co*-HEMA)[4]	15	4.9 ± 4.9	12.5

[1]CFU ml^{-1} is shown as the mean ± 1 SD and is derived from 3 repeats. Means within the column are significantly different ($p<0.05$).

[2]MIC are shown as mg ml^{-1} for a 2% (v v^{-1}) seeding of a late log phase culture of *S. aureus* in MHB media and evaluated at late stationary phase (24 hr of culture).

[3]Negative control contains only the MHB medium and *S. aureus*.

[4]All hydrogel samples were co-cultured with *S. aureus* in MHB media at 250 mg ml^{-1}.

For Peer Review

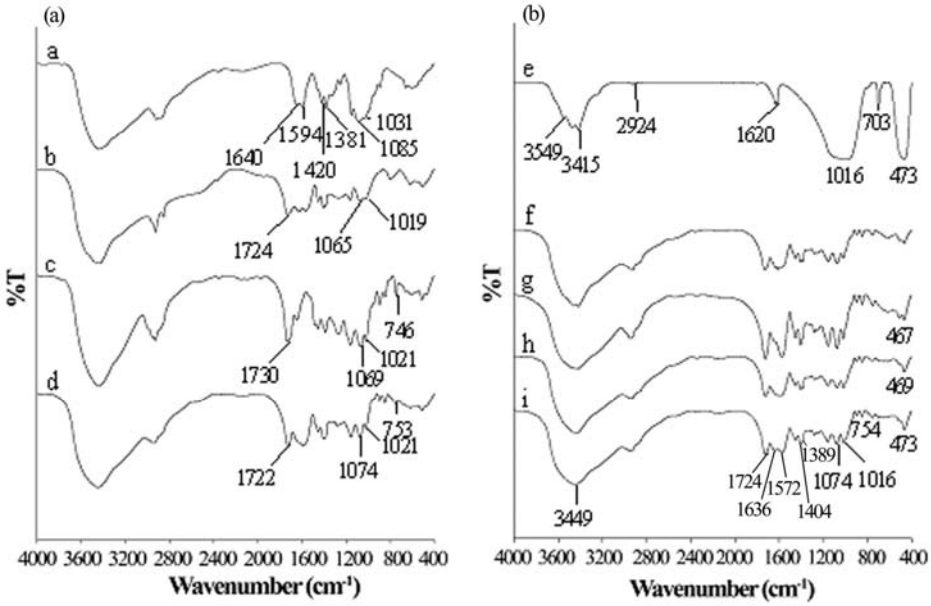

Figure 1

Representative FT-IR spectra of (A): (a) CS, and (b) CS-g-poly(AA), (c) CS-g-poly(HEMA) and (d) CS-g-poly(AA-co-HEMA) hydrogels, the last being synthesized with an AA: HEMA, N-MBA: CH, APS: CH and TEMED: CH molar ratios of 1, 0.11, 0.07 and 0.58, respectively; (B): (e) mica, and CS-g-poly(AA-co-HEMA)/mica nanocomposite hydrogels with mica loadings of: (f) 5%, (g) 7%, (h) 10% and (i) 15% w w-1 based on the monomer.
104x72mm (600 x 600 DPI)

eview

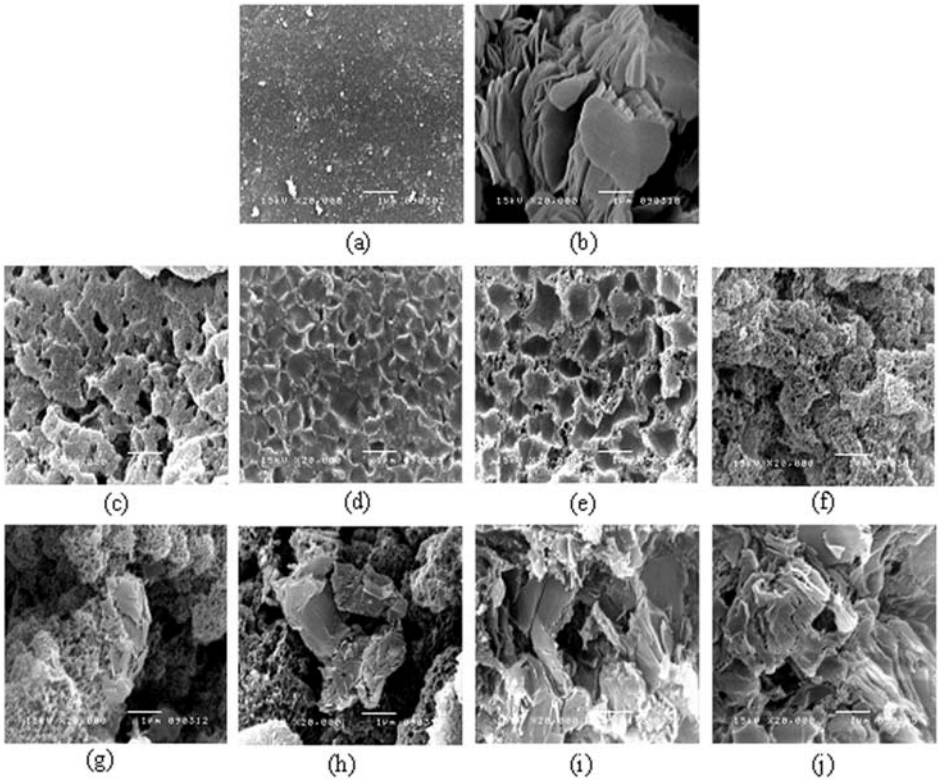

Figure 2

Representative SEM micrographs of (a) CS, (b) mica, (c) CS-g-poly(AA), (d) CS-g-poly(HEMA), (e, f) CS-g-poly(AA-co-HEMA), and CS-g-poly(AA-co-HEMA)/mica composite hydrogels synthesized with mica loading levels of (g) 5%, (h) 7%, (i) 10% and (j) 15% w w-1 of the monomer.
158x140mm (400 x 400 DPI)

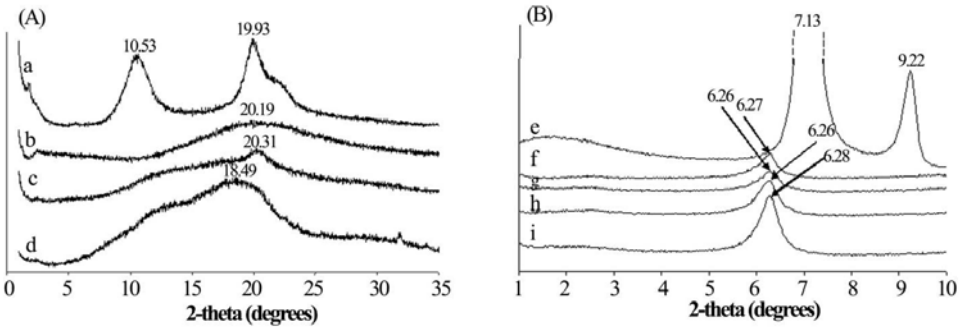

Figure 3

Representative XRD patterns of hydrogels synthesized from (A): (a) CS, (b) CS-g-poly(AA) synthesized with 1 g CS, 54 mmol AA, and N-MBA, APS and TEMED at 10%, 10% and 40% w w-1 of CS, respectively, (c) CS-g-poly(AA-co-HEMA) and (d) CS-g-poly(HEMA); (B): (e) mica, and CS-g-poly(AA-co-HEMA)/mica nanocomposite hydrogels synthesized with mica loadings of (f) 5%, (g) 7%, (h) 10% and (i) 15% w w-1 based on the monomer, 1 g CS, an AA: HEMA molar ratio of 1:1, and N-MBA, APS and TEMED at 10%, 10% and 40% w w-1 of CS, respectively.
60x24mm (600 x 600 DPI)

eer Review

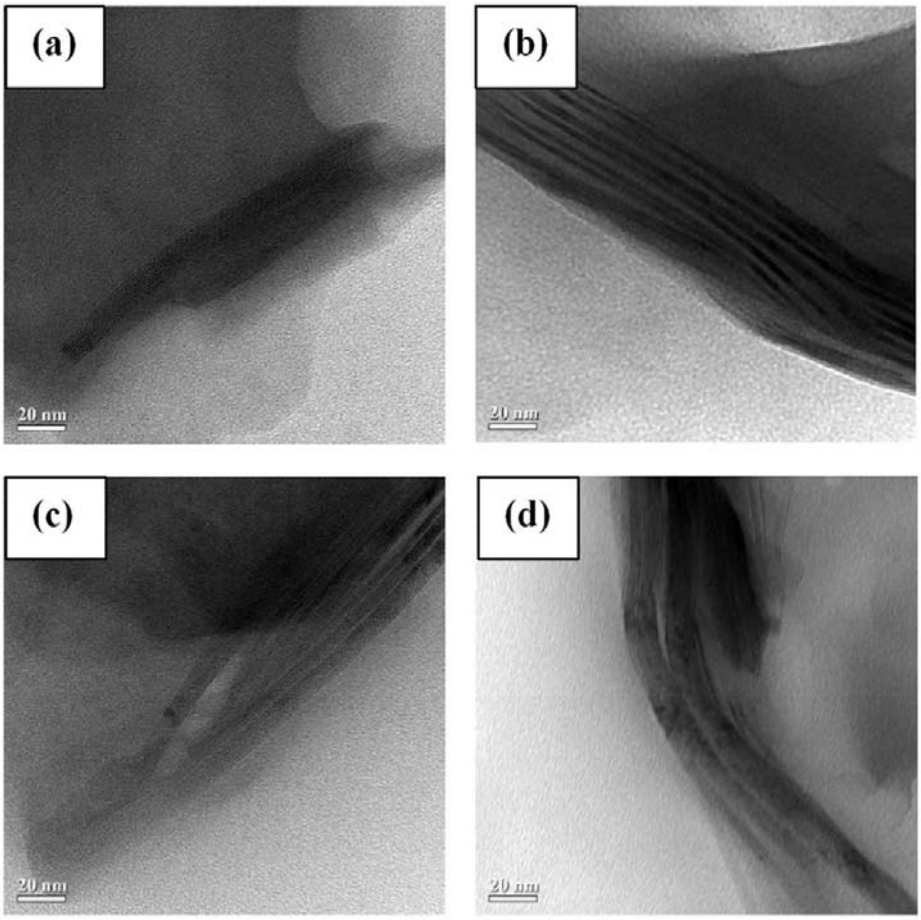

Figure 4

Representative TEM micrographs of CS-g-poly(AA-co-HEMA)/mica composite hydrogels synthesized with mica loadings of (a) 5%, (b) 7%, (c) 10% and (d) 15% w w-1 based on the monomer.
104x115mm (300 x 300 DPI)

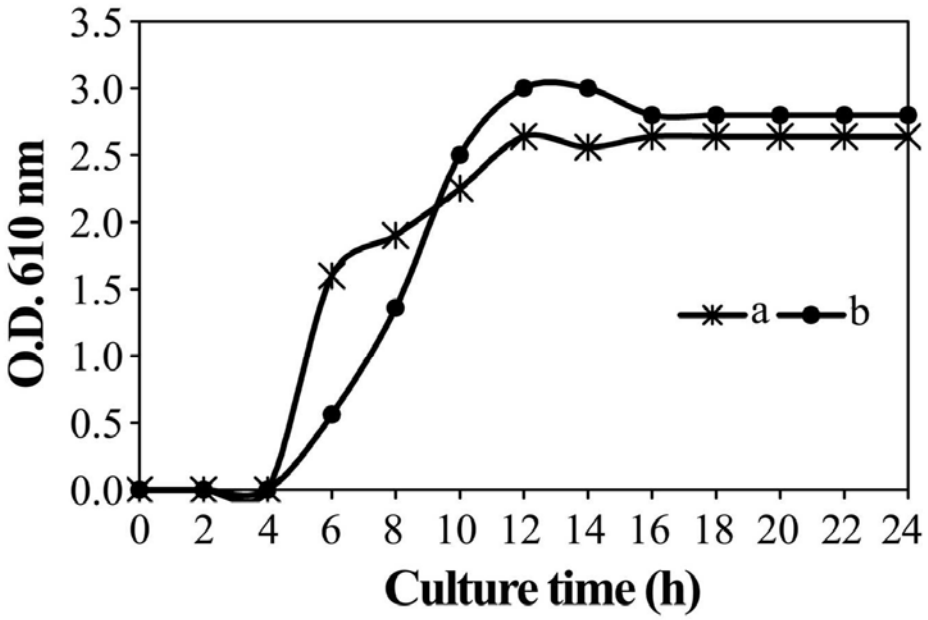

Figure 5

The optical density at 610 nm of S. aureus cultured in HMB media at various culture times with (a) the negative control, or 250 mg ml-1of (b) CS-g-poly(AA-co-HEMA) hydrogel prepared with 1 g CS, a AA: HEMA molar ratio of 1:1, and N-MBA, APS and TEMED at 10%, 10% and 40% w w-1 of CS, respectively, with polymerization performed at 250 pm and 60 °C for 60 min.
59x45mm (600 x 600 DPI)

view

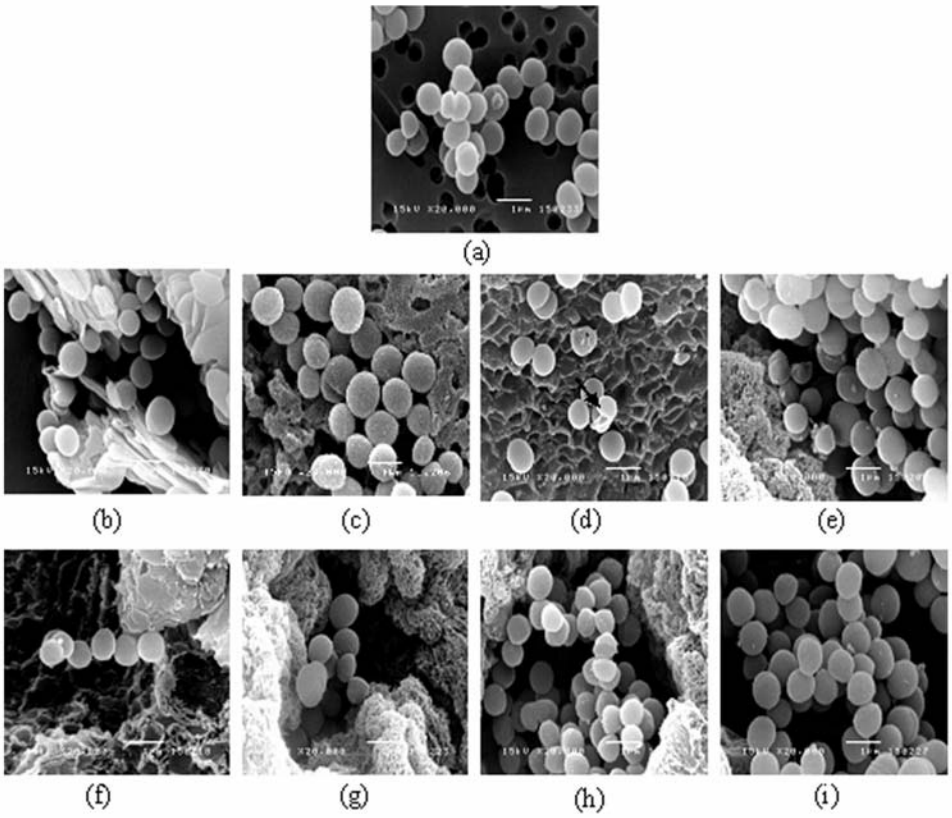

Figure 6

Representative SEM micrographs of S. aureus after co-culture for 24 h with (a) negative control, (b) mica, (c) CS-g-poly(AA), (d) CS-g-poly(HEMA), (e) CS-g-poly(AA-co-PHEMA) and CS-g-poly(AA-co-PHEMA)/mica nanocomposites with mica loadings of: (f) 5%, (g) 7%, (h) 10% and (i) 15% w w-1 based on the monomer. The arrow in (d) highlights a damaged cell.
152x142mm (600 x 600 DPI)

KAPOK I: CHARACTERISTCS OF KAPOK FIBER AS A POTENTIAL PULP SOURCE FOR PAPERMAKING

Somporn Chaiarrekij,* Apiporn Apirakchaiskul, Kuntinee Suvarnakich, and Suda Kiatkamjornwong

The potential use of kapok fiber for pulping and papermaking has been investigated. The kapok fibers were cooked using the optimal dosage of sodium hydroxide determined from the experiments. Then, the pulp was refined twice using a disc refiner with a disc gap of 1/100 inch and this kapok pulp was mixed with commercial hardwood pulp and/or softwood pulp at different blend ratios to make papers. Addition of the kapok pulp to the mixed pulps improved the tensile and burst strengths of the sheets but decreased the tear resistance and elongation. Brightness and opacity of the sheets were also dropped with the addition of kapok pulp to the mixed pulps. Water repellency of the sheets prepared from the kapok pulp mixed with the commercial pulps was also improved. These results indicate that kapok fiber can be a quality pulp source for papermaking, especially for packaging paper.

Keywords: Kapok fiber; Properties; Raw material; Papermaking

*Contact information: Department of Imaging and Printing Technology, Faculty of Science, Chulalongkorn University, Phayathai Road, Bangkok, 10330 Thailand; *Corresponding author: Huaja@hotmail.com*

INTRODUCTION

The kapok tree, *Ceiba pentandra (L.)* Gaertn. (Malvales: Malvaceae), formerly Bombacaceae family, is cultivated widely in Southeast Asia, as well as other parts of East Asia and Africa. The kapok fiber is an agricultural product obtained from the fruits of the kapok tree (Tang et al. 2008; Qiuling and Lin 2009). Kapok fibers have a hollow structure with a thin fiber wall and large lumen (Hong et al. 2005; Lim and Huang 2007). The diameter including the fiber wall is 16.5 ± 2.4 μm. The lumen diameter is 14.5 ± 2.4 μm and the fiber length is 25 ± 5 μm (Huang and Lim 2006). Kapok fibers are fluffy, light-weight and too inelastic to be spun, and so are good for stuffing beds, pillows and cushions. Chemical compositions of kapok fiber were differently reported by two groups of researchers. The first one mentioned that kapok fiber is chemically composed of 64% cellulose, 13% lignin and 23% pentosan on a weight basis (Kobayashi et al. 1977) while the other stated that it comprises of 35% cellulose, 21.5% lignin, 22% xylan and 13% of acetyl groups on a weight basis (Hori et al. 2000). Besides all those mentioned chemical compositions, they also contain a waxy cutin on the fiber surface which makes them water repellent and oil absorbent. Thus, they are also useful in oil removal applications (Hori et al. 2000; Khan et al. 2004; Huang and Lim 2006; Rengasamy et al. 2011).

There are few reports on utilizing blended kapok fibers for papermaking, such as, the blend of 75:25 (w/w) kapok fibers: bamboo pulp was treated with detergent and

sodium hydroxide before being used to produce paper (Malab et al. 2001). In this case, the combination of the two non-wood fibers significantly reduced the volume of the bamboo pulp, and the amounts of chemical reagents and energy consumption, without adversely affecting the paper strength properties. Another study has indicated that kapok fibers could potentially be pulped to produce paper (Chaiarrekij et al. 2008), but this claim has not been established and any products have not been further characterized. However, it has been observed that paper sheets made from kapok pulp seemed to demonstrate superior water resistant behavior even without any sizing agents being added.

Consequently, the optimum set of pulping conditions for the kapok fibers to give the best strength properties was investigated. This optimal set of pulping conditions was then employed to produce kapok pulp. The influence of kapok pulp on paper properties when the kapok pulp was mixed with commercial hardwood pulp and softwood pulp was also determined. The hypothesis being tested was that kapok pulp might increase the strength properties of the hybrid paper prepared from mixtures of kapok pulp with conventional commercial softwood pulp and/or hardwood pulp. It was thought that as well as providing better strength, paper made of kapok pulp might possess superior water resistance, which is generally required for a packaging paper.

EXPERIMENTAL

Materials

Before pulping, the kapok fibers (sourced from the north eastern part of Thailand) were washed, cleaned, and immersed in water for three weeks prior to manually squeezing out the excess water and cutting to 3-5 cm in length. The moisture content was determined using the moisture balance (FD-600, Kett Electric Laboratory, Japan). The commercial softwood (SW) pulp from Pine and hardwood (HW) pulp from Eucalyptus were obtained from the Crofton Pulp & Paper Mill, Canada and the Phoenix Pulp & Paper Public Co., Ltd, Thailand, respectively.

Methods

The experiment was divided into 2 parts. The first part was about determination of optimal pulping condition for kapok fiber, while the second part was about examining the effects of kapok pulp addition to commercial softwood and hardwood pulps on the properties of the resultant pulp and paper.

Determination of optimal pulping condition for kapok fiber

Kapok fibers were separately pulped using 10, 15, 20, and 25% (w/w) NaOH, based on the oven-dried pulp weight. The liquor-to-wood ratio was 17:1. The pulping was carried out in an autoclave digester, (UEC-2017A, Universal Engineering, India) with an initial digesting temperature at 40 °C. The pulp matrix was then gradually heated to 120 °C over 30 min. Pulping was proceeded at this temperature for another 120 min. The pulp was then extensively washed with tap water to remove the alkalinity from the pulp by controlling with a pH meter (Hanna HI 98128, Hanna Instrument, U.S.A.).

Kapok pulps were refined twice through a disc refiner, using a 1/100 inch disc gap (Andritz Sprout, U.S.A.). The degree of refining was determined following the Canadian Standard Freeness (CSF) standard, using a freeness tester (CF/A, Regmed, Brazil) according to TAPPI Standard Method T227 om-04. Kapok pulps were disintegrated in a standard disintegrator (Formax T-100, Adirondack, U.S.A.) for 100,000 revolutions in hot water (80 °C) to remove latency. The average length of 5,000 fibers per sample was automatically determined using a fiber quality analyzer (FQA, Optest, Canada) according to the TAPPI Standard Method T271 om-98 using the following equations.

The arithmetic average length of individual fibers (L) is calculated from equation (1):

$$L = \frac{\Sigma n_i l_i}{\Sigma n_i} \quad (1)$$

The length-weighted average length of the fibers (L_l) is calculated from equation (2):

$$L_l = \frac{\Sigma n_i l_i^2}{\Sigma n_i l_i} \quad (2)$$

The weight-weighted average length of the fibers (L_w) is calculated from equation (3):

$$L_w = \frac{\Sigma n_i l_i^3}{\Sigma n_i l_i^2} \quad (3)$$

where the number of fibers (n_i) is the number of fibers in each class of length (l_i).

The chemical composition of each pulp was determined using TAPPI Standard Method T222 om-98 for lignin determination, TAPPI Standard Method T203 cm-99 for alpha cellulose (α-cellulose) determination, and Browning's method for holocellulose determination (Browning 1963). The amount of hemicellulose was calculated from the difference between the holocellulose content and the alpha cellulose content.

Kapok pulp was also made into 60 g/m^2 handsheets on a Rapid-Köthen sheet former (RK-2A KWT, PTI, Austria) according to the ISO Standard Method 5269-2. The brightness and opacity of the handsheets were measured using an optical tester (Color Touch PC, Technidyne, U.S.A.), based on ISO Standard Methods 2470 and 2471, respectively. The tensile, burst, tear, and zero-span tensile strengths were measured using a tensile strength tester (Strograph E-S, Toyo Seiki, Japan), a burst strength tester

(SE002P, Lorentzen & Wettre, Sweden), a tear strength tester (Protear, Thwing-Albert, U.S.A.), and a modified tensile strength tester (Pendulum Tensile Strength Tester with special clamps adjustable to zero, Toyo Seiki, Japan), according to TAPPI Standard Method T494 om-01, T403 om-02, T414 om-04 and T231 cm-96, respectively. The contact angle of water in contact with surface of handsheet was automatically measured using the Pocket Goniometer PG-3 (Fibro System, Sweden) by capturing and processing the water droplet images. The dynamic mode was used to measure the rate of change of the contact angle as a function of time. The test was done following TAPPI standard T558 om-06.

The effects of the addition of kapok pulp to commercial softwood pulp and hardwood pulps on the properties of the resultant paper samples

Kapok pulp produced by using the set of optimal conditions previously described was bleached using 3% (w/w) aqueous hydrogen peroxide at a 1.5% consistency and 80 °C for 120 min. The product was disintegrated using a disintegrator (Formax T-100, Adirondack Machine, U.S.A.) for 100,000 revolutions in hot water (80 °C) to remove latency. Each commercial pulp was beaten in a valley beater (UEC-2018A, Universal Engineering, India) in which 360 g of the oven-dried pulp in 23 L of water was accommodated, according to TAPPI Standard method T200 sp-01. The softwood pulp and hardwood pulp were separately beaten to meet the Canadian Standard Freeness of 350 mL and 300 mL, respectively. Then, the bleached kapok pulp was mixed with the commercial beaten hardwood pulp, softwood pulp and mixed pulp (25:75 (w/w) softwood: hardwood) to make handsheets. These procedures of papermaking and paper characterization were repeated in the manner as described.

Statistical analysis

Parametric data were analyzed using the analysis of variance (ANOVA). In all cases, a p-value smaller than or equal to 0.05 was accepted as being a statistically significant difference. For all of the experiments, three replicates were performed.

RESULTS AND DISCUSSION

Determination of Optimal Pulping Condition

Chemical composition of kapok pulp

The effects of the sodium hydroxide solution on the chemical composition of the kapok pulp are summarized in Table 1. Analysis of the chemical composition of the pulps showed that an increased amount of sodium hydroxide in cooking liquor resulted in lower percentages of lignin, higher percentages of holocellulose and alpha cellulose, with lower percentages of hemicellulose. It should be noted that holocellulose is composed of alpha cellulose and hemicellulose. This finding was to be expected, since sodium hydroxide solution dissolves lignin. Carbohydrates, especially hemicellulose, can also be easily destroyed by sodium hydroxide, leaving a higher ratio of alpha cellulose behind. Since all of the P-values of the chemical compositions were lower than 0.05, the effects of sodium

hydroxide solution on kapok pulp chemical compositions were thus statistically significant.

Table 1. Effects of Sodium Hydroxide Concentration on the Chemical Composition of the Kapok Pulp

Pulp Chemical Composition	NaOH Dosage (% w/w)				
	10	15	20	25	P-value
Lignin (%)	19.20	18.27	17.57	17.53	0.0109*
Holocellulose (%)	76.12	76.53	78.49	78.50	0.0005*
Alpha cellulose (%)	65.63	69.87	69.65	69.96	0.0002*
Hemicellulose (%)	10.49	6.66	8.84	8.54	0.0007*
* Statistically significant since P-value is lower than 0.05					

Kapok pulp and fiber characteristics

The effects of sodium hydroxide treatment level on pulp yield, freeness and the average fiber length, characterized in terms of arithmetic, length-weighted, and weight-weighted criteria are summarized in Table 2, along with the percentage of fines.

Table 2. Pulp and Fiber Characteristics of the Kapok Pulp after Soda Pulping

Pulp and Fiber Properties	NaOH Dosage (% w/w)			
	10	15	20	25
Pulp yield (%)	62.40	51.25	44.69	40.46
Freeness (CSF, mL)	401	362	296	277
Average fiber length-Arithmetic (mm)	0.91	0.91	0.83	0.81
Average fiber length-Length weighted (mm)	1.51	1.49	1.32	1.28
Average fiber length-Weight weighted (mm)	2.26	2.17	1.93	1.83
Fines (%)	21.5	21.6	22.7	23.7

The results in Table 2 indicate that high sodium hydroxide concentration could also result in a lower pulp yield because of the removal of lignin and extractives. Also, high sodium hydroxide dosage could lead to carbohydrate degradation, especially with the hemicellulose, due to a peeling reaction. This might also contribute to the lower pulp yield.

Table 2 shows that increasing the concentration of sodium hydroxide significantly decreased the degree of the pulp freeness. Thus, there was a decrease in the pulp's drainage capacity. This was probably due to an increasing amount of fines which would have a significantly greater surface area than fibers for water absorption. Also relevant are the removal of hydrophobic lignin, the dissolution of hemicellulose and possibly the saponification of the cutin wax by the alkali with "solvation" of the cellulose. The latter two possibilities were supported by the results from contact angle studies in which the contact angle with water decreased when the amount of alkali was increased (Fig. 1).

Figure 1 also shows that the handsheets in the dry state (at a zero contact time) had the greater water contact angles. However, after contact with the water, the contact angles decreased due to wetting, absorption, penetration, and spreading of the water under the influence of the cellulosic hydrophilic interactions.

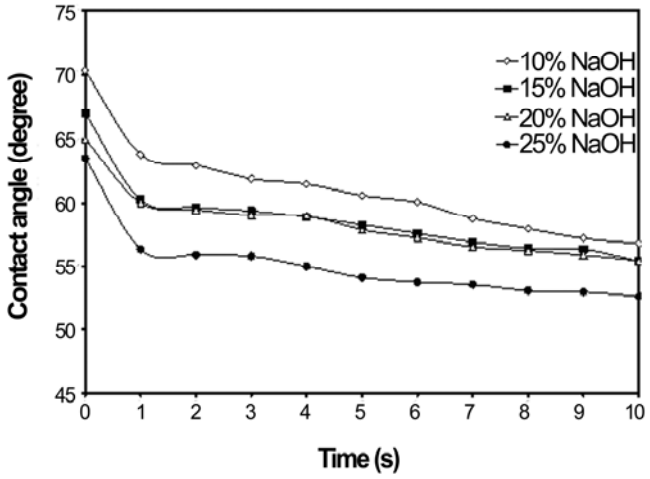

Fig. 1. The effects of different sodium hydroxide concentrations on water contact angles of the kapok fiber sheets.

It should be noted that weight weighted average fiber length is one of the average fiber length values, but it emphasizes more on the content of long fibers as compared to the length weighted fiber length and the arithmetic average fiber length, respectively. When the amount of sodium hydroxide increased, the average fiber length significantly decreased, whilst the fines content was increased (Table 2). This was likely to have occurred because the fibers were damaged by a peeling reaction under the strong alkali conditions leading to carbohydrate degradation (Sjöström 1993). Thus, the greater the amount of carbohydrate that was degraded by the alkali, the lower would be the mean fiber length and the greater would be the amount of fiber fines.

Kapok handsheet properties

The effects of the sodium hydroxide solution on the kapok handsheet properties are summarized in Table 3.

Table 3. Effects of Sodium Hydroxide Concentration on the Kapok Handsheet Properties

Pulp and Paper Properties	NaOH Dosage (% w/w)				
	10	15	20	25	P-value
Apparent density (g/cm^3)	0.68	0.80	0.82	0.88	0.1264
ISO opacity (%)	97.9	97.5	97.4	97.0	0.0235*
ISO brightness (%)	21.3	19.1	18.6	18.1	0.1917
Tensile index (N m/g)	80.3	100.4	111.5	101.3	0.0002*
Elongation (%)	1.75	2.01	2.10	2.05	0.0335*
Burst index (kPa m^2/g)	4.44	5.73	5.96	5.98	0.0348*
Tear index (mN m^2/g)	1.78	1.68	1.60	1.59	0.4005
Zero span tensile index (N m/g)	59.5	58.2	56.7	55.9	0.9801
* Statistically significant since P-value is lower than 0.05					

Increasing the amount of sodium hydroxide solution led to an increase in the apparent density of the sheets which was defined as handsheet grammage divided by

handsheet thickness, but a lower opacity (Table 3). Such effects are likely to be due to the role of sodium hydroxide solution in breaking up lignin molecules within the fiber cell wall. As the hydrophobic lignin was removed, the fiber surface became more hydrophilic, encouraging fiber swelling and conformability. This would result in a more compacted sheet that in turn, which could lead to fewer air-to-fiber interfaces and a lower opacity. In addition, the increasing content of fines and the greater amount of fiber contact areas would help to improve fiber bonding, leading to denser sheets, as indicated by the higher apparent density. Shorter fibers and a greater amount of fines also provided a basis for more effective filling of existing voids, which might also have contributed to lower opacity of the sheet. However, the effect of sodium hydroxide solutions on the apparent density appeared in this case to be statistically insignificant while its effect on opacity was statistically significant.

Pulp brightness would be expected to increase when greater amounts of sodium hydroxide solution were used, since more lignin would be removed. However, the observed trend was the opposite of this expectation, as indicated by the statistical evaluation (Table 3). However, greater concentrations of sodium hydroxide solution might reduce pulp brightness through an alkali darkening reaction, resulting in structural changes of the chromophoric groups in the residual lignin. These groups could also absorb light and thus cause the brightness of the pulp to decrease. An additional plausible explanation might be that the sodium hydroxide solution mediated the removal of lignin and caused greater sheet compactness with a resultant reduced level of light scattering of the sheet, whilst the greater amount of fines might also lead to sheet compactness.

The tensile index defines the tensile strength of paper. It is the tensile strength divided by the grammage. The burst index defines the burst strength of the paper and is equal to the burst strength divided by the grammage. Fiber bonding is highly likely to affect the tensile strength and burst strength. Increasing sodium hydroxide dosage provided higher tensile and burst strengths due to increasing fiber bonding, since lignin was removed and fibers became more conformable (Table 3). Increased fiber bonding caused by the greater sodium hydroxide dosage also led to the higher elongation. However, it should be noticed that using too high dosage of sodium hydroxide was detrimental to tensile and burst strengths as a result of carbohydrate degradation by peeling reaction at a strong alkali condition. The effects of the sodium hydroxide concentration in cooking liquor on the tensile index, the elongation and the burst index were statistically significant.

The tear index, the tear resistance value divided by the grammage, defines the tear resistance of the paper. Tear resistance is affected by many factors, such as the intrinsic fiber strength, the fiber length, and fiber bonding. The most important factor for well-bonded sheets is the fiber strength. The zero span tensile index is defined by the zero-span tensile strength divided by the grammage. Generally, zero span tensile index is a function of both the intrinsic fiber strength and the fiber bonding; however, the intrinsic fiber strength is a major contributing factor. The tear index decreased when the sodium hydroxide concentration increased (Table 3). The same observation was found for the zero span tensile index. This effect could be caused by the peeling reaction that destroys endwise, the chains of cellulose and hemicellulose and by the alkaline hydrolysis that leads to a drop in the degree of polymerization of the fibers (Shatalov and Pereira 2005).

The decrease in tear resistance might also be caused by the shorter fiber length and the greater amount of fines that are created. However, the effects of sodium hydroxide dosage on the tear and zero span tensile index values were so small that they were statistically insignificant.

Overall, the optimum condition for kapok fiber pulping was that of the cooking liquor containing 20% (w/w) of sodium hydroxide, which gave the maximum tensile properties as discussed. Thus, kapok pulp that was prepared using a 20% (w/w) sodium hydroxide dosage was used in subsequent experiments. However, the pulp was bleached before being mixed with commercial pulps.

Effects of Kapok Pulp Addition to Commercial Softwood and Hardwood Pulps on the Properties of the Resultant Pulp and Paper

Fiber length distributions of kapok, softwood and hardwood pulps

The fiber length distributions of the kapok pulp that was produced using the cooking liquor of 20% (w/w) sodium hydroxide and the commercial softwood pulp and hardwood pulp are shown in Fig. 2.

The kapok pulp had an intermediate amount of short fibers that was less than that of the hardwood pulps. The softwood pulp gave the lowest short fiber content. The kapok pulp was also intermediate in the amount of both medium and long fibers. These were lower than that from the hardwood pulp. The softwood pulp contained the greater amount of long fibers.

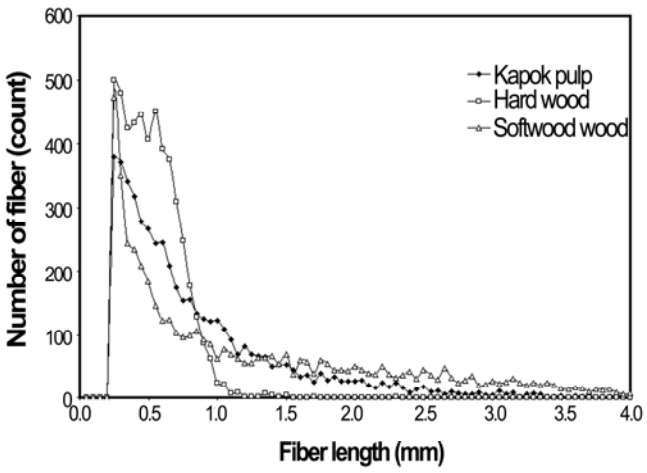

Fig. 2. Fiber length distributions of the kapok, hardwood and softwood pulps.

Fiber length, fines content and zero span tensile index of kapok, softwood and hardwood pulps

Fiber length, fines content and zero span tensile index of kapok, softwood and hardwood pulps are compared and illustrated in Table 4.

Table 4. Fiber Length, Fines Content and Zero Span Tensile Index of Kapok and the Commercial Pulps

Pulp Properties	Pulp Types		
	Kapok	Softwood (SW)	Hardwood (HW)
Average fiber length-Arithmetic (mm)	0.83	1.25	0.50
Fines (%)	22.7	43.2	34.0
Zero span tensile index (N m/g)	56.7	82.6	44.2

After being refined to the freeness of 300 mL as shown in Table 4, the average fiber length of the kapok pulp (0.834 mm) was between those of the softwood pulp (1.253 mm) and hardwood pulp (0.496 mm). The kapok pulp also had the lowest level of fines, followed by the hardwood pulp and softwood pulp, respectively.

As shown in Table 4, the sheets made from the softwood and hardwood pulps had the greatest and least zero-span tensile index at 82.6 and 44.2 N m/g, respectively. That made from kapok pulp was 56.7 N m/g. Since kapok fiber was brittle, this led to the lower zero span tensile index of kapok pulp.

Apparent density

The apparent densities of the sheets that were prepared from different ratios of the kapok pulp to the commercial softwood (SW), hardwood (HW) and softwood-hardwood mixed pulps, are shown in Fig. 3.

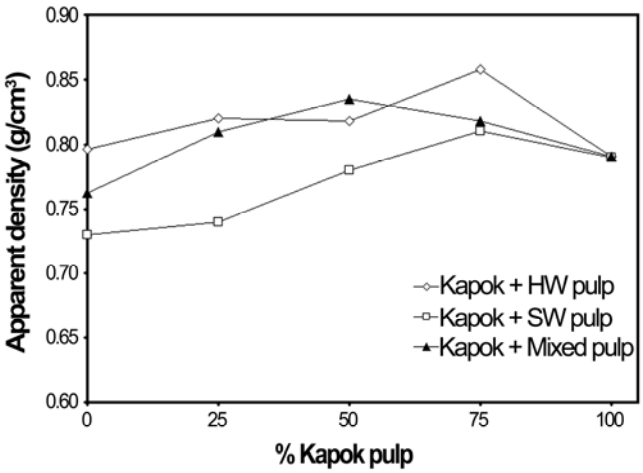

Fig. 3. Apparent density of the sheets made from kapok pulp mixed with the commercial hardwood (HW) pulp and softwood (SW) pulp at the indicated percentages.

The sheets made from the hardwood pulp had a greater apparent density than those containing either the softwood pulp or the kapok pulp. That is because the shorter fibers of the hardwood pulp fill the voids and pores in the sheet structure, making the sheets more compact. The inclusion of kapok pulp increased the apparent density of the sheets in all of the pulp mixtures. This could be because the kapok fibers have very thin cell wall, being easily collapsed, making more compact sheets. However, sheets derived

from the pure kapok pulp were not greater in apparent density, as seen by the fact that the kapok fibers become easily entangled. Thus, pure kapok sheets gave poor sheet formation and an irregular sheet surface.

Tensile index and burst index

The sheets made from kapok pulp gave the highest tensile index (Fig. 4). This could be because the kapok fibers were long and the lumens were easily collapsed when forming paper, producing highly bonded regions and denser sheets with a resulting superior sheet tensile index.

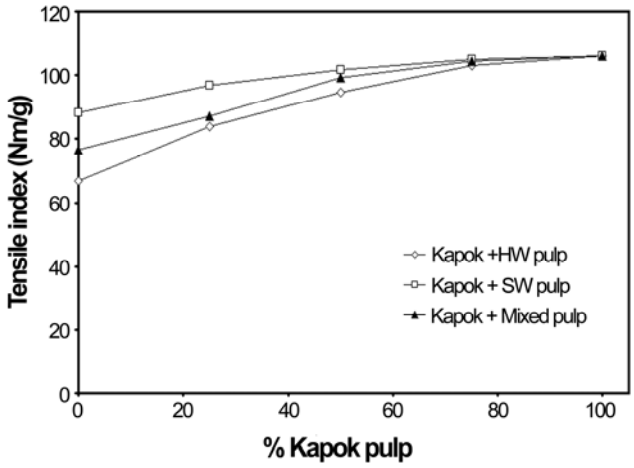

Fig. 4. Tensile index of the sheets made from kapok pulp mixed with the commercial hardwood (HW) pulp and softwood (SW) pulp at the indicated percentages.

The sheets made from the hardwood pulp produced the lowest tensile index. Those made from a 75:25 (w/w) blend of the hardwood: softwood pulps had a medium tensile index. Those made from the pure softwood pulp gave the greatest tensile index. With respect to kapok-commercial pulp mixtures, as the ratio of kapok pulp increased, the tensile index also increased (Fig. 4). However, the results were more prominent when the kapok pulp was mixed with the hardwood pulp than with the softwood pulp.

The sheets derived from the pure kapok pulp gave the highest burst index, the values being somewhat similar to those of the sheets made from the softwood pulp (Fig. 5). This is because both kapok fiber and the softwood fiber are long and have extensive contact areas that are available for fiber bonding. The sheets made from the hardwood pulp had the lowest burst index. This is because the hardwood pulp contained a greater amount of short fibers, resulting in poor bonding. As the ratio of the kapok pulp in mixtures with the hardwood pulp or the 75:25 ratios (w/w) of hardwood pulp: softwood pulp increased, the burst indexes of the resultant paper significantly increased, because fiber bonding was greatly improved.

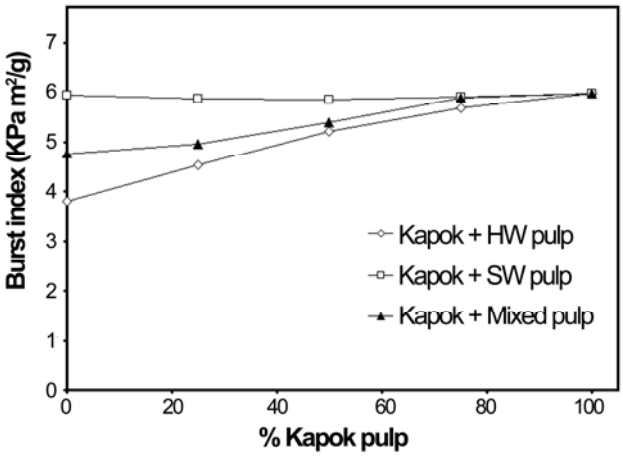

Fig. 5. Burst index of the sheets made from kapok pulp mixed with the commercial hardwood (HW) pulp and softwood (SW) pulp at the indicated percentages.

Tear index and elongation

One of the key characteristics of kapok fibers is their brittleness. Thus, the sheets made from the kapok pulp had the lowest tear index relative to those made from the commercial softwood pulp, the hardwood pulp, and the softwood-hardwood mixed pulp. For kapok-commercial pulp mixtures at different ratios, it was clearly observed that as the ratio of kapok pulp increased, the tear index significantly decreased (Fig. 6).

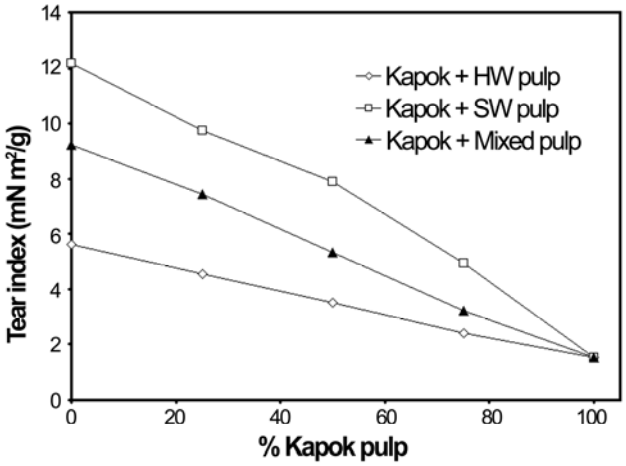

Fig. 6. Tear index of the sheets made from kapok pulp mixed with the commercial hardwood (HW) pulp and softwood (SW) pulp at the indicated percentages.

The elongation of the sheets that were prepared from different ratios of the kapok pulp is compared in Fig. 7. Sheets made from kapok pulp had the lowest elongation. This is because the key characteristics of kapok fibers are their brittleness and inelasticity, which might reduce the elongation of the sheets when a load was applied. Thus, as the

ratio of the kapok pulp was increased, the elongation significantly decreased in all pulp mixtures.

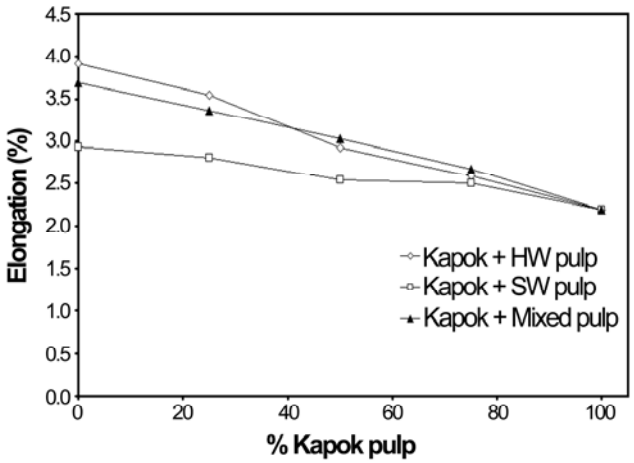

Fig. 7. Elongation of the sheets made from kapok pulp mixed with the commercial hardwood (HW) pulp and softwood (SW) pulp at the indicated percentages.

Water contact angle

The water contact angles of the sheets made from kapok pulp mixed with the commercial softwood pulp and hardwood pulp are shown in Fig. 8. As seen in Fig. 8, K 100 represented handsheets made from 100% kapok pulp. HW100 indicated handsheets made from 100% hardwood pulp while SW100 illustrated handsheets made from 100% softwood pulp. M100 designated handsheets made from mixed pulp (25:75 (w/w) softwood pulp: hardwood pulp). Handsheets prepared from kapok pulp mixed with hardwood, softwood and mixed pulps with different percentages characterized by K: HW, K: SW and K: M with the percentage indicated in parenthesis.

The results indicated that as the time of contact increased, the water contact angles decreased because of absorption and penetration of the water droplets into the sheet. Those made from 100% kapok pulp gave the greatest values for the water contact angle. This effect was due to the unique characteristics of the kapok fibers having a wax coating on the surface. Although the kapok fibers were pulped, some of the wax was still present. When mixed with the commercial pulps (softwood, hardwood and mixed pulps), as the ratio (w/w) of the kapok pulps increased, the water contact angle values increased.

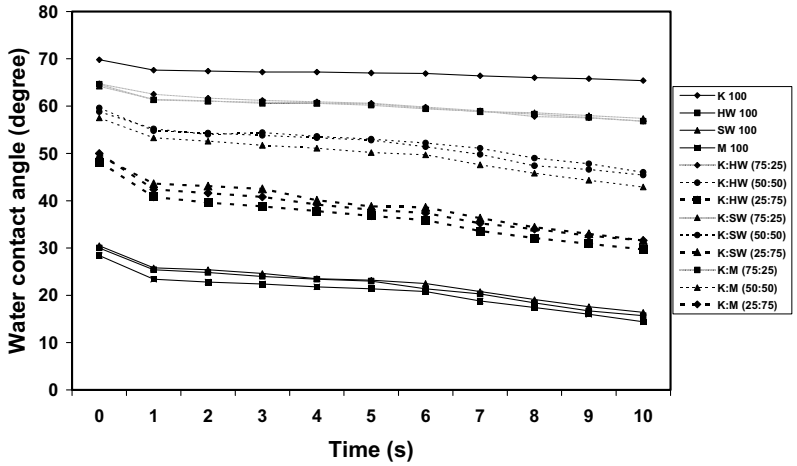

Fig. 8. Water contact angles of the sheets from the kapok (K) pulp mixed with the commercial hardwood (HW) pulp, softwood (SW) pulp and mixed (M) pulp at the indicated percentages.

CONCLUSIONS

1. When kapok pulp was mixed with the commercial softwood pulp and/or hardwood pulp, the tensile and burst strengths of the blended sheets increased but with the lower tear resistance and elongation due to the excellent tensile strength and brittleness of kapok pulp.
2. Brightness and opacity of the blended sheets decreased when higher amounts of kapok pulp were added in the pulp mixture due to the yellowness of the kapok pulp.
3. Handsheets containing kapok pulp gave greater water contact angles due to the hydrophobic nature of kapok fibers.
4. Thus, kapok pulp can potentially be mixed with the commercial softwood pulp and/or hardwood pulp to produce commercial packaging paper when the strength and light weight characteristics are required.

ACKNOWLEDGMENTS

This research was financially supported by a Research Team Aid Grant from the Thailand Research Fund and Commission of Higher Education under the contract number RTA5080004. The authors would like to thank the Department of Imaging and Printing Technology of Chulalongkorn University, and the Product and Technology Development Center of Siam Cement Group Paper Company Limited for providing relevant research facilities.

REFERENCES CITED

Browning, B. L. (1963). *Methods in Wood Chemistry*, Interscience Publishers, New York.

Chaiarrekij, S., Wongsaisuwan, U., and Watchanakit, S. (2008). "Papermaking from Kapok fiber," *Thai Petty Patent, 4279*, June 13, 2008.

Hong, X., Wei-dong, Y., and Mei-wu, S. (2005). "Structure and Performances of the Kapok Fiber," *Journal of Textile Research* 26(4), 4-6.

Hori, K., Flavier, M. E., Kuga, S., Lam, T. B. T., and Liyama, K. (2000). "Excellent oil absorbent kapok [*Ceiba pentandra (L.) Gaertn*.] fiber: Fiber structure, chemical characteristics, and application," *J. Wood Sci.* 46(5), 401-404.

Huang, X. F., and Lim, T. T. (2006). "The performance and mechanism of hydrophobic–oleophilic kapok filter for oil/water separation," *Desalination* 190(1-3), 295-307.

Khan, E., Virojnagud, W., and Ratpukdi, T. (2004). "Use of biomass sorbents for oil removal from gas station runoff," *Chemosphere* 57, 681-689.

Kobayashi, Y., Matsuo, R., and Nishiyama, M. (1977). "Method for adsorption of oils," *Japanese Patent*, 52,138,081, November, 17, 1977.

Lim, T.-T., and Huang, X. (2007). "Evaluation of Kapok (*Ceiba pentandra* (L.) Gaertn.) as a Natural Hollow Hydrophobic-Oleophilic Fibrous Sorbent for Oil Spill Cleanup," *Chemosphere* 66, 955-963.

Malab, S. C., Agrupis, S., Cabalar, L., and Ballesteros, R. (2001). "Paper sheets from bamboo and kapok," *PCARRD Press Release* No.153, December, 14, 2001.

Qiuling, C., and Lin, W. (2009). "Structure and Property Contrast of Kapok Fibre and Cotton Fibre," *Contton Textile Technology* 37(11), 668-670.

Rengasamy, R.S., Dipayan, D., and Karan, P.C. (2011). "Study of Oil Sorption Behavior of Filled and Structured Fiber Assemblies Made from Polypropylene, Kapok and Milkweed Fibers," *Journal of Hazardous Materials* 186(1), 526-532.

Shatalov, A. A., and Pereira, H. (2005). "Kinetics of polysaccharide degradation during ethanol–alkali delignification of giant reed-Part 1. cellulose and xylan," *Carbohydr. Polym.* 59(4), 435-442.

Sjöström, E. (1993). *Wood Chemistry-Fundamentals and Applications*, 2nd ed., Academic Press, San Diego.

Tang, A.-m., Sun, Z.-h., Fu, X., Zi, M., Zhang, H.-w., Chen, G., and Lin, Y. (2008). "Chemical and Structural Characteristics of Kapok Fibers," *Zhongguo Zaozhi Xuebao/Translations of China Pulp and Paper* 23(3), 1-5.

Article resubmitted: July 31, 2011;

Elsevier Editorial System(tm) for Journal of Chromatography A
Manuscript Draft

Manuscript Number:

Title: Comparative study of the mesostructure of natural and synthetic polyisoprene by SEC-MALS and AF4-MALS

Article Type: Full Length Article

Keywords: Field flow fractionation; size exclusion chromatography; polyisoprene; multi angle light scattering; rubber

Corresponding Author: Mr. Stéphane Dubascoux,

Corresponding Author's Institution: Montpellier SupAgro

First Author: Stéphane Dubascoux

Order of Authors: Stéphane Dubascoux; Chalao Thepchalerm; Eric Dubreucq; Suwaluk Wisunthorn; Laurent Vaysse; Suda Kiatkamjornwong; Charoen Nakason; Frédéric Bonfils

Suggested Reviewers: Stepan Podzimek
stepan.podzimek@synpo.cz
expert in AF4 and polymer science

Bruno Grassl
bruno.grassl@univ-pau.fr
expert in polymer science

Yacine Hemar
y.hemar@auckland.ac.nz
expert in physico-chemistry of colloidal system

Opposed Reviewers:

Montpellier SupAgro

CENTRE INTERNATIONAL D'ETUDES SUPERIEURES EN SCIENCES AGRONOMIQUES

DEPARTEMENT DES SCIENCES POUR LES AGRO-BIOPROCEDES

UMR INGENIERIE DES AGROPOLYMERES ET TECHNOLOGIES EMERGENTES
(UMR 1208 IATE, CIRAD-INRA-MONTPELLIER SUPAGRO-UM2)

République Française

Dr. Stéphane Dubascoux
Tel : +33 (0) 499613016
Email : stephane.dubascoux@supagro.inra.fr

Montpellier, 05th July 2011

Cover letter

Dear Managing Editor,

Please find enclosed the submission of our regular research paper entitled: "*Comparative study of the mesostructure of natural and synthetic polyisoprene by SEC-MALS and AF4-MALS*". In this article, we present the first original results about natural and synthetic rubber characterization by asymmetrical flow field flow fractionation (AF4). Mesostructure evaluation by AF4 is compared with that obtained with size exclusion chromatography.

Up to now, there is a real lack of information concerning natural rubber mesosctructure and more precisely about the presence and the nature of microaggregates (gel content) among the linear polyisoprene chains. AF4 allows assessing simultaneously both the distribution of polyisoprene chains and gel content. Results obtained allow to validate the AF4 fractionation (compared to SEC results) and to consider the gel part of polyisoprene samples.

For these reasons, we think that our article matches with the topic of your journal and is appropriate for publication in journal of chromatography A.

Sincerely yours,

The authors: Stephane Dubascoux, Chalao Thepchalerm, Eric Dubreucq, Suwaluk Wisunthorn, Laurent Vaysse, Suda Kiatkamjornwong, Charoen Nakason, Frederic Bonfils

*Manuscript
Click here to view linked References

Comparative study of the mesostructure of natural and synthetic polyisoprene by SEC-MALS and AF4-MALS.

Stephane Dubascoux*[1], Chalao Thepchalerm[1,2,6], Eric Dubreucq[1], Suwaluk Wisunthorn[3], Laurent Vaysse[4], Suda Kiatkamjornwong[5], Charoen Nakason[2], Frederic Bonfils*[6]

[1] *Montpellier SupAgro, UMR IATE 1208, 2 Place Viala, 34060 Montpellier, France*

[2] *Center of Excellence in Natural Rubber Technology, Faculty of Science & Technology, Prince of Songkla University, Pattani campus, Thailand*

[3] *Faculty of Science and Industrial Chemistry, Prince of Songkla University, Surat Thani campus, Thailand*

[4] *CIRAD, UMR IATE 1208, KU-CIRAD laboratory, Agroindustry building 3, 7th Floor, Kasetsart University, Bangkok 10900, Thailand*

[5] *Faculty of Science, Chulalongkorn University, Bangkok, Thailand*

[6] *CIRAD, UMR IATE 1208, 2 Place Viala, 34060 Montpellier, France*

Abstract

This paper presents results from the first analyses of the mesostructure of natural rubber (NR) by asymmetrical flow field flow fractionation (AF4). The results are compared with those obtained by size exclusion chromatography (SEC) in terms of average molar masses, radius of gyration and insoluble part (or gel quantity). Comparable results were obtained for the sample not containing gel. Conversely, for samples with gel, significant differences were found due to the presence of microaggregates. In fact, contrary to SEC, AF4 fractionation enables partial fractionation of polyisoprene chains and microaggregates in a single run without preliminary treatment. The results presented here also highlight the special structure (very compact spheres) of microaggregates in NR compared to chemical crosslinked microaggregates in synthetic polyisoprene. The advantages and drawbacks of both techniques for analysing NR samples are also discussed.

Introduction

For natural rubber (NR), as for numerous biopolymers, it is rather simplistic to speak about macromolecular structure. Indeed, biopolymers often exhibit a complex associative structure, a mixture of macromolecular chains, microaggregates and macroaggregates [1,2]. Because of that, the term mesoscopic structure or mesostructure, which includes both macromolecular structure and aggregate characterization, is increasingly being used. Although NR mesostructure has been studied for many years, the origins of its unique properties are not yet fully clear. Recently, Kim *et al*. [3,4] revisited the mesostructure of NR. Kim *et al*. [3,4] analysed NR samples with SEC-MALS and showed that the soluble part injected into a SEC system contained very few branched macromolecules, contrary to earlier published studies [5-7]. Kim *et al*. [3,4] showed that the soluble part of NR in solution in tetrahydrofuran (THF) was composed of a mixture of linear chains and assumed compact microaggregates ($R_g \approx$ 110-130 nm). They showed that to more effectively ascertain the mesostructure of NR, as is the case with most polymers, a MALS detector coupled with SEC is required to avoid a misunderstanding of the structure. From a mechanistic point of view, many mechanisms have been proposed to explain the associative structure of NR [8-11]. The most recent proposal is Tanaka's group scheme involving a protein and a phospholipid at each end of the poly(*cis*-1,4-isoprene) chain. These two reactive end chains would appear to be involved in what they called the "naturally occurring network" of NR [12,13].

Today, many tools are available for macromolecule analysis. Of these techniques, size exclusion chromatography (SEC) and field flow fractionation (FFF) are tools of choice to fractionate macromolecules according to their sizes. SEC is beyond doubt the most popular and developed technique for polymer separation. However, a recent study has also highlighted some difficulties for NR separation with SEC coupled with a multi-angle light scattering (MALS) detector because of an abnormal elution phenomenon [3]. This abnormal elution is

due to co-elution of microaggregates with short chains. Kim *et al*. [3] showed that the abnormal elution occurring with NR could be overcome by treating the SEC columns with an ionic surfactant. After treatment, it was possible to separate these compact microaggregates from linear random coil polyisoprene chains [3]. However, it is difficult to be sure whether or not all microaggregates elute and the procedure is rather cumbersome. The solution to this SEC limitation for NR sample analysis might be the use of techniques based on field flow fractionation. Recent reviews have demonstrated the potentiality of FFF in various fields, such as polymer science [14], biomolecule characterization [15], nanoparticles [16] or the environment [17]. Moreover, FFF could easily be coupled on-line with different detectors, such as a refractive index detector, an ultra-violet detector, a light scattering or inductively coupled plasma mass spectrometer [18]. Recently, Messaud *et al*. [14] emphasized the fact that field flow fractionation techniques can provide effective simultaneous separation of polymer and microgel. The most popular FFF techniques used for polymer fractionation are thermal flow field flow fractionation (Th-FFF) and Flow Field Flow Fractionation (Fl-FFF or F4) [14]. The main difference between these two sub-techniques is the field used for the fractionation. Fractionation takes place in a channel and the field is a thermal gradient for Th-FFF, while it is a crossflow stream carried through an ultrafiltration membrane in the case of Fl-FFF [19]. Up to now, only Th-FFF has been used for NR characterization [20-23]. However, during Th-FFF, macromolecules are separated according to their size and their chemical composition. Thus, heterogeneity in the chemical composition of a given polymer can complicate the determination of macromolecular structure. Asymmetrical Fl-FFF (AsFl-FFF or AF4) is Fl-FFF where the channel is semi-permeable and asymmetric, involving less sample dilution [19]). Natural rubber has been analysed by Th-FFF using either the polyisoprene calibration curve [20,22,23] or a multi-angular light scattering detector (MALS) [21]. Lee and Molnar [23] compared the analysis of natural rubber by Th-FFF and SEC. They

used a calibration curve made with linear standards poly(*cis*-1,4-isoprene). The analysed NR samples (RSS1 type) had a number-average molar mass (M_n) of about 0.8 million g.mol^{-1} and a weight-average molar mass (M_w) of about 29 million g.mol^{-1}, M_w being three times higher than that given by SEC. Lee and Molnar **[23]** showed that the high molar masses and microgels disappeared after mastication of a NR sample in an extruder. The range of molar masses found was between 10,000 and 10 million g.mol^{-1} (non-masticated RSS). Filtration of the solution through filters with 5 µm pores led to a shift in the fractogram towards lower retention times. This phenomenon was observed for non-masticated rubber but not for masticated rubber. This shift to lower molar masses was attributed to the removal and/or degradation of microgels (or ultra-high molar mass species). They quantified the gel rate (as a % of total rubber, w/w) in the NR samples by Th-FFF and found slightly lower values (RSS 13%, masticated RSS 0%) than with their conventional method – i.e. filtration through a 125 µm wire mesh after 24 h in toluene (RSS 15%, masticated RSS 0%). Fulton and Groves **[21]** analysed two synthetic polyisoprenes (IR305, Natsyn2200), a polybutadiene (Europrene BR40) and a natural rubber (SMR5L) in cyclohexane by Th-FFF-MALS without any filtration. They showed that the IR305 sample was essentially linear with no gel, as confirmed later by Kim *et al.* **[3]** by SEC-MALS, contrary to the Natsyn2200 sample, which had a 25% gel rate and was branched for molar masses above 5.10^5 g.mol^{-1}. While there was no steric effect in the separation process for the two synthetic polyisoprenes, they observed such an effect for the polybutadiene and the NR samples. As a consequence of this phenomenon, very large entities eluted together with the smaller molecules. Bang *et al.* **[24]** used AF4 to characterize and determine the molar mass distribution of styrene–butadiene rubber.

This paper presents the first study of synthetic and natural polyisoprene fractionation by AF4 coupled with MALS in an organic solvent (tetrahydrofuran). The peak shape is discussed and the results in terms of average molar masses, radius of gyration and gel content are compared

105 with those obtained by SEC-MALS. The comparison of AF4-MALS with SEC-MALS also
106 made it possible to evaluate the discrepancies between the two techniques for analysing NR
107 samples.
108

Material & methods

Samples

In order to compare SEC and AF4 results on synthetic polyisoprene and natural rubber (NR), four samples were chosen for their differences in mesostructure. The two synthetic poly(*cis*-1,4-isoprenes) were Kraton IR 307 (Kraton polymer, Houston, USA) and Nippol 2200 (Zeon Corporation, Louisville, USA). The main difference between these two synthetic polyisoprenes is the gel rate: no gel in the IR307 sample and presence of microgel in Nippol 2200. The two natural rubbers, M160 and M121, were TSR5CV (Technically Specified Rubber with a Constant Viscosity) made from monoclonal *Hevea brasiliensis* latex. The preparation of the samples was described previously **[25]**.

In order to reach a sample concentration of 1 $mg.mL^{-1}$, 30 ± 5 mg of the samples was dissolved in about 30 mL of HPLC grade tetrahydrofuran (THF, VWR, West Chester, USA) stabilized with 2,6-di-tert-butyl-4-methylphenol – BHT – (Sigma Aldrich, Saint Louis, USA) at 250 $mg.L^{-1}$. The flasks were precisely weighed (± 0.01 mg) before and after filling with THF to determine the exact concentration of the solutions. The solvent (THF + BHT) was filtered at 0.1 µm before use. Each sample was analysed in triplicate to evaluate measurement repeatability. All solutions were stored in the dark in a water bath at 30°C for 7 days and gently shaken at 30 rpm (rotational agitator REAX 2, Heidolph, Schwabach, Germany) for 1 hour each day for optimum dissolution. Before injection, the macrogel and part of the microgels were removed from all the solutions by filtration at a 1 µm cutoff with Acrodisc glass filters (Pall, Port Washington, USA) to avoid both clogging of the column during SEC analysis and a steric effect (resulting in inverse elution) on AF4 fractionation **[21]**.

Two monodisperse polystyrene standards at 200 and 1460 kDa from Polymer Standard Service (PSS, Mainz, Germany) were used to assess the quality of the separation/fractionation and detector response for each SEC/AF4 injection series.

134

135 ***AF4 experiments***

136 The AF4 system was a Postnova AF2000 MT series (Postnova Analytics GmbH, Landsberg,
137 Germany) equipped with a channel adapted for organic solvents and a 350 µm spacer. The
138 membrane was made of cellulose material treated for compatibility with organic solvents with
139 a cut-off of 5 kDa (Postnova Analytics GmbH, Landsberg, Germany). The temperature
140 setpoint of the AF4 oven containing the channel was 45°C. The detector flow was kept
141 constant at 0.65 $mL.min^{-1}$. The focusing step consisted of a flow delivered by the injection
142 port of about 0.2 $mL.min^{-1}$ with a crossflow of 1 $mL.min^{-1}$ for 6 minutes. Then, a 1 min
143 transition time was applied to avoid a major pressure drop during the switch from the focus
144 step to the elution step. The programme to decrease the linear crossflow during the elution
145 step was as follows:

146

147 ***Table 1***

148

149 An autosampler (PN 5300 model, Postnova Analytics GmbH) was used to carry out the
150 100 µL sample injections.
151 Detection was carried out with a 7-angle multi-angle light scattering detector (PN 3070
152 model, Postnova Analytics GmbH) in line with a refractive index detector (2414 model,
153 Waters Corporation, Milford, USA). The data gathered were processed with AF2000 software
154 (Postnova Analytics GmbH) after blank subtraction for the DRI signal (used as a
155 concentration detector) and according to the Berry model with 2^{nd} order polynomial
156 formalism. In fact, it has been shown that this formalism is well adapted for entities with a
157 radius up to 50 nm **[26]**. As the refractive index detector signal changes during transition steps
158 due to the AF4 functioning principle, five blank (mobile phase) injections were carried out in

each injection series. The refractive index detector signal from the blank injections was subtracted for each sample injected.

For one series, each sample triplicate was injected once. Two series were carried out (i.e. a total of 6 injections was carried out for each sample) with different operators in order to evaluate the reproducibility of the analysis. Prior to each series of injections, the membrane was replaced and the detector was recalibrated.

SEC experiments

The SEC system was based on an on-line ERC 3112 degaser (ERC, Saitama, Japan), a Waters 515 pump (Waters Corporation, Milford, USA) and 3 MIXED-A columns in series: 2 styragel columns (porosity 20 µm, 300 mm × 7.5 mm I.D.) from Waters and 1 PLgel column (porosity 20 µm, 300 mm × 7.5 mm I.D.) from Varian (Varian, Walnut Creek, USA). All the columns were kept in an oven at 45°C. The detectors were an 18-angle multi-angle light scattering detector (Dawn DSP model, Wyatt Technology, Santa Barbara, USA) and a refractive index detector (Optilab rEX model, Wyatt Technology). Data from angles 5 to 16 were collected and processed with Astra software version 5.3.1 (Wyatt Technology) according to the Berry method with a 2^{nd} order polynomial model. Similarly to the AF4 injection series, each sample triplicate was injected once. Two series were carried out (i.e. a total of 6 injections carried out for each sample).

Theory/calculation

Light scattering theory

For the Berry method with a 2nd order polynomial fit, $[Kc/\Delta R(\theta)]^{1/2}$ is plotted against $\sin^2(\theta/2)$. According to the light scattering theory, this plot makes it possible to determine M_{wi} and R_{gi} for each slice of the fractogram from AF4 or the chromatogram from SEC, respectively, according to equation 1.

$$\left[\frac{Kc}{\Delta R(\theta)}\right]_i^{1/2} = \left[\frac{1}{M_{wi}} + \frac{16\pi^2}{3_0^2}\frac{\langle R_g^2\rangle_i}{M_{wi}}\sin^2\left(\frac{\theta}{2}\right)\right]^{1/2} \quad \textit{Equation 1}$$

where $\mathbf{K}$ is an optical constant
c is the solute concentration (in $g.mL^{-1}$)
θ is the scattering angle
$\Delta R(\theta)$ is the excess Rayleigh ratio, the ratio of scattered and incident light intensity
M_{wi} is the weight-average molar mass of the solute
λ_0 is the wavelength of the laser beam in a vacuum (in nm)
R_g is the gyration radius of the solute (nm)

The optical constant $\mathbf{K}$ is given by equation 2.

$$K = \frac{4\pi^2 n_0^2}{N_{A0}^2}\left(\frac{dn}{dc}\right)^2 \quad \textit{Equation 2}$$

where n_0 is the refractive index of the solvent
N_A is Avogadro's number
$\left(\frac{dn}{dc}\right)$ is the differential refractive index increment of the polymer in the solvent used

For detailed information about the light scattering theory, refer to **[27,28]**.

Molar mass and radius definitions

The different molar masses calculated and presented are defined as:

$$M_n = \frac{\sum_i N_i M_i}{\sum_i N_i} \qquad M_w = \frac{\sum_i N_i M_i^2}{\sum_i N_i M_i} \qquad M_z = \frac{\sum_i N_i M_i^3}{\sum_i N_i M_i^2} \quad \textit{Equation 3, 4 \& 5}$$

Where N_i is the number of polymers with molecular weight M_i

The radius of gyration ($<R_g>$ or R_z) or root mean square radius (r.m.s) is defined for a non-rigid particle as:

$$< R_g >= \frac{\sum_i c_i M_i \langle R_g^2 \rangle_i}{\sum_i c_i M_i} \quad \textit{Equation 6}$$

Gel content calculation

In order to evaluate the amount of gel retained by the 1 µm filter, the whole peak from the concentration detector (refractive index detector) observed in SEC or AF4 separation was integrated using 0.13 as the value of $^{dn}/_{dc}$ [29]. This gel content was called the "filtrate gel on 1 µm" or $Gel_{>1\mu}$. In previous papers this quantity of aggregates (macro and micro) was called "total gel". However, as shown by Kim *et al*. [3] and as we will see later in this paper, a not insubstantial quantity of microaggregates passes through the 1 µm filter. As a consequence, the real total gel (G_T) is:

$$G_T = Gel_{>1\mu} + Gel_{<1\mu} \quad \textit{Equation 7}$$

$Gel_{<1\mu}$ is the quantity of microaggregates with a size smaller than 1 µm. $Gel_{<1\mu}$ cannot be determined by SEC-MALS, except by treating the columns with tetrabutylammonium bromide (TBABr) as shown previously [3]. This procedure is rather cumbersome, whereas it will be shown that $Gel_{<1\mu}$ can easily be estimated using AF4 analysis of NR samples. Indeed, by knowing the initial concentration of the sample before filtration, it is possible to determine from the fractogram (DRI signal) the concentration of the two populations in solution after filtration: polyisoprene chains and microaggregates smaller than 1 µm.

Thus:

$$Gel_{>1\mu m} = \frac{C_1 \times 100}{C_0} \quad \textit{Equation 8}$$

$$Gel_{<1\mu m} = \frac{C_2 \times 100}{C_0} \quad \textit{Equation 9}$$

Where C_0 is the initial concentration of the analysed sample, C_1 the concentration of the analysed sample passing through the 1 µm filter (polyisoprene chains + microaggregates) and C_2 the concentration of only the microaggregates passing through the 1 µm filter. C_1 can be determined either by SEC or AF4 by integrating the whole peak of the concentration detector (DRI). C_2 can be calculated only by AF4 integrating the part of the DRI peak containing microaggregates.

Results & Discussion

Qualitative description of fractograms

SEC-MALS profiles for the different samples are presented in Figure 1. M_w variations started with a linear decrease corresponding to a normal elution from large chains to small chains but displayed a deviation of the slope of this curve for samples containing gel (i.e. Nippol, M121 and M160, figure 1B, C & D). As described in the introduction and as previously detailed **[3]**, SEC separation of rubber generally presents this abnormal elution due to co-elution of delayed large macromolecules, assumed to be microaggregates ($GEL_{<1\mu}$), with the small chains of poly(*cis*-1,4-isoprene). This particular elution was highlighted when either a change or an inversion of the slope presenting the variation in weight-average molar mass versus elution volume occurred. Regarding the detectors, the differential refractive index (DRI) signal during the SEC elution profile corresponded to a main Gaussian peak (with slight back-tailing) for Nippol and M121, and to a bimodal molar mass distribution for the IR307 and M160 samples. The LS signal was more unimodal with back-tailing varying depending on the sample.

Figure 1

Unlike SEC, AF4 fractionated the macromolecules from small to large ones and the peak shapes appeared quite different. For poly(*cis*-1,4-isoprene) with gel (i.e. Nippol 2200, M160 and M121), the shape of the LS fractograms did not correspond to a Gaussian peak. The fractograms displayed a long front tailing, (i.e. a long and low signal increase) and an abrupt increase in the LS signal from 25 to 30 min (corresponding to a crossflow ranging from 0.5 to

0.3 $mL.min^{-1}$) (Figure 2). For the IR307 sample, the fractogram exhibited a clearly less pronounced increase in the LS signal (Figure 2A). As the IR307 sample did not contain gel, unlike the Nippol 2200 sample, this abrupt increase in the signal was due to microaggregates, as observed by Andersson *et al.* **[30]** for AF4 analysis of ethylhydroxyethyl cellulose. For the refractive index detector signal, the behaviour was unfamiliar, with a first peak close to void volume (elution starting at 7 min), corresponding to small chains, followed by either a slight increase in the concentration signal (for IR 307), or a decrease (for Nippol 2200), or quite a constant signal up to the end of the peak (for the two natural samples) (Figure 2). With both the DRI and LS detectors, the fractograms gave a continuous elution whatever the entities eluting, be they random coil or compact microaggregates (sphere-like). However, the evolution of the molar masses (M_{wi}) in line with the elution time was not linear from a qualitative viewpoint (Figure 2). For the IR307 sample, Figure 2A shows a change in slope for an elution time of 17-18 min ($M_{wi} \approx 600$ kg mol^{-1}). A clear decrease in the variability of the measured R_{gi} was observed from this elution time (t_e = 17-18 min) (Figure 2). Indeed, for the first 18 minutes of the fractogram, R_{gi} values were very dispersed whatever the samples analysed using Berry 2 formalism (Figure 2), compared to SEC-MALS. This high dispersion of R_{gi} may have occurred because the concentrations of the injected solutions were too low (≈ 1 $mg.mL^{-1}$) for LS detection or because there was a lack of resolution for small molecule fractionation under our AF4 conditions. This initial slope change in M_{wi} was observed for other samples at times that varied depending on the sample (from 13 up to 17 min). With the Nippol sample, a second marked change appeared in the M_{wi} slope at an elution time of about 31 min (Figure 2B). This abrupt slope change was accompanied by a dramatic increase in the LS signal due to huge entities eluting ($250 < R_{gi} < 1000$ nm). This second change in the M_{wi} slope in line with the elution time was not visible for the other synthetic polyisoprene

(IR307), but was visible to a lesser extent for the two NR samples (M121 and M160) at an elution time of about 26-27 min (Figure 2C & D).

Figure 2

The M_{wi} AF4 profile for IR 307 confirmed the presence of only one population of chains with a M_{wi} ranging from 60,000 g.mol^{-1} to 5 million g.mol^{-1} (Figure 2A). Conversely, the Nippol AF4 profile clearly showed the presence of 2 distinct populations (Figure 2B). The first population was composed of isolated polyisoprene chains and the second one (starting at 32 min) was composed of microaggregates with sizes under 1 µm (Gel$<_{1\mu}$) with a drastic increase in the M_{wi} slope. For the two NR samples (M121 and M160) (Figure 2C and 2D), the M_{wi} profiles were quite different from that for Nippol. Isolated polyisoprene chains seemed to elute first up to about 27 min. After this elution time, the M_{wi} profile exhibited an increase in slope (from 27 to about 35 min), reaching a quasi-plateau (from 35 min). This behaviour suggests that this population was quite monodisperse. These two parts could be attributed to co-elution of isolated polyisoprene chains and Gel$<_{1\mu}$ in the first case and Gel$<_{1\mu}$ only for the plateau.

Large differences were observed for the $M_{wi}=f(V_e)$ and $R_{gi}=f(V_e)$ slopes, the sizes (R_{gi}) and the molar masses (M_{wi}) of the second populations for Nippol compared to the two natural polyisoprene samples (Figure 2). These results tend to confirm that the gel was not intrinsically the same for natural and synthetic polyisoprene. Indeed for NR, the radius for the Gel$<_{1\mu}$ was about 150 nm for a molar mass close to 15 million g.mol^{-1} whereas for Nippol for the same molar mass the radius was about 240 nm (i.e. 60% higher), as illustrated in Figure 3. Moreover, there was no "plateau effect" for Nippol compared to the NR samples. Thus, with a lower R_{gi} for the same M_{wi}, the microaggregates in the NR samples seemed more compact

316 than in the Nippol synthetic polyisoprene. However, some of the difference observed in the
317 slopes may have been due to an underestimation of M_{wi} for the microaggregates of the NR
318 samples. Indeed, it cannot be ruled out that the dn/dc of NR microoaggregates is not constant.
319 Changes in the non-isoprene composition (lipids and/or proteins) of microaggregates cannot
320 be excluded. A change in the proportion of non-isoprene compounds versus polyisoprene in
321 the microaggregates could lead to a change in the dn/dc and so in the M_{wi} determined.
322
323 ***Figure 3***
324
325 One of the main difficulties encountered with AF4 fractionation is to define a correct and
326 unbiased integration range. For our data, the integration range for average molar mass and
327 radius of gyration assessment was started when the M_{wi} and R_{gi} signals were stabilized (out of
328 void peak influence) and stopped just before the end of the peak (shown as the red box in
329 figure 4 for M160, for example). This choice of integration area was made in order to have
330 results including almost all the peak surface and to avoid a decrease in repeatability for the
331 AF4 results due to pre- and post-peak radius and mass dispersion and heterogeneity because
332 of a low LS signal. This method was applied for the AF4 signals from IR307, M160 and
333 M121. On the other hand, the treatment for Nippol 2200 was different. Indeed, the variation in
334 M_{wi} in the second part of Nippol 2200 fractionation was quite high due to the presence of
335 microaggregates with ultra high molar masses (over 10^{10} g mol^{-1}). Moreover, this final M_w
336 increase was quite noisy and unrepeatable, probably due to the low associated RID signal. In
337 fact, as presented in table 2 for example, increasing the Nippol 2200 integration range (from
338 9.5 - 35 min to 9.5 - 40 min), drastically increased the average molar masses, but also the
339 standard deviation. Lastly, a 7% increase in RID integration area (hence in quantity) led to an
340 increase of 4 orders of magnitude for the M_w and resulted in an increase in the standard

deviation from 25% to 71%. Consequently, for Nippol, the integration range was shortened,compared to the other samples, to avoid excessive variability in the results.

Table 2

In order to quantify aggregates exceeding 1 µm ($Gel_{>1\mu}$) (estimation of C_1 in eq. 9), the whole peak was integrated (green box in figure 4). The quantity of microaggregates smaller than 1 µm ($Gel_{<1\mu}$) (estimation of C_2 in eq. 10) was calculated according to a third integration range (the blue box in figure 4) starting from the middle of the zone we considered as a mixture of polyisoprene chains and microaggregates (data $R_g=f(V_e)$) up to the end of the peak.

Figure 4

<u>Comparison of data between SEC-MALS and AF4-MALS</u>

Average molar masses

M_n, M_w and M_z were calculated from the SEC and AF4 results for each sample. The results are presented in Figure 5.

Figure 5

The number average molar mass M_n did not present significant differences whether determined by SEC or AF4 (Figure 5). The ratio of M_n obtained by AF4 to that obtained by SEC was ranged between 0.85 and 1.0. Unlike M_n, M_w and M_z were different, with a higher M_w and M_z obtained for AF4. As described previously, these larger M_w and M_z can be

366 explained by the presence of large microaggregates not observed with SEC. This observation
367 is confirmed by the fact that for IR 307 (poly(*cis*-1,4-isoprene) without gel), M_w and M_z
368 exhibited no significant difference between SEC and AF4 results. The difference between
369 AF4 and SEC in terms of average molar masses was, as expected, higher for M_z than for M_w.
370 The M_w ratios ($M_{w\text{-}AF4}$:$M_{w\text{-}SEC}$) ranged from 1.0 to 4.3 (for IR 307 and M121 respectively)
371 whereas the M_z ratios ($M_{z\text{-}AF4}$:$M_{z\text{-}SEC}$) ranged from 1.0 to 18.6 (for IR 307 and Nippol
372 respectively). For the three average molar masses considered (i.e. M_n, M_w or M_z), the AF4
373 results showed greater heterogeneity than for the SEC results, with high standard deviations.
374 This lower reproducibility and repeatability was mainly due to the difficulty in defining the
375 integration range, as previously explained, but also to the substantial variability generated by
376 the refractive index detector baseline position. Indeed, the AF4 principle resulted in some
377 noise, deviations and jumps in the DRI baseline and thus to some doubts / uncertainties on the
378 baseline position, despite the blank subtraction. The large M_z difference (from AF4 to SEC)
379 and RSD for Nippol was due to the large amount of microaggregates with ultra high molar
380 masses and to the poor repeatability in the high mass range, as explained later on.
381
382 ***Determination of gel rates***
383 The gel rates in the samples were calculated after SEC and AF4 analysis. $Gel_{>1\mu}$ was
384 calculated for both the SEC and AF4 analyses whereas $Gel_{<1\mu}$ was only calculated after AF4
385 analysis. Figure 6 presents the $Gel_{>1\mu}$ rate after SEC and AF4 analyses. For the IR 307 and
386 Nippol samples, the $Gel_{>1\mu}$ rate did not display any significant difference (no gel for IR307
387 and average $Gel_{>1\mu}$ slightly higher for Nippol with AF4). For the two NR samples, only M160
388 exhibited a significant difference in the $Gel_{>1\mu}$ rate between SEC and AF4 determination
389 (23.8% for SEC and 17.2% for AF4). For M121, the lack of significant difference was due to
390 the high variance of the AF4 result. The $Gel_{<1\mu}$ calculation was estimated at 9.5% for Nippol,

27% for M160 and 29% for M121 (no $Gel_{<1\mu}$ for IR 307). These large quantities of $Gel_{<1\mu}$ explained the large differences observed for M_w and M_z in the NR samples and the Nippol sample (higher M_w and M_z for AF4 analyses compared to SEC). However, as a result of such a large quantity of $Gel_{<1\mu}$ for the NR samples, assumed to be "lost" in not insubstantial proportions in SEC, the $Gel_{>1\mu}$ rate should have been much lower with AF4 compared to SEC for Nippol, M160 and M121. The slight difference observed between AF4 and SEC for the $Gel_{>1\mu}$ rate could be explained either by the large measurement variability for AF4, or by an overestimated $Gel_{>1\mu}$ calculation in AF4 analysis (potentially due to concentration peak area determination and therefore to blank subtractions). For the $Gel_{<1\mu}$ calculation, Kim *et al*. **[3]** obtained $Gel_{<1\mu}$ values close to 10% (calculated by SEC after ionic surfactant treatment of the columns) for NR samples similar to M160 and M121, meaning a difference with our $Gel_{<1\mu}$ values of about 15%.

Figure 6

<u>Comparison of radii of gyration</u>

As for the average molar masses, the R_g values obtained with AF4 were higher than those obtained with SEC, except for the IR307 sample, whose R_g was the same for both separation techniques (see table 3). Nevertheless, the differences in R_g obtained with the two techniques were less pronounced than for M_z. This was due to the narrower radius of gyration size range observed (typically varying from 20 to 200 nm) compared to the 10^2 - 10^3 order of magnitudes for the masses over the whole fractionation (up to 10^5 for Nippol). The variation in R_{gi} depending on the elution time with AF4 displayed a similar behaviour to that for M_{wi} (Figure 2). As the variation in R_{gi} was less significant than for M_{wi}, it implies that the material was becoming increasingly compact (greater increase for masses than for radii) towards the

416 end of the elution, especially for the second population, as previously illustrated in figure 3.
417 This observation confirms the presence of compact microaggregates highlighted by Kim *et al.*
418 **[3]**.
419
420 ***Table 3***
421

Conclusions

This work demonstrates the ability of AF4 to fractionate natural and synthetic poly(*cis*-1,4-isoprene). Distinct populations (characterized by a clear slope change in M_{wi} variation) corresponding to isolated polyisoprene chains and microaggregates smaller than 1 µm ($Gel_{<1\mu}$) were detected. Average molar masses were determined and compared with those obtained by SEC. Similar M_n values were obtained but large differences were observed for M_w and M_z. These differences could be explained by a microgel population observed in AF4 but not during SEC separation. Moreover, microaggregates in the NR samples exhibited quite a different structure, appearing more compact than the microaggregates in the Nippol synthetic polyisoprene. Some problems (difficulties in defining the baseline, DRI signal jumps, etc.) due to the use of DRI with AF4 were encountered, in particular for gel rate determination. It seems obvious that some analytical developments are needed to optimize fractionation, increase the resolution for small polyisoprene chains and enable better reproducibility. However, these results are promising and microgel ($Gel_{<1\mu}$) can be considered for further individual studies and physico-chemical characterization.

Acknowledgements

The authors gratefully thank Emilie Croizat and Christine Char for their valuable contribution to this project. A4F-MALS and SEC-MALS analyses were carried out on the LipPol-Green platform (http://www.supagro.fr/plantlippol-green/). We kindly thank CIRAD DRS and Agropolis fondation (http:// http://www.agropolis-fondation.fr) for financial support, and the Hubert Curien Programme for funding Miss Chalao Thepchalerm's scholarship.

References

[1] Hongsheng Liua, Fengwei Xiea, Long Yua, Ling Chena, L. Li, Prog. Polym. Sci. 34 (2009) 1348.

[2] L. Vaysse, F. Bonfils, P. Thaler, J. Sainte Beuve, in D.R. Höfer (Editor), Sustainable Solutions for Energy Generation, Royal Society of Chemistry, Cambridge, 2009, p. 335.

[3] C. Kim, M. Morel, J. Sainte Beuve, A. Collet, S. Guilbert, F. Bonfils, J. Chromatogr. A 1213 (2008) 181.

[4] C. Kim, J. Sainte Beuve, S. Guilbert, F. Bonfils, Eur. Polym. J. 45 (2009) 2249.

[5] Angulo-Sanchez JL, Caballero-Mata P, Rubber Chem. Technol. 54 (1981) 34.

[6] K.N.G. Fuller, W.S. Fulton, Polymer 31 (1990) 609.

[7] J. Tangpakdee, Y. Tanaka, J. Rubber Res. 1 (1998) 14.

[8] S.N. Gan, J. Membrane Sci., Pure Applied Chemistry A33 (1996) 1939.

[9] J. Tangpakdee Sakdapipanich, T. Kowitteerawut, K. Suchiva, Y. Tanaka, Rubber Chem. Technol. 72 (1999) 712.

[10] F. Ngolemasango, E. Ehabe, C. Aymard, J. Sainte-Beuve, B. Nkouonkam, F. Bonfils, Polym. Int. 52 (2003) 1365.

[11] Y. Tanaka, L. Tarachiwin, Rubber Chem. Technol. 82 (2009) 283.

[12] S. Amnuaypornsri, J. Sakdapipanich, S. Toki, B.S. Hsiao, N. Ichikawa, Y. Tanaka, Rubber Chem. Technol. 81 (2008) 753.

[13] J. Carretero–Gonzalez, T. A. Ezquerra, S. Amnuaypornsri, S. Toki, R. Verdejo, A. Sanz, J. Sakdapipanich, B.S. Hsiaod, M.A. Lopez–Manchadoa, Soft Matter 6 (2010) 3636.

[14] F.A. Messaud, R.D. Sanderson, J.R. Runyon, T. Otte, H. Pasch, S.K.R. Williams, Prog. Polym. Sci. 34 (2009) 351.

[15] R. Qureshi, W. Kok, Anal. Bioanal. Chem. 399 (2011) 1401.

[16] G. Lespes, J. Gigault, Anal. Chim. Acta 692 (2011) 26.

[17] L.J. Gimbert, K.N. Andrew, P.M. Haygarth, P.J. Worsflod, Trends Anal. Chem. 22 (2003) 615.

[18] S. Dubascoux, I. Le Hecho, M. Hassellov, F. Von der Kammer, M.P. Gautier, G. Lespes, J. Anal. At. Spectrom. 25 (2010) 613.

[19] M.E. Schimpf, K.D. Caldwell, G.J. C., Field Flow Fractionation Handbook, Wiley Interscience, 2000.

[20] W.-S. Kim, C.H. Eum, A. Molnar, J.-S. Yu, S. Lee, Analyst 131 (2006) 429.

[21] W.G. Fulton, SA, J. Nat. Rubber Res. 12 (1997) 154.

[22] S. Lee, C. Eum, A. Plepys, B. Korean Chem. Soc. 21 (2000) 69.

[23] S. Lee, A. Molnar, Macromolecules 28 (1995) 6354.

[24] D.Y. Bang, D.Y. Shin, S. Lee, M.H. Moon, J Chromatogr. A 1147 (2007) 200.

[25] C. Kim, M. Morel, J. Sainte Beuve, S. Guilbert, F. Bonfils, Polym. Eng. Sci. 50 (2010) 240.

[26] M. Andersson, B. Wittgren, K.-G. Wahlund, Polymer 46 (2003) 4279.

[27] I. Teraoka, Polymer Solutions: An Introduction to Physical Properties, New York, 2002.

[28] P.J. Wyatt, Anal. Chim. Acta 272 (1993) 1.

[29] C. Kim, A. Deratani, F. Bonfils, J. Liq. Chromatogr. Relat. Technol. 33 (2010) 37.

[30] M. Andersson, B. Wittgren, K.G. Wahlund, Anal. Chem. 73 (2001) 4852.

Figure 1

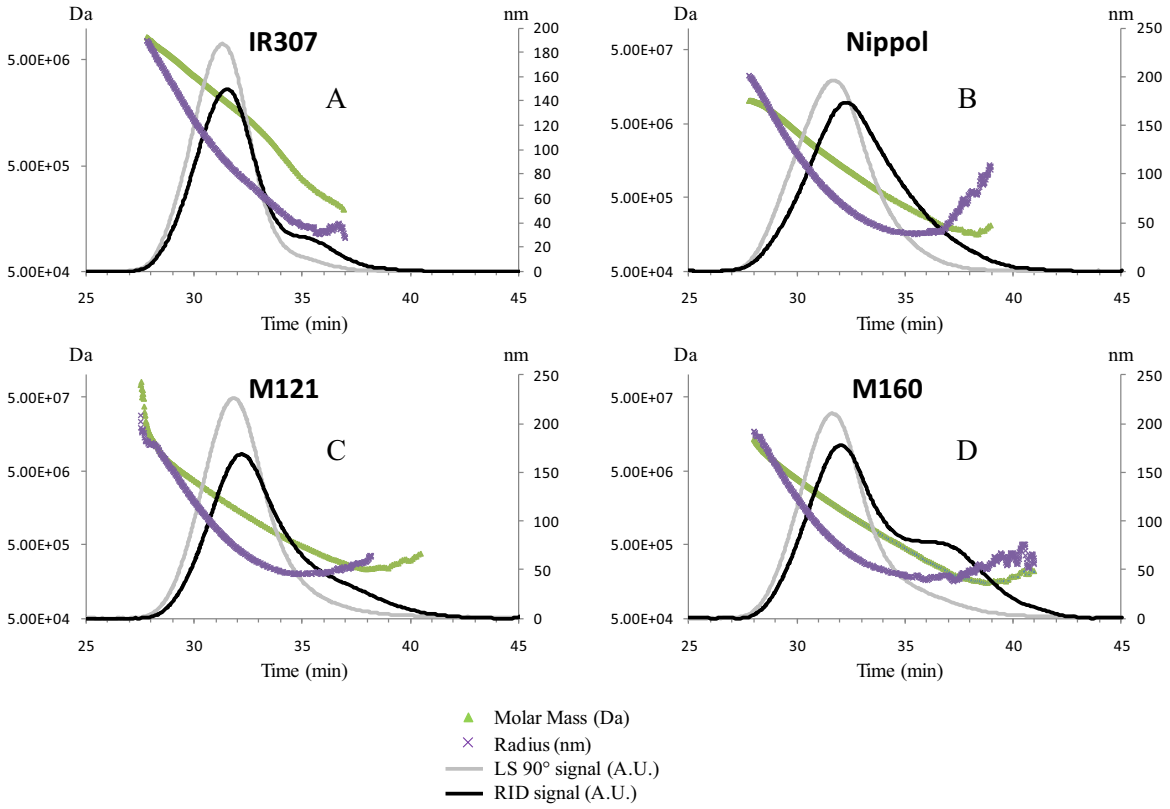

Figure 1: Chromatograms (from the RID and LS detector at 90°) and variation in R_g and M_i depending on the elution time during SEC analysis

Figure 2

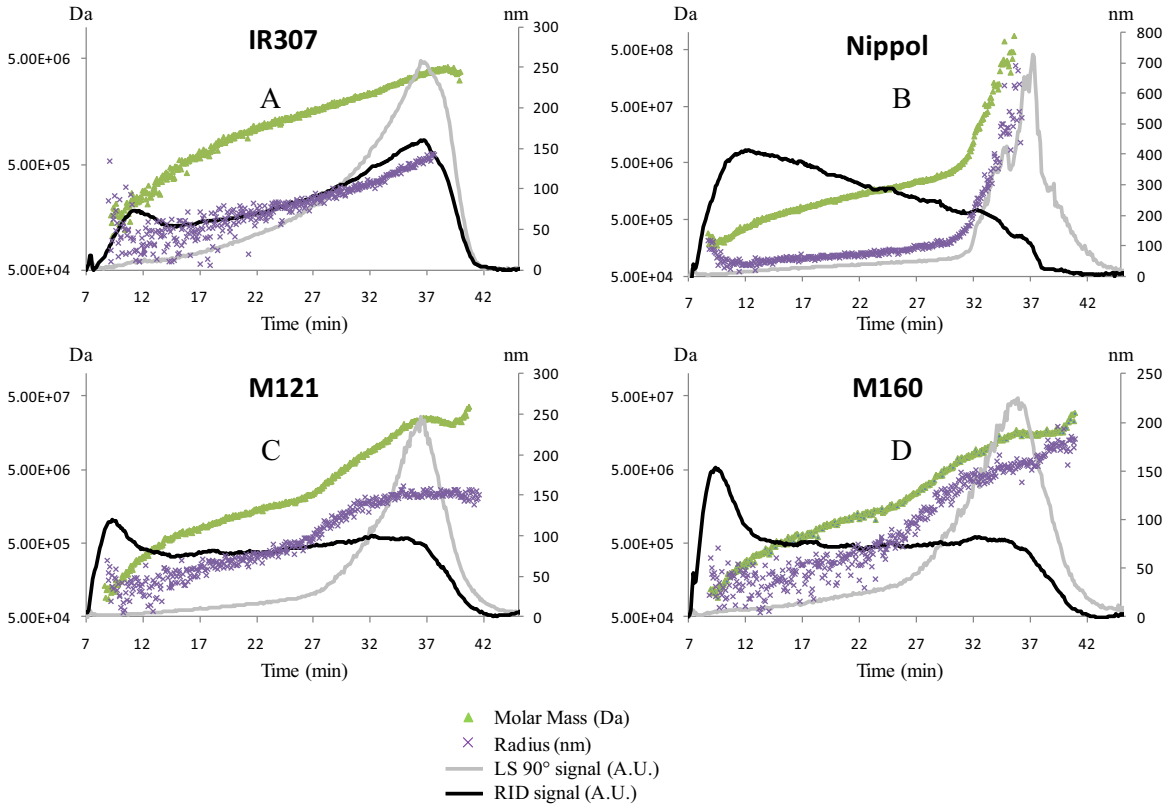

Figure 2: Fractograms (from the RID and LS detector at 90°) and variation in R_g and M_i depending on the elution time during AF4 analysis

Figure 3

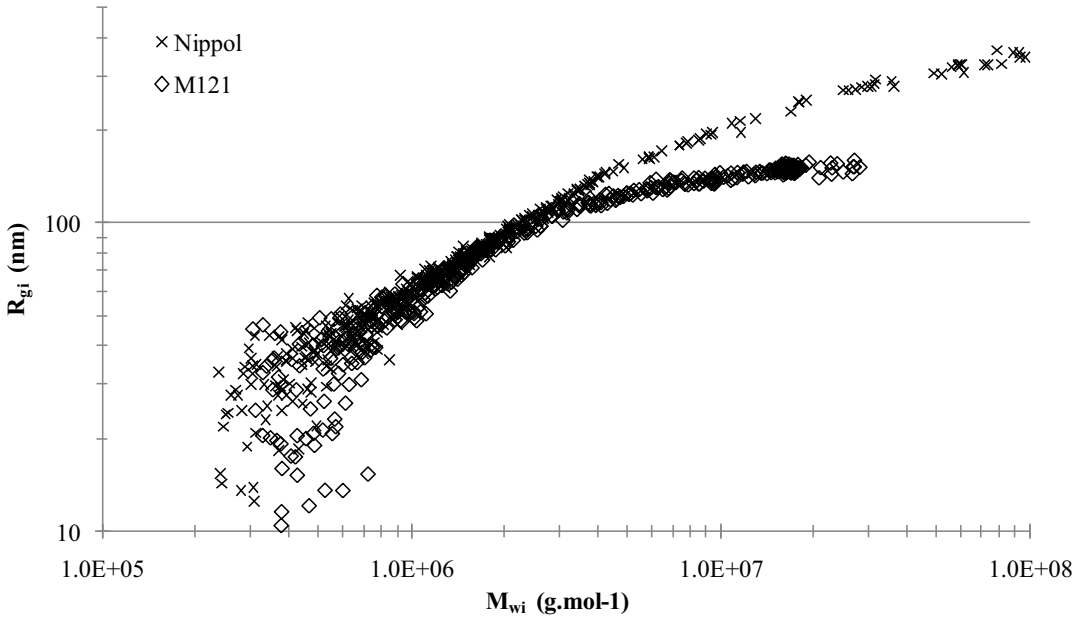

Figure 3: Variation of the radius of gyration (R_{gi}) depending on molar masses (M_{wi}) for the Nippol 2200 and M121 samples.

Figure 4

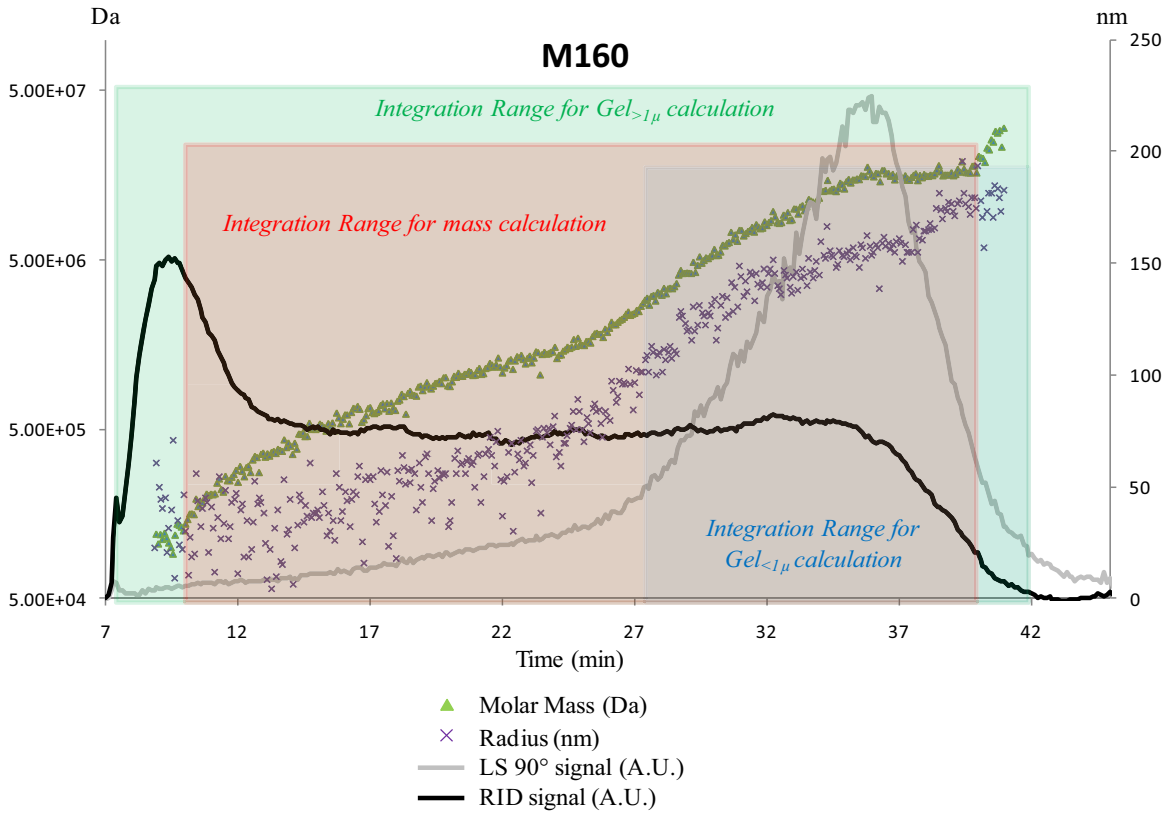

Figure 4: Determination of the AF4 integration range for the M160 sample

Figure 5

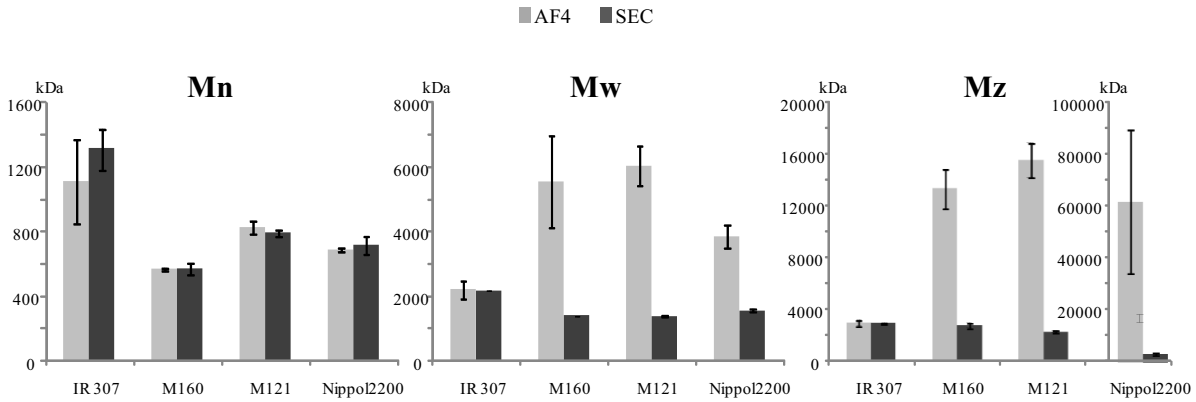

Figure 5: Comparison of masses obtained by SEC and AF4

Figure 6

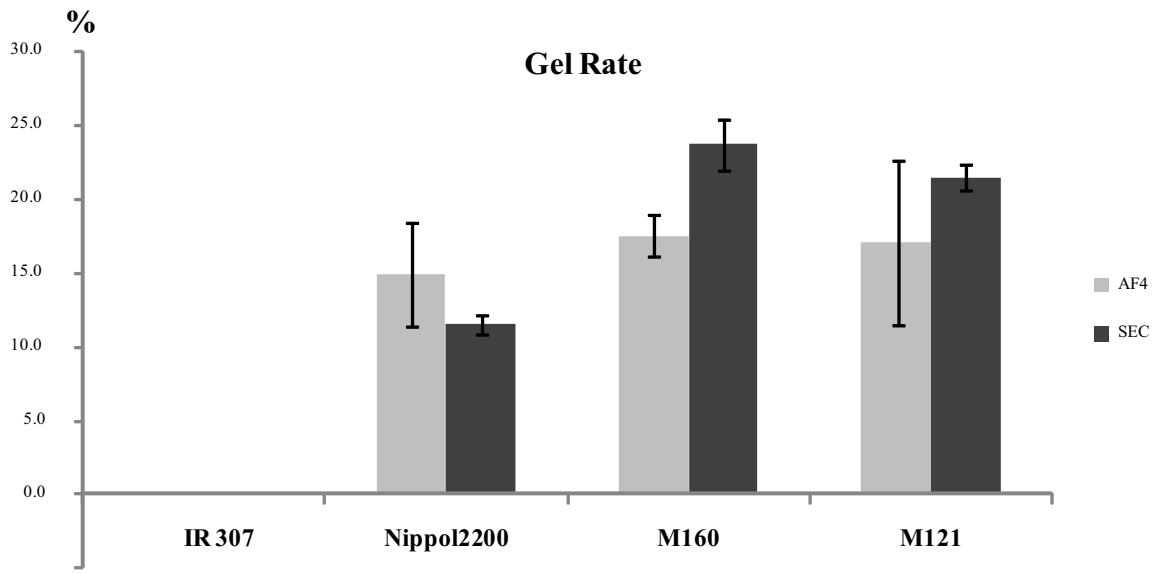

Figure 6: Comparison of filtrate gel on 1 µm ($Gel_{>1\mu}$) rate calculated by AF4 and SEC

Tables 1

Step	***Duration (min)***	***Crossflow ($mL.min^{-1}$)***	***Type of rate***
1	*1.5*	*1*	*Constant*
2	*30*	*From 1 to 0.08*	*Linear*
3	*9*	*0.08*	*Constant*
4	*7*	*0*	*Constant*

Table 1: AF4 crossflow programme during elution

Tables 2

	integration start	integration end	M_n (Da)	RSD	M_w (Da)	RSD	M_z (Da)	RSD
Nippol 2200	9.5 min	35 min	6.95E+05	4%	3.61E+06	25%	4.24E+07	62%
	9.5 min	40 min	7.48E+05	4%	9.36E+10	71%	1.40E+14	81%

Integration : +7% of surface area

Table 2: Nippol 2200 mass calculation (M_n, M_w and M_z with respective RSD from one AF4 series) with different integration ranges

		R_g (nm)	SD (nm) (1)	CV (1)
IR307	AF4	*115.8*	*3.8*	*4.0%*
	SEC	*112.1*	*1.4*	*1.3%*
Nippol	AF4	*249.9*	*28.8*	*28.8%*
	SEC	*108.5*	*4.2*	*3.9%*
M160	AF4	*136.5*	*7.0*	*4.3%*
	SEC	*102.8*	*2.3*	*2.2%*
M121	AF4	*133.5*	*7.8*	*3.4%*
	SEC	*92.5*	*2.4*	*2.6%*

(1) SD: standard deviation, CV: coefficient of variation ((SD/mean) x 100)

Table 3: R_g determined by AF4 and SEC

Elsevier Editorial System(tm) for Colloids and Surfaces B: Biointerfaces
Manuscript Draft

Manuscript Number:

Title: Surface-quaternized chitosan particles as an alternative and effective organic antibacterial filler

Article Type: Full Length Article

Keywords: chitosan; particle; heterogeneous quaternization; minimum inhibitory concentration.

Corresponding Author: Dr. Voravee Hoven, Ph.D.

Corresponding Author's Institution: Chulalongkorn University

First Author: Oraphan Wiarachai, MS

Order of Authors: Oraphan Wiarachai, MS; Nuttha Thongchul, PhD; Suda Kiatkamjornwong, PhD; Voravee Hoven, Ph.D.

Abstract: Taking advantage of the large surface area that is covered with permanent positive charges of quaternary ammonium entities, this research aimed to develop environmentally friendly, organic antibacterial fillers from quaternized chitosan particles that may be applicable for biomedical devices, health and textile industries. The particles were formulated by ionic crosslinking of chitosan with tripolyphosphate followed by quaternization that was conducted under heterogeneous condition via either direct methylation or reductive N-alkylation with a selected aldehyde followed by methylation. Sub-micron, spherical, and positively charged quaternized chitosan particles were formed, as determined by 1H-NMR, FT-IR, PCS, and TEM analysis. Antibacterial activity tests performed by viable cell counts suggested that all quaternized chitosan particles exhibited superior antibacterial activity against the model Gram-positive bacteria, S.aureus, as compared to the native chitosan particles at neutral pH. Only some quaternized chitosan particles, especially those having a high charge density and bearing large alkyl substituent groups, were capable of suppressing the growth of the model Gram-negative bacteria, E. coli. The inhibitory efficiency of the quaternized chitosan particles was quantified in terms of the minimum inhibitory concentration (MIC).

June 12, 2011

Dear Sir/Madam:

I would like to send a manuscript, entitled **"Surface-quaternized chitosan particles as an alternative and effective organic antibacterial filler"** to be considered for publication as a full paper in **Colloids and Surfaces B: Biointerfaces**. On behalf of all authors, namely, Oraphan Wiarachai, Nuttha Thongchul, Suda Kiatkamjornwong, Voravee P. Hoven, I hereby confirm that this manuscript or its contents in some other form has not been published previously by any of the authors and/or is not under consideration for publication in another journal at the time of the submission.

This work introduces surface-quaternized chitosan particles as an effective, environmentally friendly, organic antibacterial filler that may be incorporated into materials that require antibacterial activity. Based on the minimum inhibitory concentration, it was found that some surface-quaternized chitosan particles are more effective in inhibiting the bacterial growth than the quaternized chitosan solution. The fact that the heterogeneous quaternization used for the preparation of surface-quaternized chitosan particles can simply be done without the requirement for tedious purification process opens up an opportunity to produce such effective antibacterial filler at a large scale and that is very beneficial from industrial perspective.

The authors believe that the content of this contribution would be of interest to **Colloids and Surfaces B: Biointerfaces** audiences. Should there be any further information which may be required or if any problems arise, please contact me at the address shown below.

Sincerely yours,

Vp. Hoven

Voravee P. Hoven, Ph.D.
Corresponding Author

Organic Synthesis Research Unit, Department of Chemistry, Faculty of Science, Chulalongkorn University
Phayathai Road, Patumwan, Bangkok 10330, THAILAND
Telephone +(662) 218-7626-7 ext 102, Facsimile +(662) 218-7598
e-mail: vipavee.p@chula.ac.th

*Graphical Abstract

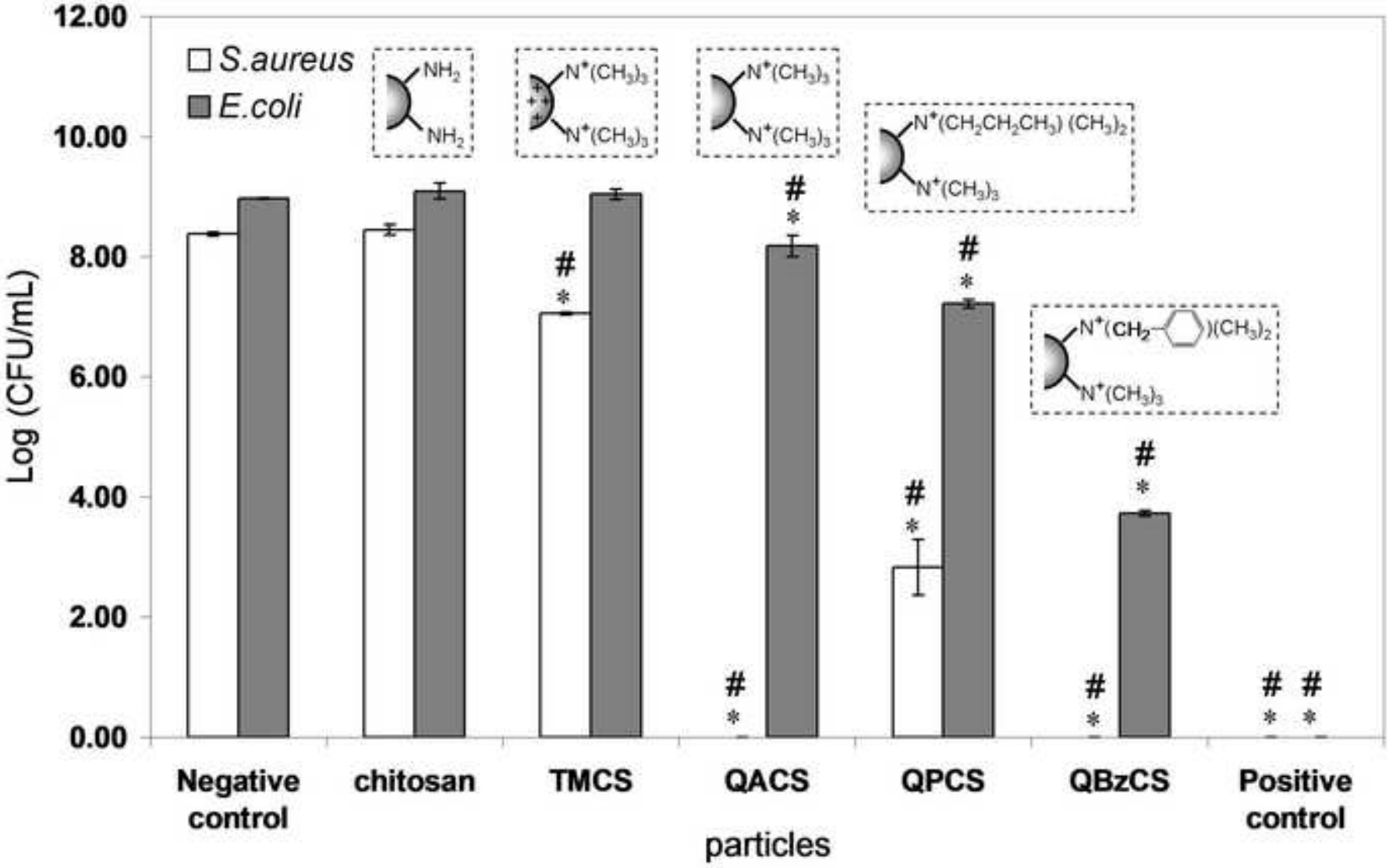

[*p < 0.01 (compared with the negative control), #p < 0.01 (compared with the chitosan particles)]

Research highlights

- Quaternized chitosan particles prepared by heterogeneous quaternization exhibited significantly higher antibacterial activity against *S. aureus* (Gram positive bacteria) and *E. coli* (Gram negative bacteria) than the particles prepared by homogeneous quaternization.
- Only some quaternized chitosan particles, especially those having a high charge density and bearing a large alkyl substituent, were capable of suppressing the growth of *E. coli*, the Gram-negative bacteria.

*Manuscript
Click here to view linked References

Surface-quaternized chitosan particles as an alternative and effective organic antibacterial filler

Oraphan Wiarachai[a,b], Nuttha Thongchul[c], Suda Kiatkamjornwong[d], Voravee P. Hoven[e*]

[a] *Program in Petrochemistry and Polymer Science, Faculty of Science, Chulalongkorn University, Phayathai Road, Pathumwan, Bangkok 10330, Thailand*

[b] *Center for Petroleum, Petrochemicals, and Advanced Materials, Chulalongkorn University, Phayathai Road, Pathumwan, Bangkok 10330, Thailand*

[c] *Institute of Biotechnology and Genetic Engineering, Chulalongkorn University, Phayathai Road, Pathumwan, Bangkok 10330, Thailand*

[d] *Department of Imaging and Printing Technology, Faculty of Science, Chulalongkorn University, Phayathai Road, Pathumwan, Bangkok 10330, Thailand*

[e] *Organic Synthesis Research Unit, Department of Chemistry, Faculty of Science, Chulalongkorn University, Phayathai Road, Pathumwan, Bangkok 10330, Thailand*

* Corresponding author. Tel: +66-2218-7626-7 ext 102; fax: +66-2218-7598

E-mail address: vipavee.p@chula.ac.th.

ABSTRACT

Taking advantage of the large surface area that is covered with permanent positive charges of quaternary ammonium entities, this research aimed to develop environmentally friendly, organic antibacterial fillers from quaternized chitosan particles that may be applicable for biomedical devices, health and textile industries. The particles were formulated by ionic crosslinking of chitosan with tripolyphosphate followed by quaternization that was conducted under heterogeneous condition via either direct methylation or reductive *N*-alkylation with a selected aldehyde followed by methylation. Sub-micron, spherical, and positively charged quaternized chitosan particles were formed, as determined by ^{1}H-NMR, FT-IR, PCS, and TEM analysis. Antibacterial activity tests performed by viable cell counts suggested that all quaternized chitosan particles exhibited superior antibacterial activity against the model Gram-positive bacteria, *S.aureus*, as compared to the native chitosan particles at neutral pH. Only some quaternized chitosan particles, especially those having a high charge density and bearing large alkyl substituent groups, were capable of suppressing the growth of the model Gram-negative bacteria, *E. coli*. The inhibitory efficiency of the quaternized chitosan particles was quantified in terms of the minimum inhibitory concentration (MIC).

Keywords: chitosan; particle; heterogeneous quaternization; minimum inhibitory concentration

1. Introduction

Incorporation of antibacterial fillers is an efficient approach to introduce antibacterial activity to materials. There are many types of filler that can be incorporated into the materials to induce their antibacterial activity such as antibiotic [1], nitric oxide [2], halogen species [3, 4] , biocide [5] and heavy metal [6-8]. From several types of antibacterial fillers, heavy metal in the form of silver nanoparticles (AgNPs), are well recognized to exhibit an effective antibacterial activity and are widely used in many applications such as medical devices [9], paint [10], coating [11] and textiles [12]. Recently, it has been reported that the AgNPs could affect human tissues from diverse routes of exposure including the respiratory system, skin, and gastrointestinal tract [13]. It has been proposed that AgNPs may interact with thiol groups of proteins and enzymes within mammalian cells, some of which are key components in the antioxidant defense mechanism of the cell. Inhibition of this mechanism would then result in an increase in the concentration of reactive oxygen species that can alter or damage the function of the cells. Also, it has been found that the AgNPs can be released from commercial clothing (socks) into the wash water [14], and so could increase the risk of environmental contamination. Therefore, it is highly desirable if the antibacterial fillers can be developed from natural, nontoxic and environmentally friendly material.

Chitosan is a natural biopolymer derived from the deacetylation of chitin, an abundantly available biopolymer found in the exoskeletons of insects, the shell of crustaceans, and fungal cell walls. It is nontoxic, biodegradable, biocompatible and possesses antibacterial properties [15]. In fact, the potential of chitosan particles as an effective antibacterial agent/filler has been realized and continuously reported. Early work by Qi and co-workers demonstrated that chitosan in the form of nanoparticles exerted a higher antibacterial activity against *E. coli, S. choleraesis, S. typhimurium, and S. aureus* than chitosan solution, and it was proposed that the greater surface area of the particles provided a

more intimate contact with the surface of bacterial cells [16]. Ye and co-workers, on the other hand, have shown that cotton fabrics coated with core-shell particles, having poly(*n*-butyl acrylate) as the core and chitosan as the shell, exhibited an excellent antibacterial activity against *S. aureus* with a reduction in viable bacteria numbers of more than 99% [17].

In general, chitosan would exhibit its antibacterial activity only in acidic medium, due to the poor solubility of chitosan above its pKa (pH 6.5). Quaternization of the amino groups to introduce permanent positively charged quaternary ammonium groups has been recognized as a potential way to enhance the antibacterial activity of chitosan over a broader pH range. The reaction can simultaneously introduce the permanent positive charge and hydrophobicity, the two parameters that are believed to affect the antibacterial activity [18-20]. Synthetic routes and applications of quaternized derivatives of chitosan have been recently reviewed and published [21, 22], whilst the application of quaternized chitosan particles has been reported. For example, particles fabricated from chitosan that was formerly quaternized by hexyl bromide were incorporated as bactericidal fillers in poly(methyl methacrylate) bone cement and tested against *S. aureus* and *S. epidermidis* under a neutral pH environment [23].

In order to promote ionic interactions with the negatively charged components of the bacterial cell membrane, the incorporation of metal ions [24-26] or cationic polymer [27] into chitosan particles has also been recently reported as an alternative approach. Qi and co-workers have suggested that the antibacterial activity can be enhanced by incorporating Cu^{2+} into chitosan particles [25]. Later, Du and co-workers have shown that chitosan particles loaded with various metal ion such as Ag^{+}, Cu^{2+}, Zn^{2+}, Mn^{2+}, Fe^{2+}, exhibited higher antibacterial effect against *E. coli*, *S. choleraesuis*, and *S. aureus* than chitosan particles [24, 26]. In addition, Inphonlek and coworkers have found that core-shell nanoparticles having poly(methyl methacrylate) core coated with polyethyleneimine, and chitosan-mixed-

polyethyleneimine shells exhibited higher antibacterial activity against *S. aureus* and *E. coli* than chitosan nanoparticles [27].

Here in this research, we attempt to develop an environmentally friendly, organic antibacterial filler from chitosan particles. The permanent positive charges in the form of quaternary ammonium groups were introduced to the surface of pre-fabricated chitosan particles under heterogeneous condition via direct methylation or reductive *N*-alkylation using two different aldehydes, propionaldehyde and benzaldehyde, followed by methylation with methyl iodide. This method has the advantage that it can be performed conveniently in the absence of tedious purification process that is generally required for homogeneous quaternization. The success of this type of method for enhancing antibacterial activity especially in a neutral pH environment has been previously reported for the chitosan films [28]. And the fact that the addition of cationic metal species or polymers is no longer necessary truly simplifies the fabrication method.

2. Materials and methods

2.1. Materials

Chitosan flake (DAC 85%, M_V = 45,000 Da) was purchased from Seafresh Chitosan (Lab) Co., Ltd (Thailand). Propionaldehyde, methyl iodide (CH_3I), sodium borohydride ($NaBH_4$), sodium chloride (NaCl), sodium hydroxide (NaOH), sodium iodide (NaI) and tripolyphosphate (TPP) were purchased from Fluka (Switzerland). Acetic acid, benzaldehyde, ethanol (EtOH), and methanol (MeOH) were purchased from Merck (Germany). Dialysis membrane (cut-off molecular weight of 12,400 g/mol) was purchased from Sigma (USA). All reagents and materials were of analytical grade and used without further purification. *E. coli* and *S. aureus* were provided by National Center for Genetic Engineering and Biotechnology (BIOTEC), Thailand. Mueller-Hinton agar (MHA) and Mueller-Hinton broth (MHB) were

purchased from Difco (USA). Mueller Hinton agar plates were supplied by Department of Medical Science, Ministry of Public Health, Thailand. Ultrapure distilled water was obtained after purification using a Millipore Milli-Q system (USA) that involves reverse osmosis, ion exchange, and a filtration step.

2.1. Preparation of surface-quaternized chitosan particles

Chitosan particles were prepared using TPP as a crosslinking agent according to the published procedure by Qi *et al.* [16] Preparation of quaternized *N*-alkyl chitosan particles were done following the method of Vallapa *et al.* [28]. In brief, an anhydrous methanol solution of a selected aldehyde (10 mL) having a desired concentration was added into a flask containing chitosan particles (0.03 g). After stirring for a given time at ambient temperature (~ 28-30^{o}C), $NaBH_4$ (0.3 g, 0.8 mol) was added into the reaction mixture and the solution was stirred for 24 h. The resulting *N*-alkyl chitosan particles were then isolated by centrifugation at 12,000 rpm for 30 min. The supernatant was discarded and the particles were centrifugally washed as above with methanol three times and then dried *in vacuo*. An anhydrous methanol solution (10 mL) containing NaI (0.30 g, 2 mmol) and NaOH (0.13 g, 3 mmol) was then added into a flask containing chitosan or *N*-alkyl chitosan particles (0.03 g) and CH_3I was then added via syringe. The reaction mixture was stirred at 50°C for a given time. The particles were isolated and purified as above mentioned.

2.2. Characterization of surface-quaternized chitosan particles

Fourier Transform-Infrared (FT-IR) spectra were collected using a Nicolet Impact 410 FT-IR spectrometer. All samples were prepared as KBr pellets. All ^{1}H NMR spectra were recorded in a 1% (v/v) solution of CF_3COOH/D_2O or D_2O using a Varian model Mercury-400 nuclear magnetic resonance spectrometer (USA) operating at 400 MHz. Chemical shifts

(δ) are reported in parts per million (ppm) relative to tetramethylsilane (TMS) or using the residual protonated solvent signal as a reference. The size and the morphology of all particles were examined by transmission electron microscope (TEM, Model JEM-2100, Japan) with the average diameter calculated using Semafore software and reported from the measurement of 100 randomly selected particles. The ζ-potential values of the particles were determined using a Nanosizer Nano-ZS (Malvern Instruments, UK) at 25^{o}C with a scattering angle of 173^{o}. All data are displayed as the mean $\pm$ one standard deviation and are derived from at least three independent experiments. The data were calculated using the Helmholtz-Smoluchowski equation.

2.8. Evaluation of antibacterial activity

All glasswares used for the tests were sterilized in an autoclave at 121°C for 15 min prior to use. All particles were sterilized by exposing to UV radiation for 60 min prior to the tests. The antibacterial test was performed according to a modified method of Qi *et al*. [16]. Chitosan and quaternized chitosan particles (2.5 mg) were added to 5 mL of MHB in test tubes and aseptically inoculated with 50 μL of the freshly prepared bacterial suspension in distilled water (OD_{600} = 0.5). The pH of the broth was about 7.4. The negative and positive controls were a broth solution alone and a broth solution with ampicillin (50 mg/mL), respectively. After mixing, broth cultures were incubated at 37°C in a shaking incubator (Model G-25, New Brunswick Scientific Co., Inc., USA), at 110 rpm for 24 h. Then, 100 μL of the bacterial solution was removed and 10-fold serially diluted down to 10^{6}-fold the original level. A 100 μL aliquots of each diluted bacterial suspension was then spreaded onto the MHA plates for total plate counting. After incubating at 37°C for 18 h, the number of colonies, and thus replication competent bacteria, were then counted as a measure of the

assumed viable number of bacteria. The results after correction for the dilution factor were expressed as mean colony forming units per volume (CFU/mL).

To determine the minimum inhibitory concentration (MIC) of all particles, the particles were first suspended in 5 mL of MHB and two-fold serial dilutions prepared. Each set of serial dilutions was then inoculated under aseptic conditions with 50 μL of the freshly prepared bacterial suspension in distilled water (OD_{600} = 0.5). After incubating at 37°C for 24 h, the total plate count enumeration of the CFU/mL was evaluated as described above. The lowest concentration of the particles that inhibited the growth of bacteria was considered as the minimum inhibitory concentration (MIC).

All tests of antibacterial activity were performed in triplicate per sample, upon at least three independent samples and expressed as mean ± standard deviation (SD). Statistical analysis was performed using the Statistical Package for the Social Science (SPSS) version 17.0 software. Statistical comparisons made by One-Way Analysis of Variance (ANOVA) with the Least Square Difference (LSD) tests were used for post hoc evaluations of differences between groups. The threshold level for accepting statistical significance was set at $p < 0.01$.

3. Results and Discussion

3.1. Preparation and characterization of surface-quaternized chitosan particles

Chitosan particles were first fabricated by ionic crosslinking between positively charged chitosan and negatively charged TPP. The process was conducted at ambient temperature in the absence of any surfactant or oil phase. The resulting chitosan particles appeared as fine white powder after drying and were insoluble in water, dilute acidic and alkali solutions. As outlined in Scheme 1, chitosan particles were then surface-modified by heterogeneous reductive *N*-alkylation with selected aldehyde, namely propionaldehyde and

benzaldehyde which yielded *N*-propyl chitosan particles and *N*-benzyl chitosan particles, respectively. Subsequent methylation with CH_3I thus formed quaternized *N*-propyl chitosan (QPCS) particles and quaternized *N*-benzyl chitosan (QBzCS) particles, respectively. Furthermore, the quaternization (Scheme 1) was also conducted directly on chitosan particles by methylation with CH_3I and gave quaternary ammonium-containing chitosan (QACS) particles as products. The optimized conditions for the preparation of each surface-quaternized chitosan particles via heterogeneous quaternization, so as to yield the highest degree of quaternization in terms of reaction time and reagent concentration were empirically identified (Table S1, Supplementary Material) based on the results from water contact angle and ζ-potential measurements following the criteria as previously described [28]. Another type of quaternized particles designated as *N,N,N*-trimethylchitosan (TMCS) particles were prepared for comparison. Although the quaternary ammonium entity (trimethyl, $-N(CH_3)_3$) of the TMCS particles is similar to that of the QACS particles, the TMCS particles were prepared differently by ionic gelation of *N,N,N*-trimethylchitosan synthesized homogeneously from chitosan according to the method reported by Sieval *et al*. [29]. In other words, TMCS particles should not only bear positive quaternary ammonium groups at the particles' surface which is the case for the QACS particles, but also inside the particles.

Chemical functionalities of all quaternized chitosan particles were first identified by FT-IR analysis. As shown in Fig. 1, absorption peaks at 1650 and 1544 cm^{-1} can be assigned to the C=O stretching (Amide I) and N-H bending (Amide II) of the glucosamine unit of chitosan, respectively. The decrement of the N-H bending signal at 1544 cm^{-1} and the appearance of the C-H deformation signal in a range of 1470-1460 cm^{-1} in the spectra of all quaternized chitosan particles implied that the amino groups were functionalized by alkyl substituents introduced by either reductive *N*-alkylation/methylation or direct methylation. Nonetheless, the C-H deformation peak belonging to the TMCS particles was obviously weak

as opposed to those observed for other particles implying that there was smaller content of quaternary ammonium groups in the TMCS particles.

The degree of success in the quaternization of chitosan particles was also confirmed by ^{1}H NMR analysis. As illustrated in Fig.2, the multiplet in the range of δ3.3 - 4.4 ppm comes from the six carbon atoms at the 2', 3, 4, 5, 6, and 6' positions, while the two singlets at δ1.9 and δ2.9 ppm are due to the methyl protons from the acetyl groups (position A) and at the 2 position of *N*-acetyl glucosamine unit, respectively. For the QPCS and QBzCS particles, it should be emphasized that not all of the amino groups of chitosan were alkylated in the first step of reductive *N*-alkylation. As a consequence, the signals of the methyl protons appearing in Fig.2(d-e) would come from methyl groups attached to both alkylated and non-alkylated amino functionalities. The signal at δ3.1-3.3, δ3.0, and δ2.7 ppm can be assigned to the methyl protons of the trisubstituted (-$N^{+}(C\underline{H}_3)_3$ or $NR^{+}(C\underline{H}_3)_2$, position B), disubstituted (-$N(C\underline{H}_3)_2$ or -$NR(C\underline{H}_3)$, position C) and monosubstituted (-$NH(C\underline{H}_3)$, position D) amino groups, respectively. The trace signals of methylene protons (δ1.0 ppm) and methyl protons (δ0.85 ppm) observed on the spectrum of QPCS particles (Fig.2(e)) can be used as additional evidences confirming the attachment of propyl groups at the amino moieties of chitosan in the step of reductive *N*-alkylation. For the QBzCS particles (Fig.2(f)), the signals of aromatic protons at δ7.4 ppm together with the benzylic protons at 1.0 ppm could be used to verify the attachment of benzyl groups at the amino positions of chitosan.

Based on the ^{1}H NMR analysis, the degree of quaternization (%DQ) can also be estimated. To simplify the calculation, it was assumed that the majority of quaternary ammonium groups existed in the form of -$N^{+}(C\underline{H}_3)_3$ and only a few were present in the form of $NR^{+}(C\underline{H}_3)_2$. This assumption is based on the fact that the non-alkylated or free amino groups (-NH_2) left after the *N*-reductive alkylation step are less bulkier than the alkylated amino group (-NHR) and should thus be more accessible for nucleophilic substitution of CH_3I. Such

characteristics should favor the formation of $-N^{+}(C\underline{H}_3)_3$ as opposed to that of the $NR^{+}(C\underline{H}_3)_2$. The %DQ can thus be calculated from the relative ratio between the integration of the nine protons from the three methyl groups of the quaternized *N*-alkyl chitosan at the position δ3.1-3.3 ppm and the peak integration of the six protons of chitosan (δ3.3-4.4 ppm). Accordingly, the calculated %DQ value based on the content of $N^{+}(C\underline{H}_3)_3$ was 2.1, 7.1, 4.2, and 5.7 % for TMCS, QACS, QPCS, and QBzCS particles, respectively. It should be taken into account that the quaternized chitosan particles were not completely soluble in the CF_3COOH/D_2O, the solvent used for NMR analysis. As a result, the %DQ values obtained from ^{1}H NMR analysis are not capable of reflecting the actual degree of surface quaternization, they can only be used as a qualitative measure of the extent of surface substitution. The fact that %DQ of TMCS particles was the lowest agrees quite well with the data formerly described based on FT-IR analysis (Fig.1).

TEM analysis revealed that all particles were quite spherical in shape and had average diameters in a sub-micron range of 260 -490 nm (Fig. 3). The dimension of QACS particles was quite comparable to that of the TMCS particles implying that the preparation method did not have significant impact on the particle size and morphology. On the other hand, the size of chitosan particles seemed to be greater when being modified by a larger alkyl substituent (propyl, benzyl) which came from the aldehyde used in the reductive *N*-alkylation step. The charge characteristic of the quaternized chitosan particles was determined by photon correlation spectroscopy (PCS). As shown in Fig. 3, all particles prepared by heterogeneous quaternization via reductive *N*-alkylation followed by methylation (QPCS and QBzCS particles) or direct methylation (QACS particles) exhibited greater zeta potential values than those of chitosan and TMC particles. Indeed, comparing TMCS and QACS particles, it seems that the heterogeneous quaternization approach was more efficient in enhancing positive charges of the chitosan particles than the homogeneous one. This may stem from the fact that some positive charges of

TMC were neutralized following ionic crosslinking with the negatively charged TPP upon the particle formation. In accord with this notion is that the TMCS particles formed by the crosslinking of TMC and TPP were not completely soluble in CF_3COOH/D_2O. As a result, the %DQ of TMC particles (2.1%) was much lower than that of the originally synthesized TMC (%DQ = 11.8%) indicating the consumption of the positive charges during crosslinking. Unlike the TMCS particles, the introduction of trimethyl groups to chitosan particles via direct methylation to yield the QACS particles was performed after the particle formation. Thus, the positive charge density generated thereafter was not depleted by the crosslinking. A similar explanation can be applied for the QPCS and QBzCS particles, where again the quaternization was applied after the particle formation. Interestingly, the presence of the larger alkyl substituents (propyl and benzyl) somewhat promoted the subsequent methylation accounting for why the ζ-potential was raised above +35 eV for both the QPCS and QBzCS particles. It is postulated that the more hydrophobic environment created by the propyl and benzyl substituents may increase a chance of CH_3I, a small organic molecule of low polarity, to reach the amino active sites of chitosan chain during methylation. Previous work has also demonstrated that the degree of surface quaternization can be tailored by adjusting the CH_3I concentration used in the methylation step [28].

3.2 Antibacterial efficacy of surface-quaternized chitosan particles

The antibacterial activity of surface-quaternized chitosan particles were tested against the representative Gram-positive and Gram-negative bacteria, *S. aureus* and *E. coli*, respectively, and reported as the total number of replication competent (viable) cells as mean colony forming units per volume (CFU/mL). In the case of *S. aureus*, all quaternized chitosan particles, TMCS, QACS, QPCS and QBzCS particles, exhibited significantly higher antibacterial ratio (> 95%) than the chitosan particles at pH 7.4 (Fig. 4), supporting that the

introduction of the positive charges via quaternization can effectively improve the antibacterial activity of chitosan particles especially in neutral media. In contrast, the antibacterial action of chitosan particles cannot be detected given that their viable counts closely resembled those of the negative control. This outcome is in line with our previous observation on chitosan film implying that chitosan particles would exhibit its potential in suppressing the bacterial growth only when they are in acidic media in which they are positively charged [28]. This also further suggested that the chelation of the amino groups of chitosan as proposed by others [30, 31] is definitely not the major mechanism that controls the antibacterial activity at this particular condition. These evidences support that the superior antibacterial activities of some quaternized chitosan particles, especially QPCS and QBzCS particles, to the chitosan particles are mainly due to their higher charge density in near neutral pH condition than the latter (See Fig. 3 for ζ-potential data). Overall, this trend is in accordance with previously observed data reported by Qi and coworkers [16], who proposed that the positively charged chitosan particles should interact favorably with negatively charged cell membranes, causing an increase in membrane permeability and eventually rupture and leakage of intracellular components. This proposed mechanism is particularly reasonable in the case of the Gram-positive bacteria, such as *S. aureus* since their outer membrane consists of negatively charged teichoic acid, that is believed to be responsible for the electrostatic binding with the positively charged particles.

Although the TMCS particles exhibited a slightly lower ζ-potential than the chitosan particles, they still inhibited the growth of *S. aureus*, potentially suggesting that the inhibition did not solely rely on the contact-inhibitory mechanism which should be charge density-dependent, but may also be influenced by the charge inside the particles or the ability to dissolve in the media considering that TMC is water soluble and not all of the TMC molecules were crosslinked by TPP during the particle formation. In fact, this release-inhibitory

mechanism involving surface leaching of soluble chitosan and/or its quaternized derivatives has been recently proposed by Fernandez-Saiz and co-workers [32] and also in our earlier work on the surface-quaternized chitosan films [28]. Similar explanations may also be applied in the case of QACS particles whose charge density (ζ-potential = +29.3 mV) was slightly higher than those of both chitosan particles (ζ-potential = +27.1 mV) and TMCS particles (ζ-potential = +23.2 mV). Having the same type of quaternary ammonium groups (-$N(CH_3)_3$), the QACS particles exhibited better antibacterial action against *S. aureus* than the TMCS particles indicating that the heterogeneous quaternization was potentially a more effective route to promote the antibacterial activity of chitosan particles than the homogeneous one. This is extremely important considering that the higher charge density can be achieved via heterogeneous route without sacrificing the positive charges to the crosslinking process. The lowering of the ζ-potential upon ionotropic crosslinking of TMC by TPP has also been reported by Sadeghi and co-workers [33]. It is also conceivable that the uncrosslinked surface-modified quaternized layer on the surface of QACS particles may leach out easier than the quaternary entities trapped or crosslinked by TPP inside and/or on the surface of TMCS particles.

The trend observed for the representative Gram-negative bacteria, *E. coli* is quite different from that seen with the Gram-positive *S. aureus* described above. In comparison with the negative control and chitosan particles, the quaternized chitosan particles with only slightly higher charge density, namely TMCS, and QACS particles, did not possess significant antibacterial activity against *E. coli* (Fig. 4). QACS particles exhibited % antibacterial activity of 82.9% whereas the detrimental action of TMCS cannot be detected. On the other hand, the quaternized chitosan particles with larger alkyl groups having higher charge density, namely QPCS and QBzCS particles, exerted much higher antibacterial action against the *E. coli.* With a similar ζ-potential, the QBzCS particles displays a greater inhibitory action than the QPCS particles which is reasonable considering that the uppermost

layer of the outer membrane of *E. coli* contains lipopolysaccharide that should interact favorably with hydrophobic entities of the particles. In addition, the fact that QACS film was reported to exhibit much lower % antibacterial activity against *S. aureus* (26%antibacterial ratio) and *E.coli* (29% antibacterial ratio) [28], in comparison with the QACS particles apparently suggests that the antibacterial efficacy can be magnified by the enhanced surface area of the particles.

Comparatively, as outlined in Fig. 4, it was found that *E. coli* had a greater resistance to quaternized chitosan particles than the *S. aureus*. This can be explained by three reasons. Firstly, the absence of an outer membrane and the presence of negatively charged teichoic acid within a thick peptidoglycan layer (20-80 nm) on the surface of *S. aureus* should make them more attractive to the positively charged, quaternized chitosan particles and more specific to be damaged by positively charged molecules than *E. coli*. Secondly, the presence of a number of small channels of porins within the outer membrane of *E. coli* may help block the entrance of the particles into the bacterial cell, making them more difficult to inhibit than *S. aureus*. Finally, the smaller dimension of *S. aureus* (sphere, i.d. ~ 0.5-1 μm) may partly account for more intimate contact with the quaternized chitosan particles, making the antibacterial activity more effective than the *E. coli* (rod, 0.3-1.0 × 1.0-6.0 μm) .

Minimum inhibitory concentration (MIC) is the lowest concentration of an antimicrobial agent that can inhibit the growth of the target microorganism. From a practical perspective, this value is a key indication of the inhibitory efficiency of the substance against the microorganism. In this study, the MIC values of chitosan, TMCS, QACS, and QBzCS particles were evaluated by viable cell counting methods. The MIC values for each type of particle were identified by comparing the viable cell counts (log (CFU/mL)) between the suspension having the designated particles and the negative control). Results for all quaternized chitosan particles are displayed in Table 1. The fact that the concentration of as

high as 1000 mg/mL was neccessary for chitosan particles to express their inhibitory power explained why no inhibitory action was detected when previously tested with 0.5 mg/mL or 500 μg/mL chitosan particles (Fig.4). To start suppressing the growth of *E. coli* by chitosan particles demanded a concentration as high as 2000 μg/mL. These results support the previous assumption that *E. coli* is more tolerant than *S. aureus*. However, using the same growth media for bacteria, MHB, much lower MIC values of 234 and 117 μg/mL against *S. aureus* and *E. coli*, respectively have been reported for the chitosan particles also prepared by ionotropic crosslinking by TPP [24]. It is suspected that this difference may be a result of their particles having a much smaller size (~54 nm) and so possess a greater available surface area than ours (~320 nm). Therefore, a significantly lower quantity of chitosan particles was required in their case. In contrast, Sadeghi and co-workers [33] reported a two-fold higher MIC value for the TPP-crosslinked chitosan particles against *S. aureus*. This is reasonable given that their particles had a comparable size (~250 nm) to ours but with less ζ- potential (+15.9 eV).

As anticipated, the QACS particles with lower MIC were more potent in prohibiting bacterial growth than the TMCS particles. This MIC value (62.5 μg/mL) was apparently lower than those reported for TMC solutions with various degree of quaternization (%DQ) [33, 34] indicating their superior antibacterial efficacy. This outcome truly indicated the potential of heterogeneous route for the preparation of quaternized chitosan particles as opposed to the conventional homogeneous one which is obviously suffered from the drawback of a deteriorated antibacterial activity because the particles have to be formed after quaternization. The data demonstrated by Sadeghi and co-workers (also shown in Table 1) can be used as a good example [33]. The variation in experimental parameters such as molecular weight and degree of deacetylation of chitosan, %DQ, growth media, pH, initial bacteria concentration, bacterial source, method used for determination of the antibacterial

activity (i.e. optical density (OD), total plate counts for viable cells) should be taken into account when comparing the results. Eventhough a greater quantity of QPCS and QBzCS particles was required to start their detrimental effect on both bacterial strains as compared with the QACS particles, their antibacterial action was more effective when the quantity of all particles were as equal to or above the MIC values of the QPCS and QBzCS particles. This can be evidenced from the data shown in Fig.4 (tested with 500 μg/mL particles). Interestingly, the MIC values of both QACS and QBzCS particles were independent on the bacterial strain.

4. Conclusions

Quaternized chitosan particles having different alkyl substitutents can be successfully prepared by heterogeneous direct methylation or reductive *N*-alkylation/methylation as verified by ^{1}H NMR and FT-IR analyses. The particles were spherical in shape, having an average diameter in a range of 230-490 nm and carried positive charges with ζ-potential ranging from +23.2 to +46.8 mV. As determined by viable count method, it was found that all quaternized chitosan particles exhibited higher antibacterial activity against *S. aureus* (Gram positive bacteria) than the chitosan particles in neutral media. It is believed that the electrostatic binding between the positive charges on the particles and the negatively charged teichoic acid on the outer membrane of *S. aureus* was responsible for their superior antibacterial activity. In contrast, only the QPCS and QBzCS particles, which have a high charge density and relatively large alkyl groups, were capable of suppressing the growth of *E. coli* (Gram-negative bacteria). The fact that *E. coli* had greater resistance to all quaternized chitosan particles than the *S. aureus* may be explained as a result of their difference in shape and outer membrane properties. The minimum inhibitory concentration (MIC) data led to two important conclusive remarks: (1) the antibacterial efficiency of each particle was dose-

dependent and (2) having the same alkyl substituent as TMCS particles, QACS particles were a more potent antibacterial material indicating that the heterogeneous quaternization was a more effective method than the homogeneous one. The results obtained from this research suggested that the surface-quaternized chitosan particles may potentially be used as effective antibacterial fillers for biomedical applications.

Acknowledgments

This research was financially supported by Research Team Promotion Grant from the Thailand Research Fund (RTA50800004). The authors appreciated a language editing service provided by Dr. Robert Butcher, the Publication Counselling Unit (PCU), Faculty of Science, Chulalongkorn University.

References

[1] M. Changez, V. Koul, A. K. Dinda, Efficacy of antibiotics-loaded interpenetrating network (IPNs) hydrogel based on poly(acrylic acid) and gelatin for treatment of experimental osteomyelitis: in vivo study, Biomaterials 26 (2005) 2095-2104.

[2] B. J. Nablo, A. R. Rothrock, M. H. Schoenfisch, Nitric oxide-releasing sol-gels as antibacterial coatings for orthopedic implants, Biomaterials 26 (2005) 917-924.

[3] Y. Y. Sun, G. Sun, Novel refreshable *N*-halamine polymeric biocides: *N*-chlorination of aromatic polyamides, Ind. Eng. Chem. Res. 43 (2004) 5015-5020.

[4] Y. Sun, G. Sun, Synthesis, characterization, and antibacterial activities of novel *N*-halamine polymer beads prepared by suspension copolymerization, Macromolecules 35 (2002) 8909-8912.

[5] S. M. Iconomopoulou, G. A. Voyiatzis, The effect of the molecular orientation on the release of antimicrobial substances from uniaxially drawn polymer matrixes, J. Control. Release 103 (2005) 451-464.

[6] N. Cioffi, L. Torsi, N. Ditaranto, G. Tantillo, L. Ghibelli, L. Sabbatini, T. Bleve-Zacheo, M. D'Alessio, P. G. Zambonin, E. Traversa, Copper nanoparticle/polymer composites with antifungal and bacteriostatic properties, Chem. Mater. 17 (2005) 5255-5262.

[7] M. Rai, A. Yadav, A. Gade, Silver nanoparticles as a new generation of antimicrobials, Biotechnol. Adv. 27 (2009) 76-83.

[8] V. K. Sharma, R. A. Yngard, Y. Lin, Silver nanoparticles: Green synthesis and their antimicrobial activities, Adv. Colloid Interf. 145 (2009) 83-96.

[9] F. Furno, K. S. Morley, B. Wong, B. L. Sharp, P. L. Arnold, S. M. Howdle, R. Bayston, P. D. Brown, P. D. Winship, H. J. Reid, Silver nanoparticles and polymeric medical devices: A new approach to prevention of infection, J. Antimicrob. Chemoth. 54 (2004) 1019-1024.

[10] A. Kumar, P. K. Vemula, P. M. Ajayan, G. John, Silver-nanoparticle-embedded antimicrobial paints based on vegetable oil, Nat. Mate. 7 (2008) 236-241.

[11] M. Wagener, Antimicrobial coatings, Polym. Paint Colour J. 196 (2006) 34-37.

[12] N. Duran, P. D. Marcato, G. I. H. De Souza, O. L. Alves, E. Esposito, Antibacterial effect of silver nanoparticles produced by fungal process on textile fabrics and their effluent treatment, J. Biomed. Nanotechnol. 3 (2007) 203-208.

[13] X. Chen, H. J. Schluesener, Nanosilver: A nanoproduct in medical application, Toxicol. Lett. 176 (2008) 1-12.

[14] T. M. Benn, P. Westerhoff, Nanoparticle silver released into water from commercially available sock fabrics, Environ. Sci. Technol. 42 (2008) 4133-4139.

[15] M. N. V. R. Kumar, R. A. A. Muzzarelli, C. Muzzarelli, H. Sashiwa, A. J. Domb, Chitosan chemistry and pharmaceutical perspectives, Chem. Rev. 104 (2004) 6017-6084.

[16] L. F. Qi, Z. R. Xu, X. Jiang, C. H. Hu, X. F. Zou, Preparation and antibacterial activity of chitosan nanoparticles, Carbohyd. Res. 339 (2004) 2693-2700.

[17] W. J. Ye, M. F. Leung, J. Xin, T. L. Kwong, D. K. L. Lee, P. Li, Novel core-shell particles with poly(*n*-butyl acrylate) cores and chitosan shells as an antibacterial coating for textiles, Polymer 46 (2005) 10538-10543.

[18] X. L. Ye, X. G. Li, L. J. Yuan, L. H. Ge, B. S. Zhang, S. B. Zhou, Interaction of houttuyfonate homologues with the cell membrane of gram-positive and gram-negative bacteria, Colloid Surf. A-Physicochem. Eng. Asp. 301 (2007) 412-418.

[19] M. E. I. Badawy, Structure and antimicrobial activity relationship of quaternary *N*-alkyl chitosan derivatives against some plant pathogens, J. Appl. Polym. Sci. 117 (2010) 960-969.

[20] C. H. Kim, K. S. Choi, Synthesis and antibacterial activity of quaternized chitosan derivatives having different methylene spacers, J. Ind. Eng. Chem. 8 (2002) 71-76.

[21] W. Sajomsang, Synthetic methods and applications of chitosan containing pyridylmethyl moiety and its quaternized derivatives: A review, Carbohyd. Polym. 80 (2010) 631-647.

[22] V. K. Mourya, N. N. Inamdar, Trimethyl chitosan and its applications in drug delivery, J. Mater. Sci.-Mater. Med. 20 (2009) 1057-1079.

[23] Z. L. Shi, K. G. Neoh, E. T. Kang, W. Wang, Antibacterial and mechanical properties of bone cement impregnated with chitosan nanoparticles, Biomaterials 27 (2006) 2440-2449.

[24] W. L. Du, S. S. Niu, Y. L. Xu, Z. R. Xu, C. L. Fan, Antibacterial activity of chitosan tripolyphosphate nanoparticles loaded with various metal ions, Carbohyd. Polym. 75 (2009) 385-389.

[25] L. F. Qi, Z. R. Xu, X. Jiang, Y. Li, M. Q. Wang, Cytotoxic activities of chitosan nanoparticles and copper-loaded nanoparticles, Bioorg. Med. Chem. Lett. 15 (2005) 1397-1399.

[26] W. L. Du, Y. L. Xu, Z. R. Xu, C. L. Fan, Preparation, characterization and antibacterial properties against *E. coli* K88 of chitosan nanoparticle loaded copper ions, Nanotechnology 19 (2008) 085707.

[27] S. Inphonlek, N. Pimpha, P. Sunintaboon, Synthesis of poly(methyl methacrylate) core/chitosan-mixed-polyethyleneimine shell nanoparticles and their antibacterial property, Colloid Surf. B-Biointerfaces 77 (2010) 219-226.

[28] N. Vallapa, O. Wiarachai, N. Thongchul, J. S. Pan, V. Tangpasuthadol, S. Kiatkamjornwong, V. P. Hoven, Enhancing antibacterial activity of chitosan surface by heterogeneous quaternization, Carbohyd. Polym. 83 (2011) 868-875.

[29] A. B. Sieval, M. Thanou, A. F. Kotze, J. C. Verhoef, J. Brussee, H. E. Junginger, Preparation and NMR characterization of highly substituted *N*-trimethyl chitosan chloride, Carbohyd. Polym. 36 (1998) 157-165.

[30] M. Kong, X. G. Chen, C. S. Liu, C. G. Liu, X. H. Meng, L. J. Yu, Antibacterial mechanism of chitosan microspheres in a solid dispersing system against *E. coli*, Colloid Surf. B-Biointerfaces 65 (2008) 197-202.

[31] R. G. Cuero, G. Osuji, A. Washington, *N*-Carboxymethylchitosan inhibition of aflatoxin production: Role of zinc, Biotechnol. Lett. 13 (1991) 441-444.

[32] P. Fernandez-Saiz, J. M. Lagaron, M. J. Ocio, Optimization of the biocide properties of chitosan for its application in the design of active films of interest in the food area, Food Hydrocolloids 23 (2009) 913-921.

[33] A. M. M. Sadeghi, F. A. Dorkoosh, M. R. Avadi, P. Saadat, M. Rafiee-Tehrani, H. E. Junginger, Preparation, characterization and antibacterial activities of chitosan, *N*-trimethyl chitosan (TMC) and *N*-diethylmethyl chitosan (DEMC) nanoparticles loaded with insulin using both the ionotropic gelation and polyelectrolyte complexation methods, Int. J. Pharm. 355 (2008) 299-306.

[34] W. Sajomsang, P. Gonil, S. Saesoo, Synthesis and antibacterial activity of methylated *N*-(4-*N,N*-dimethylaminocinnamyl) chitosan chloride, Eur. Polym. J. 45 (2009) 2319-2328.

List of Figure and Scheme Captions

Scheme 1 Preparation of surface-quaternized chitosan particles by reductive *N*-alkylation/methylation (top row) and direct methylation (bottom row).

Fig. 1. FT-IR spectra of (a) chitosan particles, (b) TMCS particles, (c) QACS particles, (d) QPCS particles, and (e) QBzCS particles.

Fig. 2. ^{1}H-NMR spectra of (a) chitosan particles, (b) TMCS particles, (c) QACS particles, (d) QPCS particles, and (f) QBzCS particles.

Fig. 3. Representative TEM micrographs (x 12,000), average particles sizes and ζ- potentials of chitosan and quaternized chitosan particles. Micrographs shown are representative of at least 10 such fields of view per sample and 3 independent samples.

Fig. 4. Total replication competent (viable) cell counts of *S. aureus* and *E. coli* in suspension after incubation with different chitosan particles (0.5 mg/mL) for 24 h. Statistical significance with $p < 0.01$ of the viable count is compared with the negative control (*) and the chitosan particles *(#*). Below in the table is the corresponding antibacterial ratio.

Figure(s)
Click here to download high resolution image

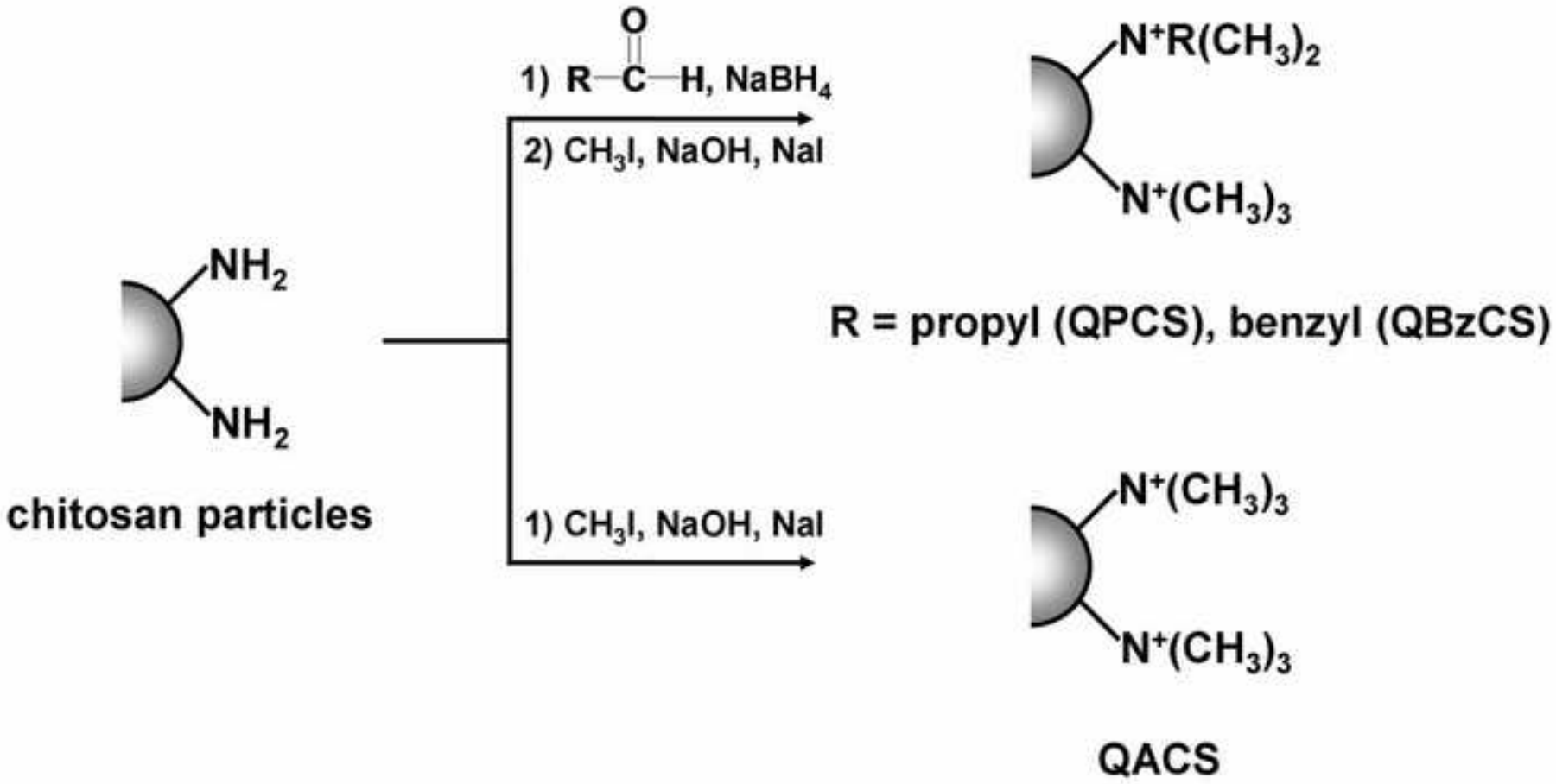

Figure(s)
Click here to download high resolution image

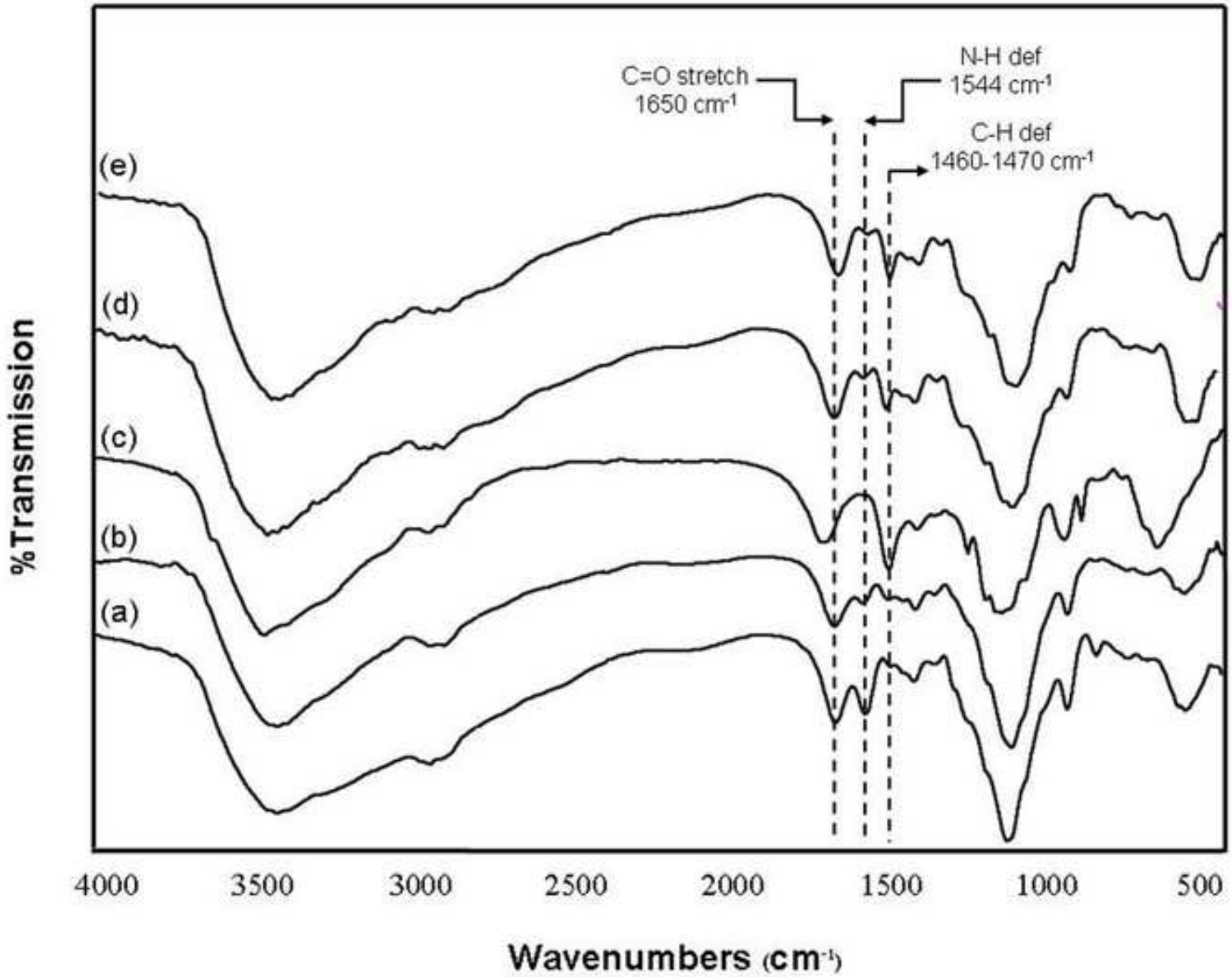

Figure(s)

Click here to download high resolution image

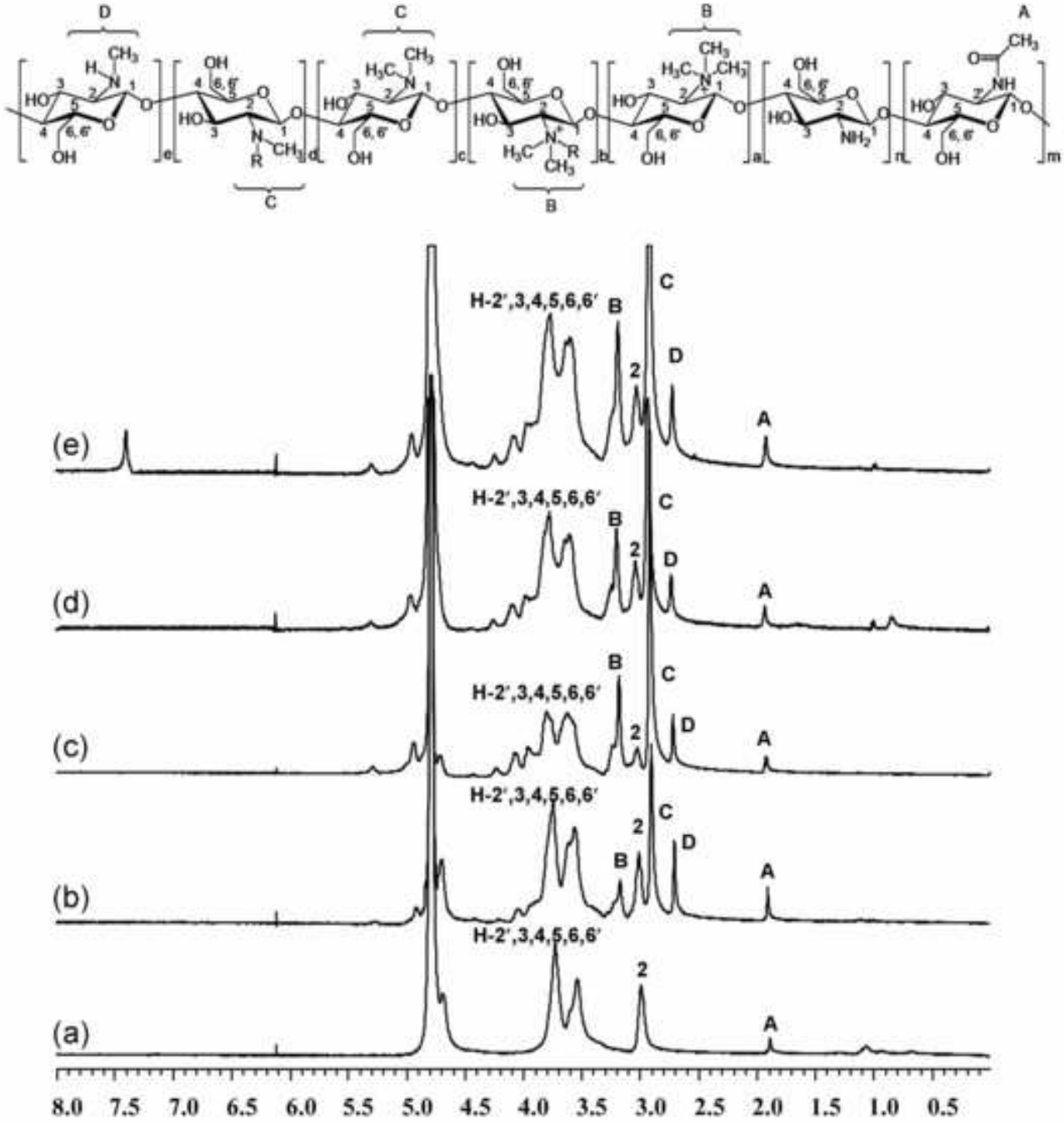

Figure(s)
Click here to download high resolution image

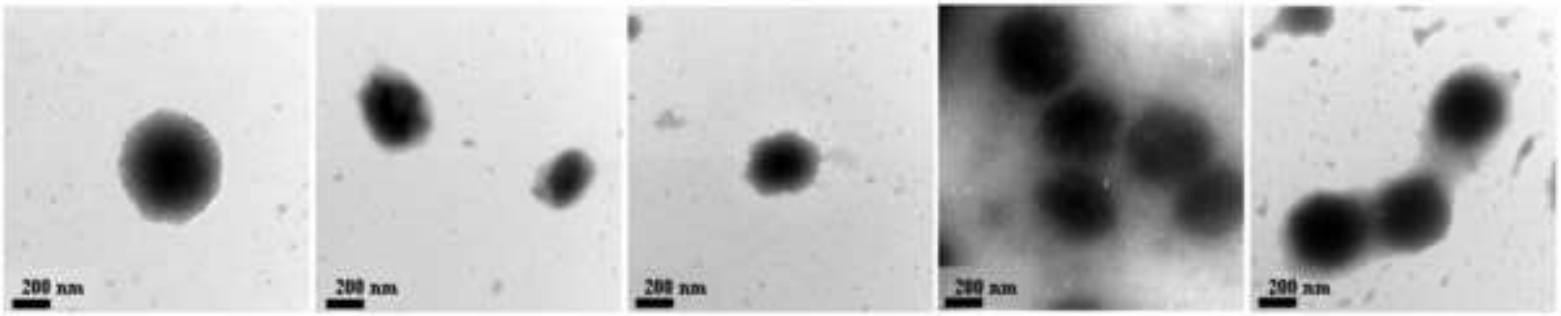

	chitosan	TMCS	QACS	QPCS	QBzCS
size (nm)	320 ± 160	290 ± 210	260 ± 90	440 ± 120	490 ± 210
ζ-potential (mV)	+27.1	+23.2	+29.3	+45.9	+46.8

Figure(s)
Click here to download high resolution image

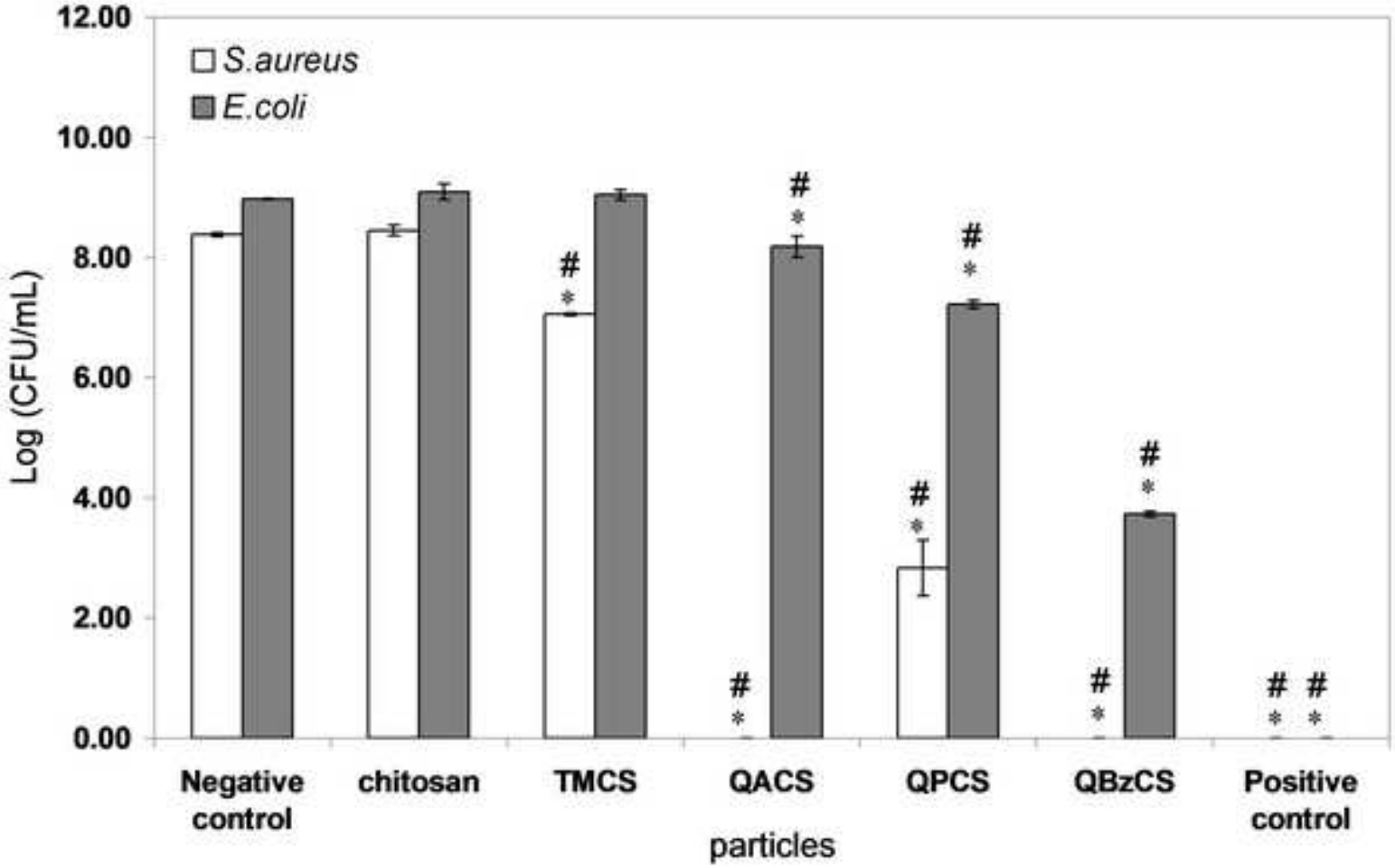

	% Antibacterial ratio						
S. aureus	0.0	ND	95.3	100.0	99.9	100.0	100.0
E. coli	0.0	ND	ND	82.9	98.2	99.9	100.0

ND (Not Detected)

Table(s)

Table 1. MIC values of chitosan and quaternized chitosan particles prepared in this work against *S. aureus* and *E. coli* in comparison with those of chitosan particles and quaternized chitosan both in the form of solution and particles as reported in the literatures

Materials	MIC (μg/mL)	
	S. aureus	*E. coli*
chitosan particles; size = 320 ± 160 nm [TS]	1000	2000
chitosan particles; size = 54 nm [24]	234	117
chitosan particles; size = 250 nm [33]	2000	N/A
TMCS particles; size = 290 ± 210 nm [TS]	250	125
QACS particles; size = 260 ± 90 nm [TS]	62.5	62.5
TMC particles; size = 215 nm [33]	500	N/A
TMC solution; 55±5%DQ [33]	250	N/A
TMC solution; MW = 120 kDa, 64%DQ [34]	125	250
TMC solution; MW = 200 kDa, 28%DQ [34]	500	1000
QPCS particles; size = 440 ± 120 nm [TS]	125	250
QBzCS particles; size = 490 ± 210 nm [TS]	125	125

[TS] = this study; N/A = not available

Supplementary Material

Click here to download Supplementary Material: Wiarachai_CSB_Supplementary_Final.doc

Polymer International

Improvement of tensile modulus and tear strength of natural rubber dipped films by vinylated silica generated in situ

Journal:	*Polymer International*
Manuscript ID:	PI-11-0382
Wiley - Manuscript type:	Original Article
Date Submitted by the Author:	06-Jun-2011
Complete List of Authors:	Rachanark, Navagan; Chulalongkorn University, Program of Petrochemistry and Polymer Science Tangpasuthadol, Varawut; Chulalongkorn University, Chemistry Kiatkamjornwong, Suda; Chulalongkorn University, Department of Imaging and Printing Technology
Key Words:	composite, silica, sol-gel process, natural rubber

For Review

SCHOLARONE™
Manuscripts

submitted to 'Polymer International'

Improvement of tensile modulus and tear strength of natural rubber dipped films by vinylated silica generated in situ

Navagan Rachanark, Varawut Tangpasuthadol*, Suda Kiatkamjornwong

Vinylated silicas were generated in natural rubber latex. The silica-rubber vulcanizates showed high tensile modulus and tear strength, possibly due to vinyl group participation in the sulfur curing of rubber.

For Peer Review

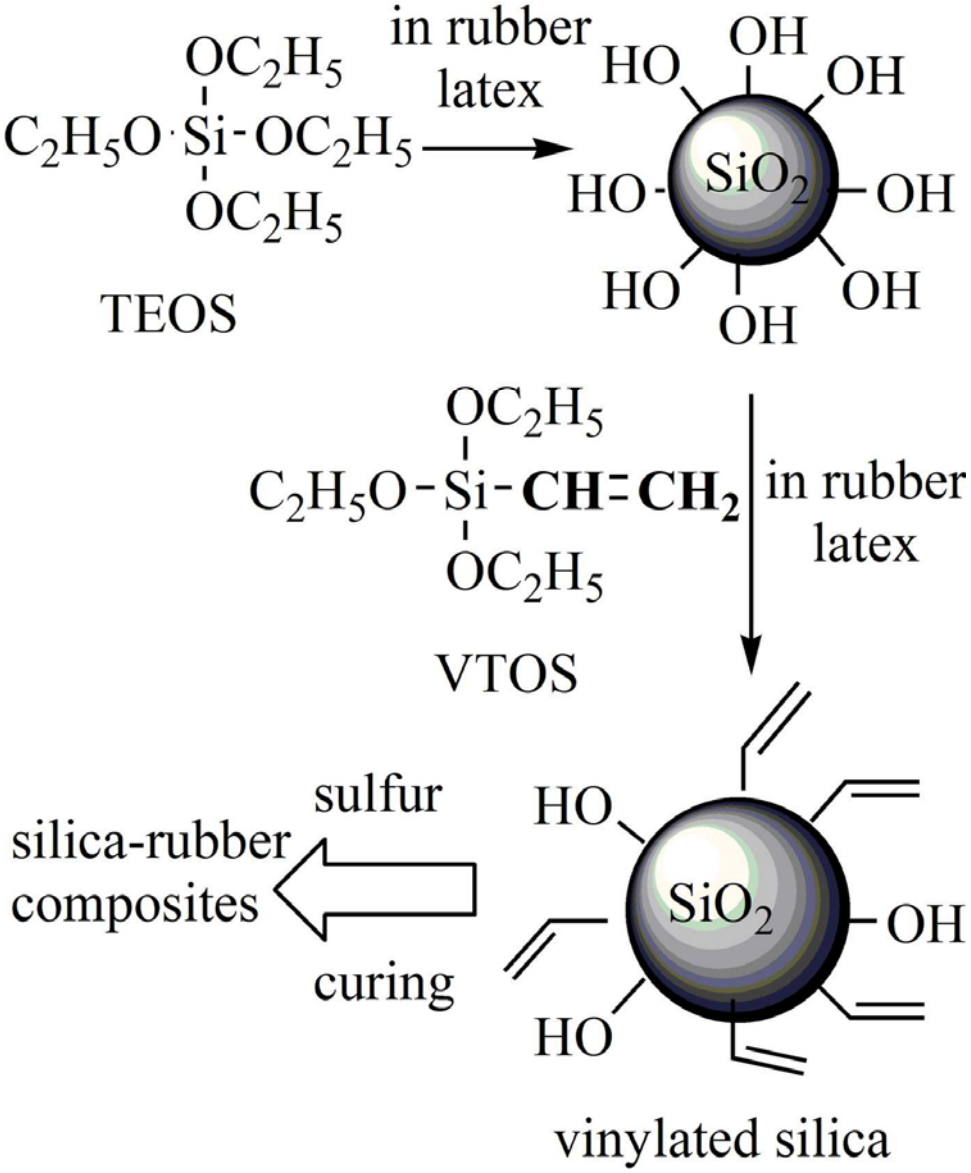

59x71mm (600 x 600 DPI)

submitted to 'Polymer International'

Improvement of tensile modulus and tear strength of natural rubber dipped films by vinylated silica generated in situ

Navagan Rachanark[1], Varawut Tangpasuthadol[2,*], Suda Kiatkamjornwong[3]

[1]Program of Petrochemistry and Polymer Science, Faculty of Science, Chulalongkorn University, Bangkok, Thailand 10330

[2]Organic Synthesis Research Unit, Department of Chemistry, Faculty of Science, Chulalongkorn University, Bangkok, Thailand 10330

[3]Department of Imaging and Printing Technology, Faculty of Science, Chulalongkorn University, Bangkok, Thailand 10330

*Corresponding author: Tel. 66-2218-7626, Fax. 66-2218-7598

E-mail address: varawut.t@chula.ac.th

Email: navagan@hotmail.com, suda.k@chula.ac.th

For Peer Review

Abstract

Alkylated silica particles were generated in dipped natural rubber films by sol-gel process of tetraethoxysilane (TEOS) and alkyltrialkoxysilane that were mixed with rubber latex before dipping process. Vinyltriethoxysilane (VTOS), ethyltriethoxysilane (ETOS), and methacryloxypropyltrimethoxysilane (MPS) were three alkyltrialkoxysilanes investigated as surface-treating reagents for the silica formed in the system. After heating the mixed alkaline latex at 80°C, the conversions from the silane to silica were in the range of 38-77% by mole of the total added silanes, depending on the size and polarity of the alkyl group in the silane. By TEM, the *in situ* silica particles were observed around rubber particles in the latex. Among the three

silanes, only the addition of VTOS in the TEOS-mixed latex led to significantly increases of tensile modulus and tear strength of the vulcanized films as compared to the addition of TEOS alone, possibly due to the participation of vinyl groups in the curing process.

Keywords: composite; silica; sol-gel process; natural rubber

For Peer Review

Introduction

Natural rubber (NR) latex is used to produce thin film products such as gloves and condoms, which require high elongation and excellent resilience. Nevertheless, NR has some weak characteristics, such as low tensile strength and modulus. A conventional technique to reinforce NR products is to physically mix fine silica powder with solid rubber or to mix aqueous slurry of silica with NR latex.[1] However, in the mixing process, silica particles tend to aggregate and agglomerate due to intermolecular hydrogen bonding between the hydroxyl groups on the silica surface. This often results in poor particle dispersion in the rubber matrix and high viscosity during mixing.[2] Silica can also adsorb or react with curing agents and accelerators on its surface which results in the reduction of curing efficiency.[3]

A method for overcome these problem is to generate silica particles right in the NR matrix. *In situ* silica formation is achieved by the sol–gel process of a silica precursor, such as tetraethoxysilane (TEOS), within the rubber matrix. There have been many reports on the *in situ* silica formation methods in solid rubber sheet,[3,4] rubber solution,[5,6] and rubber latex.[7-10] However, the use of TEOS alone as the silica precursor results in silica with polar hydroxyl groups on its surface. These polar groups potentially cause incompatibility between silica and rubber. One way to reduce the number of hydroxyl groups on the silica surface was to utilize alkyltrialkoxysilane to form 'alkylated' silica. The alkyltrialkoxysilane is a compound that carries three alkoxy groups and an alkyl substituent. The three alkoxy arms are required for bonding with silica, while the alkyl substituent is designated for *bonding* or *interacting* with the rubber matrix. They were regularly used under the name 'coupling agent' in rubber processing industry to chemically modify silica powder, in order to improve the filler

For Peer Review

dispersion and prevent adsorption of curing agents on the silica surface. Some functional groups such as alkyl, phenyl, amine, and vinyl groups can be introduced by selecting the right choice of alkyltrialkoxysilanes.[11,12]

The mixing of TEOS and alkyltrialkoxysilanes in NR latex for the preparation of *in situ* silica reinforced rubber vulcanizates were reported recently. The composite containing *in situ* silica had higher tensile modulus and tear strength than the composite prepared by conventionally mixing with silica powder.[9] A combination of bis-(3-triethoxysilylpropyl)tetrasulfide (TESPT) and TEOS that was mixed with the latex was shown to improve the mechanical properties and sulfur curing rates during milling and compression process.[7] Triethoxysilanes carring either vinyl, ethyl, and iso-butyl group were reportedly used to generate silica in sulfur-cured NR sheets obtained by melt-compression process.[9] Among them, vinyltriethoxysilanes was the most promising silane that was able to enhance the tensile modulus and resistance to tear of the rubber vulcanizates.

In this work, the focus was to utilize a mixed silane system in the reinforcement of natural rubber films that were prepared by 'latex-dipping' process. TEOS was used in combination with either VTOS or methacryloxypropylmethoxysilane (MPS) to prepare *in situ* silica having carbon-carbon double bonds on the particle surface. ETOS was also used in the film preparation for the purpose of investigating the role of C=C double bond in the reinforcement capability of the resulting silica. The structures of TEOS, VTOS, ETOS, and MPS are shown in Fig. 1. It was hypothesized that the *in situ* 'vinylated' silica particles can improve the dispersibility and mechanical properties of the NR/silica dipped films.

For Peer Review

Experimental

Materials

Concentrated natural rubber latex with 60% weight content of dry rubber (DRC) incorporated 0.7% NH_3 was purchased from the Rubber Research Institute of Thailand. Liquid dispersion of vulcanizing agents was donated from Polymer Innovation Co., Ltd., Nonthaburi, Thailand. Tetraethoxysilane (TEOS, >98%), vinyltriethoxysilane (VTOS, >98%), ethyltriethoxysilane (ETOS, >97%), methacryloxypropyltrimethoxysilane (MPS, >98%) were purchased from Aldrich, Germany.

Preparation of pre-vulcanized NR latex

The concentrated NR latex was diluted with 0.7% v/v ammonia solution to obtain 30% DRC latex. It was then mixed with the dispersion of vulcanizing agents formulated as shown in Table 1. Then a predetermined amount of TEOS was added to the latex compound with stirring. After maturated at room temperature for 24 hr, a predetermined amount of VTOS, ETOS, or MPS was mixed with the latex mixture as listed in Table 2. The homogeneous milky mixture of silane-latex was maturated for an additional 24 hr before it was used in the dipping process. During the maturation period, the reaction of silane slowly took place in the presence of water and base in the latex. The total amount of alkoxysilanes added into the latex was limited to 30 phr, because the latex tended to be unstable if a higher amount of the silanes was added.

For Peer Review

Table 1 Composition of vulcanization reagents in the form of dispersed liquid used in the latex dipping process

Ingredients	Amount (phr[a])
Natural rubber	100
Sulfur	2.5
ZMBT[b]	0.5
ZDEC[c]	1.5
ZnO[d]	2.0

[a] part per hundred part of rubber by weight, [b]zinc salt of 2-mercaptobenzothiazole, [c]zinc-diethyldithiocarbamate, [d]zinc oxide

Table 2 Variation of alkoxysilane amounts mixed into NR latex for *in situ* silica-NR composites preparation

Entry	Silane amount (phr)			
	TEOS	VTOS	ETOS	MPS
VNR	-	-	-	-
30T	30	-	-	-
25T	25	-	-	-
25T5V	25	5	-	-
20T10V	20	10	-	-
25T5E	25	-	5	-
20T10E	20	-	10	-
25T5M	25	-	-	5
20T10M	20	-	-	10

For Peer Review

Dipping process

In situ silica-NR vulcanized films were prepared by dipping glass cylinders (pre-dipped in $Ca(NO_3)_2$ solution, 40 mm in diameter) in the prepared latex-silane-vulcanizing agent mixtures. The coated former was then heated in an oven at 80°C for 24 hr to initiate the vulcanization and sol-gel process of the added silanes. On average, the film thickness obtained was 0.15 mm.

Determination of silica content in the *in situ* silica-NR dipped films

The silica content was determined by cutting the NR/silica dipped films into small pieces (~50 mg). After an exact weight was determined, the sample was heated at 850°C for 15 min in an oven. The weight of the remaining ash was calculated for the silica content in the composite by equations 1 and the conversion of the alkyltrialkoxysilane to silica was calculated using equation 2,

$$\text{Silica Content (phr)} = 100\ (W_1/W_2) \quad (1)$$

$$\text{Conversion (\%)} = 100\ (W_3/W_4) \quad (2)$$

where, W_1 is the weight of silica in the sample, W_2 is the weight of the organic rubber, W_3 is the obtained amount of the *in situ* generated silica in the sample, and W_4 is the theoretical amount of silica generated from the added amount of alkoxysilane in the latex. The calculation of W_4 was based on the chemical equation shown in Fig. 2 by assuming a quantitative conversion of TEOS and alkyltriethoxysilane to silica and alkylated silica, respectively. The results reported were averaged from three specimens.

Microscopic Analysis

For Peer Review

A scanning electron microscope (JOEL JSM-6480LV SEM) was used to analyze silica distribution in the NR matrix at 15 keV. The analysis was performed on the fractured surface of silica-NR dipped films prepared by breaking the film specimens while it was immersed in liquid nitrogen. Energy dispersive X-ray spectrometric (EDX) detector was carried out at an elevation angle of 35° in order to determine atomic types on the analyzed surface. A transmission electron microscope (JOEL JEM-2100) was used to examine the morphology of rubber and silica particles in the latex mixed with the silane precursors. The silane-latex mixture was diluted with distilled water to obtain a DRC of 0.75%. The substrate was stained by exposure to RuO_4 vapor before TEM analysis.

Mechanical properties

Tensile properties were measured with an H10KS universal testing machine (Hounsfield, Redhill, UK), according to JIS K6251-8 at a grip length of 10 mm, and a crosshead speed of 500 mm/min. Each data point was an average value obtained from four replicates of specimens. Tear properties were measured using a Hounsfield H10KS universal testing machine, following ASTM D624-91. The die C-cut specimens were tested at a gauge length of 70 mm and a crosshead speed of 500 mm/min. The values reported for each sample were averaged from three specimens.

Tension set measurement

All dipped film samples were cut into the size of 5×60 mm. Two lines about 10 mm apart were marked at the center of the sample strip. The sample was extended until the distance between the two lines was twice that of the original length, and was held for 10 min. After that, the sample was allowed to retract for 10 min. The final distance

For Peer Review

between the two lines was then measured. All measurements were made by using a vernier caliper. The tension set was calculated using equation 3 where L_i and L_f were the initial and final distances between the two lines.

$$\text{Tension set } (\%) = ((L_f - L_i)/L_i) \times 100 \quad (3)$$

Results and Discussions

Silica content and percentage conversion of silanes to silica

Earlier, we reported a cross-condensation of TEOS and alkyltrialkoxysilanes that were mixed together in the NR latex to form 'alkylated' silicas *in situ*.[9] In this work, TEOS was first mixed into the latex in order to form the silica particles during the maturation period. Then one of the alkyltrialkoxysilanes was added so that it could condense with the pre-formed silica, resulting in silica particles with selected alkyl groups (R) on the surface (Fig. 3).

The amounts of silicas formed in the rubber matrix are listed in Table 3. The conversion of TEOS to silica in the silica-NR dipped film was the highest at 77%, resulting in 6.7 phr of silica. Although the sol-gel process of the silane took place preferably in an alkaline latex, the conversion obtained here for TEOS was somewhat lower than our previous reports of >90%.[7-9] In those reports, the concentration of NR latex was 60% DRC but in this work the latex was diluted to 30% to suit the dipping process. The diluted latex contained a large amount of water, possibly suppressing the chemical equilibrium back to silicic acid, and thus reducing the silicon dioxide network formation. At various ratios of TEOS and alkyltrialkoxysilanes (Table 3), the degree of silane-to-silica conversions in the rubber vulcanizates decreased when the relative amount of alkyltrialkoxysilane was increased. This was because each of the selected

For Peer Review

alkyltrialkoxysilanes contained only three hydrolysable siloxane arms as compared to four siloxanes in the structure of TEOS. In addition, the degree of silane-to-silica conversion was also affected by the structure and polarity of the alkyl substituent in the silanes used, i.e. TEOS-VTOS > TEOS-ETOS > TEOS-MPS. In highly polar aqueous medium, a polar and small alkyl group on the silane molecule should allow higher access of water and another silanol group (-Si-OH) at condensation site than does the non-polar and bulky substituent. In this case, the vinyl group (in VTOS) is more polarized than the ethyl (in ETOS), the mixed VTOS-TEOS silanes therefore results in a higher conversion than the ETOS-TEOS. In the case of MPS, the methacryloxypropyl group is long and bulky. It therefore partially inhibits the sol-gel process, resulting in slightly lower silica formation than does the VTOS system. This result is in fact in good agreement with our earlier finding.[9]

Table 3 Silica content and degree of conversion from alkoxysilane to silica in rubber.

Entry	Silica content (phr)	Conversion (%)
30T	6.7 ± 0.3	77 ± 3.0
25T	5.1 ± 0.1	70 ± 1.0
25T5V	5.6 ± 0.3	61 ± 3.5
20T10V	5.2 ± 0.1	52 ± 0.6
25T5E	5.0 ± 0.2	54 ± 2.2
20T10E	4.8 ± 0.2	48 ± 2.2
25T5M	5.2 ± 0.4	48 ± 3.2
20T10M	4.9 ± 0.1	38 ± 0.8

For Peer Review

Moreover it was believed that the alkoxysilane precursors could evaporate from the mixed latex during the dipping and drying steps. To overcome the loss of starting silane reagents, the silane-mixed latex was maturated (or stored) at room temperature for 1-2 days in order to allow partial sol-gel process to take place. This hypothesis was tested with results shown in Fig. 4, in which the degree of conversion was determined after one and two days of maturation. Without the maturation, the conversion of TEOS to silica in the rubber matrix was only 25% but increased dramatically to almost 80% (or about 7 phr) after one day of storage at room temperature.

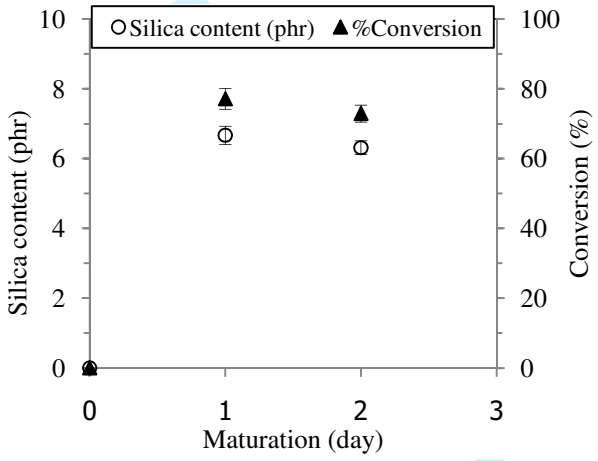

Figure 4 Changes of silica content and degree of conversion of TEOS (30 phr) mixed in the NR latex (30% DRC) as a function of latex maturation time

Morphology of *the in situ* silica and NR

The image from transmission electron microscope (TEM) was used to locate the silica particles in the rubber latex (Fig. 5). Analysis of the ruthenium-stained latex sample showed that the shape of NR particles appeared to be spherical with size ranging from 0.1-1 μm (Fig. 5a). The *in situ* generated silica were observed as dark irregular-shaped

particles, with the size of about 100 nm or less, surrounding the rubber particle in the latex compound mixed with TEOS (Fig. 5b), TEOS-VTOS (Fig. 5c), and TEOS-MPS (Fig. 5d).

The distribution of silica particles in the fractured surface of the composite films was analyzed by scanning electron microscope (SEM) (Fig. 6). The silica formed in the vulcanizate was visualized as aggregates among ZnO particles, an activator used in the vulcanization process (Fig. 6a). The identity of silicon atoms was confirmed by its characteristic peak at 1.7 keV in the EDX spectrum, while the ZnO was identified by the signal at 1.0 keV (Fig. 6b).

Comparison of the characteristic of *in situ*-formed silica generated from the mixed silanes was made as shown in Fig. 7. The silica particles of all precursor types form aggregates with sizes ranging from <1 to several μm and are dispersed throughout the rubber matrix. The particles obtained appear to be quite similar in terms of size and shapes, regardless of its precursor type.

Mechanical properties

In order to investigate the effect of alkyltrialkoxysilane types on the tensile properties of the *in situ* silica-NR dipped films, four rubber samples filled with approximately equal amounts of *in situ* generated silica (5.0 ± 0.4 phr) were prepared and named as 25T, 20T10V, 20T10E, and 20T10M. Their analyses for modulus value at 300% & 500% elongation and tensile strength at break were performed in comparison with the silica-free vulcanized film (VNR) as shown in Fig. 8. The modulus at 500% elongation of the 20T10V was significantly higher than the others. The use of mixed TEOS-ETOS and TEOS-MPS were slightly less effective in reinforcing the rubber film than using TEOS-

For Peer Review

VTOS or only TEOS. It seemed that MPS, also containing the vinyl group, was not as efficient as a reinforced precursor as VTOS for the dipped system.

The elongations at break of these selected vulcanizates, with or without the *in situ* silica, were between 630-690% (Fig. 9). No relation between the ultimate elongation and the type of silane precursor was observed. Tear testing of all NR/silica composites was performed on cast rubber sheets (~0.6 mm thick) that were prepared from the same latex compound as used for the dipping process. From the results shown in Fig. 10, only two samples, 20T10V and 20T10E, had significantly higher tear strength than did the VNR. The highest tear strength belonged to 20T10V.

From the tensile and tear test results of the *in situ* silica-NR vulcanizates, the vinyl group in VTOS that was mixed with TEOS in the ratio of 1:2 (VTOS:TEOS) plays an important role in the mechanical properties of the rubber films. The vinyl group on the *in situ* generated vinylated silica can most likely take part in the sulfur vulcanization process. In other words, the sulfur crosslinking takes place not only among the isoprene units of NR chains but possibly also with the vinylated silica particles. Unfortunately using a spectroscopic method such as IR to detect the disappearance of vinyl group after sulfur cure step would be inconclusive, since the NR matrix also contains a large number of double bonds. Nevertheless this type of participation was reported in other works, such as the preparation of wood fiber/PE and PP composites, in which the vinyl group was reportedly bonded with polyolefin backbone via radical grafting while the ethoxy silyl group on the other end of VTOS reacted with the hydroxyl groups of cellulose structure.[13,14]

For Peer Review

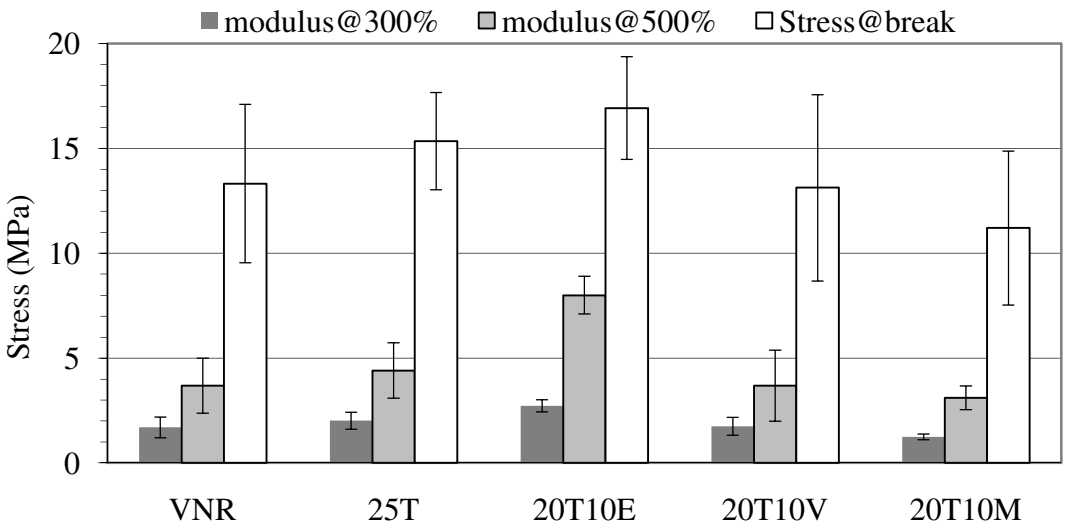

Figure 8 Modulus at 300&500% elongation and tensile strength of the dipped NR films filled with *in situ* silica generated by various types of alkoxysilane precursor, compared with silica-free dipped film (VNR).

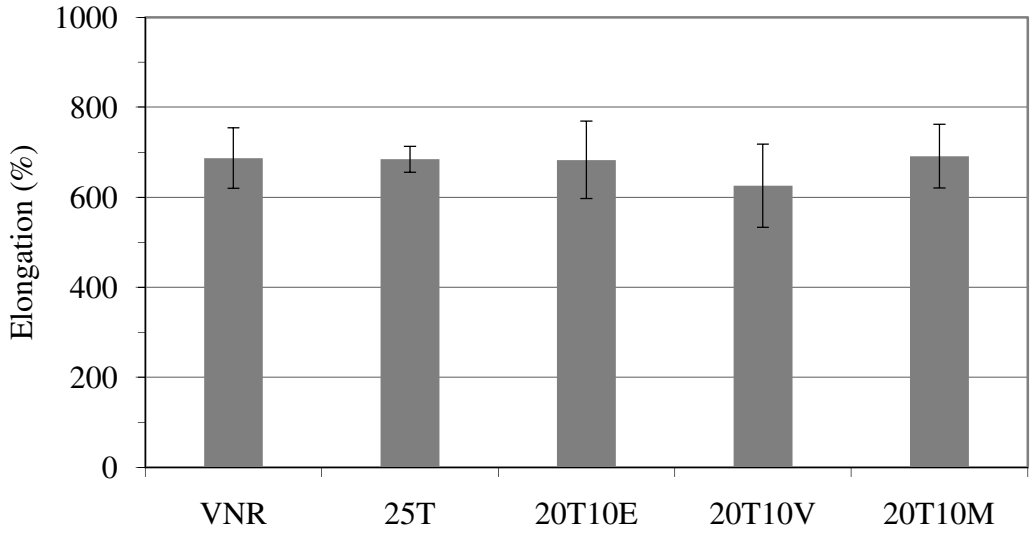

Figure 9 Elongation at break of the dipped NR films filled with *in situ* silica generated by various types of alkoxysilane precursor, compared with silica-free dipped film (VNR).

For Peer

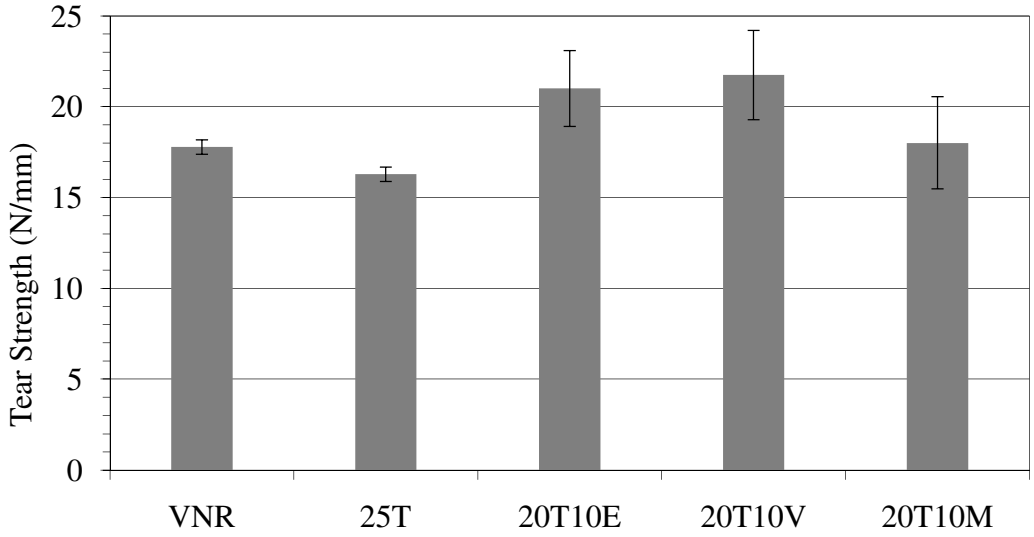

Figure 10 Tear strength of the vulcanized cast NR sheets filled with *in situ* silica generated by various types of alkoxysilane precursor, compared with silica-free sheets (VNR).

Figure 11 shows the results of tension set study. The tension set parameter, reflects the elasticity of rubber. It is the extent to which vulcanized rubber is permanently deformed after the film is stretched for a certain length and time. Here the tension set percentages of all *in situ* NR/silica dipped films were between 2.3 to 4.3%. No difference between the *in situ* silica-reinforced and non-reinforced samples was observed. The use of TEOS and other alkyltrialkoxysilanes to generate silica in the dipped film did not significantly affect to the tension set.

For Peer Review

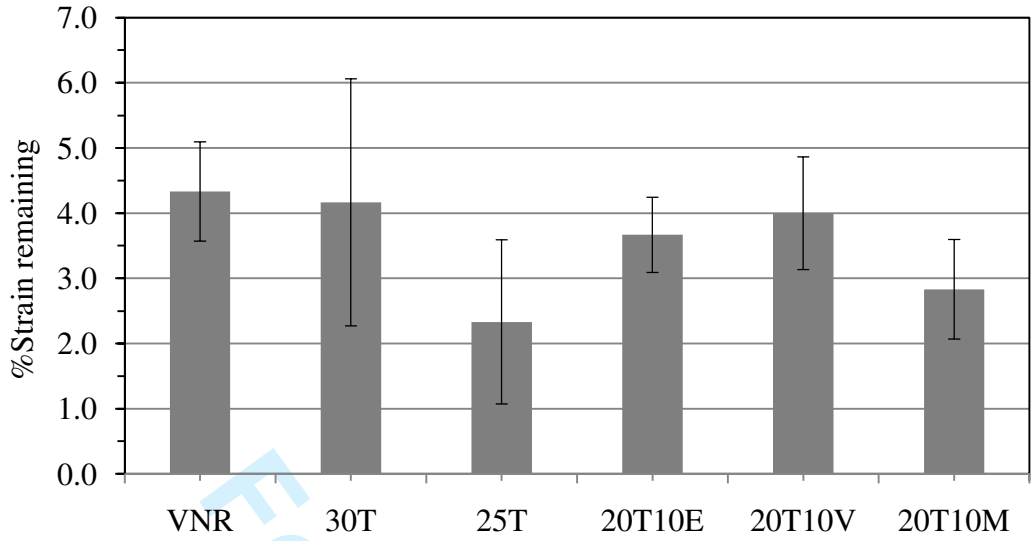

Figure 11 Result of tension set study of the dipped rubber films filled with *in situ* silica generated by various types of alkoxysilane precursor, compared with silica-free dipped rubber film (VNR).

For Peer Review

Conclusion

Silicas with different alkyl groups were successfully generated in the vulcanized dipped NR films by the use of TEOS/alkyltriethoxysilane as precursors. Maturation of the silane-latex mixture for at 2 days was required in order to obtain high degree of silane-to-silica conversion. A single heating step was used to initiate sulfur-vulcanization of the rubber films as well as silica formation in the rubber matrix. By TEM, the *in situ* silica particles were observed around the NR particle. The size of silica particle was less than 100 nm, but it did not depend on the silane types. The SEM images and EDX analysis confirmed that the *in situ* silica particles were fairly dispersed inside the rubber matrix. The use of vinyl containing alkoxysilane to treat the surface of *in situ*-formed silica resulted in the vulcanizate that possessed higher tensile modulus than the other silanes. Based on the mechanical testing results, we believed that the unsaturation

nature of the C=C double bond on the *in situ* formed silica could involve in the sulfur vulcanization process of the NR.

Acknowledgement

The research funding provided by Research Team Assistance Grant under Contract Number RTA5080004 from the Thailand Research Fund was highly acknowledged. Many thanks also go to Chemical Innovation Co., Ltd., Thailand, for mechanical testing facilities**.**

For Peer Review

REFERENCES

1. Mathew S, Varghese S, Rajammal G and Thomas PC, *J Appl Polym Sci* **104**: 58-65 (2007).
2. Castellano M, Conzatti L, Codta G, Falqui L, Turturro A, Valenti B and Negroni F, *Polymer* **46**: 695-703 (2005).
3. Kohjiya S and Ikeda Y, *Rubber Chem Technol* **73**: 534-550 (2000).
4. Ikeda Y, Poompradub S, Morita Y and Kohjiya S, *J Sol-Gel Sci Technol* **45**: 299-306 (2008).
5. Poompradub S, Chaichua B, Kanchanaamporn C, Boosalee T and Prasassarakich P, *Kgk-Kaut Gummi Kunst* **61**: 152-155 (2008).
6. Chaichua B, Prasassarakich P and Poompradub S, *J Sol-Gel Sci Technol* **52**: 219-227 (2009).
7. Tangpasuthadol V, Intasiri A, Nantivanich D, Niyompanich N and Kiatkamjornwong S, *J Appl Polym Sci* **109**: 424-433 (2008).
8. Satraphan P, Intasiri A, Tangpasuthadol V and Kiatkamjornwong S, *Polym Adv Technol* **20**: 473-486 (2009).
9. Siramanont J, Tangpasuthadol V, Intasiri A, Na-Ranong N and Kiatkamjornwong S, *Polym Eng Sci* **49**: 1099-1106 (2009).
10. Watcharakul N, Poompradub S and Prasassarakich P, *J Sol-Gel Sci Technol* **58**: 407-418 (2011).
11. Hsiue GH, Chen JK and Liu YL, *J Appl Polym Sci* **76**: 1609-1618 (2000).
12. Chen G, Zhou S, Gu G, Yang H and Wu L, *J Colloid Interface Sci* **281**: 339-350 (2005).

For Peer Review

13. Bengtsson M and Oksman K, *Compos Sci Technol* **66**: 2177-2186 (2006).

14. Xie Y, Hill CAS, Xiao Z, Militz H and Mai C, *Composites Part A* **41**: 806-819 (2010).

For Peer Review

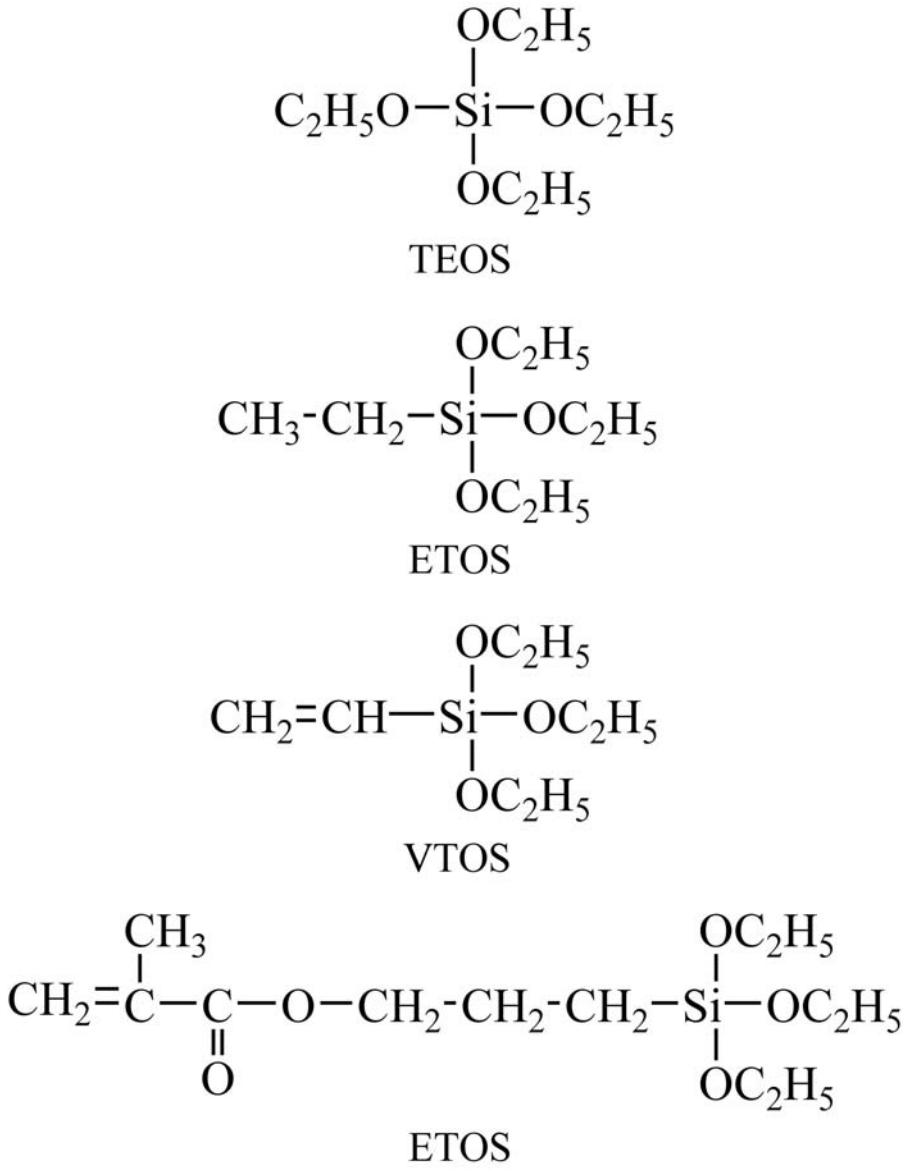

Figure 1 Structures of tetraethoxysilane (TEOS), ethyltriethoxysilane (ETOS), vinyltriethoxysilane (VTOS), and methacryloxypropyltrimethoxysilane (MPS).
118x154mm (600 x 600 DPI)

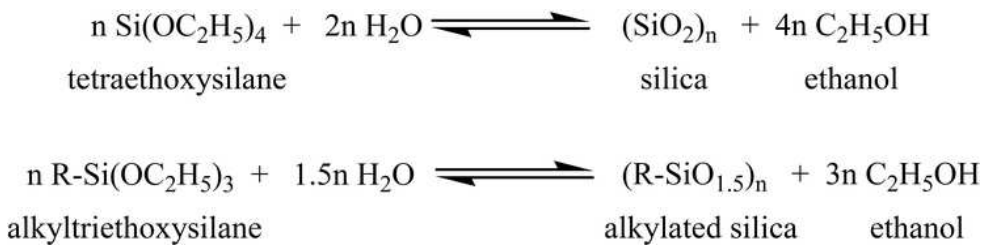

Figure 2 Chemical equations of the conversion of TEOS to silica (top) and alkyltriethoxysilane to alkylated silica (bottom).
31x7mm (600 x 600 DPI)

For Peer Review

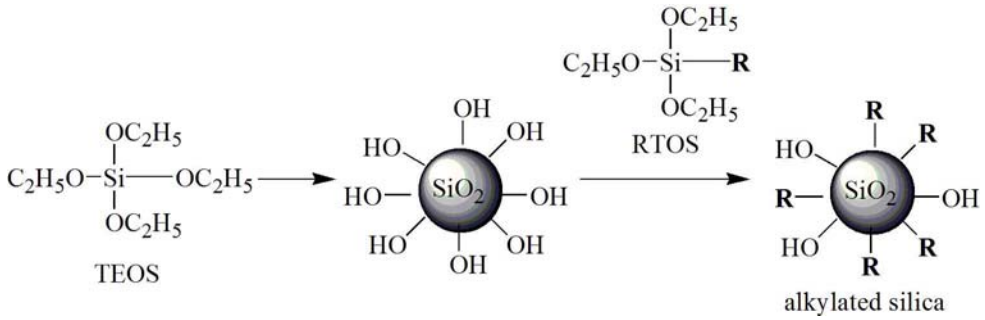

Figure 3 Cross-condensation of alkyltrialkoxysilane (RTOS) and a silica particle from tetraethoxysilane (TEOS) precursor.
128x41mm (300 x 300 DPI)

For Peer Review

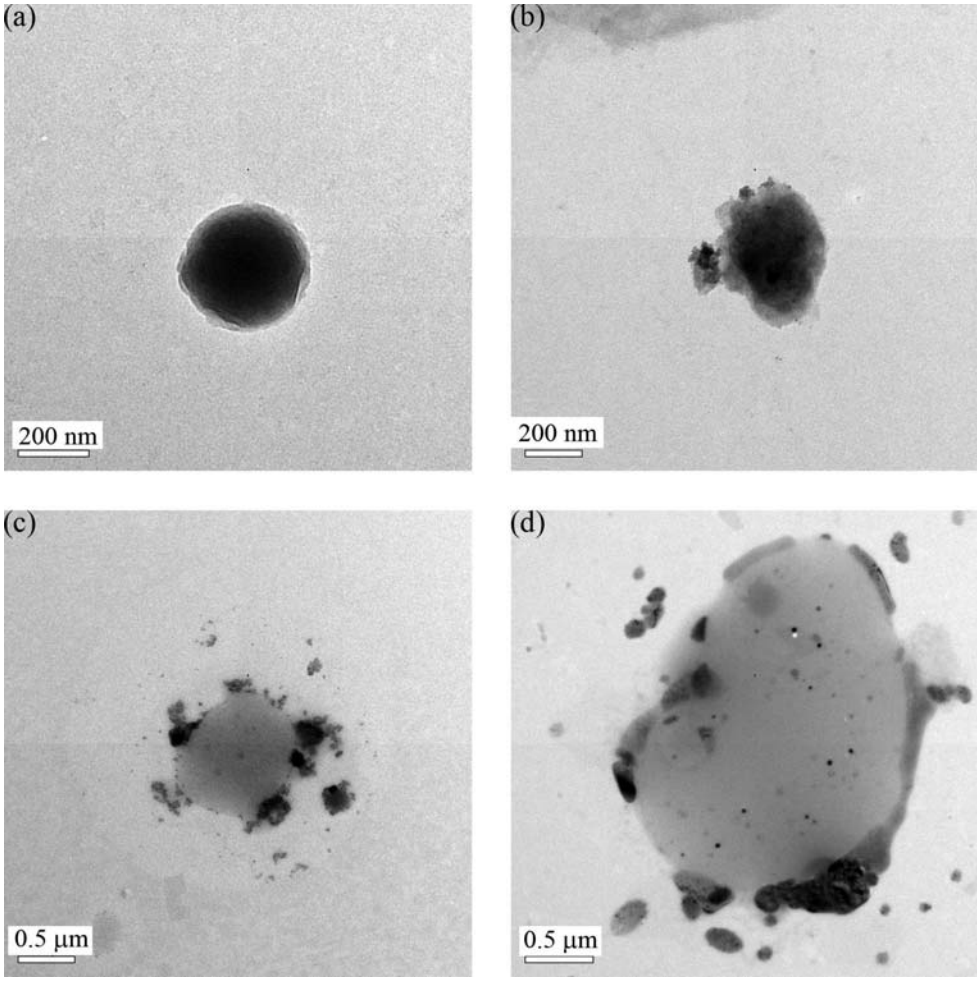

Figure 5 The TEM image of NR particle in (a)non-modified latex in comparison the images obtained from the latex that was mixed with (b)TEOS, (c)TEOS-VTOS, and (d) TEOS-MPS. The in situ-formed silica particles were seen as the dark spots surrounding the rubber core.
158x158mm (300 x 300 DPI)

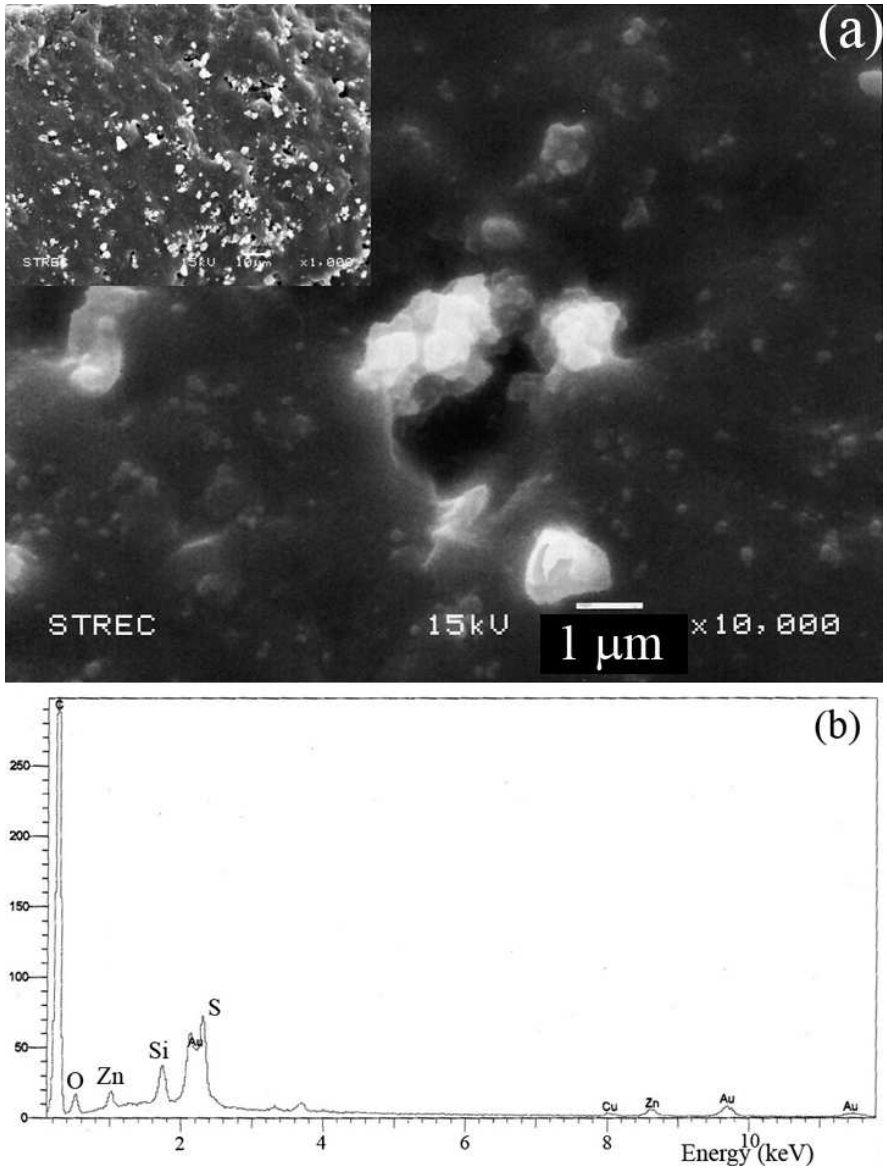

Figure 6 (a)The inset figure (1,000×) shows the distribution of in situ-formed silica obtained from the fractured surface of silica-NR vulcanizates (sample: 30T; 6.7 phr silica). The main image (10,000×) shows close-up detail of the silica aggregates. (b)The EDX spectrum of the shown area in the main image displays a series of elements, including Zn and Si.
60x81mm (300 x 300 DPI)

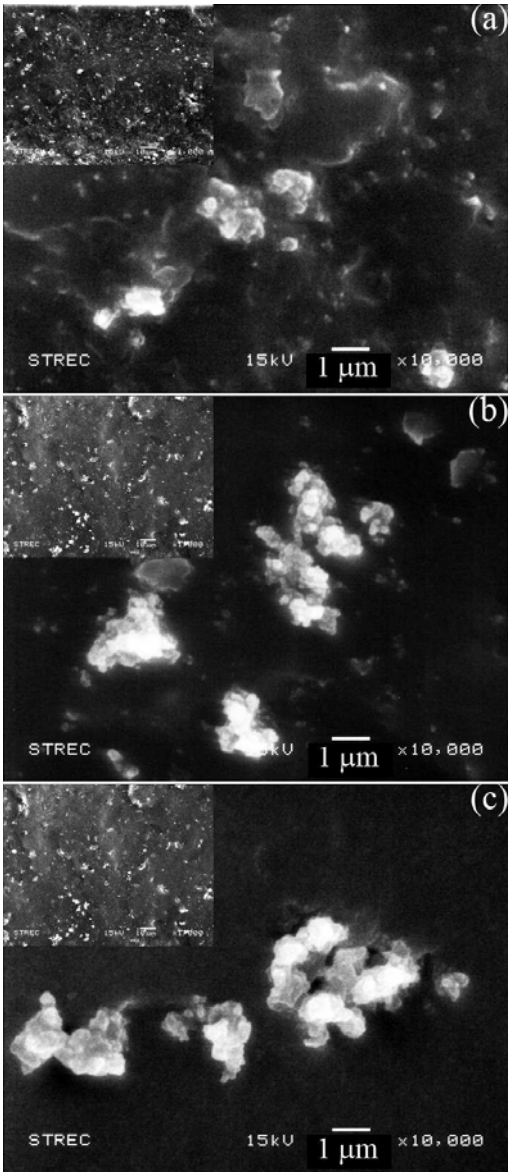

Figure 7 The SEM images show the distribution of in situ-formed silica (inset; 1,000×) and detailed silica aggregates (main; 10,000×) obtained from the fractured surface of silica-NR vulcanized films of (a)20T10V (silica: 5.2 phr), (b)20T10E (silica: 4.8 phr), and (c)20T10M (silica: 4.9 phr).
60x140mm (300 x 300 DPI)

Draft

Multilayer Film Assembled from Charged Derivatives of Chitosan: Physical Characteristics and Biological Responses

Wilaiporn Graisuwan[1,2], Cheeraporn Ananthanawat[3], Oraphan Wiarachai[1,2], Songchan Puthong[4], Suphan Soogarun[5], Suda Kiatkamjornwong[6], Voravee P. Hoven[7]*

[1] Program in Petrochemistry and Polymer Science, Faculty of Science, Chulalongkorn University, Phayathai Road, Pathumwan, Bangkok 10330, Thailand

[2] Center for Petroleum, Petrochemicals, and Advanced Materials, Chulalongkorn University, Phayathai Road, Pathumwan, Bangkok 10330, Thailand

[3] Program in Macromolecular Science, Faculty of Science, Chulalongkorn University, Phayathai Road, Pathumwan, Bangkok 10330, Thailand

[4] The Institute of Biotechnology and Genetic Engineering, Chulalongkorn University, Phayathai Road, Pathumwan, Bangkok 10330, Thailand

[5] Department of Clinical Microscopy, Faculty of Allied Health Sciences, Chulalongkorn University, Phayathai Road, Pathumwan, Bangkok 10330, Thailand

[6] Department of Imaging and Printing Technology, Faculty of Science, Chulalongkorn University, Phayathai Road, Pathumwan, Bangkok 10330, Thailand

[7] Organic Synthesis Research Unit, Department of Chemistry, Faculty of Science, Chulalongkorn University, Phayathai Road, Pathumwan, Bangkok 10330, Thailand

RECEIVED DATE (to be automatically inserted after your manuscript is accepted if required according to the journal that you are submitting your paper to)

TITLE RUNNING HEAD. Multilayer film of charged chitosan

*To whom correspondence should be addressed. Tel: +66-2218-7627 ext 102. Fax: +66-2218-7598. E-mail: vipavee.p@chula.ac.th

ABSTRACT. Polyelectrolyte multilayer films were assembled from charged derivatives of chitosan: *N*-[(2-hydroxyl-3-trimethylammonium)propyl]chitosan chloride (HTACC), *N*-succinyl chitosan (SCC), and *N*-sulfofurfuryl chitosan (SFC) and selected oppositely charged polyelectrolytes which are poly(acrylic acid) (PAA) and poly(allylamine hydrochloride) (PAH) successfully deposited on the surface-treated poly(ethylene terephthalate) (treated PET) substrates by alternate layer-by-layer adsorption. The assembly process was monitored by quartz crystal microbalance with dissipation (QCM-D). Stratification of the multilayer films was demonstrated by water contact angle data. The coverage of the assembled films was characterized by AFM. Biological responses of the assembled films were assessed in terms of *in vitro* cell adhesion and proliferation of fibroblasts, antibacterial activity, and protein adsorption. The *in vitro* cells study showed slightly alternating trend depending on the outermost layer. The multilayer film containing HTACC exhibited greater antibacterial activity against *E. coli* and *S. aureus* than the treated PET substrate and the control. The blood compatibility study suggested that (PAH/SFC) can reduce protein adsorption.

KEYWORDS. Charged derivative, Chitosan, Muitlayer film, Layer-by-layer, Cytocompatibility, Antibacterial activity, Antithrombogenicity

Introduction

The layer-by-layer (LBL) assembly technique,[1] typically based on the alternating adsorption of oppositely charged polyelectrolytes, has been widely employed for the modification of biomaterial surfaces in order to render them bioactive, adhesive or non-adhesive for cells or specific microorganisms so that they can be used for biomedical applications. This versatile strategy, involving building up of thin multilayer film, is mostly driven by electrostatic interactions between a charged polyelectrolyte and an oppositely charged surface. The first adsorbed layer of polyelectrolyte from aqueous solution leads to the surface charge reversal and enables second adsorption of an oppositely charged polyelectrolyte. The process is simple and can be adapted for any type of substrate as long as the surface charge is present without the limitation of substrate topology. In principle, the thickness of the multilayer film can be varied as a function of adsorption variables as well as the number of deposition. Most importantly, the surface properties of the supported films are determined by the outermost layer that is last deposited.

Chitosan is considered as one of the most attractive natural polyelectrolyte often used for generating biocompatible surfaces via multilayer assembly. It is the partially deacetylated form of chitin, the second-most abundant natural polymer, mainly harvested from the exoskeleton of insects, marine crustaceans and fungal cell walls. Its favorable physico-chemical and biological characteristics such as biocompatible,[2] biodegradable,[3,4] non-toxic,[5] and antibacterial activity[6] makes chitosan suitable for many bio-related applications. Besides, charged derivatives of chitosan exhibit diversified bioactivities. Quaternary ammonium chitosan, a positively charged derivative possesses superior antimicrobial activity[7,8]. Succinyl chitosan, a negatively charged derivative, has favorable properties such as low toxicity and long-term retention in the body so it

was applied as a drug carrier.[9] Sulfonated chitosan, another negatively charged derivative, on the other hand, is antithrombogenic.[10-12]

Several researches have been reported on the formation of polyion complex multilayer films between chitosan and a number of anionic polyelectrolytes. Serizawa, *et al.*[13,14] have revealed the alternating anti-vs procoagulation activity of ultrathin polymer films prepared from dextran sulfate and chitosan by the layer-by-layer assembly technique against human blood. Zhu, *et al.*[15] assembled the multilayer films of poly(styrene sulfonate, sodium salt) (PSS) and chitosan to improve cytocompatibility of the poly(L-lactic acid) surface. Cai, *et al.*[16] constructed a multilayer film using chitosan and gelatin on titanium in order to improve their biocompatibility. Fu, *et al.*[17] generated multilayer films from heparin (anti-adhesive agent) and chitosan (antibacterial agent) on aminolyzed PET films. It was found that the multilayer films not only reduced the bacterial adhesion but also kill the bacteria adhered onto the surface. This desirable feature renders the multilayer film a powerful anti-infection coating for cardiovascular devices. Liu, *et al.*[18] modified a surface of poly(ethylene terephthalate) (PET) by hydrolysis and built up multilayer films by alternative adsorption of chitosan and chondroitin sulfate. The *in vitro* cell culture revealed that the adherence of endothelial cells was enhanced on the multilayer-deposit PET film with their preserved function.

In our previous publication,[19] we have demonstrated that the multilayer films can be successfully assembled from charged derivatives of chitosan (CHI), *N*-sulfofurfuryl chitosan (SFC) and *N*-[(2-hydroxyl-3-trimethylammonium)propyl]chitosan chloride (HTACC) on the plasma-treated PET. Alternate bioactivity of the multilayer assembly of three pairs of polycation/polyanion: CHI/poly(styrene sulfonate sodium salt) (CHI/PSS), poly(allylamine hydrochloride)/SFC (PAH/SFC), and HTACC/poly(acrylic acid) (HTACC/PAA) were realized

by testing against four proteins having different size and charge characteristic which are albumin, fibrinogen, γ-globulin, and lysozyme.

In the present study, we explore further on the insight into the physical characteristics of the multilayer films assembled from those charged derivatives that have been reported earlier (SFC and HTACC) as well as an additional negatively charged derivative, *N*-succinyl chitosan (SCC). For the first time, the internal structure, water content, and viscoelastic properties of the multilayer films were assessed by quartz crystal microbalance with dissipation mode (QCM-D). Three pairs of oppositely charged polyelectrolytes were investigated: HTACC/PAA, PAH/SCC, and PAH/SFC (Figure 1). Biological responses of selected multilayer systems were tested against fibroblast cells, bacteria, plasma proteins, and platelets. The consequence of this study should provide fundamental information that should be very useful for further development of these charged derivatives of chitosan for biomedical applications.

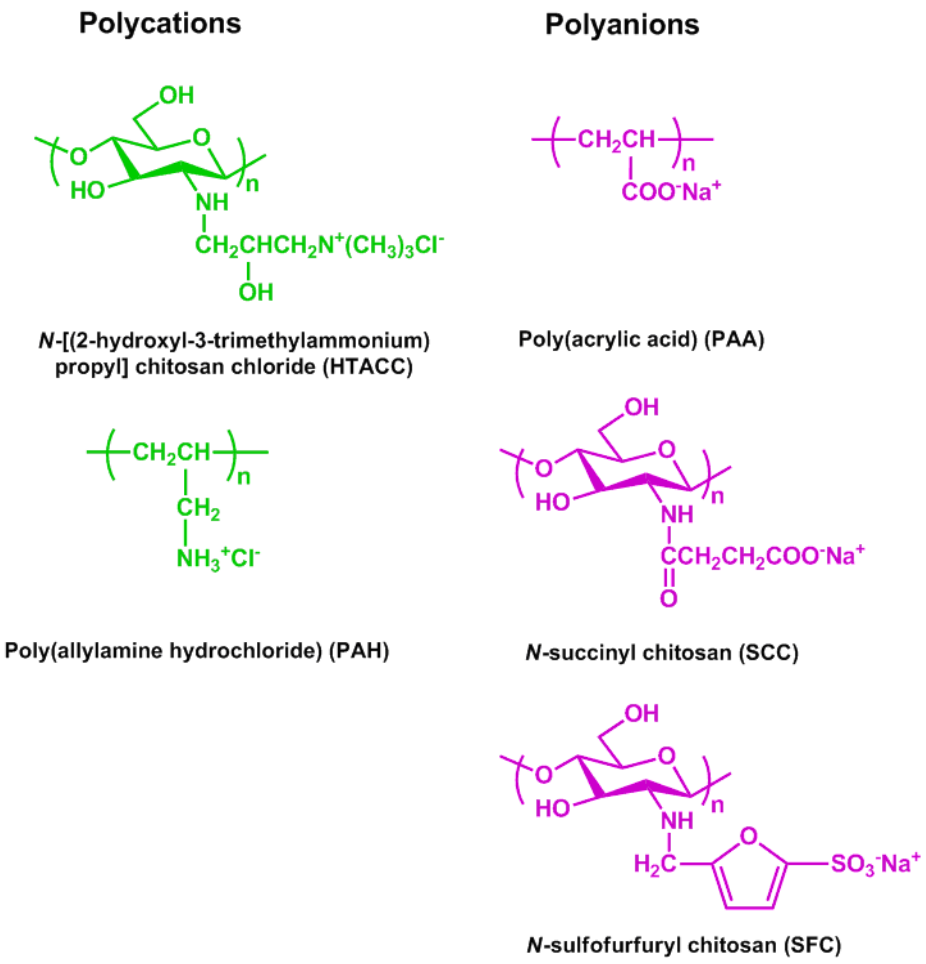

Figure 1. Polycations and polyanions used for multilayer assembly.

Experimental Section

Materials. Chitosan flakes (DAC of 95%, M_w = 100,000 g·mol^{-1}) were obtained from Seafresh Chitosan (Lab) Co., Ltd. (Thailand). Succinic anhydride (SA) was purchased from May&Baker (England). 5-Formyl-2-furan-sulfonic acid, sodium salt (FFSA), poly(allylamine hydrochloride) (PAH), M_w = 70,000 g·mol^{-1}, phosphate buffered saline (PBS), glycine, and a bicinchoninic acid assay kit (QuantiPro^{TM} BCA assay) were supplied by Sigma-Aldrich (USA). Heparin (HEP), M_w = 4,000-6,000 g ·mol^{-1} was purchased from Fluka (USA). Triethanolamine, sodium borohydride

($NaBH_4$), glycidyltrimethylammonium chloride (GTMAC), and poly(acrylic acid) (PAA), M_w = 60,000 $g \cdot mol^{-1}$ were purchased from Fluka (Switzerland). Plasma-treated poly(ethylene terephthalate) films (i.d. = 14 mm) were supplied by Wako Pure Chemical Industry, Ltd. (Japan). Fibroblast L929 cells were purchased from American Type Culture Collection (ATCC) (USA). Fetal bovine serum (FBS) and RPMI medium 1640 were purchased from InVitromex (USA). Penicillin was purchased from General Drugs House Co.,Ltd. Streptomycin was purchased from M&H manufactureing Co.,Ltd. (Thailand). *E. coli* and *S. aureus* were provided by National Center for Genetic Engineering and Biotechnology (BIOTEC), Thailand. Mueller-Hinton agar (MHA) and Mueller-Hinton broth (MHB) were purchased from Difco (USA). Mueller Hinton agar plate was supplied by Department of Medical Science, Ministry of Public Health, Thailand. The chemicals were of analytical grade and used as received without further purification. Ultrapure distilled water (Milli-Q water) was obtained after purification using a Millipore Milli-Q system (USA) that involves reverse osmosis, ion exchange and a filtration step. *N*-[(2-hydroxyl-3-trimethylammonium)propyl] chitosan chloride (HTACC), *N*-sulfofurfuryl chitosan (SFC), and *N*-succinyl chitosan (SCC) were synthesized according to the method modified from that of Seong *et al*.[7] Amiji.[10] and Aoki *et al.*,[20] respectively. Detailed experimental procedures and chemical characteristics of all derivatives characterized by FT-IR spectrometer (Nicolet, model Impact 410, USA) and ^1H NMR spectrometer (Varian, model Mercury-400, USA) are available in Supporting Information Section.

Multilayer Assembly. Plasma-treated PET substrates were immersed in a solution of 1 M NaOH (aq) at 60°C for 1 h. After incubated for a given time, the substrates were taken out, washed with 0.1 M HCl (aq) for 10 min to rinse off NaOH. Finally, the substrates were rinsed thoroughly with Milli-Q water and air-dried at ambient temperature to obtain the surface-hydrolyzed PET films. After surface hydrolysis, the treated PET substrates were subjected to

multilayer assembly by sequentially dipping in a polycation solution (2 mg/mL of PAH, or 2 mg/mL of HTACC) and a polyanion solution (1 mg/mL of SCC, 2 mg/mL of SFC, or 2 mg/mL of PAA) for 20 min interval. The optimal concentration of each polyelectrolyte was identified by conventional QCM measurements as previously described.[19] All polyelectrolytes were not buffered. For most of the experiments, the salt concentration of 0.1 M NaCl (aq) was added in both solutions. The pH of the solution was adjusted by using 0.1 HCl (aq) or 0.1 NaOH (aq). The substrates were rinsed thoroughly with Milli-Q water between each dipping and after the final adsorption. Three pairs of polyelectrolyte self-assemblies were fabricated: at pH 7 for HTACC/PAA and PAH/SCC, and at pH 8 for PAH/SFC.

Characterization of Deposited Multilayer Film. A contact angle goniometer model 100-00 equipped with a Gilmont syringe and a 24-gauge flat-tipped needle (Ramé-Hart, Inc., USA) was used for the determination of water contact angles. A droplet of Milli-Q water was placed on the tested surface by bringing the surface into contact with a droplet suspended from a needle on the syringe. The measurements were carried out in air at ambient temperature. The reported angle is an average of 5 measurements on different areas of each sample. The structure and morphology of the multilayer films were examined by atomic force microscopy (AFM). AFM images were recorded with a Scanning Probe Microscope; model NanoScope®IV, Veeco, USA. Measurements were performed in air at ambient temperature using a tapping mode. Silicon nitride tips with a resonance frequency of 267-298 kHz and a spring constant 20-80 N/m were used.

Analysis by Quartz Crystal Microbalance. The apparatus and the quartz crystals used for QCM measurements were obtained from Maxtek, Inc. (USA). An AT-cut quartz crystal with a fundamental resonance frequency of 5 MHz, model SC-501-1 was used. The plating crystal (1

inch in diameter) was covered by evaporated gold on both faces. The frequency shift of the gold-coated QCM plate was monitored by a Maxtek plating monitor (model PM-710) coupled with an MPS-550 sensor probe. The Data-Log Software (Maxtek) was used for data acquisition and monitoring. For QCM measurements with dissipation mode (QCM-D), a Q-Sense D300 (Q-Sense, Götenborg, Sweden) fitted with a Q-sense axial flow chamber was used for real-time simultaneous measurement of frequency and dissipation changes. An AT-cut piezoelectric crystal coated with gold electrodes on its two faces having a fundamental resonance frequency of 5 MHz (Q-Sense AB, Götenborg, Sweden) was excited at its fundamental frequency (n=1) as well as at the third, fifth, and seventh overtones (n = 3, 5, and 7, respectively) corresponding to 15, 25, and 35 MHz, respectively. The gold-coated QCM plate was cleaned by soaking in piranha solution (3:1 H_2SO_4:30% H_2O_2) for 5 min, rinsing thoroughly with Milli-Q water and drying with a light stream of nitrogen gas prior to use. The surface modification of the gold-coated QCM plate was carried out by immersion in an ethanolic solution containing 1:1 (v/v) of 10 mM 11-mercaptoundecanoic acid and 10 mM 11-mercapto-1-undecanol at ambient temperature. After 24 h, the plate was rinsed with ethanol and dried with a light stream of nitrogen gas. For the QCM measurements in the conventional mode, one side of the gold-coated QCM plate was covered with a designated polyelectrolyte solution for a desired period of time, rinsed with Milli-Q water, dried with a light stream of nitrogen gas after each step of deposition and then the resonance frequency was measured in air. For the QCM-D measurements in real-time, one side of the gold-coated quartz crystal was kept in permanent contact with a designated polyelectrolyte solution and the frequency change was recorded continuously at ambient temperature.

Cell Adhesion and Proliferation Tests. The Fibroblast L929 cells were cultured in RPMI 1640 medium supplemented with 5% fetal bovine serum (FBS), penicillin (100,000 U/L) and

streptomycin (100 mg/mL). They were incubated at 37°C in atmosphere containing 5% CO_2 where the culture medium was changed every 3 days. Both the treated PET substrates with and without multilayer films were sterilized by soaking in 70% ethanol in water for 30 min and washed twice with RPMI medium 1640. The substrates were then transferred to cover the bottom of 96-well tissue culture polystyrene (TCPS) plate. Three replicated samples were used for each condition. Approximately $5x10^3$ of L929 cells in 0.2 mL culture medium were pipetted into each well containing the substrates as well as blank wells made of tissue culture polystyrene (TCPS) as a control and then incubated under 5% CO_2 at 37°C. MTT assay was used to investigate cell adhesion and proliferation. After 12 h of incubation, the culture medium was removed to discard the unattached cell and the 0.2 mL fresh culture medium was pipetted into each well followed by 10 μL of 0.5 mg/mL MTT/normal saline solution. After incubation for 4 h, the supernatant solution was removed and 150 μL of DMSO was pipetted into each well to dissolve the purple crystals of formazan. Next, 25 μL of 0.1 M glycine (pH 10.5) was added. The optical density of the solution was measured using a microplate reader (MK II, Titertek Multiskan MCC/340, Finland) at the wavelength at 540 nm.

Antibacterial Activity Test. The antibacterial activity of the multilayer film of HTACC/PAA assembled on the treated PET substrates against the Gram-positive bacteria, *S. aureus* and Gram-negative bacteria, *E. coli* was assessed by viable cell-counting method. The treated PET substrates carrying multilayer films were sterilized by exposing to UV irradiation for 1 h prior to the tests. The substrates were placed one per well of a 24-well plate containing 2 mL Mueller-Hinton broth (MHB). Then 12 μL of bacterial suspension in distilled water (OD_{600} = 0.1) was pipetted into each well and the plate incubated in a shaking incubator (Model G-25, New Brunswick Scientific Co., Inc., USA) at 37°C, 110 rpm, for 24 h. A 100 μL of each of the

bacterial suspensions was then transferred from each well and then diluted 10^4 times and 100 μL of this diluted bacterial suspension was then spread onto Mueller-Hinton agar (MHB). After incubating at 37°C for 24 h, the number of colonies, and thus replication competent bacteria were then counted as a measure of assumed viability. The results, after correction for the dilution factor, were expressed as the mean number of colony forming units per volume (CFU/mL). All tests of antibacterial activity were performed in triplicate per sample and upon at least three independent samples.

Preparation of Platelet-rich Plasma (PRP) and Platelet-poor Plasma (PPP). Human whole blood (100 mL) from a healthy volunteer was collected into a sterile plastic syringe and mixed with 3.8 %(wt/v) sodium citrate in PBS (1 mL:10 mL blood). To obtain the platelet-rich plasma (PRP) for *in vitro* static platelet adhesion testing,[21,22] the human whole blood was centrifuged at 1,200 rpm for 10 min. After centrifugation, the red blood cells and platelets were separated into 2 layers. The PRP as yellowish solution (top layer) was carefully withdrawn via micropipette. Subsequently, a portion of PRP was taken and then centrifuged at 2,000 rpm for 15 min to obtain the platelet-poor plasma (PPP) to be used for protein adsorption test.[21,22]

Determination of the Total Amount of Adsorbed Human Plasma Protein. The multilayer films of PAH/SFC and PAH/HEP assembled on the treated PET substrates were placed into 24-well tissue culture plate containing deionized water and hydrated overnight to reach an equilibrium hydration before experiment. Triplicate samples were used (n = 3). Each sample was removed from deionized water and suspended into the well containing 1.0 mL of PPP and incubated at 37°C for 3 h. After incubation, the samples were removed from PPP and followed by rinsing twice with PBS to remove any loosely attached protein. The adsorbed protein on the

sample surface was detached by soaking each sample in 1.0 mL of 1 %(wt/v) aqueous solution of sodium dodecyl sulfate (SDS) for 30 min. A 100 μL of SDS solution which socked each sample was pipetted into 96-well tissue culture plate. The solution was then mixed with 100 μL of BCA working solution in each well and followed by incubation the well-plate at 37^{o}C for 2 h. The absorbance of the solution was measured at 562 nm by UV microplate reader (Microtiter plate reader; Model Sunrise, Tecan Austria GmbH). The amount of protein adsorbed on the samples was calculated from the protein concentration in SDS solution. The data were express as mean ±standard deviation (S.D). A protein analysis kit based on the bicinchoninic acid (BCA) method was used to determine the concentration of the protein dissolved in the SDS solution.

Evaluation of Platelet Adhesion. The multilayer films of PAH/SFC and PAH/HEP assembled on the treated PET substrates were put into the 24-well TCPS and hydrated overnight in PBS. After PBS was removed, the samples were immersed in 1 mL of freshly prepared PRP and incubated at 37^{o}C for 1 h. After incubation, samples were gently rinsed with PBS to remove loosely adherent platelets from the surface and then treated with 2.5% glutaraldehyde in PBS to fix the platelets adhered to the surfaces for 1 h at ambient temperature. Finally, the samples were washed again with PBS and then subsequently dehydrated with gradient immersion of ethanol/water solutions (50, 60, 70, 80, 90, 95, and 100 vol.-%) for 10 min each and dried *in vacuo* overnight. The substrates were then sputter-coated with gold for the scanning electron microscope characterization (JEOL Model JSM-5410LV, Japan).

Statistical Analysis. Statistical analysis of cell adhesion/proliferation tests, antibacterial activity test, and protein adsorption are expressed as the means±standard deviations (S.D.) of a representative of three similar experiments carried out in triplicate. Statistical analysis was

performed using the Statistical Package for the Social Science (SPSS) version 14.0 software. Statistical comparisons made by One-Way Analysis of Variance (ANOVA) with the Least Square Difference (LSD) tests were used for post hoc evaluations of differences between groups. The threshold level for accepting statistical significance was set at $p < 0.05$.

Results and Discussion

Physical Characteristics of Multilayer Assembly. QCM is an effective tool to investigate the growth of multilayer film. It is an ultrasensitive mass sensor, consisting of a piezoelectric quartz crystal sandwiched between a pair of electrodes. When a suitable RF voltage is applied across the electrodes, the quartz crystal oscillates at its resonant frequency; a small layer added to the electrodes induces a decrease in resonant frequency ($\triangle F$). If a rigid layer is deposited on one or both sides of the electrodes, the resonant frequency will decrease proportionally to the mass of the absorbed layer according to the Sauerbrey equation: [23]

$$\Delta F = \frac{-2F_0^2 \Delta m}{A (\rho_q \mu_q)^{1/2}} \qquad (1)$$

In Equation (1), ΔF = measured frequency shift, F_0 = fundamental frequency of the crystal, Δm = mass change per unit area, A = piezoelectrically active area, ρ_q = density of quartz (2.648 g/cm^3), and μ_q = shear modulus of quartz (2.947×10^6 N/cm^2). Typically, the relationship between the frequency shift and the adsorbed mass per unit area (Δm) is linear obeying the Sauerbrey equation, Equation (2):

$$\Delta m = -C\Delta F/n \quad (2)$$

where C is the mass sensitivity constant (17.7 ng·cm^{-2} Hz^{-1} at 5 MHz), and n is the overtone number. In addition, dissipation can be characterized by the dissipation factor D, which is defined by Equation (3):

$$D = \frac{E_{dissipated}}{2\pi E_{stored}} \quad (3)$$

where $E_{dissipated}$ is the energy dissipated during one oscillation and E_{stored} is the total energy stored in the oscillating system. With the QCM-D measurements, the change in dissipation factor, $\Delta D = D\text{-}D_0$ is deduced, where D_0 is the dissipation factor of the pure crystal in solvent before adsorption and D is the dissipation factor after adsorption.

In this research, QCM analysis was conducted on a thiol-modified gold-coated QCM plate containing an equal composition of COOH and OH groups which is used as a model for treated PET substrates which were later subjected to multilayer assembly and determination of biological responses. Its water contact angle of 55° being close to that of the treated PET substrate (53°) suggests that it can satisfactorily mimic the treated PET substrate. Figure 2 displays the evolution of the normalized frequency changes ($\Delta F/n$) on the 3rd, 5th, and 7th overtone numbers and the corresponding changes in energy dissipation on the 3rd overtone number versus time of three multilayer systems as measured by QCM-D. At time (t) = 0 min, a stable baseline starting with 0.1 M NaCl was first established prior to adsorption of polyelectrolyte. At t = 5 min, a polycation (HTACC or PAH) solution was injected into the measurement chamber and allowed to adsorb for

5 min before the rinsing step began. After rinsing with 0.1 M NaCl for 5 min, at t = 15 min, the polyanion (PAA, SCC, or SFC) solution was then introduced followed by the same rinsing procedure. The adsorption and rinsing cycles were repeated until 10 individual layers of the polyelectrolyte were deposited. The change in frequency (ΔF) and dissipation (ΔD) throughout the building-up process were continuously observed indicating the stepwise deposition of the polyelectrolyte molecules to the QCM substrate. The fact that the $\Delta F/n$ of all three overtones can be superimposed throughout the whole range investigated strongly indicates that the assembled films are relatively rigid, not viscoelastic and that the adsorbed mass can be calculated from the observed frequency shift following Sauerbrey relationship.

For the HTACC/PAA system, an increase in ΔD and a decrease in $\Delta F/n$ were apparently more dramatic in the step of HTACC deposition (odd layer) as opposed to those in the step of PAA adsorption (even layer) suggesting that the HTACC layer was less rigid and perhaps greater in thickness than the its negatively charged counterpart, PAA. To explain such scenario, it is conceivable to take the comparative charge density of the HTACC and PAA into consideration. With 78% degree of substitution (%DS) of positively charged quaternary ammonium entities ($N(CH_3)_3^+$), HTACC should be less charged than PAA, a weak polyelectrolyte having a p*Ka* of 4.3[24] at pH 7. Therefore, HTACC can adopt less extended conformations at the interface with a higher proportion of loops and tails than PAA. Not only can that bring in more HTACC chains to adsorb and yielded a thicker layer than did the PAA, but such coil-like conformation should also be able to trap more water molecules within its structure. These two reasons are believed to be responsible for the substantial difference in the decrease in $\Delta F/n$ and the increase in ΔD upon the adsorption between HTACC and PAA. It was not totally unexpected to observe a collapse of the entire multilayer film towards the interface upon the adsorption PAA. Its greater charge density as compared with HTACC makes the interpenetration and complexation/crosslinking between

the oppositely charged polyelectrolytes resulting in intrinsic charge compensation at the interface much more efficient. The stiffening of the adsorbed multilayer together with the preferably extended conformation led to a thinner layer of PAA having presumably less coupled water within its structure.

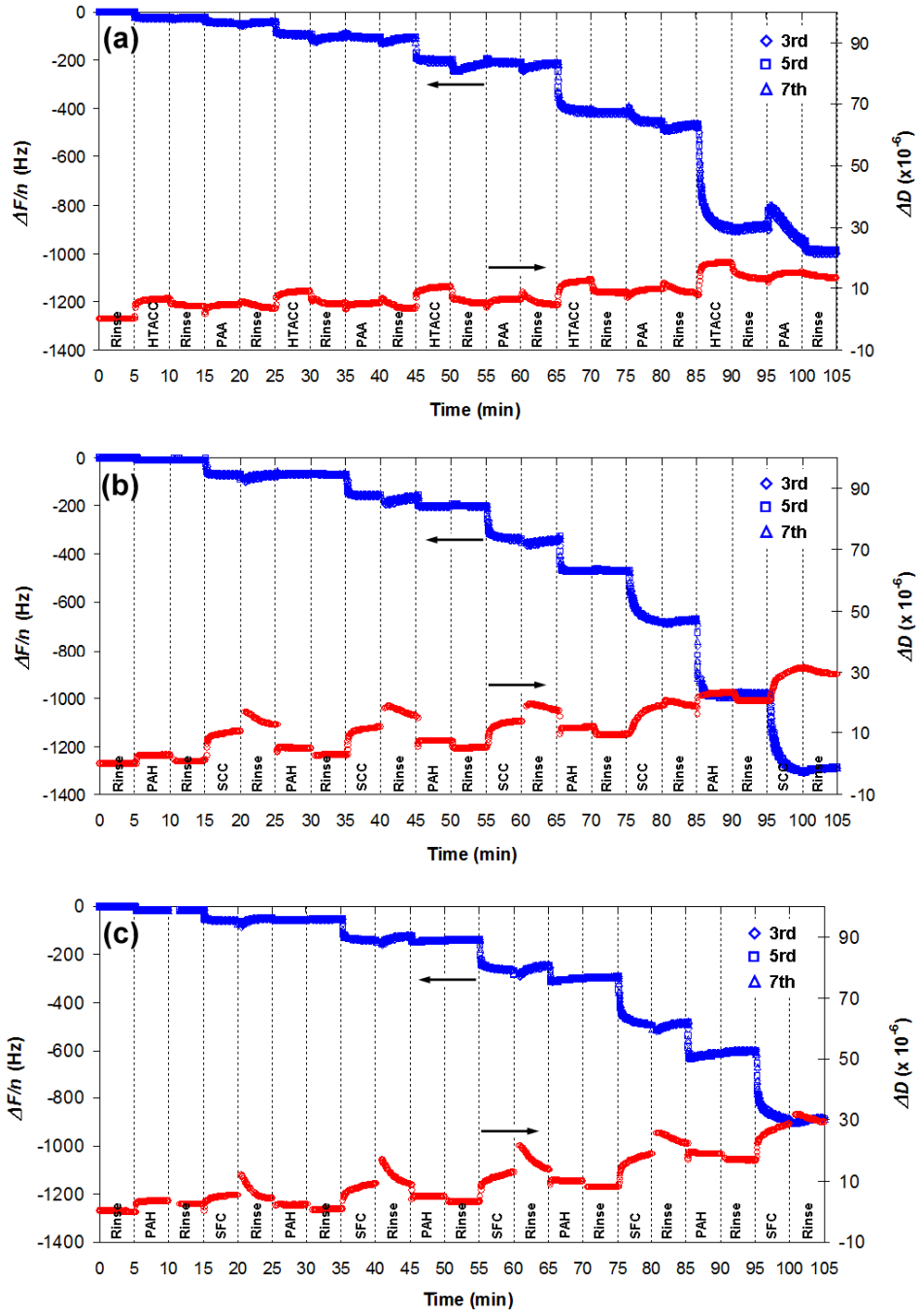

Figure 2. The change in normalized frequency ($\Delta F/n$) on the 3rd, 5th, and 7th overtones and the energy dissipation change (ΔD) on the 3rd overtone as a function of time upon consecutive adsorption of polyelectrolytes for 3 multilayer systems: (a) HTACC/PAA, (b) PAH/SCC, and (c) PAH/SFC.

The odd-even effect in terms of *ΔF/n* and *ΔD* variation was also evidenced on other two multilayer films, PAH/SCC and PAH/SFC, both of which were assembled from the same cationic polyelectrolyte, PAH (Figure 2 (b) and (c)). The explanation based on the charge density should also be valid. As a consequence of the incomplete substitution of negatively charged entities at the NH_2 position on the chitosan backbones, SCC with 44% DS (of *N*-succinyl groups) and SFC with 68%DS (*N*-sulfofurfuryl groups) should be less charged than PAH, a weak polyelectrolyte having a p*Ka* of 9.67.[25] At pH 7-8 at which PAH/SCC and PAH/SFC multilayer films were assembled, 98-99% of $-NH_3^+$ of PAH remained undissociated. This is the reason why an increase in *ΔD* and a decrease in *ΔF/n* were appreciably much greater in the step of SCC and SFC deposition (even layer) than those in the step of PAH adsorption (odd layer) suggesting that the SCC and SFC layers were thicker and presumably more water-rich than their positively charged counterpart, PAH. The higher charge density of the PAH facilitated interfacial crosslinking between the oppositely charged polyelectrolytes and so thus imparted the collapse of the film upon its deposition. This suggests that the properties of multilayer thin film depend on which the adsorbed layer in the outermost layer. Evidently, it can be concluded that all three multilayer films have a relatively compact, rigid internal structure and the differences in the observed dissipation are determined by the interfacial properties of the last deposited layer.

The water content of each individual layer for all three multilayer systems can be estimated from the mass per unit area for dry films (m_d) and wet film (m_w) following Equation (4): [26] It should be emphasized that m_d and m_w were calculated based on the assumed density of the dry films (1.2 g/cm^3)[27] by Sauerbrey equation from ΔF obtained from QCM and QCM-D measurements, respectively.

$$\% \text{ water content} = \frac{m_w - m_d}{m_w} \times 100 \qquad (4)$$

According to the results shown in Figure 3, the water contents of all three multilayer pairs are relatively high with all values being above 60%. The alternating trend of the water content between the odd and even layer was only observed at initial stage of assembly process (up to 4-7 layers). The water contents tended to level out at 85-90% between 7-10 deposited layers. Together in the same figure, the dried adsorbed mass determined by QCM was plotted to demonstrate that the odd-even effect of $\Delta F/n$ and ΔD variation analyzed by QCM-D as previously shown in Figure 2 and the m_w displayed in Figure S1 (Supporting Information) at the early stage of deposition was very much influenced by the different content of associated water within each individual layer between the odd and even layer. Once the assembly process was well established (from 5 layers onward), the odd-even fluctuation of both $\Delta F/n$ and ΔD was no longer governed by the entrapped water, but mainly dictated by the varied amount of the adsorbed polyelectrolyte which is dependent on its charge density and conformation

It is not unprecedented to see an exponential growth of deposited mass and thickness (Figure S2 in Supporting Information) in the investigated range for all three multilayer systems. Schlenoff and Dubas[28] described this initial nonlinear growth regime as a result of excess charge profile being truncated by the impenetrable multilayer. Ladam and co-workers[29], on the other hand, suggested that there are polyelectrolyte chains diffusing into and out of the film during the buildup process. It was proposed that free polyelectrolyte chains within the multilayer film diffuse out to form complexes with the oppositely charged polyelectrolytes at the surface upon the change of the bulk solution to one with polyelectrolytes of opposite charge. And that would

promote the adsorption of more material on the surface in each adsorption step than that should be expected from the regular charge compensation.

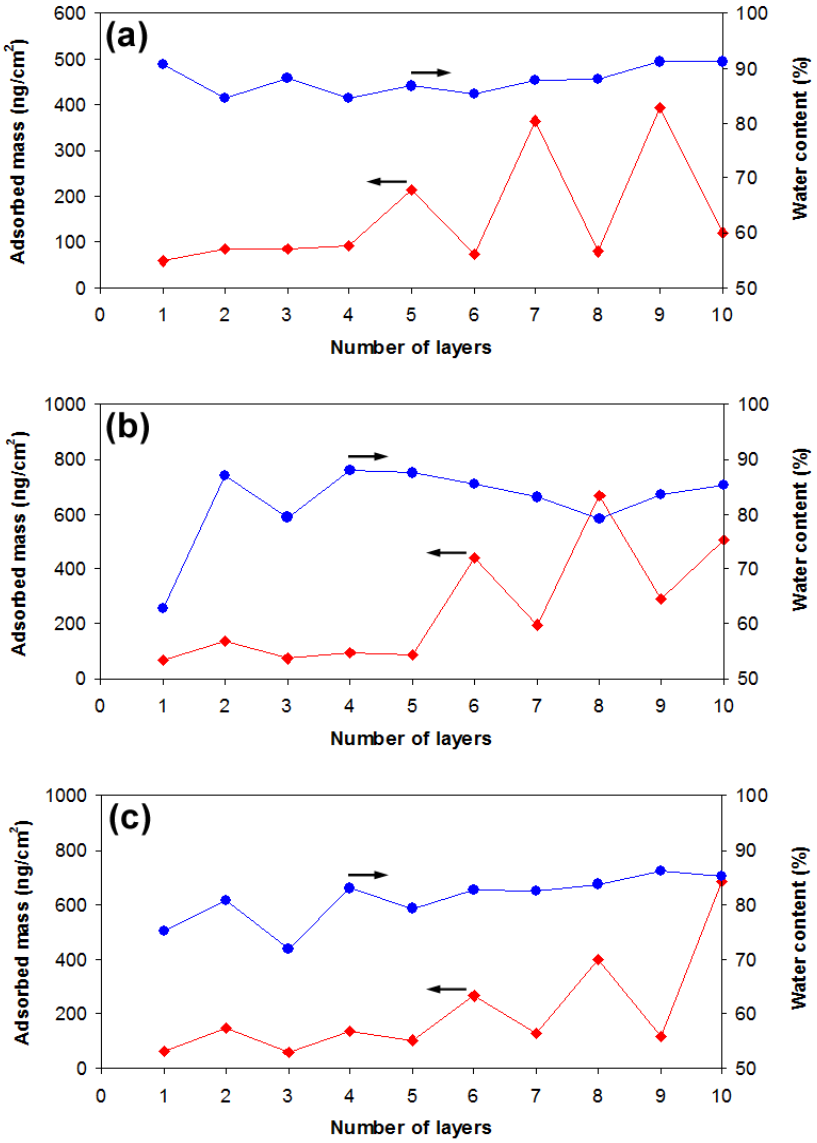

Figure 3. Water content (•) and mass per unit area for dry films (m_d) determined by QCM (◆) as a function of layer number for 3 multilayer systems: (a) HTACC/PAA, (b) PAH/SCC, and (c) PAH/SFC

Surface Coverage and Wettability of the Multilayer Films. In this research, the plasma-treated PET plates, commercially available and commonly used polymeric materials for biomedical and biomaterials applications, were employed as substrates for multilayer assembly. After the treatment by basic hydrolysis, the treated PET substrate with a water contact angle of 53º and carboxyl group density of 1.46 x 10^{-8} mol/cm^2 as estimated by Toluidine blue O assay were obtained.[19] The coverage of the deposited multilayer films was monitored by AFM analysis. Upon basic hydrolysis, the treated PET substrate became rougher as can be evidenced from the root-mean-square roughness (R_{rms}) being increased from 1.76 to 7.68 nm (micrographs not shown). As illustrated in Figure 4, the surfaces became apparently smoother after the deposition of HTACC/PAA multilayer. A similar trend was also observed for the system of PAH/SCC, except that the roughness of the even layer (having SCC as the outermost layer) seemed to be rougher than their adjacent odd layer (having PAH as the outermost layer). In contrast, the assembled PAH/SFC film became increasingly rougher upon the growth of the multilayer film implying that the defects or aggregates generated during the deposition of the first layers have been accumulated in the consecutive layer. The adsorbed polyelectrolyte that was expected to fill previously formed valleys on the surface and smoothened the film, in turn made the film rougher. This may be explained as a consequence of the loosely bound polyelectrolyte form complexes upon partial or total desorption and deposited back into the assembled layer during the adsorption process. Apparently, the interdigitation was less perfect in this particular case. The fact that the surface roughness of the film having the chitosan derivative (HTACC, SCC or SFC) as the top layer were always greater than that having its oppositely charged polyelectrolyte (PAA or PAH) as the top layer agree quite well with the QCM data which previously indicated that all chitosan derivatives with their lower charge density than their counterparts adsorbed in the less extended and more loop-like conformations and yield thicker

individual layer. And that can be the origin of the odd-even topographic variation. Nonetheless, it can be assumed that the assembled films grow homogeneously when the size of the roughness and the pores is far larger than molecular sizes of polyelectrolytes and smaller than the average thickness of a single bilayer. (Table S1 in Supporting Information)

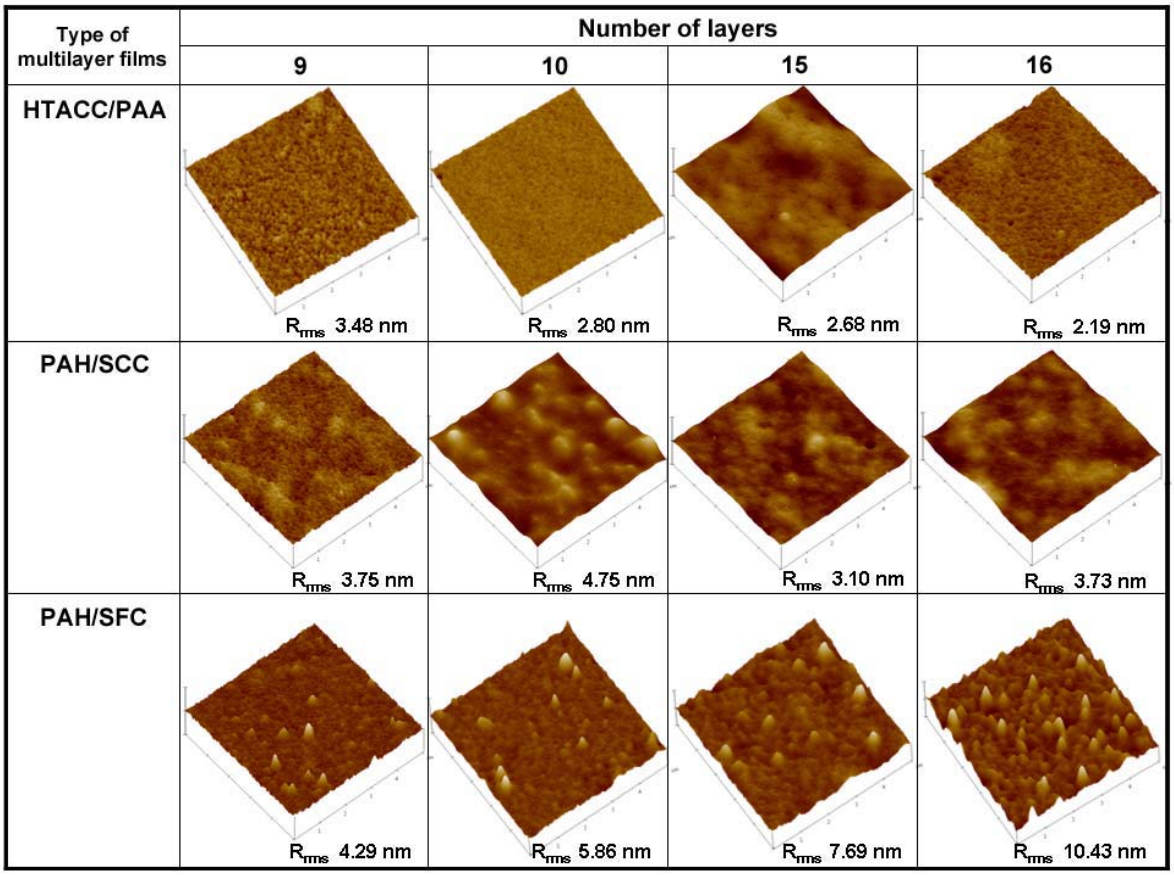

Figure 4. AFM images (5x5 μm^2) of treated PET substrates with three multilayer systems: HTACC/PAA, PAH/SCC, and PAH/SFC. The value listed under each micrograph is the corresponding root-mean-square roughness ($R_{rms.}$) for each micrograph.

The wettability of the multilayer film was probed by water contact angle measurements. The results depicted in Figure 5 suggested that the assembled film was stratified. And the films

having the odd number of deposited layer and positively charged was more hydrophobic than those having an even number of deposited layer and negatively charged. The odd-even wetting behavior coincides with the fact that each individual layer based on QCM analysis (half of the bilayer thickness shown in Table S1) is thicker than the sampling depth of contact angle measurement (a few Å) so that the wettability of the multilayer film is strongly determined by the last layer deposited and the influence of the underlying layers was not observed.

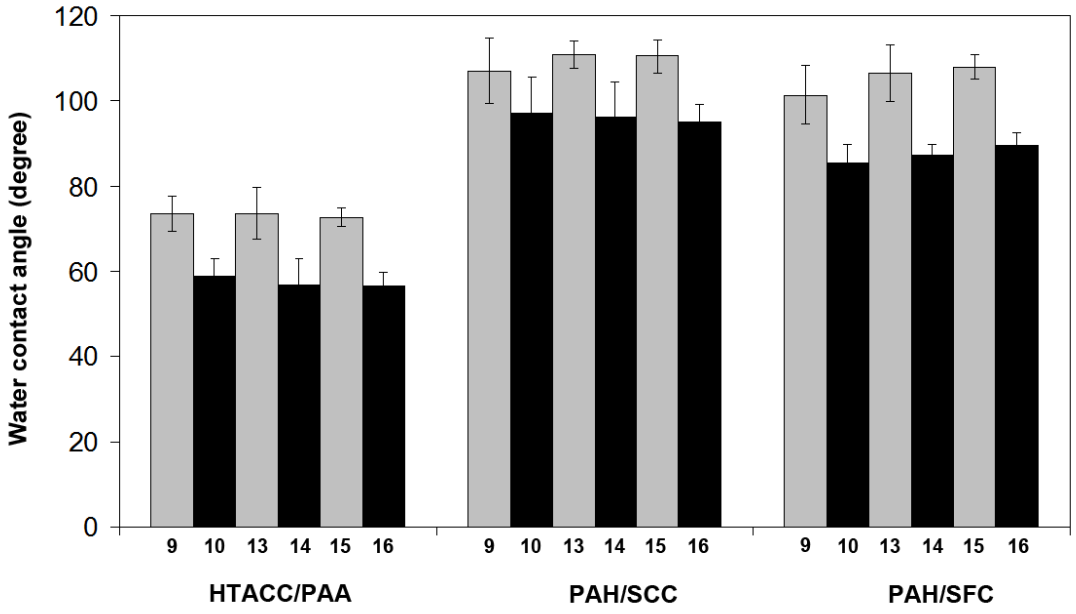

Figure 5. Water contact angle of multilayer films assembled on treated PET substrates. The number appearing on the horizontal scale represents the number of depositions.

Cell Adhesion and Proliferation. The *in vitro* cytocompatibility of three multilayer systems, on the treated PET substrates was carried out against L929 fibroblasts. To investigate the mitochondrial functions of the cultured L929, reduction of MTT reagent was used as an assay to measure mitochondrial redox activity. MTT reagent is a pale yellow substance that is reduced to a dark blue formazan product when incubating with viable cells by mitochondrial succinate

dehydrogenase in complex II, which plays a critical role in both oxidative phosphorylation and tricarboxylic acid cycle. Therefore, the production of formazan can reflect the level of cell viability. The results shown in Figure 6 are reported in terms of the cell adhesion (after 12 h incubation) and proliferation ratio (after 48 and 96 h incubations) with relative to TCPS. The number appearing on the horizontal scale represented the number of deposition. If the number of layer is odd, the charge of the outermost layer is positive. If the number of layer is even, the charge of the outermost layer is negative.

Considering the HTACC/PAA system, the multilayer film having the even number of layer with PAA as the top layer seems to be more favorable for both cell adhesion and proliferation than those having the odd number of layer with HTACC as the top layer. The effectiveness of PAA in promoting positive cellular responses is equivalent to the TCPS which was used as a positive control. It is generally known that the cell membrane possesses negative charges. The opposite charges of HTACC should lead to a strong attraction with the cells and causes detrimental influence on the cells. The effect is more pronounced after 4 days of incubation. It has been previously reported that HTACC exhibit potent antibacterial activity.[7,8] And this may be the reason why it is not a favorable substrate for promoting cell growth and maintaining cell viability.

As opposed to the system of HTACC/PAA, the PAH/SCC multilayer films exhibit the opposite tendency. After 2 and 4 days of incubation, a significant improvement of cell adhesion was observed, especially when the number of layer was equal to 15 and PAH was the top layer. Unlike HTACC, PAH is a weak synthetic polyelectrolyte that has been found to enhance early cell adhesion in the multilayer system of (PSS/PAH)[30] when it is the outermost layer of the film. The fact that SCC bears some negative charge, which is the same charge as the cell membrane, can explain why it is unfavorable for cell attachment. Evidently, the hydrophilic nature is not

enough to counteract the charge repulsion. However, the same explanation cannot be applied with PAA. A similar trend was observed in the case of PAH/SFC system. In particular, the 9-layer multilayer film with PAH as the outermost layer gave significantly higher in both cell adhesion and proliferation than the treated PET substrate. The charge repulsion may also account for the inferior cellular responses of the multilayer films having SFC as the top layer. The cellular responses seem to be worse as a larger number of layers were deposited. There may be some influence from the increased roughness (See AFM data).

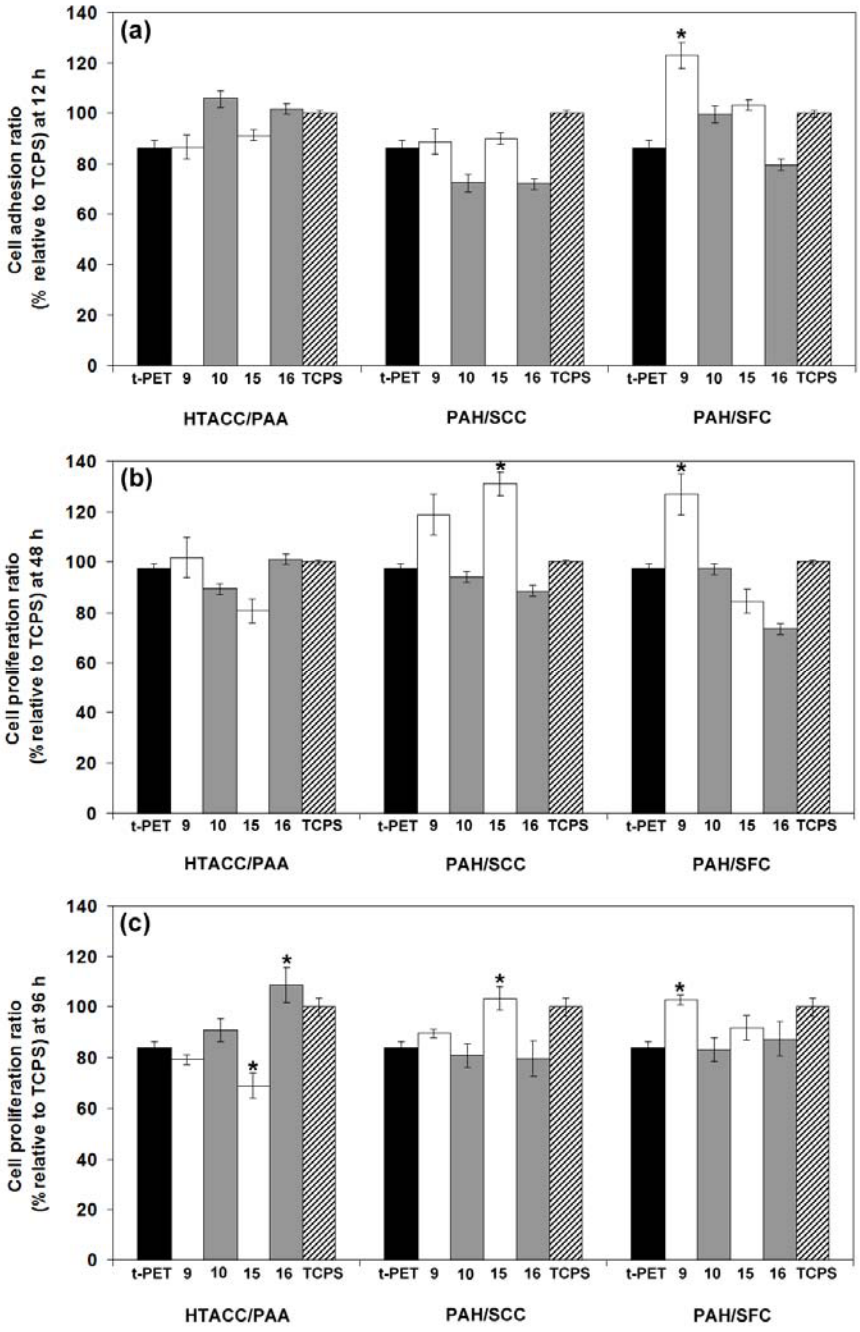

Figure 6. Responses of L929 cells (% relative to TCPS) with a seeding density of 5.0×10^3 cells/well on treated PET substrates with three multilayer systems in terms of (a) cell adhesion ratios at 12 h and cell proliferation ratios at (b) 48 and (c) 96 h. Statistical significance with $p < 0.05$ is compared with the control (t-PET) (*).

Antibacterial activity of the HTACC/PAA Multilayer Film. HTACC has been known to deliver desirable antibacterial activity when used in the soluble form[31,32] and chemically grafted or coated on materials.[7] Here, we anticipate that a similar antibacterial action can also be achieved when HTACC is deposited as assembled layers on any substrates. In this research, the antibacterial activity of the HTACC/PAA multilayer deposited on the treated PET substrate was tested against the Gram-positive and Gram-negative representative bacteria, *S. aureus* and *E. coli*, respectively, in terms of the total number of replication competent (viable) cells as mean colony forming units per volume (CFU/mL). The tested results are displayed in Figure 7 in which the number appearing on the horizontal scale represents the number of depositions. If the number of layers is odd (9 and 15), HTACC was the last layer deposit. If the number of layers is even (10 and 16), PAA was the last layer deposit. In the case of *S.aureus,* the detrimental effect was detected for the HTACC/PAA multilayer films having 15 and 16 layers. The former seemed to possess greater activity than the latter considering its %antibacterial ratio reached 70.5% as opposed to 57.8% of the latter. This can be expected taking into account that the surface of *S. aureus* consists of negatively charged teichoic acid within a thick peptidoglycan layer and lacks of an outer membrane. Such characteristic should render the bacterial cell more attractive to and easier to be damaged through the contact-inhibitory mechanism when exposed to the positively charged 15-layer film than the negatively charged 16-layer film.

In contrast, the damaging impact on *E.coli* was observed on the multilayer film having at least10 layers with only a slight odd-even effect was observed between the multilayer film having 15 and 16 deposited layers. The lower antibacterial potency of the multilayer film against *E.coli* than that against *S. aureus* may be explained as a result of the different bacterial membrane structures. Unlike *S. aureus*, *E. coli* has a double protective layer: the outer lipopolysaccharide layer embedded with a number of small channels of porins and the inner peptidoglycan layer (7-8

nm). The fact that it does not contain the negatively charged entities that can electrostatically interact with HTACC makes it less sensitive to be destroyed by positively charged molecules like HTACC. Although HTACC was not the top layer of the 16-layer HTACC/PAA film, the substrate exhibits favorable cellular responses (See Figure 6), it can introduce a reasonable antibacterial property (~50% antibacterial ratio) against both bacterial strains to the multilayer film. This is a desirable characteristic for biomaterials applications given that the film supported cell attachment and proliferation and at the same time appreciably prevented bacterial growth. Also, it should be emphasized that HTACC can be used as an effective material for antibacterial coating especially against bacterial strains having negatively charged cell membrane, *S. aureus* in this particular case.

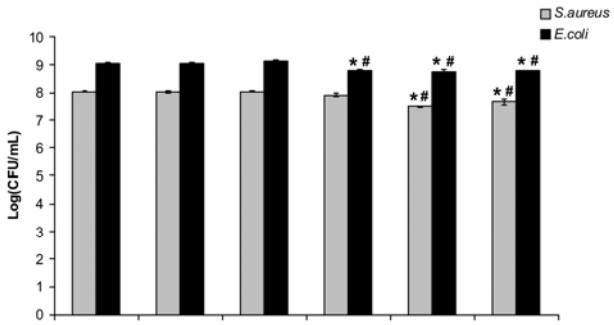

% Antibacterial ratio						
S. aureus	0.0	3.7	ND	20.6	70.5	56.9
E. coli	0.0	1.7	ND	46.3	48.6	45.7

ND = Not Detected

Figure 7. Total replication competent (viable) cell counts of bacteria grown for 24 h in media alone (control) or in the presence of treated PET substrate (t-PET) and multilayer film of HTACC/PAA assembled on treated PET substrate. The number appearing on the horizontal scale represents the number of depositions. Statistical significance with $p < 0.05$ of the viable count is compared with the control (*) and t-PET (#). Below in the table is the corresponding antibacterial ratio.

Antithrombogenic Properties of the PAH/SFC Multilayer Film. It has been previously demonstrated that SFC in a soluble or a surface-coated form expresses antithrombogenic property[10,11,33] a necessary feature for the development of materials to be used in contact with blood. This can be derived from the presence of sulfonic acid groups in its structure, the same negatively charged moieties present in heparin (HEP), a well-known and widely used anti-blood coagulation polymeric material. In principle, when a material is in contact with blood, a surface-induced thrombosis is initiated by adsorption of plasma proteins, followed by the adhesion and activation of platelets.[21] Herein, for the first time, the anticoagulating characteristic of SFC in the assembled form (PAH/SFC) was assessed in terms of amount of adsorbed plasma protein/surface area (mean±S.D.) and platelet adhesion of which results are illustrated together in Figure 8. The investigation was done in comparison with the multilayer films assembled from HEP and the same cationic polyelectrolyte, PAH.

As anticipated, the amount of adsorbed protein on the multilayer film having the odd number of layer with PAH as the top layer (9-layer and 15-layer) was greater than those having the even number of layer with SFC and HEP as the top layer (10-layer and 16-layer). It is generally known that under normal physiological condition at pH 7.4, the human serum carries negative charge due to the presence of albumin, its major protein component having the isoelectric point of 4.8.[22] Thus, the plasma proteins can favorably interact with cationic polyelectrolyte, PAH with a p*Ka* of 9.67[25] in this particular case, mainly through electrostatic interactions. On the other hand, the amount of adsorbed protein was approximately 31-33% and 48-62 % reduced on the assembled films terminating with SFC and HEP (the 10-layer and 16-layer), respectively when compared with that on the treated PET surface. This can be described as a result of the electrostatic repulsion between the negatively charged entities in the SFC and HEP layer and the plasma proteins. It should be emphasized that the negative charges in HEP do not only come from the

sulfonate groups (in the form of $–NHSO_3^-$), but also from the sulfate groups ($–CH_2OSO_3^-$ and OSO_3^-) and carboxylate groups (COO^-). Thereby, there are two negative entities in each repeat unit of HEP. Unlike HEP, SFC used in this investigation only bears 68% of negatively charged sulfonate groups substituted on the chitosan backbone. This is the reason why the ability of the films terminating with SFC in preventing plasma protein adsorption is inferior to that terminating with HEP. It should be noted that the level of antithromboginicity was varied as a function %DS of sulfofurfuryl groups on chitosan backbone in SFC. Upon mixing with 5 mL of whole blood for 15 min, 0.2 mg of SFC having 68%DS (dissolved in 0.85% NaCl(aq)) showed the lowest degree of partial blood coagulation as opposed to the SFC derivative having lower %DS. The real time coagulation of whole blood mixed with SFC having %DS of 68 and 55 can be viewed from Video S1 and S2 in Supporting Information, respectively. In contrast, the blood coagulation of whole blood mixed with the same amount of HEP (Video S3) was entirely suppressed whereas the blood became totally clotted within 3 min of mixing with chitosan (Video S4).

The results from static platelet adhesion assay (Figure 8) are in excellent agreement with the protein adsorption test. Aggregation of adherent platelets at partially activated stage having extensions of pseudopods were apparent on the substrates with high amount of adsorbed plasma proteins such as the treated PET substrate alone or the treated PET substrates with the 9-layer assembled PAH/SFC film. Fewer numbers of platelets adhered with insignificant degree of activation on the assembled PAH/SFC films terminated with SFC (10-layer and 16-layer) than those adhered on the PAH/SFC films terminated with PAH (9-layer and 15-layer). The alternating trend of platelet adhesion was also observed on the assembled PAH/HEP films confirming that the anticoagulant property is surface-dependent with the 16-layer assembled PAH/HEP showing an absolute anti-platelet adhesion. Although SFC is not as effective as HEP in suppressing plasma protein adsorption and platelet adhesion, its anticoagulating property is at

a satisfactory level given that its negative charge density is much less than HEP so that it can be considered as an alternative, nature-derived antithrombogenic material, being capable of forming assembled layer on materials to be used in blood-contacting applications.

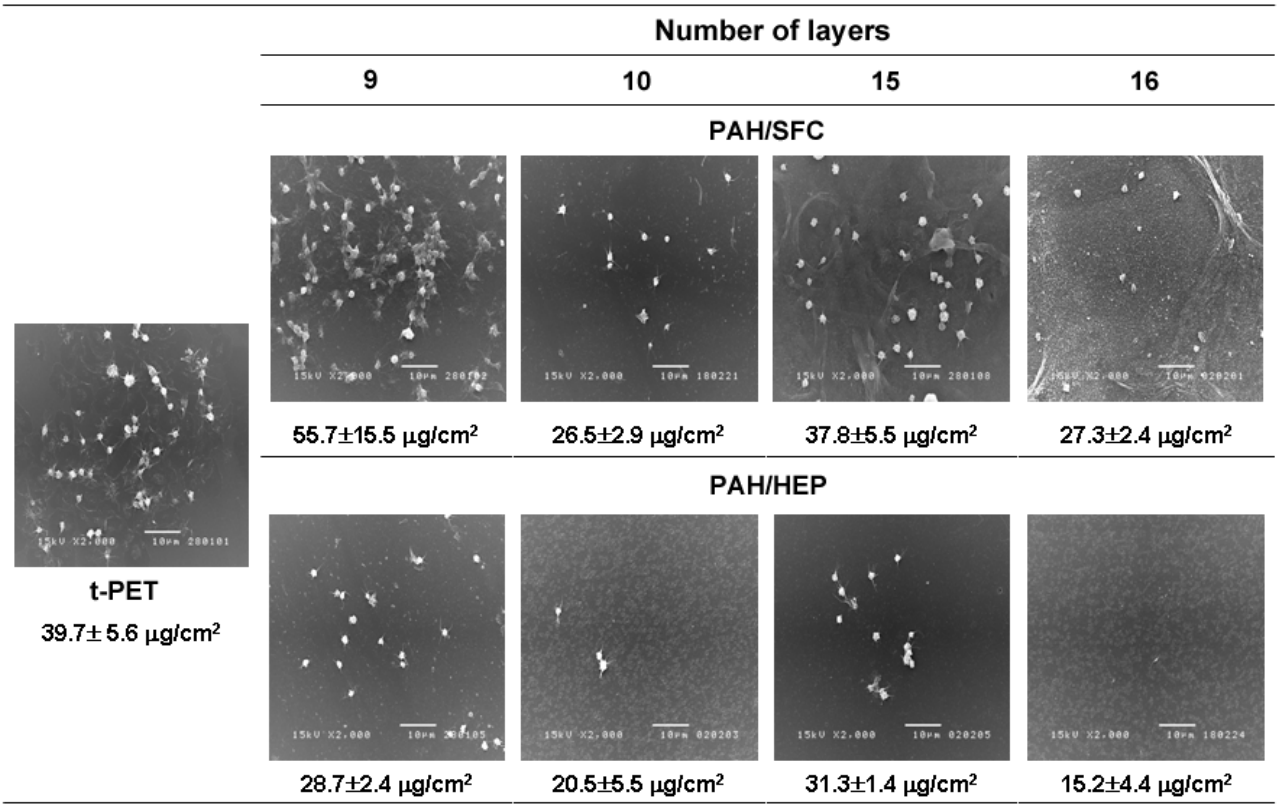

Figure 8. Representative SEM micrographs of treated PET substrates with multilayer systems after exposure to PRP for 1 h. Micrographs shown are representative of at least 10 such fields of view per sample and 3 independent samples. Below each micrograph is the corresponding amount of plasma protein adsorption ($\mu g/cm^2$) after the substrates were exposed to PPP for 3 h.

Conclusion

QCM analysis suggested that multilayer films of these 3 pairs of polyelectrolytes: (HTACC/PAA), (PAH/SCC) and (PAH/SFC) have been successfully formed by alternate layer-

by-layer adsorption. The stratification of the multilayer films deposited on the plasma-treated poly(ethylene terephthalate) (treated PET) substrates was verified by water contact angle measurements, respectively. As characterized by AFM, the multilayer films can homogeneously cover the substrate and have the ability to smooth-out a rough surface of the treated PET substrates. The *in vitro* cell adhesion and proliferation of fibroblasts showed that the degree of cytocompatibility of the multilayer films depends strongly on the polyelectrolyte used for the assembly process and the last layer deposited. The antibacterial activity of (HTACC/PAA) showed that the multilayer film is able to inhibit the growth of *E. coli* and *S.aureus* which was consistent to cell study. The results from blood compatibility indicated that the (PAH/SFC) multilayer film terminating with SFC can reduce protein adsorption. All above results of this study demonstrated that multilayer film assembled from charged derivatives of chitosan are potential candidates for biomedical applications.

Acknowledgment. This research is financially supported by a Research Team Promotion Grant, the Thailand Research Fund (RTA4780004 and RTA5080004). The authors are indebted to Dr.Xiaodi Su of Institute of Materials Research and Engineering, Singapore for providing a QCM-D facility.

References

(1) Decher, G. *Science* **1997**, *277*, 1232-1237.

(2) Shahidi, F.; Arachchi, J. K. V.; Jeon, Y.-J. *Trends Food Sci. Technol.* **1999**, *10*, 37-51.

(3) Sashiwa H, S. H., Shigemasa Y, Ogawa R, Tokura S. *Int. J. Biol. Macromol.* **1990**, *12*, 295-296.

(4) Shigemasa, Y.; Saito, K.; Sashiwa, H.; Saimoto, H. *Int. J. Biol. Macromol.* **1994**, *16*, 43-49.

(5) Iwasaki, N.; Yamane, S. T.; Majima, T.; Kasahara, Y.; Minami, A.; Harada, K.; Nonaka, S.; Maekawa, N.; Tamura, H.; Tokura, S.; Shiono, M.; Monde, K.; Nishimura, S. I. *Biomacromolecules* **2004**, *5*, 828-833.

(6) Rabea, E. I.; Badawy, M. E. T.; Stevens, C. V.; Smagghe, G.; Steurbaut, W. *Biomacromolecules* **2003**, *4*, 1457-1465.

(7) Seong, H. S.; Whang, H. S.; Ko, S. W. J. *Appl. Polym. Sci.* **2000**, *76*, 2009-2015.

(8) Lim, S. H.; Hudson, S. M. *Carbohydr. Res.* **2004**, *339*, 313-319.

(9) Kato, Y.; Onishi, H.; Machida, Y. *Biomaterials* **2004**, *25*, 907-915.

(10) Amiji, M. M. *Colloids Surf. B* **1998**, *10*, 263-271.

(11) Jayakumar, R.; Nwe, N.; Tokura, S.; Tamura, H. *Int. J. Biol. Macromol.* **2007**, *40*, 175-181.

(12) Vongchan, P.; Sajomsang, W.; Subyen, D.; Kongtawelert, P. *Carbohydr. Res.* **2002**, *337*, 1239-1242.

(13) Serizawa, T.; Yamaguchi, M.; Matsuyama, T.; Akashi, M. *Biomacromolecules* **2000**, *1*, 306-309.

(14) Serizawa, T.; Yamaguchi, M.; Akashi, M. *Biomacromolecules* **2002**, *3*, 724-731.

(15) Zhu, Y. B.; Gao, C. Y.; He, T.; Liu, X. Y.; Shen, J. C. *Biomacromolecules* **2003**, *4*, 446-452.

(16) Cai, K.; Rechtenbach, A.; Hao, J.; Bossert, J.; Jandt, K. D. *Biomaterials* **2005**, *26*, 5960-5971.

(17) Fu, J.; Ji, J.; Yuan, W.; Shen, J. *Biomaterials* **2005**, *26*, 6684-6692.

(18) Liu, Y.; He, T.; Gao, C. *Colloids Surf. B* **2005**, *46*, 117-126.

(19) Channasanon, S.; Graisuwan, W.; Kiatkamjornwong, S.; Hoven, V. P. *J. Colloid Interface Sci.* **2007**, *316*, 331-343.

(20) Aoki, N.; Nishikawa, M.; Hattori, K. *Carbohydr. Polym.* **2003**, *52*, 219-223.

(21) Hoven, V. P.; Chombanpaew, K.; Iwasaki, Y.; Tasakorn, P. *J. Appl. Polym. Sci.* **2009**, *112*, 208-217.

(22) Lin, W.-C.; Liu, T.-Y.; Yang, M.-C. *Biomaterials* **2004**, *25*, 1947-1957.

(23) Sauerbrey, G. *Zeitschrift fuer Physik* **1959**, *155*, 206-222.

(24) Notley, S. M.; Eriksson, M.; Wågberg, L. *J. Colloid Interface Sci.* **2005**, *292*, 29-37.

(25) Yu, Y.; Wang, F.; Shi, W. Q.; Wang, L. Y.; Wang, W. B.; Shen, J. C. *Chin. Sci. Bull.* **2008**, *53*, 22-26.

(26) Garg, A.; Heflin, J. R.; Gibson, H. W.; Davis, R. M. *Langmuir* **2008**, *24*, 10887-10894.

(27) Lvov, Y.; Ariga, K.; Onda, M.; Ichinose, I.; Kunitake, T. *Colloids Surf. A* **1999**, *146*, 337-346.

(28) Schlenoff, J. B.; Dubas, S. T. *Macromolecules* **2001**, *34*, 592-598.

(29) Ladam, G.; Gergely, C.; Senger, B.; Decher, G.; Voegel, J. C.; Schaaf, P.; Cuisinier, F. J. G. *Biomacromolecules* **2000**, *1*, 674-687.

(30) Boura, C.; Menu, P.; Payan, E.; Picart, C.; Voegel, J. C.; Muller, S.; Stoltz, J. F. *Biomaterials* **2003**, *24*, 3521-3530.

(31) Kim, J. Y.; Lee, J. K.; Lee, T. S.; Park, W. H. Int. *J. Biol. Macromol.* **2003**, *32*, 23-27.

(32) Liu, C. X.; Zhang, D. R.; He, Y.; Zhao, X. S.; Bai, R. *J. Membr. Sci.* **2010**, *346*, 121-130.

(33) Sagnella, S.; Mai-Ngam, K. *Colloids Surf. B* **2005**, *42*, 147-155.

Graphic for Table of Contents

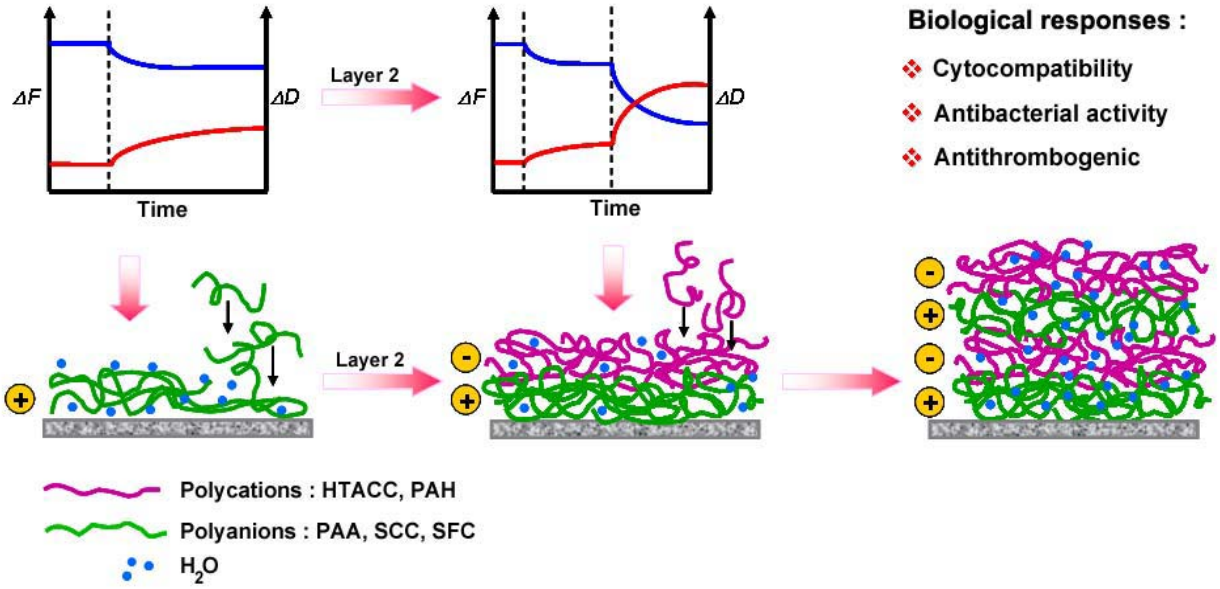

Supporting Information

Multilayer Thin Film Assembled from Charged Derivatives of Chitosan: Physical Characteristics and Biological Responses

Wilaiporn Graisuwan, Cheeraporn Ananthanawat, Oraphan Wiarachai, Songchan Puthong, Suphan Soogarun, Suda Kiatkamjornwong, Voravee P. Hoven

Page

2 Synthesis and Characterization of Charged Derivatives of Chitosan

4 **Figure S1.** The mass per unit area for wet films (m_d) determined by QCM-D as a function of layer number for 3 multilayer systems

5 **Figure S2.** Thickness of multilayer film assembled on the thiol-modified gold-coated QCM plate, obtained from QCM analysis as a function of the number of depositions.

6 **Table S1.** Average frequency shift and thickness of deposited multilayer film analyzed by QCM measurements using conventional mode**.**

Synthesis and Characterization of Charged Derivatives of Chitosan

***N*-[(2-hydroxyl-3-trimethylammonium)propyl] chitosan chloride (HTACC).** Chitosan flakes (0.50 g, 1 equiv. of NH_2) were dissolved in 1 vol. % (v/v) aqueous acetic acid (25 mL) to prepare a 2.0 % (w/v) chitosan solution. GTMAC (1.82 g, 4 equiv.) was added. The reaction was performed at 70°C for 24 h. After the reaction, the solution was poured into the dialysis tubing and dialyzed in deionized water for 5 days and then the solution was lyophilized to obtain a cotton-like white material.

IR (KBr): ν = 1,598 cm^{-1} (N-H bending of amino groups of chitosan), and 1,480 cm^{-1} (C-H bending of methyl groups of quaternary ammonium groups)

^{1}H NMR (D_2O): δ = 2.6 ppm (-NHC$\underline{H}_2$-), 3.1 ppm (N^+-(C$\underline{H}_3$)$_3Cl^-$), 4.4 ppm (-NHCH$_2$C$\underline{H}$-), and 3.3-4.3 ppm (m, $H^{2'}$,H^3, H^4, H^5, H^6, and $H^{6'}$). Degree of substitution of HTACC calculated from ^{1}H NMR data was 78%

***N*-sulfofurfuryl chitosan (SFC).** Chitosan flakes (0.50 g, 1 equiv. of NH_2) were dissolved in 1 % (v/v) aqueous acetic acid (25 mL) to prepare a 2.0 % (w/v) solution. Methanol (10 mL) containing 1.0 % (w/v) triethanolamine was slowly added to the chitosan solution. The mixture was stirred for 6 h at ambient temperature. FFSA (2.38 g, 4 equiv.) was slowly added to the chitosan slurry. The reaction was allowed to proceed for 24 h at ambient temperature. As the reaction continued, the Schiff's base thus formed was reduced by a slow addition of sodium borohydride ($NaBH_4$) (0.70 g, 6 equiv.). After the reduction for 6 h, the Schiff's base slowly dissolved to form a viscous solution. After the reaction, the solution was poured into the dialysis tubing and dialyzed in deionized water for 5 days and then the solution was lyophilized to obtain a cotton-like white material.

IR (KBr): ν = 1,237 cm^{-1} (O=S-O stretching of the sulfonate salt), and 1,040 cm^{-1} (S=O stretching of sulfonic acid)

^{1}H NMR (D_2O): δ = 4.4 ppm (-NHC$\underline{H}_2$-), 3.3-4.1 ppm ($H^{2'}$, H^3, H^4, H^5, H^6, and $H^{6'}$), and 6.3-6.7 ppm (=C$\underline{H}_2$C$\underline{H}_2$=). Degree of substitution of SFC calculated from ^{1}H NMR data was 68%.

***N*-succinyl chitosan (SCC).** Chitosan flakes (0.50 g, 1 equiv. of NH_2) were dissolved in 1 % (v/v) aqueous acetic acid solution (25 mL) to prepare a 2.0 % (w/v) chitosan solution. The chitosan solution was diluted with 40 mL of methanol. SA (1.20 g, 4 equiv.) dissolved in a minimum amount of acetone, was then added to the chitosan solution. The mixture was

vigorously stirred for 2 h at ambient temperature. The obtained viscous solution was diluted with 50 mL of water and the pH of the solution was adjusted to 10 using 2 M NaOH solution. After dialysis for 5 days, the solution was lyophilized to obtain a cotton-like white material.

IR (KBr): ν = 1,650 cm^{-1} (amide I, increase from chitosan), 1,560 cm^{-1} (amide II, increase from chitosan), and 1,598 (N-H bending of amino groups of chitosan, decrease from chitosan)

^{1}H NMR (CF_3COOH/D_2O): δ = 2.2-2.5 ppm (-NHCOC$\underline{H_2}$C$\underline{H_2}$-), and 3.0-3.8 ppm (m, $H^{2'}$, H^3, H^4, H^5, H^6, and $H^{6'}$). Degree of substitution of SFC calculated from ^{1}H NMR data was 44%.

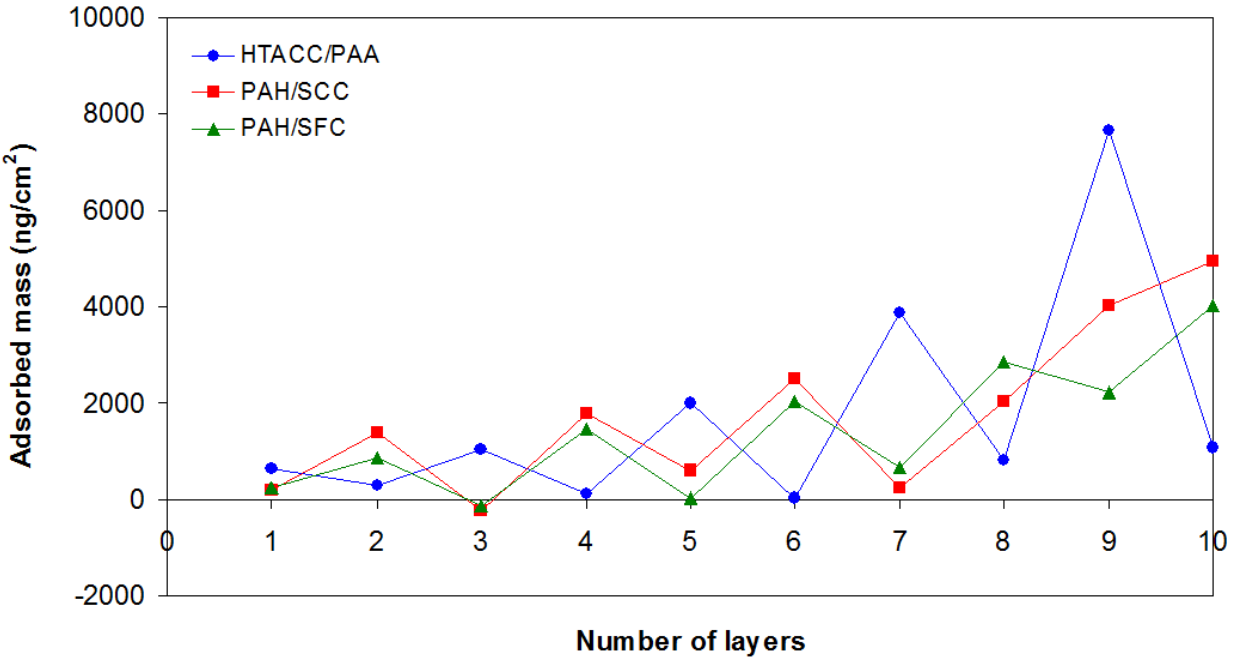

Figure S1. The mass per unit area for wet films (m_d) determined by QCM-D as a function of layer number for 3 multilayer systems

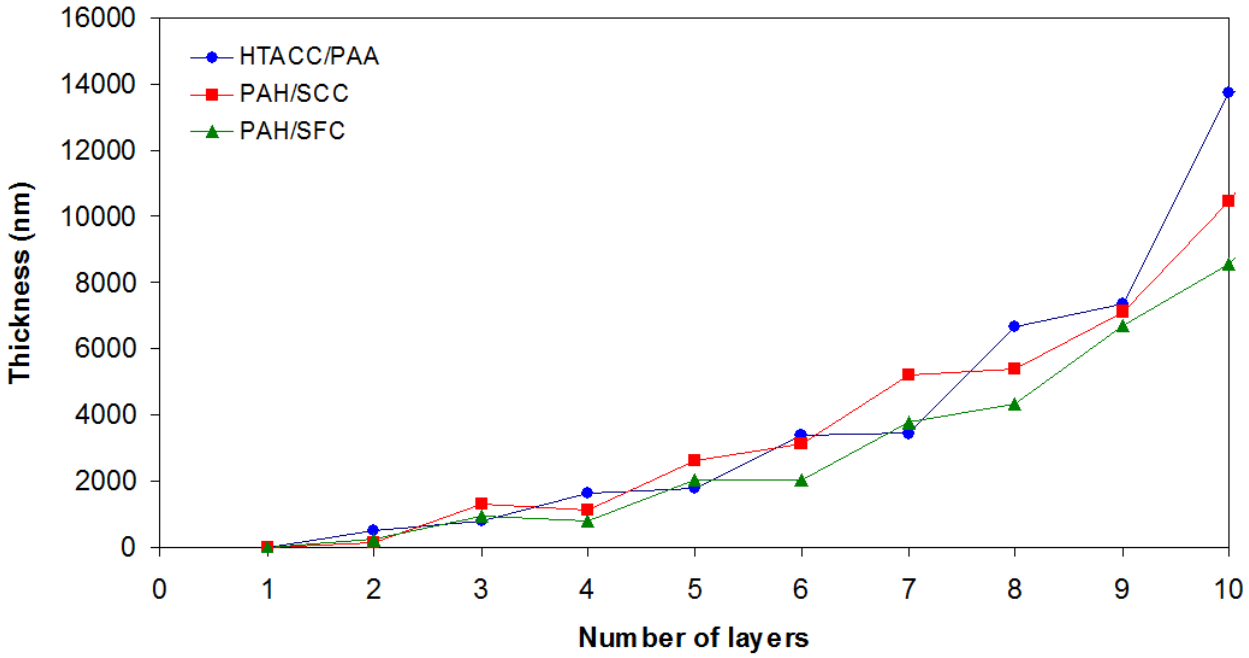

Figure S2. Thickness of multilayer film assembled on the thiol-modified gold-coated QCM plate, obtained from QCM analysis as a function of the number of depositions.

Table S1. Average frequency shift and thickness of deposited multilayer film analyzed by QCM measurements using conventional mode**.**

Multilayer system	Average ΔF_{odd} (Hz)	Bilayer thickness, $d_{b,odd}$ (nm)	Average ΔF_{even} (Hz)	Bilayer thickness, $d_{b,even}$ (nm)
HTACC/PAA	81.3	11.9	85.5	12.6
PAH/SCC	142.5	20.9	148.3	21.8
PAH/SFC	81.0	11.9	118.5	17.4

All VDO clips listed below are attached as separated files

Video S1. Real time monitoring for coagulating property of 5 mL whole blood in a closed test tube upon mixing for 15 min with 0.2 mg of SFC having 68%DS, dissolved in 0.85% NaCl(aq).

Video S2. Real time monitoring for coagulating property of 5 mL whole blood in a closed test tube upon mixing for 15 min with 0.2 mg of SFC having 60%DS, dissolved in 0.85% NaCl(aq)**.**

Video S3. Real time monitoring for coagulating property of 5 mL whole blood in a closed test tube upon mixing for 15 min with 0.2 mg of SFC having 55%DS, dissolved in 0.85% NaCl(aq).

Video S4. Real time monitoring for coagulating property of 5 mL whole blood in a closed test tube upon mixing for 15 min with 0.2 mg of HEP, dissolved in 0.85% NaCl(aq).

Video S5. Real time monitoring for coagulating property of 5 mL whole blood in a closed test tube upon mixing for 15 min with 0.2 mg of chitosan, dissolved in 0.85% NaCl(aq).

Draft Manuscript

Kapok II: PRETREATMENT OF KAPOK FIBERS FOR PULPING AND PAPERMAKING

Somporn Chaiarrekij[a*] Thippawan Hommaivai[b], Kuntinee Suvarnakich[a], and Suda Kiatkamjornwong[a]**

[a]Department of Imaging and Printing Technology, Faculty of Science, Chulalongkorn University, 254 Phayathai Road, Bangkok 10330, Thailand.
*Tel: +662 218 5572; e-mail: huaja@hotmail.com
**Tel: +662 218 5587; Fax: +662 255 3021; e-mail: ksuda@chula.ac.th

[b]Pulp and Paper Technology Program, Faculty of Science, Chulalongkorn University, 254 Phayathai Road, Bangkok 10330, Thailand.

Abstract

Kapok fibers are naturally coated with wax and cutin which renders them hydrophobic. To obtain fibers that are suitable for pulping, they must first be immersed in tap water for up to three to four weeks which is very time consuming. This research then investigated the effects of fiber pretreatment with sodium hydroxide (NaOH) or lipase for varied immersion times before it was subjected to soda pulping, in comparison with the control fibers that were pretreated by immersion in tap water for 3 weeks. For chemical pretreatment, two doses of NaOH (5 and 10% (w/w) based on the O.D. kapok fiber weight) were used with three immersion times (1, 2 and 3 weeks). For biological pretreatment, a commercial lipase with the enzyme activity of 100 KLU/g with the dosages of 0.25 and 0.5% (w/w) based on O.D. kapok fiber weight was used for three immersion times (1, 3 and 5 hours) of the fibers. After soda pulping and latency removal of the kapok fibers, the pulp and their sheets formed (60 g/m^2) from each pretreatment were characterized for the pulping efficiency, and physical and optical properties. It was found that both alkali and lipase pretreatments provided the pulp with the lower lignin content but higher opacity. However, higher tensile and burst strengths were obtained when the pulp was pretreated with NaOH while higher tear resistance was acquired with lipase pretreatment.

Key words: Lipase, Pulping, Paper making, Chemical pretreatment, Biological pretreatment

Introduction

In a previous study of the pulping of kapok fibers for papermaking, it was concluded that kapok fiber can be a quality pulp source for papermaking, especially for strengthening tensile strength of paper (Apirakchaiskul, 2008). However, the idea of using kapok fibers as one of the new potential fiber sources for the demands of the pulp and paper industries is intimidated by the inherent difficulty in soaking the hydrophobic kapok fibers prior to processing them to soda pulping. Indeed, wetting kapok fibers is not easy and practically takes around three weeks for kapok fibers to get wet after being immersed in plain tap water. This is due to the waxy cutin on the fiber surface that provides strong water repellency. So, the pretreatment of kapok fibers before soda pulping is required in order to remove the surface waxy material, and this might also increase the soda pulping efficiency of kapok fibers. In turn, this would make the process more economically and ecologically viable with a lower chemical consumption and/or shorter immersing time and pulping time of kapok fibers.

Fiber pretreatment involves modification of the fibers before the pulping process, and can be divided into two broad types. The first is chemical pretreatment, which utilizes chemicals, typically alkali, such as NaOH or potassium hydroxide (KOH), to digest or soften the material (woodchips or, as in this case, fibers) and to open the fiber surface so that

pulping becomes easier and more efficient. The second broad approach is that of biological pretreatment, which uses micro-organisms or enzymes to digest the woodchips or fibers before processing them by the pulping process. Enzymes that have been used in this method include cellulases, hemicellulases, xylanases, pectinase and cutinase. These micro-organisms and enzymes may react with waxy fiber surface, cellulose, hemicellulose and lignin, including the lignin-carbohydrate complex. This causes the opening of more fiber surfaces to the aqueous environment and therefore provides a better reaction between the fibers and cooking chemicals during the pulping processes.

For biopulping, the fungus *C. subvermispora* has been applied to spruce woodchips for two weeks before processing them in a refiner to produce the mechanical pulp (Scott *et al*., 1998). The bio-pretreatment of these woodchips provided an energy saving of 24 to 38% during the refining process. Moreover, the bio-treated pulp had a higher strength than that of the control pulp, as indicated by the higher tensile, burst and tear indexes. Although the pulp brightness obtained from the bio-treated pulp was lower than the control pulp, it could, if required, be improved by pulp bleaching. Wax elimination from the surface of cotton fibers was also evaluated using a mixture of mechanical and biological action with cutinase and pectinase (Agrawal *et al*., 2008). The temperature required for wax elimination decreased from 100 °C, when NaOH was used, to 50 °C, when pectinase was used. In addition, using pectinase with cutinase was able to further reduce the required temperature to 30 °C and the reaction time to 15 min.

In this work, chemical pretreatment using NaOH for kapok fibers was evaluated, along with the biological pretreatment of kapok fibers using lipase. The objectives of the present work are to investigate the effects of these chemical and biological pretreatments on the soda pulping efficiency of the kapok fibers; to determine the optimum condition of each chemical and biological pretreatment of the kapok fibers; and to compare the results from the optimum condition of the chemical pretreatment with those from the biological pretreatment.

Experimental

The kapok fibers sourced in Thailand were subjected to chemical or biological pretreatment. Both pretreated fibers were then pulped by the soda process and analyzed with respect to the control pulp. The control pulp in all cases was derived by replacing the pretreatment stage with simply immersing the fibers in tap water for three weeks. Three replicates were done for all control and pretreated pulps.

Pretreatment of kapok fibers

500 g of Kapok fibers were pretreated by either immersion in tap water for three weeks (control) or chemical (NaOH) or biological (lipase enzyme) pretreatment. For the chemical pretreatment, the kapok fibers were treated with NaOH at 5% or 10% (w/w, based on the oven dried (O.D). kapok fiber weight) in 13 L of tap water for 1, 2 and 3 weeks. For the biological pretreatment, kapok fibers were pretreated with the Lipolase 100L, the commercial enzyme from Novozymes having the enzyme activity of 100 KLU/g (KLU stands for kilo lipase unit) at two different dosages (0.25% and 0.50% w/w, based on O.D. fiber weight) in 13 L of tap water and three times (1, 3 and 5 hours). After the pretreatment, the kapok fibers were washed prior to squeezing out the excess water and cut to 3-5 cm in length before being processed by soda pulping.

Soda pulping of kapok fibers

Kapok fibers with and without the pretreatments were separately pulped using NaOH at 20% (w/w, based on O.D. kapok fiber weight). The liquor-to-wood ratio (L: W) was 17:1 (v/w). The pulping was carried out in an autoclave digester, (UEC-2017A, Universal Engineering, India) with an initial digesting temperature at 40 °C. The pulp matrix was then gradually heated to 120 °C over 30 min. The pulping was proceeded at this temperature for

another 120 min. The pulp was then extensively washed with tap water to remove the excess alkali from the pulp by controlling with a pH meter (Hanna HI 98128, Hanna Instrument, U.S.A.). The net pulp yield and residual alkaline level were then determined.

Kapok pulp at 5% pulp consistency (w/w) was refined twice through a disc refiner, using a 1/100 inch disc gap (Andritz Sprout, U.S.A.). Then, refined kapok pulp was disintegrated at 1.5% pulp consistency (w/w) in a standard disintegrator (Formax T-100, Adirondack, U.S.A.) for 50,000 revolutions in hot water (80 °C) to remove latency.

Evaluation of pulp and paper properties

The chemical composition of each pulp was determined using TAPPI Standard Method T222 om-98 for lignin determination, TAPPI Standard Method T203 cm-99 for alpha cellulose (α-cellulose) determination, and Browning's method for holocellulose determination (Browning, 1963). The amount of hemicellulose was calculated from the difference between the holocellulose content and the alpha cellulose content.

Kappa number, an indication of lignin content in the pulp, was analyzed according to TAPPI Standard Method T236 om-99. Kapok pulp drainage was also determined following the Canadian Standard Freeness (CSF) standard, using a freeness tester (CF/A, Regmed, Brazil) according to TAPPI Standard Method T227 om-04. Kapok pulp was also made into 60 g/m^2 handsheets on a Rapid-Köthen sheet former (RK-2A KWT, PTI, Austria) according to the ISO Standard Method 5269-2. The brightness and opacity of the handsheets were measured using an optical tester (Color Touch PC, Technidyne, U.S.A.), based on ISO Standard Methods 2470 and 2471, respectively. The tensile, burst and tear strengths were measured using a tensile strength tester (Strograph E-S, Toyo Seiki, Japan), a burst strength tester (SE002P, Lorentzen & Wettre, Sweden), and a tear strength tester (Protear, Thwing-Albert, U.S.A, according to TAPPI Standard Method T494 om-01, T403 om-02, and T414 om-04, respectively.

Results and discussion

Chemical pretreatment of the fibers

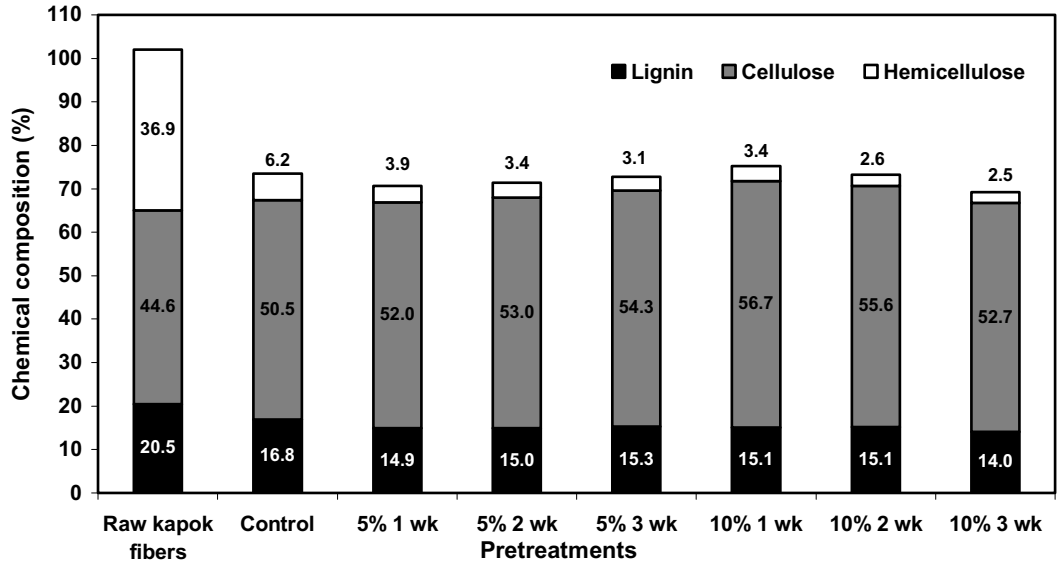

Figure 1. Effects of chemical pretreatment on chemical composition of kapok pulp.

As shown in Figure 1, the analysis of the pulp chemical composition indicated that the alkali pretreated samples had the lower lignin contents than the control pulp since NaOH dissolved the lignin. In addition, NaOH pretreatment was observed to produce a lower hemicellulose content but a higher cellulose content than the control pulp because NaOH partly dissolved the hemicellulose in the pulp leaving the cellulose content mostly intact. It was also noticed that hemicellulose content decreased with the higher dosage and longer alkali pretreatment time. However, cellulose content potentially increased with the higher alkali dosage while the effect of alkali pretreatment time on cellulose content was apparently indistinguishable. The effects of alkali pretreatment dosages and times seemingly have no different impacts on the lignin content of the alkali pretreated pulp except for the extreme case that used the highest alkali dosage with the highest pretreatment time which inevitably provided the lowest lignin content.

Table 1. Effects of chemical pretreatment on pulp yield, residual alkali, and kappa number

Pretreatment condition		Pulp yield (%)	Residual alkali (%)	Kappa number
NaOH dosage (%)	Number of weeks			
0 (Control)	3	76.02 ± 1.79	2.00 ± 0.59	108 ± 2
5	1	73.71 ± 0.06	2.90 ± 0.14	99 ± 2
	2	75.02 ± 2.25	3.50 ± 0.14	98 ± 2
	3	76.00 ± 2.06	3.60 ± 0.28	98 ± 1
10	1	78.20 ± 1.06	4.00 ± 0.00	116 ± 2
	2	76.08 ± 0.41	4.60 ± 0.28	130 ± 3
	3	72.66 ± 7.17	5.80 ± 0.28	132 ± 5

The control experiment as indicated by 0% NaOH dosage was for immersing kapok fibers in tap water for 3 weeks.

The results tabulated in Table 1 indicate that the alkali dosage and pretreatment time used in this study seemed to have a small effect on pulp yield. However, the residual alkali increased with the higher NaOH concentration and longer pretreatment time. The residual alkali levels imply that the alkali consumption during the soda pulping was lower with the alkali pretreated samples than the control. Thus, there was probably less chance for carbohydrate degradation during the pulping leading to the pulp yields comparable to that of the control.

The Kappa numbers of the NaOH pretreated pulp were lower than that of the control pulp only when the lower dosage (5% w/w) of NaOH was used. In contrast, the kappa numbers increased significantly with the higher NaOH pretreatment concentration (10% w/w) and with the longer pretreatment times at this higher dose. Perhaps the presence of cutin interferes with the permanganate oxidation of lignin. At the higher NaOH concentration for the longer pretreatment times, the cutin could be much easier to dissolve during the subsequent soda pulping stage, which might markedly disrupt the permanganate oxidation of lignin.

The results from Table 2 illustrate that the effects of NaOH dosage and pretreatment time on the density were indistinguishable. Opacity typically increased with increasing NaOH dosage and reacting time, the only exception being that seen for the pretreatment with 5% (w/w) alkali for three weeks (Table 2). This might probably cause by the alkali pretreatment which led to the higher fines contents of the pulp and thus could increase light scattering of these handsheets. However, NaOH pretreatment seemed to initially lower the brightness at

the short pretreatment times, and then increase it with the longer treatment times or higher NaOH concentrations. This might be due to the alkali induced darkening effect to render the pulp yellow. Nevertheless, increasing the pretreatment time produced a brighter pulp, which was caused by the result of more wax removed from the fiber surface and so the cooking liquor could penetrate into and react better with more fibers. Thus, more lignin was removed and the pulp became brighter.

Table 2. Effects of chemical pretreatment on density, brightness and opacity

Pretreatment condition		Density (g/m^3)	Brightness (%)	Opacity (%)
NaOH dosage (%)	Number of weeks			
0	3	0.72 ± 0.03	21.3 ± 0.5	81.2 ± 1.0
5	1	0.73 ± 0.05	21.0 ± 0.4	85.8 ± 0.6
	2	0.78 ± 0.04	20.9 ± 0.2	86.1 ± 1.5
	3	0.78 ± 0.05	21.5 ± 0.4	81.2 ± 0.4
10	1	0.72 ± 0.04	20.0 ± 0.5	86.5 ± 1.1
	2	0.79 ± 0.04	21.2 ± 0.5	88.8 ± 1.0
	3	0.76 ± 0.05	22.5 ± 0.5	91.4 ± 0.7

The control experiment as indicated by 0% NaOH dosage was for immersing kapok fibers in water for 3 weeks.

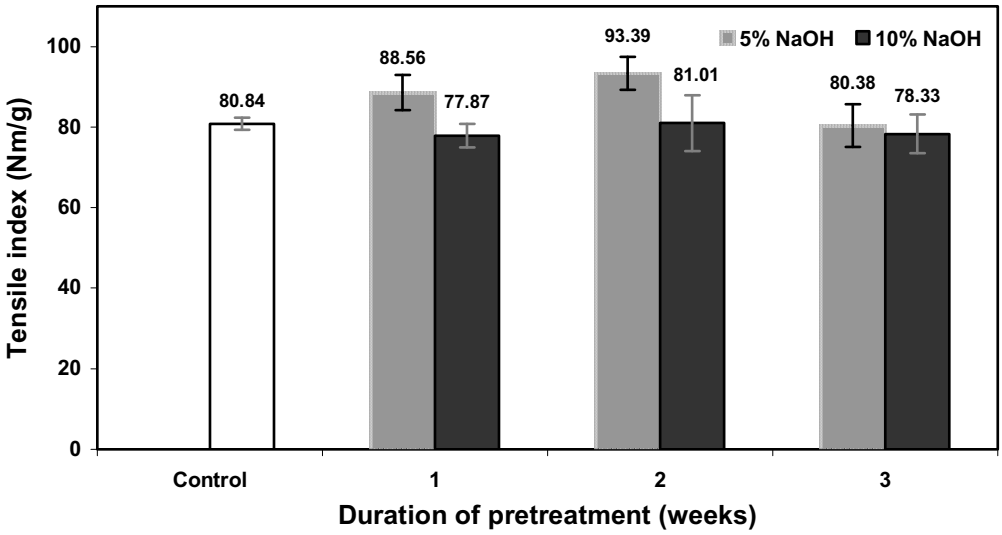

Figure 2. Effects of chemical pretreatment on tensile index.

As shown in Figures 2 and 3, after the pretreatment with the lower concentration of NaOH, the pulp displayed the highest tensile index and burst index, higher than those derived from the control pulp. However, the effects of the NaOH pretreatment time on the tensile index and burst index were somewhat variable but important. The pulp became stronger when it was pretreated with NaOH for two weeks yet three weeks of the pretreatment was detrimental to both the tensile and burst strengths, reducing them to essentially the same level as the control pulp. This could be because NaOH aided in not only removing the fiber surface wax but also attacked the lignin leading to a better fiber bonding in the sheets, at least when pretreated at the optimal NaOH concentration and time. Also, the NaOH led to a higher

cellulose content which might in turn helped increase the fiber strength. However, when too high a NaOH dose was used for a long time, the tensile and burst strengths declined, and this is likely to be due to carbohydrate degradation by the peeling reaction under a strong alkali condition.

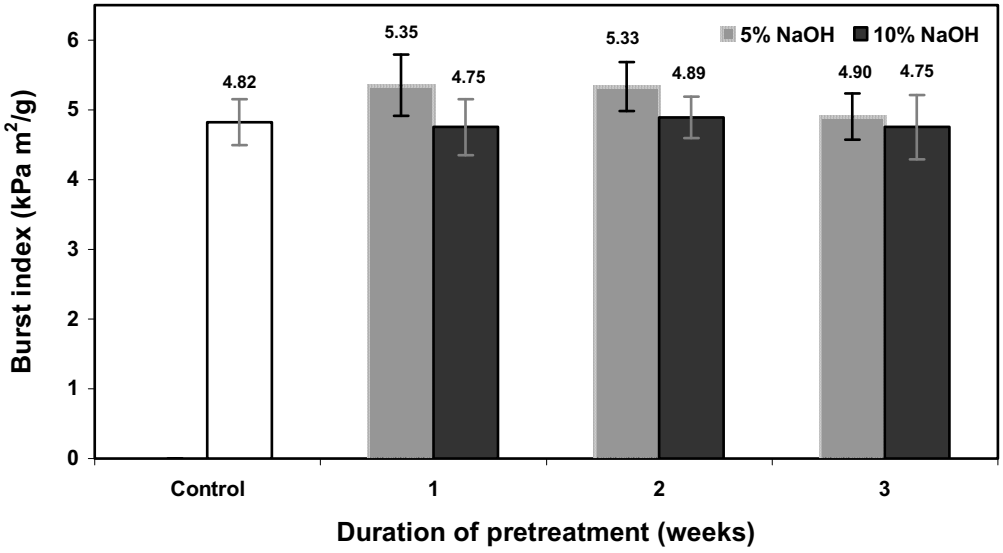

Figure 3. Effects of chemical pretreatment on burst index.

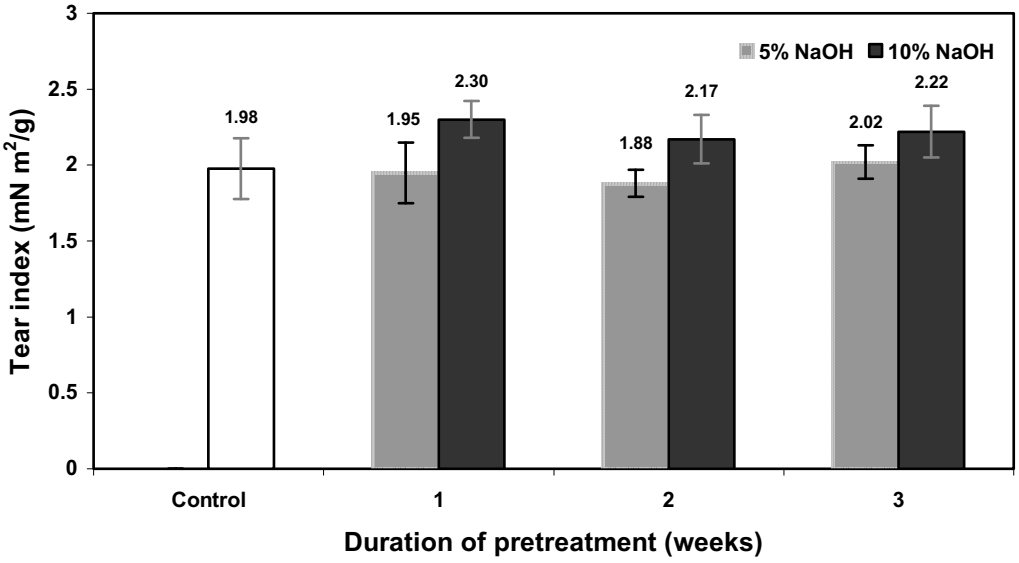

Figure 4. Effects of chemical pretreatment on tear index.

The pulp pretreated with the higher concentration (10% w/w) of NaOH potentially provided a higher tear index (Figure 4), which is opposite to the cases for the tensile and burst indexes. Generally, in contrast to tensile and burst strengths, tear resistance depends mostly on the strength of individual fibers rather than the strength of inter-fiber bonding. The higher NaOH concentration produced pulp with the higher cellulose content but the lower

hemicellulose contents (Figure 1), which might increase the fiber strength and then tear strength of the pulp as a whole.

Based on the overall results, pretreatment of the kapok fibers with NaOH at 5% (w/w) for two weeks was selected as the optimal condition. Under these pretreatment conditions, the kapok pulp provided the highest tensile strength with the lowest kappa number. Burst and tear strengths were acceptable and it also gave a suitable residual alkali level which was in the optimal range for pulping.

Biological pretreatment of the fibers

Pretreatment of the kapok fibers with lipase beneficially resulted in a lower lignin content than that seen in the control pulp, whilst the lignin content was further reduced with the higher lipase dose (Figure 5). Likewise, the hollocellulose contents were lower in pulp pretreated with any lipase dose than that seen in the control, suggesting that the lipase had reacted with the wax at the kapok fiber surface. This might then cause the fiber surface to open more and allow greater access to NaOH during the soda pulping. That the resulting holocellulose and especially alpha cellulose of the lipase pretreated pulps were lower implies that the cellulose was attacked more than was the hemicellulose after the lipase pretreatment. It was also noticed that the effects of the pretreatment time on the chemical composition were more evident only in the case of higher dosage of lipase as indicated by the lower lignin and cellulose contents but the higher hemicellulose content with the longer pretreatment time.

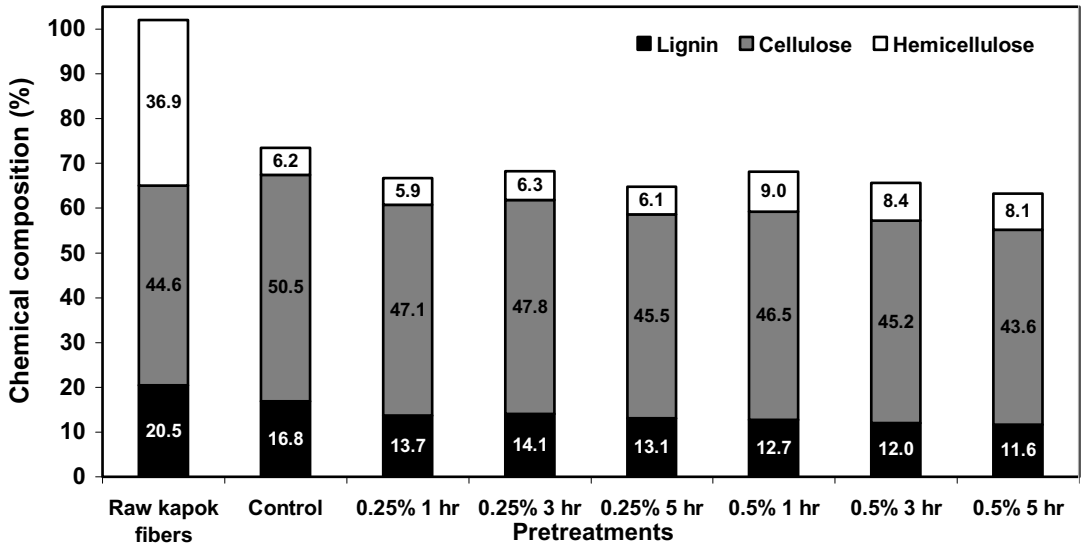

Figure 5. Effects of lipase pretreatment on chemical composition of kapok pulp.

Table 3 reveals that the lipase pretreated pulps gave a lower pulp yield than that of the control pulp, and the yield decreased with a higher enzyme dosage and pretreatment times. The residual alkali content was lower in the lipase-pretreated samples and was minimal after two-hour exposure. This also implied that the alkali consumption during the soda pulping stage was higher following the lipase pretreatment. The lipase pretreated pulp also produced a slightly lower kappa number, compared to that of the control, at the low lipase dose; but at the higher lipase dose, it was lower than the control only after a three-hour exposure. The kappa number and pulp yields obtained indicated that lipase eventually reacted with cutin at

the fiber surface and caused the surface to open for the alkali to react with the kapok fibers more easily in the pulping stage.

It should also be noted that the lipase enzyme pretreated pulp gave a lower pulp yield and residual alkali content than did the NaOH pretreated pulp (Tables 1 and 3). Thus, the enzyme pretreatment provided a better accessibility of the kapok fibers for the NaOH in the pulping reaction than did the NaOH pretreatment.

Table 3. Effects of lipase pretreatment on pulp yield, residual alkali, and kappa number

Pretreatment condition		Pulp yield (%)	Residual alkali (%)	Kappa number
Lipase dosage (%)	Number of hours			
0 (Control)	504	76.02 ± 1.79	2.00 ± 0.59	108 ± 2
0.25	1	70.52 ± 1.04	1.60 ± 0.57	106 ± 0
	3	72.10 ± 0.12	0.80 ± 0.00	105 ± 2
	5	68.73 ± 1.70	1.05 ± 0.07	107 ± 0
0.50	1	71.59 ± 1.70	1.20 ± 0.00	108 ± 3
	3	69.22 ± 1.07	0.90 ± 0.14	108 ± 3
	5	66.92 ± 1.68	1.25 ± 0.07	105 ± 3

The control experiment as indicated by 0% NaOH dosage was for immersing kapok fibers in tap water for 3 weeks

Table 4. Effects of lipase pretreatment on density, brightness and opacity

Pretreatment condition		Density (g/m^3)	Brightness (%)	Opacity (%)
Lipase dosage (%)	Number of hours			
0	504	0.72 ± 0.03	21.3 ± 0.5	81.2 ± 1.0
0.25	1	0.68 ± 0.03	22.7 ± 0.7	87.7 ± 1.1
	3	0.67 ± 0.04	22.2 ± 0.7	87.1 ± 1.2
	5	0.71 ± 0.02	22.8 ± 0.7	88.3 ± 1.4
0.50	1	0.65 ± 0.02	22.2 ± 0.8	88.9 ± 1.3
	3	0.70 ± 0.03	23.0 ± 0.7	87.6 ± 1.3
	5	0.70 ± 0.03	22.3 ± 0.6	85.4 ± 1.9

The control experiment as indicated by 0% NaOH dosage was for immersing kapok fibers in tap water for 3 weeks

Lipase pretreatment hardly impacted sheet density but provided the pulp with a higher brightness and opacity as compared to the control pulp (Table 4). Higher brightness of lipase pretreated pulp was caused by a higher level of lignin removal while higher opacity might probably be caused by higher fines contents which then increased the light scattering coefficients of these handsheets. This might implied that lipase pretreatment improved accessibility of the kapok fibers for NaOH in pulping reaction. However, the effects of enzyme dosage and treatment time on density, brightness and opacity seemed to be very small.

When comparing the effects of the lipase pretreatment on the density, brightness and opacity to those of the NaOH pretreatment, it was found that both pretreatments provided

essentially the same effects on the density and opacity, but the lipase pretreatment potentially produced a higher brightness level.

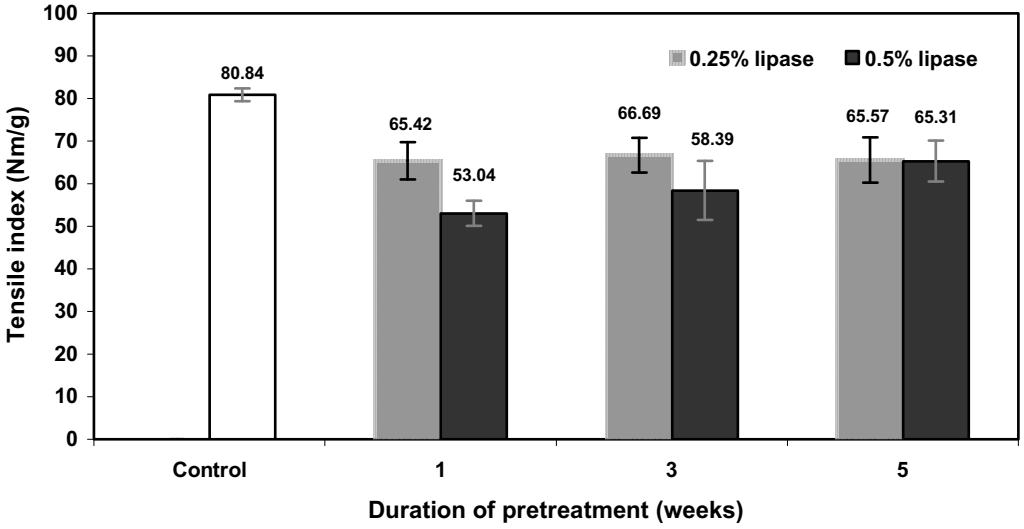

Figure 6. Effects of lipase pretreatment time on tensile index.

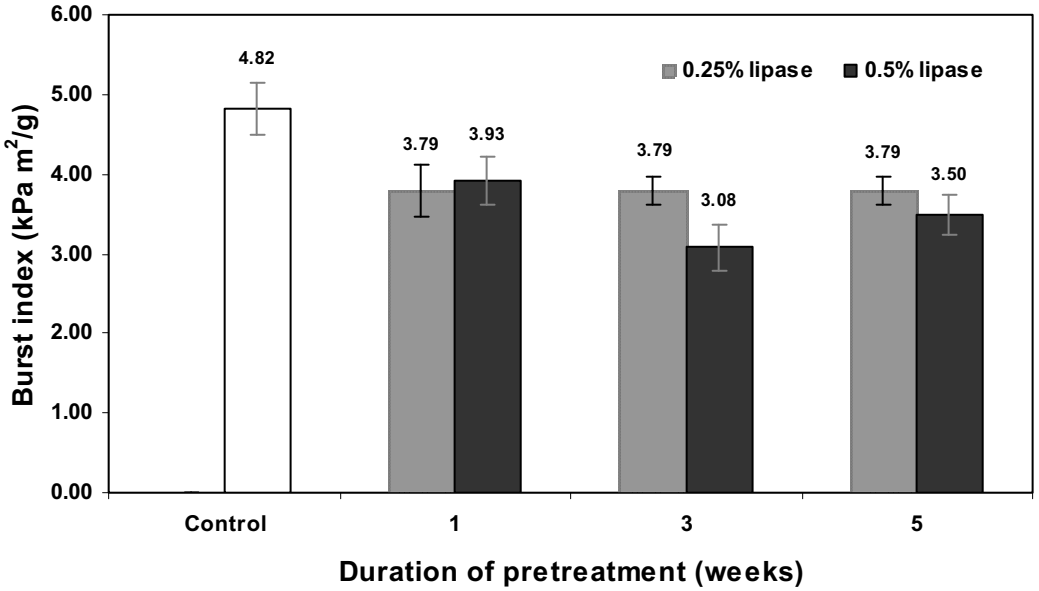

Figure 7. Effects of lipase pretreatment time on burst index.

The tensile and burst strengths of all lipase pretreated pulp were lower than those of the control pulp (Figures 6 and 7). This could be because the cellulose content was lower whilst the hemicellulose content was higher for the lipase pretreated pulp (Figure 5). Thus, the individual fiber strength of the enzyme pretreated pulp might be diminished due to the lower cellulose content and this might decrease the tensile and burst indexes. It should also be noted that these tensile and burst strength of lipase pretreated pulp typically decreased with pretreatment at the higher lipase dose, while effects of the longest enzyme treatment time on the tensile and burst index.

The lipase pretreated pulp gave lower tensile and burst strengths than that of the NaOH pretreated pulp (Figures 2 and 3 compared to Figures 6 and 7), which emphasizes that the enzyme pretreatment could provide a better accessibility of the NaOH into the kapok fibers in the pulping stage than did the NaOH pretreatment.

Unlike the tensile and burst indexes, the tear index of the lipase pretreated pulp was surprisingly higher than that of the control pulp, and this was more markedly at the higher lipase dose, although the preincubation time at both lipase doses seemed irrelevant (Figure 8).

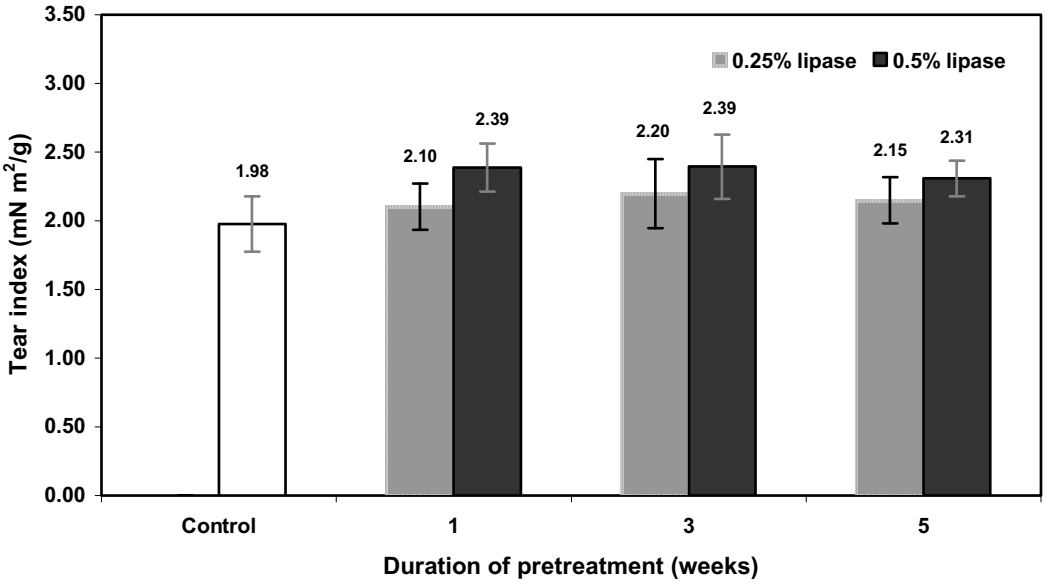

Figure 8. Effects of lipase pretreatment on tear index.

Based on the overall results, the biological pretreatment with a lipase dosage of 0.25% (w/w), based on the O.D. fiber weight, for three hours was selected as the optimal condition, since at this condition the kapok pulp provided the highest tensile strength and pulp yield with the lowest kappa number and residual alkali content.

Overall comparison between the chemical and biological pretreatments

Based on the results obtained from both the NaOH and lipase pretreatments in comparison with respective control pulp, the pulp and paper properties obtained at the optimal conditions for each of the pretreatments are summarized in Table 5. The optimal conditions for the alkali pretreatment was NaOH at 5% (w/w) based on the O.D. fiber weight for two weeks, whilst those for the lipase pretreatment was a lipase dose at 0.25% (w/w) based on O.D. fiber weight, for three hours.

The benefits of both chemical and biological pretreatments are the lower kappa number and higher opacity obtained compared to that of the control pulp. Perhaps the pretreated kapok pulp has more opened structures and more fines content which could lead to the higher light scattering and opacity.

The advantages of using the alkali pretreatment are better tensile and burst indexes. The residual alkali content of the chemical pretreatment was also higher than that of the control and lipase enzyme pretreated pulps, which implied that the alkali content in the pulping reaction can be decreased in future work. The lower kappa number also indicated that the cooking liquor could penetrate through the kapok fibers and react with a greater proportion of the total number of reaction sites.

The advantages of utilizing the lipase pretreatment were the lower kappa number with the higher tear index, brightness and opacity. Finally, it was recommended that mechanical or physical parameters such as a proper mixing and suitable reaction temperature for the lipase enzyme, which were not evaluated and optimized here, might be selectively employed for the biological pretreatment in order to increase the rate of enzyme reaction at the kapok fiber surface.

Table 5. Comparison of the control, alkali (chemical) and lipase (biological) pretreatments of kapok fibers

Pulp and paper properties	Control	NaOH pretreatment	Lipase pretreatment
Lignin (%)	16.8 ± 0.3	15.0 ± 0.2	14.1 ± 0.2
Cellulose (%)	50.5 ± 0.0	53.0 ± 0.2	47.8 ± 1.0
Hemicellulose (%)	6.2 ± 0.2	3.4 ± 0.0	6.3 ± 0.9
Pulp yield (%)	76.02 ± 1.79	75.02 ± 2.25	72.10 ± 0.12
Residual alkali (%)	2.00 ± 0.59	3.50 ± 0.14	0.80 ± 0.00
Kappa number	108 ± 2	98 ± 2	105 ± 2
Tensile index (N m/g)	80.8 ± 1.5	93.4 ± 4.1	66.7 ± 4.0
Burst index (kPa m^2/g)	4.82 ± 0.33	5.33 ± 0.35	3.79 ± 0.18
Tear index (mN m^2/g)	1.98 ± 0.20	1.88 ± 0.09	2.20 ± 0.25
Density (g/m^3)	0.72 ± 0.03	0.78 ± 0.04	0.67 ± 0.04
Brightness (%)	21.3 ± 0.5	20.9 ± 0.2	22.2 ± 0.7
Opacity (%)	81.2 ± 1.0	86.1 ± 1.5	87.1 ± 1.2

The control experiment as indicated by 0% NaOH dosage was for immersing kapok fibers in water for 3 weeks

Conclusions

Chemical (NaOH) and biological (lipase enzymatic) pretreatment of kapok fibers were shown to be beneficial to the soda pulping of kapok fibers, because the immersing time and NaOH consumption could be reduced. The pretreated pulp also had a lower kappa number and higher opacity. The chemical pretreatment with NaOH should be employed when increases in tensile and burst index are demanded, whilst the biological pretreatment with lipase is more attractive when the tear resistance of sheets is desired. Combining both chemical and biological pretreatments is also supposition since both treatments can provide beneficially synergistic effects to the soda pulping of kapok fibers.

Acknowledgements

This research is fully financially supported by the Research Team Aided Grant from the Thailand Research Fund and the Commission of Higher Education under the Contract number RTA5080004. Some research facilities provided by the Product and Technology Development Center of Siam Cement Group Paper Company Limited are also gratefully appreciated.

References

Apirakchaiskul, A., “The Use of Kapok Fiber to Improve Strength of Paper”, M.S. Thesis, Department of Imaging and Printing Technology, Faculty of Science, Chulalongkorn University, 2008.

Scott, G.M., Akhtar, M., Lentz, M.J., Kirk, T.K., and Swaney, R., “New Technology for Papermaking: Commercializing Biopulping”, TAPPI Journal, 81(11), 1998, 220-225.

Zhang, W., Okubayashi, S., and Bechtoid, T., “Fibrillation Tendency of Cellulosic Fibers-Part 3. Effects of Alkali Pretreatment of Lyocell Fiber”, Carbohydrate Polymers, 59(2), 2005, 173-179.

Browning, B. L. (1963). *Methods in Wood Chemistry*, Interscience Publishers, New York.

Comments to Archan Somporn: More corrections are needed. Suda

Draft Manuscript

Colloids and Surfaces A: Physicochemicals and Engineering Aspects

Manuscript Number:

Title: Microencapsulation of menthol by crosslinked chitosan via porous glass membrane emulsification technique and their controlled release properties

Article Type: Research Paper

Keywords: Microcapsules; chitosan; menthol; SPG membrane emulsification; encapsulation

Abstract: Chitosan encapsulated menthol microcapsules were successfully prepared by the oil-in-water emulsion process using Shirasu porous glass (SPG) membrane emulsification technique. The SPG membrane with a membrane pore size of 5.2 μm was found to be suitable for a high viscosity dispersion phase containing light mineral oil. The effect of operating pressure, the amount of menthol loading and crosslinking time on the size and size distribution of microcapsules were systemically investigated. The size of the menthol-loaded chitosan microcapsules was strongly dependent on the mean pore size of the SPG membrane and the amount of menthol loading in the dispersion phase. The average diameter of emulsion droplets of 28.3 μm with a coefficient of variation of 24.7% was obtained. Increasing the menthol loading in the dispersion phase from 5 to 10 wt% of chitosan decreased the emulsion droplets with a broad droplet size distribution. The crosslinked microcapsule size and size distribution of the o/w emulsion droplets decreased with increasing crosslinking time. The mechanism of menthol release was a diffusion control which depended on the proportion of amino group in chitosan-to-tripolyphosphate and crosslinking time.

Microencapsulation of menthol by crosslinked chitosan via porous glass membrane emulsification technique and their controlled release properties

Roongkan Nuisin[a)], Jaruwan Krongsin[b)], Supaporn Noppakundilograt[c)], Suda Kiatkamjornwong[c)*]

[a)] Department of Environmental Science, Faculty of Science, Chulalongkorn University, Bangkok 10330, Thailand

[b)] Multidisciplinary Program of Petrochemistry and Polymer Science, Faculty of Science, Chulalongkorn University, Bangkok 10330, Thailand

[c)] Department of Imaging and Printing Technology, Faculty of Science, Chulalongkorn University, Bangkok 10330, Thailand

Short running title: Microencapsulation of menthol by crosslinked chitosan via porous glass membrane

[*]Corresponding author

Suda Kiatkamjornwong
Address: Department of Imaging and Printing Technology, Faculty of Science, Chulalongkorn University, Bangkok 10330, Thailand
Telephone: +66-02-218-5587
E-mail: ksuda@Chula.ac.th

Abstract

Chitosan encapsulated menthol microcapsules were successfully prepared by the oil-in-water emulsion process using Shirasu porous glass (SPG) membrane emulsification technique. The SPG membrane with a membrane pore size of 5.2 μm was found to be suitable for a high viscosity dispersion phase containing light mineral oil. The effect of operation pressure, the amount of menthol loading and crosslinking time on the size and size distribution of microcapsules were systemically investigated. The size of the menthol-loaded chitosan microcapsules was strongly dependent on the mean pore size of the SPG membrane and the amount of menthol loading in the dispersion phase. The average diameter of emulsion droplets of 28.3 μm with a coefficient of variation of 24.7% was obtained. Increasing the menthol loading in the dispersion phase from 5 to 10 wt% of chitosan decreased the emulsion droplets with a broad droplet size distribution. The size and size distribution of o/w crosslinked microcapsules decreased with increasing crosslinking time.

Keywords: Microcapsules; chitosan; menthol; SPG membrane emulsification; homogenizing

1. Introduction

Menthol is a cyclic terpene alcohol with three asymmetric carbon atoms. Among the optical isomers, menthol is the one that occurs most widely in nature and it is endowed with the peculiar property to be a fragrance and flavor compound. For this reason, it is widely used as flavoring for toothpaste, oral hygiene and personal care products [1]. Menthol is generally available in the form of crystals or granules with a melting point of 41–43°C. However, its high volatility and whisker growth are the very important problems concerning its applications and shelf life. The microencapsulation method is an accountable and appropriate technique to solve these problems [2]. Chitosan is derivatized by deacetylation of chitin. Chitosan has been used in many applications because of its biocompatibility, biodegradability, non-toxicity and antibacterial activity [3]. Chitosan can form microcapsules by various methods such as spray drying, emulsification/solvent evaporation, ionotropic gelation, coacervation techniques, and so on. It can prevent loss of volatile flavors, and enhance stability of the flavor core materials [2]. The capsule is kept stable during the release time. However, the size of the microcapsules prepared by these methods is difficult to control, and the size distribution is thus very broad [4].

In conventional emulsification devices, such as high-pressure homogenizer, mechanical stirring, and rotor-stator systems, these methods produce rather polydisperse emulsions and consume high energy [5]. A membrane emulsification system produces emulsions by permeating a dispersed phase into a continuous phase through a membrane having a uniform pore diameter. The membrane emulsification method makes it possible to produce monodisperse emulsions and consume less energy [6, 7]. The most commonly used microporous membrane for the emulsification is a Shirasu Porous Glass (SPG) membrane. The SPG membrane is made from SiO_2–Al_2O_3, with a very narrow pore size distribution. It was fabricated by Nakashima and Shimizu [8] via a series of sophisticated heat treatments,

an induced phase separation created a bi-continuous structure of $CaO\text{-}B_2O_3$, and $SiO_2–Al_2O_3$. Commercially, the pore sizes ranging from 0.1 to 18.0 μm have been available. The SPG membrane is inherently hydrophilic and it is much easier to get the monodisperse oil-in-water (o/w) emulsions than water-in-oil emulsion (w/o) due to the presence of negatively charged silanol groups on the surface [9]. Kiatkamjornwong et al. [10] had successfully prepared the microcapsules of chitosan (0.5–40 μm in diameter) by the conventional stirring method in which chitosan is the shell of microcapsules encapsulating the core material of menthol. The size distribution of the conventional method is rather polydisperse and thus a better technique of porous glass membrane emulsification can remedy the large size distribution to a narrow size distribution of microcapsules.

In this study, the SPG membrane emulsification method was applied to prepare menthol-loaded sodium tripolyphosphate crosslinked chitosan microcapsules. The effects of membrane pore size, the amount of menthol loading and crosslinking time were investigated on the microcapsule size and size distribution. Release kinetics of menthol from microcapsules correspondence to crosslinking time, concentration, and molar ratio of amino and tripolyphosphate were studied.

2. Experimental

2.1 Materials

Chitosan (Sea fresh Chitosan Lab Co., Ltd., Bangkok, Thailand) with a degree of deacetylation of 95% with a viscosity-average molecular weight ($\overline{M}_v$) of 100,000 g/ mol was used as received. Sodium tripolyphosphate (TPP, Merck, Hohenbrunn, Germany) was used as a crosslinker. Light mineral oil (Hopewell International Co., Ltd., Thailand) was used as an oil phase. Menthol with a molecular weight of 156.27 g/mol (Hong Huat Co., Ltd., Thailand) was used as an encapsulating material. Poly(oxyethylene-2-stearyl ether) (Brij 72,

Greensville Co., Ltd., Thailand) was used as an oil-soluble surfactant. Sodium dodecyl sulfate (SDS, Merck, Germany) and cetyl stearyl alcohol (Kao Co., Ltd., Thailand) were used as a surfactant and a co-surfactant, respectively. Poly(vinyl alcohol), PVA-220, (Kuraray Co., Ltd., Japan) with 87-89% of hydrolysis degree was used as a stabilizer.

2.2 Apparatus

A miniature kit for emulsification with an SPG module was purchased from Kiyomoto Co., Ltd (Japan). A tubular porous glass membrane with the size of 2 cm length and 1 cm diameter was installed in the module. The dispersed phase (oil phase) was stored in a Teflon vessel (20 ml) which was connected to nitrogen gas inlet, the continuous phase (water phase) containing a mixture of SDS and PVA in a 250-ml beaker was stirred at 300 rpm with a magnetic bar to prevent creaming of the droplets. With an optimum pressure of nitrogen gas, the dispersed phase can permeate through the uniform pores of the membrane into the continuous phase to form droplets. The droplets were then stabilized by the PVA and SDS dissolved in the continuous phase.

2.3 Preparation of chitosan microcapsules

The procedures of preparing oil-in-water emulsion of chitosan/menthol microcapsules were manufactured as follows: continuous phase was composed of 50.0 g of deionized water, 0.05 g of sodium dodecyl sulfate, then pour 1w/v% chitosan solution in acetic acid 1v/v%. Oil phase consist of 5.0 g of mineral oil, the solution were then mix using high speed homogenizer at 6000, 10000, 14000 and 16000 rpm for 30-120 minutes. The mixture was continuous stirred at 400 rpm to prevent the coagulation.

2.3.1Preparation of chitosan microcapsules via SPG emulsification

The SPG membrane with an average pore size of 1.4 and 5.2 μm was used for the emulsification. The preparative condition for the emulsification is shown in Table 1. The

SPG membrane was pre-wetted in the aqueous phase. Menthol was dissolved in a mixture of light mineral oil, surfactant and co-surfactant by heating up to 40-43°C and was used as a dispersed phase. The aqueous phase where PVA and SDS had been dissolved was used as a continuous phase. The oil phase permeated through the uniform pores of the SPG membrane by the pressure of nitrogen gas into the aqueous phase to form the o/w emulsion. Sodium tripolyphosphate (TPP) solution was slowly dropped into the o/w emulsion to crosslink the chitosan droplets by stirring at 200 rpm for 1 to 5 h. Finally, the chitosan microcapsules were collected and washed repeatedly two times with petroleum ether and acetone by centrifugation at 3000 rpm, and then the microcapsules were freeze dried. A pressure used was slightly above the critical pressure. In this study, the ranges of the permeation pressures at 48.9 to 88.8 kPa for the 1.4 μm pore size, and 14.1 to 67.0 kPa for the 5.2 μm membrane pore size were used.

Insert Table 1

2.3.2 Preparation of chitosan microcapsules via double emulsion methods

Primary and secondary emulsions in a ratio of 1:1 were mixed and stirred in mild condition of 200 rpm for 1 hr. Sodium tripolyphosphate (TPP) with various concentration of 1, 5, 10, and 15% was dropped into the mixture as crosslinkng agent. Varying amount of amino group of chitosan to TPP of 2:1, 4:1, 6:1, and 8:1, the mixtures were then stirred at 400 rpm using different time interval of 30, 60, 90, and 120 minutes. The pH was adjusted to 3, 5, 7, and 9 using acetic acid and sodium hydroxide solution. A simple flowchart for the preparation of chitosan microcapsules by the double emulsion is shown in Fig. 1.

Insert Figure 1

2.4. Characterization of chitosan microcapsules

2.4.1. Measurement of size distribution of the droplets

Droplets before and after the crosslinking were observed with an optical microscope. Diameters of approximately 150 droplets were measured to calculate the average diameter. The number average diameter ($\overline{d_e}$) was calculated according to eq. (1). The coefficient of variation (CV) was determined using the formula in eq. (2).

$$\overline{d_e} = \sum_{i=1}^{n} d_i / N \quad (1)$$

$$CV = \left(\sum_{i=1}^{n} \frac{(d_i - \overline{d}_e)^2}{N} \right)^{1/2} \Big/ \overline{d}_e \quad (2)$$

where, d_i is the diameter of each droplet, N is total number of the droplets measured, and $\overline{d_e}$ is the number average diameter of the droplets.

2.4.2 Observation of morphology of the microparticles

Morphology of the emulsion microparticles was observed using an optical microscope (model BH2, Olympus Optical Co., Ltd, Tokyo, Japan).

2.4.3 Controlled release study

The 5 ml of prepared chitosan microcapsules were transferred to 15 ml test tube and centrifuged at 3000 rpm for 30 minutes. The creamy layer was separated from aqueous layer, and then transferred to vacuum oven at 30°C for 12 hr. The encapsulation efficiency was calculated as shown in eq.3. Release profiles were calculated in term menthol release (%) with time as shown in eq. 4. All samples were assayed in triplicate for 60 hr.

$$\text{Encapsulation efficiency} = \frac{W_m - W_0}{W_m} \times 100 \quad (3)$$

$$\text{Release } (\psi) = \left[\frac{W_m - W_m(t)}{W_m - W_0} \right] \times 100 \quad (4)$$

where, W_m is the weight of dried microcapsule after vapor evaporation, $W_{(t)}$ is the weight of microcapsules in a 40°C oven at time *t* (hr). The samples were weight at different time interval of 1, 3, 5, 7, 12, 24, 48, and 60 hr. The W_o is the weight of microcapsules after menthol evaporated in a 120°C [11, 12].

2.5 Release kinetic studies of menthol from microcapsules

The release profile of menthol from chitosan microcapsules was studied using the release (%) calculated from eq. 4. The release data of microcapsules were analyzed following mathematical models: Zero-order kinetic; first-order kinetic; Higuchi equation (square-root of time equation) [13]; Baker-Lonsdale equation; Hixson-Crowell; and Ritger-Peppas equation [14], as shown in Table 2. Linear regression value has been used for calculation the correlation coefficient (R^2) in order to predict the release behavior from microcapsules.

Insert Table 2

3. Results and discussion

3.1. Effect of the pore size of membrane on the droplet size and size distribution

The SPG membranes with the average pore diameter of 1.4, and 5.2 μm were used to prepare the o/w emulsion. The uniform emulsion droplets were prepared, and the average diameter ($\overline{d_e}$) of 10.2 and 19.6 μm for the membrane pore sizes of 1.4 and 5.2 μm obtained. It was found that the diameter of droplets in the o/w emulsion was approximately 8 and 4 times the diameters of membrane pore. The dispersed phase containing light mineral oil without menthol as an additive was difficult to permeate through the SPG membrane pore size of 1.4 μm. The possible cause was occurred from the high viscosity of light mineral oil. Furthermore, due to the high molecular weight of PVA stabilizer used, the PVA molecules were covered onto the membrane surface and plugged the pores, the oil phase was thus

retained and could not be permeated. As a resulted, the SPG membrane pore size of 5.2 μm was used for further studied.

3.2. Effect of the amount of menthol loading on droplet size and size distribution

The menthol dissolved in the dispersed phase affected the o/w emulsion. The permeation pressure decreased from 7.4 kPa to 2.5 kPa and 0.6 kPa when increasing the amount of menthol from 0 to 5 and 10 wt%, respectively. The hydrophilic in the disperse phase increased with increasing the amount of menthol loading in disperse phase. The hydroxyl group of menthol enhances the hydrophilicity of the oil phase, thus to permeate it easily through the hydrophilic pore wall of the SPG membrane. The permeation pressure was then decreased. Optical micrographs and the histogram of size distribution of the droplets in oil phase at different amounts of menthol loadings are shown in Fig. 2. Without the menthol, an average diameter of emulsion droplets of 28.3 μm with the CV of 24.7% was obtained. When the amounts of menthol loading in the disperse phase increased from 5 to 10 wt%, the average diameters of emulsion droplets decreased from 24.2 to 16.8 μm with the CV of the droplets increased from 34.4 to 57.6%. The size distributions expressed as histograms in Figure 2 a-c) indicate that more menthol loading in the dispersed phase produced the smaller size droplets in the range of 10 μm. This effect is caused by the increases in hydrophilicity of the hydroxyl groups when increasing the menthol loadings.

Insert Fig. 2

Insert Fig.2a, Fig 2b, Fig 2c

3.3. Effect of crosslinking time on the size and size distribution

Chitosan as the shell of o/w emulsion droplets was crosslinked with TPP solution. TPP was dissociated into OH^- and $P_3O_{10}^{5-}$ anions. The positively charged amino group of chitosan reacted with $P_3O_{10}^{5-}$ anions to form crosslinking bonds [15]. The crosslinked microcapsule

sizes of the o/w emulsion droplets decreased from 47.4 to 27.6 μm with increasing crosslinking time (Fig. 3) due to the increase of crosslink density of chitosan-TPP matrix [16]. The less crosslinking time of 1 h could not form the small droplet size for the subsequence process in this research. Very interestingly, the longer crosslinking time gave the narrow size distribution.

Insert Fig. 3

3.4Preparation of microcapsules via conventional homogenizing method

The preparation of o/w emulsion with narrow size distribution by SPG emulsification technique is that the o/w emulsion should be stable with a narrow emulsion droplets size distribution. Since, the oil phase composed of chitosan with different amount of menthol, a hydrophilic properties was reviewed. Therefore, it is necessary to find a condition where a large amount of chitosan can be maintained and performed microcapsules. The ultrasonic homogenizer was used with high homogenizing rate. The effects of homogenizing speed, time, and chitosan concentration were studied.

3.4.1 Effect of homogenizing speed

Chitosan microcapsules with broad coefficient of variation of 55.9% were obtained using the lower homogenizing speed of 6000 rpm. Increasing the homogenizing speed from 14000 to 16000 rpm, the microcapsules with CV of 38.9 and 39.7%, were obtained, respectively. However, the homogenizing speed at 10000 rpm was found the lowest CV% of 31.5. The phase separation of emulsion was observed at the beginning of emulsification process approximately within 1 hr after the homogenizing process. As shown in Table 3, the homogenizing speed of 10000 rpm was selected for further study since the emulsion droplets in size of 39.1±12.3 μm.

Insert Table 3

3.4.2 Effect of homogenizing time

Chitosan microcapsules was prepared and used as a secondary emulsion for combination with a primary emulsion obtained via SPG emulsification process. The homogenizing speed of homogenizer was used at 10000 rpm. The effect of homogenizing time of 30, 60, 90, and 120 second were studied. As shown in Table 4, the emulsion droplets with coefficient of variation of 30.8 and 34.8% were obtained with homogenizing time of 30 and 60 second, respectively. The broad droplets size distribution was reviewed comparison with using the homogenizing time of 60 and 120 second. The coefficient of variation of 24.8 and 24.6% was calculated. The short period of homogenizing time, the droplets disruption with less stability occurred. The micelles formation was unstable. The oil droplets distribution related to the stirring time that affected to the micelles of oils in water phase was reviewed [10]. An increasing in stirring time from 90 to 120 minute, an emulsion droplets size was increased from 39.8±9.9 to 41.2±10.1 μm. The stirring time of 90 second were then selected for further studies.

Insert Table 4

3.4.3 Effect of chitosan concentration

Preparation of chitosan microcapsules was prepared with various concentration of chitosan in acetic acid solution. As shown in Table 5, the amount of chitosan was varied from 1, 1.5, and 2.0 w/v% of acetic acid. It was found that the emulsion droplets of chitosan in size of 17.9±8.1, 17.0±6.3, and 16.7±6.9 μm was obtained, respectively. The 1.5 w/v% chitosan solution in acetic acid was considered as a suitable concentration for further experiment since the viscosity is concerned for emulsification processing [17].

Insert Table 5

3.5 Preparation of menthol encapsulated chitosan microcapsule

Menthol encapsulated microcapsules was prepared via double emulsion method. The emulsions from SPG emulsification using SPG membrane pore size of 5.2 μm as a primary, and high-speed homogenizer at 14,000 rpm for 90 minutes as secondary emulsion was prepared. The miscibility of two emulsions was studied in terms of size and encapsulation efficiency. In this experiment, the primary emulsion of 24.2±8.3 μm was mild stirred with secondary emulsion of 17.0±6.3 μm, and left for 1 hr. The emulsion droplets in size of 31.0±8.5 μm was obtained and the narrow coefficient of variation observed as shown in Table 6. It was found that the small size of secondary emulsion was diffused and absorbed into the primary emulsion, the swelling droplets obtained with narrow size distribution. The mechanism is followed the non-destructive swelling [18]. Since, the less thermodynamics stability of secondary emulsion tend to migrate to the more stable droplets of primary emulsions, the absorption were then occurred.

Insert Table 6

3.5.1 Effect of pH on size and size distribution of microcapsules

The effects of pH adjusted solution onto size and size distribution of swollen microcapsules was studied. The pH in ranges of 5 to 7 was preferred for the use of microcapsules in further application as an additive in leave-on conditioners. The pH values of 3.6, 5.0, 7.0, and 8.9 were studied. As shown in Fig. 4, the droplets size of microcapsules tend to decreased with increasing coefficient of variation at pH of 3.6 (Figure 4a, and 4b). The affects of microcapsules degradation may results from the non-crosslinked chitosan molecules dissolved from microcapsule at low pH. The pH of 5.0, 7.0, and 8.9 in emulsions were adjusted using sodium hydroxide. The menthol encapsulated chitosan microcapsules in size of 26.8, 28.6, and 28.0 μm were obtained, respectively. The narrow emulsion size

distribution as increasing pH was reviewed. The coefficient of variation of 20.6, 23.7, and 30% was calculated. Then, the workable pH for microcapsules in further uses was considered in ranges of 5 to 7.

Insert Figure 4a

Insert Figure 4b

3.6 Efficiency of encapsulation and controlled release of menthol from microcapsule

The efficiency of encapsulation and controlled release of menthol from microcapsules were studied as follows:

3.6.1 Effects of crosslinking time

Menthol encapsulated chitosan microcapsules were prepared via double emulsion, 5 w/w% sodium tripolyphosphate (TPP) as crosslinking agent. The crosslinking time was varied for 30, 60, 90, and 120 min. The encapsulation efficiency profiles of microcapsules were graphically presented in Figure 5. The results revealed that the menthol encapsulated in chitosan microcapsules was increased with increasing crosslinked time. The order of menthol encapsulated in microcapsules was 9.9±0.1, 35.6±0.1, 35.5±1.0 and 36.1±0.3% when the crosslinking time of 30, 60, 90 and 120 min, respectively. The encapsulation pattern indicated that the menthol was released and controlled by the thickness of microcapsule wall. The ionic interaction between a negatively charged counterion of tripolyphosphate and a positively charged amino group of chitosan was an important role on degree of crosslinking [16]. Encapsulation efficiency of menthol in microcapsules was retained when the longer period of crosslinking time was applied. The release of menthol was very slow which could be due to the thickness of chitosan wall. Figure 6 shows release behavior of menthol from chitosan microcapsules prepared with TPP solution as ionic crosslinking agent at various crosslinking times.

Insert Fig. 5

Insert Fig. 6

3.6.2 Effects of crosslinking concentrations

Figure 7 shows release behavior of menthol from chitosan microcapsules prepared with tripolyphosphate solution at various concentrations. As previously described, the amount of crosslinking agent influenced the ionic-crosslinking density of TPP-chitosan. As shown in Figure 7, the encapsulation efficiency of menthol was improved by the increasing amount of TPP concentration. The amount of TPP solution of 1, 5, 10, and 15 w/w% was applied, the encapsulation efficiency values of 14.8±7.8, 36.1±0.3, 38.1±1.7 and 37.7±3.3% were obtained. The higher the amounts of TPP is, the thicker the microcapsule walls became. Figure 8 shows the effect of the TPP as the crosslinking agent on the release behavior of menthol. There was a release 95% of menthol at 60 hr in 1 w/w% TPP-chitosan microcapsules. The amount of TPP of 5, 10, and 15 w/w%, the amount of menthol releasing from microcapsules were 46.1±1.5, 43.8±2.3, and 38.3±2.5, respectively. The higher concentration of TPP, the lower amount of menthol released from chitosan microcapsules. It depends on the crosslinking density of TPP-chitosan.

Insert Fig. 7

Insert Fig. 8

3.6.3 Effects of molar ratio of amino group in chitosan to tripolyphosphate

Encapsulation efficiency increases with increasing the molar ratio of amino group in chitosan to TPP, as shown in Figure 9. The effects of molar ratio of amino group in chitosan to tripolyphosphate of 2:1, 4:1, 6:1, and 8:1 to encapsulated efficiency of menthol was carried out. Chitosan microcapsules with encapsulated efficiency of 47.5±3.5, 52.7±0.5, 67.0±1.5 and 69.2±1.3% was obtained, respectively. In Figure 10, the comparative releasing

profile of menthol from chitosan microcapsules decreased with increasing amount of molar ration of amino group to TPP. The menthol diffusion was reduced after 12 hours. It was found that the amount of menthol releasing of 34.0±2.0, 22.9±2.9, 18.4±2.9 and 16.2±2.8% obtained when the molar ratio of amino group-to-TPP of 2:1, 4:1, 6:1, and 8:1, respectively. The slope of releasing profiles for all molar ratio of amino and tripolyphosphate increased at the initial stage and declined after 60 hr. From the graph, the release rate of menthol could find slows down when the molar ratio of amino and tripolyphosphate increases. The chitosan wall membrane almost completely seals up when increasing degree of crosslinked.

Insert Fig. 9

Insert Fig. 10

3.7 Release kinetics studies of menthol from microcapsules

The release kinetics of menthol from various conditions based upon crosslinking time, crosslink concentration, and molar ratio of amino and tripolyphosphate was determined by comparing their respective co-relation coefficients. Various models and equations of zero order, first order, Higuchi, Hixson-Crowell, Baker-Lonsdale, and Ritger-Peppas [19, 20] have been used after linearization to predict mechanisms of menthol release. Ritger-Peppas plots were found to be the highest linearity with correlation coefficient greater than that of the other kinetics as shown in Fig. 11a-c. The results indicating that the menthol release mechanism from these chitosan microcapsules was diffusion controlled with diffusion index (n) calculated from slope. In Table 7, the n values revealed that the releasing menthol was found from spherical capsules. The diffusion index n was ≤ 0.43, which indicates a Fickian diffusion, and $0.43 \leq n \leq 1.00$ indicates a non-Fickian [19]. The value of "n" in Ritger-Peppas is approximately 0.5, which implies that the menthol follows non-Fickian transport.

The resulted demonstrated that the transportation of menthol was controlled by crosslink density [21]. The crosslinking density increases, the value of *n* was increased.

Insert Fig. 11

Insert Table 7

4. Conclusion

Chitosan as the wall membrane material, menthol as volatile core material microcapsules were prepared using high speed homogenizer and SPG membrane emulsification techniques. The effects of membrane pore size, the amount of menthol loadings and crosslinking time were affected to size and size distribution of droplets. The uniform-sized chitosan microcapsules can also be prepared when the membrane pore size used was 5.2 μm; the higher amount of menthol gave the smaller mean diameter of the emulsion droplets with narrow size distribution. The longer crosslinking time, the smaller microcapsules with a narrow size distribution was produced. The emulsion droplets with average size of 31.0±8.5 μm and coefficient of variation of 27.4% were obtained. The suitable pH for microcapsules stability was found at pH in range of 5 to 7. To control release of menthol by changing manufacturing conditions of crosslinking time, amount of tripolyphosphate, and molar ratio of amino group in chitosan to tripolyphosphate were studied. The resulted indicated that encapsulation efficiency and release properties of menthol were depended on the crosslinking time, amount of tripolyphosphate, and molar ratio of amino group to tripolyphosphate. The menthol release curve shows an exponential release normally at a higher rate in the beginning. Non-Fickian diffusion was described behavior of menthol release from microcapsules. The diffusion patterns were found to be dependent on the crosslinking density.

Acknowledgements

The authors thank the Thailand Research Fund for funding the research under the Senior Scholarly Consolidation Grant no. RTA5080004. Research facilities from the Department of Imaging and Printing Technology are highly appreciated.

References

[1] N. Galeotti, L. Di Cesare Mannelli, G. Mazzanti, A. Bartolini, C. Ghelardini, Menthol: a natural analgesic compound. Neurosci. Lett. 322 (2002) 145–148.

[2] A. Soottitantawat, K. Takayama, K. Okamura, D. Muranaka, H. Yoshii, T. Furuta, M. Ohkawara, P. Linko, Microencapsulation of l-menthol by spray drying and its release characteristics. Innovat. Food Sci. Emerg. Tech. 6 (2005) 163–170.

[3] M. Rinaudo, Chitin and chitosan: Properties and applications. Prog. Polym. Sci. 31 (2006) 603–632.

[4] W. Wei, L.Y. Wang, L. Yuan, X.D. Yang, Z.G. Su, G.H. Ma, Bioprocess of uniform-sized crosslinked chitosan microspheres in rats following oral administration. Eur. J. Pharm. Biopharm. 69 (2008) 878–886.

[5] G.T. Vladisavljevic, H. Schubert, Preparation and analysis of oil-in-water emulsions with a narrow droplet size distribution using Shirasu-porous-glass (SPG) membranes. Desalination 144 (2002) 167–l72.

[6] M. Yasuno, M. Nakajima, S. Iwamoto, T. Maruyama, S. Sugiura, I. Kobayashi, A. Shono, K. Satoh, Visualization and characterization of SPG membrane emulsification. J. Membr. Sci. 210 (2002) 29–37.

[7] S.M. Joscelyne, G. Trägårdh, Membrane emulsification – a literature review. J. Membr, Sci. 169 (2000), 107–117.

[8] T. Nakashima, M. Shimizu, Porous glass from calcium alumino boro-silicate glass. Ceramics 21 (1986), 408.

[9] G.T. Vladisavljevic, I. Kobayashi, M. Nakajima, R.A. Williams, M. Shimizu, T. Nakashima, Shirasu Porous Glass membrane emulsification: Characterization of membrane structure by high-resolution X-ray microtomography and microscopic observation of droplet formation in real time. J. Membr. Sci. 302 (2007) 243–253.

[10] S. Kiatkamjornwong, S. Phansomboon, V. Hoven, Chitosan microencapsulation of menthol and its controlled release, The Journal of the Royal Institute of Thailand 34 (2009) 337–371.

[11] C.P. Chang, T.K. Leung, S.M. Lin, C.C. Hsu, Release properties on gelatin-gum Arabic microcapsules containing camphor oil with added polystyrene. Colloids Surf. B Biointerfaces 50 (2006) 136–140.

[12] W.C. Hsieh, C.P. Chang, Y.L. Gao, Controlled release properties of chitosan encapsulated volatile citronella oil microcapsules by thermal treatments. Colloids Surf. B Biointerfaces 53 (2006) 209–214.

[13] T. Higuchi, Mechanism of sustained-action medication. Theoritical analysis of rate of release of solid drugs disperse in solid matrices. J. Pharm. Sci. 52 (1963) 1145–1149.

[14] R.W. Korsmeyer, R. Gurny, E. Doelker, P. Buri, N.A. Peppas, Mechanisms of solute release from porous hydrophilic polymers. Inter. J. Pharm. 15 (1983) 25–35.

[15] F.M. Hsieh, C. Huang, T.F. Lin, Y.M. Chen, J.C. Lin, Study of sodium Tripolyphosphate-crosslinked chitosan beads entrapped with *Pseudomonas putida* for phenol degradation, Process Biochem. 43 (2008) 83–92.

[16] J.A. Ko, H.J. Park, S.J. Hwang, J.B. Park, J.S. Lee, Preparation and characterization of chitosan microparticles intended for controlled drug delivery. Inter. J. Pharm. 249 (2002) 165–174.

[17] L.Y. Wang, G.H. Ma, Z.G. Su, Preparation of uniform sized chitosan microspheres by membrane emulsification technique and application as a carrier of protein drug. J. Control. Release 106 (2005) 62–75.

[18] G.H. Ma, M. Nagai, S. Omi, Synthesis of uniform microspheres with higher content of 2-hydroxyethyl methacrylate by employing SPG emulsification Technique followed by swelling process of droplets. J. Appl. Polym. Sci. 66 (1997) 1325–1341.

[19] P.L. Ritger, N.A. Peppas, A simple equation for description of solute release I. Fickian and non-Fickian release from non-swellable devices in the form of slabs, spheres, cylinders or discs. J. Control. Release 5 (1987) 23–36.

[20] K. Shi, Y. Jiang, M. Zhang, Y. Wang, F. Cui, Tocopheryl succinate-based lipid nanospheres for paclitaxel delivery: Preparation, characters, and in vitro release kinetics. Drug Delivery 17(1) (2010) 1–10.

[21] R.V. Kulkarni, B.S. Mangond, S. Mutalik, B. Sa, Interpenetrating polymer network microcapsules of gellan gum and egg albumin entrapped with diltiazem–resin complex for controlled release application. Carbohydr. Polym. 83 (2011) 1001–1007.

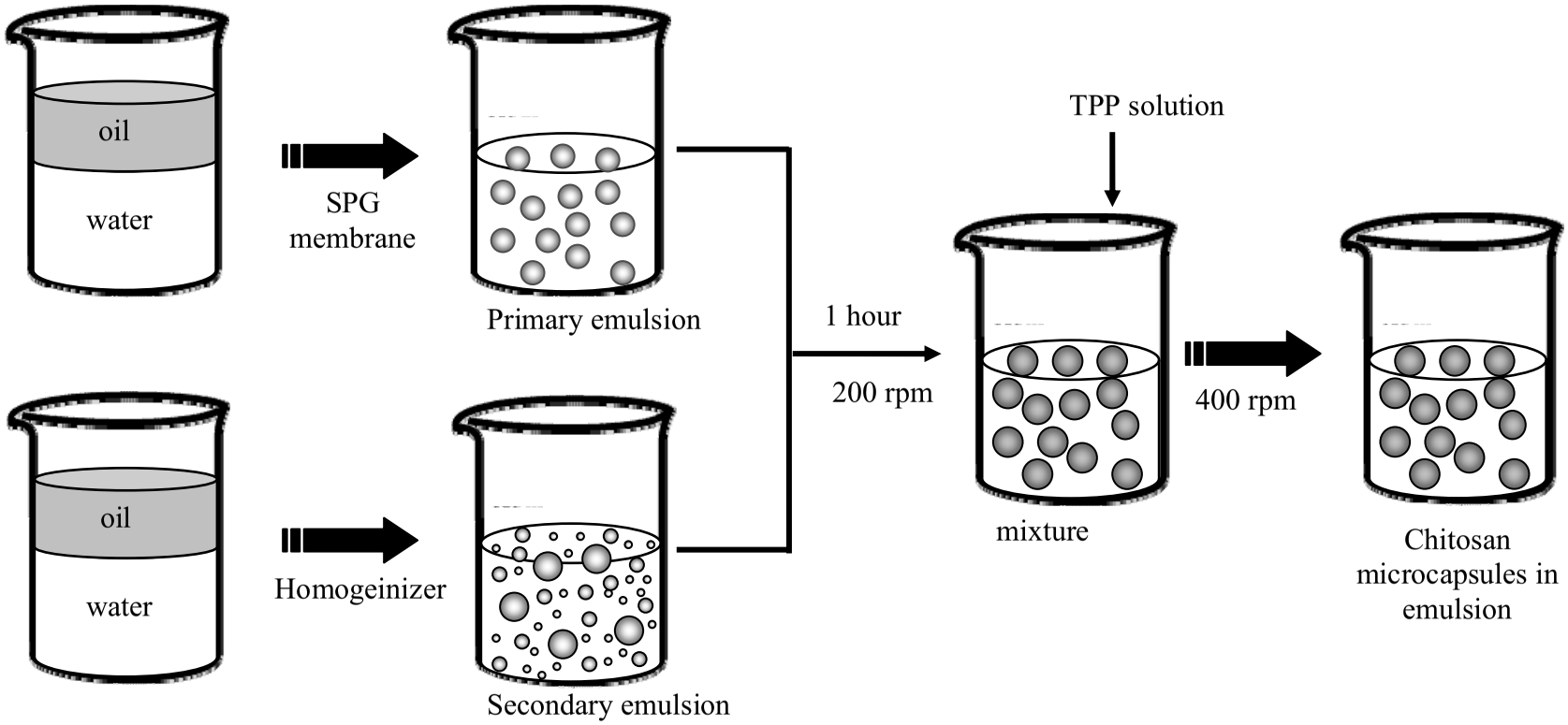

Figure 1 Flowchart for preparation of chitosan microcapsules by double emulsification

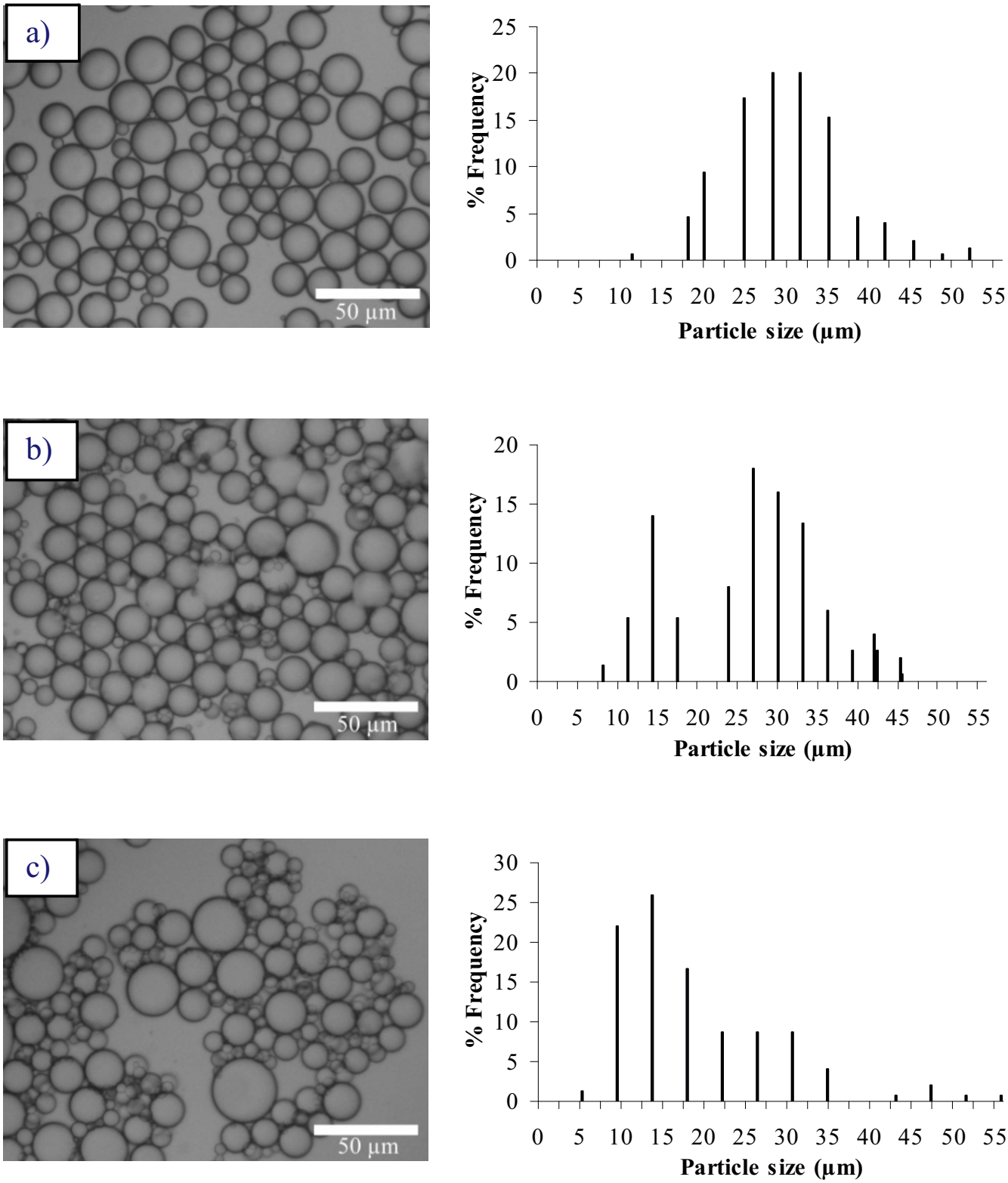

Figure 2 Optical micrographs (left) and histograms of the size distribution (right) of o/w emulsion with different amounts of menthol loadings for a) without menthol, b) 5 wt% menthol, c) 10 wt% menthol

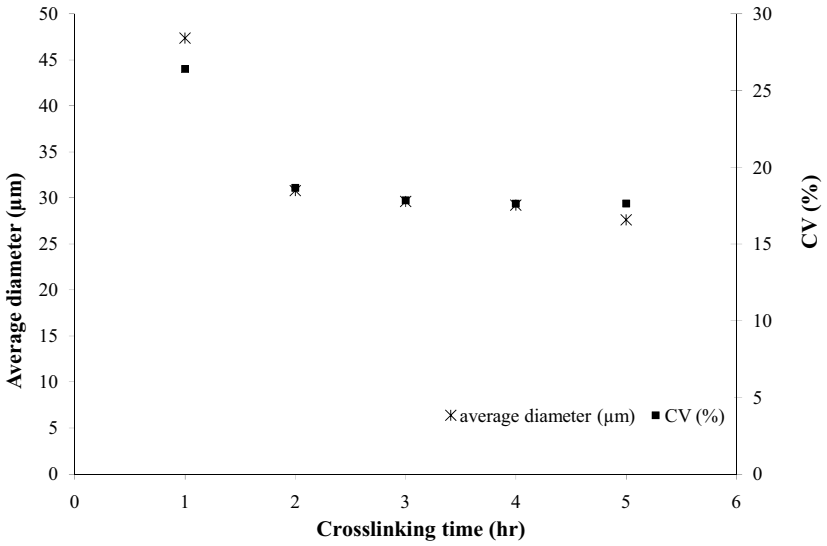

Figure 3 Relationship between the crosslinking time, the average size and the coefficient of variation

a) size

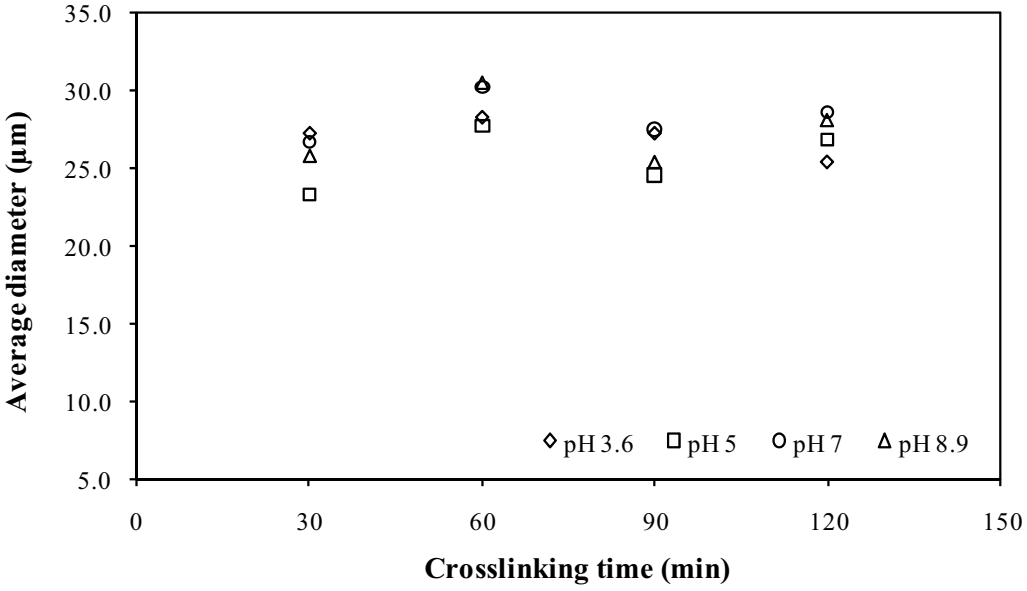

Figure 4 Relationship of microcapsules with different pHs: a) size, b) coefficient of variation

b) coefficient of variation

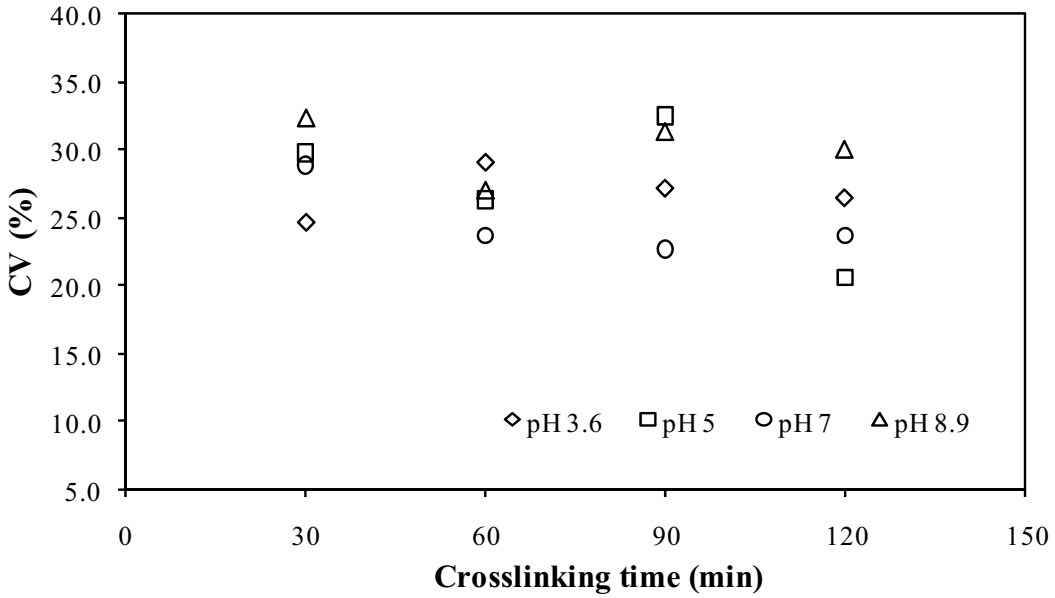

Figure 4 Coefficient of variation Vs. crosslinking time at various pHs

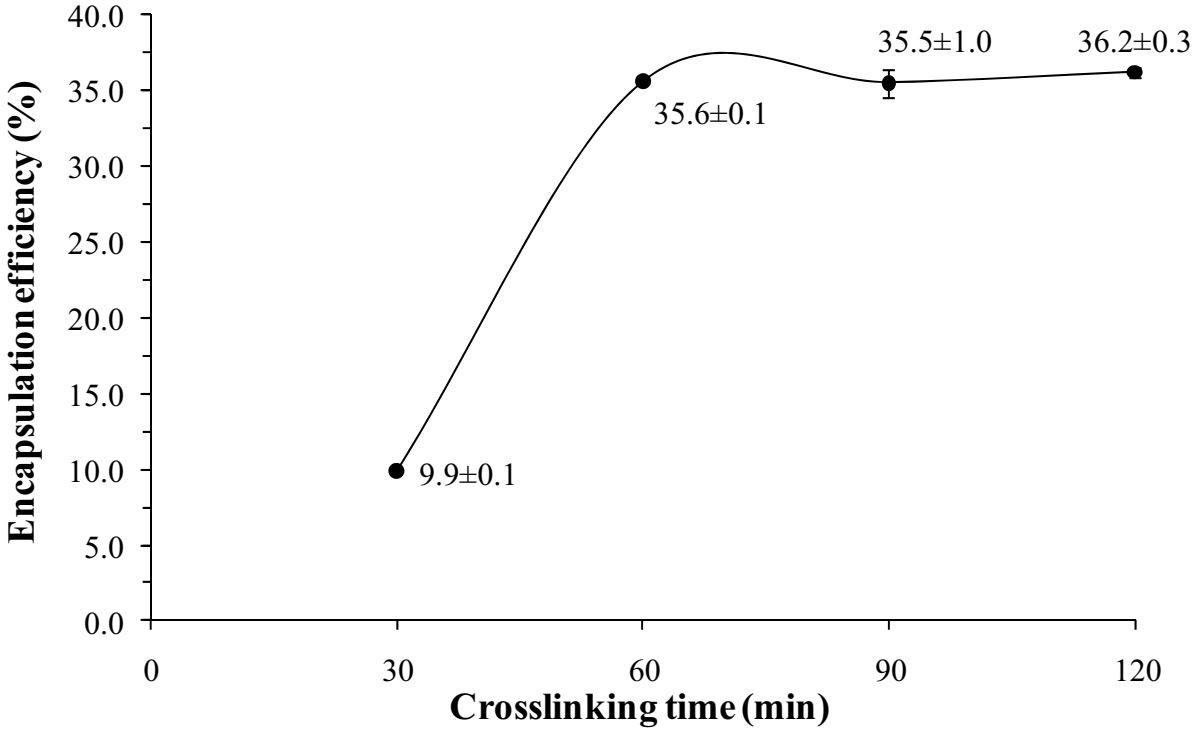

Figure 5 Encapsulation efficiency curves of menthol at 72 hr with various crosslinking times with 5w/w% of TPP, and molar ratio of amino group in chitosan to TPP of 1:1.

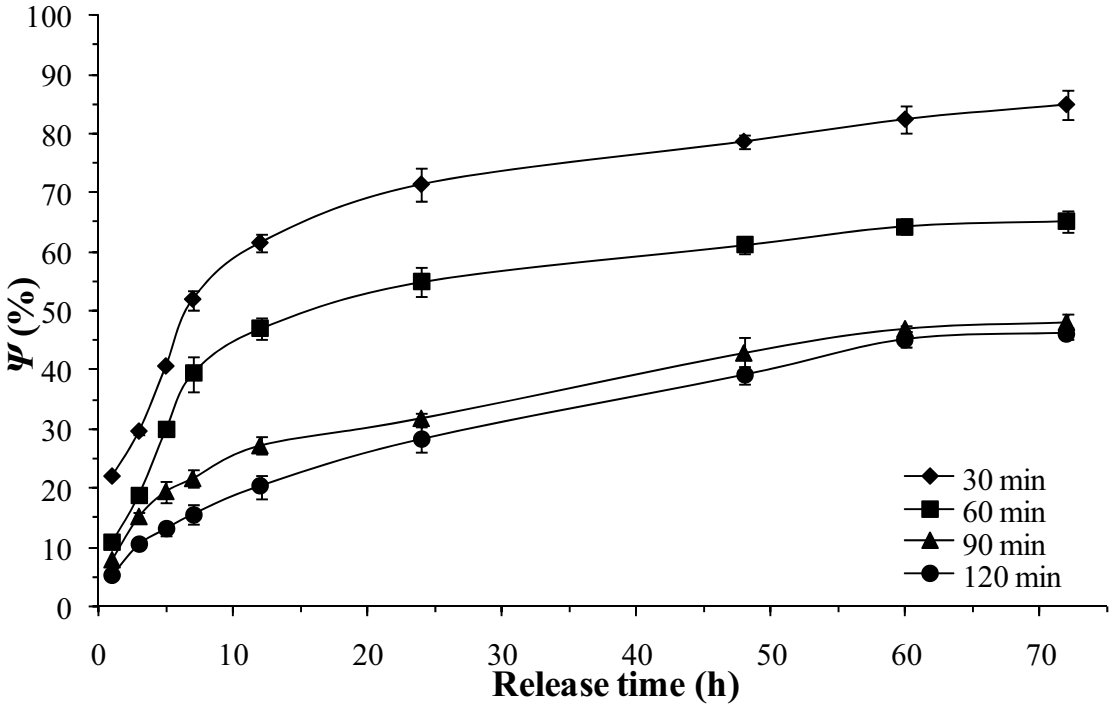

Figure 6 Comparative curves of menthol at 72-hr release, the chitosan amino group-to-TPP mole ratio of 1:1 at various crosslinking times

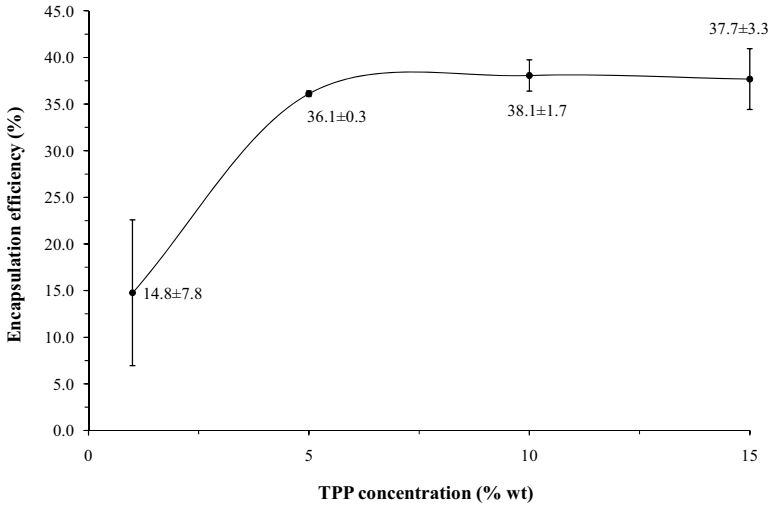

Figure 7 Menthol releasing curve at 72 hr with various TPP concentrations

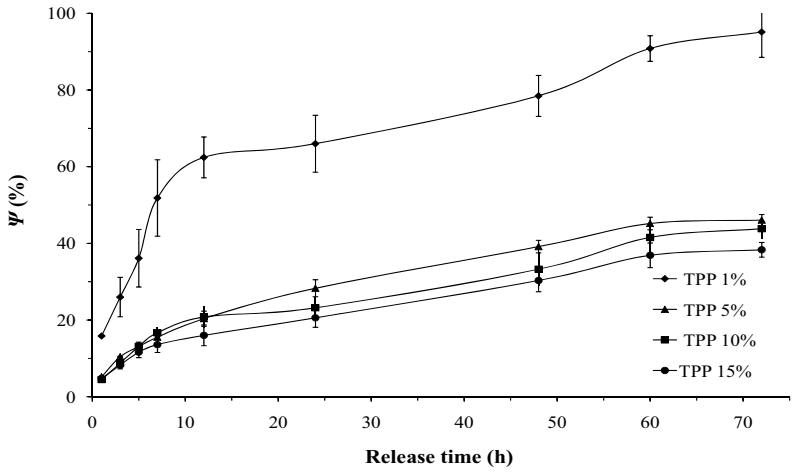

Figure 8 Menthol release curves as a function of TPP concentrations at the crosslinking time of 120 min.

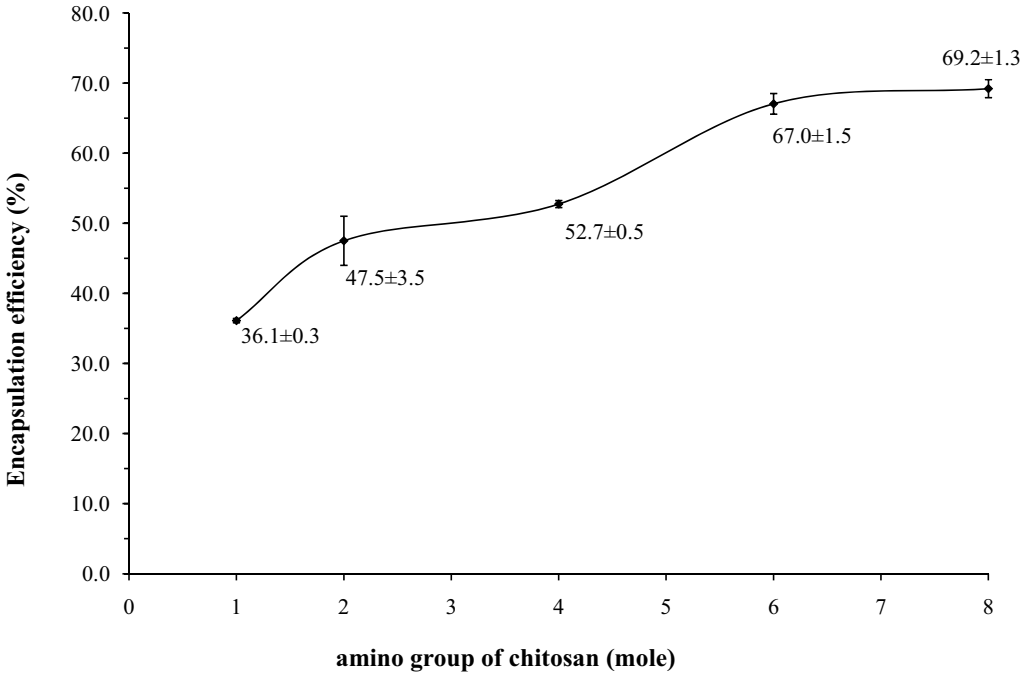

Figure 9 Encapsulation efficiency curve of menthol at 72 hr at various molar ratios of amino group in chitosan, 5 w/w% TPP at a crosslinking time at 120 min.

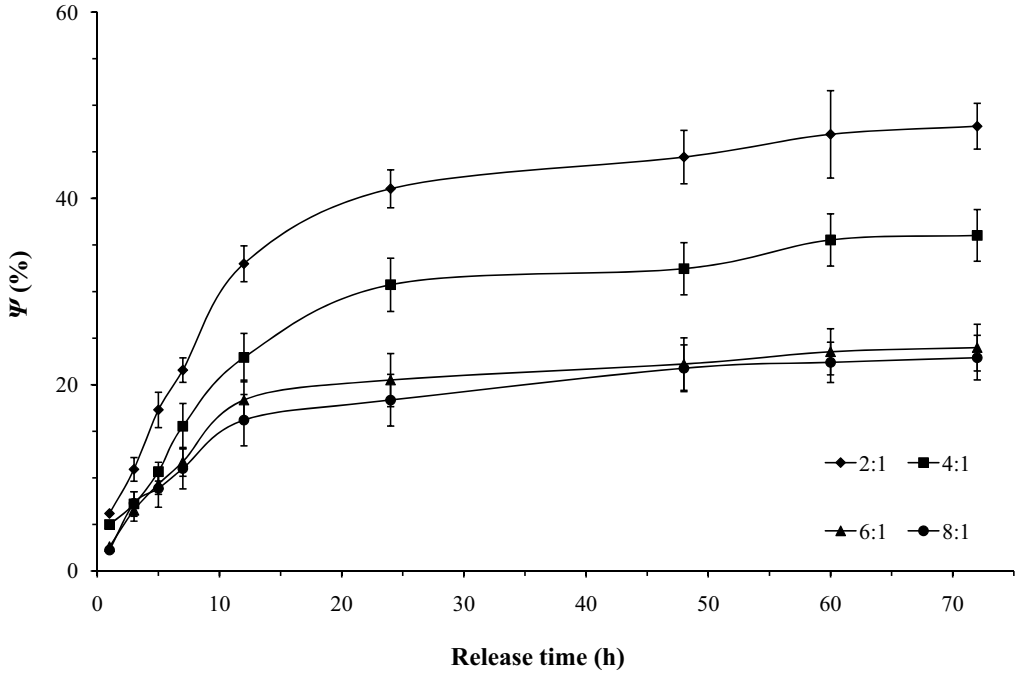

Figure 10 Effect of release time at the function of molar ratios of amino group in chitosan to TPP with 120 min crosslinking time

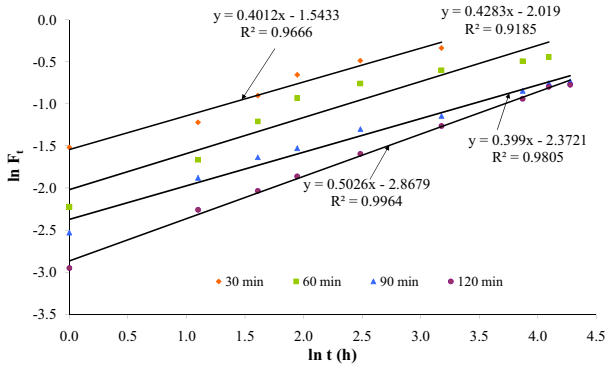

a) crosslinking time

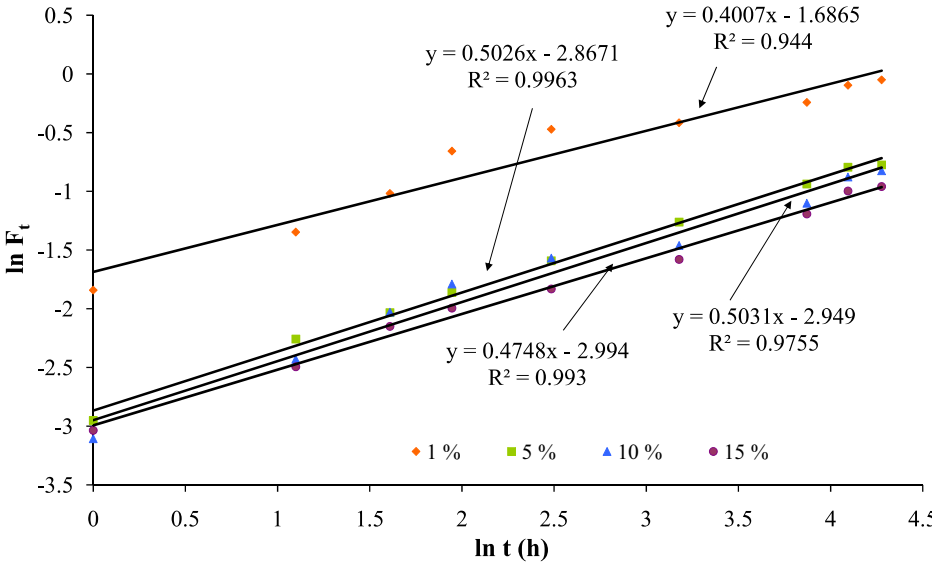

b) concentration of TPP

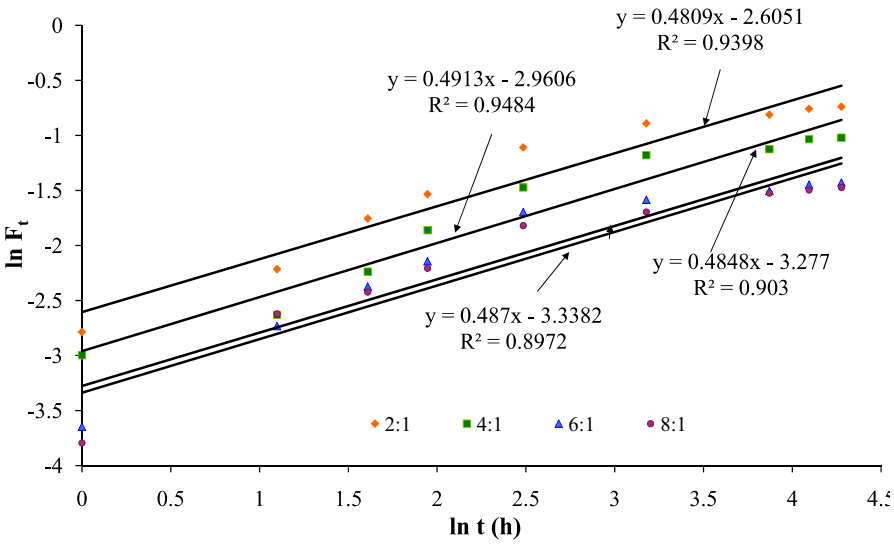

c) molar ratio of an amino group to TPP

Figure 11 Linear regression of Ritger-Peppas models for release kinetics of menthol; a) crosslinking time, b) concentration of TPP, and c) molar ratio of an amino group to TPP

Table 1 A recipe for the o/w emulsion

Component	Weight (g)
Continuous phase	
water	220
chitosan solution (1% w/v in 1 M acetic acid)	20
PVA	3.0
SDS	1.5
Disperse phase	
light mineral oil	20
menthol	0.5-2.0
Brij 72	0.5
cetyl-stearyl alcohol	0.5

Table 2 The o/w emulsion droplets (without menthol) obtained by two pore size membranes

Particle property	pore size (μm)	
	1.4	5.2
Number average diameter, $\overline{d_e}$ (μm)	10.2	19.6
CV (%)	10.1	11.5

Table 3 Size and size distribution of emulsion with different homogenizing speeds

Run no.[a]	Speed (rpm)	$\overline{d_e}$ (μm) ±SD	CV (%)
D001	6000	62.6±34.9	55.9
D002	10000	39.1±12.3	31.5
D003	14000	20.2±7.9	38.9
D004	16000	30.5±12.1	39.7

[a] Chitosan solution 1 w/v% of 2 M acetic acid, the amount of chitosan was 10.0 g.

Table 4 Size and size distribution with various homogenizing times

Run no.	Time (second)	$\overline{d_e}$ ±SD (μm)	CV (%)
T30	30	38.7±11.9	30.8
T60	60	38.7±13.5	34.8
T90	90	39.8±9.9	24.8
T120	120	41.2±10.1	24.6

Table 5 Size and size distribution of microcapsules with various chitosan concentrations

Run no.	Chitosan concentration (%w/v)	$\overline{d_e}$ ±SD (μm)	CV (%)
CH1	1.0	17.9±8.1	45.6
CH1.5	1.5	17.0±6.3	37.1
CH2	2.0	16.7±6.9	41.0

Table 6 Size and size distribution of emulsion droplets prepared with double emulsion method

Conditions	$\overline{d_e}$ ±SD (μm)	CV (%)
Primary emulsion	24.2±8.3	34.4
Secondary emulsion	17.0±6.3	37.1
Double emulsion	31.0±8.5	27.4

Primary emulsion was prepared using homogenizing speed at 14,000 rpm for 90 minutes.
Secondary emulsion using SPG pore size having 5.2 micrometers.

Table 7 Mathematical models for controlled release kinetics understudy

Model	Equations	X	y
Zero-order	$Q_t = Q_0 + k_0 t$	Q_t	t
First order	$\log Q_t = \log Q_0 + kt/2.303$	$\log Q_t$	t
Higuchi	$Q_t = k_H t^{1/2}$	Q_t	$t^{1/2}$
Baker-Lonsdale	$3/2[1-(1-F_t)^{2/3}]-F_t = kt$	$3/2[1-(1-F_t)^{2/3}]-F_t$	t
Hixson-Crowell	$(1-F_t)^{1/3} = 1-kt$	$(1-F_t)^{1/3}$	t
Ritger-Peppas	$\text{Ln } F_t = \ln k + n \ln t$	$\ln F_t$	ln t

Table 8 Release exponent (k), diffusion index (n), and correlation coefficient (R^2) from the linear regression using Ritger-Peppas model with $\ln F_t = k + n \ln t$

Condition	k	R^2	n
Crosslinking time (min)			
30	-1.5433	0.9666	0.4020
60	-2.0190	0.9185	0.4283
90	-2.3721	0.9805	0.3990
120	-2.8679	0.9964	0.5026
Concentration of TPP (%)			
1	-1.6865	0.9440	0.4007
5	-2.8671	0.9963	0.5026
10	-2.9490	0.9755	0.5031
15	-2.9940	0.9930	0.4748
Molar ratio of CS:TPP			
2:1	-2.6051	0.9398	0.4809
4:1	-2.9606	0.9484	0.4913
6:1	-3.2770	0.9030	0.4848
8:1	-3.3382	0.8972	0.4874

Draft Manuscript

Synthesis and Characterization of Water Swellable Natural Rubber Composites

Charoen Nakason[1]*, Yeampon Nakaramontee [1], Azizon Kaesaman[1], Wiyong Kangwansukpamonkon, and Suda Kiatkamjornwong[2]**

[1]Center of Excellence in Natural Rubber Technology, Department of Rubber Technology and Polymer Science, Faculty of Science and Technology, Prince of Songkla University, Pattani, 94000, Thailand;

*[1]*e-mail:ncharoen@bunga.pn.psu.ac.th*

[2]Multidisciplinary Program of Petrochemistry and Polymer Science, Department of Imaging and Printing Technology, Faculty of Science, Chulalongkorn University, Bangkok, 10330, Thailand;

*[2]**e-mail: ksuda@chula.ac.th*

Synthesis and Characterization of Water Swellable Natural Rubber Composites

ABSTRACT

A superabsorbent polymer (SAP) based on cassava starch-*g*-polyacrylamide (CSt-*g*-PAM) was prepared by a reactive batch processing using a specially designed batch reactor. SAP composites (SAPCs) were prepared from the CSt-g-PAM by blending with 20 phr of bentonite clay to increase the water absorbency of the SAP from 605 g/g up to 730 g/g for the SAPC. Water swellable natural rubber (WSNR) was then prepared by blending high-ammonia natural rubber (HANR) latex, or dry blending either epoxidized natural rubber (ENR) or maleated natural rubber (MNR) with the SAPC, coupled with poly(ethylene oxide) (PEO) and/or trimethylol propane trimethacrylate (TMPTMA). The curing, mechanical and morphological properties and the water absorbency of the different WSNRs were characterized. The WSNRs with both 10 phr PEO and 2 phr TMPTMA gave a higher mechanical strength and water absorbency. Increasing the PEO loadings to 20 or 40 phr rendered a higher absorbency but with a lower mechanical strength. A higher scorch time and cure time with a lower crosslinking density and cure rate index were found in the MNR based WSNRs compared with the WSNRs derived from the unmodified NR or ENR. The ENR base WSNR exhibited the highest water absorbency with lower mechanical strength compared with the unmodified NR base WSNR.

Keywords: Water swellable natural rubber, Superabsorbent polymer composite, Poly(ethylene oxide), Trimethylol propane trimethacrylate coupling agent.

INTRODUCTION

Superabsorbent polymers (SAPs) have been synthesized by modifying the molecular structure of cassava starch (CSt), and thus has gained in interest since such CSt based SAPs are claimed to be biodegradable products [Nakason, Wohmang, Kaesaman & Kiatkamjornwong, 2010; Lanthong, Nuisin & Kiatkamjornwong, 2006]. In contrast, most of the current SAPs are synthetic polymers that have a poor biodegradability that then leads to environmental problems upon their disposal. The development of starch-based SAPs could potentially be used to solve this problem. Potential applications of starch-based SAPs are fairly diverse and include, amongst others, personal care products, fire-fighting gels and agricultural uses [Willette & Finkenstadt, 2006]. Starch-based SAPs are developed by grafting starch with unsaturated hydrophilic monomers, such as acrylic acid (AA), acrylamide (AM) [Nakason, Wohmang, Kaesaman & Kiatkamjornwong, 2010; Lanthong, Nuisin & Kiatkamjornwong, 2006; Willette & Finkenstadt, 2006; Athawale & Lele, 1998; Karadage, Uzum & Saraydin, 2005; Lostafa, 1995] and ε-caprolactone [Chen, Ni, Bian, Qiu, Zhang & Chen, 2005], by a chemical initiated radical chain copolymerization [Athawale & Lele, 2000; Chen, Park & Park, 1999], or by using γ-ray irradiation [Kiatkamjornwong, Mongkolsawat & Sonsuk, 2002]. A reactive extrusion process has been used to prepare starch-based graft copolymers [Carr, Kim, Yoon & Stanley, 1992; Yoon, Carr & Bagley, 1992]. Starch-*g*-polyacrylamide (St-g-PAM) has been successfully prepared using a co-rotating twin screw extruder [Willette & Finkenstadt, 2003, Finkenstadt & Willette, 2005], but the maximum water absorbency capacity of the St-g-SAPs obtained using this process was relatively low at only approximately 300 times their dry weight [Carr, Kim, Yoon & Stanley, 1992]. However, our previous work based on the reactive blending process [Nakason,

77 Wohmang, Kaesaman & Kiatkamjornwong, 2010] with a specially designed batch
78 reactor gave St-g-SAPs with a higher maximum water absorbency capacity at ~ 730
79 times their dry weight.

80 In recent years, the development of water swellable (natural) rubbers
81 (WS(N)Rs) has been developed. WS(N)Rs are functional polymers that expand their
82 volume up to more than 1.5 times their original weight by absorbing surrounding
83 water. They can be used as a sealing material or in calking applications, preventing
84 water leakage from pipes or blocking connections in civil constructions, such as
85 subways and subsea tunnels [Park & Kim, 2001].

86 Any given WS(N)R is typically prepared by dispersing SAP particles in
87 common hydrophobic rubbers, such as chloroprene rubber [Wang, Li & Chen, 1999;
88 Liu, Ding, Zhou & Chen, 2006], chlorohydrin rubber [Zhang, Zhang, Wang, Liu, Liu
89 & Chen, 1999; Zhang, Zhang, Wang, Liu, Liu & Chen, 2000] and NR [Park & Kim,
90 2001, Wang, Zhang, Dong, Chen & Tan, 2002]. This special type of rubber possesses
91 not only the properties of general rubber, such as a high mechanical strength, set and
92 resilience properties, but also has high water absorbency. These properties are due to
93 the presence of the crosslinking network in the rubber and water absorbing material.

94 A specially designed batch reactor was used to prepare St-*g*-PAM based SAPs
95 via reactive processing, based on the optimum conditions found in Nakason *et al*.
96 [2010]. In this work, SAP composites (SAPCs) of the St-*g*-PAM mixed with bentonite
97 clay were prepared and later blended with NR and other important ingredients. That
98 is, each WSNR was prepared by mixing SAPC particles with the NR, poly(ethylene
99 oxide) (PEO) and trimethylol propane trimethacrylate (TMPTMA). Each ingredient
100 was then compounded and cured by the sulfur vulcanization system. The effects of the
101 addition of SAPC, PEO and TMPTMA on the water absorbency, curing, mechanical

and morphological properties of the resulting WSNR compound and vulcanizate were then investigated.

2. EXPERIMENTAL

2.1 Materials

High ammonia (HA) NR latex having a dried rubber content of approximately 60% was manufactured by Yala Latex, Co., Ltd (Yala, Thailand). Epoxidized natural rubber (ENN)) with 25% mol epoxide (i.e., Epoxyprene 25 (ENR-25)) was manufactured by Muang Mai Guthrie Public Co., Ltd. (Surathani, Thailand). Maleated natural rubber (MNR) was prepared in-house by blending the rubber air-dried sheet (manufactured by Khuan Pun Tae Farmer Co-operation, Phattaluang, Thailand) with 8 phr of maleic anhydride at 150 °C using an internal mixer (Brabender Plasticorder, model PLE331, Brabender OHG Duisburg, Germany) at a rotor speed of 60 rpm. Details of the preparation and characterization procedures of MNR are described by Nakason and Saiwari [2008].

CSt, used as a polymer substrate, was obtained from Siam Starch (1966) Co., Ltd., Rayong, Thailand. AM, used as a grafting monomer, and *N, N'*-methylenebisacrylamide, used as a crosslinker were from Fluka (Buchs, Switzerland). Potassium persulfate, used as a free radical initiator, was obtained from Asia Pacific Specialty Chemicals Ltd., (Seven Hills, Australia). Hydroquinone, used as a free radical scavenger, was from Merck (Darmstadt, Germany). Sodium lauryl sulfate was prepared in-house by reacting lauric acid (Imperial Industrial Chemicals (Thailand) Ltd.) with sodium hydroxide (BDH, England). For the preparation of SAPCs, bentonite clay, grade SAC-1, was from Thai Nippon Chemical Industry, Co., Ltd., (Samut Sakhon, Thailand), and TMPTMA, used as a coupling agent for functional

groups, was obtained from Behn Meyer Chemical Co., Ltd, Rayong, Thailand. PEO was from Alkox E-30, Meisei Chemical Works, Ltd., Kyoto, Japan, and was used to enhance the water absorbing properties of the rubber. Zinc oxide (white seal) and stearic acid, used as the activators in the sulfur vulcanization system, were supplied by Metoxide Thailand Co., Ltd. (Pathumthani, Thailand) and Imperial Industry Chemical Co., Ltd. (Pathumthani, Thailand), respectively. *N*-tert-butyl-2-benzothiazyl sulphenamide (TBBS), used as an accelerator, was manufactured by Flexsys America L.P. (Reliance Technochem Co., Ltd., Bangkok, Thailand). Sulfur, used as a curing agent, was manufactured by Ajax Chemical Co., Ltd. (Auckland, New Zealand).

Figure 1 A illustrates Infrared spectra of the major raw materials (a) poly(ethylene oxide), (b) starch-*g*-polyacrylmide and bentonite 20 phr, and (c) TMPTMA. The neat natural rubber peaks (not shown here) contained the following peaks: 3224 cm^{-1} (w), ν_{O-H} OH (moisture in the rubber); 3037 cm^{-1} (s) $\nu_{=C-H}$; 2960, 2916 and 2850 cm^{-1}, ν_{-C-H}; 1661 cm^{-1}, $\nu_{C=C}$; 1447 and 1375 cm^{-1}, ρ_{C-H}; 833 cm^{-1} ν_{C-H} on cis C=C of polyisoprene, or $\delta_{=C-H}$ polyisoprene. For the neat PEO, the following peaks were found. 3450 cm^{-1}, ν_{-OH} (hydration of PEO); 2889 cm^{-1}, ν_{-CH}; 1632 cm^{-1}, $\nu_{-C=O;}$ 1467 cm^{-1}, $\delta_{asH-C-H}$; 1360 cm^{-1}, δ_{sH-C-H}; 1149 cm^{-1}, ν_{C-O-C}; 916, 842 cm^{-1}, ρ_{CH_2} (guache) (Manoratne, Rajapake &Dissanayake, 2006; Zain & Arof, 1998). For the neat TMPTMA, 2980, 2920, 2900 cm^{-1}, ν_{CH} (ali); 1870 cm^{-1}, $\nu_{as\ C=O}$ (w); 1720 cm^{-1}, $\nu_{as\ C=O}$ (s); 1640 cm^{-1}, $\nu_{C=C}$ (m); 1480 cm^{-1}, δ_{C-H}.

150 ***2.2 Preparation of Cassava Starch-Graft-Polyacrylamide Superabsorbents (CSt-***
151 ***PAM SAPs) and Associated Composites (SAPCs) by Reactive Blending***

152 CSt-PAM was prepared by reactive batch processing using a specially
153 designed batch reactor, with the preparation and characterization as described before
154 [1]. The SAPC loaded with 20 phr of bentonite clay was prepared from the CSt-PAM
155 according to the described procedures [1].

156

157 ***2.3 Preparation of WSNR***

158 The HA concentrated NR latex was first mixed with the SAPC loaded with 20
159 phr bentonite clay and 2% (w/w) of SDS surfactant for 1 h at room temperature, and
160 then the mixture was aged for another 24 h to allow it to reach equilibrium. The
161 mixture was then cast into 10 x 10 cm thin films and dried at room temperature for 24
162 h followed by in a hot air oven for another 24 h at 40 °C. The ENR and MNR derived
163 WSNRs or called modified WSNRs were produced by a dry blending process with the
164 internal mixer at 40 °C and a rotor speed of 60 rpm, with the formulation and mixing
165 schedule shown in Table 1.

166

167 ***2.4 Influence of PEO and TMPTMA loadings on properties of WSNRs***

168 WSNR composites from the CSt-PAM SAP loaded with 20 phr bentonite clay
169 were prepared according to the procedure described in section 2.3. Each dried
170 composite was mixed at 50 °C using the internal mixer (capacity of 80 cm^3) at a rotor
171 speed of 60 rpm following the formulations shown in Table 2. In this work, the
172 properties of the WSNR composites and also with the addition of PEO with or
173 without the coaddition of TMPTMA were investigated.

174

175 ***2.5 Water absorbency***

176 Each WSNR composite (0.1 - 0.5 g) was immersed in distilled water (250 mL)
177 for 24 h at ambient temperature (25 - 30 ºC) to reach equilibrium swelling. The
178 residual water was removed by filtration through an 80-mesh stainless steel screen
179 with the WSNR composite left on the screen for at least 1 h to drain off the
180 unabsorbed water. During this period, the screen was gently shaken with a declining
181 angle of 15 - 20º to ensure that most of the unabsorbed water was separated. The
182 water absorbency was determined by weighing the fully swollen WSNR and its dried
183 composite as follows:

184 $$Water\ absorbency\ (g/g) = \frac{(W_1 - W_0)}{W_0} \quad (1)$$

185

186 where W_0 is the weight of the dried WSNR and W_1 is the weight of the swollen
187 WSNR. In this work, the water absorbency of the WSNR composites before
188 vulcanization (rubber compound) and after vulcanization (rubber vulcanizate) was
189 carried out.

190

191 ***2.6 Cure characterization***

192 A rotorless rheometer (Rheo Tech MD+, Tech Pro, Inc., from Cuyahoya Falls,
193 U.S.A.) was used to determine the curing characteristics of the rubber composites at
194 160 °C with 1° arc and 60 min. The optimum cure time (tc_{90}) and scorch time (t_{s1}), the
195 minimum and maximum torque (M_L and M_H, respectively), and delta torque (M_H -
196 M_L) were determined from the curing curves. Cure rate index (CRI) was measured
197 based on ASTM D5289 and the formula for the calculation is shown below.

198

199 $$CRI = 100/t_{c90}\text{-}t_{s1} \quad (2)$$

where t_{s1} is the time required to increase one unit torque from the minimum torque, t_{90} is the time required to reach 90% of the total cure.

Vulcanizates with a thickness of approximately 550 ± 50 μm were then prepared by compression molding at 160 °C according to the determined optimum cure time (tc_{90}). The mechanical, morphological and water absorbency properties of the composite vulcanizates were investigated.

2.7 Infrared Spectroscopic Analysis

The existence of the functional groups of the rubber samples and raw materials was investigated by Fourier Transform Infrared Spectroscopy (FT-IR; System 2000, Perkin Elmer, U.S.A.). The dried sample and KBr powder were mixed, ground, pressed, and then subjected to the FT-IR spectrometry.

2.8 Microstructure studies

Scanning electron microscopy (SEM) (model JSM-6510LA, Jeol Ltd., Akishima, Japan) was used to characterize microstructures of the cryogenic fractured surfaces of the WSNR composites. The samples were coated with a thin layer of gold under vacuum before characterization.

2.9 Thermal properties analysis

Thermal behavior of the WSNR composite at different PEO contents was investigated using differential scanning calorimetry (DSC) (Mettler Toledo DSC823e/400, USA) and thermogravimetric analysis (TGA) (Mettler Toledo). In the case of DSC, the powder sample sealed into the aluminum pan was heated up at the rate of 10 °C min^{-1} from -50 to 100 °C. During the heating, nitrogen gas (N_2) was

flowed into the furnace at a flow rate of 20 cm^3 min^{-1} for 5 min. In TGA, the samples were put inside alumina pans hanged in the heating furnace. The weight of remaining material was recorded while the furnace was heating from 25 °C to 500 °C at a rate of 10 °C min^{-1}. Oxygen (O_2) was fed into the furnace at 20 cm^3 min^{-1} as a purge gas.

2.10 X-ray diffraction analysis

X-ray diffraction measurements of WSNR composite at different PEO contents were carried out using an X-Ray Diffractometer: Bruker AXS Germany (Model D8 Advance with the target and wavelength (CuK_{∞} radiation, λ = 0.15406 nm, 40 kV, 30 mA). The X-ray diffraction (XRD) patterns were recorded from 5° to 80° with an increment of 0.02 degree in a 2θ mode at a scanning rate of 1° min^{-1}. The dried composite powder was mounted on a sample holder with smooth double-sided adhesive tape.

2.11 Mechanical properties

Dumbbell shaped specimens were prepared from a sheet of the rubber vulcanizates by die cutting according to ASTM die type C. The stress-strain behavior of the vulcanizates was then investigated using a universal tensile testing machine (Hounsfield Tensometer, model H 10KS, Hounsfield Test Equipment Co., Ltd, Surrey, U.K.) at a speed of 500 mm/min and an initial gauge length of 25 mm, according to ASTM D412. The tensile strength and elongation at break were then determined based on the stress-strain behavior.

3. RESULTS AND DISCUSSION

3.1 IR studies

The materials derived were investigated for IR spectroscopic information to look for some interaction. Figure 1 B illustrates the peaks of the unmodified NR synthesized with bentonite-modified SAP and compounded with PEO with/without TMPTMA, the additional peaks are found as follows.

Sample A [NR+bentonite]: one can see the peak at 3318 cm^{-1} ν(-OH) of Si-OH group; the peak at 1646 cm^{-1} for deformation vibration of the interlayer water in the clay; the peak at 1263 cm^{-1} ρ_s(-Si-CH_3), peaks at 1100 cm^{-1} ν(-Si-O) in-plane, and 1030 cm^{-1} ν(-Si-O) out-of-plane (Alabarse, Conceição, Balzaretti, Schenato & Xavier, 2011; Paluszkiewicz, Holtzer & Bobrowski, 2008; Madejova, Janek, Komadel, Herbert & Moog, 2002; Özcan & Özcan, 2004).

Sample B ([NR+ bentonite + PEO (10 phr)]: the additional peak at 3318 cm^{-1} ν(-OH) of Si-OH group; 873 cm^{-1} ρ(Al-Fe-OH) bentonite.

Sample C [NR+ bentonite + PEO (10 phr) + TMPTMA (2 phr)]: the additional peaks were found as follows: 3318 cm^{-1} ν(-OH) of Si-OH group; 1725 cm^{-1} ν(C=O) TMPTMA, and 1145 cm^{-1} ν(C-O-C) PEO.

Sample D [NR+ bentonite + PEO (20 phr) + TMPTMA (2 phr)]: additional peaks were found: 3318 cm^{-1} ν(-OH) of Si-OH group; 1725 cm^{-1} ν(C=O) TMPTMA; 1637 cm-1 ν(C=O) PEO; 1342 cm^{-1} $\delta_s CH_2$ PEO; and 1143 cm^{-1} ν(C-O-C) PEO.

Sample E [NR+ bentonite + PEO (40 phr) + TMPTMA (2 phr)]: additional peaks were found: 3318 cm^{-1} ν(-OH) of Si-OH group; 1725 cm^{-1} ν(C=O) TMPTMA;

1360 cm^{-1} $\delta_S(CH_2)$ PEO; 1145 cm-1 ν(-C-O-C) PEO; 916, 842 cm^{-1}, ρ_{CH_2} (guache) (Manoratne, Rajapake &Dissanayake, 2006; Zain & Arof, 1998).

Sample F [ENR+ bentonite + PEO (10 phr) + TMPTMA (2 phr)]: 3318 cm^{-1} ν(-OH) of Si-OH group; 1725 cm^{-1} ν(C=O) TMPTMA; 1539 cm^{-1}???; 1342 and 1360 cm^{-1} δ_s CH_2 PEO; 1144 cm^{-1} ν(C-O-C) PEO; 962, 946 and 873 cm^{-1} ν(oxirane ring) epoxide (Zong-Qiang, He-Ping, Qi-Fang & Guang, 2008; Yoksan,2008)

Sample G [MNR+ bentonite + PEO (10 phr) + TMPTMA (2 phr)]:)]: 3318 cm^{-1} ν(-OH) of Si-OH group; 1793 cm^{-1} ν(C=O) succinic anhydride rings; 1723 cm^{-1} ν(C=O) succinic acid (hydrolysis of succinic anhydride ring); 1146 cm^{-1}, ν(C-O-C) PEO; 872 cm^{-1} ν(oxirane ring) maleic anhydride (Saelao & Phinyocheep, 2004; Nakason, Kaesaman & Supasanthitikul, 2004; Vicente, Campos, Bordado & Ribeiro, 2008).

3.1 Influence of PEO and TMPTMA on Curing Properties

The curing curves of the WSNR composites and those with the addition of PEO with and without the co-addition of TMPTMA reveal that all of the composites have a curing equilibrium state (the plateau curves), with equilibrium being obtained with 20 min (Figure 2). Furthermore, the NR-based composites alone (i.e. without PEO and TMPTMA) showed the longest delayed action at the beginning of the curing with the longest scorch time of 4.0 min (Table 3). Incorporation of 10 phr PEO produced a significantly shorter scorch time (1.43-fold) of the composites due to reactivity of PEO with polar functinal groups in the composite system. Moreover, co-incorporation of 2 phr TMPTMA with the PEO induced only a slight reduction in the scorch time compared with the one without PEO and TMPTMA, and much less than

with the addition of the same content (10 phr) of PEO alone. This is attributed to the fact that, besides the role of crosslinking agent, TMPTMA could react with the TBBS accelerator and delay the scorching of the materials while a shorter scorch time resulted from the incorporation of the PEO. In this scenario then, these two effects overshadow and compensate each other with a net unchanged scorch time. Basically, the addition of zinc oxide (ZnO) as an activator for the sulfur vulcanization of rubbers enhances the vulcanization efficiency and vulcanizate properties and reduces the vulcanization time. The co-addition of 2 phr TMPTA and 10 phr PEO reduced the scorch time by 1.11-fold compared to that with no addition, but to a lower extent than the addition of 10 phr PEO alone (Table 3). Moreover, the incorporation of 10 phr PEO and 2 phr TMPTMA also slightly decreased the crosslinked density (M_H - M_L) and the cure rate index (CRI), by significantly decreasing both the minimum and the maximum torque, of the rubber composites.

3.2 Influence of PEO and TMPTMA on Water Absorbency

Figure 3 illustrates the water absorbency capabilities of the WSNR composites and vulcanizates, either alone or with the addition of 10 phr PEO with or without the coaddition of 2 phr TMPTMA. With each given blend system, the WSNR composite compounds exhibited a higher water absorbency (e.g. 2.6-fold to 4.7-fold higher at two days of immersion) than that of the corresponding vulcanizate at all time points. This is attributed to the crosslinked structure that is formed in the rubber vulcanizates and provides a lower free volume for water to enter into the bulk of the rubber. As a result of the hydrophilic nature of PEO, its incorporation at 10 phr rendered a higher water absorbency capacity of the products. Furthermore, the PEO contributed to a better dispersion of the SAP and SAPC in the rubber matrix. The highest water

absorbency was obtained in the WSNR containing both 10 phr PEO and 2 phr TMPTMA. The hydrophilic nature of both PEO and TMPTMA has the capability to form a strong hydrophilic network with NR, SAP, PEO and SAPC to generate the highest water absorbency.

Three PEO loadings (10, 20 and 40 phr) at a fixed concentration of 2 phr TMPTMA used to prepare WSNR composite compounds and their associated vulcanizates are shown in Figure 4. The water absorbency capabilities of these vulcanized and unvulcanized WSNR composites differed, where as expected, at each given loading of PEO, the water absorbency capabilities of the unvulcanized composite compounds were higher than those of the corresponding vulcanizates at all time points of water immersion (e.g. from 1.4-fold to 2.6-fold after two days immersion). The water absorbency of the unvulcanized composite compounds with and without PEO differed, showing a slightly decreasing trend with increasing immersion times of longer than 6 days in the absence of PEO, but remained constant (10 phr PEO) or continued to increase (20 & 40 phr PEO) after six days of immersion. Probably the SAP was prone to be eluted from the composite compounds into the water phase due to lack of interaction between the different phases of the composite compounds. Certainly, increasing the PEO loading to 20 and 40 phr increased the water absorbency at each time point of water immersion and lead to increasing water absorbency with increasing water immersion times. A corresponding trend, but with a lower magnitude, was observed for the water absorbency in the vulcanizates. This suggested a stronger network because of the interaction between the polar functional groups and the reactive groups of different components in the composites. The WSNR composite vulcanizates showed the highest water absorbency capacity of 530% (w/w) at a PEO loading of 40 phr after 14 days of water immersion.

3.3 Influence of PEO and TMPTMA on Mechanical Properties

The tensile strength and elongation at break of WSNR composite vulcanizates decreased and increased slightly, respectively, with increasing water immersion time (Table 4). This suggests that a certain portion of the water sensitive SAP or SAPC still present in the composites is not damaged by a long-term immersion in water, and so the strength of these materials can potentially be used in damping conditions. It was also noted that the inclusion of 10 phr PEO to the vulcanizates significantly (1.24-fold to 1.1-fold at 0 to 14 days immersion time, respectively) increased the elongation at break but had only a marginal affect on the tensile strength due to the presence of the crosslinked network that is capable of a higher elongation. In contrast, the co-addition of 2 phr TMPTMA with 10 phr PEO to the WSNR composite vulcanizates and compounds resulted in the highest tensile strength properties, but essentially the same elongation at break values (Table 4). The WSNR with PEO or with PEO plus TMPTMA showed the same trend of a decreasing tensile strength with increasing water immersion time and an opposite but weaker trend for the elongation at break.

The influence of the PEO loading levels on the tensile strength and elongation at break of the WSNR composite vulcanizates is shown in Table 4, respectively. As expected, for all four PEO loadings (0, 10, 20 and 20 phr), increasing the water immersion time rendered a decreasing trend of the tensile strength, which is attributed to the swelled hydrophilic components of the WSNR composites. At any given immersion time larger than 2 days, the composite loaded with 10 phr PEO exhibited the highest tensile strength and that with a PEO of 40 phr exhibited the lowest strength. The tensile strength of the WSNR composites with different PEO loadings could then be ranked as follows: 10 phr > 0 phr > 20 phr > 40 phr. The WSNR composite vulcanizate loaded with 10 phr PEO is presumed to have the appropriate

371 amount to react and interact between the different components. Wang et al [1999]
372 found that when increasing the amount of PEO in the blends, it could not only
373 decrease the intermolecular forces of the NR phase functioning as a plasticizer, but
374 also produced more flaws in the rubber phase and also increase the low crosslinking
375 density moieties. The mechanical properties thus decreased in which they found
376 coincided with the decreases in crosslinking density.

377 The elongation at break (Table 4) is increased by incorporation of PEO into
378 the WSNR composite vulcanizate at all three levels examined (10, 20 and 40 phr vs. 0
379 phr), but to essentially the same extent for all three PEO inclusion levels at any water
380 immersion time. However, the WSNR composite vulcanizates without PEO exhibited
381 the lowest extension capability. It is likely that the swelling network of PEO could
382 lubricate the WSNR composite system to gain more extensibility. These properties
383 then mean that these WSNR composite vulcanizates can likely be used for sealing and
384 caulking applications.

385

386 ***3.4 Influence of PEO and TMPTMA on Morphological Properties***

387 SEM micrographs of the WSNR composite vulcanizates with PEO loadings at
388 20 and 40 phr before and after immersion in water for 14 days show clear differences
389 in morphologies in Figure 5a and 5c and Figure 5b and 5d, respectively. The white
390 particulates and agglomerates of SAP, SAPC, PEO and ZnO are clearly observed as
391 particulate in nature before immersing in water (Figure 5a and 5b), but after
392 immersion in water for 14 days, a large number of holes were seen while the white
393 particulates or agglomerates had disappeared (Figure 5c and 5d). The higher (40 phr)
394 PEO loaded WSNR composite vulcanizates (Figure 5 d) had larger holes in the
395 surface after a long time immersion in water, suggesting that some of the PEO, SAP

and SAPC, the hydrophilic nature materials, were removed from the composites. This appearance could be related to the inferior mechanical strength of the WSNR composites (Table 4).

3.5 Thermal properties analysis

Figure 6A shows the DSC curves of WSNR composites with different contents of PEO in which the WSNR composite without PEO exhibited no peak while two transition peaks at approximately –12 °C and 38 °C were observed when the PEO contents were 20 and 40 phr, respectively. The first peaks may be caused by PEO which was well-dispersed and interacted with the WSNR composites whereas the second peak might be caused by the phase separation due to the excess PEO content. The intensity of PEO peaks at 38 °C increased with increasing amounts of PEO loading in the WSNR composite (Figure 6A (c, d)). This result indicates that the crystallization of PEO in the WSNR composite is strictly confined.

Thermal stability is an ability of a material to maintain its physical properties when being exposed to high temperatures. The TGA curves in Figure 6B show that the neat PEO in curve (a) is the most thermally stable material, whereas the WSNR composites having higher PEO content (Figure 6B (c, d)) are more stable materials than the WSNR composite without PEO (Figure 5B (b)). This is additional evidence that the PEO crystalline phases were dispersed in the polymer matrix in the XRD work to be discussed below.

3.5 Effect of PEO amount loaded in unmodified WSNR *on mechanical properties*

The XRD patterns of bentonite, PEO and SAP (all starting materials for preparing WSNR), unmodified WSNR composites in the different contents of PEO,

421 and the modified NR are graphically represented in Figure 6. The XRD pattern of
422 bentonite was found at 6.02° with a d-spacing value of 14.7 Å, while those of PEO at
423 19.6° and 23.7° had the d-spacing values of 4.5 and 3.8Å. The starch-*g*-PAM had
424 only one intense peak at 22.1° with a d-spacing of 4.0Å. Table X illustrates the
425 effect of PEO and TMPTMA loadings on XRD pattern. The XRD pattern of WSNR
426 composite without PEO (Figure 7 (a)) showed a strong peak at $2\theta = 9.54°$ which
427 involves that the layers of bentonite were partially exfoliated in the polymer matrix.
428 The absence of diffraction peaks for WSNR composite with PEO 10 phr (Figure 7
429 (b)) suggests that the bentonite clay has been totally exfoliated and dispersed in the
430 polymer matrix to form a nanocomposite structure. The WSNR composites with
431 various contents of PEO (Figure 7 (c, d)) produced the peaks at approximately $2\theta =$
432 19.2° and 23.3° correspond to the 011 and 210 planes of the crystalline structure of
433 PEO in the polymer composite [Wang, Li & Chen, 1999]. The intensity of the
434 characteristic PEO peaks increased more intensely with increasing amounts of PEO
435 loadings in the WSNR composite, in comparison with the WSNR composite with less
436 PEO loadings (Figure 7 (b, c)). Thus, mechanical properties of the swollen rubber
437 samples decreased with an increase in the amount of PEO as mentioned above due to
438 increases in the absorbed water.
439
440 ***3.6 Influence of NR Type on Curing Properties.***
441 The curing curves of the WSNR composites derived from three different types
442 of rubber bases (NR, ENR and MNR) revealed that the unmodified NR and the ENR
443 exhibited broadly similar curing characteristics (Figure 8) and a broadly similar
444 scorch time (Table 4). Likewise, the curing curves revealed they reached an
445 equilibrium state by about 10 min for NR to 20 min for ENR. In contrast, the curing

curve of the MNR containing WSNR compound exhibited a very slow and delayed action, not beginning to cure until after some 10 min and then proceeding slowly such that equilibrium was still not attained after 60 min, a characteristic marching curve, where only a slight increase in the torque with increasing time was observed. In addition, the MNR compounds exhibited a significantly longer scorch time (3.3- and 3.83-fold) and cure time (3.19- and 4.46-fold) than did the ENR and NR vulcanizates, respectively, together with the lowest cure rate index (2.92- and 5.71-fold) and crosslinked density (2.53- and 2.17-fold, respectfully) (Table 3). This effect is induced by the remaining maleic anhydride, and maleic acid from the reaction with moisture, which then react with the TBBS accelerator. As a direct consequence there is insufficient TBBS accelerator left for the vulcanization process leading to the inferior curing characteristics. Also seen in Figure 8 and Table 4 is that the ENR compound exhibited the longest cure time and the lowest cure rate index compared with the unmodified NR compound. However, the ENR compound gave the highest crosslinked density. This could be caused by the chemical interaction from the polar functional groups in ENR molecules with the blend components, and the coupling reaction among the blend components with TMPTMA.

3.7 Influence of the NR Type on Water Absorbency

The water absorbency of the WSNR composite compounds and vulcanizates derived from NR, ENR and MNR show marked differences (Figure 9). In all cases the water absorbency of the WSNR composites increased with increasing immersion time and were still increasing after 14 days of water immersion (the longest time point assayed), although this was less marked for the vulcanized samples than the unvulcanized ones. The modified NR (i.e., ENR and MNR) showed a markedly

471 higher (from 2.8- and 3.4-fold to 2.0- and 2.5-fold higher for ENR and MNR at two
472 and 14 days immersion, respectively) water absorbency of the WSNR composite
473 compounds (unvulcanized) than NR. Indeed, ENR showed the highest water
474 absorbency followed by MNR and the unmodified NR showed by far the lowest water
475 absorbency and this trend was maintained over the entire 14 days of water immersion.
476 This is attributed to the stronger chemical interactions and bonding between the
477 modified NR, PEO and SAPC that are assisted by the TMPTMA. However, note that
478 although the vulcanizates showed the same trend of water absorbency and the same
479 ranked order of ENR > MNR > NR, a lower level of water could enter into the
480 crossliked structure of the vulcanizates and the difference in magnitude between the
481 three different rubber types was less marked than in the non-vulcanized samples.
482 Thus, the water absorbency of the ENR based WSNR vulcanizate showed the highest
483 value with the maximum value at approximately 600 wt% for the vulcanizate.
484

485 ***3.8 Influence of type of natural rubber on Mechanical properties***

486 The tensile strength and elongation at break of the WSNR vulcanizates derived
487 from the NR, ENR and MNR show clear differences (Table 6). As with the higher
488 water absorbency, the WSNR of ENR and MNR showed a dramatic reduction in the
489 tensile strength. It is possible that some NR molecules might be degraded during the
490 modifying process. Additionally, a number of polar functional groups along the chain
491 of NR that form weak linkages, such as –C-O, and -O-O-, are removed in the
492 modification process. The elongation at break of the WSNR vulcanizates increased
493 slightly with increasing immersion time, but the ENR- and MNR-based WSNR
494 vulcanizates yielded lower elongation at break values that were still within the range

of good extensibility of the rubber vulcanizates. Therefore, it is concluded that the ENR and MNR base WSNR vulcanizates exhibited a superior water absorbency but

One can see that the peak intensity at 873 cm^{-1} in (e) and (f) for the inclusion of 10 phr PEO decreased sharply which is in agreement with the XRD and thermal properties. As mentioned by Wang et al (1999) that increases in PEO content had a significant effect on the crystallinity of the vulcanized rubber, i.e., the PEO contents higher than 10 phr are not used in the process and cause increases in water absorption which reduce tensile strength.

CONCLUSION

SAPs of CSt-*g*-PAM were prepared by a reactive batch process using a specially designed batch reactor. The SAPCs were then prepared with the addition of 20 phr bentonite clay to the SAP mixture. WSNRs were prepared by blending HANR latex, or dry blending of ENR or MNR, with the SAPC alone or with the addition of various loadings of PEO with or without the co-addition of 2 phr TMPTMA. The WSNR compounds and vulcanizates with PEO and TMPTMA gave the highest mechanical strength and water absorbency. A PEO loading of 10 phr gave the highest mechanical strength and water absorbency compared with the WSNR without PEO. Increasing the PEO loading increased the water absorbency and lowered the mechanical strength, with the lowest tensile strength being observed at a 40 phr PEO loading. The curing behavior of the WSNR depended on the NR type. The highest scorch time and cure time with the lowest crosslinked density and cure rate index were obtained in the MNR based WSNR, whilst the ENR based WSNR exhibited the highest water absorbency but with a lower mechanical strength than that of the WSNR made from the unmodified NR.

ACKNOWLEDGEMENTS

The authors are indebted to the Thailand Research Fund for funding the research project under the Research Team Aid (Grant no. RTA5080004). Sincere thanks and appreciation are given to the Prince of Songkla University (Pattani Campus) and Chulalongkorn University for provision of the research facilities. Language editing from Publication Consultation Unit of the Research Division, Faculty of Science, Chulalongkorn University, is acknowledged.

REFERENCES

Alabarse, F. G.; Conceição, R. V.; Balzaretti, N. M.; Schenato, F.; Xavier, A. M. (2011). In-situ FTIR analyses of bentonite under high-pressure. *Applied Clay Science 51*, 202-208.

Athawale, V.D, Lele, V. (1998). Graft copolymerization onto starch. II. Grafting of acrylic acid and preparation of its hydrogels. *Carbohyd. Polym.*, **35**, 21.

Athawale, V.D., Lele, *V.* (2000). Thermal Studies on Granular Maize Starch and its Graft Copolymers with Vinyl Monomers. *Starch/Starke*, **52**, 205.

Carr, M. E., Kim, S., Yoon, K. J., & Stanley, K. D. (1992). Graft polymerization of cationic methacrylate, acrylamide, and acrylonitrile monomers onto starch by reactive extrusion. *Cereal Chem*, **69**, 70–75.

Chen, J., Park, H., and Park, K. (1999). Synthesis of superporous hydrogels: hydrogels with fast swelling and superabsorbent properties, *J Biomed Mater Res*, **44**, 53.

Chen, L., Ni, Y., Bian, X., Qiu, X., Zhang, X., Chen, X. A novel approach to grafting polymerization of ε-caprolactone onto starch granules (2005). *Carbohyd. Poly*m., **60**, 103.

545 Finkenstadt, V.L., Wilett, J.L. (2005). Reactive Extrusion of Starch-Polyacrylamide
546 Graft Copolymers: Effects of Monomer/Starch Ratio and Moisture Content
547 Karadag, E; Uzum, OB; Saraydin, D. (2005). Water uptake in chemically crosslinked
548 poly(acrylamide-*co*-crotonic acid) hydrogels*, Mater Design*, **26 (4)**, 265–270.
549 Kiatkamjornwong, S., Mongkolsawat, K., Sonsuk, M. (2002). Synthesis and property
550 characterization of cassava starch grafted poly[acrylamide-*co*-(maleic acid)]
551 superabsorbent via γ-irradiation *Polymer*, **43**, 3915.
552 Lanthong, P., Nuisin, R., Kiatkamjornwong, S. (2006). Graft copolymerization,
553 characterization, and degradation of cassava starch-*g*-acrylamide/itaconic acid
554 superabsorbents *Carbohyd. Polym.* **66**, 229.
555 Liu, C., Ding, J., Zhou, L., Chen, S. (2006). Mechanical properties, water-swelling
556 behavior, and morphology of water-swellable rubber prepared using
557 crosslinkedsodium polyacrylate *J. Appl. Polym. Sci.*, **102**, 1489**.**
558 Madejova, J., Janek, M.; Komadel, P., Herbert, H.-J., Moog, H. C. (2002) FTIR
559 analyses of water in MX-80 bentonite compacted from high salinity salt solution
560 systems. *Applied Clay Science 20*, 255- 271.
561 Manoratne, C. H.; Rajapakse, R. M. G.; Dissanayake, M. A. K. L. (2006). Ionic
562 Conductivity of Poly(ethylene oxide) (PEO)-Montmorillonite (MMT)
563 Nanocomposites Prepared by Intercalation from Aqueous Medium.
564 *International Journal of Electrochemcal Science, 1*, 32-46.
565 Mostafa, K.H.M. (1995). Graft polymerization of acrylic acid onto starch using
566 potassium permanganate acid (redox system) *J. Appl. Polym. Sci.*, **56**, 263.
567 Nakason, C., Saiwari, S. (2008). Effect of Grafted Maleic Anhydride Content
568 Recyclability of Dynamically Cured Maleated Natural Rubber/Polypropylene
569 Blends.*J. Appl. Polym. Sci.*, **110,** 4071.

570 Nakason, C., Wohmang, T., Kaesaman, A., Kiatkamjornwong, S. (2010). Preparation
571 of cassava starch-graft-polyacrylamide superabsorbents and associated
572 composites by reactive blending *Carbohyd. Polym.*, **81,** 348.

573 Özcan, A. S., Özcan, A. (2004). Adsorption of acid dyes from aqueous solutions onto
574 acid-activated bentonite. *Journal of Colloid and Interface Science 276*, 39-46.

575 Paluszkiewicz, C., Holtzer, M., Bobrowski, A. (2008). FTIR analysis of bentonite in
576 moulding sands. *Journal of Molecular Structure 880*, 109-114.

577 Park, J.H., Kim, D. (2001). Preparation and characterization of water-swellable
578 natural rubbers *J. Appl. Polym. Sci.*, **80**,115.

579 Wang, C., Zhang, G., Dong, Y., Chen, X., Tan, H. (2002). Study on a water-
580 swellable rubber compatibilized by amphiphilic block polymer based on
581 poly(ethylene oxide) and poly(butyl acrylate). *J. Appl. Polym. Sci.*, **86**, 3120
582 (2002).

583 Wang, G., Li, M., Chen, X. (1999). Effects of fillers on mechanical properties of a
584 water swellable rubber *J. Appl. Polym. Sci.* **72**, 577.

585 Willet, J.L., Finkenstadt, V.L. (2003). Preparation of starch-graft-polyacrylamide
586 copolymers by reactive extrusion, *Polym. Eng. Sci*, **43**, 1666.

587 Willette, J.L., Finkenstadt, V.L. (2006). Reactive Extrusion of Starch–Polyacrylamide
588 Graft Copolymers Using Various Starches. *J. Polym. Environ*, **14**, 125.

589 Yoksan, R. (2008). Epoxidized Natural Rubber for Adhesive Applications. *Kasetsart*
590 *Journal: Natural Science 42*, 325 - 332.

591 Yoon, D. J., Carr, M. E., & Bagley, E. B. (1992). Reactive extrusion vs. batch
592 preparation of starch-*g*-polyacrylonitrile. *J. Appl. Polym. Sci.,* **45**, 1093–1100.

593 Zain, N. M.; Arof, A. K. (1998). Structural and electrical properties of poly (ethylene
594 oxide)-cadmium sulphate complexes. *Materials Science and Engineering: B 52*,
595 40-46.

596 Zhang, G., Zhang, Z., Xie, F., Hu, X., Luo, X. Chen, X. (2000). Chlorohydrin water
597 swellable rubber compatibilized by an amphiphilic graft copolymer. I. Synthesis
598 and characterization of compatibilizer PVA-*g*-PBA *J. Appl. Polym. Sci.*, **75**,
599 977.
600 Zhang, Z., Zhang, G., Li, D., Liu, Z., Chen, X. (1999). Chlorohydrin water-swellable
601 rubber compatibilized by an amphiphilic graft copolymer. II. Effects of PVA-*g*-
602 PBA and CPA on water-swelling behaviors, *J. Appl. Polym. Sc.i*, **74**, 3145.
603 Zhang, Z., Zhang, G., Wang, C., Liu, D., Liu, Z., Chen, X. (2001). Chlorohydrin
604 water-swellable rubber compatibilized by an amphiphilic graft copolymer. III.
605 Effects of PEG and PSA on water-swelling behavior, *J. Appl. Polym. Sci.*, **79**,
606 2509
607 Zong-Qiang, Z.; He-Ping, Y.; Qi-Fang, W.; Guang, L. (2008). Effects of Coagulation
608 Processes on Properties of Epoxidized Natural Rubber. *Journal of Applied*
609 *Polymer Science 109*, 1944-1949.